CONTENTS

Acta Technica *62* No. 2B/2017, 1–10

Early warning of pirate attacks based on decision tree[1]

Sun Mao-jin[1,2], Lv Jing[1], Gao Tian-hang[1], Sun Xiao-shan[1]

Abstract. Considering the pirates threats to the international transport ships, a constructed forewarning model of pirates attack can provide warning information before it happens, and it will reduce the probability of attack substantially. Therefore, a forewarning model based on decision tree is constructed to study the correlation between the severity of pirates attack and other factors. This method takes the ships types and geographic areas as input data, pirates attack consequence as output data, and the pirates attack in the waters of east Africa as study subjects. After the validation, the results show that the predictions are much better than random guesses. This proves that the method is effective and scientific.

Key words. Ship security, pirates attack, forewarning, decision tree.

1. Introduction

As the trades among various countries in the world gets frequent, marine transport has been becoming more and more important in international society, which has turned into one of the foremost transportation modes. However, transport ships have been affected greatly by the traditional and unconventional security threats. The security issue is one of the problems the practitioners concern most. With the development of technologies, the security issues of marine transport system, primarily caused by climate and geographical factors, have been decreased greatly. But the unconventional security threats still exist violently, which is mainly reflected as piracy and maritime terrorism. By taking the piracy incidents with most extensive impact as examples, as for the international waters, the piracy activities frequently occurs in several areas, including Aden Gulf, Indian Ocean, West Africa coast, Malacca and sea areas belonging to South China Sea. To deal with these situations, it is particularly necessary to make clear how to build the piracy forewarning

[1]College of Transportation Management, Dalian Maritime University, Dalian 116026, Liaoning, China
[2]Corresponding author

model by reasonable algorithm for warning the passing transport ships before pirates attack based on the current information, guiding them to deviate and take effective measures.

At present, the direction of research on the pirate attacks are diversified, covering politics, society, military affairs and management, etc. For settling the matter of Somali pirates, [1] has discussed and analyzed its multifaceted problem, such as formation history, organization and operation, countermeasures taken by various countries internationally, etc. [2] has studies the economic losses of marine transport ships brought about by the pirate attacks. [3] treats the private attacks as one of dynamic behaviors, analyzes the number and movement area of privates by using the dynamic model, and takes the areas in Aden Gulf as case to study. Literature [4] proposes a new escort maneuver for warships combating pirates by adopting the idea about covering priority area first, so as to improve navy's combat efficiency. References [5—6] respectively uses the Stackelberg game and evolutionary game to simulates the game process between navy and pirates; afterwards, naval escort area has been selected while the decision-making process between both of them has been refined. Reference [7] adopts the game theory to study the fairway programming in order to provide the navigation route, of which can avoid the private attacks, for the transport ships. There are no researches on forewarning of privates attacks despite the fact that privates attacks studies are relatively plentiful. To build a better forewarning model of pirate attacks, this paper chooses the researches related to forewarning as references. Paper [8] applied the combination of fuzzy comprehensive evaluation and analytic hierarchy process (AHP) to forewarning classification of public emergencies; on that basis, forewarning classification model is formed. Reference [9] built the BP neural network model by using neural network method based on the characteristics of petroleum safety precaution. Paper [10] built the alarm index system and forewarning model for spatial agglomeration suitability of manufacturing industry by catastrophe series method, which achieved great forewarning results. Reference [11] set up the incident-based forewarning system of supply chain so as to supervise and alert the timeliness of supply chain. Liu et al. [12] created a public information space for urban flood disaster in order to forewarn this kind of natural hazard. In conclusion, many attempts in the other forewarning study are done by the relevant scholars, which offers the formed thoughts and approaches that play an enlightening role in the research of this paper. This paper builds a forewarning model of pirate attacks by selecting the proper method and referring to the historical data characteristics and forming processes of pirate attacks

1.1. Decision tree overview

Decision tree is a common method with supervised classification in machine learning. In a generated decision tree, a node represents an attribute, and its branch is the optional value of corresponding attribute. When a sample is going to be classified, node will be sought out in accordance with the attribute value correspondingly based on the sample characteristics; and then, the previous step shall be run repeatedly till leaf node is reached. Prediction classification of this sample is the leaf

classification, thereby the classification is completed. As for construction algorithm of decision tree, this paper set ID3 algorithm as example. ID3 is one of algorithms constructing the decision tree that are built on the information theory while taking the information entropy and information gain degree as valuation criterion. Intuitively, a higher information gain can distinguish various samples better. Sample points are classified to a node (e.g. root node); ID3 calculates the information gain partitioned by each attribute. Afterwards, the attribute with highest gain is selected as the classification attribute, which is also the standard to partition the sample to the next child node of corresponding value, and then this step should be repeated starting from the child node till there are no more attributes to be used, or new information gain to be partitioned.

Mathematical formulation of decision tree: the expression of information entropy is $H(S) = -\sum_{x \in X} p(x) \log_2 p(x)$. Symbol S represents the data set, X is the classification result of S, x is one member set of classifications in S, $p(x)$ is the proportion of Class x. It can thus be seen that, when there is only one classification in S, the information entropy is 0. But if there are more classification in S, the more the proportion, the higher the information entropy. That is to say, the information entropy reflects the impurity level of data. The information gain is built on the information entropy, thus it shows the change of information entropy both before and after data set is partitioned, namely the impurity level variation of pre- and post-data. The information gain is represented by $IG(A)$. In the formulation $IG(A) = H(S) - \sum_{t \in T} p(t)H(t)$, where $H(S)$ is the information entropy before partitioned, t is one of multiple data set get from the partitioned attribute A, T is aggregate of these date sets, $S = \bigcup_{t \in T} t$, $p(t)$ is the proportion of member numbers of t in S, and $H(t)$ is the information entropy of data set t. If a given data set is partitioned by different attributes, the information entropy results are always different. The attribution with higher information gain enables to get nodes with higher purity after partitioned. Actually, ID3 adopts this logic to lower the classified information entropy fast.

1.2. Forewarning model construction for pirate attacks

In the forewarning model of pirate attacks, the navigation risk is predicted and judged according to the characteristics of this navigation, such as ship types, the waters covered by the lane, longitude and latitude, the relation with coastline, etc. Longitude and latitude, a single data, cannot provide any valuable information. Hence, this paper selects the space region formed by integrated conditions as characteristics of navigation risk. Specifically, the entire waters are divided into multiple areas based on the pirate attack time, and each area contains a class of pirate attack incidents. One classification has various elements related to pirate attack possibly. The elements are similar with each other in one classification, but different among classifications. This classification represents the different characteristics of pirates in different areas, for example, some pirates, who value the money, are used to kidnap the hostages for getting ransom; and some others do not care about sailors' lives, they will kill the sailors who put up a desperate struggle when they are opposed. This

situation is ascribed to the different movement range of pirates. Obviously, pirate characteristics in different areas have done a great deal to affect the danger levels in different areas. Except the basic characteristics, like ship types, the factor of pirate having different characteristics in different areas must be considered, too; in the meantime, ships sailing navigating into an area should be added into the judgment conditions of decision tree. Thus, for decision tree method, the best characteristic should be filtered for running the partition, which conforms to the conditions about one of attribute value and risk level. And then a new attribute will be searched to its child node. The decision tree is going to be constructed in this way. When steps are done, a navigation characteristic is put into the generated decision tree, finally getting a risk level as the prediction result. The specific algorithm of constructing a decision tree is shown as Fig. 1.

Data: Pirate Incident Sample X, available classification attribute A

Result: Root node of decision tree

If all samples are belonged to a same classification **then**

Return to the root node, the classification is sole classification

end

If there is no attribute to be used **then**

Return to the root node, the classification is value of majority samples

else

Find out the attribute T with largest information gain in the stand-by attribute A

Set T as root node

for possible value v of attribute T **do**

Add a new branch under the root node, corresponding valve v of T

if $Ex(v)$ of sample set is null under the branch $T = v$ **then**

Suppose the corresponding node of value v as leaf node, the classification is the majority classifications in all samples.

else

Execute $ID3(Ex(v), A - \{T\})$ and set this node as the returned result.

end

end

end

Fig. 1. ID3 algorithm

2. Case study

To demonstrate that the forewarning model of pirate attack constructed based on the decision tree algorithm in this paper has certain practical value, this paper selects the statistic pirate attacks of GISIS database occurred in the waters of East Africa

as research objects, and set the ship types and geographic areas as the forewarning information for verifying the pirate-attack-result-oriented forewarning result.

2.1. Data processing

The first step is to quantify the data. The quantitative method is determined by the data characteristics, and the quantitative objects mainly include ship types, geographic areas and consequence of pirate attack. The output variable calculated by the decision tree method related to consequence of pirate attack is easy to understand, which is used to represent the severity of pirate attack Here, this paper simply states why two factors, ship types and geographic areas, are chosen as the initial data. First reason is that different cargoes are loaded on the types of ships, which enable board height of ships are not same. For instance, the board of ship loading container cargo is higher than the others', because the container weight is lighter. Conversely, the board of ship loading dry and liquid bulk cargo is lower, because this kind of goods is heavier. The advantage of ship with high board is that pirates hardly climb up to embark for hijacking. But the ship with lower board is easy to attempt hijacking. From the perspective of earnings, pirates tend to hijack the ship with lower board generally. Second reason is about the geographic areas. Currently, pirates operate the mother ship mainly, who are going to unionized and scale up, but pirates cannot go to the place where is far away form their base on the coastline generally. That is to say, pirates from the different areas always appear in area where they often go due to the different centralized location of pirates. Furthermore, pirates from the different areas have attack preferences to different ship, which even causes various consequences due to diverse equipment and preferences. In general, ship types and geographic areas have a certain influence on the consequences of pirate attack. In database statistics, there are over 40 statements about ship type; and according to the research results provided by the author, there are 9 movement areas with different characteristics in waters of East Africa. In term of pirate attack consequence, ships are got the different result after robbed by pirates. However, the reports saved in the database describe those situations with some qualitative words, which makes that the two attributes mentioned above cannot be quantified simply. After the data is compared carefully, this paper finally decides to quantify depending on different keywords, and the selected specific keywords are:

1. Is there any sailor died: killed, dead;
2. Is there any sailor injured or missing: injured (badly, seriously), missing.
3. Is there any ship damaged, is there any cargo missing: broken, stolen, miss.

By quantified the basic data, this paper has processed the quantitative outcome further, mainly including categories of ship types and levels of pirate attack consequence. As for categories of ship types, there are over 40 types concluded from the first step, and it shows big quantity variance among each of types. This paper decides to divide these ships according to the type of cargoes after the specific ship type is analyzed. Finally, ships are divided into 5 categories, and the quantity variance of each category has been improved greatly. The specific category result is:

1st category: Ship loading dry and bulk cargo;

2nd category: Ship loading containers;
3rd category: ship loading liquid and bulk cargo;
4th category: ship loading sundry goods;
5th category: the others.

And speak of area selection, this paper divides the waters into numerous disjoint areas. If pirate attacks occur in a certain area, it means the area in attribute is the area number. For example, the waters of East Africa has been divided into 9 valid areas, so that there are 11 possible values from 0 to 11 totally by considering the areas are not classified and out of bounds. At last, the consequence levels are acquired from the keywords statistics, the result are: dead: 11; badly injured: 4; injured: 19; broken: 495; N/A: 670. Considering the casualty status of crew and damaged conditions of ships have different impact, this paper classified the consequences, and the specific levels are: 1st level: no crew casualties and damaged ships (N/A); 2nd level: the crew is injured slightly, or the ship is broken(injured, broken); 3rd level: the crew is injured slightly and the ship is broken (injured, broken); 4th level: Some crew members are dead, or the crew members are injured badly (dead or badly-injured). Based on the levels information, the statistical result is given as below: 1st level: 670 incidents; 2nd level: 486 incidents; 3rd level: 12 incidents; 4th level: 14 incidents.

2.2. Generation and verification of decision tree

The test is operated based on the processed data. By the consequence levels, it is found that the statistical differences between 1st and 2nd levels is large; and relatively speaking, the consequences of 3rd and 4th levels are worse badly. Thus, this paper adopts the sampling method used by re-sample method [15] to duplicate this part of data for enabling the data size of 1st and 2nd levels are equal basically. Afterwards, all the data are processed to generate the decision tree, shown as Fig. 2. The 1st layer is area, and the 2nd layer is ship type.

When the decision tree is constructed, the reasonability of generated decision tree should be verified. In consequences processing of pirates attack, the decision tree is constructed by all the data, this method brings the fitting risk undoubtedly. For this reason, this paper uses [16] the cross validation method to verify the validity of model and algorithm. Cross validation means that the original data is divided into two parts that respective are training set and test set. The training set is used to learn model, and the test set is applied for verifying the model regarded as learning outcome. The measurement standards obtained by this way are more persuasive. The model built by the data A is not used to verify A, but B, so there is no circulatory verification. This paper uses 5-fold cross validation, namely dividing into 5 parts at random. Four parts of them trains one test each time. This step should be repeated 5 times. In this paper, four evaluation criterions are adopted. Accuracy means the correct proportion; precision rate refers to the proportion of true normal sample in the predicted normal samples (precision rate = TP/(TP + FP)); recall rate means the how many normal samples are predicted correctly in all true normal samples (recall rate = TP/(TP + FN)); f1-score is a comprehensive score (fl = (2*precision

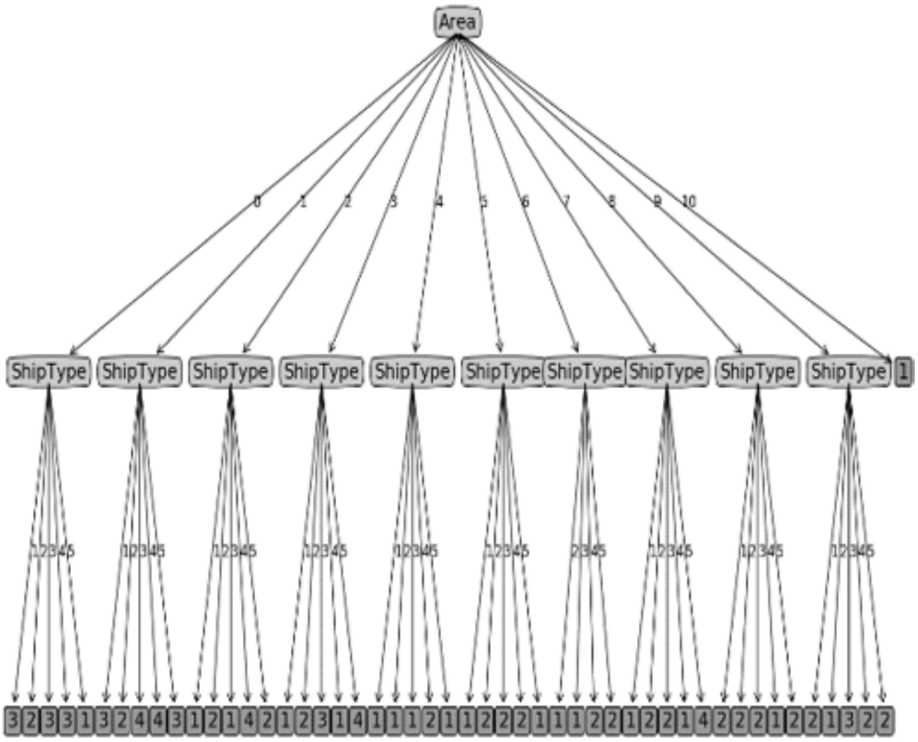

Fig. 2. Decision tree of pirate attack incidents

rate*recall rate/(precision rate+recall rate)). By calculated and verified, it is found that overall comprehensive accuracy is 57.1 %; severity level 1's precision rate, recall rate and f1-score respectively are 49.6 %, 20.2 % and 28.1%; severity level 2's are 55.0 %, 16.4 %, and 23.3 %; severity level 3's are 55.5 %, 84.8 % and 66.9 %; severity level 4's are 63.9 %, 100 % and 77.9 %. Because there are 4 severity levels, precision rate, recall rate and f1-score are only 25 % if predicted at random. It is thus observed that synthetically, the result concluded from the forewarning model of pirate attack with decision tree algorithm is far superior to the results of random guessing. Thus, this model is quite reasonable; especially the precision rate exceeds 50 %.

3. Conclusion

For forewarning transport ships early with the current information before pirates attack, this paper constructs the forewarning model of pirate attack based on the decision tree algorithm. This algorithm mainly considers the types of transport ships and geographical areas, and set them as the input data to predict risk levels of pirate attack. On that basis, this paper executes the practical calculation and verification according the basic data of pirate attack in East Africa area saved in GISIS database.

The verification result shows that compare with the random prediction, this model has obvious advantage because its precision rate of predicting pirate attack is over 50 %. However, due to the data characteristics of East Africa waters, this paper chooses two attributes, ship types and geographic areas, which can improve the predictive effect further, especially in the part of recall rate. The current result has proved the validity of this method. Meanwhile, when this model is used in practice, some diacritical attributes can be added to learn decision tree so as to realize better predictive effect.

References

[1] A. R. Andres, S. A. Asongu: *Fighting software piracy: which governance tools matter in Africa.* Journal of Business Ethics *118* (2013), No. 3, 667–682.

[2] B. S. Sergi, G. Morabito: *The pirates' curse: Economic impacts of the maritime piracy.* Studies in Conflict & Terrorism *39* (2016), No. 10, 935–952.

[3] E. Marchione, S. D. Johnson, A. G. Wilson: *Modelling maritime piracy: A spatial approach.* Journal of Artificial Societies and Social Simulation *17* (2014), No. 2, 1–9.

[4] L. Carral, C. F. Garrido, J. J. de Troya, J. A. Fraguela: *Considering anti-piracy ship security: Citadel design and use.* Brodogradnja/Shipbuilding *66* (2015), No. 3, 75–90.

[5] E. R. Gregorio: *The Filipino seafarers' lived experiences aboard international shipping vessels: A basis for health promotion intervention.* Acta Medica Philippina *45* (2012), No. 3, 69–74.

[6] M. Neocleous: *The universal adversary will attack: pigs, pirates, zombies, Satan and the class war.* Critical Studies on Terrorism *8* (2015), No. 1, 15–32.

[7] J. J. Dabrowski, J. P. de Villiers: *Maritime piracy situation modelling with dynamic Bayesian networks.* International Fusion *23* (2015), 116–130.

[8] J. Wei, F. Wang, M. K Lindell: *The evolution of stakeholders' perceptions of disaster: A model of information flow.* Journal of the Association for Information Science and Technology *67* (2016), No. 2, 441–453.

[9] C. H. Chen, C. M. Hong, T. C. Ou: *Hybrid fuzzy control of wind turbine generator by pitch control using RNN.* International Journal of Ambient Energy *33* (2012), No. 2, 56–64.

[10] S. Ota, Y. Kawatake, R. Kikuchi, K. Tamura: *Analysis on effectiveness of countermeasures against piracy based on incident data.* The Journal of Japan Institute of Navigation *128* (2013), 73–80.

[11] E. D. Carter: *Where's Che? Politics, pop culture, and public memory in Rosario, Argentina.* FOCUS on Geography *55* (2012), No. 1, 1–10.

[12] C. Liu, X. Zhao, M. Li: *Pre-alarm technique for gas disaster and comprehensive solution scheme of computer system construction.* Mining Safety & Environmental Protection *36*(2009), No. s1, 60–63.

[13] L. Nanni, C. Fantozzi, N. Lazzarini: *Coupling different methods for overcoming the class imbalance problem.* Neurocomputing *158* (2015), 48–61.

[14] M. Townsley, A. Oliveira: *Space-time dynamics of maritime piracy.* Security Journal *28* (2015), No. 3, 217–229.

[15] W. Dai, W. Ji: *A mapreduce implementation of C4. 5 decision tree algorithm.* International Journal of Database Theory and Application *7* (2014), No. 1, 49–60.

[16] A. Vehtari, A. Gelman, J. Gabry: *Practical Bayesian model evaluation using leave-one-out cross-validation and WAIC.* Statistics and Computing *27* (2017), No. 5, 1413–1432.

Received October 12, 2017

Acta Technica *62* No. 2B/2017, 11–20

Simulation analysis of interaction mechanism between triangular track and ground based on Bekker theory

Zhang Jinzheng[2, 3, 4], Wang Qi[2, 3], Jin Qichun[2], Zhang Peng[2, 3]

Abstract. Based on the Bekker theory, the relationship between the triangular track mechanism and the ground is analyzed in this paper. Based on this analysis, the interaction between the track plate and the soil was simulated under two working conditions: uniform straight climbing and spot turn is simulated in the ABAQUS, and the relationship between the stress change and the deformation of the track shoe under various working conditions was clarified. The relationship between the soil settlement amount under the track shoe and the ground pressure was obtained, and the change regulation between the triangular track mechanism and the ground action was obtained. Therefore, interaction analysis model of triangle crawler mechanism and elastic-plastic ground under various working situations was established. Based on the perfected prophase research, the important basic data can be provided for the optimal design of the triangle tracked mechanism.

Key words. Bekker theory, triangular track, soil settlement, ground pressure.

1. Introduction

For engineering vehicles, the walking environment is more complex, and they need to face various situations in actual walking. The traditional four-wheel walking wheel is unable to meet practical demands, and the inflexible traditional track cannot cope with different complicated landforms. Therefore, a more flexible walking device is needed to assist in going forward [1]. The triangular track developed on this is not only adaptable to complex landforms, but also as flexible as general wheeled devices. At present, the triangular track, with broad space in development [2], is gradually

[1]This work was supported by University Science Research Project of Jiangsu Province.

[2]Suzhou Institute of Technology, Jiangsu University of Science and Technology, Zhangjiagang, 215600, China

[3]School of Mechatronic and Power Engineering, Jiangsu University of Science and Technology, Zhangjiagang, 215600,China

[4]Corresponding author

applied to many fields, such as industry, agriculture, and military. Triangular track is inevitably the trend of the development of future engineering vehicle walking devices [3]. Bearing its own and the vehicle's weight, triangular track will cause deformation of the ground in actual walking. The part that subsides meets Bekker theory and, on this basis, should be analyzed by the theory [4]. Currently, triangular track has been put into use in more than 50 countries and regions around the world [5], and there are a number of relevant agencies, including the famous American companies such as MATRACKS and TRACK [6], being involved in the development of triangle track. At present, the research on triangular track mainly focuses on light devices, and its application in this area is quite mature. However, the research of heavy equipment remains insufficient and is still in the initial stage [7]. In the future, triangular track will definitely become an important component of walking devices. Based on previous studies carried out by experts and scholars, this thesis conducts a simulation analysis on the interaction process between triangular track and the ground with Bekker theory, expecting to contribute to the development of triangular track system.

2. Analysis of triangular track structure and ground effects

2.1. The structure and function of triangular track system

Triangular track shows the future development direction of walking devices. It is a kind of modernized walking device [8] which is established partly based on wheeled structure and partly on track structure, and has both advantages of the two structures. The structure of the triangular track is shown in Fig. 1. Analyzed with the stability of triangles in actual process of walking, this structure has advantages in moving obtained from wheeled structure and stability from track structure. It is able to perform on different landforms with greater walking advantages [9].

Fig. 1. Structure of a type of triangular track

2.2. Ground stress analysis based on Bekker theory

The direct contact between track and soil will produce ground pressure. Ground pressure is an important parameter of triangular track. It has an important impact on factors like traction and resistance in using triangular track devices. The ground pressure of triangular track is affected by many factors, such as track flexibility,

thrust wheel data, and track rigidity. The influence of the number of thrust wheels is determined by factors such as the center distance of adjacent thrust wheels S and the pitch of tracks t. When walking on the ground, the track will cause ground pressure and settlement, which in turn, will react to the track. This kind of situation belongs to the category of Bekker theory. Therefore, it is necessary to study the mechanism of the interaction between triangular track and the ground with this theory. Triangular track is a kind of narrow-pitch track. When it is moving on the ground, its pressure can be regarded as in linear distribution. To study the mathematical model of track ground pressure on this basis, the model should be simplified first. During the operating process, the ground pressure of the track is related to its own gravity, mechanical resistance, center-of-gravity position, ground slope, velocity and other factors. The angle that the track forms with the ground and shift of the center of gravity can be negligible [10]. Under the conditions above, the stress analysis of triangular track was carried out.

The interaction between the track and the ground accords with Bekker theory, thus the soil is subjected to the pressure of the structure when it is acting on the ground. Here the term, soil pressure bearing capacity, can be introduced. It refers to the functional relationship between the depth that the track subsides and the compressive stress of the soil under the action of the triangular track. This thesis studies the walking process of triangular track in the sand. Because of the poor bearing capacity when walking in the sand, the track will be resisted by the ground subsidence. In the stress analysis of this process, it is not difficult to find that the effects of the stress are in a dynamic change. On this account, the stress can be treated in segments. In the movement of triangular track, it will lead to ground deformation under resistance and the resistance F_{c} can be calculated by the formula

$$F_{\mathrm{c}} = \frac{2b}{(n+l)\,K^{\frac{1}{n}}} \left(\frac{W}{A}\right)^{\frac{n+1}{n}} \tag{1}$$

.

Here, l is the track length, b is its width, the single track width is denoted as n, K is constant, W is the action force perpendicular to the plane and A is the area on which the force acts.

In actual moving process, the loading process can be quantified using the formulae (2) and (3). During the process, formula (4) can be obtained by combining Bekker theory and the and shear force deformation relationship by Jia Nokia. On this basis, supposing the track is under pressure both from movement and from interaction with the ground, put $j = ix$ (j being the shear displacement and i the track slip rate) and $\sigma = W/(2bL)$ into the formula, then formula (5) can be obtained:

$$\mathrm{d}F_r = \tau b\,\mathrm{d}x\,, \tag{2}$$

$$F_r = 2b\int_0^l \tau\,\mathrm{d}x\,, \tag{3}$$

$$\tau = (C + \sigma \tan \varphi) \left(1 - \mathrm{e}^{\frac{j}{k}}\right) , \tag{4}$$

$$F_r = (A_\mathrm{c} + W \tan \varphi) \left[1 - \frac{K}{iK} \left(1 - \mathrm{e}^{\frac{iL}{k}}\right)\right] . \tag{5}$$

Here, τ is the shear stress, C denotes the bond coefficient, σ is the soil compressive stress, and φ is the soil internal friction angle.

The formulae above show that the greater gravity the triangle track carries, the more pressure it exerts on the ground, and the deeper the ground subsides. When it is within the range of soil bearing capacity, the shear stress of triangular track will increase to further enhance the resistance over triangular track, which can be transformed into a kind of thrust from the perspective of structure in design. Based on this, simulation on the walking performance of triangular track can be further improved.

3. Transient analysis of interaction between track shoe and ground

Because the non-linear factors such as soil are contained in the model, the force relationship between the crawler and the soil is more complex [11]. The transient analysis step of the interaction between the track shoe and the soil is different from the ordinary transient analysis process. Since the stiffness setting of the contact pair has a direct effect on the convergence of the analysis results, so it is necessary to complete the model simulation through repeated selection and debugging of the experimental materials.

3.1. Establishment of finite element model

During the operation of the track, the deformation of the soil is caused by its squeezing on the ground, and the deformation of the soil also made the track suffered the change of the normal force and tangential force from the soil. The relationship between the force and the deformation of the two is mainly transmitted through the track shoe, the one-piece rubber track shoe would suffer the adjacent track shoe tension, the pressure and the shearing force of the thrust wheel, the soil would suffer the anisotropic force from track shoe, resulting in deformation, thus led to the reaction to the track shoe, so the track board would suffer tangential force and normal force from the soil.

The material of the track shoe in the track shoe-soil model is rubber, and the isotropic constitutive relationship in line elasticity is used in ABAQUS to simulate the track shoe. Its modulus of elasticity E is 5.5 MPa, Poisson's ratio ν is 0.43, tensile strength is 1.26 MPa, yield strength is 8.21 MPa, and density ϱ is 1.05 g/cm^3.

The soil material model is more complex because the deformation of the soil is not only related to the size of the load, but will be different because of the different stress path, which can engender elastic deformation and plastic deformation, the Drucker-

Prager material model in the ABAQUS can meet the requirements above. Drucker-Prager material model is generally used for granular materials; in the calculation, the total deformation is divided into elastic deformation and plastic deformation to be solved separately, Hooke's law is used in the calculation of elastic deformation part, while the plasticity theory is adopted in the calculation of plastic deformation part. The main characteristic parameters of the selected Drucker-Prager material model include modulus of elasticity–19.6 kPa, Poisson's ratio 0.23, internal friction angle 17.7° and the cohesive force 1.917 N.

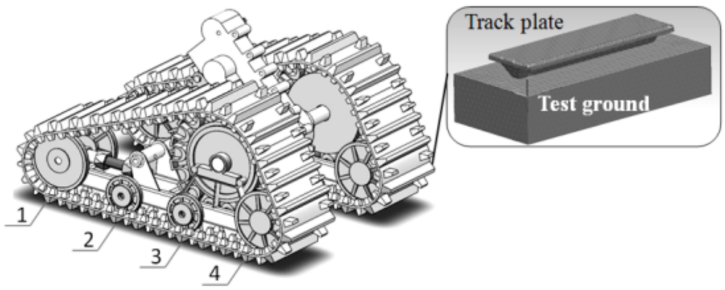

Fig. 2. Three-dimensional model of triangular track system

The rubber track shoe 1, the track shoe 2, the track shoe 3 and the track shoe 4 under the thrust wheel are taken as the research objects. The interaction model between the rubber track shoe and the soil are shown in Fig. 2. The interaction between the track shoe and the soil is simulated by ABAQUS, so the relationship between the track plate and the soil is analyzed for we have acquired results like the track shoe and soil deformation diagram and stress diagram. The relationship between the track plate and the soil was analyzed. The preliminary study has clarified the interaction relationship between the crawler plate and the soil under the stationary condition and the uniform linear motion condition. The continuous analysis and study on the two basic working conditions of climbing and turning are required in this paper, then the mechanism of the interaction between the triangle track and the ground is clarified further.

3.2. Simulation on climbing condition

Tracked vehicles conduct uniform straight climbing at 30° angle, and the stress condition of track shoe is relatively complex. The stress condition of the every track shoe under the thrust wheel remains the same as that in the uniform linear motion. The main forces are the pressure of the wheel on the track wheel, the friction force of the thrust wheel on the track shoe in an inclined direction, the tension between the track shoes in an inclined direction, as well as the vertical tension between the track shoes. For thrust wheel, its time of passing the track shoe is about 0.6 seconds under the conditions of constant speed, and the a transient analysis of 0.6 seconds on track shoe-ground model is implemented. The simulation results are shown in the following figure. Figure 3 shows the stress diagram of each track plate. The relationship between the stress change and the displacement change of each track

shoe is shown in Fig. 4. It can be seen from the figure that the stress extremes of the track plates show a tendency to increase linearly from the front to the rear along the crawler's rolling direction, and the displacement extremes also show the same trend. Under the 30° angle uniform straight climbing condition, the track shoe's stress and deformation variable rate is slightly higher than that of uniform linear motion condition according to the different locations. Therefore, greater interaction force need be exerted between the track and the ground to enable the triangular track to maintain a uniform linear climbing state.

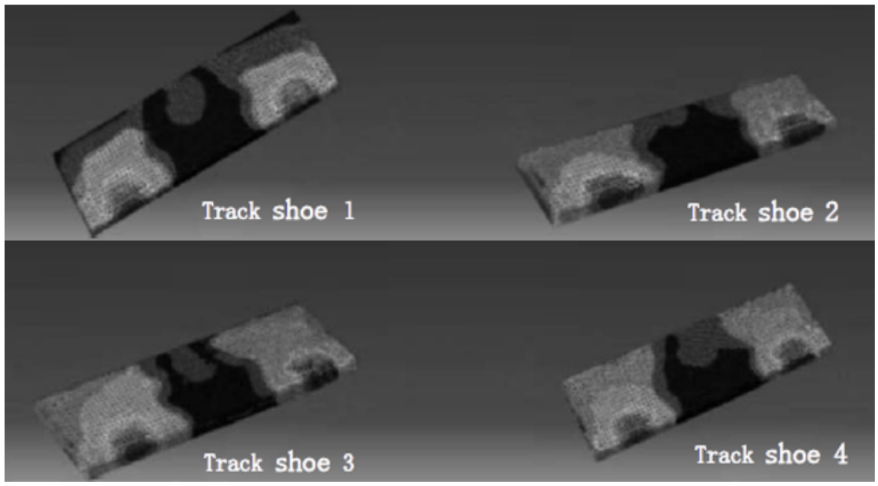

Fig. 3. Stress nephogram of track shoe under climbing condition

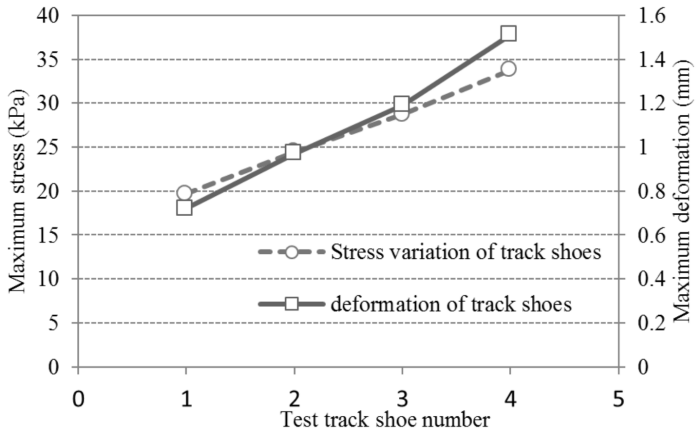

Fig. 4. Variation of stress and deformation of track shoe under climbing condition

At the same time, the change of soil settlement and the distribution of ground pressure under each track plate under this condition were analyzed. The soil settlement and ground pressure nephogram under different track plate were obtained, the

relationship between the settlement and ground pressure of soil is shown in Fig. 5. As is shown in the picture, the maximum soil settlement and ground pressure under the track plate showed an increasing trend from front to back, especially soil settlement of track shoe 4 changed obviously. Under this condition, the maximum soil settlement is 1.05–1.08 times lager than the soil settlement under uniform linear motion condition. The maximum ground pressure is 1.01–1.02 times lager than ground pressure under uniform linear motion condition. The change rate of soil ground pressure and settlement is relatively fast under climbing condition.

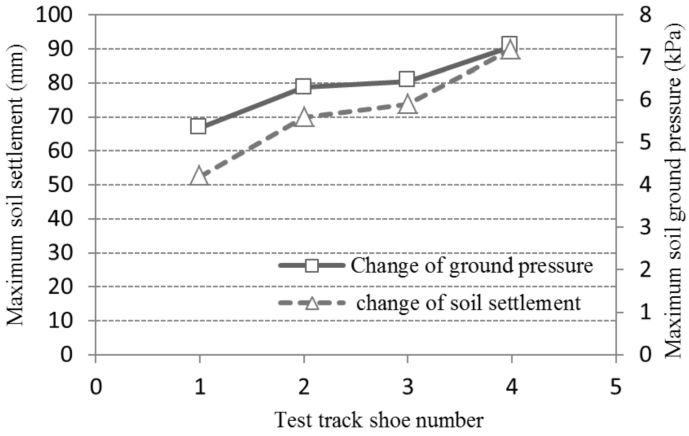

Fig. 5. Variation of soil ground pressure and settlement under climbing condition

3.3. Simulation on spot turn condition

In the simulation experiment under spot turn condition, the outside track shoe of steering process is taken as the object. The main forces are the pressure of the wheel on the track wheel in three directions, the tension between the track shoes in three directions. For support wheel, its time of passing the track shoe is about 1.0 seconds under the conditions of spot turn, and the a transient analysis of 1.0 seconds on track shoe-ground model is implemented. The simulation results are shown in the following figure. Figure 6 shows the stress diagram of each track plate. The relationship between the stress change and the deformation change of each track shoe is shown in Fig. 7. According to the picture, we can conclude that the stress extremum and displacement extremum of each track plate did not show obvious increased tendency, the maximum stress and maximum deformation of each track plate were basically the same.

Pointing to this condition, soil settlement and ground pressure of each track plate are simulated and analyzed. The soil settlement and ground pressure nephogram under different track plate were obtained, the relationship between the settlement and ground pressure of soil is shown in Fig. 8. As is shown in the picture, the maximum soil settlement and ground pressure under the track plate showed the trend of decreasing first and then increasing without showing a trapezoidal distribution. The

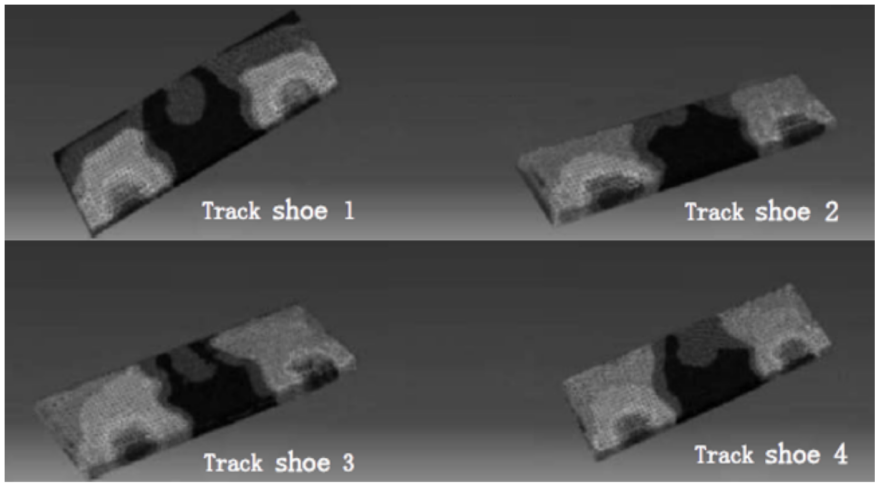

Fig. 6. Stress nephogram of track shoe under spot turn condition

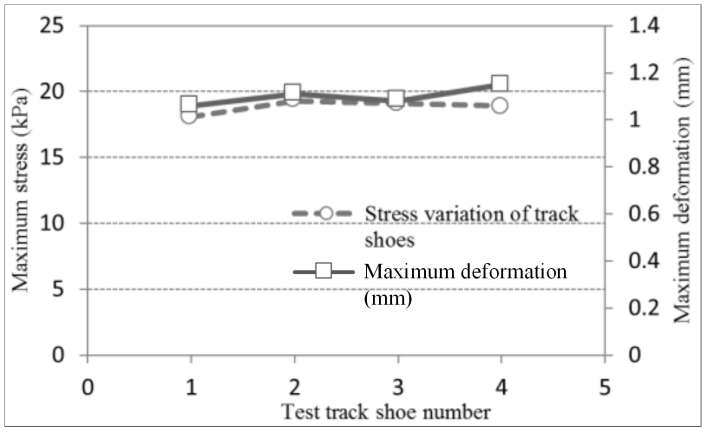

Fig. 7. Variation of stress and deformation of track shoe under spot turn condition

variation trend of soil ground pressure and settlement under the track is consistent, average value is 1.06–1.72 times lager than the value under uniform linear motion condition. According to the above analysis, it can be concluded that the triangle track mechanism still meets the relationship between the soil ground pressure and the settlement based on Bekker theory in the case of turning process.

4. Conclusion

Aiming at the analysis of the design process of triangular track, this research worked out the basic parameters by analyzing its stress condition through Bekker theory and from the perspectives of statics and dynamics. Combining with Bekker theory, relevant parameters can be worked out on the basis of force analysis. Af-

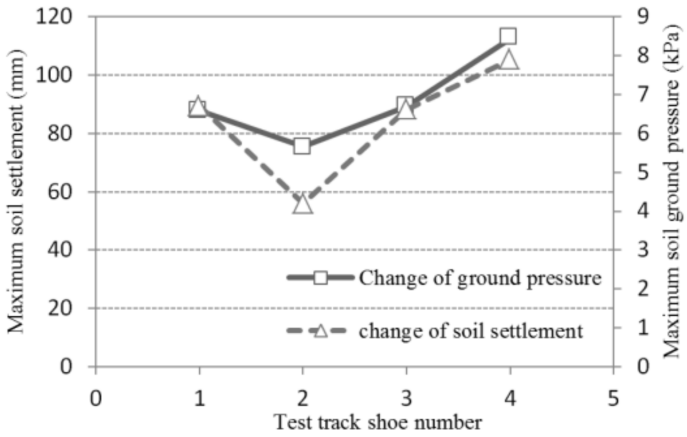

Fig. 8. Variation of soil ground pressure and settlement under spot turn condition

terwards, corresponding structural analyses and simulation analysis of interaction mechanism between triangular track and ground can be carried out. Analyzing based on the research above, according to the basic theory of ground mechanics and the contact theory, the finite element analysis method was used to establish the mechanical model of the interaction between the track shoe and the soil under the two basic conditions: uniform linear climbing at 30° angle and the spot turn in the ABAQUS model, and the numerical simulation analysis was carried out, so as to provide further supplement and improvement on the previous relevant research. Through the analysis of the numerical simulation results, the relationship between the stress change and the displacement change of the track shoe under the two conditions was defined. The relationship between the soil settlement amount under the track shoe and the ground pressure was obtained, and the change regulation between the triangular track mechanism and the ground action was obtained. Therefore, the triangle track mechanism-elastic-plastic ground interaction analysis model under various working situations was established, and based on the perfected prophase research, the important basic data can be provided for the optimal design of the triangle tracked mechanism.

References

[1] F. Qian, T. Zhang, W. Korff, P. B. Umbanhowar, R. J. Full, D. I. Goldman: *Principles of appendage design in robots and animals determining terradynamic performance on flowable ground.* Bioinspiration & Biomimetics *10* (2015), No. 5, paper 056014.

[2] G. E. Halkos, K. D. Tsilika: *Programming identification criteria in simultaneous equation models.* Computational Economics *46* (2015), No. 1, 157–170.

[3] W. Domcke, S. Mishra, L. V. Poluyanov: *The relativistic E×E Jahn–Teller effect revisited.* Chemical Physics *322* (2006), No. 3, 405–410.

[4] V. T. Lai, R. M. Willems, P. Hagoort: *Feel between the lines: Implied emotion in*

sentence comprehension. Journal of Cognitive Neuroscience *27* (2015), No. 8, 1528–1541.

[5] X. Lu, L. Xie, H. Guan, Y. Huang, X. Lu: *A shear wall element for nonlinear seismic analysis of super-tall buildings using OpenSees.* Finite Elements in Analysis and Design *98* (2015), 14–25.

[6] V. Chatziioannou, M. van Walstijn: *Energy conserving schemes for the simulation of musical instrument contact dynamics.* Journal of Sound and Vibration *339* (2015), 262–279.

[7] A. F. Aubeneau, J. D. Drummond, R. Schumer, D. Bolster, J. L. Tank, A. I. Packman: *Effects of benthic and hyporheic reactive transport on breakthrough curves.* Freshwater Science, *34* (2015), No. 1, 301–315.

[8] J. Chen, M. Gauci, W. Li, A. Kolling, R. Gross: *Occlusion-based cooperative transport with a swarm of miniature mobile robots.* IEEE Transactions on Robotics *31* (2015), No. 2, 307–321.

[9] P. Ocùoñ, D. Taler, P. Cisek, M. Pilarcyk: *Fem-based thermal analysis of underground power cables located in backfills made of different materials.* Strength of Materials *47* (2015), No. 5, 770–778.

[10] T. N. Tran, S. Hou, X. Han, M. Q. Chau: *Crushing analysis and numerical optimization of angle element structures under axial impact loading.* Composite Structures *119* (2015), 422–435.

[11] Y. Dai, S. J. Liu: *Multi-rigid-body modeling and simulation analysis for tracked vehicle.* Computer Simulation *26* (2009), No. 3, 281–285.

Received August 7, 2017

Acta Technica *62* No. 2B/2017, 21–30

Performance improvement of streaming media QoS based on behavior feature and content analysis

Furong Li[1]

Abstract. In order to improve the performance of streaming media QoS, an enhanced QoS-supported streaming media service system model based on behavioral characteristics and content analysis. By adding the media filter module and the feedback processing module, the improved system model can support different characteristics of the heterogeneous multimedia terminal, such as resolution, color display attributes and so on, and then realize the QoS support of the streaming media service. Because the traditional Internet network was originally designed for ordinary data traffic transmission, its best effort (best effort) features cannot provide real-time multimedia data transmission for the corresponding quality of service (QoS) guarantee. In order to improve QoS support for network streaming media applications, a streaming media service system model with enhanced QoS support is proposed based on the traditional streaming media application system model. By adding the media filter module and the feedback processing module, the improved system model can support different characteristics of heterogeneous multimedia terminals, such as resolution, color, display, attributes and so on. And then the support of streaming media service QoS is realized. The necessity and feasibility of the system model are demonstrated by setting up an experimental platform, designing test cases and analyzing experimental results. The performance of the core module algorithm in the system model is verified. The results show that the streaming media system model with enhanced QoS support can effectively improve the performance of streaming media QoS. For different broadcast terminals and their QoS requirements, QoS support for network streaming media applications has been effectively improved.

Key words. Streaming media, QoS, media filters.

1. Introduction

As streaming media transmission compared with traditional data transmission has its own characteristics, so the streaming media transmission has a special request to the network QoS (Quality of Service) compared to the traditional data transmission. Streaming media transmission on the network delay and delay jitter have more stringent requirements, end to end transmission delay and delay jitter

[1]Mechanical and Electrical Professional Technology Institute of Hunan, 410151 Hunan, China

in the transmission will affect the streaming media applications. Streaming media transmission on the packet loss rate has a higher requirement. Due to the inconsistency of the importance of streaming media data, the loss of a small amount of critical data can cause a sudden drop in service quality, and continuous packet loss will make the quality of service completely unacceptable. Streaming media transmission has a higher bandwidth requirement, requires adequate bandwidth and has a smooth throughput. Bandwidth, delay and packet loss rate have a great impact on the quality of streaming media service, but because of the traditional Internet transmission characteristics, it cannot provide the corresponding QOS guarantee [1]. Therefore, streaming media applications on the Internet often play pause, audio and video images are not synchronized or mosaic and other phenomena, seriously affect the streaming media application quality of service. To expand the application of streaming media in various fields, it is necessary to provide a corresponding guarantee mechanism for the QoS of the media, so as to improve the service quality of streaming media applications.

Compared with the real-time characteristics of streaming media, the traditional TCP protocol needs more overhead and is not suitable for streaming media transmission. Therefore, HTTP/TCP is used to transmit control information, and RTP/UDP is used to transmit real-time sound data [2]. Unfortunately, UDP does not have the TCP congestion control mechanism. Sally Floyd proposes an equal congestion control mechanism for unicast traffic. Internet The existing "best effort" traffic in Internet uses the traditional TCP protocol. In contrast to the streaming media, a TCP friendly (TCP-friendly) congestion control mechanism needs to be found to avoid the mechanism of using TCP to reduce the speed of packet loss when congestion is generated. For the same problem, some researchers have proposed a new congestion control algorithm and give a performance simulation. By analyzing the shortcomings of the Padhye'S TCP throughput model, a new congestion control mechanism for streaming media based on the dynamic TCP throughput model is proposed [3]. It can guarantee the TCP friendliness in the dynamic environment, and has good response to the change of the network status. In order to improve the QoS support for the application of network streaming media, the current research work is mainly focused on the following two aspects:

1. From the physical / network level to improve the service performance of network QoS, including the network equipment, network-protocol and network infrastructure transformation, the streaming media QoS needs mapping to the underlying network, thereby enhancing network support for streaming media applications QoS.

2. From the application layer to improve the service quality of streaming media application, the service quality optimization strategy is adopted in the server side and the client side, so as to improve the adaptability of the streaming media application to the network environment.

Based on the traditional streaming media application system model, this paper presents an enhanced QoS-supported streaming media service system model. By adding the media filter module and the feedback processing module, the improved system model can support different characteristics of the heterogeneous multimedia terminal, such as resolution, color display attributes and so on, and then realize the

QOS support of the streaming media service.

2. Methods

2.1. Enhanced QoS supported streaming media system model

In order to increase the support of streaming media service QoS, this paper proposes an improved streaming media service system model, in which the media filter module is added in the existing streaming media system model to support the different characteristics of different multimedia terminals, such as resolution, color display attributes, etc., and increase the player feedback mechanism to enhance QoS support, as shown in Fig. 1.

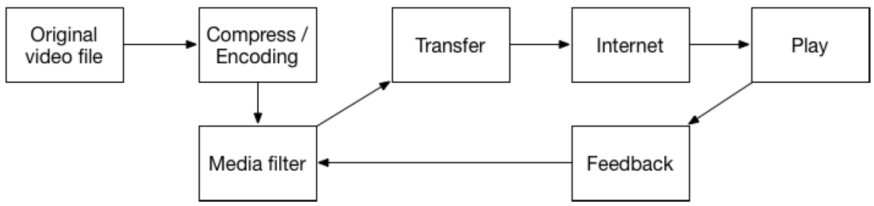

Fig. 1. Enhanced QoS supported streaming media model

2.2. Design of core algorithm for media filter

The main function of the media filter is to process the compressed data according to the feedback information (resolution, color display attribute, etc.) sent by the player, so as to adjust the transmission rate according to the different QoS requirements of the broadcasting end, in meeting the requirements of the playback side QoS is more conducive to network transmission [4]. As an example, for large screen resolution of the player to receive the data transmission rate faster than the screen resolution of the smaller player. In order to achieve this effect, the transmission rate can be increased by adjusting the priority of the transmitted data stream. To achieve the different QoS requirements for the player to adjust the sending rate of data timely, we can consider the congestion control mechanism applied to the streaming media application based on the implementation. Congestion control mechanism should be used to ensure smooth delivery rate (to meet the requirements of streaming media applications), but also for different data streams for different sending priority adjustment [5].

First, the feedback information processing module collects the feedback information from the broadcasting end, maps the feedback information to the sending priority of the transmission data according to the specific algorithm, and then the media filter module determines the transmission data priority according to the feedback information processing module, calculates the transmit data rate that is appropriate for the current playback QoS requirements [6]. Specifically, the media filter takes

the following algorithm:

The media filter uses the same mechanism as the TFRC to detect the performance parameters of the current network, including the probability P_{e} of the lost event, the number of packets b received by an ACK, the average round-trip time RTT, the packet retransmission time T, and packet loss probability P_{r}.

According to the feedback information processing module, the data transmission priority n can be obtained, and the data transmission rate is calculated according to the following algorithm.

In the TFRC protocol, n TCP data stream average transmission rate is calculated as follows (unit: bit/s)

$$X_{\mathrm{Bps}} = \frac{S}{R\sqrt{2bp/3} + t_{\mathrm{RTO}} 3\sqrt{3bp/8}p(1+32p^2)}, \tag{1}$$

where S is the size (in bits) of each data fragment, R is the average round trip time in seconds, b is the maximum number of packets in a TCPACK advertisement, p is the loss event rate, whose value lies between 0–1, and t_{RTO} is the time of retransmission of TCP timeout.

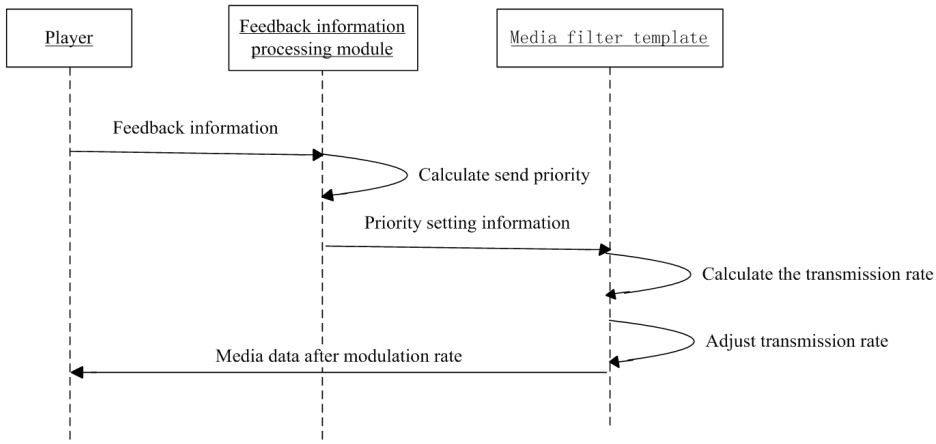

Fig. 2. Collaboration diagram of media filters with other modules

As shown in Fig. 2, the player sends the feedback information (video file resolution requested by the player) to the feedback information processing module, the feedback information processing module determines the priority of the transmission data according to the mapping algorithm and transmits the priority setting information to the media filter module. The media filter module runs the transmission rate algorithm to start the data transmission according to the adjusted transmission rate.

3. Results

From the system model shown in Fig. 1, it can be seen that the media filter module is the key function module in the enhanced streaming media system model supported by QoS. Therefore, to verify the performance of the model, the key is to verify the media filter module for streaming media performance improvement contribution. In order to verify the value of the above system model, this paper builds an experimental test platform, and uses a self-developed tool with data transfer function, which implements MulTFRC protocol implementation code. The MulTFRC protocol was used to provide different transmission priorities for different transmit data streams compared to other congestion control protocols such as DCCP and TFRC [7]. Its priority is set by setting the aggression value of the data flow to achieve. In the transport layer is still using the UDP protocol implementation code, the relevant MulTFRC protocol control code is added to the tool's application layer code. After each data transmission, the receiver will calculate the transmission time; receive the packet size and other information. In addition, the sender can set the sending data of the aggression value, that is, set the parameter n value, it indicating that the transmitted data stream will simulate the performance of n TCP data streams, the default value of the parameter n is 1, representing a standard TCP data stream.

3.1. Test Scenario A - Verify the tunability of the media filter transmission rate

This experimental scenario mainly validates the tunability of the media filter module transmission rate in the enhanced streaming media system model supported by QoS. As the core module in the model, the function of the media filter is: when the media filter receives the feedback information from the player, it finds that the media quality of the player is high (such as the screen resolution is high, or high quality). Now it is possible to adjust the priority of the transmission data stream accordingly. By increasing the priority of the transmission, the high priority data stream obtains a higher throughput than the lower priority data stream, thereby satisfying the QoS requirement of the broadcasting end [8]. On the contrary, when the media filter module receives the player feedback information, if the media quality of the player is low, the media filter adjusts the priority of the transmission data to a lower value to make it more effective. Reasonable is here use of network bandwidth. In order to test the above performance, the experiment needs to test the performance of the data flow with different sending priority. The priority is set by the aggression value (n value in MulTFRC protocol). Table 1 and Fig. 3 show some important experimental data.

3.2. Test Scenario B - Verify the friendliness of the media filter

This experimental scenario mainly validates the TCP-friendliness of the media filter in the enhanced streaming media system model supported by QoS, i.e. whether TCP-friendly transmission data flow and TCP traffic adjusted by media filter are

TCP-friendly. In the enhanced QoS-supported streaming media system model, the media-adjusted transmitted data stream requires both a smooth delivery rate and a TCP-friendly nature. In order to study the TCP-friendly (competing with each other) between data streams with different transmission data priorities, the experiment uses a stream with an aggression value of 1 as the background traffic, other experimental scenario settings are the same as for test scenario A. Table 2 and Fig. 4 show some experimental data.

Table 1. Test Scenario A

File size (Mb)	Aggression value	Transmission time (s)	Average transmission rate (kb/s)
12.8	1	24.2	529
12.8	2	18.2	703
12.8	3	17.8	719
12.8	4	16.6	771
12.8	5	16.3	785
12.8	6	15.8	810
12.8	7	15.5	821
12.8	8	15.3	833
12.8	9	15.2	840
12.8	10	14.9	851

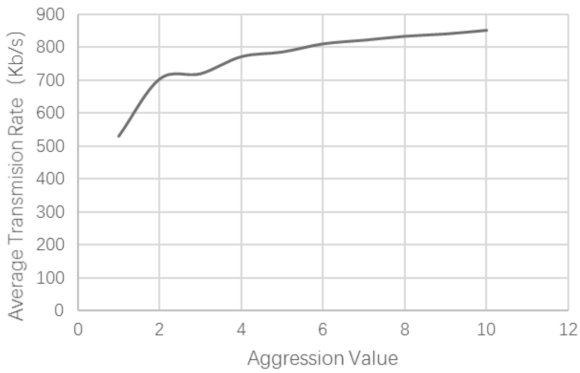

Fig. 3. Data of the test scenario A

4. Discussion

4.1. Verification of tunability of the media filter send rate

In the course of the experiment, each experiment is transmitted with a size of 12.8 M media files. When the priority of sending data is set to 1, the file transfer time is 24.25, the average transmission rate is 529 Kbs; when the priority of the transmission data is set to 2, the file transfer time is 18.25, the average transmission rate is increased To 703 Kbs. With the sending data priority increases, the file transfer time is getting shorter and shorter, the average sending rate is faster and faster. From this it can be concluded that the data flow with higher transmission priority in the same network environment can obtain higher throughput than the data flow with lower transmission priority. Corresponding to the enhanced QoS support streaming media system model, when the player needs higher QoS quality (such as the player screen is larger, higher resolution), the media filter by adjusting the priority of the data flow to a The higher the value to get a higher transmission throughput, and then meet the player QoS requirements; the contrary, when the player requires QoS quality is low, the media filter to reduce the priority of sending data streams, to meet the player QoS Requirements while more rational use of network bandwidth.

Table 2. Test Scenario B

File size (Mb)	Aggression value	Transmission time (s)	Average transmission rate (kb/s)
2.8	2	18.7	684
12.8	3	17.3	739
12.8	4	17.2	744
12.8	5	17.2	744
12.8	6	17.1	748
12.8	7	17.0	752
12.8	8	17.1	760
12.8	9	16.8	764
12.8	10	16.6	768

4.2. Verification of tunability of media filter's friendliness

In the course of the experiment, each experiment transmits the same media file with a size of 12.8 M, and sends the TCP data stream with a rate of 50 Kbs as the background traffic. The experimental results show that when the priority of the transmitted data is set to 1, the file transfer time is 29.95 and the average transmission rate is 427 Kb/s. When the priority of the transmitted data is set to 2,

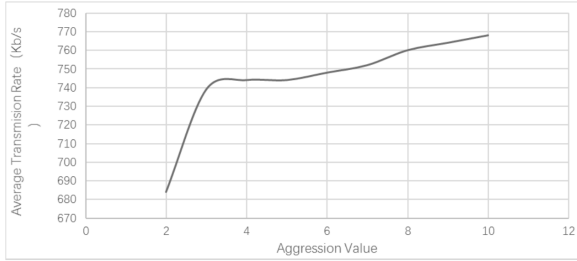

Fig. 4. Data of the test scenario B

the file transfer time is 18.75 and the average transmission rate is 624 Kb/s. As the priority of the transmitted data increases, the transmit data throughput also grows smoothly. It can be concluded that the data streams of different transmit priority and TCP data streams are friendly in the competitive bandwidth, and are still able to maintain the characteristics of the transmission rate as the transmission priority is improved. In the streaming media system model with enhanced QOS support, the data stream output through the media filter module can maintain good TCP friendliness while maintaining its inherent characteristics.

5. Conclusion

The results show that the QoS-supported streaming media system model can effectively improve the QoS performance of streaming media, and meet the QoS requirements of different playing terminals. Media filter module as the core module in the model, when the player needs higher QoS quality (such as the player screen is larger, higher resolution), the media filter by adjusting the priority of sending data to a more high value to get a higher transmission throughput, and then meet the player QoS requirements. On the contrary, when the quality of the QoS is required to be low, the media filter can reduce the bandwidth of the transmitted data stream and make more reasonable use of the network bandwidth while satisfying the QoS requirements. On the other hand, the transmission rate adjusted by the media filter can ensure smooth transmission rate and good TCP friendliness (data streams with different transmission priorities have good friendliness with each other, and TCP data flow is also friendly). Experimental results show that the improved QoS model built in this paper can effectively improve the performance of streaming media QoS, and meet the QoS requirements for different broadcast terminals. The main contribution of this paper is to study the traditional model of streaming media service system. On the basis of this, the concept of media filter is introduced, and a streaming media system model is proposed to enhance QoS support. By building an experimental platform, the performance of the core module in the system model is demonstrated. However, the system model is currently in the theoretical research stage. It only has a preliminary demonstration model that is not fully realized. In future research, this enhanced QoS support for streaming media system implementation and actual data validation also requires a lot of work.

References

[1] F. Furqan, D. B. Hoang: *LTE_FICC: A new mechanism for provision of QoS and congestion control in LTE/LTE–advanced networks.* International Conference on Mobile and Ubiquitous Systems: Computing, Networking, and Services MobiQuitous, 2–4 December 2013, Tokyo, Japan, Lecture Notes of the Institute for Computer Sciences, Social Informatics and Telecommunications Engineering (LNICST) *131* (2013), 768–781.

[2] W. Chen, Q. Guan, S. Jiang, Q. Guan, T. Huang: *Joint QoS provisioning and congestion control for multi-hop wireless networks.* EURASIP Journal on Wireless Communications and Networking (2016), No. 1, paper 19.

[3] H. Liu, F. Sun: *Intermediate node congestion control mechanism for QoS-oriented satellite network.* Press of Tsinghua University *54* (2014), No. 10, 1344–1349.

[4] H. Matsumoto, H. Obata, K. Ishida: *Characteristics evaluation of flow QoS guarantee method using both TCP congestion control and MAC frame priority control over wireless LAN.* IEICE Technical Report *113* (2013), No. 140, 101–106.

[5] M. Mayandi, K. V. Pillai: *Probabilistic QOS aware congestion control in wireless multimedia sensor networks.* Scientific Research, Circuits and Systems (2016), No. 7, 2081–2094.

[6] S. Rajeswari, Y. Venkataramani: *Congestion control and QOS improvement for AEERG protocol in MANET.* International Journal on AdHoc Networking Systems (IJANS) *2* (2012), No. 1, 13–21.

[7] N. Yeadon, F. Garcia, D. Hutchison, D. Shepherd: *Filters: QoS support mechanisms for multipeer communications.* IEEE Journal on Selected Areas in Communications *14* (1996), No. 7, 1245–1262.

[8] C. Krasic, J. Walpole, W. Feng: *Quality-adaptive media streaming by priority drop.* International workshop on Network and operating systems support for digital audio and video (NOSSDAV), 1–3 June 2003, Monterey, CA, USA, Published ACM New York (2003), 112–121.

Received August 7, 2017

Acta Technica *62* No. 2B/2017, 31–40

Synchronization design of shape and structure of petroleum machinery and equipment

Dehua Feng[1], Yaoguang Qi[1]

Abstract. The purpose is to study the synchronous design of the form and structure of petroleum machinery equipment. The size of the four-bar mechanism of the conventional pumping unit determines its dynamic performance, kinematic performance and energy consumption. Based on the rated torque value of the reducer 1824 inlbs (210 kN.m), the suspension load value 427 1b (190 kN) and the maximum stroke length 240 in (6.09 m), the size of the four rod mechanism is optimized. The optimum performance of the four-bar mechanism size is studied. At the same time, according to the basic theory and installation dimensions, the size of the three bearing housings is designed. Its influence on the movement and force of the four-link structure of the pumping unit is discussed. The results show that this design can reduce the manufacturing cost of the product. In addition, it meets the demand of small quantity and specification. Therefore, it can be concluded that the design can meet the needs of production.

Key words. Pumping unit, four connecting rods, oil machinery, equipment.

1. Introduction

According to different working conditions of different oil wells, the requirements of the mechanical oil production methods for oil equipment technology are constantly improving. As a result, the design and manufacturing level of the oil recovery equipment has been greatly improved [1]. The pumping units also develop and innovate from their initial forms. In the process of continuous development, there are hundreds of technical inventions of pumping units [2]. In this paper, the model C1824D-427240 of the largest beam pumping unit in China is studied.

In recent years, the pumping unit industry has been developing in a new direction [3]. The main features of these new pumping units are the adoption of many modern technologies and advanced structural schemes, as well as new materials and processes [4]. The adaptability, economy, reliability, advancement and technical level of pumping units have reached the highest level ever. It has made outstanding

[1]China University of Petroleum (East China), 266580, Qingdao, China

contributions to the efficient, economical, safe and reliable exploitation of petroleum resources [5]. Here is a brief outline of the general development. It not only develops towards large pumping equipment and low energy consumption, but also develops towards automation and intelligence [6]. The high adaptability is very important. The special working condition pumping unit is developed [7]. The design concept of C1824D-427-240 pumping unit is designed strictly according to API standard. According to the domestic multinational mining units and the Middle East and other countries on the demand for pumping units, the production of API conventional pumping unit is imminent [8]. In this way, it is used to improve the series standards of API conventional pumping units. At the same time, the market competitiveness of pumping units in our country has been enhanced. It has important guiding significance for our occupation of the international market share [9].

The top drive rig was originally used for drilling in marine areas. At present, it is gradually applied to land drilling, desert areas and alpine regions. It evolved from conventional strata to more complex geological and stratigraphic structures. It should reduce the system height and save the cost of derrick reconstruction, so that the device can be effectively applied to various drilling systems. Although some of China's petroleum machinery plants have the ability to produce some types of top drive drilling equipment, the oil fields are gradually being popularized. However, due to the late start of China's top drive, it is still in the stage of development. Domestic top drive product model is relatively simple, which cannot meet the needs of China's offshore and land oil drilling rigs. It is still necessary to further strengthen the research of the top drive device, develop new products, increase specifications, and gradually form the top drive series in China, so as to realize the domestic production of top drive. At present, the development of top drive device has entered a mature stage. Its main features are as follows: first, the power motor (electric motor or liquid motor) with high power and large torque is adopted to achieve the torque speed characteristic suitable for drilling. Second, the drilling and unloading device is adopted, so that the drill string can be unloaded at any position in the derrick, thus giving prominence to the advantages of the top driving mode. Third, the rigid rail is added to the derrick to withstand the reverse torque of the derrick during drilling. The top drive drilling system is suitable for marine, desert, Arctic and other poor environmental conditions. The number of applications in foreign countries is more, and it accounts for more than 90 %.

2. Methodology

2.1. Determination of dimension of four connecting rods

The design of pumping unit type is discussed in C1824D-427-240 [10]. The size of the four bar linkage of the pumping unit is shown in Fig. 1. The height of the bottom plane of the pumping unit to the center of the support bearing is H. It is determined according to the maximum stroke length of the pumping unit. In addition, it also determines the height of the pumping unit. The specific calculation

method of H is

$$H = s_{\max} + H_{\mathrm{h}} + 0.2 \sim 0.25\,\mathrm{m} \tag{1}$$

In the formula, $s_{\max}$ is the maximum stroke length (m), H_{c} denotes the wellhead height (m), which is generally 1.2–1.5 m and H_{h} is the height of the rope (m), which is generally 0.35–0.4 m.

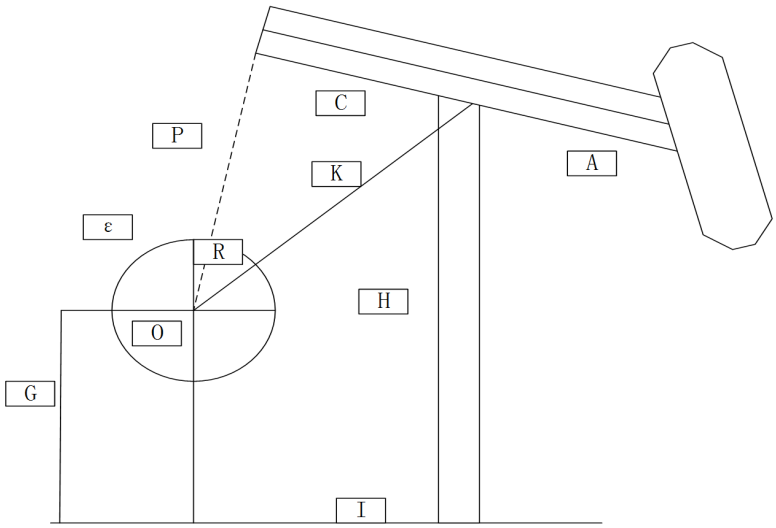

Fig. 1. Size diagram of four-bar linkage mechanism of beam-type pumping unit

The design of the "C" type pumping unit of the four linkage size of the beam, forearm length A is 6600 mm. The length of the rear arm of the beam is 3460 mm. The horizontal distance I of the center of the bracket bearing to the center of the output shaft of the gear unit is 3505 mm. The connecting rod length P is 5095 mm. The vertical distance (H–G) of the center of the bracket bearing to the center of the output shaft of the gear unit is 5080 mm. In addition, it was determined that the distance G between the center of the output shaft of the reducer and the bottom of the base was 3433 mm. The distance H from the center of the bracket bearing to the bottom of the base is 8515 mm.

2.2. Theoretical calculation of pumping unit

Figure 2 shows the mechanism of the conventional pumping unit.

The geometric calculation follows. According to the known condition and the triangular residual u theorem, the angle values are obtained, that is, the degrees of β, a, σ, θ', θ and the length of the pumping stroke [11]. The motion calculation: The velocity of the suspension point V_t and the acceleration point a_A are calculated. The process of calculation: under different pump diameters and different strokes, the maximum pump depth is calculated. The daily amount Q of fluid is calculated

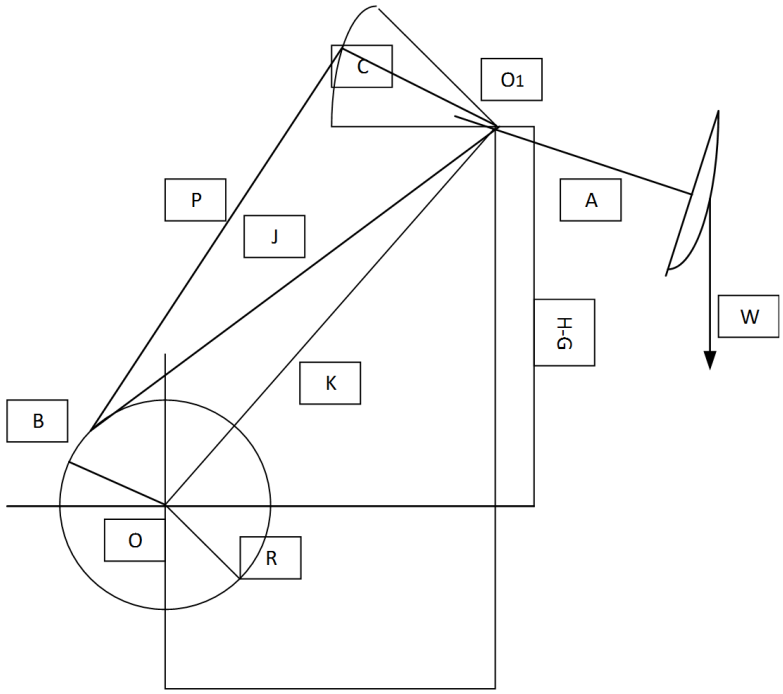

Fig. 2. Mechanism motion diagram of pumping unit

by the single well theory [12]. The working torque T_{W}, the balance torque T_{R}, the net torque T_{N} and the offset angle τ are calculated. The actual stroke length s_{i} and the actual output Q_1 are calculated. The power of the motor is calculated. The formulae for particular quantities are:

Connecting force:

$$F_{\mathrm{L}} = \frac{A}{C \sin \beta} W' \,. \tag{2}$$

Crank tangential force:

$$F_{\mathrm{ct}} = F_{\mathrm{L}} \sin \alpha \,. \tag{3}$$

Crank legality:

$$F_{\mathrm{cl}} = F_{\mathrm{L}} \cos \alpha \,. \tag{4}$$

Horizontal component of support:

$$F_x = F_{\mathrm{L}} \cos(\delta + \beta) \,. \tag{5}$$

Vertical component of support:

$$F_y = F_{\mathrm{L}} \sin(\alpha + \beta) + 1.15W \,. \tag{6}$$

Support force:

$$F_{\mathrm{s}} = \sqrt{F_x^2 + F_y^2}\,. \tag{7}$$

Stretch force direction:

$$\lambda = \arctan\frac{F_x}{F_y}\,. \tag{8}$$

Working torque:

$$T_{\mathrm{W}} = \frac{AR\sin\alpha}{C\sin\beta}W'\,. \tag{9}$$

2.3. Checking calculation of main bearing elements

The moving mechanism of a conventional pumping unit is a four-link mechanism. According to the foregoing, the main load-bearing components are: support, beam, beam, rod, crank and base. Then, there are support bearings, end bearings and crank pin bearings for connecting them. In addition, there are pins, bolts and other parts of the force. In the process of checking, the following calculation is carried out mainly: beam, beam, strength calculation, bearing, and strength and life calculation. The suspension load, the stroke and the strike stroke of the light rod are different. When checking calculation, the maximum load, maximum stroke and the maximum thrust are taken together. If the "three most important" conditions cannot be met at the same time, the calculation should be carried out in descending order.

The section size of the beam is 1050×350 mm, that is to say, the selected H-steel is made of 350×350 mm formed welding. The overall structure is welded by the upper and lower wings and the side plates. According to the loading condition of the traveling beam and the relevant knowledge of the mechanics of the material, the stress of the beam in the center section is the largest. When considering the role of the shim plate, it is safe to calculate the main body of the beam. In addition, the beam is a square structure. The flexibility of u is generally no more than 10, which does not require fatigue calculation and stability check. The beam is a H steel formed by welding, and the flexural modulus (S_x) of the section is 16804713 mm^3. From the above conditions, the maximum bending moment of the beam is calculated as

$$M_y = A \cdot W_{\max} = 6600 * 190000 = 1254000000(\mathrm{Nm}) \tag{10}$$

and the maximum stress of the beam is

$$\sigma_y(fcb) = \frac{M_y}{W_n(SX)} = 74.62\,\mathrm{MPa} < 74.62\,\mathrm{MPa} \sim 1000\psi\,. \tag{11}$$

By calculation, the beam meets the requirements specified by API and these requirements can be obtained. The strength of the beam is calculated. The transverse beam is connected to the connecting rod through the connecting rod pin and mainly bears the force of the connecting rod. Among them, the length of the transverse beam body is 2993 mm. The distance between the two pin holes is 2800 mm, and the span of the bolt hole is 592 mm. The main material of the cross element is H steel of cross section 606×201 mm. Its flexural rigidity is $W_n(Sx) = 3000000\,\mathrm{mm}^3$.

According to the force of the cross beam, the transverse beam can be simplified as simply bent beam with simply supported ends. The intermediate one is acted by pure bending moment. Through analysis, it can be seen that bolt hole is the most dangerous section. Its structure is checked and calculated. According to the load spectrum of the crossbeam in the schedule, it is known that the maximum load of the two center hole of the crossbeam is 202.247 kN. According to the stress analysis and the size of the structure, the maximum bending moment of the dangerous cross section of the beam is $M_y = 239258.201\,\mathrm{Nm}$. Therefore, the maximum bending stress of the cross section is

$$\sigma_y = \frac{M_y}{M_n} = \frac{239258.201}{3000} = 79.75\,\mathrm{MPa} > 77.4\,\mathrm{MPa}\,. \tag{12}$$

Since the calculation only considers the main body of the beam, and the effect of the strengthening plate is not considered, the strength of the girder can be considered sufficient. Similarly, the beam structure is not subjected to stability calculations and fatigue calculations. In the analysis of connecting rod of API conventional pumping unit with crank balance, the force of connecting rod can be simplified as two force pole, and the connecting rod is only subjected to pull force. In general, the size of the connecting rod is smaller than the size of the upper and lower connecting rod, and the strength is considered sufficient. Therefore, only the strength of the connecting rod can be calculated.

2.4. Checking of crank pin bearing

The crank pin bearing also rotates at low speed, which is subjected to unstable periodic variation load. According to the load spectrum, the maximum value $P_{\max}$ of the bearing force of the crank pin is 20224.7 kg, and the minimum force $P_{\min}$ is 12983 kg. According to the known conditions, it can be obtained

$$F_r = \frac{1}{3}(2P_{\max} + P_{\min}) = 17810.8\,\mathrm{kg}\,. \tag{13}$$

For the installation of a pair of bearings, the bearing force is $F_r = 17810.8\,\mathrm{kg}$. To check the "mechanical design manual", for the 22328 double row spherical roller bearing (53628) $C = 1040\,\mathrm{kN}$, $c_\mathrm{o} = 1770\,\mathrm{kN}$, $X = 1$, $Y = 1.8$ and $F_\mathrm{a} = 0$. Therefore, $P = F_\mathrm{r} + F_\mathrm{a} = F_\mathrm{r} = 178.11\,\mathrm{kN}$, $p_\mathrm{o} = XF_\mathrm{r} + YF_\mathrm{a} = Fr = 178.11\,\mathrm{kN}$.

The static strength check: according to its working characteristics, the instantaneous dynamic load factor is $\mu = 2.0$, and the static safety factor is $S_\mathrm{s} = 1.35$. It can be concluded that

$$S_\mathrm{o} = \frac{c_\mathrm{o}}{up_\mathrm{o}} = \frac{1770}{2 \cdot 178.11} = 4.79 > S_\mathrm{s}\,. \tag{14}$$

The process of life calculation is

$$L_\mathrm{H} = \frac{10^6}{60n}\left[\frac{f_\mathrm{T}C_\mathrm{r}}{F_\mathrm{f}p}\zeta\right]. \tag{15}$$

According to the working conditions of this bearing, check the "mechanical design manual", take $\varepsilon = 1.2$, $f_{\mathrm{T}} = 1.0$, $F_{\mathrm{f}} = 1.35$, $n = 4.0$, then, these parameters are brought into the formula. After calculation, it is obtained $L_{\mathrm{H}} = 549321.14$ hours. It can be seen that the bearing life is sufficient.

2.5. General design structure diagram of pumping unit

Figure 3 shows the general design structure diagram of pumping unit

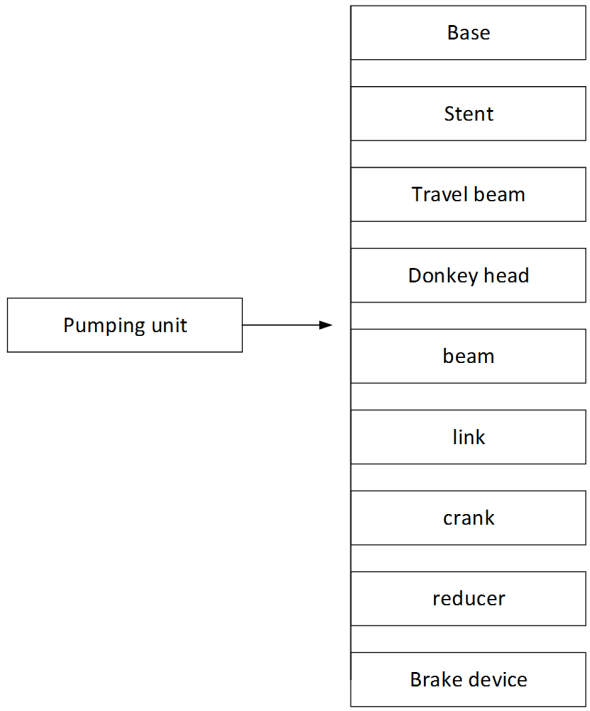

Fig. 3. General design structure diagram of pumping unit

3. Result analysis and discussion

The design dimensions of the pumping unit are shown in Table 1.

The specific data for designing other components are as follows. The total length of the transverse beam is 2993 mm. The distance between the two pin holes is , and the span of the bolt hole is 592 mm. The main material of the cross element is H steel of cross section 606×201. The connecting rod selection size is 102×10 mm^2 steel tubes. The maximum tensile force is 202.247 kN. The maximum value of the bearing capacity of the support shaft is 66641.63 kg, and the minimum force is 45110.96 kg. The maximum bearing capacity of the tail shaft is 40449 kg, and the minimum force is 25966 kg. The maximum value of the bearing force of the crank pin is 20224.7 kg,

and the minimum force is 12983 kg. According to the data in the table, the maximum stress of the beam is 74.62 MPa, less than 77.4 MPa under the condition of maximum load, maximum stroke and maximum thrust. This calculation only considers the beam body, and does not consider the role of the enhanced version. Therefore, it can be considered that its strength is enough. The strength of the connecting rod meets the requirement of use and the size is reasonable. The static strength of the bracket bearing is greater than 2.1 S_s, and the service life is 14537.05 hours, and all the requirements are satisfied. The static strength of the tail bearing is greater than 4.5 S_s, and the life span is 274972 hours. Therefore, they meet the requirements. The static strength of crank pin bearing is greater than 4.97 S_s, and the life span is 549321.14 hours. All of these elements meet the requirements. All parts meet the requirements of stress and service life, so the design can meet the needs of production.

Table 1. Design of components of pumping unit

Pumping unit parts	Design dimension (mm)
Forearm length A	6600
The length of the rear arm of the beam C	3460
Bracket bearings to the horizontal distance of the reducer I	3505
Connecting rod length P	5095
The vertical distance of the support bearing to the reducer (H-G)	5080
Distance between the output shaft of the reducer and the base plane of the base G	3433
The distance between the center of the bearing and the base plane H	8515

4. Conclusion

The size of the four bar linkage of the beam pumping unit determines its movement performance, dynamic performance and energy consumption. According to the principle of determining the four link mechanism, the parameters of the four link structure are obtained. Through the determination of the size of the four connecting rod of the pumping unit and related theoretical calculations, structural design and verification, the size of C 1824D-427-240 pumping unit is determined. The structure design of the pumping unit is designed according to the standard of API. According to the size of the four link structure of the pumping unit, the structure size of the parts is determined, and the structure and size of the pumping unit are determined. According to the design theory of pumping unit, an analytical model of C 1824D-427-240 pumping unit is established. According to the standard of API and related theoretical calculation, the structure type and size parameter of pumping unit are

obtained. The basic calculation of the model pumping unit is completed.

References

[1] H. Zhao, Y. Qi, H. Du, H. Wang, G. Zhang, W. Liu, H. Lu: *Cloud computation processing for oilfield block data and chain drive pumping unit polished rod motion model.* Journal of Signal Processing Systems *89* (2017), No. 1, 41–50.

[2] Y. Yu, Z. Chang, Y. Qi, X. Xue, J. Zhao: *Study of a new hydraulic pumping unit based on the offshore platform.* Energy Science & Engineering *4* (2016), No. 5, 352–360.

[3] H. Fu, L. Zou, Y. Wang, Z. Feng, Z. Song: *Study on design and simulation analysis of the double horse-head pumping unit based on the compound balance structure.* ARCHIVE Proceedings of the Institution of Mechanical Engineers, Part C: Journal of Mechanical Engineering Science *229* (2015), No. 16, 3034–3046.

[4] G. Takacs, L. Kis, A. Koncz: *The calculation of gearbox torque components on sucker-rod pumping units using dynamometer card data.* Journal of Petroleum Exploration and Production Technology *6* (2016), No. 1, 101–110.

[5] K. Li, X. Gao, Z. Tian, Z. Qiu: *Using the curve moment and the PSO-SVM method to diagnose downhole conditions of a sucker rod pumping unit.* Petroleum Science *10* (2013), No. 1, 73–80.

[6] G. Han, H. Zhang, K. Ling: *The optimization approach of casing gas assisted rod pumping system.* Journal of Natural Gas Science and Engineering *32* (2016), 205–210.

[7] A. T. Nguyen, S. Reiter, P. Rigo: *A review on simulation-based optimization methods applied to building performance analysis.* Applied Energy *113* (2014), 1043–1058.

[8] C. R. Vistas, D. Liang, J. Almeida, E. Guillot: *TEM_{00} mode Nd:YAG solar laser by side-pumping a grooved rod.* Optics Communications *366* (2016), 50–56.

[9] I. N. Iskenderli, V. A. Narimanov: *Choice of alternative steel grade for manufacturing bottom-hole pumping rod joint couplings.* Chemical and Petroleum Engineering *51* (2015), Nos. 7–8, 536–539.

[10] J. A. Villasante, L. O. Mantovano, H. A. Ernst, M. G. Pereyra: *Development of a new hollow sucker rod family for rotating pumping (progressive cavity pump systems).* Journal of Petroleum Science and Engineering *134* (2015), 277–289.

[11] S. A. Mahrooqi, M. Gonzalez, M. Marcano, L. Vargas, A. A. Harthy: *Oil spillage environment impact reduction based on automated leak detection on rod pumping wells in south of Oman.* Proc. SPE Middle East Oil & Gas Show Conference (MEOS), 8–11 March 2015, Manama, Bahrain, Publisher Society of Petroleum Engineers, Document ID SPE-172613-MS.

[12] M. Xing: *Response analysis of longitudinal vibration of sucker rod string considering rod buckling.* Advances in Engineering Software *99* (2016), 49–58.

Received August 7, 2017

Acta Technica *62* No. 2B/2017, 41–52

Research on high-dimensional clustering algorithm based on information entropy change trend

Zhang Yunfeng[1], Fang Haoshuai[1]

Abstract. The rapid development of computers and network technology has caused the explosive growth of scale and dimension of data in the Internet. How to cluster, analysis and mine massive high-dimensional data automatically is a research hotspot in the area of information retrieval and data mining. In order to meet the need for high-dimensional data clustering algorithm at present preset parameters, the computational complexity is high, according to the information retrieval system in data distribution characteristics of proposed high-dimensional clustering algorithm based on edge distribution entropy and the change trend. The algorithm firstly, the samples are mapped to each dimension, according to the principle of edge differential entropy decrease monotonically separate hierarchical clustering, and then use the single dimensional clustering results to maximize the edge of differential entropy and the principle of sample data are divided according to the, to get the final clustering result.

Key words. Clustering algorithm, high dimension, information entropy, scale out, query suggestion, relevancy evaluation.

1. Introduction

With the development of computer and Internet technologies, the amount of social information has taken on an explosive growth tendency so information that users can obtain is dramatically increasing. In order to better screen, store, index, retrieve and assess the massive data, the information retrieval system came into being [1]. Clustering analysis and application of massive high dimensional data is a challenge in the present field of data mining. Researches on theories and methods suitable for high-dimensional clustering are of great significance to improvement of data mining theories and extension of clustering application [2].

[1]North China Institute of Aerospace Engineering Computer and Remote Sensing Information Technology Institute Hebei, Langfang, 065000, China

2. Clustering algorithm model based on changing tendency of information entropy

2.1. Relative definitions

The attribute set $A = \{A\_1, A_2, \cdots, A_d\}$ is composed of d continuous real number fields and S is a d-dimensional hyperspace $S = A\_1 \times A_2 \times \cdots \times A_d$. The input is a d-dimensional data point set $V = \{v_1, v_2, \cdots, v_n\}$, $v_j = \langle v_{j1}, v_{j2}, \cdots, v_{jd}\rangle$, where the ith component u_i is the value of A_i in S. The component values of different data points in each dimension can be the same. Suppose that u_i are different values of $v_{i1}, v_{i2}, \cdots, v_{iu_i}$ in the ith dimension, respectively. The lengths between values are, respectively, $l_{i1}, l_{i2}, \cdots, l_{iu_i}$, where $l_{ix} = v_{i(x+1)} - v_{ix}$. The number of data points $v_{i1}, v_{i2}, \cdots, v_{iu_i}$ is $k_{i1}, k_{i2}, \cdots, k_{iu_i}$. When $j = u_i$, it can be considered that $l_{i(j+1)} = \infty$, where

$$\sum_{x_1=1}^{u_1} k_{1x_1} = \cdots = \sum_{x_i=1}^{u_i} k_{ix_i} = \cdots = \sum_{x_d=1}^{u_d} k_{dx_d} = n\,. \tag{1}$$

When applying the single dimensional clustering algorithm to the data, each point will move in the positive or negative direction of the coordinate axis. We use s_{ij} to indicate the moving direction of v_{ij}: 1 for positive direction and –1 for negative direction. Symbol H_i indicates the edge differential entropy of the data in the ith dimension and $H_{i\left[v_{ij},\, v_{i(j+1)}\right]}$ indicates the edge differential entropy calculated within the interval $\left[v_{ij},\, v_{i(j+1)}\right)$ in the ith dimension.

2.2. Clustering algorithm

The clustering algorithm based on changing tendency of information entropy can be divided into three steps.

Step 1: Map the data sample to each dimension and sort the data in each dimension.

Step 2: Move the data points according to Theorem 1 in each dimension. When two points meet, merge them and recalculate k (the k value of the new point is the sum of the k values of the merged points), l and H_i and re-determine the moving direction s of each data point. Move in this way until only one point is left in each dimension. Thus we can obtain d-hierarchical cluster trees $CT = \{CT_1, CT_2, \cdots, CT_d\}$, as shown in Fig. 1.

In CT_i, the data point $V = \{v_1, v_2, \cdots, v_d\}$ is only located in the leaf node and the clustering node $C_i = \{c_{iLayer_yNoz} \,|y \in [1,n]\,, z \in [1,n]\}$ is only located in the non-leaf node. All clustering nodes in the path from the root to each leaf node are the category of this leaf node. The leaf nodes with the same ancestor belong to the category indicated by this ancestor [3].

Each hierarchy of the hierarchical cluster tree indicates the merging process of one clustering. Only two clusters are merged in each clustering, so for each hierarchy except the bottom hierarchy, only one clustering node has two child nodes. Other

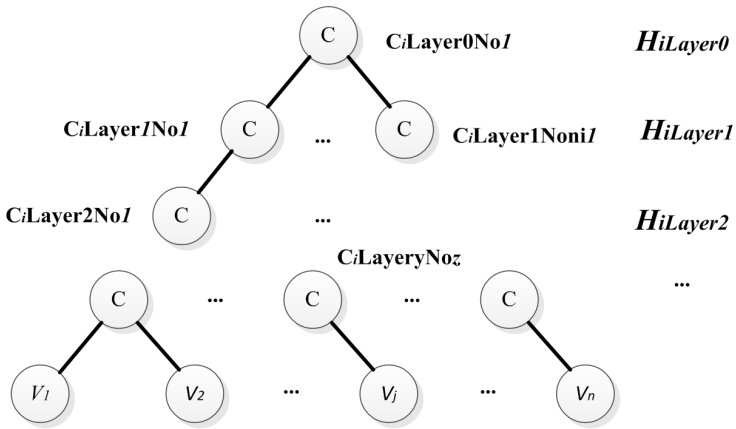

Fig. 1. Single dimensional hierarchical cluster tree

clusters with only one cluster merely change their positions rather than be merged with other clustering points during this clustering process [4].

Step 3: Each time, re-partition of the already-made data clustering results by choosing one from the d hierarchical cluster trees to maximize the increment of the sum of edge entropies. Each hierarchy of the hierarchical cluster tree indicates the partition method of a data sample. Partition is defined as follows.

Suppose the data sample has a partition $p_{i_1} = \{c_{i_1 1}, c_{i_1 2}, \cdots, c_{i_1 m}\}$ in the i_1th dimension and has another partition $p_{i_2} = \{c_{i_2 1}, c_{i_2 2}, \cdots, c_{i_2 n}\}$ in the i_2th dimension, where $i_1 \neq i_2$. Define $p_{i_1 i_2} = p_{i_1} \times p_{i_2}$ as the result by re-partitioning the p_{i_1} partition result with p_{i_2}. The calculation method is as follows:

$$p_{i_1 i_2} = p_{i_1} \times p_{i_2} =$$

$$= \left\{ c_z \left| c_z = c_x \bigcap c_y,\ x \in [1, i_1 m]\,,\ y \in [1, i_2 n]\,,\ z \in [1, i_1 m \times i_2 n] \right. \right\}. \qquad (2)$$

2.3. Time complexity and space complexity of the algorithm

The algorithm complexity can usually be classified into time complexity and space complexity. Time complexity can be expressed as CPU cost and I/O cost while space complexity can be expressed as memory cost [5]

First we will analyze CPU cost. This algorithm can be divided into three steps: initialization, single dimensional clustering and overall partition. The complexity of each step is shown in Table 1.

Secondly we will analyze I/O cost. The process of initialization requires reading-in of all data of the data points and then, respectively, writing-into d files indicating data of different dimensions. The cost of this process is $2nd$. The process of single dimensional clustering requires reading-in of single dimensional data and writing the merged result into the result file after each merging. This cost is n, so the general

I/O cost of d dimensional merging is nd [6]. Each partition requires reading-in of a clustering result so a maximum of $c-1$ clustering results are needed to produce c clusters. This cost is $c-1$. The I/O cost of the export is 1. Therefore, the general I/O cost of this algorithm is$3nd+c$.

Table 1. Algorithm complexity

Step	Operating complexity	Description
Data partition	$nd+dn\log n$	Partition the data points to the single dimensional data and sort them in ascending order.
Single dimensional clustering	$dn(n+1)$	Cluster in each dimension until one point is obtained.
Data set partition	$c(n\log n+n)$	Partition the data set to obtain c clusters.
General complexity	$dn^2+(d+c)n\log n+2nd+cn$	General computational complexity of the algorithm.

The memory occupied by the algorithm or "space complexity" is also one of the important performance indexes. When moving the single dimensional data, we should load data of a certain dimension of all data points into the memory and then move them until one merged point is obtained, so the memory cost is $O(n)$. When merging data points, we should keep on inquiring serial numbers of data points in a certain interval in a certain dimension (if after sorting the d-dimensional data of the data points in ascending order, we merge the points in the $[x_1,\ x_2]$ interval with the points in the $[x_3,\ x_4]$ interval, then during the partition process, we need to inquire which points are included in $[x_1,\ x_2]$ and which points are included in $[x_3,\ x_4]$ in order to obtain the intersection with the current data set.). This requires loading the values and serial numbers of all points in all dimensions in ascending order into the memory for inquiries. However, we needn't operate these data so we can load them into several servers according to interval and dimension and start the inquiry service program for the partition program to inquire. Therefore, theoretically, it can meet the data set with infinite n and d. So, the limitation of this algorithm on the memory exists in the merging stage. The required memory or space complexity is $O(n)$.

3. Experiment design & result analysis

3.1. Experiment assessment indexes

This study tests efficiency and accuracy of this algorithm with random and public data:

1. Efficiency: Test relations between operating time, data quantity, dimension and cluster quantity:

2. Accuracy: Test discrepancy between the clustering result derived from this algorithm and the standard result and compare it with other algorithms.

3.2. Generation method of synthetic data

The methods for randomly generating data sets in this experiment include uniform distribution and normal distribution. Parameters in the generation program for uniform distribution data sets can be seen in Table 2, which includes coordinates $\langle c_{i1}, \cdots, c_{id} \rangle$ of k d-dimensional core points $core_1$, $core_2$, ..., $core_k$, $core_i$, data point quantity n_k produced by $core_i$ and generation radii $< ri_1, ri_2, \cdots, ri_d >$ of $core_i$. The method of generating data points: choose the core points in sequence to produce data points of the designated quantity. The coordinate of a certain data point in a certain dimension j equals to the coordinate c_{ij} of $core_i$ plus a value randomly and uniformly produced from $[-r_{ij}, \cdots, r_{ij}]$. Thus the data point produced by each core point is located within a hyper-rectangle cube with the core point as the center.

The generation program for normal distribution data sets is to randomly produce data samples in each dimension according to normal distribution. The number of parameters needed is the same as the number of parameters needed in the generation program for uniform distribution data sets, but c_{ij} indicates the average μ_{ij} of the ith normal distribution in the jth dimension, r_{ij} indicates the standard deviation σ_{ij} and n_i indicates the data point quantity of the ith normal distribution.

Table 2. Generation parameter of data samples

	Coordinate	Radius	Quantity
$core_1$	$\langle c_{11}, \cdots, c_{1d} \rangle$	$\langle r_{11}, \cdots, r_{1d} \rangle$	n_1
$core_2$	$\langle c_{21}, \cdots, c_{21d} \rangle$	$\langle r_{21}, \cdots, r_{2d} \rangle$	n_2
$\cdots$	$\cdots$	$\cdots$	$\cdots$
$core_k$	$\langle c_{k1}, \cdots, c_{k1d} \rangle$	$\langle r_{k1}, \cdots, r_{kd} \rangle$	n_k

3.3. Experiment result and analysis of synthetic data

3.3.1. Test generation of data set. In order to test the performance of this algorithm, this research has tested the performance and quality of this algorithm with the randomly generated data samples derived with the generation method of synthetic data sets. The performance test includes relations between running time, data points, dimension quantity and cluster quantity. Each experiment will record total running time of clustering, reading/writing time of the hardware I/O and reading/writing & computing time of the program in the memory. Accuracy test includes clustering quality assessment of this algorithm and comparison of clustering quality with other clustering algorithms [7].

The following is the performance result derived from synthetic data. The testing machine used is Pentium 4CPU 2.66 GHz with memory of 1.49 GB.

Figure 2 displays the running time for data points to increase from 1000 to 100000.

The data sample is composed of 10 dimensions, including 10 clustering centers. The algorithm presets the cluster quantity to be 128. It can be seen that the curves for total running time and computing time in the memory have shown quadratic characters while the reading/writing time of the hardware I/O are linearly related to data point quantity. All conform to the description of algorithm complexity.

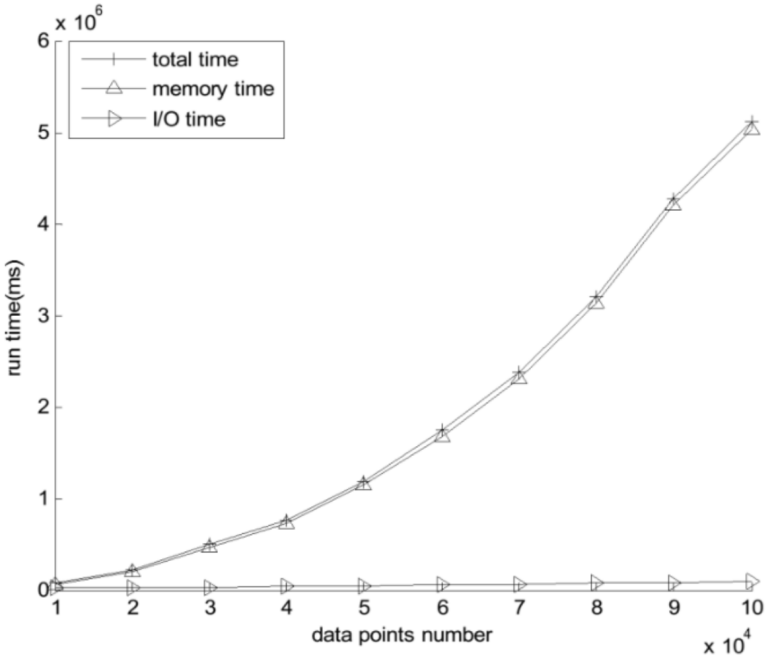

Fig. 2. Relationship between data point quantity and running time

Figure 3 displays the running time for data dimension to increase from 10 to 100. The data sample is composed of 10000 data points, including 10 clustering centers. The algorithm presets the cluster quantity to be 128. It can be seen that the total running time, the computing time in the memory and the reading/writing time of the hardware I/O are all linearly related to dimension quantity. All conform to the description of algorithm complexity.

3.3.2. Cluster quantity. Figure 4 displays the running time for cluster quantity to increase from 2 to 1000. The data space is composed of 10000 data points, including 10 dimensions. It can be seen that the total running time and the computing time in the memory have shown quadratic characters while the reading/writing time of the hardware I/O remains basically unchanged. All conform to the description of algorithm complexity.

3.3.3. Accuracy. In order to test clustering quality, this research adopts the Davies–Bouldin index method as the parameter for internal assessment. The external assessment will adopt the Rand measure (William M. Rand 1971) method and at the

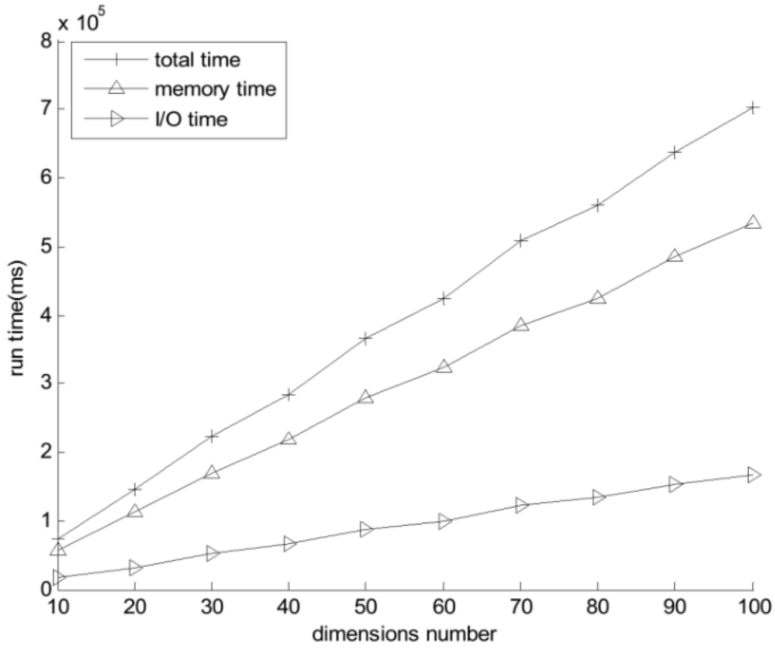

Fig. 3. Relationship between dimension and running time

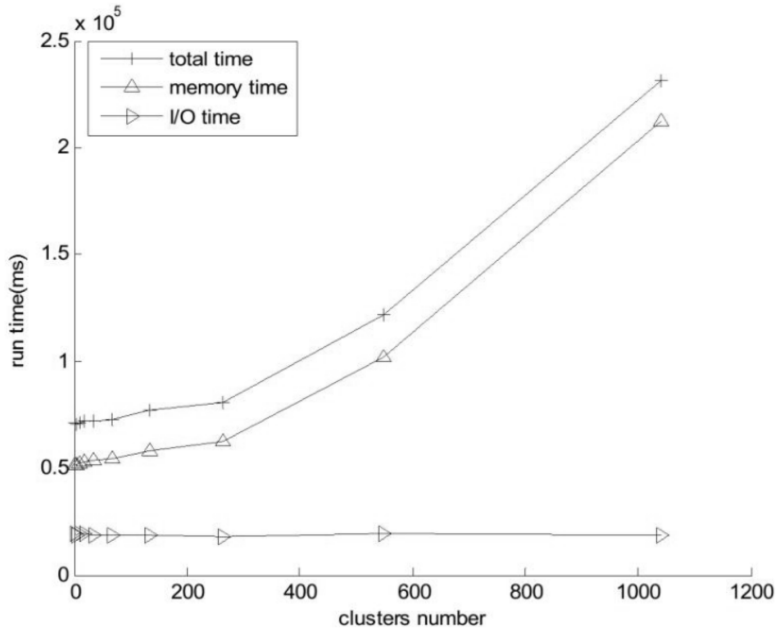

Fig. 4. Relationship between cluster quantity and running time

same time test the two clustering quality parameters from algorithms of CLIQUE[70] and DBSCAN[57] as a horizontal comparison.

This research mainly focuses on overall accuracy and stability of the algorithm. The formula for calculating Rand Index is

$$R = \frac{TP + TN}{TP + FP + FN + TN}, \tag{3}$$

where TP refers to the quantity of pairs which are in one category in the X clustering method and also in one category in the Y clustering method, TN refers to the quantity of pairs which are not in one category in the X clustering method and not in one category in the Y clustering method, FP refers to the quantity of pairs which are in one category in the X clustering method but not in one category in the Y clustering method, and FN refers to the quantity of pairs which are not in one category in the X clustering method but in one category in the Y clustering method.

The value range of Rand Index is [0,1]. The closer it is to 1, the better is the clustering quality.

This research tests accuracy and stability of DBSCAN, CLIQUE and this algorithm with the same synthetic data. DBSCAN represents the method based on density and CLIQUE represents the high dimensional subspace clustering method. Use randomly chosen radii, core points and data point quantity to produce 8 data sample generation program and then use these programs. Each program can randomly produce 100 samples whereas range of core point quantity is $[2, 32]$, range of dimension quantity is $[1, 20]$ and range of core point coordinate is [-500, 500]. The value range of radius is two times the range of core point coordinate divided by core point quantity. The value range of the data sample quantity is $[50, 5000]$. CLUQUE & DBSCAN clustering algorithm requires presetting of parameters. For every 100 data samples, this experiment will use optimal parameters derived from previous experiments of the same dimension and the same data sample quantity.

Cluster each sample with the above three clustering methods and calculate Rand Index of each clustering result. Average the experiment results produced by 100 samples using the same program. Figure 5 is the RandIndex histogram of the results of each clustering algorithm.

In perspective of average and variance, we can see that this method is not only superior to CLIQUE and DBSCAN methods in average accuracy but also remarkably enhances stability. The significant difference results derived by testing this algorithm and the other two algorithms with F-test are 0.009542 and 0.001241. This shows that there is a significant difference in RandIndex variance between this algorithm and CLIQUE or DBSCAN algorithm, that is, stability of this algorithm is superior to that of CLUQUE or DBSCAN algorithm.

According to the display of Rand Index, this method is more stable and accurate in performance while DBSCAN or CLIQUE methods will cause big fluctuations due to poor matching of its preset parameters with the data. This is caused by limitation of the method itself. This is because other algorithms require presetting of some thresholds but the optimal thresholds are usually hard to be set for a new

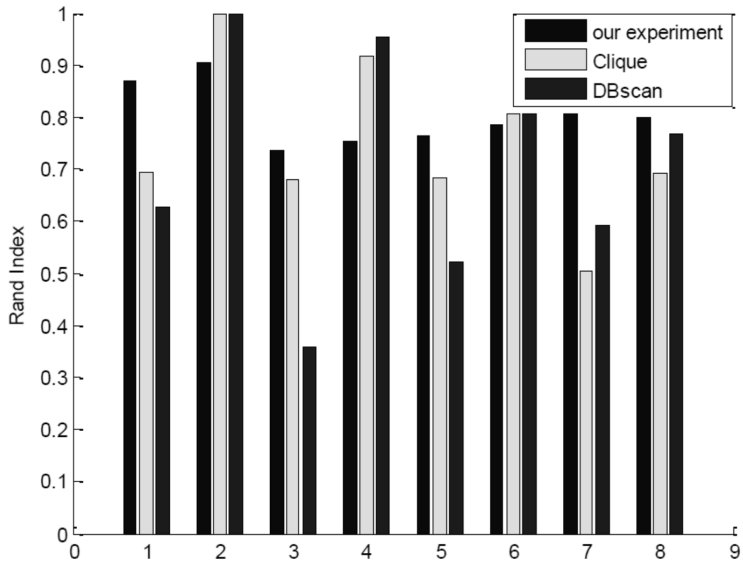

Fig. 5. Rand index of each clustering algorithm

data sample. Sometimes DBSCAN presents very low accuracy especially in handling high dimensional data. Sometimes this algorithm also has lowered accuracy for the clusters of these data samples cannot be divided by the axial hyperplane.

This research adopts the publicly downloaded data sets for specially testing clustering algorithms provided by School of Computing, University of Eastern Finland [1]. The data set is Aggregation, including 788 data points and 7 pre-labeled clusters.

Table 3 displays parameters corresponding to cluster quantity. It can be seen that when cluster quantity is 12 or 16, the sum of single dimensional entropy tends to be stable; when cluster quantity is 12, RandIndex reaches its optimal value 0.897855. So a good clustering result is achieved.

Table 3. Experimental results of actual data

Cluster Number	Sum of entropy	DB index	Rand index	Wk Index
2	0.114169	1.282283	0.250901	3109.942
3	0.26294	4.400401	0.303001	3012.798
4	1.580926	3.78385	0.719845	2364.641
5	1.625217	3.177317	0.720025	2334.227
9	1.731556	2.75222	0.727604	2241.779
12	3.387532	2.528866	0.897855	1217.795
16	3.763777	1.844235	0.890344	898.7305
20	4.001007	1.497016	0.887028	767.9188
23	3.964119	1.417218	0.880108	753.0749
29	4.046071	1.48137	0.865389	712.2116
35	4.3863	1.727795	0.840908	664.814

3.4. Summary of algorithm

Through the above analyses, we can see the following advantages of this algorithm:

1. Stable. The results of many clustering algorithms such as K-MEANS and DBSCAN have a lot to do with preset parameters. Some algorithms, BIRCH for example, are sensitive to input sequences of data. But in this algorithm, the output for a definite input is also definite. Moreover, there is no need to set parameters so it requires no knowledge from any particular fields. This is of great significance to applications in different fields.

2. Parallel process in a distributed way. The data can be split into single dimensional data for clustering separately, so the single dimensional data can be sent to distributed servers for parallel process.

3. It has overcome the problem of intervals between data points of high dimensional data tending to be equal. This algorithm does not adopt intervals to calculate similarities between data points so it can overcome this problem.

4. Discussion

High dimensional data clustering is a very complicate problems so there are still many areas to be further studied and perfected. Though the method proposed in this paper has made some improvements in computational complexity and stability, the long-time study finds that the essence of this study is to divide the data set with a plane parallel to the coordinate axis of the hyperspace. For data sets that cannot be divided by a plane parallel to the coordinate axis, this method cannot achieve good results. This research proposes to first reduce dimensionality with the principal component analysis (PCA) and then employ this method for clustering.

5. Conclusion

Taking reduction of algorithm complexity and dependence on preset parameters as the target, this research proposes a clustering algorithm based on changing tendency of the sum of edge differential entropy according to basic principles of information theory. It first performs separate hierarchical clustering to the data sample mapped to each dimension in the principle of monotone decrease of information distribution entropy and then obtains the final results by partitioning the single dimensional clustering results in the principle of maximizing the sum of single dimensional information entropy. The research verifies this algorithm with synthetic data and actual data.

The study shows that this algorithm, by adopting the method of first performing clustering in a single dimension and then repartitioning the data samples with the single dimensional clustering results in the whole data space, can remarkably enhance its computational efficiency compared with other existing algorithms such as CLIQUE ad DBSCAN. In additional, both experimental results derived from syn-

thetic data and actual data samples show that this method is not only superior to other existing algorithms in accuracy but also has remarkably increased its stability.

References

[1] H. Sun, Y. Du, D. Jiang: *ESCHCD: Entropy-based algorithm for subspace clustering with high dimensional categorical datasets.* Journal of Shandong University (Engineering Science) *41* (2011), No. 5, 37–45.

[2] L. Tang: *Text feature selection method based on information entropy and dynamic clustering.* Computer Engineering and Applications *51* (2015), No. 19, 152–157.

[3] C. Bellenguez, A. Strange, C. Freeman, P. Donnelly, C. C. Spencer: *A robust clustering algorithm for identifying problematic samples in genome-wide association studies.* Bioinformatics *28* (2012), No. 1, 134–135.

[4] M. Mutwil, B. Usadel, M. Schütte, A. Loraine, O. Ebenhöh, S. Persson: *Assembly of an interactive correlation network for the Arabidopsis genome using a novel heuristic clustering algorithm.* Plant physiology *152* (2010), No. 1, 29–43.

[5] L. Cao, H. Zhang, Z. Wang: *EB-SVM: Support vector machine based data pruning with informatior entropy.* Journal of Shandong University (Natural Science) *47* (2012), No. 5, 59–62.

[6] P. Jiang, M. Singh: *SPICi: A fast clustering algorithm for large biological networks.* Bioinformatics *26* (2010), No. 8, 1105–1111.

[7] U. Doraszelski, K. L. Judd: *Avoiding the curse of dimensionality in dynamic stochastic games.* Quantitative Economics *3* (2012), 53–93.

[8] H. Ouyang, X. Dai, Z. Wang, M. Wang: *Rough K-prototypes clustering algorithm based on entropy.* Computer Engineering and Design (2015), No. 5, 1239–1243.

Received August 7, 2017

Acta Technica *62* No. 2B/2017, 53–62

Exploration and implementation of user behavior forensics analysis system of computer network based on system log[1]

Wenzhe Lu[2, 3, 4]

Abstract. In order to make the forensic analysis of crime occurred in the computer system and computer network, and access to the electronic evidence of invasion, based on the background of "research on security guarantee system for large-scale network", the forensic analysis of computer network user behavior based on log system is made. First of all, the computer network intrusion forensics technology is analyzed, and then the functions of forensic analysis system are designed. In addition, the working flow and function of two subsystems of log collection agent and forensics server are focused on and realized. Moreover, the performance of the system is tested and analyzed from the system log collection performance, data transmission performance and other aspects. The test results show that the system has the basic function of network forensics, and meets the design requirements. In a word, the system designed basically meets the expected purpose.

Key words. Computer crime, forensic analysis, system log, log collection.

1. Introduction

With the development and popularization of computer and network technology, the current computer crime shows a growing trend. The loss brought about by the computer crime is incalculable, which brought great damage to the national life and social stability and development. But when the criminals made use of computer for crime, there was no body description nor fingerprints, let alone others to be used as circumstantial evidence. While the evidence is always in the form of electronic information, easily broken and changed, so the research on computer

[1]The author acknowledges the National Natural Science Foundation of China (Grant No. 51578109), the National Natural Science Foundation of China (Grant No. 51121005).

[2]Computer Network Information Center, Chinese Academy of Sciences, Beijing, 100080, China
[3]University of Chinese Academy of Sciences, Beijing, 100080, China
[4]North Long net (Beijing) science and Technology Co., Ltd., Beijing, 100190, China

forensics technology is particularly important [1]. As a result, this paper intends to take the system log records of criminal behavior as the foundation, to study the methods of computer network forensics. A LAN oriented distributed computer network user behavior forensics based on system log is designed. It is expected to make statistics and correlation analysis of the system log through the system, and to supply it for emergency response reference or as the court evidence. As a result, criminals should pay the price for their crimes and consequences, so as to purify the network environment, renovate the network order, and safeguard the national security and social stability.

2. Experimental procedure

2.1. Computer network intrusion forensics based on system logs

The implementation model of computer network forensics based on system logs: Based on the feasibility and legal requirements of the system log as electronic evidence, this paper first of all proposes a computer network user behavior forensics analysis system model based on system log. The main idea of designing computer network user behavior forensics analysis system is to collect the system logs of the key servers in a LAN to a special forensic server for collective storage and forensics analysis. The theoretical model of the system is shown in Fig. 1.

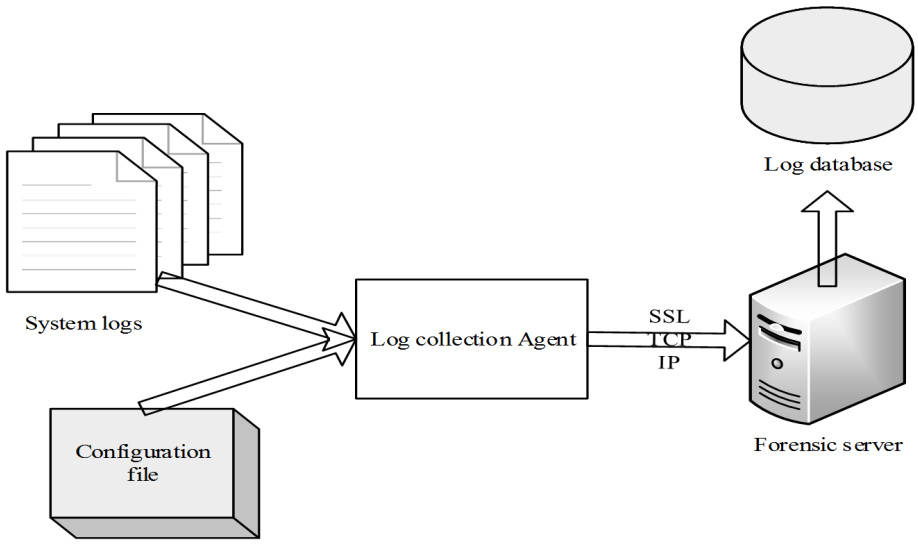

Fig. 1. The computer network user behavior forensics analysis system model based on system log

Figure 1 shows that the system consists of two parts: log collection agent and forensics server. The system uses client/server structure, and the log collection Agent is the client side, deployed in the protected servers in the LAN, responsible

for the integrity verification, acquisition and sending of system log information on the target machine. The configuration file defines the parameters of collection agent; forensics server is the server terminal of system, which is responsible for the receiving and preservation of log data sent by Agent. In addition, it is also necessary to make the integrity protection and verification of the original log data [2]. At the same time, the forensics server is responsible for preprocessing and management of log data. The forensics analysis of log data is the most important function of forensics server. According to the instructions of forensic personnel, statistics analysis and association analysis is needed for log data in the database.

Log forensics analysis:

Computer forensics analysis is confronted with massive data and it cannot be analyzed manually one by one. It is necessary to use computer system to screen evidence materials related to computer crimes. The log statistics analysis process is shown in Fig. 2.

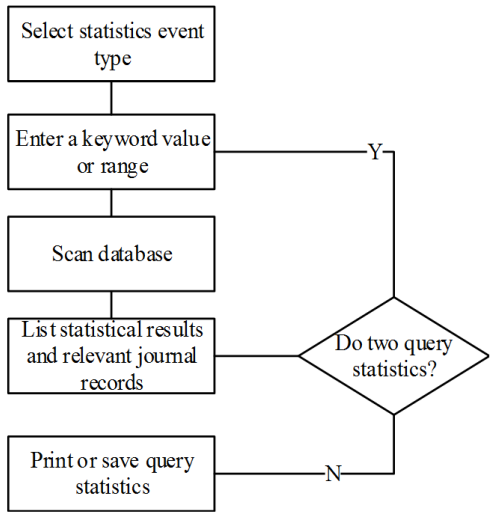

Fig. 2. Statistical analysis flow chart

2.2. Functional module design of computer network user behavior forensics analysis system

The system is a distributed computer network forensics system based on agent. It takes a LAN as the application background, and the system log of server in LAN for forensics object. The overall goal is to make a forensic analysis of the intrusion occurred in the important LAN server, and to dig out the illegal behavior evidence of network users in the system log [3]. In this paper, for the computer network user behavior forensics analysis system based on the system logs, the specific module is shown in Fig. 3.

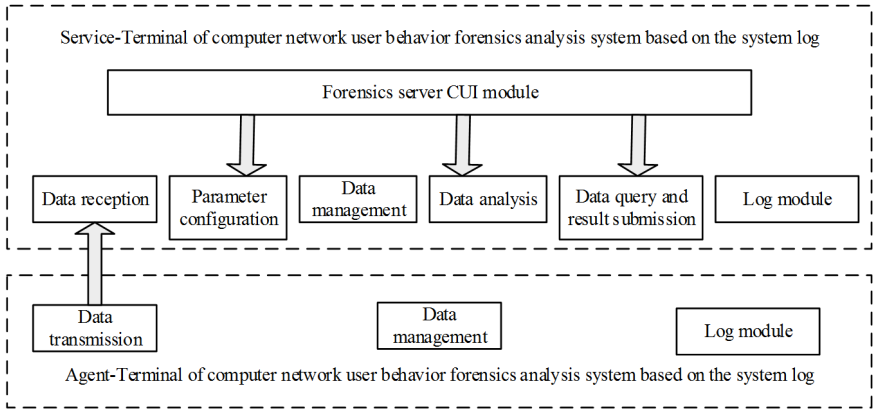

Fig. 3. System overall function module diagram

2.3. Major functions implementation of computer network user behavior forensics analysis system

Log collection agent sub-function implementation:

The log collection agent subsystem consists of three modules. Among them, the data management module is responsible for the data storage format conversion, data integrity verification and calling action and the corresponding time stamp in the log module recording of data management process, and the abnormal changes of system log. The data transmission module is responsible for collecting the initialization parameters and dynamic adjustment, the establishment and management of the SSL channel, regular acquisition of data log according to the configuration parameters. And through the SSL channel, it is transmitted to the server, and at the same time, it completed the recording of data transmission process and history. The log module is mainly responsible for accepting the calling of other modules, recording the process of collection agent end forensics operating, abnormal cases of system log files, and the corresponding time stamp information, so as to maintain the integrity of evidence chain. The work-flow of the log collection agent is shown in Fig. 4.

Implementation of log forensics server sub-functions:

The log forensics server module is one of the core modules of the system, which is mainly responsible for the acquisition of log information on the server. Among them, the data receiving module mainly receives the log data from the log collection agent entity, which can complete the establishment of SSL channel, receive data and synchronization, and record the receiving process. The data management module can store all kinds of logs in layers according to the source IP address, log type, and receiving time. For log files in the same type and the same source, they are merged to a paper file. At the same time, this part functions, for the log data received, can carry out data integration, data cleaning, data reduction and so on pretreatment [4]. And the CES algorithm is adopted to make signature encryption of original files received, to conduct ACL control of the log file, so as to ensure that only those who have the administrator privileges can access to. The data analysis module is mainly

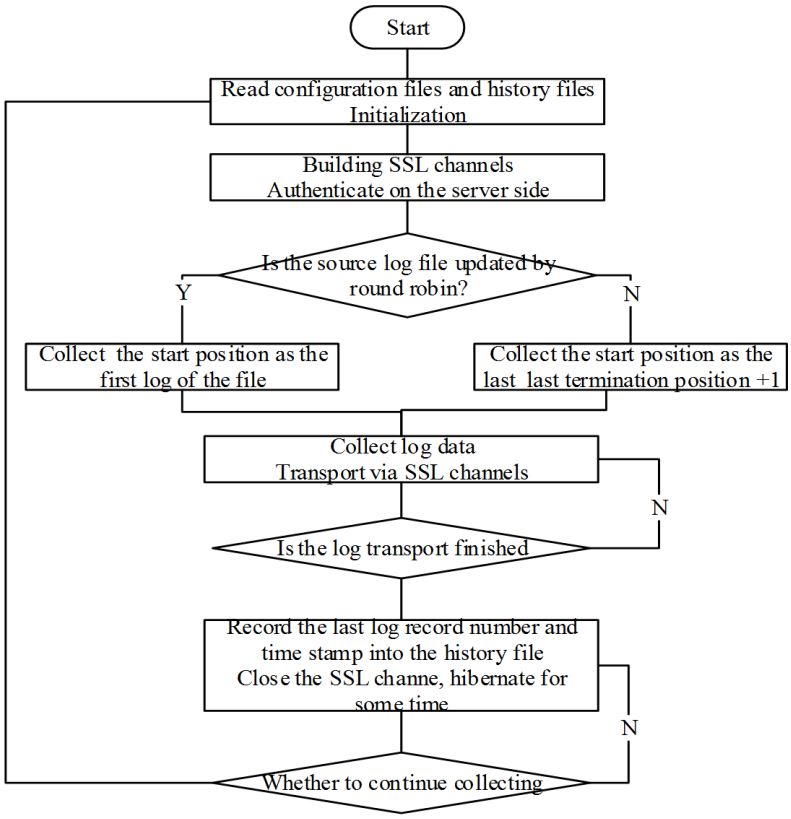

Fig. 4. Work-flow chart of log collection agent

based on the instructions of forensics personnel for statistical analysis, clustering and correlation analysis of log data, to form the forensic analysis report, and to send the forensic analysis results to the GUI module and display in an appropriate way. The data query and submit module can make all kinds of queries of the original log files according to forensics analysis results, extract the query result, and perform the signature lock using CES algorithm, so as to form the log evidence file. This module should also have the function to verify the integrity of the extracted log file. The parameter configuration module is responsible for receiving the instructions sent by the GUI module about modifying server parameters configuration. Modify the corresponding parameter in the configuration file can control the corresponding parameters configuration in the data receiving module and data processing module. The log module is designed for being called by the other modules and recording the whole process of data processing and abnormal situations in the forensics process [5]. Gu I module is mainly responsible for modifying the server configuration parameters, accepting statistical analysis, association analysis, query extraction and so on request operations on the interface of users, and transmitting the request to other modules. In the meanwhile, it calls the data of log module and displays the data processing

record. The work-flow of the forensics server is shown in Fig. 5.

The users interact with the forensics server through the GUI interface, and start the log receiving module, parameter configuration module, data analysis module, and query module through the start menu items. In addition, uses complete the server configuration, receiving and management of log data, forensic analysis of log data, query and log data extraction and submit, forensic results integrity verification and so on. The data management module and forensics log module are called by other modules in the process of forensics.

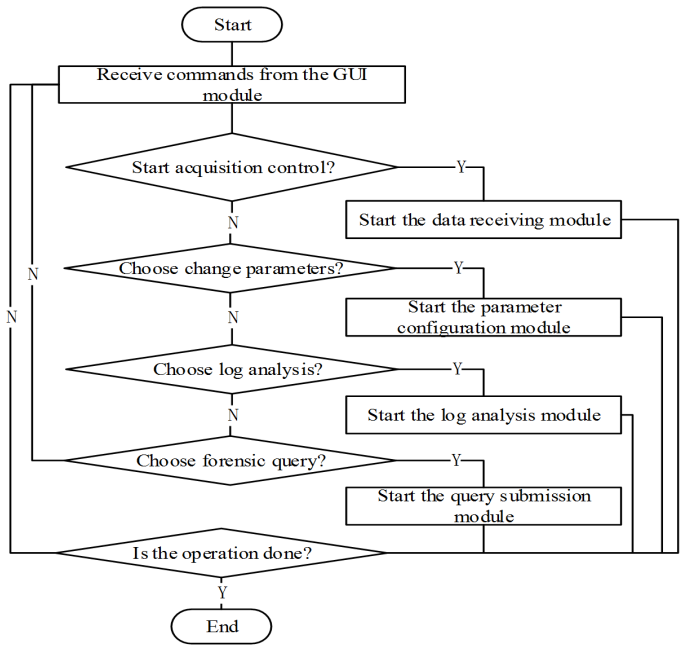

Fig. 5. Work-flow chart of log forensics server

Interface implementation:

The log collection agent interface is shown in Fig. 6. The client configuration file ssl_client.conf provides the relevant parameters setting of client, including client certificates and keys, evidence server IP address and port, acquisition time interval and acquisition object, client log file name and storage path and so on information. By directly editing the file, we can change the parameters of client; history record file send_history.txt records the history information that each log transfers, for the reference for the next transmission, so as to achieve the integrity verification of incremental transmission and log files. The client log file records the process, log management, abnormal cases and so on information in the process of each log transfer, and it is filled in and inquired by the client log module. The interface relationship of the forensics server subsystem is shown in Fig. 7.

Design and implementation of forensic database:

The forensic database is used to save the processed log data, and the database can

provide us with quick queries. Relational databases can also realize the association query of multiple database tables. Database queries can be simply implemented only by using SQL statements, which are incomparable for queries bade on file. Therefore, this system uses the database based scheme in statistical analysis and correlation analysis of logs.

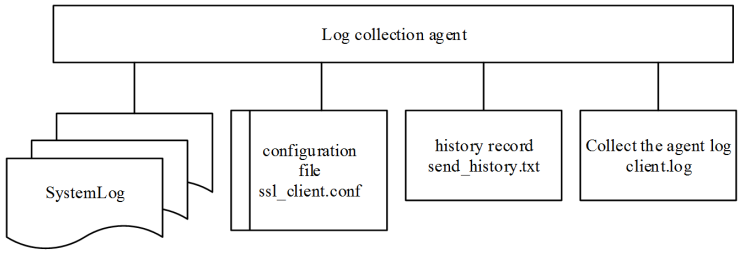

Fig. 6. Interface to a forensic server subsystem

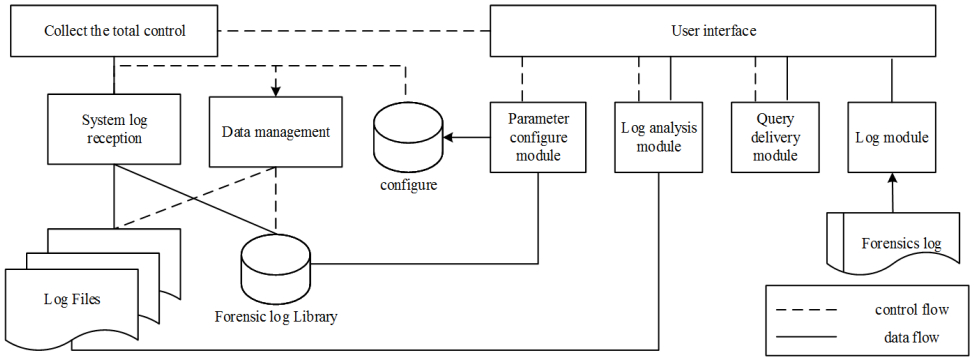

Fig. 7. Interface to a forensic server subsystem

The system uses relational database, using open source database software MySQL to build the database, MySQL has cross platform, simple management and operation, able to handle large data, quick query and so on advantages. The database is defined based on a log, a data table. The field of table is basically corresponding to attribute domain of various log record tables, just removing some irrelevant attribute domains and adding Logsource (log source, the source host IP address), Result (possible outcome of events) and Condnion (event condition) [6]. The fields are set to facilitate the subsequent forensic analysis, and to fill in the value of these fields in the data preprocessing of log data written to the database.

3. Results and discussion

After the completion of construction of computer network user behavior forensics analysis system based on the system log, it is necessary to test various functions of the system and determine the performance of the system, so as to verify the feasibility of

the system. For the design of the computer network user behavior forensics analysis system, part of the test results are as follows.

3.1. Acquisition performance test

It mainly tests the adaptability of collecting agents to load changes and the rationality of acquisition model. The test method is to change the generation speed of system log through the conscious file, directory operations and process operations.

During the test process, when the speed of the log data changes rapidly, the acquisition agent can automatically adjust the acquisition time interval, and timely collect and transfer the log data, which executively protect the log security. When the speed of log data generation varies little, the acquisition time interval remains stable. Experiments show that the system has a certain self-adaptability. However, there is a certain lag in the adjustment action, and the choice of time interval increments affects the sensitivity of adjustment. The calculation of the initial time interval will also affect the subsequent dynamic adjustment. If it is too large or too small, it will lead to frequent adjustment of the time interval during the acquisition process. The choice of the minimum time interval should be determined by the maximum load of the system.

3.2. Transmission performance test

Through the SSL channel packet transmission, the speed and accuracy between the acquisition agent and forensic agent are mainly tested. Table 1 gives the time taken for different size log data transmissions with different lengths of the RSA key (the data transmission buffer takes 4096 bytes). As can be seen from the table, the length of the RSA key has little effect on the transmission time. This is because in the SSL protocol, the RSA public key algorithm is used to exchange the session key, the data transmitted is encrypted with a symmetric key algorithm DES and CBC3 [7]. The changes in key length RSA only affect DES session key encryption speed. DES key is only 64 bits long, and a data acquisition only exchanges for a session key. In the case of software implementation, the DES algorithm is 10 times faster than the RSA algorithm, and 100 times faster than the hardware implementation. As can be seen from the table, the data transmission time is directly proportional to the data size. The SSL channel transmission data can reach an average of 600 KByte/second, which fully meets the needs of log transmission of server in a medium-sized and small-sized LAN. As long as the suitable acquisition time interval is selected, it will not cause the evidence server congestion and denial of service.

Another factor affecting the transmission speed of the acquisition is the log buffer size, which is the size of log data for one time transmission of a client and server. Table 2 gives the effect of buffer on the log transmission speed (RSA key length is 4096 bits). As can be seen from the table, the buffer size is directly proportional to the data transmission speed. However, as discussed in [8], when a transmission data is less than the buffer size, the capacity of the buffer has little effect on the transmission speed. Of course, the buffer cannot be too large. On the one hand, it is

because the sampling interval is not too large, and the amount of log data generated will not be too great. On the other hand, the buffer is too large so that it requires fragmentation and reassembly in the TCP message, and large buffer requires large memory that it will affect the performance of the host server. In combination with the above factors, the system buffer is set to 4096 bytes in size.

Table 1. Transmission performance test

	RSA key length			
Data size	1024 bits	2048 bits	3072 bits	4096 bits
1000 kB	1.613	1.583	1.604	1.617
2000 kB	3.195	3.275	3.149	3.249
4000 kB	6.309	6.449	6.374	6.509
8000 kB	12.528	12.613	12.463	12.614
12000 kB	18.797	18.867	18.591	18.572

Table 2. Effect of buffer size on the speed of log transfer (time unit: seconds)

	Buffer size		
Data size	1024 bytes	2048 bytes	4096 bytes
8000 kB	47.874	24.419	12.614
20 kB	0.150	0.095	0.080
10 kB	0.050	0.050	0.047

3.3. Log analysis test

Log analysis test mainly tests the accuracy and reliability of system's analysis of log data. After the test, the system can count on the log data according to the type of event, establish a network and user behavior, and find the abnormal log records. The two times statistics provided by the system can further narrow the scope for analysis. The number of data in the database table is an important factor affecting the performance of statistical analysis. The greater the amount of data, the slower the query and statistics, and the greater the demand for memory at the same time. Therefore, the database must be backed up regularly, with only a week's data left in the database and reimported into the database when needed.

In association analysis, the system can find the relevant log records of security events according to the time stamp and relevant features of log records. Factors affecting the accuracy of correlation and analysis velocity are the main selection of $\triangle t$ value, correlation property, and relevant log table, and the definition of condition and result field value in the pretreatment. What is more, the accuracy of clock synchronization network is also an important factor.

The memory size of the forensic server also affects the performance of log analysis, and large memory support is required for database query, log query and extraction.

4. Conclusion

Through in-depth research and analysis of computer forensics technology, system log forensics analysis and other related technologies, computer network user behavior analysis system based on the system log is designed. In the design process, this paper chooses client/server structure as a whole system structure. At the same time, it makes specific design and implementation of two sub-systems log acquisition agent and forensics server constituting the whole system. The work flow is given, and the system database and interface are designed. Finally, the performance test of the designed system is carried out. The analysis results show that the system has basically reached the expected goal, to achieve the requirements of computer forensics.

References

[1] H. Alipour, Y. B. Al-Nashif, P. Satam, S. Hariri: *Wireless anomaly detection based on IEEE 802.11 behavior analysis.* IEEE Transactions on Information Forensics and Securityy *10* (2015), No. 10, 2158–2170.

[2] J. Yan, H. He, X. Zhong, Y. Tang: *Q-learning-based vulnerability analysis of smart grid against sequential topology attacks.* IEEE Transactions on Information Forensics and Security *12* (2017), No. 1, 200–210.

[3] S. Oh, M. Pandey, I. Kim, A. Hoogs: *Image-oriented economic perspective on user behavior in multimedia social forums: An analysis on supply, consumption, and saliency.* Pattern Recognition Letters *72* (2016), 33–40.

[4] R. Liu: *Research on IPV6-based computer crime evidence dynamic forensics technology.* IEEE International Conference on Communication Systems and Network Technologies, 4–6 April 2015, Gwalior, India, IEEE Conference Publications (2015), 720 to 724.

[5] K. C. Seigfried-Spellar, N. Villacís-Vukadinovič, D. R. Lynam: *Computer criminal behavior is related to psychopathy and other antisocial behavior.* Journal of Criminal Justice *51* (2017), 67–73.

[6] S. He, J. Zhu, P. He, M. R. Lyu: *Experience report: System log analysis for anomaly detection.* IEEE International Symposium on Software Reliability Engineering (ISSRE), 23–27 October 2016, Ottawa, ON, Canada, IEEE Conference Publications (2016), 207–218.

[7] Y. Shi: *Research of social network log analysis system based on MongoDB.* Open Automation and Control Systems Journal *7* (2015), No. 1, 1621–1628.

[8] T. Grance, S. Chevalier, K. K. Scarfone, H. Dang : *Guide to integrating forensic techniques into incident response.* NIST Special Publication (2006), Report No. 800–86.

Received August 7, 2017

Acta Technica *62* No. 2B/2017, 63–72

Security of robot wireless network remote control system

Yu Lin[1], Ding Mi[1]

Abstract. The purpose is to study the security of wireless remote-control system of robot. A new EAP-TLS Plus protocol is proposed. At the same time, the robot remote control system is simulated by using the advantages of the absolute safety of quantum technology. The security performance is analyzed and studied respectively. In the case of improving the security performance of user access authentication, the simulation and analysis of the robot remote control system based on EAP-TLS Plus protocol are carried out. A quantum secure direct communication scheme and a quantum signature scheme based on four - particle cluster state are proposed. The simulation and performance analysis are carried out. At last, the idea of applying quantum technology to robot remote control system is put forward, and theoretical analysis and research are carried out. The results show that the security performance of the new protocol is enhanced, but the time complexity (authentication delay) is also increased. Therefore, it can be concluded that the improvement is only a temporary solution. Only by physically changing its security performance can this security problem be better resolved.

Key words. Wireless local area network, robot, information security, quantum communication, remote control.

1. Introduction

Human society has entered the era of information. With the rapid development and popularization of computer information technology, people depend too much on the information life. People's awareness of the protection of information has gradually risen from the embryonic stage to a more conscious stage. All kinds of communication means are inseparable from our daily life [1]. It has become the basic requirement to ensure communication fluency and communication security. Wireless local area networks (LAN) has good mobility and low operating cost. It can also organize the network flexibly, and management is very convenient. This makes up for the lack of wired networks [2]. At present, wireless LAN has been widely used in manufacturing, robotics and other fields. With the continuous improvement of the wireless LAN transmission rate, the application of the wireless LAN in the robot

[1]Zhengzhou Shuqing Medical College, ZhengZhou Henan, 450064, China

industry is increasing. Many robots work in dangerous and harsh environments, which can greatly affect the efficiency and personal safety of the operator. Therefore, the control of robots, from traditional field control and wired network control to wireless network control, has become an urgent need for the development of robots [3].

However, the security performance of the wireless local area networks is not as stable as that of wired network. At present, the most widely used wireless LAN is the 802.11 standard. Although 802.1x makes up for some of the 802.11 standard defects, there are still some shortcomings. The reason is that the protocol lacks two-way authentication between the client and the authenticator, and lacks the encryption protection of the authentication message. Illegal users can use these defects to achieve a variety of attacks [4]. There are three main types of attacks: the first is a fake attacker attack, the second is the session hijacking attack, and the third is to refuse service attacks. These security flaws have become the bottleneck of restricting the development of robot remote control technology based on wireless network to a certain extent. Figure 1 is a schematic diagram of the IEEE802.1x protocol architecture. Figure 2 is the IEEE802.1x authentication protocol process.

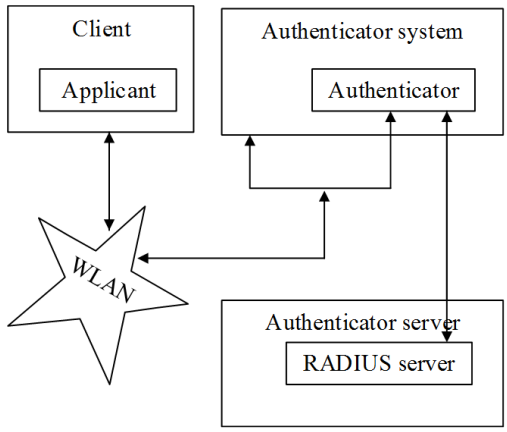

Fig. 1. 802.1x structure diagram

The security performance of robot remote control technology based on wireless network should be improved. Wireless LAN not only can play a greater role in robot development, research and application, but also can make wireless remote-control technology more secure and practical. This is conducive to the further development of robot remote control technology and the popularity of robots in various fields. At the same time, it will also help promote the industrialization of robots, especially industrial robots in our country. Therefore, it is an important task to realize secure information transmission in the wireless remote control of robot. However, so far, no attention has been paid to the security of the robot remote control system in wireless networks.

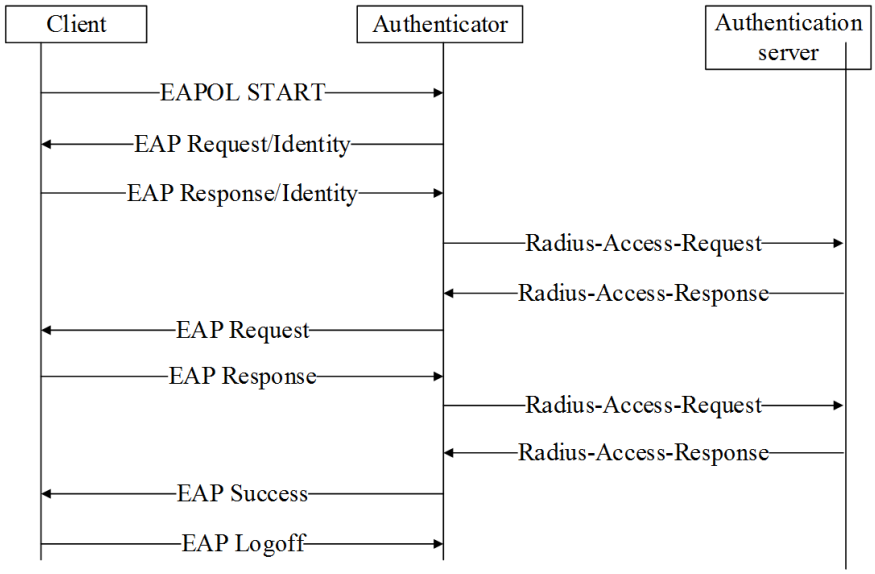

Fig. 2. IEEE802.1x authentication protocol process

2. State of the art

2.1. Research status of wireless network security

At present, both at home and abroad have put forward the wireless LAN security standards. However, they have some security flaws [5]. In 2004, in view of the DCF mechanism in the MAC layer of IEEE802.11 protocol, Ji Xiaomei conducted an analysis and improvement. The improved solution achieves better channel utilization efficiency and more stable performance through two "virtual competition" phases. In 2005, Feng Liuping and Liu Xiangnan analyzed the vulnerability of IEEE802.11 authentication protocol and denial of service attack. In 2006, based on the framework of 802.1x protocol and EAP protocol, Zhao Lin proposed a password based authentication enhancement scheme. The scheme can meet the security requirements of WLAN authentication to a certain extent, and it effectively enhances the authentication mechanism of 802.11i. In 2010, in order to enhance the security of IEEE802.1x protocol, Du Hui and Zhu Zhixiang proposed a new scheme, that is, EAP-DH. Through verification of the identity of the authenticator, the scheme can effectively prevent the impersonation of the IEEE802.1x protocol from attack, so that the security performance of the protocol has been improved. In 2011, Zhou Chao pointed out the root of the 802.1x protocol being vulnerable to attack. Protocol state machines are unequal and incomplete. It lacks protection for message integrity and source authenticity [6]. Then, an improved scheme of bidirectional challenge handshake and offline verification is proposed and implemented.

Quantum cryptography, based on quantum mechanics, is different from classical cryptography. It is the full use of physical characteristics. The quantum cryptog-

raphy can develop an absolutely secure cryptosystem. Because if there is external eavesdropping, it will disturb the original state of the quantum system. Theoretically, the quantum states of quantum channels in quantum cryptography are not allowed to be measured by illegal users, because illegal measurements are bound to disturb both sides of the communication. In terms of methods, quantum cryptography is not used to transmit secret messages, but rather to transfer and distribute encryption keys (or create a password manual). In practice, quantum cryptography can guarantee the absolute security of communication. However, there are still some shortcomings. The quantum system itself is susceptible to interference from the communication environment, resulting in a higher communication error rate. It will affect the communication quality [7].

Compared with foreign countries, China's achievements in quantum cryptography is more significant. China University of Science and Technology achieved a key distribution of 150 km. Through the use of communication fiber optic cable, the long distance QKD was completed in Beijing, Xianghe and Tianjin. After long time monitoring, the bit error rate has been stable below 6 %. At the same time, USTC (University of Science and Technology of China) has successfully developed a prototype of quantum telephone. Through the commercial optical fiber network, a quantum communication network has been set up in Hefei, and a free quantum telephone network has been set up. The network's coverage is 1000 square kilometers, and it has successfully implemented a call encrypted quantum phone. This achievement not only demonstrates the absolute security of quantum communication, but also shows that quantum communication technology can be realized completely. At the 2011 Nobel prize winner forum in Beijing, Professor Pan Jianwei announced that China plans to launch a quantum communications satellite in 2016. Quantum information technology ensures that our calls are not bugged, and quantum unique parallel computing capabilities make quantum computing extremely fast.

2.2. Research status of robot remote control

With the continuous research and exploration of human nature, more and more complex and dangerous working environment is involved in the field of space, ocean and so on. In this context, people began to study the robot remote control technology in the 60s of last century [8]. The robot remote control system (RRCS) can provide basic functions, such as remote operation, data transmission, remote monitoring, network conversation and abnormal feedback. With the continuous development of science and technology, especially the maturity of computer information and communication technology, robot remote control system has become more rapid, convenient and intelligent [9]. The robot remote control system is designed according to the specific task and the actual working environment. As shown in Figure 3, it describes a simple framework for the hardware of a robot remote control system. A robot remote control system usually performs point to point remote control by the control device and the execution device. Furthermore, it can be further designed as remote control of multi-control equipment by multi-control equipment. The robot remote control system is mainly composed of control equipment, execution equipment, wire-

less communication module and sensor. The hardware frame diagram of the robot remote control system is shown in Fig. 3.

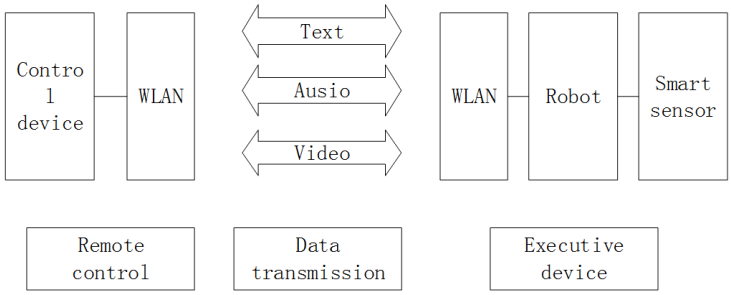

Fig. 3. Robot remote control system hardware frame diagram

When the robot remote control system is working, the staff login to the remote-control client at the control device end, and realize the remote control of the device (robot) in the human-computer interaction interface [10]. The control device communicates with the execution device through the wireless local area network. As shown in Fig. 4, it can be seen that on the basis of wireless LAN communication, this paper is mainly responsible for the authentication of client (control device) and server (execution device). It can ensure the safe communication between the control device and the executing device, and verify the origin, authenticity and integrity of the transmitted data. Further, it guarantees that the remote execution equipment is not damaged, the remote operation is free from interference, and the surrounding operating environment is not polluted and destroyed [11]. The connection and control of the robot can be realized by installing the client at the end of the control device. After the connection is successful, the man-machine conversation can be carried out. The software frame diagram of the robot remote control system is shown in Fig. 4.

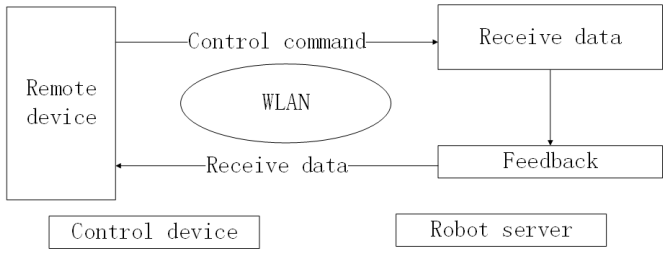

Fig. 4. Robot remote control system software frame diagram

To sum up, the robot remote control technology is an important part of robot technology. The wireless communication technology is used in the robot remote control system, which can not only realize the remote control of the robot, but also

make the robot interact with other intelligent software and intelligent sensor. It will make robots more intelligent. The remote control of robot plays an important role in deep-sea exploration, space exploration and dangerous environment operation. At present, the research of robot remote control technology is not mature enough. The security risks of user access control are not noticed. The security defects of wireless networks restrict the development of remote control technology to a certain extent. In the final analysis, its physical limitations limit the security performance of communication technology. Only through breaking through this physical limitation can we fundamentally solve the security problems of access control. Although quantum communication is a new subject, it has shown its strong security advantages. Quantum cryptography can ensure unconditionally secure communications. Therefore, a new EAP-TLS Plus protocol is proposed in this paper. At the same time, the remote control system of robot is simulated by using the advantages of the absolute safety of quantum technology, and the security performance of the robot is analyzed and studied respectively.

The following aspects are mainly studied. The basic knowledge and existing problems of IEEE802.1x protocol and EAP protocol are introduced. The authentication process and authentication method of IEEE802.1x protocol and EAP protocol are analyzed, and several security defects of IEEE802.1x/EAP authentication protocol and the specific reasons for these defects are deeply studied. The EAP-TLS Plus protocol is proposed, and the robot remote control technology is used to analyze it. First of all, the IEEE802.1x / EAP authentication protocol security flaws were studied. A kind of targeted improvement protocol is proposed and its safety performance is simulated and analyzed. Then, the robot remote control was introduced. In the case of improving the security performance of user access authentication, the simulation and analysis of the robot remote control system based on EAP-TLS Plus protocol are carried out. A quantum secure direct communication scheme and a quantum signature scheme are proposed. According to the strong correlation degree and large entanglement of four particle cluster states, a quantum secure direct communication scheme based on four particle cluster states and a quantum signature scheme are proposed. The simulation and performance analysis are also carried out. Then, the idea of applying quantum technology to robot remote control system is put forward, and theoretical analysis and research are carried out.

3. Methodology

3.1. Research on RRCS based on EAP-TLS Plus

EAP-TLS protocol is vulnerable to session hijacking. From the three points of view, the shared secret instruction, the shared encryption and decryption key and the increase of the authentication between the client and the authenticator, the EAP-TLS protocol is improved. A more secure EAP-TLS Plus authentication protocol is proposed. The pre-shared secret instruction completes the authentication of the client identity at the first time, and the legal user refuses directly. If an illegal user initiates an authentication request, when the authentication server's Challenge

is queried, the illegal user needs to submit a hash value Xi in the confidential instruction information shared by the client and the authentication server in advance. The possibility of an incorrect user submission is clearly very low. This not only saves the computing resources and storage resources for the authentication server, but also effectively avoids malicious denial of service attacks. Therefore, it effectively protects the key information frames transmitted during the authentication process. The improved EAP-TLS Plus authentication protocol is applied to RRCS. The security performance of the new authentication protocol is analyzed by simulation and compared with the EAP-TLS protocol.

3.2. Research of RRCS based on quantum technology

Traditional cryptography systems are based on mathematical calculations, whereas quantum cryptography is based on quantum mechanics. Quantum cryptography is an absolute security cryptosystem based on quantum attributes. The Heisenberg uncertainty principle shows that if a quantum state is measured, it must cause some degree of interference to the original quantum state. The measured quantum states will be different from those of the original state. Similarly, if a quantum system is measured, the resulting measurements cannot include complete information about the original system. According to the uncertainty principle, it can be known that both sides of the communication can detect the eavesdropper at the first time. Because the eavesdropper does not measure the quantum states on the quantum channel, it cannot guarantee the undisturbed state. Once disturbed, the measurement results of both sides of the communication will change, and then it will find the existence of eavesdroppers. At present, the safety of the principle of quantum state uncertainty has been proved. Therefore, even a computer with supercomputing power is of no avail. In addition, the quantum has the characteristics of non-cloning. In the case of communication under the conditions of channel security, the third party cannot steal any useful messages. The quantum technology is applied to robot remote control technology. According to the process of quantum secure direct communication protocol, the flow of simulation algorithm is designed. The protocol is simulated by Microsoft Visual 2010 platform, and the information security performance is analyzed and studied.

4. Result analysis and discussion

4.1. Analysis of EAP-TLS Plus and EAP-TLS comparison results

In the simulation of the robot remote control system, the IEEE802.1x / EAP-TLS Plus protocol is simulated by the security performance. On the basis of simulation and simulation, it is found that the security of classical information cannot fundamentally eliminate the attacker's attack. On the basis of the EAP-TLS Plus protocol, the security performance of the wireless remote control system based on the wireless network is greatly improved. However, in the final analysis, its safety

performance is dependent on classical cryptography. In the simulation system based on IEEE802.1x / EAP-TLS Plus protocol, the user's authentication from the control device to the user's identity is successfully validated by the robot authentication server, which takes a longer time. In view of this, the simulation program based on IEEE802.1x/EAP-TLS protocol is also made in this paper, and several experiments have been carried out. Through experiments, it can be found that the EAP-TLS Plus protocol takes longer than the EAP-TLS protocol. According to the experimental results, it can be seen that the EAP-TLS Plus protocol has some shortcomings in the speed of authentication. As shown in Fig. 5, it is the result of the 50 times test contrast.

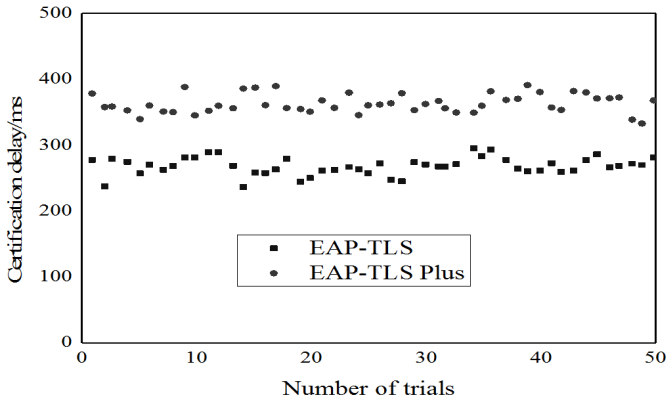

Fig. 5. Comparison of authentication delay between EAP-TLS Plus and EAP-TLS protocols

4.2. Analysis of RRCS security simulation results based on quantum technology

Through the previous analysis, in the ideal channel, the quantum communication for the non-coherent attack is safe. The communication efficiency has also been improved. Before formal access to coded communications, probe photons are introduced. It mainly carries on the second detection to the security of the quantum communication channel. The security and defense capability of the communication protocol is improved. In fact, the noise of the quantum channel influences the security of the communication scheme to a certain extent. This scheme has three advantages. First, the secret message is transmitted directly without the need to send a password. Second, the trial photon is inserted in the communication phase, so that the security performance of the communication is strengthened. With the cluster state as the information carrier, the entanglement is the largest, the correlation is the highest, and the communication efficiency is high.

Figure 6 is a statistical survey of the 20 test of channel safety before analog communication. It can be seen that before the communication, the protocol can always detect whether the channel is secure, which provides the security guarantee for the

protocol. The dotted line in the picture is a security line, which indicates that the channel is unsafe. The security performance of the protocol can be proved directly from the experimental results. It also reflects the security of quantum communications.

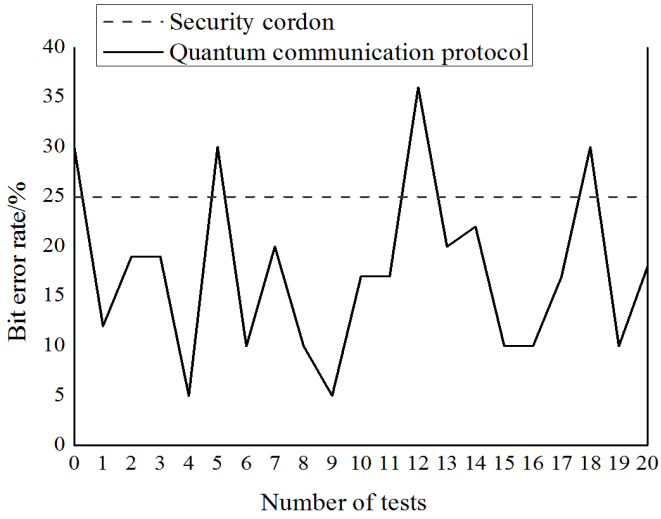

Fig. 6. Experimental results of secure detection for quantum communication channels

5. Conclusion

The security defects of IEEE802.1x / EAP authentication protocol are analyzed, and a modified protocol—EAP-TLS Plus is put forward. The EAP-TLS Plus protocol is combined with robot remote control technology. The control system is simulated, and the security performance of the access control is analyzed. Through simulation tests, the results show that the security performance of the new protocol is enhanced, but the time complexity (authentication delay) is also increased. Although the EAP-TLS Plus protocol has enhanced security performance, it can still be deciphered and attacked. Therefore, the improvement is only a temporary solution. Only by physically changing its security performance can this security problem be better resolved. The four particles cluster state is chosen as the information carrier. A quantum secure direct communication scheme and a quantum signature scheme based on four particle cluster states are proposed, and their performances are analyzed respectively. Then, based on the research of quantum technology, the security performance of the robot remote control system is analyzed and studied in detail. Finally, it comes to the conclusion that quantum technology is unconditionally secure. If human beings could design and produce quantum computers, our information would not be stolen by others. However, the quantum channel noise

is still not resolved at the moment. The future research should try to improve the feasibility and reliability of quantum experiment.

References

[1] F. Peng, X. P. Fan: *Research on safety monitor system for coal mine based on EPA.* Advanced Materials Research *433–440* (2012), 6128–6133.

[2] H. Zhao, Z. Liu: *Design and implementation of wireless communication subsystem in WLAN-based rescue robot.* Proc. IEEE International Conference on Internet Technology and Applications, 20–22 August 2010, Wuhan, China, IEEE Conference Publications (2010), 1–4.

[3] J. W. Zhao, H. C. Li, G. Q. Chen, J. J. Huang, J. Dai: *Development of numerical control system for 3-PRS-XY series-parallel machine tool.* Proc. Mechanical Engineering and Control Systems, Publisher: WSPC, International Conference on Mechanical Engineering and Control System (MECS), 15–17 April 2016, Wuhan, China, 511–517.

[4] Z. Cai, X. Ren, G. Hao, B. Chen, Z. Xue: *Survey on wireless sensor and actor network.* Proc. IEEE World Congress on Intelligent Control and Automation (WCICA), 21–25 June 2011, Taipei, Taiwan, IEEE Conference Publications (2011), 788–793.

[5] R. Modugu, Y. B. Kim, M. Choi: *Design and performance measurement of efficient IDEA (International Data Encryption Algorithm) crypto-hardware using novel modular arithmetic components.* IEEE Instrumentation & Measurement Technology Conference Proceedings, 3–6 May 2010, Austin, TX, USA, IEEE Conference Publications (2010), 1222–1227.

[6] Q. Wang, S. Liu, Z. Wang: *A new internet architecture for robot remote control.* Proc. IEEE/RSJ International Conference on Intelligent Robots and Systems, 9–15 October 2006, Beijing, China, IEEE Conference Publications (2006), 4989–4993.

[7] G. P. Biswas: *Establishment of authenticated secret session keys using digital signature standard.* Information Security Journal: A Global Perspective *20* (2011), No. 1, 9–16.

[8] X. Qin, B. Jiang, X. Deng, X. Zu, Y. Du, H. Li: *A robot remote control system based on VPN and TCP/IP protocol.* Proc. IEEE International Conference on Mechatronics and Automation, 5–8 August 2008, Takamatsu, Japan, IEEE Conference Publications (2008), 285–289.

[9] X. Xing, E. Shakshuki, D. Benoit, T. Sheltami: *Security analysis and authentication improvement for IEEE 802.11i specification.* Proc. IEEE GLOBECOM 2008–2008 IEEE Global Telecommunications Conference, 30 November–4 December 2008, New Orleans, LO, USA, IEEE Conference Publications (2008), 1–5.

[10] X. Li, G. HE, M. Gu, P. Dai: *Quantum secure direct communication protocol based on four-qubit cluster state.* Proc. International Conference on Information Engineering and Applications (IEA), 26–28 October 2012, Chongqing, China, Springer, Lecture Notes in Electrical Engineering *219* (2013), No. 4, 105–112.

[11] M. Gutiérrez, L. Svec, A. Vargo, K. R. Brown: *Approximation of realistic errors by Clifford channels and Pauli measurements.* Physical Review A *87* (2013), No. 3, ID 030302-1–030302-5.

Received August 7, 2017

Acta Technica *62* No. 2B/2017, 73–84

Text mining technology based on cloud computing

Chong Xing[1], Kunhao Wang[2,3]

Abstract. The purpose is to study the text mining technology based on cloud computing. Text mining is the process of getting user care and valuable information from unstructured text data. With the developing of informatization, the massive data processing has become an urgent problem. Based on this, the Hadoop cloud computing platform and the MapReduce programming model are described in detail. The Chinese word segmentation and the new word recognition algorithm are mainly studied. In addition, based on the Hadoop platform, the MapReduce solution of the two algorithms were presented. By setting up Hadoop experiment platform, the two improved algorithms are programmed. Finally, the performance and advantages of the new algorithm are analyzed by experiments. The results show that the MapReduce programming model can improve the efficiency of processing large-scale data. Therefore, it can be concluded that it is very meaningful to combine cloud computing with text mining to deal with massive text data.

Key words. Chinese word segmentation, new word recognition, cloud computing, mining.

1. Introduction

At present, most of the information on the Internet is in the form of text. Therefore, it is important to extract resources efficiently from a large number of unstructured text messages [1]. The study of text mining effectively solves this problem. As an important research direction of data mining, mining has been applied to many fields such as search, classification, recommendation system, public opinion and viewpoint mining. It has social and economic significance for scientific research and enterprise applications [2]. Today, the blowout of the Internet's massive information also poses a serious challenge to traditional information processing methods. The traditional information processing methods cannot deal with large amounts of data [3]. The vast majority are in the stand-alone processing, which is easily restricted by computer hardware devices such as processors and storage media. When dealing with large amounts of data, it seems powerless. Nowadays, the industry has

[1]Department of Information and Technology, Changchun Finance College, Jilin, 130028, China
[2]School of information engineering , Changchun Sci-Tech university, Jilin, 130600, China
[3]Corresponding author

paid more and more attention to this problem, and has accumulated some experience. Among them, the parallel processing of data is an important and effective means [4]. Cloud computing is the development and continuation of parallel computing, distributed computing, and grid computing. It is the result of a combination of virtualization, utility computing, Iaas (infrastructure as a service), Paas (platform as a service), Saas (software as a service), and so on [5]. The basic principles of cloud computing are as follows. By distributing computing on a large number of parallel computers, the operation of enterprise data centers is more similar to the use of the internet. As a result, the enterprise can switch the resource to the required application at any time, and access the computer and storage system according to the requirements [6]. It is foreseeable that cloud computing technology has a broad development prospects. Therefore, the application of cloud computing to other areas has become the focus of the current research. Based on this, text mining and cloud computing technology have been studied. Combining the classical algorithm of text mining and cloud computing technology, the improved text mining algorithm overcomes the shortcomings of traditional algorithms. It meets the requirement of dealing with mass data [7].

2. State of the art

2.1. The word segmentation algorithm

An example is given to illustrate the main flow of the segmentation algorithm. Entering a sentence "Liu Shuang welcomes you", the participle of the body flow is as follows. First, Participle Liu / double / welcome / you"; second, posTagging (part of speech tagging) Liu /q double j/ welcome /v you /r"; third, NE identification (name, transliteration name, place name), identification "Liu /q, double j/, welcome /v, you /r", Liu Shuang /nr"; fourth, re-word: "Liu Shuang / welcome / you"; fifth, re-posTagging (verbose) "Liu Shuang / nr / welcome / v you / r". finally, the participle is finished. The main idea of Chinese segmentation algorithm is to segment the word by CHMM (cascaded Markov model) first. Through layering, it not only increases the accuracy of word segmentation, but also ensures the efficiency of word segmentation. It is divided into five layers. The Chinese lexical analysis framework based on CHMM is shown in Fig. 1.

First, the dictionary is loaded. Then, the atoms are segmented. On this basis, the N- shortest path segmentation is carried out, and the segmentation results of the previous N are found out. The binary wordbook is generated. Then, the word formation result is generated. Finally, the part of the annotation is carried out and the main word segmentation step is completed.

2.2. The new word recognition algorithm

New words are one of the unregistered words. It is a word that does not appear in the dictionary [8]. Language develops with the development of society. In vocabulary, its big performance is the new words and the emergence of new phrases.

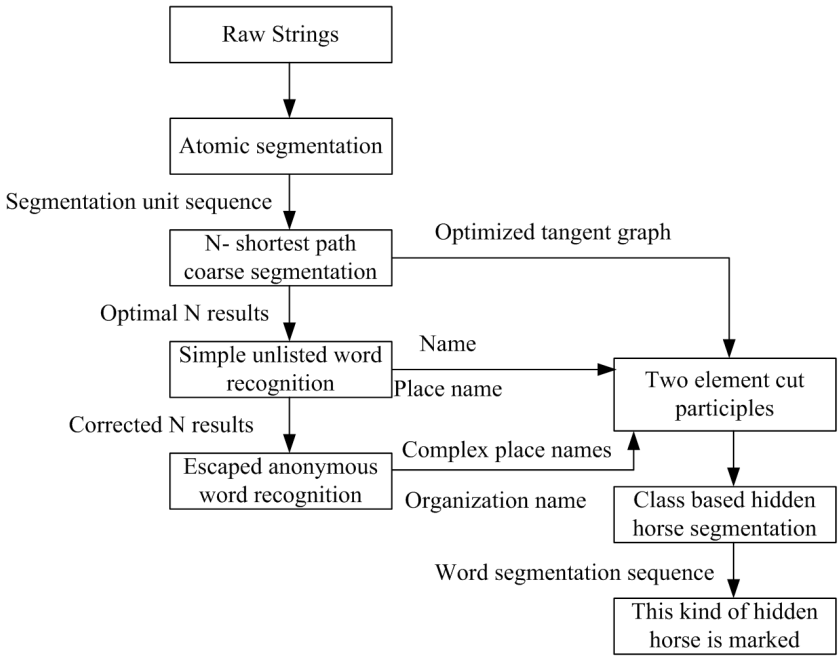

Fig. 1. The Chinese lexical analysis framework based on CHMM

The new words are first proposed in a particular field. After that, the frequency of its repetition increases. Finally, the new words stabilize [9]. It not only appears many times in a document, but also occurs repeatedly in many documents, which is a prerequisite for the recognition of new words. The emergence of new words reflects the emerging of new things, but it brings challenges to the processing of new Chinese words. Therefore, the emergence of new words has aroused special attention of linguists in recent years [10].

The new words mainly fall into two categories: the first category is named entities. It includes geographical names, names and institutional names. The second category is the emergence of new things with the words, such as "Super Girl", "Ray", "scientific concept of development" and so on [11]. The two main indicators to judge the pros and cons of the new word recognition algorithm are accuracy rate and recall rate. The following are the definitions of these two indicators:

$$\text{Accuracy rate P} = \frac{\text{Identification of new words correctly}}{\text{Total number of candidate words}} \times 100\%\,, \tag{1}$$

$$\text{Recall R} = \frac{\text{Identification of new words correctly}}{\text{New number of candidate words in total}} \times 100\%\,. \tag{2}$$

Among them, the total number of new words in the candidate words is generally calculated by manual.

3. Methodology

MapReduce is a major feature and core part of the Hadoop platform [12]. Therefore, the focus of the algorithm design is how to make the original single machine algorithm reasonably MapReduce, and transplant it to Hadoop. The proposed new word recognition algorithm based on cloud computing uses the combination of rules and statistics to identify [13]. It cooperates with the dictionary and noise dictionary. In order to achieve better accuracy and recall rate, a pruning strategy is used to filter out noise words. The new word recognition algorithm MapReduce process is shown in Fig. 2.

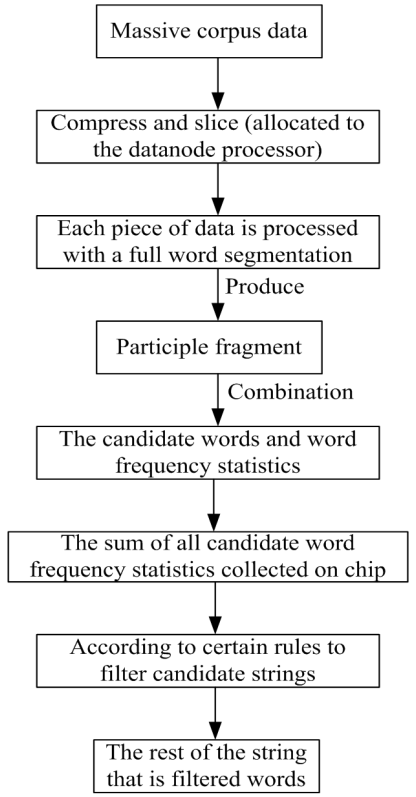

Fig. 2. Process of new word recognition algorithm

The new words are extracted from the word segmentation after the word processing. The recognition process of the new words is essentially the process of fusing these successive string fragments. That is, to find a string that is adjacent to each other and should not be cut, and combine them to form new words. According to statistics, most new words are combinations of single words or combinations of single words and multiple words. The combination of multi-word and multi-word is less frequent. Therefore, the candidate string extracted from the corpus data is mainly concerned with the string that contains the single word. Due to the relationship

between massive data, the corpus data that used in this paper is handled by pre-compression. The compression format is Sequence File Input Format. This format is the compression method that used on the Hadoop platform. It can reduce the size of the data and can effectively improve the speed of reading and writing.

3.1. MapReduce design of Chinese word segmentation

Since the Chinese word segmentation process is a global serial structure, it cannot be split into parallel processing. So, this approach is as following. First, the system configures the parameters globally and initializes the dictionary, so that each Data node does not have to separate the dictionary separately. It saves a lot of overhead and time to initialize the dictionary. Second, the input data is fragmented, and then assigned it to each Datanode for a complete word segmentation process. After the Map operation, the effective word segmentation has been obtained. Therefore, this algorithm does not require Reduce operation, as long as the segmentation results of each segmentation is compressed and output to the file directly. The flow chart is shown in Fig. 3. MapReduce parameters and logic instructions is as shown in Table 1.

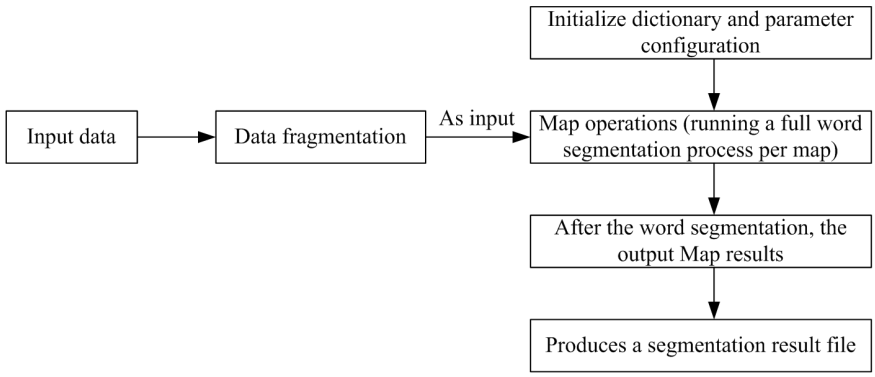

Fig. 3. Chinese word segment MapReduce process

3.2. The MapReduce design of new word recognition algorithm

The MapReduce flow chart is shown in Fig. 4. The main idea of the new word recognition algorithm MapReduce is as follows. On Namenode, configuration information such as dictionaries and parameters is initialized. This information is shared by all nodes in the cluster (including Namenode and Datanode). According to the size of the input data and the number of machines in the cluster, the input data is sliced and sent to the corresponding Datanode to wait for processing. A Chinese word segmentation is performed on the data fragmentation, and each Datanode performs a complete and independent Chinese word segmentation process for the assigned slice data. The advantage of our Hadoop platform design is that the designer cannot care about this data allocation and communication problem at

all, because the platform itself provides a stable and intelligent solution for distribution. The extraction of candidate words integrates the successive words remaining in the segmentation fragments after the end of the participle, and forms the candidate words.

Table 1. MapReduce logic instructions

	Map function	Reduce function
Input data segmentation logic	Sequence file A key-value pair is a cut	
Enter Key, value	Key: it is the key of the Sequence file, that is, the path of the source text file Value: the contents of the text	
Output Key, value	Key: the path of the source text file; Value: word segmentation result	
Function calculation logic	The value corresponding to each input key, that is, the text, is processed by word segmentation	
Global data	Word segmentation dictionary and part of speech display parameters	

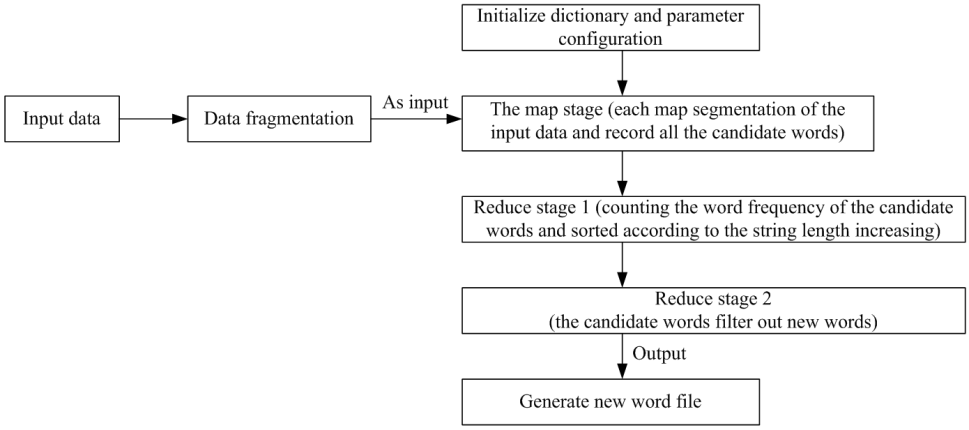

Fig. 4. The new word recognition algorithm MapReduce process

The so-called continuous word, refers to a combination of two or more consecutive words. For example, the "melamine incident is a hot spot of recent concern", the result of word segmentation (without part of speech) is "three / poly / cyanide / amine / event / yes / near / attention / a /". The single words are "melamine", "one", which can generate candidate words for "trimeric", "melamine", "cyanide", "melamine", "cyanamide", " one "and so on. The candidate word frequency statistics collects the candidate words and word frequency statistics processed on all Datanodes (the same word frequency is added). The candidate words are filtered first, and the frequency

of candidate candidates is counted. By comparing it with the pre-set threshold, the candidate words whose frequency is smaller than the threshold are filtered out. Then, in conjunction with a stop dictionary, a noisy dictionary, a pruning strategy is used to filter the remaining candidates. The candidates left by the above steps are considered new words.

3.3. New word filtering method based on pruning strategy

Because the garbage strings and the redundant information exists in a large number of candidate words from the word fragments, such as melamine". If "melamine" is selected, then "trimer" and "cyanuric chloride" must also be selected. However, these are redundant information, and they should be deleted. Based on the frequency filtering of candidate words, and combined with the stop word dictionary and noise dictionary, a pruning strategy to effectively filter the noise words and redundant information is proposed. The pruning strategy is defined as follows.

First, if $N(c_ic_{i+1}...c_{i+j}) = N(c_{i+1}c_{i+2}...c_{i+j+1}) = N(c_ic_{i+1}...c_{i+j}c_{i+j+1})$, then, $N(c_ic_{i+1}...c_{i+j})$ and $N(c_{i+1}c_{i+2}...c_{i+j+1})$ are deleted.

Second, if $N(c_ic_{i+1}...c_{i+j}) > N(c_ic_{i+1}...c_{i+j}c_{i+j+1})$ or $N(c_{i+1}c_{i+2}...c_{i+j+1}) < N(c_ic_{i+1}...c_{i+j}c_{i+j+1})$, then, $N(c_ic_{i+1}...c_{i+j}c_{i+j+1})$, where N is the frequency at which strings appear, and c is a single word.

If the frequency of a parent string is equal to the frequency of its two largest substrings, it is also assumed that the parent string is a word, the substring is deleted, and the pruning ends. On the contrary, if any of the largest substring frequencies are greater than the parent string, the parent string is not considered a word and the parent string is deleted. The cycle was repeated until no string substring, and the pruning is ended. The overall filtration process is shown in Fig. 5.

The new word recognition algorithm only takes into account the recognition of four words (including four words). The reason is that after statistics, the word more than four words is little, and the frequency is not high. Through the experimental summary, the frequency of the occurrence of four words and more than four words is obviously different. Therefore, this paper proposes a double threshold strategy to deal with four words and four words respectively. It achieves better results.

4. Result analysis and discussion

4.1. Chinese word segmentation

The test data uses lab internal data for plain text files, and the total size of the source file is 1.6 G, totaling more than 9000 files. After transformation, the size of sequence file was 635 MB. The test result is related to the machine condition and network at that time. The tests were conducted in a cluster with Datanode numbers of 2 units, 4 units, 6 units, and 8 units. After several tests, the acceleration ratio curve is obtained. The test acceleration is shown in Fig. 6.

It can be seen from the figure that as the number of clusters increases, the acceleration ratio is getting higher and higher. Due to the use of a specific compression

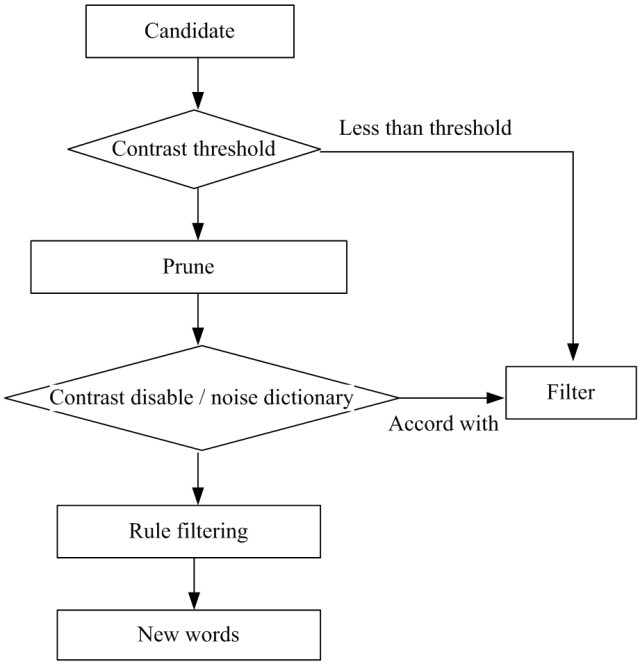

Fig. 5. Filtering process of candidate words

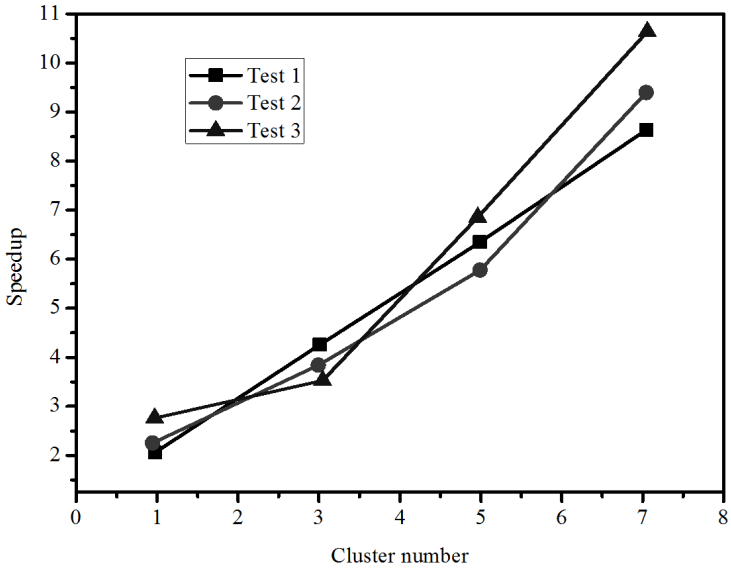

Fig. 6. Test of acceleration ratio

format, it saves a lot of time compared to processing the raw data directly. However, the experimental results show that the number of cluster machines is relatively small when the overall performance increase is not obvious. There are two main reasons for this situation. The communication between clusters takes a certain amount of time. The advantage of Hadoop platform is to deal with massive data through large-scale cluster mode. The number of experimental clusters is small, and the test data is small. It is difficult to play Hadoop platform of this advantage.

From this, it can be guessed that if the data scale is increased, the speedup ratio will be improved obviously. To verify the conjecture, another experiment is carried out in this paper. The scale of the experimental data is increased by two times to 4.8 G. After compression, it is 1.8 G, and the experiment is repeated many times with the number of two Datanode added. The experimental results are shown in Fig. 7.

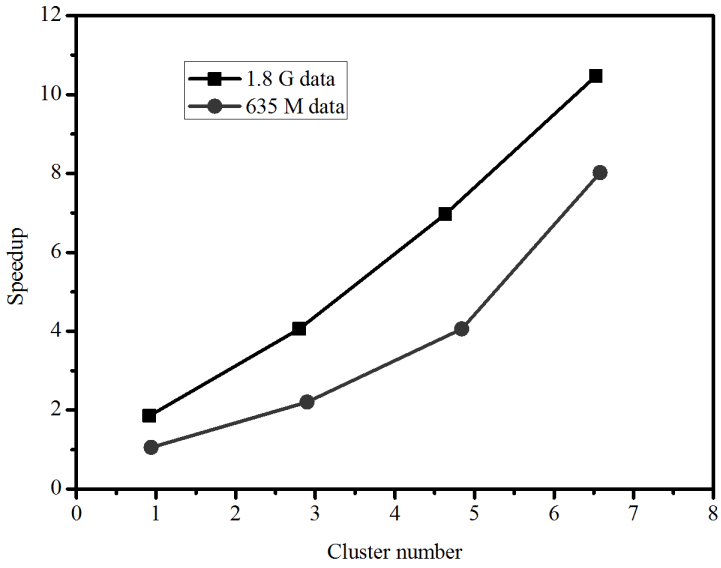

Fig. 7. Acceleration of ratio comparison

As can be seen from the Fig. 7, as the amount of data increases, the acceleration ratio is significantly improved. Moreover, as the number of clusters increases, the speedup is faster. The experimental results are in line with the expected conjecture, which verifies the advantages of the Hadoop platform for processing large data. The test data used in this article, even if it has reached nearly 5 G. However, in the mass storage and massive data of today, it is not too large. And the size of the 9 cluster is also small. Because of the constraints of these experimental hardware, this article has not done more testing. However, it can be inferred that the advantages and efficiency of the Hadoop platform, especially the MapReduce programming model in dealing with large-scale data, are quite objective.

5. Conclusion

On the Hadoop platform, the MapReduce improvements of the two text mining algorithms are implemented. It solves the problem that traditional mining algorithms are relatively difficult to deal with large-scale mass data sets. By briefly introducing the principle of Chinese word segmentation and new word recognition algorithm, a method of MapReduce of these two algorithms is proposed. At the same time, through the cluster experiment, the feasibility of the method is verified. It gets the ideal speedup effect.

References

[1] A. M. Espín, F. Exadaktylos, B. Herrmann, P. Brañas-Garza: *Short- and long-run goals in ultimatum bargaining: Impatience predicts spite-based behavior.* Frontiers in Behavioral Neuroscience (2015), No. 9, 214.

[2] S. Bennett, T. Wernberg, S. D. Connell, A. J. Hobday, C. R. Johnson, E. S. Poloczanska: *The 'Great Southern Reef': Social, ecological and economic value of Australia's neglected kelp forests.* Marine and Freshwater Research *67* (2016), No. 1, 47–56.

[3] L. A. Woodham, R. H. Ellaway, J. Round, S. Vaughan, T. Poulton, N. Zary: *Medical student and tutor perceptions of video versus text in an interactive online virtual patient for problem-based learning: A pilot study.* Journal of Medical Internet Research *17* (2015), No. 6, e151.

[4] K. Kirubhakaran, K. M. Parammasivam: *Understanding blowout phenomena to the induced angle of V-gutter-stabilized flames.* International Journal of Turbo & Jet-Engines *33* (2016), No. 1, 81–85.

[5] B. J. Ellis, A. A. Volk, J. M. Gonzalez, D. D. Embry: *The meaningful roles intervention: An evolutionary approach to reducing bullying and increasing prosocial behavior.* Journal of Research on Adolescence *26* (2016), No. 4, 622–637.

[6] L. Qian, R. Agarwal, G. Hoetker: *Configuration of value chain activities: The effect of pre-entry capabilities, transaction hazards, and industry evolution on decisions to internalize.* Journal Organization Science *23* (2012), No. 15, 1330–1349.

[7] D. Dai, H. Wu, W. Zhang: *Utilization of field enhancement in plasmonic waveguides for subwavelength light-guiding, polarization handling, heating, and optical sensing.* Materials (Basel) *8* (2015), No. 10, 6772–6791.

[8] H. Santos, A. Latgé, J. E. Alvarellos, L. Chico: *All-electrical production of spin-polarized currents in carbon nanotubes: Rashba spin-orbit interaction.* Physical Review B *93* (2016), No. 16, paper 165424.

[9] J. Liu, W. Zhu, T. Ebrahimi, J. Apostolopoulos, X. S. Hua, C. Wu: *Introduction to the special section on visual computing in the cloud: Fundamentals and application.* IEEE Transactions on Circuits and Systems for Video Technology *25* (2015), No. 12, 1885–1887.

[10] T. Hirai, H. Masuyama, S. Kasahara, Y. Takahashi: *Performance analysis of large-scale parallel-distributed processing with backup tasks for cloud computing.* Journal of Industrial and Management Optimization *10* (2014), No. 1, 113–129.

[11] S. L. Smith, M. K. Pichora-Fuller, G. Alexander: *Development of the word auditory recognition and recall measure: a working memory test for use in rehabilitative audiology.* Ear Hear *37* (2016), No. 6, e360–376.

[12] T. R. McRackan, J. B. Ahlstrom, W. B. Clinkscales, T. A. Meyer, J. R. Dubno: *Clinical implications of word recognition differences in earphone and aided conditions.* Otology & Neurotology *37* (2016), No. 10, 1475–1481.

[13] T. Aitamurto: *Crowdsourced democratic deliberation in open policymaking: Definition, promises, challenges.* International Reports on Socio-Informatics (IRSI), Proc. CSCW 2016 – Workshop: Toward a Typology of Participation in Crowdwork *13* (2016), No. 1, 79–90.

Received August 7, 2017

Acta Technica *62* No. 2B/2017, 85–94

Design and implementation of improved distributed data mining algorithm

Ang Li[1]

Abstract. Faced with the rapid growth of data, the traditional data mining algorithm is not capable of dealing with this issue. Although the existing data mining algorithm has taken into account the distributed operation, it does not apply to wireless sensor networks. Therefore, a method of data mining algorithm for wireless sensor networks is proposed. The design and implementation of improved distributed data mining algorithm DDMAW is described, and its performance is analyzed. Based on the performance comparison of finding events algorithm based on distributed K-means with the improved distributed algorithm DDMAW. After that, the DDMAW algorithm itself is discussed in parallel. The comparison results show that DDMAW algorithm has the characteristics of low time complexity and high accuracy, and it is more suitable for use in wireless sensor networks.

Key words. Wireless sensor network, data mining, distributed.

1. Introduction

In recent years, the research on all aspects of wireless sensor network has increased, and the research on distributed clustering algorithm and anomaly detection algorithm is growing to be more. But applying the traditional, centralized data mining algorithm to the wireless sensor network environment is not feasible [1]. The traditional data mining algorithm processes data in a unified and centralized way, but not the use of distributed processing method. If a large amount of data is processed in a centralized data analysis algorithm, it is possible to cause significant traffic and computational complexity, and cost a lot of time, which rapidly consumes the energy of the sensor and increase the overhead, which leads to the reduction of the sensor life. The wireless sensor network technology and distributed data mining technology should be dynamically integrated [2].

[1]Nanjing University of science & Technology Zijin College, Nanjing, 210023, China

2. Design and implementation of distributed clustering algorithm

2.1. The algorithm overview

As the basic algorithm of data mining in wireless sensor networks, it is accordingly improved to be centralized K-means algorithm. The improvement can make it can apply to the distributed environment [3]. The K-Dmeans algorithm solves the parallel problem, but there are still problems that will delete part of the point sets. For wireless sensor networks, the above method may lose some data points, resulting in the loss of observed events [4]. However, it is feasible to divide the detection area into grid.

2.2. The improved DMAW algorithm

In the wireless sensor network, the normal working sensor nodes are able to receive data. But only a part of the sensor nodes can detect the occurrence of the event. Therefore, in the process of data mining, there is only need to do the clustering analysis of selected point set including events rather than each data [5]. And the selected data, not only contains the observed data, but also should be attached with the data information of the geographical coordinates. After selecting the point sets containing events, the geographical position range of the point set is delineated to determine the area of the event. Within this range, the event and the location of occurrence can be obtained through the data mining algorithm [6]. The whole algorithm is divided into two parts. The first is the data processing, and the other part is the determination of the K value, finding clustering centroids, returning the observed value and the corresponding position coordinates.

Before data mining, the data is pre-processed so that the observed data is in an effective detection environment. Then SSE is calculated starting from $K = 1$ iteration. If the threshold is exceeded, iteration will continue. Otherwise stop, output K value, and event center point coordinates.

The time complexity of the grid-based algorithm is mainly the time complexity of the assignment point set to the grid cell, and the time complexity of deleting the sparse grid and induction [7]. Therefore, the time complexity based on the grid algorithm is $O(N)$. The time complexity of the improved algorithm—DMAW algorithm is approximately $O(N)$. And the time complexity based on the grid algorithm is also $O(N)$. That is to say, the time complexity of the DMAW algorithm is basically the same as the time complexity of the grid algorithm. The communication complexity of DMAW algorithm is also analyzed. The communication complexity of the DMAW algorithm is denoted as: T_{M}. According to the description of the DMAW algorithm, it can be assumed that the traffic is generated in the following parts.

1. Scan data points and finds data that exceeds the normal values
2. Determine the effective detection area
3. Iterate starting from $K = 1$ for the preprocessed data

Scan the data points and find out the data exceeds the normal value, and operate this on N points respectively. The communication complexity of this part is

$$T_{\mathrm{M1}} = N \times (T_{\mathrm{D}} + T_{\mathrm{C}}) . \tag{1}$$

Next, the process of determining the effective detection area is to compare the values of x and y, respectively. The communication complexity required for this process is:

$$T_{\mathrm{M2}} = N_{\mathrm{a}} \times (\log N_{\mathrm{a}}) . \tag{2}$$

Then, iterate the processed data.

The first traversal communication complexity is

$$T_{\mathrm{M31}} = T_{\mathrm{D}} . \tag{3}$$

The second traversal communication complexity is

$$T_{\mathrm{M32}} = 2 \times T_{\mathrm{D}} . \tag{4}$$

The Kth traversal communication complexity is

$$T_{\mathrm{M3K}} = K \times T_{\mathrm{D}} . \tag{5}$$

Therefore, the communication complexity of the iteration process is

$$T_{\mathrm{M3}} = (1 + 2 + \cdots K) \times T_{\mathrm{D}} + T_{\mathrm{C}} . \tag{6}$$

Based on the analysis above, the communication complexity of DMAW algorithm is

$$T_{\mathrm{M}} = T_{\mathrm{M1}} + T_{\mathrm{M2}} + T_{\mathrm{M3}} . \tag{7}$$

Namely,

$$T_{\mathrm{M}} = (N + N_{\mathrm{a}} \log N_a + K(K+1)/2) T_{\mathrm{D}} . \tag{8}$$

Since the connection setup time is much smaller than the actual communication time, the communication complexity of the DMAW algorithm can be approximated by formula (8).

The data set points in the whole detection area are 1000, 2000, 4000, 8000, 16000, 32000, respectively. The number of events in each detection area is 2, SNR is 10 dB. The analysis and discussion is undergone through the computation time and data mining effect of DMAW algorithm. The experimental results show that the computation time of DMAW algorithm is proportional to the number of nodes in the case of different nodes. The corresponding DMAW algorithm computing time at 16000 points is 146.767 milliseconds. And the corresponding DMAW algorithm computing time is 350.784 milliseconds at 32000 points. That the time complexity of the DMAW algorithm is $O(N)$, it can be obtained in the case of different numbers of nodes.

2.3. The improved DDMAW algorithm

The centralized algorithm can only be applied to local parts as for distributed environments [7]. As for the distributed, not only the local processing of data is necessary, but also it needs to consider how to improve in the overall situation [8]. In view of this problem, this paper proposes DDMAW algorithm. The core idea of the DDMAW algorithm is the parallel implementation of DMAW algorithm in each detection area, and then fuses data when the local model is aggregated to the global level.

The idea of data fusion is listed as follows:

1. To determine whether there exists a value v falling on the detection area boundary or the coordinates of the two events are close to each other.
2. For both centroids, find the effective detection area before the calculation.
3. Integrate the effective detection areas corresponding to the two centroids.
4. Implement the data mining in the new area.
5. Return the new centroids of events.

The DDMAW algorithm is based on the improvement of DMAW algorithm. The DMAW algorithm is used for local models. Multiple detection areas simultaneously use the DMAW algorithm to work in parallel to form a distributed underlying architecture. Each detection area reports its own event centroid after computation, and then on the basis of this to implement the data fusion. After the integration, a new event center is created [9].

As for DDMAW algorithm, it is analyzed by means of time complexity and communication complexity. It is assumed that the time complexity of the DDMAW algorithm is T_{D}. The communication complexity of DDMAW algorithm is T_{C}. The number of data points per detection area is N. Suppose the number of detection areas is M. The computation time is mainly composed of the parallel data mining time and the time of data fusion to the data reintegration. Thus, the time complexity of the DDMAW algorithm should be $O(N)$.

The communication complexity of DDMAW algorithm is discussed hereby. Assuming that T_{D} is the data communication time, and T_{C} is the connection setup time, the communication complexity of the DMAW algorithm is given by the formula (8) mentioned above.

Since $\ll N$, and $N_a \log N_a \ll N$, the communication complexity of the DMAW algorithm can be approximated as: $T_M = N \times T_{\mathrm{D}}$. Considering that there are four detection areas, then $T_{\mathrm{MM}} = N \times M \times T_{\mathrm{D}}$.

In the process of transmitting $K_1 + K_2 + \cdots + K_M$ event centroids to the upper level, the needed communication complexity is $(K_1 + K_2 + \cdots + K_M) \times T_{\mathrm{C}}$ which is negligible.

Extract the two effective detection areas for the event. Since the extracted area is given in the parallel execution of the DMAW algorithm, and the comparison is for

the values of the x and y values of the region. Thus, the communication complexity of this part is approximately $4T_{\mathrm{D}}$. Calculate the communication complexity for the new effective detection area event computation center. The DMAW algorithm is still adopted here. So, the communication complexity of this part of is $T_{\mathrm{M}} = N \times T_{\mathrm{D}}$. Based on what is discussed above, the communication complexity of DDMAW algorithm is $T_{\mathrm{M}} = (N \times M + 5) \times T_{\mathrm{D}}$. Since $N \times M \gg 5$, the communication complexity of the DDMAW algorithm can be approximated as $T_{\mathrm{M}} = N \times M \times T_{\mathrm{D}}$.

The data set points of all the detection area are 1000, 2000, 4000, 8000, 16000, 32000. The number of events of each detection area is 6, SNR is 10 dB. The analysis and discussion is undergone through the computation time and data mining effect of DMAW algorithm. Experiments show that in the detection area, you can accurately find its centroids as for the occurrence of specific events, and the event falls on the edge of the detection area. The DDMAW algorithm fuses the data for this event and other events may occur in the adjacent area according to its principle.

1. The number of nodes in the detection area is different, the number of events is the same and the noise condition is the same. The DDMAW algorithm can accurately find out each event and its centroid point in the case of the variation of the number of nodes in the detection area. Therefore, the DDMAW algorithm can also be used if the detection area node is small. The running time of DDMAW algorithm is basically linear with the number of nodes in the detection area. And the computation time of the algorithm increases with the increase of the number of nodes in the detection area.

2. The number of nodes in the detection area is different, the number of events is the same and the noise condition is the same. The DDMAW algorithm can accurately determine the number of event, its time and position in the case of the variation of the number of events in the detection area. Therefore, the DDMAW algorithm can apply to the case of single event occurrence and multi-events occurrence. The running time of DDMAW algorithm is basically linear with the number of events in the detection area. And the computation time of the algorithm increases with the increase of the number of nodes in the detection area.

3. The number of nodes in the detection area is the same, the number of events is the same and the noise condition is different. The negative value of SNR is regarded that the noise power exceeds the signal power. The DDMAW algorithm set a threshold for excluding most of the noises in data processing. The result of finding the centroids of event points may drift to some degree due to the noise disturbance, but the disturbance is little under the condition of a certain SNR. The event could be accurately found out when the SNR value is negative.

3. Comparison of the DMAW algorithm and other algorithms

3.1. Performance analysis and comparison

The time complexity of the iteration is $O(KTN)$ through analyzing the time complexity of K-means. Since $K, T \ll N$, so the time complexity of this part is approximately $O(N)$. The spatial complexity of K-means algorithm is $O((K+N)m)$ through analyzing the spatial complexity of K-means algorithm. Analyze the communication complexity of K-means algorithm, and the communication complexity of K-means algorithm is

$$T_{\mathrm{K}} = T \times N \times K \times T_{\mathrm{D}} \,. \tag{9}$$

The time complexity of DMAW algorithm is $O(N)$, and the communication complexity of DMAW algorithm is given by formula (9).

3.2. Experimental analysis and comparison

The method to find the event based on the K-means is the analysis and computation of, all the data points, including the points of the normal circumstances. Therefore, there is a certain error in the determination of the event and the event centroids. The DMAW algorithm is more accurate in finding events, since it only processes the event area and excludes the redundant data in the sensor network.

This paper also explores the time required to find an event based on the K-means. The time required to find the event based on K-means is analyzed through MATLAB simulation. The DMAW algorithm runs faster because it only processes the event occurrence area. And the number of events in the DMAW algorithm is determined by iteration, which greatly improves the accuracy of determining the number of events. In addition, the data mining of the effective detection area of the event can accurately determine the event position.

Analyze the cases that the number of nodes of each detection area is 1000, 2000, 4000, 8000, 16000, and 32000, respectively. Assume that there is one event in each detection area, and the SNR is 10 dB. The required time comparison is shown in Fig. 1.

4. The comparison of the DMAW algorithm and other algorithms

4.1. Performance analysis and comparison

The time complexity and communication complexity of K-Dmeans are analyzed, and compared with DDMAW algorithm.

The time complexity of K-Dmeans algorithm is $O(N^2)$. Then the communication complexity of K-Dmeans algorithm is analyzed, and the result is $O(N^2)$.

The time complexity of DDMAW algorithm is $O(N)$. The time complexity of the distributed algorithm based on K-means is much larger than that of the DDMAW

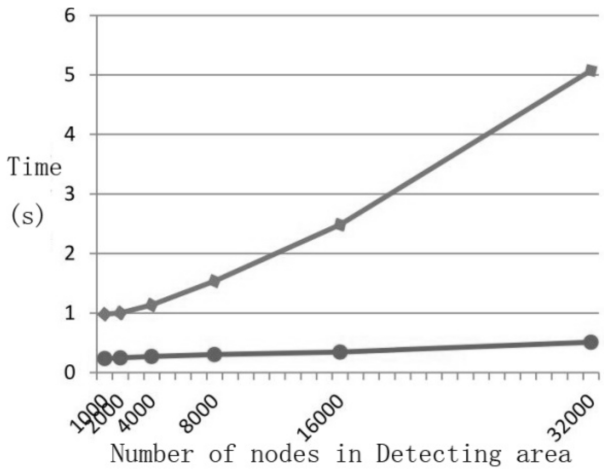

Fig. 1. Required time comparison of the two algorithms

algorithm. Therefore, the DDMAW algorithm performs better than the distributed K-means algorithm theoretically. The communication complexity of the K-Dmeans algorithm and the DDMAW algorithm are $O(N^2)$ and $O(N)$ respectively. Therefore, the DDMAW algorithm is superior to the distributed K-means algorithm in communication complexity.

4.2. Experimental analysis and comparison

The event centroids based on the K-means event finding algorithm is not consistent with the pre-assumed event in the detection area. In the same situation, DDMAW algorithm can accurately find all six events. Therefore, the accuracy of the DDMAW algorithm is better than that of the K-means in terms of the algorithm effect. For the computation time, the time required for the event finding algorithm based on K-means and the DDMAW algorithm both increases with the number of nodes in the four parallel areas. The time required for the event finding algorithm based on K-means is much higher than that of the DDMAW algorithm. The time required to find an event based on K-means is significantly higher than that of the DDMAW algorithm. The computation time for the event finding algorithm based on K-means and the DDMAW algorithm both increases with the number of nodes in the four parallel areas in the case of 8 parallel areas. Moreover, the time required of event finding algorithm based on K-means is higher than that of the DDMAW algorithm. Therefore, the event finding algorithm based on K-means has the drawbacks in determining the number of events, and the DDMAW algorithm can find out the number and the centroids of the event accurately.

4.3. The comparison of self- performance of DDMAW algorithm

The DDMAW algorithm is improved based on the DMAW algorithm. The DMAW algorithm and the DDMAW algorithm are compared, and the experiment adopts the man-made data sets. The number of data set points in all detection areas are 100, 1000, 4000, 8000, 16000, and 32000, respectively. The computation time and data mining results of the DDMAW algorithm parallel in 4 areas and the DDMAW algorithm parallel in 8 areas are analyzed and discussed. Assuming that there are 1000 nodes in the local area, and two events in the area, namely (4, 5), (16, 15), and the SNR is 10 dB. In the case of four areas in parallel, the DDMAW algorithm can still accurately find the location of the event.

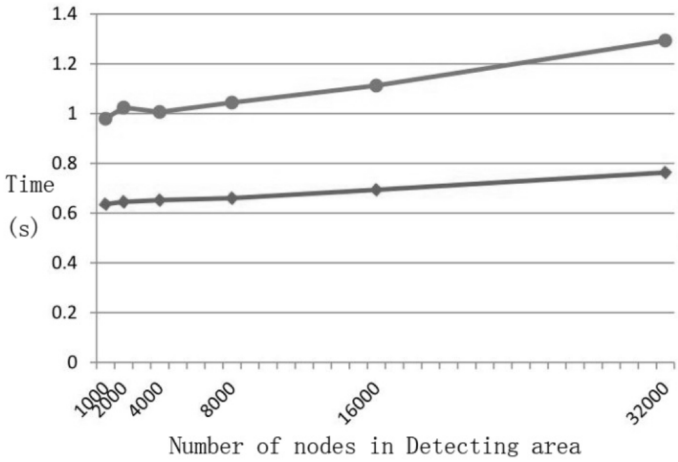

Fig. 2. Average required time of each area in different cases of parallel area number

Figure 2 compares the average time for each area of the four parallel areas and eight parallel areas respectively. It can be seen from the figure that the average time spent on each detection area in the four parallel areas (dots) is slightly higher than that of 8 parallel areas (square points). Among them, in the case of four parallel areas, there is a higher value when the data set point number is 2000. To explore the reasons, it is possible that in the four 2000-points parallel areas, the number of event occurrence is relatively more, therefore the computation time is relatively long. In the case of more parallel areas, the average computing time of DDMAW algorithm in each detection area is less adversely. This shows that the DDMAW algorithm efficiency is higher in the cases of relative more parallel areas.

5. Conclusion

In a wireless sensor network environment, the collected data is distributed across many nodes. If the data of these nodes are processed uniformly, the amount of data will be extremely enormous. And the large amount of data will lead to a

long computation time, which lacks timeliness in data application. Therefore, the distributed data mining technology is applied to wireless sensor networks, which can improve the computation efficiency and effectively find useful information. As the fact that it is not practical to apply the distributed data algorithm directly to the wireless sensor network for actual situation, the relevant data mining algorithm is improved, making it suitable for wireless sensor network structure.

Firstly, a new distributed model for wireless sensor networks is proposed according to the principle of distributed data mining algorithm. The model is divided into multiple parallel detection areas. There are several nodes in each detection area. The data of each node in the work is collected to one of the nodes. In the parallel process, each node aggregates the data to the cluster node. Then the cluster nodes fuse the data of the information. Then, an improved DMAW algorithm is proposed. The algorithm firstly determines the area of events. Secondly, it determines the number of events in the area and find the centroid of the event. At the same time, a distributed DDMAW algorithm is proposed based on the DMAW algorithm. The results show that the comprehensive performance of the DMAW algorithm and the DDMAW algorithm is better.

As for the distributed data mining technology in the sensor network in this paper, the algorithm design idea of the algorithm determines that the algorithm can accurately determine the number of events and find out the centroids of the events. Moreover, the algorithm time is superior to other data mining technology. However, considering the abnormal points in the experimental analysis, it is obvious that there may exist other factors impacting the running time of algorithm except for the number of data set point. The next work will specifically explore other factors that affect the running efficiency of the DMAW algorithm and the DDMAW algorithm.

References

[1] H. S. Shi, Y. X. Li, S. P. Zhang: *An energy-efficient MAC protocol for wireless sensor network*. Proc. IEEE International Conference on Advanced Computer Theory and Engineering(ICACTE), 20–22 August 2010, Chengdu, China, IEEE Conference Publications *4* (2010), V4-619–V4-623.

[2] K. Sohrabi, J. Gao, V. Ailawadhi, G. J. Pottie: *Protocols for self-organization of a wireless sensor network*. IEEE Personal Communications *7* (2000), No. 5, 16–27.

[3] J. Paek, K. Chintalapudi, R. Govindan, J. Caffrey, S. Masri: *A wireless sensor network for structural health monitoring: Performance and experience*. IEEE Workshop on Embedded Networked Sensors(EmNetS-II), 30–31 May 2005, Sydney, Queensland, Australia, IEEE Conference Publications (2005), 1–10.

[4] G. Werner-Allen, K. Lorincz, M. Ruiz, O. Marcillo, J. Johnson, J. Lees, M. Welsh: *Deploying a wireless sensor network on an active volcano*. IEEE Internet Computing *10* (2006), No. 2, 18–25.

[5] A. Arora, P. Dutta, S. Bapat, V. Kulathumani, H. Zhang, V. Naik, V. Mittal, H. Cao, M. Demirbas, M. Gouda, Y. Choi, T. Herman, S. Kulkarni, U. Arumugam, M. Nesterenko, A. Vora, M. Miyashita: *A line in the sand: A wireless sensor network for target detection, classification, and tracking*. Computer Networks *46* (2004), No. 5, 605–634.

[6] G. Werner-Allen, J. Johnson, M. Ruiz, J. Lees, M. Welsh: *Monitoring volcanic eruptions with a wireless sensor network*. IEEE Proceeedings of the Second European

Workshop on Wireless Sensor Networks, 31 Januar–2 Februar 2005, Istanbul, Turkey, IEEE Conference Publications (2005), 108–120.

[7] I. H. Witten, E. Frank: *Data mining: Pratical machine learning tools and techniques, second edition.* Morgan Kaufmann, San Francisco, CA, USA, (2005).

[8] T. Hastie, R. Tibshirani, J. H. Friedman: *The elements of statistical learning: Data mining, inference, and prediction, second edition.* Springer Series in Statistics, New York, USA (2016).

[9] D. R. Rhodes, J. Yu, K. Shanker, N. Deshpande, R. Varambally, D. Ghosh, T. Barrette, A. Pandey, A. M. Chinnaiyan: *ONCOMINE: A cancer microarray database and integrated data-mining platform.* Neoplasia *6* (2004), No. 1, 1–6.

Received August 7, 2017

Acta Technica *62* No. 2B/2017, 95–104

Modular design of electronic control for automatic production line of brasque burdening packing

Wang Liliang[1]

Abstract. The electronic control modularization technology of the automation production line of brasque burdening packing provides a positive impetus to the development of related industries. In order to further improve the theory and technology of electronic control module in China, in this paper, the related theories were first outlined, and the design of the electronic control modularization technology for automation production line of brasque burdening packing was discussed, and the associated diagnostic system was further referenced to analyze the constructed modules. The results show that the control module hardware and software equipment are running normally, and the system has higher productivity than traditional technology. The aim of the study is to provide reference for the development of related technologies.

Key words. Brasque burdening packing, automatic production line, electronic control modular.

1. Introduction

With the development of the times, today's international environment has begun to gradually toward the direction of development, and has begun to take economic and scientific development as the theme of the development of the times. Under the theme and background of new era development, each country and region have begun to regard scientific development as the first productive force of its economic development. In this context, many new technologies and theories have been continuously introduced and applied in the production of various industries, which have had a significant positive impact on the further development of the industry and the improvement of production efficiency. With the rapid development of the times, the world economy has been greatly improved. At the same time, various industries in the world have begun to develop in a more automated and concise way. Especially since the industrial revolution, each country and region has greater demand for the

[1]Beijing Union University, Beijing, 100101, China

promotion of economic strength. Due to the further liberation of human hands, the process of automation has made human resources more efficient. Because of the reduction of the negative influence caused by subjective factors, the development of the whole enterprise is more sustainable. China has also begun to apply automation technology in the production process of some industries, and has achieved some results in the development of the times. This study will design and research the electronic control modularization of automatic production line of brasque burdening packing. The research aims to provide theoretical support and reference for the improvement and development of related technology and theory in China.

2. State of the art

In the new era of economic development, a number of new enterprises and fields began to be developed, such as the development of the electronic control module, which gradually becomes one of the basic industries for the production of various electronic products in the high-speed development of the electronic age [1]. Through the analysis of the current status of the development of electronic control module, many research scholars found that the production of the electronic control module has the defects in the manual operation, which makes the packaging of the ingredients not perfect enough, which has a negative impact on the development of other electronic industries [2]. With the gradual increase in the importance of electronic control module, now the industry has gradually become an important industry in the development of today's era, which can provide some parts for the development of other electronics industry, so as to provide a great impetus to the economic development of the world electronics industry [3]. In the demand of the times, many scholars have put forward new technologies and theories and have applied them to the practical development of electronic control modular production [3]. As a new technology, computer technology has brought more new technology to the development of today's era and has had a positive impact on the development of various industries [4]. Now a lot of research scholars believe that computer aided technology has enabled many industries to become more automated, and enabled enterprises to collect large amounts of related basic data, at the same time, it also further enhanced the production efficiency of related enterprises, thereby enhancing the level of enterprise's comprehensive competition [5]. Therefore, the automated production line processes are also being gradually applied to the development of electronic control modules.

3. Methodology

Since the first industrial revolution, the world has gradually entered the era of industrialization, making people's production and life greatly changed. Since the modern industrial revolution, the world has gradually entered the era of electronic information. The development of this era is characterized by the gradual emergence of some electronic products and the application of people's production and life, so

as to bring more comprehensive joy to people's life. In the new era background, China has further followed the course of the development of the times, and gradually entered the era of electronic information, China's electronic industry has begun to develop. With the rapid development of some electronic industries and the inevitable trend of the times, nowadays, in order to make our electronic products more colorful, our electronic industry needs to design the control module of all kinds of electronic products [6]. A lot of control module production has been applied to the actual electronic products, such as television sets, air conditioning and other control modules, which makes it more satisfied with some of the needs of people compared with the early electronic products, and then makes its function have a more perfect development [7]. With the increasing diversity of electronic products, the design of electronic control templates has gradually been required and put into actual industrial production. More perfect electronic control template production technology plays an important role in the development of production in the electronic industry, and gradually becomes an indispensable technology for the development of the times [8]. In this study, through the investigation of the current electronic module design enterprises in China, the author found that nowadays, in the top ten electronic module design enterprises in our country, foreign-funded enterprises accounted for a larger proportion, Sino foreign joint ventures enterprises followed. There are only one local electronic module enterprises in our country (Fig. 1), which indirectly shows that the comprehensive level of electronic module design enterprises in China is still relatively backward.

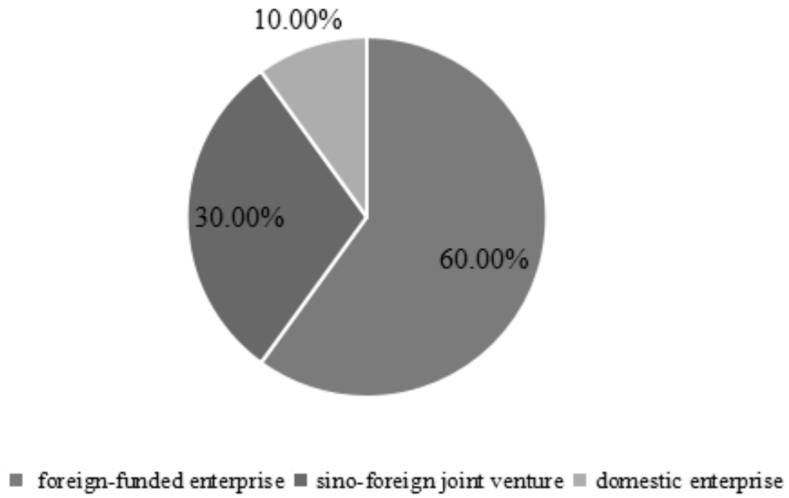

Fig. 1. China's top ten electronic module design enterprises

On the basis of understanding the present situation of the development of electronic module design enterprises in our country, the author summarized the causes of the backward production of electronic control module in China (see Fig. 2). The main reasons are as follows: (1) because the electronics industry started relatively

late, China has not yet formed a more perfect development model, therefore, the continuity of the production structure has further affected the development of the electronic model design enterprise; (2) the electronic model design enterprises in our country use more traditional methods of manual production because of more, so that the production efficiency is low, and the cost of human resources increases, which further indirectly affects the improvement of comprehensive level of the industry; (3) because the enterprise has not formed the pillar enterprises of our country, which makes the country pay less attention to it and leads to less research on this industry in China, China has not formed a more perfect theoretical system, which makes the development of this enterprise suffer some theoretical restrictions; (4) because the enterprise is deeply affected by the traditional technology, the enterprise cannot integrate with the new technology and theory, and then cannot form a new production mode suitable for the development of the times. On the basis of research on the related problems, many research scholars have begun to put forward some new technology into the production of electronic module design enterprises, which promotes the continuous improvement of production efficiency, further makes its products more perfect, so as to provide certain technical support for the development of the entire industry scale [9]. As an important innovation link in the design of electronic control module, the automatic production line of brasque burdening packing has a positive influence and a great impetus to the development of this enterprise. However, due to the backward development concept of some enterprises in our country, the introduction and combination of this technology are not enough, which has a negative effect on the improvement of the design of the electronic control module [10]. In view of this situation, this study researched and analyzed the relevant theories of the electronic control module design of the automated production line of brasque burdening packing, and summarized the advantages of the technology. The research aims to provide some reference and theoretical support for the continuous development of related products and industries.

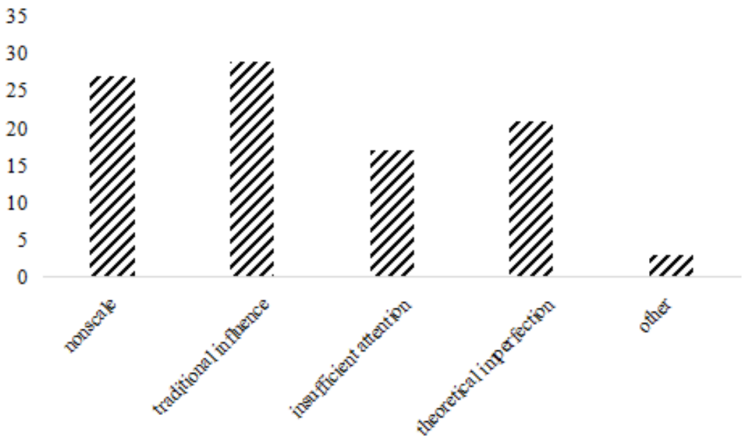

Fig. 2. Lack of enterprise development of electronic control module in China

Firstly, through the reading of relevant materials, this study summarized the process flow of the production line of brasque burdening and its related subsystems to determine the design principle of the production line process and comprehensively analyzed the characteristics of its various subsystems, thus forming a clearer theoretical basis.

Secondly, according to the relevant theoretical basis, this study chose and designed the main hardware equipment of the electronic control module of the brasque burdening production line. The design of electronic control module was mainly based on SIMATIC S-300 system. The module is highly scalable and has relatively high performance. On the basis of the acute design of the control system of the main control module, the author designed and studied the sensor and transmitter of the production line, including temperature, temperature, weighing and speed measurement and other main sensors. The model formulas for the working process of weighing and speed measuring sensors are formulas (1) and (2). Only by optimizing the parameters of the system can the sensor be more efficient. The model formula is as follows

$$\frac{M}{0.7 \times N} \leq m \leq \frac{M}{0.6 \times N}\,, \tag{1}$$

where M is the total weight of the product delivered by the production line, N is the number of weighing sensors in the whole production line, and m is the weight of a single weighing sensor.

$$w(t) = qv\,, \tag{2}$$

where $w(t)$ is the comfortable flow of a speed sensor, q is the actual load value of the material on the sensor (kg/m), and v is the speed of the conveyor belt of the production line (m/s).

Thirdly, after the selection of the hardware equipment for the entire brasque burdening production line was completed, the author further designed the system communication of the entire production line. The main application technology was the PROFIBUS system. Through the network information link way, the research enabled each link to obtain certain connection through the local area network, thus realizing the final basic data sharing.

Fourthly, based on the design of all the programs, the study further introduced the PR0RIBUS theory to carry out anti-jamming diagnosis of the whole transmission system. The basic characteristics of this kind of theory are shown in Table 1.

Table 1. Basic features of a transport medium based on PR0RIBUS-DP

Network topology	Linear bus, there are active bus terminals at both ends of the bus, bait rate ≤ 1.5 Mbit/s allows the use of short wiring
Medium	Shielded twisted pair cable
Station count	Without repeater, each divided into 32 stations; with repeaters, there can be assigned up to 127 stations
Plug connector	9-pin D-type plug

This research finally put the related production line to the actual electronic products enterprises, studied and discussed the modular design of electronic control of automatic production line for brasque burdening packing and the advantages of its applications from an example point of view.

4. Result analysis and discussion

All aspects of the traditional packaging production line mainly include the charging of the raw material of the product, the storage of raw materials, the weighing of raw materials, raw material delivery of the conveyor belt, mixing and packaging of raw materials. The associated process is shown in Fig. 3 (Mishra et al. 2009) [11].

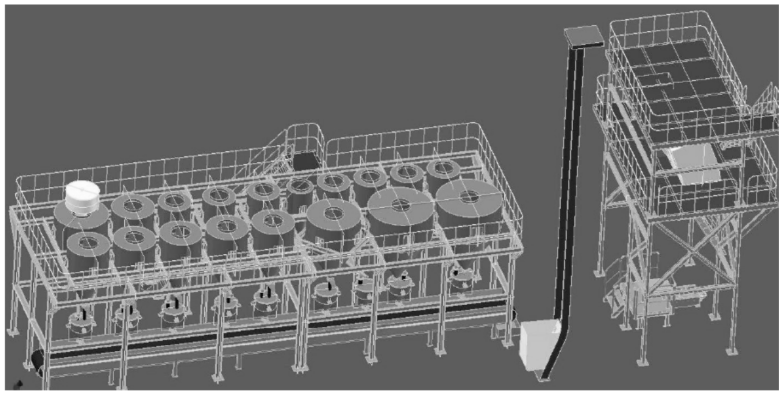

Fig. 3. Process flow of brasque material production line

As an important part of the automated production line of brasque burdening packing, the electronic control module can meet the needs of people, and can also effectively improve the production efficiency in the whole production process. Studies have pointed out that the electronic control module of automatic production line for brasque burdening packing is mainly composed of workstations that monitor and control the entire operation process (see Fig. 4) and related SIEMENS PLC S7-300 systems. The whole control module collects the data of all the links and sends the commands generated by the central system into the control module of each link through the monitoring equipment, and carries on the relevant parameter operation to the whole process, monitors the whole operation process, so that the parameters produced by all links can be recorded and adjusted in a timely manner, which can effectively help the central control system for real-time monitoring of all sectors, and further help the staff to conduct real-time monitoring, so as to realize the whole operation process and improve the production efficiency, and convenient for the management.

Based on the understanding of the relevant theories, this paper further analyzed and discussed the application of the electronic control module of the automatic production line for SIMATIC S-300 brasque burdening packing in the actual electronic products enterprises (Rashid et al. 2015) [12]. The author introduced the

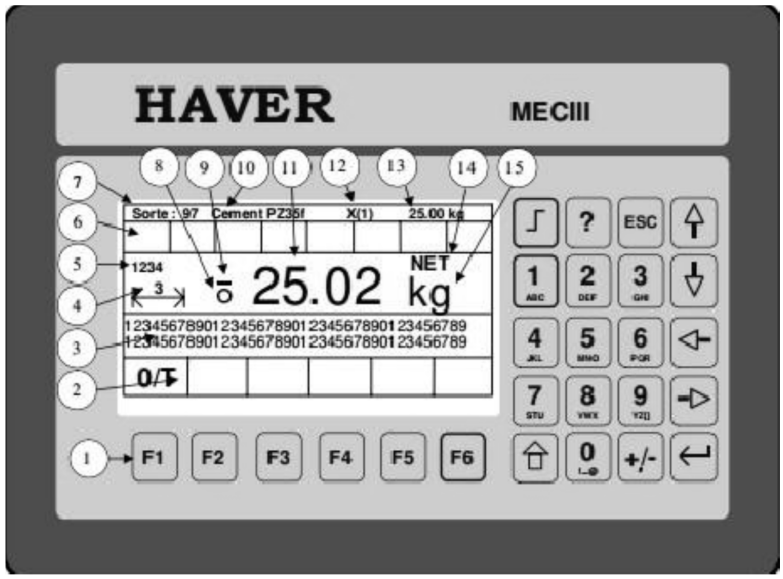

Fig. 4. Construction of automatic electronic control module for brasque burdening packing

PRORIBUS system to diagnose the hardware and software of the automated production line to determine the safety and reliability of the control system (Francisca, et al. 2010) [13]. Firstly, this study analyzed and diagnosed the hardware of the electronic control module. Among them, the diagnosis of hardware equipment was mainly in its sensor and calculator and analysis of operation process of electromagnetic valve, so as to determine whether the operation process was normal, and ensure the normal operation of the whole automation production line (Arasan et al. 2008) [14]. The related hardware test results are shown in Table 2. The results show that all the sensors, transmitters and actuators of the electronic control module used in this system can be operated normally, which can provide technical support for the subsequent applications (Srivastava et al. 2014) [15].

Table 2. Hardware device test results of electronic control module system of automatic production line of brasque burdening packing

Sensors and transmitters					
Temperature sensor	Weighing sensor	Speed sensor	Displacement sensor	Flow sensor	Level sensor
30–40 °C	0.6–0.8 kg	1–1.5 m/s	1–1.5 m	0.4–0.5 M	4–20 mA
Actuator					
Solenoid valve			Electric control valve		
Magnetic force can operate normally			After collecting the relevant data, it can be adjusted automatically		

Then, this study further studied and analyzed the software equipment of the whole system. The diagnosis of software was mainly based on the transmission rate of its basic data. In connection with different links, it is necessary to diagnose the length of the network cable, and the cable should be selected first without a screw lines. This study compared and used three different cables, A, B and C. The parameters of different cables are shown in Table 3. Then, the author analyzed the relationship between baud rate of three different cables and the length of cable, as shown in Table 4. Through the analysis, it can be seen that in three different cables, the performance of cable A is better, which has stronger impedance strength under the influence of the electromagnetic radiation environment, so it has higher anti-interference performance, so as to make the operation process more stable. And the results show that when the baud rate exceeds 500, this may have a higher requirement for the length of the cable, so the author believes that in order to ensure the transmission efficiency of the cable for the relevant basic data, it is necessary to determine the length of the cable used

Table 3. Cable parameters of different models

Cable type	Impedance	Capacitance	Loop resistance	Gauge	Conductor area
Type A	135–165 Ω	<30 pf/m	110 Ω/km	0.66 mm	>0.34 mm^2
Type B	95–125 Ω	<20 pf/m	140 Ω/km	0.82 mm	>0.34 mm^2
Type C	65–80 Ω	< 20pf/m	120 Ω/km	0.66 mm	>0.52 mm^2

Table 4. Correlation analysis of baud rate and cable length of different types of cables

Baud rate (kbit/s)	Distance/segment (m)		
	Type A cable	Type B cable	Type C cable
9.6	1200	1100	950
19.2	1200	1100	950
93.75	1200	1000	950
187.5	1000	900	700
500	400	350	350
1500	200	170	190
12000	100	90	50

Finally, this study compared and analyzed the electronic control modularization of the automatic production line for brasque burdening packing and the traditional production line technology. The results are shown in Fig. 5. The results show that the electronic control modularization technology of the automatic production line for brasque burdening packing can effectively improve the production efficiency of the production line, and further save human resources, thereby reducing the cost and making the production benefit higher. Therefore, in the subsequent development of related industries, it is necessary to continuously improve and develop the electronic

control module technology of the automatic production line for brasque burdening packing, so as to provide technical support for the development of related industries.

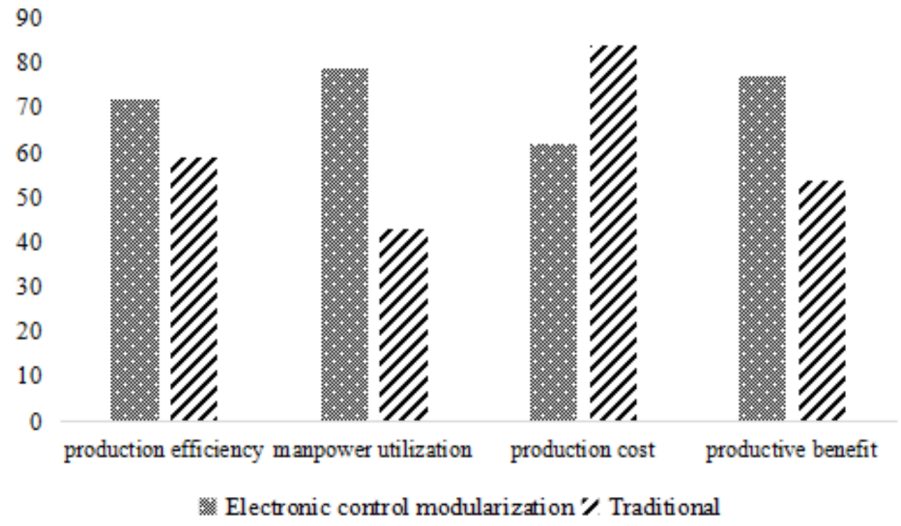

Fig. 5. Comparison and analysis of the electronic control modularization of the automatic production line of brasque burdening packing and the traditional production line technology

5. Conclusion

With the development of the times, every industry has developed a lot, especially the development of electronic enterprises has brought a very important impetus to the development of the comprehensive economic level of the world. In this trend, the electronic control module technology of the automatic production line for brasque burdening packing has brought a positive impetus to the development of various electronic industries. However, the relevant industry in our country still lacks a deep understanding of the technology and theory, the technical development of the relevant industry in our country is not perfect enough. In order to provide theoretical basis for the development of related technologies and theories in China, the relevant theories were summarized, the design theory of hardware and software facilities was further described, and the hardware and software performance of the electronic control module was diagnosed. It is concluded that the electronic control module technology of the automatic production line for brasque burdening packing has a positive influence on the development of the related industry. Because of the lack of cognition of the relevant theories, the research has some shortcomings, but it can provide the theoretical basis for the related research.

References

[1] S. Ryalat, R. Darwish, W. Amin: *New form of administering chlorhexidine for treatment of denture-induced stomatitis.* Therapeutics and Clinical Risk Management (2011), No. 7, 219–225.

[2] L. A. Casemiro, C. H. G. Martins, F. C. P. Pires-de-Souza, H. Panzeri: *Antimicrobial and mechanical properties of acrylic resins with incorporated silver-zinc zeolite–part I.* Gerodontology *25* (2008), No. 3, 187–194.

[3] H. Gupta, A. Bhat, K. D. Prasad, K. M. S. Prasad, K. V. Kumar: *An innovative method of incorporating antifungal agents into tissue conditioners: An in vitro study.* Trends in Biomaterials and Artificial Organs *25* (2011), No. 2, 63–66.

[4] V. R. Santos, R. T. Gomes, R. A. de Mesquita, M. D. de Moura, E. C. Franca: *Efficacy of Brazilian propolis gel for the management of denture stomatitis: A pilot study.* Phytotherapy Research *22* (2008), No. 11, 1544–1547.

[5] N. Emira, S. Mejdi, M. Aouni: *In vitro activity of Melaleuca alternifolia (tea tree) and eucalyptus globulus essential oils on oral candida biofilm formation on polymethylmethacrylate.* Journal of Medicinal Plants Research *7* (2013), No. 20, 1461–1466.

[6] A. Mertas, A. Garbusinska, E. Szliszka, A. Jureczko, M. Kowalska, W. Król: *The influence of tea tree oil (Melaleuca alternifolia) on fluconazole activity against fluconazole-resistant candida albicans strains.* BioMed Research International (2015), ID. No. 590470, 1–9.

[7] B. T. Bal, H. Yauzyilmaz, M. Yücel: *A pilot study to evaluate the adhesion of oral microorganisms to temporary soft lining materials.* Journal of Oral Science *50* (2008), No. 1, 1–8.

[8] W. M. Amin, M. H. Al-Ali, N. A. Salim, S. K. Al-Tarawneh: *A new form of intraoral delivery of antifungal drugs for the treatment of denture induced oral candidosis.* European Journal of Dentistry *3* (2009), No. 4, 257–266.

[9] H. Komine: *Predicting hydraulic conductivity of sand–bentonite mixture backfill before and after swelling deformation for underground disposal of radioactive wastes.* Engineering Geology *114* (2010), Nos. 3–4, 123–134.

[10] Z. Minghua, F. Xiumin, A. Rovetta, H. Qichang, F. Vicentini, L. Bingkai, A. Giusti, L. Yi: *Municipal solid waste management in Pudong New Area, China.* Waste Management *29* (2009), No. 3, 1227–1233.

[11] A. K. Mishra, M. Ohtsubo, L. Y. Li, T. Higashi, J. Park: *Effect of salt of various concentrations on liquid limit, and hydraulic conductivity of different soil-bentonite mixtures.* Environmental Geology *57* (2009), No. 5, 1145–1153.

[12] H. M. A. Rashid, K. Kawamoto, T. Saito, T. Komatsu, Y. Inoue, P. Moldrup: *Temperature effects on geotechnical and hydraulic properties of bentonite hydrated with inorganic salt solutions.* International Journal of Geomate *8* (2015), No. 1, 1172–1179.

[13] F. M. Francisca, D. A. Glatstein: *Long term hydraulic conductivity of compacted soils permeated with landfill leachate.* Applied Clay Science *49* (2010), No. 3, 187–193.

[14] S. Arasan, T. Yetimoglu: *Effect of inorganic salt solutions on the consistency limits of two clays.* Turkish Journal of Engineering & Environmental Sciences *32* (2008), No. 2, 107–115.

[15] A. Srivastava, S. Pandey, J. Rana: *Use of shredded tyre waste in improving the geotechnical properties of expansive black cotton soil.* International Journal Geomechanics and Geoengineering *9* (2014), No. 4, 303–311.

Received August 7, 2017

Acta Technica *62* No. 2B/2017, 105–116

The analysis and application of B-H curves shearing in adjustable inductors[1]

Zhengrong Jiang[2], Jingjiang Qu[2], Jiahui Li[2]

Abstract. The desirable characteristics of the orthogonal inductor are explained by the mathematical and experimental analysis, and those important characteristics are derived from an inclining $B-H$ curve. The effective constitution of the grain oriented lamination core presented here is capable of representing the response of the core subject to the orthogonal magnetization. Considering the DC bias field as an additional anisotropy and magnetostrictive energy, the effective constitutive is satisfactory for describing the effect on hysteresis loop caused by the DC orthogonal bias current. Thus it is anticipated that the method will provide a helpful base for the designing of such kind of inductor. The conclusion can be summarized as the following: The orthogonal bias field can be regarded as an extra energy, which changes the magnetization characteristics of the core of inductor. The inclining B-H plane is created with various DC bias currents put on the inductor, and when the working point is in the linear region of the plane, the linearity of the control characteristics can be gained. The characteristic of the orthogonal inductor is suitable for improving the performance of the passive filter, and the harmonic content can be decreased remarkably with the application of the orthogonal technology. Due to the arrangement of the AC winding and DC bias winding, the decoupling effect is significant. The advantage is beneficial for the application in EVH and UVH transmission system.

Key words. Adjustable inductor, $B-H$ curve, magnetization, harmonic, simulation.

1. Introduction

An adjustable inductor based on orthogonal magnetization shows that it offers some desirable advantages, such as linear regulation, and higher safety in the application of EVH or UVH and lower loss. Most of advantages are derived from the special magnetization mechanism, which must be analyzed, taking into account the movement of domains. A magnetization relation of DC exciting field and AC ex-

[1]This work was sponsored by National Natural Science Foundation of China (51377006) and Beijing Natural Science Foundation (3132008).

[2]School of Electrical and Control Engineering, North China University of Technology, Beijing, 100144, China

citing field has been researched in [1]. In [2],the extra energy is used to analyze the magnetizing process and deduce the mathematical formulas. For the analysis of the DC bias field, the finite element method is applied to model the magnetic distribution on the ferrite inductor [3]. Due to the domain moving involved in the orthogonal magnetization, it requires to study the characteristics of $B-H$ curves to figure out how the bias field affects magnetizing process. In the proposed work, the analysis differs from above-mentioned methods, and here the analysis mainly considers tensor permeability in the core which is subject to orthogonal fields; it is a special consideration under an orthogonal magnetization [4], so $B-H$ curves under the orthogonal bias field are investigated firstly, and then the hysteresis is modeled by comparing the performance of the magnetic material under the action of compressive stress; finally, a prototype inductor is presented, the characteristics are measured and the filter application is discussed. With the calculation and measurement results, relative conclusions are deducted for the magnetization mechanism and applications.

2. State of the art

The strong correlation between the inductance and reluctance has not only been used to elucidate the magnetic mechanism, the design of magnetic structure and decomposition of all kinds of losses, but it has also been selected to change the inductance, and the specific strategic adjustment of the inductive reactive power often becomes the concept of the electromagnetic table.

As an important component for limiting overvoltage, improving power quality and providing reactive power compensation, reactor plays an important role in the stable operation of power network. The expansion of network capacity makes the system short-circuit capacity ratings increase rapidly. In order to limit the short-circuit current, power transmission line protection device must be installed, reactor, that can reduce the short-circuit current and voltage of the short-circuit while the system remains unchanged. Series reactors are mainly used to limit short circuit currents, while shunt reactors are used to adjust the operating voltage of power lines. Shunt reactors are widely used on long distance AC transmission lines, for absorbing excessive reactive power of light load or no-load lines. In UHV and EHV transmission systems, shunt reactor is of special significance, it can improve the transmission capacity of the power system, reduce over-voltage and so on. In the application of the arc suppression coil, shunt reactor provides an inductive current to counteract the capacitive current when the arc suppression coil is grounded, therefore protecting the power equipment.

However, a fixed reactor has some disadvantages, such as:

(1) A fixed reactor reduce the voltage regulating ability when system characteristic changes.

(2) A fixed reactor bring about the power loss when the transmission system is in heavy load.

(3) A fixed reactor increases the equivalent impedance, weakening the line power transmission capacity. In addition, it becomes an additional burden of the transmis-

sion line under heavy load conditions.

2.1. Methodology

The schematic structure of the orthogonal adjustable inductor is shown in Fig. 1. It contains a cylindrical hollow core made of grain-oriented Fe-Si lamination. The overall size of the core is 120×150×80 mm. The toroidal DC winding with 150 turns goes through the bore of the core; outside of the cylinder core, there is a main coil with 220 turns which is connected with power system and creates the AC exciting field in the axial direction. The toroidal winding, like DC bias winding, is connected with DC power to create bias field in the circumferential direction. The two fields are orthogonal to each other.

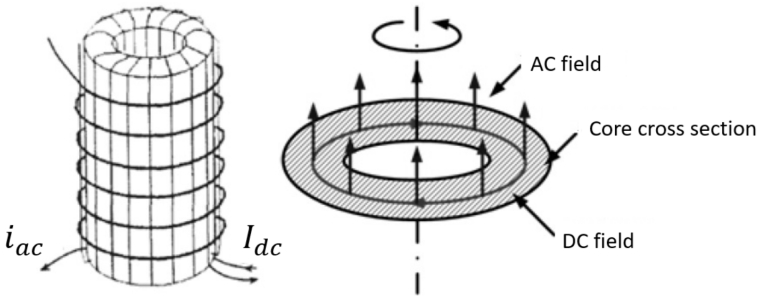

Fig. 1. Configuration of the orthogonal inductor

In order to reduce the effect of demagnetization, two yokes made up of grain-oriented silicon lamination are used, and $B-H$ curves are measured on S&T tester platform. The platform is used to measure the magnetization process of the inductor core under AC field and DC field. It is obvious that $B-H$ curves change with the increase of DC field when the alternating excitation gives $H_{\mathrm{ac}} = 50\,\mathrm{A/m}$ and the $B-H$ curves inclines with the increase of the DC field. Meanwhile, the area of $B-H$ curves decreases simultaneously, which means that the remanence and coercivity descend as well [5].

It appears that $B-H$ curve rotates clockwise in the loci plane remarkably with the increase of the DC bias field. When DC bias current reaches 5 A, the $B-H$ curve becomes a straight line and the enclosed area nearly decreases up to zero, but the magnetization curve has no noticeable hysteresis. However, in case of open path, there is a strong demagnezation field in two terminals [6], even when the AC exciting and DC bias fields have a higher amplitude, and the magnetization process is not completely reversible. In this case, the bias field can be used to adjust the inductance of inductor with this kind of core by altering the effective internal AC field, and the variable range becomes more pronounced due to the shortening of the air path. For the semi-core variable inductor, the inductance is described as

$$L = \frac{\overline{\mu} n^2 D\delta}{l}\,. \tag{1}$$

Here, n is the number of main winding turns, D is the external diameter of the core, δ is the net thickness of the core and l is the core length. Symbol $\overline{\mu}$ is determined by DC bias current while the main current is constant.

Measurement results show that the linearity of the $B-H$ curves is increasing with the increase of the DC bias current. The fact brings about a characteristic of linear permeability. This derives from two facts: one is that the bias winding independent on the ac winding, so there is no mutual inductance between the two windings. The other is that the reversible domain motion is the main process in the initial magnetization, while domain rotation plays a role in the later magnetization [7]. It is contrary to the magnetization in the axial direction. Hence the DC bias field strengthens the reversibility motion ac flux. Due to the demagnetization in the iron core, the effect of the DC bias field on the ac direction is no longer pronounced even if the bias field is higher.

The domain movement is studied toward a perpendicular direction when a press strain works on magnetic material [8]. The effect on hystersis of magnetic material is similar to that of the orthogonal field. So the orthogonal magnetization modeling can be derived referring to the effect caused by the compressive stress.

The magnetization movement in Cartesian coordinates is as shown in Fig. 2.

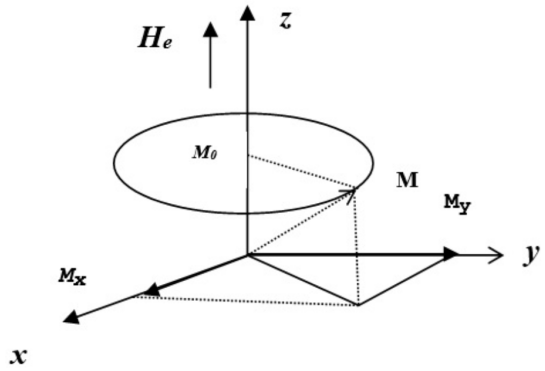

Fig. 2. Magnetization movement in Cartesian coordinates

When the DC bias field increases, an additional anisotropy energy and elastic energy can be effectively calculated and included into the generalized anhysteretic function described previously [9], and the energy E of domains can be described as

$$E = -\mu_0 m \cdot (H_{\parallel} + H_{\perp} + \alpha M) + \widetilde{E}_{\mathrm{an}} + \widetilde{E}_{\sigma}\,. \tag{2}$$

Here, $H_{\parallel}$ means the DC H field whose direction is parallel to AC H field and $H_{\perp}$ means the DC H field whose direction is perpendicular to AC H field.

From the minimum energy theory, the magnetic material will get elastic distortion when the magnetization changes, so the modeling of domain rotating can be established to analyze the changing of the system energy [10]. All these phenomena are connected with the magneto mechanical field, which can be described as follows:

$$E_H = -\mu_0 M_\mathrm{s} H(\cos\theta_1\cos\phi_1 + \cos\theta_2\cos\phi_2 + \cos\theta_3\cos\phi_3)\,, \tag{3}$$

$$\widetilde{E}_\mathrm{an} = E_0 + K_1(\cos^2\theta_1\cos^2\theta_2 + \cos^2\theta_2\cos^2\theta_3 + \cos^2\theta_3\cos^2\theta_1)\,. \tag{4}$$

$$\begin{aligned}\widetilde{E}_\sigma = -\frac{3}{2}\lambda_{100}\sigma(\cos^2\theta_1\cos^2\beta_1 + \cos^2\theta_2\cos^2\beta_2 + \cos^2\theta_3\cos^2\beta_3) + \\ - 3\lambda_{111}\sigma(\cos\theta_1\cos\theta_2\cos\beta_1\cos\beta_2 + \cos\theta_2\cos\theta_3\cos\beta_2\cos\beta_3 + \\ + \cos\theta_3\cos\theta_1\cos\beta_3\cos\beta_1)\,,\end{aligned}$$

$$\overline{\mu_{ij}} = \frac{1}{8\pi^2}\int_0^\pi\int_0^{2\pi}\int_0^{2\pi}\mu_{ij}(\theta,\varphi,\psi)\sin\theta\,\mathrm{d}\psi\,\mathrm{d}\varphi\,\mathrm{d}\theta\,. \tag{5}$$

Here, $\widetilde{E}_\mathrm{an}$ is the effective anisotripic energy, E_H is the exciting field energy, $\widetilde{E}_\sigma$ is the effective magnetostrictive energy, θ_{1--3}, ϕ_{1--3}, β_{1--3} are the mean three directions of the turning magnetic domains in the local coordinate system (indices 1–3 correspond to three conditions) M and H, effective strain force and grain axial direction, respectively. The total energy is

$$E_\mathrm{total} = E_\mathrm{H} + \widetilde{E}_\mathrm{an} + \widetilde{E}_\sigma\,. \tag{6}$$

The effective constitutive equation can be presented as

$$B_i = q_{ijk}\sigma_{kl} + \mu_{ij}H_j + J_i^r\,, \tag{7}$$

where q_{ijk} is the magnetostrictive coefficient, σ_{kl} is the stress tensor, μ_{ij} is the permeability tensor, and J_i^r is the remanent magnetization. Because of the hysteresis of the grain oriented lamination, the direction of M deviates the sum vector of two H fields. Like the analysis mentioned above, the bias field is effective on an additional magnetostrictive energy. In order to explain the magnetization process under the bias field, a perturbation equations is necessary [2].

The anhysteretic function can be quoted as

$$M_\mathrm{aniso} = M_\mathrm{s}\frac{\sum_{\mathrm{all-moments}}\mathrm{e}^{-\frac{E}{k_\mathrm{B}T}}\cos\theta}{\sum_{\mathrm{all-moments}}\mathrm{e}^{-\frac{E}{k_\mathrm{B}T}}}\,. \tag{8}$$

When the orthogonal bias field is increased according to equation (8) (k_B denoting the Boltzmann constant), the change of E makes $B-H$ hysteresis "shearing", which is a quantitative agreement with the experimental result.

The additional anisotropy energy affects the magnetization of the grain-oriented core, which can be calculated from the following equation [11]. The corresponding anhysteresis can be gained and the result curves are shown in Fig. 3.

$$\frac{\mathrm{d}M}{\mathrm{d}H} = (1-c)\frac{M_\mathrm{an}-M}{\delta k - \alpha\,(M_\mathrm{an}-M)} + c\frac{\mathrm{d}M_\mathrm{an}}{\mathrm{d}H}\,. \tag{9}$$

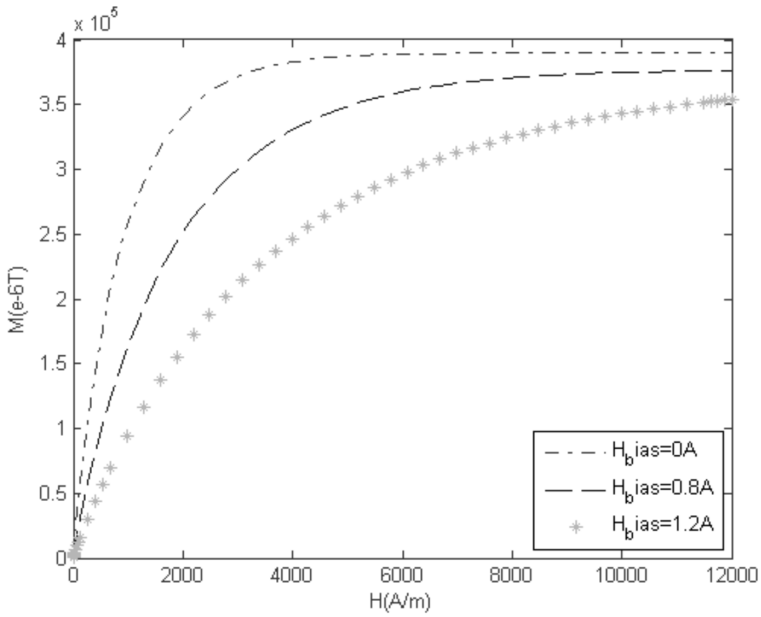

Fig. 3. Anhysteresises under various DC bias currents

3. Result analysis and discussion

Generally, a saturation adjustable inductor is based on the controlled saturation in part of the magnetic circuit, and the permeability and saturation are two of the critical magnetic properties [12]. A constant permeability is nearly a flat magnetization curve across the origin of the $B-H$ plane, and the saturation magnetization at a high field can be described by a horizontal line in the $B-H$ plot, as is shown in Fig. 4. When the DC bias current increases, the magnetization curve will vary gradually from the constant permeability regime to the saturation one. Therefore, the core operating point is critical for the accurate changing of the reactance of the inductor [6].

When the DC bias current increases, a bias flux sums the ac flux in the core and the working point shifts into the non-linear area; the output current becomes distorted due to the non-linearity [13]. For example, when the working point moves from b to a, the output current waveform is changed from 3' to 2'. So the inductance changes with the DC bias flux. With the continuing increase of the DC current, the working point gets closer to the saturate area, and the inductance decreases remarkably. Accordingly, the harmonic content becomes worse.

It is obvious that the non-linearity of the magnetization curve leads to a substantial harmonic distortion. On the contrary, when the operating points are retained in the linear region of $B-H$ "cluster", the output current waveform can be expected to retain sinusoidally in a wide control region, as is shown in Fig. 5. The FEM analysis

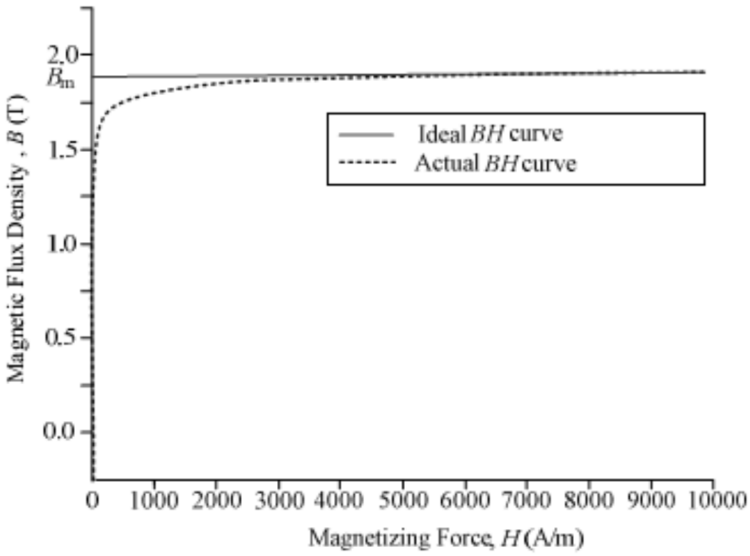

Fig. 4. Ideal and actual $B - H$ curves

also supports the estimation [14].

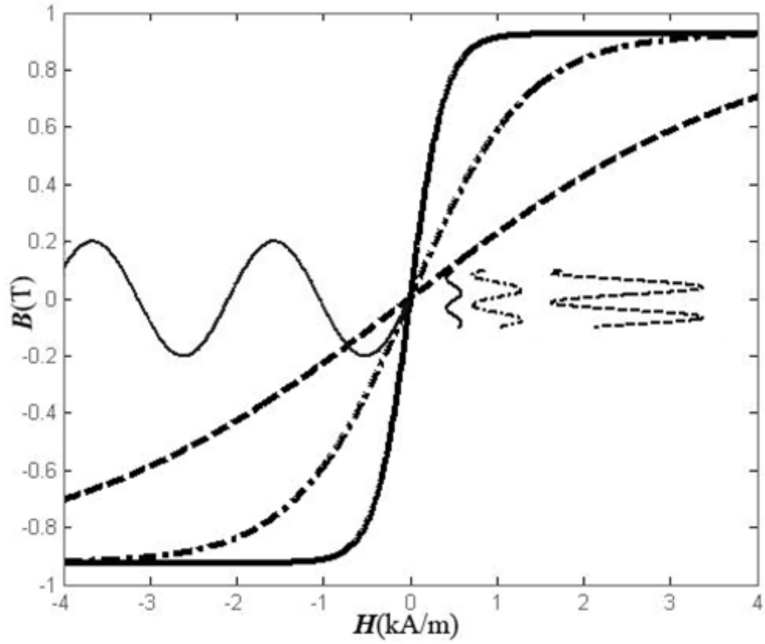

Fig. 5. $B - H$ clusters result in sinusoidal wave

Here, the particular curves represent the typical $B - H$ loops—characteristics of

the magnetic material.

The orthogonal adjustable inductor is expected to achieve the goal mentioned above. In the case of $B-H$ cluster, each curve can be expressed as two lines, and the cluster can be simply described as a lot of lines with differential incline angles, as are shown in Fig. 6.

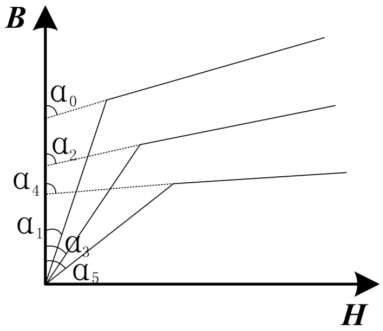

Fig. 6. $B-H$ simple descriptions

Then $B-H$ curve can be described as

$$H = B\tan\alpha_1 \quad \text{for} \quad B < B_{\mathrm{s}}\,,$$

$$H = (B - B_{\mathrm{s}})\tan\alpha_0 \quad \text{for} \quad B > B_{\mathrm{s}}\,. \tag{10}$$

So the working winding current is described as

$$i_{\mathrm{ac}} = (1/2B_{\mathrm{m}}\tan\alpha_0)\bullet$$

$$\begin{gathered}(-B_m\cos\omega t + B_0)\tan\alpha_1 - B_m\cos\omega t + B_0 < B_s \\ (-B_m\cos\omega t + B_0 - B_s)\tan\alpha_1 - B_m\cos\omega t + B_0 > B_s\end{gathered} \tag{11}$$

Using Fourier series analysis, the harmonic current values are gained, as is shown in Fig. 7.

Here the horizontal axis represents the angle between B and H and vertical axis denotes the harmonic content per unit.

It is obvious that the linearity of the permeability is improved with the increase of the orthogonal field , so the harmonic characteristic of the inductor becomes better with the increase of the orthogonal field.

In order to verify the harmonic characteristic of the inductor, an experiment is performed and the experiment circuit is shown in Fig. 8.

Here, U_{e} is AC power which is connected with the working winding of the inductor, U_{s} is the DC power which is connected with DC bias winding, R1 and R2 are changeable resistances, and X1 is the adjustable inductor. Given $U_{\mathrm{e}} = 220\,\mathrm{V}$, through changing DC bias current, based on the experiment results, the harmonic

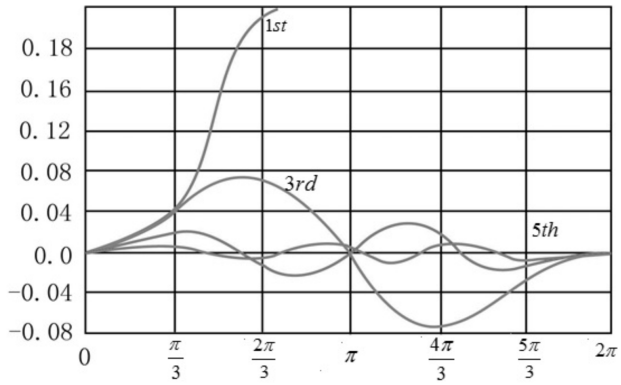

Fig. 7. Incline angles versus harmonics per unit

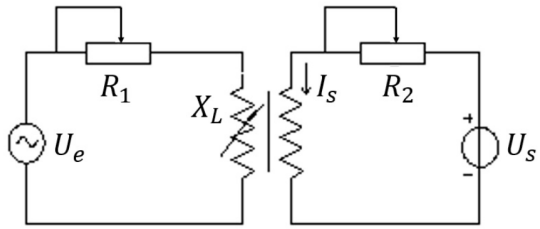

Fig. 8. Experimental platform

characteristic is gained, as is shown in Fig. 9.

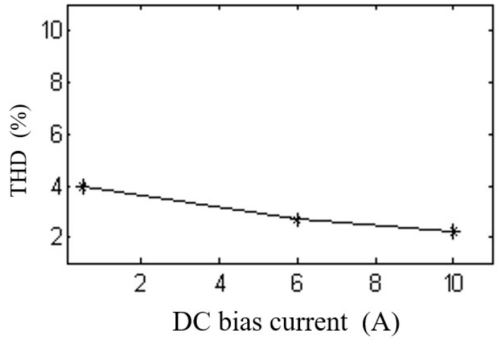

Fig. 9. Harmonic characteristics of the orthogonal magnetization inductor

4. Conclusion

The desirable characteristics of the orthogonal inductor are explained by the mathematical and experimental analysis, and those important characteristics are

derived from an inclining B-H curve. The effective constitution of the grain oriented lamination core presented here is capable of representing the response of the core subject to the orthogonal magnetization. Considering the DC bias field as an additional anisotropy and magnetostrictive energy, the effective constitution is satisfactory for describing the effect on hysteresis loop caused by the DC orthogonal bias current. Thus it is anticipated that the method will provide a helpful base for the designing of such kind of inductor. The conclusion can be summarized as the following: The orthogonal bias field can be regarded as an extra energy, which changes the magnetization characteristics of the core of inductor. The inclining B-H plane is created with various DC bias currents applied to the inductor, and when the working point is in the linear region of the plane, the linearity of the control characteristics can be gained. The characteristic of the orthogonal inductor is suit for improving the performance of the passive filter, and the harmonic content can be reduced remarkably with the application of the orthogonal technology. Due to the arrangement of the AC winding and DC bias winding, the decoupling effect is significant. The advantage is beneficial for the application in EVH and UVH transmission systems.

References

[1] Q. Yu, X. Wang, Y. Cheng: *Electromagnetic modeling and analysis of can effect of a canned induction electrical machine*. IEEE Transactions on Energy Conversion *31* (2016), No. 4, 1471–1478.

[2] D. Hu, J. Sheng, J. Ma, L. Yao,Z. Y. Li, Z. Hong, Z. Jin: *Characteristic tests and electromagnetic analysis of an HTS partial core transformer*. IEEE Transactions on Applied Superconductivity *26* (2016), No. 4, Article No. 5500305.

[3] S. Shen, Y. Tang, L. Ren, Z. Wang: *Electromagnetic calculation of a 35 kV/3.5 MVA single-phase HTS controllable reactor with field–circuit coupled-FEM*. IEEE Transactions on Applied Superconductivity *26* (2016), No. 7, Article No. 5603305.

[4] B. Gustavsen, M. Runde, T. M. Ohnstad: *Wideband modeling, field measurement, and simulation of a 420-kV variable shunt reactor*. IEEE Transactions on Power Delivery *30* (2015), No. 3, 1594–1601.

[5] S. Mukhopadhyay, D. Maiti, A. Banerji, S. K. Biswas, N. K. Deb: *A new harmonic reduced three-phase thyristor-controlled reactor for static VAr compensators*. IEEE Transactions on Industrial Electronics *64* (2017), No. 9, 6898–6907.

[6] M. Young, Z. Li, A. Dimitrovski: *Modeling and simulation of continuously variable series reactor for power system transient analysis*. Proc. IEEE Power and Energy Society General Meeting (PESGM), 17–21 July 2016, Boston, MA, USA, IEEE Conference Publications (2016), 1–5.

[7] Z. Deng, X. Wang, F. Zhou, X. Lei, K. Yu, Y. Qiu: *Modeling of extra-high voltage magnetically controlled shunt reactor*. Proceedings of the CSEE *28* (2008), No. 36, 108–113.

[8] S. S. Sinha, J. Shah, H. Nerkar: *Harmonics measurement using FFT algorithm in digital signal controller for smart micro-grid system*. Proc. IEEE Region 10 Humanitarian Technology Conference (R10-HTC), 21–23 December 2016, Agra, India, IEEE Conference Publications (2016), 1–5.

[9] Y. Yao, B. Chen, C. Tian: *Modeling and characteristics research on EHV magnetically controlled reactor*. Proc. IEEE International Power Engineering Conference (IPEC), 3–6 December 2007, Singapore, Singapore, IEEE Conference Publications (2007), 425–430.

[10] R. Bramanpalli: *Accurate calculation of AC losses of inductors in power electronic applications*. Proc. PCIM Europe 2016; International Exhibition and Conference for Power Electronics, Intelligent Motion, Renewable Energy and Energy Management, 10–12 May 2016, VDE Conference Publications (2016), 1–8.

[11] X. Wei, Y. Ji, J. Wang, G. Tan: *Orthogonal core harmonic model analysis with magnetization curve and magnetic saturation*. Proc. IEEE International Conference on Industrial Technology (ICIT), 15–17 December 2006, Mumbai, India, IEEE Conference Publications (2006), 2148–2153.

[12] B. Chen, Y. Gao, M. Nagata, K. Muramatsu: *Investigation on harmonics suppression of saturable magnetically controlled reactor using nonlinear magnetic field analysis*. Proc. IEEE International Conference on Electromagnetic Field Problems and Applications (ICEF), 19–21 June 2012, Dalian, Liaoning, China, IEEE Conference Publications (2012), 1–4.

[13] K. Nakamura, S. Hayakawa, S. Akatsuka, T. Ohinata, K. Minazawa, O. Ichinokura: *Three-dimensional reluctance network analysis considering an iron loss characteristic for an EIE-core variable inductor*. IEEE Transactions on Magnetics *41* (2005), No. 10, 4033–4035.

[14] A. Lamecki, L. Balewski, M. Mrozowski: *Effect of mesh deformation on the accuracy of 3D FEM electromagnetic analysis*. Proc. IEEE MTT-S International Conference on Numerical Electromagnetic and Multiphysics Modeling and Optimization (NEMO), 27–29 July 2016, Beijing, China, IEEE Conference Publications (2016), 1–2.

Received May 7, 2017

Acta Technica 62 No. 2B/2017, 117–128

Vehicle continuity tracking in traffic monitoring video based on mean hash[1]

Honghui Fan[2], Hongjin Zhu[2,4], Jiawei Li[2], Dongming Yuan[3]

Abstract. To further improve the vehicle detection and tracking accuracy, the detection and tracking of target vehicles in traffic surveillance video were discussed. Depending on the characteristics of the traffic video monitoring, Gaussian mixture model algorithm and the improved background subtraction algorithm were discussed and optimized to detect vehicle. And mean hash algorithm was used on the target vehicle continuously. Cloudy and foggy surveillance monitoring videos were utilized to verify the proposed proposal. At the same time, vehicle detection and tracking at different speeds were also verified. Through these experiments, it was verified that the target vehicle could adapt to the background model and update when it was traveling at low speed, and it was possible to maintain a relatively stable detection and tracking of the target vehicle. Verification experiments meant it had a beneficial effect on the influence of the weather environment.

Key words. Gaussian mixture model, background difference, vehicle detection, mean hash, vehicle continuity tracking.

1. Introduction

In recent decades, with the rapid development of information technology and greatly improve the performance of hardware, video monitoring system has been widespread deployment, around the city roads everywhere [1]. In the field of computer vision detection and tracking of moving targets has been a research hot spot, in robot navigation, intelligent transportation systems, and other fields have a wide range of applications. Tens of thousands of cameras can produce huge amounts of traffic monitoring data every day, through the traffic surveillance video data real-time

[1]The authors acknowledge the Changzhou Science and Technology Support Projects (CE20175026, CE20165028), IUR Prospective Joint Project of Jiangsu Province (BY2016030-05) and Liyang science and technology planning project(LA2016007).

[2]School of Computer Engineering, Jiangsu University of Technology, Changzhou, 213001, China
[3]Shenzhi Elevator Co., Ltd, Jilin, Liyang, 213300, China
[4]Corresponding author

analysis and processing, can build a lot of smart services: such as vehicle tracking, traffic control and traffic violation detection and so on [2, 3]. Therefore, the intelligent transportation system (ITS) becomes research and development hot spots in the world transportation vying [4, 5]. Although the intelligent transportation system has been got rapid development and a series of significant achievements have been made, but still have a certain gap with people's expectations. Collins and others using multiple cameras to realize intelligent traffic detection system, can identify the target vehicle state, and can be updated road information in real time [6, 7]. These research works have improved the intellectuality of the intelligent transportation system, but continuities of tracking of the same vehicle needs to be improved.

Continuous tracking of moving targets, the first thing to the moving object of video sequence detected in the frame, to provide initial targets information for follow-up. Moving target detection is mainly divided into two parts, background model and foreground detection. General methods of background model include mean filter method, median filter method and Gaussian mixture model (GMM) method [8–10]. Which of Gaussian mixture model method can detect the moving objects more completely, and adaptable to changes in the scene [11]. In the background after the success of the modelling, the use of background difference algorithm, can get the foreground image-moving targets. Using background subtraction algorithm would be influenced by external factors, such as light, weather and other factors, and if using the improved background subtraction algorithm, can eliminate these problems [12–14].

In this paper, Gaussian mixture model was used to the background model and update. Then improved background subtraction algorithm foreground detection to detect the moving vehicles. Finally, the hash algorithm was adopted to the same continuous tracking of the vehicle for monitoring video.

2. Background update and foreground detection principle

2.1. Background updating based on Gaussian mixture model

Gaussian model could represent the characteristics of each pixel in image [15]. For any pixel in the tth moments the observed values of $X_t = [r_t, g_t, b_t]^{\mathrm{T}}$. So the probability representation of the background is given by the equation

$$P(X_t) = \sum_{i=1}^{k} \omega_{(i,t)} \eta(X_t, u_{(i,t)}, \sum_{(i,t)}) \,. \tag{1}$$

In (1), $\omega_{(i,t)}$ is the weight of the ith Gauss components at the T moment. Quantity $\eta(X_t, u_{(i,t)}, \sum_{(i,t)})$ is the probability density function of the ith Gaussian component at time T, and the mean value is $u_{(i,t)}$. The covariance matrix is $\sum_{(i,t)}$. The current value of pixels is matched with the$K$-th Gaussian distribution of the Gaussian mixed model. If new pixel values and Kth Gaussian distribution match successfully, determine the pixels as the background, otherwise the prospects for

points.

If a new pixel value with one of the Gaussian distribution satisfies $\left|X_{(i,t)} - u_{(i,t)}\right| \leq D\sigma_i$ (D representing custom parameters for the user, typically 2.5, and σ_i is variance), the weight w of the kth Gaussian distributions in the model is adjusted according to the equation

$$\omega_{(k,t)} = (1-\alpha)\omega_{(k,t-1)} + \alpha(M_{(k,t)})\,, \tag{2}$$

where, α is the learning rate, and its size determines the speed of the background update. If the detected pixel value $X_{(i,t)}$ matches the kth Gaussian distribution, then $M_{(k,t)} = 1$, the other values of $M_{(k,t)} = 0$. To match the success of the Gaussian distribution, the mean $u_{(i,t)}$ and variance $\sigma^2_{(i,t)}$ also need to be updated according to the formulae

$$\rho = \alpha\eta(X_t\,|u_k, \sigma_k)\,, \tag{3}$$

$$u_{(i,t)} = (1-\rho)u_{(i,t-1)} + \rho X_{(i,t-1)}\,, \tag{4}$$

$$\sigma^2_{(i,t)} = (1-\rho)\sigma^2_{(i,t-1)} + \rho \times (X_{(i,t-1)} - u_{(i,t-1)})^{\mathrm{T}} \times (X_{(i,t-1)} - u_{(i,t-1)})\,. \tag{5}$$

For matching of unsuccessful Gaussian distribution, the mean and variance remain unchanged when the background is updated. Therefore, the algorithm of mixed Gaussian model can update background accurately. The experimental results are shown in Figure 1.

Figure 1 is the result of a background update using a mixed Gaussian model algorithm in a complex environment. From Figure 1(A) to 1(F), there are shown respectively the numbers of frame 1, 50, 100, 200, 100, and 350. In the experimental results, we can see that the 350th frame is basically recovered from the original background. This result verifies the validity of the background update of the mixed Gaussian model algorithm

2.2. Foreground detection based on improved background difference algorithm

The common background difference algorithm is similar to the image subtraction operation, that is, the two images are point-to-point subtracted. Background different results are finalization processing. Mathematical expression is shown in (6). Symbol $R(i,j)$ is the difference image, $F(i,j)$ is the current frame, and $G(i,j)$ is the background image. Where the value of $R(i,j)$ is 1, the region is the target area to be detected. Symbol T is a gray scale threshold whose size is related to the sensitivity of the recognition target.

$$R(i,j) = \begin{cases} 1, & |F(i,j) - G(i,j)| > T, \\ 0, & \text{otherwise.} \end{cases} \tag{6}$$

The conventional background difference algorithm is simple to implement, but

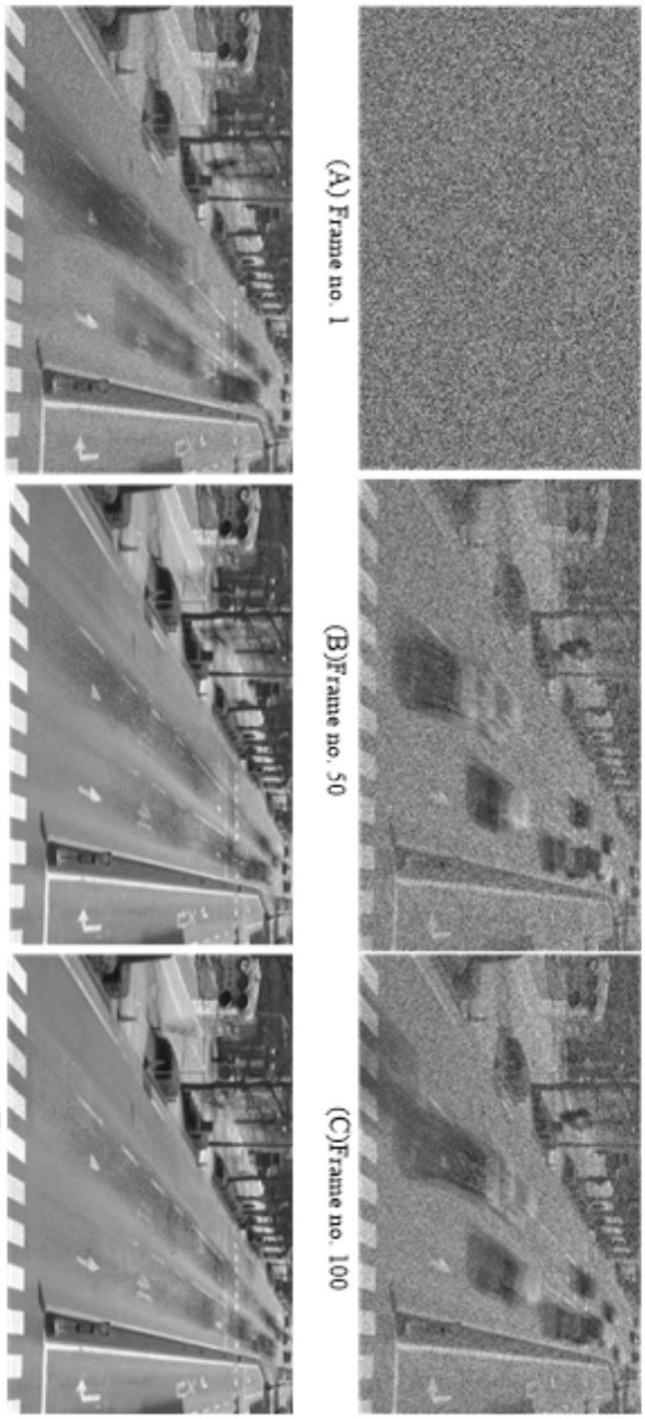

Fig. 1. The algorithm of the Gaussian mixture model realizes background update

because the gray scale threshold T is a fixed value, the segmentation effect is greatly affected in a complicated environment. Dynamic thresholds can solve this problem. It can automatically find the appropriate threshold for segmentation. Therefore, a background difference algorithm based on dynamic threshold is proposed, the basic principle is built on the two images have been obtained when the light changes, which can dynamically adjust the threshold. Therefore, the background difference algorithm could be improved based on the original algorithm to increase the dynamic threshold increment T. The corresponding mathematical expression is

$$\Delta T = \lambda \times \frac{1}{M \times N} \sum_{i=0}^{N-1} \sum_{j=0}^{M-1} |F(i,j) - G(i,j)| \tag{7}$$

$$R(i,j) = \begin{cases} 1, & |F(i,j) - G(i,j)| > T + \Delta T, \\ 0, & \text{otherwise.} \end{cases} \tag{8}$$

Symbol λ in (7) is the suppression factor. It could be accorded with the actual situation value. Product $M \times N$ represents the size of each processed image, the numerical result indicates the number of pixels in the detection area. Symbol ΔT reflects the overall environment changes. It changes with the change of the light. As a result, the background subtraction algorithm based on dynamic threshold could effectively inhibit the effects of the light changes. The experimental results as shown the Fig. 2.

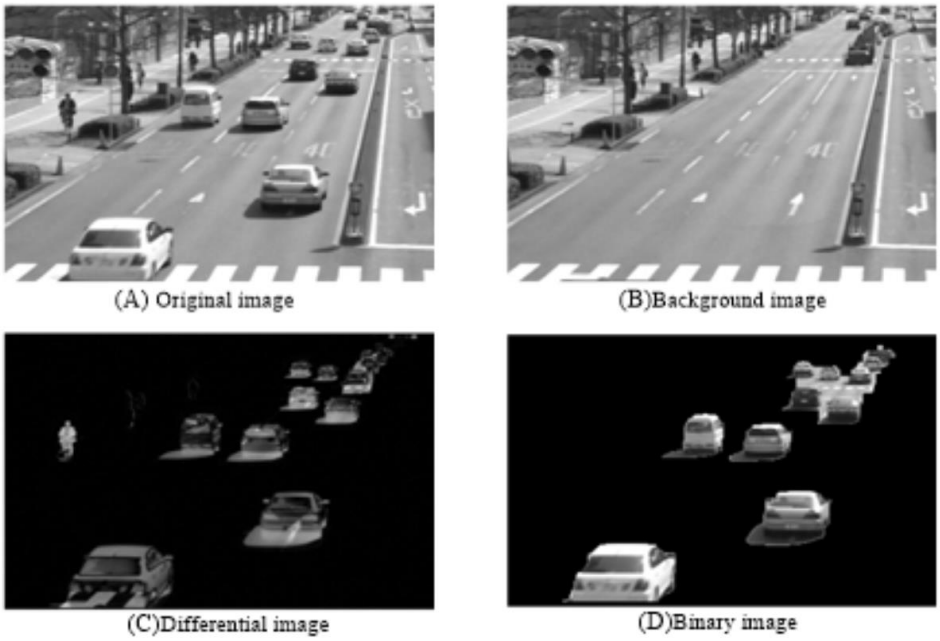

Fig. 2. Application of improved difference method in complex background

3. Persistence tracking based on mean hash principle

Hash algorithm maps a binary value of any length to a fixed-length binary value, which is called a hash value [16]. So hash value is a unique and extremely compact numerical data representation, so as long as the hash of a letter is changed, then the subsequent hash value will change. For two different inputs it is not possible to have the same hash value, so the hash value of the data can verify the integrity of the data.

Average hash algorithm is used primarily for a similar image search. Average hash of their main role is to each image to create a "fingerprint" string, then compare different fingerprint images. The result of the hash is very close, and it means that the image is very similar. Average hash algorithm is mainly using images of low frequency information, and the working process was illustrated in Fig. 3.

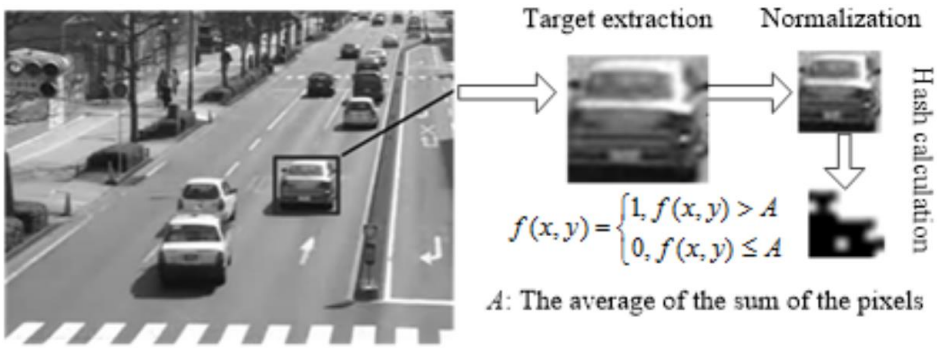

Fig. 3. Hash calculation process diagram

A picture is a two-dimensional signal. It contains the different frequency components, and the low frequency component is the region where the brightness changes are low and describe a wide range of information. The place of intense brightness change is the high-frequency component (such as the edge of the object), which describes specific details. This means that the high frequency can provide the details of images, and low frequency can provide a framework of images. In general, the frequency of large and detailed images is high, and small images lack the details of the image, so the miniature image seems to have a lot of low frequency components. The down sampling in image process, that has also the form of narrowing the pictures, is actually a process of loss of high-frequency information.

Hamming distance could compare the similarity of two images. The first is to calculate the hash of two images, that is, 64-bit 0 or 1, and then calculate the separate digits. If the Hamming distance value is 0, it means that the two images are very similar, if the Hamming distance is less than 5, it means there are some differences, if the Hamming distance is greater than 10, it shows the two images are different. As it can measure the similarity of two images, it should be used for target tracking. In the process of processing, as long as each frame to find the closest target location, according to the threshold of the same target can be matched. The principle of matching the template is similar, but the similarity measure used by the

template match is the correlation of the two images.

Assume the original image size is $m \times n$, distribution range of pixel value is from 0 to 255, reduce image size is 8×8, so the pixel value distribution range is from 0 to 63. Assume that the image is $f(x, y)$. Then the specific steps are as follows:

Step 1: The quickest way to eliminate the high frequency and detail is to reduce size of the image. The image is reduced to 8×8 sizes, and it is comprised of 64 pixels.

Step 2: Convert 8×8 small images into gray-scale images.

Step 3: Calculate the average gray scale level in the all 64 pixels.

Step 4: The gray scale of each pixel is compared with the average. A mark greater than or equal to the average is 1 and the rest is 0.

Step 5: Combine the previous comparison results into a 64 bit integers, which is the hash key for this picture. The order of the combinations is a need, just make sure all the pictures are in the same order.

Thus, continuous tracking of the same vehicle based on the mean hash algorithm can be achieved. The target vehicle is to be tracked to find and then save, calculate its hash code, scan the next frame image and calculate the hash code of each scan window, and compare the target vehicle hash code. The distance from the smallest scanning window is the most similar to the target vehicle, which is the image of the target vehicle location. In order to expedite, only the image area around the previous frame is scanned. In order to accommodate changes in the target, it is also necessary to update the target vehicle to be tracked for each frame after successful tracking.

4. Experimental results

In order to verify the validity of the proposed method two groups of test experiment were used. Group 1 was under the condition of the same vehicle speed, and the vehicle in different weather conditions under the condition of continuous tracking. Group 2 was under the condition of the same weather environment, and the vehicle at unusual speed under the condition of continuous tracking. The experimental environment was based on Windows 7, visual studio 2010 and opencv2.4.9. We used foggy and low speed vehicle, cloudy and low speed vehicle and high speed vehicle to verify the vehicle tracking result. The three videos with a size of 240×360 pixels and the frame rate was 30. In order to quantitatively compare the performance of the proposed method, three metrics were used to evaluate the tracking performance.

The first set of video images (cloudy and low speed vehicle) had the total of 311 frames. The tracking results were shown in Fig. 4. A second set of video images (foggy and low speed) had the total of 313 frames, and tracking results were shown in Figure 5.

The first and second set videos were used for a group of comparative experiments. In the experiments, under the condition of vehicles running at low speed (less than 60 km/hour), the weather environment was different. In the cloudy and foggy weather for the same vehicle continuous tracking test, number of successful tracking was recorded. For this group of experiments, in the case of cloudy weather, the target vehicle in the first group of video appeared in a total of 188 frames, using

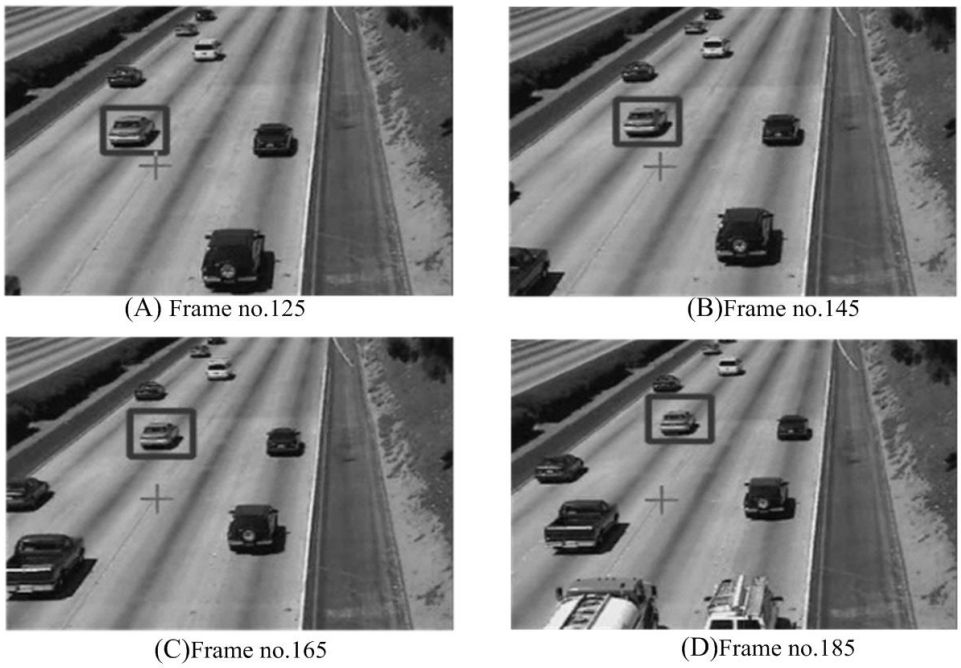

Fig. 4. Cloudy and low speed vehicle tracking experimental result

the proposed method in this paper could successfully track 181 frames. In the foggy weather, the target vehicle in the second group of video appeared in a total of 118 frames, target vehicle could be successfully tracked 101 frames.

Group 3 video images (cloudy and high speed vehicle) had a total of 353 frames, tracking results were shown in Fig. 6.

The first and second set video was used for a group of comparative experiments. In the experiments, under the condition of vehicles running at low speed (less than 60 km/hour), the weather environment was different. For the cloudy and foggy weather for the same vehicle and continuous tracking test, a number of successful tracings were recorded. For this group of experiments, in the case of cloudy weather, the target vehicle in the main group of video appeared in a total of 188 frames, using the proposed method in this paper could successfully track 181 frames. In the foggy weather, the target vehicle in the second group of video appeared in a total of 118 frames, target vehicle could be successfully tracked 101 frames.

In order to quantitatively compare the performance of the proposed method, using an accuracy rate, omission rate and error rate three metrics to evaluate the tracking performance. Accuracy rate relates to the target vehicle has success tracking number of frames and the target vehicle in the ratio of total number of frames. Omission rate refers to the target vehicle has no success tracking the number of frames and the target vehicle in the ratio of total number of frames. Error rate relates to the target vehicle has error tracking number of frames and the target

Fig. 5. Foggy and low speed vehicle tracking experiment result

vehicle in the ratio of total number of frames. The first group, the second and third group detailed performance parameters of the video image tracking results were shown in Table 1.

Table 1. Vehicle continuous tracking performance evaluation

Video sequence number	Evaluation factors	Accuracy rate (%)	Omission rate (%)	Error rate (%)
1	Cloudy Low speed	96.28	3.19	0.53
2	Fog Low speed	85.59	5.08	9.33
3	Cloudy High speed	55	36.5	8.5

As shown in Table 1, the first set of video tracking accuracy was highest, the third set of video omission rate was highest, the second set of video error rate was highest. The first and second groups of video tracking results could be seen that the weather environment affect the target vehicle tracking accuracy. Accuracy rate had fallen by about 10 %. In the first group and the third group of video tracking results it could be seen that vehicle speed affects the target vehicle tracking accuracy. Accuracy rate had fallen by about 40 %. The weather environment changes and vehicles run

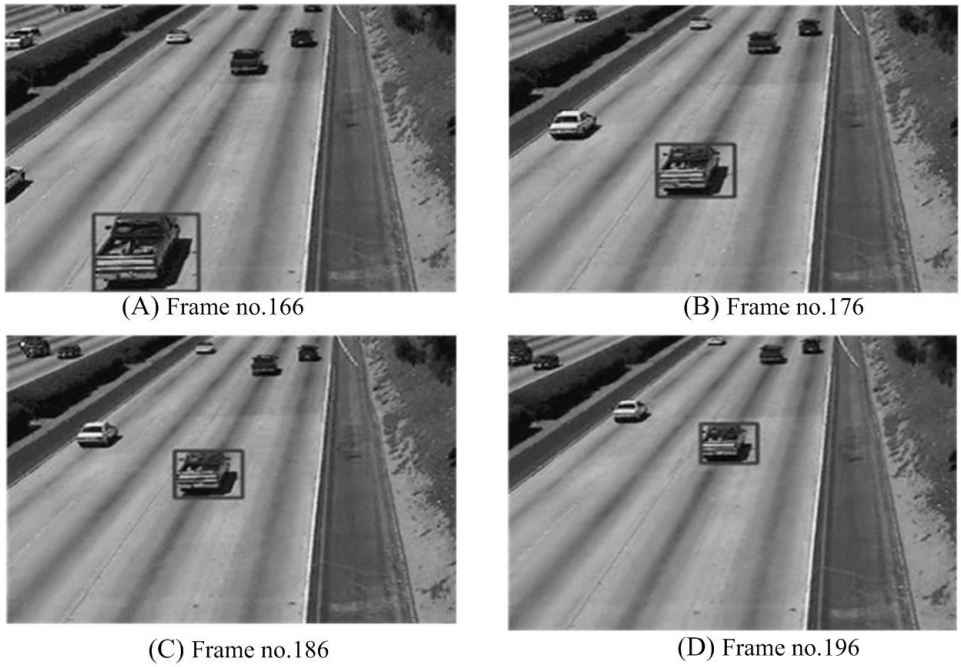

Fig. 6. Cloudy and high speed vehicle tracking experiment result

at low speed. Using the proposed method to keep track of the same vehicles, good results can be achieved. But there was no confirmation that the weather changes with vehicle speed would affect the vehicle tracking accuracy. By comparison, vehicle speed had a greater impact on the vehicle continuous tracking in proposed method.

5. Conclusion

In this paper, moving target vehicle detection and tracking were discussed. In the intelligent transportation system we used a Gaussian mixture model to update road background, and the improved background different algorithm was used to detect foreground. Simulation experiments were conducted in different weather conditions and vehicle speeds. Experiments showed that the proposed method could adapt to the background model and update when the target vehicle was running at low speed, and had a beneficial effect on the influence of the change of the weather environment. And the proposed method could remain relatively stable detection of the target vehicle and tracking.

However, when the vehicle was traveling at high speed, the accuracy of the target vehicle's continuous tracking using the proposed method was not satisfactory. At the same time, this study had not been compared with other algorithms, which were a future research direction.

References

[1] H. J. Zhu, H. H.,Fan, F. Y. Ye, S. S. Zhu, P. Z. Gan: *A novel method for moving vehicle tracking based on horizontal edge identification and local autocorrelation images.* DYNA - Ingeniería e Industria *91* (2016), No. 1, 61–68.

[2] X. J. Wang, F. Pan, W. H. Wang: *Tracking of moving target based on video motion nuclear algorithm.* Journal on Smart Sensing and Intelligent Systems *8* (2015), No. 1, 181–198.

[3] E. Taniguchi, H. Shimamoto: *Intelligent transportation system based dynamic vehicle routing and scheduling with variable travel times.* Transportation Research Part C: Emerging Technologies *12* (2004), Nos. 3–4, 235–250.

[4] H. H. Fan, H. J. Zhu: *Separation and extraction of moving vehicles in traffic images based on horizontal roof edges.* International Review on Computers and Software *7* (2012), No. 3, 1347–1351.

[5] rederick J. Engelbrecht, M. J. Booysen, G. J. van Rooyen, F. J. Bruwer: *Survey of smartphone-based sensing in vehicles for intelligent transportation system applications.* IET Intelligent Transport Systems *9* (2015), No. 10, 924–935.

[6] H. J. Zhu, H. H. Fan, F. Y. Ye, X. R. Zhao: *Improving vehicle detection accuracy based on vehicle shadow and superposition elimination.* Open Mechanical Engineering Journal *9* (2015), No. 1, 1039–1044.

[7] H. J. Zhu, H. H. Fan, S. Q. Guo: *Moving vehicle detection and tracking in traffic images based on horizontal edges.* TELKOMNIKA Indonesian Journal of Electrical Engineering *11* (2013), No. 11, 6477–6483.

[8] X. M. Zhang, Y. L. Xiong: *Impulse noise removal using directional difference based noise detector and adaptive weighted mean filter.* IEEE Signal Processing Letters *16* (2009), No. 4, 295–298.

[9] S. Shrestha: *Image denoising using new adaptive based median filters.* Signal & Image Processing: International Journal (SIPIJ) *5* (2014), No. 4, 1–13.

[10] W. Li, S. Prasad, J. E. Fowler: *Hyperspectral image classification using gaussian mixture models and Markov random fields.* IEEE Geoscience and Remote Sensing Letters *11* (2014), No. 1, 153–157.

[11] T. Bouwmans, J. Gonzàlez, C. F. Shan: *Special issue on background modeling for foreground detection in real-world dynamic scenes.* Machine Vision and Applications *25* (2014), No. 5, 1101–1103.

[12] H. J. Zhu, T. Koga: *Face detection based on adaboost algorithm with local autocorrelation image.* IEICE Electronics Express *7* (2010), No. 15, 1125–1131.

[13] J. Zhang, J. L. Tang, H. H. Fan: *Variable length niche algorithm and application in fuzzy image edge detection.* Metallurgical & Mining Industry *7* (2015), No. 6, 368–372.

[14] H. J. Zhu, H. H. Fan: *Face detection based on adaboost algorithm with normalized differential images.* International Review on Computers and Software *7* (2012), No. 2, 845–849.

[15] H. H. Santosh Dadi, P. Venkatesh, P. Poornesh, L. N. Rao, A. Kumar: *Tracking multiple moving objects using gaussian mixture model.* International Journal of Soft Computing and Engineering *3* (2013), No. 2, 114–119.

[16] G. Wu, W. X. Kang: *Vision-based fingertip tracking utilizing curvature points clustering and hash model representation.* IEEE Transactions on Multimedia *19* (2017), No. 8, 1730–1741.

Received May 7, 2017

Acta Technica *62* No. 2B/2017, 129–140

Design and implementation of meteorological prediction and early warning information system for slope geologic hazard based on the WebGIS of RIA

Guan Xinbang[1]

Abstract. In geological disasters, heavy rainfall is the cause of slope geological collapse, debris flow and other disasters, and will lead to greater property, life and safety crisis. Meteorological prediction and early warning information system for slope geologic hazard based on the WebGIS of RIA was designed and implemented; first of all, the present situation of geological disasters was introduced, and the main technologies of the WebGIS of RIA and the algorithms of weather forecast and early warning for slope geological hazard were analyzed; and then meteorological forecast and warning information system of slope geological hazard based on WebGIS of RIA was designed; finally, the application status of early-warning information system in high incidence area of slope geological hazards in China was analyzed. Therefore, the system is helpful for the rescue personnel to carry out remote consultation and decision-making command of the slope geological disaster area.

Key words. RIA, WebGIS, weather forecast of slope geological hazard, early warning information system.

1. Introduction

With the expansion of the population of the world, the scope of human activities expands, and the natural environment is deteriorating, and the occurrence of geological disasters is more and more frequent, which brings more and more serious losses to human society, the incidence of geological disasters is high in China [1]. Geological disasters are widespread, and characterized by extensive distribution, which will produce serious threat to the safety of people's lives and property, affect social and economic development, and restrict the long-term sustainable development of society. Especially in recent years, China's geological disasters occur frequently, the

[1]China University of Mining and Technology (Beijing), Beijing, 100083, China

flood season is affected by meteorological factors, slope geological disasters occur frequently, and any disaster prevention must be based on early warning [2]. The occurrence of geological disasters is a dynamic process of change, and also a very big project for the study and early warning of geological disasters. Therefore, it is necessary to use modern science and technology, information technology and multidisciplinary collaboration to assist in the study.

Up to now, all countries in the world have set up special geological disaster prevention and prediction institutions. Combined with the knowledge of computer science and geographic information system, a specific information management system for geological disaster prediction and early warning has been developed. With the rise of Internet technology, some countries have basically realized WebGIS based on the publication and application of the geological disaster prediction information system [3]. The researchers have carried out the deformation monitoring of the landslide and timely captured the relevant information of the landslide indications, so as to effectively prevent and control the geological disasters of the landslide. Deformation monitoring generally includes surface deformation monitoring and depth deformation monitoring, and surface monitoring includes geological inspection, simple monitoring of surface instruments, geodetic leveling network [4].

2. State of the art

Since 1980s, great progress has been made in the research and development of the geographic forecast and early warning information system. The geographic information system (GIS) is a tool based computer, which can be used to map objects on the earth and analyze events in detail according to the research and development of the techniques and methods for the prediction of sudden geological disasters [5]. Based on the analysis of boundary conditions and structural elements of geological disasters, the geological hazard environment and various parameters are determined by the number of parameters (experimental or instrumental determination) or linear change values, then the rigid body equilibrium equilibrium theory or the improved limit equilibrium theory is used to establish mathematical expressions or empirical expressions to predict the distribution of geological hazards and dynamic processes [6]. This method is applicable to the prediction and assessment of a single geological hazard (falling gradient), but not suitable for large area regional forecasting [7]. Although specific (especially early) engineering examples play a part, this simple problem gradually exposes the approximate defects of geological disasters and it is always unsatisfactory when predicting the dynamic disaster of instability with the continuous recovery of geological disasters [8].

3. Methodology

3.1. The main technology of WebGIS based on RIA

RIA technology can be introduced, and its visual effects can be added into WebGIS applications to suit the user-friendly needs of the system. Therefore, it's feasible to construct WebGIS architecture under RIA, and the design and implementation of the system are more in line with the idea of object-oriented software development. The main techniques include the following:

The spatial database management system and relational database management system are quite mature, commercial RDBMS not only supports B/S and C/S mode, but also supports data distribution, through SQL and ODBC, almost all GIS software can work together based on public identification numbers. Object relational database technology and object oriented database technology are mature gradually, and become the main technologies of GIS spatial data management in the future.

Life cycle of the whole information system includes object -oriented, object-oriented (OOA), object-oriented design (OOD) and object-oriented language (OOL), and object-oriented data management (OODBM). The object-oriented control database technology is gradually mature, spatial object query language (SOQL), spatial object relational analysis, object-oriented database management, object-oriented software technology and GIS are closely related, and this is a good way to describe geography from the development of object-oriented technology [9].

Client/server has a wide range of meanings, database technology and distributed processing technology are closely related. Data communications and geography operations of client / server are balanced to take advantage of the server's high-performance benefits, handle complex critical services, and reduce network traffic, and users can make full use of the various resources of the network by planning the client / server model of the GIS system [10].

WebGIS not only has the functionality of most or all of the traditional GIS software, but also has the advantage of using Inetmet's unique features. These unique features include that users don't have to install GIS software on the local computer to access remote GIS data and applications on the Internet, perform GIS analysis, and provide interactive maps and data on the Internet. The main features of WebGIS are object-oriented, distributed and interoperable. Any data and functions of GIS are an object. These are deployed on different servers on the Internet and are assembled and integrated when needed, and any other system on the Internet can exchange and interact with these objects. Architecture of WebGIS is as follows (see Fig. 1):

The client will complete three operations:

(1) The first one is to manage user interfaces and deal with application logic.

(2) The second one is to generate a database request and send a request to the GIS server, and then accept the result from the GIS server.

(3) The third one is the formatted result, which is published to the user, and the corresponding function of the network server is to accept the request of the client user and generate the dynamic web page content to return to the client.

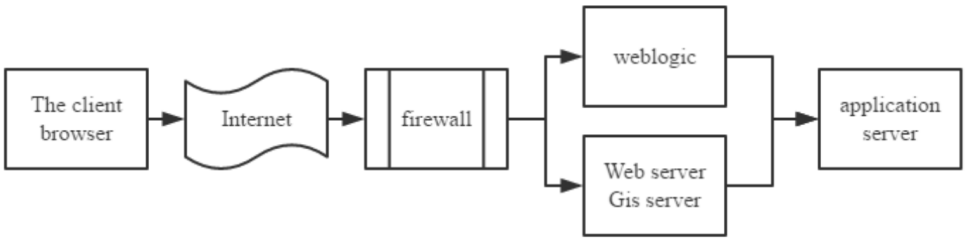

Fig. 1. Architecture of WebGIS

The corresponding functions of the GIS server are as follows:
(1) The first one is to accept database requests from the client.
(2) The second one is the processing of requests of the database.
(3) The third one is the formatted result, which is sent to the client.
(4) The fourth one is to maintain the database.

The implementation of this system architecture is based on the implementation of the server (thin client), that is, clients only need browsers, and no other Java plug-ins need to be downloaded; the server is responsible for dealing with customer's requests, as well as related space calculation, data query and other high load operations, non-map requests are executed on the network server side, while map requests are switched to the ArcIMS application server via the network server, and the result is returned after the server processing of the ArcIMS is established.

3.2. Warning algorithm for meteorological forecast of slope geological hazard

The occurrence of meteorological disasters and geological disasters is a process from chronic change to a variety of natural factors, including human factors. Geological condition is a necessary regulation of MGD, and rainstorm is a sufficient condition for occurrence of MGD. Thus, MGD is a function of geological factors (d), human factors (m), and precipitation (r). That is, MGD $= f(d, m, r)$. For specific regions, MGD is a function of precipitation (R) in the medium and short term forecast of MGD, that is, MGD $= f(r)$, geological conditions and human factors are basically the same. Precipitation monitoring and prediction produce MGD short-term, medium term forecasts and alarms. The prediction of the risk (possibility) of MGD is calculated by the formula

$$\mathrm{MGD}(r) = \sum_{i=1}^{n} Y_i(r) + g\,, \tag{1}$$

where Y represents the cumulative rainfall of multiple storm periods, $_i$ represents the value in the sample, n is the number of sample data, and g denotes the threshold of the non resistance factor. The principle of the formula is calculated and the relationship between weather conditions and prediction, establish the prediction equation, and assuming that the numerical prediction results exactly, and the numerical re-

sults as predictor equation (Hofer et al. 2015 [11]). In addition, the MGD forecast is similar to the strong rainfall forecast, and the general statistical method is used as the model. In daily and fixed-point MGD forecasts, small probability events rarely occur in daily precipitation events (Youssef et al. 2015) [12].

The ETA numerical prediction model is simply referred to as η prediction model, which is a way to forecast by analyzing the intensity prediction of precipitation centers above regional moderate rainfall that is basically consistent with the actual situation. According to the different configuration of weather system, and degree of deviation between rainfall and actual weather is predicted by η model, precipitation predicted by η model is treated as a post process. That is correct for the intensity of center of the rain, position of the rain, and precipitation of each point in the predicted rainfall

$$R_{\mathrm{b}} = \frac{R_{\mathrm{a}}}{R_{\max}} \times R_i + R_i \,. \tag{2}$$

Here, R_i is a forecast of the ETA model rainfall rainfall in value, R_a is the fixed point correction before rainfall, $R_{\max}$ denotes the maximum rainfall data collected before the correction value, R_{b} needs to be corrected after correction for point rainfall. The rain area should be considered in the drift correction effect of average wind speed forecast area and direction on drift. The weather forecast system area forecast rainfall correction and intensive rain drift process of rainfall products using the ETA model (Kadiyala et al. 2015) [13]. Then using the weight method and successive correction method, the prediction of the ETA model lattice into rainfall weighting method is

$$y_0 = \frac{\sum_{i=1}^{n} W_i y_i}{\sum_{i=1}^{n} W_i} \,. \tag{3}$$

Here, y_0 is the ETA model grid point precipitation interpolation to forecast the precipitation forecast value of single station and Y_i is the forecast value of precipitation lattice precipitation at the ith grid point near the single station. Symbol W_i is the weight coefficient of the ith grid point, and n is the total number of samples.

3.3. Design of meteorological forecast and early warning information system for slope geological hazard

The prediction and warning information system for sudden geological disaster makes use of the various functions of GIS which are determined by the characteristics of geological disasters. The uncertainty of geological disasters and the complexity of the interaction among geological factors cause that GIS is used to manage the data of these geological disasters after a large number of basic geological environment data are collected. Effective treatment methods, temporal and spatial distribution of geological disasters are presented in the analysis of the probability of occurrence of geological disasters. Slope geological disaster area and its prevention are shown in Fig. 2.

The system uses GIS technology, network technology and decision support system, and provides decision support system for designing and developing meteorological early warning for geological disasters. The real-time weather information and the

Fig. 2. Meteorological forecast and early warning information system for slope geological disasters

prediction of geological disasters are analyzed through the study of the relationship between geological disasters and their induced factors-meteorological factors [14]. The system automatically receives weather information, once there is the possibility of inducing disaster, the system will reach the threshold of the weather information displayed on the map, a preset warning prediction scheme is automatically entered, a warning device is used to trigger through an alarm device. Through the warning forecast with light sound, alert messages are automatically sent to related personnel of the group defense system and mobile terminals of the population threatened to achieve the purpose of early warning and prediction [15]. The framework of the meteorological forecast and early warning information system for slope geological disasters is depicted in Fig. 3.

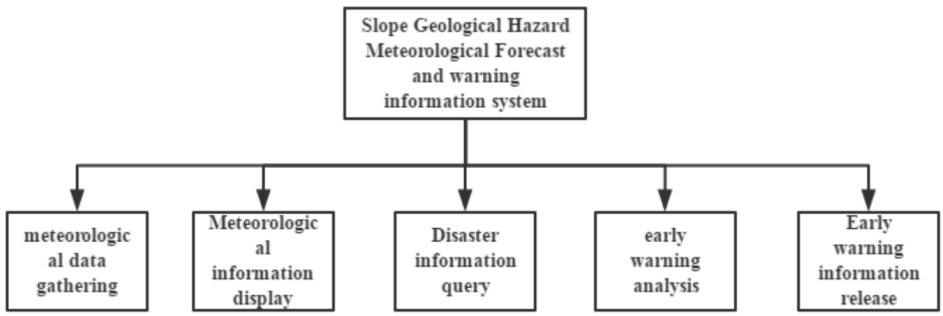

Fig. 3. Meteorological forecast and early warning information system for slope geological disasters

4. Result analysis and discussion

4.1. Configuration and implementation of meteorological forecast and warning information system for slope geological hazard of based on WebGIS of RIA

The meteorological forecast and warning information system for slope geological hazard of based on WebGIS of RIA needs to be equipped with advanced spatial data server software, provides users with greater support for spatial databases, and supports multi-user editing, a large number of spatial databases and any number of users. The system consists of a unified ArcSDE data management for geological disaster, database for prediction and release of sudden geological hazard. The data contained in this database includes: special data of sudden geological disasters, thematic data of rainfall observations reported by flood stations, and the auxiliary basic terrain data. The spatial database is organized according to Table 1.

Table 1. Composition of a spatial database

Data of sudden geological disasters	Forecast map of disaster probability	Ground fissure
		Caving-in
	Disaster spots and disaster prone areas	Mud-rock flow
		Hill-creep
Data of margin observation of news station	Rainfall in the past 1 hour	-
	Rainfall in the past 2 hour	-
Data of basic terrain	Administrative boundaries, water systems, roads	-

The background service program will carry on the real-time update to maintain the updating of the data. Attribute structure of disaster probability forecast chart is set with the field of "Probability", and attribute structure for observing rainfall element class is set with the field of "Rainfall", which are used for thematic symbol rendering respectively.

The configuration of the ArcIMS application server: ArcIMS maps are configured in two main ways: Author and ArcMap. The LAPS system is selected in the map configuration selection ArcMap to publish more complex thematic maps. Two topics need to be published respectively: disaster probability prediction and rainfall monitoring station, they all use basic terrain data to assist in thematic maps and communications. Each observed rainfall elemental class is based on the “rainfall” field, and represented by graduated value and magnitude of rainfall, different sizes and different colors. The prediction of sudden geological disaster is divided into five grades. Among them, the third and fourth levels represent the release of forecast and the fifth level represents the release of alerts with yellow and orange as signs

respectively, as shown in the following Table 2.

The probability value of characteristic class stores of the probability field (range 0–1) of prediction of sudden geological disasters is based on the value of field, and presented as unique value. Basic ground features are mainly used to assist display, and display the proportion of different distribution according to management level and visual effect, so that the location of the disaster area is very clear through the realm and place names.

Table 2. Grade of prediction and early warning of geological disaster

Rank	The first level	The second level	The third level	The fourth level	The fifth level
Probability	0.0–0.2	0.2–0.4	0.4–0.5	0.5–0.8	0.8–1.0
Possibility	Little	Less	Large	Larger	Great

4.2. Analysis of application of meteorological forecast and warning information system for slope geological hazard based on WebGIS of RIA

China's slope geological disasters occur mainly in Sichuan and Yunnan Provinces.

Meteorological forecast and early warning information system was applied in the above two areas. The meteorological forecast and warning information system for slope geological hazard based on WebGIS of RIA showed that the relationship between MGD and the current precipitation in Yunnan was: the MGD during period of rainstorm was the pre 0–4 days, the number of storms was between the sixth and the eleventh day. In the precipitation patterns caused by rainstorm and MGD relation models, the key rainfall periods of rainstorm induced in many days were 0–5 days and 6–12 days, the key rainfall period of continuous rainy induction was 0–40 days, as shown in Fig. 4.

Collection and analysis of debris flow and landslide disaster in Sichuan basin were carried out through the application of geographic information early warning and forecasting system based on RIA. In the prediction model η, through the analysis of the precipitation of the same day, the precipitation of the first 3 days and the rainy days of the first 30 days of debris flow landslide, the relevant threshold values for the associated weather forecast and warning information of slope geological hazard were obtained and listed in Table 3.

Table 2. Correlation threshold of meteorological forecast and warning information for slope geological hazard

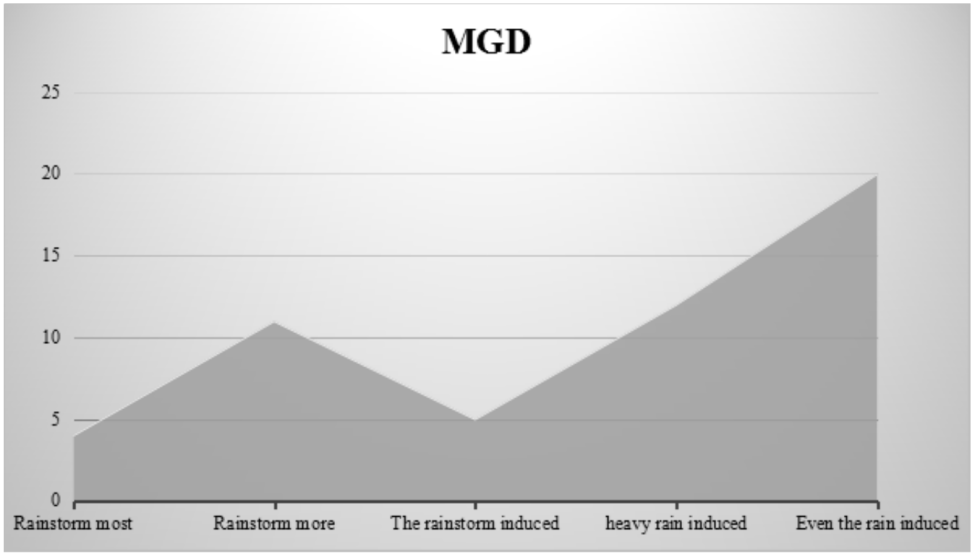

Fig. 4. Information area map of MGD

Forecast precipitation	Rainfall for the first 3 days	The first 30 days before the rain/precipitation rain fall	The possibility of slope geological hazard
Above 200 mm	$\geq$ 100 mm	$\geq$ 16 days	Great possibility
Below 200 mm	Between 12 and 36 hours 100–200 mm	-	Small possibility
50–10 mm	$\geq$ 40 mm	$\geq$ 16 days	Large possibility
30–50 mm	-	$\geq$ 100 mm	Little possibility

As can be seen from the above data, in the prediction model η, the meteorological information in the time period was all taken into account, the meteorological information such as rainfall during the period of time was compared with the meteorological information of slope and geological disaster, an alarm was issued once the threshold was exceeded to remind local authorities and personnel to take appropriate defensive measures. In addition, according to the forecast data model η, efforts should be made to build appropriate protective structures and equipment on hardest hit areas of slope geological disasters.

5. Conclusion

The prediction information system of slope geological hazard is based on the condition that rainfall is relatively slow in the case of geological disasters caused by geological environment factors, and combines the geological disasters caused by

geological and meteorological conditions with slope geology and weather. From the point of view of system analysis engineering, it is necessary to put forward a meteorological forecast and warning information system for slope geological disaster which is cooperative and suitable for the application of prefecture level business by using advanced GIS technology, database technology and computer programming technology. In this paper, the meteorological forecast and warning information system for slope geological hazard based on WebGIS of RIA was studied and designed, first of all, the present situation of slope geological hazard and its loss for people's life were introduced; then, the current situation of the related information technology system of prediction and early warning for slope geological disaster was introduced, and WebGIS of RIA technology, correlation algorithm of prediction and warning, and design framework of the whole system were introduced in detail; finally, the configuration, implementation and application of the weather prediction and early warning information system for Slope Geological Hazard based on the WebGIS of RIA were analyzed. The results show that the system can meet the urgent requirements of disaster prevention and mitigation, and can effectively reduce the slope geological hazards induced by meteorological factors, but there is still a lack of geographical positioning technology.

References

[1] T. Wu, M. Qi, Y. Li, H. Yan: *On the application of RIA technique in WebGIS development.* Bulletin of Surveying and Mapping (2006), No. 6, 208–211.

[2] F. G. Xiong, X. Han, L. Q. Kuang: *Design and implementation of geological hazard forecast system based on WebGIS.* IEEE International Conference on Computational Intelligence and Software Engineering, 11–13 December 2009, Wuhan, China, IEEE Conference Publications (2009), 1–4.

[3] L. Zhong, S. Xiao, Y. Zhou: *Research on the early warning and forecast system of geologic hazards in Hubei province based on WEBGIS.* IEEE International Workshop on Education Technology and Computer Science (ETCS), 7–8 March 2009, Wuhan, Hubei, China, IEEE Conference Publications *1* (2009), 602–606.

[4] W. Li, W. Wang: *Design and implementation of the early warning and forecast system of abrupt geological hazard based on WebGIS.* Journal of Zhejiang University of Technology *37* (2009), No. 6, paper 002.

[5] N. Wang, T. Shi, Y. Li, Z. Lian, P. Ke: *Quantitative assessment on the influence of rainfall on landslides in Jianshi county of Qing river basin, China.* Environmental Earth Sciences *75* (2016), No. 3, paper 241.

[6] W. Chen, B. He, L. Zhang, D. Nover: *Developing an integrated 2D and 3D WebGIS-based platform for effective landslide hazard management.* International Journal of Disaster Risk Reduction *20* (2016), 26–38.

[7] J. N. Munyendo, D. Kuria, K. Mubea: *Development of AWebGIS supported road traffic accident data management system: A case study of Nairobi county.* International Annual Conference on Sustainable Research and Innovation (SRI), 6–8 May 2015, Nairobi, Kenya, Published in the Journal of Sustainable Research in Engineering (2015), 218-227.

[8] M. Ding, F. Wei: *GIS and DWR based short-term and impending landslide forecasting for Liangshan prefecture (China).* Tehnicki Vjesnik - Technical Gazette *22* (2015), No. 3, 695–702.

[9] M. A. Abdelfattah, A. T. Kumar: *A web-based GIS enabled soil information system*

for the United Arab Emirates and its applicability in agricultural land use planning. Arabian Journal of Geosciences *8* (2015), No. 3, 1813–1827.

[10] O. Rahmati, A. N. Samani, M. Mahdavi, H. R. Pourghasemi, H. Zeinivand: *Groundwater potential mapping at Kurdistan region of Iran using analytic hierarchy process and GIS.* Arabian Journal of Geosciences *8* (2015), No. 9, 7059–7071.

[11] B. Hofer: *Uses of online geoprocessing technology in analyses and case studies: A systematic analysis of literature.* International Journal of Digital Earth *8* (2015), No. 11, 901–917.

[12] A. M. Youssef, B. Pradhan, H. R. Pourghasemi, S. Abdullahi: *Landslide susceptibility assessment at Wadi Jawrah basin, Jizan region, Saudi Arabia using two bivariate models in GIS.* Geosciences Journal *19* (2015), No. 3, 449–469.

[13] M. D. Kadiyala, S. Nedumaran, P. Singh, S. Chukka, M. A. Irshad, M. C. S. Bantilan: *An integrated crop model and GIS decision support system for assisting agronomic decision making under climate change.* Science of The Total Environment *521–522* (2015), No. 6, 123–134.

[14] A. Chybicki: *Innovative web-based geographic information system for municipal areas and coastal zone security and threat monitoring using EO satellite data.* Marine Geodesy *38* (2015), No. 3, 203–224.

[15] K. Sowmya, C. M. John, N. K. Shrivasthava: *Urban flood vulnerability zoning of Cochin City, southwest coast of India, using remote sensing and GIS.* Natural Hazards *75* (2015), No. 2, 1271–1286.

Received May 7, 2017

Acta Technica *62* No. 2B/2017, 141–150

Production prediction model of coalbed methane wells at stable production stage

Jia Liu[1], Yinghong Liu[1], Ruyong Feng[1], Kailei Yang[1]

Abstract. To calculate the production capacity of coalbed methane wells at stable production stage, a seepage mathematical model suitable for coalbed methane wells at stable production stage is established based on the theory of seepage and the adsorption and desorption characteristics of coalbed methane to get the productivity equation of coalbed methane production so that the production capacity of coalbed methane wells can be predicted. The results show that the low critical desorption pressure leads to the lack of energy in the course of methane production. The weakness of gas expansion energy and the difficulty in pressure dropping will also seriously affect the gas production. The reduction of bottomhole flowing pressure can effectively improve the productivity of coalbed methane wells, and the increase in gas production is more prominent when the bottomhole flowing pressure is relatively high. It is advisable to install pump hanging tools in coalbed methane wells whose bottomhole flowing pressure is greater than 1.5 MPa

Key words. Coalbed methane, capacity prediction, critical desorption pressure, bottomhole flowing pressure, pump hanging tools.

1. Introduction

Since a vast majority of the coalbed methane adsorbed into the solid matrix of the coal, the main method of coalbed methane mining is depressurization. The coalbed methane is different from conventional natural gas in terms of hydrocarbon accumulation mechanism, occurrence state, distribution law and exploration and development mode [1–3]. During the period of 2011–2015, China has accelerated the construction of two industrial bases in the Qinshui Basin and the eastern Ordos. The new proven geological reserves in China are 350.41 billion m^3, and the accumulated proven geological reserves are 629.27 billion m^3. However, in terms of coalbed methane production, the production of a single well is still too low [4–5].

[1]CNOOC Research Institute, 100028, Beijing, China

Therefore, it is of great importance to predict the methane production capacity of coalbed wells since it is helpful for decision-makers in selecting wells and predicting the single production capacity of a single well when it is comes to new wells and to determine whether the current production is normal or whether the gas production has reached the peak in terms of old wells so that the data can be used to guide the work and adjust the work system. Thus, how to effectively predict coalbed methane production capacity and how to effectively determine the production possibility curve of coalbed methane wells becomes an important research topic in the development of coalbed methane.

Currently, there is no deep understanding on the prediction of coalbed methane production capacity. One approach to obtain the methane production capacity in coalbeds with artificial cracks and stress-sensitive coalbeds based on the seepage theory [6–7]. By calculating the production capacity of coalbed methane wells under different production pressures, they found that the extraction of coalbed methane needs to set up reasonable production pressures and strictly control the mining intensity. However, these models treat coalbed methane as a conventional reservoir, considering nothing about the adsorption and desorption properties of coalbed methane reservoirs. The coalbed methane production capacity could be predicted by he numerical method with taking desorption, diffusion and seepage processes of coal seam methane into consideration [8]. A neural network back propagation (BP) model was established for time series forecasting the dynamic production capacity of coalbed methane wells, with the modern artificial intelligence theory and mathematical statistics theory. The model could well fit the production history of coalbed methane wells and can make accurate quantified prediction [9–10]. Another method has established a type curve to analyze the correlation between the dimensionless production and time and established an equation to show the relationship between dimensionless production under different Langmuir pressures and practice and proposed some methods to use the type curve to predict the coalbed methane production [11]. However, the two above-mentioned formulas are established only on practice and do not take the seepage into consideration. This paper, based on the theory of seepage and the adsorption and desorption characteristics of coalbed methane, establishes a seepage mathematical model for coalbed gas wells at stable production stage. By introducing the pressure variable into the model and solve it, we can get an equation to predict the coalbed methane production, which is helpful to guide the efficient extraction of coalbed methane.

2. Analysis methods

Suppose in a mean circular strata whose temperature is in a constant state and of equal-thickness, a coalbed methane well located at the center of it is producing gas at a small time step with a fixed production. If the seepage flow is steady at

this time, the differential equation can be expressed as

$$\frac{\mathrm{d}}{\mathrm{d}r}\left(r\frac{\mathrm{d}\tilde{P}}{\mathrm{d}r}\right)=0\,. \tag{1}$$

Equation (1) is a second-order ordinary differential equation, whose general solution is

$$\tilde{P}=C_1\ln r+C_2\,, \tag{2}$$

where r is the radius and $\tilde{P}$ is the pressure coefficient given by the relation

$$\tilde{P}=\int\rho\,\mathrm{d}P+C\,. \tag{3}$$

Here, P denotes the pressure. The pressure coefficient $\tilde{P}$ was created to make the calculation easier.

Substituting the following boundary conditions

$$\text{borehole wall}: r=r_{\mathrm{w}} \qquad \tilde{P}=\tilde{P}_{\mathrm{w}}\,, \tag{4}$$

$$\text{external boundary}: r=r_{\mathrm{e}} \qquad \tilde{P}=\tilde{P}_{\mathrm{e}}\,. \tag{5}$$

As the coalbed methane is adsorbed gas, only when the pressure is lower than the critical desorption pressure the coalbed methane can desorb from surfaces, diffuse through the coal matrix and become free gas. However, the strata not in the range of desorption sees no gas flow. Therefore, in equation (5), $\tilde{P}_{\mathrm{e}}$ is the critical desorption pressure, r_{e} is the desorption radius, $\tilde{P}_{\mathrm{w}}$ is the bottomhole flowing pressure, and r_{w} is the radius of the wellbore.

Then we obtain:

$$C_1=\frac{\tilde{P}_{\mathrm{e}}-\tilde{P}_{\mathrm{w}}}{\ln\frac{r_{\mathrm{e}}}{r_{\mathrm{w}}}}\quad C_2=\tilde{P}_{\mathrm{w}}-\frac{\tilde{P}_{\mathrm{e}}-\tilde{P}_{\mathrm{w}}}{\ln\frac{r_{\mathrm{e}}}{r_{\mathrm{w}}}}\ln r_{\mathrm{w}}\,. \tag{6}$$

Substituting C_1 and C_2 into (2) we can obtain the equation for the pressure function in the form

$$\tilde{P}=\tilde{P}_{\mathrm{e}}-\frac{\tilde{P}_{\mathrm{e}}-\tilde{P}_{\mathrm{w}}}{\ln\frac{r_{\mathrm{e}}}{r_{\mathrm{w}}}}\ln\frac{r_{\mathrm{e}}}{r}\,. \tag{7}$$

In order to obtain the production Q, Darcy's law is used. Usually the volume of gas will change with the pressure. However when seepage flow is stable, the mass flow rate is a constant which can be obtained by multiplying area of the cross-section and mass flow rate.

$$M=\frac{2\pi Kh(\tilde{P}_{\mathrm{e}}-\tilde{P}_{\mathrm{w}})}{\mu\ln\frac{r_{\mathrm{e}}}{r_{\mathrm{w}}}}\,. \tag{8}$$

In the above equation, h is the formation thickness, K is the cleavage permeability, Q is the gas production in standard conditions and μ is the gas viscosity.

The volume flow rate of the planar radial flow well under the standard condition is then

$$Q = \frac{\pi K h}{\mu} \frac{T_{\mathrm{a}}}{P_{\mathrm{a}} \bar{z} T_{\mathrm{f}}} \frac{P_{\mathrm{e}}^2 - P_{\mathrm{w}}^2}{\ln \frac{r_{\mathrm{e}}}{r_{\mathrm{w}}}} . \tag{9}$$

Here, T_{a} is the temperature under standard conditions, T_{f} is the formation temperature, P_{a} is pressure under standard conditions and $\bar{z}$ is the compression factor.

3. Analysis and discussion

In order to verify the applicability of this model, this paper chooses the real block to carry on the contrast simulation. Since the southeastern part of the Shizhuang South Block has been recovered for a relatively long time and its control system is relatively stable, this paper will take this block as the example to test the veracity of this model by comparing the prediction results of this model separately with the data in numerical simulation and actual mining process.

First, the result difference between the capacity prediction model and the commercial numerical simulation software is compared. By analyzing the geological parameters of the existing mining wells, among which, the thickness, porosity and initial pressure etc. are measured values while permeability, gas content, and critical desorption pressure etc. are calculated values based on the production data. Then, a typical coalbed methane geological model suitable for the target block is established on the average of the above-mentioned parameters. The parameters used in the model are shown in Table 1. Based on these parameters, capacity prediction model and numerical simulation software will be used separately to predict the gas production of coalbed methane wells.

Table 1. Typical model parameters in the target block of four kinds of light sources

Well control area	300 m×300 m	Thickness	6 m
Permeability	10^{-3} μm^2	Porosity	5.82 %
Gas content	17.2 m^3/t	Initial pressure	6.0 MPa
Critical desorption pressure	2.2 MPa	Bottomhole pressure	0.2 MPa

Then, the commercial numerical simulation software is used to simulate the geological model. The dynamic fluid level will be declined at a speed of 3 m/d in the process of water-pumping and depressurization, that is, the descent speed of the bottomhole flowing pressure will be controlled at 0.03 MPa/d. After gas comes to the surface, slow the descent speed of the dynamic fluid level to 0.1 m/d. The simulation results are shown in the Fig. 1. This coalbed methane well enters the stable yield period after experiencing the water-pumping and depressurization period and the production-rising period, whose gas production remains at about 1350 m^3/d.

Then the capacity prediction model will be used to calculate the coalbed methane production under the same geological parameters. It can be seen from the formula (9) that the gas production in the coalbed methane wells is mainly related to the

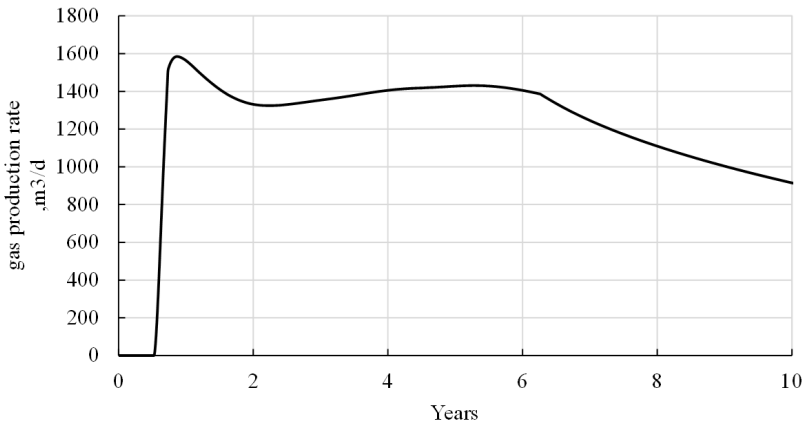

Fig. 1. Curve of numerical simulation results of gas production in target area

desorption radius. The larger the desorption radius is, the smaller the daily gas production is. This is because the larger the desorption radius is, the smaller the pressure drop of each grid can get from the same water production, and therefore the less the desorbed gas will be. However, it can be seen from the calculation result that the gas production is reduced at a small rate and basically maintains stable.

For the convenience of comparison, we will use the daily gas production data whose desorption radius is 70 m. The results show that the calculated gas production at stable stage is about 1400 m^3/d in the capacity prediction model (see Fig. 2), and the error between the results of the capacity prediction model and the numerical simulation is within the reasonable range. Therefore, it can be concluded that the capacity data derived from the prediction model and the numerical simulation are in good agreement.

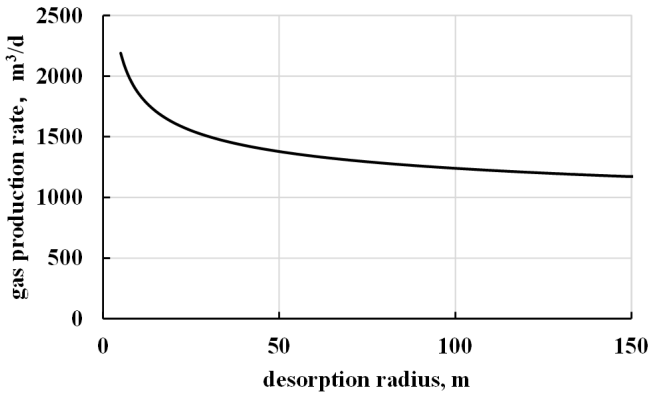

Fig. 2. Calculated results of gas production of a single well in target area

The production data of 32 single wells in Shizhuang South block that have pro-

duced gas and whose drainage system is stable and production rate per hour is high are selected in the calculation process. The calculation parameters are selected according to the actual well test data, among which, the viscosity is 0.013 mPa s and the well diameter is 0.1 m. The permeability is 0.25 mD–3.74 mD according to the coalbed well gas test. The thickness of the coal seam is based on the actual test data of each well, and the critical desorption pressure and the bottom hole pressure are taken from the actual production data. The critical desorption pressure is the bottomhole flowing pressure when the gas comes to the surface of the wells. The results are shown in Fig. 3.

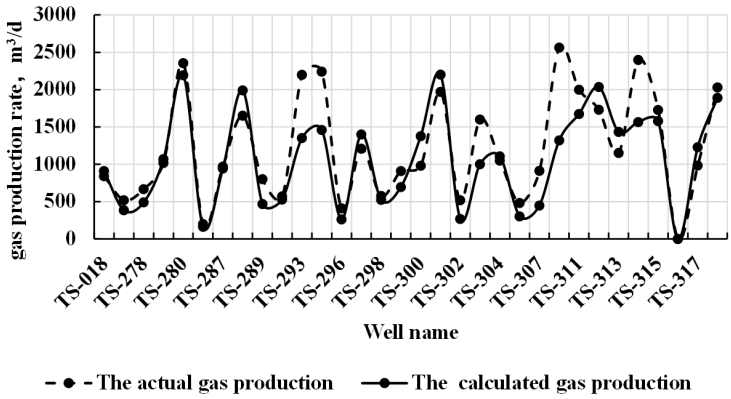

Fig. 3. Comparison between the theoretical gas production and the actual gas production in target area

The results show that 85 % of the predicted results are in good agreement with the actual mining data, with an average error of 10 % and a minimum error of less than 3 %. Therefore, it can be concluded that this model can be used to predict coalbed gas production. Some of the wells (15 %) have poor prediction of gas production. There are two main reasons accounting for this poor prediction. First, the permeability of coal seam is unclear, and the underground permeability cannot be truly reflected. Second, there is some error in the measurement of bottomhole flowing pressure.

Based on the capacity prediction model, the influencing factors of coal seam permeability, coal seam thickness, critical desorption pressure and bottomhole flowing pressure are analyzed respectively.

The results show that the gas production of coalbed methane wells increases with the increase of coal seam permeability, thickness and critical desorption pressure and there is a linear relationship between the permeability, coal thickness and gas production.

The critical desorption pressure is proportional to the gas production in terms of power function, i.e., with the increase of the critical desorption pressure, the daily production is increased.

However, the above-mentioned three parameters (permeability, coalbed thickness, critical desorption pressure) all are the attributes of coal seam itself, so it is difficult

to increase the production through the existing technology. Although the artificial fracturing technology can increase the permeability to a certain extent, its function is only limited to the range around the coalbed methane wells, and the secondary fracturing will not only increase the cost but also bring higher risk, so it is unlikely to adjust the coal seam permeability after the production. Therefore, the bottomhole flowing pressure becomes one of the important parameters to control the production of coalbed methane wells. Reducing the bottomhole flowing pressure can improve the gas production of coalbed methane wells and the bottomhole flowing pressure can be further reduced in the well site by the installation of pump hanging tools.

The calculation results show that the gas production of coalbed methane increases with the pressure drop of the bottom hole, and the increase rate is getting smaller and smaller. So, when the bottom hole pressure is high, reducing the bottomhole flowing pressure can get a larger increase in gas production.

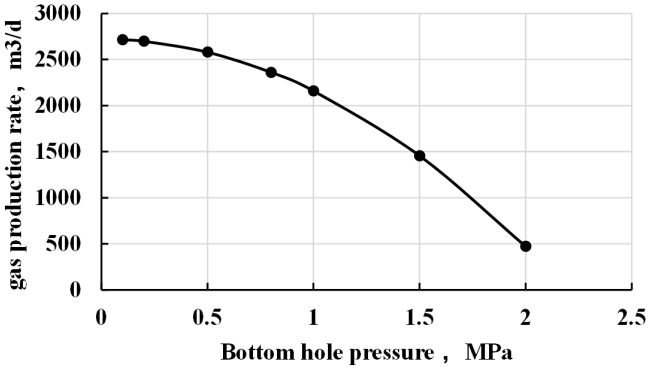

Fig. 4. Curve of coalbed methane production and bottomhole flowing pressure

Presently, there are some wells in the southeastern part of the Shizhuang South Block have installed pump hanging tools in their operation and the daily gas production has increased to a certain extent. The following figure shows the relationship between the bottomhole flowing pressure before the operation and the increase of gas production after installing the pump hanging tools. The results show that the larger the bottomhole flowing pressure is, the larger the growth rate is, which is in agreement with the theoretical results of this study. In order to obtain a better yield effect, it is suggested to select the coalbed methane wells with the bottomhole flowing pressure greater than 1.5 MPa t before installing the pump hanging tools.

4. Conclusion

Currently, there is no deep understanding on the prediction of coalbed methane production capacity. This paper establishes capacity prediction model of coalbed methane wells at stable production stage based on the classic theory of seepage and the special mining rule of coalbed methane. Based on the geological parameters of

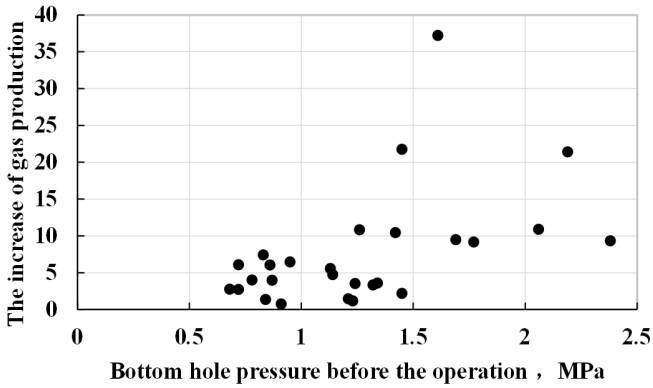

Fig. 5. Curve between the bottomhole flowing pressure and production increase with pump hanging tools of the coalbed methane wells in the target area

the southeastern part of the Shizhuang South Block, the gas production capacity of coalbed methane wells at stable production stage is calculated by the capacity prediction model, which is then compared with data produced by the numerical simulation and the data in the actual production. The results show that this model has good applicability. The influencing factors: permeability, coal seam thickness, critical desorption pressure and bottomhole flowing pressure, are analyzed separately by the capacity prediction model and the finding shows that the gas production of coalbed methane wells increases with the increase of coal seam permeability, thickness and critical desorption pressure, and decreases with the increase of bottomhole flowing pressure. The results of this paper provide a theoretical basis for the rational selection of wells and layers before the production and how to increase the coalbed methane production and keep it stable after production.

The results of this study are only suitable for the stable stage of coalbed methane wells, but the gradual decrease in coalbed methane production is also a relatively long stage in the coalbed methane development. So it is the future research direction to predict the production capacity of coalbed methane wells when the coalbed methane production is gradually decreasing.

References

[1] X. J. Shao, C. F. Wang, D. Z. Tang, Y. B. Sun, H. Xu: *Productivity mode and control factors of coalbed methane wells: A case from Hancheng region.* Journal of China Coal Society *38* (2013), No. 2, 271–276.

[2] S. A. Zhang, L. H. Cao, C. X. Du: *Study on CBM production mechanism and control theory of bottom-hole pressure and coal fines during CBM well production.* Journal of China Coal Society *39* (2014), No. 9, 1927–1931.

[3] D. M. Smith, F. L. Williams: *Diffusional effects in the recovery of methane from coalbeds.* Society of Petroleum Engineers *24* (1984), No. 5, 529–535.

[4] J. Q. Shi, S. Durucan: *Modelling laboratory horizontal stress and coal permeability*

data using S&D permeability model. International Journal of Coal Geology *131* (2014), 172–176.

[5] B. Yan, Y. Wang, J. E. Killough: *Beyond dual-porosity modeling for the simulation of complex flow mechanisms in shale reservoirs*. Computational Geosciences *20* (2016), No. 1, 69–91.

[6] Y. Fu, X. Guo, H. Long: *Productivity method of fractured horizontal wells in coalbed gas*. Journal of Southwest Petroleum University(Science & Technology Edition) *25* (2003), No. 3, 44–46.

[7] M. P. Yang, G. Wang, S. Y. Xu, C. Gao: *Steady flow productivity equation for stress sensitivity coal-bed methane gas well*. Natural Gas Geoscience (2011), No. 2, paper 023.

[8] A. Khanna, A. Keshavarz, K. Mobbs, M. Davis, P. Bedrikovetsky: *Stimulation of the natural fracture system by graded proppant injection*. Journal of Petroleum Science and Engineering *111* (2013), 71–77.

[9] X. D. Wu, G. Q. Wang, A. Li, X. Wang: *Productivity prediction of coal-bed gas wells*. Natural Gas Industry *24* (2004), No. 8, 82–84.

[10] Y. Deng, R. Huang, D. Guo, S. Zhang: *Affecting factors of coal-bed gas production and production prediction of unstable percolation*. Natural Gas Industry *25* (2005), No. 1, 117–119.

[11] B. X. Xu, X. F. Li, X. H. Hu, S. M. Hu: *Type curves for production prediction of coalbed methane wells*. Journal of China University of Mining & Technology *40* (2011), No. 5, 743–747.

Received September 12, 2017

Acta Technica *62* No. 2B/2017, 151–162

Design and implementation of automatic assembly software system based on machine vision

Yao Liying[1]

Abstract. At present, relative technology and research of high precision measurement and automatic assembly have attracted extensive attention. In this paper, optical measurement theory, image processing technology and visual positioning technology were used, and a precise part measuring and assembling system was set up. Then the image preprocessing algorithm was analyzed and compared, and a mixed distortion model considering radial distortion and centrifugal distortion was proposed. The camera calibration method was adopted, and the camera was calibrated, and thus the effect of camera lens distortion on measurement accuracy was reduced. In addition, an improved Canny algorithm combined with elliptic curve fitting algorithm was adopted, and the sub-pixel precision edges of the parts were extracted. And the accuracy of measurement and positioning were further improved, thus providing the basis for automatic assembly of parts. The experimental results prove that the system can meet the industrial requirements.

Key words. Machine vision, automatic assembly, distortion model.

1. Introduction

With the quickening pace of human life, mobile, portable, micro machinery and electronic equipment have become the mainstream. Most of these devices are made of tiny, precision parts, usually of micron size. At present, the measurement and assembly of most micro precision parts require manual micrometer or microscope, which greatly reduces the detection efficiency, and may damage parts, and is also very easy to cause eye fatigue, low efficiency. In addition, assembly personnel should have a certain professional knowledge, which increases the cost of product production, and assembly consistency is poor, and stability is low. Therefore, high precision micro size measurement and precise assembly method are required, so as to further improve the detection efficiency, and have important significance to the actual production. In recent years, machine vision has made great progress in quality inspection, size measurement, and object recognition and so on. Machine vision is a

[1]Mianyang Teachers' College, Mianyang 621000, Sichuan, China

multidisciplinary field, and requires the support of related fields such as biology, digital vision processing, and communication and so on. With the increase of computer processing speed, the research and development of algorithms, and the deepening of theoretical research, high speed and stable image processing and control system has been developed more and more, thus widening the applicable areas of machine vision.

2. State of the art

Machine vision technology abroad has developed earlier and has been widely studied and applied. Moreover, it has been heading for a higher rate of development, higher accuracy, unknown detection environment and diversified testing objects [1]. Machine vision technology was first used in the manufacturing industry in the United States. Through the analysis of the development of machine vision to all the applications now, in the world, there are: printed circuit board inspection field, automobile parts inspection field, parts defect field and agricultural products detection [2]. In China, the research and application of machine vision have been developing rapidly. Yue Xiaofeng and others have developed the automatic detection system of engine cylinder bore by using digital image processing algorithm and theory, and have achieved higher detection accuracy; Chen Yongguang and others have realized the defect edge morphology according to the gray morphological characteristics of wood and using threshold segmentation algorithm; Liu Xuefang has analyzed and compared two edge detection algorithms from the point of view of whether the edges are continuous or consistent, and has come to an ideal conclusion [3]; Zhang Xiaobo and others have developed automatic detection and classification methods which are independent of subjective factors and can quantitatively analyze the effect of detection; aiming at the defect detection, size measurement and analysis of aeroengine turbine blade, Cheng Yunyong and others have developed a nondestructive testing system based on CT technology [4]; according to the optimization theory, Ma Qiang and others have used affine transformation technology, and have studied the contour detection system based on machine vision; Feng Bin and others have studied the rapid processing algorithms for fruit morphology and defects, and have summarized the related techniques and theories [5].

3. Methodology

In order to realize the vision measurement and automatic assembly of the parts, the coordinate value of the target position and the central position of the assembly parts are required, and so two vision systems are needed in this paper. Moreover, the correct selection of visual system is the prerequisite and guarantee for subsequent image processing. Through the correct selection of the visual system, image acquisition can be carried out and high-quality images will be obtained. Thus the difficulty of image preprocessing can be reduced, so as to facilitate the extraction of image features, and ultimately to reduce visual measurement errors and assembly

errors (Ma et al. 2004) [6]. The visual hardware system is mainly composed of industrial cameras for photographic imaging, lenses for changing light paths, and light sources providing illumination. The selection of these three kinds of vision acquisition hardware is analyzed.

Industrial cameras can obtain more stable images, and can transmit image signals quickly while resisting external interference. At present, the industrial camera's photosensitive sensors include CCD or CMOS sensors. In the process of image acquisition, the CCD camera firstly performs photoelectric interchange, stores the obtained charge, and then realizes the transmission of the electrical signal through the charge movement, and finally reads the signal. The CCD sensor is a typical imaging sensor with charge as signal [7]. CCD is not easy to be burned in the process of imaging, with fast response, no delay and low working power. With the development of large-scale integrated silicon manufacturing process, CMOS sensors are also developing rapidly. In the process of CMOS imaging, the weak image signals are modulated and transformed, and the digital signals are analyzed and processed on the signal processor, and finally the image signals are output. CMOS sensors can integrate photosensitive devices and processing circuits on small chips. Its power is small, and the speed of signal transmission is fast, thus becoming the first choice for users.

The camera lens acts on the camera just as the lens does to the eye, which enables the object to be imaged clearly on the image sensor. When the lens is imaged, there may be aberrations that can affect the quality of the image, which can make the beam of light unable to meet the spherical aberration at the same location of the main axis, and sharp points, astigmatism can't be formed on the ideal plane. Therefore, it is necessary to select the proper parameters of the lens according to the environment and object of the lens, so as to reduce the aberration effect on output image [8]. Generally, it is necessary to judge the industrial lens selection according to the resolution, the maximum relative aperture, and the depth of field. Resolution reflects the extent where the lens senses the detail, and the depth of field reflects the extent of the spatial depth range in the image plane, and the maximum relative aperture location reflects the degree of illumination of the lens. Since the assembled parts may vary in thickness, if the zoom lens is used, the measurement plane of all parts can't be guaranteed on the focal plane. Two telocentric lenses were selected in this paper, in which, the magnification of the lens used to determine the center of the component was 0.2, the focal length of the object was 118 mm, and the view size was $15\times20\,\mathrm{mm}^2$; the magnification of the lens having the position of the assembly target was 0.34, the focal length of the object was 113 mm, and the view size was $33\times36\,\mathrm{mm}^2$.

In the vision system, the light source plays an important role in guaranteeing the quality of the image. Choosing the appropriate light source can improve the contrast between the target and the background, and provide convenience for feature extraction and analysis. Common light sources are shown in Table 1.

Depending on the visual system, the incident angle of the light source can be different [9]. When the angle between the illumination direction and the target is small, the contour of the object to be measured can be displayed better; when the

angle between the illumination direction and the target is larger, the brightness of the image is higher, which is used for the illumination of the object with more rough surface; when illuminated from multiple angles, the image is softer and used to detect curved surfaces; when the backlight is illuminated, the object is black and the surface details of the object can't be seen, so that the size of the object to be measured is detected; and when the light is irradiated by the coaxial light, the light is uniform, and the utility model is suitable for detecting the defect of the surface of the object.

Table 1. Performance comparison of four kinds of light sources

Light source	Fluorescent lamp	Halogen lamp	LED lamp	Laser
Lifetime (h)	5000–7000	5000–7000	6000–10000	more than 10000
Brightness	bright	bright	bright	very bright
Response speed	slow	slow	fast	fast
Other features	less expensive, less fever	less expensive, more fever	less expensive, less fever	good quality and low power consumption

In traditional camera calibration methods, the size of calibration objects must be known. By establishing the relative relation of the points in the two coordinate systems, the internal parameters that reflect the property of the camera itself and the external parameters that can reflect the spatial position of the camera can be obtained according to the related algorithms. And the calibration object can be two-dimensional or three-dimensional [10]. Since the former is easy to manufacture and preserve, the method of calibrating multiple images from different angles is used to find all the parameters. When the requirement of the application is higher and the camera parameters do not change frequently, the traditional camera calibration method can achieve higher calibration accuracy. The calibration method of self-calibration camera is a very flexible calibration method. It can be calibrated according to the image of the object which is used to determine the motion information. Table 2 shows the comparison of the three classes of calibration methods in four ways.

When assembling precision parts, it is necessary to determine whether the assembly is qualified according to specific technological requirements, technical requirements, and through inspection. In this paper, the process and technical requirements for the assembly problem are based on the thickness of the parts. There are three kinds of parts to be assembled. The first class includes the base and nut, and the second class consists of metal parts, including parts 3, parts 4, parts 7, and the third kind is quartz flake. Moreover, the second and third kinds are round.

The mathematical model for the problem is as follows: the thickness of the part 5 which is assembled in a set is x_{1j}, the number of slices is e, the thickness of part 6

is x_2, the thickness of part 3 is x_3, the thickness of part 4 is x_4, the thickness of part 1 is x_{5k}, the number of pieces outside the part 3 is a, the number of pieces outside the part 4 is c, the thickness of part 2 is x_{6l}, the number of pieces outside the part 3 is b, the number of pieces outside the part 4 is d, the thickness of part 7 is x_8.

Table 2. Comparison of three calibration methods

Calibration method	Accuracy	Calibration process	Dependence on device	Dependence on calibration objects
Traditional calibration method	high	tedious	low	high
Active vision method	higher	more complicated	commonly	commonly
Self-calibration method	low	simple	high	low

If the ith suit is qualified, then $y_i = 1$; if the ith suit is not qualified, then $y_i = 0$. The model consists of six following equations:

$$1.02 < x_3 - \left(\sum_{k=0}^{a} x_{5k} + \sum_{l=0}^{b} x_{6l}\right) < 1.15\,, \tag{1}$$

$$1.02 < x_4 - \left(\sum_{k=0}^{c} x_{5k} + \sum_{l=0}^{d} x_{6l}\right) < 1.15\,, \tag{2}$$

$$4 < \sum_{j=1}^{e} x_{1j} + x_2 + x_3 + x_8 + x_4 < 4.1\,, \tag{3}$$

$$1.57 < \left(\sum_{k=0}^{a} x_{5k} + \sum_{l=0}^{b} x_{6l}\right) < 1.61\,, \tag{4}$$

$$2.05 < \left(\sum_{k=0}^{c} x_{5k} + \sum_{l=0}^{d} x_{6l}\right) < 2.12\,, \tag{5}$$

$$y_i = \begin{cases} 1, i \text{ sets of assembly qualified,} \\ 0, i \text{ sets of assembly unqualified.} \end{cases} \tag{6}$$

The objective function is

$$f_{\max}(y) = \sum_{i}^{4} y_i\,. \tag{7}$$

Aiming at the precise parts which make up the precision products, the require-

ments of high-precision measurement and automatic assembly are achieved, a high precision measurement and automatic assembly system is designed, and an experimental prototype is built. The overall block diagram of the system is shown in Fig. 1.

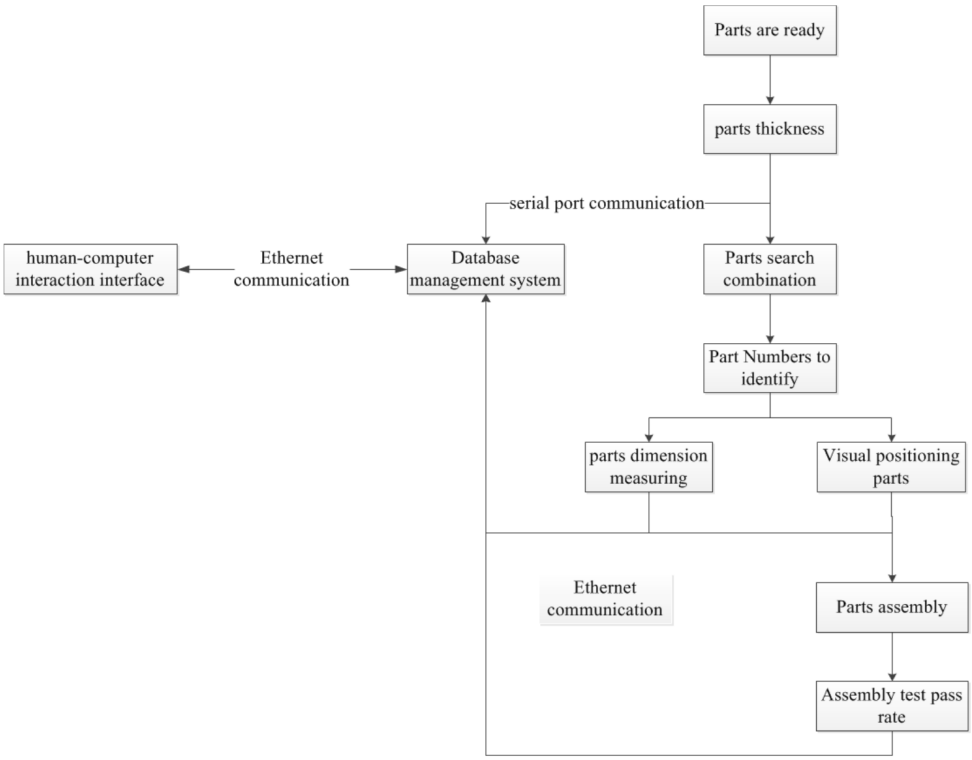

Fig. 1. Overall block diagram of the system

As can be seen from Fig. 1, the overall design of the prototype includes software system design and hardware system design. The software system design mainly includes: the visual system program design, combination search algorithm design, character recognition program design, program design, database management system and communication system design and human-computer interface design; the hardware system design includes: the mechanical structure design, the origin of the manipulator, and the establishment of the tool coordinate system.

Mechanical structure design is the basis of the whole system design. The machining and installation accuracy of the mechanism will directly affect the realization of the system function. And perfect and reasonable mechanical structure can reduce the difficulty of software system design and make the whole system more stable. The three-dimensional appearance of the experimental prototype of the system designed in this paper is shown in Fig. 2.

The main mechanical structure of the prototype is as follows:

Feed mechanism: the mechanism consists of a tray for placing precise parts, a

parallel guide rail, and a servo motor that drives the tray into and out of the assembly space, and is used to deliver the assembly parts to the measuring and assembling stations.

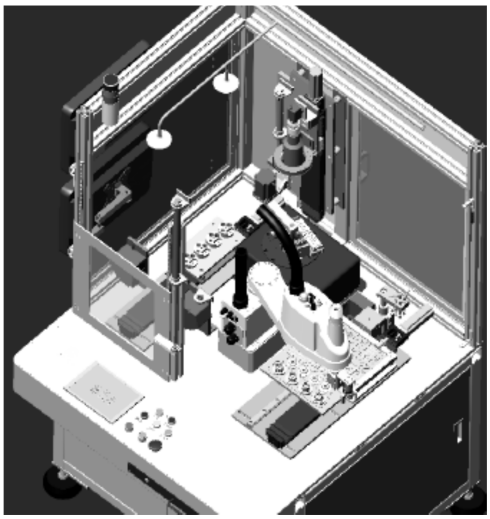

Fig. 2. 3D appearance of the prototype

Discharging mechanism: the discharging mechanism is composed of a servo motor, a discharging tray and a sealing guide rail, a finished product is arranged on the discharging tray, the adjusting nut is used to adjust the levelness of the tray, and the pallet level is guaranteed as much as possible, and the specifications and models of the servo motor are the same as that of the feeding mechanism. In the process of finished product delivery, the qualified rate of the finished product is tested. In order to meet the requirements of non-contact measurement of polishing parts and parts with surface topography requirements, Keyence high-speed and high-precision CCD measuring instruments are selected. Through servo drive system, the finished product is controlled by the detecting device in turn. The system will obtain the height of the finished product, so as to determine the qualified rate of the assembly.

Thickness measurement mechanism for precision parts: the measurement of the thickness of precision parts is the premise of assembly. In assembly, the search combination of parts is based on the thickness of the parts superimposed, and the thickness measuring device is mainly composed of a rotating cylinder, a magnetic grating ruler, a thickness gauge and a measuring platform.

Part holding mechanism: the part holding mechanism is used to measure and assemble parts during the process of parts measurement or assembly. In this paper, there are three kinds of parts to be taken, so the clamping mechanism of the parts must be multi-functional, and the three parts can be taken out. For different parts of the different ways to grab, the three point air is used to claw the base, and then parallel finger driven U card groove is used to take the nut. Finally, the vacuum suction head is used to absorb the precision sheet parts. There are four metal vacuum suction heads, and the vacuum suction is the maximum -101 kPa vacuum generated

by a vacuum generator.

Nut tightening mechanism: tightening the nut on the base is the last step in the assembly process. Before tightening, the assembly shall be pressed with a pressure bar to prevent the shift of the parts.

4. Result analysis and discussion

According to the above research results, the final experimental prototype is shown in Fig. 3.

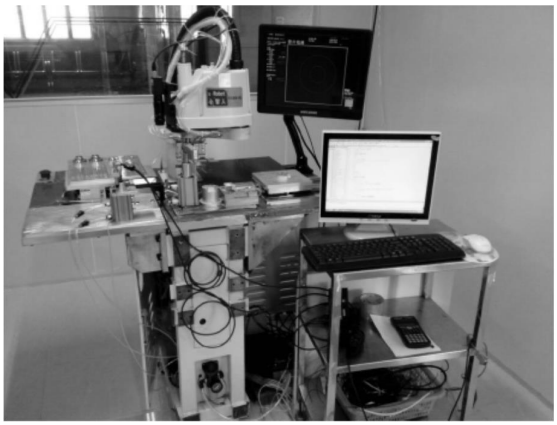

Fig. 3. Sample drawing of experimental prototype

In the system studied in this paper, the two processes of measurement and assembly should be completed. The high precision measuring procedure refers to the measurement of the outer diameter of each precise circular part, and the measuring accuracy is 0.01 mm. In order to verify the accuracy of the system for measuring the diameter of parts, measurements were made on the components of the 1 set of ligands. In each package, in addition to the base, nuts, and parts 8, the different parts in the 7 also remained to be measured, and each part was measured 10 times. The concrete steps are as follows:

Firstly, a part was repeatedly taken to the camera position, so as to obtain the part image.

Secondly, the target image was pretreated.

Thirdly, the sub-pixel outer diameter edge was extracted from the preprocessed image, and the outer diameter pixel size was obtained, as shown in Table 3.

Fourthly, the internal and external parameters of the camera were obtained by calibrating the camera, and the actual size of the outer diameter in the world coordinate was calculated. The measurement results are shown in Table 4.

According to the camera calibration, the imaging model was established and the distortion model was considered. The internal and external parameters of the camera were calculated, and the outer diameter results in pixels were converted to the actual size results in mm.

Table 3. Measurement results of outer diameter of parts (unit: pixel)

	Part 1	Part 2	Part 3	Part 4	Part 5	Part 6	Part 7
1	653.27	615.04	672.41	433.82	542.36	622.41	667.64
2	653.54	615.36	672.54	433.95	452.50	622.32	667.41
3	653.41	615.17	672.36	433.73	452.59	622.23	667.36
4	653.09	615.27	672.18	434.00	452.45	622.45	667.59
5	653.23	615.45	672.27	433.86	452.41	622.18	667.50
6	653.14	615.09	672.14	433.73	452.54	622.00	667.54
7	653.45	615.32	672.41	433.68	452.68	622.14	667.77
8	653.00	615.18	672.59	433.91	452.64	622.09	667.73
9	653.27	615.41	672.50	434.10	452.36	622.50	667.36
10	653.32	615.23	672.23	433.95	452.18	622.32	667.45

Table 4. Measurement results of outer diameter of parts (unit: pixel)

	Part 1	Part 2	Part 3	Part 4	Part 5	Part 6	Part 7
1	14.372	13.531	14.793	9.544	9.952	13.693	14.688
2	14.378	13.538	14.796	9.547	9.955	13.691	14.683
3	14.375	13.533	14.792	9.542	9.957	13.698	14.682
4	14.368	13.536	14.788	9.548	9.954	13.694	14.687
5	14.371	13.540	14.790	9.545	9.953	13.688	14.685
6	14.369	13.532	14.787	9.542	9.956	13.684	14.686
7	14.376	13.537	14.793	9.541	9.959	13.687	14.691
8	14.366	13.534	14.797	9.546	9.958	13.686	14.690
9	14.372	13.539	14.795	9.551	9.952	13.695	14.682
10	14.373	13.535	14.789	9.547	9.948	13.691	14.684
Average value	14.372	13.536	14.792	9.545	9.954	13.690	14.686

According to the above table, the standard deviation of the average value of the outer diameter of the 7 parts was obtained. The result is shown in Table 5.

Table 5. Average deviation of parts outside diameter (unit: mm)

Parts category	1	2	3	4	5	6	7
Standard deviation (‰)	3.7	3.1	3.4	3.1	3.3	3.6	3.2

Available from Table 5, in measuring the diameter of the 7 parts, the maximum standard deviation was $\sigma_{1\,\max} = 0.0037$ mm.

In order to further validate and calibrate the visual measurement accuracy, in this paper, the 0 stage length standard block was used for calibration, and the length limit deviation was 0.14 m. The visual measurement method was adopted, and the standard blocks of nominal length 15 mm, 14 mm, 13 mm, 12 mm, 11 mm, 10 mm and 9 mm were measured respectively. And each standard block was measured 10 times. The measurement results are shown in Table 6.

The standard deviations of the 7 standard blocks were calculated. The results

were shown in Table 7.

Table 6. Measurement results of standard blocks (unit: mm)

	Block 1	Block 2	Block 3	Block 4	Block 5	Block 6	Block 7
1	9.002	10.001	11.002	12.002	12.999	14.002	15.001
2	9.002	10.002	11.003	12.004	12.998	14.004	15.004
3	9.001	10.004	11.004	12.002	12.997	14.002	15.002
4	9.003	10.000	11.000	12.003	12.996	14.003	15.003
5	8.999	9.999	11.002	12.001	13.000	14.002	15.003
6	9.001	9.998	11.003	12.003	13.001	14.001	15.001
7	8.999	10.003	11.003	12.004	12.998	14.002	15.002
8	9.004	10.002	11.004	12.002	12.997	14.002	15.004
9	9.003	10.004	11.002	12.001	12.997	14.003	15.001
10	9.003	10.003	11.004	12.004	12.996	14.003	15.003

Table 6. Average deviation of parts outside diameter (unit: mm)

Standard block	1	2	3	4	5	6	7
Standard deviation (‰)	2.3	2.5	2.9	2.0	2.6	2.2	2.6

Available from Table 7, through the method of visual measurement in this paper, the maximum standard deviation of the standard block length was $\sigma_{2\max} = -0.0029$ mm. For measuring the precision parts, the maximum standard deviation of the parts' outer diameter measurement value relative to the parts' true value was set as $\sigma_{\max}$, where $\sigma_{\max} = \sigma_{1\max} + \sigma_{2\max} = 0.0066$ mm, thus meeting the industrial requirements.

5. Conclusion

In this paper, the precision measurement and automatic assembly system of precision parts based on machine vision was studied. Then software system design, related algorithm design, and visual system hardware design were completed. And the problem of measurement and assembly in automated production of precision electromechanical products was solved. The results of this paper were obtained as follows: the edge detection algorithm based on pixel precision was analyzed and compared; through the algorithm simulation, the detection effect of each detection algorithm was obtained; on this basis, the method of improving Canny edge detection algorithm was proposed, and the best edge extraction effect of the improved algorithm was proved; then, the sub-pixel edge detection algorithm was analyzed, and a sub-pixel edge detection algorithm was proposed according to the shape characteristics of the detected part; in addition, an improved Canny edge detection algorithm was used to obtain the pixel precision edge, and then the sub-pixel edge was obtained by ellipse fitting method. The experimental results show that the measurement and assembly system in this paper can achieve the measurement accuracy of 0.0066 mm, as well as the assembly accuracy of coaxiality of 0.017 mm. Both of the measurement

accuracy of 0.01 mm and the coaxial assembly accuracy requirements of 0.05 mm for industrial design can be achieved. Of course, there are still some shortcomings in the process of system research and design, which need further studies. For example, the calibration process of the camera calibration algorithm used in this paper is done manually, and it is tedious.

References

[1] H. Golnabi, A. Asadpour: *Design and application of industrial machine vision systems.* Robotics and Computer-Integrated Manufacturing *23* (2007), No. 6, 630–637.

[2] S. Li, Y. Tan: *Image fully thinning algorithm based on spanning tree.* Computer Engineering and Design (2006), No. 21, paper 015.

[3] D. J. Lewis, J. O. Michelini, O. J. Cullen, J. D. Russell: *Electromagnetic valve control in an internal combustion engine with an asymmetric exhaust system design.* Patent US 7031821 B2 (2006).

[4] Y. Chen, S. G. Wang, G. C. Chen: *Development of static characteristic automatic testing system about brake valves of automobile.* Journal of Chongqing University *29* (2006), No. 1, 19–21.

[5] Y. Zhang, J. Han, X. Fu, H. Lin: *An online measurement method based on line laser scanning for large forgings.* International Journal of Advanced Manufacturing Technology *70* (2014), Nos. 1–4, 439–448.

[6] W. Tang, D. Ye, F. Yuan, G. Chen: *Independent distortion correction algorithm in vision measurement system.* Journal of Optoelectronics.Laser *24* (2013), No. 2, 308–315.

[7] Y. Xichen: *Laser processing robot and its industrial applications.* Chinese Journal of Lasers (2009), No. 11, paper 001.

[8] Y. Zhang: *Automatic inspection of industrial sheetmetal parts with single non-metric CCD camera.* International conference on Advanced Data Mining and Applications (ADMA), 22–24 July 2005, Wuhan, China, Springer-Verlag Berlin, Heidelberg (2005), 654–661.

[9] R. Duan, H. Duan, Q. Li, Y. Li, Z. Yang: *Micro-assembly auto-focusing system based on image processing.* Optics and Precision Engineering (2006), No. 3, paper 023.

[10] S. Yi, R. M. Haralick, L. G. Shapiro: *Automatic sensor and light source positioning for machine vision.* IEEE International Conference on Pattern Recognition, 16–21 June 1990, Atlantic City, NJ, USA, IEEE Conference Publications *70* (1990), 55–59.

Received August 7, 2017

Acta Technica *62* No. 2B/2017, 163–172

Water quality model for the influence of riparian materials on the purification ability of riverine organic pollutants[1]

He Fei[2,3], Xie Yufeng[2], Liu Aiping[2], Hang Xiaoshuai[2], Li Weixing[2], Gao Jixi[2]

Abstract. Because China has only focused on economic development but ignored environmental protection in the past few decades, which has caused serious water pollution and water shortage in China. Rivers are flooded with all kinds of pollutants, including organic pollutants. In this paper, the construction of water quality model for the influence of riparian materials on the purification ability of riverine organic pollutants was studied. The present situation of water pollution in China was first introduced, and then the process of constructing water quality model which affected the purification ability of organic pollutants was studied, finally, the water quality model was established for ecological river course. Correlation analysis shows that organic pollutants are similar to model parameter coefficients, and the model can accurately reflect the overall purification ability of riparian materials to organic pollutants in water.

Key words. River water quality model, organic pollutants, riparian materials, ecological river course.

1. Introduction

In recent years, the importance of river ecology has been widely recognized, concept of river hardening has been abandoned gradually, and the ecological river channel has been introduced into the river improvement project, more attention has been paid to the study of quality of river water in rivers and streams, and the results have showed the influence of ecological river channel mechanism. However, there is little research on riparian water quality models, and there is no reliable

[1]The work presented in this paper is supported by Major Science and Technology Program for Water Pollution Control and Treatment(2014ZX07503-004) and Basic Research Project for State Level Public-benefit Research Institutes (20160405).

[2]Nanjing Institute of Environmental Sciences, Ministry of Environmental Protection, Nanjing 210042, Jiangsu, China

[3]Corresponding author

mathematical model to explain the impact of riparian resources on water quality. The mature water quality model can be used to simulate the characteristics and rules of water pollutants migration and transformation, and study the influence of pollutants on water quality development. According to the mechanism of river bed degradation affecting organic pollutants in water bodies, the river water quality model issued by the International Water Association was simplified, and the river water quality model was simplified to simulate the different ecological processes. In addition to the degradation of organic pollutants, references can be provided for water environment pollution control planning and decision analysis to improve the existing river water quality model, and evaluate the ecological effects of rivers.

2. State of the art

Ecological restoration of rivers refers to the restoration of rivers by means of integrated methods, resulting in the loss or degradation of natural functions [1]. At present, the ecological restoration methods at home and abroad are mainly physical methods, chemical methods and biological ecology methods, some successes in pollution control of rivers are achieved. Physical means mainly refers to sediment dredging, machinery, algae and so on, this method can quickly deal with the eutrophication of rivers in the short term, however, because the process of pollutants itself will not degenerate and transform, this method is often used to cure and cannot completely improve the water environment [2]. Chemical methods, such as condensation, precipitation, chemical removal of algae, the chemical method is faster than the physical remediation method, and the operation is more convenient [3]. But a lot of drugs can cause damage to rivers in other organisms, causing two pollution, the repeated use of drugs can cause resistance to water in algae and affect treatment outcomes [4]. In recent years, the method of biological ecological restoration is a fast developing new technology, and it is also one of the hot spots of scholars at home and abroad [5]. The purpose is to realize purification pollution of the river water by using the water purification facilities in the river space with the advantages of good effect, low cost, low energy consumption and low running cost. The viewpoint of ecology and ecological restoration technology is starting from the overall optimization of the ecological system to gradually restore damaged ecosystems, improve water purification capacity, improve the water quality of the environment, and establish a healthy aquatic ecosystems [6]. Usually the cultured plants or inoculated microorganisms are used for life activities; pollutants in the water are transferred, transformed and degraded so that water can be purified. Ecological restoration of landscape water technology includes: channel aeration technique, microbial enhancement techniques (bacteria), biofilm technology and biological contact oxidation process, constructed wetland technology, pond stabilization techniques and aquatic phytoremediation techniques.

3. Methodology

It is generally believed that rivers are naturally flowing water that has a considerable amount of water on its surface or perennial or seasonal. Some scholars believe that the urban river water environment covers the city's linear water (natural rivers, artificial channels, and moat) and the composition of the water cycle space. Compared with natural rivers, urban rivers and regional human activities interact greatly [7]. On the one hand, the region's healthy rivers provide a variety of services for socio-economic activities [8]. On the other hand, the river water, water cycle, water quality, health conditions are also affected by high-intensity social and economic activities. With the rapid growth of population and the rapid development of economy, more and more pollutants are discharged into rivers, much more than the self-purification capacity of rivers [9]. In addition, due to changes in environmental conditions, river pollutants enter the river bed sediments, with the river water temperature, change of pH and biodegradation, the function of water flow back to the river makes it difficult to control the source of pollution, the concentration of dissolved oxygen in highly polluted river water is very low, or even zero, which causes the smell of rivers, or even massive death of fish, and seriously damages the river's ecosystem. The specific pollution phenomenon is shown in Fig. 1.

Fig. 1. Current situation of organic pollution in rivers

The total amount of industrial wastewater and domestic wastewater has reached more than 5000 tons, and many rivers have become the retention areas of sewage [10]. The total length of rivers in the United States is about 420 thousand km, accounting for about 29 % of the river pollution. The content of pesticides, phenol, arsenic, mercury, and chloride in the famous Mississippi River far exceeds the required standard, the turbidity and the smell of black of the river lead to the extinction of many aquatic animals. Half of the main river suffers serious damage, and rare shrimp is near extinction due to serious water pollution. Rivers in China are also seriously polluted. According to China's environmental status bulletin issued by the State Environmental Protection Administration in 2012: the pollution cross section ratio of Yangtze River, the Yellow River, the Pearl River, Songhua River, Huaihe River, Haihe River, Liaohe River, Zhejiang Minji River, Northwest River and Southwest River was about 20.9, rivers in China's cities were experiencing a series of environmental problems with the rapid development of cities. At present, more than 80 % of the city's rivers are polluted. The problems of water pollution and ecological degradation in China's urban rivers highlight the deterioration of the water quality and even the stench of life, water ecology is seriously degraded and even destroyed, the dike art and river geometry, urban flood, and river landscape are greatly hurt. In short, urban rivers in China are faced with a variety of environmental problems, as shown in Table 1.

Table 1. Results statistics of watershed segmentation

The impact of accelerated urbanization	With the accelerated pace of urbanization, a large number of industrial waste water and some domestic sewage are discharged directly (or not up to standard) to the river without treatment, resulting in serious pollution of water quality, and COD, BODS, ammonia nitrogen, total nitrogen and total phosphorus exceed the standard.
The effect of one-sided pursuit of function	In the process of urban construction, only the flood control function of the river channel or the beautification function of the river channel are taken into account, but the resources functions and ecological functions of the river course are ignored, bending and straightening, stone revetment and high building are adopted.
The influence of river bank hardening on channelization	Many of the city's black odor rivers covered the underground river, the hardening and channelization of the river banks lead to the loss of water space, which reduces the habitat of aquatic organisms and has many negative impacts.

In this paper, RW QM 1 model is studied. The components involved in the RW QM 1 model are complex, and their mathematical models are more complex, and it is difficult to apply the full model directly to practice. Therefore, the RW QM 1 model is simplified for the problems that need to be addressed in this study. Preliminary studies show that riparian substances have important effects on microbial

biomass and enzyme activities, which will affect the enzyme activities of microbial biomass and key biochemical reactions such as nitration, and affect the degradation of organic pollutants in rivers. Therefore, it is assumed that the degradation process of organic pollutants is only related to suspended bacteria, the effects of algae and plankton are ignored. Based on the RW QM 1 model, it is necessary to establish a solution containing biodegradable dissolved organic matter, and seven components and six biochemical reactions such as heterotrophic bacteria, ammonia nitrogen, nitrite nitrogen, nitric acid nitrogen, dissolved inorganic phosphorus, and dissolved oxygen. River biochemical reaction model is simplified. S-RW QM 1 control equation is selected for the continuous mixing reaction tank (CSTR)

$$\frac{\partial c}{\partial t} = \frac{Q}{V}(c - d)\,, \tag{1}$$

where Q is the influent flow, V is the volume of the reach, c is the concentration of the influent concentration, and d is the component effluent concentration. The upper formula is the rate equation of component transformation process.

Organic pollutants are characterized by TOC, in RWQM 1 model, COD is expressed as organic matter, and the RWQM 1 model is used to classify COD components. The model converts conventional COD data into component data that meets the model requirements. TOC COD Total organic carbon (TOC) is an indicator of the total amount of organic matter in carbon bodies. Chemical oxygen demand is the amount of oxidant consumed by the reducing substance in the water that is easily oxidized by the strong oxidizing agent; the results are expressed in terms of oxygen content. In the river body, the composition of the reducing material is relatively stable, or the proportion of inorganic reducing substances in COD is small, the change is not enough to cause the linear relationship between COD, TOC and COD can be used, TOC data can enter the model's available COD data. In the present study, the experiment was conducted with water obtained from the new port of Guangzhou; the TOC content of the river was stable at 21.01 to 24.99 mg/l, COD and TO were used to analyze six batches of water samples, content of organic pollutants in experimental water. The results of linear regression analysis, detection and regression analysis are shown in Table 2 and Table 3.

Table 2. Content of organic pollutants in experimental water

TOC	COD1
20.03	23.63
20.39	24.58
20.83	29.63
20.64	31.25

Due to the lack of simple and effective heterotrophic bacterial methods, hypothesis modeling was commonly used in model simulations. In this study, COD accounted for 10 % of the total COD. The reduction rate of COD in the experimental water body reached 94 %, and the inert organic matter S was 6 % of the total COD.

The content of ammonia nitrogen in the experimental water was 0.41∼0.54 mg/L, the content of nitrate nitrogen was 1.04∼1.35 mg/L, content of nitrite nitrogen was 0.11 to 0.18 mg/L, the proportion of organic nitrogen that accounted for 80 total phosphorus percentage was neglected, with a content of 0.45 to 0.54 mg/L.

Table 3. Linear regression analysis of TOC and COD

R	Standard error	P	Regression constant	Regression coefficient
0.8536	0.2363	0.0086	15.3665	0.5693

The model stoichiometry and kinetic parameters used in this study were based on the typical values given by the International Water Association (IWA) as the initial values of the simulations. Sensitivity analysis was used to analyze the effect of parameter variations on the results. According to the hydrophilicity of different riparian materials, it can be seen that microbial biomass and adjustment of MK/UQ value can affect the kinetic parameters of simulated COD values and improve the accuracy of simplified RW QM 1 model. The sensitivity was calculated by the formula

$$S = \frac{Y - X}{X}, \tag{2}$$

where S is the sensitivity and Y, X are the concentrations of components before and after the change of kinetic parameters. When S is greater than 1, the parameter values have a great influence on the computation results of the model components.

The ecological riparian based on the ecological characteristics is the main ecological problem of riparian. According to the basic principle of ecology, the river construction of ecological riparian comprehensive evaluation index and evaluation method was discussed, and some technical extension systems of urban ecological riparian construction in the middle reaches of the Yangtze River were summarized. Most ecological riparian ecological problems are mainly reflected in the destruction of ecological balance, low plant diversity, river heterogeneity decreased in the case of serious water pollution. The principle of ecological river bank planning should not only follow the principles of nature and rational allocation of plants to avoid biological invasion, maintain sustainable development and unity, but also increase the riparian hydrophilic space, strengthen the comprehensive management of rivers, parks and surrounding parks, and form distinctive waterfront landscape according to the natural characteristics of the original river bank and ecological problems. In the ecological river bank planning and construction, the engineering measures and plant measures should be organically integrated. Species and communities are the main considerations for the restoration of aquatic vegetation in the construction of riparian ecosystems. Selection of species and allocation of community are one of the key factors for the success of vegetation restoration. The choice of pioneer species is to screen species that are tolerant and adapted to river water quality as a pioneer species in restoration of aquatic plant communities on the basis of biological characteristics and pollution tolerance of aquatic plants, at the same time, community species are provided for the restoration of communities. In combination with

domestic and international studies on the ecological management of aquatic plants in lakes and rivers, the pioneer species of aquatic plant communities should comply with the following principles. The ecological disasters caused by improper species selection have many precedents in China, the ecological safety of species is considered, in principle, it's generally possible to consider local or existing species or historical species (including the introduced species that grow safely) as pioneer species and constructive species. The selected species should have better adaptability to climate and water temperature in the river basin, plants with strong reproductive ability, resistance to wind and waves, low transparency requirements, and adapted to the survival of deep water are selected. In the process of water ecological restoration, there are many adverse habitats such as high pollution load, large phytoplankton reproduction and single spatial structure of communities. Therefore, pioneer plants must have a strong ability to resist pollution, survive and grow in harsh polluted water bodies, and form a fixed community.

Plant design has been applied to native trees. The banks of the park will be divided into different functional departments. Upstream can be designed for use in water management areas, water management area retains the original dike foundation and returns along the road, the original vertical embankment can be used to enter the planting pool, at the side of the dam, hydrophilic area is designed in high cruise terminal, the hydrophilic area retains the original cement embankment foundation and returns along the road, the planting area is formed in the original vertical embankment slope soil, and pebbles are laid on the embankment to form a hydrophilic interface, the water level is above the water level platform. The lower reaches are designed as play areas, the iris is planted to form obstacles of wind and waves, the original pieces are transformed into embankment to reduce the slope of the river bank and form a gentle slope, lawns and local plants are planted, visitors can close hydrophilic footprint of low water network at the interface of water, as the scene designed in Fig. 2.

4. Result analysis and discussion

The content of lipid, metabolic state and organic pollutant of microorganisms in the experimental water was simulated at the end of the river circulation. The results show that microbial biomass, dehydrogenase, fluorescein, ethylidene diacetate and nitrate reductase activities are significantly different under the influence of different river bed materials. The enzymes involved in microbial, nitrifying, and other key biochemical reactions differ in their activity, so that degradation of organic pollutants in rivers is different. The mole ratio of methyl naphthoquinone and ubiquinone can reflect the metabolic state of microorganism, the higher the ratio is, the more pronounced anaerobic metabolism will be. From the experimental results, it is can be seen that the better the hydrophilicity of the riparian materials is, the higher the microbial biomass will be, and the lower value of the aerobic metabolism is, the higher the degradation rate of organic pollutants will be. The characteristics of the West Jinye filler affect the growth of microorganisms on their surfaces. In the three fillers of Gebin Bank, the pebbles are porous, the most sediment in the

Gobbin structure can provide the largest surface area for microorganisms, and is more conducive to the growth and reproduction of microorganisms. The larger microbial biomass per unit volume of filler leads to higher dehydrogenase activity, resulting in a strong degradation of organic pollutants. It can be seen that the kinetic parameters which affect the biodegradation of organic compounds in the COD component of RW QM 1 are microbial biomass. According to the results of microbial biomass, MK/UQ and sensitivity analysis, the constants of aerobic growth rate of heterotrophic bacteria and the constants of aerobic absorption rate of heterotrophic bacteria were investigated respectively; the simulation accuracy was improved by constant value calculation. The results are shown in Table 4.

Fig. 2. Ideal state after processing

Table 4. Results of simulation calculations

Category	Material	End time of the run cycle	Simulated value after check	Fractional error
Riparian materials	Permeable brick	60.36	57.36	–2.36
	Pine wood chips	46.36	59.36	–3.35
Gabion revetment	Granite	17.86	17.56	5.36
	Pebbles	12.96	16.34	6.31

After adjusting the kinetic parameters, the relative error between the COD simulation value and the measured value during the operation of the river channel was

small. Model parameters and the content of microbial lipids, and the relationship between MK/UQ molar ratio and organic pollutant were analyzed. Correlation analysis shows that microbial index is highly correlated with organic matter and riparian matter; it is consistent with the degradation of organic pollutants in rivers. Therefore, the model can reflect the influence of riparian substances on the purification ability of organic pollutants in water, and simulate the degradation of organic pollutants in rivers.

5. Conclusion

In this paper, in view of the degradation mechanism of organic pollutants in the water body, the river simulation results of "simplified river water quality model 1" (S-RW QM 1) based on river water quality model 1 (RW QM 1) were established to simulate the process of biochemical reaction and degradation of organic pollutants in riverbed. After adjusting the relative parameters, it can be found that the relative error of COD simulation is small; S-RW QM 1 has good simulation results. In addition, sensitivity analysis of the kinetic parameters indicates that the parameter affecting the COD fraction simulation is molar ratio. According to the influence of riparian resources on microbial biomass and metabolic status, the adjustment of the molar ratio can improve the accuracy of COD simulation. S-RW QM 1 can reflect the effects of riparian substances on the purification ability of organic pollutants in water, and simulate the degradation of organic pollutants in rivers. There are still some shortcomings in this study because of the limited time and ability, for example, the results of this study may not be suitable for other areas due to the imbalance in the level of organic pollution in rivers, and the further research is needed.

References

[1] Y. Wang, P. Wang, Y. Bai: *Assessment of surface water quality via multivariate statistical techniques: A case study of the Songhua river Harbin region, China.* Journal of Hydro-environment Research *7* (2013), No. 1, 30–40.

[2] J. Qu, M. Fan: *The current state of water quality and technology development for water pollution control in China.* Critical Reviews in Environmental Science and Technology *40* (2010), No. 6, 519–560.

[3] B. Spänhoff, R. Bischof, A. Böhme, S. Lorenz, K. Neumeister, A. Nöthlich, K. Küsel: *Assessing the impact of effluents from a modern wastewater treatment plant on breakdown of coarse particulate organic matter and benthic macroinvertebrates in a lowland river.* Water, Air, and Soil Pollution *180* (2007), Nos. 1–4, 119–129.

[4] J. Soininen: *Responses of epilithic diatom communities to environmental gradients in some Finnish rivers.* International Review of Hydrobiology *87* (2002), No. 1, 11–24.

[5] R. C. Nijboer, P. F. M. Verdonschot: *Variable selection for modelling effects of eutrophication on stream and river ecosystems.* Ecological Modelling *177* (2004), Nos. 1–1, 17–39.

[6] R. F. Spalding, M. E. Exner: *Occurrence of nitrate in groundwater: A review.* Journal of environmental quality *22* (1993), No. 3, 392–402.

[7] P. F. Wang, X. R. Wang, C. Wang: *Experiment of impact of river hydraulic char-*

acteristics on nutrients purification coefficient. Journal of Hydrodynamics, Ser. B *19* (2007), No. 3, 387–393.

[8] F. Wang, J. K. Burton: *Second life in education: A review of publications from its launch to 2011.* British Journal of Educational Technology *44* (2013), No. 3, 357–371.

[9] E. O. Igbinosa, A. I. Okoh: *Impact of discharge wastewater effluents on the physico-chemical qualities of a receiving watershed in a typical rural community.* International Journal of Environmental Science & Technology *6* (2009), No. 2, 175–182.

[10] D. F. Juang, W. P. Tsai, W. K. Liu: *Treatment of polluted river water by a gravel contact oxidation system constructed under riverbed.* International Journal of Environmental Science & Technology *5* (2008), No. 3, 305–314.

Received May 7, 2017

Design and research of pulsed vacuum sterilizer based on digital PID

Bian Jiang[1,2], Cao Hong-Ying[2]

Abstract. The design and application of pulsed vacuum sterilizer based on digital PID can provide a certain technical support for the development of related industries. In order to make the theory and technology of pulsed vacuum sterilizer more perfect in our country, a simple design of the sterilizer was made, and the influence of air pressure on pulsed vacuum sterilizer was also compared and analyzed based on a clear overview of relevant theories in this study. The results show that the high pressure pulsed vacuum sterilizer has better sterilization effect. Compared with the traditional sterilizer, the pulsed vacuum sterilizer based on digital PID has better sterilization performance. The purpose of this study is to provide a scientific basis and reference support for further studies.

Key words. Digital PID, pulsed vacuum, sterilizer.

1. Introduction

A certain number of microbial communities live in the living environment of the human body, these microbial communities may have a damaging effect on people's bodies depending on their own skills, while some microbial communities may have some positive effects on the normal functioning of the organism and some physiological activities. These microbial communities include microbes, fungi, and other microorganisms. The quantity and kind of microorganisms existing in the human organism's living environment may be closely related to human health and disease, which have a certain impact on the health of the human body. For example, they may cause certain damage to the human immune system, and allow more bacteria or fungi to stimulate the human organism, thereby reducing the body's own immune levels and increasing the recurrence and severity of the disease. Therefore, the elimination of some harmful microorganisms has gradually been paid attention to by some countries. More timely measures have begun to be gradually applied to the actual sterilization process, which has provided a guarantee for human beings to

[1]Corresponding author
[2]Kaifeng University Institute of Electrical and Electronic Engineering, Kaifeng, Henan, 475004, China

create a better living environment. This research will study and discuss the design of pulsed vacuum sterilizer based on digital PID technology. The purpose of this research is to provide a theoretical basis and reference for the follow-up research and technical improvement and development.

2. State of the art

In the production and life of people, some microorganisms always affect people's normal life more or less. Many medical researchers believe that the presence of harmful bacteria in the environment for a long time may have an impact on people's health and may be an increase in people's disease outbreaks [1]. In recent years, the relevant international medical organizations and biological organizations have fully realized the negative impact of harmful microorganisms on human health and stability. And some western developed countries have been gradually carry out the relevant work and human body micro-biome research through some related techniques and methods, and obtained some achievements [2]. The sterile environment, especially the environment without harmful bacteria is necessary in many industries. In some hospital systems, some premature neonate can't complete its invasion of the external bacteria through its own immunity because of its relatively weak immune capacity. A sterile environment can help them go through this difficult period [3]. In some biological industries, a sterile environment is extremely important for the design and operation of industry related biological experiments. Only in a sterile environment can the process of the experiment be smoother and the results obtained are more reliable [4]. There are many researches on sterilization instruments, and the gradual improvement of sterilization instruments has made more industries develop. Under this trend, pulsed vacuum sterilizer based on digital PID technology has been studied more and achieved more achievements [5].

3. Methodology

In the present era, the economic level of our country has been greatly improved. However, our country's economic development model is more extensive mode of development, which has caused great damage to the relevant environment of our country to a certain extent. The harmful microorganisms in our environment have been increasing. And it does harm to the survival of people and other organisms [6]. It can be found in more reports in our country that with the development of the times, the physical quality of our citizens has declined. This trend is not only due to the lack of a certain amount of physical exercise, but also partly because of the gradual deterioration of people's living environment [7]. Many reports indicate that the harmful microorganisms in the soil and water bodies in our country are showing a gradual trend with the accumulation, which may have a great negative impact on our national health in the future to a certain extent. Under this trend, the research on killing some harmful bacteria in our country began to increase in the selection of better technology and theory. And in the development of some

industries, the creation of a sterile environment is also extremely demanding. To some extent, it may promote the development and progress of some industries in our country, and obtains more research results directly or indirectly. Especially in the development of the medical and biological industries in China, the use and operation of these industries may require the use of certain sterile environments, which can promote the human body to obtain a greater degree of health. Especially in the development of the biological industry, due to the operation of some pathological experiments, it may cause the relevant researchers to adhere to the harmful bacteria during the experiment. If it is not possible to sterilize the body or related tools and clothes in time, it may cause some harm to its health. The development of the food industry in our country also attaches great importance to the sterilization of related raw materials so that more healthy foods have been developed and put into market production [8]. Under this trend, sterilizer has been gradually applied to the development of various industries in our country (see Fig. 1).

Fig. 1. Development and application of sterilizer

Under this kind of demand, the related profession in our country has begun to increase for the sterilizer research. The sterilizers with different sterilization properties have been gradually put into practical industrial application, and have provided certain technical guarantee for the safety production and the safe use of products in related industries. However, due to lack of knowledge about sterilization theory in some industries or fields in our country, this makes the development and application of sterilization equipment still have certain limitations, and has laid a certain security risk for subsequent development. Nowadays, the design and research of pulsed vacuum sterilizer based on PID technology have provided certain positive impetus for the demand of sterilization treatment in various industries [9] (Fig. 2).

However, because of the high production cost of the sterilization technology, and the lack of mastery of the technology in some sectors of our country, it makes it impossible to better integrate the technology with the actual demand of the industry. This limits the further development of some industries to a certain extent [10]. Therefore, a clear overview of the design theory of digital PID based pulsed vacuum sterilizer was given and the feasibility of its practical application was analyzed in this study. The purpose of this study is to provide theoretical support for the gradual improvement of this technology, and to provide technical support for the integration of this technology with other industries.

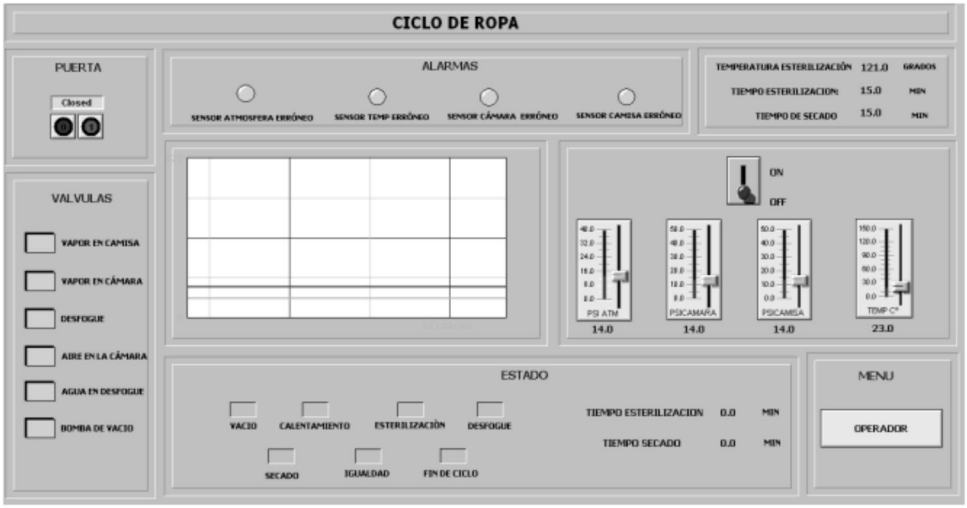

Fig. 2. The use of digital PID technology in the development of sterilizers

In order to obtain more accurate and reliable analysis results, the study was further carried out by the following related research analysis. The detailed methods of study are as follows:

First of all, the relevant information was read and summarized in this study. On this basis, the relevant theories were clarified, and the main deficiencies of the commonly used sterilization system in our country were explained and analyzed. Then, the sterilizer was designed and optimized on the basis of the cognition of the design principles of the sterilizer.

In view of the pressure and temperature detecting system of sterilizer, the control algorithms of steam generator and temperature in the sterilization cavity were studied and discussed. The algorithm model of PID was introduced in the design concept of pulsed vacuum sterilizer [11]. The related formulas of the algorithm model were introduced as follows in this study.

(1) The deviation between the preset value of the pulsed vacuum sterilizer and the actual output value of the sterilizer was calculated. The formula model is

$$e(t) = r(t) - c(t)\,, \tag{1}$$

where $r(t)$ and $c(t)$ represent the set value and actual output value respectively.

(2) The control expression of PID was analyzed. Because this kind of control is composed by many different links, the model equation is constructed as follows:

$$u(t) = K_{\mathrm{p}} \left[e(t) + \frac{1}{T_1} \int_0^1 \mathrm{e}(\tau)\, \mathrm{d}\tau + T_{\mathrm{D}} \frac{\mathrm{d}e(t)}{\mathrm{d}t} \right], \tag{2}$$

where K_{p}, T_1 and T_{D} represent the proportion of each link, integral time and differential time, respectively.

(3) In order to better reduce the static error in the PID control process, the stability of the vacuum sterilizer was higher. The study further optimized the above formula so that the system could maintain the maximum output value and speed up the control. The model equation is

$$u(k) = K_{\mathrm{p}} \left\{ e(k) + \frac{T_{\mathrm{D}}}{T} \left[e(k) - e(k-1) \right] \right\}. \tag{3}$$

Finally, the actual case was introduced, and the sterilization efficiency and performance of pulsed vacuum sterilizer based on digital PID were analyzed and compared under different pulse modes. The comparative study was mainly based on the current international standard of ISO11140-4/5, and the judgments and measurements of final elimination effect (BD) of steam sterilizer on air pre-vacuum pressure of pulsed vacuum sterilizer at high and low atmospheric pressure and whether all links can meet the anticipated conditions (PCD) of the sterilizer in the process of recycling were conducted. A common sterilizer was introduced as a negative control. Thus, a better condition for the application of the pressure of the pulsed vacuum sterilizer based on digital PID technology was determined. Furthermore, the advantages of this technology were summarized and analyzed. The research aimed at providing a theoretical basis for further improvement and development of sterilizer technology and providing technical support for the development of other subsidiary industries.

4. Result analysis and discussion

Nowadays, with the increasing attention of science and technology, various new technologies begin to appear constantly. Computer technology is one of the most influential sciences and technologies in the development of various industries in the world [12]. Many fields have begun to apply this technology to the development of themselves field. In recent years, the demand for aseptic conditions has increased gradually in some industries. Many fields in the world begin to develop the traditional disinfection equipment into the pre-vacuum and fully automatic way. In particular, researchers have a better understanding of the structure and properties of certain microorganisms. This provides some positive effects on the research and development of some disinfection and sterilization instruments [13]. Under this background, pulsed vacuum sterilizer based on digital PID has been developed and applied in actual industry or field (Fig. 3). The sterilizer combines with the digital

PID technology of computer technology, so it has more advanced R & D technology. It can achieve better disinfection effect in the absence of unattended, so it begins to be popularized gradually (Fu et al. 2011) [14]. The performance advantage of pulsed vacuum sterilizer based on PID technology in our country is mainly manifested in the vacuum validity. Thus, a plurality of bacteria and viruses can be killed so as to achieve better sterilization effect. And because of the more pre-vacuum validity, the sterilization equipment has relatively high validity and efficiency. Its system structure is relatively simple and the system function is more perfect, which can be used by more industries [15].

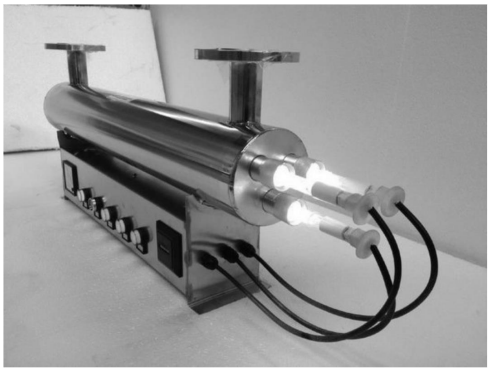

Fig. 3. The use and development of pulsed vacuum sterilizer

On the basis of understanding the relevant theories, the author studied and designed the pulsed vacuum sterilizer used in this research. The control system of the pulsed vacuum sterilizer designed in this paper is mainly composed of a single-chip microcomputer based on PIC technology and a generator that can control the steam and integrate it. In the design process of the sterilizer, the perfection of the circuit has a very important influence on the normal use of the pulsed vacuum sterilizer with digital PID technology. The utility model can further improve the service life and time of the sterilizer on the basis of ensuring that the sterilization process of the sterilizer is more reliable. Therefore, more attention should be paid to the scientificality and the systematicness of the pulsed vacuum sterilizer so that the final instrument sterilization effect is better. According to reading relevant information, the circuit of this sterilizer was summarized and perfected, so as to provide the basis for the performance of the sterilizer. The circuit design of the sterilizer in this study is shown in Fig. 4.

Based on the relevant theories and the basic design of sterilizer, the judgments and measurements of final elimination effect (BD) of steam sterilizer on air pre vacuum pressure of pulsed vacuum sterilizer at high and low atmospheric pressure and whether all links meet the anticipated conditions (PCD) of the sterilizer in the process of recycling were conducted in this study. The results of the measurements are shown in Table 1 and Table 2. The results show that the rate of BD negative test of pulsed vacuum sterilizer at high pressure is as high as 99.34 % and 95.18 % at low pressure. Therefore, the evacuation efficiency of the pulse sterilizer at high

pressure for cold air is obviously higher than that at low pressure. When the cold air is not completely discharged, the steam in the sterilizer can not penetrate more effectively, which may affect the sterilization effect. In order to verify the BD effect of autoclave under different pressure, further validation was carried out by positive experiments. The results show that the autoclave with high pressure has a higher pass rate that 46.38 %, which has better penetrating effect.

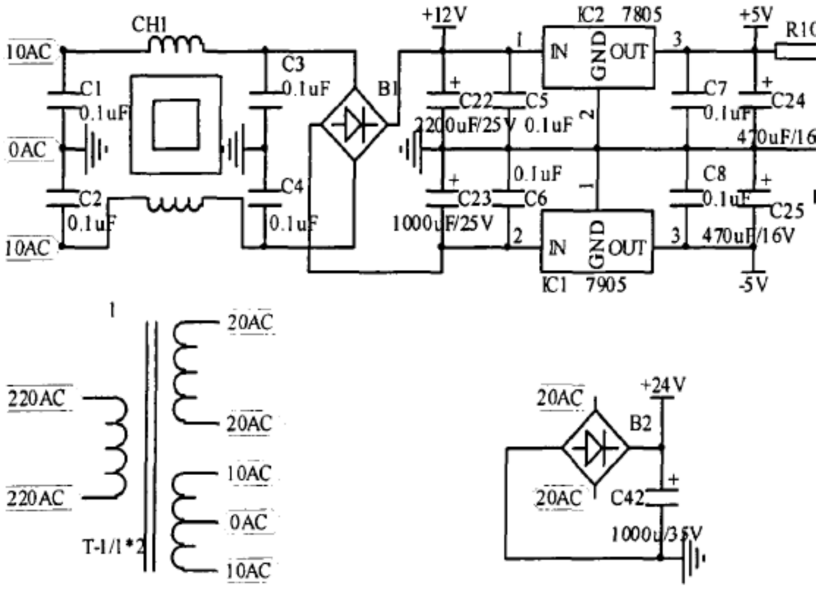

Fig. 4. The circuit operation flow of the sterilizer used in this study

Table 1. Comparison of BD test results of pulse sterilizer at low atmospheric pressure and high pressure

Test cycle negative	Experiment times	Low atmospheric pressure pulse BD test		High pressure pulse BD test	
		Qualified number	Qualified rate (%)	Qualified number	Qualified rate (%)
Positive	457	435	95.18	454	99.34
Test cycle	457	25	5.47	212	46.38

The effects of different pulse modes on PCD in sterilization pot were analyzed in this study. The results show when the negative test is carried out, the sterilization effect of the pulse sterilization pot is higher than that in the low pressure air, and its qualification is up to 99.76 %. However, the risk of sterilization may still be incomplete under qualified sterilization conditions. Therefore, positive detection was further carried out in this study. The results show that the qualified rate of pulse sterilization is higher in high pressure, which can reach 42.49 %.

Table 2. Comparison of BD test results of pulse sterilizer at low atmospheric pressure and high pressure

Test cycle negative	Experiment times	Low atmospheric pressure pulse PCD test		High pressure pulse PCD test	
		Qualified number	Qualified rate (%)	Qualified number	Qualified rate (%)
Positive	859	850	98.95	857	99.76
Test cycle	859	12	1.39	365	42.49

The experiment confirmed that the PID vacuum pulse sterilizer with high pressure has better effect. Then, the disadvantage reasons of the pulsed vacuum sterilizer for PID technology at low atmospheric pressure were analyzed. The analysis results are shown in Table 3.

Table 2. Comparison of BD test results of pulse sterilizer at low atmospheric pressure and high pressure

	Low atmospheric pressure pulse negative				High pressure pulse negative			
	Failure times	Improper handling of staff	Sterilizer leak	Poor performance of vacuum pump	Failure times	Improper handling of staff	Sterilizer leak	Poor performance of vacuum pump
BD	22	11	7	4	3	1	1	1
PCD	9	2	3	4	2	2	0	0

Finally, the performance of pulsed vacuum sterilizer based on digital PID technology and traditional sterilizer was analyzed in the study. The analysis results are shown in Fig. 5. The results show that the sterilization efficiency of this kind of sterilization pot is high, and the sterilization is more thorough. And the operation is simple, so it is more suitable for the application of related industries.

5. Conclusion

With the development of the times, the demands for aseptic conditions have gradually increased in the development of many industries, so that the research of sterilizer has gradually become one of the necessary needs for the development of the industry. In this trend, more sterilizers have been developed and applied to the actual industry development. Because the traditional sterilizer is difficult to operate and the sterilization efficiency is low, which cannot meet the actual needs of the industry. The research of pulsed vacuum sterilizer based on PID technology can provide some technical support for solving this problem. However, the research of pulsed vacuum sterilizer in our country is still few, and the related theories and techniques are

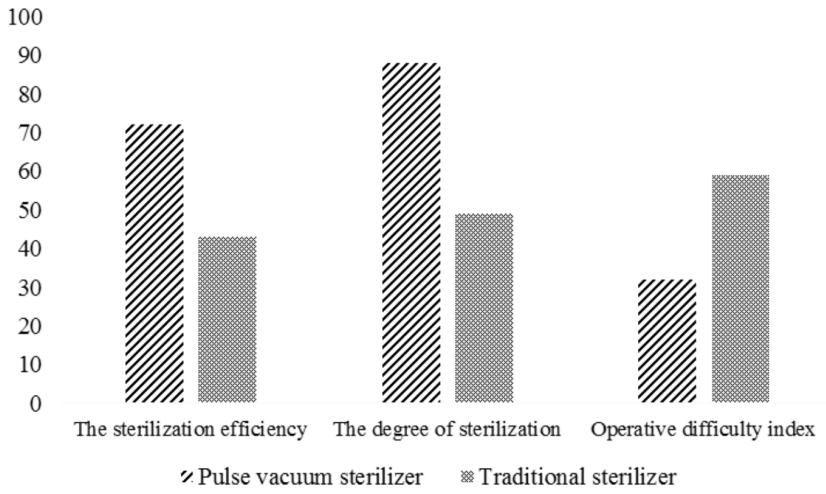

Fig. 5. Performance comparison between a pulsed vacuum sterilizer and a conventional autoclave based on digital PID technology

not perfect enough. In view of this deficiency, relevant concepts were defined and outlined by reading relevant data in this study. On this basis, the simple design of pulsed vacuum sterilizer based on digital PID technology was studied, and the performance of the sterilizer under different conditions was compared and analyzed. The results show that the pulsed vacuum sterilizer based on digital PID technology has better sterilization effect. Only the influence factor of air pressure has been studied in this study, which makes the research have certain deficiency. But this study still can provide the theoretical basis and support for the follow-up research.

References

[1] S. Killeen, M. McCourt: *Decontamination and sterilization.* Surgery *30* (2012), No. 12, 687–692.

[2] C. Ackert-Burr: *Low-temperature sterilization: Are you in the know?.* Perioperative Nursing Clinics *5* (2010), No. 3, 281–290.

[3] S. Govindaraj, M. S. Muthuraman: *Systematic review on sterilization methods of implants and medical devices.* International Journal of ChemTech Research *8* (2015), No. 2, 897–911.

[4] C. S. Sousa, L. M. Torres, M. P. F. Azevedo, T. C. de Camargo, K. U. Graziano, R. A. Lacerda, and R. N. T. Turrini: *Ozônio na esterilização de produtos para assistência à saúde: Revisão integrativa da literatura.* Revista da Escola de Enfermagem da USP São Paulo *45* (2011), No. 5, 1243–1249.

[5] T. Batakliev, V. Georgiev, M. Anachkov, S. Rakovsky, G. E. Zaikov: *Ozone decomposition.* Interdisciplinary toxicology *7* (2014), No. 2, 47–59.

[6] R. S. Somalwar, V. U. Janekar, B. Umate: *Advance method for calculating ozone chamber parameters.* IOSR Journal of Electrical and Electronics Engineering (2014), No. 1, 33–38.

[7] F. Mitsugi, T. Nagatomo, K. Takigawa, T. Sakai, T. Ikegami, K. Nagahama, K. Ebihara, T. Sung, S. Teii: *Properties of soil treated with ozone generated by surface discharge*. IEEE Transactions on Plasma Science *42* (2014), No. 12, 3706–3711.

[8] S. Botelho da Silva, M. de Mello Luvielmo, M. Curtinovi Geyer, I. Prá: *Potencialidades do uso do ozônio no processamento de alimentos - Potential use of ozone in the food processing*. Semina: Ciências Agrárias *32* (2011), No. 2, 659–685.

[9] A. Mahfoudh, M. Moisan, J. Séguin, J. Barbeau, Y. Kabouzi, D. Kéroack: *Inactivation of vegetative and sporulated bacteria by dry gaseous ozone*. Journal Ozone: Science & Engineering *32* (2010), No. 3, 180–198.

[10] M. Jerrett, R. T. Burnett, C. A. Pope, K. Ito, G. Thurston, D. Krewski, Y. Shi, E. Calle, M. Thun: *Long-term ozone exposure and mortality*. New England Journal of Medicine *360* (2009), No. 11, 1085–1095.

[11] Q. Wang, I. Balasingham: *Wireless sensor networks - An introduction, Wireless sensor networks: Application-centric design*. InTech, Edited by G. V. Merrett and Y. K. Tan (2010).

[12] M. Winkler, K. Tuchs, K. Hughes, G. Barclay: *Theoretical and practical aspects of military wireless sensor networks*. Journal of Telecommunications and Information Technology *2* (2008), No. 2, 37–45.

[13] G. Zhao: *Wireless sensor networks for industrial process monitoring and control: A survey*. Network Protocols and Algorithms *3* (2011), No. 1, 46–63.

[14] X. Fu, W. Chen, S. Ye, Y. Tu, Y. Tang, D. Li, H. Chen, K. Jiang: *A wireless implantable sensor network system for in vivo monitoring of physiological signals*. IEEE Transactions on Information Technology in Biomedicine *15* (2011), No. 4, 577–584.

[15] P. W. Rundel, E. A. Graham, M. F. Allen, J. C. Fisher, T. C. Harmon: *Environmental sensor networks in ecological research*. New Phytologist *182* (2009), No. 3, 589–607.

Received May 7, 2017

Acta Technica *62* No. 2B/2017, 183–192

A text information extraction algorithm based on label path clustering[1]

Jing Qiu[2,3], Yuhan Chai[2]

Abstract. XML documents are widely used in computer and Internet technology. Based on XML documents, data exchange can be effective. However, the extraction of text information determines the utilization and efficiency of the data. The traditional text information extraction algorithm has low accuracy and low efficiency. Therefore, a text information extraction algorithm based on label path clustering was proposed in this paper. Then the traditional PBClusreing algorithm was improved. Finally, the verification test was carried out. As can be seen from the result, compared with the traditional algorithms, the improved text information extraction algorithm has significant advantages in noise elimination and efficiency. Therefore, the improved text information extraction algorithm can be applied to the specific practice, which is conducive to promoting communication and utilization of Internet data, and has positive significance for the development of the Internet.

Key words. Clustering, information extraction, frequent path, XML.

1. Introduction

With the continuous development and application of modern computer technology and Internet technology, people rely more and more on the Internet, and the Internet has greatly changed people's way of life [1]. When people use computers and the Internet to communicate with each other, there are more extensible markup language applications (hereinafter referred to as XML), which can exchange data among different data sources [2]. In terms of structure and function, XML can not only represent structured data, but also represent unstructured data of the Web class, which is widely used in database, data exchange, e-commerce, natural language conversion and so on, and has become a standard language for data representation and exchange [3]. With the increasing of XML class data, how to effectively carry

[1]This paper is supported by the National Natural Science Foundation of China (project No. 61300120).

[2]Department of Information Science and Engineering, Hebei University of Science and Technology, Shijiazhuang, Hebei, 050026, China

[3]Corresponding author

out this kind of data information has become more important. XML data is mostly represented in the form of XML, and in the XML document, the two main forms are hierarchical and semi-structured. At present, the data mining methods for this kind of document include classification processing, clustering analysis and structure mining (Yan et al. 2015) [4]. The clustering processing of XML documents is usually done in two aspects: structured clustering processing and content clustering processing [5]. In this paper, a text information extraction algorithm based on label path clustering was proposed to achieve the rapid and accurate extraction of XML class information. And the algorithm was compared with the traditional method. Thus, the accuracy and practical value of the algorithm were understood.

2. State of the art

The development of information technology leads to exponential growth of Internet information, and it is harder and harder for people to acquire the knowledge they want. It is a challenge to find the desired information from heterogeneous, dynamic and distributed Web information library and convert it into the information and knowledge that users need [6]. When using Web retrieval to query relevant information, a list of results is returned to the user, and according to the correlation algorithm, a variety of factors are calculated to carry out sorting [7]. In these sorting algorithms, the frequency, location, number, importance, and number of clicks being queried are considered synthetically [8]. At present, the related clustering analysis of HTML language files applied in Internet has been studied more and more, and the fast and accurate extraction of text information has been realized. However, the research of information extraction algorithms for XML documents is relatively small, which is not conducive to the use and communication of Internet information [9]. At present, TreeFinder and Tag-based are the main methods to extract structural information of XML documents. In this paper, a collection of paths from roots to leaf nodes was used to represent XML documents [10].

As extensible markup languages, both XML and HTML belong to the category of SGML, and there are many similarities between them. They are the common standard languages in the world [11]. XML is a subset based on the SGML language, but different from the SGML language, it avoids the complex features of SGML language to some extent [12]. As for the basic functions of XML, in terms of file data, documents are varied and diversified by description, and its technology is mainly oriented to data applications, in which, the meaning of some data and material can be explained by marking [13]. In processing patterns, XML documents are often abstracted into semantic layer, syntax layer, character layer, structure layer, binary file and so on, which are similar to network protocol TCP/IP [14].

3. Methodology

3.1. Preprocessing of XML documents

The XML document can be represented in the form of a tree. The main idea of the new algorithm proposed in this paper is to use sequential pattern mining to obtain frequent path sets among different XML documents. XML documents with similar structure have similar frequent paths, while, for XML documents of different structure, similar frequent paths will be relatively few. Therefore, the clustering documents, frequent paths can be used as their characteristics. Converting the XML document into a tree structure, then each node in the tree corresponds to an element of the XML document. In this paper, tree structure was represented based on path. In this way, each tree is represented by a collection of paths, and the ordered nodes form the root node to the leaf node together form the paths. In the study, a simplified XPath was used to represent the path. It contains both element information and hierarchical information in the path, so that the XML document can be represented by a simple collection of XPath expressions [15]. Firstly, the XML document was preprocessed, to extract the corresponding path set from the tree structure. And then the duplicate path was deleted. The specific process is shown in Fig. 1.

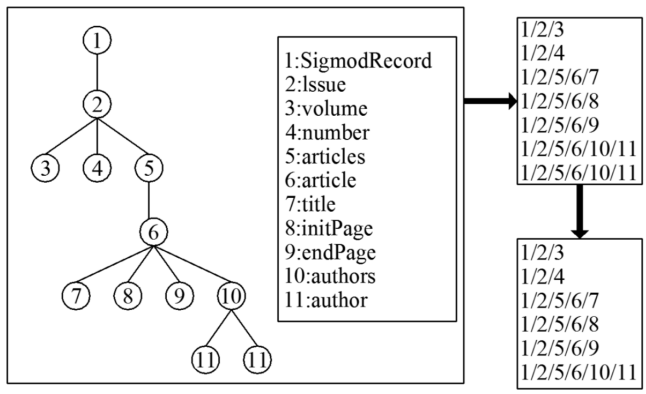

Fig. 1. The path set for the XML document

When using this representation, in the path, in order to indicate a change in the hierarchy of the different elements, a "/" will be added behind the element. Therefore, the Xpath paths obtained after preprocessing include both path element information and hierarchical information. Since the XML path is a relatively simple sequence, each element is a XML node and can't be a collection containing multiple items. Then, in the XML path, if a path is not included in all other paths, then the path is the maximum path. Path support is involved, the computational method of which is the ratio of the number of occurrences of a path to the number of documents in a path set. If in the XML document the path A is contained in the path B, then the path A can be called a subsequence of path B. It is assumed that a XML path

set is D, which can be determined by the document number and serial numbers to which each path belongs, respectively $doc - id, seq - id$.

The number of occurrences used to compute path support refers to the number of XML documents that s is contained in D. In this paper, only the frequent paths among different documents were searched, while the XML paths that were repeated in the same document were not counted repeatedly. If the given support threshold is $\min\sup p$, the support number of the sequence database for path$s$ in XML is no less than $\min\sup p$, and s is known as the path model. The document set of XML is converted to the corresponding path set. According to the given minimum support threshold $\min\sup p$, the sequential pattern mining algorithm is used to find the path patterns of all XML. After removing all the paths contained by other paths, the maximum path pattern can be obtained.

3.2. Frequent path mining process and document clustering

The two XML document trees are input to sample the mining process of the XML frequent path pattern, as shown in Fig. 2. The minimum support is set to 100 %. Preprocessing is performed in the manner described earlier to obtain a XML path set.

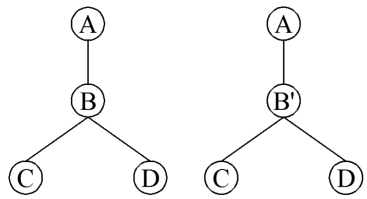

Fig. 2. Two XML document counts

The specific steps of XML frequent path mining are:

(1) All frequent nodes satisfying minimum support, referring to the frequent paths of length 1, should be found out.

(2) According to the frequent nodes found, a Hash mapping table based on frequent node sets is constructed. By using this mapping table, the path of the XML document machine can be converted and represented. Each frequent node name is replaced by a corresponding integer, and the result of the conversion is shown in Fig. 1. After the processing and transformation, the integer sequence can be used to represent the path, thus reducing the identification space of the XML document path sequence set, and improving the subsequent mining speed.

(3) AprioriAll algorithm is used to carry out iteration, and thus a collection of frequent sequences of lengths from 1 to maximum length can be obtained.

(4) The path contained in other patterns in the frequent sequence is eliminated, so as to obtain the maximal frequent sequence.

The path transformation representation is described in Table 1.

The XML frequent path is used as clustering feature. The number of its maximum path patterns is affected by the minimum support of the path mining phase.

The appropriate minimum support can effectively eliminate noise data and avoid excessive features missing, so as to ensure that the classification features of the XML document set can be effectively represented in the smaller dimension feature space.

Table 1. Path transformation representation

Document number	1	1	2	2
Path number	1	2	1	2
Original path	A/B/C	A/B/D	A/B'/C	A/B'/D
Converted path	A//C	A//D	A//C	A//D
After mapping	1,2,2,3,	1,2,2,4	1,2,2,3	1,2,2,4

In the vector intermediate model, the PBClusreing algorithm represents the XML document set. If the number of maximal frequent paths obtained by XMNL frequent paths in the excavation stage is n, then an n dimensional vector is used to represent each XML document. If an XML document contains the maximum frequent path m, then in the corresponding vector $S_m = 1$ or $S_k = 0$. When PBClusreing algorithm calculates the similarity between documents, the traditional Euclidean distance is used to perform calculations, and then the clustering algorithm is adopted to perform clustering.

3.3. Improvement of text information extraction algorithm

There are some problems in the existing information extraction algorithms, and previous studies have also tested the performance of the PBClusreing algorithm. The problems existing in the traditional PBClusreing algorithm are mainly embodied in the following aspects. The accuracy of clustering is not high. Even if the minimum support of very frequent and verifiable frequent paths is selected, the accuracy of the final clustering results is only about 70%, which is also the reason for the improvement of the algorithm. In addition, the sensitivity of PBClusreing algorithm to noisy data is high. In the performance of artificial data and actual high noise data, the actual noise situation has not been fully considered. And the scalability of the traditional PBClusreing algorithm is poor. Due to the use of aggregation hierarchical clustering algorithm and AprioriAll algorithm, the time complexity required is higher. In the face of large amounts of data, it is difficult to effectively deal with the data, and its processing efficiency is low. Therefore, aiming at many problems existing in the algorithm, some targeted improvements and research were made in this paper.

The principle of PBClusreing algorithm is to define the distance between documents directly through Euclidean distance. Although it is very easy to understand in the low latitude space, the distribution of the data will obviously improve the noise level when the high-dimensional data is encountered. And thus, in the conventional sense, Euclidean distance definition is no longer valid, and cosine similarity can be used to document similarity calculation.

Boolean vectors are often used when documents containing frequent paths are

represented by the PBClusreing algorithm. However, the differences among the lengths of the frequent paths are not fully taken into account. There are nowa, b, c documents, and two documents a, b contain the frequent path s_1, and b, c documents contain the frequent path s_2. If the frequent pathss_1 is longer than s_2, it is considered that a is closer to the document b than c. The vector of the XML document can be weighted, and integer vectors are used to represent an XML document, such as $\{s_1, s_2, \cdots, s_n\}$. If there is a k maximum path model in a XML document, then its corresponding length assignment is s_k, or $s_k = 0$. The key codes based on experiments to obtain weighted paths are shown in Fig. 3.

```
public AprioriAlgorithm(double minsupp, string[] files)
        {
            StringBuilder strb = new StringBuilder();
            strb.AppendFormat("{0}:start reading {1} xml docs. . . .",
                System.DateTime. Now. ToString(),
                files.Length;
             strb.AppendLine();
             ininInfo = strb. ToString();
            this. sequenceData = new SequenceDataSet(minsupp, files);
              StringBuilder strb2 = new StringBuilder();
              strb2.AppendFormat("{0} :generate length of 1:{1}",
                  Sysytem.DateTime.Now. ToString(),
           . . . . . .
```

Fig. 3. Key codes for weighted paths

In the use of PBClusreing algorithm, the relatively classic AprioriAll algorithm is applied, the principle of which is anti-monotone. If a sequence fails to pass the test, all sequences that contain it are considered impossible to pass the test. Based on this feature, the search space can be cut to make sequential pattern mining more efficient. But whether it is AprioriAll algorithm or agglomerative hierarchical clustering algorithm, the time complexity is still relatively large, and can't meet the requirements of large document set processing. On this basis, the more efficient PrefixSpan algorithm can be applied. In addition, the K-mean algorithm can be used in the clustering division, and the efficiency of the algorithm is also higher. In this paper, different types of XML document formats can be considered as clustering centers, and the high-dimensional vector space was relatively sparse, so that the K-mean algorithm was also applicable. The K-hierarchy algorithm was used to replace the hierarchical clustering algorithm. Thus, the improved PBClusreing algorithm based on the K-mean algorithm and the PrefixSpan algorithm can be obtained.

4. Result analysis and discussion

4.1. Similarity calculation of documents

In this study, a comparative analysis of different clustering algorithms was carried out. In the four classes of use, each class contained 150 documents. When the minimum support degree of the frequent path was 5 %, Euclidean distance and cosine similarity coefficients were compared and analyzed. And the clustering hierarchy and

K-mean clustering algorithm were adopted. The specific results are shown in Fig. 4.

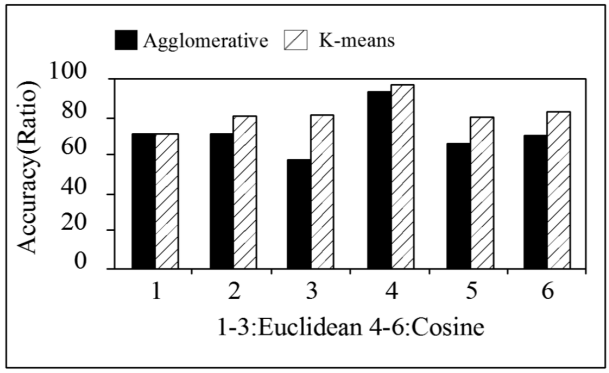

Fig. 4. Contrastive analysis of two methods of measurement

It can be seen from Fig. 3 that the clustering accuracy obtained by cosine similarity coefficients is better than that of Euclidean distance under the same algorithm. And in the case of using the same metric method, the K-mean clustering algorithm has better effect than the hierarchical clustering algorithm. It can be seen that, when calculating the document similarity of the path schema, the cosine similarity coefficient can achieve better results compared with the traditional Euclidean distance method.

The path weighted analysis was further carried out. In 11 classes of documents, each type of document contained 150 files. When the minimum support of the frequent path was 8 %, the contrast experiments were conducted to analyze whether the 10 groups joined the path length weight. From the results of the study, it can be seen that when the path length is added, the accuracy of clustering is improved, and the range of improvement is about 5–10 %. Therefore, the path model can effectively reduce noise and eliminate the influence of short path noise.

4.2. Algorithm comparison

In the case of frequent path with minimum support of 5 %, PrefixSpan algorithm and AprioriAll algorithm were compared in terms of the time efficiency. The size of the document, ranging from 200 to 1400, was divided into 7 levels. The specific results are shown in Table 2.

Table 2. Comparison and analysis of time efficiency between PrefixSpan and AprioriAll algorithms

Time (s)	200	400	600	800	100	1200	1400
PrefixSpan	0.29	0.85	1.21	1.51	1.76	1.82	2.03
AprioriAll	13	40	57	58	53	111	125

As can be seen from Table 2, the PrefixSpan algorithm is more efficient and has a significant advantage compared with the AprioriAll algorithm. Four types of

documents were further selected, 150 in each category. When the support was 5 % and 15 %, respectively, 117 and 49 frequent paths were obtained. Then the K-mean clustering and aggregation hierarchy were compared and analyzed in terms of time and accuracy. The specific results are shown in Table 3. As can be seen from Table 3, the clustering accuracy obtained by the two algorithms is comparable in the 117 and 49 dimensions. However, further analysis shows that the K-mean algorithm has a more significant advantage than the aggregation level algorithm.

Table 3. Comparative analysis of time efficiency between aggregation level and K-mean

Time (s)	Aggregation level	K-mean
49 dimensional	112 (100 %)	0.017 (98 %)
117 dimensional	173 (96 %)	0.03 (94 %)

5. Conclusion

XML documents are used more frequently in data usage. However, there are many problems such as low efficiency and low accuracy in the traditional text information extraction algorithm. Therefore, a more efficient and reliable algorithm for text information extraction is urgently needed. Based on the traditional PB-Clusreing algorithm, the K- mean algorithm and the PrefixSpan algorithm were introduced in this paper, and the large data text set can be processed. In order to verify the practicability of the algorithm, the computation of document similarity and the performance of other algorithms were compared and analyzed. It can be seen that the cosine similarity coefficient has better effect, and the path model can reduce the influence of noise effectively. In addition, the PrefixSpan algorithm will have higher time efficiency than the traditional AprioriAll algorithm. As for the accuracy of clustering, the K- mean algorithm also has a more prominent advantage. In summary, compared with the original algorithm, the improved text information extraction algorithm has better application effects, especially for high noise and large number of processing. And the accuracy is also improved by 10–20 %, and the time efficiency is also significantly improved.

References

[1] J. S. Leu, J. H. Chen, K. H. Li: *Hybrid search scheme for social networks supported by dynamic weighted distributed label clustering.* IEEE Transactions on Computers *64* (2015), No. 9, 2586–2594.

[2] M. Piernik, D. Brzezinski, T. Morzy, A. Lesniewska: *XML clustering: A review of structural approaches.* Knowledge Engineering Review *30* (2015), No. 3, 297–323.

[3] S. He, P. Samara, J. Burgers, L. Schomaker: *A multiple-label guided clustering algorithm for historical document dating and localization.* IEEE Transactions on Image Processing *25* (2016), No. 11, 5252–5265.

[4] W. Yan, F. Suo: *Top-k ranking of preference query results for XML based on simi-*

larity of contextual states. Journal of Computational Information Systems *11* (2015), No. 12, 4439–4446.

[5] M. Piernik, D. Brzezinski, T. Morzy: *Clustering XML documents by patterns.* Knowledge and Information Systems *46* (2016), No. 1, 185–212.

[6] Y. Xia, L. Nie, L. Zhang, Y. Yang, R. Hong, X. Li: *Weakly supervised multilabel clustering and its applications in computer vision.* IEEE Transactions on Cybernetics *46* (2016), No. 12, 3220–3232.

[7] N. Shafieian: *A novel method for transforming XML documents to time series and clustering them based on delaunay triangulation.* Applied Mathematics *6* (2015), No. 6, 1076–1085.

[8] L. Guo, W. Zuo, T. Peng, L. Yue: *Text matching and categorization: Mining implicit semantic knowledge from tree-shape structures.* Mathematical Problems in Engineering *2015* (2015), Article ID No. 723469, 1–9.

[9] K. Li, Y. Liu, Q. Wang, Y. Wu, S. Song, Y. Sun, T. Liu, J. Wang, Y. Li, S. Du: *A spacecraft electrical characteristics multi-label classification method based on off-line FCM clustering and on-line WPSVM.* Plos One *10* (2015), No. 11, e0140395.

[10] M. L. Zhang, L. Wu: *Lift: Multi-label learning with label-specific features.* IEEE Transactions on Pattern Analysis & Machine Intelligence, *37* (2015), No. 1, 107–120.

[11] N. Piroonsup, S. Sinthupinyo: *Semi-supervised cluster-and-label with feature based re-clustering to reduce noise in Thai document images.* Knowledge-Based Systems *90* (2015), 58–69.

[12] M. Hucka, F. T. Bergmann, S. Hoops, S. M. Keating, S. Sahle, J. C. Schaff, L. P. Smith, D. J. Wilkinson: *The systems biology markup language (SBML): Language specification for level 3 version 1 core.* Journal of Integrative Bioinformatics *12* (2015), No. 2, paper 266.

[13] S. Cheng, M. T. Martinez-Ingles, D. P. Gaillot, J. M. Molina-Garcia-Pardo, M. Liénard, P. Degauque: *Performance of a novel automatic identification algorithm for the clustering of radio channel parameters.* IEEE Access: Toward Ubiquitous Real-Time Radio Propagation Modeling *3* (2015), 2252–2259.

[14] C. Bothorel, J. D. Cruz, M. Magnani, B. Micenkova: *Clustering attributed graphs: Models, measures and methods.* Network Science Journal *3* (2015), No. 3, 408–444.

[15] J. Levatić, D. Kocev, S. Džeroski: *The importance of the label hierarchy in hierarchical multi-label classification.* Journal of Intelligent Information Systems *45* (2015), No. 2, 247–271.

Received May 7, 2017

Acta Technica *62* No. 2B/2017, 193–204

Study on seismic shear strength of concrete hollow block masonry[1]

Jintao Cui[2,3], Yue Zhang[2]

Abstract. Concrete hollow block masonry is a common method used in civil and commercial buildings. However, inadequate brittleness, tensile and shear strength of concrete hollow block masonry, especially the performance of masonry collapse and ductility under the action of earthquake, have seriously restricted the development of masonry structure. In this paper, the basic mechanical properties of concrete block masonry, such as seismic and shear strength, were studied according to standard test method. The seismic shear strength tests of 24 sets of standard specimens of 36 hollow concrete block masonry structures were carried out. Finally, the formulas for calculating the seismic shear strength of hollow block masonry were obtained, and the recommended values were given.

Key words. Concrete, hollow block masonry, shear strength, friction coefficient.

1. Introduction

The structure of hollow concrete masonry has a wide range of applications all over the world because of better convenience for the construction, good fire resistance, excellent chemical stability and atmospheric stability, long safe service life, good heat insulation and sound insulation performance [1]. The structure of masonry concrete hollow masonry is a complex anisotropic material composed of hollow brick, block, mortar, and so on [2]. In the aspect of mechanical properties of materials, the average tensile strength, flexural tensile strength and shear strength of unreinforced masonry are only about 10 % of their axial compressive strength [3]. There are three ways to improve the seismic and shear strength of concrete hollow masonry structures:

[1]The authors acknowledge the financial support of the Project of National Science and Technology Supporting Plan (2015BAL03B02), the National Natural Science Foundation of China (Grants Nos. 11402166 and 51408400), the General Projects in Tianjin Research Program of Application Foundation and Advanced Technology (Grant No. 13JCYBJC39100), the Youth Projects in Tianjin Research Program of Application Foundation and Advanced Technology (Grant No. 12JCQNJC05000).

[2]School of Civil Engneering, Tianjin Chengjian University, Tianjin, 300384, China

[3]Corresponding author

increasing the strength of the material, changing the structure form and exerting a certain degree of pre stress [4].

After the prestressing force is applied to the masonry structure, the shear capacity will be greatly improved, and the integrity and resilience of the structure will be improved. Under the action of prestressing force, the masonry structure can bear more deformation, and it also includes the improvement of crack resistance. In this case, the masonry structure can be subjected to greater deformation, and it can even further reduce the cracking caused by temperature changes and mortar shrinkage. Cracks due to occasional loads will also tend to close after the load disappears due to preload (Yu et al. 2015 [5]). Therefore, the study on the shear behavior, the relative mechanical properties and the seismic capacity of masonry structures under the combined action of shear and compression is carried out, which is of great significance to the application of prestressed masonry structure in China.

2. State of the art

He [6] systematically collected and sorted out the failure modes of masonry during shearing, and considered that vertical joint did not transfer stress, especially shear stress. In 1990s, the concrete hollow block had gradually replaced the solid clay bricks become the mainstream in bulk. The masonry structure code revised by the American Masonry Standards Federation included the prestressed masonry structure as a separate structural form, and gave the corresponding calculation indexes [7]. Incerti carried on the shear test of masonry specimens, and proved that the experimental values of the shear strength of masonry under shear compression composite were in good agreement with Coulomb friction theory [8]. Sathiparan carried on the shearing proof and the compression test to the hollow brick masonry standard brick, and he proved the comprehensive influence of various factors such as surface treatment and groove shape of block [9]. Elmenshawi analyzed the results of double brick single shear strength test of solid brick and hollow brick masonry, and proved that it was elastic before breaking [10]. Buch conducted the two-way shear compression interaction test, and it was proved that the shear strength of standard joints was approximately linearly related to the increase of compressive strength [11]. Min carried out the masonry shear test under axial compression, and he proved that processing the bulk surface could improve the shear strength of masonry [12]. Mansouri proved that the wetting of block before masonry and maintenance could improve the shear strength of masonry [13]. The shear tests of masonry walls were carried out by Janaraj. It was proved that the calculated strength of the main tensile stress failure theory was close to the experimental results [14]. The single shear test of brick masonry was carried out by Chourasia, and the tension and compression model of masonry under shear was put forward. The results of microscopic numerical analysis and finite element analysis showed good agreement with the test [15].

3. Methodology

3.1. Design and manufacture of specimen

The study applied the prestressing force to masonry structures, so as to give some advantages to prestressed concrete structures. The channels of prestressed masonry structure can avoid the complicated procedures of the channel reservation and the second grouting construction during the construction of prestressed concrete, which can not only save the project cost, but also enhance the efficiency of the project. In general, the prestressing force of prestressed masonry structures is low, so that even relatively simple equipment, such as jacks and torque wrenches, can be used to perform prestressing tensioning. As a result of prestressed tensioning, the material of masonry block has basically been completed contraction. Therefore, its shrinkage and creep are smaller than the prestress loss of prestressed concrete. However, the prestressed masonry structure also has some shortcomings. For example, the prestressing bars can only be arranged in a straight line due to different type and manner of the blocks. Due to the prearranged prestressed steel bars, there will be some inconveniences in the subsequent construction process. The shear specimens used in this study were made of three skin staggered masonry, which consisted of 2 plates and 2 standard blocks. The size of the sample was 590 mm×390 mm×190 mm. The arrangement is shown in Fig. 1.

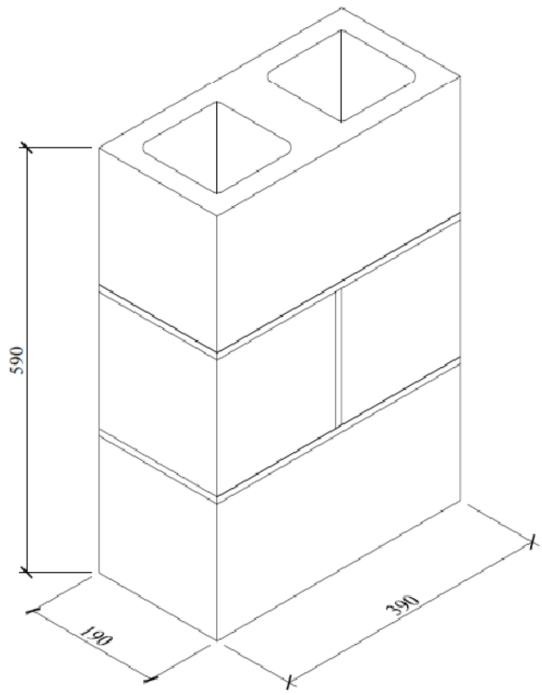

Fig. 1. Sketch map of standard parts (units: mm)

In the process of testing, the basic mechanical properties of specimens were obtained by compression test of standard parts, and further analysis was conducted. In order to ensure the consistency of the compressive and shear specimens, the shear standard component specification and the three-skin and non-five-skin staggered joint masonry standard were adopted. In this way, it can be more standardized to point out that the compressive strength of the specimens was not significantly different when the ratio of height to thickness of masonry was 3 and 5, respectively. The test method for shear strength of masonry along the through section is shown in Fig. 2.

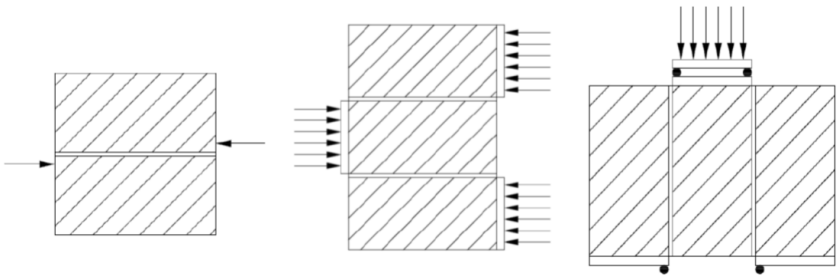

Fig. 2. Test method for shear strength of masonry along the through joint

In this experiment, the orthogonal design method was adopted to complete the one-way shear test of 24 hollow block standard parts, tests on pre compression joint shear of 12 hollow block masonry standard pieces, and uniaxial compressive test of 15 hollow block masonry standard parts. The orthogonal combination of the strength grade of block and mortar was mainly considered in the hollow standard parts. The specific design scheme is shown in Table 1.

Table 1. Design scheme of standard parts for hollow block masonry

Block strength	Mb5	Mortar strengthMb10	Mb15
MU10	K1\MK1	K2	
MU15	SK2\MK2	K3\SK1\MK3	K4\SK3
MU20		MK4	K5\MK5

The letter number K represented the shear specimen of the through seam with EN loading method. The letter number SK represented the shear specimen of the through seam with GB loading method. The letter number MK represented the uniaxial compression specimen. There were 3 specimens in each group. The material used in the pre compression joint shear test had the same strength grade as MU15, Mb10 and Cb20. The variable was the magnitude of the preload. The specific design is shown in Table 2. The letter number YK represents the prestressed hollow masonry shear specimens.

Since the standard block had very strong water absorption, it was necessary to ensure that all the blocks were adequately wetted before masonry. All the smooth boards were prepared in advance, and all the standard pieces were made on the

boards. In order to ensure the smoothness of the boards, cement mortar was used before the masonry. In the construction process, we effectively discriminate the plasma surface and bulk surface, so as to avoid the reverse situation. Because the bulk was inevitable certain difference, it was difficult to ensure bulk of the two planes parallel. Therefore, in carrying out specific construction, the main task was to ensure the parallelism of each paste surface and each surface. The plumpness of mortar directly affected the shear area of the ash joint, and then affected the shear strength. Therefore, it was necessary to ensure the mortar plumpness of the test block. The mortar was cleaned or removed if the mortar was smoothed.

Table 2. Design standard for shear compression standard piece of pre compression joint

Specimen	Preload size				
	0.28	0.41	0.55	0.68	1.02
Hollow	YK1	YK2		YK3	YK4

After the completion of masonry, it needed to be cured and sealed with test film. Continuous watering during the maintenance period was needed to ensure a moist environment for 7 days. Grouted standard parts needed pouring column 7 days later in the masonry. The adopted concrete was fabricated by field mixing, and the method of layered casting was adopted in the pouring process. After pouring, the vibrator should be vibrated to ensure the compactness of the concrete. In the 30 days after the completion of the casting, the sealed moisture conservation was needed, so as to ensure the strength of concrete.

In the building design of standard parts, because the bulk may have rough surface inequality defects and construction error, it was difficult to ensure absolute flatness and surface parallel test on the surface. If the masonry surface was not smooth, it may cause uneven stress within the masonry and affect the mechanical properties in the shear stress and compression test. Therefore, during the construction process, reasonable measures must be taken to ensure the smoothness of the surface of the specimen and ensure the uniformity of the specimen.

3.2. Measurement scheme

In the test process, the concrete steps of loading scheme were as follows.

(1) Firstly, the initial limit load of block and mortar strength specimens were estimated.

(2) The appearance breakage and defects of the specimen were inspected and recorded, and the force surface size of the standard parts was measured in detail. In particular, it was necessary to measure the height difference between the upper and lower surfaces of the shear and prestressed specimens, so as to ensure their parallelism.

(3) The installation of the specimens was carried out. The relevant measuring instruments were checked, calibrated and reset to ensure the normal use of the measuring instruments.

(4) The loading of the specimens: the loading schemes of different specimens were

different, and the shear standard parts were subjected to continuous loading with constant rate. The standard component of prestressing force adopted horizontal pressure loading. Preloading was used for compression of standard parts.

(5) As long as a shear surface was destroyed, the one-way shear criterion determined the loss of its bearing capacity. The prepressed standard continued to load when the peak was reached, until a sudden drop or slippage of the load occurred. The pressure gauge continued to load until it was broken.

(6) The loading of the specimen: the cracks and characteristics of the specimens were observed, and the corresponding load values were recorded. After loading the load, a crack map and took pictures were drawn.

In the process of testing, the data of shear standard parts should be continuously measured, including shear load, shear deformation, horizontal axial pressure and so on. Among them, the load sensor was used to measure the load size, and high precision displacement sensors were used to measure shear deformation. In addition, the measurement of horizontal and vertical deformation of standard parts was also included. The vertical load was measured by force sensors.

In the test of the compressive strength, according to the test requirements in the test method, the 190 mm standard block with the same batch of masonry blocks was selected. In order to minimize the influence of the uneven surface of the block on the results of the test, it was necessary to use high-strength gypsum (1:2) to process the upper and lower surfaces of the block and test it on the 5000KN press. Sand filling method was used to measure the void ratio of standard blocks, and the final porosity was 46.7%. The mean strength and coefficient of variation of compressive strength of each block are shown in Table 3.

Table 3. Block compressive strength

Strength grade	Average compressive strength	Single block minimum strength	Coefficient of variation	Rating of strength
MU10	13.51	11.73	8.15%	MU10
MU15	19.86	16.05	9.68%	MU15
MU20	20.91	19.01	12.61%	MU20

Standard blocks were leveled and damaged, as shown in Fig. 3.

4. Result analysis and discussion

The failure state and crack propagation of concrete hollow compression specimens are shown in Fig. 4.

Based on the comprehensive research at home and abroad, the experimental phenomena and results, the study was carried out in this paper. When the concrete block masonry was subjected to uniaxial compression, the loading failure process could be divided into the following four stages according to the development of

cracks.

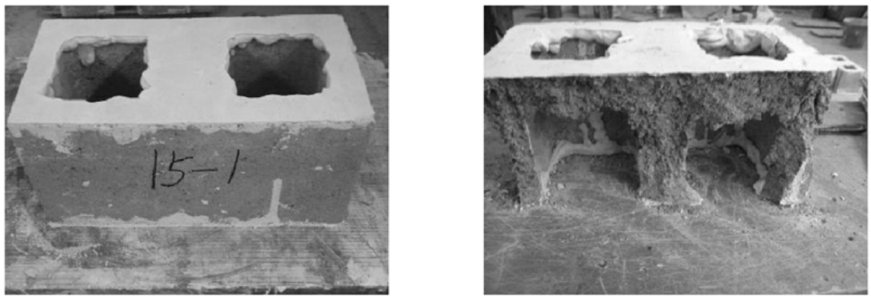

Fig. 3. Setting and destruction of building blocks

Fig. 4. Failure state of hollow compression standard parts

The first stage was the compression of the standard piece and the presence of the first crack. In this stage, the vertical deformation of the standard parts was relatively small. This stage was the elastic force state, and the load displacement had the linear relationship. The strain at this stage failed to produce initial microcracks. The second stage had the first crack. As the load continued to increase, the standard parts began to make minor noises from the inside, and cracks began to appear at the chamfer of the specimen. The cracks in this stage were slender and developed slowly, and the load displacement was linear.

The third stage: as the load increased to the peak, the cracks continued to expand, and the final specimen had plastic deformation. Cracks expanded with the increase of load, and more narrow vertical cracks appeared in the narrow surface of standard parts, which showed a remarkable nonlinear load displacement curve. The slope decreased until the final plastic deformation occurred.

The fourth stage: when the load exceeded the peak value, the specimen presented a brittle failure and lost the ability to continue bearing. When the load exceeded the peak value, the bearing capacity of the specimen continued to decline, and the specimens began to appear through the vertical cracks, which had eventually brittle fracture and the loss of carrying capacity. The initial load, the peak load, the compressive strength, the initial crack coefficient and the coefficient of variation measured by the hollow compression standard are shown in Table 4.

Table 4. Compressive strength of hollow standard parts

Group	Number	Initial crack load (kN)	Peak load (kN)	Compressive strength (MPa)	Compressive strength average (MPa)	Coefficient of variation of Compressive strength	Initial crack coefficient	Mean of initial crack coefficient	Coefficient of variation of initial crack coefficient (%)
MK1	MK1-1 MK1-2 MK1-3	268 523 276	482 640 401	6.49 8.61 5.38	6.82	19.5	0.556 0.816 0.688	0.687	10.5
MK2	MK2-1 MK2-2 MK2-3	404 333 569	711 739 741	9.60 9.94 9.99	9.84	1.74	0.568 0.450 0.767	0.595	6.19
MK3	MK3-1 MK3-2 MK3-3	422 466 589	734 797 911	9.95 10.68 12.29	10.94	9.24	0.576 0.584 0.646	0.602	6.10
MK4	MK4-1 MK4-2 MK4-3	411 464 385	569 938 687	7.63 12.55 9.19	9.79	20.9	0.722 0.494 0.560	0.592	7.75
MK5	MK5-1 MK5-2 MK5-3	1147 614 830	1229 1069 966	16.53 14.34 2.89	14.59	10.2	0.932 0.574 0.878	0.788	4.76

Through the analysis results, it can be seen that under the action of load, the specimen usually cracked from the hole of the block. The stress tended to focus on the block than rib thickness reduced parts, so that the transverse tensile specimen stress was much greater than its tensile strain limit of material. Furthermore, it could be seen from the table that the initial split coefficient of hollow standard parts was in the range of 0.6∼0.8. Because of the great brittleness of the specimen, the crack was developed rapidly and finally destroyed.

The compressive strength of mortar with block and mortar were f_1 and f_2. The coefficient of masonry category and the coefficient of mortar strength were k_1 and k_2, respectively. For hollow masonry with the strength grade of MU20, the compressive strength needed to be multiplied by 0.95 of the correction factor. A formula for calculating the average compressive strength of concrete hollow block masonry f_{m}^0 is as follows.

$$f_{\mathrm{m}}^0 = k_1 f_1^{0.9}(1 + 0.07 f_2) k_2 \,. \tag{1}$$

The comparison between the measured compressive strength and the calculated

values is shown in Table 5.

Table 5. Comparison of compressive strength test values and calculated values of hollow standard parts

Group	f_1 (MPa)	f_2 (MPa)	f_{m} (MPa)	f'_{m} (MPa)	f^0_{m} (MPa)	$f_{\mathrm{m}}/f^0_{\mathrm{m}}$
MK1	13.49	5.78	6.82	12.81	6.78	1.006
MK2	19.84	5.96	9.84	18.47	9.59	1.025
MK3	19.84	10.48	10.94	20.53	11.68	0.936
MK4	20.89	10.48	9.79	18.38	11.62	0.842
MK5	20.98	13.72	14.59	20.89	12.71	1.146
Average value						0.991
Coefficient of variation						10.1 %

From the further analysis in Table 5, it could be seen that the results obtained from this test had a good fitting effect with the calculated results based on the specifications, which showed that the data was relatively reasonable. However, there were still some problems. When calculating the compressive strength of masonry, the ratio of the load value to the gross sectional area was obtained. This was not sufficiently related to the failure criteria of mortar and block materials. Therefore, it was difficult to carry out the relevant mechanical analysis and formula deduction based on theory. Even when considering the coefficient of 1.1 times, because the void ratio was small, the hollow block masonry was still low in formula calculation. In the calculation of high strength block and mortar, we must consider the correction factor, which increased the complexity of calculation.

In fact, the compressive strength of hollow block masonry was determined by the compressive strength of the material and its net cross sectional area A. The formula for calculating the compressive strength f'_m of material per unit area is

$$f'_m = \frac{N}{A(1-\alpha)}\,, \tag{2}$$

where N is the pressure, A denotes the per unit area, α is the effect of hole ratio coefficient on compressive strength of masonry (this formula considering the effect of hole ratio on compressive strength of masonry with $A(1-\alpha)$ net section area, calculated in the calculation of compressive strength of f'_m). Even the masonry bearing capacity to meet the requirements, but due to the void ratio are not satisfied with limited time and the compressive strength of material f'_m is insufficient, the calculating method for bearing hollow block masonry in numerical value is the same. In the design and construction practice, should be void ratio δ as a control index.

5. Conclusion

Based on the seismic shear strength test of standard parts of hollow concrete block masonry and the existing research results, the influences of loading mode,

material strength, structure form and pre-stress on the seismic and shear resistance of masonry were analyzed. Main results were as follows: the modulus of elasticity of hollow block masonry was higher than the calculation value of masonry in the present standard, and the value of masonry was improved to a certain extent. The results of the compression test coincided with the calculated results. The shear stress composite stress coefficient given in the present masonry specifications was not applicable to concrete hollow block masonry built with special mortar, which presented a low state. Therefore, it was necessary to cancel the correction factor of the average formula on the basis of the original standard, and the friction coefficient was 0.7. Based on the measured shear load displacement curve, the coefficient expressions of seismic shear strength of prestressed hollow brick masonry were obtained. Furthermore, a piecewise expression of the dimensionless load displacement curve of masonry under seismic shear was obtained. In this paper, the seismic shear strength of hollow block masonry was studied in this paper, and the seismic shear strength of grouted masonry will be studied in the next step. Because of the higher shear capacity of grouted masonry, the grouted masonry test under different axial compression ratio was used to establish the intact shear compression bearing capacity curve of masonry.

References

[1] D. A. Hidalgo-Leiva, L. P. Beneit, A. H. Barbat, D. Acuña-García: *Experimental analysis of in-plane shear strength of reinforced concrete masonry wall and its seismic behavior.* International Brick & Block Masonry Conference (IBMAC), 26–30 June 2016, Padova, Italy, CRC Press (2016), 2295–2302.

[2] M. Betti, L. Galano, M. Petracchi, A. Vignoli: *Diagonal cracking shear strength of unreinforced masonry panels: A correction proposal of the b-shape factor.* Bulletin of Earthquake Engineering *13* (2015), No. 10, 3151–3186.

[3] J. G. Eixenberger, F. S. Fonseca: *Shear strength of dry-stack masonry walls.* International Brick & Block Masonry Conference (IBMAC), 26–30 June 2016, Padova, Italy, CRC Press (2016), 1539–1544.

[4] L. Facconi, A. Conforti, F. Minelli, G. A. Plizzari: *Improving shear strength of unreinforced masonry walls by nano-reinforced fibrous mortar coating.* Materials and Structures *48* (2015), No. 8, 2557–2574.

[5] J. Yu, F. Zhang, G. Bai: *Experimental study on shear behaviour of recycled concrete hollow block masonry.* Materials Research Innovations *19* (2015), No. S8, 579–583.

[6] X. X. He, Y. Lins: *Test & research on the shearing strength of the continuous seams in the mortar-less fabricated block & masonry.* Applied Mechanics and Materials *777* (2015), 194–200.

[7] M. Sedlmajer, J. Zach, V. Novak, J. Hroudova, A. Horsky: *Alternative technology of constructing masonry structures designed for areas with increased seismic activity.* Procedia Engineering *151* (2016), 177–182.

[8] A. Incerti, V. Rinaldini, C. Mazzotti: *The evaluation of masonry shear strength by means of different experimental techniques: A comparison between full-scale and laboratory tests.* International Brick & Block Masonry Conference (IBMAC), 26–30 June 2016, Padova, Italy, CRC Press (2016), 1645–1652.

[9] N. Sathiparan, W. A. V. Anjalee, K. K. S. Kandage: *The scale effect on small-scale modelling of cement block masonry.* Materials and Structures *49* (2016), No. 7, 2935–2946.

[10] A. Elmenshawi, N. Shrive: *Assessment of multi-wythe stone masonry subjected to seismic hazards.* Journal of Earthquake Engineering *19* (2015), No. 1, 85–106.

[11] S. H. Buch, D. M. Bhat: *Performance of hollow concrete block masonry under lateral loads.* Advances in Structural Engineering, Edition: I, Publisher: Springer India (2015), 2435-2444.

[12] E. Yu, M. J. Kim, S. H. Lee, C. M. Kim: *Relation between shear strength of masonry infills and seismic performance of masonry-infilled frames.* Journal of the Earthquake Enginerring Society of Korea *19* (2015), No. 4, 173–181.

[13] A. Mansouri, M. S. Marefat, M. Khanmohammadi: *Experimental evaluation of seismic performance of low-shear strength masonry infills with openings in reinforced concrete frames with deficient seismic details.* Structural Design of Tall and Special Buildings *23* (2014), No. 15, 1190–1210.

[14] T. Janaraj, M. Dhanasekar: *Design expressions for the in-plane shear capacity of confined masonry shear walls containing squat panels.* Journal of Structural Engineering *142* (2016), No. 2, paper 04015127.

[15] A. Chourasia, S. K. Bhattacharyya: *Influence of plaster thickness of shear strength of solid clay brick masonry.* International Brick & Block Masonry Conference (IBMAC), 26–30 June 2016, Padova, Italy, CRC Press (2016).

Received May 7, 2017

Acta Technica *62* No. 2B/2017, 205–218

Inertial/celestial integrated navigation algorithm for long endurance unmanned aerial vehicle[1]

Fang Ting[2,3], Huang Xiaoming[2]

Abstract. In recent years, unmanned aerial vehicle (UAV) technology has been widely used in military and civil fields because of many advantages, such as low cost and no need of personal operation, among them, the most strategic value is long endurance UAVs. The strapdown inertial navigation system proposed in this paper was an inertial navigation algorithm for such long endurance UAVs. Simulation analysis and practical application of the algorithm were carried out to verify the feasibility of the algorithm in specific applications. In addition, the characteristics of pure inertial navigation system without correction and the reasons for the occurrence of navigation error were analyzed, so as to provide a reference for modular design of integrated navigation system.

Key words. Long endurance unmanned aerial vehicle (UAV), strapdown inertial navigation system (SINS), integrated navigation system.

1. Introduction

The development of UAVs makes our production, life and other fields have undergone great changes. Whether it is in agriculture or military applications, it is hoped that UAVs can have longer time navigation. However, high-altitude long endurance UAVs has higher requirements for navigation, such as higher accuracy and autonomy, which is difficult to achieve for traditional single navigation systems [1]. It can be seen from the analysis that both celestial navigation and inertial navigation system have their own characteristics. After combining them, they can give full play to the advantages of the two, realize complementary advantages, and eventually build a strong anti-interference, high precision navigation system [2]. The success of high-altitude long endurance UAVs is inseparable from a stable and reliable navigation system. Compared with other types of UAVs, its particularity of operating environment makes it more demanding for navigation system [3]. For the

[1]School of Electrical and Information Engineering, Anhui University of Technology, Maanshan, Anhui, 243000, China
[2]Corresponding author

high-altitude photography, measurement and control, and reconnaissance tasks conducted by aerial high-altitude (HALE) unmanned aerial vehicle, it is necessary to equip with optical/electronic detection equipment and provide accurate positioning accuracy and a stable working environment for the equipment [4].

In addition to aerial reconnaissance and control class UAVs, when the HALE UAV is engaged in similar work such as geographical mapping, it also requires navigation systems to provide very high precision for these devices, so as to guarantee high resolution images and other information in the process of geographical mapping [5]. In the long standing environment, the internal and external environment of UAVs is relatively complex, and there is a great deal of interference. Therefore, the UAV navigation system must be highly reliable and have high anti-interference capability [6]. In view of this special demand, the UAV navigation sensor, whether it is configuration or system structure, has a higher demand. Therefore, the algorithm of relative integrated navigation has certain application value.

2. State of the art

The UAV technology of our country is relatively advanced in the world. From the initial development so far, it has experienced forty years. A series of different purposes, different properties of the drone reconnaissance aircraft, and general UAVs have been successfully developed, which are now widely used in various industries [7]. The UAV technology of our country is relatively mature, and the UAVs have excellent performance, which are loved by domestic and overseas users. One of the most typical representatives of the long endurance UAV is Xianglong UAV. Its continued sailing time has reached more than 10 h, which is prominent in the same type of UAVs [8].

After decades of development, the current methods of celestial navigation used by UAVs mainly include direct and indirect sensitive horizon. The latter uses the principle of starlight refraction to make a higher progress [9]. The existing indirect sensitive horizon method has to be realized on the basis of orbital dynamics. But for long endurance UAVs, their kinematic characteristics do not meet the conditions of use [10]. In this case, it is necessary to design a strapdown inertial navigation algorithm that can be used in engineering practice. According to different installation methods of measurement devices, the inertial navigation system can be divided into two types, platform type and strapdown inertial navigation system [11]. Because inertial platform is relatively large in volume and quality, it results in higher cost of platform inertial navigation system. In addition, because of its complicated structure, the failure rate is relatively high, and its reliability is difficult to be effectively guaranteed. The development of inertial sensors has led to strapdown inertial navigation gradually replacing platform type systems. With the development of modern computer information technology, an inertial/satellite integrated navigation system has come into being in order to satisfy the rapid development of UAV industry.

3. Methodology

3.1. The basic principle of strapdown inertial navigation

Strapdown inertial navigation system (SINS) used in UAVs is an inertial accelerometer, such as accelerometer and gyroscope, which is fixed on UAV platform. These sensors are used to carry out the UAV body coordinate system, as well as acceleration and angular increments. The accelerometer calculates the projection of the acceleration component in the inertial coordinate system in the body coordinate system. What are measured by the gyro include the projection of the UAV in the body coordinate system and the angular rate of rotation relative to the inertial space. The coordinate system of UAV is relative to the navigation coordinate system, which is the required navigation information. According to the situation, the Northeast terrain coordinate system is adopted. In order to obtain the strapdown matrix, it is necessary to convert the volume of the body coordinate system relative to the inertial coordinate to that of the geographic coordinate system. The strapdown attitude can be used to calculate the relative information of the body, and the relative information can be transformed from the relative coordinate system to the geographical coordinate system.

An example of long endurance unmanned aerial vehicle that could be equipped with the strapdown inertial navigation is shown in Fig. 1.

Fig. 1. Long endurance unmanned aerial vehicle

The working principle of strapdown inertial navigation system is that when the initial conditions are determined, the attitude, position and velocity of the vector

are computed by the measured results of the inertial component, and the navigation parameters in the navigation coordinate system are converted into the navigation parameters. For only a simple inertial navigation system, the accurate navigation parameters cannot be obtained if the accuracy of the inertial period is low. In the case of integral action, there will be cumulative errors. Therefore, it is necessary to combine it with visual navigation or satellite navigation, and the Kalman filter is used to correct the initial and parameter errors in inertial navigation to ensure the accuracy of navigation parameters. The principle of strapdown inertial navigation system is shown in Fig. 2.

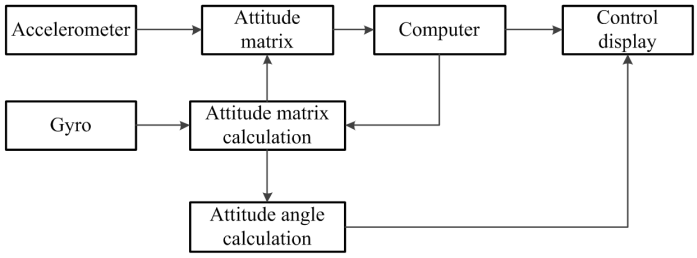

Fig. 2. Scheme of strapdown inertial navigation system

The design scheme of the UAV navigation development contains many contents, including the measuring information of simulated gyroscope and accelerometer, the output of the GPS module design, trajectory generation module planning, the design of strapdown inertial navigation module and the design of visual measurement module [12]. The first step is to simulate the track according to the actual situation of the planning, and obtain the UAV attitude, velocity, acceleration and angular speed and position of the ideal information. In addition, the error is added to the real error model to simulate the outputs of inertial devices, satellite systems and visual system measurements. Finally, the outputs of the inertial navigation system are calculated. Then, according to the needs of UAV navigation, the appropriate data fusion method is chosen, and the corresponding sensor output is called to estimate the parameters of the strapdown inertial navigation system. The error correction is also included in the calculation result, which includes the deviation of the sensing element. Finally, the output of the combined system is shown, and finally the simulation design of the UAV integrated navigation system is completed.

3.2. Design of linked inertial navigation algorithm

The attitude of UAV is solved by using strapdown navigation system, which is to solve the attitude differential equation by using the angular increment information produced by inertial component. Finally, the angle information rotation relationship between the machine system and the navigation system is obtained by using the calculated results. By calculating the attitude matrix values, the attitude information in different directions of the UAV can be obtained, and the attitude information matrix can be updated by using the continuous output of the inertial components, so that the attitude update can be carried out. Whether it is speed, posture, or po-

sition, the navigation parameter information must have a reference standard when it is expressed. On the other hand, the output information of inertial devices such as inertial sensors in inertial navigation systems is relative to the inertial coordinate system. Therefore, the definition of the common coordinate system must be carried out. In the process of navigation, the types of coordinate systems used by UAVs are very large. According to this demand, the department of geography is chosen as the navigation system of unmanned aerial vehicle during flight. Based on the needs of the research, the conversion of the full text and the analysis of the coordinate system are carried out in this paper.

A rigid body acts as a fixed point at one point of the body and rotates on an axis, so that it can rotate to achieve any gesture. The rotation process of the quaternion can be expressed as follows:

$$q = \cos\frac{\theta}{2} + \sin\frac{\theta}{2} \cdot \boldsymbol{n} = \cos\frac{\theta}{2} + \sin\frac{\theta}{2}\cos\alpha \cdot i + \sin\frac{\theta}{2}\cos\beta \cdot j + \sin\frac{\theta}{2}\cos\gamma \cdot k\,. \quad (1)$$

In formula (1),

$$q_0\,(0) = \cos\frac{\theta_0}{2}\sin\frac{\varphi_0}{2}\cos\frac{\gamma_0}{2} - \sin\frac{\theta_0}{2}\sin\frac{\varphi_0}{2}\sin\frac{\gamma_0}{2},$$

$$q_1\,(0) = \sin\frac{\theta_0}{2}\cos\frac{\varphi_0}{2}\cos\frac{\gamma_0}{2} - \cos\frac{\theta_0}{2}\sin\frac{\varphi_0}{2}\sin\frac{\gamma_0}{2},$$

$$q_2\,(0) = \cos\frac{\theta_0}{2}\cos\frac{\varphi_0}{2}\sin\frac{\gamma_0}{2} + \sin\frac{\theta_0}{2}\sin\frac{\varphi_0}{2}\cos\frac{\gamma_0}{2},$$

$$q_3\,(0) = \cos\frac{\theta_0}{2}\sin\frac{\varphi_0}{2}\cos\frac{\gamma_0}{2} + \sin\frac{\theta_0}{2}\cos\frac{\varphi_0}{2}\sin\frac{\gamma_0}{2}.$$

In the upper form, q represents the displacement vector of the rigid body and has a directionality. Symbol θ represents the angle of rotation of a rigid body with an axis, and α, β, γ represent the angles between the motion direction of the rigid body and coordinate axes, respectively. In addition, in order to facilitate full text coordinate conversion, the subscripts are interpreted as follows: geographic coordinate system - subscript t, earth coordinate system - subscript e, inertial coordinate system - subscript i.

It is assumed that the rotation angle speed of UAV is ω. When the quaternion differential equation and its own coordinate system are in line with the coordinate system of the UAV, the attitude calculation formula of the UAV can be obtained:

$$\dot{q} = \frac{1}{2} q \cdot \omega\,. \quad (2)$$

Formula (2), since the true value corresponding to the quaternion can be seen as

0, can be rewritten and the corresponding matrix is obtained

$$\begin{bmatrix} \dot{q}_0 \\ \dot{q}_1 \\ \dot{q}_2 \\ \dot{q}_3 \end{bmatrix} = \frac{1}{2} \begin{bmatrix} 0 & -\omega_x & -\omega_y & -\omega_z \\ \omega_x & 0 & \omega_z & -\omega_y \\ \omega_y & -\omega_z & 0 & \omega_x \\ \omega_z & \omega_y & -\omega_x & 0 \end{bmatrix} \begin{bmatrix} q_0 \\ q_1 \\ q_2 \\ q_3 \end{bmatrix} \tag{3}$$

The calculation of the angular rate in formula (3) is

$$\omega_{tb}^b = \omega_{ib}^b - \omega_{it}^b = \omega_{ib}^b - C_t^b \left(\omega_{eb}^t + \omega_{ie}^t\right) \tag{4}$$

By solving the differential equations of the quaternion, the real-time attitude of the UAV can be obtained by using the result of the calculation, and the strapdown attitude matrix T (C_b^t) is obtained in the form

$$T = \begin{bmatrix} q_0^2 + q_1^2 - q_2^2 - q_3^2 & 2\left(q_1 q_2 - q_0 q_3\right) & 2\left(q_1 q_3 + q_0 q_2\right) \\ 2\left(q_1 q_2 + q_0 q_3\right) & q_0^2 - q_1^2 + q_2^2 - q_3^2 & 2\left(q_2 q_3 - q_0 q_1\right) \\ 2\left(q_1 q_3 - q_0 q_2\right) & 2\left(q_2 q_3 + q_0 q_1\right) & q_0^2 - q_1^2 - q_2^2 + q_3^2 \end{bmatrix}. \tag{5}$$

The Picard solution method is selected for the solving the quaternion may be written as

$$\dot{q}\left(t\right) = \frac{1}{2} \Omega_b q\left(t\right). \tag{6}$$

It is further converted into an iterative form

$$q\left(t\right) = \left\{ \cos \frac{\Delta\theta_0}{2} \cdot I + \frac{1}{\Delta\theta_0} \sin \frac{\Delta\theta_0}{2} \Delta\Theta \right\} q\left(0\right), \tag{7}$$

$$q\left(n+1\right) = \left\{ \cos \frac{\Delta\theta_0}{2} \cdot I + \frac{1}{\Delta\theta_0} \sin \frac{\Delta\theta_0}{2} \Delta\Theta \right\} q\left(n\right). \tag{8}$$

The solution of the differential equation can be calculated. The attitude angle is calculated by using strapdown matrix, and the following parameters are included

$$\theta = \sin^{-1} T_{32}, \tag{9}$$

$$\gamma = \tan^{-1}\left(-\frac{T_{31}}{T_{33}}\right), \tag{10}$$

$$\varphi = \tan^{-1}\left(-\frac{T_{12}}{T_{22}}\right). \tag{11}$$

Here $\gamma = \begin{cases} \gamma & T_{33} > 0, \\ \gamma + 180^o & T_{33} < 0, \gamma < 0, \\ \gamma - 180^o & T_{33} < 0, \gamma > 0, \end{cases} \quad \psi = \begin{cases} \varphi & T_{22} > 0, \psi > 0, \\ \varphi + 360^o & T_{22} > 0, \psi < 0, \\ \varphi + 180^o & T_{22} < 0. \end{cases}$

On this basis, the most important information about the navigation, including pitch, roll and yaw can be obtained. With the rotation of the earth, the angular

velocity component of the geographic system in three directions is calculated as

$$\begin{cases} \omega_{ieE}^{t} = 0, \\ \omega_{ieN}^{t} = \omega_{ie} \cos L, \\ \omega_{ieU}^{t} = \omega_{ie} \sin L. \end{cases} \tag{12}$$

With the UAV movement, the change of angular velocity between the geographical coordinate system and the earth coordinate system can be expressed as

$$\begin{cases} \omega_{etE}^{t} = -\frac{V_N^t}{R_m+h}, \\ \omega_{etN}^{t} = \frac{V_E^t}{R_n+h}, \\ \omega_{etU}^{t} = \frac{V_E^t}{R_n+h} \tan L. \end{cases} \tag{13}$$

Thus, the sum of the angular velocity components between the geographical coordinate system and the earth coordinate system can be calculated. And the tracking angle rate of sins is obtained:

$$\begin{cases} \omega_{itE}^{t} = -\frac{V_N^t}{R_m+h}, \\ \omega_{itN}^{t} = \omega_{ie} \cos L + \frac{V_E^t}{R_n+h}, \\ \omega_{itU}^{t} = \omega_{ie} \sin L + \frac{V_E^t}{R_n+h} \tan L. \end{cases} \tag{14}$$

In the above formula, R_m represents the radius of curvature on the meridian of the earth ellipsoid, R_n represents the radius of curvature of the earth reference meridian, and $\omega_{itE}^{t}, \omega_{itN}^{t}, \omega_{itU}^{t}$ represent the matching information of the white noise measured by the gyro in all directions of the earth. Symbol ε represents the platform equivalent error rotation caused by gyro drift, ϕ denotes the attitude deviation of the UAV mathematical platform written in the corresponding variables in the geographic system and L denotes latitude information. Finally, V represents the speed vector of the UAV in all directions.

The output measured by the accelerometer on the UAV is not the data of the aircraft system relative to the navigation system, so the geographic system t is needed as the navigation system of the UAV. By using the matrix C_b^t, the relative information of the machine system relative to the inertial system is converted into the comparative information relative to the geographic system

$$f^t = C_b^t f^b \,. \tag{15}$$

In the upper form, f^t represents the comparative information of the geographic system, C_b^t represents the transformation matrix, and f^b represents the comparative information of the machine system.

The formula (15) is unfolded and we can obtain the formula as follows

$$\begin{bmatrix} f_E^t \\ f_N^t \\ f_U^t \end{bmatrix} = \begin{bmatrix} T_{11} & T_{12} & T_{13} \\ T_{21} & T_{21} & T_{23} \\ T_{31} & T_{32} & T_{33} \end{bmatrix} \begin{bmatrix} f_E^b \\ f_N^b \\ f_U^b \end{bmatrix} . \tag{16}$$

In summary, the basic equation of inertial navigation system can be obtained

$$\dot{V}_{et} = f - (2\omega_{ie} + \omega_{et}) \times V_{et} - g\,. \tag{17}$$

The formula (17) is unfolded and we can obtain the formula as follows.

$$\begin{bmatrix} \dot{V}_E^t \\ \dot{V}_N^t \\ V_U^t \end{bmatrix} = \begin{bmatrix} f_E^t \\ f_N^t \\ f_U^t \end{bmatrix} - \left(- \begin{bmatrix} 0 & -(2\omega_{ieU}^t + \omega_{etU}^t) & 2\omega_{ieN}^t + \omega_{etN}^t \\ 2\omega_{ieU}^t + \omega_{etU}^t & 0 & -(2\omega_{ieE}^t + \omega_{etE}^t) \\ -(2\omega_{ieN}^t + \omega_{etN}^t) & 2\omega_{ieE}^t + \omega_{etE}^t & 0 \end{bmatrix} \cdot \begin{bmatrix} V_E^t \\ V_N^t \\ V_U^t \end{bmatrix} + \begin{bmatrix} 0 \\ 0 \\ -g \end{bmatrix} \right). \tag{18}$$

3.3. Flow arrangement of linked inertial navigation algorithm

By inertial navigation, a very accurate horizontal attitude can be provided. On this basis, the platform type astronomical positioning can further obtain the accurate two-dimensional position information through the height difference method. The study of inertial celestial navigation is the analysis of integrated navigation based on the whole platform model. When using celestial navigation positioning, in order to avoid the accuracy of positioning due to the lack of height information, the pressure altimeter is usually used for auxiliary positioning to ensure the observability of the height channel. Through the combination of navigation system design, the autonomy and navigation precision of the navigation system can be guaranteed.

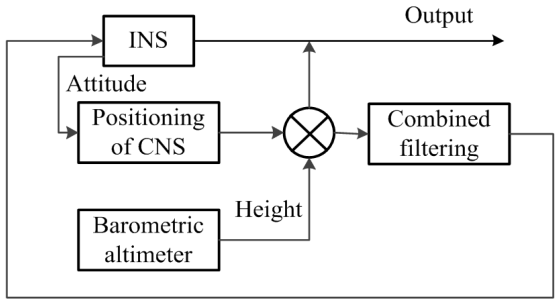

Fig. 3. Scheme of inertial/astronomical position combination

In the design of strapdown inertial navigation algorithm, the initial velocity, attitude and location information must be calculated or given. Each of these initial parameters contains both the true initial information and the initial error. By using the initial information alignment method in inertial navigation, the initial attitude

misalignment angle can be determined, and the integrated navigation can also be estimated under static conditions. After the initial state of UAV operation is determined, the strapdown inertial navigation algorithm can be used to calculate. The flow of the design using this algorithm is shown in Fig. 4.

4. Result analysis and discussion

Based on the above mentioned UAV integrated navigation system algorithm and related design, the simulation research was carried out. The simulation time was 84 h, and the acceleration time of the accelerometer and gyroscope in the UAV navigation system was 0.01 s. The initial attitude was a stationary condition, and the velocity was 0. The initial parameters are as follows:

(1) Initial position: latitude and longitude were 105.63 and 45 degrees, and the height was 1 km.

(2) Initial error: the deviation of initial position and velocity was zero, and the deviation of pitch angle was 0.2 degrees.

(3) Gyro error: measurement noise and Changzhi drift were 0.05 and 0.5 degree/h, respectively.

(4) The error of accelerometer: noise measurement and bias error were 10^{-5} g and 10^{-4} g, respectively.

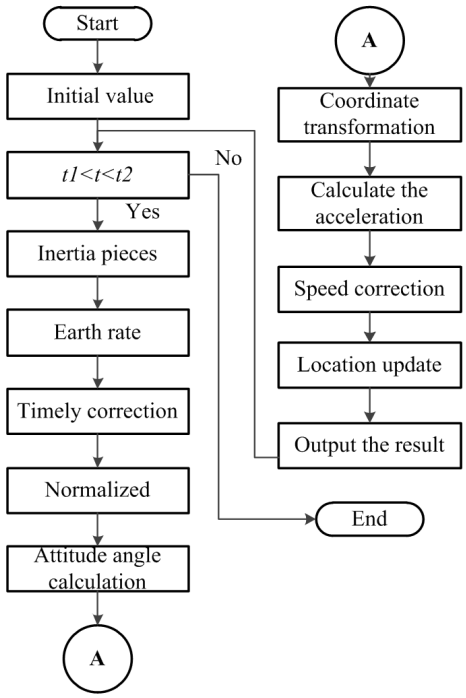

Fig. 4. Trapdown inertial navigation system algorithm

In simulation, the period of Kalman filtering information fusion was 1 s, and the output frequency of INS CNA data was 1 Hz. In order to facilitate the analysis, it was assumed that the positioning accuracy and altimeter measurement accuracy of CNS were 300 m and 50 m, respectively. The initial value of the filter is shown in Table 1.

Table 1. Working initial value of Kalman

Error term	Horizontal attitude	Heading angle	Speed	Latitude and longitude	Height
Initial value	360 °	1800 °	0.6 m/s	100 m	100 m

During the flight of the UAVs, the gyro and accelerometer were set to 0.01 s. After the take-off, the UAVs climbed 7 times in succession. Finally, the UAVs finally climbed to the highest position, and maintained the current position for 800 s flat flight. After the flat flighted, they gradually were downhill and landing. The test time was a total of 2500 s. The sensing elements used throughout the flight included micro accelerometers and mechanical gyroscopes. Under static conditions, the navigation simulation results of UAV Based on sins are shown in Figs.5–8.

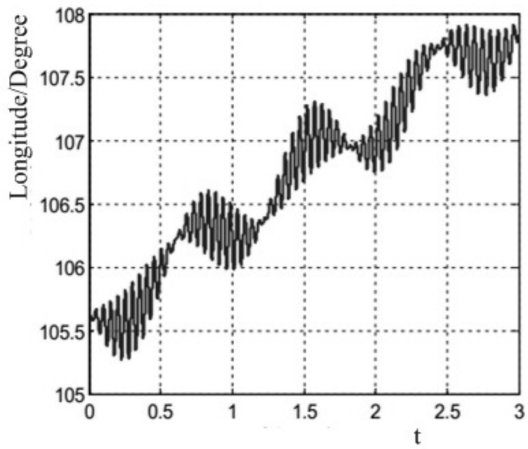

Fig. 5. Longitude error characteristic curve

In the stationary state, the accuracy of celestial navigation and positioning of UAV was simulated and analyzed, and the inertial navigation system was simulated by computer. The selected inertial navigation system was equivalent to gyro drift 0.1 degrees/h and acceleration zero bias to 10^{-4} g. The error of inertial attitude angle was not taken into account, and the observation error of celestial navigation sensitive phase was . Under the simulation condition, since the inertial navigation system provided the horizontal datum for the astronomical positioning under the

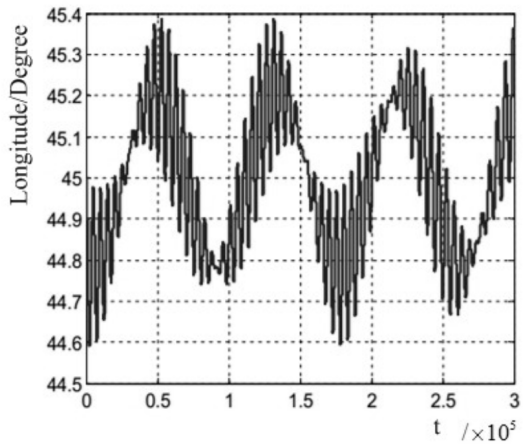

Fig. 6. Latitude error characteristic curve

airborne environment, it was necessary to take full account of the accuracy of the astronomical positioning, which was affected by the inertial attitude error angle. The error was the superposition effect of steady state and random error. Through the synthetic analysis of the simulation curves, it can be seen that the results obtained by the strapdown inertial navigation system are consistent with the error propagation equations under static conditions. The conclusions are as follows:

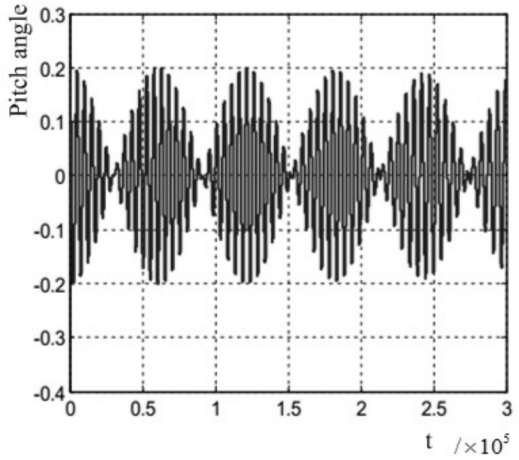

Fig. 7. Pitch angle error characteristic curve

If the initial errors of gyro, accelerometer and navigation parameters are considered at the same time, the height, accuracy, direction, velocity and other positional parameters of the UAV will be divergent, and the deviation of angle and latitude will occur. In addition, position information, posture, and speed all oscillate in three directions. The oscillation errors can be divided into positional oscillation,

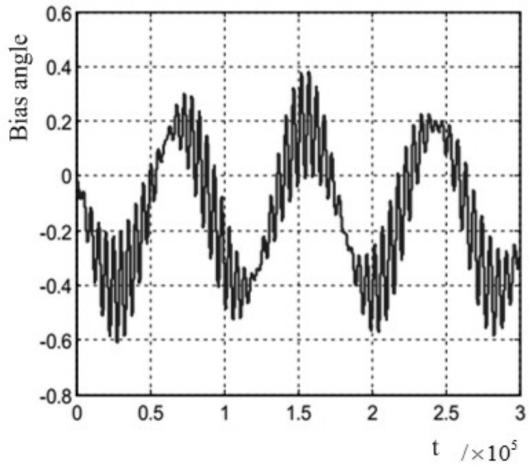

Fig. 8. Bias angle error characteristic curve

earth oscillation and Foucault oscillation, and their periods are 84.4 min, 24 h and 51 h respectively. The Foucault oscillator is the longest in the cycle time. As the dimension changes, the value of the dimension determines the length of the cycle directly. At the equator, the Foucault oscillation period is 0. But at the poles of the earth, Foucault oscillations degenerate and eventually degenerate into earth oscillations. Finally, the oscillation law of navigation parameters can be summed up as follows. There are earth oscillation and Schuler oscillation existing in navigation information such as heading angle, precision and dimension. The oscillation of the earth Schuler oscillation plays an obvious inhibitory effect. In the horizontal direction of the velocity and attitude information is the existence of Foucault and Schuler oscillation, and Foucault oscillation has a significant inhibitory effect on Schuler oscillation.

5. Conclusion

High altitude long endurance UAVs are now more and more popular, but they have very high precision and autonomy requirements for navigation systems. The traditional single navigation system is difficult to meet its performance requirements. Therefore, according to the actual demand, the strapdown inertial navigation algorithm was proposed in this paper on the basis of the advantages of celestial navigation and inertial navigation system. On this basis, the simulation and application analysis of related algorithms were carried out. Through analysis, the scheme of integrated navigation system for unmanned aerial vehicle (UAV) which is oriented to engineering practice planning was successfully carried out. The design of time inertial navigation algorithm was studied according to the system principle. Finally, the simulation of the algorithm was improved under static conditions, and the feasibility and efficiency of the algorithm were verified. The specific analysis was carried

out by the measured data. Through the analysis of the measured results, it can be seen that the error of this algorithm is relatively small, which effectively solves the autonomy problem of the traditional GPS integrated navigation system and can be widely used in engineering practice, and it plays a very active role in promoting the development of UAV at high altitude and long endurance in China, which has a very strong application value

References

[1] I. K. Nikolos, K. P. Valavanis, N. C. Tsourveloudis, A. N. Kostaras: *Evolutionary algorithm based offline/online path planner for UAV navigation.* IEEE Transactions on Systems, Man, and Cybernetics, Part B (Cybernetics) *33* (2003), No. 6, 898–912.

[2] A. Cesetti, E. Frontoni, A. Mancini, P. Zingaretti, S. Loghi: *A vision-based guidance system for UAV navigation and safe landing using natural landmarks.* Journal of Intelligent and Robotic Systems *57* (2010), Nos. 1–4, 233–257.

[3] I. K. Nikolos, K. P. Valavanis, N. C. Tsourveloudis, A. N. Kostaras: *Evolutionary algorithm based offline/online path planner for UAV navigation.* IEEE Transactions on Systems, Man, and Cybernetics, Part B: Cybernetics *33* (2003), No. 6, 898–942.

[4] Y. Kuroki, G. S. Young, S. E. Haupt: *UAV navigation by an expert system for contaminant mapping with a genetic algorithm.* Expert Systems with Applications *37* (2010), No. 6, 4687–4697.

[5] J. Zhang, Y. Wu, W. Liu, X. Chen: *Novel approach to position and orientation estimation in vision-based UAV navigation.* IEEE Transactions on Aerospace and Electronic Systems *46* (2010), No. 2, 687–700.

[6] A. G. Shem, T. A. Mazzuchi, S. Sarkani: *Addressing uncertainty in UAV navigation decision-making.* IEEE Transactions on Aerospace and Electronic Systems *44* (2008), No. 1, 295–313.

[7] J. Zhang, W. Liu, Y. Wu: *Novel technique for vision-based UAV navigation.* IEEE Transactions on Aerospace and Electronic Systems *47* (2011), No. 4, 2731–2741.

[8] J. Y. Chen: *UAV-guided navigation for ground robot tele-operation in a military reconnaissance environment.* Ergonomics *53* (2010), No. 8, 940–950.

[9] S. T. Goh, O. Abdelkhalik, S. A. Zekavat: *A weighted measurement fusion kalman filter implementation for UAV navigation.* Aerospace Science and Technology *28* (2013), No. 1, 315–323.

[10] Y. Gui, P. Guo, H. Zhang, Z. Lei, X. Zhou, J. Du, Q. Yu: *Airborne vision-based navigation method for UAV accuracy landing using infrared lamps.* Journal of Intelligent & Robotic Systems *72* (2013), No. 2, 197–218.

[11] E. Michaelsen, J. Meidow: *Stochastic reasoning for structural pattern recognition: An example from image-based UAV navigation.* Pattern Recognition *47* (2014), No. 8, 2732–2744.

[12] F. Lindsten, J. Callmer, H. Ohlsson, D. Törnqvist, T. B. Schön, F. Gustafsson: *Geo-referencing for UAV navigation using environmental classification.* IEEE International Conference on Robotics and Automation (ICRA), 3–8 May 2010, Anchorage, Alaska, USA, (2010), Publ: Curran Associates, Inc., 1420–1425.

Received August 7, 2017

Acta Technica *62* No. 2B/2017, 219–230

Mechanism analysis of mechanochemical action in preparation of polymer composites[1]

Yinan Jiang[2], Huiyong An[2,3], Caiya Qi[2], Weiwei Si[2]

Abstract. Mechanochemistry is one of the most important methods for preparing polymer composite materials, and there are not many studies on the mechanism of its preparation. Therefore, the mechanism of mechanochemical action in the preparation of polymer composite materials was analyzed in this paper. After discussing the development of mechanochemistry, the green cellulose polymer, nano cellulose, was studied as an example. The results show that in the process of preparation, mechanochemistry changes the morphology of cellulose, and also makes the molecular chain of cellulose recombine, which leads to the change of crystal structure.

Key words. Mechanochemistry, polymers, materials, preparation, cellulose.

1. Introduction

Since people began using cremation rubber as a representative of the modified natural polymer materials in nineteenth century, polymer materials have developed toward the direction of composite materials with the gradual progress of science and technology, and have played an increasingly important role in the production and life of human society [1]. The polymer composite materials are found everywhere in various kinds of plastic products which are very common in people's life and in the aerospace industry. It is precisely because of this polymer composites have had an important impact on the change in the world outlook since twentieth century. Therefore, Time Magazine has named polymer composite as the most important

[1]This work reported in National Natural Science Foundation of China, Application of the radical polymerization method in the high-grade insoluble sulfur, Grant(No. 21304042); Natural Science Foundation of Liaoning Province of China, Toughening mechanism and application research of hydrophobically associating hydrogels, Grant (No. 211602466).

[2]College of Chemistry, Chemical Engineering and Environmental Engineering, Liaoning Shihua University, Fushun, 113001, China.

[3]Corresponding author

invention in human society [2]. In addition, polymer composite materials also have important influence on the cultural field and life style of human society. Therefore, the preparation of polymer materials has become the most important production activities in the society [3].

In general, the preparation of polymer composites involves many aspects, such as formula design, processing technology and processing equipment. Formulation design refers to the combination design of the properties and structure of various raw materials, which is the most important process for the preparation of polymer composite materials [4]. After the formulation design is completed, it is necessary to make use of various processing techniques and processing equipment to complete the manufacture of polymer materials. At present, due to the rapid development of science and technology, the preparation methods of polymer composites are also various [5]. Among them, mechanochemistry is one of the methods of preparing polymer composites in recent years. However, there are few studies on the application of mechanochemical methods in polymer materials. Therefore, in this paper, the mechanism of mechanochemical action in the preparation of polymer composite materials was proposed.

2. State of the art

Mechanochemistry is a technique that uses mechanical energy to stimulate chemical reactions to alter the structure and properties of materials. This technique is mainly used to prepare new materials or to modify materials. These materials are often unable to be treated or prepared by conventional chemical methods [6]. The mechanochemical method first appeared in the early part of the last century and was first proposed by German scholar W. Ostwald. He defined the mechanochemical method first and explained the two by theoretical analysis, but the basic principle was not clearly explained [7]. After nearly thirty years of silence, the golden age of development was ushered in. As time went on, mechanochemistry began to develop from the original high value-added materials to the fields of chemistry, metallurgy and alloy. Nowadays, mechanochemistry has been widely used in many fields, such as nanocomposites, minerals and waste treatment, synthesis of new materials and metal refining [8].

Mechanochemistry has been applied in more and more material fields, which has prompted scholars from all over the world to study the theory and application of mechanochemistry [9]. Takahashi used the mechanochemical process to grind the clay so that the part of the clay was dehydrated and its structure changes. China's research in this field has focused on the application of biomaterials, and has made great progress. Scholar Shi Junli once used the mechanical force to carry on the success research to the rice starch structure. In addition, some scholars have applied it in the Chinese herbal medicine treatment of traditional Chinese medicine, and it can improve the curative effect of Chinese medicine by superfine mechanical treatment of Chinese herbal medicine. It is believed that with the deepening of national research, the application of mechanochemistry will be more extensive [10].

3. Methodology

Nowadays, with the development of science and technology, there are many kinds of polymer composite materials. Therefore, in this paper, when analyzing the mechanism of mechanochemical action in the preparation of polymer composite materials, Nano-cellulose was chosen as the object of this study, which was the most important raw material of polymer composite. Cellulose is a kind of natural biomass polysacharide formed by glycosidic linkage of glucose units, which belongs to natural polymer materials [11]. Because of its wide range of sources, renewable nature, biodegradable nature and good biocompatibility, it has become a kind of green and environment-friendly biomass energy. Today, with the worsening of the ecological environment, the characteristics of its green environment protection will be widely used in more and more fields. Fig. 1 shows a kind of common cellulose [12]. However, cellulose as a natural polymer material, its strength and chemical resistance are relatively poor, and it is difficult to be dissolved in general solvents. These disadvantages have severely limited the development and utilization of natural cellulose [13]. Therefore, people can obtain Nano-cellulose by means of retaining the amorphous region of cellulose and decomposing the crystalline region by specific means. While retaining the advantages of cellulose degradation and broad source, Nano-cellulose has been greatly optimized for its physical and chemical properties, which makes it one of the most widely used materials in composite materials [14]. Because of its environmental protection and wide application, it is the important reason that Nano-cellulose is chosen as the object of this study.

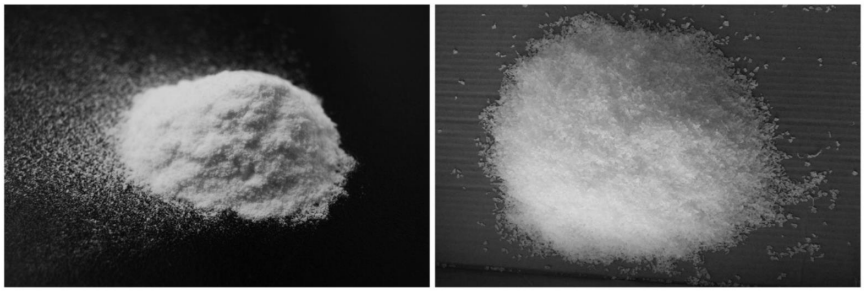

Fig. 1. Currently more common cellulose

In the analysis and study of Nano cellulose, Nano cellulose was firstly prepared by mechanochemical method. Then, the mechanism of the preparation of cellulose by mechanochemical method was analyzed. First of all, the experimental materials and methods involved in the experiment were described in detail. The raw material of this experiment is rayon grade pulp, phosphotungstic acid, and anther. α-cellulose content of rayon grade pulp exceeded 94 %, which was the main raw material in this experiment and purchased from Nanzhi Limited by Share Ltd. in F province. Phosphotungstic acid and ether were purchased from the National Pharmaceutical Group Chemical Reagents Co., Ltd. Phosphotungstic acid is a kind of solid heteropoly acid with mild conditions. It has high catalytic activity, low toxicity, easy recovery, good

thermal stability and so on. It belongs to the green environmental protection catalyst [15]. It is widely used as catalyst in condensation, esterification and oxidation reactions, and this is also an important factor in the use of phosphotungstic acid in this experiment. The related instruments and equipment involved in the test are shown in Table 1.

Table 1. The related instrument and equipment used in the test

Instrument	Model	Manufacturer
Standard fiber breaker	GBT-A	Changchun on small test machine limited liability company
Variable frequency planetary ball mill	BXQM-0.4L	Nanjing special wheel new instrument Co., Ltd.
Heat collection type constant temperature heating magnetic stirrer	DF-101S	Gongyi Hua Hua Instrument Co., Ltd.
Numerical control ultrasonic cleaner	KQ-250DB	Kunshan Ultrasonic Instrument Co., Ltd.
Electrothermal constant temperature blower drying box	DHG-9246A	Shanghai precision experiment equipment Co Ltd.
TGA	STA449C	NETZSCH
Vacuum freeze drying apparatus	TB-1B-50	Beijing boyikang experimental instrument factory
Fu Liye transform infrared spectrometer	NICole80	Thermo electron, USA
High speed freezing centrifuge	GL-20G-I	Shanghai Anting Scientific Instrument Factory
Transmission electron microscope	JEM-1010	JEOL
X-ray diffractometer	MiniFlex	Japan Science Corporation
Fiber analyzer	Morfi Compact	French Techpap

Before the test, the mill was used to break the raw material, rayon grade pulp, so as to obtain cellulose pulp and dry it at the temperature of 60 °C. 2 g cellulose slurry and 40 ml phosphotungstic acid were dissolved in two ball milling tanks of 90 ml in volume. Each pot used 20 agate balls with a radius of 3 mm for ball milling in 0.5 h to 2.5 h. The 600 r/min of agate ball speed was appropriate. After completing the above procedure, the sample was transferred to a round bottomed flask with a volume of 200 ml for a certain period of time with a temperature of 90 °C. After cooling, the sample was centrifuged several times until the reactants were neutral. The obtained acid solution was treated with ethyl ether to obtain phosphotungstic acid and recovered. The reactant suspension was subjected to ultrasonic treatment for 1 h, and the ultrasonic treated suspension was centrifuged using a centrifuge.

After treatment, the upper layer of white latex suspension was collected to obtain Nano-cellulose. Cellulose powder was obtained by drying with a vacuum freeze drying apparatus.

0.03 g rayon grade pulp was extracted and diluted to 1000 ml. The morphology of the fiber was observed with an instrument, and the length and width of the fiber were analyzed. The projection electron microscope was used to observe the morphology and size of Nano-cellulose to disperse the situation. Subsequently, cellulose suspensions with a content of 0.01 % were disposed and adsorbed by copper nets. After the use of phosphotungstic acid solution for dyeing 1 min or so, it was naturally dried. The 100 kV accelerated voltage was used in this paper. The rayon grade pulp was blended with Nano-cellulose to form powder and then mixed with KBR at a ratio of 1:100 to be fully ground and pressed. Fourier transform infrared spectroscopy was used to analyze the chemical structure of cellulose. The crystallinity analysis of cellulose was carried out by X-ray diffractometer. The cellulose sample was to be powdered in the experiment. Using Ni filter and Cu Kα ray, the range of scan and step scan was 6–900. The cellulose crystallization strength was calculated using the crystalline index CrI, and the cellulose type I was calculated as follows

$$C_{\mathrm{rI}} = \frac{I_{002} - I_{\mathrm{Iamorph}}}{I_{002}} \times 100\,\%\,, \tag{1}$$

where, I_{002} represents the maximum diffraction intensity of the main crystallization peak 002 with a value of 22.60 and I_{Iamorph} indicates the diffraction intensity of the scanning range of 180.

The formula for cellulose type II is as follows:

$$C_{\mathrm{r}\|} = \frac{I_{101} - I_{\mathrm{Iamorph}}}{I_{101}} \times 100\,\%\,, \tag{2}$$

where, I_{101} in the formula represents the maximum diffraction intensity of the 101 peak with a scanning range of 20.8 °C, and I_{Iamorph} indicates the diffraction intensity of the trough at the scanning range of 160.

The thermogravimetric analysis of nanofibers was carried out by thermogravimetric analyzer. The experimental condition was that the temperature under argon protection rose to 550 °C at a rate of 5 °C/min, and the gas flow rate was 30 ml/min.

4. Result analysis and discussion

Firstly, morphological analysis of nanofibers was carried out. Fig. 2 shows the fiber morphology of the rayon grade pulp. As can be seen from the diagram, the fiber state of the raw material was elongated, and some short fibers were mixed. Fiber length and width were measured by fiber morphology. The final results showed that the length of the fiber was between 0.68–5.31 mm and the width of the fiber was between 15–60 nm.

After observing the fiber morphology of the rayon grade pulp, the morphology of cellulose jelly and nanofiber was observed by transmission electron microscopy. First

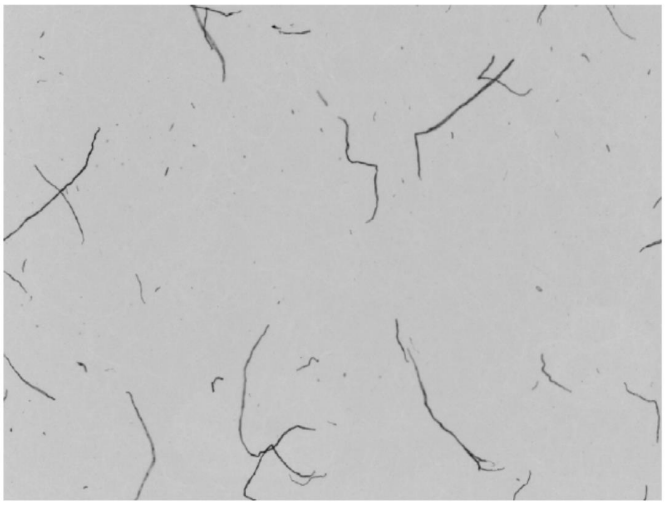

Fig. 2. Fiber morphology of the rayon grade pulp

of all, the aqueous solution of nanofiber paste was mainly white in appearance. A transmission electron microscope was used to observe cellulose jelly, and it could be seen that the length of the fiber was between 200–300 nm and the width was between 20–40 nm. In terms of length and width, nanofibers underwent a mechanochemical process, and their fiber length and width underwent significant physical changes. The fibers presented a microfibril state, and the structure was a network of intertwining structures. Under transmission electron microscopy, the length and width of nanofibers were shorter than those of the gel. The length was about 100–300 nm, and the width was between 10–40 nm. The nanofibers were in the shape of bars, and they were also intertwined with each other into a network. The results show that the fibers of the nanofibers become finer and shorter under ultrasonic action, but their structure is not destroyed, as shown in Fig. 3.

Fig. 4 shows the infrared spectra of the rayon grade pulp, jelly, and Nano-cellulose in Fourier infrared spectrometer. It can be seen from the infrared spectrum that the characteristic peaks of the rayon grade pulp, jelly and Nano-cellulose were basically the same, and three of them had the basic structure of cellulose. This spectrum showed that acid hydrolysis did not change the basic structure of cellulose during the preparation of Nano-cellulose. There was a broad and strong hydroxyl absorption peak at the 3445/cm position in the three, and the absorption peak belonged to the stretching vibration of -OH. The characteristic peak around 2900/cm was the C–H symmetric stretching vibration of $-CH_2-$. The peak around 1640/cm was formed by water absorption of the cellulose samples, and the emergence of this characteristic peak showed that the water absorption capacity of cellulose samples was very strong. The absorption peaks around 1382/cm belonged to the C-H symmetric stretching vibration. The C–O stretching vibration around 1060/cm and the rocking vibration around 897/cm belonged to cellulose alcohol. The only big difference between the

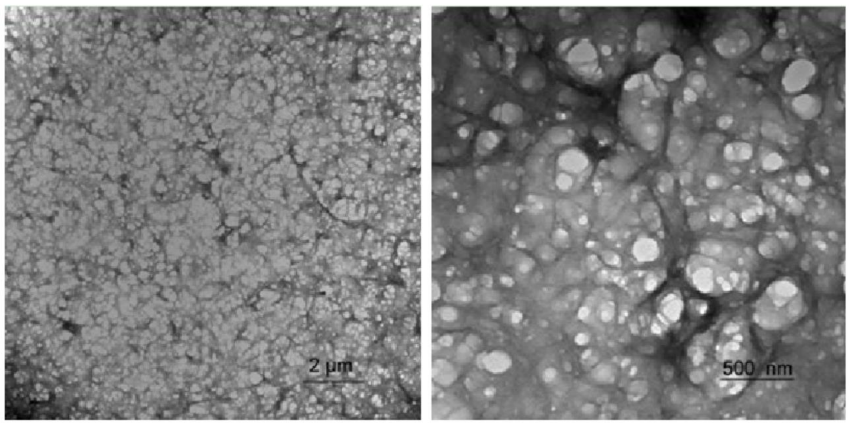

（1）10000×　　（2）50000×

Fig. 3. Nanofiber under transmission electron microscope

three infrared spectra was the peak around 1429/cm. There was a small absorption peak in the human plasma, which was due to the $-CH_2-$ symmetric bending vibration. The peak intensity of the other two in this position was obviously weakened, which was accompanied by a slight blue shift. The reason for this may be that the mechanochemical action leads to fracture and reconstruction of hydrogen bonds around C_66 in cellulose molecules. The appearance of this phenomenon indicates the emergence of cellulose II crystalline variants.

Fig. 5 shows a diffraction diagram of raw material, the rayon grade pulp, and the finished product of Nano cellulose under X-ray diffractometer. First of all, from the diffraction curve of the rayon grade pulp, the diffraction peaks were located around 14.50, 160 and 22.50 of the scanning range. This result indicated that the fibrous crystal belonged to the fiber type I. The analysis of the diffraction peaks of Nano cellulose showed that the position of the nanofibers was within 12.10, 19.50 and 220 of the scanning range. This result showed that the crystal of cellulose belonged to the fiber type II. From the diffraction of X-ray diffractometer, it indicated that in the process of mechanochemical preparation of nanometer cellulose, phosphotungstic acid was used as reagent to promote the dissolution of natural cellulose, and then to regenerate. Mechanochemical changes led to changes in the crystal type of cellulose. The crystallinity of the rayon grade pulp and Nano cellulose was calculated by crystallization index CrI. The final calculation results showed that the crystallinity of the rayon grade pulp was 66.44 %, and the crystallinity of Nano cellulose was 59.62 %. The results showed that the crystallinity of Nano cellulose was less than that of human cellulose. In the preparation of Nano cellulose by mechanochemistry, the crystallinity of cellulose decreased. The reason was probably that during the mechanochemical process, the small molecular chains of cellulose underwent the reorganization when the rayon grade pulp was dissolved and reconstituted.

Fig. 6 shows a thermogravimetric diagram of the nanofibers prepared from raw material, rayon grade pulp, and mechanical power. Firstly, the raw material and

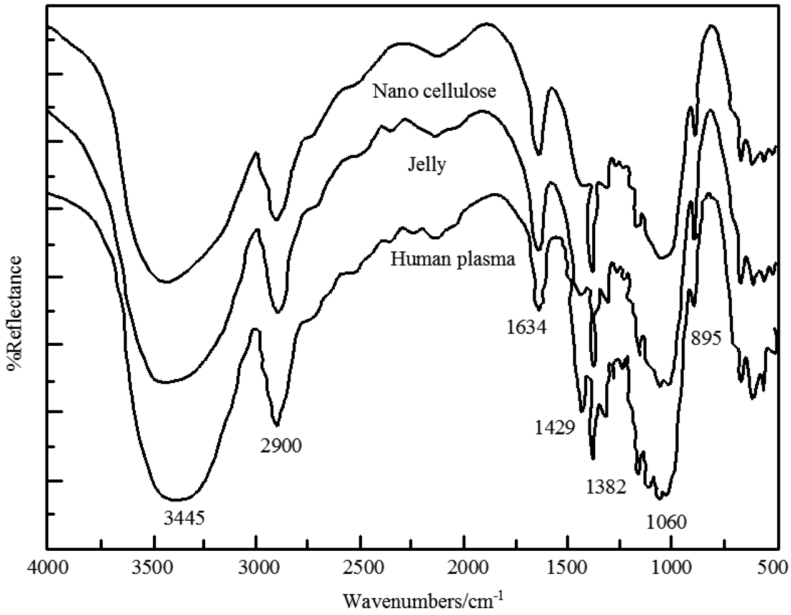

Fig. 4. Infrared spectra of different cellulose samples

pulp were analyzed.

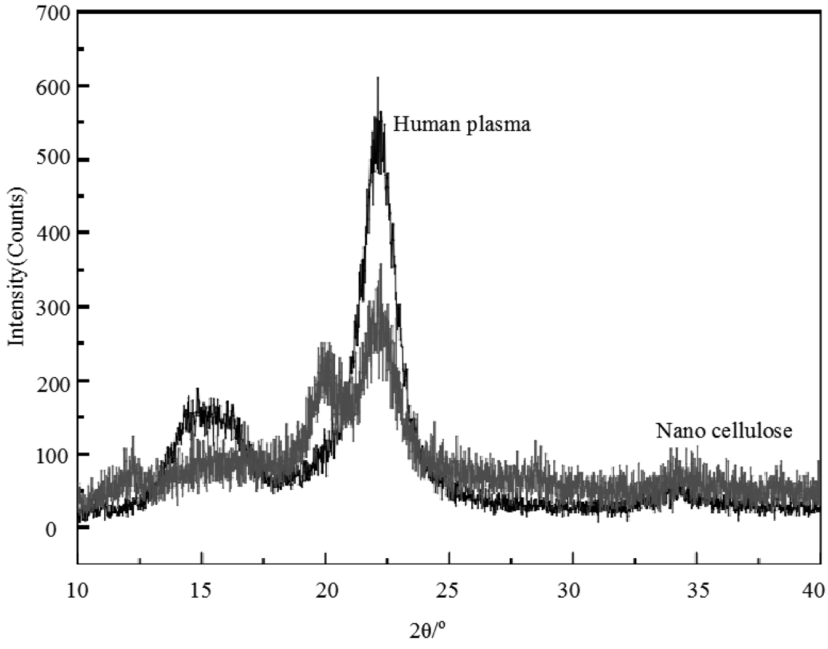

Fig. 5. X-ray diffraction patterns of human plasma and Nano-cellulose

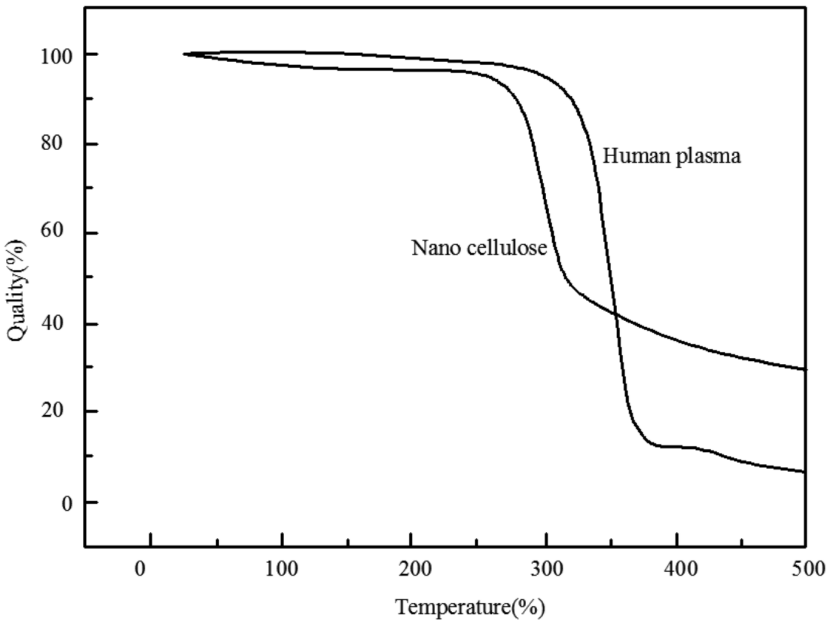

Fig. 6. Thermogravimetric diagram

It could be seen from Fig. 6 that there was no weightlessness in the rayon grade pulp at about 150°C, which showed that the water in the pulp contained less water. Starting from 200°C, the thermogravimetric curve of the sample began to decline rapidly until slowly at 375°C. At the temperature of 200–375°C, the total mass loss of the sample was about 85 %. From 375 to 500°C, the rate of thermal degradation decreased very slowly, and the total mass loss was about 90 %. Thermogravimetric analysis of Nano cellulose showed that the thermogravimetric curve of Nano-cellulose decreased slowly at 35–150°C. The main reason was that there was a slow evaporation of water at this stage, and the total mass loss was about 3%. The thermal gravimetric curve of the cellulose decreased rapidly at 200°C and slowed down at 325°C. The total mass loss was 49 % mainly because of the decomposition of Nano-cellulose. When the temperature reaches 500°C, the total mass loss was about 70 %. By comparing the thermogravimetric curves of two samples, it could be seen that the thermal decomposition temperature of Nano-cellulose was lower than that of the rayon grade pulp. The results showed that the stability of Nano-cellulose was less than that of human plasma. The main reason was that the size of the Nano-cellulose became much smaller than the size of the raw material through mechanochemical action. In addition, the surface area increased considerably, and the exposed active group changed more.

5. Conclusion

Nowadays, with the rapid development of science and technology, all kinds of industrial products made of polymer composite materials have become one of the most important factors in the production and life of human society. In this context, the mechanism of mechanochemical action in the preparation of polymer composite materials was proposed in this paper. Nano-cellulose, a green and environmentally friendly polymer material, was chosen as the object of this study. Firstly, Nano-cellulose was prepared and analyzed by mechanochemical method. It can be seen from the analysis that the fiber morphology of the human fiber changed under the action of mechanochemistry. The main reason is that the length and width of the fiber become smaller, but the whole structure is not destroyed. However, the crystal structure of cellulose was changed, and the crystallinity of cellulose was reduced. The reason is that the small molecular chains of the cellulose undergo recombination when the rayon grade pulp is dissolved and reconstituted by mechanochemical action.

References

[1] J. Thévenot, H. Oliveira, O. Sandre, S. Lecommandoux: *Magnetic responsive polymer composite materials.* Chemical Society Reviews *42* (2013), No. 17, 7099–7116.

[2] X. Sun, H. Sun, H. Li, H. Peng: *Developing polymer composite materials: Carbon nanotubes or graphene?.* Advanced Materials *25* (2013), No. 37, 5153–5176.

[3] M. Ma, L. Guo, D. G. Anderson, R. Langer: *Bio-inspired polymer composite actuator and generator driven by water gradients.* Science *339* (2013), No. 6116, 186–189.

[4] N. Saba, M. T. Paridah, M. Jawaid: *Mechanical properties of kenaf fibre reinforced polymer composite: A review.* Construction and Building Materials *76* (2015), 87–96.

[5] W. L. Song, M. S. Cao, M. M. Lu, S. Bi, C. Y. Wang, J. Liu, J. Yuan, L. Z. Fan: *Flexible graphene/polymer composite films in sandwich structures for effective electromagnetic interference shielding.* Carbon *66* (2014), 67–76.

[6] A. F. Fuentes, L. Takacs: *Preparation of multicomponent oxides by mechanochemical methods.* Journal of Materials Science *48* (2013), No. 2, 598–611.

[7] K. Y. Shin, S. Lee, S. Hong, J. Jang: *Graphene size control via a mechanochemical method and electroresponsive properties.* ACS Applied Materials & Interfaces *6* (2014), No. 8, 5531–5537.

[8] A. Echresh, M. Z. Shoushtari: *Synthesis of Al-doping ZnO nanoparticles via mechanochemical method and investigation of their structural and optical properties.* Materials Letters *109* (2013), 88–91.

[9] B. C. Yadav, R. Singh, S. Singh: *Investigations on humidity sensing of nanostructured tin oxide synthesised via mechanochemical method.* Journal of Experimental Nanoscience *8* (2013), No. 5, 670–683.

[10] W. K. Dong, K. H. Park, S. C. Hong: *The influence on SCR activity of the atomic structure of V_2O_5/TiO_2, catalysts prepared by a mechanochemical method.* Applied Catalysis A: General *451* (2013), 227–235.

[11] S. Maiti, J. Jayaramudu, K. Das, S. M. Redy, R. Sadiku, S. S. Ray, D. Liu: *Preparation and characterization of nanocellulose with new shape from different precursor.* Carbohydrate Polymers *98* (2013), No. 1, 562–567.

[12] M. I. Aranguren, N. E. Marcovich, W. Salgueiro, A. Somoza: *Effect of the nanocellulose content on the properties of reinforced polyurethanes. A study using mechanical tests and positron anihilation spectroscopy.* Polymer Testing *32* (2013), No. 1, 115–122.

[13] C. J. Chirayil, M. Lovely, T. Sabu: *Review of recent research in nano cellulose preparation from different lignocellulosic fibers.* Reviews on Advanced Materials Science *37* (2014), Nos. 1–2, 20–28.

[14] Z. Song, H. Xiao, Y. Zhao: *Hydrophobic-modified nanocellulose fiber/PLA biodegradable composites for lowering water vapor transmission rate (WVTR) of paper.* Carbohydrate Polymers *111* (2014), 442–448.

[15] E. Robles, I. Urruzola, J. Labidi, L. Serrano: *Surface-modified nanocellulose as reinforcement in poly(lactic acid) to conform new composites.* Industrial Crops and Products *71* (2015), 44–53.

Received May 7, 2017

Acta Technica *62* No. 2B/2017, 231–240

Numerical simulation and experimental study of smelting reduction furnace based on oxygen-rich top-blowing[1]

Yiqin Liu[2,3], Shan Qing[2], Yingchun Liu[2,4], Aimin Zhang[2], Zhao Gui[2]

Abstract. The development and the progress of modern society have made the iron and steel industry facing increasingly severe environmental pressure load and the risk of a shortage of resources. Therefore, it is necessary to develop a new ironmaking technology that can meet the needs of modern economic development and environmental protection. Factor analysis of the numerical simulation of the oxygen-rich top-blowing smelting furnace was carried out by using software of fluid mechanics and related effects. Through the numerical simulation and industrial test monitoring results of comparative analysis, it was found that the results of the two were relatively consistent. This shows that the technology can be applied in specific engineering practice and can promote the healthy development of China's iron and steel industry.

Key words. Oxygen-rich top-blowing, numerical simulation, experiment.

1. Introduction

Since the establishment of Chinese, a thousand things wait to be done. The economy of our country is developing rapidly. In order to meet the production and construction of our country, the output of iron and steel is increasing year by year.

[1]This work reported in National Natural Science Foundation of China: The transfer characteristics and strengthening mechanism of Al2O3/TiO2 nanoparticles in the organic Rankine cycle under multi-field driving, (No. 51566005) and National Natural Science Foundation of China: Phosphorus behavior in smelting reduction process of high phosphorus iron ore in Yunnan based on HIsmelt (No. 51064015).

[2]Department of Metallurgical and Energy Engineering, Kunming University of Science and Technology, Kunming, 650093, China

[3]Department of Communication and Information Engineering, Yunnan Open University, Kunming 650000, China

[4]Corresponding author

China's crude steel production increases from 450 thousand tons in the founding to 100 million tons by 1996. The annual output reached 6.02 tons in 2015 [1]. It is foreseeable that the demand for steel is still great in a long period of time. As long as the supply of coke is enough, the blast furnace ironmaking process is needed to produce and supply the steel. However, the process of blast furnace ironmaking has many deficiencies. On the one hand, the coal resources needed are relatively small. On the other hand, a large amount of air pollution is produced in the process of ironmaking. This is clearly not in line with China's current strategy for the protection of the ecological environment. At the same time, China's coke oven imports from abroad mainly. But the aging of coke ovens in the major steel producing countries around the world makes the supply of coke more stressful, which makes the traditional process of blast furnace facing severe challenges.

Internationally, various countries have begun to carry out extensive research on the new ironmaking process of non-coking coal and iron ore. The utilization of resources is improved and environmental pollution is reduced through new processes. After nearly 30 years of development time, the United States, Japan, Australia and other foreign countries has achieved remarkable results in the new iron making process of the developer, and it has been widely used in actual application promotion. China's iron and steel production has increased year by year, which means that the demand for focusing coal is increasing year by year. The amount of coking coal needed per year must reach 57 thousand and 400 tons [2]. According to the reserves of China's coking coal resources and the demand of our country, it is likely that China will be faced with the depletion of coking coal resources in 2026. Under such circumstances, it is imperative for China to carry out a new type of ironmaking process to reduce or no longer use the coking coal resources.

2. State of the art

Since the latter half of the last century, people have begun to actively attempt to develop and study new types of non-coking coal iron making process. From the initial reduction process to the current smelting reduction process, many countries in the world have invested a lot of material and financial resources, and made outstanding achievements in South Korea. Among them, there are typical Jindal steel mills in India, Saldanha in South Africa and POXCO. They have built many large demonstration plants by using the new smelting reduction process, and actively seek investment in order to achieve commercial production [3]. The most important feature of the new iron making process is the direct use of iron ore and coal that have not been treated. It uses direct reduction process to directly iron ore into solid iron, or it uses the smelting reduction process to realize the reduction reaction of iron ore in the high temperature slag phase [4].

Through the existing research and new technology, it can be seen that the new iron smelting process can skip the sintering of iron ore and the process of coking coal compared to the traditional iron smelting process. In this way, the economic benefits of ironmaking can be improved while the pollution to the environment is reduced. The comparison and analysis of all kinds of new iron making process shows

that smelting reduction method has very good potential and research value. It can make use of the high temperature environment provided by the combustion of coal so that the molten iron can be melted and reduced to be molten iron. The reaction rate is faster. The strength of molten iron smelting by this method is more than 5 times of that of blast furnace [5].

3. Methodology

3.1. Mathematical model for oxygen-rich top-blowing smelting reduction furnace

The flow of fluid is satisfied with the conservation equations of physics, which includes the conservation of energy, the conservation of mass, and the conservation of momentum (Weiland et al. 2013 [8]). If the flow of fluids has different components and can be burned with each other, additional component transport equations are needed. If the studied fluid is turbulent, the turbulent transport equation needs to be further considered [6]. We need to consider the turbulent combustion reaction to construct the mathematical model, and the basic equations are as follows:

The continuity equation of mass conservation equation is

$$\frac{\partial(\rho)}{\partial t} + \operatorname{div}\ (\rho U)\ , \tag{1}$$

where ρ is the fluid density, U is the free velocity and t is the time.

The momentum conservation component equations may be written in the form

$$\frac{\partial(\rho u)}{\partial t} + \operatorname{div}\ (\rho u U) = \operatorname{div}\ (\mu \operatorname{grad}\ u) - \frac{\partial p}{\partial x} + S_u\,, \tag{2}$$

$$\frac{\partial(\rho v)}{\partial t} + \operatorname{div}\ (\rho v U) = \operatorname{div}\ (\mu \operatorname{grad}\ v) - \frac{\partial p}{\partial x} + S_v\,, \tag{3}$$

$$\frac{\partial(\rho w)}{\partial t} + \operatorname{div}\ (\rho w U) = \operatorname{div}\ (\mu \operatorname{grad}\ w) - \frac{\partial p}{\partial x} S_w\,, \tag{4}$$

where u, v, w are the components of velocity in three dimensions and p is the internal stress tensor of fluid.

The energy conversation equation is

$$\frac{\partial(\rho T)}{\partial t} + \operatorname{div}\ (\rho T U) = \operatorname{div}\ \left(\frac{\lambda}{C_{\mathrm{r}}} \operatorname{grad}\ T\right) + S_r\,. \tag{5}$$

Here, T is the fluid temperature, λ is the fluid volume viscosity and C is an empirical coefficient.

By arranging the equations in front, the following general equation can be obtained

$$\frac{\partial(\rho\phi)}{\partial t} + \operatorname{div}\ (\rho\phi U) = \operatorname{div}\ (\Gamma_\phi \operatorname{grad}\ \phi) + S_\phi\,. \tag{6}$$

In the preceding equation, ϕ represents a generic variable that can be used to represent variables such as u, v, w and T in the governing equations. Symbols S_ϕ and Γ_ϕ represent diffusion and generalized source terms [7]. In formula (6), the items from left to right are represented as transient terms and convection terms, respectively. And from left to right, they are diffusion terms and source terms, respectively.

3.2. Establishment of geometric model of smelting reduction furnace

The main research model is used in cylindrical geometry of the model is relatively simple, less difficult when rendering 3D geometry of the GAMBIT can be used to draw three-dimensional graphics rendering of the smelting reduction furnace, as shown in Fig. 1. The calculation area is mainly composed of a smelting reduction furnace, in addition to a combustion nozzle and a part of the flue area. In the process of simulation, it is unnecessary to carry out the calculation of the combustion nozzle, so the modeling of the spray gun is not necessary when the geometric model is built, but only the exit section of the nozzle jet flow is taken into account. After the completion of the collection model, it is necessary to partition the grid, and the quality of grid partition will have a very important impact on the accuracy of the entire process and the accuracy and economy of the results.

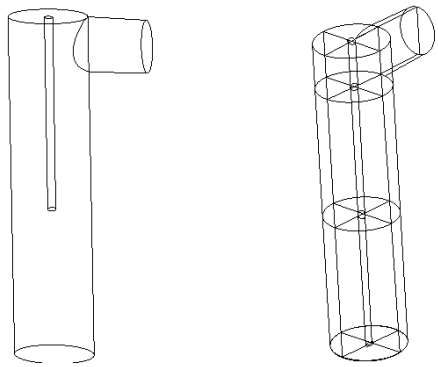

Fig. 1. The model for the reduction of oxygen top blown melting furnace

In order to obtain excellent mesh quality, (Milbourne et al. 2013) [9], it can be divided into different regions. According to this method, the main part of the smelting reduction furnace can be divided into 3 zones, and the results are shown in Fig. 2 (furnace mesh and flue grid, respectively). In order to improve the mesh quality as much as possible, the cylinder is divided into 4 equal volume fan-shaped columns along the axial direction. Each column is 90 degrees in the ground, and is divided into hexahedral regular network. But the flue and the cylinder intersecting part to be divided into hexahedron regular mesh is difficult, and divide it into tetrahedral meshes according to the situation, because this part is only in the whole grid occupies a small proportion, this also shows that the quality of the entire grid. When the

central cylinder is meshed, it is necessary to take into account the characteristics of the jet region in the central cylinder region, and its gradient is relatively large, so it is necessary to encrypt the mesh.

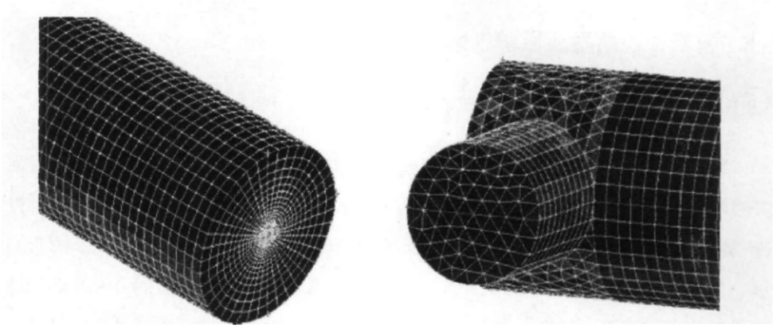

Fig. 2. Mesh diagram of oxygen top blown smelting reduction furnace

In the simulation of the model, the fuel oil is injected from the source into the furnace with the form of discrete phase, in which the air is joined by continuous phase [10]. The burner is not involved in the calculation, which simplifies the calculation. The fuel injector and the air inlet can be simplified into two surfaces [11]. The fuel oil can be selected according to the actual needs of the appropriate atomization model, and will not be affected by the model inlet conditions.

By studying the combustion temperature distribution of different fuels, the temperature field distribution under 21 %, 35 % and 46 % oxygen-enriched concentration was analyzed respectively [12]. The analysis results show that the average temperature of fuel combustion increases with the increase of oxygen enrichment concentration, and the combustion state tends to be stable. This is mainly because the effect of volume of combustion products on combustion temperature is remarkable. If oxygen or air is replaced by oxygen enriched air or nitrogen as an oxidant in combustion reactions, the volume of combustion products will be reduced significantly. The combustion temperature increases with the increase of oxygen concentration, and the distance of ignition is shortened, and the high temperature zone at the bottom of the furnace is further expanded [4]. However, because of more than 70 % heat and mass transfer in the furnace are realized based on the radiation, the increase of the oxygen content is accompanied by a decrease in radiation gases such as carbon dioxide, which is not conducive to the temperature in the furnace to improve the heat transfer and radiation. It is also true that when the oxygen enrichment concentration in the furnace is greater than 50 %, the effect of oxygen concentration on the temperature rise is not obvious.

In the numerical simulation, the exit cross section of the model is monitored. The parameters of different combustion furnace outlet oxygen concentration under top-blowing smelting reduction furnace, and the specific test results are shown in Table 1 [2]. As a result of the monitoring of the export section, the total amount of oxygen, nitrogen, water, and nitric oxide and nitrogen dioxide is about 100 %. In addition, carbon smoke is not monitored. The amount of carbon monoxide in the

monitoring results is relatively small, indicating that the furnace then reacts fully. The oxygen content is too large, and it shows that the combustion in the furnace is an excessive combustion of air, which is conducive to the full and complete combustion of combustion [13].

Table 1. Exit parameter

Oxygen density (%)	Average temperature (K)	Mass fraction of each component (%)					Exit velocity (m/s)
		O_2	CO	N_2	H_2O	CO_2	
21	1715.2	4.32	0.64	78	3.74	12.30	4.56
35	1853.3	4.12	0.57	66	7.47	22.84	4.04
46	1920.5	9.98	0.52	53	9.96	31.56	3.68

3.3. Raw materials and test scheme in the oxygen top-blowing smelting reduction experiment

According to the previous design ideas, the oxygen top-blowing smelting reduction experiment was studied. The raw materials used included anthracite and high phosphorus iron ore. They were mixed with MgO, fluorite and lime in a certain proportion, and then added to the furnace after mixing. The design idea of the test scheme is as follows:

The smelting reduction of high phosphorus iron ore was carried out by using P = 0.9 % alone, so as to obtain the best control parameter for smelting high phosphorus iron ore. The smelting reduction of high phosphorus iron ore was carried out using root mineral (P = 0.305 %) alone. The industrial test of amalgamation and reduction of Huimin mine and root ore according to the ratio of P = 0.7 % and P = 0.5 % was carried out. In the reduction reaction, high phosphorus iron ore and bituminous coal with C/O = 1.1 and R = 2.0 were added. In order to improve the fluidity of slag iron and be easy to separate, 1% CaF_2 of slag and 4% MgO were added.

Table 2. Test parameters

Oxygen density (%)	Oxygen flow rate (m^3/h)	Thermocouple temperature (°C)	Smoke analyzer reading							
			O_2 (%)	CO (mg/m^3)	NO (mg/m^3)	NO_2 (mg/m^3)	SO_2 (mg/m^3)	CO_2 (%)	Speed (m/s)	Temperature (°C)
21–30	30–37	1350–1410	2.31	327	623	731	156	14.65	4.33	1029
31–40	27–33	1450–1530	4.01	436	568	607	190	25.24	3.78	1137
41–50	23–30	1495–1580	3.14	355	495	533	186	33.52	3.46	1190
51–60	21–27	1500–1590	2.55	334	467	512	167	33.46	3.19	1216
61–70	20–25	1480–1590	2.71	319	451	598	182	34.25	2.89	1215

After the prepared reduced molten iron was cooled, it was put into the crucible for grinding and the sample of 500 g was obtained. The sample was placed in a high temperature furnace and was continuously heated up to 1450°C. At this temperature level, it was cooled down gradually after holding the temperature for 1.5 h. When the temperature was reduced to normal temperature, samples were taken and analyzed accordingly. The chemical analysis, SRD analysis and SEM analysis at different stages of molten iron and slag prepared by the oxygen-rich top-blowing smelting reduction ironmaking furnace were carried out. During each experiment, measurement and analysis were needed to determine the effect of smelting under different experiment parameters.

4. Result analysis and discussion

4.1. Comparison of the results of oxygen-rich top-blowing smelting reduction experiments and numerical simulation results

The chemical analysis of oxygen-rich top-blowing smelting reduction experiments under different conditions of molten iron and slag is shown in Table 3.

Table 2. Test parameters

Fused reduced iron							Temperature	Smelting reduction slag			
T.F	M.F	S	P	C	Si	M	°C	MgO	CaO	SiO_2	Al_2O_3
98.01	95.36	0.16	0.15	0.95	0.37	75.68	1526	13.26	47.19	8.23	15.32

The sample obtained was subjected to X-ray diffraction analysis to observe the presence of reduced iron. As a result, the comparison results of the standard diffraction pattern of metal iron X-ray diffraction and ray diffraction were obtained, as shown in Fig. 4. It could be seen from the figure that in the X-ray diffraction patterns of smelting reduction iron, the most important was the line of iron, and the iron was in the form of iron, as well as part of the Fe_2O_3, FeO and Fe_3O_4. In addition, the spectra of some small amounts of C were also included in the spectra, which was due to the excess pulverized coal. In addition to heating and reducing agent consumption, this part of coal powder also had C penetration in some pulverized coal.

4.2. Comparison of smoke monitoring at outlet

Through simulation and experimental monitoring of temperature, the analysis and comparison was carried out. The numerical simulation results showed that when the oxygen concentration was 21 %, 35 % and 46 %, the corresponding 2100 K, 2250 K and 2280 K were converted, and the actual combustion temperature was 1386 °C, 1504.5 °C and 1528.3 °C, respectively. Based on the comparative analysis

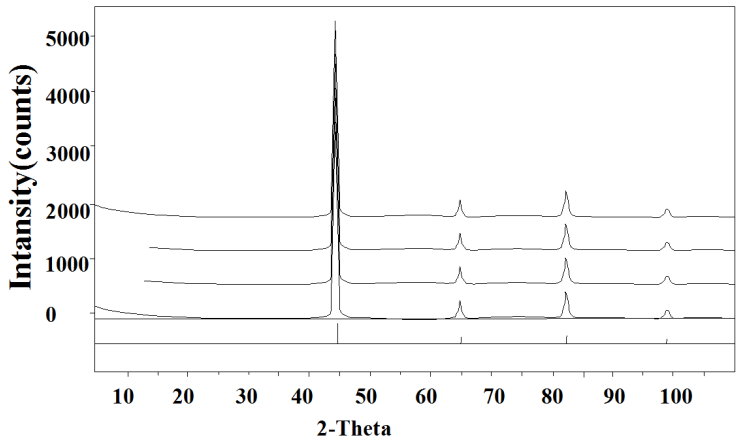

Fig. 3. XRD diagram of fused reduced iron

of the results of the oxygen-rich top-blowing smelting reduction experiments, it was found that the oxygen concentration of 21 %∼30,% corresponded to the temperature of 1350 °C to 1410 °C. When the concentration of oxygen was between 31 % and 40 %, the corresponding temperature was between 1450 °C and 1530 °C. When the concentration of oxygen was between 41 % and 50 %, the corresponding temperature was between 1495 °C and 1580 °C. After the numerical simulation, the converted temperature is 1386 °C, 1504.5 °C and 1528.2 °C, respectively, and the temperature was fluctuated in the range of the experimental data. This showed that the measured results of thermocouples were in good agreement with the numerical simulation results.

Numerical calculation and experimental monitoring results were compared and analyzed. By simulation, it could be seen that when the oxygen concentration was 21 %, 35 % and 46 %, the average temperature of flue gas outlet is 1081.6 °C, 1176.7 °C and 1239.5 °C, respectively. The temperature under the different oxygen concentration measured by the smoke analyzer in the test was shown as follows. When the oxygen concentration was 21 %∼30 %, 31 %∼40 %, and 41 %∼50 %, the corresponding flue gas temperature was 1029 °C, 1136 °C, and 1198 °C, respectively. By comparing and analyzing, it could be seen that the results measured by the experiments and the results of numerical simulation were close. However, the temperature of flue gas analyzer was slightly lower because of the loss of energy in the process of the experiments.

A comparative analysis of smoke flow velocity was carried out by monitoring and numerical simulation. In the numerical simulation, when the oxygen concentration was 21 %, 35 % and 46 %, the average velocity of flue gas at the corresponding outlet was 4.57 m/s, 4.03 m/s, 3.68 m/s, respectively. Correspondingly, when oxygen concentrations were 21 %∼30 %, 31 %∼40 %, and 41 %∼50 %, the average speed of smoke monitoring at the exit was 4.32 m/s, 3.97 m/s, 3.41 m/s, respectively. By comparing and analyzing, it could be seen that the results measured by the exper-

iment was similar to the results of numerical simulation analysis. However, due to the possibility of collisions between the fly ash and flue gas in the process of flue gas flow, partial energy loss occurred, which led to a decrease in velocity.

Through monitoring and numerical simulation of oxygen content in flue gas outlet, we could see that in the numerical simulation, when the oxygen concentration was 21 %, 35 % and 46 %, the corresponding oxygen content in the flue gas at the outlet was 4.31 %, 4.13 %, 3.97 %, respectively. When the concentration of oxygen in the flue gas at the exit was 21 %∼ 30%, 31 %∼ 40%, and 41 %∼50 %, the oxygen content in the flue gas at the corresponding outlet was 2.31 %, 4.01 %, 3.14 %, respectively. The comparison found that the two of them were identical, and no oxygen was found.

5. Conclusion

Under the new social situation, the traditional iron and steel production process is difficult to meet the needs of economic efficiency and environmental protection. Therefore, more economical and environmentally friendly production processes need to be replaced. In this paper, the mathematical model of oxygen-rich top-blowing smelting reduction furnace was constructed by software. Firstly, the study on air coefficient, furnace temperature and oxygen enriched combustion was carried out, so as to construct the mathematical model. The influence factors of oxygen jet, combustion, combustion temperature distribution and combustion characteristics were analyzed. By comparing and analyzing the monitoring results and the results of numerical simulation in the furnace, the deviation of the results of industrial test and numerical simulation were obtained. The results show that under different oxygen concentrations, the temperature of the furnace, the average temperature of the flue gas outlet, the velocity of the smoke flow and the oxygen content of the smoke outlet are in good agreement with the monitoring results. However, it is necessary to further improve the applicability and reliability of the model, so as to achieve better application results in engineering practice.

References

[1] S. J. Mangena, J. R. Bunt, F. B. Waanders: *Mineralogical behaviour of North Dakota lignite in an oxygen/steam blown moving bed reactor*. Fuel Processing Technology *106* (2013), 474–482.

[2] J. H. Wei, T. Li: *Study on mathematical modeling of combined top and bottom blowing VOD refining process of stainless steel*. Steel Research International *86* (2015), No. 3, 198–211.

[3] J. Krzywanski, W. Nowak: *Artificial intelligence treatment of SO_2 emissions from CFBC in air and oxygen-enriched conditions*. Journal of Energy Engineering *142* (2016), No. 1, paper 04015017.

[4] A. C. Gujar, J. Baik, N. Garceau, N. Muradov, A. T-Raissi: *Oxygen-blown gasification of pine charcoal in a top-lit downdraft moving-hearth gasifier*. Fuel *118* (2014), 27–32.

[5] Y. D. Kim, C. W. Yang, B. J. Kim, K. S. Kim, J. W. Lee, J. H. Moon, W. Yang,

T. U. Yu, U. D. Lee: *Air-blown gasification of woody biomass in a bubbling fluidized bed gasifier.* Applied Energy *112* (2013), 414–420.

[6] J. H. Kim, S. Schouten, M. Rodrigo-Gámiz, S. Rampen, G. Marino, C. Huguet, P. Helmke, R. Buscail, E. C. Hopmans, J. Pross, F. Sangiorgi, J. B. M. Middelburg, J. S. Sinninghe Damsté: *Influence of deep-water derived isoprenoid tetraether lipids on the $TEX_8$6 H paleothermometer in the Mediterranean Sea.* Geochimica et Cosmochimica Acta *150* (2015), 125–141.

[7] Z. Y. Wang, J. L. Zhang, X. D. Xing, Z. J. Liu: *Congregated electron phase and Wagner model applied in titanium distribution behavior in low-titanium slag.* Transactions of Nonferrous Metals Society of China *25* (2015), No. 5, 1640–1647.

[8] F. Weiland, H. Hedman, M. Marklund, H. Wiinikka, O. Öhrman, R. Gebart: *Pressurized oxygen blown entrained-flow gasification of wood powder.* Energy & Fuels *27* (2013), No. 2, 932–941.

[9] R. J. Milbourne, T. R. Meadowcroft: *The use of an oxygen-blown open hearth to feed a multistrand casting machine.* Canadian Metallurgical Quarterly *7* (1968), No. 4, 247–253.

[10] M. Naqvi, J. Yan E. Dahlquist: *System analysis of dry black liquor gasification based synthetic gas production comparing oxygen and air blown gasification systems.* Applied Energy *112* (2013), 1275–1282.

[11] E. Simeone, M. Siedlecki, M. Nacken, S. Heidenreich, W. de Jong: *High temperature gas filtration with ceramic candles and ashes characterisation during steam–oxygen blown gasification of biomass.* Fuel *108* (2013), 99–111.

[12] G. Zhang, Y. Yang, H. Jin, G. Xu, K. Zhang: *Proposed combined-cycle power system based on oxygen-blown coal partial gasification.* Applied Energy *102* (2013), 735 to 745.

[13] P. Jin, Z. Jiang, C. Bao, Y. Lu, J. Zhang, X. Zhang: *Mathematical modeling of the energy consumption and carbon emission for the oxygen blast furnace with top gas recycling.* Steel Research International *87* (2013), No. 3, 320–329.

Received May 7, 2017

Acta Technica *62* No. 2B/2017, 241–252

An improved stable election protocol based on node energy consumption (EC)

Peng Duo[2,3], Li Suoping[3,4], Zhang Qiuyu[3]

Abstract. Sensors and wireless communication technology are embedded in wireless sensor networks, which are widely used in industrial production and defense, military and other industries. However, the sensor nodes' energy compensation is limited, which affects the service life of wireless sensor networks. Therefore, it is very important to design an improved network routing election protocol based on node energy saving. Based on the SEP protocol introduced by DEEC, a stable clustering election protocol was proposed in this paper to achieve the energy loss of balanced nodes. In addition, Matlab software was used to simulate and analyze the improved election protocol, so as to prove the scientific validity of the protocol.

Key words. Routing protocols, energy consumption; election protocols, wireless sensor networks.

1. Introduction

The twenty-first century is the era of the Internet and the electronic information. With the continuous development of science and technology, people's detection space is more and more broad. Therefore, the detection system cannot be limited to a single operating system. A large number of sensors are required to cooperate, so as to perform more accurate detection tasks [1]. At the same time, the test results are passed to the actual users, so that users can complete the detailed calculation and analysis. With such a strong market demand, wireless sensor networks have become the focus of research of experts and scholars. The modern wireless sensor

[1]This work reported in The National Natural Science Foundation of China (No. 61663024, No. 61363078); The open research fund of National Mobile Communications Research Laboratory, Southeast University (2014D13).

[2]College of Electrical and Information Engineering, Lanzhou University of Technology, Lanzhou, Gansu, 730050, China

[3]School of Computer and Communication, Lanzhou University of Technology, Lanzhou, Gansu, 730050, China

[4]Corresponding Author

network, which combines sensing technology and wireless communication technology, is the industrial revolution of computer network communication technology since the computer revolution [2]. WSN is a wireless sensor technology with sensing and computing power, which is the world's second largest network structure that keeps pace with the Internet. At the same time, WSN has broad application prospects in the civil, military, agricultural and environmental monitoring. Because WSN is the key factor to transmit information efficiently in wireless networks, the performance of the network itself has a great impact on the overall operation of the network [3]. The traditional network routing protocol nodes are controllable in number. WSN network nodes are huge, and the storage and energy consumption of nodes is very large, which makes that the traditional ADHOC routing algorithm cannot meet the actual application of multi-node and multi-energy WSN. Therefore, according to the characteristics of WSN, it is necessary to develop a routing protocol suitable for WSN [4]. Aiming at the above problems, this paper proposed an improved and stable routing voting protocol based on the characteristics of node energy consumption equalization, so as to achieve the purpose of WSN normal operation.

2. State of the art

Wireless sensing network (WSN) originated from the early warning system of military operations in America. At the beginning of the invention, only a single signal acquisition could be carried out, and the collected signals were only be transmitted between nodes. Later, American military research experts set up a research team for distributed sensing networks, which officially opened the door to WSN's research [5]. In the late 1990s, the research team established a simulated dynamic environment which could adapt to the military battlefield and transmit the actual data of the military battlefield in real time. Wireless sensor networks were moving into people's field of vision. After entering the twenty-first century, industry and academic fields began to be more interested in WSN, and research funding began to be heavily invested in WSN research projects [6]. In 2003, Japan's science and technology enterprises jointly launched the "IPV6 sensor networks" industry plan to accelerate the application of WSN in environmental detection range, so as to establish long-term strategic development goals in environmental testing and national defense military [7]. The distributed sensing networks deploy more sensor terminals in their own system structures. The peripheral nodes need energy supplement to keep the running off. But sometimes the energy cells of these nodes are not able to effectively replenish the power, which causes some of the peripheral nodes to die prematurely during normal operation [8].

In the actual application phase of distributed sensor networks, data transmission is constantly fluctuating and changing, and it is not fixed. The peripheral sensor nodes of WSN are the basic detection unit of distributed sensing network, which are responsible for detecting random detection of objects, and passing the detected data to the users. If in the actual application process, the node's premature death will lead to the detection blind spot. The test data returned will be distorted and the result will be unstable and stable [9]. Domestic and foreign have carried on the

related research work to this kind of question, and proposed many kinds of routing protocols, including LEACH, HEED, DD and other routing protocols. According to the topology ontology structure, the network routing protocols are divided into hierarchical and planar routing protocols [10]. Hierarchical routing protocol is a cluster structure, which has more advantages in application in terms of energy saving and adaptability. LEACH routing protocol is a node energy-saving routing protocol designed based on this idea.

3. Methodology

The design of WSN routing protocol must first consider the efficient supplementary energy of nodes. Although the energy consumption of a single node needs to be monitored and supplemented, the overall energy loss balance is also the focus of consideration. The long distance transmission of WSN needs to consume a great deal of node energy. In order to avoid such a situation, a multi-level jump data transmission is used within a limited range [11]. Because the calculation of nodes is too complex, the computation and storage capacity of sensor nodes is greatly impacted. Therefore, it is more important to design simple and efficient routing protocols to meet the cost of resources. In addition, environment differences also need to design heterogeneous features of nodes. In view of the above design characteristics of WSN wireless network routing, the improved routing protocol has the characteristics of low energy consumption, scalability and heterogeneous features [12].

The classification of routing protocols mainly consists of planar routing protocol and clustering routing protocol. The planar routing protocols are divided into flooding routing protocol, chatting method, SPIN center routing protocol and so on. The late development of directed diffusion routing protocol improves the speed of data transmission, but the data transmission gradient leads to data transmission delay. Directed diffusion transport protocol is a data inquiry type data transmission mode, and it cannot meet the practical application of continuous detection and sensing data [13]. Clustering routing protocol divides the network structure into several cluster regions, and each well divided cluster can be divided into several nodes. Figure 1 shows the basic structure diagram of a clustered routing protocol. As can be seen from Fig. 1, the cluster heads of each cluster are based on the high-level network structure of the original network. The high level network clusters cluster into clusters to push to a higher level network structure. The role of each cluster is not only to fuse and collect node data, but also to transmit data to a higher level cluster head. Therefore, the energy consumption of nodes is relatively large. In order to maximize the lifetime of the network, clustering routing protocols need to improve algorithms and update voting protocols.

Compared with the traditional network protocol, LEACH network transport protocol can reduce the energy consumption of the network and realize the energy balance of the network. In the actual operation process, the data transmission can meet the transfer within the cluster. Because the distance of information transmission is relatively close, only a few cluster heads can transmit data with remote sink nodes in actual operation. For data transmission and information communica-

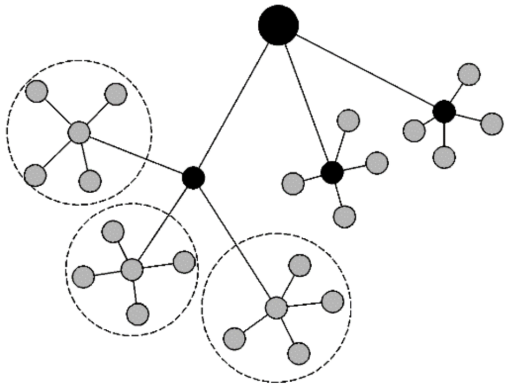

Fig. 1. Basic structure of clustering routing protocol

tion, the shorter the distance, the lower the node energy consumption, the longer the network life. In addition, the LEACH network protocol guarantees that each end node can achieve the same probability as the cluster head. Thus, the energy consumption of the network nodes can be balanced. Combined with data fusion computing, redundant data can be removed, the data of the collected nodes can be efficiently calculated and processed. According to the current usage, the use of the network protocol reduces the energy consumption of the network, and confirms that the LEACH network protocol can increase the service life of the network by at least 10 %.

Figure 2 shows an energy consumption model for LEACH protocols in wireless network applications. As shown in Fig. 2, the nodes of the sensor are evenly distributed in the effective monitoring area, and the nodes do not move randomly when they are used. The energy initial values of the whole network sensor are the same, and the node energy of sink is unrestricted. Sensor nodes do not die randomly during work, and only die out in constant consumption. Wireless communication between sensor nodes and the outside world is unrestricted, and energy consumption is lost in each direction. The system's sensors are controllable in terms of power usage. In the process of transmitting data transmitted by nodes, reasonable radio power can be given according to the actual detection and calculation of distances. Based on the characteristics of the network energy consumption, the energy consumption is mainly the energy consumption of the node when the data is transmitted and transmitted back to the node.

The sensor node is the relay station and amplifier for data transfer. After the data transmission enters the node, it needs to calculate the distance transmitted to the next node, and the reasonable transmission power is then arranged. The data sent consumes a certain amount of energy. The expression of energy consumed during the computation of node sending is calculated as follows [14]

$$E_{\mathrm{Tx}}(L,d) = \begin{cases} LE_{\mathrm{elec}} + Ld^2, & d \le d_0, \\ LE_{\mathrm{elec}} + Ld^4, & d > d_0. \end{cases} \tag{1}$$

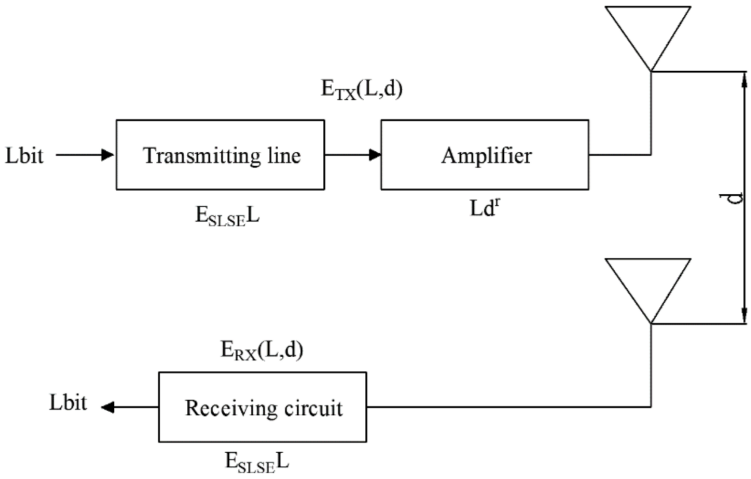

Fig. 2. Energy consumption model of LEACH protocol in wireless network application

Symbol E_{elec} in the formula represents the node energy value consumed by the wireless network when transmitting one section of data, and d represents the effective distance between the previous node's transmission and the location of the latter node. According to the law of conservation of energy in the transmission process, the nodes that receive data also need to consume part of their energy. The energy value consumed by the node that receives one section of data is calculated as

$$E_{\text{RX}}(L) = LE_{\text{elec}}\,. \tag{2}$$

The clustering process for wireless network transmission needs to be made by an election protocol. Each node can determine which node as the cluster head, which mainly depends on the distributed network WSN in cluster head probability, and whether a node become cluster head in the transmission of data in the previous stage. The threshold formula for a node to become a cluster head is [15]

$$T(n) = \begin{cases} \dfrac{p}{1-p\left(r \mod \frac{1}{p}\right)} \text{ if } n \in G, \\ 0 \text{ if } n \notin G. \end{cases} \tag{3}$$

In formula (3), p represents the proportion of nodes that become cluster heads at each node, which is the basic probability value that we often call cluster heads, r is the data transmission cycle in wireless networks and G represents the overall integration of nodes into cluster heads.

In the current cycle, the node that becomes the cluster head is announced to all nodes in the message inside the node, which expresses the ID information of the node. Cluster heads adopt protocol broadcast, and each cluster capital sends energy consumption information broadcast. The nodes of non-cluster heads decide which

cluster header to join according to the incoming message. Typically, non-cluster heads choose the nearest cluster head, which reduces the energy consumed by signal transmission.

Compared with the establishment stage of the cluster, the stable transmission nodes consume much longer time, and the energy consumption of each node is also the largest. After the cluster is determined, the gap table can be confirmed, and data transmission is officially initiated. The gap table divides the transmission phase into frames at each time frame. Each frame is divided into a plurality of gaps according to the node condition in the cluster. The nodes in the cluster randomly assign a reasonable gap and send the received information to the cluster head within the gap. Fig.3 shows the detailed operation of the agreement. The protocol assumes that the nodes in the cluster keep the data transmission and ensure that each node does not conflict with the competition.

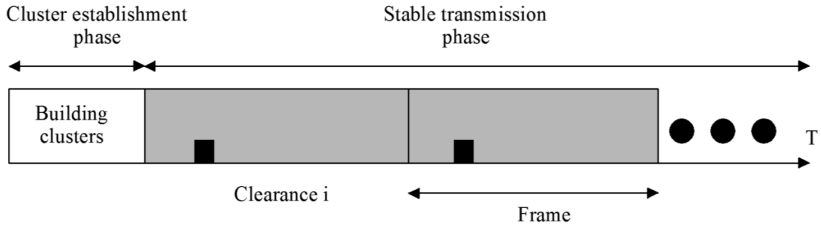

Fig. 3. Specific operation flow of network transport protocol

According to the requirements of the above process, when the node becomes a cluster head, it must always be ready to receive data from other nodes in the cluster. After the data is collected, the data is fused and the redundant data is removed by itself. First, the converged data is passed to the sink node. At the same time, the cluster head is far away from the sink position at this stage. Therefore, the process consumes the most energy, and the specific output transmission process is shown in Fig. 4. In the stable transmission phase, the LEACH protocol adopts periodic cluster head election, which makes the distributed network transmission structure with more balanced energy consuming.

In order to propose an improved stable election protocol, the cluster head election method is used to compute the residual node energy with the expression as follows

$$p(s_i) = \frac{np_{\text{opt}}(1+a_i)}{n+\sum_{i=1}^{n} a_i} \frac{E_i(r)}{\overline{E}(r)} . \tag{4}$$

In the formula, $p(s_i)$ represents the cluster head probability of a single node, a_i denotes the multiples of the node s_i above a certain base energy, and p_{opt} is the cluster head probability, which can be solved by the ratio of the optimal cluster head number to the total number of nodes n in the network. Symbol $E(r)$ represents the residual energy of the node in the rth cycle, and $\overline{E}(r)$ represents the average residual energy value of all nodes in the entire network in the rth cycle.

The threshold expression for which the node becomes the cluster head is

$$T(s_i) = \begin{cases} \frac{p(s_i)}{1-p(s_i)(r \mod \frac{1}{p(s_i)})} \ fi, s_i \in G, \\ \\ 0 \text{ otherwise.} \end{cases} \tag{5}$$

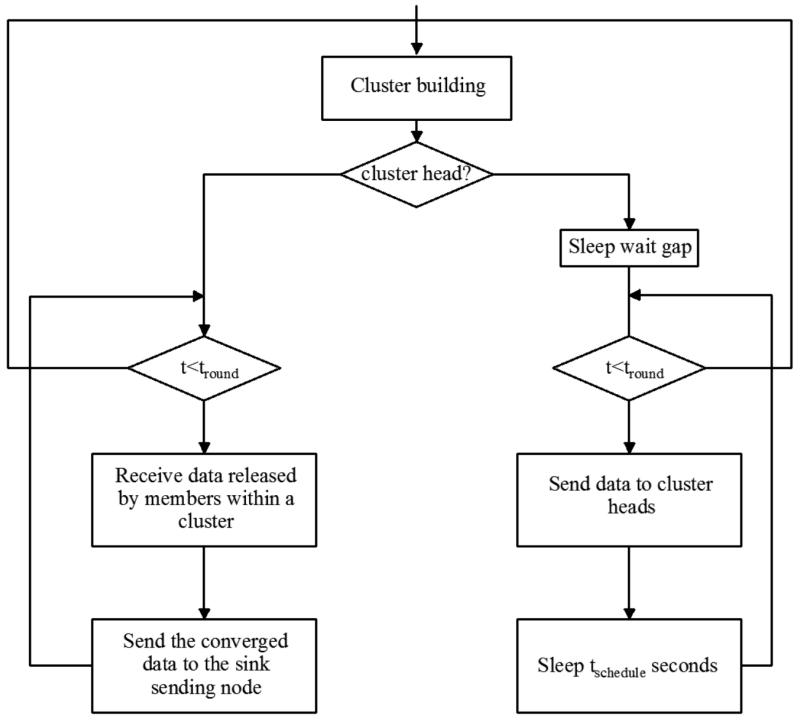

Fig. 4. The receiving and sending process of node energy

In the above formula, $T(s_i)$ represents the threshold of each node, and r is the cycle of node calculation. It is assumed that the energy consumption of each node in the energy cycle of each node is the same. Symbol E_{tot} is the initial total energy of the network and R is the total number of the network. Then, the average energy consumption $\overline{E}(r)$ of the round nodes is the average energy consumption of the network

$$\overline{E}(r) = \frac{1}{n} E_{\text{tot}}(1 - \frac{r}{R}) \tag{6}$$

According to the energy loss calculation method of average node, the election mechanism of cluster head in traditional DEEC protocol is improved. In order to select the cluster head intelligently for the remaining nodes, the energy of other nodes should be estimated. Elections can't be held beyond the threshold. Since the energy consumption in the process of the cluster head's receiving data, fusing data and sending data, the nodes with high residual energy should be elected as

cluster heads during the next round of election. In this study, the design of dynamic threshold interval is proposed. The reason for this design is that the nodes with higher residual energy value become larger, so that the energy consumption of each node is uniform, and the network transmission lifetime is extended.

4. Result analysis and discussion

Figure 5 shows a curve relation between the number of messages and the time in the process of data transmission in the sink node of a multistage network protocol, which shows the changes of protocol nodes' receiving and transmitting information over time. When receiving and transmitting messages with the same amount of energy consumed, DEEC-TA nodes receive more information. This shows that the protocol has more information throughput, and it can transmit more efficient data under the same energy consumption. In addition, it is found that the ability of sink to transmit data between DEEC and the improved DEEC protocol is relatively large. This is because the traditional DEEC protocol predicts the running cycle, which makes the average energy value of nodes too large, the election number of cluster heads in the whole operation cycle relatively small, and the total number of sink too small to explain. The optimized DEEC protocol can optimize the threshold interval. According to the nodes of different energy values, different threshold intervals are designed. In this way, the cluster heads formed in each cycle of the network are more reasonable, and the data received and sent by sink is more uniform.

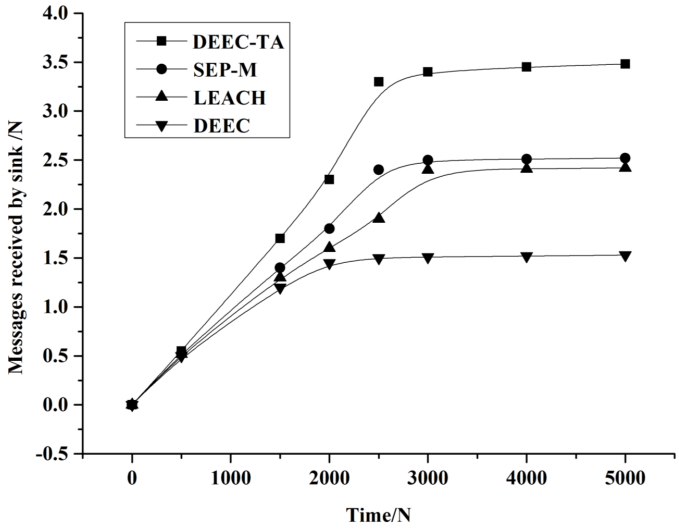

Fig. 5. Node data transmission message and time relation curve

Figure 6 shows the relation between the energy loss and the time of the nodes in the multistage heterogeneous wireless network transmission. As we can see from Fig. 6, when the wireless network is running, the total energy consumption of each

protocol is increasing. Before 1200 weeks, the total energy consumption of the network transmission protocol selected in this paper has no significant difference in the actual operation process. After the curve equal ratio method is adopted, the total energy consumption of the improved DEEC network transmission protocol proposed in this paper is minimal. When the cycle time is more than 1200 weeks, the total energy consumption of LEACH is the least, the total energy consumption of DEEC is the most, and the total energy consumption of SEP-M is centered. At this time, the running time of LEACH and SEP-M has exceeded the stable stage of normal operation, and the survival of nodes has been reduced, so that the total energy consumption has been reduced. Therefore, when the cycle is greater than 1200 weeks, the DEEC and the modified DEEC protocol do not have the research value of comparative analysis. To sum up, in the stable data transmission phase, the improved DEEC protocol has the least total energy consumption. According to the simulation of the improved protocol simulation results, compared with other protocols, the improved network transfer protocol can better balance the energy consumption of the network nodes, enhance the data throughput of the network and stabilize the data transmission cycle.

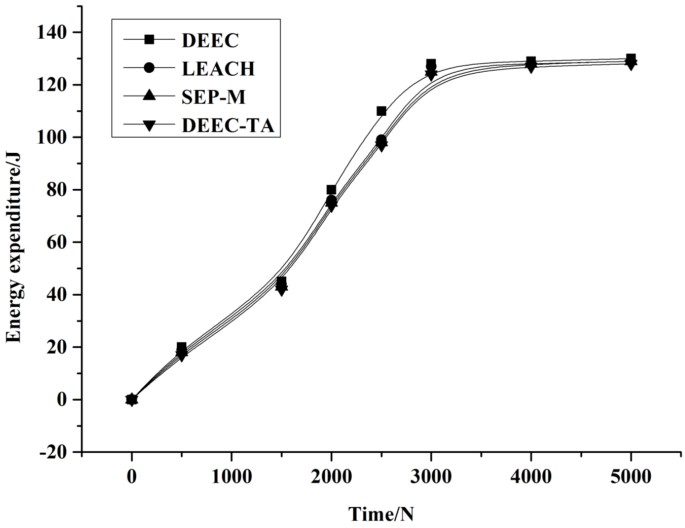

Fig. 6. Relationship between energy loss and time of nodes in multistage heterogeneous wireless network transmission

5. Conclusion

WSN is a comprehensive subject technology, involving interdisciplinary fields of many subjects, which is widely used in information collection, defense, and military and natural environment detection. Based on the lowest comprehensive energy consumption of wireless network node and the minimum maximum data throughput as the research object, the research of WSN routing protocol was carried out, and

the heterogeneous cluster election protocol of wireless network was improved in this paper. The key technologies of WSN wireless network structure were summarized and analyzed. On the basis of discussing the characteristics of routing technology in wireless networks, the traditional DEEC protocol defects were improved and an improved DEEC algorithm was proposed. The objective of the improvement is to minimize the energy consumption of nodes and to change the election of cluster heads into more reasonable agreements. The improved protocol and its calculation method of extremum interval can set the dynamic extreme range of the cluster head election, which can greatly improve the probability of high energy nodes being elected as cluster heads, and reduce the probability of low energy for nodes to be elected as cluster heads. In addition, the energy consumption is more balanced throughout the network operation. In this study, it was assumed that the transmission positions of sensor nodes and sink remained unchanged, whereas nodes had moving characteristics in practical applications. Therefore, the research of wireless network routing protocol also needs to incorporate the node's mobile features into the research factors, which needs to be considered.

References

[1] O. Rehman, N. Javaid, B. Manzoor, A. Hafeez, A. Iqbal, M. Ishfaq: *Energy consumption rate based stable election protocol (ECRSEP) for WSNs*. Procedia Computer Science *19* (2013), 932–937.

[2] H. Jing: *Routing optimization algorithm based on nodes density and energy consumption of wireless sensor network*. Journal of Computational Information Systems *11* (2015), No. 14, 5047–5054.

[3] Y. X. Zhai, L. Y. Li, C. L. Li: *An energy efficient communication routing protocol based on LEACH for WSN*. Advanced Materials Research *905* (2014), 595–599.

[4] K. G. Qian, M. Li, Z. C. Dai: *A sensor network flooding routing algorithm based on sector area nodes selection*. Advanced Materials Research *765–767* (2013), 1766–1769.

[5] Z. P. Liu: *Based on base station control management protocol in heterogeneous sensor network*. Applied Mechanics and Materials *273* (2013), 519–523.

[6] S. Y. Zhang, J. D. Wu, X. D. Wang, Y. G. Fan, T. T. Leng: *An energy consumption balanced clustering routing algorithm for wireless sensor network*. Computer Engineering *40* (2014), No. 8, 6–9.

[7] Z. M. Li: *Energy consumption balance LEACH routing protocol for wireless sensor networks*. Applied Mechanics and Materials *536–537* (2014), 744–747.

[8] C. Divya, N. Krishnan, T. Gandhimathy: *Energy efficient stable election protocol for clustered heterogeneous wireless sensor networks*. IOSR Journal of Computer Engineering *12* (2013), No. 5, 55–61.

[9] A. Razaque, K. M. Elleithy: *Energy-efficient boarder node medium access control protocol for wireless sensor networks*. Sensors (Basel) *14* (2014), No. 3, 5074–5117.

[10] R. Azizi: *Energy consumption and fault tolerance in the MAC protocols for WSN*. Journal of Computer & Communications *3* (2015), No. 6, 118–130.

[11] J. Yu, L. Feng, L. Jia, X. Gu, D. Yu: *A local energy consumption prediction-based clustering protocol for wireless sensor networks*. Sensors (Basel) *14* (2014), No. 12, 23017–23040.

[12] A. M. Khedr: *Effective data acquisition protocol for multi-hop heterogeneous wireless sensor networks using compressive sensing*. Algorithms *8* (2015), No. 4, 910–928.

[13] S. RaniS, J. Malhotra, R. Talwar: *Energy efficient chain based cooperative routing protocol for WSN*. Applied Soft Computing *35* (2015), 386–397.

[14] T. Cevik, F. Ozyurt: *Impacts of structural factors on energy consumption in cluster-based wireless sensor networks: a comprehensive analysis.* International Journal of Ad hoc, Sensor & Ubiquitous Computing (IJASUC) *6* (2015), No. 1, 1–19.

[15] Z. H. Yuan, B. Li, N. Wang, X. L. Zhang: *The improvement of LEACH router protocol based on geography and energy.* Applied Mechanics and Materials *678* (2014), 482–486.

Received May 7, 2017

Acta Technica *62* No. 2B/2017, 253–262

Indoor location algorithm based on RBF neural network[1]

Xushan Peng[2,3], Yongping Li[2], Xiaoming Zhang[2], Shui Wang[2]

Abstract. At present, indoor location technology is widely used in the field of wireless communication network. Due to the relatively complicated indoor environment, the wireless signal changes at any time, which brings great difficulty to the establishment of fingerprint map. In this study, a location algorithm based on RBF neural network was designed for the indoor location technology. Then, the prediction model of radial RBF neural network was adopted by the prediction technique and the K neighborhood algorithm was used to test the performance of this method. In order to make the fingerprint map adapt to the changing state of the environment at any time, the map construction method of the dynamic RF fingerprint was adopted. After optimizing the algorithm, the map was compensated according to the environmental parameter value.

Key words. RBF neural network, indoor positioning, wireless sensor network.

1. Introduction

Wireless sensor network is a comprehensive interdisciplinary. In practical applications, the number of nodes of the wireless sensor network is relatively large, and after the detection, the sensor passes the data to customers. Wireless sensor network location technology is the core technology of the wireless sensor network technology, which has a strong application value [1]. Then, the indoor location application is to use the navigation system, and the global application is to use GPS

[1]This paper is supported by projects: 1) Zhejiang public welfare Technology Application Research Project, Study of chaotic synchronization and information flow in large scale coupled nonlinear systems (2017C35013). 2) Zhejiang Provincial Natural Science Foundation, Research on Multi-order Brillouin Scattering Mode Locked Laser in RoF systems (LQ13F01004). 3) Ningbo science projects, he development of Dendrobium automatic screening grading equipment of machine vision technology (2016C10056). 4) The scientific research project of Ningbo Dahongying University, Research on Frequent Itemsets Mining Based on block transaction data (1320133017).

[2]School of Information Engineering, Ningbo Dahongying University, Ningbo, Zhejiang, China, 315175

[3]Corresponding author

outdoor location system, the location effect shows that the anti-interference ability is relatively strong. However, GPS is only suitable for outdoor open environment. Without the block of buildings or other objects, the energy consumed in the process of completing the task is relatively large. Thus, GPS is not suitable for being applied to WSN [2]. Indoor location can bring great convenience for human life, such as the office object location and the rescue location in the emergency circumstances. As a result, the market demand for indoor location technology is relatively large, more researchers are concerned about this aspect, furthermore, the value of research has a very broad prospect [3]. Indoor location technology uses the distance measurement and the non-distance measurement location calculation methods. The distance measurement location technology can carry out the time difference location, angle location, the location accuracy is relatively high, and meanwhile, the original cost is reduced. The non-distance measurement location algorithm includes the mass center calculation method and the RSSF RF fingerprint matching algorithm [4]. The requirements on the nodes are relatively low and the influence of the indoor environment is relatively low. RSSI radio frequency (RF) maps have low technical costs for the indoor RBF neural networks, while the achievement efficiency of the installation and operation is high. As a result, more scholars are focusing on this research.

2. State of the art

Wireless sensor network was launched in the US military industry in last century. In the later period of development, the wireless sensor network has made great progress in theory and practical application [5]. Then, key technologies are widely used in the fields of environmental observation, medical care and building inspection. The foreign countries have attached great importance to the application given in this respect, which have provided a lot of manpower and material resources [6]. Although the domestic WSN research starts relatively late, the country's policy support in this area is more. With the development and progress of wireless sensor networks, indoor location technology has also been widely studied. Then, the non-distance measurement location technology has obtained great attention in the academic field in the indoor location technology research and development [7]. The research on the RF map matching method based on RSSI is more concentrated, and the location algorithm and the latter part of the training location phase also obtain researchers' attention. In the offline trial, the construction of the fingerprint RF map requires the acquisition of most of the reference position signals. If the indoor area is large, the construction of RF fingerprint map will consume relatively large human and material resources [8]. In addition, the signal will encounter the role of obstacles in indoor communication, and the changes with the time and space are relatively large.

If the map can not adapt to the current real environment, then, the node geographical position of the calculated position needs to be reestablished [9]. Therefore, the offline algorithm training stage is the core technology of indoor location. And it has become the key to indoor location technology about how to optimize the algorithm, so as to build dynamic RF fingerprint [10]. RADAR indoor location system proposed by the scholars is the design work completed by adopting the WSN indoor

location technology. In the system, using the method of collecting data point by point to create a fingerprint RF is special, which is relatively close to the actual results. However, the workload is relatively large, which is not suitable for the indoor environment location system [11]. The difference calculation method given in the literature can reduce the work of collecting data point by point, and the workload of training can be reduced in the later stage. The method is more suitable in the case of that there are a few obstacles in the indoor environment [12]. The classical algorithm in the location phase is the calculation method of K value approaching location, the advantages and disadvantages of the localization algorithm are analyzed, and the algorithm is further optimized and transformed into RSSI's RF fingerprint map internal location calculation method.

3. Methodology

Indoor location algorithm is applied into the location process of RF fingerprint. In order to obtain high algorithm accuracy and practical application effect, the sample point fingerprint data needs to undergo a lot of training, so that the better spatial characteristics of the indoor environment can be show. However, the collection of the fingerprint data for indoor spatial characteristics requires a point-by-point measurement to each position, and this work method consumes physical strength [13]. At the aspect of nonlinear measurement, the neural network shows the advantages of this, and RBF neural network convergence performance is better, which makes up for the BP neural network's local shortcomings and restrictions in many places. The precision of the method of taking data point by point is higher than that of the prediction method, and the main idea is to conduct the derivation according to the grid data acquisition part, then, the correlation between the basic coordinates of the measurement point and the signal intensity is obtained, so that a map of the RF fingerprint is constructed in accordance with the signal strength of the model prediction grid [14]. Figure 1 shows a prediction method of the propagation model, this method can efficiently establish the radio frequency fingerprint map in a short time, and the workload of the later data training is relatively small. At the same time, the data predicted by this model will also have errors, so it is the best to use the point sampling method with higher precision.

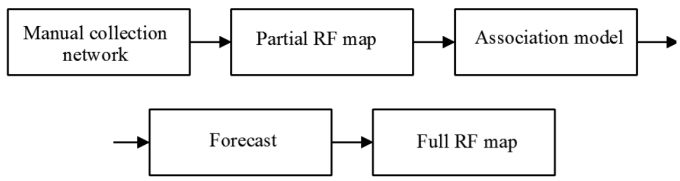

Fig. 1. Propagation prediction model

According to the propagation model, the linear interpolation algorithm is more widely used. The algorithm is simple to use, and the signal strength of the detected nodes is predicted according to the propagation distance of the theoretical signal

and signal. Linear interpolation can reduce the intensity of training. Set up $\mathrm{RSSI_R}$ and $\mathrm{RSSI_L}$ respectively for the interpolation points on the right and left position of the adjacent signal strength value, set $\mathrm{RSSI_D}$ and $\mathrm{RSSI_U}$ for the interpolation point of the lower and upper position near the signal strength value, horizontal direction interpolation $\mathrm{RSSI_H}$, vertical interpolation with $\mathrm{RSSI_V}$. The expressions calculated by interpolation in horizontal and vertical directions are considered as follows

$$\mathrm{RSSI_H} = \frac{\mathrm{RSSI_L} + \mathrm{RSSI_R}}{2}\,, \tag{1}$$

$$\mathrm{RSSI_V} = \frac{\mathrm{RSSI_U} + \mathrm{RSSI_D}}{2}\,. \tag{2}$$

Although the linear interpolation method can reduce the workload of offline training, there will be non-line-of-sight problem in the actual application process. Therefore, the indoor location calculation effect is relatively poor in the case of that there are obstacles. The fingerprint database established by adopting the interpolation method by neural network can save training time. Most of the indoor location systems can use the method of taking the average after the point-by-point sampling to establish a fingerprint map. In the stage of offline training, evenly divided small grids can be divided in the locating area. The average value of the signal strength of each grid node is collected, and the data is summarized into the database, at the same time, more data points are required to collect, therefore, the workload is relatively large and the measurement accuracy obtained is relatively high.

According to the radial basis function of multivariable interpolation, Darken proposed neural network structure (RBF). This kind of network structure also belongs to a kind of forward neural network structure, which can realize the continuous function of infinitely approximating to the real value. The RBF neural network uses three layers of structure, the first layer belongs to the input layer, which constitutes the initial structure of the signal source; the second layer is the hidden layer, which determines the specific requirements of the specific problem; the third layer is the output layer, and the corresponding value is made for the input signal. The data transformation between the first and second layers is non-linear and the data conversion between the second and third layers is linear. Figure 2 is a schematic diagram of the neuron structure of neural network structure. The distance between the weight and the input vector is used as an independent variable.

The expression for the activation function R is

$$R(\|\mathrm{dist}\|) = \mathrm{e}^{-\|\mathrm{dist}\|^2}\,. \tag{3}$$

In the formula, $\|\mathrm{dist}\|$ is the distance between the weight vector and the input vector, and it is also the independent variable of the formula.

According to the structure function role of the input layer, output layer and hidden layer of the neural network structure, the input layer is only responsible for the transmission of the signal, and the works of the output layer and the hidden layer are only different learning strategies. The output layer needs to adjust the

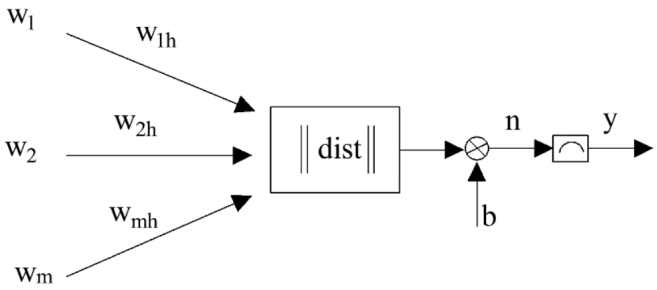

Fig. 2. Schematic diagram of neural structure of neural networks

linear weight, which has a strong learning speed. The hidden layer simply calls and activates the function, and the learning strategy is not linear, so the learning speed is relatively slow. Then, the learning method used by RBF neural network is the center selection method of the intelligent self-organization. The radial basis function used by RBF neural network is generally a Gaussian selection function, the expression is

$$R(x_{\mathrm{p}} - c_i) = \mathrm{e}^{-\frac{\|x_{\mathrm{p}} - c_i\|^2}{2\sigma^2}} . \tag{4}$$

In the formula, $x_{\mathrm{p}} - c_i$ represents the constant, c_i represents the center value of the Gaussian function, and σ is the variance of the Gaussian function.

Neural network is the total intelligent information processing technology in the future, which can build the model according to the data's ontology characteristics, and it has strong self-learning and adaptive features. RBF can conduct the adaptive learning and self-regulation in accordance with the specific problems described, so as to make the network have a good practicality. In addition, RBF neural network training algorithm can realize the adjustment of intelligent hidden layer unit data, the excellent learning performance is shown.

According to the description above, the prediction method based on radial nerve RBF network was proposed and the uniform indoor sampling was selected for fingerprint database finishing. In order to minimize the impact brought by the signal acquisition fluctuations, the average of the collected 100 200 data was taken as the basic database of the radial basis function neural network. Figure 3 shows a predictive model of the network. According to the coordinates of the nodes, the receiving intensity of different signal nodes was predicted and the node signal strength of the trained network prediction target was used effectively. This algorithm can restrain the incomplete map problem of the fingerprint radio frequency training method.

Affected by the indoor environment, after matching the measured values received during the location calculation process with the previous RF fingerprint map, it is found that the effect of location is not ideal. According to the RSS value of the node received by the reference node, the calculated expression for the compensation is

$$\mathrm{RSS}'_i = \mathrm{RSS}_i - \frac{\sum_{j=1}^{n} (\mathrm{RSS}'_{ij} - \mathrm{RSS}_{ij})}{n} . \tag{5}$$

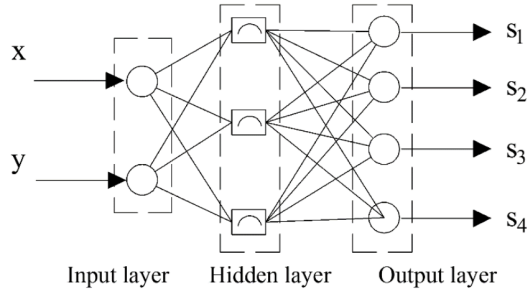

Fig. 3. Prediction model of network

In the formula, n represents the number of reference nodes and RSS_i is the average value of the offline training. This kind of calculation method can compensate the dynamic error of spatial data motion measurement to a great extent, and the periodic precision is relatively high. At the same time, the position reference point arranged will increase the input cost of the hardware, sometimes the dynamic compensation formula (5) and the actual environmental signal changes may not be consistent.

The mobile node and the prearranged reference node are set as the receiving node, and then, the emission signal of the confidence node is received. Assuming that the signal strength values received establish a mapping relationship at different spatial positions, the mapping relationship is relatively stable, then, a prearranged signal acquisition point can be used as an estimated value of the signal strength of the spatial location. The calculation expression is:

$$s = f((r_j)_{j=1}^{J})\,. \tag{6}$$

In the formula, f is the mapping function expression and $(r_j)_{j=1}^{J}$ represents a wireless signal received by a prearranged reference node.

The offline training phase selects massive beacon nodes to construct RF fingerprint maps. According to the previous research results, it is shown that the influencing factors of RF fingerprint map have time variability. In this paper, a dynamic RF fingerprinting method based on environmental status parameters was proposed in accordance with RBF neural network optimization indoor location algorithm. The method can be divided into two stages for the arrangement of the algorithm. The first stage is the calibration environment parameter confirmation of the fingerprint database, the previous RBF neural network prediction model is established and the data is sent out through the mobile node, then, the convergence node signal is transmitted to the computer through the serial port, and the RF fingerprint composition is completed. The map is constructed according to the RF fingerprints of the established environmental status parameters. Assuming the environmental state parameters and combining with the signal intensity values, the calculation formula of the environmental change degree is

$$C = \frac{(\mathrm{RSS}_2 - \mathrm{RSS}_2') + (\mathrm{RSS}_3 - \mathrm{RSS}_3') + (\mathrm{RSS}_4 - \mathrm{RSS}_4')}{3}\,, \tag{7}$$

where RSS_2, RSS_3 and RSS_4 are the assumed environmental state parameters.

4. Result analysis and discussion

In this paper, the interpolation calculation method and the algorithm proposed in this study were compared and analyzed. The RBF neural network prediction algorithm and the linear interpolation calculation method were used to construct RF fingerprint maps respectively. When the value of k was 3, the location verification analysis of the indoor environment was carried out, and the probability of sampling was 0.9, 0.7, 0.5 and 0.3 respectively. The cumulative results of the two methods are shown in Table 1. Due to the impact of indoor obstructions, the collected data may show that the signal of some points is weak, while the signal of some points is very strong, so the calculated results may not be in line with the actual situation. And furthermore, the data of the random two collection points uses the interpolation method to calculate will bring a lot of data error. RBF neural network is the total intelligent information processing technology in the future, and the model is established according to the correlation of the data itself. The algorithm can have a good nonlinear ability of approximating to the actual value. In addition, it also has good adaptability and good learning performance, which has strong superiority in the intelligent processing of data. The experimental results show that the smaller the probability value of the collected data is, the more reasonable the neural network prediction result of the interpolation method is. The experimental results show that when the probability of the acquisition point was greater than 0.9, the cumulative error would be between 1.5 m and 3 m, and the algorithm in this paper was superior to the interpolation method. When the probability of collecting data was about 0.5, the indoor location error reached the cumulative error ratio of 2.5 m to 3.5 m. Besides, the RBF neural network prediction method is superior to the precision control of the interpolation calculation method. In the status of using the point-by-point acquisition method, and the indoor location RF fingerprint map building process, the indoor location algorithm of RBF neural network can be reduced at least half of the work, and the location accuracy can be improved by at least 5 %.

Table 1. Cumulative results of two methods

Error	Linear interpolation ratio (70%)	Paper algorithm (70%)	Linear interpolation ratio (50%)	Paper algorithm (50%)	Linear interpolation ratio (30%)	Paper algorithm (30%)
0.5	25	23	18	18	5	11
1.5	54	60	51	58	25	46
2.5	88	91	81	88	57	77
3.5	98	100	93	98	80	91
4.5	100	100	100	100	96	100
5.0	100	100	100	100	100	100

Figure 4 shows the location comparative results of the proposed reconstructed updating algorithm and the linear compensation algorithm. In order to show the results more clearly, when the c value was less than or equal to 1.34, the curve changed relatively gentle. The results show that the impact of the environmental state parameters to the results was relatively small, and the errors of the reconstructed updating calculation method and linear compensation algorithm to the indoor location calculation were basically the same. According to the previous algorithm features, it was considered that the stage that c was less than or equal to 1.34 was more suitable for dynamic compensation algorithm. When c was greater than 1.34, the slope of the curve changes was relatively large, which showed that the influence of the environment state parameters to the results was relatively large. However, in contrast, the indoor location error of the reconstructed updating algorithm method was smaller than the linear compensation calculation method. Therefore, this stage is more suitable for the reconstructed calculation method with higher accuracy.

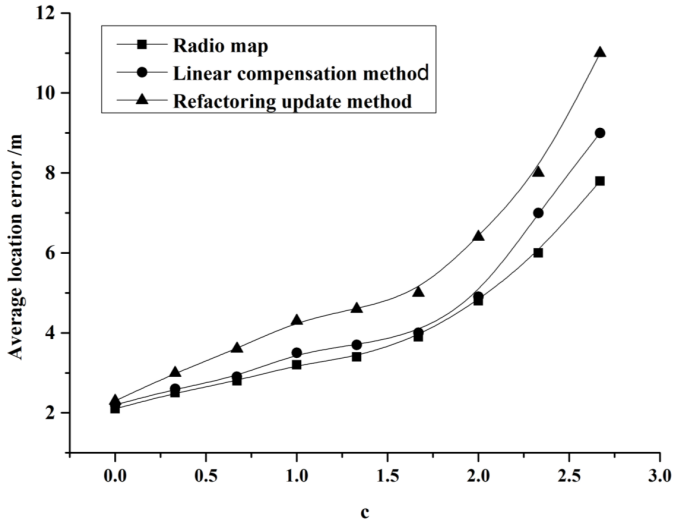

Fig. 4. Location comparison results between the reconstructed update algorithm and the linear compensation algorithm

In the indoor online location based on RBF neural network, the first was to confirm the observation value to the environment, and what kind of algorithm was adopted to optimize the RF fingerprint map database to build the database was determined according to the consignment of the measured value c. Then, the comparative analysis was carried out to the dynamic RF fingerprint map construction algorithm and the static RF fingerprint map construction algorithm. The results are shown in Fig. 5. It can be seen from Fig. 5 that the indoor location error rate of the environment adaptive dynamic RF fingerprint map construction algorithm was reduced and the reduction value was about 20 %. Due to the signal in the network environment, the indoor location had time variability, therefore, there might be the static RF fingerprint data map location matching defects. Then, a dynamic RF fin-

gerprint mapping algorithm was proposed. According to the algorithm advantages and disadvantages of the fingerprint database which is nearly mature application currently, this paper proposed a two algorithm tradeoff selection algorithm based on the environmental parameter values. The experimental results show that the indoor location algorithm based on RBF neural network dynamic environment can improve the location accuracy.

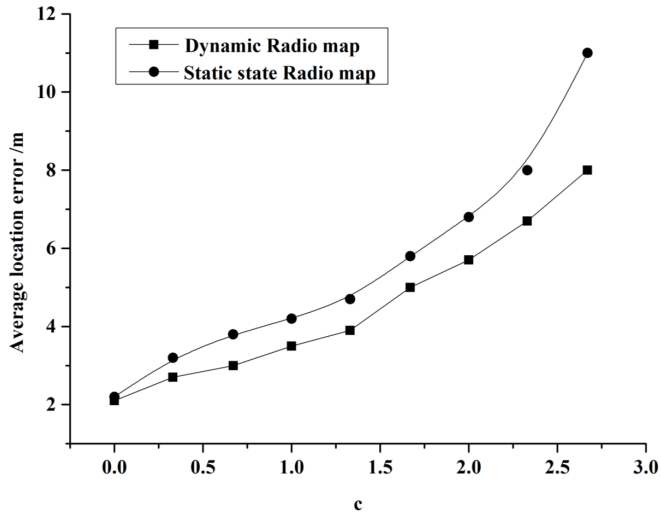

Fig. 5. Construction algorithm of dynamic RF fingerprinting map and construction algorithm of static radio frequency fingerprinting map

5. Conclusion

The convenience of the location technology to the mankind is obvious, GPS location also provides a great help for driving and navigation, and human life environment is mostly indoors. However, the indoor location data collection will be affected by obstacles, so it is necessary to set a reasonable indoor location algorithm according to different environmental state parameters. In this study, a prediction algorithm based on RBF neural network was proposed, and an indoor location RF fingerprint database was established. At the same time, this algorithm was compared with the linear interpolation algorithm, and it was considered that the indoor location algorithm based on RBF neural network was superior to the linear interpolation algorithm. As the indoor wireless signal environment changed with time, the environmental state parameter values were used to determine the positioning algorithm under the online location state. Then, 1.34 was taken as the boundary of environmental state parameter, when the environmental parameter was less than or equal to 1.34, the dynamic compensation algorithm was adopted to match. When the environmental parameter was greater than 1.34, the RBF reconstructed updating algorithm was used for the indoor location. The experimental results showed

that the location error value of the dynamic RF fingerprint was smaller than that of static error value, and the ratio of error reduction was about 20 %. The algorithm proposed in this paper can effectively balance the calculation complexity of the algorithm and the precision effect of indoor location. Under the premise of not adding the computational cost and the hardware cost, the algorithm and the corresponding location method can show good environmental adaptability.

References

[1] J. Ren, J. Chen, L. Feng: *A novel positioning algorithm based on self-adaptive algorithm of RBF network.* Open Electrical & Electronic Engineering Journal *10* (2016), No. 1, 141–148.

[2] D. P. F. Cruz, R. D. Maia, L. A. da Silva, L. N. de Castro: *BeeRBF: A bee-inspired data clustering approach to design RBF neural network classifiers.* Neurocomputing *172* (2016), 427–437.

[3] M. Mirrashid: *Earthquake magnitude prediction by adaptive neuro-fuzzy inference system (ANFIS) based on fuzzy C-means algorithm.* Natural Hazards *74* (2014), No. 3, 1577–1593.

[4] N. Li,R. Wang, Y. L. Tian, W. Zheng: *An effective strategy to build up a balanced test suite for spectrum-based fault localization.* Mathematical Problems in Engineering (2016), Article ID No. 5813490, 1–13.

[5] W. Jia, D. Zhao, T. Shen, C. Su, C. Hu, Y. Zhao: *A new optimized GA-RBF neural network algorithm.* Computational Intelligence and Neuroscience (2014), Article ID No. 982045, 1–6.

[6] W. Jia, D. Zhao, L. Ding: *An optimized RBF neural network algorithm based on partial least squares and genetic algorithm for classification of small sample.* Applied Soft Computing *48* (2016), 373–384.

[7] N. Shao, H. Li, L. Liu, G. Li: *Distributed containment control with dynamic leaders based on binocular vision.* Journal of Computational Information Systems *12* (2015), No. 4, 1319–1327.

[8] J. Ren, J. Chen, W. Bai: *A new localization algorithm based on taylor series expansion for NLOS environment.* Cybernetics and Information Technologies *16* (2016), No. 5, 127–136.

[9] S. Z. Nie, Y. H. Zhong, M. Hu: *Short-time traffic flow prediction method based on universal organic computing architecture.* Advanced Materials Research *756-759* (2013), 2785–2789.

[10] Z. H. Deng, Y. Q. Zhang: *AN improved RBF neural network model based on hybrid learning algorithm.* Advanced Materials Research *718–720* (2013), 2202–2207.

[11] X. S. Gan, H. L. Gao: *Research on learning algorithm of RBF neural network based on extended Kalman filter.* Advanced Materials Research *989–994* (2014), 2705–2008.

[12] J. Y. Zhao, H. Guo, X. N. Li: *Research on algorithm optimization of hidden units data centre of RBF neural network.* Advanced Materials Research *831* (2014), 486–489.

[13] S. Y. Song, B. H. Zhang, Y. Ma: *The RBF neural network based on Kalman filter algorithm and dual radial transfer function.* Advanced Materials Research *971–973* (2014), 1816–1819.

[14] F. Q. Xu, Y. T. Tao: *Variables screening method based on the algorithm of combining fruit fly optimization algorithm and RBF neural network.* Advanced Materials Research *756–759* (2013), 3225–3230.

Received August 7, 2017

Acta Technica *62* No. 2B/2017, 263–272

Multi-terminal data integration analysis of internet of things based on middleware[1]

Weiqing Qu[2,3], Yuedou Qi[2], Qi Zhang[2], Chunliang Zhou[2]

Abstract. With the emphasis on environmental protection in China, the development of electric vehicles in China is getting bigger and stronger. However, traditional electric vehicles still have the problem of mobile terminal positioning, which is not only inefficient but also low in reliability. Therefore, in order to solve these problems, in this paper, the method of multi-terminal data integration analysis of Internet of things based on middleware was proposed, and the network physical structure of charging station of electric vehicle was constructed. By adjusting routing configuration and topology structure, the design of the middleware of the electric vehicle charging station network was completed. Through the simulation test, it can be seen that the system has the function of fast locating and searching electric vehicle charging station by means of mobile terminals, which specifies a number of data for the mobile terminal device, and has good data integration performance.

Key words. Internet of things, middleware, electric vehicle, RFID technology.

1. Introduction

In order to provide effective information for mobile terminal equipment, this paper explored that how to locate and search the electric vehicle charging station with the help of mobile terminal, and solved the problems of charging pile navigation, communication and fast positioning during the use of the electric vehicle. With the help of gateway equipment, including the Internet of things, sensor networks and mobile Internet network and other network interfaces, wireless sensor networks are

[1]This work reported in this research was supported by Zhejiang Province public nonprofit technology applied research plan project (No. 2015C33236), Zhejiang Province University youth discipline leader academic climbing program (No. pd2013443), and Ningbo Natural Science Foundation project (No. 2012A610071).

[2]Ningbo Dahongying University, Ningbo 315175, China

[3]Corresponding author

integrated with the Internet to solve heterogeneous network convergence issues after accessing the Internet through the use of design gateways, which provides charging pile navigation and communication technology support for electric vehicles [1]. This paper described the traditional electric vehicle mobile terminal positioning problem. With the RFID technology as the breakthrough point, this paper discussed the non-contact automatic identification technology, improved the algorithm and design level of traditional problems, such as low location search efficiency and poor data integration performance. In the charging station search, this paper entered the low frequency transmitting antenna area through the RFID card, and designed the method of multi-terminal data integration analysis of Internet of things based on middleware, discussed the system construction and hardware model design and the problem of Internet of things gateway from the following two aspects: With the help of gateway technology, software platform design and hardware platform design can complete the task of heterogeneous network integration of cloud computing, and achieve the goal of data fusion of the information resources of the electric vehicle charging station, can highlight the good performance of the equipment in the process of system testing, so as to better serve the owners of electric vehicles.

2. State of the art

Since 2005, the International Telecommunication Union (ITU) has proposed "ITU Internet Report 2005: Internet of Things", the report formally declared that the Internet of things is an extension of Internet applications, the following core technologies can achieve the Internet of things: RFID, Sensor technology, intelligent embedding technology and nanotechnology [2]. In 2009, IBM proposed the concept of "wisdom of the earth", many countries incorporated the Internet of things into the strategic system for future information development [3]. Up to now, the world has not made a unified definition of the Internet of things. The European Internet of Things project research team argues that the Internet of Things is an important part of the Internet, belonging to a dynamic global network architecture that contains self-organizing capabilities for communication protocols [4]. Physical and virtual "objects" include features: physical attributes, virtual properties, identity, and it can be applied to the information network [5]. The definition of the current setting of Internet of things: With the help of various information sensing equipment, including the integration of global positioning system, laser scanning, infrared sensor and RFID device with Internet, it constitutes a huge network, the main objective is to make the network accessible to all objects, which improves the efficiency of management in the process of integrating identification resources. In the Internet of things, "CPS" "M2M" belongs to the key application forms [6].

3. Methodology

3.1. Internet of things technology

In the current environment, the Internet of Things is used in many fields, including logistics sales, intelligent transportation, public services, furniture life, environmental monitoring and so on, involving industrial agriculture and logistics industry and other fields. Among them, smart grid is one of the key fields of Internet of things [7]. Power transmission and transformation equipment has many characteristics as rich species, large quantity, which makes the equipment information sources more abundant. The access methods are also different. At the same time, the equipment evaluation and decision making technology is uneven, which brings a series of influence to the operation state of power transmission and transformation equipment, and makes the operation safety of power grid be impacted to varying degrees. According to China's data grid report, since the 21st century, due to natural disasters and equipment failure problems, the grid accident rate increased significantly. The use of Internet of Things technology can effectively reduce the risk, reduce the irrationality of equipment condition maintenance, help the equipment to achieve the goal of optimal management, improve the detection performance level of substation equipment and standardize the standard detection framework [8]. For the power transmission and transformation equipment of Internet of things, it is closely related to information space and physical space and belongs to the extension of the smart grid in the intelligent environment of the equipment. For the Internet of things, by using intelligent perception technology, it can improve the efficiency of on-line monitoring of equipment and solve the demand of smart grid for equipment status data. As shown in Fig. 1, the modern Internet of things technology connects all fields to integrate communication, so as to carry out information exchange and management. The standardization construction function in the Internet of things technology makes the information model of power transmission equipment more scientific, which is of great significance to the scientific framework of the grid, and has a positive impact on the integration of the information system and detection system of power transmission and transformation equipment, so as to better serve the equipment [9].

ITU Internet pointed out in its report in 2005 that the Internet of things covers four key application technologies, namely, RFID technology, sensor technology, intelligent technology, nanotechnology, its functions include tagging things, perceiving things, thinking about things, and reducing things [10]. The research center of Internet of things technology in China focuses on communication network technology, information processing technology and perceptual identification technology. The extension application of Internet of things is based on perceptual identification technology, which can sense and identify a range of data, including components such as radio frequency identification, smart sensors, electronic code, and two-dimensional code [11]. For the communication network technology, its role is to enhance the realization of perceived identification information reliability, to build a more secure transmission environment. The network covers the wireless self-organizing network,

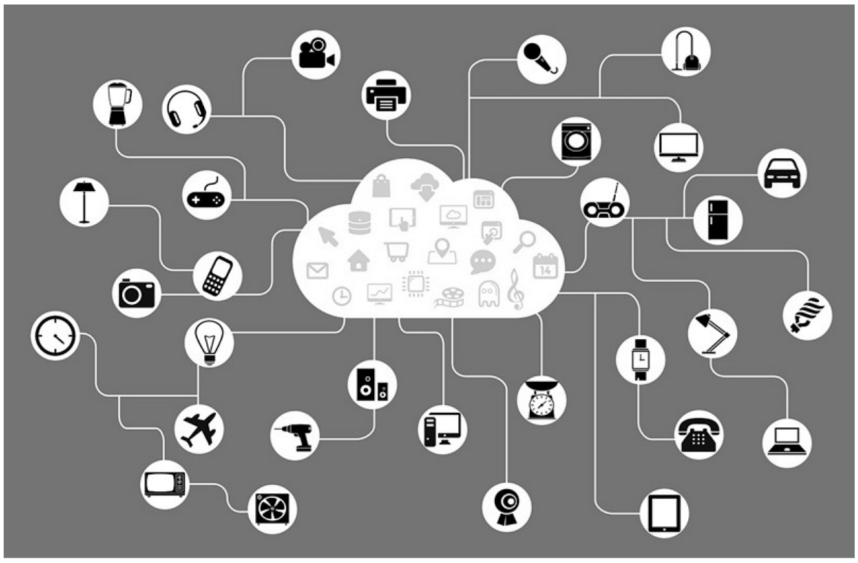

Fig. 1. Sketch map of modern Internet of things

the sensor network, the next generation network with the Internet protocol version as the core. In terms of communication technology, it mainly involves ultra-wideband, global microwave interconnection, Bluetooth, wireless fidelity, near field communication, 3U and so on. It is necessary to deal with more difficulties after expanding the scale application of Internet of things, including: data storage, information fusion, information mining and knowledge update. The Internet of things is an information processing technology based on cloud computing, which is based on efficient use of information [12].

With the rapid development of smart grid, non-renewable energy is becoming increasingly depleted. The important components of the smart grid construction, such as the new distributed energy of electric vehicles, can meet the demand for the rational use of energy in time by adjusting the price and peak shaving of the power grid [13]. The application of IT technology in the Internet of things in electric vehicles will enable them to play an important role in rechargeable batteries, charging facilities and electric vehicles. In addition, the use of smart sensors can help cities achieve full coverage. The Internet of things has a series of advantages, including low investment cost, extensibility, flexibility and applicability of network topology. The application of Internet of things technology in the charging facilities can give full play to the advantages of dispatching and make the metering and accounting functions scientific and reasonable. In the configuration of intelligent sensors for electric vehicles, it sets the electronic tag, which can transfer data messages to the charging facilities scheduling platform by means of Internet of things wireless technology. The platform is based on the following issues: car operation status, the number of electric vehicles charged, the use of charging facilities and so on, so as to improve service efficiency [14]. This paper designed the main controller of the system as S3C2440

module, interface circuit, 485 network and Ethernet communication-based interface circuit, made many improvements to the multi-terminal data integration algorithm, and finally completed the data integration goal of the multi-terminal of the electric vehicle charging station information resource.

3.2. Construction of network physical architecture for electric vehicle charging station

When the electric vehicle enters the charging pile area, the owner of the electric vehicle uses the electronic tag, and the reader in the charging station can automatically scan the identity and basic information of the user, including personal name, identity card number and telephone and so on, while sensing the corresponding battery charge information. This information will be automatically transferred to the automatic toll collection system, and then the charging charge will be measured. The settlement center will pay automatically according to the value, and will obtain the consumer information on the user's SMS with the form of short message. With the help of Internet, users can query their personal account information. Internet of things not only has the charging facilities management functions, but also has a series of advantages in the rechargeable battery. This paper combined the different intelligent charging service network operation mode, charging assets change two issues, analyzed battery management in network operation mode and developed a series of system solutions.

Based on the perspective of multi-terminal equipment, in order to achieve the goal of resource sharing and data integration, electric vehicle charging station is set as the research subject, so that it can provide a series of services for the owners, including the search charging station, accurate positioning, searching charging pile. Based on the design of the system model, the designed electric vehicle charging station has the characteristics that in the monitoring area, the isomorphism is set as a micro sensor node with data acquisition function, at the same time, it guarantees that the communication distance, energy supply and computing ability of each node can be well coordinated. In the cloud node control environment, that is, wireless sensor network, efficient algorithm is used to make the adjacent nodes trust each other by monitoring the behaviors of two adjacent nodes, so as to obtain the comprehensive trust value after tradeoff. In the process of loop computing, the communication link data of wireless sensor networks can be assigned a series of tasks. At the same time, the transmission results can be sent to the data to achieve the purpose of data transmission and distribution. Based on the above principle, the structure of the physical system of the electric vehicle charging station in the framework of the Internet of Things system is shown in Fig. 2.

According to the above principles, the electric vehicle charging station network physical architecture is constructed. In this paper, the middleware technology is used to complete the following contents: the heterogeneity of charging station network, hierarchical structure design, some common functions of the business layer based on sensor network infrastructure. The hierarchical structure and heterogeneity of the charging station for electric vehicles are shown in Fig. 3. As shown in Fig. 3, the use of network middleware technology can achieve the following service functions:

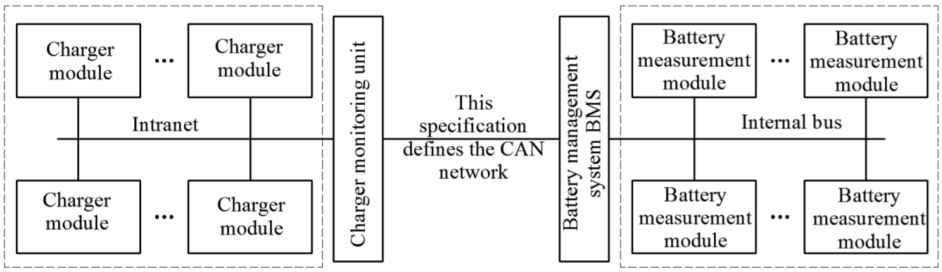

Fig. 2. Station network physical architecture of electric vehicle charging

network generation services, network connectivity services, wireless sensor network access services and network self-healing services. Middleware can be used as the carrier to transmit interactive messages. It is worth noting that the node of the key way of completing middleware is information transmission. Applications can be applied to the OS environment and multiple platforms through middleware.

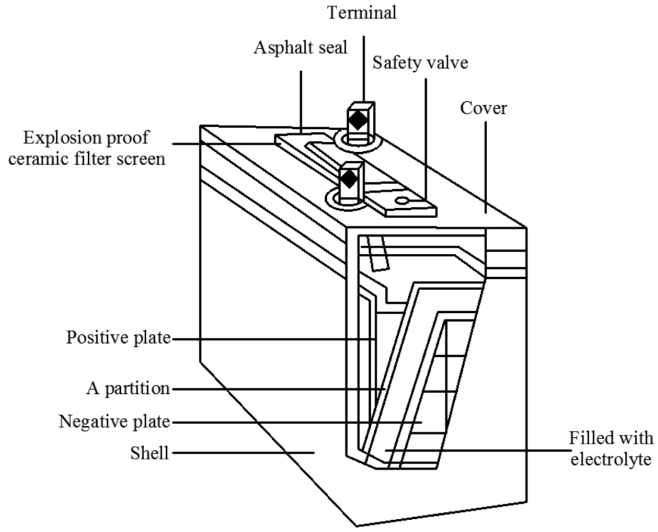

Fig. 3. Heterogeneous and hierarchical structure of electric vehicle charging station network

3.3. Heterogeneous network hierarchical data fusion model for electric vehicle charging station

In this paper, the NES C design idea is used to construct the heterogeneous hierarchical data fusion model of the charging station network. The component takes the connected interface as a carrier, and describes a set of functions command() and event() in the gateway structure, among them, the former is provided by the

interface provider, and the latter is implemented by the interface user. Components have the function to implement the logic function module, which belongs to the basic unit of the program NES C. In the whole Tiny0S node, many components constitute a program. In the electric car charging station, Fig. 4 shows its network node application program and communication hardware design and module design system.

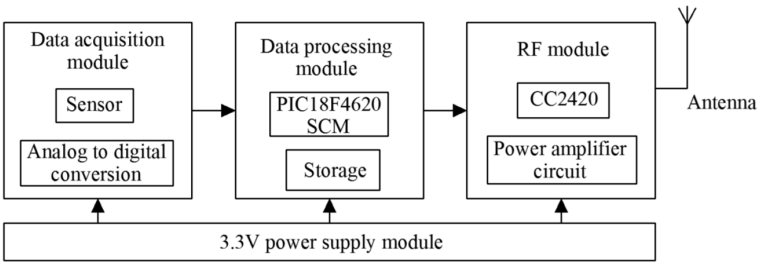

Fig. 4. Station network heterogeneous hierarchical data fusion diagram of electric vehicle charging based on Tiny0S

4. Result analysis and discussion

Through the hardware module synthesis, this paper puts forward the concept of multi-terminal data integration algorithm, and used the gateway technology to achieve the goal of cloud computing heterogeneous network convergence, and dealt with the following problems: the real time and validity of network transmission, data integration strategy. In order to improve the efficiency of network data transmission, this paper proposed an access algorithm to enable heterogeneous network networks to improve problem processing efficiency during convergence. For the algorithm design, it is described as follows: by using the above-mentioned branch situation, the number of scheduling task instructions is predicted. After the terminal data integration analysis, the number of scheduling task instructions is measured by the corresponding formula. In this formula, $p(q|e)$ is mainly used for the description of the time interval, so that the distribution of q is more logical, δ is a collection that consists of the total number of location instructions in the charging station, this formula is used to complete the description:

$$\delta = \{q\,|el + 2eq \leq q \leq Q\} \tag{1}$$

Among them, based on the middleware task in the Internet of Things, Q is the maximum value of the allocation period. According to the above algorithm, this paper used the network technology to integrate and realize the heterogeneous network of cloud computing, so that multi-terminal of information resources for the electric vehicle charging station achieved data integration, and met the requirement of fast and accurate positioning of the electric vehicle during the use, meanwhile, it dealt with the navigation and communication of power station, charging pile.

In order to test the design proposed in this paper, from the perspective of multi-terminal data integration of Internet of things based on middleware technology, this paper tested the performance of data gateway terminal fusion, that was, the location and search performance of electric vehicle charging station. Firstly, the gateway serial port based on middleware technology was constructed. Computer gateway port was taken as a carrier, telos B node and another telos B node were connected, a data was output every 1 s, and the search for the electric car charging station was completed. According to the simulation background design, the search positioning and data integration function of the electric car charging station was completed. The serial port debugging tool software allowed the system to output interface data after completing multi-terminal data integration, as shown in Fig. 5.

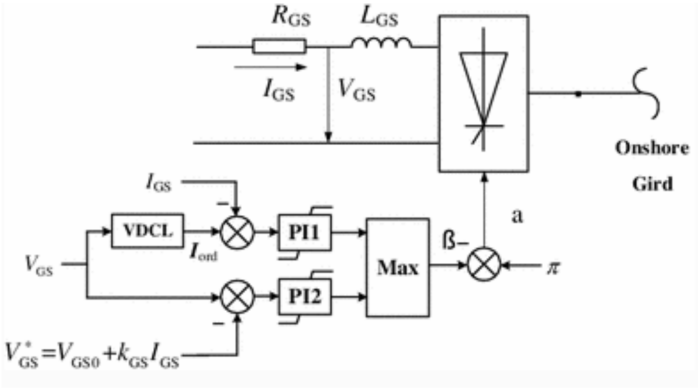

Fig. 5. Multi terminal data integration analysis results

The results of the data location experiment of the charging station of the electric vehicle in city A are shown in Table 1.

Table 1. Station data information localization results of electric vehicle charging in city A

Number	Real data location	Traditional algorithm results	Algorithm results in this paper
1	(21, 48)	(22, 49)	(20, 47)
2	(46, 35)	(49, 36)	(49, 35)
3	(56, 73)	(55, 75)	(54, 74)

According to the results of data integration described in Figure 4 to charge high search station detection, assuming the charging station distribution area belongs to random distribution, on the basis of cloud computing in heterogeneous network proposed fusion principle, can realize the fast charging station coordinates, during the search for the best navigation, take the mobile terminal fast positioning function to search for electric vehicles the charging station, by mobile terminal equipment can obtain effective information, after a series of testing system can obtain different

charging city of A in the simulation environment the station coordinate map, we conducted a total of three positioning experiments, as shown in Table 1, the actual position location respectively (21, 48), (46, 35), (56, 73), and the traditional positioning method for the position (22, 49), (49, 36), (55, 75), by using the method of this paper is (20, 47), (49, 35), (54, 74), obviously, this method is more close to the true position, positioning is more accurate, complete data integration in the mobile terminal, can effectively improve the charging station location coordinates positioning accuracy, guarantee the precision of navigation, the networking gateway designed load balance display in this paper, the Balanced Routing system has higher, reflecting the data integration and network communication function, so as to electric vehicle charging pile in navigation and communications to provide technical support.

5. Conclusion

The use of smart sensors and electronic tags in the charging station can sense the position and running state of the electric vehicle in real time, which helps the owner understand the performance of the rechargeable battery profile. When the charging facilities have problems, the deficiencies can be solved in time. In this paper, the rapid positioning of mobile terminals and the search of electric vehicle charging stations were discussed, so as to provide service information for mobile terminals and effectively solve a series of problems for owners in the use of electric vehicle, including rapid positioning, charging pile navigation and communication. In this paper, the method of multi-terminal data integration analysis of Internet of things based on middleware was proposed. System construction and hardware model were designed and analyzed. From the point of view of software platform design and hardware platform design, the Internet of things gateway was analyzed, the convergence goals of cloud computing heterogeneous networks were accomplished by relying on network management techniques, the multi-terminal data integration of information resources of long power station of electric vehicle was realized. According to the system test, the multi-terminal data integration system of Internet of things of the electric vehicle charging station designed in this paper can locate and search the coordinates of the charging station, and improve the efficiency of network communication and data integration, which makes it easier for the owners of electric vehicles to finish rapid positioning, charging pile navigation and communications during the use. Of course, the results of the study also reflect the room for further improvement. Therefore, the lack of continuous improvement research is a weakness.

References

[1] D. Gao, J. Cao, Y. Zhang, X. Wang: *Communication networking schemes for wide area electric vehicle energy service network*. Energy and Power Engineering *5* (2013), No. 4B, 1415–1420.

[2] W. Jiang, X. Wang, Y. Yang, J. Wang, Q. Xu, G. Zhou: *Electric vehicle smart*

battery management and its wireless sensor network protocol. Automation of Electric Power Systems *39* (2015), No. 18, 62–68.

[3] M. M. Rana: *Attack resilient wireless sensor networks for smart electric vehicles.* IEEE Sensors Letters *1* (2017), Article Sequence No. 5500204, 1–4.

[4] J. Lin, K. C. Leung, V. O. K. Li: *Optimal scheduling with vehicle-to-grid regulation service.* IEEE Internet of Things Journal *1* (2014), No. 6, 556–569.

[5] L. Yu, T. Jiang, Y. Zou: *Distributed online energy management for data centers and electric vehicles in smart grid.* IEEE Internet of Things Journal *3* (2016), No. 6, 1373–1384.

[6] H. Chu, D. Xie, Y. Lou, Y. Zhang, M. Yang, J. Sun: *Grid-connection control based on information fusion for intelligent integrated power station.* Electric Power Automation Equipment *35* (2015), No. 6, 37–43.

[7] Y. Lin, J. Yang, Lv Z, W. Wie, H. Song: *A self-assessment stereo capture model applicable to the Internet of Things.* Sensors (Basel) *15* (2015), No. 8, 20925–20944.

[8] V. Pande, C. Marlecha, S. Kayte: *A review-fog computing and its role in the Internet of Things.* International Journal of Engineering Research and Application *6* (2016), No. 10, Part No. 4, 7–11.

[9] S. M. R. Islam, D. Kwak, M. H. Kabir, M. Hossain, K. S. Kwak: *The Internet of Things for health care: A comprehensive survey.* IEEE Access *3* (2015), 678–708.

[10] F. Chen, P. Deng, J. Wan, D. Zhang, A. V. Vasilakos, X. Rong: *Data mining for the Internet of Things: Literature review and challenges.* International Journal of Distributed Sensor Networks, Special issue on Big Data and Knowledge Extraction for Cyber-Physical Systems (2015), Article ID No. 431047, Article No. 12, 1–14.

[11] J. Granjal, E. Monteiro, J. S. Silva: *Security for the Internet of Things: A survey of existing protocols and open research issues.* IEEE Communications Surveys & Tutorials *17* (2015), No. 3, 1294–1312.

[12] M. Gorlatova, J. Sarik, G. Grebla, M. Cong, I. Kymissis, G. Zussman: *Movers and shakers: Kinetic energy harvesting for the Internet of Things.* IEEE Journal on Selected Areas in Communications *33* (2015), No. 8, 1624–1639.

[13] M. Ehret: *The zero marginal cost society: The Internet of Things, the collaborative commons, and the eclipse of capitalism.* Journal of Sustainable Mobility *2* (2015), No. 2, 67–70.

[14] M. A. Razzaque, M. Milojevic-Jevric, A. Palade, S. Clarke: *Middleware for Internet of Things: A survey.* IEEE Internet of Things Journal *3* (2016), No. 1, 70–95.

Received August 7, 2017

Acta Technica *62* No. 2B/2017, 273–282

Unmanned aerial vehicle (UAV) intelligent wayfinding system based on inertial navigation technology

Yunjie Qu[1]

Abstract. In the modern war, UAVs play an important role. With the increasing complexity of the war environment, the army's demand for unmanned aerial vehicle systems is getting higher and higher. In this paper, the inertial navigation technology of unmanned aerial vehicle (UAV) and the technical problems of intelligent wayfinding system were studied. According to the algorithm characteristics of inertial navigation path, the ant colony fusion particle algorithm was designed, and the calculation method of inertial guided solution was discussed. Based on the inertial navigation technology, the related algorithms and the simulation of the intelligent navigation system were studied. The verification results show that the intelligent wayfinding system designed in this paper has good reliability.

Key words. Unmanned aerial vehicle (UAV), inertial navigation, intelligent algorithm.

1. Introduction

Compared with manned aircraft, UAVs can save a lot of money in terms of design, manufacturing and training maintenance. UAVs are relatively light and agile in operation, and have strong air combat capability, which can be used for radar attack in the course of reconnaissance operations [1]. Infrared detectors are installed on UAVs to acquire information about each other's operations in the air. In combination with the above performance characteristics, UAVs are irreplaceable in military power. UAVs need to avoid military threats in the air during their actual use. Because they do not have the air-to-air combat strike capability, the enemy's air strike firepower should be predicted in advance [2]. Therefore, unmanned aerial vehicle (UAV) requires intelligent navigation of the flight path for man-machine safety, so as to perform the task efficiently. Scientific UAV path guidance system is the safeguard of UAV's reconnaissance operations. Intelligent flight operations of UAVs can be realized only by using optimizing intelligent algorithms and calculating the optimal flight path in the process of air operation. In order to achieve the

[1]School of Astronautics, Harbin Institute of Technology, Harbin, 150001, China

strategic role of UAVs in the air, it is necessary to have a predetermined optimal flight path reference and combine intelligent precise navigation system to provide precise location information for UAVs [3]. In order to improve the flight reliability of UAVs, the UAV navigation guidance system should be equipped with sensors. Therefore, the requirement for the precision of the UAV intelligent navigation system is higher [4]. More and more researches have been done on the precision promotion of the intelligent navigation and wayfinding system of UAVs, and the problem has become a hot research topic.

2. State of the art

The intelligent wayfinding problem of UAVs also belongs to the optimal path problem, which means that under certain environmental constraints, the UAV navigation system can plan the path algorithm and accomplish the best flight path from the starting flight position to the end point [5]. The path selection and planning of combat UAVs are different from those of conventional trajectory planning problems. The optimal solution for the variability of the three-dimensional space and the complex features of the environment makes the optimal planning process of the flight path more difficult [6]. The UAV flight path planning problem can be divided into the following steps. The simulation system of UAV flight environment should be established. In addition, the optimal route of flight path should be evaluated. In order to ensure the safety performance of flight, a reasonable planning algorithm must be adopted to calculate the safe and efficient flight path [7]. UAV flight path planning algorithm needs a certain evaluation to complete. And it is necessary to predict the flying distance and the threats that may occur in the flight path. In order to verify the superiority of UAV flight path planning method, a certain path evaluation condition and principle should be established.

The UAV mission planning is the main part of the UAV design, which is composed of many modules, and can form comprehensive and detailed functions through different functions and task planning [8]. The initialization function module contains the preset settings for related parameters of the job, the maximum flight angle of the UAV and the corresponding constraints. In the course of flight, in order to avoid radar detection and protect its flight concealment, the flying radar detection blind zone should be set up in the UAV flight guidance system [9]. Although a radar network composed of several radars can narrow the detection blind area, it cannot completely eliminate the blind area. UAVs usually fly close to the ground, and such a flight may experience ups and downs of the terrain. However, in order to satisfy the concealment and flight safety, it is necessary to make such a challenging flight strategy [10]. The navigation system studied in this paper is close to the actual situation, and the environment threat module is established. Finally, the flight environment of UAV in 3D space is effectively fused, and then the real combat flight characteristics of UAVs can be simulated completely.

2.1. Methodology

The navigation control system of unmanned aerial vehicle (UAV) is the main link to realize the scheduled flight target. The requirements for the flight performance of UAVs are relatively high, so that UAVs need to exhibit specific performance for different battlefield environments. In order to realize the intelligent navigation system of UAV, it is necessary to analyze and discuss the navigation control system of unmanned aerial vehicle (UAV). Figure 1 shows a control chart of an UAV navigation and wayfinding system. In order to control the UAV to fly effectively, the control system and navigation system need excellent performance, and each module needs to work cooperatively. In a real combat environment, UAVs need to overcome the interference environment, thus putting forward higher requirements for the intelligent navigation system of UAVs.

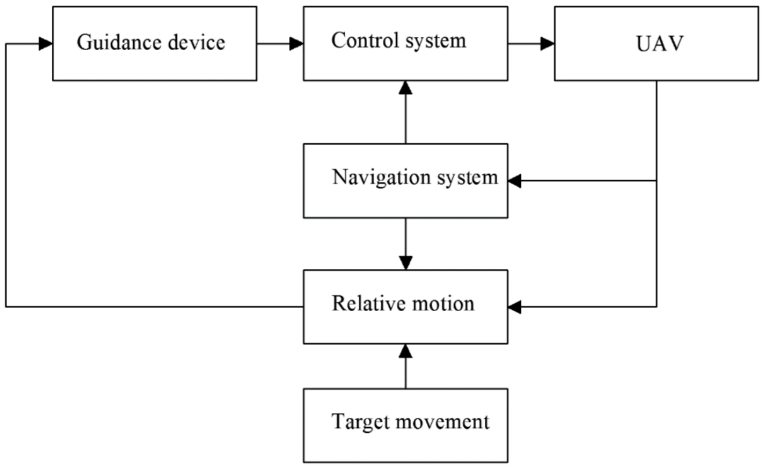

Fig. 1. Control chart of UAV navigation and wayfinding system

The particle swarm optimization (PSO) algorithm for the flight path choice of UAVs is a computational method proposed in the 1990s. The principle of this method is derived from the competition mechanism among microscopic particles, and the optimal solution is selected by competition elimination. In the particle swarm optimization algorithm, firstly, the population of particles should be initialized. The feasible solution of the search space is expressed by random particles in the population, and is endowed with a special fitness function. By random motion, the particle has a regular change of position trajectory, representing the degree of motion fitness of particles. And according to the degree of motion fitness of particles in the trajectory, the optimal solution of particles in motion and in the whole trajectory can be searched. Each movement updates the particle, and eventually the synthetic optimal solution is obtained [11].

It is assumed that the range of motion of the particles in three-dimensional space is represented by D. The total number of particles is represented by m, and the coordinates of the particles in the three-dimensional space are represented by

$x_i,\ i = 1, 2, 3$. The optimal value of the particle motion and the optimal value of the swarm are updated with the coordinates of p_g. The trajectory of particles in three-dimensional space is regular. According to the update speed of the particle's own optimal solution, the updating formula for the optimal solution of particles is established as follows:

$$x_{id}(t+1) + x_{id}(t) + v_{id}(t+1)\,, \tag{1}$$

$$v_{id}^{k+1} = wv_{id}^{k} + crand_1^k(pbest_{id}^k - x_{id}^k) + crand_2^k(gbest_d^k - x_{id}^k)\,. \tag{2}$$

In the formula, v_i denotes the velocity vector, subscript d means that the dimension of the particle has the degree d, superscript k represents the number of iteration, r_1 and r_2 stand for the stochastic constants between [0,1] ω is the adaptive weight factor, c_1 is the self learning factors, including self learning ability, and learning environment factor c_2 regulates the social learning ability. From the above formulae, it can be seen that the particle search results are limited by three levels of factors. The three factors are the particle velocity, particle self learning ability, and other learning ability of particles. The particle motion rate can balance the global search ability of particles, and the self reinforcement ability of particles can avoid the falling into [12] in the process of particle movement.

The design of ant colony algorithm, inspired by ants foraging in groups, belongs to an optimization method for simulating bionics. Through the transformation of several feasible solutions in space, a series of operator transformations and corresponding transformations, finally, the optimal solution can be obtained. Ants release information and receive information from other ants in the course of a random path, which is the information sharing process of ant colony algorithm. The movement of the ant colony will be concentrated with the colony effect of the ant colony, and the ants will move constantly toward a large amount of information [13]. Ant colony algorithm has the mechanism of effective information feedback. The more the selection path, the greater the amount of information will be, and the higher the probability of eventually obtaining the optimal solution will be. The expression of the path selection probability of ant colony algorithm is

$$p_{ij}^k(t) = \frac{[\tau_{ij}(t)]^\alpha [\eta_{ij}]^\beta}{\sum_{j \in U} [\tau_{ij}(t)]^\alpha [\eta_{ij}]^\beta}\,. \tag{3}$$

In the formula, p indicates the movement rate of ants from one point to another, τ_{ij} represents the basic strength of the trajectory, η_{ij} denotes an inducer, and U represents the collection of all trajectories.

Ants may form a concentration gradient in the course of movement. Therefore, in the process of ant movement, the concentration of information at random locations will change, and the formula for calculating the concentration of information is. There holds

$$\tau_{ij}(t+n) = \rho\tau_{ij}(t) + \Delta\tau_{ij}\,, \tag{4}$$

and

$$\Delta\tau_{ij} = \sum_{k=1}^{m} \Delta\tau_{ij}^{k} \,. \tag{5}$$

In the above formulae, $\Delta\tau_{ij}^{k}$ describes the information intensity that ants release at the edges of trajectories and ρ indicates that the retention strength of information may change over time.

By analyzing the characteristics of ant colony algorithm and particle swarm algorithm, it can be found that particle swarm optimization method can achieve relatively strong search results, but it may fall into the loop of search. Ant colony algorithm is not easy to fall into the loop, but the early calculation speed is slow and the latter calculation speed is faster. In this paper, combining the advantages of the two algorithms, the global search feature of particle swarm optimization algorithm was utilized to carry out the global search. Then, the ant colony algorithm is used to calculate the optimal solution.

In order to give full play to the maximum performance of the two algorithms, the computational advantages of the two algorithms should be complementary. The key of calculation is the grasp of the computational time node, which refers to the critical value of particle swarm optimization and ant colony algorithm. The confirmation of the time point of the two algorithms will affect the overall application of the fusion algorithm. Figure 2 shows the convergence rate of the particle swarm optimization method and the ant colony algorithm. As illustrated in Fig. 2, in the practical T range, the convergence of particle swarm optimization method is more obvious, and as time goes on, the rate of convergence is speeding up. Over the T range, the ant colony algorithm is better. Therefore, from the point of view of fusion calculation, the method of particle swarm optimization is adopted within the range of T, and after the time is greater than T, the ant colony algorithm can be adopted.

In this paper, the flight path planning of unmanned aerial vehicle (UAV) in three-dimensional space is analyzed. It is considered that before the plane takes off, according to the existing information, the fusion method of particle swarm algorithm and ant colony algorithm can be used to obtain the optimal path of UAV from the starting position to the termination position. In this paper, the particles are divided into sub layer particles and low dimensional particles according to the flight state of UAVs. When the particle search of the parent layer is completed, the particle is transferred to the sub layer. Finally, the sub layer completes the search process of the parent layer and guides the optimal solution to find the location.

Figure 3 shows the principle frame diagram of an inertial navigation system. As shown in Fig. 3, the gyroscope is used to determine the acceleration of the UAV in the inertial navigation system. After the acceleration is measured, the two are compensated for the error control, and the result is used as the effective input of the four element method. The effective output of the four element method is the attitude matrix. The attitude angle is calculated by inertial navigation system, and after the integral solution, the velocity and position information of the final calculation point can be obtained.

In inertial navigation system, the result of signal measurement based on inertial

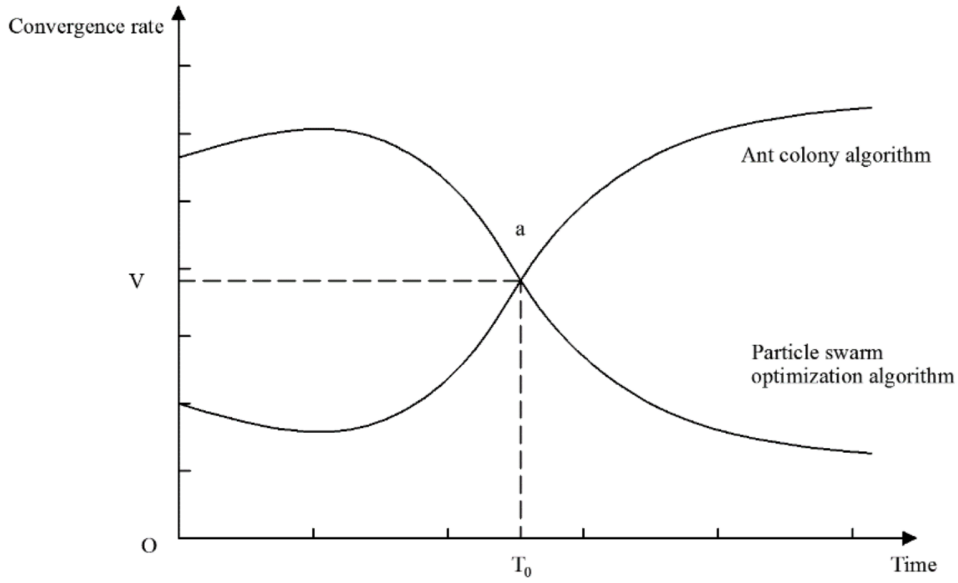

Fig. 2. Convergence rate diagram of particle swarm optimization method and ant colony algorithm

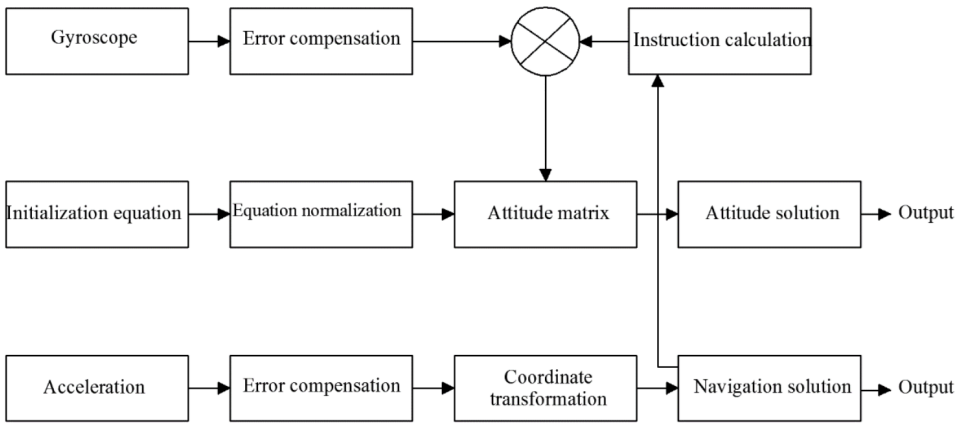

Fig. 3. Principle frame diagram of inertial navigation system

component is the key of attitude angle position information. In a coordinate system of an inertial component, the signal is converted into the data of the navigation coordinate system. There is a certain degree of data association between the navigation coordinate system and the carrier coordinate system. And a relative coordinate system can be established by the angle of flight deviation and the rolling angle of the

UAVs. The four element method is used to solve the inertial navigation algorithm:

$$C_b^n(q) = \begin{bmatrix} C_{11} & C_{12} & C_{13} \\ C_{21} & C_{22} & C_{23} \\ C_{31} & C_{32} & C_{33} \end{bmatrix}. \tag{6}$$

The method for calculating the optimal flight path of unmanned aerial vehicle (UAV) was given. The working mechanism of inertial navigation system was analyzed by combining the particle swarm calculation method and ant colony algorithm, and the algorithm of inertial navigation system's working mechanism was studied. It is necessary to design an intelligent and digital simulation system to simulate the above algorithms and the UAV intelligent wayfinding system. And then in the MTALAB platform, the system calculation method can be verified scientifically, and the structure of the system is shown in Fig. 4. UAV intelligent wayfinding simulation system based on inertial navigation technology is divided into: path calculation module, emulator module, anaphase solution module and data output module.

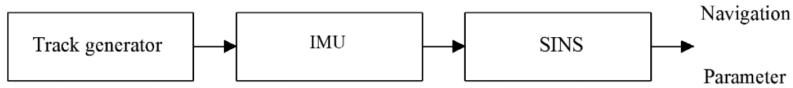

Fig. 4. Composition structure of the system

3. Result analysis and discussion

In order to verify the excellent algorithm performance after the fusion of particle swarm algorithm and ant colony algorithm, in this study, the fusion method and standard ant colony algorithm and standard particle computing method were compared and analyzed. It was assumed that the flying environment of UAVs was a number of overlapping peaks. And the central position of a mountain peak was different. In order to facilitate the simulation, cone structure was used to replace the mountain structure between peaks. The central coordinates between peaks were (22, 67), (23, 19), (44, 54), (44, 26), (54, 78), (74, 26), (76, 68), (82, 44). The starting position of the UAV was (0, 0), and the terminal position was (89, 69). The parameters of each algorithm should be pre-set, and the particle self-learning factor and other self-learning factors were constant 2 in the particle swarm optimization method. The total number of particles was set to 50, the number of iterations was 5500, and the total number of searches was 6 layers. In ant colony computation, the number of ants was 50, and the total number of iterations was 5500. The constant parameter values of the fusion method were consistent with the standard calculation methods, and the iteration times of the two methods were 2900 and 2600 times respectively. According to the operating parameters, the simulation curves obtained in the MATLAB simulation platform are shown in Fig. 5.

It can be seen from the simulation results that the standard particle computing method can't completely solve the problem of unmanned aerial vehicle (UAV) in

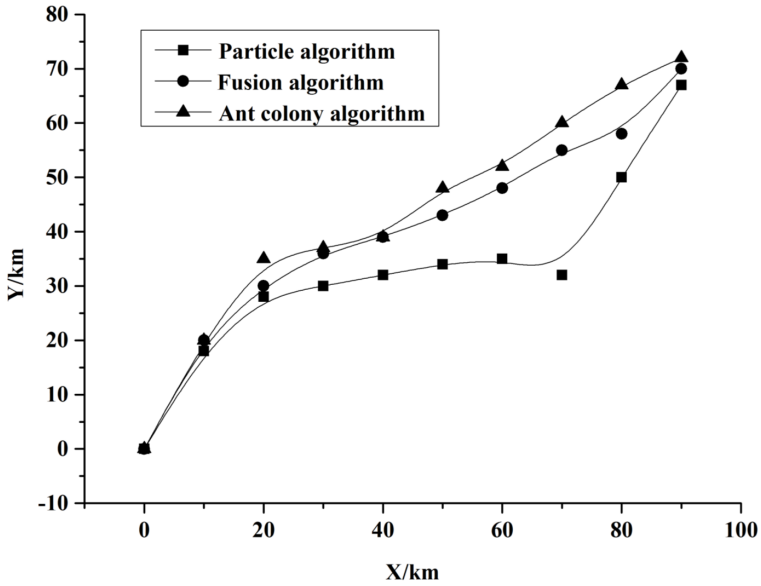

Fig. 5. Simulation curves of different calculation methods

case of emergency danger, and the UAV flight path planning is relatively long, even the route is also relatively tortuous; although the path calculated by the standard ant colony algorithm is relatively smooth, it can also minimize the possibility of an emergency. However, the flight path is still relatively long; while the fusion method allows the planning of the nearest flight path, thus making the use time shortest. The experimental results show that the convergence performance of the global optimization algorithm can be obtained by the fusion method. To sum up, the fusion computing method can obtain a better flight path planning scheme for UAVs.

The flight path of unmanned aerial vehicle (UAV) can be obtained through the UAV flight path simulation calculation. By varying the associated analog parameters, different flight trajectories can be set. And the flight path is generated by UAV trajectory generator, including attitude angle, acceleration and other flight parameter data. The actual output of the simulated gyroscope is completed by the IMU simulation accelerator. And then in the process of actual use, the calculation model of the error is added to the calculation model of gyroscope. Figure 6 is the result of acceleration related information obtained by using the IMU simulator. As can be seen from Fig. 6, the true output of the X axis forms a straight line curve, the output data of the Y axis and the Z axis forms a wave curve; the output data of the X axis and the Y axis of the acceleration line forms straight lines, and the true output of the Z axis is the curve. As can be seen from Fig. 6, the IMU simulation element designed in this research can truly reflect the flight situation of UAVs, and the data of acceleration and gyroscope is closer to the real state of operation. By calculating the drifting characteristics, the two are of great value in actual use.

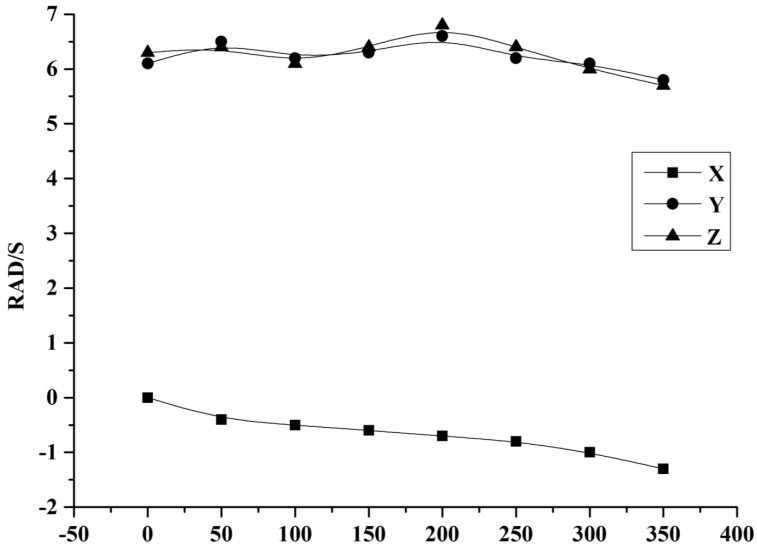

Fig. 6. Results of acceleration related information

4. Conclusion

The flight path of unmanned aerial vehicle (UAV) has always been the focus of research on UAV navigation technology. In this paper, the segmented fusion method of particle algorithm and ant colony algorithm was proposed for UAV trajectory calculation. Subsequently, the simulation of related algorithms was studied. From the theoretical and practical point of view, inertial navigation technology and intelligent wayfinding system were organically combined. Then the characteristics of particle swarm optimization and ant colony algorithm were analyzed. The fusion method proposed can not only complement the disadvantages of the two methods, but also retain the advantages. In addition, in the MATLAB platform environment, the performances of two independent algorithms and fusion algorithms were compared and analyzed. Simulation results show that the fusion method combined with inertial navigation system can perform great performance in UAV navigation design. Due to the limitation of time, the experimental simulation research of UAV's hardware in the loop navigation system has not been completed in this paper. Therefore, in engineering practice, further empirical analysis and discussion are needed.

References

[1] T. Wang, C. Wang, J. Liang, Y. Chen, Y. Zhang: *Vision-aided inertial navigation for small unmanned aerial vehicles in GPS-denied environments.* International Journal of Advanced Robotic Systems *10* (2013), No. 5, 1–12.

[2] K. K. Veremeenko, V. M. Savel'ev: *In-flight alignment of a strapdown inertial nav-*

igation system of an unmanned aerial vehicle. Journal of Computer and Systems Sciences International *52* (2013), No. 1, 106–116.

[3] D. Wang, L. Chen, J. Wu: *Novel in-flight coarse alignment of low-cost strapdown inertial navigation system for unmanned aerial vehicle applications.* Transactions of the Japan Society for Aeronautical and Space Sciences *59* (2016), No. 1, 10–17.

[4] R. Sabatini, S. Ramasamy, A. Gardi, L. R. Salazar: *Low-cost sensors data fusion for small size unmanned aerial vehicles navigation and guidance.* International Journal of Unmanned Systems Engineering *1* (2013), No. 3, 16–47.

[5] Y. Kim, W. Jung, H. Bang: *Visual target tracking and relative navigation for unmanned aerial vehicles in a GPS-denied environment.* International Journal of Aeronautical and Space Sciences *15* (2014), No. 3, 112–121.

[6] M. Ushaq, F. J. Cheng: *Reliable multi-sensor navigation system for an unmanned aerial vehicle realized through integration of SINS with GPS, CNS and doppler radar.* Applied Mechanics and Materials *392* (2013), 312–318.

[7] E. Fresk, G. Nikolakopoulos, T. Gustafsson: *A generalized reduced-complexity inertial navigation system for unmanned aerial vehicles.* IEEE Transactions on Control Systems Technology *25* (2017), No. 1, 192–207.

[8] R. V. Shul'z, P. D. Krel'shtein, I. A. Malina: *The research of inertial navigation system systematic errors at aerial photography from unmanned aerial vehicles.* Kharkiv Polytechnic Institute, Technical Sciences, Scientific Journal "Science Rise" *9* (2015), No. 14, paper 6.

Received August 7, 2017

Acta Technica *62* No. 2B/2017, 283–294

BP neural network based on wolf pack algorithm optimization

Xushan Peng[2], Yongping Li[2], Xiaoming Zhang[2], Shui Wang[2]

Abstract. BP neural network has a good ability to fit nonlinear functions. But the convergence speed of traditional BP algorithm is slow, so that it is difficult to achieve the desired results. Many scholars begin to study the initial weights and thresholds of BP neural networks, so as to strengthen the reliability of BP algorithm by optimizing initial weights and thresholds. In this paper, a BP neural network algorithm based on wolf pack optimization was proposed. Then the initial weights and thresholds were obtained by the wolf optimization algorithm. Finally, a nonlinear function was used, and the reliability of the algorithm was verified. The results show that the BP neural network based on wolf pack algorithm optimization has been greatly improved in terms of prediction accuracy and reliability, and it takes less time to process, which not only improves reliability, but also saves a lot of time.

Key words. Wolf pack algorithm, BP neural network, optimization.

1. Introduction

Traditional BP neural networks often suffer from slow convergence and local minimum. One of the reasons is that the connection weights and thresholds are arbitrarily taken between $< -1, 1 >$ [1]. Particle swarm optimization, genetic algorithm and ant colony algorithm have the function of global search and optimization Therefore, many researchers use these algorithms to study the optimization of initial

[1]This paper is supported by projects:
1) Zhejiang public welfare Technology Application Research Project, Study of chaotic synchronization and information flow in large scale coupled nonlinear systems (2017C35013).
2)Zhejiang Provincial Natural Science Foundation, Research on Multi-order Brillouin Scattering Mode Locked Laser in RoF systems (LQ13F01004).
3)Ningbo science projects, he development of Dendrobium automatic screening grading equipment of machine vision technology (2016C10056).
4)The scientific research project of Ningbo Dahongying University, Research on Frequent Itemsets Mining Based on block transaction data (1320133017).
[2]School of Information Engineering, Ningbo Dahongying University, Ningbo, Zhejiang, China, 315175

weights and thresholds of networks [2]. These algorithms have more or less defects, and the optimization results of genetic algorithms are not accurate [3]. In the wolf pack algorithm, based on individual ability difference, the wolves are divided into leader wolf, detective wolf and fierce wolf. And iterative optimization is performed by three intelligent behaviors. The choice of the leader wolf and the regeneration of population reduce the chances that individuals will fall into local minima. The wolf pack optimization method is a kind of intelligent algorithm which is summarized after an analysis of a large number of hunting behaviors [4]. The algorithm has a good advantage in optimizing the multidimensional parameter matrix of neural networks. At present, there is no wolf pack algorithm to optimize BP neural network in the existing research [5]. Therefore, the wolf pack algorithm and BP neural network are combined together to form an improved BP neural network model, so as to prevent the network from falling into local extremum, and to improve the network performance [6].

2. State of the art

BP neural network has a good ability to fit nonlinear functions, but the traditional BP algorithm is easy to diverge. Many scholars begin to study the initial weights and thresholds of BP neural networks, hoping to strengthen the reliability of BP algorithm by optimizing initial weights and thresholds [7]. Therefore, the improved BP neural network algorithm came into being. A BP neural network algorithm based on wolf pack optimization has been proposed, in which, the initial weights and thresholds can be obtained by the wolf pack optimization algorithm [8]. Artificial neural networks based on wolf pack optimization can also be used for spectrum sensing, and can realize the neural network spectrum sensing with the optimal structure of neural networks [9]. In the algorithm, on the basis of spectrum sensing algorithm including self-organizing neural networks, the training sample generation is described in detail. And after the training of neural network and the training phase of neural network, the weight matrix is further optimized by using the wolf pack optimization method [10]. Recently, a method of handwriting identification of probabilistic neural network (WAPNN) based on wolf pack optimization algorithm has been proposed [11]. The method contains the advantages of probabilistic neural networks (PNN) and wolf pack algorithm (WA), forming WAPNN. By using wolf pack algorithm, the optimal smoothing parameter α of PNN can be obtained, and the structure of probabilistic neural network can be optimized. The application shows that the method of probabilistic neural network based on wolf pack optimization algorithm can greatly improve the reliability of machine identification and save a lot of time, which can provide scientific theory support for further development of handwriting identification, and has certain application value [12]. Aiming at the problem of the extraction accuracy of fault signal frequency components and the accuracy of fault location, the Prony algorithm is used to extract the natural frequency of the fault voltage signal as a sample, and then the wolf pack algorithm is applied to optimize the structure of BP neural network and train it, thus to improve the defects that are easy to generate multiple local minima, enhance the training ef-

ficiency and convergence speed of the network, and make the distance measurement more accurate [13]. The BP neural network based on wolf pack algorithm optimization has been greatly improved in terms of prediction accuracy and reliability, and it takes less time to process, which not only improves reliability, but also saves a lot of time. ERNN is one of the most efficient feedforward neural networks learning algorithms. In the ERNN training process, the gradient descent technique is used, and therefore, there are no problems such as local minima and slow convergence. The new heuristic search algorithm, known as wolf search (WS) based on predatory behavior of wolves, can achieve faster convergence and avoid local minimization by training weights in ERNN [14].

3. Methodology

3.1. Wolf algorithm principle

The wolf pack optimization algorithm is an intelligent algorithm derived from the natural behavior of the wolf race in nature, which has high accuracy and good reliability, and can optimize other algorithms accurately. Based on the behavior of wolf colony hunt, the bottom-up design concept was adopted. As shown in Fig. 1, after a great deal of behavioral analysis, the specific process of information exchange and responsibility allocation among wolf groups is summed up. Thus, the wolf algorithm is defined, and the specific wolf hunting model is shown below. The specific wolf hunting model is shown below [15].

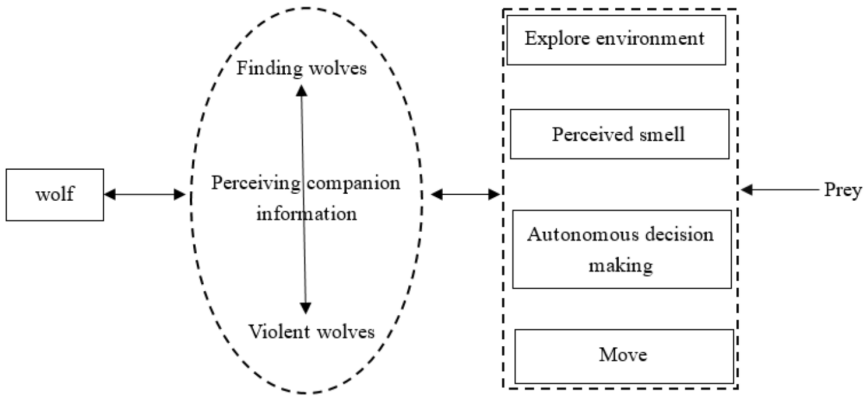

Fig. 1. Wolves hunting model

A resource for wolves to hunt is an $N \times D$ space. Here, N is the number of wolves in a wolf pack, and D is a hunted quantity. The state of an artificial wolf i can be expressed as $X_i = (x_{i1}, x_{i2}, \cdots, x_{id})$, where x_{id} is the position of the ith artificial wolf in the d-dimensional ($d = 1, 2, \cdots, D$) variable space. The concentration of artificial wolf hunting can be perceived as $Y = f(X)$, Y being the expected value. The distance between the wolf p and wolf q is defined the Manhattan distance

between their state vectors $L(p,q) = \sum_{d=1}^{D} |x_{pd} - x_{qd}|$. Other methods may be used to define distance without affecting actual results and research steps.

The specific steps of the wolf algorithm are as follows.

Step 1: Initially, the data is computed to obtain some values. The wolf positions X_i and their number N are initialized in the wolves. The maximum allowable number of iterations is $k_{\max}$, the wolf scale factor is α, the maximum number of trips is $T_{\max}$, the distance determination factor is ω, the step size factor is S, and the update scaling factor is β.

Step 2: As the optimal individual in the group, the position of the leader wolf is extremely important. It is necessary to iterate to determine the relationship between the odor concentration Y_i of detective wolf i and Y_{lead}. Then, Step 3 can be executed.

Step 3: If the odor concentration perceived by fierce wolf $Y_i > Y_{\text{lead}}$, then$Y_{\text{lead}} = Y_i$, and then the convening behavior can be carried out; on the contrary, if $Y_i < Y_{\text{lead}}$, Step 4 cannot be executed until $d_{is} \leq d_{\text{near}}$.

Step 4: With the formula in Step 3 as standard, the location update and execution of group siege are carried out.

Step 5: According to the mechanism of survival of the fittest, the position of the leader wolf should be constantly updated. In this way, the entire wolf pack can be renewed to ensure overall consistency.

Step 6: It is necessary to determine whether the maximum allowable number of iterations has been reached.

The flow chart of the algorithm is depicted in Fig. 2.

3.2. The principle of fitting function of BP neural network

Neural network is a new method to imitate the working mode of human brain. In recent years, many scholars have done a lot of research and simplification on it. The traditional neural network learning experience shows that one layer is good enough. However, recent depth learning denies the claim. Just like every update value of the gradient descent function, every time a sample is updated, the cost function becomes smaller and smaller. Similarly, weights are firstly given with random initial values. Then, the calculations are carried out until the last layer (output layer). If there is an error between the output and the actual value (which is certain in the normal case), then the error back propagation algorithm is used to optimize the value of each layer (the weight value).

(1) Node output model

Hidden node output model:

$$O_j = f(\sum W_{ij} \times X_i - q_j)\,. \tag{1}$$

Output model of output node:

$$Y_k = f(\sum T_{jk} \times O_j - q_k)\,. \tag{2}$$

(2) Interaction function model

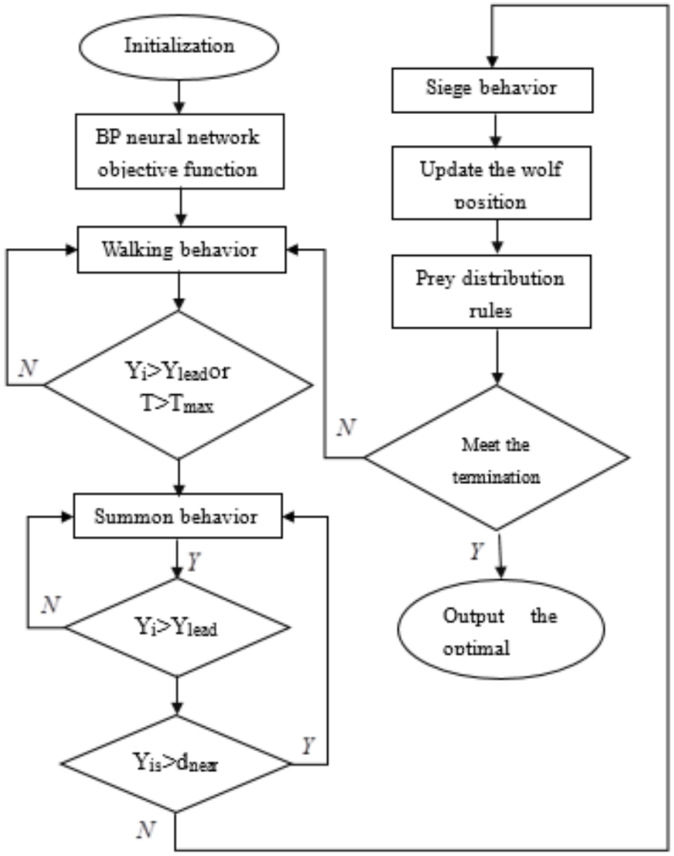

Fig. 2. Flow chart of WPA

The activation function is generally a continuously valued Sigmoid function in (0,1):

$$f(x) = \frac{1}{1 + \mathrm{e}^{-x}}\,. \tag{3}$$

(3) Error calculation model

$$E_p = 1/2 \sum (t_{pi} - O_{pi})^2\,, \tag{4}$$

where t_{pi} is the theoretical output value of the ith node and O_{pi} is the actual result of the ith node.

(4) Self-learning model

The network output error is reduced to an acceptable level (or to the preset number of studies). The error between the output and expected output is obtained through the output layer to adjust the weight of the hidden layer indirectly. Self-

learning model is

$$\Delta W_{ij}(n+1) = h \times \Phi_i \times O_j + a \times \Delta W_{ij}(n)\,. \tag{5}$$

The optimization strategy of BP network model includes:

(1) Optimization of learning factor h

The step size can be adjusted to make the target value the best, and then the number of operations can be reduced and the efficiency of calculation can be improved.

$$h = h + a \times (E_{p(n)} - E_{p(n-1)})/E_{p(n)}\,, \tag{6}$$

where a is the adjustment step size, and its value is 0∼1.

(2) Optimization of node number in hidden layer

The number of hidden nodes has a great influence on the performance of the algorithm, and the empirical formula can be used to determine the number of hidden nodes. In the BP algorithm, the weights and thresholds are adjusted once every training session. Firstly, the weights are assigned with a random initial value, and then the calculation is run until the last layer (output layer). If the output result is in error with the actual value, it is necessary to continue to judge; if there is no error, the discriminant can be terminated. It is difficult to determine the optimal value among the neurons in the actual hidden layer, which is usually determined by trial and error method or optimization algorithm. The number of nodes in the input layer is 3, the number of nodes in the output layer is 1, and the number of nodes in the hidden layer can be within 2–8. The empirical formula of the best hidden node number L is

$$L = (m+n)^{1/2} + c\,. \tag{7}$$

(3) Algorithm optimization

In the BP algorithm, a gradient descent method is used. Weights are firstly given with random initial values. Then, the calculations are carried out until the last layer (output layer). If there is an error between the output and the actual value (which is certain in the normal case), then the error back propagation algorithm is used to overcome the shortcomings.

3.3. BP neural network based on wolf pack algorithm optimization

The basic idea of the BP neural network based on wolf pack algorithm optimization is derived from the natural behavior of the wolf race in nature. The algorithm has high precision and good reliability, and can optimize the BP neural network algorithm accurately. Based on the behavior of wolves during hunting, a bottom-up design concept is adopted. According to the specific process of information exchange and responsibility allocation among wolf groups, an algorithm can be obtained to optimize the BP neural network. In other words, the state of the artificial wolf is used to represent the weights and thresholds of the BP neural network. Then through the process of information exchange and responsibility allocation among wolf groups, the best weights and thresholds can be found as initial values. After screening the

initial values in the above steps, the BP neural network can be trained to achieve the prediction effect. Because its initial value is derived from the wolf pack optimization algorithm, instead of artificial substitution according to experience, this method is more accurate and rigorous compared with the traditional prediction model. After the Wolf algorithm optimization, training was carried out. Under the same conditions, the BP neural network based on wolf pack algorithm optimization has been greatly improved in terms of prediction accuracy and reliability, and it takes less time to process, which not only improves reliability, but also saves a lot of time. Thus, this method is rigorous in theory and is clear in logic, and is suitable for theoretical research and practical application in engineering. The main steps of the algorithm are as follows:

(1) Initialization parameter, including the number of individual wolves, the maximum number of iterations, the wolf scale factor, the maximum number of trips, the distance determination factor, the step factor, and the update scaling factor.

(2) Determination of odor concentration function. This method can obtain two values at the same time, one is the expected value, and the other is the predictive value. The size of the two is generally unequal, and the odor concentration function is the sum of the absolute error between the expected value and the predicted value. Formula (8) shows the concrete operations.

$$F = \sum_{i=1}^{n} |y_i - o_i| \ . \tag{8}$$

(3) Detective wolf's wandering behavior. As the optimal individual in the group, the position of the leader wolf is extremely important. It is necessary to iterate to determine the relationship between the odor concentration Y_i of detective wolf i and Y_{lead}. Then, steps can be executed.

$$x_{id}^{p} = x_{id} + \sin(2\pi p/h)\text{step}_a^d \tag{9}$$

In the formula, step_a is the wandering length.

(4) Fierce wolf approaches prey by formula (9), if $Y_i > Y_{\text{lead}}$, and then $Y_{\text{lead}} = Y_i$, and the fierce wolf can replace the leader wolf; if $Y_i < Y_{\text{lead}}$, then fierce wolf continues to approach the prey until $d_{is} \leq d_{\text{near}}$. The distance between individual wolves a and b is defined as Manhattan, and the distance is $L(a,b) = \sum_{d=1}^{D} |x_{ad} - x_{bd}|\, d_{\text{new}} = \frac{1}{D_{gw}} \sum_{d=1}^{D} |\max_d - \min_d|$. The range of variable d to be optimized is $[\min_d, \max_d]$. The value step_b is the step size of fierce wolf approximating leader wolf.

$$x_{id}^{k+1} = x_{id}^{k} + \text{step}_b^d g(g_d^k - x_{id}^k) / \left|g_d^k - x_{id}^k\right| \ . \tag{10}$$

(5) Using the above formula, the status of the besieged individual wolf is updated:

$$x_{id}^{k+1} = x_{id}^{k} + \lambda g \text{step}_b^d g \left|G_d^k - x_{id}^k\right| \ . \tag{11}$$

In the formula, λ is the random number between <-1, 1>, and step_c is the siege step of the ith wolf.

(6) According to the mechanism of survival of the fittest, the position of the leader wolf should be constantly updated. In this way, the entire wolf pack can be renewed to ensure overall consistency.

(7) The state of the artificial wolf is used to represent the weights and thresholds of the BP neural network. Then through the process of information exchange and responsibility allocation among wolf groups, the best weights and thresholds can be found as initial values. After screening the initial value.s in the above steps, the BP neural network is trained to achieve the prediction effect.

The flow chart of the above algorithm is depicted in Fig. 3

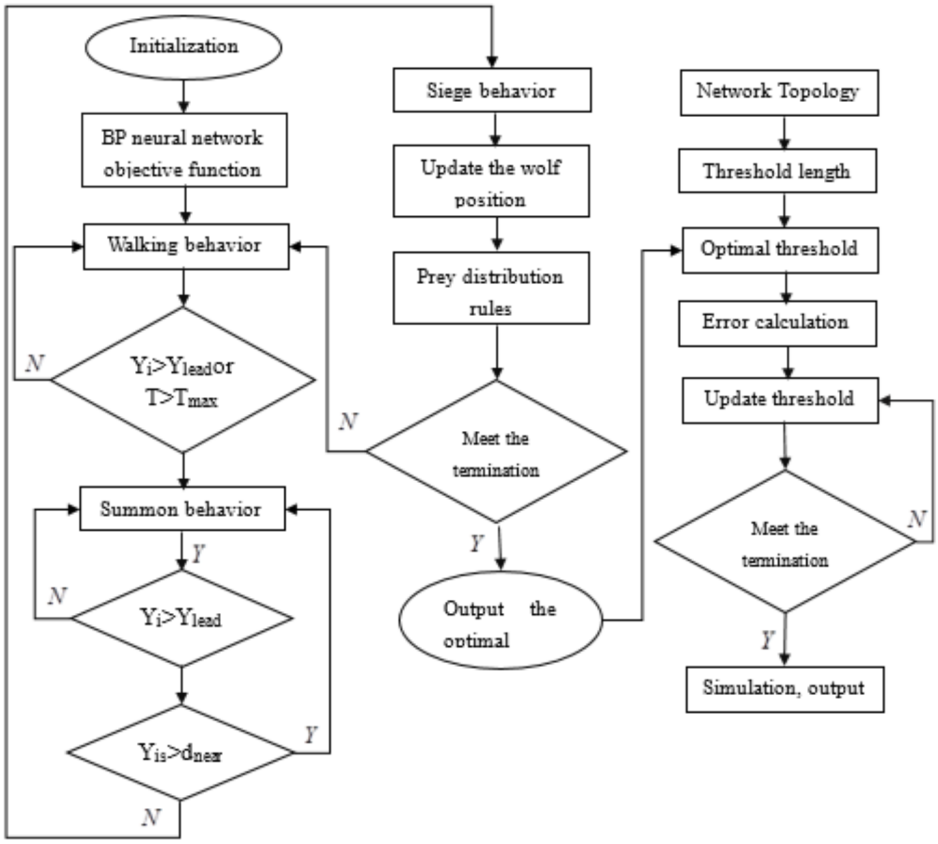

Fig. 3. Flow chart of algorithm

4. Result analysis and discussion

MATLAB software was used to carry out simulation experiments. MATLAB is the very powerful data processing software, which has a huge advantage in matrix computing, also known as the matrix laboratory. Thus, using MATLAB to solve

such problems is a good method. MATLAB software is used to write the m file of these algorithms and then carry out nested calls. First of all, the state of the artificial wolf is used to represent the weights and thresholds of the BP neural network. Then through the process of information exchange and responsibility allocation among wolf groups, the best weights and thresholds can be found as initial values. After that, the initial weights and thresholds are optimized to enhance the reliability of the BP algorithm. After screening the initial values in the above steps, the BP neural network is trained to achieve the prediction effect.

The above algorithms were written in MATLAB2012b by using MATLAB language. MATLAB2012b is a classic MATLAB software series, which can carry out simulation, numerical analysis, and graphics processing at the same time. To verify the effectiveness of the BP neural network model based on wolf pack algorithm optimization (WPABP model) in fitting function, the BP neural network (BP model) without optimization and the BP neural network (GABP model) based on genetic algorithm optimization were compared in terms of the accuracy of function fitting. The following figure shows comparison results. The fitting error comparison is depicted in Fig. 4.

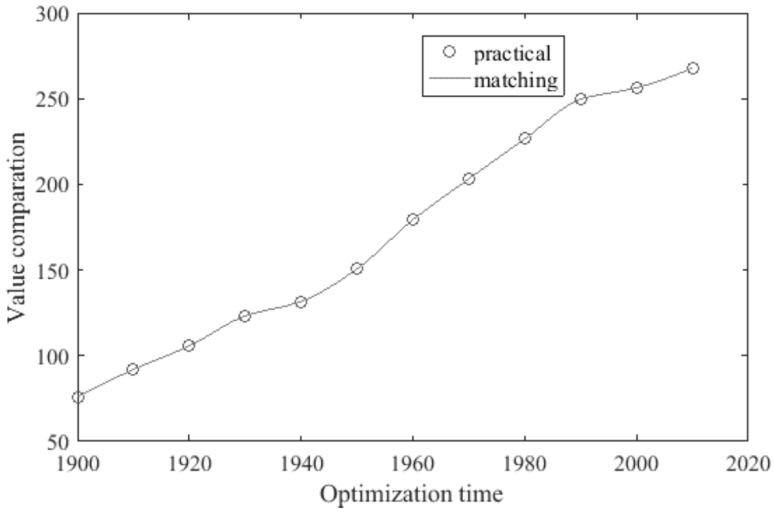

Fig. 4. Fitting error comparison

As can be seen from the diagram above, the predicted result fluctuates from top to bottom near the expected value, and as the number of runs increases, the error becomes bigger and bigger. This result is in line with the actual situation. In most cases, as the number of runs increases, the computational burden of the computer increases greatly, and a variety of problems such as storage space become prominent, thus affecting the accuracy of the results to a certain extent. The results are shown in Table 1.

Table 1. Results comparison

	Correct rate	Test probability	Time
Before optimization	0.8808	0.9903	7.7524
After optimization	0.9126	0.9966	7.6509

As can be seen from the table, after the Wolf algorithm was optimized, and then the training was carried out. Under the same conditions, the results of comparison were: in the case of no wolf algorithm optimization, the accuracy of the prediction was 0.8808, and the training reliability was 0.9903, and the time required from the start of the operation to the completion of the forecast was 7.7524 s; while in the case of wolf algorithm optimization, the accuracy of the prediction was 0.9126, and the training reliability was 0.9966, and the time required from the start of the operation to the completion of the forecast was 7.6509 s. According to these specific data, it can be found that the BP neural network based on wolf pack algorithm optimization has been greatly improved in terms of prediction accuracy and reliability, and it takes less time to process, which not only improves reliability, but also saves a lot of time.

5. Conclusion

In this paper, a BP neural network based on wolf pack algorithm optimization was proposed. The initial weights and thresholds were obtained by the wolf pack optimization algorithm. Finally, a nonlinear function was used to perform simulation experiments on MATLAB software, and then the reliability of the algorithm was verified. Under the same conditions, the results of comparison were: in the case of no wolf algorithm optimization, the accuracy of the prediction was 0.8808, and the training reliability was 0.9903, and the time required from the start of the operation to the completion of the forecast was 7.7524 s; while in the case of wolf algorithm optimization, the accuracy of the prediction was 0.9126, and the training reliability was 0.9966, and the time required from the start of the operation to the completion of the forecast was 7.6509 s. According to these specific data, it can be found that the BP neural network based on wolf pack algorithm optimization has been greatly improved in terms of prediction accuracy and reliability, and it takes less time to process, which not only improves reliability, but also saves a lot of time.

References

[1] R. Wang, N. Wang: *Research on BP neural network optimization based on ant colony algorithm.* Applied Mechanics and Materials *513–517* (2014), 1819–1821.

[2] H. Y. Li, X. X. Wu, T. Wang, D. Zhao: *A simulation and prediction method of the height of wheat based on BP neural networks and the ant colony algorithm.* Advanced Materials Research *659* (2013), 113–117.

[3] Q. D. Zhao, Y. Yu, M. M. Jia: *Applied-information technology in short-term wind*

speed forecast model for wind farms based on ant colony optimization and BP neural network. Applied Mechanics and Materials *662* (2014), 259–262.

[4] E. Emary, H. M. Zawbaa, C. Grosan: *Experienced Gray Wolf optimization trough reinforcement learning and neural networks*. IEEE Transactions on Neural Networks and Learning Systems *PP* (2017), No. 99, 1–14.

[5] W. Jia, D. Zhao, T. Shen, S. Ding, Y. Zhao. C. HU: *An optimized classification algorithm by BP neural network based on PLS and HCA*. Applied Intelligence *43* (2015), No. 1, 176–191.

[6] G. Sun, T. Chen, Z. Wei, Y. Sun, H. Zhan, S. Chen: *A carbon price forecasting model based on variational mode decomposition and spiking neural networks*. Energies *9* (2016), No. 1, paper 54.

[7] W. Jia, D. Zhao, Y. Tang, C. Hu, Y. Zhao: *An optimized classification algorithm by neural network ensemble based on PLS and OLS*. Mathematical Problems in Engineering (2014), Article ID No. 395263, 1–8.

[8] K. Zhang, F. Yuan, J. Guo, G. Wang: *A novel neural network approach to transformer fault diagnosis based on momentum-embedded BP neural network optimized by genetic algorithm and fuzzy c-means*. Arabian Journal for Science and Engineering *41* (2015), No. 9, 3451–3461.

[9] M. Diao, R. Qian, H. Gao: *Spectrum sensing algorithm based on neural network with wolf pack optimization*. Computer Engineering and Applications *52* (2016), No. 19, 107–110.

[10] M. Madhiarasan, S. N. Deepa: *Long-term wind speed forecasting using spiking neural network optimized by improved modified grey wolf optimization algorithm*. International Journal of Advanced Research *4* (2016), No. 7, 356–368.

[11] D. Wang, H. Luo, O. Grunder, Y. Lin, H. Guo: *Multi-step ahead electricity price forecasting using a hybrid model based on two-layer decomposition technique and BP neural network optimized by firefly algorithm*. Applied Mechanics and Materials *190* (2017), 390–407.

[12] S. Amirsadri, S. J. Mousavirad, H. Ebrahimpour-Komleh: *A Levy flight-based grey wolf optimizer combined with back-propagation algorithm for neural network training*. Neural Computing and Applications (2017), Nos. 3–4, 1–14.

[13] W. Han, X. Shen, E. Hou, J. Xu: *Precision time synchronization control method for smart grid based on wolf colony algorithm*. International Journal of Electrical Power & Energy Systems *78* (2016), 816–822.

[14] Y. Yang, G. Wang, Y. Yang: *Parameters optimization of polygonal fuzzy neural networks based on GA-BP hybrid algorithm*. International Journal of Machine Learning and Cybernetics *5* (2014), No. 5, 815–822.

[15] S. Lahmiri: *Comparing variational and empirical mode decomposition in forecasting day-ahead energy prices*. IEEE Systems Journal *PP* (2015), No. 99, 1–4.

Received August 7, 2017

Acta Technica *62* No. 2B/2017, 295–306

Spatial data integration of 3D GIS and visualization technology

Yiping Tian[1], Peng Chen[1], Junhao Yang[1]

Abstract. GIS technology is more and more widely used in production and life, but the study and apply of 3D GIS are urgent because the traditional two-dimensional model is difficult to meet the needs of people. The application facing the geometric field was combined with the discrete fitting idea, the spatial database was converted through AutoCAD graphical data, the automatic modeling was achieved by the hierarchical representation strategy and discrete algorithm, finally, the OpenGL was used to exaggerate the visualization of 3D models. In order to verify the feasibility and reliability of the technology, the drilling data information of geological exploration and production exploration in a mine was selected for analog simulation, therefore, the 3D model that can slit, browse and roam, and can be applied in specific engineering practice was successfully constructed.

Key words. 3D GIS, spatial data, visualization, geology.

1. Introduction

In the information age, the demand for information is increasing, and the requirements for its accuracy and real-time are higher. In this social situation, geographic information system (referred to as GIS) comes into being, and it is applied to production and life [1]. GIS can carry on the storage and processing of the spatial location information of the research object, which makes the GIS more widely used and have more functions. With the extension of the application of GIS technology, it has developed into a new science which integrates information science, surveying and mapping remote sensing, environmental science, computer science, management science and so on [2]. Western developed countries have already started the research and application of GIS technology. According to statistics, they have doubled their investment in the GIS system every two or three years [3]. However, the research in GIS in China started late. Although it has developed rapidly and achieved some results, the related technologies are not still mature enough to be popularized widely [4]. The results of existing GIS research are more focused on the description of

[1]School of Computer, China University of Geosciences, Wuhan City, Hubei Province, 430074, China

two-dimensional spatial information, so it is difficult to give people the most original feelings of nature [5]. In this case, three-dimensional GIS technology needs to be used to truly show the three-dimensional spatial information for building the information system which integrates the collection, analysis, management and reproduction of information data. The research aims at the analysis of 3D GIS spatial data integration and visualization technology for geological applications, which has certain research value for the development of 3D GIS technology in our country.

2. State of the art

The earliest research of GIS originated in the 80s of last century, and more and more scholars began to study the three-dimensional GIS with the deepening of research and the promotion of application of GIS [6]. In the initial study, the three-dimensional GIS system is used mainly in the special applications of geology and mining and other similar areas, and the spatial analysis is realized by constructing a gridded data model, in this case, the functions of GIS are relatively single [7]. Thus, the initial three-dimensional GIS system can only perform simple spatial analysis, the three-dimensional GIS system has considerable technological progress in spatial analysis ability with the in-depth study of people, but it is still not put into practical engineering applications [8]. With the development of computer technology, the three-dimensional query and display functions of 3D GIS system are unable to meet the needs of people, many analog systems begin to combine traditional GIS technology with 3D visualization technology, so as to realize the access and visualization of mass data on the basis of database [9]. In recent years, with the development of network technology, GIS research has begun to develop towards the Internet network, formed a Web-GIS on the basis of the Internet, and published spatial data on Web, so as to provide users with relevant analysis, query and browse functions of spatial data [10]. At present, many commercial GIS systems are added with 3D GIS modules, and terrain analysis and real-time three-dimensional flight browsing are implemented by using three-dimensional terrain data related to data sets of remote sensing image [11]. However, the focus of these 3D GIS systems is the analysis of topography with two-dimensional surface, and the two-dimensional data which is displayed in the three-dimensional environment cannot really be called the three-dimensional GIS system. [12]. However, it is necessary to carry out research on modern 3D GIS technology based on visualization technology as the demand for 3D GIS system is getting higher and higher. The combination of GIS and visualization technology can greatly enhance the realism and the operability of GIS graphics

2.1. Methodology

2.2. Construction of three-dimensional hierarchical model

In order to construct a 3D entity that can be applied to the geological field, it is necessary to combine the idea of discrete fitting; the automatic construction of the model is realized by using the hierarchical representation strategy and discrete

algorithm of the 3D GIS model. The amount of data that 3D GIS needs to process is enormous, the real-time spatial analysis and operation are required, which make the visualization of 3D GIS model more difficult. Based on the existing research, the idea of combining discrete approximation was put forward in this study, the automatic construction of the model was realized by using the hierarchical representation strategy and discrete algorithm of the GIS model, and the OpenGL technology was used to exaggerate the visualization of the 3D model. The specific principle is shown as shown in Fig. 1.

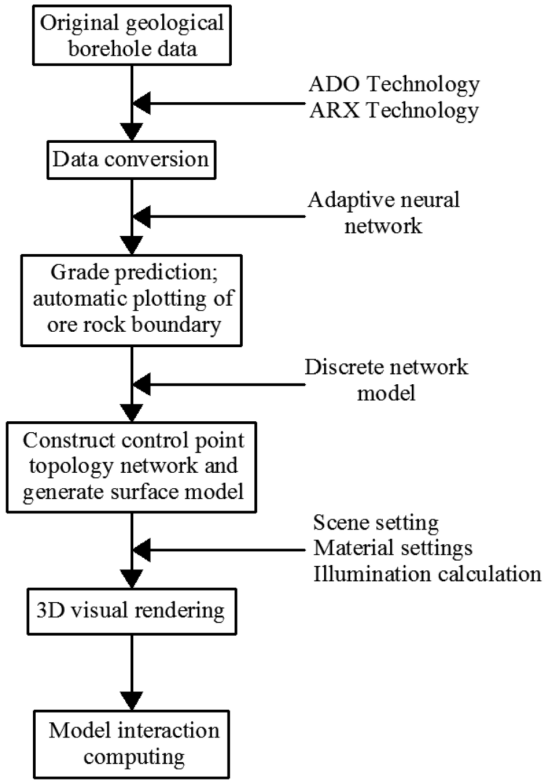

Fig. 1. Construction principle of 3D model

After the data of the original geological borehole was given, ARX and ADO technology was used to conversion of storage format in CAD graphics and GIS spatial database, the information region in the position of transverse section was predicted by an adaptive neural network, and the boundaries of ore and rock according to the grade threshold of the boundary were determined. The 3D surface model could be generated after constructing the topological relation between the control points in the data hierarchy, finally, the OpenGL technology was used to exaggerate the visualization of the model. This method can effectively reduce the influence of human factors on model construction, so the model constructed can reflect the original

spatial structure characteristics of geological bodies more truly; the whole modeling process can achieve higher automation and avoid excessive interaction, which greatly improves the efficiency of modeling.

2.3. Conversion between CAD graphics data and GIS spatial database

According to the habit of existing engineering practice, almost all of the data is stored in the CAD graphics format either in the process of geological exploration or in the production design. Building 3D model of geological body requires the storage in the form of spatial database Therefore, in order to facilitate the operation and improve the applicability, the realization of the conversion between CAD graphics data and GIS spatial database was put forward based on ARX, MFC and spatial database technology. Not only can the transformation of specific CAD primitives be made, but also batch conversions can be made, so as to provide a perfect spatial database support for the construction of 3D model. AutoCAD is a computer aided software developed by American companies, and provides three embedded programming languages: ARX, ADS, and AutoLISP. The call relationship between them and AutoCAD is shown in Fig. 2.

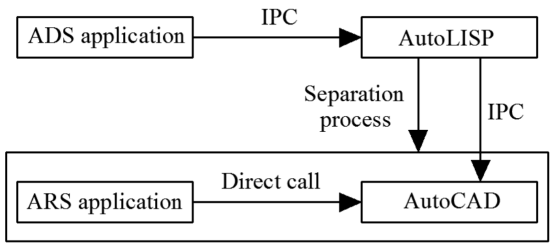

Fig. 2. Call relationships for ARX, ADS, AutoLISP, and AutoCAD

The graphical data file in CAD was defined as an object of AcDbDatabase class and organized in a hierarchical structure, as shown in Fig. 3. Each hierarchy object has two relations synchronously: including and being contained; the root of its collection is the object of graphic database.

The technology combined with ARX, MFC and database was used to realize the conversion of graphic database to spatial database, so that a 3D model was successfully constructed. The first step is that ARX extracts the attribute information of the basic entities in the CAD graphics file, and then the attribute information of the graph area is written into the spatial database by using the object-oriented database programming interface (ADO), so that the data can be converted smoothly. In addition, the attribute data can be obtained from the spatial database, and then drawn and displayed by ARX technology, so the reverse conversion of the spatial database can be realized.

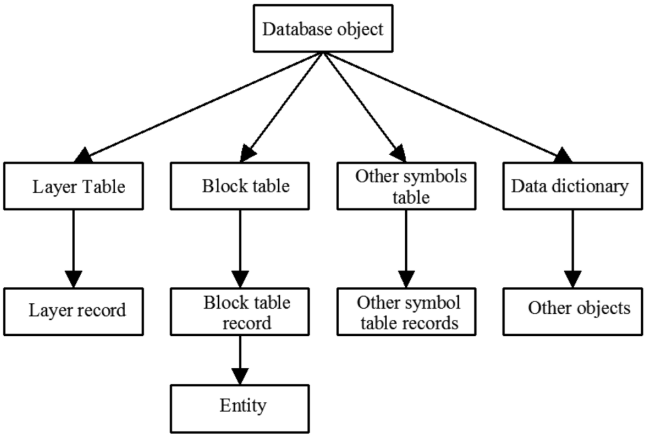

Fig. 3. The graphical data structure of AutoCAD

2.4. Three-dimensional hierarchical model and visualization

The construction of a hierarchical indexing mechanism is to facilitate the localization of spatial objects, so as to achieve various retrieval operations. Different entities are made up of different layers or sections, the layers contained in each entity can be maintained with the corresponding ID current table, and the spatial semantics is used to illustrate the binding attribute of the entity. In the same entity, different layers may also be composed of one or more closed polygons. The vectors of the control points are connected together by turns and form polygons, the linear table of the control point is stored in the three-dimensional data point of the underlying operation, and each control point is treated as an object with 3D data attribute. Based on hierarchical indexing mechanism, localization of spatial target and retrieval operations can be implemented more succinctly, and the operation is more convenient for computer programming. The hierarchical indexing mechanism is shown in Fig. 4

In order to construct a 3D model successfully, the key point is to establish the topological relation between the control points correctly, which determines the adjacency relation between the discretized surface triangles. When the topological relation is properly established correctly, the distortion of surface of the model can be reduced to a great extent, and the geometric features of the surface of the 3D model can be reflected more really. In traditional methods, the method which is made in advance is often adopted; the data structure of this method is relatively complex and has more work, so it is difficult to make dynamic changes after the creation of a three-dimensional model. Therefore, the neural network model was used for reference and a discrete network model was proposed to dynamically construct the control point of the topology network. The geometric and attribute information of the surface of the model are affected by the discrete topological relation of the triangle plane, however, the surface model cannot really reflect the spatial structure

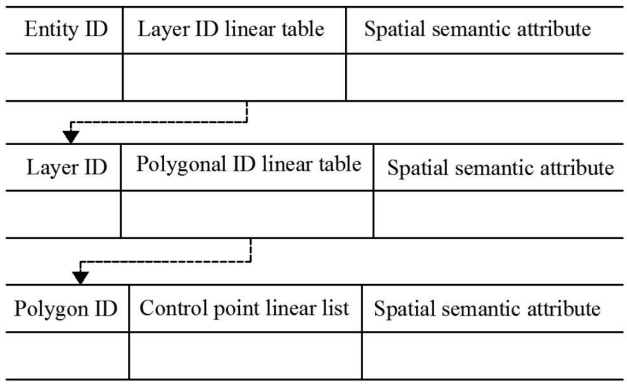

Fig. 4. Hierarchical indexing mechanism

relationship of the model, so it is necessary to exaggerate its visualization, specific steps are included: settings for model scene variables, settings for color and environment variables, and material properties; calculation of light conditions, and the use of chained library OpenGL of open graphics to realize visual operation.

2.5. Dynamic interaction and algorithm of 3D hierarchical model

In the process of specific application of GIS, engineering designers should carry out the dynamic interaction in real time. The model system not only can change from many angles, arbitrarily cut and observe its internal structure at random, but also realize the display of features of spatial structure from all directions.

In computer graphics, the introduction of homogeneous coordinate representation can be more convenient for the description of various algorithms of graphic transformation. After the use of homogeneous coordinates, two-dimensional, three-dimensional, or even three-dimensional high dimensional space graphics can successfully achieve the easy and efficient transformation from one coordinate system to another coordinate system; in addition, the homogeneous coordinate system can be used to represent infinite points, and even make them transformed into finite distant points by using perspective changes.

In the production design in the geological field, the model should be able to cut so that the internal structure of the model can be observed and thus the engineering drawings can be generated, which is of great significance to the whole field of geology. The new cutting algorithm which combined the characteristics of 3D GIS hierarchical data model was proposed, based on the principle of optimized search, the triangles with small plane intersected with the cut section were searched according to the data structure of hierarchical model. The schematic diagram of cutting is shown in Fig. 5

In Fig. 5, the vertical plane perpendicular to the surface of the paper is a straight line AB, the entry edge and the exit edge are defined as l_1, l_2, respectively, the former is formed by intersecting the section and the triangular sides of surface of entity, one

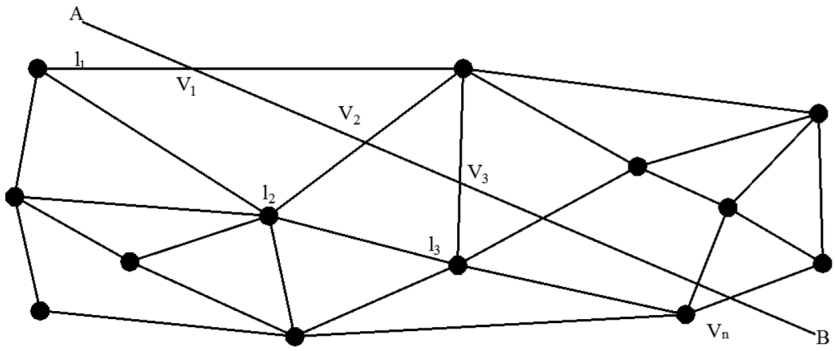

Fig. 5. Sketch map of model cutting algorithm

of the other two sides of a triangle is l_2. Symbol Q denotes a triangle with a single edge, and the exit edge is changed into the exit edge according to the topological relation between discrete triangle planes, the first step of the cut algorithm is to set the state variable, followed by the search the first edge intersecting the tangent plane. On the basis of the two endpoints on the entry edge, the small triangles intersecting the cut plane were searched, of which the edge that intersected the cut plane was the exit edge, and intersection point was preserved after calculation. Three-dimensional dissection can provide a virtual platform for engineering designers to observe the geological structure from a wide range, so that they can propose a more reasonable engineering design.

3. Result analysis and discussion

The related data was simulated based on the related techniques of 3D GIS spatial data sets and visualization, the data used in this paper was the spatial data and related attribute data of primary geological exploration and production exploration drilling of a mine in China. The mine has been running for 8 years since 2008. Therefore, the geological data obtained during the production process is relatively perfect, there are also data provided by geological exploration boreholes in the areas without construction. These figures contain the spatial coordinates and grade attribute information of the corresponding sampling section. The platform used in the experiment was Windows2003, Server, OpenGL1.3 and MapInfo, and its hardware was configured as 512DDR memory, 2.4 GHz CPU, 128 M NVIDIA graphics card.

First of all, the graphic data in CAD was transformed into the storage format of extended SQL Server2003 by using the transition mechanism between CAD graphics data and GIS spatial database. Secondly, the adaptive neural network prediction was used to automatically generate the boundaries of ore and rock in each section so as to form a three-dimensional profile of geology. Figure 6 shows the two-dimensional section of the 3D cut and its sectional correspondence. After the conversion of data, the two-dimensional data was converted into a spatial database that can be used.

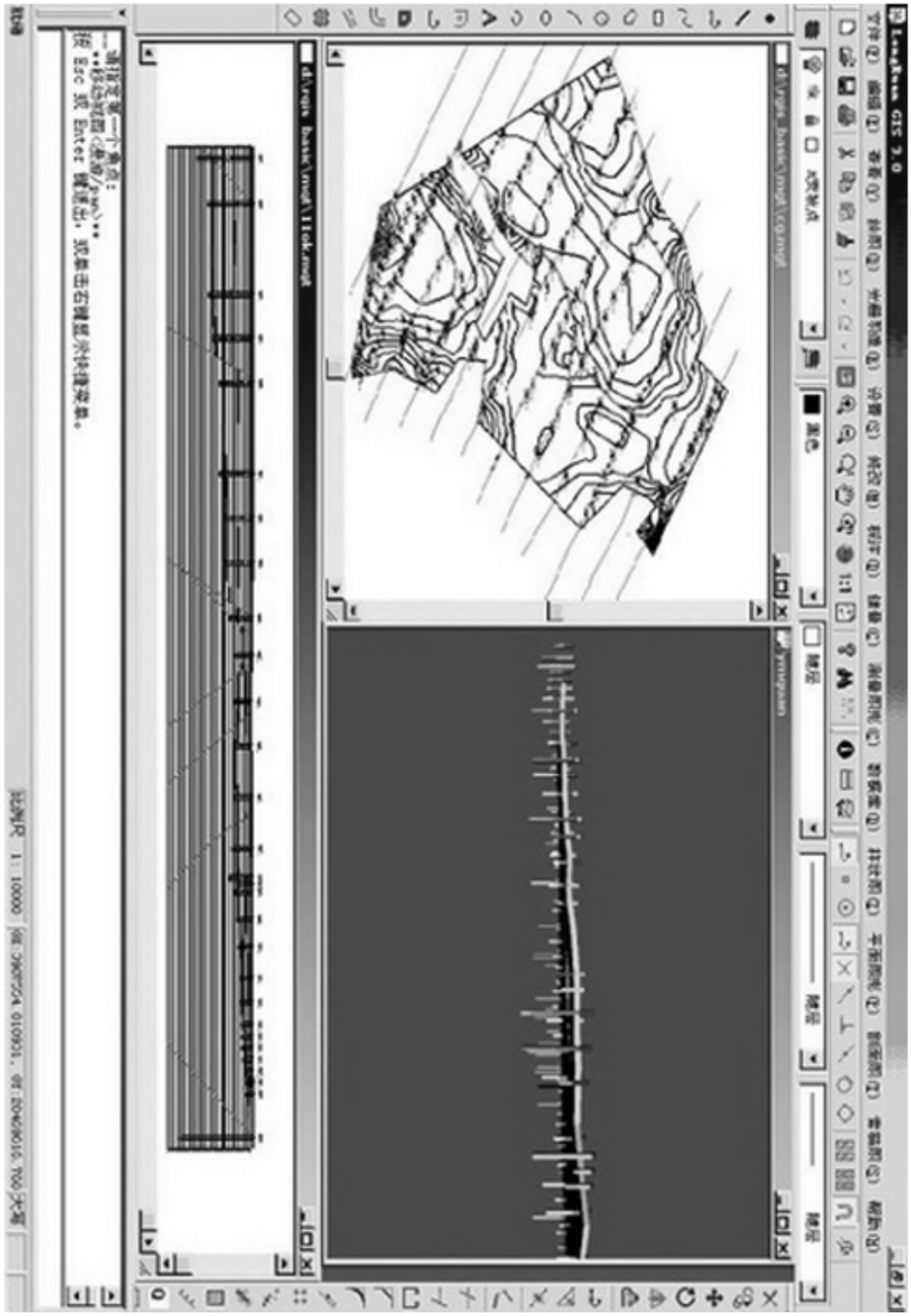

Fig. 6. Three-dimensional dissection forms two dimensional sections and its plane section correspondence

In the formed section, each section is composed of one or more closed polygons which do not intersect each other, and different colors represent different geological bodies. As long as the data is complete, the topological relation between the inner control points of adjacent cross sections can be successfully established. The topological relation was constructed by the discrete network model, and the topological relation of the control points in other adjacent sections was established according to analogy, and then the wireframe model of geological body was constructed. Finally, OpenGL was used for visual rendering, and the wireframe model composed of topological relation was transformed into surface model. After loading all kinds of attribute data, the normal vector of triangle plane was calculated respectively; and under the condition of illumination, different material was represented by different colors, and a 3D solid model of geological body was generated.

The tools provided in the system can scale, rotate, and translate and so on, so that the model can be cut arbitrarily. After the additional clipping planes were set, the rest of the work was done automatically by the system. Figure 7 shows the typical cut of a model, it is very clear to observe the construction of concrete structure through the three-dimensional dissection results. Two dimensional mapping of the model's cutting results was carried out to obtain the geological section of the two-dimensional coordinate plane. In addition, the system can meet the needs of different statistical analysis and production.

After the 3D visualization model of the mine was built, the 3D visualization and roaming of the corresponding area were carried out. Figure 8 shows a three-dimensional view of the mine floor.

From the point of comprehensive analysis, the system can not only realize geological, equipment, plant, terrain and other 3D models building based on GIS spatial data set and visualization technology, but also realize the panorama and browsing of the whole picture from the ground surface to the ground floor. Three-dimensional visual editing platform with relatively perfect function can be used to realize data editing, coating management, automatic modeling, import and export and other functions, and implement and the import and export of 3DMax; in addition, the association between 3D virtual scene and integrated automatic data, the inquiry, modification and input of data of relevant equipment, as well as the real-time monitoring in the process of operation can be realized.

4. Conclusion

Based on the three-dimensional spatial data model of GIS, the presentation of geological structure from all aspects can be realized, and many limitations and shortcomings of the traditional two-dimensional GIS plane can be effectively solved. Based on ARX, MFC and spatial database technology, the conversion of CAD graphics data and GIS spatial database was realized, and the visual rendering operations of the model were carried out by OpenGL. This method can realize the conversion of AutoCAD graphics data better, overcome the influence of human factors in the process of model building, and automatically generate any section map. The actual data of a mine in China was exploited in the analog simulation. It can be seen

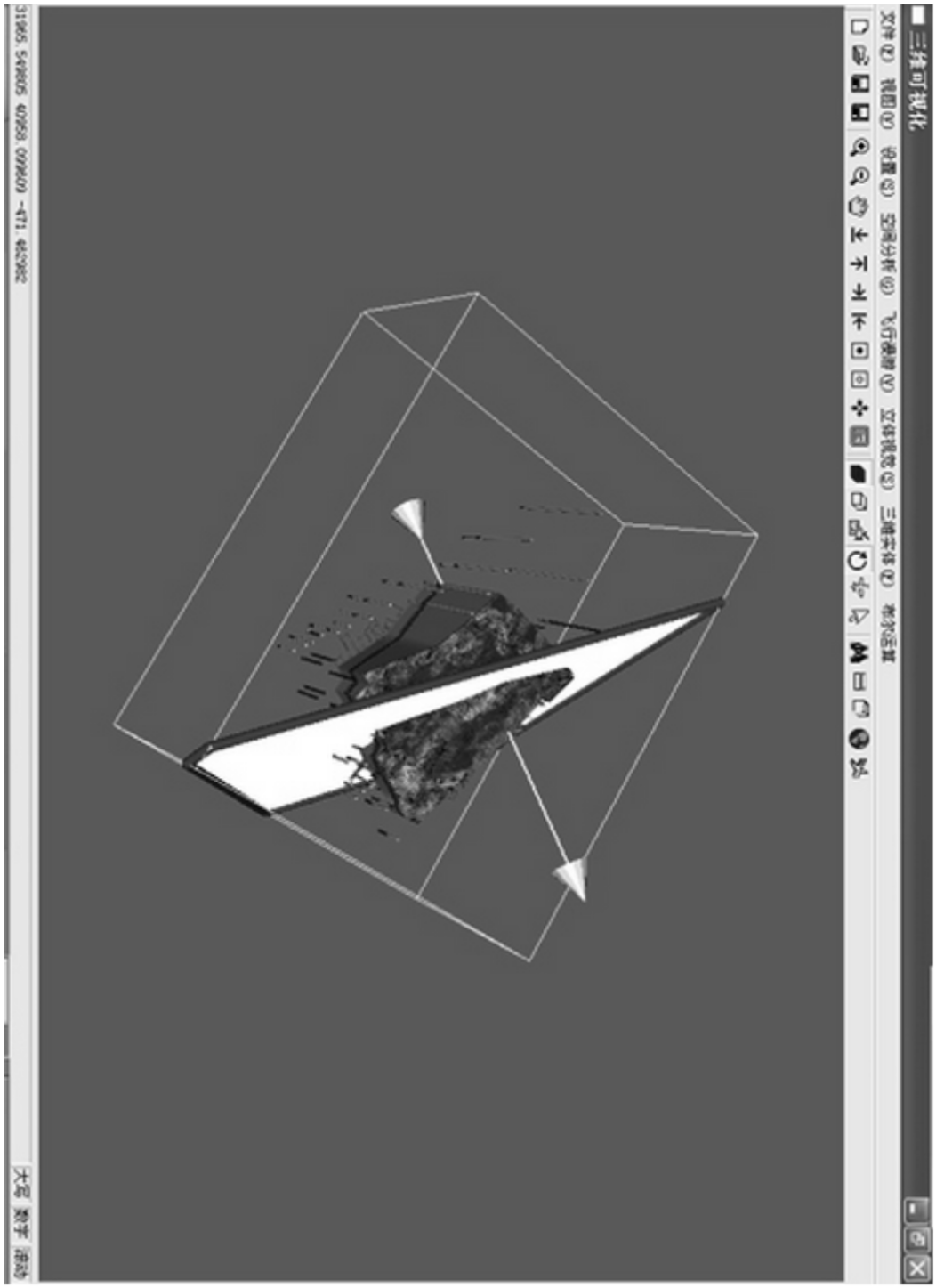

Fig. 7. Model cutting

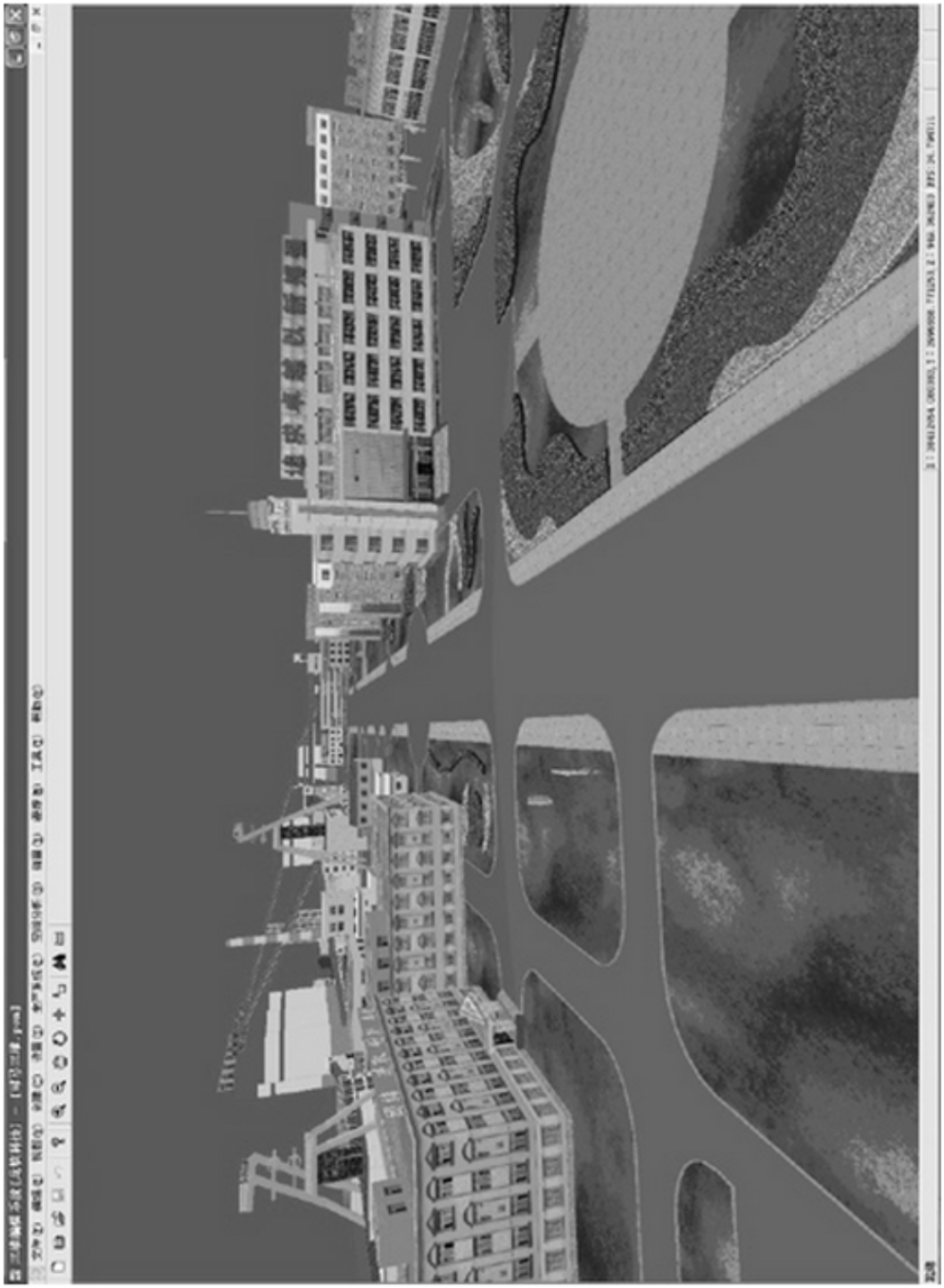

Fig. 8. Three-dimensional visualization and navigation of mine surface

that a 3D model for geological application can be successfully constructed after the conversion of CAD graphics data to the spatial database. The tools provided in the system can realize the scaling, rotation, and translation of graphics, and the model can be cut arbitrarily, and the section of corresponding model can be obtained. In addition, roaming and browsing can also be carried out to facilitate the daily management of mines. However, the experimental system needs to be further improved, and a whole set of platform for 3D GIS modeling, analysis and visualization can be formed.

References

[1] Q. Hamid, M. H. Chauhdry, S. Mahmood, M. S. Farid: *Arc GIS and 3D visualization of land records: A case study of urban areas in Punjab.* National Academy Science Letters *39* (2016), No. 4, 277–281.

[2] M. Alcaraz, E. Vázquez-Suñé, V. Velasco, M. Diviu: *3D GIS-based visualization of geological, hydrogeological, hydrogeochemical and geothermal models.* Zeitschrift der Deutschen Gesellschaft für Geowissenschaften (German J. Geol.) *167* (2016), No. 4, 377–388.

[3] B. Li, J. Wu, M. Pan, J. Huang: *Application of 3D WebGIS and real-time technique in earthquake information publishing and visualization.* Earthquake Science *28* (2015), No. 3, 223–231.

[4] N. Dell'Unto, G. Landeschi, A. M. Leander Touati, M Dellepiane, M. Callieri, D. Ferdani: *Experiencing ancient buildings from a 3D GIS perspective: A case drawn from the Swedish Pompeii Project.* Journal of Archaeological Method and Theory *23* (2016), No. 1, 73–94.

[5] j. Huang, R. Huang, N. Ju, Q. Xu, C. He: *3D WebGIS-based platform for debris flow early warning: A case study.* Engineering Geology *197* (2015), 57–66.

[6] X. Y. Wei, Y. Wang, X. P. Yan, Y. F. Tian, B. Wu: *Design and realization of the 3D electronic chart based on GIS and virtual reality technology.* Applied Mechanics and Materials *744–746* (2015), 1669–1673.

[7] A. S. Harvey, G. Fotopoulos, B. Hall, K. Amolins: *Augmenting comprehension of geological relationships by integrating 3D laser scanned hand samples within a GIS environment.* Computers & Geosciences *103* (2017), 152–163.

[8] H. Huang, J. Ni, Y. Zhang, T. Qian, D. Shen, J. Wang: *Web3DGIS-based system for reservoir landslide monitoring and early warning.* Applied Sciences *6* (2016), No. 2, paper 44.

[9] C. Tao, Q. K. Wang: *GIServices-based 3D internet GIS: GeoEye 3D.* Acta Geodaetica Et Cartographic Sinica *31* (2002), No. 1, 17–21.

[10] Y. Li: *Street level urban design qualities for walkability: Combining 2D and 3D GIS measures.* Computers, Environment and Urban Systems *64* (2017), 288–296.

[11] C. Xiong, X. Lu, M. Hori, H. Guan, Z. Xu: *Building seismic response and visualization using 3D urban polygonal modeling.* Automation in Construction *55* (2015), 25–34.

[12] A. Tiwari, K. Jain: *A detailed 3D GIS architecture for disaster management.* International Journal of Advanced Remote Sensing and GIS *4* (2015), No. 1, 980–989.

Received August 7, 2017

Acta Technica *62* No. 2B/2017, 307–318

Design of detection robot of fault oil well[1]

Hangxin Wei[2,3], Wei Wu[2], Wenkui Xi[2]

Abstract. The exploration instrument is very important for the breakdown maintenance of the production of oil wells, and it can help to understand the internal conditions of the oil wells. However, the traditional detection robot can not adapt to the complicated channel environment and realize the function of detection in the well. The combination of traditional pipeline robot was used for the design of a new detection robot of fault oil well, and virtual simulation technology was used to design the structure of key parts, and the robot hydraulic system and the state of force in different states were calculated respectively. Finally, through the test, the force test of the pipeline robot's performance was carried out. It is proved that the robot can satisfy the demand of the movement and the force, which provides some reference for the design of detection robots of fault oil well in our country.

Key words. Pipeline detection, robot, kinematics, oil well.

1. Introduction

Oil well is an important production device for oil and gas exploitation, and the radial size is small and the depth degree is into the ground. According to their different types, the oil wells can be divided into oil wells, gas wells and injection wells [1]. With the continuous development of China's economy, a large number of oil-related resources have been mined. According to statistics, by the end of 2006, China has developed more than 100 thousand oil wells in service. According to different operations, the production unit of oil and gas can be divided into the production operation well and the fault operation well [2]. Among them, the fault operation wells refer to the oil wells which are in fault, and these oil wells need troubleshooting. In our country, about 1/3 of the oil wells have faults every year, and they need to be repaired so that they can continue to ensure that the well can

[1]This work reported in this National natural science foundation of China, Study on multidisciplinary collaborative design modeling and deep knowledge acquisition for high parameter rotor system with coupled flow force and small clearance force, No. 51405385.

[2]School of Mechanical Engineering, Xi'an Shiyou University, Xi'an, Shanxi, 710065, China

[3]Corresponding author

carry out the normal production operation smoothly [3].

The oil wells still rely mainly on water flooding in China: it raises the pressure by injecting water into the ground, thus eventually getting the resources we want. However, due to the complex underground environment and difficult judgment on the geological condition, it is easy to cause serious faults, which makes workover operations more important [4]. Now, when downhole operations are performed, it is often possible to use the cables to put the detected instruments and operating equipment into the well, but under self-weight, this can only be done with simple ascending and descending operations [5]. The downhole production or maintenance operation of the oil well can be carried out in a timely and accurate manner through the downhole video detection system, and it also can distinguish and detect the inside of the well [6]. In order to further expand the ability of downhole detection instruments, improve the accuracy and effect of downhole detections, and accurately determine the type and situation of downhole faults, the design of the fault oil well robot is carried out to realize the intelligent detection of the downhole fault.

2. State of the art

Cable power is still the main power source of the existing downhole detection equipment, which uses its own motor or fluid as the power and relies on the inertial navigation robot to realize the active walking in the well, and the robot sends the relevant instruments to the correct position [7]. The downhole robot has been used as a downhole tractor or downhole retractor, and according to their different driving modes, they can be divided into wheeled downhole tractor, telescopic downhole tractor, high-pressure jet recoil downhole tractor, and propeller downhole tractor [8]. In 2000, Smart Tract developed a retractable cable tractor that was the most new type of tractor at that time and it could be operated in double ways [9]. This kind of tractor is not only larger in size than moving through the urine, but also requires less power, and the ground equipment is very compact, which is easy to operate specific engineering applications. Sondex Company has also developed a wheeled cable tractor that is much different from the conventional tractor, which uses a non-hydraulic pump. The maximum outer diameter is 54 mm and the maximum pulling force is 2.68 kN, and the bidirectional drive can be realized, and this tractor has been perforated in Southeast Asia to recover remaining oil deposits [10]. "Bore-shuttle" and "Baker-Hughes" downhole robots of Shell Oil Company can completely be operated autonomously, which can realize the tube walking of robots by using the built-in power source [11]. Based on pipeline robot, fault detection technology and application in oil well can be further improved, and new fault detection technology of robot in fault well is developed [12].

3. Methodology

3.1. Conceptual design of robot

The research robot can realize the free intelligent walking in the complex environment of the oil well, and it is possible to detect the conditions in the well. Based on the design idea of the existing oil well exploration robot (as shown in Fig. 1), this detection robot mainly consists of hydraulic components, electrical components, components that support upper and lower and detection components. The hydraulic components are connected together to the components that support walking, and they form a closed-type system together, which is the control unit and drive unit of the whole components that support walking. The pressure compensated fuel tank is designed because of adopting the variable amplitude supercharging mode, and with the increase of the depth of the robot and the increase of the well fluid pressure, the tank pressure in the robot will also rise, and the working pressure of the whole hydraulic system is a variable pressure working state. The electrical components of the robot are in the rear position, and are mainly composed of communication components, electrical control components, and drive motors, which can realize the signal transmission, power transmission and power control of the robot with the ground during the downhole operation.

Fig. 1. Common pipe robots

The detection module is located at the front end of the detecting robot. In this selection of conventional ultrasonic imaging and other detection instruments, more advanced downhole video detectors can be installed as required. The components that support walking and the detecting components are connected together, which is an important execution part of the mobile carrier of the robot, and it adopts the

hydraulic driving mode. The driving principle of this kind of drive is the slip piston type, and when the robot moves through the well, the upper and lower supporting components will move, loosen, extend and shrink alternately. The walking component with upper and lower support adopts a universal hinge joint, thus, the robot can achieve the horizontal or directional wells of different directions in the well.

3.2. Hydraulic system design of fault detection robot in oil well

The hydraulic system of the robot is designed with a closed hydraulic system, and the pressure compensating tank is operated with variable amplitude supercharging. With the increasing depth h of the robot in the well, the fluid pressure P_1 of the well will also increase gradually, and correspondingly, the pressure in the tank is gradually increasing. The pressure in the tank is greater than or equal to the hydraulic pressure of the well, and the hydraulic pump pressure is ΔP. From this it can be seen that the working pressure of the pump is equal to the sum of P_1 and ΔP. In the process of operation, when the oil flow in the hydraulic circuit, there will be a certain pressure loss, and coupled with the pressure damage of the pipeline and each valve, the total pressure loss of the whole oil circuit is $P_\mathrm{s} = 1\,\mathrm{MPa}$.

The structural representation of the support cylinder is shown in Fig. 2. It is assumed that inner diameter and the cross sectional area of the support cylinder are, respectively, $S_1\,, D_1$, the outer diameter and cross sectional area of the piston rod are $S_2\,, D_2$, and the left cross section of the piston is $\Delta S = S_1 - S_2$.

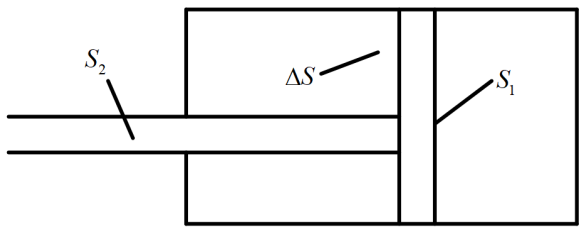

Fig. 2. Chart of the support hydraulic cylinder

As the piston advances to the right, the force acting on the left and right end of the piston is shown in the formulas

$$F = P\Delta S = (P_1 + \Delta P - P_\mathrm{s})\,\Delta S \tag{1}$$

and

$$F = PS_1 = P_1 S_1\,. \tag{2}$$

Then the force acting on the piston rod by the well fluid can be calculated as

$$F = P_1 S_2\,. \tag{3}$$

The force analysis and calculation formula of the whole piston is

$$F = (P\Delta S_1 - PS_1)\,\eta_{\mathrm{m}} + P_1 S_2 \approx (\Delta P - P_{\mathrm{s}})\,\Delta S\,. \tag{4}$$

The minimum force required to support the cylinder piston and the minimum card effort required for the support foot are both greater than the maximum load that the piston receives. The main dimensions of the walking cylinder are shown in Fig. 3. It is assumed that the inner diameter and the cross sectional area of the walking cylinder are respectively $D_3\,, S_3$, and the outer diameter and cross sectional area of the piston rod are $D_4\,, S_4$. Thus, the left cross section of the race can be obtained in the form $\Delta S' = S_3 - S_4$.

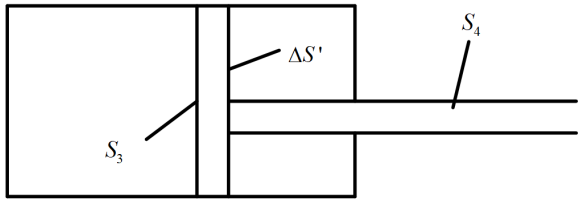

Fig. 3. Chart of move of hydraulic cylinder

As the piston advances to the right, the force of the piston's left and right ends is shown in formula (5) and formula (6), separately:

$$F = PS_3 = (P_1 + \Delta P - P_{\mathrm{s}})\,S_3\,, \tag{5}$$

$$F = P\Delta S' = P_1 \Delta S'\,. \tag{6}$$

Then the force acting on the piston rod by the well fluid is

$$F = P_1 S_1\,. \tag{7}$$

The force analysis and calculation formula of the whole piston is

$$F_1 = (PS_3 - P\Delta S')\,\eta_{\mathrm{m}} F \approx (\Delta P - P_{\mathrm{s}})\,S_3\,. \tag{8}$$

In summary, combined with the design parameters, the flows, pressures and power values of the hydraulic cylinder at different stages are shown in Table 1.

3.3. Structural design of fault detection robot for oil wells

The operating conditions in the pipeline are relatively complex, which requires that the detection robot must be flexible, so the shell of the robot is composed of 2 cylinders. The robot uses a wheeled carrier, with 3 sets of support wheels that are uniformly distributed in the circumferential direction of the pipe, and the wheel telescopic mechanism is used to ensure that the support wheel can be extended and changed within the range of 300 mm$\sim$400 mm in the pipe diameter, and the tight

joint of the support wheel and the pipe wall can be realized by using the torsion spring. Among them, the first section of the cylinder is instrument cabin, and the second section is the battery cabin. The instrument cabinet contains modules such as signal acquisition, data storage, electrode drive, etc., and the battery compartment contains batteries for the entire instrument. With the joint of the universal joint, the second section of the cylinder is more flexible, so that the robot can walk better. The casing of the robot is nested and linked together, including a clamping cylinder and a walking cylinder, and all the valves are embedded in the shell of the robot, and the hydraulic circuit of the robot is also completed inside the shell.

Table 1. Pressure, flow and power value of hydraulic cylinder in different stages

Working condition		Load	Oil return chamber pressure	Inlet chamber pressure
Support cylinder	Fast forward	$-P_1S_2$	P_1	P_1
	Feeding	$F - P_1P_2$	P_1	$P_1 + \Delta P - P_s$
	Rewind	P_1S_2	P_1	P_1
Walking cylinder	Fast forward	P_1S_3	P_1	P_1
	Rewind	$F - P_1S_3$	P_1	$P_1 + 10^3F$

The clamping cylinder and the end cover of the running cylinder are connected to the cylinder by welding, and end caps on the rod side of the hydraulic cylinder are connected with the cylinder when the outer thread is used, but the rear end cap still uses a welded joint. Through this connection, it is possible to reduce the exposure of various parts of the cylinder as far as possible, so as to ensure the smaller size and smooth appearance, and it can improve the robot's bearable impact load to a certain extent and adapt to more adverse external environments. In the design of the piston structure, the slip ring combination of piston - car foot type is selected, and the direct guide sleeve of end cap type is used at the outer end of the piston rod. The virtual design of the pipe robot is shown in Fig. 4

3.4. Kinematics analysis of fault detection robot for oil wells

Because the environment in the oil well is complex, the requirement on the performance of the fault detection robot is higher. The main factors that influence the performance include the robot's supporting foot, clamping force, traction force and piston thrust, which affect the stability and flexibility of the robot walking in the mine. Among them, the traction force determines the robot's walking ability, and the size of the supporting foot of the robot is affected by the thrust of the piston, and there is a certain mathematical relationship between the two. Figure 5 illustrates the force diagram of the supporting foot, and then uses a simple mathematical model to represent the mathematical relationship between the three parameters. From their mathematical relationship, it can be seen that the traction force of the robot is pro-

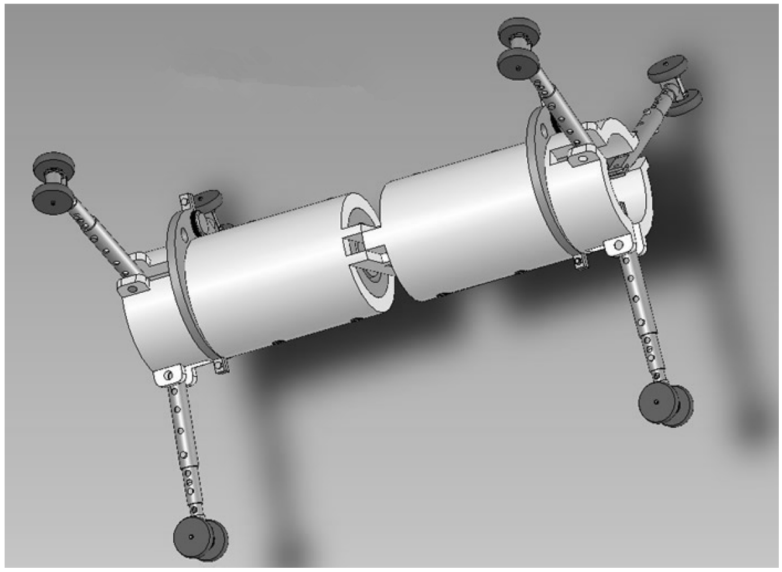

Fig. 4. Virtual modeling of pipeline robot

portional to the supporting force of the foot, that is, the increase in the clamping force of the foot will increase the traction of the robot accordingly.

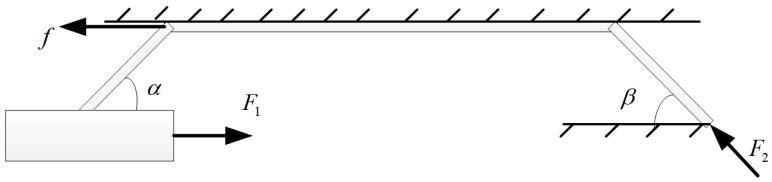

Fig. 5. Force diagram of robot's feet

When the diameter of the borehole is in the range of 90 to 130 mm, the stability of the robot walking will also decrease as the bore diameter becomes smaller, similarly, as the cable drag increases, the stability of the robot will also decrease. The fault detection robot of oil well can keep relatively stable running state when walking in vertical shaft, and the single walking distance can reach 160 mm, and the average walking speed is 7.1 mm/s. Under the pulling force of the cable, the robot will be locked between the support foot and the shaft lining, however, the self-locking will decrease with the decrease of the bore diameter, which will lead to lower stability. Taking the walking of the fault detection robot in the well with an inner diameter of 90 mm as an example, when the pulling force of the cable reaches 5 kN, the support foot of each walk will slide 10 mm to ensure the stability of the robot while walking in the well.

The upper and lower support legs of the robot are clamped to the shaft wall to ensure its stability, but as the robot moves, this clamping force will change slightly. Because of the impact of the weight of the robot, the force of the lower support foot

varies greatly, and contact forces between the support foot and the shaft wall will also change a little, so this change is directly reflected in the specific stress changes. When the support leg of the robot is clamped in the shaft wall, the cylinder piston force under its support is 3 kN, and its range of change is 2.7–3.3 kN, which is due to the fluctuation of the piston force caused by the change of the foot clamping force.

4. Results analysis and discussion

4.1. Environment condition

The modular design of the detection robot for the fault oil well is shown in Fig. 6. The robot uses a three-axle differential type, and its main parameters are: the mass of the robot is 26 kg, the normal running speed is 80 mm/s, the axial length is 0.55 m, the pipe diameter is 0.31 m, the input power is 120 W, and the output tractive force is 0.24 kN.

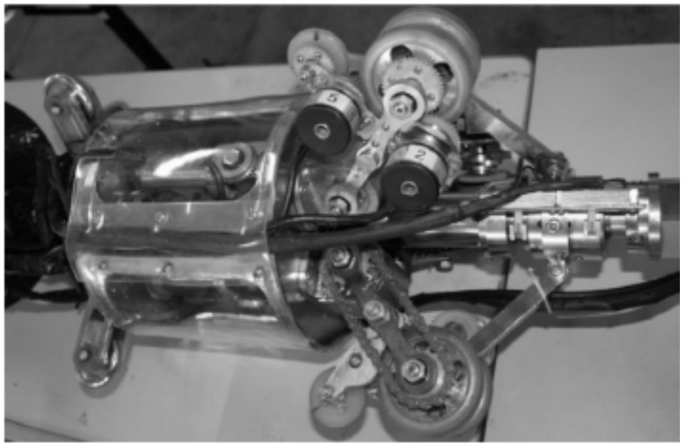

Fig. 6. Pipeline robot prototype

A test tube of the robot is made of a steel tube and an organic glass tube which is connected by flanges, and the inner diameter and outer diameter of the pipeline are 0.31 m and 0.325 m respectively. The material of the bent pipe in the pipe is a steel tube, while the straight pipe is made of plexiglass tube, and the radius of curvature is 0.93 m.

4.2. Robot test

Speed sensor was installed at the driving wheel and driven wheel, and through the measured results, the running speed was compared and analyzed, so as to determine whether the robot is locked, turned or skidded during the operation. The robot was set to move into the bent pipe according to different attitude angles. The walking test shows that the robot can smoothly pass through the elbow. Further

comparison and analysis of the relative data show that the driven wheel has better following effect, and slipping and motion interference do not occur in the driving wheel. During the operation of the elbow, the robot walks at a uniform speed, and its smooth walking shows that the three-axis differential actuator plays a good role in differential regulation.

The differential effect of the robot attitude angle of 0° and 30° in the operation of the elbow was analyzed respectively. When the attitude angle was in 0°, the curve of the angular speed of the driving wheel was obtained, as shown in Fig. 7. Furthermore, the average angular velocity of the drive wheel and the result of the theoretical calculation were compared and analyzed during the operation of the bent pipe, and at the same time, the error analysis was carried out. By comparing and analyzing the results, it can be seen that the analysis results of the two are equal and the error is quite small, which further shows that the robot has very good differential speed effects.

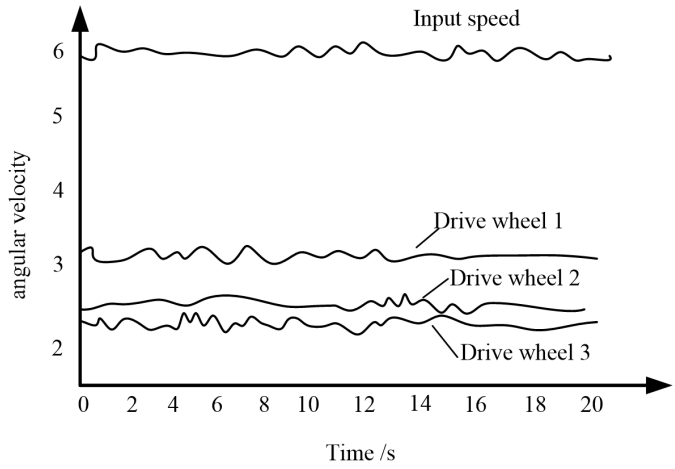

Fig. 7. Angular velocity curve of driving wheel

4.3. Traction test of robot

In order to ensure the stability of the load during the test and the real-time adjustment function, a robot's end pipe friction tester was used to provide the load. The traction test of the robot was carried out in the plexiglass tube section. The preload of the robot was set at 0.35 kN, and its initial speed was 0.08 m/s. When the load was loaded to 0.24 kN, the robot could still run normally, and the robot did not slip during the operation.

The maximum traction test of robot under different preload was carried out, and the friction tester was locked, so that the robot's drag force could be run by sensors. When the driving wheel of the robot was slipping, the maximum tractive force of the corresponding robot could be measured under the action of the pull force. In the process of testing, the pretension was gradually increased, and the tractive force

of the robot was gradually increased, but ultimately it was limited by the power rating of the drive motor, and when the preload increased to 0.5 kN, there was a stall phenomenon in the motor. The friction factor between the drive wheel and the tube wall was 0.8, and the included angles of the pretightening mechanism α and β were 44° and 42°, respectively. By comparing the theoretical and experimental values of the traction force under different pretensions, the maximum error was only 6.3 %. This shows that the experimental results are in good agreement with the theoretical results.

From the test results, it can be seen that the robot preload is the same as the result in the robot traction test with different attitude angles, and the maximum tractive force measured at the end is in good agreement with the theoretical result. It also shows that there is no significant relationship between the traction force and the attitude angle of the robot.

5. Conclusion

The fault oil well can be detected through the use of pipeline robot, which can walk autonomously in the well by carrying sensors or other operating devices, thus transmitting information from the well to the ground. Considering the size of the drive wheel and the attitude model of the robot running in the elbow, the shortcomings of the previous model were made up by the model that can be used as a general model for solving the position and orientation problem of the bent pipe of a robot, and the theoretical speed ratio relationship of the drive wheel was verified when the pipe was running. The bend test of the detection robot of fault oil well was carried out further, and results of each parameter measured by the test were compared with the results of the simulation analysis, so as to verify the performance of the robot. Through the test results, it can be seen that the robot can run smoothly in the bent pipe and meet the functional requirements, which coincides with the simulation results. Compared with the traditional detection robot, the robot has better stability and lower cost, so it has certain popularization values. But research on robot intelligence is relatively small, so it can strengthen the intelligence research of robot, thus further improving its performance.

References

[1] N. Mohamed, J. Al-Jaroodi, I. Jawhar: *A cost-effective design for combining sensing robots and fixed sensors for fault-tolerant linear wireless sensor networks.* International Journal of Distributed Sensor Networks *10* (2014), Article ID No. 659356, 1–11.

[2] S. Bhowmick: *An approach to design a simple human detecting robot for cost effective home security system as well as various rescue missions.* Communications on Applied Electronics (CAE), Foundation of Computer Science FCS *1* (2015), No. 8, 5–8.

[3] M. Van, H. J. Kang, Y. S. Suh, K. s. Shin: *A robust fault diagnosis and accommodation scheme for robot manipulators.* International Journal of Control, Automation and Systems *11* (2013), No. 2, 377–388.

[4] M. A. Kamel, X. Yu, Z. Zhang: *Fault-tolerant cooperative control design of multiple wheeled mobile robots.* IEEE Transactions on Control Systems Technology *PP* (2017), No. 99, 1–9.

[5] L. H. Zhang, Y. D. Chi, C. P. Board, J. P. Grid: *The research and design of overhead transmission line insulator detecting robot.* Electronic Design Engineering *23*(2015), No. 16, 164–166.

[6] J. Zhou, C. Huang, B. Liu, T. T. Wang: *A control system design of underwater robot for detecting underwater structures.* Applied Mechanics and Materials *536–537* (2014), 1105–1109.

[7] X, Tian, Y. Liu, Y. Zhang, R. Lin, Y. Xi: *Fault diagnosis research of submarine casing cutting robot for abandoned oil wellhead.* International Journal of Security and Its Applications *8* (2014), No. 1, 213–224.

[8] B. H. Wu, J. J. Xi: *Design and research of synchronous-style clamping mechanism for cable-detecting robot.* Advanced Materials Research *1028* (2014), 127–133.

[9] F. Xu, J. Hu, X. Wang, G. Jiang: *Helix cable-detecting robot for cable-stayed bridge: Design and analysis.* International Journal Robotics and Automation *29*(2014), No. 4, 406–414.

[10] B. Sun, B. Cai, Y. Zhang, Q. Fan, S. Yu: *Fault diagnosis research of submarine electro discharge cutting robot for abandoned oil wellhead.* Computer & Digital Engineering (2013), No. 7.

[11] H. W. Wang, X. N. Wang, X. Tian, G. H. Du, Y. M. Tian, q. M. S. Rong, W. K. Zhang: *Software and hardware design of a acoustic fault detecting instrument.* Applied Mechanics and Materials *432* (2013), 246–252.

[12] R. R. Kalia, P. Abrol: *Design and implementation of wireless live wire fault detector and protection in remote areas.* International Journal of Computer Applications *97* (2014), No. 17, 14–20.

Received August 7, 2017

Acta Technica *62* No. 2B/2017, 319–328

Design and implementation of computer simulation laboratory construction system

Liu Na[1]

Abstract. The design and development of computer simulation laboratory construction system provide certain technical supports for the improvement of relevant theories in all sectors of our country. By reading and summarizing the related data, the related concepts of computer virtual laboratory construction system were summarized, and the simulation of the meteorological laboratory construction system was also taken as an example. Compared with the actual setting value, the error was relatively small. The results show that the computer simulation laboratory construction system is more suitable for today's industry development. The purpose of this research is to provide theoretical basis and technical support for the development of related industries in China.

Key words. Computer, simulation, laboratory construction system.

1. Introduction

With the development of the times, the world economic level has been greatly improved. In this trend, various industries have also been greatly improved. Various new theories and techniques have been gradually applied to the development of the industry. However, how to determine whether a theory or technology is necessary for the development of the times and the progress of enterprises is necessary, and how to judge a theory is more accurate and more reliable is of great importance. Under this problem, the importance of the laboratory is beginning to be highlighted. The laboratory is extremely important for the development of the industry, it can further improve the relevant theories through the experimental design of some problems raised by the industry, so that the relatively imperfect parts of these theories are improved, and the relevant theories and techniques can provide greater impetuses to the development of the industry. Therefore, as an important link of theoretical and technical verifications, the development of laboratory is of great importance to the

[1]School of Information Engineering, Chongqing Industry Polytechnic College, Chongqing, 401120, China

development of an industry or an area. Especially in today's era of theoretical and technological innovations, it is necessary to make real-time evaluation and analysis on all relevant theories, so that more advanced theories can be created and perfected continuously, thus providing a scientific basis for the promotion of the overall level of the industry as a whole. However, in the construction of laboratory, there are great risks and high costs. For example, in the laboratory construction, if the relevant laboratory construction link in a timely manner cannot be controlled, risks may arise in the construction of certain links during the process, which has some negative effects on the subsequent experimental operations and theoretical verifications.

2. State of the art

In the current era, with the development of various industries in the world, the demand for more new theoretical knowledge has become one of the main concerns of various industries [1]. In many industries, many theories in these industries are presented in the form of hypotheses. Therefore, in the development of these industries, it is necessary to guarantee the relevant theoretical knowledge can be combined with the actual development of the industry in the process of development, so as to achieve the organic combination of industrial practices and theories and provide more positive impacts for the development of the industry [2]. Therefore, the construction of laboratories has become a top priority in the development of various industries, and many industries have constantly updated their related laboratory equipment, so that the final evaluation results of the experiment have higher credibility, and the data is more authentic and reliable, so as to provide a certain technical support for the progress of the industry ultimately [3]. In the traditional laboratory construction, the whole experiment is done through manual operations, and there are many risks, for example, there are a large number of toxic and harmful gases, so that the body of the relevant personnel will suffer a certain degree of damages. And in the construction, if the relevant links cannot be timely controlled to assess its various links on the basis of the completion of the comprehensive evaluation of the entire laboratory construction, it will have a negative effect on the construction process of the laboratory, and then it will also affect the whole operation process of the laboratory [4]. The appearance of computer simulation system provides technical supports for the development of the laboratory construction, and many research scholars begin to study and analyze this link, which provides more theoretical supports for the improvement of the laboratory construction process.

3. Methodology

With the development of the times, the overall economic level of the world has been greatly improved. In this trend, countries around the world have begun to pay more attentions to the development of their various industries, and more advanced theories and techniques have been introduced into the development of various industries. And with the rapid development of the industry, many more correct and

reliable theories are applied gradually, while there are many inaccurate assumptions which cause some limitations for the development of the industry [5]. Therefore, the relevant theories and technologies need to be verified in a timely manner, so as to ensure that more accurate information can be applied to the development of the industry, which is extremely important to enhance the overall strength of the industry. Since China's reform and opening up, the contact with the developed countries has gradually increased, and the comprehensive strength of various industries in China has been greatly improved. In this situation, China has also begun to introduce related theories and technologies from many developed countries [6]. However, whether the relevant theories and technologies that are introduced can be combined with the actual situation and demand of our country is one of the important issues that should be considered when introducing relevant theories and technologies. Many advanced theories and techniques have been verified to some extent in the later stage, so the development of our country's industry level, China's economic level, the overall strength of the country and the international status have been greatly improved [7]. However, because of the blind use in the process of introduction, there are some theories that cannot be better combined with the actual situation of our country and the actual demand of the industry development, they have a certain negative impact on the development of China's industry, and the related costs in the development of some industries in China increase, so they fail to obtain relevant incomes, thereby hindering the progress of the industry [8]. In this uncoordinated phenomenon, our country begins to build various types of laboratories, and the laboratory is verified firstly through the introduction of relevant theories and techniques. On the basis of the expected effect in a small environment, the relevant theory is further applied to actual industrial production, which can greatly reduce the risk of the development of the industry, and it may also provide a basis for the development of some new theories and innovative technologies in our laboratories [9]. Therefore, the establishment of laboratories is very important for the development of various industries in our country (Figure 1). However, in the process of increasing the number of our laboratories, although it provides more related theories and techniques with innovative values for the development of the industry, there are also some unharmonious factors that also need to be further considered. For example, in the construction of laboratory, the arrangement and use of related instruments and equipment in laboratories are important links of laboratory constructions. Because our country still lags behind the developed countries in some aspects, the construction of some specialized laboratories remains at a relatively backward level, so that the initial construction of the laboratory is not reasonable. This may result in the harmful poisonous gases produced by some chemical experiments or biological experiments in the course of experiments, which cannot be eliminated in time because of the construction, thus causing certain losses to people's bodies; because some of the more expensive instruments are not properly placed, which may do damage to the equipment during use, thereby increasing the overall experimental costs or indirect costs; in the course of some experimental operations, some of the more important laboratory links may not be better connected because of the unreasonable design of the laboratory, which may have an impact on the accuracy and reliability of the

experimental results, thus affecting a series of subsequent verification processes, and it will also result in an increase in the cost or time cost of certain experiments or a failure of the experiment. In serious cases, it may lead to erroneous theories and cause irreparable damages to the development of subsequent industries. Therefore, the design of the laboratory is very important for the development of the whole link of the experiment [10].

Fig. 1. Laboratory development

In view of a series of discordant phenomena above, through the analysis of the relevant data, the relevant theories of the computer simulation laboratory construction were determined, and the advantages of laboratory construction under this technology were further analyzed, so as to determine the theoretical basis of this study; on the basis of the theory, the main influencing factors of the computer simulation technology for laboratory construction were generalized; and based on the importance and advantage of computer simulation technology, the comprehensive evaluation of its related construction links and the final construction were obtained by taking the laboratory construction of a university as an example, so as to validate the study from an example point of view; through the questionnaires for relevant university laboratory managers, a comparative analysis of the mode of laboratory construction based on computer simulation and the traditional laboratory construction method was made in this paper, so as to confirm the necessities of the development of this technology and provide more authentic and reliable data supports for the follow-up researches.

The computer simulation technology in traffic weather laboratory was selected as the actual laboratory operating platform. Firstly, the atmospheric visibility correlation model of fog simulation systems in the meteorological observation was established by the computer simulation system. Among them, the formulas of the extinction coefficient, visibility and other parameters in the meteorological observa-

tion are shown as follows:

$$Vis = -\frac{\ln \varepsilon}{\beta}\,, \tag{1}$$

$$\beta = \pi \sum_{i=1}^{N} Q_{\mathrm{ex}} n_i r_i^2\,, \tag{2}$$

$$u(t) = K_{\mathrm{p}}[e(t) + \frac{1}{T}\int_0^t e(t)\,\mathrm{d}t + T_{\mathrm{d}}\frac{\mathrm{d}e(t)}{\mathrm{d}t}]\,. \tag{3}$$

In the above equations, Vis represents the extinction coefficient, ε and β represent the correlation coefficients, Q denotes the actual observation, n denotes the number of actual observations, $u(t)$ represents the visibility parameters, T is the model of associated value and values of K_{p} represent P.

Then, the coefficients of the related model were optimized to make the model better. The main optimization scheme is shown in Table 1. By analyzing several schemes of correlation coefficients, the optimal operational parameters for the study were determined.

Table 1. Optimization schemes of correlation coefficients

Parameter estimation scheme	Extinction coefficient model	a	b
Kunkel scheme	$\beta = 144.7W^{0.88}$	144.7	0.88
Eldridge scheme	$\beta = 91.0W^{0.65}$	91.0	0.65
Pinnick scheme	$\beta = 145.0W^{0.63}$	145.0	0.63
Tomasi scheme	$\beta = 65.0W^{0.67}$	65.0	0.67

4. Result analysis and discussion

Today, our country has begun to take the design of laboratories as an important part of the experiment, and it has attracted more attentions of scholars. With the emergence and development of computer technology, many scholars have begun to apply the computer simulation technology to the construction and evaluation of the laboratory, and they have achieved considerable results [11]. However, the research in China is still in the initial stage, and the related theories and techniques are not mature enough. In order to improve the related theories and technologies, the design theories of computer simulation laboratory construction system were analyzed and generalized in this research. The research aims at providing a reference for the development of computer simulation laboratory construction system in our country, and further providing technical supports for the development of related industries.

The development of laboratory and its role have become more and more impor-

tant in the current era of rapid economic developments. No matter what the industry is, it is inseparable from the understanding of the development of relevant theories and knowledge. On this basis, more theories are verified and analyzed, so as to put forward more innovative theories and technologies and provide a theoretical basis for the development of the industry as a whole. The construction of the laboratory is one of the most important prerequisites for the accurate operation of the entire experimental operation [12]. In the various industries of the world, many scholars have started to take the construction link of laboratories as an important prerequisite for laboratory researches. For example, in the chemical or biological industry, a large number of experiments are needed to verify the relevant theoretical knowledge in the field. In the course of the experiment, there are more polluting drugs in the chemical or biological industries, and the design of the laboratory may be harmful to the human body because of the unreasonable design of the laboratory; or in the physics industry, the related instruments and equipment with radiation may be exposed to the industry and the structure of the laboratory is irrational, it may cause more radiations, which will restrict the development of the whole industry. Moreover, some experimental operations may involve the use of expensive instruments and equipment. If the design of the lab is not reasonable, it may cause some mistakes in the process of use, thus affecting the integrity of the expensive equipment in the laboratory, which will lead to an increase in the cost of some experiments and have a negative impact on the further development of laboratories [13]. Therefore, in the laboratory construction, it is necessary to evaluate and analyze the relevant aspects of laboratory construction in a timely manner, so as to confirm the perfection of the whole construction link and then provide certain guarantees and positive influences for the follow-up experiments. There are many related links in the construction of laboratory, and many scholars have analyzed and explored them and have made great achievements. The advent of computer technology has brought a new technical support for the development of various industries. And because of the existence of related characteristics of the computer technology, this technology can be better combined with related industries, thus forming a new model of development [14]. Under this trend, some of the computer's techniques such as computer simulation systems have also been gradually introduced into the laboratory building (Figure 2). In the construction of simulation laboratory system based on computer, the main thing is to introduce the computer simulation technology into the actual laboratory construction, and through the use of the system, all kinds of evaluation indexes are collected in real time in the whole laboratory construction. And through the computer simulation system, the whole construction process can be analyzed and evaluated, so that the late construction has some basis and the whole construction process is monitored in real time, thus evaluating the rationality of the whole process construction [15]. Therefore, compared with the traditional construction model of subjective judgments, the construction of laboratory based on computer simulation system can obtain relatively large basic data and more perfect evaluation models, and it considers the problem more comprehensively, so that there are more reliable basis and data supports in the late construction.

On the basis of the clarity of relevant theories, a laboratory for fog detection in a

Fig. 2. Development of computer simulation laboratory construction

weather processing laboratory was further built. The main links in the construction of the fog laboratory based on computer simulation system included data acquisition, data processing and data analysis. The major simulation building facilities are shown in Table 2.

Table 2. Components for the construction of this computer simulated fog laboratory

Visibility setting point (m)	Conventional laboratory measurements (m)			Computer simulation laboratory measurements (m)			Error value	
	1#	2#	3#	4#	5#	6#	Absolute error (m)	Relative error (%)
200	203	208	210	204	213	212	9	4.5
150	153	161	156	151	159	159	6	4
100	94	98	93	97	94	93	7	3
50	53	52	54	53	49	52	2	4

Then, by setting different visibilities and using the constructed computer simulation techniques, the laboratory technique and the traditional laboratory technique were compared and analyzed, as shown in Table 3. The absolute error and relative error of the set value of visibility in experiments and computer simulation systems were analyzed. The results show that the error of computer simulations of the fog laboratory is relatively small, and it is more convenient and reliable for laboratory operations.

Table 2. Components for the construction of this computer simulated fog laboratory

Name	version	Technical parameter specification	Number
Touch screen	version	Technical parameter specification	Number
Programming cable		6ES7 810-4CC07-0YA5	1

5. Conclusion

With the development of the times, every industry has made a great progress, and more advanced theories and technologies have been introduced from developed countries to some backward countries because of the increasing exchanges between countries. In this trend, a large number of laboratories have been set up and established for validation of relevant theories. However, in the traditional laboratory construction, some non-standard construction methods may cause certain harm to human health and increase the cost of researches. The theories and techniques of computer simulations of laboratory designs have begun to be used in traditional laboratory operations. The related theories and techniques of the laboratory design of computer simulation technology were summarized in this study, and the model was used in the fog laboratory as a practical case to compare and analyze the computer model laboratory construction system. The purpose of this research is to provide a theoretical basis for the construction of computer virtual laboratory in China. Due to the lack of relevant theories, the depth of the discussion needs to be improved. The following researches should consider all kinds of influencing factors in the construction of computer virtual laboratories, so as to provide better references for the development of computer virtual laboratories in China.

References

[1] V. K. Decyk, T. V. Singh: *Adaptable Particle-in-Cell algorithms for graphical processing units.* Computer Physics Communications *182* (2011), No. 3, 641–648.

[2] H. Bura, R. Widera, W. Honig, G. Juckeland, A. Debus, T. Kluge, U. Schramm, T. E. Cowan, R. Sauerbrey, M. Bussmann: *PIConGPU: A fully relativistic Particle-in-Cell code for a GPU cluster.* IEEE Transactions on Plasma Science *38* (2010), No. 10, 2831–2839.

[3] G. Stantchev, W. Dorland, N. Gumerov: *Fast parallel Particle-to-Grid interpolation for plasma PIC simulations on the GPU.* Journal of Parallel and Distributed Computing *68* (2008), No. 10, 1339–1349.

[4] S. Lee, C. T. C. Nguyen: *Influence of Automatic Level Control on micromechanical resonator oscillator phase noise.* IEEE International Frequency Control Symposium and PDA Exhibition. Jointly with the 17th European Frequency and Time Forum (IEE Cat. No.03CH37409), 4–8 May 2003, Tampa, FL, USA, IEEE Conference Publications (2003), 341–349.

[5] B. Gerfault, B. Godara: *Novel methodology for choosing detectors for the Automatic Level Control of high power amplifiers.* IEEE International Conference on Anticounterfeiting, Security, and Identification in Communication, 20–22 August 2009, Hong Kong, China, IEEE Conference Publications (2009), 378–381.

[6] U. R. Pfeiffer, D. Goren: *A 20 dBm fully-integrated 60 GHz SiGe power amplifier with Automatic Level Control.* IEEE Journal of Solid-State Circuits *42* (2007), No. 7, 1455–1463.

[7] J. Yuan, P. Darabi, M. Salcudean: *Modelling of flow, combustion, clinker formation and NOx emissions in long rotary cement kilns.* ZKG International *60* (2007), No. 12, 54–67.

[8] Z. Wang, J. Zhou, Z. Wen, J. Liu, K. Cen: *Effect of mineral matter on NO reduction in coal reburning process.* Energy & Fuel *21* (2007), No. 4, 2038–2043.

[9] M. Moser, S. Akhtar, V. Sakthithamn, F. C. Lockwoods: *NOx reduction*

through a combination of reburn and SNCR. ZKG International *61* (2008), No. 5, 46–57.

[10] J. Chen, M. Shi: *A universal model to calculate cyclone pressure drop.* Powder Technology *17* (2007), No. 3, 184–191.

[11] A. Raoufi, M. Shams, H. Kanani: *CFD analysis of flow field in square cyclones.* Powder Technology *191* (2009), No. 3, 349–357.

[12] C. Cortés, A. Gil: *Modeling the gas and particle flow inside cyclone separators.* Progress in Energy and Combustion Science *33* (2007), No. 5, 409–452.

[13] C. Tao, L. Zhao, W. Yu, R. Liu, Z. Hu, Q. Qian: *An evaluation method for combustion characteristics of coal in cement industry.* Journal of Wuhan University of Technology-Materials Science *25* (2010), No. 1, 174–178.

[14] B. T. Zhao: *Modeling pressure drop coefficient for cyclone separators: A support vector machine approach.* Chemical Engineering Science *64* (2009), No. 19, 4131–4136.

[15] C. Tao, L. Zhao, W. Yu, X. Peng, X. Wang: *Mechanism of resistance characteristics in cyclone.* Journal of the Chinese Ceramic Society *37* (2009), No. 12, 2124–2129.

Received May 7, 2017

Acta Technica *62* No. 2B/2017, 329–340

Application of adaptive ant colony algorithm in optimization of machine process manufacturing route

Wang Chuan[1], Xu Zhi[2], Zhang Daoshun[3]

Abstract. Because there is no a standard design management concept in the mechanical manufacturing industry, the quality of process design results is not high. Therefore, the application of adaptive ant colony algorithm in the optimization of machine process manufacturing route was discussed and analyzed in this paper. The principles of bionics ant colony algorithm, the mechanical process route optimization based on adaptive ant colony algorithm and its scheduling design and route optimization verification algorithm were introduced. Taking the manufacturing process of the gear shaft of Company A as an example, the adaptive ant colony optimization design was carried out, and the manufacturing scheduling problem was verified. The results show that the optimized manufacturing route based on adaptive ant colony algorithm can effectively improve the enterprise's machinery manufacturing efficiency and corporate profits.

Key words. Adaptive ant colony algorithm, mechanical process manufacturing route, optimization.

1. Introduction

With the fierce market competition in recent years, the demand for diversified customers has rapidly developed, but also the speed of the product life cycle has become shorter and shorter. Therefore, the society has also put forward higher requirements for part of the process design [1]. As a bridge connecting product design and manufacture, the design process of parts processing is empirical highly. This process has a high degree of dependence on the environment. At present, most enterprises in the quality of our process design still rely on the quality and

[1]China Tobacco Jiangsu Industrial CO.LTD Nanjing Cigarette Factory, Jianyei District, Nanjing, Jiangsu, China, 210019

[2]Institute of Electrical and Automation Engineering, Sanjiang University, Yuhuatai District, Nanjing, Jiangsu, China, 210012

[3]College of Computer Science and Technology, Zhejiang University, Hangzhou, Zhejiang, China, 310058

experience of designers [2]. Although there are a number of mature process examples, its inheritance cannot be used effectively, thus wasting a lot of time and effort in some repetitive design work. At the same time, because there is no standard design and management concept and standard, the quality of process design result is not high, which makes the process design restrict the development of the enterprise. Therefore, it is necessary to optimize the process design process. The quality of process design needs to be improved and the existing mature design examples need to be reused, which can be used as the research focus of process design [3].

In view of the optimization of mechanical manufacturing process, foreign scholars have analyzed the design of CAPP process in the process of product design. Foreign scholars have found that contemporary design cannot take into account the product features while considering the characteristics of complex and diversified manufacturing resources fully. And foreign scholars believe that the integration of product design is to improve product flow route design efficiency. In order to prevent the algorithm from falling into the local optimal solution or the excessive number of components and the complexity of the part structure causing the iterative speed to be too slow, domestic scholars have adaptively treated the evaporation of pheromone in the process of ant transfer on the basis of ant colony algorithm, so as to guarantee the convergence speed of the ant colony algorithm and improve the efficiency of the process route generation [4].

2. State of the art

Attention to bionics from people originated in the middle of 50 s. Artificial immune algorithm, neural network, ant colony algorithm, genetic algorithm and other new algorithms are proposed based on the principle of bionics. Researchers have done a lot of experiments and optimization deficiencies for the shortcomings of ant colony algorithm. The application field of ant colony algorithm is mature, and the application field is expanded gradually [5]. Ant colony algorithm: the ants begin to explore food from the cave without knowing where there is food. Ants will be able to use their own path to make other companions aware of chemicals in this process to exchange information for each other and find the best path finally [6]. A new heuristic optimization algorithm which is called ant colony algorithm is proposed in this way. Ant colony algorithm can be regarded as a mathematical model to solve the spatial parameterized probability distribution model [7]. In fact, according to the pheromone concentration, the algorithm updates the optimal solution of the algorithm by searching in the probability distribution model continuously.

2.1. Methodology

2.2. Principles of ant colony algorithm

When ants are looking for food sources, they can release unique pheromones on their routes. Ants can sense the presence and intensity of matter during movement, and guide the direction of movement so that ants tend to move toward high intensity

of matter [8]. When they encounter intersections that have not yet passed, they select a path randomly and release the pheromone associated with the path length. The longer the ant's path, the less information it releases. The more ants on the path, the more likely the latter will choose the path. Thus, the collective behavior of ant colonies represented by a large number of ants shows positive feedback phenomena. The amount of information on the optimal path is more and more, and the amount of information on the other path decreases as time goes on. Finally, the entire ant colony will find the best path [9].

The number of ants is set to m. These ants have the memory function and have the following characteristics:

(1) According to the concentration of network pheromone and heuristic information, ants are moved to the next city that is the next node, they have corresponding transition probability.

(2) The visited nodes are placed in the tabu list, and the ants will no longer access the existing city or node in the tabu table.

(3) The ants will have certain rules at the edge of the pheromone just becoming part of the local update after a step. And the ants will select global updates after they have gone through the entire network [9].

2.3. Optimization of machine manufacturing process based on adaptive ant colony algorithm

The core of the process route optimization design is the design process of all processing methods to optimize the structural features of each component. Process route optimization selects machining methods, processing equipment and mechanical information to achieve design dimensions and accuracy of parts. This process is a multi-objective optimization problem because of the need of considering various machining accuracy, location reference, working time and cost. Routing optimization and constraints include processing order and manufacturing resource constraints [10]. The optimization of routing is to find a sequence of processes that is optimal for multiple objectives (precision, cost, work hour, etc.) under these constraints. There are three hypotheses when we build ant colony algorithm:

(1) Ants communicate with each other by making pheromones as medium. Each ant responds only to a small fraction of its surroundings.

(2) The direction of action of ants is entirely based on the concentration of pheromones, that is to say, the direction of action is the highest concentration of pheromone.

(3) The behavior of a single ant is random. The group behavior is highly ordered because of the internal self-organization process [11].

The choice of each processing element to the next processing element requires consideration of various factors. Therefore, in addition to determining the pheromone concentration, the subordinate group should also consider some constraints when transferring the nodes. The constraints fall into the following two categories in the process of optimizing the design process:

The first is to deal with the order of constraints. The "baseline first" principle determines that the scheduling process requires a fine work base to provide a more

accurate benchmark for subsequent processing. The principle of "first thick, later fine" refers to the finishing order of rough processing from one to half. As a result of the above principles, it is necessary to establish a priority processing matrix at initialization

$$p_{ij} = 1\,. \tag{1}$$

Formula (1) indicates that the machining primitive j is processed prior to the primitive i. If $p_{ij} = 0$ is 0, it means other. The priority processing design route matrix is as follows:

$$P(p_{ij}) = \begin{bmatrix} 0 & 0 & \cdots & 1 & \cdots & 0 \\ 1 & 0 & \cdots & 0 & \cdots & 1 \\ \vdots & \vdots & & \vdots & & \vdots \\ 0 & 1 & \cdots & 1 & \cdots & 0 \\ \vdots & \vdots & & \vdots & & \vdots \\ 1 & 1 & \cdots & 0 & \cdots & 0 \end{bmatrix}. \tag{2}$$

The entire priority processing matrix is updated after each processing element is completed. The corresponding column of the machining primitive is set to 0. One is that the processing element has been processed and will not constrain the processing of other primitives [12].

The other is the restriction of processing equipment. The machining design is often restricted by the existing processing equipment to a great extent. Enterprise or processing unit determines the type of processing equipment on the basis of consideration of cost. The model is certified by experts, and the cost is optimal under the condition of meeting the processing requirements [13]. However, the processing of resources is limited to some extent, and the design process should consider how to ensure the utilization and processing efficiency of manufacturing resources. Frequent replacement of machine tools, tools, fixtures will increase the processing auxiliary time greatly and reduce processing efficiency. Therefore, in order to ensure the efficiency of mechanical manufacturing process, the best machining accuracy and cost, it is necessary to try to adjust the order of processing in the design process. Number of machines replaced times replaces tools to replace minimum quantities. At the same time, the utilization rate of various processing resources is ensured [14]. In addition to considering the characteristics of the parts, it is necessary to integrate geometric constraints, feature accuracy, manufacturing resource selection, process personnel experience and other factors. Mechanical process manufacturing site is shown in Fig. 1.

2.4. Optimization of mechanical manufacturing scheduling design and verification

The effects of manufacturing results on the interests of enterprises are manifold. The merits of manufacturing results should be a comprehensive evaluation of a series of issues such as order time, production cost, inventory cost and so on. However, the evaluation of manufacturing solutions is usually performed on a small number

Fig. 1. Mechanical process manufacturing site

of questions or on the relative validity of each indicator in previous manufacturing studies. Business managers considering all aspects of corporate interests cannot be reflected adequately without flexibility. This scheme can only be extensible to describe the way in which business interests are presented. Therefore, in order to make that the optimization results of mechanical manufacturing process are in line with the interests of enterprises, the enterprise benefit evaluation system was established in this paper, and the default cost or profit, direct production costs, inventory costs were considered as a measure of the composite index.

The solution of manufacturing scheduling is defined as x, and each factor that affects the interests of an enterprise has an evaluation function f_i. Each factor that affects the interests of an enterprise has an evaluation value $y_i = f_i(x)$. The evaluation of enterprise benefits can be expressed as

$$y = f(y_1, y_2, \cdots, y_n)\,. \tag{3}$$

Function f in the above formula must not be a simple function.

However, several manufacturing modes commonly used in enterprises include Make To Stock (MTS), Make To Order (MTO), Assembly To Order (ATO) and Engineering To Order (ETO). In addition to the inventory model oriented manufacturing, the order determines the revenue of the enterprise in other manufacturing models. Therefore, enterprises can increase their interests only by reducing their costs. For the inventory model oriented manufacturing, the income of the enterprise is also predictable after the master manufacturing plan is determined at the market level. Therefore, the way to increase business interests is often to cut costs rather than expand revenues at the manufacturing scheduling level.

In consideration of that part of the impact of corporate interest is the loss of intangible costs or the benefits of monetary measurement, the impact of other units of measurement will be assessed as a monetary measurement company according to the specific values and cultural circumstances. Finally, the evaluation of various costs in monetary terms is an assessment of the interests of the enterprise. Depending on the importance of the customer to the business, the same order is the invisible loss caused by the delayed delivery of the enterprise. The customer should handle the relationship with the customer and avoid important customer orders as late as

possible. The second point is that the size of the product value will also affect the default loss. The greater the volume is, the greater the default loss is. Finally, the longer the order delivery delay, the greater the adverse impact on the enterprise, and the higher the default loss. The main verification and parameter analysis theory should be considered in the design of the system architecture. Therefore, the results that are convenient for case studies and analyses should be given priority. As a result, data storage uses text file format modified easily, and the output of the algorithm uses a machine friendly form. When it is required, the machine friendly output of the algorithm is transformed into a user friendly form by using separate modules. The snapshot of the production resource stored at the lower level is the BOM, the list of devices, and the scheduling target [15]. In general, there are user friendly data structure forms and machine friendly data structure forms mainly. User friendly data forms are stored in text files for ease of generation and modification. The system architecture is shown in Fig. 2.

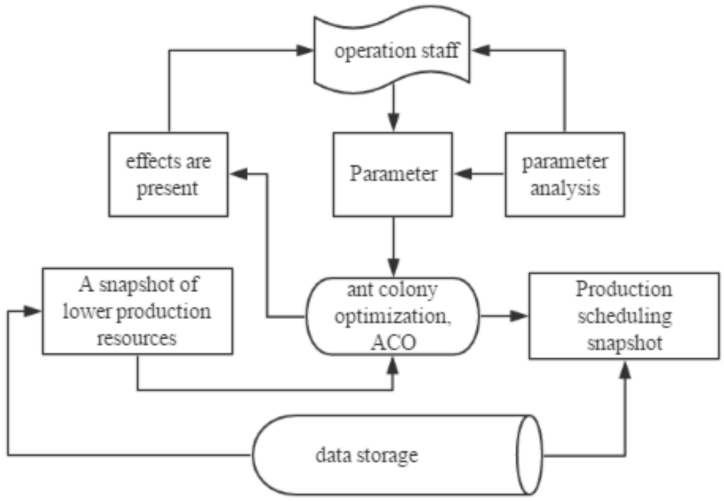

Fig. 2. Ant colony algorithm validation architecture design

3. Result analysis and discussion

The mechanical manufacturing process of the gear shaft of the company A was taken as an example. Pheromone is the most important parameter factor in ant colony algorithm. The snail ants give birth to inherent information that is used to communicate with each other in search of the shortest path during the cruise. According to the relationship between the pheromone and the processing primitives, the route matrix is shown in Table 1.

Then, adaptive route length, iteration number and the evaluation of enterprise's benefit were obtained by simulation of company A' gear shaft mechanical process manufacturing route. The number of ants was set to 50. The data is shown in Table

2.

Table 1. Part of the route matrix

Processing primitives	1	2	3	4	5
1	0	1	1	0	0
2	1	1	0	1	1
3	1	0	0	1	1
4	1	1	0	0	1
5	0	1	0	1	1

Table 2. Variable value of mechanical process route

Serial number	Adaptive route length	Iteration number	Benefit evaluation (y)
1	26.9	76	88.57
2	28.6	22	84.21
3	30.5	15	79.22
4	32.6	8	73.45
5	35.1	5	70.78

It can be seen from Table 2 that the global search capability was related to the number of mother ants directly. The larger mother ant number was a good thing to improve the global search ability, but it would reduce the convergence speed of the algorithm. If the complexity of the problem was high, the number of mother ants was relatively small. The path length of mechanical process was related to the number of iterations based on adaptive ant colony. The more of the number of iterations, the higher the degree of optimization of the manufacturing route was. Moreover, as far as the evaluation of enterprise interests, the shorter of the manufacturing process, the more effective the production efficiency would be, and the benefit of the enterprise would increase. When the number of iterations was as high as 76, the adaptive mechanical manufacturing route was 26.9, and the benefit evaluation was 88.57.

The results of the optimization of the mechanical manufacturing process must be validated to avoid the effects of non-quantifiable factors in the manufacturing process. Adaptive ant colony algorithm and the correctness of production scheduling problem in solving manufacturing environment with complicated process route were verified. Firstly, the same parameter runs, including random number seeds, were used to validate the system. The correctness of the algorithm was verified by two scheduling objectives, namely, the shortest processing time and the maximization of enterprise benefits. And the correctness of the algorithm was verified when the work center had an expected downtime. Supposing that the design process manufacturing route of company A is shown in Fig. 3: (letters represent the chain of operations needed for this process, and data after letters represent assembly quantities).

The enterprise manufacturing work center table is set out as follows, and this table applies to the production flow of such process products:

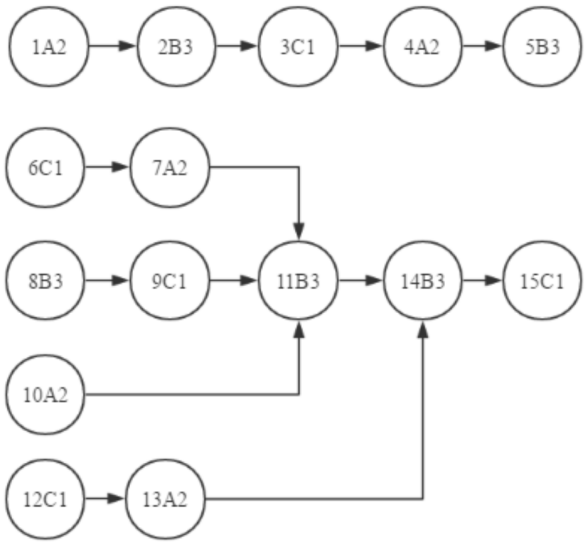

Fig. 3. Process route

Table 3. Work center table

Work center number	Process chain	Processing rate	Unit cost	Predictable downtime
1	A	800	400	NULL
2	B	200	300	NULL
3	B	300	300	NULL
4	C	400	200	NULL
5	C	500	300	NULL
6	C	600	400	NULL

The order form is shown in Table 4.

Table 3. Work center table

Order number	Final process	Batch	Delivery time	Liquidated damages
1	5	600	100	200
2	15	400	100	300

The production cost and the default cost were used as the basis of the enterprise benefit evaluation, and the calculation of the default cost was simplified as the tardiness time multiplied by the liquidated damages rate. The optimization results

are shown in Fig. 4.

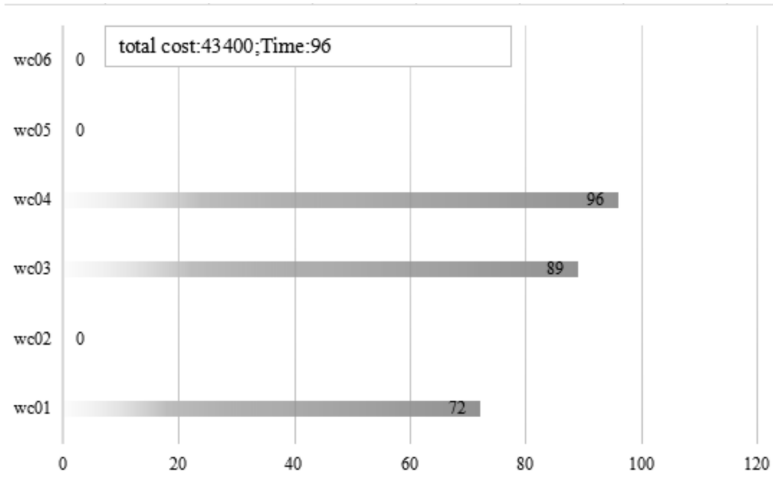

Fig. 4. Optimization results

The scheduling results show that the completion time of the last process was 96. No breach occurred at this time, and the total cost 43400 was the direct production cost. The order delivery time was revised to 70. The optimization results are shown in Fig. 5.

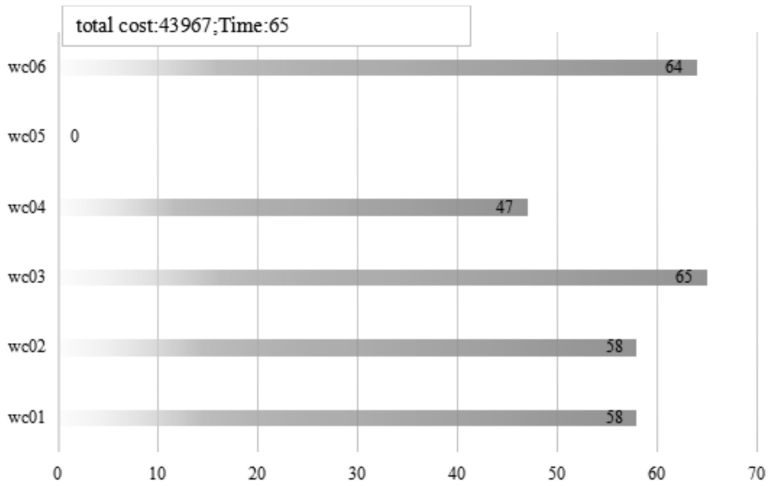

Fig. 5. Optimization results that can be met by order times

When the delivery time was 70, the total cost was 43967, which was greater than the previous scheduling result of 43400. This is because the time will cause the cost of default, and the algorithm arranges a part of the process to the work center with higher production cost. Although this will increase the cost of direct production, it also avoids the occurrence of breach of contract so that the total cost

is lowest. That is to say, the interests of enterprises are maximized. Therefore, the ant colony algorithm can solve the production scheduling problem with multiple optimization objectives, complex process routes and environments defined by this example effectively. Ant colony algorithm is better for the optimization of mechanical process route.

4. Conclusion

As the link of product design and manufacture, process design affects the machining efficiency and quality of products to a great extent. However, there is diversity in process design due to the characteristics of parts structure, manufacturing accuracy, processing methods and manufacturing resource selection. Therefore, how to choose the best manufacturing route for the various processing routes for product manufacturing to save costs and improve manufacturing quality is particularly important. The decision making problem of mechanical process manufacturing is transformed into the optimal ordering problem of manufacturing resource substitution rate under the constraints of processing sequence and manufacturing resource. The application of adaptive ant colony algorithm in the optimization of machine process manufacturing route was analyzed in this paper. Firstly, the background and the present situation of the optimization of the mechanical manufacturing route were introduced, and the bionic ant colony algorithm was analyzed. Secondly, the principles of ant colony algorithm, the optimization of mechanical process route based on adaptive ant colony algorithm, the optimization of mechanical manufacturing scheduling design and verification method were analyzed. Finally, the optimized design was carried on by taking the gear shaft mechanical processing route of Company A as the example. And the route verification analysis was carried out based on its manufacturing scheduling factors. Experiments show that ant colony algorithm can optimize the design of mechanical manufacturing process according to the manufacturing process factors, and improve the operation and production efficiency of enterprises.

References

[1] H. Shi, Y. Dong, L. Yi, D. Zheng, H. Ju, E. Ma, W. Li: *Study on the route optimization of military logistics distribution in wartime based on the ant colony algorithm.* Computer and Information Science *3* (2010), No. 1, 139–143.

[2] J. F. Wang, X. Wu, X. Fan: *A two-stage ant colony optimization approach based on a directed graph for process planning.* International Journal of Advanced Manufacturing Technology *80* (2015), Nos. 5–8, 839–850.

[3] T. Zhang, W. A. Chaovalitwongse, Y. J. Zhang, P. M. Pardalos: *The hot-rolling batch scheduling method based on the prize collecting vehicle routing problem.* Journal of Industrial and Management Optimization *5* (2009), No. 4, 749–765.

[4] P. Vijayalakshmi, S. A. J. Francis, J. A. Dinakaran: *A robust energy efficient ant colony optimization routing algorithm for multi-hop ad hoc networks in MANETs.* Wireless Networks *22* (2016), No. 6, 2081–2100.

[5] M. Tong, Y. Chen, F. Chen, X. Wu, G. Shou: *An energy-efficient multipath routing algorithm based on ant colony optimization for wireless sensor networks.* Interna-

tional Journal of Distributed Sensor Networks *11* (2015), No. 6, Article ID 642189, 1–12.

[6] J. Li: *Logistics distribution route optimization based on chaotic cuckoo algorithm.* Advanced Materials Research *1049–1050* (2014), 1681–1684.

[7] H. Zhang: *Closure to "Ant colony optimization for multimode resource-constrained project scheduling" by Hong Zhang.* Journal of Management in Engineering *28* (2012), No. 2, 150–159.

[8] Q. Fan, X. X. Nie, K. Yu, X. L. Zuo: *Optimization of logistics distribution route based on the save mileage method and the ant colony algorithm.* Applied Mechanics and Materials *448–453* (2014), 3683–3687.

[9] Q. Yi, C. Li, X. Zhang, F. Liu, Y. Tang: *An optimization model of machining process route for low carbon manufacturing.* International Journal of Advanced Manufacturing Technology *80* (2015), Nos. 5–8, 1181–1196.

[10] O. Quevedo-Teruel, E. Rajo-Iglesias: *Application of ant colony optimization based algorithm to solve different electromagnetic problems.* EuCAP 2006: proceedings of the European Conference on Antennas and Propagation, 6–10 November 2006, Nice, France.

[11] C. Y. Liu, J. Yu: *Multiple depots vehicle routing based on the ant colony with the genetic algorithm.* Journal of Industrial Engineering and Management *6* (2013), No. 4, 1013–1026.

[12] D. K. Sharma, R. K. Jana: *A hybrid genetic algorithm model for transshipment management decisions.* Wireless Networks *122* (2009), No. 2, 703–713.

[13] N. A. M. Sabri, A. S. H. Basari, B. Husin, K. A. F. A. Samah: *The utilisation of Dijkstra's algorithm to assist evacuation route in higher and close building.* Journal of Computer Science *11* (2015), No. 2, 330–336.

[14] R. Kohad, V. Ahire: *Application of machine learning techniques for the diagnosis of lung cancer with ant colony optimization.* International Journal of Computer Applications *113* (2015), No. 18, 34–41.

[15] M. Yousefikhoshbakht, N. Malekzadeh, M. Sedighpou: *Solving the traveling salesman problem based on the genetic reactive bone route algorithm whit ant colony system.* International Journal of Production Management and Engineering *4* (2016), No. 2, 65–73.

Received August 7, 2017

Acta Technica *62* No. 2B/2017, 341–350

Hierarchical protection mechanism of network information based on computer security model algorithm terminal

Yue Peng[1], Zhao Limin[1]

Abstract. With the continuous development of computer communication technology, people's life, work and other aspects have undergone major changes, and have become more and more dependent on the network information. At the same time as the network information continues to increase, the increasing demand for its security has become the focus of its research. Therefore, the research and implementation of hierarchical protection mechanism for network information based on computer security model algorithm terminal was proposed. Through the construction of the computer security model, the computer terminal network information was hierarchized and protected. The experimental results show that the protection mechanism can effectively classify the network information and effectively protect the network information.

Key words. Computer security model, algorithm terminal, network information level, protection mechanism.

1. Introduction

With the continuous development and popularization of computer communication technology, people's lives, work and other aspects have been inseparable from the network, and the network has brought convenience to people's lives and work. However, with the continuous increase of network information, its security problems become increasingly prominent. In order to be able to provide users with better security services, the concept of security platform has been widely extended and widely used. The protection measures are mainly for the protection of the platform outside, if the back of the platform is entered, there is no difference in its grade [1]. It is precisely because of this, that seemingly safe protection is actually very fragile, once someone enters the security platform inside, its security does not make any sense. Therefore, how to protect the network confidence has become a hot topic in

[1]College of Management, Xinxiang Medical University, Xinxiang, Henan, China, 453003

the field of computer and the community [2]. Our country has a large population, although the level of computer development is still a certain distance from the international level, China's Internet users have reached 100 million, ranking first in the world. This also means that people enjoy the convenience and favorable information brought about by the network, at the same time, the demand for the protection of network information is growing, so China needs to strengthen step in this respect.

2. State of the art

Since the advent of the information age, all countries in the world have strengthened their investment in network information security, and have continuously researched and widely applied the technology of network information security protection, so that a series of security concept and corresponding protection methods have been formed, and a number of network information security management and protection systems have been established. For example, the United States has proposed Protection of Critical Infrastructure in the United States, and has carried out a number of organizations for the establishment of information security, including the National Information Security Committee, the Chief Information Officer Committee and the Federal Computer Event Response Action Group and other more than 10 national institutions and organizations [3]. Subsequently, the US National Security Agency developed the Information Security Technology Framework based on the actual situation and future needs, and proposed the "deep defense strategy" concept, determined the goals of network and infrastructure defense, as well as the defense of environmental defense and supportive infrastructure [4].

Our country started relatively early in the construction of network information security. The state has made great efforts to support and promote the construction of this aspect. After several years of efforts, our country has achieved relatively good results, and the network information security technology has been rapidly developed and applied [5]. For example, the Regulations of the People's Republic of China on Computer Security Protection formulated by the State Council of the People's Republic of China stipulates that the computer information system should carry out security grade protection, and carry out the management through the security of network information classification standards and classification management related measures, in addition, the Ministry of Public Security in conjunction with relevant departments should formulate the standards for the classification of grades and the measures for their administration. At the same time, the Opinions of the National Informatization Leading Group on Strengthening Information Security Work forwarded by the general office of the Central Committee and the general office of the State Council clearly illustrates the importance of network information management, information classification and related management measures [6].

2.1. Methodology

Hierarchical protection of network information is the rational classification protection and the guidance of classification for the basic network information and

important information systems related to the national economy and the people's livelihood according to the degree of importance and actual demand. The phased implementation and security information system can secure the normal operation of information and improve the comprehensive ability of information security protection, so that national security can be guaranteed, social stability and sustainability can be maintained, and the construction of information technology can be carried out in a benign way [7]. Therefore, China has conducted a unified management standard and technical standard for the hierarchical protection of network information, and has implemented an effective hierarchical protection mechanism for the information system through the organization of citizens, legal persons and institutions [8]. According to the provisions of Guidelines for the Classification of Computer Information System Security Protection, the information security level can be divided into five levels, that is, the first level is the user's independent protection level, which is primarily the way of users to protect resources. The second level is the level of system audit protection, that is, the security protection mechanism of this level is to provide technical support for improving the ability of users to protect themselves, especially in the ability to access audits [9]. The third level is the security tag protection, that is, the mandatory access control for visitors and interviewee is increased on the basis of the second level protection capability, so as to access the permissions set through different tags. The fourth level is structural protection, which extends the protection of the previous three levels to all visitors and interviewee, which has a strong resistance to penetration [10]. The fifth level is access verification, that is, the arbitration of the visitor's ability to access is increased on the basis of the fourth level of protection, which has a strong resistance to penetration. Fig. 1 shows the computer network information level protection mechanism publicity map.

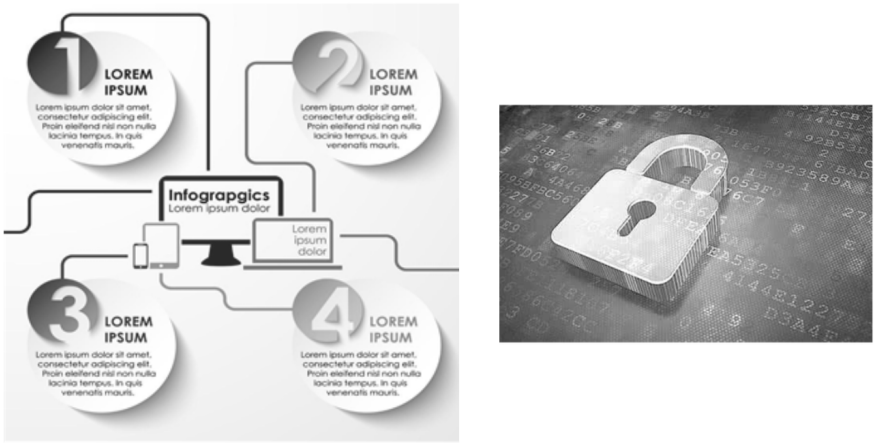

Fig. 1. Propaganda diagram of the computer network information level protection mechanism

In the process of building the network information level protection mechanism based on the computer security model algorithm terminal, for the terminal security evaluation, it is necessary to classify the information security according to the

test results in each structure, so as to realize the safe use of different security level requirements [11]. Therefore, the author chooses the support vector machine classification algorithm to construct the terminal security classification model. The ultimate goal is to realize the objective and accurate classification of terminal security level information. According to the literature, it is known that the support vector machine belongs to a two-class algorithm, which is obtained by super-plane acquisition through a high-dimensional space, and the sample is divided into two categories by the minimum error probability [12]. Support vector machine has the characteristics of global optimization, simple structure and easy popularization in the construction of terminal security classification model, especially it has obvious advantages in solving small samples, nonlinear recognition and high dimensional pattern recognition [13]. The model construction of the support vector machine architecture is carried out: firstly, sample data set training is carried out in a space of a given feature, that is, $T = \{(x_1, y_1), (x_2, y_2), ..., (x_N, y_N)\}$, $x_i \in \chi = R^n$ in the formula and $y_i \in \gamma = \{+1, -1\}, i = 1, 2, 3, ..., N$. Then, the model is constructed and the constrained optimization problem is solved, as shown in equation (1):

$$\begin{array}{l} \min\limits_{\alpha} \frac{1}{2} \sum_{i=1}^{N} \sum_{j=1}^{N} \alpha_i \alpha_j y_i y_j (x_i \times x_j) - \sum_{i=1}^{N} \alpha_i, \\ \text{s.t. } \sum_{i=1}^{N} \alpha_i y_i = 0, \\ \alpha_i \geq 0, \ i = 1, 2, ..., N. \end{array} \tag{1}$$

By combining the theorem with the optimal solution $\alpha^* = (\alpha_1, \alpha_2, ..., \alpha_N)$in equation (1), the calculation is carried out, and the results are shown in formula (2) and formula (3):

$$w^* = \sum_{i=1}^{N} \alpha_i^* y_i x_i \,, \tag{2}$$

$$b^* = y_i - \sum_{i=1}^{N} \alpha_i^* y_i (x_i \cdot x_j) \,. \tag{3}$$

In combination with the above results, the hyperplane needed by the model can be obtained, as shown in equation (4):

$$w^* \cdot x + b^* = 0 \,. \tag{4}$$

So, the decision function can be drawn as shown in equation (5):

$$f^*(x) = sign(w^* \cdot x + b^*) \,. \tag{5}$$

According to the characteristics of the support vector machine, the author divides the security of the network information level of the computer terminal into four levels. So the model of this part chooses the hierarchical model to construct the classification. In the model structure, the decision function in the ith layer structure is expressed as $f^{(i)}(x)$, and when $f^{(i)}(x) = 1$, the $y = i$ sample points can be separated. When $f^{(i)}(x) = -1$, it will enter the next level of the decision. Figure 2

shows the module's hierarchical structure.

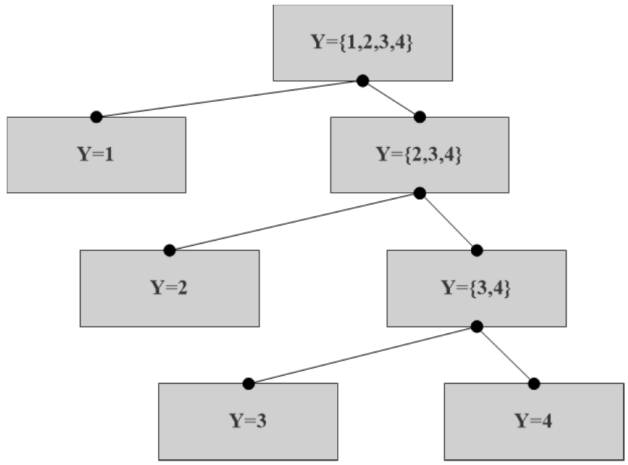

Fig. 2. Hierarchical diagram

As can be seen from the hierarchical structure diagram, in the first layer, the sample is divided into 1 class, and the division of the grade 2, 3, 4 is performed, so the new sample set is

$$T^{(1)} = \left\{ \left(M_1, y_1^{(1)} \right), \left(M_2, y_2^{(1)} \right), ..., \left(M_N, y_N^{(1)} \right) \right\},$$

$$T^{(2)} = \left\{ \left(M_1, y_1^{(2)} \right), \left(M_2, y_2^{(2)} \right), ..., \left(M_{N_1}, y_{N_1}^{(2)} \right) \right\},$$

$$T^{(3)} = \left\{ \left(M_1, y_1^{(3)} \right), \left(M_2, y_2^{(3)} \right), ..., \left(M_{N_1}, y_{N_2}^{(3)} \right) \right\}.$$

The following is the initial optimization problem, with the first layer as an example. In the sample set of the first layer

$$\begin{cases} y^{(1)} = 1, y = 1; \\ y^{(1)} = -1, y \in \{2, 3, 4\}; \end{cases} , i = 1, 2, ..., N.$$

The structural optimization problem is shown in equations (6) and (7):

$$\min_{\alpha} \frac{1}{2} \sum_{i=1}^{N} \sum_{j=1}^{N} \alpha_i \alpha_j y_i y_j \left(x_i \bullet x_j \right) - \sum_{i=1}^{N} \alpha_i , \tag{6}$$

$$\text{s.t.} \sum_{i=1}^{N} \alpha_i y_i = 0, \alpha_i \geq 0, i = 1, 2, ..., N . \tag{7}$$

And then, the optimal solution is $\alpha^{(1)} = \left(\alpha_1^{(1)}, \alpha_2^{(1)}, ..., \alpha_N^{(1)} \right)^T$ and $w^{(1)} = \sum_{i=1}^{N} \alpha_i^{(1)} y_i x_i$ is calculated, and the positive component of $\alpha^{(1)}$ is chosen to cal-

culate $b^{(1)} = y_j - \sum_{i=1}^{N} \alpha_i^{(1)} y_i \left(x_i \cdot x_j\right)$. Then, the decision function of the required hyperplane $w^{(1)} \cdot x + b^{(1)} = 0$ can be obtained, as shown in equation (8)

$$f^{(1)}(x) = \operatorname{sign}\left(w^{(1)} \cdot x + b^{(1)}\right). \tag{8}$$

So, when $f^{(1)}(M_i) = 1$, the network information security level is 1, when $f^{(1)}(M_i) = -1$, the network information security levels are 2, 3, 4, which then enter the next level of the decision. After entering the second and third layers, the decision functions are obtained by the above methods, as shown in equations (9) and (10):

$$f^{(2)}(x) = \operatorname{sign}\left(w^{(2)} \cdot x + b^{(2)}\right), \tag{9}$$

$$f^{(3)}(x) = \operatorname{sign}\left(w^{(3)} \cdot x + b^{(3)}\right). \tag{10}$$

Then, the network security level is judged and divided into the sample set.

In the aspect of the implementation of computer security model terminal network information level protection mechanism, the author believes that the implementation of module multilevel security mechanism mainly involves the following three aspects: the first is the access control decision module, which mainly marks the subject and object information and checks the information security strategy, accesses the request information of the resource access and the related security policies according to the subject and object, so as to provide corresponding ruling results for access control enforcement [14]. The second is the access control execution module, that is, according to the decision result of the upper module, it performs or rejects the access to the subject and object. In addition, the implementation of identity authentication module is needed. The authentication module mainly validates the users who use the information through the trusted hardware device to obtain the information authentication whose identity and user rights are consistent. At the same time, during the verification process, the system will perform mandatory access control, the provider's markup, and permissions [15]. The third is the security agent module, which mainly communicates with each other through the need of Windows node system and the security management control center, including the subject and object marking synchronization information, security policy download, audit information submission and other information. Table 1 shows the function index of Windows node subsystem.

3. Result analysis and discussion

This paper studied the implementation of the network information level protection mechanism based on the computer security model algorithm terminal. According to the above, the network information level security model was constructed. The model of the network information level protection mechanism was tested. Therefore, according to the principle of network information level protection, the model in this test first controlled the user's access behavior in the network communication on the

basis of the rule. Among them, the subject in the system was the user, the object was the keyword. For subject of different levels, there was a difference in the right to use the object, so subjects with lower security levels had more restrictions on network communications than subjects with higher security levels. Thus, subjects with different levels of security could only use objects that were consistent with their security levels. If the subject had unauthorized use of the process of using the network information, the system would handle violations according to relevant regulations. The author divided the objects into five levels in the system, which were open, secret, confidential, top secret and prohibited. The security intensity of the five grades was: public <secret <confidential <top secret <prohibited. Therefore, the security level for the main body was divided into four levels, namely, open, secret, confidential and top secret. Table 2 shows the control authority of the subject access object.

Table 1. Function index of Windows node subsystem

Index type	Index content
Mark	It provides two-dimensional markings to mark the confidentiality level, integrity level, and security class of the entities in the system. The tagged objects include users in the system, all files and processes, ensuring that the tagged information is accurate, complete, and consistent throughout the lifecycle.
Forced access control	The mandatory access control mechanism implements the same security policy as the system two-dimensional security model, which can control all the operations of the process on the file. The mandatory access control mechanism should have some flexibility to combine the application process to check the behavior of processes that do not conform to the system's mandatory access control policies. This ensures that those that meet business needs without compromising system security can be enforced; mandatory access control mechanisms are always valid and will not be bypassed.
Identification	It can provide a secure identity authentication mechanism based on trusted hardware devices to ensure that unauthorized users cannot access system information.

Table 2. Subject access object control authority

Subject/object	Public	Secret	Confidential	Top secret	Prohibit
Public	allow	prevent	prevent	prevent	prevent
Secret	allow	allow	prevent	prevent	prevent
Confidential	allow	allow	allow	prevent	prevent
Top secret	allow	allow	allow	allow	prevent

In the case of the classification of the sample set, the security level of the sample set also needed to be divided according to the above-mentioned subject authority, in which the network information of the public level could be divided when the sample

set was divided. Therefore, this experiment mainly divided four levels of secret, confidential, top secret and forbidden; secret was level 1, confidential was level 2, top secret was level 3, forbidden was level 4. Therefore, the three threshold values were set to the positive number, that was, η_1, η_2, η_3 and $\eta_1 = 25,\ \eta_2 = 50,\ \eta_3 = 75$. According to the three thresholds set, the four diversity points of the terminal were divided, symbol y representing the level and $y \in \{1, 2, 34\}$, then the available expression of y was:

$$\begin{cases} y = 1,\ 0 \leq Y \leq Y_1, \\ y = 2,\ Y_1 \leq Y \leq Y_2, \\ y = 3,\ Y_2 \leq Y \leq Y_3, \\ y = 4,\ Y_3 \leq Y \leq 100. \end{cases}$$

Here, the numbers 1, 2, 3 and 4 are the corresponding levels; the higher the security level was, the higher the security was. In this paper, by testing N computer network terminals 1 time, the resulting test results could be expressed with $M_1, M_2, ..., M_N$, and each test project was composed of various types of test items, there were all out of 100 points; the higher the score was, the better the security was, which could be expressed by $M_i = [m_1, m_2, ..., m_N]^{\mathrm{T}}$, $0 \leq m_i \leq 100$. At the same time, the total score for each calculation was expressed as $\overrightarrow{Y} = \overrightarrow{M_i^{\mathrm{T}}} \cdot \overrightarrow{H}$. Therefore, according to the above experimental process, the network information terminal of 55 known results was tested on the network information security protection mechanism. The test results are shown in Table 3. From the data in the table, it can be seen that the computer security model algorithm constructed in this paper can differentiate the hierarchical protection of network information. The result of the differentiation is consistent with the actual situation. Therefore, it can be proved that the network information level protection mechanism based on the computer security model algorithm terminal can effectively divide and classify network information and protect it effectively.

Table 3. Test results of network information security mechanism of network information terminal

Subject/object	Public	Secret	Confidential	Top secret	Prohibit
Public	5	7	2	3	1
Secret	6	9	3	0	2
Confidential	1	3	5	1	0
Top secret	0	1	1	3	2

As shown in Fig. 3, the statistical results of the effectiveness of the hierarchical protection mechanism for 55 network information terminals were presented. It can be seen from the figure that the network information level protection mechanism based on the computer security model algorithm terminal can achieve almost 100 % protection requirements, especially for information protection with high security level. But for the information protection mechanism with slightly lower security level, its efficiency is weak, which needs further improvement and analysis.

In conclusion, the network information level protection mechanism based on the computer security model algorithm terminal can effectively classify the computer

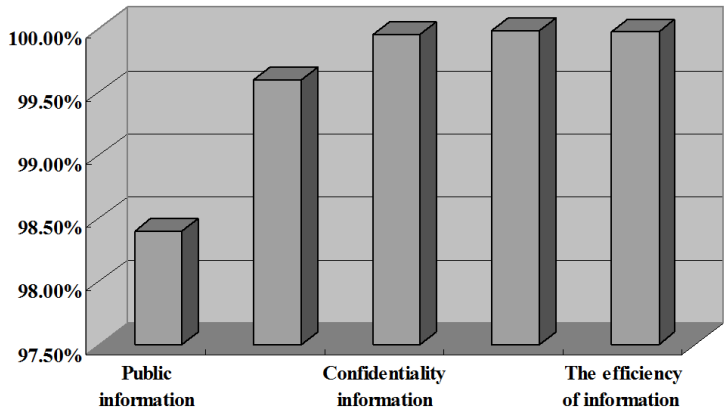

Fig. 3. Statistical results of the effectiveness of the hierarchical protection mechanisms for 55 network information terminals

network terminal information and protect it according to the security level of the network information. At the same time, the protection mechanism also divides users into different grades and uses different request limits for network users in different grades, so as to protect different levels of network information. And the experimental results show that the network information level protection mechanism based on the computer security model algorithm terminal is effective in network information protection. However, the protection of network information with low security level needs to be improved.

4. Conclusion

Network information plays an important role in people's life and work, and people depend more and more on it. At the same time, the increasing of network information also makes its security problems increasingly prominent. How to improve the security of network information has become the focus of the computer security model. In this paper, through the construction of computer security model, the network information security level division model was constructed according to the actual situation, and the user's level and the security level of the network information were divided. Through the computer terminal test, it can be found that the computer security model constructed in this paper can effectively divide the network information, and optimize the structure of the model to improve the efficiency of information classification. In addition, the user's level division can effectively protect the network information, users of different grades open corresponding network information, thus reducing the request rate of network information with high security level, thereby improving the protection of network information. However, it can be seen from the test results that the protection of low-security network information is not in place, in certain probability, network information cannot be protected, which needs further improvement.

References

[1] S. Kajioka, N. Wakamiya, H. Satoh: *Implementation and evaluation of multichannel multi-interface routing mechanism with QoS-consideration for ad-hoc networks.* EURASIP Journal on Wireless Communications and Networking (2010), Article ID No. 4074927, 1–14.

[2] K. Gopalakrishnan, R. V. Uthariaraj: *Acknowledgment based reputation mechanism to mitigate the node misbehavior in mobile ad hoc networks.* Journal of Computer Science *27* (2011), No. 8, 1157–1166.

[3] M. Ahn, J. Kwon: *Design and implementation of ontology-enabled context-aware platform in ubiquitous environment.* Angewandte Makromolekulare Chemie *86* (2006), No. 1, 203–213.

[4] T. E. Carroll, D. Grosu: *An incentive-based distributed mechanism for scheduling divisible loads in tree networks.* Journal of Parallel and Distributed Computing *72* (2012), No. 3, 389–401.

[5] D. V. Prieto, L. R. I. Quiñones, D. G. Ramírez, G. Z. Fuentes, P. T. Labrada, H. O. Pérez, V. M. Montero: *Impact of the information andc ommunication technologies in education and new paradigms in the educational approach.* Revista Cubana de Educación Médica Superior *25* (2011), No. 1, 95–102.

[6] L. Caviglione, M. Gaggero, J. F. Lalande, W. Mazurczyk, M. Urbański: *Seeing the unseen: Revealing mobile malware hidden communications via energy consumption and artificial intelligence.* IEEE Transactions on Information Forensics and Security *11* (2016), No. 4, 799–810.

[7] M. Alsaleh, P. C. van Oorschot: *Revisiting network scanning detection using sequential hypothesis testing.* Security and Communication Networks *5* (2012), No. 12, 1337–1350.

[8] P. Szwed, P. Skrzyński: *A new lightweight method for security risk assessment based on fuzzy cognitive maps.* International Journal of Applied Mathematics and Computer Science *24* (2014), No. 1, 213–225.

[9] P. Zand, S. Chatterjea, K. Das, P. Havinga: *Wireless industrial monitoring and control networks: The journey so far and the road ahead.* Journal of Sensor and Actuator Networks *1* (2012), No. 21, 123–152.

[10] Y. L. Chong, K. B. Ooi: *Collaborative commerce in supply chain management: A study of adoption status in Malaysian electrical and electronic industry.* Journal of Applied Sciences *8* (2008), No. 21, 3836–3844.

[11] M. S. Babu: *Operating systems-functions, protection and security mechanisms.* Resonance – Journal of Science Education *7* (2002), No. 4, 60–66.

[12] A. Nafarieh, S. Sivakumar, W. Robertson, W. Phillips: *SLA-based time-aware provisioning mechanisms in shared mesh protected optical networks.* The Computer Journal *58* (2015), No. 8, 1717–1731.

[13] Y. Jian, s. Chen, Z. Zhang, L. Zhang: *A novel scheme for protecting receiver's location privacy in wireless sensor networks.* IEEE Transactions on Wireless Communications *7* (2008), No. 10, 3769–3779.

[14] J. Sprague, D. Clements, T. Conlin, P. Edwards, K. Frazer, K. Schaper, E. Segerdell, P. Song, B. Sprunger, M. Westerfield: *The zebrafish information network (ZFIN): The zebrafish model organism database.* Nucleic Acids Research *31* (2003), No. 1, 241–243.

[15] Y. Jiang, J. Zhao: *An empirical research of the creative process of collaborative e-business capability in service industry.* International Journal of Networking and Virtual Organisations *10* (2012), No. 1, 73–870.

Received August 7, 2017

Acta Technica *62* No. 2B/2017, 351–362

Logistics service transformation and its system construction in colleges and universities based on the "Internet plus"

Chen Chaochao[1]

Abstract. With the continuous development of computer technology and network technology, more and more people hope to establish a new logistics service model that can make full use of the Internet. In order to study the new logistics service mode, in this paper, with the university logistics service as an example and the method of literature research, sample analysis and other methods, the information technique was introduced to construct the "Internet plus logistics system"; the university logistics service mode based on Internet plus new services and micro video resources as the core was constructed. The final experimental results show that the new logistics service mode can promote the transformation of traditional logistics system upgrade, improve the management efficiency, and innovate the education service industry state, so it is conducive to improve the quality of university logistics service.

Key words. Internet plus, university logistics, strategic transformation.

1. Introduction

Pony Ma, a pioneer of Internet technology application and the chairman and CEO of Tencent, put forward the "Internet plus" strategy at the National People's Congress in 2015. In simple terms, "Internet plus" strategy is to use the Internet platform, information and communication technology, and big data to combine the Internet with all walks of life, including traditional industries, so as to create a new ecology in the new field.

"Internet plus university logistics system can fully optimize the optimization and integration function of Internet in the allocation of logistics resources, so as to realize the rational allocation of resources and the resource sharing. It can integrate the innovative achievements of the Internet into management and services, construct the digital work platform, build good and efficient management teams, form a mechanism

[1]Logistics Department of China West Normal University, Nanchong, Sichuan, China, 637000

with scientific decision, fine management fine, and quick response, and improve the management and service level of education. In short, the Internet work is the comprehensive concentration of pain and fatigue in everyone's eyes. According to previous experience, the logistics staffs rely on manual form, so not only the labor is dense and heavy, but also the efficiency is relatively low. The traditional mode of logistics management cannot meet the growing demands of the contemporary teachers and students for food, shelter, transportation, study, purchase, medical treatment, water conservancy and electricity, greening environment and so on. The logistics department must quickly take advantage of "Internet plus" and the Internet, big data, e-commerce technology and platform to carry out a full range of services, so as to truly respond to demands of public and improve service satisfaction. Therefore, the construction of "Internet plus university logistics" system is of great significance.

2. State of the art

As the "Internet plus" in today's society is becoming increasingly popular, many foreign experts and scholars have carried out comprehensive studies on specific Internet plus. Based on the institutional drawbacks of many colleges and universities over the years, some people have put forward the practice of the service system of "big logistic view" in colleges and universities [1]. Among them, the two stage model can simply and completely present the characteristics of the traditional university logistics model. With the increasing demands of the group, the model can no longer satisfy the needs of the modern people [2]. After research and comparison, the logistics service and management mode of universities in China and America were compared. By comparing the logistics services of Chinese universities and the rear service of American universities, the gap between the logistical services of Chinese universities and colleges was found [3].

At present, China's colleges and universities are faced with many "bottleneck" problems that need to be broken through in the reform of social reform. Especially, the dilemma of logistics service management caused by the pattern of individual schools needs to be solved urgently. In addition, the improvement of service quality, low work efficiency, scientific and reasonable performance distribution also need innovation policy urgently [4]. In the mobile Internet, the repaid development of cloud computing, big data, networking, new media as the representative of the information technology has undoubtedly become the bottleneck of logistics cracking in Chinese universities, which is also a key factor to realize the transformation of traditional logistics to modern logistics [5].

2.1. Methodology

The daily operation of today's society is more and more inseparable from the Internet. The report shows that as of December 2015, China university computer usage rate, the proportion of computer usage in Chinese universities, the proportion of Internet usage, and fixed broadband access ratio increased by 4.8, 10.3 and 8.9 percentage points, respectively, reaching 95.2 %, 89 % and 86.3 % [6]. The total

number of Chinese websites was 4 million 230 thousand, which was 880 thousand higher than in 2014, and the annual growth rate reached 26.3 %. At the same time, the number of Chinese web pages has exceeded 200 billion for the first time [7]. Chinese colleges and universities have been increasingly using Internet tools to carry out communication, information acquisition and distribution, internal management and other aspects of work, which has laid a good foundation for the "Internet plus application".

Chairman Yu Yang of the domestic well-known consulting firm Yiguan International first proposed the concept of "Internet plus" in public. On November 14, 2012, Yu Yang first proposed the "Internet plus" in the fifth session of the mobile Internet Expo, and carried out the related interpretation: the nature of the "mobile Internet" can't do without "Internet plus". In the future, "Internet plus" should be a way for our industry's current products and services to achieve promotion and sales through the network, and to combine the network platform and entity platform [8]. The board of directors of the Tencent chairman Ma Huateng has carried forward the concept of "Internet plus". Ma Huateng proposed that: the integration of the Internet and traditional industries represents a need for the market now, and in the case of multi resources and multi environments, it can improve various industries [9].

With the development of a series of Internet technologies, they have been applied to daily life and teaching practice. Figure 1 show the present situations of the Internet application in the university logistics service in several universities for the past ten years.

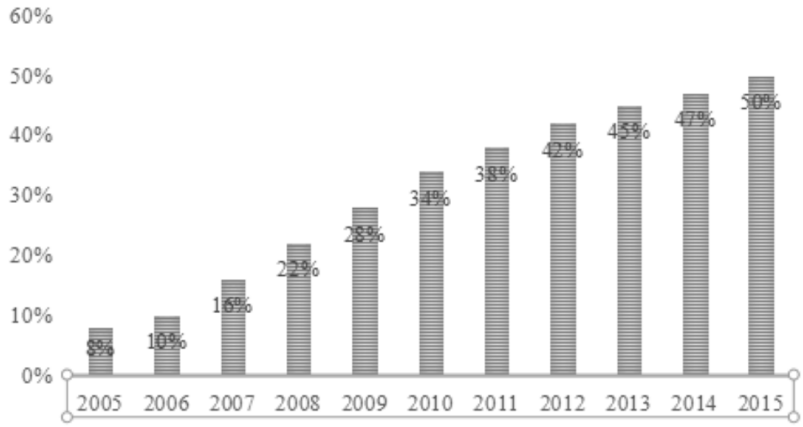

Fig. 1. Development of situation in the Internet application in the university logistics service at several universities for the past ten years

According to Fig. 1, it can be seen that in the past ten years, the development of Internet application in university logistics is showing a benign growth. In 2005, Internet applications accounted for only 8 % of logistics services. Within ten years, the proportion of Internet applications in late service has reached 50 % [10]. During the ten years, it has maintained a growth rate of 2 % to 6 % per year.

"Internet plus" is the integration of the two upgrade, and it regards the Internet as the core feature of informatization development, and the key factor is innovation. Only innovation can make this "+" really valuable and meaningful. Internet plus logistics service mode gives the autonomy to the hand of the party being served: under the support of information technology, service party can use a party to provide services by making services, media services, software and service channels and a series of service resources to accept service independent and complete logistics support staff; and students can use activities of Internet plus service with high efficiency, high quality and low interactive service to solve problems encountered in life, learning, and work, with the realization of intelligence [11]. In brief, logistics services have been integrated into the daily life of students and teachers, and the disadvantages of the fixed time of traditional logistics services have been changed to services at any time. Its comparisons with the traditional logistics service are shown in Table 1.

Table 1. Comparative analysis of traditional logistics and Internet plus logistics

	Traditional logistics	Internet plus logistics
Teaching staff	The process is inefficient and material is tedious	Quick, convenient and efficient
Student	Unable to choose independently	Self-choice
Service time allocation	Working hours of service personnel	Non-working hours for service personnel
service content	Areas of human services that can be reached	Human and computer services
Application of service means	Artificial services	Internet intelligent service
Service evaluation	Paper test	Multidimensional evaluation

The mobile phone client APP in the intelligent Internet plus post service should not be ignored. As a third-party smartphone, few people use it in logistics. In this field, Ocean University of China has made a positive exploration, and it has the courage to try and come out of a new path. APP has the advantage of being more convenient, quick and intelligent, and it can give people a new experience of mobile terminals. It uses the same database as the digital logistics lobby website and the logistics WeChat public number, so all the information is displayed synchronously, which can avoid duplication and omission, and set up the "trinity" logistics online service pattern of universities. In the maintenance declaration, after entering the APP repair module, according to the prompts, teachers and students can enter the corresponding information. Upon completion of the submission, according to the project category, the system will automatically send information to the corresponding maintenance staff on the mobile phone, and then the staff can go the scene

according to information for inspection and maintenance. At the same time, the repair will also receive information that the maintenance personnel have accepted the project information [12]. When the staff member submits the completion of the maintenance task, the maintenance personnel will receive SMS alerts, and then he can confirm and evaluate the maintenance results.

Next, from the logistics department, this paper will set examples to analyze the importance of the construction and transformation system on university logistics service Internet plus.

Decentralized financial management model costs too high and it is inefficient, and financial personnel are busy all day on the basic accounting work and accounting data collation, so they are very difficult to have the energy to understand and support the business work. Financial personnel and business people cannot communicate in a timely manner, and can't accurately analyze data.

With the increasing population of China, the number of students in higher education is increasing day by day. Under this kind of big premise, the university enrollment expansion is the inevitable trend. The continuous expansion of the financial departments of colleges and universities and how to reduce financial costs and avoid financial risks has become the focus of attention of the financial departments of colleges and universities. The existing management model of the financial department of the university has exposed many problems, so the financial management model should be designed according to the development strategy of the university [13]. With the use of Internet plus in financial aspects, the construction of financial shared services can help colleges and universities to reduce financial costs by improving financial efficiency and avoiding risks, to optimize and refine the financial process, to monitor the company's financial condition and operating costs, and to achieve the ultimate support of college enrollment strategy. Therefore, the logistics management mode of Internet plus university has been gradually recognized and applied.

As shown in Fig. 2, in the "Internet plus" era, under the cloud computing and mobile internet background, the future trend of shared services is the use of cloud computing and mobile Internet to push financial sharing services onto the "cloud", so as to realize the service whenever and wherever possible. As the financial departments of colleges and universities that are keeping pace with the times, they are closely following the trend of the times and conforming to the times. They use cloud computing, Internet plus mode to make SSC (shared service center) change to the financial cloud services. Financial cloud is based on shared services, and it can use cloud computing, big data and other emerging technologies to expand the sharing center to more adapt to the development of the era of financial information systems. The advantage of financial cloud is the sublimation of the advantages of financial shared services [14].

The development of Internet economy in China started late, so it is not enough concerned about the knowledge level and operation ability of financial personnel. The relative shortage of talent also makes enterprises unable to innovate in the Internet economy, and related work is also in a more difficult situation. In the "Internet plus", financial practitioners not only need to have accounting professional

skills, but also need to keep pace with the development of changes to increase. This kind of talent is a complex type of accountant. Complex talents require accountants to have both professional knowledge of accounting and proficiency in the operation of the Internet, and they should skillfully use a variety of methods of accounting professional analysis, prediction and evaluation [15]. These requirements have brought great impacts to accounting practitioners the under the "Internet plus". For the older generation of accountants, the accounts on paper have fallen short of the needs of the times. Modern accounting requires financial personnel not only excellent in professional knowledge, but also qualified in business. They need to improve their knowledge and skills in line with policies and the direction of the times. The transformation of financial personnel will also promote the deeper integration and development of financial accounting under the "Internet plus". The university logistics service network is depicted in Fig. 3.

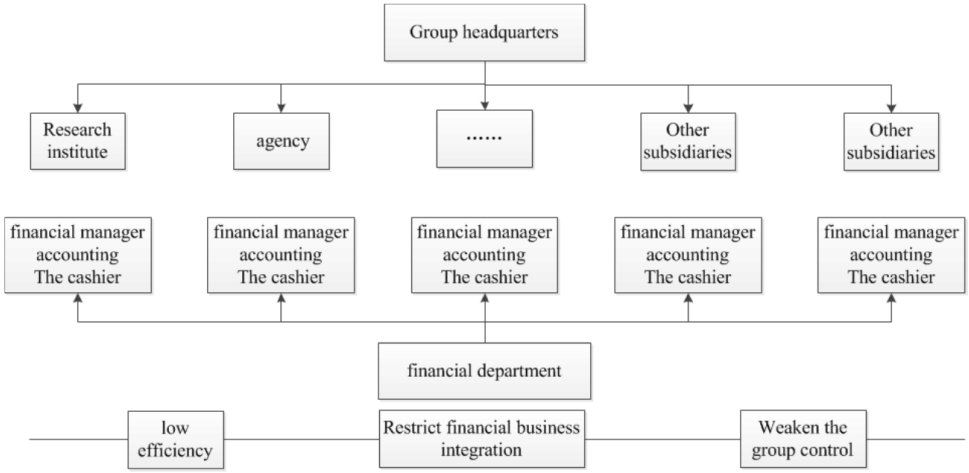

Fig. 2. Sketch map of university finance department

Fig. 3. University logistics service network

3. Result analysis and discussion

In order to prove that the above Internet plus model of university logistic service is feasible and advanced, the staff service was chosen to carry out experiments. Through a year's staff logistics support service, according to the school's standards and requirements, the service system was examined in practice, accompanied by the ten points system. Comparisons between the experimental faculty group and the control staff are shown in Table 2.

Table 2. Group comparison of laboratory staff and control staff

	Experimental population (A)	Control population (B)	A-B	P
Payroll	6.99	5.01	1.98	<0.05
Research cost	6.98	5.69	1.29	<0.05
Campus welfare	7.45	6.20	1.25	<0.05
social security	7.10	5.95	1.15	<0.05
Service supervision	6.78	5.55	1.23	<0.05
Maintenance declaration	7.73	6.10	1.63	<0.05

Note: in the table, A, B are the average of the selected samples, respectively; P is the probability value of significance test; A-B show that after the use of Internet plus in the experimental group of staff, the indicators of the experimental faculty group were higher than those of the control staff; staff and faculty group control experiment showed a normal distribution.

As can be seen from the table, the T value was tested by a significant level of 0.05. SPSS11.0 computational statistics show that the contrast values between the experimental staff group and the control staff group were significantly different, and this difference should be interpreted as experimental factors and be summarized as study results. The above chart can fully illustrate that the university logistics service model based on the environment of Internet plus can improve the work efficiency and convenience of teaching staffs, enhance the teaching efficiency of teaching staffs, enhance staff's concentration on class, and stimulate teaching effects.

According to the sample comparison in Fig. 4, the enthusiasm, efficiency, and recognition of faculty were improved after the implementation of Internet plus service in colleges and universities. Based on a numerical comparison of the figures, the efficiency of the staff was particularly pronounced on the basis of the contrast between the new service and the traditional service, which rose from 23 % to 78 %. The amount of increase was up to 55 percentage points. From this point of view,

compared with the traditional service mode, the university rear service based on the Internet plus had remarkable effects on the efficiency of teaching staff. The validity, feasibility and advanced logistics service mode of university Internet plus were verified.

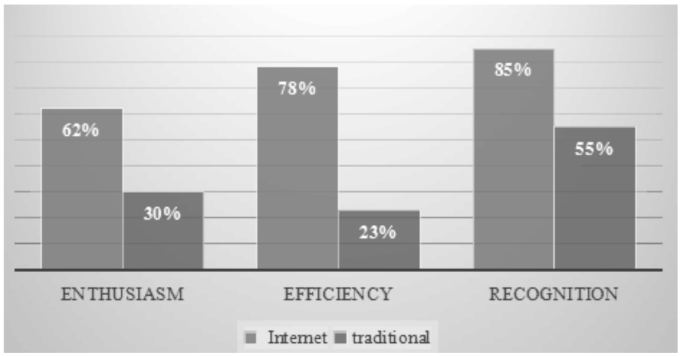

Fig. 4. Data comparison after the implementation of Internet plus service

At the same time, Internet plus university logistics service has been introduced into the students' daily life. According to statistics, as of September 2015, there were 370 student canteens in the whole province's colleges and universities. Among them, there were 131 self-operated university logistics, accounting for about 35%; universities with the introduction of service management Internet plus management accounted for about 65 %. Figure 5 shows the comparison chart of the introduction of Internet plus service mode and traditional service mode in the college canteen. About 80 % of the colleges and universities in the province have opened the catering market to varying degrees, and more than 90 catering enterprises have entered the universities.

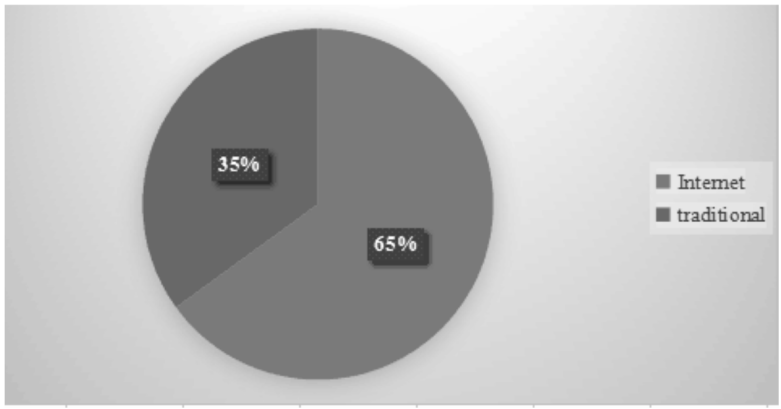

Fig. 5. The comparison chart of the introduction of Internet plus service mode and traditional service mode in the college canteen

Not only in the cafeteria, in terms of the student apartment management, there were 223 flats for student apartments in the province which adopted the Internet

plus management mode, and the number of students that it served accounted for 18 % of college students throughout the province. Figure 6 shows the comparison chart of the introduction of Internet plus service mode and traditional service mode in the college dormitory.

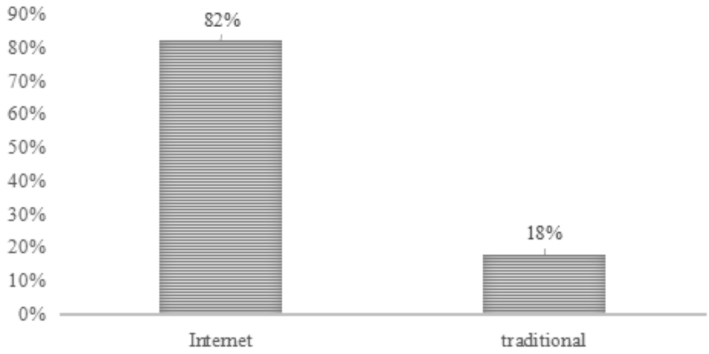

Fig. 6. The comparison chart of the introduction of Internet plus service mode and traditional service mode in the college dormitory

In addition, many colleges and universities have introduced high-quality social enterprises to carry out hosting services in the green, cleaning, supermarkets, laundry, bathroom, maintenance services and other aspects, we are not going to explain them in detail with data here.

The difference of sample data show that, after the implementation of Internet plus logistics "one-stop" service, colleges and universities can avoid duplication of posts and waste of resources, save costs, and increase revenues, efficiency and quality of service, and people-oriented management service model has won the recognition and praise of teachers and students. Logistics services, on the other hand, can become more efficient and transparent. The evaluation of teachers and students and the big data analysis become important references for the performance appraisal and awards. In this regard, the staffs are sincerely convinced, and their work enthusiasms are greatly improved.

4. Conclusion

At present, computer technology and network technology are developing rapidly. In order to study the logistics service model, through the analysis and summary of theoretical basis of the Internet plus and the existing modes, with the university as an example, the computer technology was introduced into the existing model to construct the new service model, and all aspects of the model were introduced in detail. Through this research, some conclusions were obtained as follows: compared with the traditional logistics services in colleges and universities, the new logistics service in colleges and universities is more practical, and it needs a lot of practice related activities, so it is suitable for the independent and exploratory research universities to study, so as to make the logistics service well develop. Internet plus

service model has more service modes and more flexible business hours arrangement. At the same time, the current colleges and universities have the conditions of access to the Internet, and students and faculty members have the ability to accept Internet plus new service, which is conducive to the advancement of Internet plus new service in the university. Rear service in universities can use the Internet plus mode, and can obtain good service effects. However, there are still shortcomings in this study. For example, due to the lack of front-line work experience in the university logistics services, this paper lacks the understanding of the logistics service practice process, so the service design and completion process may not be complete.

References

[1] P. Dulbecco: *The dynamics of the institutional change and the market economy: Understanding contemporaneous market development processes.* The Review of Austrian Economics *16* (2003), Nos. 2–3, 231–251.

[2] Y. J. Lv, S. B. He: *The socialization of logistics and the management of students' affairs under the internet on modern university campus.* Journal of Guangdong University of Technology(Social Sciences Edition) *48* (2004), No. 4, 1335–1343.

[3] Y. Wei: *The construction of colleges and universities library unified information system based on guangxi regional features.* Applied Mechanics and Materials *543–547* (2014), 3151–3155.

[4] J. Jerit: *Reform, rescue, or run out of money? Problem definition in the social security reform debate.* The International Journal of Press/Politics *11* (2006), No. 1, 9–28.

[5] X. Wang: *The reform on administrative management for sustainable development in China.* Journal of Convergence Information Technology. *7* (2012), No. 18, 481–488.

[6] Y. Yin: *Application research of "The Kite" law in Chinese universities logistics reform.* Creative Education *14* (2014) No. 5, 1260–1264.

[7] L. Sha: *Research on the integration of medical quality management module in office automation system.* Chinese Medical Record *554* (2013), No. 8, 60–68.

[8] J. Henri, P. Sanders, H. Lelievre, N. Cadieu: *Implementation and assessment of the quality management system in research in a laboratory of the french food safety agency: Application to PhD student work.* Accreditation and Quality Assurance *14* (2009), No. 4, 207–217.

[9] H. Ke, L. Yue, Z. P. Hu: *Research on grading standard of the project quality management system under comprehensive evaluation method.* Applied Mechanics and Materials *638–640* (2014), 2332–2337.

[10] Q. Lei, S. Q. Yi, L. W. Pan, Y. C. Song: *Research on the intelligent quality management system of supply chains based on six sigma theory.* Key Engineering Materials *439–440*, (2010), 646–651.

[11] F. Bennett: *Audio-visual services in colleges and universities in the United States.* College and Research Libraries *16* (1955), No. 1, 11–19.

[12] M. Vernuccio, A. Cozzolino, L. Michelini: *An exploratory study of marketing, logistics, and ethics in packaging innovation.* European Journal of Innovation Management *13* (2010), No. 3, 333–354.

[13] W. C. Zeng: *An analysis on the strategies of the construction of logistics service teams in local undergraduate universities.* Journal of Yichun College *33* (2011), No. 2, 285 to 303.

[14] L. Dong: *A comparative study on a reform pattern of the socialization of logistics management in colleges and universities.* Social Sciences Journal of Colleges of Shanxi *26* (2014), No. 4, 195–203.

[15] L. J. Zhang, Y. Wen: *A study on existence and development of medical work in socialization of logistic service in colleges and universities.* Journal of Chengdu University (Natural Science Edition) *21* (2002), No. 2, 11–24.

Received August 7, 2017

Acta Technica *62* No. 2B/2017, 363–374

Establishment of building energy conservation and green building model system and database based on the discussion of key technologies[1]

Hao Zhanguo[2,3], Su Xiaoming[3]

Abstract. The concept of green building aims to provide a safe, healthy and comfortable environment for people, make efficient use of resources and minimize the impact on the environment. Therefore, based on key technologies, the establishment of building energy conservation and green building model system and database was discussed and analyzed in this paper. By constructing the building energy conservation and green building model system framework and database, the environment required for building energy conservation and green building database was analyzed. Through the analysis of energy consumption of A building within the third ring road in Beijing, the conclusion that its efficiency of energy consumption equipment is high was obtained. In the future, it is necessary to strengthen the efforts to complete and update the green energy saving database, so as to provide the information technology support to the promotion of the development of green buildings around China.

Key words. Key technologies, building energy conservation, green building, model systems and database.

1. Introduction

A large number of energy consumption has seriously affected China's sustainable economic development strategy, so how to reduce building energy consumption and

[1]The study was supported by the General fund of Inner Mongolia Education Department 2016" Quantitative Control on Energy Saving Reconstruction Technology of Buildings Thermal Environment in Inner Mongolia Universities" (Fund No. NJZY16088), the General Fund of Inner Mongolia University of Technology 2015" Research on temperature field model of building space in Hohhot Universitys " (Fund No. X201512), the Key fund of Inner Mongolia University of Technology 2015 "Research on envelope thermal performance optimization of low energy consumption buildings in Inner Mongolia" (Fund No. ZD201513).

[2]School of Architecture, Tianjin University, China, 300072

[3]School of Architecture, Inner Mongolia University of Technology, Hohhot, China, 010051

improve building energy conservation has become a problem that can't be ignored. China should reduce building energy consumption and improve building energy conservation, and also needs to find a powerful tool to promote the realization of this goal in the premise of the development of green energy-saving buildings [1]. At the same time, database is the latest technology in data management. As the core and foundation of information system, database technology has been widely used in all walks of life [2]. The development situation of building energy conservation and green building is relatively satisfactory, but there are still many problems, such as the lack of perfect laws and regulations and the neglect of technology integration and; at the same time, it has not yet formed a complete set of technical system and standard system; a comprehensive system of geographical and functional suitability for green building technology has not been formed; the promotion and demonstration scale of green buildings is still small; and it has not yet played a guiding role widely [3].

There are few researches on the actual operation performance of green public buildings in China, and the systematic analysis is deficient. Relevant research scholars have defined the incremental cost of green building technology, including the corresponding benchmark program of each technology and the impact of interactive costs [4]. In addition, scholars have calculated the energy per unit area of the green public buildings of different stars, and evaluated the commonly used energy-saving emission reduction technologies with the cost effectiveness. Cost effectiveness is the incremental cost of a single technology brought about by annual energy efficiency.

2. State of the art

The key technologies of building energy conservation are mainly embodied in the construction of buildings and the construction of artificial materials with very light and transparent textures. Low-E membranes can effectively block winter heat and prevent heat loss during the summer. This open and closed electronic chrome film can darken or completely opaque the building's housing. Placing ultra-thin photovoltaic cells on the outer surface of the building's skin structure can absorb 20 % of the light, thereby providing the vast majority of the energy needs of the building [5]. Generally, the load-bearing structure of a building is made of carbon material. The load-bearing floor is made of lightweight carbon composite panels, and the intelligent floor which is used for installing electrical, water, fresh air and wire connections is located in the intermediate layer. In addition, it can be controlled according to the temperature requirement of the temperature board [6]. The design concept of green building uses the recycling of building materials in terms of the construction quality, so the environmental pollution and space utilization are forward-looking [7]. Green building is the product of the times, and the rise of green building is not only conducive to social harmony and stable development, but it also can improve the human living standards and maintain the ecological balance of the building. The consumption of natural resources will continue to decrease [8].

Therefore, the general idea of building energy conservation and green building database construction is: the construction of basic database, dynamic monitoring

database, database, business service database, model database and case database [9]. From building energy conservation to green construction design and to renewable energy applications, this process includes building structures, construction equipment, water supply lines, air conditioning, energy saving, low carbon emissions, and so on. A multi-scale, multi-resolution, heterogeneous, and multiple data source data platform and an efficient data update mechanism should be established [10].

3. Methodology

3.1. The establishment of building energy conservation and green building model system framework

For the establishment of building energy conservation and green building model system, first of all, the complete energy-saving operation system, management system, monitoring system, evaluation system and a series of system frameworks should be established according to the energy consumption in different buildings [11]. Secondly, the energy benefits of various functions should be built and constantly improved, so as to guarantee the reliable data of building energy conservation data and the smooth progress of energy saving [12]. The construction of building energy conservation and green building system model needs to be carried out step by step by using the hierarchical structure. After the statistical analysis of the judgment matrix and the weight of the index above, the consistency test results can be obtained. According to the results obtained, the building energy conservation experts can carry out analysis and judgment, assess the weight indicators of various energy-saving facilities, and obtain the final combination of weighted results. The system skeleton diagram is shown in Fig. 1.

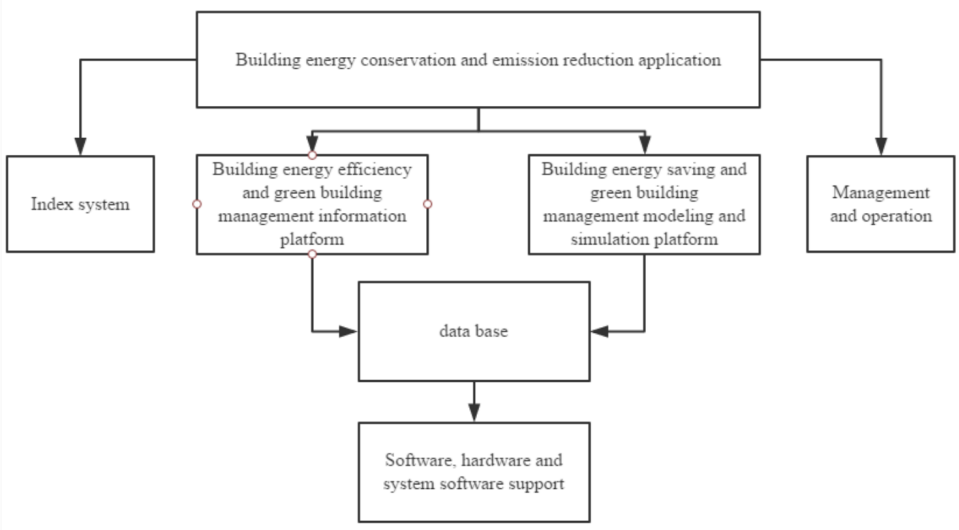

Fig. 1. Building energy conservation and green building model system diagram

The building energy conservation and green building model system framework requires the efficient operation of the platform, and it also has some configuration requirements for hardware and software facilities. Through the study of typical architectural features in various regions, the network remote transmission technology is used to carry out the analysis of the collection and storage of database data. The building energy conservation and green building management information platform and the building energy conservation and green building simulation platform can successfully complete the evaluation of building energy conservation.

3.2. The establishment of building energy conservation and green building model database

The construction of building energy conservation and green building system model not only requires the overall planning of the country, but also needs to gradually carry out all relevant indicators and standards, and various data categories formed can represent various building database systems, which can be gradually applied to the management information platform of building energy conservation and green building, so that the modeling and simulation platform built up is in good agreement with the current situation and the development trend and can make the model system always have a solid data base, which has a positive impact on building energy conservation and green building practices. Building energy conservation system needs to enter the basic characteristics, energy consumption, service direction and other information of different types of buildings in a database, so as to complete the energy assessment work according to different construction information. At the same time, according to the detailed data, the library model should be set up, and the data composition of the system model should be improved. In the building energy consumption assessment, positive conclusions can be obtained, and the building energy consumption assessment information needs to be incorporated into the building information management platform. Building energy conservation assessment information can provide corresponding data supports for building management emergencies. Building energy conservation system construction mainly needs to establish corresponding data simulation model and information service management model, so as to complete the demonstration and simulation work of building energy conservation link. In the process of building energy conservation emission reduction guidance, complete energy-saving emission reduction targets should be established; in all aspects of energy management and supervision, strict standards should be adopted; building energy conservation and green building model should be constantly improved. The database is subdivided according to Fig. 2.

In this paper, from the actual needs of green building energy consumption statistical work, the concept that the database should realize the use of green building energy consumption statistics was clearly defined, which was mainly used for the statistical management of green buildings. The required database tables, fields and keywords were determined; secondly, according to the demand analysis, the database system in the table was determined, and the fields and keywords in each table were also determined [13]. Each table contained only the topic of the relevant information, so that the table name based on the topic information was determined. In the

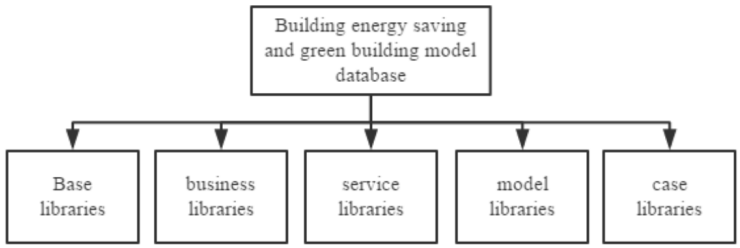

Fig. 2. Building energy conservation and green building model database

same database, tables should not have the same name; for the same table, fields should not have the same name. Then, by combining the main relationships in each table, the relationships between tables were determined, so that tables were linked to different topics [14]. Finally, the required tables, fields, and relationships between the main keywords and tables were designed to be completed; the overall design of the database was checked and the possible shortcomings for improvement were identified.

The design and implementation of green building energy conservation database system are the basic information and energy consumption based on the green public buildings, civil buildings and commercial buildings. According to statistics and summary analysis, from the point view of needs of managers, ordinary users and anonymous users, permissions settings are shown in Table 1

Table 1. Permission setting

View statistics	√	√	√
Building information input	√	√	-
Data input of energy consumption	√	√	-
Data modification	√	√	-
Data upload	√	√	-
Audit upload information	√	-	-
User information management	√	-	-
Page maintenance	√	-	-
Page upgrade	√	-	-

With the rapid development of green building, the system needs to finish the data entry of green building timely, accurately and rapidly, input data of building information, enhance information sharing, and achieve the management of user information through password management. After the data is input, data review should be carried out to prevent and modify information errors, and then the data can be uploaded. The system can realize the data statistics management of green building energy conservation. Data statistics and query is the main part, so the query and

statistics function should be the minimum response time, and the efficiency of user queries and the accurate data provided by each query should be improved through the way of presenting form.

3.3. Energy consumption analysis of green building

Database technology plays an important role in the establishment of basic information, energy consumption information, statistical analysis of energy consumption and other energy consumption statistics. Through the establishment of such database of green energy-saving buildings, the actual operation of statistical personnel and construction owners can accurately grasp related buildings, so as to realize the building operation and effective management of energy consumption. At the same time, the green building energy consumption analysis and evaluation technology can be used to comprehensively analyze all kinds of energy-saving projects at all levels from microscopic to global views, and add energy analysis data to the building energy conservation and green building model database, so as to provide important data supports for the improvement of key technologies of energy-saving green building [15].

For the analysis of green building energy conservation, energy share analysis is an intuitive method which can be easily implemented. The method of analysis can be described by the following formula:

$$\text{Input} = \sum \text{Demand} \times \text{Share}/\eta\,. \tag{1}$$

Here, the Input and Demand represent the input power and output power of building energy consumption equipment, η represents the efficiency of energy consumption device output power obtained by the improved technology and share represents the total output power of the share of equipment.

In addition, the promotion of energy-saving equipment such as energy-saving lamps will reduce the indoor heat and heating requirements. Efficiency η is not constant. At this point, the construction group splitting method will be adopted.

First of all, according to the type of building, the type of office buildings, shops, hotels, hospitals and other heat sources systems, the size of buildings and the floor planning, the clustering is carried out. In each construction category, the building model of various building categories is chosen as a reference model. Secondly, the typical building model is used, and various representative energy consumption data can be counted through the energy consumption monitoring system, including the daily cooling, heating, power and other requirements of typical buildings; modeling and simulations of energy production and distribution systems are completed to quantify typical terminal energy requirements for building models such as power and winter heating coal. The energy consumption per unit area of each building category is calculated. Finally, the total energy consumption is obtained by a method of multiplying the total energy consumption (per unit area) by the typical building type and total area. Common green energy-saving building designs are as the following shown in Fig. 3.

Fig. 3. Green energy-saving building design

4. Result analysis and discussion

4.1. Requirement analysis of database platform for building energy conservation and green building model system

In order to ensure the smooth operation of the green building energy consumption database system, one or more servers that can be accessed through the extranet should be guaranteed. The client of the system can access the system server through the extranet, and analyze the basic performance and configuration requirements of the server and the client through the analysis of the characteristics of the system. The requirements for server and client for the basic performance and configuration of the system are as listed in Table 2.

Table 1. Permission setting

	System hardware configuration		System software configuration
	Memory	Hard disk	
Server-side	2 G	200 G	Microsoft SQL Server
Client	512 M	80 G	Microsoft Windows 2000/NT/XP above

Green building energy consumption database in A building within the third ring road in the city of Beijing stores all green building information in A building within the third ring road in the city of Beijing, including building details, energy consumption data, contact information and other important information. Therefore, it is necessary to do a good job of computer virus prevention work, and regularly maintain the anti-virus function and password management of the system.

4.2. Data analysis of building energy conservation and green building model system

The energy consumption data of the A building in the third ring road in Beijing was analyzed, and the annual energy consumption of the building was audited. During the test period, the elevator in the building did not run, and the restaurant only served as an employee's dining place and did not undertake the cooking functions of the kitchen. Therefore, the building functions were relatively simple. With references to the sub node setting of the metering model, energy consumption was divided into lighting sockets, HVAC systems, communication rooms and others. The communication room was generally outside the scope of the discussion, so this part was eliminated. The monthly change chart of energy consumption and the distribution of energy consumption are shown as in Fig. 4 (energy consumption was calculated by formula 1).

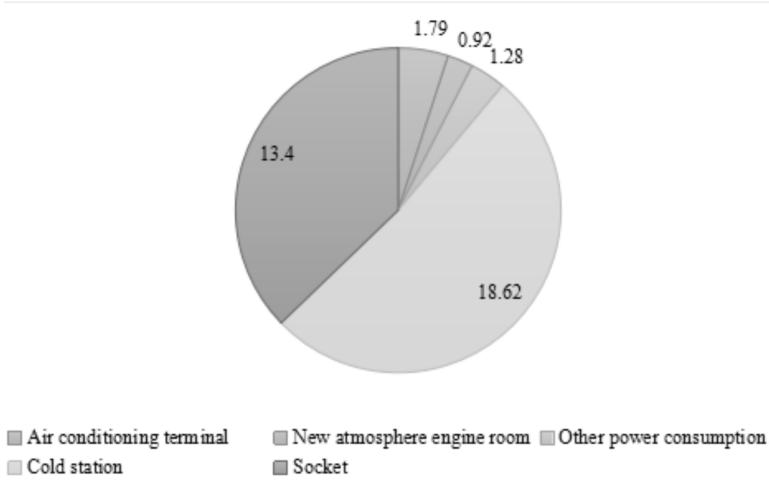

Fig. 4. Monthly energy consumption diagram of buildings and the distribution of energy consumption

Statistics show that the annual power consumption of the building was 46.03 kWh/(m^2.a). The total energy consumption of the operation was evaluated. First of all, with the database method, the electricity consumption data of 85 office buildings in Beijing were compared. Compared with 81 % of the buildings in the sample, the energy consumption was lower, so the cumulative probability level was about 19 %.

The efficiency of the building's yearly cooling and air conditioning system per-

formance is summarized in Table 3.

Table 3. Annual cumulative working condition, refrigeration and air-conditioning system, performance, efficiency

	Building refrigeration season	Survey mean	Limit
Accumulated cooling load	20.00	-	-
Air conditioning refrigeration power consumption	5.58	-	-
Air conditioning system integration	3.58	2.3	-
Cold station system EER	2.80	2.8	$\geq$3.8
Chiller EER	4.79	4.6	$\geq$4.2
Chilled water system	29.86	20.2	$\geq$30
Air conditioning terminal system	18.87	18.7	FCU:$\geq$9; FCU:$\geq$24

The above data were obtained from the building energy conservation and green building model database. The building load level, the system integrated energy efficiency and subsystem energy efficiency were all analyzed, and a more specific and comprehensive understanding of the operation of the building was made. Based on the analysis of the operation of the case, it can be seen that the building did not use special system equipment, but adopted the most traditional air-conditioning terminal equipment. Through reasonable passive design, energy-saving operation mode and good design intention in operation, it reduced the system cold and hot load, and it did not pursue the efficient equipment operation alone, but made full use of low-grade energy for cooling and heating. At the same time, it adopted flexible terminal control equipment to meet the needs of the users during the overtime period, thereby saving energy. The energy consumption assessment of the case was summarized as follows: the total energy consumption level is extremely high; the load control of the building is excellent; and the system energy efficiency level is acceptable. Although further regulation of the equipment operation mode can improve the energy efficiency, the operation performances are satisfactory in terms of the whole system.

The green performance evaluation of building A was analyzed. In the case building, 89 valid questionnaires were reclaimed. Among them, in terms of the green performance of the building, the function, aesthetic, spatial layout and maintenance management of these four aspects were rated and evaluated. The statistical scores are shown in Fig. 5.

As can be seen from the above figure, building function, aesthetic and maintenance obtained 4 points; the spatial layout score was relatively low as 3 points.

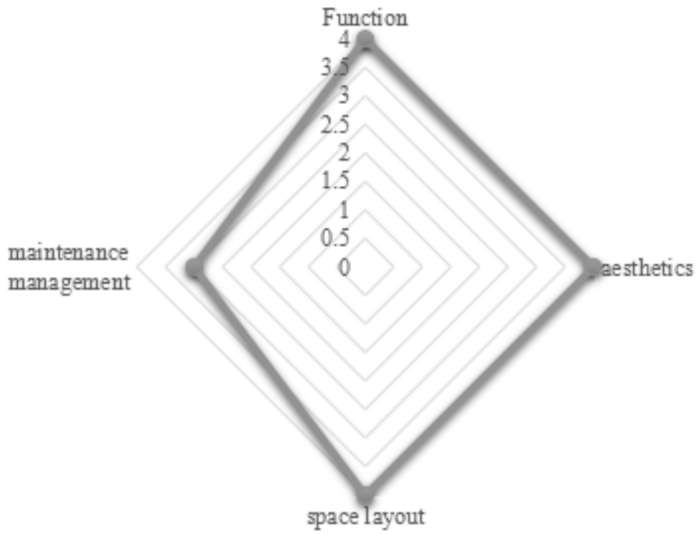

Fig. 5. Green performance Statistical score

As can be seen from data extracted from the green performance database, there were more open office spaces in the layout of the building space, so the user's space privacy and sound insulation were poor. In this regard, the user's satisfaction was relatively low. Therefore, all regions of the country should grasp the core technology of building energy conservation and green construction as soon as possible. A variety of experimental energy-saving technologies and green building technology must comprehensively utilize the building energy conservation and green building demonstration projects in different parts of China.

5. Conclusion

The establishment of building energy conservation and green building model system is conducive to promoting the promotion of green building throughout the country, so as to provide THE guarantee for the overall construction of green buildings in China. In the economic society where the building energy consumption is increasing constantly, the implementation of building energy conservation and green building technology can effectively reduce building energy consumption. Through the construction of building energy conservation and green building system, the construction of database and simulation platform, and the vigorous promotion of the green building model in various areas, a complete green energy consumption system can be constructed to achieve the energy saving and emission reduction effects. In this paper, the research on building energy conservation and green building model system and database based on key technologies was mainly carried out around the related technologies of reducing energy consumption and its detection database as the core. Through the establishment of building energy conservation and green building

system model framework and database, energy consumption of green energy-saving building was analyzed; finally, based on the building energy conservation and green building model systems and database of A building within the third ring road in Beijing, its energy consumption was studied and analyzed, and the conclusions that the energy efficiency of A building was high, and the building energy conservation methods were excellent were obtained. However, in the future database of energy-saving green building model systems, it still needs to strengthen the maintenance work, so as to provide data supports for the future green building projects.

References

[1] Y. Yuan, X. Yu, X. Yang, Y. Xiao, B. Xiang, Y. Wang: *Bionic building energy efficiency and bionic green architecture: A review.* Renewable and Sustainable Energy Reviews *74* (2017), 771–787.

[2] J. Li: *Towards a low-carbon future in China's building sector—A review of energy and climate models forecast.* Energy Policy *36* (2008), No. 5, 1736–1747.

[3] A. J. Marszal, P. Heiselberg, J. S. Bourrelle, E. Musall, K. Voss, I. Sartori, A. Napolitano: *Zero energy building – A review of definitions and calculation methodologies.* Energy and Buildings *43* (2011), No. 4, 971–979.

[4] A. I. Inayati, F. X. N. Soelami, R. Triyogo: *Identification of existing office buildings potential to become green buildings in energy efficiency aspect.* Procedia Engineering *170* (2017), 320–324.

[5] J. L. Wang, Q. Q. Wang, Y. We, G. Z. Li, Y. Yang: *Green office building retrofit optimization strategy based on building energy efficiency-predicted mean vote.* Heating Ventilating & Air Conditioning (2015), No. 11, paper 005.

[6] P. P. A. Kumar: *Overview of natural stones as an energy efficient and climate responsive material choice for green buildings.* Implementing Campus Greening Initiatives, Springer International Publishing AG., Part: World Sustainability Series, book series (WSUSE) (2015) 27–35.

[7] C. Nägeli, M. Jakob, B. Sunarjo, G. Catenazzi: *A building specific, economic building stock model to evaluate energy efficiency and renewable energy.* Proc. International Conference on Future Buildings and Districts - Sustainability from Nano to Urban Scale (CISBAT), 9–11 September 2015, Lausanne, Switzerland, Proceedings of CISBAT *1* (2015), 877–882.

[8] R. Ramírez-Villegas, O. Eriksson, T. Olofsson: *Assessment of renovation measures for a dwelling area – Impacts on energy efficiency and building certification.* Building and Environment *97* (2016), 26–33.

[9] L. Suárez, M. A. Bouraoui, M. A. Mertah, M. Morvan, L. Nuaymi: *Energy efficiency and cost issues in backhaul architectures for high data-rate green mobile heterogeneous networks.* Proc. IEEE Annual International Symposium on Personal, Indoor, and Mobile Radio Communications (PIMRC), 30 August–2 September 2015, Hong Kong, China, IEEE Conference Publications (2015), 1563–1568.

[10] J. Keirstead, M. Jennings, A. Sivakumar: *A review of urban energy system models: Approaches, challenges and opportunities.* Renewable and Sustainable Energy Reviews *16*, (2012), No. 6, 3847–3866.

[11] A. Monsalud, D. Ho, J. Rakas: *Greenhouse gas emissions mitigation strategies within the airport sustainability evaluation process.* Sustainable Cities and Society *14* (2015),414–424.

[12] W. Y. Park, S. Bae, A. A. Phadke: *Technology inventory: Energy efficiency measures for residential, commercial, and industrial sectors in the United States.* Ernest Orlando Lawrence Berkeley National Laboratory (LBNL), Report Number: LBNL-183619 (2015).

[13] V. Costantini, F. Crespi, G. Orsatti, A. Palma: *Policy inducement effects in energy efficiency technologies. An empirical analysis of the residential sector*. Springer International Publishing AG., Green Energy and Efficiency, Book Series: Green (2014), 201–232.

[14] D. Zhao, A. Mccoy, J. Du: *An empirical study on the energy consumption in residential buildings after adopting green building standards*. Procedia Engineering *145* (2016), 766–773.

[15] G. P. Henze, S. Pless, A. Petersen, N. Long, A. T. Scambos: *Control limits for building energy end use based on frequency analysis and quantile regression*. Energy Efficiency *8* (2015), No. 6, 1077–1092.

Received August 7, 2017

Acta Technica *62* No. 2B/2017, 375–384

Design and application of inventory management system for manufacturing enterprises

Liu Zhenhua[1]

Abstract. The application of manufacturing enterprise inventory management system is of great significance to the development of manufacturing enterprises in modern times. In order to improve the technology and theory of the system, in this paper, firstly, the relevant data and theories of the system design were summarized, secondly, a simple warehouse management system was constructed by relying on the database technology and the system was applied to a manufacturing enterprise. The results show that the inventory management system can effectively reduce the production cost of the enterprise while improving the production efficiency of the enterprise. The research aims to provide some theoretical basis and reference for the development of China's manufacturing enterprises.

Key words. Manufacturing enterprise; inventory; management system.

1. Introduction

With the development of the times, the world's economic level has obtained greatly improvement and progress and various industries have been a certain impetus, so that a greater degree of comprehensive strength has been achieved. In this trend, various companies begin to attach great attention on their various development links, so as to provide some protection for higher and faster development of the industry. As one of the important parts of the development of whole industry, the inventory has a very important impact on the related costs of the industry development and the profitability of the later stage. Today, the management of inventory has gradually produced a huge role in promoting the development of various industries. Traditional inventory management is more to operate by relying on the manual records, which suffers a greater degree of influence of subjective factors, and there is a negative impact for the inventory accuracy records and the effectiveness of the final assessment. With the development of the times, the current computer technology has a more advanced development trend, as one of the most influential innovative

[1]Shaanxi Technical College of Finance and Economics, China, 712000

technologies in the world today, the driving force of the computer technology for the development of various industries is beyond doubt, then, because the technology has excellent sharing and data collection and many other advantages, it can be more organically combine with the industry. Nowadays, the technology begins to be gradually applied to the inventory management of manufacturing enterprises, moreover, a certain convenience and accuracy are provided for the manufacturing enterprises' inventory management, which makes the enterprise have a greater degree of development and its comprehensive strength greatly improved. Based on relevant theory and technology development of the design and application of the inventory management system in China's manufacturing enterprises, this study compared and analyzed its advantages. The purpose of this paper is to provide a scientific basis and reference for the further improvement of related technologies and theories in China.

2. State of the art

With the development of the times, now, the world's various industries have suffered a certain impetus and positive impact under the background of the rapid development of the world economic level. As one of the key pillar industries in the rapid development of the current economic level [1], the development of manufacturing enterprises is of paramount importance for the progress of the world economy [2]. Inventory management is an important part of its normal operation and comprehensive strength promotion in the manufacturing industry. Many research scholars believe that in a manufacturing industry, only further understanding the inventory can people face up to the status of the development of the industry, and the current product production of the whole industry development can be further analyzed, then, the future product production and resource requirements can be further determined and certain theoretical and data support can be provided based on the relevant analysis. Therefore, many manufacturing companies begin to regard the inventory management as an important part and link of the development of enterprises [3]. At present, the development of the computer industry has a very important role for a variety of enterprises; in the manufacturing enterprises' inventory management process, the inventory management results can be more reliable by using the advantages of the technology and the obtained relevant data [4]. And only to have a more systematic inventory management system, a theoretical support and basis can be provided for the development of the industry ultimately, meanwhile, more technical support can be provided for the promotion of the overall strength of the entire manufacturing industry and the development of the national economic level.

3. Methodology

With the development of the times, the theme of world development is now peace and development. In this big trend of development, the world's economic level has been greatly improved, and the economic level has been unprecedented development.

As an important industry in the development of the times, the manufacturing industry has a very important practical significance for the development of the world [5]. The development of the manufacturing industry makes more products produced, which brings a very important impact for people's production and life demands in modern times, furthermore, people's lives also get a great convenience, then, some effective development is brought for people's colorful life while people's living standards are also constantly improved. In this large trend of development, China's manufacturing industry has also been a greater degree of progress. Especially since the reform and opening up, as China's manufacturing industry has brought great impetus to the improvement of China's economic level, China has gradually become an important manufacturing industry in today's world, and the products produced by related industries in China have begun to be further sold to other countries, so that the comprehensive level of China's manufacturing industry has been greatly improved (Figure 1). Then, many discordant phenomena are further exposed while massive products produced in China bring great impetus to the national economic level [6]. For example, because of the decision-making errors of the management layer in related industries, many industries have decision-making mistakes on the status of a product in the production of related products, which causes that the production of the product is more, the supply exceeds the demand and serious product backlog [7]. This series of uncoordinated phenomena has caused a certain degree of waste for the resources of related products in China, and has had a negative impact on the development of China's manufacturing industry [8]. With the progressive deterioration of related issues, China has begun to gradually pay attention to manufacturing enterprise inventory management. It is extremely necessary for an enterprise to attach great attention to the inventory management, only to timely check the inventory, the actual condition of the main raw material in the stock can be discovered, and certain raw materials that need to be purchased are bought timely, so as to avoid the delay of enterprise's production [9]. In addition, according to analyze the inventory status of some products produced, the current situation of the production of the enterprise can be realized clearly, so that the shrink production is carried out for the products with large yield, so as to avoid the product backlog. While for some products with relatively small output and relatively large demands, the production scale of this part of the product can be expanded by adjusting relevant production links [10]. Therefore, the inventory management has extremely positive impact on the development of some of China's manufacturing enterprises. However, the relevant model of inventory management in China is still in a relatively traditional calculation, the inventory check and other links are more completed by relying on manual inventory, this mode has a certain degree of subjective factors, and also has certain restricted role for the development of inventory management [11]. With the development of computer technology in China, China begins to apply computer technology to the actual manufacturing enterprise inventory management system, and then, a certain degree of progress is obtained, moreover, China's inventory management technology and related theories also begin to be gradually improved and developed. This study analyzed the current status of the development of China's manufacturing enterprise inventory management system, so as to determine the advantages of this system

model for the development of China's manufacturing enterprises through the design of inventory management system for manufacturing enterprises. The purpose of this paper is to provide some theoretical support and reference for the development of inventory management system for manufacturing enterprises in China. The time evolution of gross output value of China's manufacturing enterprises is shown in Fig. 1.

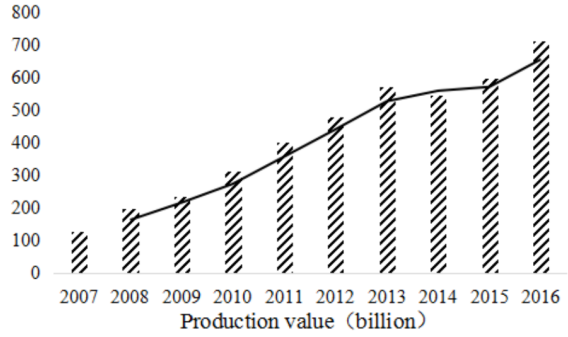

Fig. 1. Analysis of gross output value of China's manufacturing enterprises

Firstly, in this research, by reading and analyzing relevant data, the related design concept of manufacturing enterprise inventory management system was determined, and a certain theoretical foundation was laid for the further research on the basis of clarifying the relevant concept.

Then, based on ASP.NET technology, this paper constructed the related system of manufacturing enterprise inventory management. There are three layers in the main structural model. The first layer is the UI layer, its main role is the user use interface, which is mainly used to pass the user's request and submit it to the terminal, the composition structure is the client and the Web browser; the second layer is the business logic layer, this layer is mainly to use the user's related request to accept and make appropriate treatment, and then, the results are displayed to the user in the form of browsers, the main structure includes Web forms, XML Web services and component services; the third layer is the data layer, when the business logic processing layer is dealing with the request and the data processing is involved, the data processing service is provided and returned to the business logic layer, including ADO.NET and RDBMS. On the basis of the clear establishment of the relevant system, based on this system structure, some small and medium enterprises in China were adopted as the research objects to establish the database of the inventory management system; after the establishment of the database, the comparative analysis of the inventory management was conducted

4. Result analysis and discussion

With the development of the times, manufacturing enterprises have gradually become one of the important support companies to promote the world's economic

development in modern times. In the manufacturing enterprises, as an important part of the development of enterprises, the importance of inventory for the development of the enterprise is no doubt (Fig. 2). After the reform and opening up, China's various industries have also made great progress, furthermore, the exchanges and cooperation between China and other countries in the world have also gradually increased. In this trend, China's manufacturing enterprises have obtained a great degree of improvement and progress [12]. The quantity of products in certain manufacturing industries in China is increasing constantly, which makes our country have a greater influence in the world, moreover, the economic level is also further improved [13]. With the development of manufacturing enterprises, many scholars in our country have begun to put forward to improve relevant theories and systems of inventory management in some enterprises. Only in this way, the future development direction of our country can be determined, and then, the waste of resources is further reduced while making our country specify a more explicit decision-making, so as to provide a certain theoretical basis for the sustainable development of the economy.

Fig. 2. Development of manufacturing enterprises

The traditional inventory management is mainly the simple and manual record way. With the development of the times, now, computer technology has brought a certain impetus for the development and progress of various industries. The combination of technology and other industries has made more industries begin to develop towards the direction of information technology. In this trend, China's manufacturing enterprise inventory management system has also been a positive impact [14]. Initially, due to the limitations of computer hardware and software facilities, China's manufacturing enterprise inventory management system development is relatively backward and the system's function is relatively simple. While with the continuous progress of China's science and technology, nowadays, China's computer network technology has been greatly improved, and the relevant database has been established, besides, China's innovative computer network technology has further eliminated the single and relatively backward computer network technology, and the inventory management system of China's manufacturing industry has also obtained a great degree of improvement and development [15] (Fig. 3). In today's era, the

advantages of manufacturing enterprise inventory management system are shown in Fig. 3, the system is mainly composed of five kinds of databases, and the main operation way of the database is shown in Table 1.

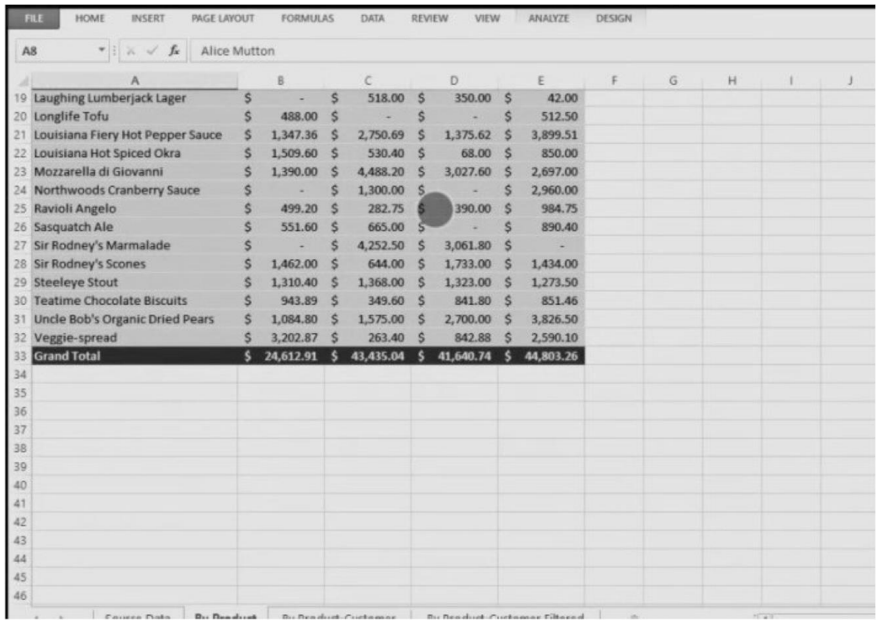

	A	B	C	D	E
19	Laughing Lumberjack Lager	$ -	$ 518.00	$ 350.00	$ 42.00
20	Longlife Tofu	$ 488.00	$ -	$ -	$ 512.50
21	Louisiana Fiery Hot Pepper Sauce	$ 1,347.36	$ 2,750.69	$ 1,375.62	$ 3,899.51
22	Louisiana Hot Spiced Okra	$ 1,509.60	$ 530.40	$ 68.00	$ 850.00
23	Mozzarella di Giovanni	$ 1,390.00	$ 4,488.20	$ 3,027.60	$ 2,697.00
24	Northwoods Cranberry Sauce	$ -	$ 1,300.00	$ -	$ 2,960.00
25	Ravioli Angelo	$ 499.20	$ 282.75	$ 390.00	$ 984.75
26	Sasquatch Ale	$ 551.60	$ 665.00	$ -	$ 890.40
27	Sir Rodney's Marmalade	$ -	$ 4,252.50	$ 3,061.80	$ -
28	Sir Rodney's Scones	$ 1,462.00	$ 644.00	$ 1,733.00	$ 1,434.00
29	Steeleye Stout	$ 1,310.40	$ 1,368.00	$ 1,323.00	$ 1,273.50
30	Teatime Chocolate Biscuits	$ 943.89	$ 349.60	$ 841.80	$ 851.46
31	Uncle Bob's Organic Dried Pears	$ 1,084.80	$ 1,575.00	$ 2,700.00	$ 3,826.50
32	Veggie-spread	$ 3,202.87	$ 263.40	$ 842.88	$ 2,590.10
33	Grand Total	$ 24,612.91	$ 43,435.04	$ 41,640.74	$ 44,803.26

Fig. 3. Development and application of enterprise inventory management system

On the basis of the extremely clear manufacturing enterprise inventory management system, this study took the discrete small and medium-sized enterprises in China as the example. Firstly, by reading relevant information, the characteristics and inventory requirements of small and medium-sized manufacturing enterprises in China were analyzed and summarized. The results are shown in Table 2. Then, according to the current development situation of discrete small and medium-sized manufacturing enterprises in China, and based on ASP.NET database technology, the warehouse and return data database of the small and medium-sized enterprises were constructed, as shown in Table 3.

The inventory system designed in this paper was applied to the inventory management process for a manufacturing enterprise in X Province in China, and then, the production costs and production benefits of the company in each quarter of 2016 were recorded and analyzed further. The results are shown in Figure 4. The results show that after the application of the stock system, the production cost of the enterprise in each quarter had a decreasing trend and the production efficiency was increasing. While with the extension of the application time, the downward trend of the production cost was large and the income of the production benefit increased constantly, then, the two indicators basically tended to a saturated state. This further indicates that the inventory management system of manufacturing enterprises has a very important positive influence and impetus to the development of

small and medium-sized manufacturing enterprises in our country, thus, the better and faster development of related manufacturing enterprises in the country can be achieved and the continuous improvement of the overall level of China's economy can be promoted through the further improvement of the system.

Table 1. Research on the theory and technology of inventory management system for manufacturing enterprises in China

Database and method	Composition	Brief description
ABC classification of the material inventory control	Class A material control	This kind of material is an indispensable material in the manufacturing process. The database mainly considers the operation cost at all aspects, such as procurement, transportation and shortage of the material, and then, further determines the best single purchase cost, thus reducing the cost as much as possible while ensuring the normal operation of the industry.
	Class B material control	The proportion of this type of the materials is between class A and class C materials, and only the general attention and protection are required in the inventory.
	Class C material control	Mostly are small materials, they have no close relationship with the industry and direct correlation, which can be purchased in large quantities.
B/S three-tier mechanism model	WEB browser, WEB server and database server	The system development, maintenance and upgrade and user aspects of the model are relatively simple, so they begin to gradually become the preferred database in the warehouse management system in China.
.Net platform framework	Language library, framework	Through the construction of the relevant code, the operation of the program can be further achieved.
ASP.NET technology	Microsoft.NET	The database often uses the code post method in the process of use, furthermore, during the calling process, the unordered compilation and program are updated, so the operation process is more high-speed, safe and powerful.
Microsoft SQL Server database	Microsoft SQL Server 2008	The database is a relatively mature and fully functional database in the inventory management system of China's manufacturing enterprises. The database is highly reliable, more efficient and intelligent.

5. Conclusion

With the development of the times, the manufacturing industry has gradually become an important support for the development of the world economy today, and the manufacturing enterprises have provided a great impetus and positive influence for the development of the world.

Table 2. Characteristics of discrete small and medium sized manufacturing enterprises in China and their special requirements of the inventory management

Research level	Illustration
Features	Production technology changes more
	Production technology changes more
	Cost control is difficult
Inventory management special needs	The practicality and miniaturization requirements of inventory management information system
	Reconfigurable requirements for inventory management systems
	Scalability requirements for inventory management systems
Inventory management link	Warehousing
	Storage
	Delivery of cargo from storage
Basic functions of inventory management system	Records of the varieties, specifications, leave the factory and other information of the storage goods
Inventory management users	General user
	Advanced user
Related business analysis	Warehousing business
	Business of delivering the cargo from storage
	Return business
	Inventory business

As an important part of the development of manufacturing enterprises, the management of inventory management link is conducive to reducing the cost of production and further increasing the benefits of business operations. However, the inventory management of China's traditional manufacturing enterprise is more dependent on the artificial form or a relatively simple computer operation program, so there are some restrictions on the management of inventory. Today, the efficient development of the computer industry provides certain technical support for the improvement of the manufacturing enterprise's database management system. In this research, through the analysis of the relevant database technology of the manufacturing en-

terprise inventory management system, a simple inventory management system was established. Through the practical application, the results show that the system has a positive effect on the reduction of the production cost and the improvement of the production efficiency of a small and medium-sized enterprise. The research aims to provide a theoretical basis for the development of China's manufacturing industry. However, due to the limitation of the author' level, a more comprehensive system construction is not understood, so there are some shortcomings in research results, while the results can still be used as a reference for the relevant industries.

Table 3. Return system of the warehouse constructed by ASP.NET database technology

Serial number	int	4	Not null	Primarykey
Product serial number	nvarchar	10	Not null	
Product code	nvarchar	20	Not null	
Product name	nvarchar	50	Not null	
Application user	nvarchar	20	null	
Application quantity	int	4	null	
Application time	datetime	8	Not null	
User confirmation	ntext	16	null	
Quantity confirmation	int	4	null	
Time confirmation	datetime	8	null	
Type of operation	nvarchar	20	Not null	
Examination and verification	nchar	4	Not null	
Remarks	ntext			

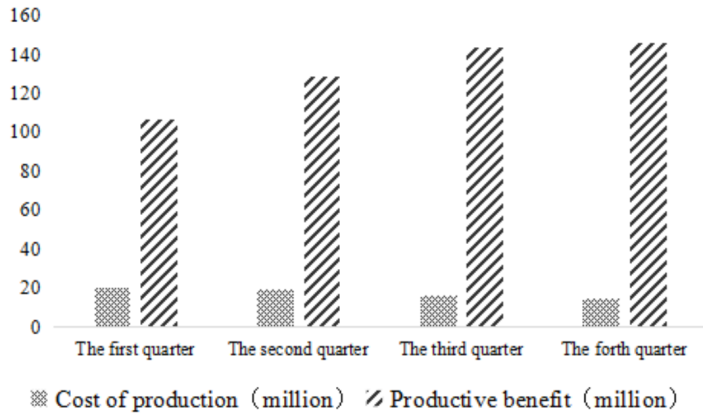

Fig. 4. Impact of the warehouse relative to an industry's production costs and benefits

References

[1] W. H. Wu, L. C. Fang, W. Y. Wang, M. C. Yu, H. Y. Kao: *An advanced CMII-based engineering change management framework: The integration of PLM and ERP perspectives.* International Journal of Production Research *52* (2014), No. 20, 6092 to 6109.

[2] B. Hamraz, N. H. M. Caldwell, D. C. Wynn, P. J. Clarkson: *Requirements-based development of an improved engineering change management method.* Journal of Engineering Design *24* (2013), No. 11, 765–793.

[3] N. Caldwell, B. Hamraz, T. W. Ridgman, P. J. Clarkson: *FBS Linkage ontology and technique to support engineering change management.* Research in engineering design *26* (2015), No. 1, 3–35.

[4] W. T. Thompson, F. Steier, W. Ostrenko: *Designing communication process for the design of an idea zone at a science center.* Journal of Applied Communication Research *42* (2014), No. 2, 208–226.

[5] L. W. Chang, S.Ṫ. Chen: *The impact of World Café on entrepreneurial strategic planning capability.* Journal of Business Research *68* (2015), No. 6, 1283–1290.

[6] J. Han, S. H. Lee, P. Nyamsuren: *An integrated engineering change management process model for a project-based manufacturing.* International Journal of Computer Integrated Manufacturing *28* (2015), No. 7, 745–752.

[7] K. R. Reddi, Y. B. Moon: *Modelling engineering change management in a new product development supply chain.* Journal of Production Research *51* (2013), No. 17, 5271 to 5291.

[8] G. Puente, O. Díaz, M. Azanza: *Refactoring affordances in corporate wikis: a case for the use of mind maps.* Enterprise Information Systems *9* (2015), No. 8, 785–834.

[9] H. Meier, R. Roy, G. Seliger: *Industrial product-service systems (IPS^2).* The International Journal of Advanced Manufacturing Technology *52* (2011), Nos. 9–12, 1175 to 1191.

[10] F. Tao, D. M. Zhao, Y. F. Hu, Z. Zhou: *Resource service composition and its optimal-selection based on particle swarm optimization in manufacturing grid system.* IEEE Transactions on Industrial Informatics *4*, (2008), No. 4, 315–327.

[11] X. Xu: *From cloud computing to cloud manufacturing.* Robotics and Computer-Integrated Manufacturing *28* (2012), No. 1, 75–86.

[12] D. H. Wu, M. J. Greer, D. W. Rosen, D. Schaefer: *Cloud manufacturing: Strategic vision and state-of-the-art.* Journal of Manufacturing Systems *32* (2013), No. 4, 564–579.

[13] D. H. Wu, J. L. Thames, D. W. Rosen, D. Schaefer: *Enhancing the product realization process with cloud-based design and manufacturing systems.* Journal of Computing and Information Science in Engineering *13* (2013), No. 4, paper 041004.

[14] K. Nagorny, A. W. Colombo, U. Schmidtmann: *A service and multi-agent-oriented manufacturing automation architecture: An IEC 62264 level 2 compliant implementation.* Computers in Industry *63* (2012), No. 8, 813–823.

[15] J. Y. Um, Y. C. Choi, I. Stroud: *Factory planning system considering energy-efficient process under cloud manufacturing.* Procedia CIRP *17* (2014), 553–558.

Received August 7, 2017

Acta Technica *62* No. 2B/2017, 385–394

Analysis of control design of quadruped robot motion based on motion stability theory

Bingqiang Yan[1,2], Weiqing Huang[2,3]

Abstract. Quadruped walking robot can not only walk on uneven ground and complex terrain by static walking, but also realize high speed walking with dynamic walking. The development of quadruped walking robot has been paid much attention to by all countries. In order to study the factors that affect the dynamic walking stability of quadruped robot, the ADAMS virtual prototype software was used to simulate the dynamic walking of quadruped walking robot. In this paper, MATLAB data was input into ADAMS by using trajectory planning of robot. According to the force and constraint imposed by ADAMS, the specific method and steps of virtual prototype of walking robot were established. The research results and the combined simulation method of MATLAB- and ADAMS have guiding significance for the design and research of quadruped walking robot and the simulation experiment.

Key words. Motion stability theory, four groups of robots, motion process.

1. Introduction

Mobile robot technology is one of the most important and active research fields in the field of robot research. A quadruped robot is a robot that mimics the form of quadruped locomotion. It not only exceeds the stability of biped robot, but also avoids the redundancy and complexity of six legged robot mechanism. It can walk slowly on complex terrain in static walking mode, and can walk at high speed with dynamic walking. It has a very attractive prospect in many fields such as military or civilian materials transportation, field exploration, star exploration, disaster rescue, agricultural production, education and entertainment in complex terrain environment. In order to realize the highly dynamic, strong adaptability and high stability of the quadruped robot, the motion control strategy is the focus and difficulty of

[1]School of Mechatronical Engineering, Beijing Institute of Technology, Haidian District, Beijing, 100081, China
[2]Hebei College of Industry and Technology, Shijiazhuang, 050091, China
[3]Corresponding author

the study, especially the multi-joint coordination control, environmental adaptability control and dynamic stability control. At present, the motion control method of biped robot is based on kinematics model and dynamics model. It adopts the idea of modeling, planning and controlling. Firstly, the robot body and environment are modeled accurately. Then, the optimal trajectory of the robot is obtained by artificial programming. The feedback mechanism is used to control the deviation between the actual motion and the ideal trajectory of the robot, so that the motion of the robot can reach the ideal trajectory as much as possible. The control method can achieve complex and precise motion of the robot. However, it needs complicated kinematics and dynamics modeling with complex motion planning, discontinuous planning process and poor real-time control, so it is difficult to improve the robot's environmental adaptability.

2. State of the art

In the aspect of CPG bionic control of quadruped robot, the research of The University of Electro and Communications is the most typical. A pioneering research on the adaptive dynamic walking of quadruped robot in unstructured environment by using neural system model was studied, and a series of quadruped robots were developed [1]. The researchers used the improved Matsuoka neuron oscillator model to construct the robot's CPG control network [2], which was the basic rhythm generator movement. The stretch reflex, vestibular reflexes, extensor flexor reflex and other biological reflection mechanisms were integrated into the CPG control network. The adaptive dynamic walking of Patrush series quadruped robot under complex terrain and the running motion on the road surface was realized. In the gait transformation of quadruped robot, researchers have made some attempts and explorations [3]. The quadruped robot with a lumbar joint was investigated, and the gait transitions were achieved by varying the robot's motion speed and the muscle tension at the lumbar joint. In addition, the researchers verified the existence of hysteresis in robot gait transformation by simulation and experiment [4]. The research on quadruped robot in our country started late, and there is still a big gap compared with foreign countries. However, in recent years, with the national attention to the robot industry and increased investment, great progress in this area has been made and a series of results have been achieved [5].

2.1. Methodology

The movement control system of higher animals is a complex network involving higher nervous centers, lower nervous centers, skeletal muscles, executive systems, receptors, and sensory organs, as shown in Fig. 1.

In Fig. 1, the high central nervous system consists of a series of motor centers, including the cerebral cortex, the basal ganglia, the brainstem and the cerebellum. Their main function is to send movement instructions, control the rhythmic motion, select sport mode, and control the movement through the central comprehensive CPG feedback, proprioceptive and visual information, so as to realize the advanced

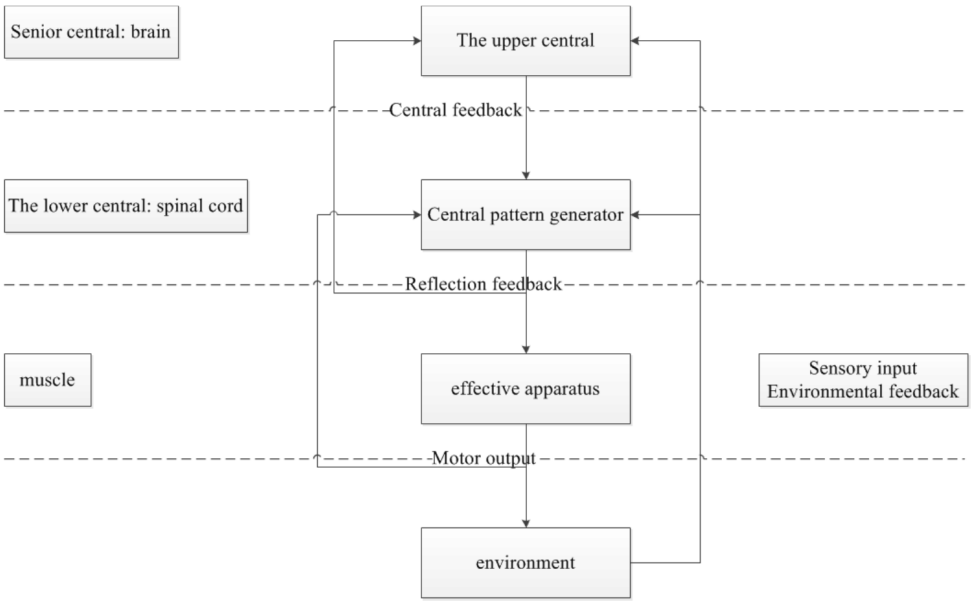

Fig. 1. Animal movement control network

movement function of obstacle avoidance and path planning in complicated environment [6]. Central mode generator (CPG) is the central control unit of rhythmic movement. The main function is to produce rhythm signals and control effector to realize motion. CPG is a distribution network composed of intermediate neurons with multiple oscillating centers. The self-oscillation is realized by mutual inhibition between neurons, and a multi-channel or one way periodic signal with stable phase interlocking relation is generated to control the rhythmic movement of the limbs or related parts of the body. In CPG, synaptic connections between neurons are malleable and a variety of output behaviors are exhibited to control animals' multiple motor patterns. Effector, the musculoskeletal system, is responsible for limb movements. There is a complex feedback network in the whole control system, including central feedback, reflective feedback and environmental feedback. These feedback loops are used to achieve biological reflex function. Central feedback is the replication of the CPG output, and the central nervous system uses central feedback to understand the control process of CPG. The feedback provides the upper body motion state or position information by using various proprioceptive sensors, and adjusts the output of CPG through the reflection mechanism, and coordinates the relationship between CPG and ontology and environment [7]. Environmental feedback monitors the relationship between the environment and the body mainly through visual and tactile sensory, so that the upper control system can ensure the appropriate command issued according to the environmental conditions or adaptive response.

In order to study the high speed walking quadruped trotting gait to achieve stable, trajectory planning and motion control curve were generated by using MAT-

LAB software firstly. And the virtual prototype was built by the ADAMS virtual prototype software [8].

In order to reduce the impact of the ground motion of the quadruped walking robot when swinging the legs to the ground, a high-speed dynamic and stable walking was carried out, and the trajectory of the foot was planned with the compound cycloidal trajectory planning method. The displacement expression in inertial coordinate system is as follows

$$x = s\left[\frac{t}{T_y} - \frac{1}{2\pi}\sin\frac{2\pi_t}{T_y}\right], \tag{1}$$

$$Z = 2H\left[\frac{t}{T_y} - \frac{1}{4\pi}\sin\frac{4\pi_t}{T_y}\right], \tag{2}$$

where, X is the displacement of the advancing direction, Z is the displacement in the high direction, S is the step length (the moving distance of the center of gravity in the unit cycle), H is the lifting height of the swinging foot, and T_y is the swinging cycle of the swinging leg.

The movement pattern of a foot animal is represented by "gait". Gait is the walking pattern with fixed phase relation between legs. The main characterization parameters of gait are defined as follows [9].

Gait cycle T: the time taken for a complete motor cycle.

Step length S: within one gait cycle, the distance that the body center of mass moves relative to the ground.

Load factor: the time at which the leg is supported on the ground, which accounts for the proportion of the entire motion cycle.

Supporting phase and oscillating phase: leg movement is divided into two processes: support and swing. The supporting phase refers to the state in which the leg meets the ground, supports the body and pushes the body forward. A swinging phase is the state of the leg lifting in the air. Load factor and phase difference are the two most important parameters of gait description. Different gait has different load factors, and the same gait can also have different load factors at different speed [10].

According to the load factor of each leg, gait can be divided into regular gait and irregular gait. Regular gait is the gait with the same load factor, the same motion rule, and the same phase difference between the legs. The typical gait of a four legged mammal has the following four kinds [11]. Walking gait: also known as "wave gait", each leg rises and falls in turn, and the phase difference is a. Trotting gait: diagonal legs rise and fall in pairs, and the phase difference between two pairs is b. Walking with the same side: the same side of the legs up and down in pairs, the difference between two pairs of c. Running gait: front and rear legs rise and fall in pairs, and the phase difference between two pairs is d. According to the rhythm of the movement, the above can be divided into double beat gait (trot gait, walking gait with the same side, running gait) and four beat gait (walking gait). The phase gait of the typical gait of a quadruped is shown in Table 1.

Table 1. Typical gait phase relation of quadruped

Gait	Leg phase			
	Left foreleg	Right foreleg	Right rear leg	Left rear leg
Walking gait	0	1/2	1/4	3/4
Trotting gait	0	1/2	0	1/2
Walking with the same side	0	1/2	1/2	0
Running gait	0	0	1/2	1/2

Nios II embedded CPG supports 32 bit instruction set, 32 bit data line width, 32 general-purpose registers, 32 external interrupt sources, and 2GB addressing space, including up to 256 user-defined CPU custom instructions [12]. The optional on-chip JTAG debug module is a debug logic based on boundary tests that supports hardware breakpoints, data triggers, and debug within an off chip. In this system, according to the corresponding requirements, the design of the system was based on the kernel, and all kinds of basic F units were added to the system development and application. The actual system design diagram is shown in Fig. 2.

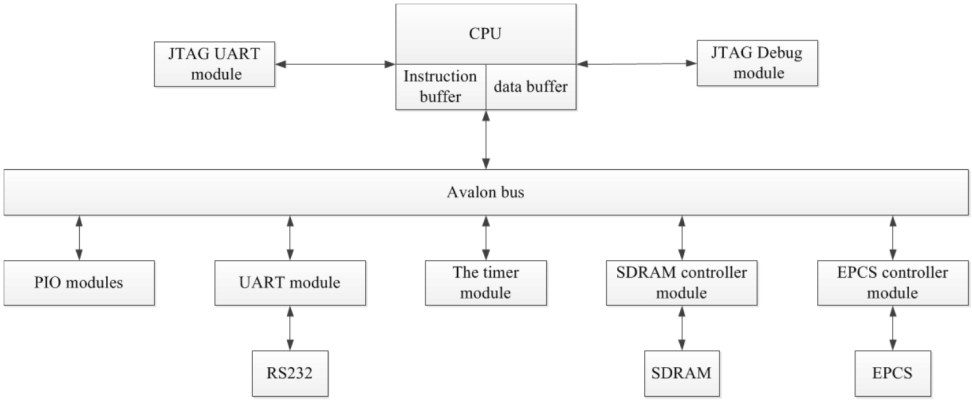

Fig. 2. Nios II system chart

It can be seen from the above diagram, the kernel of Nios II system designed in this paper includes Nios II CPU, JTAG UART module, JTAG Debug module, PIO module, UART module, timer module, SDRAM controller module, and EPCS controller module [13]. All data and programs in the system are transmitted via the Avalon bus. The whole kernel is built on the software implementation by using Altera's Quartus software and the SOPC builder tool. The whole design process adopts the SOPC technology proposed by Altera Company. SOPC technology is a flexible and efficient design scheme for on chip system SoC. Its working environment is SOPC builder in Altera of Quartus. Compared with other SoC designs [14], it has the advantage of programmability and uses the programmability of FPGA for SoC design. By using the SOPC builder tool, the user can easily connect the processor,

memory and other peripherals to form a complete embedded system. SOPC mainly consists of 2 parts: graphical user interface (GUI) and system generator from the internal point of view. Each component within the graphical user interface can also provide its own configuration graphical user interface, and GUI creates the system PTF file to describe the system. The build program creates a system HDL description for the target device [15].

3. Results analysis and discussion

In this paper, by changing the ground friction factor to simulate the movement of the robot on different ground, the paper analyzes the adaptability of the quadruped robot with different configurations to the terrain. In Adams, the static friction coefficient static coefficient and the dynamic friction coefficient dynamic coefficient are set as the design variables DV-1 and DV-2 respectively, and the different ground contact conditions are simulated by changing the values of the two design variables. DV-1 is more and less prone to relative sliding, the robot in a larger range of changes in the DV-1 stable walk reflects better terrain adaptability; DV-2 larger, the relative sliding, the robot foot and ground The greater the friction, the more easily off, the range of the two as shown in Table 2.

Table 2. Simulation data of different starting

	Design variable	Standard values	Minimum value	Maximum value
Static friction factor	DV-1	0.65	0.25	0.75
Dynamic friction factor	DV-2	0.55	0.15	0.65

It is found in the simulation experiment that when walking machine adopted symmetrical starting (the supporting foot was symmetrical at the beginning of the support and the end of the support relative to the airframe), the body soon collapsed toward the rear as the robot walks along. After careful observation and analysis, it is determined that the robot flips around the diagonal of the support (the line between two diagonal braces), which is not observed in previous physical prototype experiments. After analysis, it was determined that the value of the step size was very small in the physical prototype test, the original value was 12 cm, and the values in the simulation experiments were greater than 100 cm. The larger the step length, the greater the corner, and the more disadvantageous the walking stability was. With the subsequent step lengths were 600 mm, 450 mm and 225 mm, and the simulation results proved this point. When the step size was 600 mm, the robot fell 1 cycle after the start of the walk. When the step lengths were 450 mm and 225 mm respectively, the robot did not fall during the 20 experimental periods. When the step length was 225 mm, the attitude stability of the robot was better than that of

450 mm (see Table 3).

Table 3. Simulation data for unsynchronized length

Step size (mm)	Root mean square values of the roll angle in walking	Root mean square value of pitch angle in walking
450	1.3	3.1
225	1.2	2.9

In order to study the influence of robot walking cycle on walking stability, the robot cycle was simulated by 1.4 s, 1.0 s and 0.7 s. When the walking cycles were 1.4 s and 1.0 s, the robot fell after less than two cycles after the start of the walk. When the walking cycle was 0.7 s, the whole test cycle (20 cycles) did not fall. Obviously, smaller cycles are good for stability. The longer the cycle, the larger the change of the body of the walker's body, thus resulting in increased collisions and easy fall of the robot.

In order to solve the stability control problem of quadruped robot subjected to lateral impact, a lateral stability control strategy based on CPG and lateral step reflection was proposed. A CPG control network model considering lateral motion of robot was constructed. A trigger mechanism for the quadruped robot was introduced by constructing a trigger with a triggering property for the lateral pendulum of the hip joint. The block studies and reasonable values of CPG network connection weight matrix R were carried out, so as to make the output signal of the front and back rotation of the hip joint and the lateral oscillation oscillator keep the correct phase relationship at any time. Based on the ZMP theory and the linear inverted pendulum model, the magnitude of lateral stride of quadruped robot was predicted from the dynamics point of view. Finally, the joint simulation method of MATLAB/Simulink and ADAMS was used to verify the feasibility and effectiveness of the proposed control scheme. The simulation results show that under the influence of CPG and lateral step reflection, when the quadruped robot is subjected to lateral impact, its lateral acceleration can be restored to the threshold within a relatively short time, and then it terminates the reflection and matches the normal linear walking control scheme. The robot can successfully realize the stability control after the lateral impact of the normal walking, and its ability to resist lateral impact is improved significantly.

The principle prototype of the quadruped robot is shown in Fig. 3. The total mass of the prototype is about 100 kg. It is composed of a frame type airframe and four articulated leg mechanisms. The machine consists of 45 parts, 27 kinds of standard parts and purchased parts, totaling more than 1000 parts. The material is mainly made of 2A12 alloy aluminum, the key connection which needs to be strengthened adopts super hard aluminium 7050, and the joint shaft adopts No. 45 steel. It is mainly made up of robot, thigh side, knee joint and leg assembly, single leg and leg module.

In order to ensure the stability of the quadruped robot control system, it is

Fig. 3. Principle prototype of quadruped robot

necessary to ensure that the data communication of the control system has certain reliability, that is, the data cannot be misrepresented and lost. The purpose of this experiment is to verify the data accuracy of the CNA bus network composed of two main boards through continuous transmission and reception of large amounts of data.

The experimental principle: the gait generator sends 8 bytes to the execution drive as a set of consecutive data, and the execution driver sends the received data back to the gait generator after each data is received. The gait generator compares each received feedback data. If it is the same as the send data, count the correct variable plus 1. If it does not match the send data, count the wrong variable plus 1. Then, through the number of correct data and errors the process of sending, the correct rate of sending data can be obtained.

The prototype of quadruped robot was built in this chapter. Firstly, the CAN bus communication experiment between the gait generator and the executive driver was carried out to verify the reliability and real-time performance of the communication protocol. Secondly, with one leg experimental platform of quadruped robot, the single leg motion control experiment of robot was carried out to verify the rationality of gait generator design and the accuracy of CPG based multi-joint coordinated control method. The frequency response and load characteristics of the single leg were obtained by testing. Finally, based on the test and control performance of hydraulic drive unit, the gait planning test of the prototype was carried out to verify the correctness and effectiveness of gait generation algorithm for Quadruped Robot Based on CPG, so as to lay a foundation for the further movement of the experimental prototype.

4. Conclusion

From the point of view of design and planning, the main factors that affect the dynamic walking stability of quadruped robot were simulated and analyzed. The simulation test method was carried out using ADAMS. Through a large number of comparative analysis and theoretical analysis of simulation experiments, it can be found that there are many factors affecting the dynamic walking stability of quadruped walking robot, which are divided into the following aspects:

Stride length and walking cycle have important influence on walking stability. In order to achieve stable walking of walking robot, both stride length and walk cycle have a maximum limit value. The smaller the step size and the longer the walking cycle, the better the stability of the robot. The quality of walking robot has an obvious influence on the stability of walking. The quality of each component is reduced by employing lightweight material and reducing the size of each component, which can effectively reduce the collision between the ground and the ground when the swinging leg touches the ground, so as to improve the different effects of machine elements, such as the swing leg trajectory planning, supporting the ground, the robot's DOF configuration, damping system design and specific control plan.

However, there were still some shortcomings in this study, such as further improving the robot's ability to adapt to the environment. In this paper, the vestibular reflex and the flexor reflex have been studied, but other biological reflex mechanisms should be introduced to make the robot more abundant.

References

[1] L. Yao, E. Chen, Z. Chen, Z. Gong: *From SARS to H7N9: The mechanism of responding to emerging communicable diseases has made great progress in China.* Bioscience Trends *7* (2013), No. 6, 290–293.

[2] G. M. Xiong, T. Zhao, J. W. Gong, J. Y. Gao: *Development status and several problems of service robots.* Machine Tool & Hydraulics *35* (2007), No. 5, 212–215.

[3] Y. Zhao, C. Wu, X. Hu, G. Yu: *Research progress and problems of agricultural robot.* Transactions of the Chinese Society of Agricultural Engineering *19* (2003), No. 1, 20–24.

[4] P. Ji, H. Shen: *The current situation and development trend of service robot.* Journal of Changzhou University (Natural Science Edition) (2010), No. 2, paper 019.

[5] K. Watanabe, Y. Shiraishi, S. G. Tzafestas, J. Tang, T. Fukuda: *Feedback control of an omnidirectional autonomous platform for mobile service robots.* Journal of Intelligent and Robotic Systems *22* (1998), Nos. 3–4, 315–330.

[6] H. S. Wang, J. S. Han: *Research progress on combat trauma treatment in cold regions.* Military Medical Research (2014), No. 1, 8–8.

[7] Q. Meng, Y. Qi, S. J. Zhang: *Intelligent robot and its development.* Journal of China Ocean University Report *34* (2004), No. 5, 831–838.

[8] T. Mukai, S. Hirano, H. Nakashima, Y. Kato, Y. Sakaida, S. Guo, S. Hosoe: *Development of a nursing-care assistant robot RIBA that can lift a human in its arms.* IEEE/RSJ International Conference on Intelligent Robots and Systems, 18–22 October 2010, Taipei, Taiwan, IEEE Conference Publications (2010), 5996–6001.

[9] R. Bischoff, J. Kurth, G. Schreiber, R. Koeppe, A. Albu-Schaeffer, A. Beyer, O. Eiberger, S. Haddadin, A. Stemmer, G. Grunwald,

G. Hirzinger: *The KUKA-DLR Lightweight Robot arm-a new reference platform for robotics research and manufacturing.* International Symposium on Robotics (ISR) and German Conference on Robotics (ROBOTICS), 7–9 June 2010, Munich, Germany, VDE Conference Publications (2010), 1–8.

[10] Y. Zhao, X. Hou, L. Jia, S. Ma: *The obstacle avoidance system for mobile robot based on binocular stereo vision.* IEEE World Congress on Intelligent Control and Automation (WCICA), 7–9 July 2010, Jinan, China, IEEE Conference Publication (2010), 6461–6465.

[11] G. Campion, G. Bastin, B. D'Andrea-Novel: *Structural properties and classification of kinematic and dynamic models of wheeled mobile robots.* IEEE Transactions on Robotics and Automation *12* (1996), No. 1, 47–62.

[12] Y. Choi, B. J. You, S. R. Oh: *On the stability of indirect ZMP controller for biped robot systems.* IEEE/RSJ International Conference on Intelligent Robots and Systems (IROS) (IEEE Cat. No.04CH37566), 28 September–2 October 2004, Sendai, Japan, IEEE Conference Publications, *2* (2004), 1966–1971.

[13] J. Borenstein, Y. Koren: *A mobile platform for nursing robots.* IEEE Transactions on Industrial Electronics *IE–32* (1985), No. 2, 158–165.

[14] A. Sharkey, N. Sharkey: *Granny and the robots: Ethical issues in robot care for the elderly.* Ethics and Information Technology *14* (2012), No. 1, 27–40.

[15] L. Lei, X. J. Chen, Z. G. Hou, T. Min: *Design of the autonomous wheeled mobile robot C ASIA-1.* Chinese High Technology Letters (2003), No. 11.

Received August 7, 2017

Acta Technica *62* No. 2B/2017, 395–406

Additive manufacturing technology of laser metal deposition with high deposition rate based on Incone1718

Song Yang[1,3], Li Xu[2]

Abstract. Additive manufacturing technology is a new technique for making object entities, which is different from traditional machining technology. Laser metal deposition is a typical example of additive manufacturing technology. Compared with the traditional processing technology, laser metal deposition can effectively reduce the waste of raw materials, which is more suitable for the production of personalized parts processing. In this paper, the experimental system of the additive manufacturing of laser metal deposition with high deposition rate based on Incone1718 was studied, and the system requirements were analyzed in detail; the characteristics of the system and the characteristics of the powder materials used were also investigated; and the laser deposition process with high deposition rate based on Incone1718 was developed; the characteristics control of the process and the microstructure of the materials used were investigated and analyzed, so as to lay a solid theoretical foundation for the research of the additive manufacturing of laser metal deposition with high deposition rate based on Incone1718.

Key words. Incone1718, high deposition rate, laser metal deposition, additive manufacturing technology.

1. Introduction

Additive manufacturing is a new practical technology which is different from the traditional manufacturing technology. It is mainly through the gradual addition of materials and the accumulation of continuous form to produce a certain geometric properties of components. Compared with the traditional process, the components obtained by the process have more carrying capacity [1]. In addition to the enhanced carrying capacity, there are several other advantages [2]. For example, it can greatly reduce the waste of materials, and significantly shorten the production cycle. The production part of the product structure is more complicated, which is more able to meet the requirements of the production process and also more suitable for individual

[1]School of Manufacturing Science and Engineering, Sichuan University Chengdu, 610065, China
[2]Sichuan Conservatory of Music, Chengdu, 610000, China

parts [3]. Because of these advantages, additive manufacturing technology has been widely used in many fields, such as space, aviation, automobile and ship [4].

Although the traditional additive manufacturing technology is relatively mature, it has the disadvantage of low deposition rate [5]. The traditional process is difficult to meet the current large-scale parts processing needs, and the production cycle is longer with relatively high cost. The demand for additive manufacturing technology is also constantly improved, so it is of great practical significance to develop additive manufacturing technology with high deposition rate [6].

2. State of the art

With the widespread application of additive manufacturing technology, the research on this technology is increasing year by year in China. Published papers on the technology of making materials are increasing year by year, and the research directions and fields are becoming more and more thorough [7]. Professor Huang Weidong of the Key Laboratory of Solidification Technology of Northwestern Polytechnical University has carried out many deep researches on the additive manufacturing of laser metal deposition with high deposition rate based on Incone1718, including the microstructure of the selected material, the mechanical properties of the material, the selection of the material and the differences in the solidification process of the material. And the research results have been widely used in various fields. For example, domestic C919 aircraft used additive manufacturing technology to print the main aluminum alloy crazy block overall window frame [8].

The research on additive manufacturing technology of laser metal deposition with high deposition rate based on Incone1718 has become more and more abroad [9]. Taking the research in Germany as an example, the Fraunhofer Laser Technology Research Institute has carried out the research on additive manufacturing technology for more than 30 years. The research fields are very extensive, including the study of additive manufacturing technology based on a variety of alloys, such as titanium alloy, IN718 alloy, and WC-CO alloy [10]. At the same time, they have made a comprehensive analysis and research on the equipment used, process control, and the choice of coating oxidation resistant gas in the additive manufacturing technology. In addition, they have established a simulation model to simulate the detection of a variety of research [11]. In addition, the United Kingdom and the United States have made thorough study on the additive manufacturing of laser metal deposition with high deposition rate based on Incone1718. The specific application of additive manufacturing technology of laser metal deposition with high deposition rate based on Incone1718 is mainly divided into four parts. The first is to design the 3D model which is suitable for the parts processing; the second step is to design the appropriate processing plan for the appropriate model, and do the concrete physical processing [12]; the third step is to scan the processed 3D model by laser, compare it with the designed CAD model for the adjustment and modification, and remove the unsuitable position [13]; finally, the precise machining of the part model results in the completion of the 3D physical entity of the qualified parts [14].

3. Methodology

With the further development of science and technology in China, every industry in our country has been greatly improved and the overall strength has been improved. Especially in the related industries of machining, more technologies have gradually begun to be applied and have brought some positive effects to the development and progress of our country industry, which has enhanced the overall level of our country industry continuously, and has gradually increased the economic output value of China's industry [15]. As one of the important technologies in the development of some fields, the additive manufacturing technology has become more and more perfect, and the development of some trades in our country has been greatly influenced. Some studies have been done on the relevance of the economic output value of China's aviation industry and the improvement of additive manufacturing technology (results shown in Fig. 1). The results show that there is a positive correlation between the manufacturing output value of China's aviation industry and the improvement of China's additive manufacturing technology. With the continuous improvement of the related theories in China, the application of the industry has been gradually enhanced, and the manufacturing output value of the aviation industry in China has been increasing year by year. Therefore, from the point of view of the examples, the application of additive manufacturing technology can effectively promote the further development of related industries in China, greatly improve the relevant industry in China's economic strength, bring positive impetus to the overall strength of China's national economic promotion, and finally realize China's overall level and the improvement of international status.

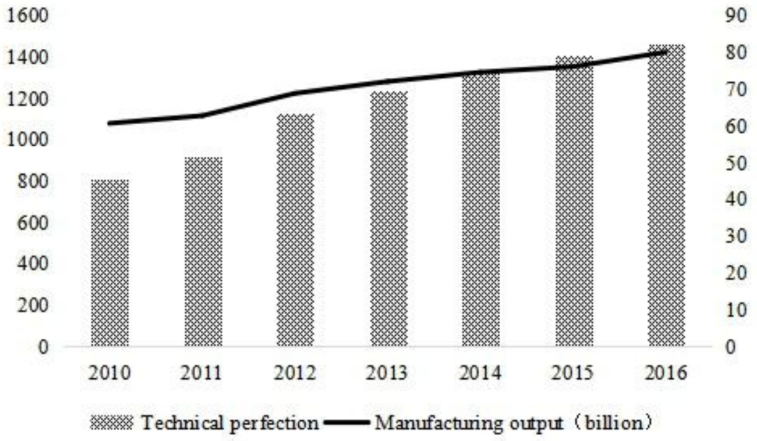

Fig. 1. Correlation analysis of manufacturing output value of aviation industry in China and the improvement of additive manufacturing technology

With the introduction and combination of the additive manufacturing technology in various fields of our country, great progress has been made in various fields. Many scholars in our country have begun to put forward some advanced science

and technology in the current era and gradually combine with the traditional additive manufacturing technology, thus forming a relatively new additive manufacturing technology. Through the improvement of this emerging technology, higher economic benefits for enterprises can be obtained, and our enterprises have more competitive performance. Laser technology with high deposition rate based on Incone1718 is one of the innovative technologies in the world manufacturing industry. The development of this technology has a positive impact on the improvement of additive manufacturing technology. Many researchers have begun to improve the two technologies and theories. At the same time, the organic integration of the two technologies is further realized to obtain some results, which brings important positive impetus to the development of manufacturing enterprises and the level of economy. In this trend, scholars in China have begun to improve the theory and application of this technology. However, due to the shortcomings of our scholars in the knowledge level, there are still some deficiencies in the related technology combination, which makes the actual performance of the technology still have some shortcomings. This indirectly affects the further development of related enterprises in China to some extent. In this study, the related theory and technology application of the additive manufacturing of laser metal deposition with high deposition rate based on Incone1718 were discussed. The research aims at providing the theoretical basis and reference for the development of the industry and the improvement of the new technology. The main methods of this study are as follows: The traditional additive manufacturing technology cannot meet the demand of high deposition rate in the production process. First of all, the requirements of all aspects of the additive manufacturing technology with high deposition rate were analyzed, so as to determine the actual needs of related technology development. On this basis, according to the actual needs of building materials, the additive manufacturing technology and related links with high deposition rate were constructed. The stability of the related system was verified on the basis of the determination of related technologies and links. The characteristics of powder spraying and laser output in the additive manufacturing technology with high deposition rate were studied and calculated. The relevant formulas are as follows:

$$v_1 = \frac{d_1}{\Delta t},\ v_2 = \frac{d_2}{\Delta t}\,, \tag{1}$$

where v_1 and v_2, respectively, indicate the velocity of powder particle ejection and the velocity of entering molten pool, and Δt is the time of powder movement.

The mathematical model of the process technology for the additive manufacturing technology with high deposition rate was established. Then, based on the related theories, different additive manufacturing techniques and models with high deposition rate were studied. The mathematical model established in this paper is as follows:

$$A_{\mathrm{T}} = \frac{2\theta}{2\pi} \times \pi R^2 - \frac{d_{\mathrm{L}}}{2}\left(R - \frac{d_{\mathrm{L}}}{r_{\mathrm{A}}}\right), \tag{2}$$

where, A_{T} represents the area size of the entire plating cross section, d_{L} represents the diameter of the spot produced by the laser emission, and r_A represents the ratio of the width and height of the coating.

For the quality of the coating, the relevant models are constructed as follows:

$$A_{\mathrm{T}} \times L \times \rho = \eta \times m \times t\,, \tag{3}$$

where,L,ρ,η and m, respectively, indicate the length of the coating, the density of the metal material used, the deposition efficiency in the powder deposition process and the weight of the powder.

The research finally analyzed and discussed the related technologies of this research from the point of view of examples. The advantages of this technique were confirmed by using actual cases. And a theoretical reference and foundation for its popularization and application was provided.

3.1. Result analysis and discussion

The additive manufacturing technology is a new kind of new manufacturing technology based on laser cladding technology. First of all, the additive manufacturing technology uses the laser to melt the metal powder, and the melted metal powder forms a molten pool on the base material. Then the laser spot moves, and then goes into the molten pool. The molten metal powder gradually solidifies, and forms metallurgical bonding with the base material. Then 3D physical entities are slowly formed in layers. Because the coating is easy to oxidize in the air, the inert gas, such as helium and argon, is used as the protective gas in the process, so as to avoid the oxidation of the coating.

There are two forms of powder feeding, namely, coaxial feeding and side feeding, as shown in Fig. 1. The principle of coaxial feeding is that the powder beam formed by laser beam and powder is the same central axis, so it is called coaxial feeding powder. There are two patterns in the process of making materials: lateral pollination and coaxial pollination, the powder beam is very concentrated in front of the nozzle, so the precision is relatively high, which is more suitable for the repair of parts and other processing technology. The side feeding is completely different from the central axis formed by the laser beam due to the powder being sent from side to side in the dissolution bath, so it is called side feeding. The lateral feeding system has a strong directionality, and there are different processing techniques in all directions. Moreover, the powder beam formed before the nozzle is not concentrated as coaxial feeding powder, but rather skewed to the rectangular shape. Therefore, the machining precision is relatively weak, but the powder feeding rate is obviously improved. Therefore, it is often used in the manufacture of metal cladding of tubular parts, which plays a role in strengthening the wear resistance of tubular parts. Material making technology in the process of physical objects as shown in Fig. 2. From Fig. 3 left, it can be found that the powder beam formed by coaxial feeding is more concentrated and more inclined to be cone shaped. In Fig. 3 right, the powder beam formed by the side feeding powder is relatively loose, and tends to be rectangular or banded, but the powder feeding rate is obviously larger.

The additive manufacturing system of laser metal deposition with high deposition rate based on Incone1718 includes the powder feeding system (powder feeder, powder distributor, powder spraying, and various connected devices), laser system

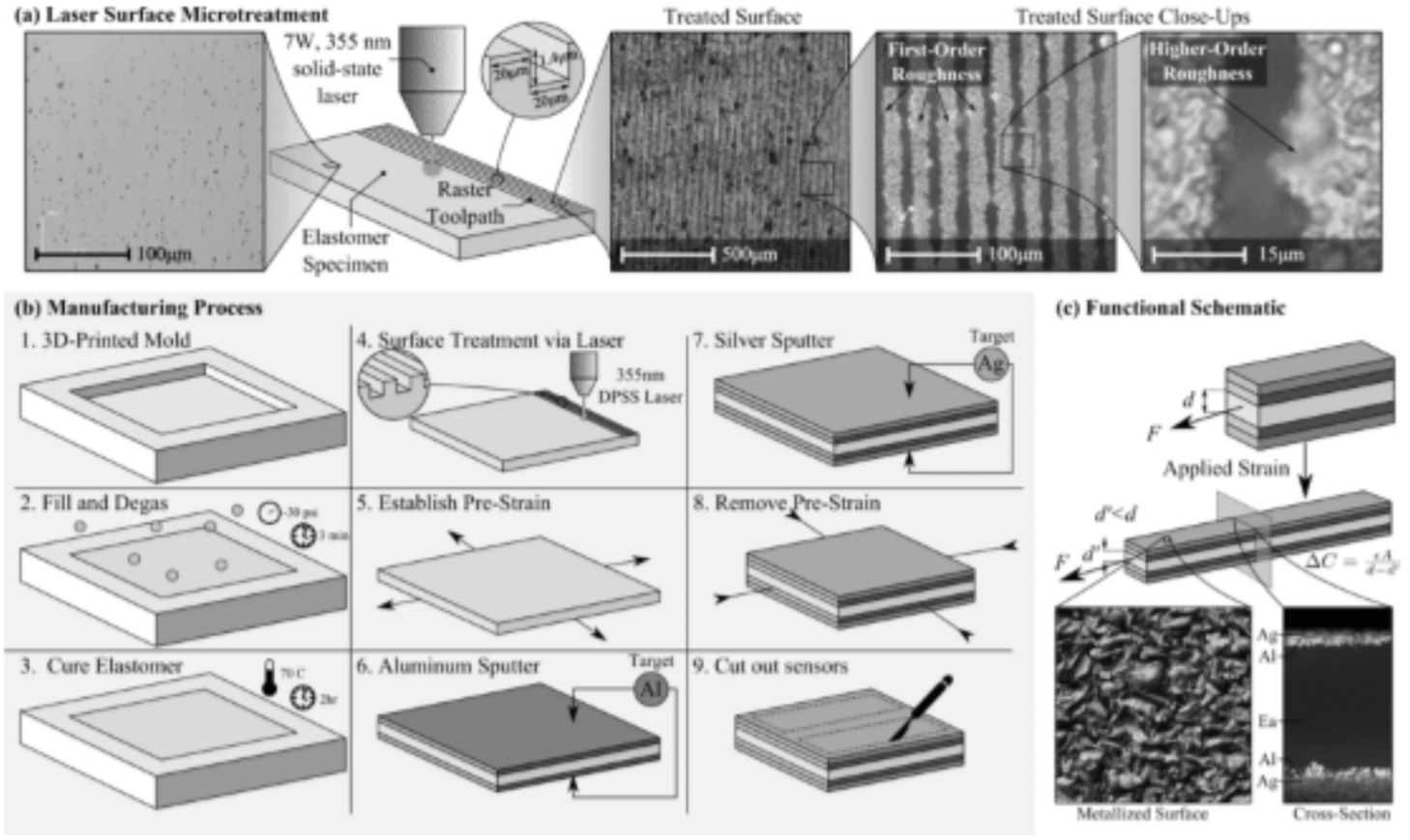

Fig. 2. Principal schematic diagram of additive manufacturing technology: top–powder feeding system of coaxial additive manufacturing technology, bottom–powder feeding system of lateral additive manufacturing technology

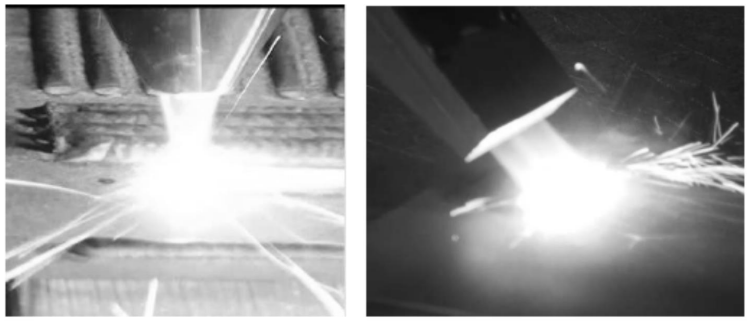

Fig. 3. Powder feeding system diagram with different additive manufacturing technologies: left–powder feeding system of coaxial additive manufacturing technology, right–powder feeding system of lateral additive manufacturing technology

(laser light source, optical system and optical fiber connection) and auxiliary system (machine, inert gas, cooling system and other monitoring system). The requirement analysis of the three systems is carried out, and each system is deeply studied. The research of powder feeding system mainly focuses on how to realize high feeding powder. The realization of high feeding powder is the necessary condition to meet the high deposition rate, and the key to realize the high feeding powder is the improvement of the component of the powder nozzle. First of all, the problems existing in the traditional material making process are analyzed. The main problems are the low powder output, the low powder mixing and powder gathering ability, and the relatively low thermal capacity. The forming state of the powder beam is studied in the case of different powder feeding rate. The results show that the powder agglomeration capacity of the powder beam is better when the feed rate is small. However, with the increase of the powder feeding rate, the powder nozzle gradually losses the power of powder gathering. In view of the above problems, a high deposition rate LMD powder nozzle is developed. The main improvements are as follows: firstly, the new nozzle should increase the distance between the inner and outer rings and adjust the internal mixing system, in this way, the damage to the inner and outer walls of the system can be avoided effectively; secondly, the new nozzle should extend the focal length of the powder beam, which can reduce the thermal load and effectively prevent the particles from sticking to the front of the nozzle; at the same time, the position of the protective mirror of the shower nozzle should be adjusted properly, so that the lens is more favorable for the protection of the lens; in addition, the aperture at the top of the nozzle should be enlarged to better adapt to the laser spot. Through the improvement above, the power of powder gathering can be strengthened under the condition of high powder feeding. As shown in Fig. 4, the top of the improved nozzle is enlarged and the focus of the powder is longer, and the beam formed by the powder is more concentrated, which can meet the requirements of precision machining.

The quality of powder material is the most important index of the quality of

the process, and the physical and chemical characteristic of the powder material is an important evaluation index to evaluate the quality of the powder material. The physical and chemical properties of powder materials seriously affect the material gain, manufacture technology and technological performance of powder. The physical and chemical properties of powder materials include the percentage of chemical elements, porosity and morphological characteristics of powder. Firstly, the percentage of chemical elements in the powder material can be measured by ICP-AES analysis. The N and O elements in the non-oxides of non-metallic elements can be obtained by means of a gas transport heat extraction (CGHE) method. C and S elements are usually selected by incineration for determination and analysis. By using the above three methods, the percentage of chemical elements in a powder material is analyzed (Table 1). From the table, it can be found that the main components of Incone1718 are Ni, Fe, Mo and Mn, and these four elements have significant influence on the LMD characteristics of the material.

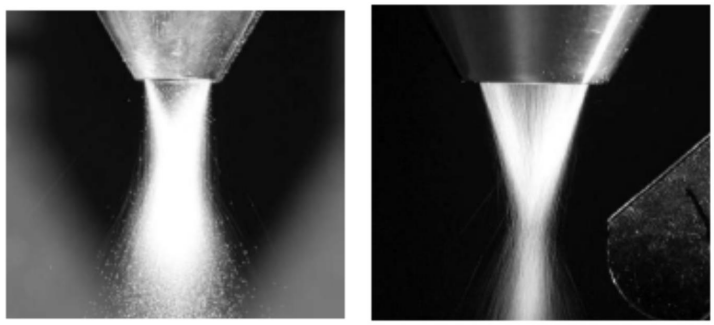

Fig. 4. Comparison of powder beam morphology between conventional powder nozzle and high deposition rate powder nozzle under high powder feeding condition: left–powder beam morphology of high deposition rate powder nozzles

Table 1. Percentage analysis results of chemical elements in powder

Ni (%)	Cr (%)	Nb (%)	Mo (%)	Ti (%)	Al (%)	Co (%)
51.3	19.2	5.2	3.0	0.99	0.56	0.038
Fe (%)	Si (%)	P (%)	Mg (%)	Cu (%)	B (%)	Mn (%)
19.0	<0.06	<0.01	<0.001	0.016	<0.005	0.037
Se (%)	Ta (%)	Ca (%)	O (%)	N (%)	C (%)	S (%)
<0.002	0.019	0.004	0.008	0.018	0.056	0.004

In this paper, the laser energy used in the calibration of the laser and the caustic curve were analyzed. It can be found that the laser source connected to the control system can effectively receive the voltage signal used by the system. The signal can also receive the output power of the laser source. Therefore, the mapping relation can be obtained by scaling the output power. Firstly, the diameter of the original

light spot of the laser optical system is set to 3 mm, and then the original dispersion curve and the laser capacity distribution at the focal point of the laser optical system are shown in Fig. 5. Caustic curve of laser optical system is symmetric hyperbolic curve style. The narrowest point of the curve is where the focus of the laser is.

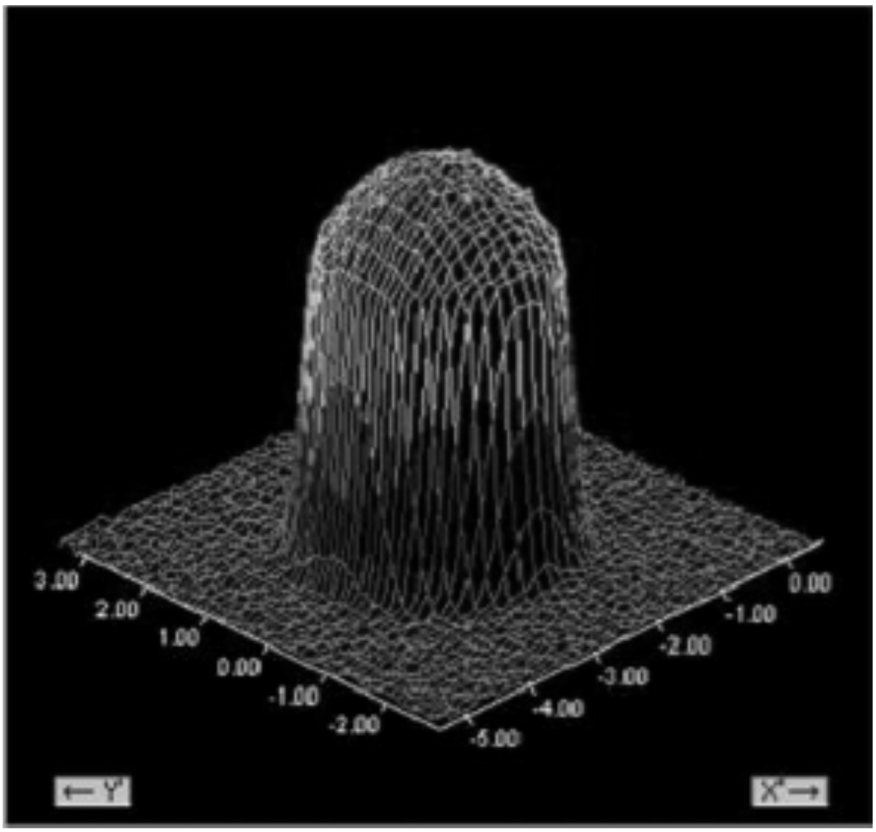

Fig. 5. Energy distribution curve and the original facula of non-zoom optical system in the focal point

The original laser spot is set to 4 mm, the distribution of laser forming caustic curve is a type of state Gauss style. Similarly, the symmetry is better, but the original spot is relatively decreased, as shown in Fig. 6.

4. Conclusion

In this paper, Incone1718 was used as the main material of research, and the additive manufacturing technology of laser metal deposition with high deposition rate based on Incone1718 was studied through the combination of theoretical literature and experimental research. The results show that the physical entity of Incone1718 used in this study is superior to the entity obtained by traditional methods in terms

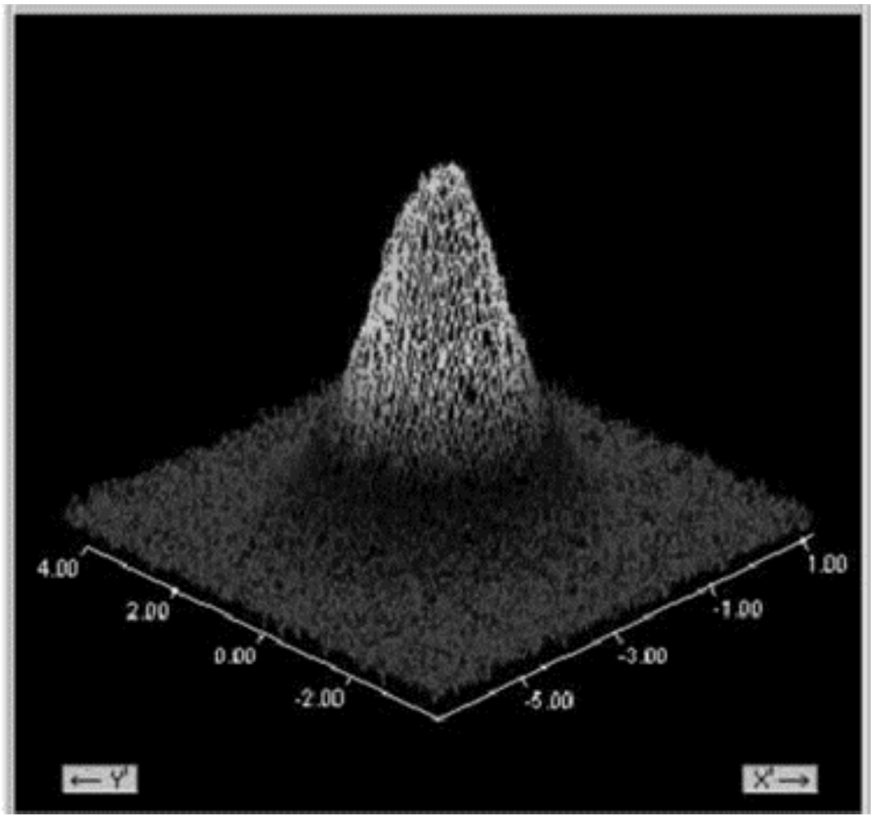

Fig. 6. Energy distribution and the original facula of zoom optical laser system in the focal point

of mechanical properties at normal temperatures, hardness of materials and ductility of materials. Firstly, the experimental system of the additive manufacturing technology of laser metal deposition with high deposition rate based on Incone1718 was studied and designed. The system has the advantages of better flexibility and high powder output. Secondly, the characteristics of powder injection and the laser characteristics of laser system were analyzed deeply. The results show that the powder beam formed by coaxial feeding powder is more concentrated and more inclined to be cone shaped, while the powder beam formed by the side feeding powder is relatively loose and tends to be rectangular or banded, but the powder feeding rate is obviously larger. Compared with the traditional process, the additive manufacturing technology of laser metal deposition with high deposition rate based on Incone1718 is improved by about 20 times. Moreover, the opening at the top of the improved nozzle is enlarged, and the focus of the powder is longer, and the beam formed by the concentrated powder is more concentrated, which can satisfy the requirement of precise processing. The research results of this paper can lay a solid theoretical foundation for the research of the additive manufacturing technology of laser metal

deposition with high deposition rate based on Incone1718.

References

[1] K. Shah, I. U. Haq, S. A. Shah, F. U. Khan, M. T. Khan, S. Khan: *Experimental study of direct laser deposition of Ti-6Al-4V and Inconel 718 by using pulsed parameters.* Scientific World Journal (2014), Article ID No. 841549, 231–248.

[2] N. Vanderesse, M. Anderson, F. Bridier, P. Bocher: *Inter- and intragranular delta phase quantitative characterization in Inconel 718 by means of image analysis.* Journal of Microscopy *261* (2016), No. 1, 79–87.

[3] K. Shah, I. U. Haq, S. A. Shah, F. U. Khan, M. T. Khan, S. Khan: *Corrigendum to "Experimental study of direct laser deposition of Ti-6Al-4V and Inconel 718 by using pulsed parameters".* Scientific World Journal (2015), Article ID No. 487439.

[4] H. T. Lee, W. H. Hou: *Study of delta phase on static recrystallization behavior of Inconel 718 alloy.* Journal Nanoscience and Nanotechnology *12* (2012), No. 9, 6987 to 6995.

[5] B. Dubiel, A. Kruk, E. Stepniowska, G. Cempura, D. Geiger, P. Formanek, J. Hernandez, P. Midgley, A. Czyrska-Filemonowicz: *TEM, HRTEM, electron holography and electron tomography studies of gamma' and gamma" nanoparticles in Inconel 718 superalloy.* Journal of Microscopy *236* (2009), No. 2, 149–157.

[6] K. Venkatesan: *The study on force, surface integrity, tool life and chip on laser assisted machining of Inconel 718 using Nd:YAG laser source.* Journal of Advanced Research Articles *8* (2017) No. 4, 407–423.

[7] J. Díaz-Álvarez, A. Tapetado, C. Vázquez, H. Miguélez: *Temperature measurement and numerical prediction in machining Inconel 718.* Sensors (Basel) *17* (2017), No. 7, paper 1531.

[8] S. Yust-Katz, P. Garciarena, D. Liu, Y. Yuan, N. Ibrahim, R. Yerushalmi, M. Penas-Prado, M. D. Groves: *Breast cancer and leptomeningeal disease (LMD): Hormone receptor status influences time to development of LMD and survival from LMD diagnosis.* Journal of Neuro-Oncology *114* (2013), No. 2, 229–235.

[9] X. Lecomte, V. Gagnaire, V. Briard-Bion, J. Jardin, S. Lortal, A. Dary, M. Genay: *The naturally competent strain Streptococcus thermophilus LMD-9 as a new tool to anchor heterologous proteins on the cell surface.* Microbial Cell Factories *13* (2014), No. 1, paper 82.

[10] B. Thevenard, C. Besset, S. Choinard, P. Fourcassié, P. Boyaval, V. Monnet, F. Ru: *Response of S. thermophilus LMD-9 to bacitracin: Involvement of a BceRS/AB-like module and of the rhamnose–glucose polysaccharide synthesis pathway.* International Journal of Food Microbiology *177*, (2014), No. 2, 89–97.

[11] M. Tasaki, K. Obayashi, M. Ueda, Y. Ando: *Amyloid typing from formalin-fixed paraffin-embedded tissues using LMD-LC-MS/MS system.* Rinsho Byori *62* (2014), No. 3, 291–296.

[12] C. Fierro-Castro, M. C. Santa-Cruz, M. Hernández-Sánchez, M. Teles, L. Tort: *Analysis of steroidogenic pathway key transcripts in interrenal cells isolated by laser microdissection (LMD) in stressed rainbow trout.* Comparative Biochemistry and Physiology Part A: Molecular & Integrative Physiology *190* (2015), No. 2, 39–46.

[13] Z. Liu, X. Chen, Z. He, Z. Shen: *LMD method and multi-class RWSVM of fault diagnosis for rotating machinery using condition monitoring information.* Sensors (Basel) *13* (2013), No. 7, 8679–8694.

[14] A. Campos-Barros, S. Benito-Sanz, J. L. Ross, A. R. Zinn, K. E. Heath: *Compound heterozygosity of SHOX-encompassing and downstream PAR1 deletions results in Langer mesomelic dysplasia (LMD).* American Journal of Medical Genetics Part A *143A* (2007), No. 9, 933–938.

[15] Y. J. Goh, C. Goin, S. O'Flaherty, E. Altermann, R. Hutkins: *Specialized adaptation of a lactic acid bacterium to the milk environment: The comparative genomics of Streptococcus thermophilus LMD-9*. Microbial Cell Factories *10* (2011), Suppl. No. 1, S22.

Received August 7, 2017

Acta Technica *62* No. 2B/2017, 407–422

Applied research on site selection for urban logistics distribution center based on fruit fly optimization algorithm

Yuan Xion[1]

Abstract. Through the optimization algorithm of fruit flies, there is a local optimum solution for the location of logistics distribution center, and it is prone to fall into the local minimum. In order to achieve reasonable allocation of the site of logistics distribution center, an improved optimization algorithm for Drosophila melanogaster is proposed in this paper, and function optimization problem and site selection of logistics distribution center are chosen as the objects of study. Function optimization problem verifies that improved fruit fly optimization algorithm exhibits faster convergence rate and higher convergence precision, so it can be applied in other research fields. A mathematical model for site selection of logistics distribution center is established according to the coordinates of logistics distribution centers in 31 cities and their demand for goods and materials. Besides, improved fruit fly optimization algorithm is applied for optimization solution to achieve the optimal allocation of distribution path and save cost. The simulation result indicates that the algorithm has the advantages of fast convergence rate and high precision.

Key words. Fruit fly optimization algorithm, logistics distribution center, chaotic system, logistic system, demand quantity.

1. Introduction

As e-commerce grows rapidly, logistics industry as an emerging industry is developing at a fast speed. The site selection method of logistics distribution center as a middle link connecting customers sand suppliers decides logistics distribution mode and distribution distance and influences work efficiency and economic benefit of logistics system. The study on site selection of logistics distribution center has important practical significance and theoretical value. Therefore, distribution center site selection model and optimization method in logistics network layout attract extensive attention of domestic and overseas research scholars.

[1]Nanchang University, Nanchang, 330031, China

Revelle and Swain [1] proposed slack linear programming algorithm for site selection problem in 1970. In 1978, for large-scale logistics site selection problem, Erlekotter [2] put forward both way slope algorithm and local search algorithm. The empirical study shows this method has good effect and high efficiency. In 1988, Kazuyoshi Hidaka [3] applied greedy heuristic algorithm and balloon search heuristic algorithm successively to solve large-scale facility site selection problem. In 1999, Yamada took minimum transportation cost and minimum CO_2 emission as the objective function[4] to select the site of logistics distribution center. Although traffic distribution was considered, this model could only handle small-scale site selection problem. In 2001, Wang Zhanquan and Yang Dongyuan [5] applied global search optimization technique, established site selection model based on genetic algorithm, compared and analyzed it with traditional mixed integer programming solution. With regard to logistics center site selection for perishable products, Jiang Dali and Du Wen [6] combined global search capacity of genetic algorithm and local search capacity of ALA method to put forward a mathematical model for logistics center site selection based on AGA integer programming in 2003. The result indicates that this algorithm can greatly increase the probability of acquiring the optimal distribution path and the optimal site. In 2006, Wu Bing, Luo Ronggui and Peng Weihua [7] came up with logistics center site selection optimization model based on genetic algorithm of priority coding. The result indicates that this method can effectively reduce the difficulty in solving site selection problem. In 2008, Zhao Dongling, Yu Longzhen and Chen Changju [8] established 0–1 integer programming model for logistics center site selection and proposed an improved single-point PMX intersection method to solve large-scale logistics distribution optimization problem by combining the thought of genetic variation. The result shows the improved algorithm has good effect, and is superior to improved single-point intersection method in terms of convergence rate and optimal solution.

2. Improved fruit fly optimization algorithm

2.1. Fruit fly optimization algorithm

Fruit fly optimization algorithm (FOA) is a new evolutionary computation method which was proposed by Pan [9] in 2011. At present, it is widely applied in function optimization, SVM parameter optimization, knapsack problem and optimization of neural network weight and threshold value, etc. Although this algorithm has such advantages as few control parameters, fast convergence rate and high convergence precision, it has local optimum problem and thus may be easily caught in local minimum. This paper combines ergodicity, regularity and randomness advantages of logistic chaotic system and proposes fruit fly optimization algorithm based on logistic chaotic system to overcome local optimum problem of FOA.

Step 1: Set fruit fly population size *popsize* and maximum iteration times of FOA; initialize fruit fly population position at random; the initialization results are expressed as X_begin and Y_begin, respectively.

Step 2: Calculate random optimizing direction and distance of fruit fly individuals according to (1) and (2):

$$x_i = X\_begin + Value \times rand()\,, \tag{1}$$

$$y_i = Y\_begin + Value \times rand()\,. \tag{2}$$

In (1) and (2), $Value$ represents search distance of fruit fly, while x_i andy_i represent the position of fruit fly individuals in the next moment.

Step 3: Estimate the distance d_i between fruit fly individuals and the original point according to formula (3); then apply formula (4) to figure out smell concentration s_i of fruit fly individuals:

$$d_i = \sqrt{x_i^2 + y_i^2}\,, \tag{3}$$

$$s_i = \frac{1}{d_i}\,. \tag{4}$$

Step 4: Substitute smell concentration s_i into formula (5)—smell concentration decision function—and calculate smell concentration of fruit fly individuals at current position

$$Smell_i = Function(s_i) \tag{5}$$

Step 5: Find out the best smell concentration and the best position of fruit fly individuals. The best smell concentration is expressed as $Smell_{\mathrm{b}}$, and the best position is expressed as x_{b} and y_{b}.

Step 6: Reserve and record the best position and the best smell concentration of fruit fly. The best smell concentration $Smellbest = Smell_{\mathrm{b}}$; the initial position of fruit fly $Y\_begin = y_{\mathrm{b}}$, $X\_begin = x_{\mathrm{b}}$; besides, fruit fly population searches towards the best position.

Step 7: Iterate for optimizing and repeat iteration steps 2–5 and judge whether the smell concentration is better than that in the last iteration. If it is better, execute Step 6.

2.2. Logistic chaotic system

Chaos phenomenon extensively exists in nonlinear system. It is an aperiodic motion form. Since the sequence generated by chaotic system has good randomness, ergodicity and regularity, chaotic sequence is widely applied in signal processing, nonlinear control, image encryption and other relevant fields.

The expression of logistic chaotic system is shown in Formula (6) [11, 12]

$$x(n+1) = ux(n)(1 - x(n)),\ x(n) \in [0,\, 1]\,. \tag{6}$$

In formula (6), n is iteration number, u represents chaos control parameter (when $u = 4$, logistic system is in the chaotic state. A transformation calculation formula

of chaos variable of Cx_i is shown in formula (7)

$$Cx(n+1)_i = 4Cx(n)_i(1 - Cx(n)_i),\ i = 1, 2, ..., N\,. \tag{7}$$

In Formula (7), $Cx(n)_i$ represents the value of the ith chaos variableCx_i of chaotic mapping after the nth chaos variable. When $Cx_i \in [0, 1]$ and $Cx_i \notin \{0.25, 0.50, 0.75\}$, the system is in the chaotic state. The optimization parameter $x_i \in [a_i,\ b_i]$ in Formula (7) can be transformed through mutual mapping of formulae (8), (9) and chaos parameter $Cx_i \in [0,\ 1]$.

$$Cx_i = (x_i - a_i)/(b_i - a_i)\,, \tag{8}$$

$$x_i' = a_i + Cx_i(b_i - a_i)\,. \tag{9}$$

In formula (9), x_i' represents the value that the ith chaos variableCx_i after chaotic mapping is transformed to conventional variable.

2.3. Improved FOA

Logistic chaos theory is introduced in FOA to improve it. The main process of improved FOA is as follows:

Step 1: Set fruit fly population size *popsize* and maximum iteration times *Iteration* of FOA; initialize fruit fly population position at random between 0 and 1, and express it as vector z_i.

Step 2: Map the $z_i$component to chaos parameter $Cz(n)_i$, $Cz(n)_i = [0,\ 1]$ according to formula (8).

Step 3: Conduct chaotic mapping for chaos parameter $Cz(n)_i$ according to formula (7).

Step 4: Carry out mapping transformation for each component according to formula (9), and the mapping is conventional variable z_i' in $[a_i,\ b_i]$; calculate fitness $f(z_i')$, choose the minimum $f(z_i')$ in the population and record the minimum $f(z_i')$, $fit(gen) = f(z_i')$.

Step 5: Optimize and iterate; repeat the steps 2–4.

Step 6: If the stop condition is met (iteration times is greater than the maximum iteration time *Iteration*), select the minimum fit and make $Smellbest = \min(fit(gen))$. At this moment, record smell concentration S_g of minimum $f(z_i')$.

Step 7: To make sure the initial value to be gained is within the small interval of optimal parameter in the initial iteration, if the parameter is greater than 0, $B \in [0,\ 1]$. Through repeated verification, $B = 0.25$ is chosen in this paper. Apply $S_i = S_g + 2B \times rand() - B$ to generate tiny disturbance population near the selected smell concentration S_g. Meanwhile, apply S_i to assess $f(S_i)$. Choose $f(S_i)$ with the smallest fitness in the population and make $Bestsmell = \min(f(S_i))$. If $Bestsmell < Smellbest$, $Smellbest = Bestsmell$ and make $S_g = S_i$.

Step 8: Carry out secondary iteration and optimization; update smell concentration S_i and repeat Step 7.

Step 9: If the stop condition is met (iteration times is greater than the maximum iteration time *Iteration*), output *Smellbest*, $P = S_g$.

2.4. Mathematical model for logistics distribution center site selection

To achieve the optimal selection of urban logistics distribution center, the following hypotheses are accepted [13]: goods capacity of logistics distribution center can satisfy the demand for goods at each demand point, and total goods amount at the logistics distribution center is decided by goods demand of distribution demand point; one distribution center only supplies a demand point; the transportation expenses from the logistics distribution center to the factory are not taken into account.

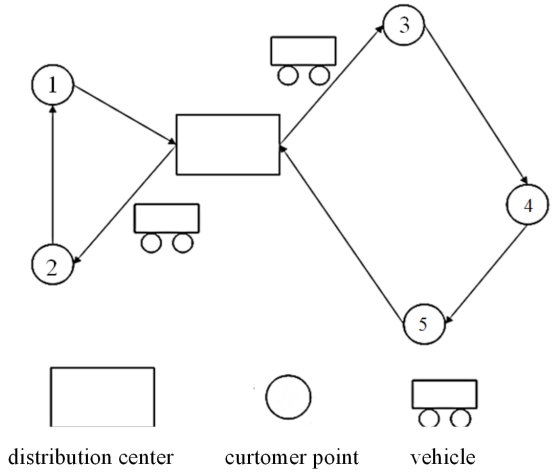

Fig. 1. Distribution diagram

Based on the above hypotheses, the mathematical model for logistics distribution center site selection can be established. The distribution diagram is shown in Fig. 1. The mathematical model is a site selection and distribution model. Under the condition of meeting upper limit of distance, it is necessary to find out the distribution center from n demand points and distribute goods to each demand point. The objective function is the minimum sum of product between the demand and distance from each distribution center to the demand point. The objective function is:

$$\min F = \sum_{i \in N} \sum_{j \in M_i} w_i d_{ij} Z_{ij} \,. \tag{10}$$

The constraint conditions are

$$\sum_{j \in M_i} Z_{ij} = 1, \; i \in N \,, \tag{11}$$

$$Z_{ij} \leq h_j,\ i \in N,\ j \in M_i\,, \tag{12}$$

$$\sum_{j \in M_i} h_j = p\,, \tag{13}$$

$$Z_{ij},\ h_j \in \{0,\ 1\},\ i \in N,\ j \in M_i\,, \tag{14}$$

$$d_{ij} \leq s\,. \tag{15}$$

In the above constraints, $N = \{1, 2, ..., n\}$ is the serial number set of all demand points, M_i represents the set of alternative distribution centers whose distances from the demand point i are less than s, $i \in N$, $M_i \subseteq N$, and w_i represent the demand quantity of demand points, d_{ij} refers to the distance from the demand point i to the nearest distribution center j, and Z_{ij} represents 0–1 variable and service demand distribution relation of users and logistics center. When $Z_{ij} = 1$, the demand quantity of demand point j is supplied by distribution center j, or else $Z_{ij} = 0$. Symbol h_j represents 0–1 variable. When $h_j = 1$, the demand point j is chosen as the distribution center. Symbol s represents the upper limit of distance from the demand point served by the newly-built distribution center.

Formula (11) guarantees that each demand point can be served by only one distribution center. Formula (12) guarantees the demand quantity of demand point can only be set to point supply of distribution center. In other words, there will be no customer where there is no distribution center. Formula (13) specifies that the number of selected distribution centers is p. Formula (15) guarantees that the demand point is within the scope that the distribution center can reach.

3. Analysis and discussion

3.1. Optimization of logistics distribution center site selection using IFOA algorithm

The steps of optimizing logistics distribution center site selection with IFOA algorithm are as follows. The flow chart is shown in Fig. 2.

Step 1: Set population size *popsize* and maximum iteration times *Iteration* of IFOA algorithm.

Step 2: Calculate fitness function value of fruit fly individuals according to formula (10) and search the position and optimal value of fruit fly individuals and global optimal individual.

Step 3: Update speed and position of fruit fly population.

Step 4: Figure out fitness and update position and speed.

Step 5: If $gen > Iteration$, save the optimal solution, otherwise $gen = gen + 1$, and turn to Step 3.

Step 6: The best position and the best distribution path of corresponding logistics distribution center according to the optimal position.

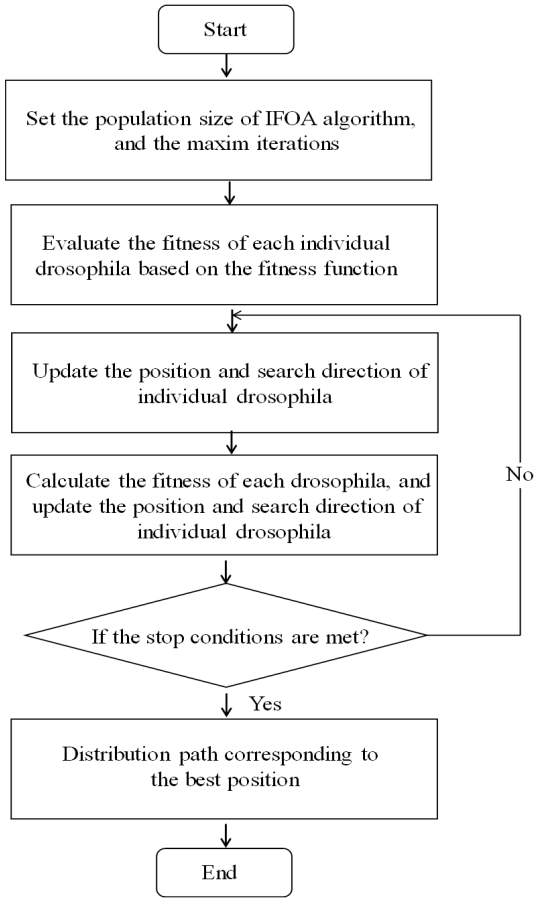

Fig. 2. Flow chart of optimizing logistics distribution center site selection with IFOA algorithm

3.2. Experimental simulation

To verify the effect and superiority of IFOA, set fruit fly population size $sizepop = 20$ and the maximum interaction times $Iteration = 100$. The optimization result is shown in Figs. 3–6 for four different standards.

1) *Rastrigin* function

$$\min f(x_1, x_2) = 20 + x_1^2 + x_2^2 - 10(\cos(2\pi x_1) + \cos(2\pi x_2)),\ x_1, x_2 \in [5, 5]\,.$$

2) *Schaffer* function

$$\min f(x, y) = 0.5 + \frac{\sin^2\sqrt{x^2 + y^2} - 0.5}{(1 + 0.001(x^2 + y^2)^2)^2},\ x, y \in [-10, 10]\,.$$

3) $F4$ function

$$\min f(x_1, x_2) = 100(x_1^2 - x_2^2) + (1 - 2x_1 + x_1^2),\ x1, x2 \in [-1, 1]\,.$$

4) *Sphere* function

$$\min f(x) = \sum_{i=1}^{n} x_i^2,\ |x_i| \le 15,\ n = 10\,.$$

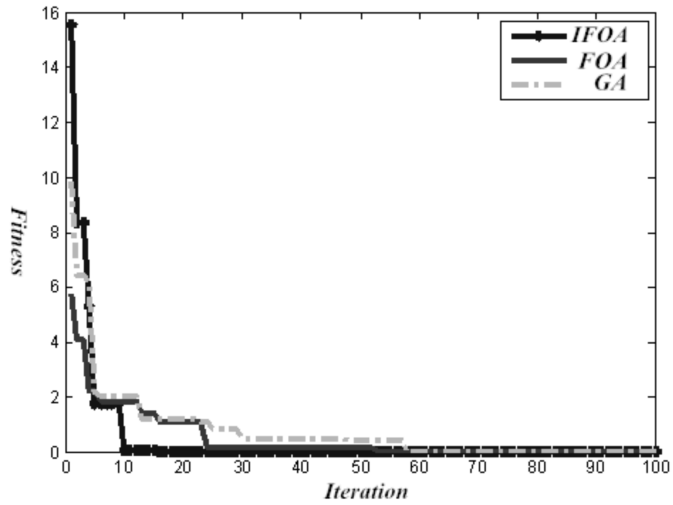

Fig. 3. Convergence graph of *Rastrigin* function

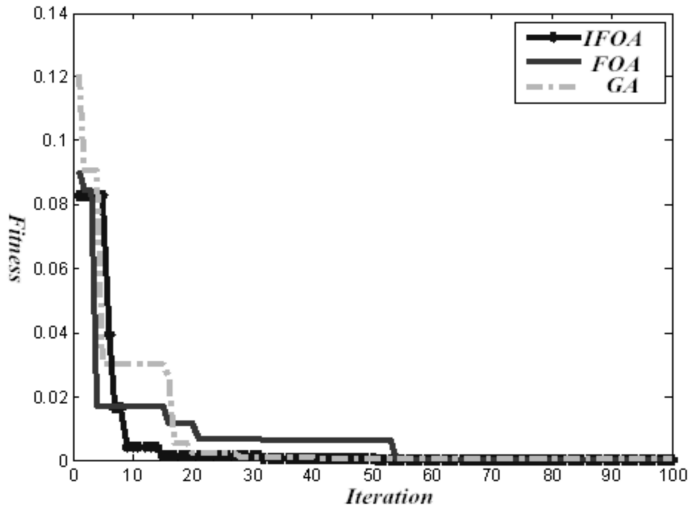

Fig. 4. Convergence graph of $Schaffer$ function

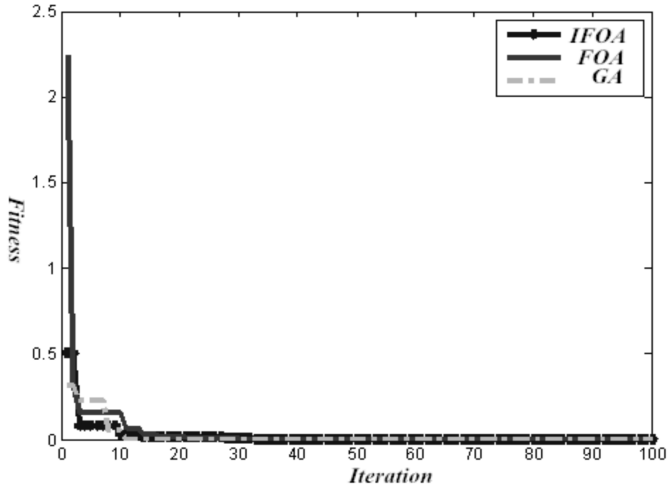

Fig. 5. Convergence graph of $F4$ function

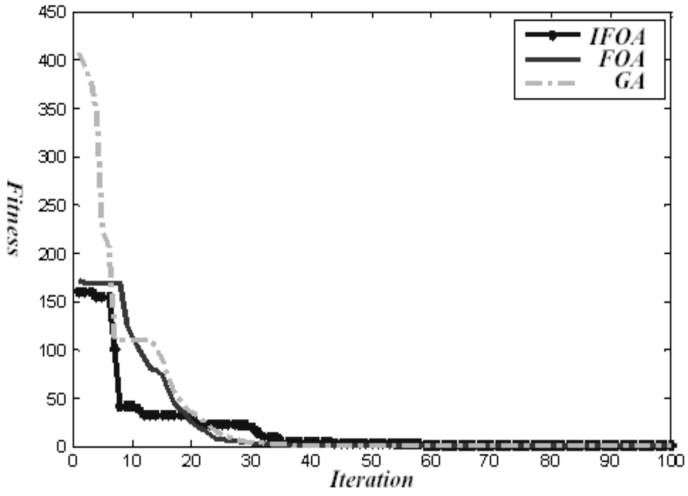

Fig. 6. Convergence graph of *Sphere* function

From Figs. 3–6 it is obvious that the convergence rate of IFOA algorithm superior to that of FOA algorithm and GA algorithm. This verifies superiority of IFOA. Its convergence rate is faster, and its fitness function value further approaches the theoretical value.

In order to prove the feasibility and effectiveness of IFOA during optimizing distribution center site selection, the coordinates of 31 cities in China are gathered, the position and the goods demand of each user are shown in Table 1. The data in this paper go through standardized processing. 6 cities are chosen as logistics distribution centers.

Table 1. Users' position and their goods demand

j	(U_j, V_j)	b_j	j	(U_j, V_j)	b_j
1	(1304, 2312)	20	17	(3918, 2179)	90
2	(3639, 1315)	90	18	(4061, 2370)	70
3	(4177, 2244)	90	19	(3780, 2212)	100
4	(3712, 1399)	60	20	(3676, 2578)	50
5	(3488, 1535)	70	21	(4029, 2838)	50
6	(3326, 1556)	70	22	(4263, 2931)	50
7	(3288, 1229)	40	23	(3429, 1908)	80
8	(4196, 1044)	90	24	(3507, 2376)	70
9	(4312, 790)	90	25	(3394, 2643)	80
10	(4386, 570)	70	26	(3439, 3201)	40
11	(3007, 1970)	60	27	(2935, 3240)	40
12	(2562, 1756)	40	28	(3140, 3550)	60
13	(2788, 1491)	40	29	(2545, 2357)	70
14	(2381, 1676)	40	30	(2778, 2826)	50
15	(1332, 695)	20	31	(2370, 2975)	30
16	(3715, 1678)	80			

Set fruit fly population size $sizepop = 20$ and the maximum iteration times $Iteration = 100$. The optimization results of logistics distribution center for 6 centers are shown in Fig. 7.

When there are 5 and 4 logistics distribution centers and the iteration times are different, the principle of calculation is similar to the above, convergence curves and distribution path maps of IFOA are shown in Figs. 8 and 9.

According to the optimization result of IFOA algorithm under different iteration times and different population size (Fig. 10), as iteration times and population size rise, the optimal iteration times and different population size tends to be better. The simulation experiment shows that IFOA algorithm has high feasibility and effectiveness during optimizing logistics distribution center site selection problem.

4. Conclusion

Although fruit fly optimization algorithm has such advantages as few control parameters, fast convergence rate and high convergence precision, it has local optimum problem and thus may be easily caught in local minimum. In order to achieve reasonable allocation of the site of logistics distribution center and improve work efficiency and economic benefit of logistics distribution system, this paper combines ergodicity, regularity and randomness advantages of logistic chaotic system and proposes fruit fly optimization algorithm based on logistic chaotic system to overcome

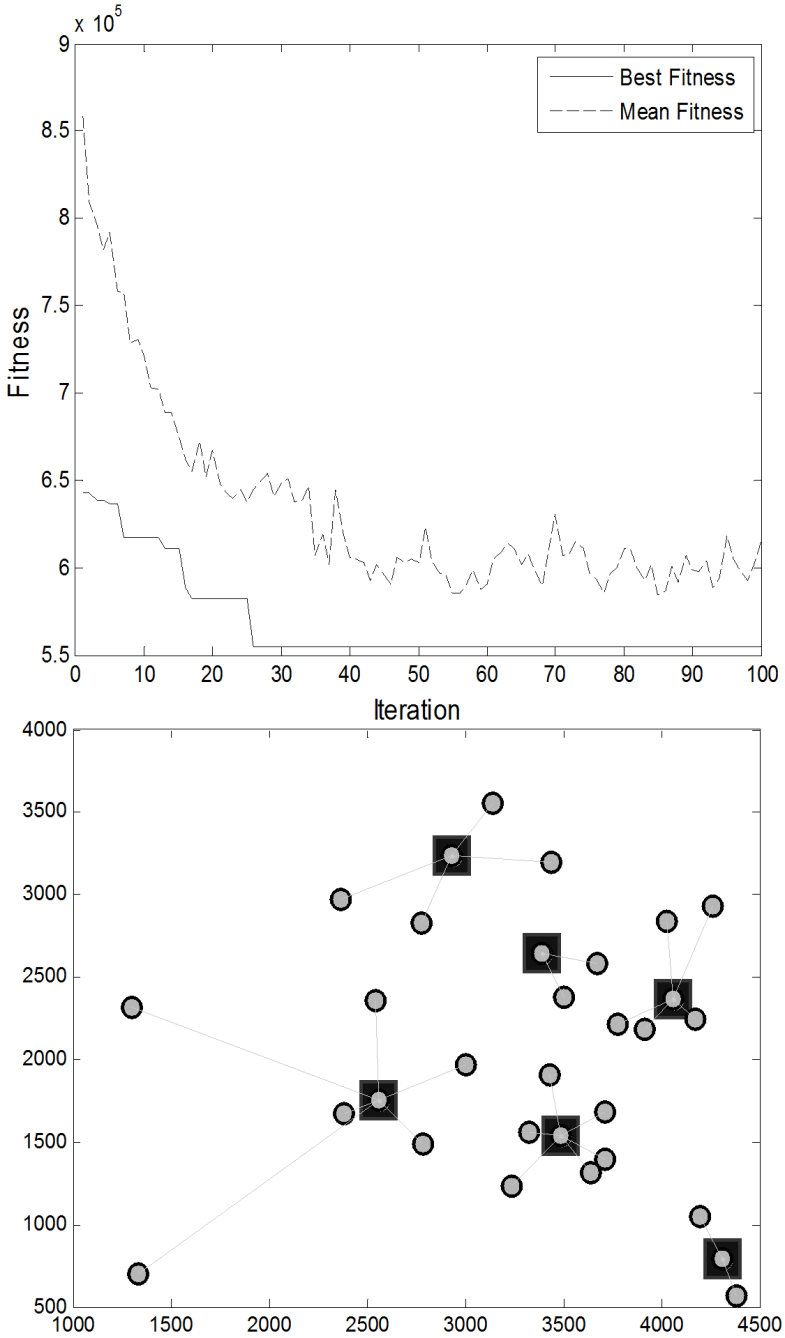

Fig. 7. Distribution path and convergence map when there are 6 distribution centers

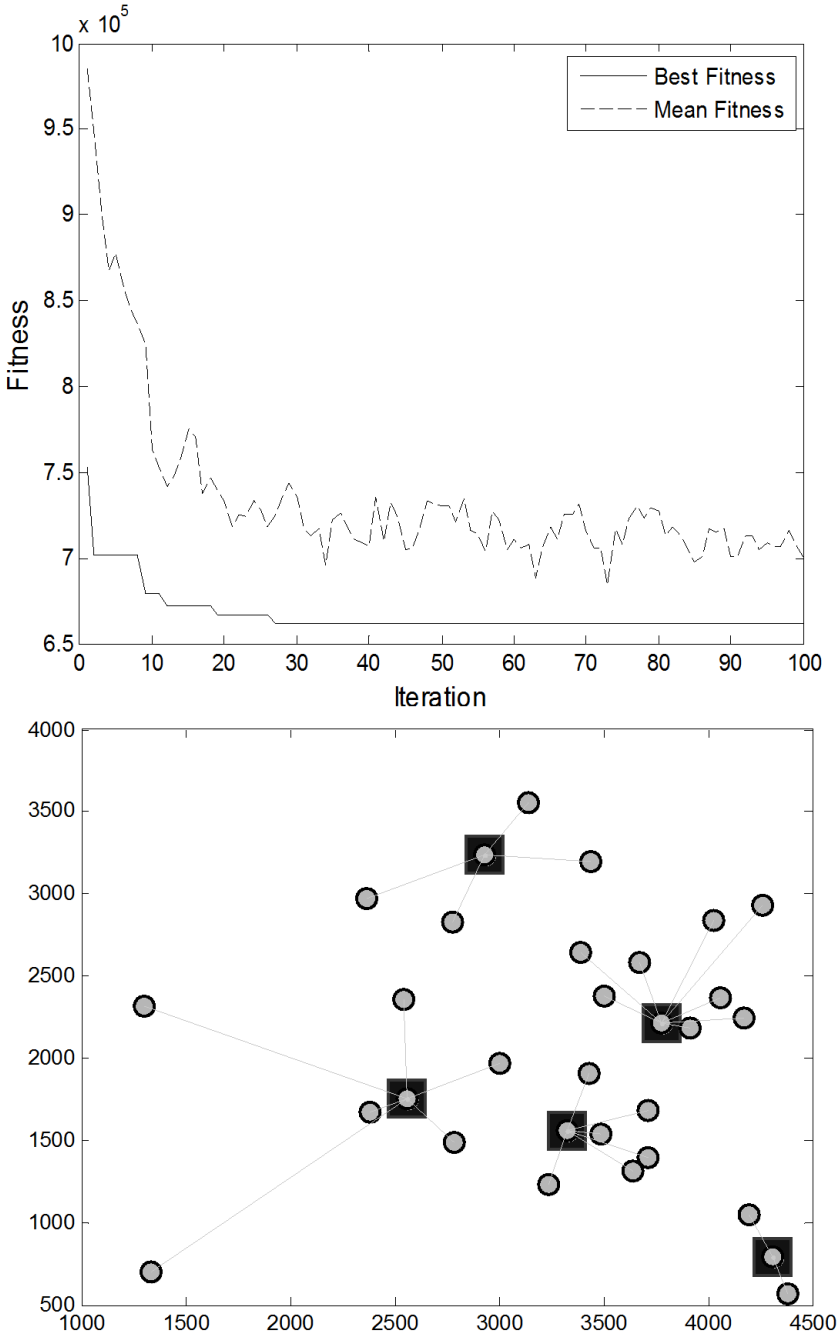

Fig. 8. Distribution path and convergence map when there are 5 distribution centers

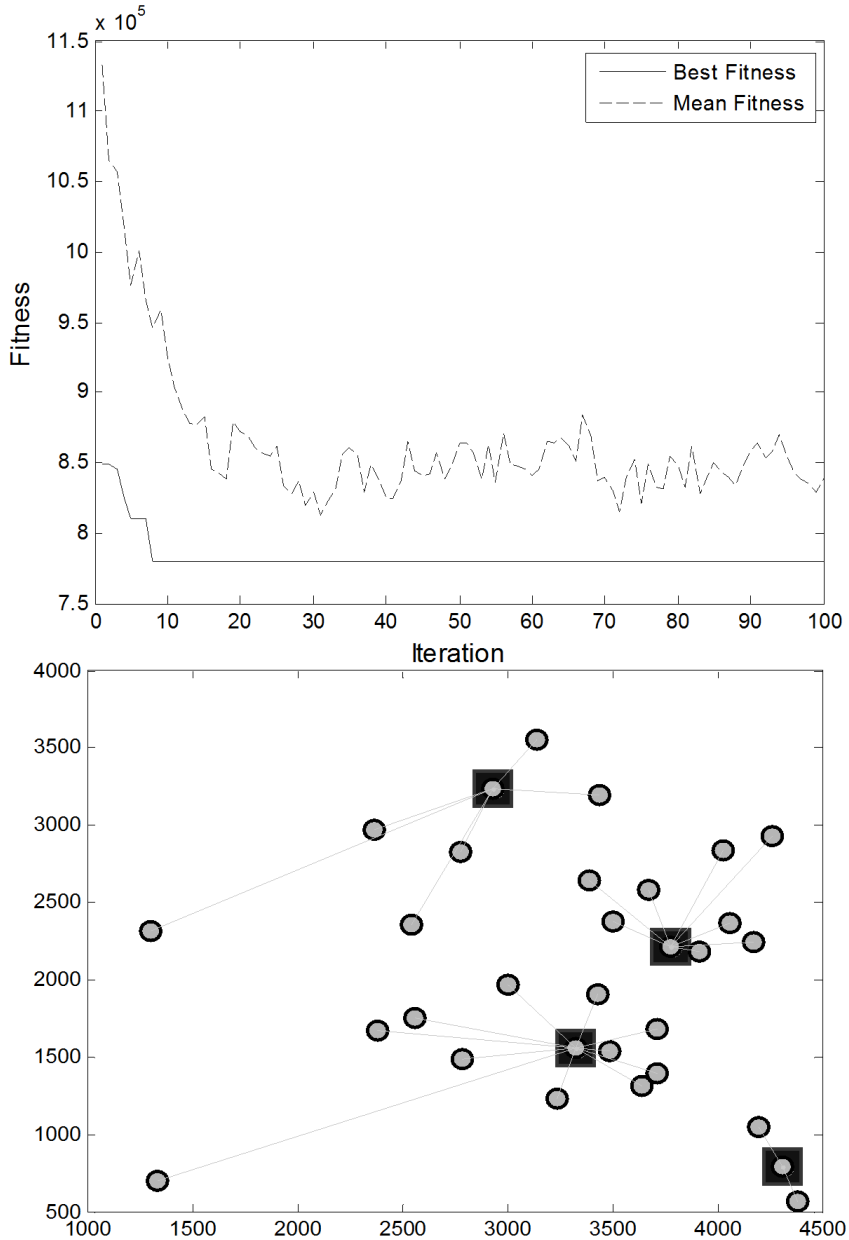

Fig. 9. Distribution path and convergence map when there are 4 distribution centers

local optimum problem of fruit fly optimization algorithm. A mathematical model for site selection of logistics distribution center is established according to the coordinates of logistics distribution centers in 31 cities and their demand for goods

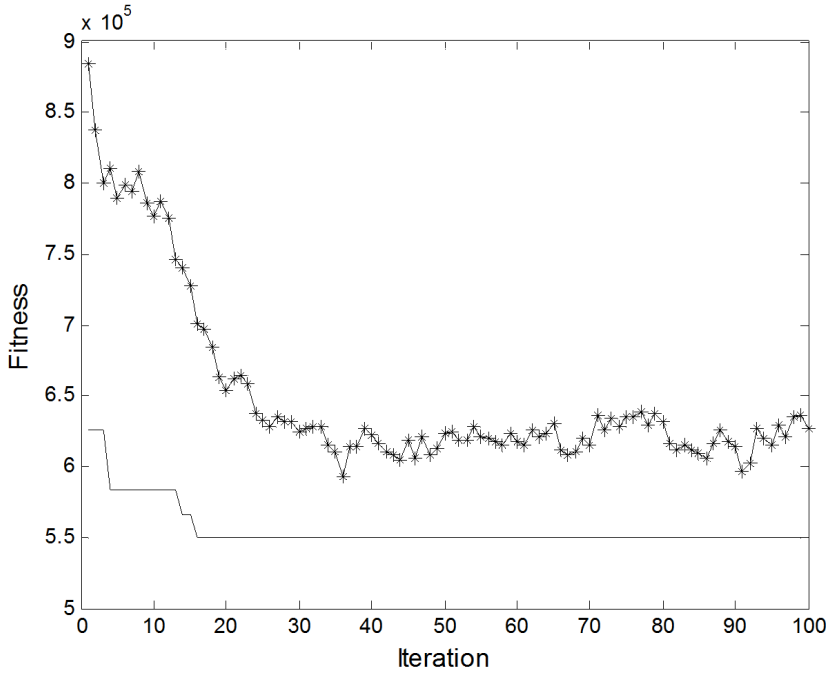

Fig. 10. Convergence comparison diagram of IFOA algorithm and FOA algorithm

and materials. Besides, improved fruit fly optimization algorithm is applied for optimization solution to achieve the optimal allocation of distribution path and save cost. The simulation result indicates that, the algorithm has the advantages of fast convergence rate and high precision. On this basis, distribution paths under different number of distribution centers and distribution paths under different iteration times and population size are compared to achieve optimization of objective function and the lowest cost.

References

[1] Z. Lv, a. Tek, F. Da Silva, C. Empereur-mot, M. Chavent, M. Baaden: *Game on, science-how video game technology may help biologists tackle visualization challenges*. PloS ONE *8* (2013), No. 3, paper 0057990.

[2] W. T. Pan: *A new fruit fly optimization algorithm: Taking the financial distress model as an example*. Knowledge-Based Systems *26* (2012), 69–74.

[3] Y. Chen, Z. Cao: *An improved MRF-based change detection approach for multitemporal remote sensing imagery*. Signal Processing *93* (2013), No. 1, 163–175.

[4] T. E. Lin, G. C. Gu, H. B. Liu, J. Shen: *A recognition method using uncorrelated discriminant locality preserving projections*. Journal of Harbin Engineering University *31* (2010), No. 1, 98–101,114.

[5] L. Ong, M. Motani: *Optimal routing for decode-forward in cooperative wireless networks*. IEEE Transactions on Communications *58* (2010), No. 8, 2345–2355.

[6] J. Yao, S. Feng, X. Zhou,Y. Liu: *Secure routing in multihop wireless ad-hoc networks with decode-and-forward relaying.* IEEE Transactions on Communications *64* (2016) No. 2, 753–764.

[7] K. Wang, K. Qiao, I. Sadooghi, X. Zhou, T. Li, M. Lang, I. Raicu: *Load-balanced and locality-aware scheduling for data-intensive workloads at extreme scales.* Concurrency and Computation, Practice and Experience *28* (2016), No. TOC 1, 70–94.

[8] Y. Lin, J. Yang, Z. Lv, W. Wei, H. Song: *A self-assessment stereo capture model applicable to the internet of things.* Sensors *15* (2015), No. 8, 20925–20944.

[9] Y. Xie, Y. He, A. Cheng, J. Zhang: *Study on medical image enhancement based on IFOA improved grayscale image adaptive enhancement.* Multimedia Tools and Applications *75* (2016), No. 22, 14379–14379.

[10] H. R. Tizhoosh, G. Krell, B. Michaelis: *Knowledge-based enhancement of megavoltage images in radiation therapy using a hybrid neuro-fuzzy system.* Image and Vision Computing *19*, (2001), No. 4, 217–233.

[11] S. K. Pal, R. A. King: *Image enhancement using smoothing with fuzzy sets.* IEEE Transactions on Systems, Man, and Cybernetics - Part A: Systems and Humans *11* (1981), No. 7, 494–501.

[12] A. Das, M. Bhattacharya: *A novel vague set approach for selective contrast enhancement of mammograms using multiresolution.* Journal of Biomedical Science and Engineering *2* (2009), No. 2, 575–581.

[13] J. J. Y. Wang, J. Z. Huang, Y. Sun, X. Gao: *Feature selection and multi-kernel learning for adaptive graph regularized nonnegative matrix factorization.* Expert Systems with Applications *42* (2015), No. 3, 1278–1286.

Received August 7, 2017

Acta Technica *62* No. 2B/2017, 423–440

Research on aircraft trajectory optimization based on reducing greenhouse effect[1]

Tian Yong[2,3], Wang Zhongfengyan[2], Wan Lili[2,3], Zhang Quan[2]

Abstract. Air transport plays an important role in people's daily life. However, the environmental impact caused by it has become increasingly serious. In order to reduce the greenhouse effect caused by global aviation, the absolute global temperature potential (AGTP) was used for the uniform quantization of aircraft emissions of CO_2 and the generated contrails. Then, considering the control boundary and mobility constraints, the aircraft level optimization model was established with the optimization objectives of minimizing greenhouse effect, and it was verified using the actual radiosonde data and operational data of Guangzhou-Beijing route. Finally in the optimized flight profile, the global surface temperature decreased, in three time level of 25 years, 50 years and 100 years, which was reduced by 36.39 %, 13.98 % and 11.21 %, respectively. Therefore, the optimization model can effectively reduce the greenhouse effect caused by aircraft operation.

Key words. Greenhouse effect, global warming potential, carbon dioxide emission, condensation.

1. Introduction

As a new industry, civil aviation industry has brought convenience, comfort and high efficiency. However, the impact of noise, fuel consumption, and pollution emissions caused by air transport on the environment has attracted more and more

[1]This paper is supported by Jiangsu Province Graduate Student Training Innovation Project, Study on green aircraft trajectory optimization (No. SJLX15_0131), Graduate Innovation Base (Laboratory) Open Fund, Research on aircraft trajectory optimization based on multi objective environmental impact (No. kfjj20150710) and National Natural Science Foundation of China, Research on the Evaluation Method of Air Traffic Volume in Airport for Enviromental Protection (Grant No. 61671237).

[2]College of Civil Aviation, Nanjing University of Aeronautics & Astronautics, Nanjing, Jiangsu, China

[3]National Key Laboratory of Air Traffic Management Technology, Nanjing University of Aeronautics & Astronautics, Nanjing, Jiangsu, China

attention. According to the United Nations Intergovernmental Panel on climate change (IPCC) statistics, 13 % of current fossil fuel is consumed by air transport, in which air transport emissions of carbon dioxide (CO_2) account for 2 % of the total global anthropogenic emissions CO_2 [1]. Another cause of climate impact is the contrail, and the impact of climate warming produced by it is even higher than the aircraft's CO_2 emissions [2]. Aircraft flying at high altitude, long duration, emissions of the gas is difficult to be absorbed compared to the ground, so the impact on the environment is a long process. Environment is a part of the future development of the aviation industry which cannot be ignored, and the altitude layer selection of aircraft is not only to follow the high level of safety and efficiency principles, but also needs to further consider the impact of the environment. Therefore, the establishment of a safe and environmentally friendly aircraft trajectory is one of the main directions of the future development of the aviation industry.

Based on the current situation of the development of Chinese civil aviation, facing to the environmental protection which should be considered in the air traffic operation, according to the characteristics of climate impact of CO_2 and contrail, the absolute global temperature potential (AGTP) [3] climate standard is used to measure the effect of CO_2 and contrail on global surface temperature, establish the weight of CO_2 and contrail, construct the aircraft altitude layer optimization model with the goal of minimizing the greenhouse effect, and compare with the global surface temperature increase value caused by the aircraft flying under the original flight profile, so as to verify that the model can effectively reduce the impact of the environment.

2. Current research status

While consuming a large amount of fuel in the upper air, the aircraft also brings about a lot of pollution to the surrounding environment and the formation of the condensate. High altitude flight usually refers to the flight altitude of 7000 m∼15000 m in altitude. For the aircraft during the height range, due to high altitude, the noise pollution of flight trajectory is negligible, and the aircraft fuel combustion CO_2 is the greenhouse gas, which can absorb and release radiation to affect global climate change, and cause a great threat to human survival. At the same time, the aircraft is easy to generate the contrail, which can block the long wave radiation from the earth's surface in the atmosphere, increasing the greenhouse effect. Therefore, the impact of high altitude flight on the environment is mainly reflected in the CO_2 emission and the contrail.

As for the twenty-first century, the research of reducing the impact of high altitude flight on the environment has been carried out by foreign countries as the following. In 2003, Victoria Williams et al. [4] proposed that the aircraft flying height layer was in favor of reducing the impact of aviation activities on the European climate. In 2008, Klaus Gierens [5] summarized a review of the methods to relieve the contrail. In 2011, Banavar Sridhar et al. [6] combined with upper wind data to optimize the horizontal direction and the height of the routes of the 12 cities in United States, and obtained the flight path with the minimal impact on

the environment by solving the nonlinear optimal control problem. In 2012, Chen et al. [7] measured the carbon dioxide and the contrail, and made the artificial determination of weighing coefficient. Although more flexible, it was greatly affected by human factors, which was not easy to unify the specification. In 2014, Manuel Soler et al. [8] described the 4D flight path planning as a multi-stage mixed integer optimization control problem, and replanned the route of the aircraft, so that the impact of contrail on the environment was minimal. In 2015, Antonio Filippone [9] evaluated the reduction measures of all kinds of contrails. There are few related researches in China, currently only focused on research of greenhouse gases on global climate change, less considering the impact of the aircraft operation on the climate, thus not carrying out the research of reducing the impact of aircraft on the aircraft environment by improving the operation. In 2011, Zhang Ruoyu et al. [10] used the assessment method of global warming potential (GWP) to study the effect of greenhouse gases on climate, and the global warming potential of greenhouse gases was reviewed comprehensively. In 2011, Liu Ping [11] pointed out in his article that China promulgated the "guidance on accelerating the work of energy conservation and emission reduction", which could reduce emissions through technology and management innovation. In 2016, Wang Zhongfengyan and others [12] preliminary discussed the aircraft flying height layer distribution program to reduce the greenhouse effect through the establishment of the climate impact assessment method of CO_2 and the contrail.

3. Aircraft trajectory optimization model and its solution

The impact of high altitude flight on the environment is mainly reflected in the formation of CO_2 emission and the formation of contrail. CO_2 emissions depend on fuel consumption and combustion efficiency. The formation of contrail is related to the atmospheric temperature and relative humidity, and the appropriate climate assessment index should be selected to establish the global warming response function. Aircraft trajectory optimization can reduce the impact of aircraft operation on the global temperature change by optimizing the altitude layer of the flight phase, thus forming an environmentally friendly path.

3.1. CO_2 emissions model

CO_2 is the main greenhouse gas, accounting for about 75 % of all greenhouse gases, no obstacle to light radiation, but it can absorb infrared and block infrared. CO_2 likes a greenhouse, and energy is easy to into and hard to go out. The more CO_2, the stronger the hindering effect of earth's heat escapes to hinder the atmosphere, so that the global warming effect is stronger. If the CO_2 content is doubled, the global temperature will rise 3∼5 °C, which may be increased by 10 °C in the Polar regions, and the climate will be significantly warmer.

With the rapid development of the global airline industry, if not to take corresponding measures to protect the environment, the proportion of gas emissions produced by air transport over the next 40 years will increase to 3 % of global

anthropogenic CO_2 emissions, and the proportion causing the climate change will reach 5 % [13]. CO_2 emissions from engines are mainly derived from fuel combustion, while combustion and combustion efficiency are the decisive factors in determining the total amount and composition of emissions.

The amount of CO_2 gas emitted by the fuel consumed during the aircraft operation can be expressed as:

$$E_{CO_2} = EI_{CO_2} \cdot FW \,. \tag{1}$$

In the formula, E_{CO_2} is the emission of CO_2, and its unit is kg, EI_{CO_2} is emission index for CO_2, and the emission index of aviation fuel is $EI_{CO_2} = 3.155\,\mathrm{kg/kg}$. Quantity FW represents the fuel consumption, and its unit is kg.

3.2. The formation model of contrail

For aircraft flying at high altitude, the tail behind will form a cloud band atomization wake. The white cloud belt is produced by condensation of condensed water from the engine and the surrounding cold air. They can be condensed into tiny droplets to form a cloud, so this article will call it the contrail. The contrail can absorb the heat of the ground radiation, thereby "adding fuel to the flames of global warming". Generally, above sea level 8000 m, the temperature is low to minus 40 °C, and the contrail will form. Therefore, the high altitude cruise phase is more likely to form the contrail.

The formation of contrails is related to the atmospheric temperature and relative humidity of the atmosphere. Air humidity refers to the degree of humidity in the air, which means the degree of vapor content in the atmosphere. At a certain temperature, the smaller the air humidity, the faster the water evaporates. Whereas the atmospheric humidity is bigger, water evaporates is more slowly. The high temperature gas discharged by the engine cold air condenses into small droplets, which is not easy evaporation, existing in the atmosphere in the form of cloud, which is the formation of contrails. When the relative humidity (RH_w) of ambient air is greater than or equal to a certain humidity, it is easy to form a continuous contrail, and the humidity is defined as the critical relative humidity RH_critical [14].

$$RH_\mathrm{critical} = \frac{G\left(T - T_\mathrm{contrail}\right) + e_\mathrm{sat}^\mathrm{liq}\left(T_\mathrm{contrail}\right)}{e_\mathrm{sat}^\mathrm{liq}\left(T\right)} \,, \tag{2}$$

$$e_\mathrm{sat}^\mathrm{liq}\left(T\right) = e_0 \cdot 10^{\frac{aT}{b+T}} \,, \tag{3}$$

$$T_\mathrm{contrail} = -46.46 + 9.43\ln\left(G - 0.053\right) + 0.72\ln^2\left(G - 0.053\right) \,, \tag{4}$$

and

$$G = \frac{EI_{H_2O} C_\mathrm{p} P}{\varepsilon Q\left(1 - \eta\right)} \,. \tag{5}$$

In the above formulas, $e_\mathrm{sat}^\mathrm{liq}\left(T\right)$ is the saturated vapor pressure at atmospheric

temperature (hPa), e_0 is the saturated vapor pressure at 0 °C and its value is 6.11 hPa. For water, $a = 7.5$, $b = 237.3$. Symbol T_{contrail} denotes the critical temperature for the formation of contrail in degrees of Celsius, $EI_{\text{H}_2\text{O}}$ represents the emission index of steam, C_{p} is the specific heat capacity of air at constant pressure (J/kg K), P denotes the atmospheric pressure (hPa), ε stands for the ratio of the molecular weight of water to the average relative molecular mass of dry air, Q is the fuel combustion value (J/kg) and η denotes the average propulsion efficiency of engine.

When the relative humidity of the atmosphere RH_{i} is greater than or equal to 100 %, the shape of the contrail can be kept.

$$RH_{\text{i}} = RH_{\text{w}} \frac{6.0612\text{e}^{\frac{18.102T}{249.52+T}}}{6.1162\text{e}^{\frac{22.577T}{237.78+T}}} . \tag{6}$$

Therefore, the conditions for the formation of the continuous contrail are as follows: the relative humidity of the water should satisfy $RH_{\text{critical}} \leq RH_{\text{w}} < 100\,\%$. And the relative humidity of ice needs to satisfy$RH_{\text{i}} \geq 100\,\%$.

3.3. Linear climate model

3.3.1. Absolute global temperature potential (AGTP). The radiative forcing and lifetime of different greenhouse gases are different, and the effect of increasing temperature is not the same. AGTP [15] is the change in global mean surface temperature caused by instantaneous or continuous release of a greenhouse gas in a future given time. In order to measure the effect of aircraft operation on the global climate, AGTP is used as the evaluation index to establish the global warming response function of the air exhaust and contrail by the linear system, so as to quantify the change of global average surface temperature by the aircraft operation. The following equation is established through the convolution from $t_0 = 0$ to $t = H$:

$$\text{AGTP}(H) = \int_0^H R\left(H - \zeta\right) \Delta F\left(\zeta\right) \, \text{d}\zeta \, . \tag{7}$$

Here, $R\left(H - \zeta\right)$ is the impulse response function, which represents the change of the global surface temperature within the H time due to the radiative forcing of $\Delta F\left(\zeta\right)$ at time ζ.

AGTP is divided into two kinds: one is the absolute global temperature change potential pulse discharge, recorded as pulse discharge AGTP, the other is the absolute global warming potential of continuous emissions, recorded as a continuous emission AGTP. Because the continuous emission of AGTP considers the influence of the gas on the surface temperature changes in the case of continuous emission, the instantaneous emission of CO_2 and the critical of the aircraft during the flight are discussed in this paper. Therefore, using the pulse emission AGTP to measure the effects of CO_2 and the critical, the effects of CO_2 and the critical are transferred to the global surface temperature change.

3.3.2. Pulse discharge AGTP of CO_2 . Pulse emission AGTP model of CO_2 describes the change of CO_2 concentration due to the transport and absorption of land and sea, which can be calculated as follows:

$$\Delta F^{\mathrm{CO_2}}(t) = A^{\mathrm{CO_2}} \left(a_0 + \sum_{i=1}^{3} a_i \mathrm{e}^{-\frac{t}{\alpha_i}} \right) . \tag{8}$$

The global surface temperature response to the radiative forcing of the unit pulse is modeled using a quadratic linear model, and the impulse response function is

$$R(t) = \sum_{j=1}^{2} \frac{c_j}{d_j} \mathrm{e}^{-\frac{t}{\alpha_i}} . \tag{9}$$

In the above formula, $A^{\mathrm{CO_2}}$ is the radiative forcing of concentration change of 1 kg CO_2, $A^{\mathrm{CO_2}} = 1.82 \times 10^{-15}$ $\mathrm{Wm^{-2}/kg}$. The values of a_i, α_i, c_j, d_j, which are the given calculation parameters, are shown in Table 1.

Table 1. Parameter values of the impulse response function of CO_2 concentration

No. of variable	0	1	2	3
a_i (dimensionless)	0.217	0.259	0.338	0.186
α_i (year)		172.9	18.51	1.186
c_j ($\mathrm{Km^2/W}$)		0.631	0.429	
d_j (year)		8.4	409.5	

From formulae (7)–(9), it can be seen that the pulse discharge AGTP of 1 kg CO_2 within H time level is as follows:

$$\mathrm{AGTP}^{\mathrm{CO_2}}(H) =$$

$$= A^{\mathrm{CO_2}} \sum_{j=1}^{2} \left[a_0 c_j \left(1 - \mathrm{e}^{-\frac{H}{d_j}} \right) + \sum_{i=1}^{3} \frac{a_i \alpha_i c_j}{\alpha_i - d_j} \left(\mathrm{e}^{-\frac{H}{\alpha_i}} - \mathrm{e}^{-\frac{H}{d_j}} \right) \right] . \tag{10}$$

The value of the parameters is added into the formula (10). The calculation shows that the value of the pulse emission $\mathrm{AGTP}^{\mathrm{CO_2}}$ at different times is only related to time level. The MATLAB is used to draw the function curve, with the step size of 0.1, and the change trend of pulse discharge $\mathrm{AGTP}^{\mathrm{CO_2}}$ with the time level is shown in Fig. 1.

3.3.3. Pulse discharge AGTP of the contrail. The AGTP modeling of the pulse discharge contrail is the same with the CO_2. The pulse discharge AGTP of the

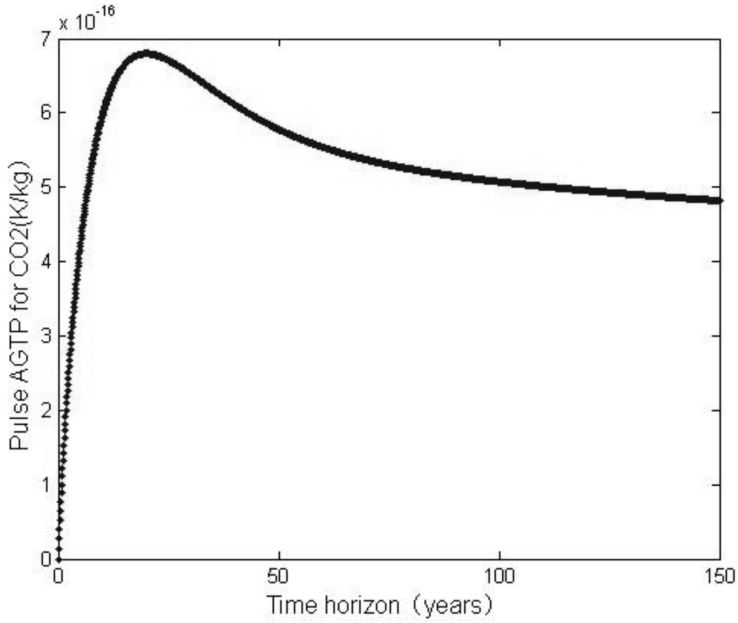

Fig. 1. Pulse AGTP for CO_2

contrail can be simply regarded as the impulse response. It is calculated as follows:

$$\mathrm{AGTP}^{\mathrm{Con}}(H) = \int_0^H R(H-\zeta)\,\delta(\zeta-0)\,\mathrm{d}\zeta = R(H)\,. \tag{11}$$

The above formula shows that $\mathrm{AGTP}^{\mathrm{Con}}(H)$ means the pulse discharge AGTP of the contrail, and its value is equal to the impulse response function $R(H)$. Net radiative forcing (RF_{net}) of the contrail includes long wave radiative forcing (RFLW) and short wave radiative forcing (RFSW):

$$RF_{\mathrm{net}} = RF_{\mathrm{LW}} + RF_{\mathrm{SW}}\,. \tag{12}$$

In the above formula, the radiative forcing has a unit of $\mathrm{W/m^2}$, which means the energy produced by the condensation in each unit area. In general, the value of RF_{net} is from $10\,\mathrm{Wm^{-2}}$ to $30\,\mathrm{Wm^{-2}}$. Due to the linear cloud of the contrail, the expression of the contrail is optimized. Optimization is for the energy generated by the unit of flight distance, and the total energy EF (GJ) of the contrail in unit length within the life cycle is calculated as follows:

$$EF = \int_{\mathrm{lifetime}} RF_{\mathrm{net}}(\zeta)\,W_{\mathrm{c}}(\zeta)\,\mathrm{d}\zeta\,. \tag{13}$$

In this formula, W_{c} is the width of the contrail, and its unit is meter.

Through formula (11)–(13), it can be seen that the pulse discharge AGTP of 1 kg

CO_2 within H time level is as follows:

$$\mathrm{AGTP}^{\mathrm{Con}}(H) = \int_0^H R(H-\zeta)\,\delta(\zeta-0)\,\mathrm{d}\zeta =$$

$$= \sum_{j=1}^{2} \frac{c_j}{d_j} \mathrm{e}^{-\frac{c_j}{d_j}} \cdot \frac{EF}{\text{Global surface area} \times \text{A year}}. \tag{14}$$

In general, the value of RF_{net} [14] is during $10\,\mathrm{Wm}^{-2}$–$30\,\mathrm{Wm}^{-2}$. And this article assumes that $RF_{\mathrm{net}} = 10\,\mathrm{Wm}^{-2}$, the width of the contrail is $W_{\mathrm{c}} = 1000\,\mathrm{m}$, life is 10000 s, and then $EF = 100\,\mathrm{GJ}$. The value of the parameters is added into the formula (14). The calculation shows that the value of the pulse emission $\mathrm{AGTP}^{\mathrm{CO_2}}$ at different time is only related to time level. The MATLAB is used to draw the function curve, with the step size of 0.1, and the change trend of pulse discharge $\mathrm{AGTP}^{\mathrm{CO_2}}$ with the time level is shown in Fig. 2.

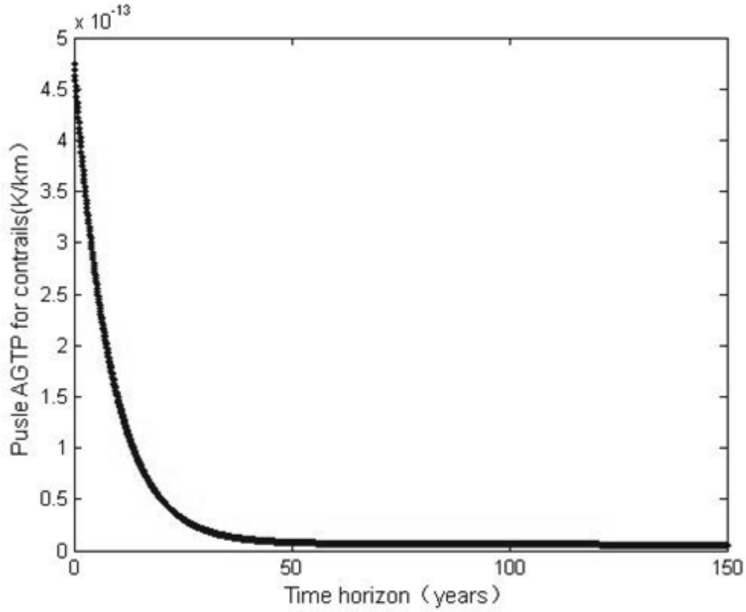

Fig. 2. Pulse AGTP for contrails

Three time levels of 25 years, 50 years and 100 years are analyzed and the $H = 25$, $H = 50$, $H = 100$ are brought into the formula (10) and (14) in this paper. The results are shown in Table 2. Comparative analysis shows that the change of global surface temperature 1 km of the contrail is the same as the effects of 44.6 kg, 12.1 kg and 9.9 kg emissions of CO_2 on the global surface temperature in 25 years, 50 years and 100 years.

Table 2. AGTP values for CO_2 and contrails at different time horizons

Time horizon H (years)	25	50	100
$\mathrm{AGTP}^{\mathrm{CO_2}}(H)$ (K/kg)	$6.73 \cdot 10^{-16}$	$5.76 \cdot 10^{-16}$	$5.13 \cdot 10^{-16}$
$\mathrm{AGTP}^{\mathrm{Con}}(H)$ (K/km)	$3.0 \cdot 10^{-14}$	$6.98 \cdot 10^{-15}$	$5.10 \cdot 10^{-15}$

3.4. Locus model

Previous studies have indicated that only changing the cruising altitude can we reduce the impact of aircraft flying on the environment during the flight phase effectively. To reduce the height of the cruise is conducive to the elimination of the contrail under normal circumstances, it is contrary to the corresponding economic cruising altitude. Therefore, it is necessary to optimize the height layer to reduce the influence of the aircraft operation on the global temperature change so as to form an environment friendly path.

3.4.1. Objective function. In order to ensure the safety and economic operation of the aircraft, it is necessary to make the following assumptions to simplify the problem:

1) Aircraft study is considered to be a moving particle, without considering the volume change of route and sector and airspace resources is adequate.

2) The assumption that Beijing time 20:00 to the next day 8:00 meteorological conditions are unchanged.

3) The meteorological data is not accurate enough in the process of changing the height layer, so the formation of the contrail is not considered.

4) Climbing or falling in the previous time slot are completed in the height of the conversion process.

The flight operation of an aircraft in the air route is assumed to be: climbing or descending. The objective function is constructed to minimize the global surface temperature variation caused by aircraft operation. The following expression is established:

$$\min T^{\mathrm{env}} = \mathrm{AGTP}^{\mathrm{CO_2}} \cdot EI_{\mathrm{CO_2}} \cdot \left(FW_m^{\mathrm{cr}} + FW_m^H\right) + r_l \gamma_{m,l} \mathrm{AGTP}^{\mathrm{Con}} L_{\mathrm{Con}} a, . \quad (15)$$

Here, r_l and $\gamma_{m,l}$ are decision variables, which are shown as follows:

$$r_l = 1$$

when the height layer l meets the conditions of the formation of the condensation layer and

$$r_l = 0 \quad (16)$$

when the height layer l does not meet the conditions of the formation of the condensation layer.

$$\gamma_{m,l} = \begin{cases} 1, & \text{Aircraft } m \text{ flies on the altitude layer } l. \\ 0, & \text{Aircraft } m \text{ does not fly on the altitude layer } l. \end{cases} \quad (17)$$

Quantities FW_m^{cr} and FW_m^H are the fuel consumption of cruise and altitude adjusted and they are calculated as follows:

$$FW_m^{\mathrm{cr}} = FF_m^{\mathrm{cr}} \cdot t_m^{\mathrm{cr}} \tag{18}$$

$$FW_m^H = \chi_m^n \cdot \left[FF_m^{\mathrm{cl}} \cdot t_m^{\mathrm{cl}} + FF_m^{\mathrm{des}} \cdot t_m^{\mathrm{des}} + (FF_m^{\mathrm{cr}} + \Delta FF_m^{\mathrm{cr}} \cdot \Delta H_m) \cdot t_m^{\mathrm{ncr}}\right] . \tag{19}$$

Here,

$$\chi_m^n = \begin{cases} 1, & \text{Height adjustment,} \\ 0, & \text{No height adjustment.} \end{cases} \tag{20}$$

Further, FF_m^{cl} and FF_m^{des} are the fuel flow of climbing and falling and the model data can be obtained from the BADA3.12, t_m^{cl} and t_m^{des} are the times of climbing and descent processes, ΔH_m and $\Delta FF_m^{\mathrm{cr}}$ are the height of the aircraft changes m and fuel flow rate changes. Finally, t_m^{ncr} is a new height layer cruise time.

3.4.2. Constraint conditions. 1. Control boundary constraints

The height of an aircraft m cannot be above the boundary of the control area:

$$FL_{\min} \le FL_m \le FL_{\max} . \tag{21}$$

2. Height layer uniqueness constraint

Each aircraft m must and can only be assigned a height layer l:

$$\sum_{n=1}^{l_x} \gamma_{m,l} = 1, \ l = 1, \ldots, l_x . \tag{22}$$

3. Mobility constraints

Up or down of aircraft m there can only change a height layer at most:

$$\Delta H_m \le |600| . \tag{23}$$

4. Aircraft performance constraints

In addition to ensure flight safety, civil aviation also needs to take into account the comfort of passengers. Therefore, the aircraft's rate of climb and descent cannot exceed the maximum rate of climb and descent:

$$\mathrm{ROC} \le \mathrm{ROC}^{\max} , \tag{24}$$

$$\mathrm{ROD} \le \mathrm{ROD}^{\max} . \tag{25}$$

Here, ROC and ROD are the rate of climb and descent, respectively. $\mathrm{ROC}^{\max}$ and $\mathrm{ROD}^{\max}$ are the aircraft's maximum rate of climb and the maximum rate of decline, respectively.

4. Example analysis and discussion

This article selects Beijing - Guangzhou route and the CA1336 flight from Guangzhou to Hong Kong in January 2rd, 2016 20:38 of Beijing time as the research object. Arrival time in Beijing is 23:17 and the route points are: Chenzhou, Changsha, Yueyang, Wuhan, Zhumadian, Zhengzhou, Handan and Tianjin. Horizontal track, height profile and velocity profile are shown in Figs. 3–5.

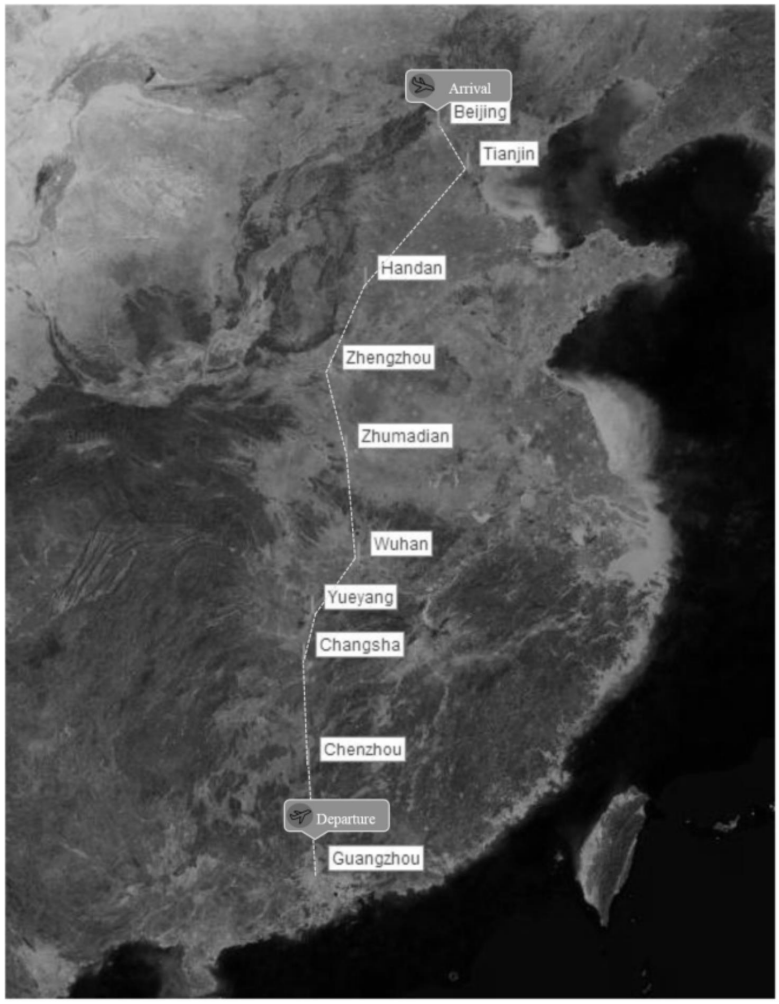

Fig. 3. Horizon track from ZGGG to ZBAA

The difference between the 3 sample points around the insertion point is treated and the power exponent is 2 in the method of inverse distance weighting by means of the available meteorological data from the University of Wyoming (Upperair air data) according to the latitude and longitude information of route point. The esti-

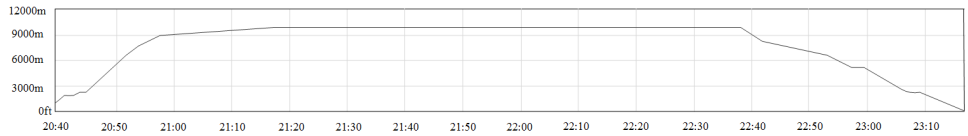

Fig. 4. Altitude profile from ZGGG to ZBAA

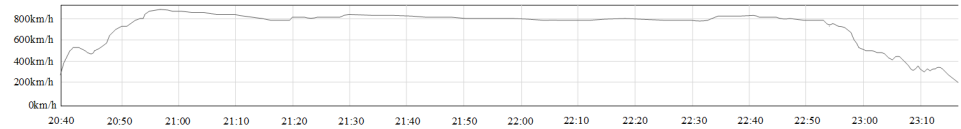

Fig. 5. Velocity profile from ZGGG to ZBAA

mated value of the insertion point is calculated is follows:

$$Z = \left(\sum_{n=1}^{3} \frac{Z_n}{s_n^2}\right) \Bigg/ \left(\sum_{n=1}^{3} \frac{1}{s_n^2}\right). \tag{26}$$

Here, Z_n is the measured value of the first n sample point and s_n was the distance between the first n sample and the point to be inserted in the formula. The weather information of the aircraft flying over the route point is estimated from the known meteorological site information. 118 national meteorological sounding station distributions are known and the route is divided into different layers when conducted subtraction operation. Three characteristic values are used for a single sample point: geographic longitude, latitude and air pressure (or temperature or relative humidity). For example, the difference calculation is conducted according to the distance and the selection principle of Yichang, Wuhan, Changsha radiosonde meteorological information, and meteorological information when calculating the way of Yueyang. The calculation results are shown in Table 3.

The weather information of route point can be calculated by interpolation method. Aircraft flying height layer is a single layer according to the requirements of the Chinese flying height layer due to the route direction is from east to west. The formation of the condensate at different points in different height layers was determined by using formulae (25)–(6) and the results are shown in Table 4. ("$\surd$"represents formation of the contrail, and "$\times$" indicates not generating the contrail).

The flight model of CA1336 is A321-231 and Table 5 is $M = 0.78$. FFcr, FFcl, ROC, FFdes and ROD are as follows when the models are at different heights (Data source come from BADA3.12).

We can check the time and altitude of the flight path according to the ADS-B FlightAware real-time position report and the statistics are shown in Table 6.

It can be seen from the above calculation that the environmental impact of the contrail generation and CO_2 emission is different due to different time levels. But reducing the formation of contrail plays a major role in reducing greenhouse effect.

Data of Yichang, Wuhan, and Changsha in Table 3 are derived from the China Meteorological data network, and the value of Yueyang is calculated by formula (26).

Table 3. Atmospheric data after differential processing in some regions at 20:00 on 2 Jan 2016

Altit. (m)	Yichang			Wuhan			Changsha			Yueyang		
	atm. press.	temp. (°C)	rel humid. (%)	atm. press.	temp. (°C)	rel humid. (%)	atm. press.	temp. (°C)	rel humid. (%)	atm. press.	temp. (°C)	rel. humid. (%)
8100	357.9	-35.1	8.1	361.0	-33.7	83.3	363.3	-33.5	16.2	361.8	-33.8	33.4
8900	318.9	-40.5	7.0	345.8	-36.3	81.8	348.2	-36.0	16.6	346.7	-36.3	33.1
9500	292.2	-43.2	7.0	321.6	-40.3	78.4	324.1	-39.3	16.9	322.5	-39.8	32.2
10100	267.3	-45.9	7.0	307.7	-42.5	75.7	310.3	-39.4	17.0	308.8	-40.7	31.6
10700	255.4	-47.2	7.0	294.2	-44.6	72.5	296.9	-39.9	16.3	295.4	-41.7	30.3
11300	243.9	-48.7	7.0	281.4	-46.0	66.6	284.2	-40.8	14.3	282.7	-42.9	27.5
11900	232.8	-50.1	7.0	269.0	-47.8	61.8	271.8	-42.3	13.8	270.3	-44.4	25.9
11900	222.2	-51.6	7.0	257.0	-48.1	58.8	259.9	-44.1	14.8	258.4	-45.7	25.7

Table 4. The contrail-favorable regions at different level from ZGGG to ZBAA

Altit. (m)	Guang-zhou	Chen-zhou	Chang-sha	Yue-yang	Wu-han	Zhuma-dian	Zheng-zhou	Han-dan	Tian-jin	Bei-jing
8100	√	×	×	√	√	×	×	×	×	×
8900	×	×	×	√	√	×	×	×	×	×
9500	×	×	×	√	√	×	×	√	×	×
10100	×	×	×	√	√	√	√	√	√	×
10700	√	×	×	×	√	√	√	√	√	√
11300	√	×	×	×	√	√	√	√	√	√
11900	√	×	×	×	√	√	√	√	√	√
12500	√	×	×	×	√	√	√	√	√	√

Table 5. The fuel flow of A321-231 at different level

Altitude(m)	FF^{cr} (kg/s)	FF^{cl} (kg/s)	ROC (m/s)	FF^{des} (kg/s)	ROD (m/s)
8100	1.88275	2.99884	7.4	0.28557	9.8
8900	1.77090	2.83641	6.3	0.27475	10.0
9500	1.67235	2.63490	7.8	0.26393	14.3
10100	1.58691	2.42395	6.8	0.25311	13.5
10700	1.51445	2.23507	5.7	0.24230	12.9
11300	1.45724	2.04132	4.1	0.23148	11.4
11900	1.41602	1.84244	2.9	0.22066	11.1
12500	1.38789	1.66448	1.7	0.20984	11.0

Table 6. Live flight tracker of Flight CA1336 on 2 Jan. 2016

Waypoint	Latitude	Longitude	Time(CST)	Altitude(m)
Chenzhou	27.644	113.5167	21:26:32	10089
Changsha	28.225	113.5673	21:31:12	10089
Yueyang	28.88	113.5503	21:36:32	10089
Wuhan	30.593	114.3052	21:52:50	10089
Zhumadian	33.815	114.7294	22:17:54	10089
Zhengzhou	34.752	114.8201	22:25:39	10089
Handan	36.667	115.1591	22:41:29	10089
Tianjin	39.09	116.5129	23:04:16	5090

The aircraft is regarded as a moving particle and an aircraft trajectory optimization model based on the reduction of the greenhouse effect is established in this study. The basic modeling ideas are as follows: the vertical section of the aircraft is divided into $k \times l$ two-dimensional grid according to the route points and the height layers. Among them, $k = 1, 2, \ldots, kx$ represents the first k route points and l is the height layer. Firstly, to check whether the condensate is formed at the end of the first grid (k, l), that is to check the contrail generation coefficient $r_{k,l}$. When $r_{k,l} = 0$, there is no need to convert the height layer at the current grid without a condensation ending. While when $r_{k,l} = 1$, it generates the contrail of the current grid. And then to check the adjacent height layer of the contrail of the formation coefficient, the aircraft can only be converted to a height layer by the aircraft mobility constraints. Therefore, we consider only adjacent height layer $l + 1$ or $l - 1$. If the coefficient of condensation at the end of the high layer $l + 1$ or $L - 1$ is 0, the aircraft is moved to the high layer, and if the height of the $l + 1$ or $l - 1$ the contrail of the formation of the coefficient are both 0, the calculation does not generate the contrail of the total height of the global surface temperature T^{env} and moves the aircraft to the minimum height layer of T^{env}. However, if the adjacent height layer the contrail generation coefficient $r_{k,l+1}$ and $r_{k,l-1}$ are 1, then the adjacent height layer is formed by the contrail and then the height layer is not converted. The flow chart is shown in Fig. 6.

Comparison between the optimized flight profile and the original flight profile is shown in Fig. 7. The real-time position report shows that CA1336 began to reach the altitude of 10700 m from Chenzhou. Route points are: Changsha–Yueyang–Wuhan–Zhumadian–Zhengzhou–Handan–Tianjin–Chenzhou. It does not form the contrail due to the height of the arrival of Tianjin has been reduced to 5090 m and there is no need to optimize the height of the route point. Therefore, it is only necessary to optimize the remaining 7 point height and the height of the optimized layer are: 10700 m–10700 m–10700 m–10100 m–9500 m–9500 m–8900 m. Comparison of global surface temperature changes before and after CA1336 trajectory optimization is shown in Table 7.

It can be seen from Table 7 that the use of a high degree of adjustment can reduce the global surface temperature changes greatly. The global surface temperature changes are different at different time levels. Global surface temperature decreases

at 36.39 %, 13.98 % and 11.21 % in 25, 50 and 100 years, respectively.

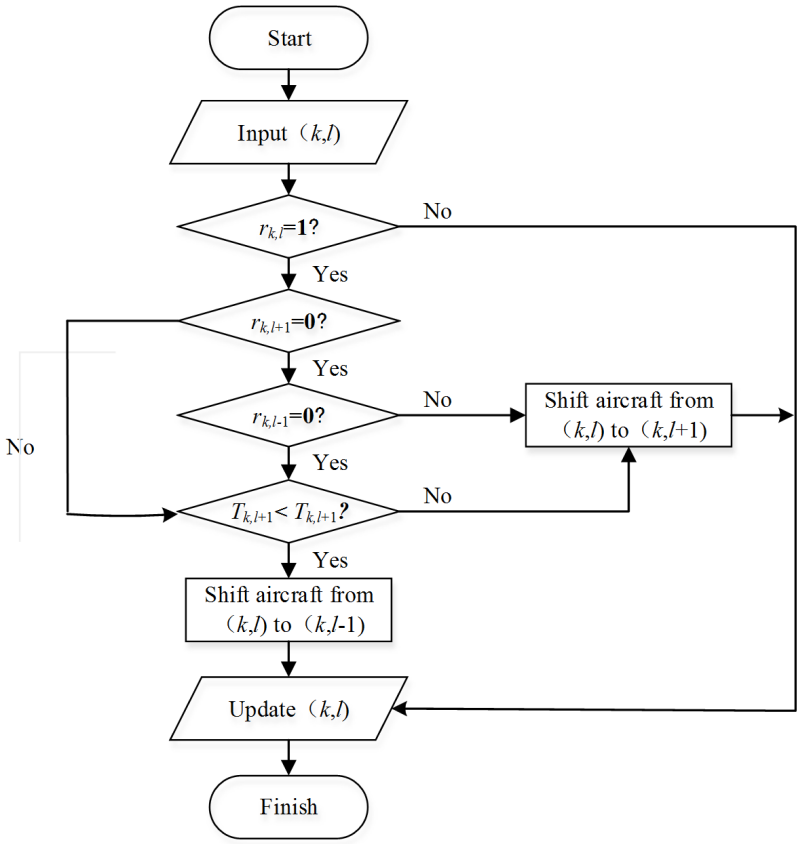

Fig. 6. Flow chart of aircraft trajectory optimization

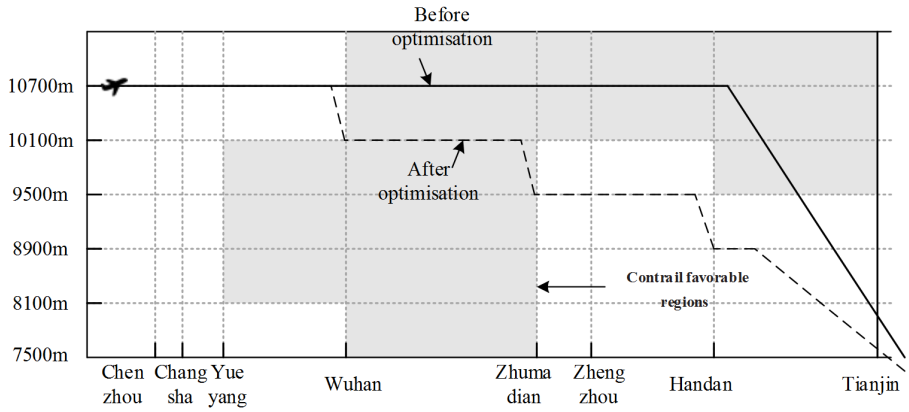

Fig. 7. The flight profile comparison before and after optimization

Table 7. The global temperature change due to flight CA1336 at different time horizons

	$H = 25$	$H = 50$	$H = 100$
The global temperature change due to flight CA1336 before optimization (K)	3.52×10^{-11}	1.72×10^{-11}	1.46×10^{-11}
The global temperature change due to flight CA1336 after optimization (K)	2.24×10^{-11}	1.48×10^{-11}	1.29×10^{-11}
The change rate of global temperature after optimization	-36.39 %	-13.98 %	-11.21 %

5. Conclusion

Aircraft altitude layer optimization is studied by using simulation and optimization algorithms based on the model of the contrail generation and the linear climate relying on the Guangzhou–Beijing route sounding data and flight data in order to reduce the impact of air transport on the environment. The main conclusions of this paper are as follows:

(1) The effect of the condensation and CO_2 emission on the environment is different at each time level, which causes that the global surface temperature increase is also different, but the reduction of the contrail formation plays a major role in reducing the greenhouse effect.

(2) The height of the flight after optimization are: 10700 m-10700 m-10700 m-10100 m-9500 m-9500 m-8900 m. The optimized height layer can eliminate the contrail by reducing the cruise height and reach to the economical cruising altitude as close as possible in order to reduce the influence of the aircraft operation on the global temperature change.

(3) The use of a high degree of adjustment can reduce the global surface temperature change greatly, and the different time levels of the global surface temperature change are different. The global surface temperature decreases by 36.39 %, 13.98 % and 11.21 %, respectively, within 25 years, 50 years and 100 years.

The aircraft trajectory optimization problem is studied and some useful conclusions are obtained combining with the simulation data. But in view of the complexity of the problem, the following issues needed further research: to deepen the research of multi-flight collaborative operation trajectory optimization, to consider the limit of the actual operation, such as route capacity and airspace structure, and to carry out the optimization research on the rising and falling stage of the aircraft trajectory.

References

[1] G. P. Brasseur, M. Gupta: *Impact of aviation on climate: Research priorities.* BAMS Bulletin of the American Meteorological Society *91* (2010), No. 4, 461–463.

[2] O. Boucher: *Atmospheric science: Seeing through contrails.* Nature Climate Change

5 (2011), No. 1, 24–25.

[3] C. Wang, X. Luo Xinzheng, H. Zhang: *Differences between the shares of greenhouse gas emissions calculated with GTP and GWP for major countries.* Progressus Inquisitiones de Mutatione Climatis *9* (2013), No. 1, 49–54.

[4] V. Williams, R. B. Noland, R. Toumi: *Air transport cruise altitude restrictions to minimize contrail formation.* Climate Policy *3* (2003), No. 3, 207–219.

[5] K. M. Gierens, L. L. Lim, K. Eleftheratos: *A review of various strategies for contrail avoidance.* Open Atmospheric Science Journal *2* (2008), No. 1, 1–7.

[6] Y. Tu, M. O. Ball, W. S. Jank: *Estimating flight departure delay distributions—a statistical approach with long-term trend and short-term pattern.* Journal of the American Statistical Association *103* (2008), No. 481, 112–125.

[7] N. Y. Chen, B. Sridhar, H. K. Ng: *Tradeoff between contrail reduction and emissions in united states national airspace.* Journal of Aircraft *49* (2012), No. 5, 1367 to 1375.

[8] M. Soler, B. Zou, M. Hansen: *Flight trajectory design in the presence of contrails: Application of a multiphase mixed-integer optimal control approach.* Transportation Research Part C: Emerging Technologies *48* (2014), No. 3, 172–194.

[9] A. Filippone: *Assessment of aircraft contrail avoidance strategies.* Journal of Aircraft *52* (2015), No. 3, 872–877.

[10] R. Zhang, J. He, H. Zhang: *Overview of researches on global warming potential of greenhouse gases.* Journal of Anhui Agriculture Science (in Chinese) *39*, (2011), No. 28, 17416–17419, 17422.

[11] Q. Fu: *Studies on international climate change legislation trend and chinese countermeasures: From the view of the GHG reduction of international aviation.* Journal of Beijing University of Aeronautics and Astronautics (Social Sciences Edition) *25* (2012), No. 5, 50–55.

[12] T. R. Anderson, E. Hawkins, P. D. Jones: *CO2, the greenhouse effect and global warming: From the pioneering work of Arrhenius and Callendar to today's Earth System Models.* Endeavour *40* (2016), No. 3, 178–187.

[13] G. Gu, Z. Wang: *A Research of Multi-country-Multi-sector Economic Growth and Carbon Emission Governance under Global Carbon Taxes.* China Soft Science *32* (2015), No. 12, 1–11.

[14] K. P. Shine, J. S. Fuglestvedt, K. Hailemariam: *Alternatives to the global warming potential for comparing climate impacts of emissions of greenhouse gases.* Climatic Change *68* (2005), No. 3, 281–302.

[15] O. Boucher, M. S. Reddy: *Climate trade-off between black carbon and carbon dioxide emissions.* Energy Policy *36* (2008), No. 1, 193–200.

Received August 7, 2017

Acta Technica *62* No. 2B/2017, 441–454

Assessment of terrain slope effects on GLAS waveform and canopy height retrieval using 3-D vegetation model

Lu Xue-hui[1,2], Li Ai-nong[1,3], Bian Jin-hu[1,2], Jin Hua-an[1]

Abstract. To assess the terrain effects on the Geoscience Laser Altimeter System (GLAS) waveform and canopy height retrieval, the 3-D lidar waveform model was used to simulate the GLAS waveform for the nine scenes with the slopes increasing from 0 to 30 ° in 1 °. When slope increased from 0 ° to 10 °, the magnitude of the canopy peak decreased by approximately 2/5 to 3/5, but the magnitude of the ground peak decreased by more than 4/5 for all the simulated scenes. The critical slope angle is in direct proportion to canopy height, and slightly decreases with the increased stand density. Further analysis showed that average error for the RH100 was 5.4 m when the slope was 10 °, and reached 9.4 m when the slope was 15 °. Meanwhile, the average error for the physical terrain correction method was –5.6 meters even for the slopes up to 30 °. Thus, it is suitable to retrieve tree height for areas with up to 10 ° slopes using the direct method. However, a simple physical slope correction could be used in areas with greater slopes. This work enhances our understanding of the interactions between surface topography, forest structure and waveform shape.

Key words. Canopy height, surface topography, 3-D vegetation model, GLAS waveform.

1. Introduction

Forests are the largest carbon reservoirs in terrestrial ecosystems and play a critical role in the global carbon cycle and global warming mitigation. Forest canopy height is considered to be among most useful structural parameters for estimating forest biomass and productivity. It has been widely accepted that light detection and ranging (lidar) provides the most direct measurements of forest structure including canopy and forest biomass. The Geoscience Laser Altimeter System (GLAS)

[1]Institute of Mountain Hazards and Environment, Chinese Academy of Sciences, Chengdu, China, 610041
[2]University of Chinese Academy of Sciences, Beijing, China, 100049
[3]Corresponding Author

onboard NASA's Ice, Cloud and Land Elevation Satellite (ICESat) was the first space-borne lidar system to provide fast forest canopy height solutions. Successes have been reported in many studies, in which GLAS waveform data served as the core data for estimating the forest canopy height and above-ground biomass [1, 2].

The GLAS signal is very sensitive to surface topography due to its large footprint. The terrain effect makes it a big challenge to retrieve canopy heights over mountainous regions. Modeling work allows the explicit calculation of the effects of land slope. To data, several RTM models have been developed for simulating the lidar waveforms of forest canopies. For example, Sun and Ranson (2000) developed a 3-D forest canopy model for simulating lidar waveforms from forest stands of varying geometry and complexity [3]. North et al. (2010) presented a Monte Carlo radiative transfer model for simulating lidar waveforms within the framework of the FLIGHT model [4]. Yang et al. (2011) adopted the updated analytical GORT vegetation lidar model to simulate lidar waveforms with changes of vegetation, structure, surface topography, footprint size, off-nadir pointing, pulse width and surface roughness, and ratio of the canopy and background reflectivity [5]. Although terrain effects on the large footprint have been modeled in previous studies [6, 7], the efforts were usually based on relatively simple experiment designs. The diversity of forest structures was not accounted for in these study.

The 3-D lidar model developed by Sun and Ranson [3] is designed especially for the simulating return lidar waveforms from forest canopies. It is flexible in the experiment design. We extended the three-dimensional (3-D) lidar model developed by Sun and Ranson [3] to account for land slope and applied the extended model to assess the aforementioned impacts on vegetation lidar waveforms and height retrieval.

2. Modelling lidar waveform from vegetation canopies

2.1. The 3-D lidar waveform model of forest

The 3-D lidar waveform model was based on theory from geometric optics and radiative transfer (GORT). To model the lidar waveform, the 3-D scene was divided into cells according to the vertical resolution of the lidar (Fig. 1). The cell used in this study was a 0.15 m × 0.15 m × 0.15 m cube that corresponded to the vertical resolution of GLAS. There were four different types of cells in the model: crown, trunk, air, and ground cells. Every cell was assigned to one type according to its position. The spectral reflectance and transmittance properties of the cells were also specified by type. The ground surface is described as a plane with a specified slope angle. The specific theory was shown in [3].

The assumptions in the following simulations were made:

1) Uniform tree crowns, i.e., the canopies within a waveform share the same structure, and are uniformly distributed.

2) Uniform ground surface.

3) Only single scattering was considered.

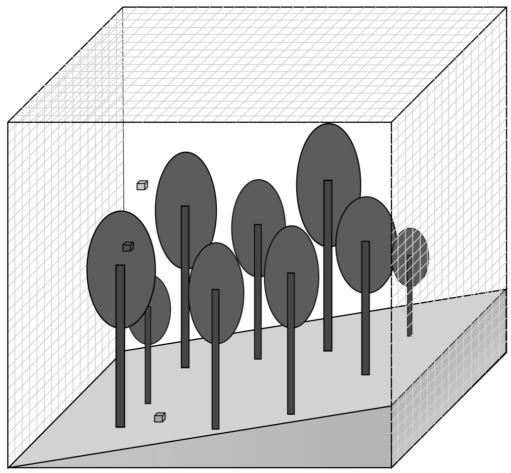

Fig. 1. The 3-D scene of a forest stand with certain slope (each cell in the model could be assigned to one type according to its position in the scene)

2.2. Tree structural model

As mentioned above, the 3-D model requires information about every tree in the laser footprint including DBH, height, crown geometry and species. In this study, tree crown shapes were modeled as ellipsoids. The structural parameters of trees were obtained from forest stand attributes. There were three tree models of different height used for the waveform simulation. The geometry parameters of every tree model are listed in Table 1.

Table 1. The parameters describing the simulated trees

Item	Tree model 1	Tree model 2	Tree model 3
DBH (Diameter at Breast Height)	15 cm	20 cm	25 cm
Tree height	10 m	15 m	20 m
Crown height	5.51 m	8.27 m	11.03 m
Crown width	2.90 m	4.35 m	5.81 m

Additional parameters used in the model were fixed to default: foliage area volume density is 1.25, $G_$factor is 0.5, leaf reflectance is 0.55, and ground reflectance is 0.2.

2.3. LiDAR sensor model

In this model, the set of parameters defining the lidar instrument were specified according to GLAS, approximating view and illumination geometry as nadir, which would produce a footprint diameter of 65 m. The angular divergence and temporal spread of the emitted pulse were assumed to be Gaussian. The width of the trans-

mitted pulse used was 5 ns, and the vertical resolution of the lidar waveform was 0.15 m. The illuminating intensity decreased from 1.0 to e^{-2} from the center to the edge of the footprint.

2.4. Experiment setup

In this study, the size of the three-dimensional stand scene was 75 m × 75 m and the diameter of the laser footprint was 65 m. Three tree distribution scenes of different densities were designed. For each scheme, trees were distributed uniformly as the hexagonal rules in the footprint. The distances separating adjacent trees in the three scenes were 10 m for scheme A, 8 m for scheme B, and 6 m for scheme C. The three tree models described in subsection 2.3 were used for each scheme, and the slope increased from 0 ° to 30 ° by 1 ° steps. Nine groups of model simulations were, therefore, used in this study.

3. Simulation results and analysis

3.1. Terrain effect on vegetation lidar waveforms

Figure 2 shows the vegetation lidar waveforms at different slope angles and footprint sizes of 65 m for the simulated forest scenes. From the figure, one can see that terrain slope stretched the length of the waveform, and decreased the canopy, particularly the ground peaks. The heights of the canopy peak and ground peak also increased slightly with slope.

It is worth noting that the slope greatly impacted on the waveform extent. As expected, greater slopes tended to generate longer waveforms. With increased slope, the waveform was extended both in the signal-end and signal-start directions. Due to the rapid decline of the ground peaks, the stretch in the signal-start directions was more significant than in the signal-end direction. For a simulated scene with a thick stand density, this trend was more obvious because the ground return was weaker and disappeared more rapidly with increasing slope under that condition.

Figure 5 shows the variation in magnitude of the ground and canopy peaks with slope. It was discovered that the decreasing tendency of the ground peaks for all the simulated senses was the same. The magnitude of the ground peak from a flat to a 10 ° slope decreased by more than 4/5. However, the decreasing rate of the canopy peak was related to canopy height. The lower the canopy height was and the faster the canopy peak decreased. The magnitude of the canopy peak from a flat to 10 ° slope decreased by approximately 2/5 to 3/5. From that, the ground returns were more distorted than the canopy returns. At a 10 ° slope, the ground peak was still noticeable for all the simulated senses except for the last one. As the slope continued to increase, the ground and canopy peaks gradually merge; at a specific slope or steeper, the ground peak disappeared.

3.1.1. The critical angle for ground peak identifying. To better address the slope effect, the concept of critical angle was introduced in this study. It is defined as the

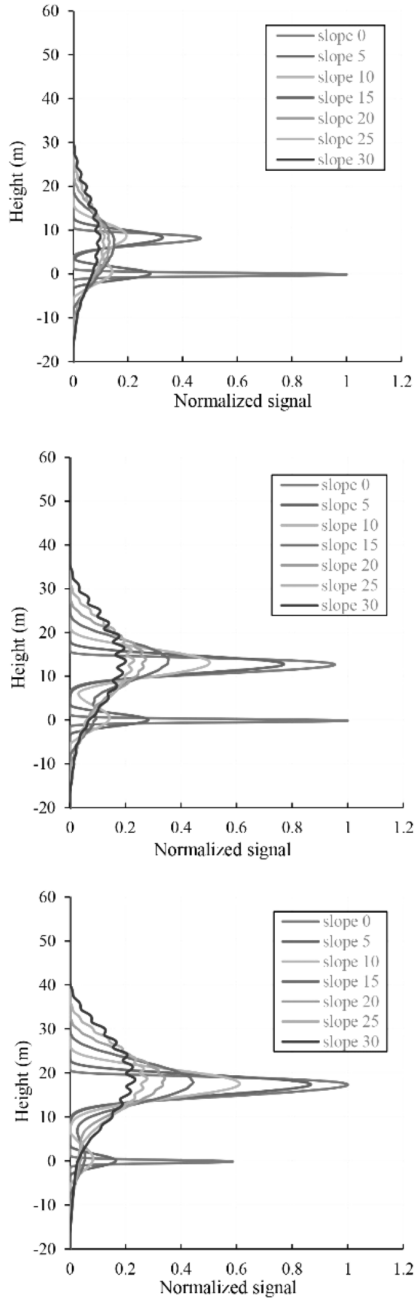

Fig. 2. The simulated waveforms over different terrain slope: from top to bottom, trees are distributed according to the scheme A in subsection 2.4 with the heights of 10 m, 15 m, and 20 m, from top to bottom, respectively

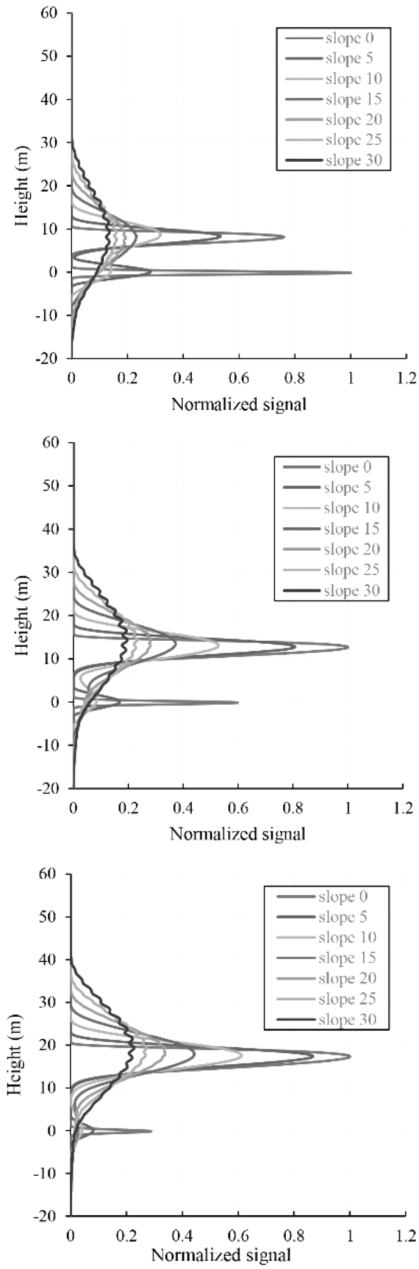

Fig. 3. The simulated waveforms over different terrain slope: from top to bottom, trees are distributed according to the scheme B in subsection 2.4 with the heights of 10 m, 15 m, and 20 m, from top to bottom, respectively

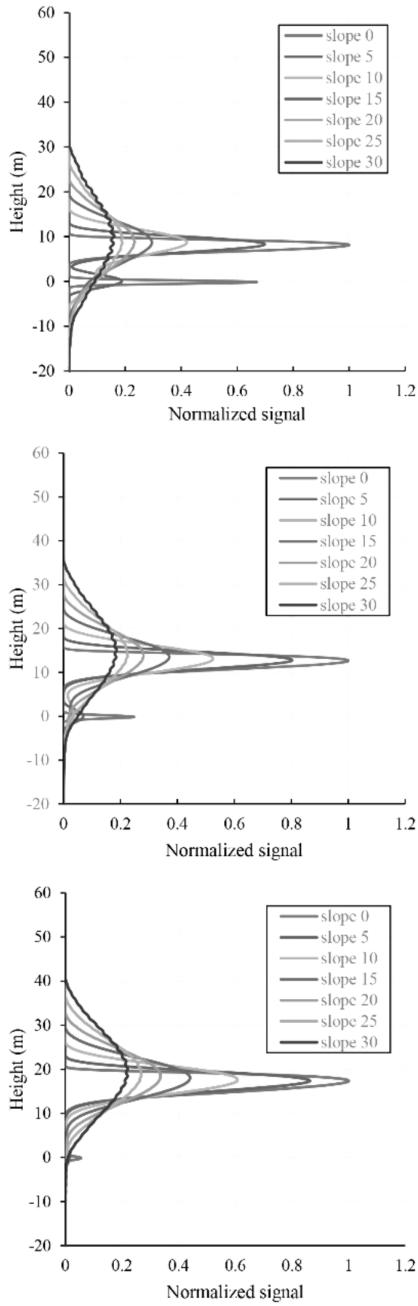

Fig. 4. The simulated waveforms over different terrain slope: from top to bottom, trees are distributed according to the scheme C in subsection 2.4 with the heights of 10 m, 15 m, and 20 m, from top to bottom, respectively

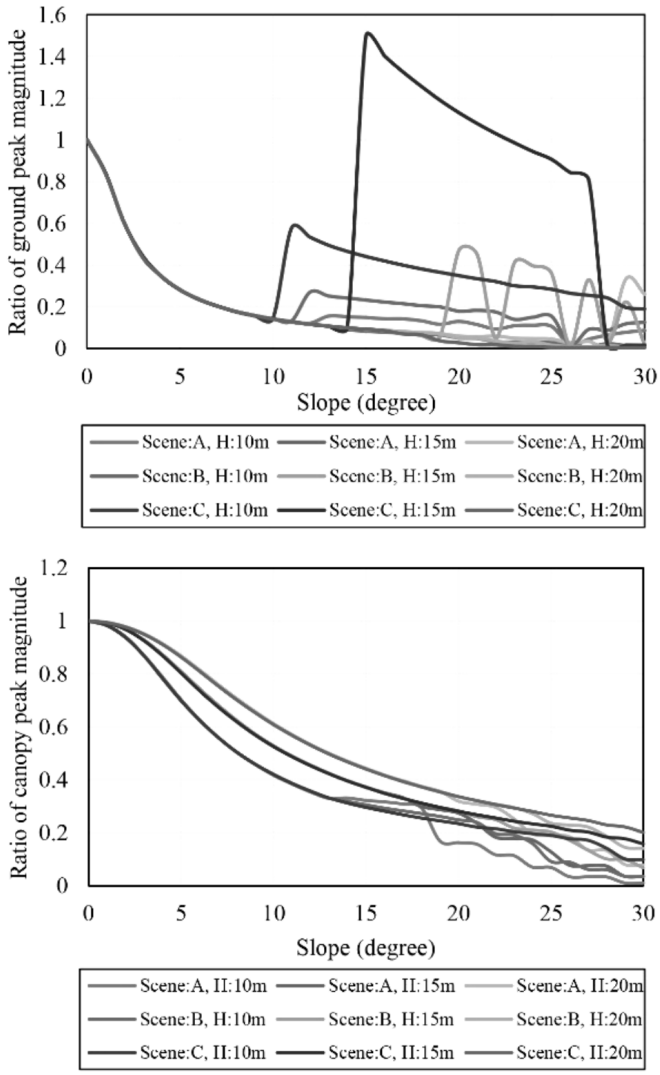

Fig. 5. The variation of magnitude of the ground (top) and canopy peak (bottom) with the slope (the oscillates of magnitude is because that ground peak mix with the vegetation peak with the increasing slope)

slope angle where the ground and vegetation returns are completely mixed [5]. When a slope exceeds the critical angle, it is quite challenging to estimate vegetation height by identifying the ground peak.

The canopy height is a major factor that influences the critical angle for the GLAS waveform. Table 2 shows the critical angle of the different simulated scenes. From the table, one can see that the critical angle was directly proportional to vegetation height. As discussed above, terrain slope leads to a mixture of the lower

part of the canopy return and the higher part of the ground return. Taller trees mean larger departures of the canopy bottom from the ground. Therefore, a larger critical angle is needed to mix the vegetation return with the ground return. As shown in Table 3, for scene A, the 20 m canopy has a critical angle of 20 °, whereas the critical angles were 15 ° and 11 ° for the 15 m and 10 m canopies, respectively. The simulated results of scenes B and C tell nearly the same story. A different case is that of C with a canopy height of 20 m. The canopy cover for that case reached 84.68 %. Under that condition, the ground return was very small on a flat terrain. With the increasing slope, the ground peak is declined rapidly, and the ground peak thus could not be identified from the waveform at a small slope angle.

Another factor that affects critical angle is canopy cover. The increase in canopy cover led to a greater laser return from the canopy or a decrease in the ground return. Table 3 shows that critical angle slightly decreased with increased canopy cover. An exception was scene C, which had a canopy of height 20 m, for the reason discussed above.

Table 2. The critical angles of the simulated scenes

Trees distribution	Canopy height (m)	Canopy coverage (%)	Critical angle (°)
Scene A	10 m	7.59	11
Scene A	15 m	17.02	15
Scene A	20 m	29.96	20
Scene B	10 m	11.89	10
Scene B	15 m	26.73	14
Scene B	20 m	47.62	19
Scene C	10 m	21.34	9
Scene C	15 m	47.44	13
Scene C	20 m	84.68	10

3.2. Canopy height error due to terrain slope

As discussed above, the topographic slope greatly affects the GLAS waveform shape and relative parameters. Therefore, the slope is expected to affect the estimation of canopy height. With the direct method, RH100 was considered as the maximum canopy height over flat terrain. Yang et al. (2011) developed an analytical equation that could be used to estimate the canopy height [5]. In this section, the estimation errors of the canopy heights calculated by the two methods are analyzed.

RH100 is the distance between the signal start and the ground return. Therefore, precise detection of the ground peak is important because it is used as a reference for calculating the quartiles. The identification of the ground peak in this study was based on the Gaussian decomposition of the waveform. The last fitted Gaussian peak was assumed to be the ground peak. In Fig. 6, top part, the canopy height error is calculated as the difference in the RH100 values and the input canopy height values of the 3-D lidar waveform model of the forest. As shown in the picture, height error was a function of terrain slope angle when the slope was less than 15 °. As the slope exceeded the critical angle, the RH100 values contained large errors from

the misidentification of the ground return, and the height errors were irregular with regard to slope. The average error for the RH100 was approximately 5.4 m when the slope was 10 °, and reached 9.4 m when the slope increased to 15 °.

In Fig. 6, bottom part, the canopy heights were estimated using the analytical equation developed by Yang et al. (2011).

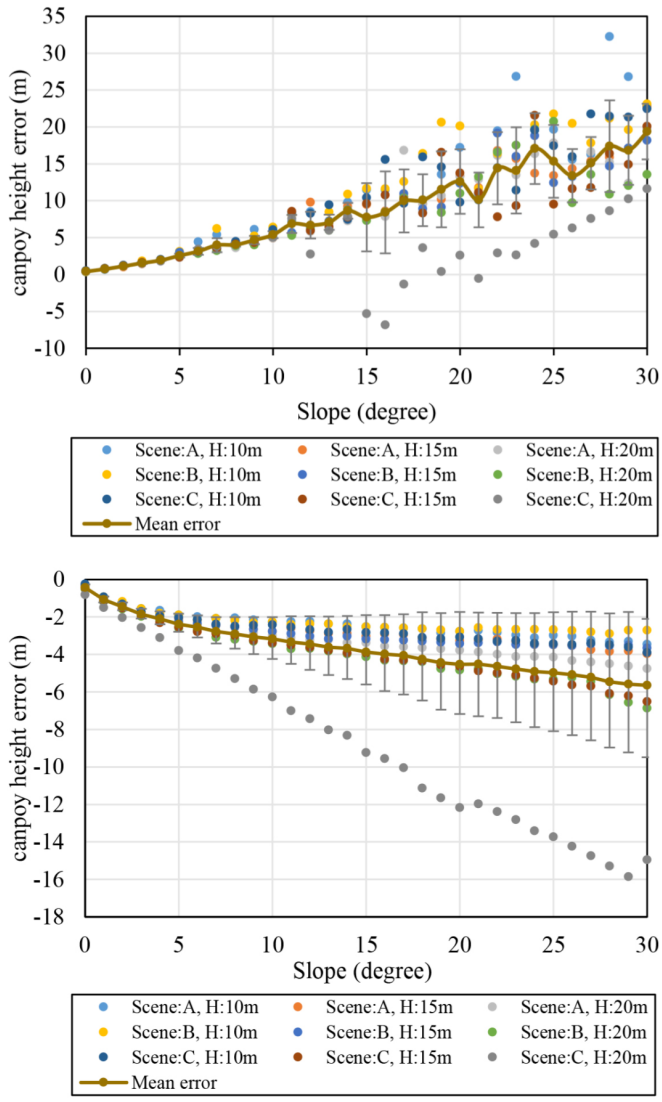

Fig. 6. Relation between maximum canopy height estimation error and slope using (top) direct method, (bottom) slope-correction model developed by Yang et al. [5], error bars represent the standard error of each mean

Due to the underestimation of waveform extents in areas with high topographic

relief, this method could be expected to result in lower height estimates. Higher slopes and stand densities would lead to more increased underestimations of forest canopy heights. For scene C with a canopy height of 20 m, the absolute errors in canopy height increased rapidly with increasing slope. The canopy height was underestimated by 6.3 m when the slope was 10 °. As the slope increased to 30 °, this value reached to almost 16 m. For other simulated scenes, the variation in the estimation errors with slope was relatively small. When the slope increased from 0 ° to 30 °, the absolute errors of canopy height increased by only a few meters. Our results have demonstrated that the GLAS height estimating approach described by Yang et al. (2011) can be used in areas with slopes up to 30 °, but there may be lager underestimations for high stand density forests.

4. Discussion

The work in this paper enhances our knowledge regarding the impact of terrain slope on GLAS waveforms. The simulation results have shown that terrain slope broadens and decreases canopy and ground peaks. This finding is in agreement with pervious simulation results [1, 5, 7]. Our study has further revealed that although the waveform extends both in the signal-end and signal-start directions, the stretch in the signal-start direction is more significant than that in the signal-end direction, especially for simulated scenes with thick stand densities. Moreover, compared with the canopy peak, the magnitude of the ground peak decreased more rapidly. The magnitude of the canopy peak from a flat to a 10 ° slope decreased by approximately 2/5 to 3/5. However, the magnitude of the ground peak from a flat to a 10 ° slope decreased by more than 4/5 for all the simulated scenes.

The critical slope angle range was 9 °–20 ° at a 65 m footprint size in this study. The model simulations showed that the critical slope angle changed depending on vegetation height and stand density. The critical angle was proportional to canopy height, and slightly decreased with increasing stand density. This means that a high and not too dense forest with a single one-layer canopy can generate a waveform from which the ground peak could be identified, even if the terrain is steep and rough. However, the critical angle can also be very small when the stand density is too large regardless of whether the canopy height is high or low. The study by Yang et al. [5] showed that the critical angles were 10.5 ° for a one-layer canopy and 12.5 ° for a two-layer canopy at a 70 m footprint size and noted out that the critical angle decision could be much more complicated. In addition, Hilbert et al. [13] found that slopes between 10 ° and 15 ° appeared to be a critical limit for the usefulness of the waveforms. The results in this paper are essentially in agreement with the predecessor conclusions and further found the critical angle could change in a wider range depending on vegetation height and stand density.

The results from the simulation aid our understanding of the overall height error caused by surface topography. The results from this study showed that average error of RH100 for the nine groups of simulation results was about 5.4 m when the slope was 10 °, and reached 9.4 m when the slope was 15 °. As the slope exceeded the critical angle, the ground peak merged with the canopy peak, making it difficult to

extract tree height using the direct method. Therefore, a conclusion was reached that it is suitable for retrieving tree heights for areas with up to a 10 ° slopes using the direct method. Some adjustment could be made according to the local conditions of study sites in the actual operational process of tree height retrieval. These results are consistent with previous studies [6, 8]. The simple physical slope correction developed by Yang et al. [5] could be used in areas with slopes up to 30 °, but may yield lager underestimation for forests with high stand densities. Previous studies have shown that large-footprint lidar estimates of maximum canopy height can be significantly improved using the simple physical slope correction [6, 9].

Modeling topographic effects on large-footprint lidar waveforms is an area of ongoing research. A simplifying assumption in the 3-D lidar waveform model was that only single scattering contributes to the returned signal. Blair and Hofton [10] demonstrated that multiple scattering was not a significant contributor to waveforms. However, North et al. explicitly modeled multiple scattering within the canopy using a Monte Carlo radiative transfer model, and found that it would cause a 'tail' beneath the ground peak in both simulated and GLAS waveforms [4]. Under this condition, the ground elevation may be underestimated due to increased path length, and such uncertainties would be reflected in calculations of waveform metrics and canopy height estimation. Some studies have suggested the presence of litter on forest floors possibly contribute to multiple scattering [11]. Further studies are needed to quantify the effects of multiple scattering in the canopies and understories on lidar pulse waveforms.

To model the impacts of surface topography on the GLAS waveforms under different forest conditions, the topography was described as a horizontal plane with specified slope angles. This method cannot model all topographic effects, but at the scale of the GLAS footprint a sloped plane will suffice. Moreover, some settings are simple and ideal in this model, such as the same vegetation structure, the uniform distribution in the footprint and ellipsoidal crown, which also affect the lidar waveform [7, 12]. The model performance need to be validated by using an actual dataset of field measurements and airborne lidar data.

5. Conclusion

In this paper, the 3-D lidar waveform model developed by Sun and Ranson [3] was used to simulate the terrain effects on a large footprint lidar waveform and on canopy height retrieval. Model simulations showed that terrain slope broadens and decreases canopy and ground peaks. Although the terrain slope stretched the waveform both in the signal-end and signal-start directions, the stretch in the signal-start direction was more significant due to the rapid decline of the ground return. The critical slope angle, where the ground and vegetation returns are completely mixed, ranged from 9 ° to 20 ° in this study. It was in direct proportion to canopy height, and slightly decreased with the increasing stand density.

The direct method and slope-correction model was employed to estimate canopy height based on the simulation results. An error analysis showed that the direct method could be used to retrieve tree height in areas with slopes up to 10 °. However,

the simple physical slope correction could be used to could be used in areas with slopes up to 30 °, but there may be increased underestimation for high stand density forests. The present study clearly demonstrates the relationship between GLAS waveform and topography. Therefore, it can help improve the accuracy of canopy height estimation using GLAS or future spaceborne lidar data.

References

[1] D. J. Harding, C. C. Carabajal: *ICESat waveform measurements of within-footprint topographic relief and vegetation vertical structure.* Geophysical Research Letters *32* (2005), No. 21, CiteID L21S10.

[2] M. A. Lefskya, M. Keller, Y. Panga, P. B. de Camargod, M. O. Hunter: *Revised method for forest canopy height estimation from Geoscience Laser Altimeter System waveforms.* Journal of Applied Remote Sensing *1* (2007), paper 013537.

[3] G. Q. Sun, K. J Ranson: *Modeling lidar returns from forest canopies.* IEEE Transactions on Geoscience and Remote Sensing *38* (2000), No. 6, 2617–2626.

[4] P. R. J. North, J. A. B. Rosette, J. C. Suárez, S. O. Los: *A Monte Carlo radiative transfer model of satellite waveform LiDAR.* International Journal of Remote Sensing *31* (2008), No. 5, 1343–1358.

[5] W. Z. Yang, W. Ni-Meister, S. Lee: *Assessment of the impacts of surface topography, off-nadir pointing and vegetation structure on vegetation lidar waveforms using an extended geometric optical and radiative transfer model.* Remote Sensing of Environment *115* (2011), No. 11, 2810–2822.

[6] X. Y. Wang, H. Huang, P. Gong, C. Liu, C. Li, W. Li: *Forest canopy height extraction in rugged areas with ICESat/GLAS data.* IEEE Transactions on Geoscience and Remote Sensing *52* (2014), No. 8, 4650–4657.

[7] X. H. Xi, R. Li, Z. Liu, X. Jang: *Forest characteristics and effects on LiDAR waveforms modeling and simulation.* International Symposium on Spatial Accuracy Assessment in Natural Resources and Environmental Sciences, 25–27 June 2008, Shanghai, China, World Academic Union (Press) (2008), 134–140.

[8] F. Enssle, J. Heinzel, B. Koch: *Accuracy of vegetation height and terrain elevation derived from ICESat/GLAS in forested areas.* International Journal of Applied Earth Observation and Geoinformation *31* (2014), 37–44.

[9] D. J. Selkowitz, G. Green, B. Peterson, B. Wylie: *A multi-sensor lidar, multispectral and multi-angular approach for mapping canopy height in boreal forest regions.* Remote Sensing of Environment *121* (2012), 458–471.

[10] J. B. Blair, M. A. Hofton: *Modeling laser altimeter return waveforms over complex vegetation using high-resolution elevation data.* Geophysical Research Letters *26*, (1999), No. 16, 2509–2512.

[11] I. A. Iqbal, J. Dash, S. Ullah, G. Ahmad: *A novel approach to estimate canopy height using ICESat/GLAS data: A case study in the New Forest National Park, UK.* International Journal of Applied Earth Observation and Geoinformation *23* (2013), 109–118.

[12] B. Hu, J. Tcherniavski, A. Dudelzak, A. Koujelev: *Modeling spaceborne lidar returns from vegetation canopies.* Lidar Remote Sensing for Environmental Monitoring VIII, SPIE Proceedings *6681* (2007).

[13] C. Hilbert, C. Schmullius: *Influence of surface topography on ICESat/GLAS forest height estimation and waveform shape.* Remote Sensing *4*, (2012), No. 8, 2210–2235.

Received September 19, 2017

Acta Technica *62* No. 2B/2017, 455–464

Automatic color grading model of foie gras based on machine vision

Pang Bin[1], Liu Tai-lian[2]

Abstract. To make up a disadvantage of traditional manual grading method, an automatic color grading model of foie gras was proposed based on machine vision and statistic recognition. Foie gras sample images from four different color grades were collected by a color CCD camera. After preprocessing and segmentation of the images, 12 color features were extracted from the foie gras area. To reduce color feature dimension, principal component analysis(PCA) was utilized. Afterwards, a multiple linear regression (MLR) model and a canonical discriminate analysis (CDA) model were set up respectively to predict color grade. The MLR model achieved the accuracy of 92 % and the CDA model of 100 %, showing that the machine vision combined with statistic recognition can provide an effective way for predicting foie gras color grades automatically.

Key words. Foie gras, color grading, machine vision.

1. Introduction

Currently, foie gras grading in China is carried out manually based on the quality indices such as weight, color, resilience and defects. Nevertheless, manual grading method relies on sensory experience of human grader, which usually lead to incompatible grading judgment. Besides, this method is costly and time-consuming for modern foie gras industry. It is evident that use of such method can not quantify the color index of foie gras. Therefore, utilization of new method such as machine vision and statistic recognition can be a substituted solution for automatic color grading of foie gras.

The machine vision technology has been considered as an objective and consistent way to estimate the quality of food product [1]. Many related studies using machine vision technology for color grading [2, 3], shape measurement [4-7] and defect detecting[8, 9] have been reported. However, although there are many studies

[1]College of Food Science and Engineering, Qingdao Agricultural University, Qingdao, Shandong, 266109, China

[2]College of Science and Information, Qingdao Agricultural University, Qingdao, Shandong, 266109, China

for meat products by using machine vision to predict color attributes, foie gras color grading by machine vision has seldom been studied. Chen et al. proposed an automatic method combined with machine vision and support vector machine(SVM) to determine color score of beef fat. Results showed that the machine vision combined with SVM discrimination method can predict color scores of beef fat effectively. Sun et al.analyzed fresh beef lean color image features for predicting beef color scores. It was reported that the machine vision combined with SVM classifier can achieve the best performance percentage of 94.7 %. Jia et al. applied a locally liner embedding (LLE) method to reduce the dimensions of pork color feature. The results showed pork color grading accuracy can be improved combined with LLE manifold learning method and SVM.

In this project, a color automatically grading method based on computer vision system was established to predict foie gras color grades. The aim of this study was to:

1) Segment foie gras sample from background using imaging processing.

2) Extract color features from RGB and $L*a*b*$ color spaces.

3) Estimate correlations between color grades and color features.

4) Reduce dimension of color features using PCA.

5) establish and test two different regression models for predicting foie gras color grades.

2. Materials and methods

2.1. Sample preparation

A total of 75 Greylag Landaise geese at age of 150 days were selected to overfeeding in the same condition. The duration of the preliminary experiment was 7 days and the duration of the formal experiment was 30 days. Then 75 geese were slaughtered and livers were classified manually by color according to Chinese foie gras standard. The 75 foie gras samples were divided into four color grades. As shown in Fig. 1, 14 pieces of grade one (G1) samples were marked with level 1, 15 pieces of grade one (G2) samples were marked with level 2, 30 pieces of grade one(G3) samples were marked with level 3, 16 pieces of grade one (G4) samples were marked with level 4.

2.2. Machine vision system

The machine vision system (Fig. 2) for collecting sample images consisted of a color CCD camera(Dimage Z1, Minolta Co.Ltd., Japan) with the maximum resolution 2048 by 1536 pixels, two adjustable LED lamps (YX-BL25040, Yongxin Ltd., China) with 400 Lux and a computer system (2.4 GHz Intel Core Duo CPU with 2 GB RAM).

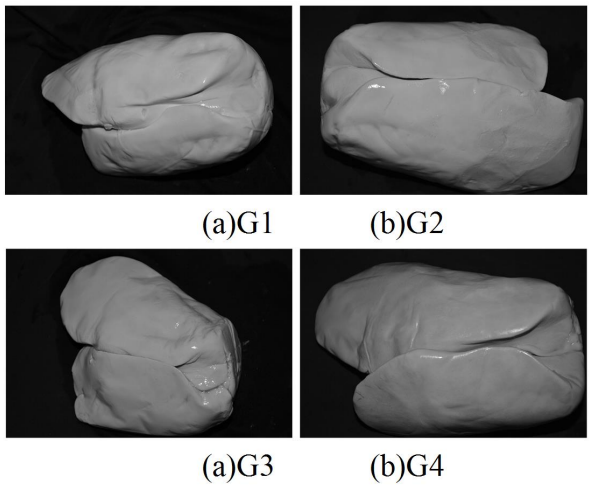

Fig. 1. Typical foie gras samples of different color grades

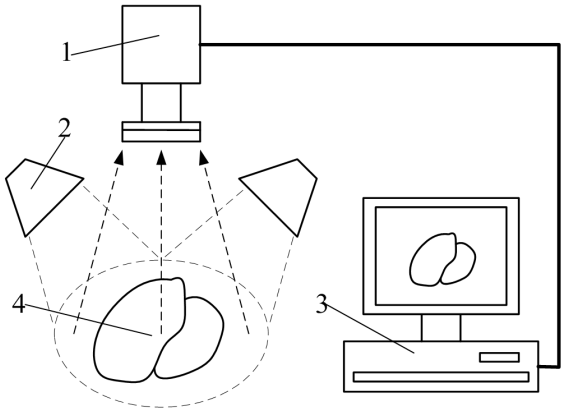

Fig. 2. Machine vision system: 1–CCD camera, 2–LED lamp, 3–computer system, 4–foie gras

2.3. Image processing and color feature extraction

Once images were collected, image processing and color feature extraction were performed using Matlab software. To remove the background, the Otsu's method was used to select the segmentation threshold value automatically. Each sample image was preprocessed to remove the background in the way and all of resulting images were subjected to extraction of color features. As resulting images were represented in RGB color space, a transformation from RGB to Lab was required. Then the mean (μ) and standard deviation (σ) were calculated in RGB and $L*a*b*$ color spaces.

2.4. Data analysis

Twelve color features(μR, μG, μB, μL, μa, μb, σR, σG, σB, σL, σa, σb) were evaluated using statistical software (SPSS 20.0). The 12 color features were reduced by principal component analysis in order to find the comprehensive features to explain foie gras color. The comprehensive features were pooled into the MLR and CDA model to quantify foie gras color grades.

3. Results and discussion

3.1. Color features extraction

As described in Section 2.3, twelve color features that characterized foie gras color were extracted from the sample images. Table 1 lists the descriptive statistics (means, standard deviations) of foie gras color features with different color score. As shown in Table 1, 12 color features (μR, μG, μB, μL, μa, μb, σR, σG, σB, σL, σa, σb) were replaced by $X_1 - X_{12}$ respectively. The standard deviation of the color features fluctuated less significantly than the mean, suggesting that the standard deviation is not a critical index.

Table 1. Descriptive statistics of foie gras color features

CF	G1	G1	G2	G2	G3	G3	G4	G4
	Mean	S.D.	Mean	S.D.	Mean	S.D.	Mean	S.D.
X_1	145.60	6.21	135.91	3.65	137.25	2.53	123.40	3.60
X_2	132.37	3.58	122.51	3.99	118.23	3.63	104.69	5.04
X_3	118.93	2.56	105.66	3.38	101.49	3.01	97.60	5.04
X_4	142.42	6.19	134.55	2.91	130.34	3.42	118.25	2.64
X_5	131.29	0.72	130.87	0.37	134.81	0.77	134.00	1.03
X_6	136.14	1.38	138.84	1.26	139.99	1.59	134.99	1.65
X_7	6.53E-02	2.66E-03	5.22E-02	3.10E-03	5.53E-02	2.36E-03	4.53E-02	1.90E-03
X_8	6.57E-02	2.21E-03	5.02E-02	2.15E-03	5.06E-02	2.36E-03	4.46E-02	2.75E-03
X_9	5.90E-02	2.83E-03	4.43E-02	3.03E-03	4.17E-02	2.72E-03	4.12E-02	2.60E-03
X_{10}	6.77E-02	1.80E-03	5.22E-02	1.97E-03	5.29E-02	3.18E-03	4.70E-02	2.59E-03
X_{11}	4.03E-03	2.57E-04	2.16E-03	2.64E-04	2.93E-03	7.02E-04	3.92E-03	3.21E-04
X_{12}	5.08E-03	2.94E-04	5.34E-03	1.87E-04	6.85E-03	2.55E-04	4.31E-03	2.82E-04

Note: CF = Color features.

3.2. PCA of color features

Twelve principal components (PC1–PC12) were calculated from the 12 color features extracted from 75 sample images. The variance contribution rates of each

principal component are shown in Table 2.

As shown in Table 2, the eigenvalues of first 3 principal components (PC1, PC2, PC3) with cumulative variance contribution rate of 86.24 % are greater than 1. Thus, the first 3 principal components (PCs) were chosen to replace the original 12 color features. Fig. 3 showed the data point distribution of the first 3 PCs. As shown in Fig. 3, the data point regions of different color grade were plotted into 4 regions clearly and had no overlap. The distribution of G3 data point region was relatively scattered. The distribution of G1, G2, G4 data point regions were relatively centralized.

Table 2. Variance contribution rate of each principal component

Principal component	Eigenvalue	Variance cntribution rate (%)	Cumulative variance contribution rate (%)
PC1	6.36	53.02	53.02
PC2	2.70	22.43	75.45
PC3	1.30	10.79	86.24
PC4	0.58	4.81	91.04
PC5	0.29	2.45	93.49
PC6	0.21	1.74	95.23
PC7	0.16	1.32	96.55
PC8	0.11	0.94	97.48
PC9	0.10	0.84	98.32
PC10	0.08	0.62	98.95
PC11	0.07	0.59	99.54
PC12	0.06	0.46	100.00

3.3. MLR model of color grade

On the premise of guaranteeing sample proportion with 2:1 in different color grade, 50 samples were drew randomly in all 75 samples as the calibration set and the rest samples were drew as the validation set. Then the first 3 PCs were calculated from calibration set and MLR model was set up. The model could be expressed as equation (1), where Y is the predict grade.

$$Y = -0.39\mathrm{PC1} + 0.01\mathrm{PC2} + 0.19\mathrm{PC3} + 2.63\,. \tag{1}$$

Figure 4 shows the calibration results of MLR model with $R^2 = 0.912$ (R^2 being the determinate coefficient of MLR model) and standard deviation of calibration set is 0.307.

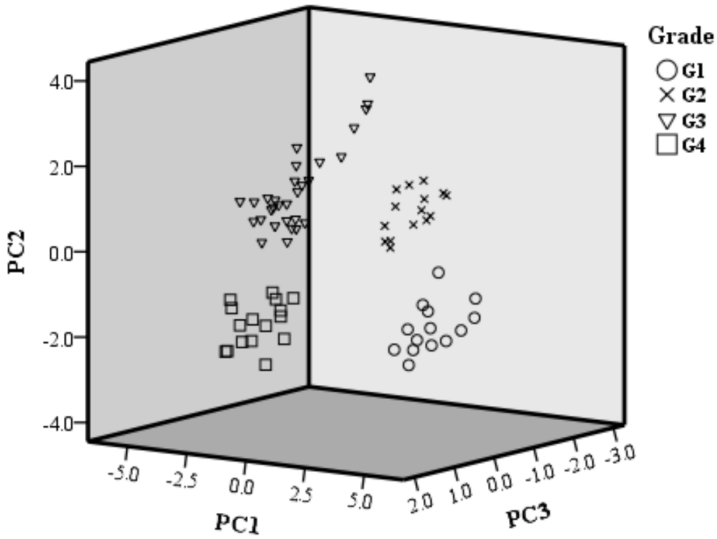

Fig. 3. Foie gras color score plot of the first 3 PCs

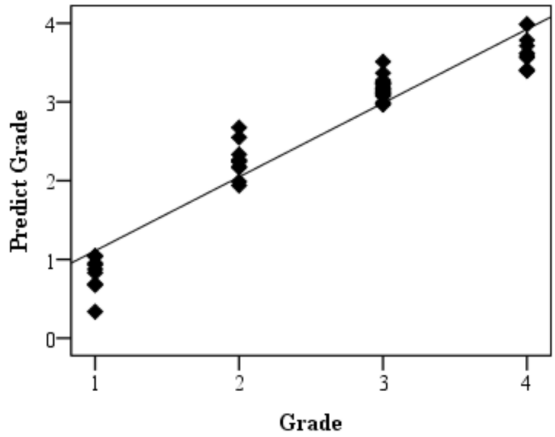

Fig. 4. Calibration results of MLR model

Figure 5 shows the validation results of MLR model with $R^2 = 0.935$ and standard deviation of validation set is 0.271. Similar predict results in two set indicated that the MLR model of color grade has some stability.

Foie gras color grade was calculated using MLR model in calibration set and validation set. The calculated results were rounded to express the estimated color grade using MLR model. Table 3 and Table 4 show the estimated results in calibration set and validation set, respectively.

As shown in Table 3, two G2 samples were wrongly estimated to 3, one G3

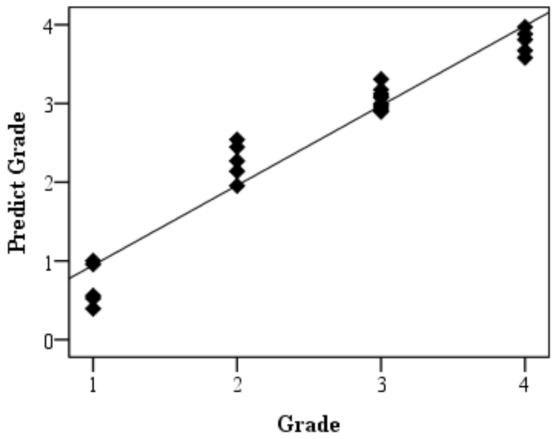

Fig. 5. Validation results of MLR model

sample was wrongly estimated to 4, two G4 samples were wrongly estimated to 3. The accuracy in calibration set was 90 %. As shown in Table 4, one G2 samples were wrongly estimated to 3 and the accuracy in validation set was 96 %. From the above, six samples of all 75 samples were wrongly estimated and total accuracy of MLR model was 92 %. Results showed that MLR model has high accuracy and stability. There were some error in MLR model, as adjacent color grade had similar color features which lead to wrong estimation.

Table 3. Estimated results in calibration set using MLR model

Grade	N	Estimated grade				Accuracy (%)
		1	2	3	4	
G1	9	9	0	0	0	100
G2	10	0	8	2	0	80
G3	20	0	0	19	1	95
G4	11	0	0	2	9	82
Total	50	9	8	23	10	90

Table 4. Estimated results in validation set using MLR model

Grade	N	Estimated grade				Accuracy (%)
		1	2	3	4	
G1	5	5	0	0	0	100
G2	5	0	4	1	0	80
G3	10	0	0	10	0	100
G4	5	0	0	0	5	100
Total	25	5	4	11	5	96

3.4. CDA model of color grade

Three canonical discriminate functions ($F1$, $F2$, $F3$) were calculated from the first 3 PCs in validation set using canonical discriminate analysis. The variance contribution rates of each function were shown in Table 5. As shown in Table 5, the eigenvalues of first 2 functions ($F1$, $F2$) with cumulative variance contribution rate of 97.18 % were chosen to replace the first 3 PCs. The transformation relation was CDA model of color grade which could be expressed as equation (2)

$$\begin{cases} F1 = -2.72\mathrm{PC1} + 1.33\mathrm{PC2} + 1.00\mathrm{PC3} - 0.23, \\ F2 = 0.50\mathrm{PC1} + 1.51\mathrm{PC2} + 1.18\mathrm{PC3} - 0.03. \end{cases} \tag{2}$$

Table 5. Variance contribution rate of each canonical discriminant function

Function	Eigenvalue	Variance cntribution rate (%)	Cumulative variance contribution rate (%)
$F1$	35.82	74.95	74.95
$F2$	10.64	22.23	97.18
$F3$	1.36	2.82	100.00

According to CDA model, data points of $F1$ and $F2$ in validation set are plotted in Fig. 6. As shown in Fig. 6, data points of different color grade are distributed around their mass center. The G1 mass center was (-11.29, 0.38), the G2 mass center was (-1.86, -1.16), the G3 mass center was (3.78, 3.16) and G4 mass center was (4.04, -5.00). Data points of different color grade around 4 mass centers have no overlap.

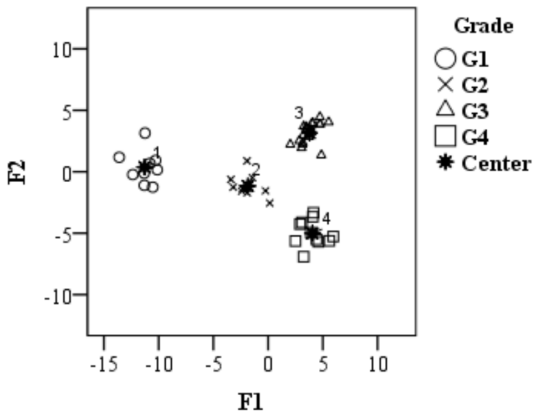

Fig. 6. Foie gras color score plot of $F1$ and $F2$ in validation set

To validate CDA model effect, data points ($F1$, $F2$) were classified according to minimum Euclidean distance from the mass centers. Table 6 shows the estimated results in validation set. As shown in Table 6, samples of 4 color grade were classified correctly and the accuracy of CDA model was 100 %. To further validate effectiveness of CDA model, data points of $F1$ and $F2$ in calibration set were plotted in Fig. 7. As shown in Fig. 7, the distribution is similar to Fig. 6. Table 7 shows the estimated results in calibration set. As shown in Table 7, samples of 4 color grades are classified correctly and the accuracy of CDA model is 100 %.

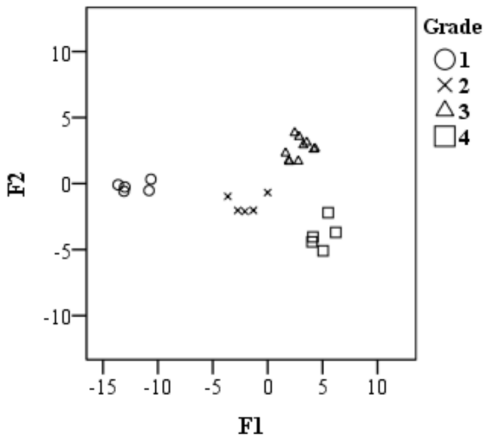

Fig. 7. Foie gras color score plot of $F1$ and $F2$ in calibration set

Table 6. Estimated results of foie gras color grade in validation set

Grade	N	Estimated grade				Accuracy (%)
		1	2	3	4	
G1	9	9	0	0	0	100
G2	10	0	10	0	0	100
G3	20	0	0	20	0	100
G4	11	0	0	0	11	100
Total	50	9	10	20	11	100

Table 7. Estimated results of foie gras color grade in calibration set

Grade	N	Estimated grade				Accuracy (%)
		1	2	3	4	
G1	5	5	0	0	0	100
G2	5	0	5	0	0	100
G3	10	0	0	10	0	100
G4	5	0	0	0	5	100
Total	25	5	5	10	5	100

4. Conclusion

In this paper, the automatic grading of foie gras color was studied by combining machine vision and statistic recognition. Conclusions were obtained:

(1) The MLR model of color grade had high accuracy and stability with total accuracy of 92 %. The model in validation set and calibration set had similar R2 and standard deviation.

(2) The accuracy of CDA model with accuracy of 100 % was higher than that of MLR model. The data points of 4 color grades in validation set and calibration set had similar distribution. Above all, on-line color grading system of foie gras could be developed using two models in order to replace manual grading in processing workshop. Furthermore, as sample number limited the accuracy and stability of the model, enlarged sample and repeated experiment were needed to make the color grading model more accurate and stable.

References

[1] B. Pang, X. Sun, C. W. Ye, K. J. Chen: *Grading of beef marbling based on image processing and support vector machine.* Computer Modelling and New Technologies *17* (2013), No. 3, 87–92.

[2] X. Sun, J. Young, J. H. Liu, L. Bachmeier, R. M. Somers, K. J. Chen, D. Newman: *Prediction of pork color attributes using computer vision system.* Meat Science *113* (2016), 62–64.

[3] Y. Zhang, W. Wang, H. Zhang, J. Zhang: *Meat sensory color grade: Mathematical simulation and its application in quality analysis of chilled pork.* Journal of Food Processing and Preservation *38* (2014), No. 4, 1957–1964.

[4] H. Chen, Q. Xia, T. Zuo: *Determination of shiitake mushroom grading based on machine vision.* Transactions of the Chinese Society for Agricultural Machinery *45* (2014), No. 1, 281–287.

[5] H. Li, H. Sun, M. Li: *Identification of cabbage ball shape based on machine vision.* Transactions of the Chinese Society for Agricultural Machinery *46* (2015), No. S1, 141–146.

[6] J. Wang, X. Cui, D. Xu, S. Zhao, H. Liu, S. Wang, J. Chen: *Plant image analysis machine vision system in greenhouse.* CCTA International Conference on Computer and Computing Technologies in Agriculture VIII, 16–19 September 2014, Beijing, China, Springer Nature, Book series (IFIPAICT) *452* (2014), No.662–690.

[7] B. Pang, X. Sun, X. Sun, K. Chen: *A fast beef marbling segmentation algorithm based on image resampling.* TELKOMNIKA Indonesian Journal of Electrical Engineering *12* (2014), No. 5, 3894–3901.

[8] B. Zhang, W. Huang, L. Gong, J. Li, C. Zhao, C. Liu, D. Huang: *Computer vision detection of defective apples using automatic lightness correction and weighted RVM classifier.* Journal of Food Engineering *146* (2015), 143–151.

[9] L. S. LeMasurier, J. F. Panozzo, C. K. Walker: *A digital image analysis method for assessment of lentil size traits.* Journal of Food Engineering *128* (2014), 72–78.

Received September 19, 2017

Acta Technica *62* No. 2B/2017, 465–476

The optimization design of Off-Highway machinery radiator based on genetic algorithm and ε-NTU[1]

Liu Yang[2], Qin Sicheng[2]

Abstract. The advantages and disadvantages of the construction machinery cooling system are closely related to the machine performance. However, it is difficult to design a high efficient radiator to manage the high heat emittance of the high-powered diesel engine. In this study, we put forward an mechanical optimization design that uses the effectiveness-number of transfer units (ε-NTU) method as the mathematical mode of the radiator performances estimation to build a radiator parameters design model, which puts the heat transfer rate and pressure drop of airside as the objective function, and also solves the alternative advantage solution set through genetic annealing algorithms (GAA). Moreover, designers could achieve the expected performance indicator or optimize the original radiators from revising radiator geometrical parameters at the beginning of the design through verifying the model effectiveness by comparing the experimental data.

Key words. Wavy fin, heat transfer, numerical simulation, genetic annealing algorithms, Off-Highway machinery.

1. Introduction

The compact heat exchanger has a broad applications in many fields due to its efficient heat transfer rate and compact volume. The research and development of current radiators are inspired by Kays et al. [1], who firstly invented various kinds of radiators in 1984, and they also obtained the original correlations between the heat transfer and resistant features of the general fins by experiences [2]. Between 2000 to 2010, Wang et al. [3] matched the laboratory correlations of the variations between the Colburn factor and fanning factor in different Reynolds numbers. Based on the previous study, in 2007 Dong [4] utilized the wind tunnel test bench to test 67 different structure parameters of five general fins and matched the laboratory correlations between their heat transfer and resistant features, which highly increased

[1]This work was supported by the National Key Technology Research and Development Program of the Ministry of Science and Technology of China (Grant No. 2013BAF07B04)

[2]School of Mechanical Science and Engineering, Jilin University, Changchun 130022, China

the fitting precision; and the deviations of correlations are only 12 %. Caputo et al. [5] applied the simulated algorithm to the solutions of industrial radiator optimized problems. Copiello et al. [6] studied the influences of cross-cut flow control on fluid resistance and heat transfer rate of radiators by improving genetic algorithm. Mostly, the traditional radiators were designed by using the method of logarithm mean temperature difference (LMTD), which used the specified parameter (inlet and outlet temperatures of hot and cold fluids) to calculate the heat transfer rate and the correction factor to decrease deviations. This method is less computed, which can fast estimate heat transfer rate, but lower accuracy. In this study, we directly applied the fins' parameters into the calculation of heat transfer rate and pressure drop by the laboratory correlations, which can accurate estimation of heat transfer rate and pressure loss of the radiator. And also we could change the appropriate heat transfer rate and pressure drop by regulating geometrical parameters of fin.

2. Mathematical model of radiator performance estimation

The design of radiators is for heat transfer rate and pressure drop of airside. This study uses the ε-NTU as the theoretical basis, the wheel loader radiator from LONKING as the vector to construct the mathematical model of radiator performance estimation. This radiator is the wavy finned tube heat exchanger. Figure 1, top and bottom parts, show its structure and geometric parameters of fin and Table 1 shows the structural parameters of the radiator.

Table 1. Structural parameters of the radiator

Parameter	Data	Parameter	Data
Core size	880 mm×858 mm×92 mm	Fin thickness δ	0.06 mm
Cooling area A	44 m^2	Wavy angle β	150 rad
Fin height F_{h}	1.5 mm	Fin space P_{f}	3.3 mm
Wavy pitch λ_{w}	12 mm	Fin number	262

Frontal area, hydraulic diameter and Reynolds number could be obtained by calculating the geometrical parameter of the wavy fins, which do not need to be mentioned more. For other kinds of fins, the design parameter is got only by changing the specified geometrical parameter. And also, the specified parameter could be obtained by operating the fin unit simulation with CFD program when there are no experimental data. In addition, the NTU of radiator could be got by computing the fin and fin facial efficiency resulted from the formula (1). The efficiency of radiator is calculated by formula (2) and Colburn factor and friction factor are calculated according to the method presented in [1]. At last, formulae (4) and (5) provide the pressure drop and heat transfer rate [7]

$$R = \frac{(q_{\mathrm{m}} C_{\mathrm{p}})_{\min}}{(q_{\mathrm{m}} C_{\mathrm{p}})_{\max}}\,, \tag{1}$$

$$\varepsilon = 1 - \exp\left\{\frac{\mathrm{NTU}^{0.22}}{R}\left[\exp\left(-R\cdot\mathrm{NTU}^{0.78}\right)-1\right]\right\} \tag{2}$$

$$\begin{cases} C_{\min} = \min\left[(\dot{m}\cdot C_{\mathrm{p}})_{\mathrm{hot}}, (\dot{m}\cdot C_{\mathrm{p}})_{\mathrm{cold}}\right], \\ C_{\max} = \max\left[(\dot{m}\cdot C_{\mathrm{p}})_{\mathrm{hot}}, (\dot{m}\cdot C_{\mathrm{p}})_{\mathrm{cold}}\right]. \end{cases} \tag{3}$$

Pressure drop:

$$\Delta P = \frac{\dot{m}}{2A_{\mathrm{c}}\rho}\left[\left(K_{\mathrm{c}}+1-\sigma^2\right)-\left(1-\sigma^2-K_{\mathrm{e}}\right)\frac{\rho_{\mathrm{in}}}{\rho_{\mathrm{out}}}+f\frac{4L}{D_{\mathrm{e}}}\rho_{\mathrm{in}}\left(\frac{1}{\rho}\right)_{\mathrm{m}}\right]. \tag{4}$$

Heat transfer rate:

$$h = j\dot{m}C_{\mathrm{p}}\left(A_{\mathrm{c}}\,\mathrm{Pr}^{\frac{2}{3}}\right)^{-1}, \tag{5}$$

$$Q = \varepsilon\cdot C_{\min}\left(T_{\mathrm{hotin}}-T_{\mathrm{coldin}}\right). \tag{6}$$

In the above equations (1)–(6), C_{p} is the specific heat of the coolant, Q denotes the heat transfer rate, ε represents the effectiveness of the heat exchanger, $\dot{m}$ stands for the mass flow, NTU is the number of the transfer units, T_{m} is log mean temperature difference, K_{c} is the entrance loss coefficient, K_{e} is the exit loss coefficient, δ is the minimum flow to face area ratio, A_{c} is the minimum cross-sectional flow area, Pr is the Prandtl number, D_{e} is the hydraulic diameter and A is the heat transfer surface area.

This predicted mathematical model is commonly used to some extent. Besides the tube-fin type shown in this study, it also can be used in plate-fin radiator and ribbon-tubular radiator, which are general in Off-Highway machinery. The only way that needs to be done is changing the specified formula of geometrical parameter and empirical formula such as the heat transfer surface area, colburn factor and friction factor [8].

3. Designed model of optimized radiator parameter

3.1. Design parameter and objective function

The objective to optimize the radiator design is to adjust the heat transfer rate and pressure drop to the range of designers' request by regulating the main structural parameter of radiators. This procedure includes the selection of designed variable, the extraction of constraint conditions, the construction of design objective and the choice of algorithm. This study gets rid of some variables that slightly affect the objective function and choose 8 parameters of radiators as the independent variables [9]. The design variables should be constrained subjected to the limited volume of production technology and power cabin. The range of design variables is shown in Table 2. The objective function 1 is heat transfer rate as shown in (5), and the objective function 4 is pressure drop as shown in equation (10), the volume of new radiator, which is less than original radiator, as the constraint conditions.

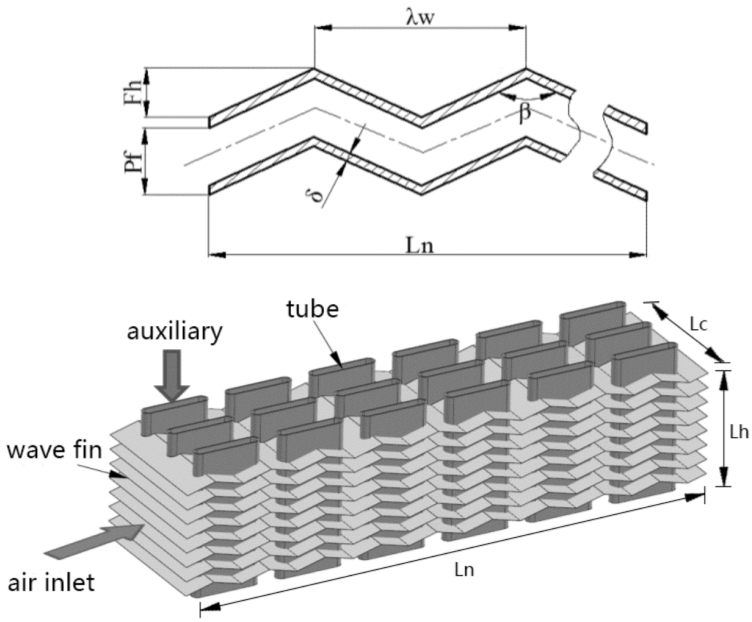

Fig. 1. Wavy fin: top–geometric parameter, bottom–structure of the fin and tube radiator

The friction factor shown in (8) and Colburn factor shown in (7) make use of the empirical formula from the wavy fin unit wind tunnel test data and the way of the next section to get the heat transfer coefficient figured in (9) and pressure drop correlation displayed in equation (10). The correction factors f_{fix1} and f_{fix2} are obtained based on the data from different fins in different radiators. This paper is in the confirmed process. So the correction factor f_{fix1} and f_{fix2} are valued 1.

Table 2. The value range of design parameter

Design parameter	Range	Design parameter	Range
L_{n}	800∼880 mm	β	130∼170 rad
L_{h}	800∼858 mm	δ	0.05∼0.07 mm
L_{c}	80∼92 mm	P_{f}	3∼3.6 mm
λ_{w}	10∼14 mm	F_{h}	9∼13 mm

$$j = \left(\frac{P_{\text{f}}}{2F_{\text{h}}}\right)^{0.1284} \cdot \left(\frac{P_{\text{f}}}{4F_{\text{h}} + \lambda_{\text{w}}}\right)^{-0.153} \cdot \left(\frac{L_{\text{n}}}{\lambda_{\text{w}}}\right)^{-0.326} \cdot 0.0836\text{Re}^{-0.2309}, \tag{7}$$

$$f = \left(\frac{P_{\text{f}}}{2F_{\text{h}}}\right)^{0.3703} \cdot \left(\frac{P_{\text{f}}}{4F_{\text{h}} + \lambda_{\text{w}}}\right)^{-0.25} \cdot \left(\frac{L_{\text{n}}}{\lambda_{\text{w}}}\right)^{-0.1152} \cdot 1.16\text{Re}^{-0.309}, \tag{8}$$

$$h = 100\eta^{-0.283} \cdot 9.2394 \cdot C_{\mathrm{p}}^{0.33} \cdot \lambda^{0.67} \cdot (\rho \cdot V)^{0.731} \cdot \sigma \cdot D_{\mathrm{e}} \cdot P_{\mathrm{f}} \cdot f_{\mathrm{fix1}}\,, \tag{9}$$

$$\Delta p = \rho^{-1} \cdot \sigma_{\mathrm{d}}^{-3} \cdot 1.07673 \cdot \left(\frac{A}{A_{\mathrm{c}}}\right)^{0.468} \cdot (\rho \cdot V)^{1.68} \cdot \left(\frac{\eta}{D_{\mathrm{e}}}\right)^{0.32} \cdot f_{\mathrm{fix2}}\,. \tag{10}$$

In the above equations, f is the friction factor, h is the heat transfer coefficient, j is the Colburn factor, Δp represents the pressure loss, ρ denotes the density of air, β is the wave angle, λ stands for the heat conductivity of air, λ_{w} is the wave pitch, σ denotes the fin thickness, η represents the dynamic viscosity of air, f_{fix1} and f_{fix2} are correction factors, F_{h} is the fin height, K denotes the heat conductivity of the radiator, P_{f} stands for the fin pitch, Re is the Reynolds number and $sigma_{\mathrm{d}}$ is the porosity of airside.

3.2. The selection of algorithm

Engineering problems always comes down to the complex multi-objective optimization problems. These functions possess the features of nonlinear, multivariable and hard redescender. Genetic algorithm (GA), as an easy computed and high efficient method, is widely used in engineering problems. However, it is limited by premature convergence and lower partial searching ability, so it cannot usually get the most optimized solution in global situation. The heuristic algorithms, such as the steepest descent, hill-climbing, simulated annealing (SA) and the list of optimization method have the strong global searching capability, and also some heuristic algorithms, which contain some information that are related to the problems, are highly effective. As hypothesized, merging the basic idea of SA in the search process of GA to construct a hybrid genetic algorithm, which contains both advantage, so as to improve efficiency of the GA operation and the quality of solution, which could help to adapt to the complex engineering problems in mechanical optimized design. GAA, used in this study, overcomes the traditional genetic algorithms and improves the search efficiency as well. The introduction of elitist preservation (the individual, which has highest fitness, will directly copy to the next generation instead of the recombination mutation) and disaster-modification (when it cannot get the optimized state after algorithms' several iterations, using probability 1 to mutate and interlace operation, at the same time, keep the optimal individuals). Do not recover to the normal cycle until a better individual is produced. The first one-the phrase has been modified to "If there is no better solution in the iteration step, the convergence of the calculation result is considered. The algorithm in this paper reduces the possibility that the algorithm falls into the local optimal solution, and improves the efficiency of calculation and the quality of solution."

The brief steps of GAA in this study are:

1) Select the original populations randomly, and compute the original fitness.

2) Repeat step 3) and 7), until satisfy the convergent roles.

3) Stochastic tournament and select the optimal father generation, then reproduce.

4) Simple mutation to the selected father generation and accept new individual by the method of probability.

5) Arithmetic crossover to the father generation and mutated sub-generation.

6) Simulate annealing operation to the father generation and produced sub-generation, then cool them down based on index.

7) Elitist preservation and judge if it need do disaster-modification. Output the global optimal results. ”

4. Experimental comparative analysis

4.1. Optimal solution analysis

This study describes the optimized problem as the style of equation 10 with the objective functions and constraint conditions that are derived from previous section, and the simulation conditions are shown in Tables 3. Set the genetic algorithm as follow: population size 100, crossover fraction 0.7, migration fraction 0.01, function tolerance 1e-6, and max generation 100. The result are shown in Fig. 2, top and bottom parts. Using NSGA-II algorithm (as shown in Figure 3) to verify the validity of the Pareto optimal solution. It can be seen that the regions of the optimal solutions are matched. However, the rate of convergence, equilibrium of distribution and the capacity of global searching of GAA are better than NGSA-II.

$$\begin{cases} \min F(x) = [f_1(x), f_2(x)], \\ f_1(x) = -Q, \\ f_2(x) = \Delta p, \\ g(x) = \Delta V = V_1 - V_2 \geq 0. \end{cases} \tag{11}$$

Here, $g(x)$ is the volume change, while $f_1(x)$ and $f_2(x)$ are the objective functions.

Table 3. Simulation boundary conditions

Parameter	Data	Parameter	Data
Ambient temperature	30 °C	Coolant flow rate	120 l/min
Airside inlet	30 °C	Coolant inlet temperature	100 °C
Ambient pressure	101325 Pa	Velocity of the airflow	12 m/s

Multi-objective optimization function does not exist a set of solutions for all constraints, replaced by an optimal solution set. The contradiction among many objective functions in real engineering problems is always met. Designers should make their choices and select the solutions that are fit to the whole designs through their own request. In this study, the design goal of radiator is to pursue the high heat transfer rate and lower pressure drop, which are obviously contradictory. However, some compromised solutions with the optimized algorithm can be obtained. Table 4. shows the result that comparing three typical preponderant solutions of GAA and the experiment data of original radiator from wind tunnel test: Type solution 1 heat

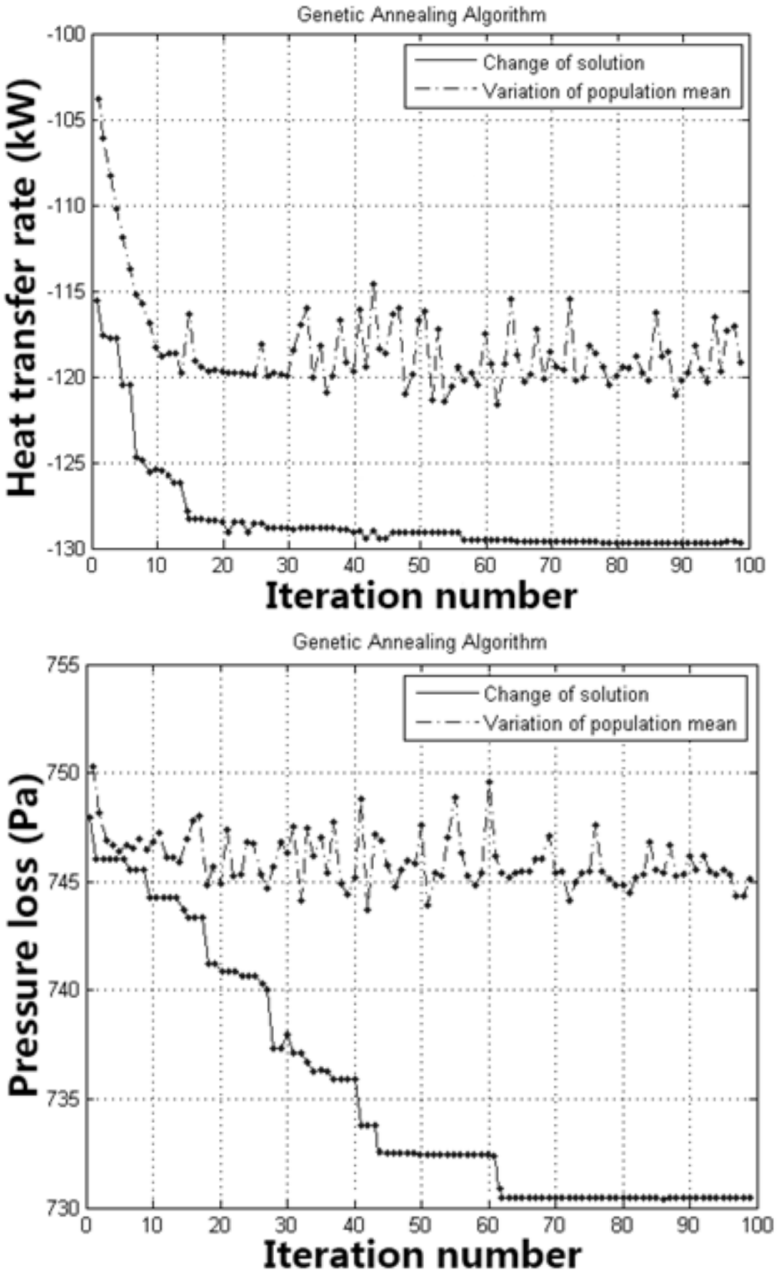

Fig. 2. Results: top–heat transfer rate of GAA, bottom–pressure drop of GAA

transfer rate increases slightly and pressure drop decreases slightly. Type solution 2 heat transfer rate and pressure drop grows significantly. Type solution 3 pressure

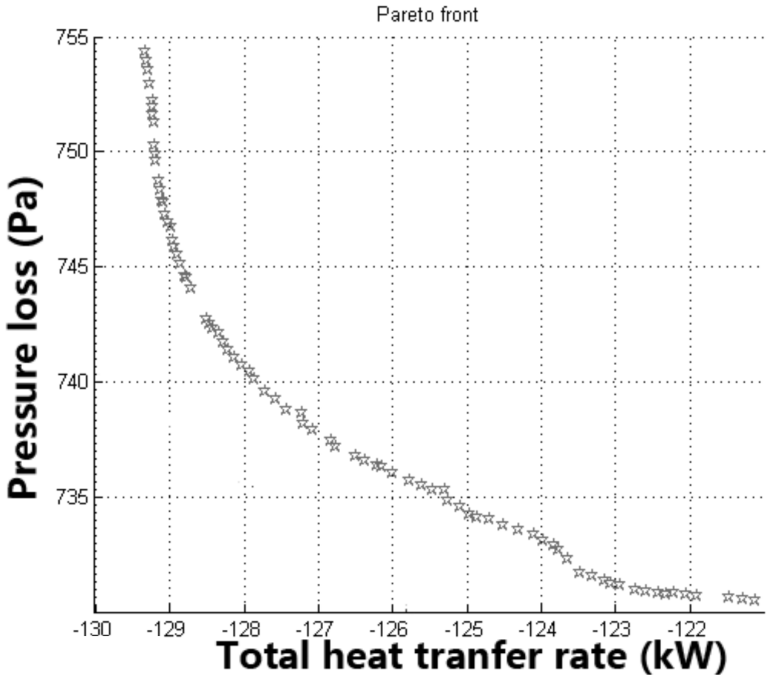

Fig. 3. Optimization results of NGSA-II

drop falls highly and the loss of heat transfer rate is higher as well. According to the actual needs, designer can choose the solution with small pressure loss or large heat transfer rate.

Table 4. Comparison of calculation results

Parameter	Experiment data	Solution 1	Solution 2	Solution 3
Q (kW)	124.55	126.65	129.74	121.41
ΔP (Pa)	140.11	137.77	148.81	131.72
L_{n} (mm)	880	872.5	870.1	869.2
L_{h}	858	849.9	846.9	846.1
L_{c}	92	91.1	91.1	90.4
ΔV (%)	N/A	−2.75	−3.36	−4.29
λ_{w} (mm)	12	11.4	11.6	11.1
β (rad)	150	135.5	153.2	147.2
δ (mm)	0.06	0.05	0.05	0.05
P_{f} (mm)	3.3	3.3	3.2	3.2
F_{h} (mm)	10	11.9	12.1	12

4.2. Analysis of radiator performance

Radiator bench test was carried out according to Fig. 4.

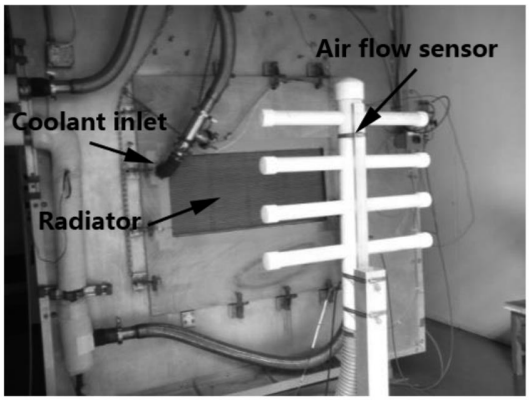

Fig. 4. Radiator bench test

Establishing the radiator model with UG, we did the stimulation by putting the viscous resistance coefficients and inertial resistance coefficients obtained from the results of fins parameters in the three groups (as shown in Table 4) into the porous media model. As shown in Fig. 5, through bench test the pressure drop curves and heat transfer curves at different inlet velocities are compared with the original radiator.

The heat transfer rate and pressure drop increase with the increase of the inlet velocity; the growth rate of pressure drop increases with the increase of inlet velocity, which is consistent with formula (4). The growing rate of heat transfer rate decreases gradually with the increasing of inlet speed. To start from the Macro-view, the increasing speed of inlet flow led to the decreasing of heat exchange time. Although the amount of air intake is increasing, the heat exchange time is reduced which causes the loss of the heat exchange efficiency. Theoretically, the heat transfer rate of radiator is mainly related to the effectiveness of radiator and $C_{\min}$. In terms of the experimental data, the effectiveness of radiator is in a convex function relationship with the NTU. The value of NTU and effectiveness of radiator varies inversely with the inlet velocity. According to the principle of heat transfer, while the inlet velocity increased to a certain size $C_{\min}$ and efficiency will be changed to a certain value, continuously increasing the inlet velocity will no longer increase the heat transfer rate.

In order to verify the accuracy of the simulation, a new radiator is made according to the fin parameters of the typical solution 1 and the bench test is carried out. The bench test experimental results are compared with the simulation results as shown in Table 5. We can figure out that the new radiator made by typical solution1 basically matches the simulation result, and the average error is about 6 %, which confirms the accuracy of the GAA calculation model.

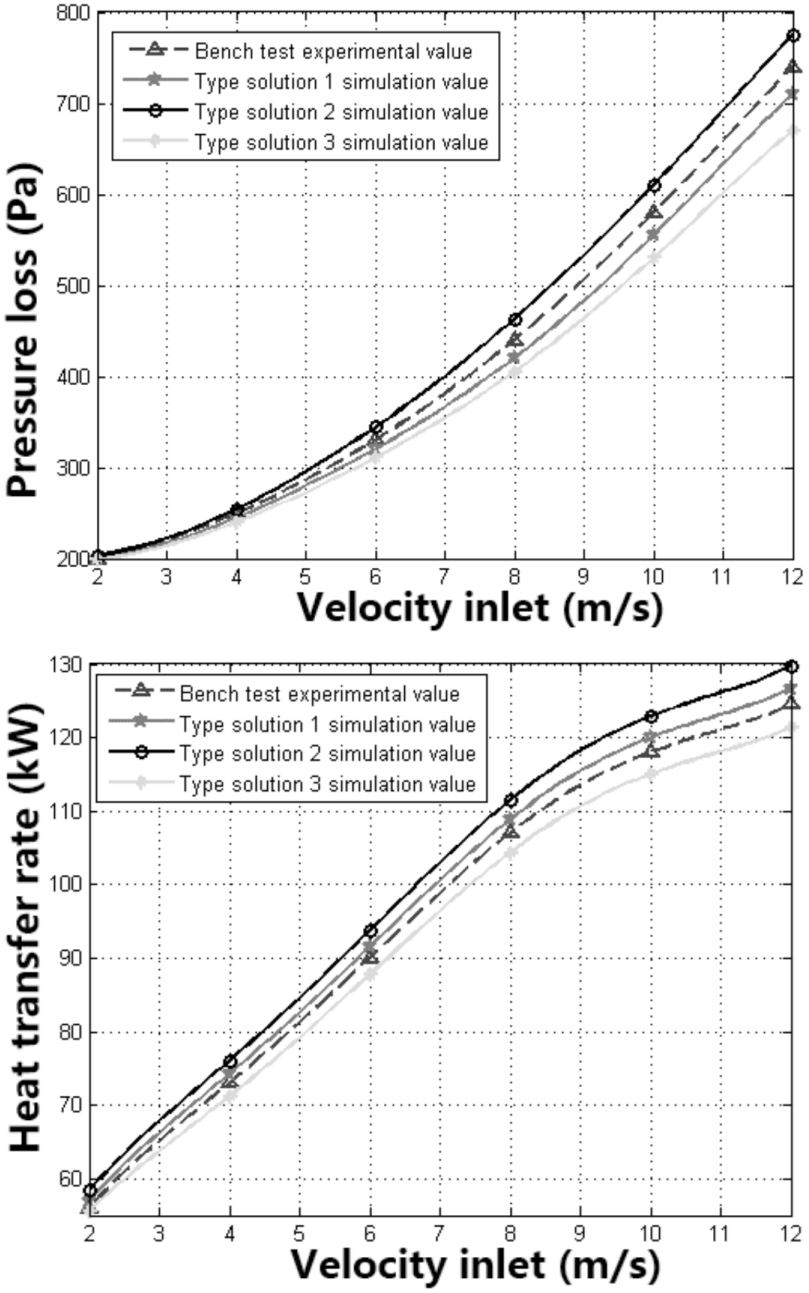

Fig. 5. Important characteristics of radiator at different inlet velocity: top-pressure loss, bottom–heat transfer rate

Table 5. Comparison of CFD simulation and experimental results

Inlet velocity	6 m/s	8 m/s	10 m/s	12 m/s
Pressure loss of type solution 1	320 Pa	420 Pa	555 Pa	710 Pa
Pressure loss of the new radiator	322 Pa	422 Pa	559 Pa	714 Pa
Heat transfer rate of type solution 1	85.43 kW	102.72 kW	116.96 kW	126.65 kW
Heat transfer rate of the new radiator	85.26 kW	102.52 kW	116.73 kW	126.42 kW

5. Conclusion

Using the ε-NTU as the theoretical basis, and the engine coolant radiator of wheel loader (wavy fin-and-tube radiator) as the research object, the mathematical model of radiator performance estimation was constructed. This model is powerful generalization, and it could be adapted to Plate-fin radiator and can be used for plate fin or Ribbon-tubular radiator when several geometrical parameters and empirical formula changed. It can also focus on the performance study in different fins of the same kind of radiators. When MATLAB to routinize mathematical model of radiator performance estimation with the mix genetic algorithm was used, the introduction of annealing algorithm complements the disadvantages of genetic algorithm in searching process. Analyzing one group of the dominant results, we find that the volume could decrease 2.7 %, and the heat transfer rate grows 1.7 %, when the pressure drop falls 1.7 % by modifying the design of the original radiator. In addition, the optimal dependability is verified by Wind tunnel test of the new radiator. The heat transfer rate and pressure drop of the radiator are greatly influenced by the fin parameters. They are increasing with the growth of inlet velocity of cold side. The increased heat transfer rate stops when the inlet velocity reaches to a certain extent. In this paper, with ε-NTU theory as the basis for the establishment of the radiator performance prediction model, combining with the genetic algorithm to optimize the size of core and fin parameters, and the optimal solution is performed by CFD simulation and wind tunnel tests to verify the effectiveness of the calculation model. This paper provides a new idea for the design and optimization of the radiator, which is conducive to shorten the development cycle and reduce the design cost.

References

[1] R. J. Moffat, W. M. Kays: *A review of turbulent-boundary-layer heat transfer research at stanford, 1958-1983.* Advances in Heat Transfer *16* (1984), 241–365.

[2] Y. Yang, Y. Li, B. Si, J. Zheng: *Performance evaluation of heat transfer enhancement in plate-fin heat exchangers with offset strip fins.* Physics Procedia *67* (2015), 543–550.

[3] B. Lotfi, B. Sundén, Q. Wang: *An investigation of the thermo-hydraulic performance of the smooth wavy fin-and-elliptical tube heat exchangers utilizing new type vortex generators.* Applied Energy *162* (2016), 1282–1302.

[4] J. Q. Dong, L. Su, Q. Chen, W. Xu: *Experimental study on thermal–hydraulic performance of a wavy fin-and-flat tube aluminum heat exchanger.* Applied Thermal Engineering *51* (2013), Nos. 1–2, 32–39.

[5] S. K. Lahiri, N. Khalfe: *Improve shell and tube heat exchangers design by hybrid differential evolution and ant colony optimization technique.* Asia-Pacific Journal of Chemical Engineering *9* (2014), No. TOC3, 431–448.

[6] L. Daróczy, G. Janiga, D. Thévenin: *Systematic analysis of the heat exchanger arrangement problem using multi-objective genetic optimization.* Energy *65* (2014), 364–373.

[7] A. A. Bhuiyan, A. K. S. M. Islam: *Thermal and hydraulic performance of finned-tube heat exchangers under different flow ranges: A review on modeling and experiment.* International Journal of Heat and Mass Transfer *101* (2016), 38–59.

[8] P.,Karthik, S. I. L. Ali Khan, K. Narasingamurthi, V. Ramalingam: *Experimental and numerical investigation of a louvered fin and elliptical tube compact heat exchanger.* Thermal Science *19* (2015), No. 2, 679–692.

[9] T. Kuvannarat, C. C. Wang, S. Wongwises: *Effect of fin thickness on the air-side performance of wavy fin-and-tube heat exchangers under dehumidifying conditions.* International Journal of Heat and Mass Transfer *49* (2006), Nos. 15–16, 2587–2596.

Received September 19, 2017

Acta Technica *62* No. 2B/2017, 477–486

Model construction and application of machinery fault diagnosis of ships based on technology of resonant demodulation[1]

Lin Chen[2], Shilai Wang[2,5], Huaming Wang[3,4], Qiaorui Wu[3]

Abstract. Resonance demodulation technology mainly adopts changing trends and the characteristics of frequency spectrum to run the equipment fault diagnosis. Resonance demodulation technology was applied to the automatic diagnosis of rolling bearings' faults has advantages of easy operation, high reliability, especially when the rolling bearing of multiple components exist random failure, analysis method is difficult to diagnose, and using the method of resonant demodulation can make accurate on such complex fault diagnosis, and the resonance demodulation technology will has wide application in ships due to its advantages of accuracy, speediness and lower cost. Firstly, this paper analyze the technology of resonant demodulation diagnosis principle. In addition, its application in vessels is discussed, specific application of the ship rolling bearing is described in detail. The application of resonant demodulation in ship fault diagnosis can enhance the overall mechanical equipment diagnosis accuracy, maintain the normal operation of equipment and reduce the economic losses of the enterprise.

Key words. Resonant demodulation, fault diagnosis, ship rolling bearing.

[1]This work is supported by the National Natural Science Foundation of China (No. 51109186), Zhejiang Provincial Natural Science Foundation (Nos: LY16E090004, LY17E090002, LQ17E090003), the doctoral scientific research foundation of Zhejiang Ocean University project, and the Open Foundation from Key Laboratory of Offshore Engineering Technology of Zhejiang.

[2]Donghai Science and Technology College, Zhejiang Ocean University, Zhoushan, 316000, China

[3]School of Naval Architecture and Mechanical-Electrical Engineering, Zhejiang Ocean University, Zhoushan, 316022, China

[4]Key Laboratory of Offshore Engineering Technology of Zhejiang, Zhoushan 316022, China

[5]Corresponding author

1. Introduction

The production of ship is very expensive and the procedure is complex. Due to extreme complexity its construction is prone to a variety of mechanical failures. The failure of the machinery [1], for example, will inevitably affect the operation of the entire ship system, and even affect the safety of the ship system [2]. Therefore, it is necessary to use modern detection technology for fault detection and prediction. There are two kinds of fault detection methods for ship mechanical system, one of them being the condition monitoring method, and the other is fault diagnosis method. The diagnosis methods of ships supercharger, gear box, motor, pump and other mechanical failures have been developed from the past "see, hear, smell, touch" [2], a simple test based on processing of suitable signals. Along with development of technology, vibration monitoring is one of the main methods. The traditional vibration signal analysis is mainly based on the fault characteristic frequency spectrum that should indicate whether a fault occurred, but in some cases, relevant information does not necessarily mean fault, but also some uncertainty. With the last development of technology, particularly technology of resonant demodulation [3—4], this becomes a line of sight of people.

Technology of resonant demodulation [5] is to detect the resonant waveform envelope detection (that is, the demodulation) and low pass filter of high frequency (more than dozens of times the impact frequency) aroused by low frequency, and obtain a relative low frequency amplifier and the broadening of the resonance demodulation impact wave, also calls the envelope. Through this resonance demodulation wave amplitude and frequency spectrum analysis, determine the fault type and quantity, so the technology of resonant demodulation is also known as shock pulse technology, envelope detection technology or the early fault detection technology. The technology of resonant demodulation is in accordance with the demodulation theory of wave [6–7], must confirm that whether the faults occur or not. Resonance demodulation technology of impact on the fault have been widely used with the advantages of correspondence, selectivity, amplification, proportionality, broadening, low frequency and multistage[8–9].

2. Resonance demodulation in the application of the ship

2.1. The choice of methods of fault monitoring

The monitoring system has been developed from the first generation of alarm system, the analysis of the second generation system, the third generation of diagnosis system, the latest development of the fourth generation of intelligent system, each generation system has its own superiority and the applicable scope, so the introduction of technology must adhere to the principle of "fit is the best", rather than "the more advanced, the better, the more expensive the better". The gear box, main motor and other key equipment should be in the fourth generation system. For ordinary motor, fan and other non-critical equipment are available to the third generation system. The centralized area of pump equipment, such as main en-

gine, auxiliary machinery and water chiller pump room is propitious to online third generation system. While, zone of noncitizen was used for half online or offline.

2.2. Judgement of characteristic signs

Spectral analysis is to look for the frequency and amplitude and the vibration signal contains a sine wave [10], and then find what kind of trouble they are produced by. The two corresponding namely, find out why, but it is not easy. As with the function of frequency spectrum analysis of vibration of the portable instrument, simple give only spectrum, spectrum varies between equipment, performance feature is different also, only a person with rich spectrum knowledge can understand. In addition, as a diagnosis of gearbox fault, each axis has two bearings, and at all levels of the gear, the acquisition of signals passed through the structural spectrum is all on the line, primary and secondary cannot be distinguished, even overlap, which causing oscillation is very high, the results of spectrum figure difficult to understand. Now the software built-in standard signs of libraries, the input parameters such as gear teeth, bearing type, will list the symptom checklist, such as imbalance, misalignment, loose information. If a theory of feature point warning, it will automatically on the spectrum. If it fits perfectly, the faults can be decided. Even if there is allowance, it will be automatically matching.

2.3. The determination of characteristic symptom standards

The determination of impact pulse spectrum and standard spectrum is different from the traditional spectrum. Now amplitude of characteristic frequency of the system can be acted as trend and set out their standard. The standard is obtained after long time data according to the data, and not directly to national or international standards. Because the latter is to use equipment overall vibration value definition, generally the velocity or displacement. However, the working condition of each device is different, even for the same equipment, such as motor, their horizontal, vertical, axial control standard of each are not identical, and also cannot use the same standards. So the standard combined with the actual data is the most suitable. Of course, the experience of the crew can also be set standards.

3. The establishment of resonance model

Resonance demodulation can be realized by the computer equipped with data collector by numerical algorithms in software implementation, and also can use the hardware circuit implementation. The difference between the two is whether through direct analysis of vibration signal spectrum to realize fault diagnosis.

3.1. The establishment software resonance demodulation model

Although there are many methods for the software to realize the shock signal resonance demodulation, the most commonly used is the Hilbert changes to the original resonant demodulation processing time domain or frequency domain signals. Software resonance demodulation of original signal processing is divided into the following four main steps:

The time domain signal FFT analysis, find the mechanical resonance frequency of the resonator, as the center frequency and frequency band pass filter; The Hilbert transform for signal after filtering; Structure of shock response signal envelope curve; The envelope curve resampling and spectrum analysis.

The Hilbert transform is a key element in software technology of resonant demodulation. Real signal $X(t)$ is defined as the Hilbert transform $\hat{X}(t)$

$$\hat{X}(t) = H\left\{\hat{X}\right\} = \frac{1}{\pi}\int_{-\infty}^{\infty}\frac{X(t)}{t-\pi}\,\mathrm{d}\tau = \frac{X(t)}{/}\pi t\,, \tag{1}$$

where H means the Hilbert transform within the brackets on the signal, the function of the Hilbert transform are $\pi/2$ phase difference with the function itself.

A new analytic function is

$$\bar{Z}_{\mathrm{m}}(t) = X(t) + j\hat{X}(t)\,. \tag{2}$$

Therefore, the signal envelope equation is expressed as

$$Z_{\mathrm{m}}(t) = \sqrt{X^2(t) + \bar{X}^2(t)}\,. \tag{3}$$

Spectral analysis was carried out on the formula (3), and get more order section of the adjustment spectrum characteristics. Figure 1 shows the flow chart of resonance demodulation method by software.

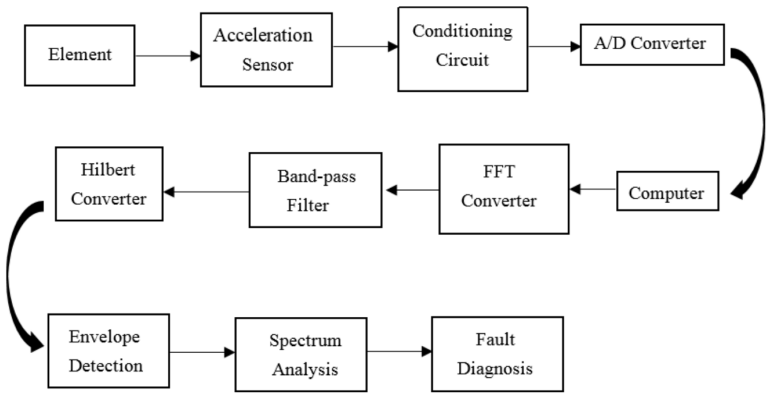

Fig. 1. Flow chart of resonance demodulation method by software

3.2. The establishment hardware resonance demodulation

Hardware technology of resonant demodulation is the application of piezoelectric and strain detection sensor technologies such as bearings, gears and other mechanical operation caused by abnormal collision impact information. Use of the electrical, mechanical, or other hardware resonator (surface acoustic wave, acoustic, etc.). By harmonic resonance response to change weak shock signal into high frequency and resonance wave attenuation oscillation of freedom, thereby gaining a weed out the resonance demodulation of low-frequency vibration interference wave after the demodulation process. Finally, through the demodulated resonance wave amplitude and frequency spectrum analysis to extract the low-frequency impact of information, and determine the fault diagnosis methods of fault detection technology. As a result, the hardware technology of resonant demodulation is not via the analysis of vibration signal spectrum directly to realize the fault diagnosis.

To extract the fault signal of the rolling bearing impact hardware resonance demodulation process, in turn in three main hardware function modules:

Figure 1 shows resonance demodulation transformation process by the analog circuit of hardware. The principle and superiority of fault detection the resonance demodulation can be observed from Fig. 1. Mixed in the vibration fault of shock wave (see Fig. 2a)) time domain pulse width is very narrow. Amplitude spectrum is rich. Using a high Q center frequency resonator for shock wave resonance response (see Fig. 2b)), get one free attenuation of high frequency in intermittent oscillation waveform. Envelope detection after the wave of resonant demodulation (see Fig. 2c)) compared with the original shock waveform, repeat same frequency, but the amplitude is amplification, broadening and time domain. Thus for demodulating resonance demodulation output pulse, compared with the low energy shock pulse, the low frequency spectrum energy is greatly enhanced. Transformation process, the resonator eliminated the interference of conventional vibration so the demodulation output signal is compared with the original signal, can obtain several orders of magnitude higher signal-to-noise ratio, made no fault, no resonance demodulation affected its spectrum of obvious effect. Demodulation signal characteristics, multistage comb spectrum diagram as shown in Fig. 2d).

When impact signal is larger, two kinds of demodulation can effectively extract the fault characteristic. When early fault signal is weak, the latter using resonator resonant amplification effect to the fault, spectrogram fault characteristics significantly, while the former effect is not ideal. But the hardware demodulation some parameters cannot be adjusted, the lack of flexibility, and the hardware equipment, weight, volume is larger, it is not easy to carry.

4. Instance analysis of ship rolling bearing

Take turbocharging system for example, bearing detection is the most important, because bearing high-speed operation, often produce fatigue pitting. The advantages of the monitoring device are high reliability and easy to install the system. At the same time, vibration detection can be carried out, which can detect the vibration of

the equipment and the imbalance between the scaling of the turbine and the carbon adhesion. Figure 3 shows turbocharger bearing status monitoring system.

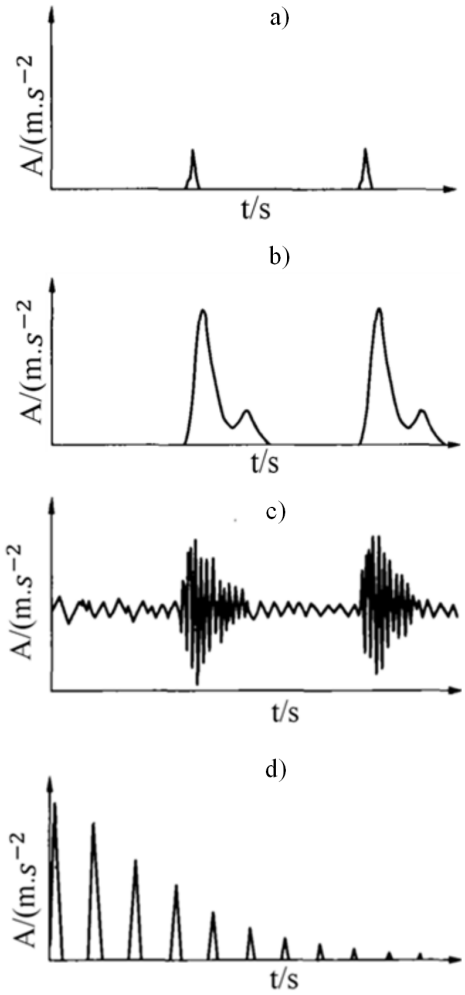

Fig. 2. Signal shift processes using hardware resonance-demodulation technology: a)–shock pulse, b)–shock wave resonance response, c)–wave of resonant demodulation, d)–multistage comb spectrum diagram

The bearings with inner ring, outer ring and rolling body maintain four parts in Marine mechanical system, each each of them having its own characteristic frequency. We use the condition monitoring equipment to judge the type and speed of the bearing, and get the characteristic frequency of the part. Different parts are characterized by different symbols, in dependence of the fault. For example, the parts without fault are characterized by number 0.07, while the parts with failure carry number 0.68. Figure 4 shows that the first node does not have a fault symbol, which indicates the system is normal. The second node has a fault sign, so that the

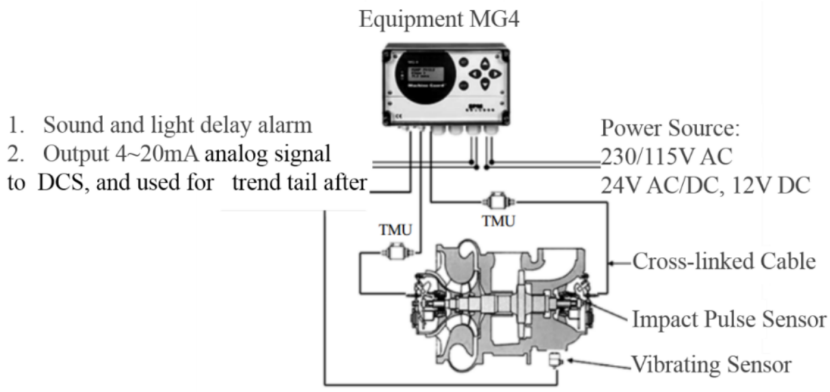

Fig. 3. Turbocharger bearing status monitoring system

maintenance personnel must replace it and then the system becomes normal again (without failure) failure.

Figure 4 shows that the first node does not have any fault symbol, which indicates that the system is normal. Further nodes have a fault sign, so that the maintenance personnel must replace the damaged parts, and the system returns from the failure state to normal state.

Figure 4 evaluates the speed and acceleration trend on the basis of comparison. It is normally hard to see what part of bearing is damaged, but from after evaluation it is easy to reflect the outer ring. In theory, with long running and aging of equipment, speed and acceleration exhibit upward and downward trends.

In this way, we are able to compare the system failure, speed and wear, to find the mechanical fault, which can be avoided by the prediction method. With the operation of machinery and equipment, the wear of each component is serious, and the probability of failure greatly increases, so that it is necessary to predict and replace the worn parts. Some parts have long running cycle and serious aging, so they can be replaced regularly to avoid serious safety faults.

Clearing relationship between the two parts is helpful to determine the stage of the fault, but the actual measured values are high and exhibit low volatility (Fig. 4 middle and bottom), which is caused by the clearance of the bearing itself. Maintenance downtime found that the bearing outer ring was serious worn and had obvious pitting and spalling pits, which might be caused by poor lubrication.

5. Conclusion

Resonance demodulation fault diagnosis is different with general vibration resonance demodulation spectrum diagnosis. The traditional fault diagnosis is mainly based on vibration signal of fault characteristic frequency spectrum to determine whether there is fault, but if only one keeps the line does not necessarily have failure, namely the uncertainty. And the technology of resonant demodulation is according to the theory of demodulation waveform, make the pledge shall order more

demodulation spectrum characteristics to determine whether there is fault, to have characteristics of the defective means to be maintained. Thus increase the reliability of the diagnosis. Its application in the ship mechanical failure promote maintenance system by the later maintenance, planned maintenance to "reliability centered", accurate prediction of initial fault, which guarantees safe and efficient navigation of the ship. However, the drawback of this method is that the signal processing is more complicated. In addition, the selection of the monitoring band has a decisive influence on the correctness of the diagnosis results when the bearing failure is diagnosed by the resonance demodulation method, so the study will be carried out in the future.

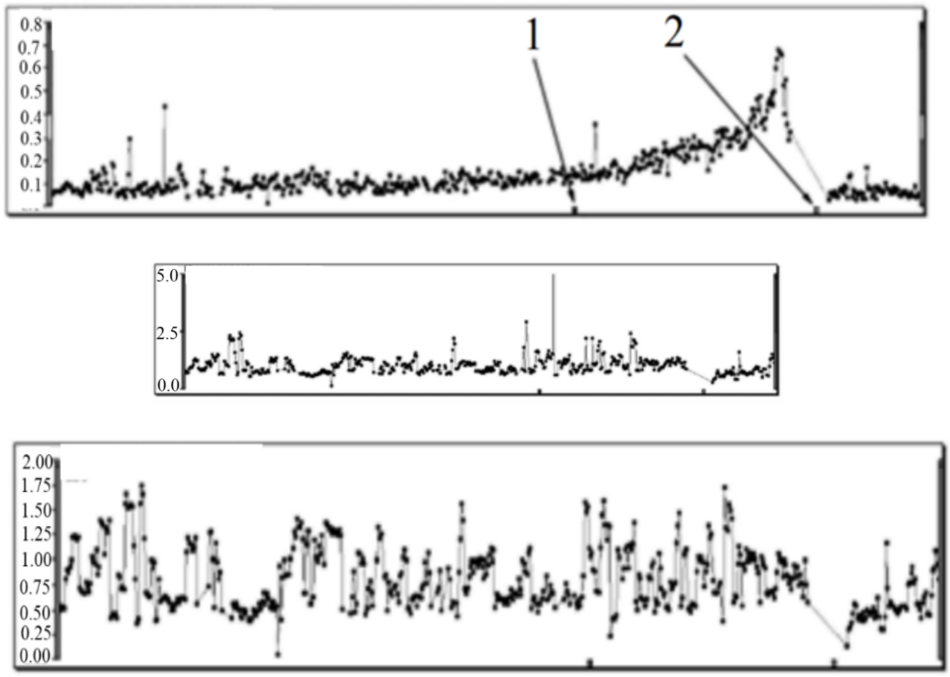

Fig. 4. The tendency of chart: top–characteristic symptom trend chart, middle–speed tendency, bottom–acceleration trend chart

References

[1] X. Yan, C. Sheng, J. Zhao, K. Yang, Z. Li: *Study of on-line condition monitoring and fault feature extraction for marine diesel engines based on tribological information.* Proceedings of the Institution of Mechanical Engineers, Part O: Journal of Risk and Reliability *229* (2015), No. 4, 291–300.

[2] R. Yan, R. X. Gao, X. Chen: *Wavelets for fault diagnosis of rotary machines: A review with applications.* Signal Processing *96* Part A, (2014), 1–15.

[3] Y. S. Sun, D. J. Yu, X. M. Chen, R. Li: *Order domain analysis based on resonance-*

based sparse signal decomposition and its application to gear fault diagnosis. Journal of Vibration and Shock *32* (2013), No. 16, 88–94.

[4] H. D. Nguyen, G. C. Steele, D. W. Bitler: *An overview of SBIR phase 2 air-breathing propulsion technologies.* Publisher: NASA (2014).

[5] Y. Lei, J. Lin, Z. He, M. J. Zuo: *A review on empirical mode decomposition in fault diagnosis of rotating machinery.* Mechanical Systems and Signal Processing *35* (2013), Nos. 1–2, 108–126.

[6] C. Li, M. Liang, T. Wang: *Criterion fusion for spectral segmentation and its application to optimal demodulation of bearing vibration signals.* Mechanical Systems and Signal Processing *64–65* (2015), 132–148.

[7] Z. Zhou, Y. S. Zhu, Y. Y. Zhang, C. F. Zhu, P. Wang: *Adaptive fault diagnosis of rolling bearings based on EEMD and demodulated resonance.* Journal of Vibration and Shock *32* (2013), No. 2, 76–80.

[8] J. Shi, X. Wu, N. Pan, S. Wang, J. Xhou: *Vibration signal analysis of bearing based on EMD and resonance demodulation.* Applied Mechanics and Materials *556–562* (2014), 1286–1289.

[9] S. Riaz, H. Elahi, K. Javaid, T. Shahzad: *Vibration feature extraction and analysis for fault diagnosis of rotating machinery-A literature survey.* Asia Pacific Journal of Multidisciplinary Research *5* (2017), No. 1, 103–110.

[10] M. Unal, Y. Sahin, M. Onat, M. Demetgul, H. Kucuk: *Fault diagnosis of rolling bearings using data mining techniques and boosting.* Journal of Dynamic Systems, Measurement, and Control *139*, (2016), No. 2, paper 021003.

Received September 19, 2017

Acta Technica *62* No. 2B/2017, 487–494

Integrated modeling and simulation of wind power generation system based on PVDF piezoelectric thin film[1]

Rui Wang[2,3], Shuchen Yang[2], Yue Li[2]

Abstract. PVDF piezoelectric film wind power generation technology is attracting more and more attention because of its high efficiency and practicability. And it has a wonderful development prospect. This paper is devoted to the study of PVDF piezoelectric thin film wind power generation technology, starting with analyzing its operation mechanism, and comparing the difference of fixed pitch, pitch and PVDF piezoelectric film wind power. Finally it selected the doubly fed PVDF piezoelectric film as the scheme: it's in the stage of low speed pitch adjustment pursuit of maximum wind energy capture, and achieve the independent regulation of stator output constant frequency and active and reactive power by controlling the rotor side power when it is in high wind speed. This paper analyzes the basic operation characteristics, points out the advantages of PVDF piezoelectric film generator that AC motor cannot match; studies the steady-state circuit and power balance, and the establishment of the state equation; realizes decoupling of the stator active and reactive power control, which makes the motor control simple. The research of this paper has promoted the development of wind power industry.

Key words. Wind power generation, PVDF piezoelectric film, doubly fed induction generator, modeling, simulation.

1. Introduction

The process of industrialization in the world has led to an increase in energy consumption and emissions of harmful chemicals. Thus caused climate anomalies, disasters, and many malignant diseases. And the energy and environmental issues become the two major issues [1–3]. The crisis caused by the energy problem and the increasingly prominent environmental problems make us recognize that the development of clean and renewable new energy is an objective need for the protection

[1]This work was supported by a grant from JiLin province science and technology development project of China (No. 20170101122JC).

[2]Changchun Normal University, Changchun, Jilin, 130032, China

[3]Corresponding author

of the ecological environment and the protection of sustainable development [4]. At present, in the development of renewable energy of wind power generation has the most potential, and the generation cost decreased gradually, and technically mature, which forms a new industry, has become the power system structure relative to the fastest growth of new energy power generation [5–6] Therefore, the research of wind power generation technology is of great significance [7]. The paper makes an analysis the basic operation characteristics, shows the advantages of PVDF piezoelectric film generator that AC motor cannot match; studies the steady-state circuit and power balance, and the establishment of the state equation; realizes decoupling of the stator active and reactive power control. The research has promoted the development of wind power industry [8–9].

2. Methodology

MATLAB 6.5/Simulink software is used to build the simulation model of each part of the system, and the simulation of the system was carried out.

The mathematical models can be expressed by the equations:

$$M_{\mathrm{w}} = \frac{\pi}{2} p c_1 w \,, \tag{1}$$

$$C_{\mathrm{p}} = 0.5 \left(\frac{rC}{L} - 0.022B - 2 \right) \mathrm{e}^{-ti\theta} \,, \tag{2}$$

$$\frac{\mathrm{d}M}{\mathrm{d}t} = \frac{1}{T(M-U)} \,, \tag{3}$$

and

$$\frac{\mathrm{d}W}{\mathrm{d}t} = \frac{1}{C(M-U)} \,. \tag{4}$$

Here, C is the piezoelectric stress constant, M is piezoelectric strain constant, B is the electric field strength, T and U are piezoelectric constant matrix and transpose matrix, L is the inductance and C_{p} is the circuit capacity.

The optimum operation principle of PVDF piezoelectric film wind turbine is depicted in Fig. 1.

The PVDF piezoelectric film wind curve is depicted in Fig. 2.

According to Fig. 2, when the wind speed changes, as long as the speed of the wind wheel is adjusted, and the tip speed ratio $\lambda_{\max} = \lambda$ is kept the same, the maximum wind power can be obtained, which is the best operation principle of the wind turbine.

The simulation models of all parts of the wind power system are built up using the software Matlab 6.5/Simulink 5.0 and simulation experiments are done, whose results show that the models are proper and the VSCF wind power system has good operating performance.

After the analysis of the essential operating characteristics, this work presents a study on the steady equivalent circuit and the power flow. Five-order-state equa-

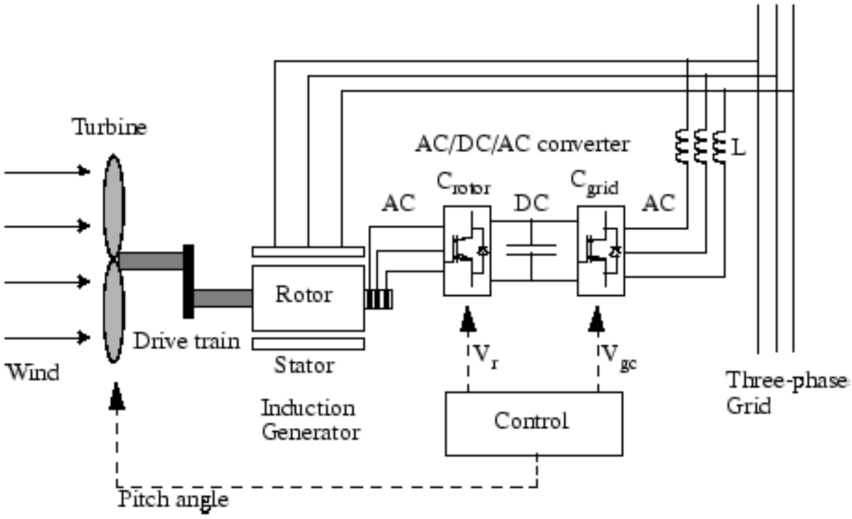

Fig. 1. Wind turbine simulation model

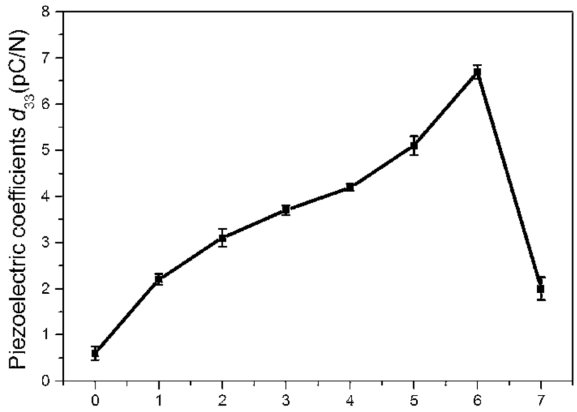

Fig. 2. PVDF piezoelectric film wind curve

tions in the M-T-0 reference frame are deducted in detail and the stator flux-oriented vector control system is built to decouple the stator active and reactive power regulations and make controlling of the motor more simple.

The main circuit structure is depicted in Fig. 3.

Matlab 6.5 software (MICROTEK Simulink/Power System Blockset model) was set up to model single-phase positive and negative rectifier circuit.

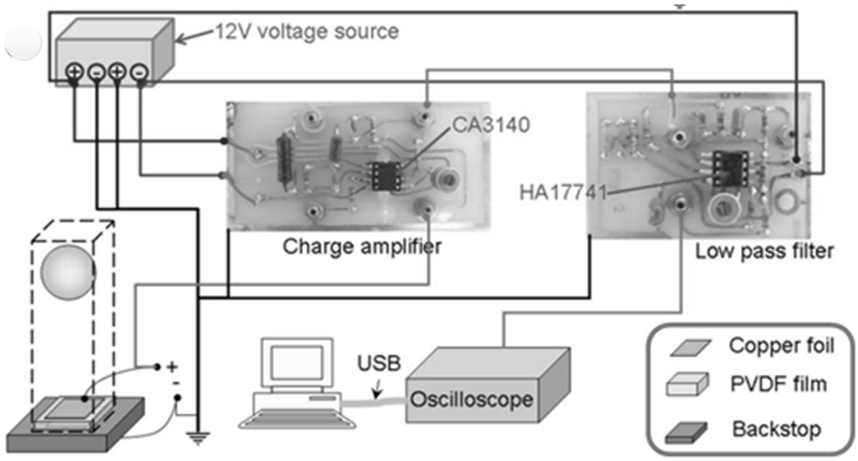

Fig. 3. Main circuit structure of system

3. Result and discussion

3.1. Simulation results of a wind turbine

Technical parameters of the model of G52-850 kW wind turbine are listed in Table 1, and the wind farm parameters are shown in Table 2.

The inverter is the key equipment to make the double-fed motor VSCF operate so the 6-pulsed AC-AC inverter, (cycloconverter) is selected as the exciting power supply. Through processing the interface between the inverter and the generator, this paper builds up the mathematical model of the inverter by analyzing its main configuration of the circuit, the method of cosine crossing and the producing of trigger pulses. Power characteristic curve and parameters of wind turbine are depicted in Fig. 4.

Table 1. Technical parameters of wind turbine

Rated power	850 kW	Hub height	55 m
Impeller diameter	52 m	Swept area	2124 m^2
Rated wind speed	13 m/s	Safe wind speed	50–70 m/s
Speed range	14.6–30.8 rpm	gearbox ratio	1:61.74

Table 2. Wind farm parameters

Air density	1.04 kg/m^3	Average speed	8 m/s
Wind frequency spacing	2 rad/s	Gap range	2000 m
Surface roughness	0.004	Max. wind speed	20 m/s
Maximum gradient wind speed	15 m/s	Distance between turbines	>260 m

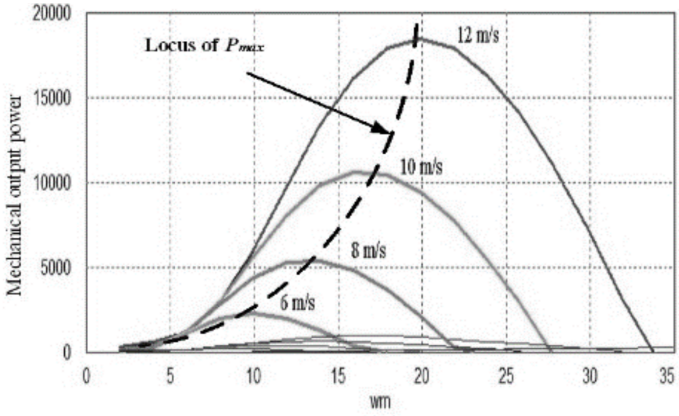

Fig. 4. Power characteristic curve and parameters of wind turbine

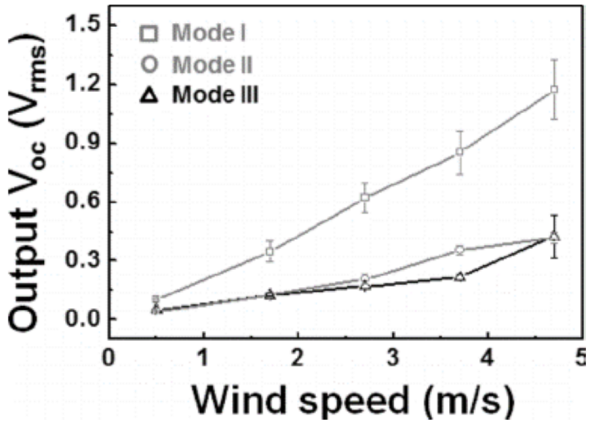

Fig. 5. PVDF piezoelectric film wind speed

Figure 5 is the power characteristic curve and parameter curve of PVDF piezoelectric film wind speed. The highest value is reached when it is about 6 seconds.

3.2. Output curve of frequency converter

Let the control voltage amplitude be 100 V and frequency 10 Hz. Then the effective value of cycloconverter fed power supplied by excitation transformer is 100 V, frequency 50 Hz and load inductance $L = 0.07$ H. Figure 6 shows the load voltage of the cycloconverter, the voltage between the two neutral points and the load current waveform.

From the simulation process it can be seen that the cycloconverter is a highly nonlinear system, containing 36 thyristors, cosine wave generator, synchronous trigger pulse generator, commutation logic control module, the system model of complex structure, and large amount of feedback.

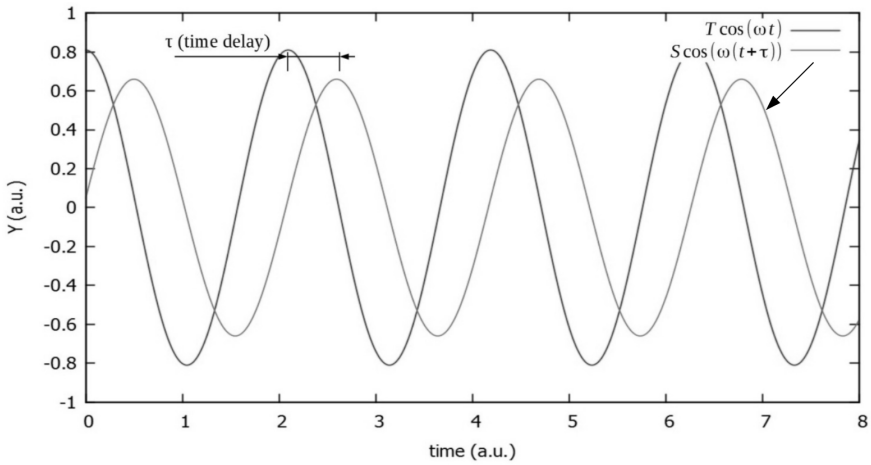

Fig. 6. Two-phase load current waveform

3.3. Simulation model of doubly fed induction generator

The stator-oriented vector control of doubly fed generator is given. The structure diagram is shown in Fig. 7, and the simulation model is similar to the block diagram, no longer tired. Before the dynamic control is implemented, the motor is in a steady state, and the following initial conditions can be determined by the equation of state of the generator.

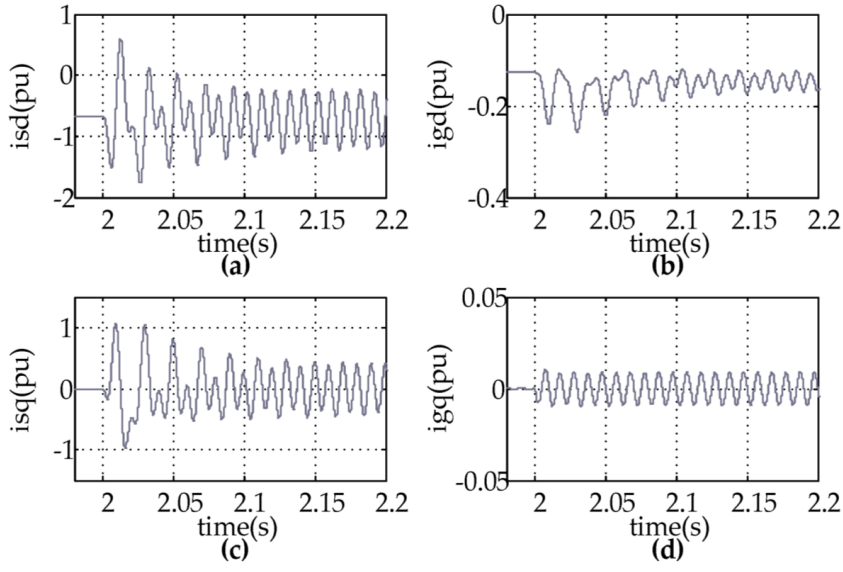

Fig. 7. Structure diagram of the doubly fed induction generator

The double-fed generator, who is superior to a general AC one in many aspects, and it is the hard core of the wind power system. After the analysis the essential operating characteristics, this thesis makes a study on the steady equivalent circuit and the power flow. Five-order-state equations in the M-T-0 reference frame are deducted in details and the stator flux-oriented vector control system is built to decouple the stator active and reactive power regulating and make controlling of the motor more simple.

4. Conclusion

This paper presented an research on PVDF piezoelectric thin film wind power generation technology, starting with analyzing its operation mechanism, and comparing the difference of fixed pitch, pitch and PVDF piezoelectric film wind power. Finally selected the doubly fed PVDF piezoelectric film as the scheme: it's in the stage of low speed pitch adjustment pursuit of maximum wind energy capture, and achieve the independent regulation of stator output constant frequency and active and reactive power by controlling the rotor side power when it is in high wind speed.Above all, the way can get a better effect in wind power generation comparing with other ways.

References

[1] P. Talemi, M. Delaigue, P. Murphy, M. Fabretto: *Flexible polymer-on-polymer architecture for piezo/pyroelectric energy harvesting.* ACS Applied Materials & Interfaces *7* (2015), No. 16, 8465–8471.

[2] Z. Wang: *Modeling and simulation of piezoelectrically driven self-charging lithium ion batteries.* ACS Applied Materials & Interfaces *9* (2007), No. 18, 15893–15897.

[3] S. Li, Q. Zhong, J. Zhong, X. Cheng, B. Wang, B. Hu, J. Zhou: *Cloth-based power shirt for wearable energy harvesting and clothes ornamentation.* ACS Applied Materials & Interfaces *7* (2015), No. 27, 14912–14916.

[4] G. Liu, Q. Leng, J. Lian, H. Guo, X. Yi, C. Hu: *Notepad-like triboelectric generator for efficiently harvesting low-velocity motion energy by interconversion between kinetic energy and elastic potential energy.* ACS applied materials & interfaces *7* (2015), No. 2, 1275–1283.

[5] S. Priya, H. C. Song, Y. Zhou, R. Varghese, A. Chopra, S. G. Kim, I. Kanno, L. Wu, D. S. Ha, J. Ryu, R. G. Polcawich: *A review on piezoelectric energy harvesting: Materials, methods, and circuits.* Energy Harvesting and Systems *4* (2017), No. 1, 3–39.

[6] B. Dudem, Y. H. Ko, J. W. Leem, J. H. Lim, J. S. Yu: *Hybrid energy cell with hierarchical nano/micro-architectured polymer film to harvest mechanical, solar, and wind energies individually/simultaneously.* ACS applied materials & interfaces *8* (2016), No. 44, 30165–30175.

[7] Y. Kim, J. Na, C. Park, H. Shin, E. Kim: *PEDOT as a flexible organic electrode for a thin film acoustic energy harvester.* ACS Applied Materials & Interfaces *7* (2015), No. 30, 16279–16286.

[8] J. H. Kang, D. K. Jeong, S. W. Ryu: *Transparent, flexible piezoelectric nanogenerator based on GaN membrane using electrochemical lift-off.* ACS Applied Materials & Interfaces *9* (2017), No. 12, 10637–10642.

[9] Y. Kang, B. Wang, S. Dai, G. Liu, Y. Pu, C. Hu: *Folded elastic strip-based triboelectric nanogenerator for harvesting human motion energy for multiple applications.* ACS Applied Materials & Interfaces 7 (201), No. 36, 20469–20476.

Received September 19, 2017

Acta Technica *63* No. 2/2018, 495–500

Dynamic obstacle detection and expression method of driverless vehicle based on laser sensor

Huan Li[1]

Abstract. In the cell technology of the driverless vehicle, the detection, prediction and collision avoidance of moving obstacles in complex outdoor environment is always the focus and difficulty of the research. Aiming at the problems encountered in detection, prediction and collision avoidance of moving obstacles in outdoor complex environment, and the overall design requirements of the system. A driverless obstacle avoidance system for driverless vehicle was designed in this paper. In this system, the methods of detection, prediction and collision avoidance were deeply studied, and some specific techniques in engineering application and experimental test were introduced. And an improved A* algorithm which can search continuous neighborhood was put forward to achieve safe and intelligent autonomous driving of driverless vehicle in dynamic environment.

Key words. Laser sensor, driverless vehicle, dynamic obstacle.

1. Introduction

Specifically, both in daily life, in military and scientific research, the research goal of unmanned vehicles is completely or partially replaced by the driver's function. The key technologies they involve are the same. In daily life, driving is not only boring but also dangerous. Drivers need to pay attention to the change of environment at all times, and at the same time, overcome their physical limitations such as fatigue and carelessness. Driverless and its derivative technology can make drivers free from boring and tedious driving behaviors to a certain extent. In military affairs, pilotless technology can replace human beings in performing dangerous missions such as reconnaissance, mine clearance, radiation and battlefield, so as to reduce casualties [1]. In scientific research, driverless vehicles can help humans engage in extraterrestrial exploration activities such as the moon and Mars. Since 2000, with the rapid development of computer vision, artificial intelligence, electronic circuits and other disciplines, these disciplines are also widely used in vehicles. In recent years,

[1]Tianjin Sino-German University of Applied Sciences, Automobile & Rail Transportation School, 300350, Tianjin, China

researchers have begun to shift the focus to auxiliary driving. Autonomous parking, self-adaptive cruise, dangerous overtaking alarm and lane departure alarm have been widely used in civil vehicles [2]. Nevertheless, there are still many problems in fully realizing driverless vehicle under complex traffic environment. Urban road environment information is large, complex and changeable. Rural road environment is tortuous and road conditions are not good. The environment of expressway is fast and dangerous. Through the research of autonomous driving technology under various traffic environments. We can improve the environmental awareness, intelligent decision-making and vehicle control ability of the driverless vehicle. It has great application prospect and strategic value [3].

2. State of the art

In the 80s of last century, our country began to study the intelligent mobile robot. In 1980, the project of remote driving anti-nuclear reconnaissance vehicle was set up in the state. Harbin Institute of Technology, Shenyang Automation Research Institute and National University of Defense Technology three units participated in the research and manufacture of the project [4]. During the 85 periods, ATB-1 unmanned vehicle was jointly developed by five units such as Beijing Institute of Technology and National University of Defense Technology. This is the first self-driving test vehicle in China, and its speed can reach 21 km/h. ATB-2 self-driving vehicle was also successfully developed in 95, compared with ATB-1. Its function has been greatly enhanced, and the linear speed can reach up to 21 meters per second. In 2005, the third-generation autonomous vehicle Autonomous Test Bed-3 was also developed. ATB-3's environmental cognition and trajectory tracking capabilities have been further strengthened. National University of Defense Technology also represents a relatively high level of research on autonomous vehicles in China. They successfully developed the self-driving car, the red flag CA7460. It can automatically change lanes according to the situation of vehicles with obstacles ahead, and its maximum speed can reach forty-seven meters per second. THMR-V self-driving vehicle was developed by Tsinghua University (Tsinghua Mobile Robot). Its maximum speed can reach 42 m/sec. Besides, vehicles can also choose two driving modes of expressways and urban roads according to different driving scenarios [5]. The Springrobot developed by Xi'an Jiaotong University is also one of the famous driverless vehicle platforms in China. It has high ability of lane detection and pedestrian detection.

3. Methodology

3.1. Searchable continuous domain A algorithm*

There are many raster-based path planning algorithms, such as A*, D*, D* Lite, Focussed D* and so on. For a known static environment, A* algorithm can solve the shortest path between two points most quickly and effectively. But raster-based

path planning algorithm has a problem. They all take the center point of grid as the searchable node in the state space. That is to say, its searchable neighborhood number is 8 (at some time, it can also be set to neighborhood number 4). The search direction of this path is also limited to 4 times the integer number, so that the path obtained is not optimal. The length of path is not the shortest and the number of turns is too much, which has great influence on large scale land robot [6]. A* is a best priority algorithm put forward by some scholars combining heuristic and conventional methods. The valuation function is as follows:

$$F(X) = g(X) + h(X) \tag{1}$$

Among them, $f(X)$ is the evaluation function from the initial point to the target point through node X. Symbol $g(X)$ denotess the actual cost from the initial point to the node X in the state space. Quantity $h(X)$ is the estimation cost from the node X to the optimal path of the target point. When the estimated cost $h(X)$ is no larger than the actual distance value from node X to the target point, the number of search points is large, and the efficiency is low. But the optimal solution can be obtained. When $h(X)$ is larger than the actual distance value from node X to the target point, the number of search points is less, and the efficiency is high. However, the optimal solution is not guaranteed. For real environment, Euclidean distance between two nodes can be selected as the estimation cost. That is:

$$h(X) = \sqrt{(x_0 - x_X)^2 + (y_0 - y_X)^2} \tag{2}$$

Among them, (x_X, y_X) are the coordinates of the node X. Quantities (x_0, y_0) are the coordinates of the target point G.

This is a static grid diagram that describes the environment. The green grid is the starting point A, the red grid is the destination B, and the blue grid is the obstacle. We need to solve the shortest path from the starting point A to the destination B in this grid graph. A* algorithm first creates two tables: open table and closed table. The open table is used to save all the nodes that are generated but not inspecting. The closed table is used to record nodes that have been visited and do not need to revisit [7]. Then operate according to the following steps. Add the starting point A to the pen table, add the raster dots adjacent to point A to the pen table. According to different requirements, we can define the adjacency differently. If we define only the upper and lower raster grids as adjacent grids, then the 4-neighborhood search. If the four rasters of the diagonal is also defined as adjacent raster, it is 8 neighborhood searches. The starting point A is moved from the pen table to the closed table, and it is defined as the parent node of its 8 adjacent grids. It is marked by a pointer from the child node to the parent node.

Then we solve the g value, H value and F value of grid points in the table. The g value is the cost from point A to the grid, which can be directly represented by distance. Suppose the length of each grid is 10, then the g value of the four grids on the top and bottom is 10, and the g value of the four grids is equal to $\sqrt{200}$. Of course, this is just the premise that grid is not occupied by obstacles. If the grid is occupied by an obstacle, then $g = \infty$. The h value is the cost of the estimate of

the grid point to the target point. In this case, the Manhattan distance between raster and terminal points is set. From the open table, select the raster dot with the smallest f value, and record it as the current node s. And move it from the open list to the closed table. Investigate all the adjacent nodes of the current node S (record, X). If X is neither in the closed table nor in the open table, it is added to the open table to solve its g value, H value and F value, and the current node S is the parent node. If point X is already in the open table, compare $g\,(S) + c\,(S, X)$ ($C(S, X)$ is the cost from point S to point X) and $G(X)$ size. When $G(S) + c(S, X) < g(X)$, $G(X)$ is $g(S)$, and the $G(X)$. And update the F value of X accordingly, and set S as its parent node. When $G(S) + c(S, X) = g(X)$, do not do any treatment. If X is already in the closed table, it will not do any processing. Repeat the above steps until the current node S is ended by 3. As shown, the raster dot of pale blue box is the point that is stored in the closed table after the whole search process is finished. The raster point of the green box is the point stored in the open table. From the end point B, find the parent node in turn until the starting point A. This path is the shortest path solved by A* algorithm. The shortest path is the path from the starting point to the end of the red marked grid. Where INSERT (x) joins node X into open table. GET_FMIN (), function returns the minimum node in the open table, and DELETE (X) moves node X from the open table to the closed table. $T(X)$ represents the current state of the node X. NEW indicates that it has not been accessed. OPEN indicates that it is stored in the open table. CLOSED indicates that it has been stored in the closed table. Quantity $b(X) - Y$ represents the parent node setting X node Y.

4. Result analysis and discussion

Based on the above model and algorithm, this paper has tested and verified it. The parameter setting of intelligent pioneers is shown in Table 1. "Intelligent pioneer" will detect the results on obstacles occupied by grid map. As shown in the figure, the black box is a clustering area based on the driving state and environment of the car, which is urgent and adaptive. When moving obstacles into the black box are successfully detected, we will compare the test results of these two moving objects with the actual results.

Table 1. Parameter setting of "smart pioneer"

t_V	t_I	a	b	c	f_0	λ	λ'
90 ms	10 ms	2	1	3	3	1.2	1.2

5. Conclusion

In this paper, an obstacle avoidance system for unmanned vehicle (unmanned vehicle) was designed based on the real-time, accuracy, security and intelligence, which was based on the data fusion of multi-laser sensors, the building of the space-

time barrier grid and the search for the continuous neighborhood A* algorithm. In addition, the theory and method of detecting, predicting and avoiding obstacles in moving vehicles were studied. Some specific technical means in engineering application and experimental test were also introduced, and collision avoidance process was divided into two sub processes: behavior choice and path planning. The spatio-temporal obstacle grid graph provided the two sub processes with obstacle information and prediction collision information description. The behavior decision module chose reasonable driving behavior based on spatio-temporal obstacle grid graph. It was also sent to the motion planning module in the form of local target points. The motion planning module used a searchable continuous neighborhood A* algorithm to plan the path on the space-time barrier grid, and finally generated an optimal path to send to the control decision layer. The path distance generated by this method is shorter and the trajectory is smoother. And it can guarantee multiple driving safety of driverless vehicle. A large number of experiments prove that this method is effective and real-time.

References

[1] P. Yao, H. Wang, Z. Su: *Real-time path planning of unmanned aerial vehicle for target tracking and obstacle avoidance in complex dynamic environment.* Aerospace Science and Technology *47* (2015), No. 31, 269–279.

[2] M. Kristian, V. S. Kenk, S. Kovačič, J. Perš: *Fast image-based obstacle detection from unmanned surface vehicles.* IEEE Transactions on Cybernetics *46*(2016), No. 3, 641–654.

[3] F. Ding, Y. Zhao, L. Guo, M. Zhang, L. Li: *Obstacle detection in hybrid cross-country environment based on markov random field for unmanned ground vehicle.* Discrete Dynamics in Nature and Society *10* (2015), No. 2, 1–8.

[4] W. Zhang, S. Wei, Y. Teng, J. Zhang, X. Wang, Z. Yan: *Dynamic obstacle avoidance for unmanned underwater vehicles based on an improved velocity obstacle method.* Sensors *17* (2017), No. 12, paper E2742.

[5] H. Wang, Y. Hou, S. Hou: *Design of laser radar obstacle detection system for unmanned vehicles.* Journal of Beijing Polytechnic College *72* (2018), No. 50, 101–105.

[6] Y. Fu, Y. Zhang, X. Yu: *An advanced sense and collision avoidance strategy for unmanned aerial vehicles in landing phase.* IEEE Aerospace & Electronic Systems Magazine *31* (2016), No. 9, 40–52.

[7] D. Hermann, R. Galeazzi, J. C. Anderssen, M. Blanke: *Smart sensor based obstacle detection for high-speed unmanned surface vehicle.* IFAC-PapersOnLine *48* (2016), No. 15, 190–197.

Received October 12, 2017

Acta Technica *62* No. 2B/2017, 501–512

Characteristics of three-phase controllable reactor under orthogonal field[1]

Zhengrong Jiang[2], Zhenkun Sun[2], Yunbo Liu[2]

Abstract. To solve the problem of additional losses, instability and harmonic currents in fixed reactors, a three-phase controllable reactor is studied by means of physical and electrical methods. The three-phase controllable reactor is based on the quadrature magnetizing energy to provide three-phase bias inductance. When the DC bias current changes, the input impedance of the three-phase reactor can be variable reactance to maintain three-phase balance. In addition, the relationship between three-phase harmonic characteristics and control is also interrelated. The magnetic mechanism of three-phase reactor under orthogonal magnetic field is introduced. A domain motion model is established. The permeability of tensor is calculated and its harmonic characteristics are analyzed. A prototype of three-phase controllable reactor is proposed, and its control characteristics are discussed. The calculated results are in good agreement with the experimental results.

Key words. B-H loop cluster, orthogonal field, tensor permeability,controllable reactor.

1. Introduction

Controllable reactor is an important equipment in power line and distribution system. Traditionally, discrete fixed shunt reactors are installed on power transmission lines and switched in or out according to the system loading. But a fixed reactor has some drawbacks, such as extra losses, less capacity of voltage stability and harmonic current generation [1]. If the fixed reactor is substituted with a controllable one, the compensation reactive power can be adjusted according to the needs of the load of the transmission and thus leads to the following advantages: lower transmission losses, higher transmission capacity of active power and less harmonics injection to the system.

[1]This work was sponsored by National Natural Science Foundation of China (51377006) and Beijing Natural Science Foundation (3132008).

[2]School of Electrical and Control Engineering, North China University of Technology, Beijing, 100144, China

There are two types of controllable reactors as an alternative to the fixed reactor: Magnetically Controlled Reactor (MCR) and Thyristor Controlled Reactor (TCR). The main difference between MCR and TCR is that MCR changes the reactance by adjusting the permeability of the iron core of the reactor, while TCR usually depends on the current through the reactor. The latter employs some power electronics to control current but results in extra harmonic current [2].

From the viewpoint of application, TCR-based SVC are suitable for some high voltage situations, such as 220 kV and below. There are some difficulties for their applications in EHV/UHV line due to the cost and insulation problems. In these cases, the MCR-based SVC has significance advantages in respect of the cost and insulation.

MCRs can be sorted into two types according to the relative direction of the DC flux and AC flux which role as DC bias control flux and main working flux, respectively. One is called Magnetic Controlled Reactor in which DC flux direction is parallel with AC flux, and the other is called orthogonal flux reactor in which DC flux direction is orthogonal with AC flux. The latter is named as MCR+ for the difference with the former one, where the "+" signal is for the orthogonal magnetization.

2. State of the art

A controllable saturation reactor generally consists of two windings on an iron core. One of the windings, which is excited by DC current source, is called control winding; another winding is the main AC working winding, which is excited by AC voltage. Changing the DC current can adjust the saturation of the iron and the reactance of the main winding [3].

Because the reactor is based on the controlled saturation in part of the magnetic circuit, the permeability and saturation are two of the critical magnetic properties [4]. A constant permeability is nearly a flat magnetization curve across the origin of the $\boldsymbol{B} - \boldsymbol{H}$ plane, and saturation magnetization at a high field can be described by a horizontal line in the $\boldsymbol{B} - \boldsymbol{H}$ plot. When the DC bias current is changing, the magnetization curve will change gradually from the constant permeability regime to the saturation one. Therefore, the core operating point must be considered in order to accurately change the permeability of the core and the reactance of the reactor [5].

The working principle of three-phase MCR and saturable reactor is the use of magnetic saturation principle, the effect of excitation DC current to change magnetic work point and magnetic properties, magnetic saturation control degree, thus changing the reactance value of AC winding to smooth the self adjusting reactor capacity.

Although MCR is developed from the traditional controllable saturable reactor, it has its own characteristics, mainly in the following aspects:

Without external DC excitation, the traditional controllable saturable reactor needs an external large capacity DC excited power supply, while the MCR itself is DC excited by the commutation of the lotus root and controlled by silicon rectifier.

The main and control winding mutual traditional saturated controllable AC wind-

ing and DC control winding of the reactor from around the core, and the working winding and control winding MCR interoperability, not only simplified the structure, save material, and reduce the loss.

The volt ampere characteristics of saturable reactor special structure of the magnetic valve with traditional nonlinear, and MCR because of its small section core, namely the magnetic valve structure, when working, the volt ampere characteristics of the magnetic valve section is only nonlinear saturation, while the remaining section is in unsaturated linear state. This reduces the harmonic content and loss, and improves the response speed.

Single phase double column MCR, because the two AC winding in parallel, winding direction, through the core of the magnetic flux direction is the same, so must add side choke, can make AC flux loop. But the three-phase six column MCR, because its three-phase voltage is symmetrical, in the magnetic circuit the three-phase alternating current magnetic flux size is equal, the phase difference is 120 degrees. Thus, in the upper and lower iron chokes, the magnetic flux vector and zero, no excess harmonic, and no need to add a side choke to form a loop, the three-phase winding adopts triangle connection mode, and can also filter the third harmonic. Compared with three single-phase combination MCR, the three-phase MCR reduces the harmonic content, saves the material, reduces the occupation area, and improves the economic benefit to a great extent.

2.1. Methodology

The theory of controllable saturation reactor is shown as following Fig. 1.

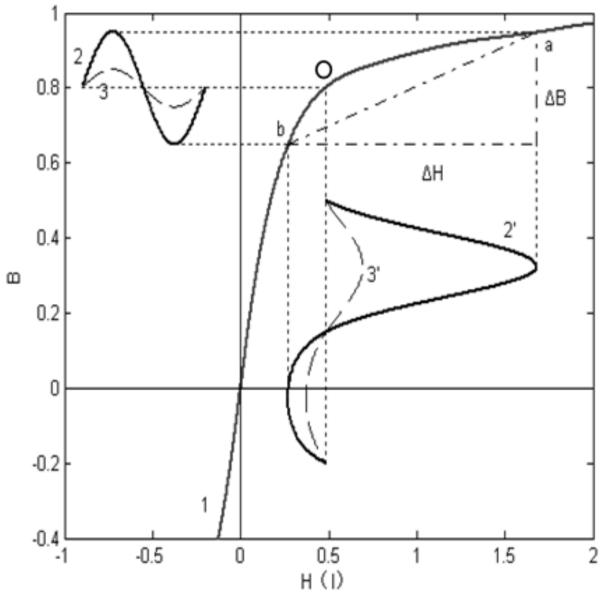

Fig. 1. Theory of saturation controllable reactor

When the operating point close to the non-linear region of the $\boldsymbol{B}-\boldsymbol{H}$ curve, a harmonic current is created inescapably. For example, the point is moving from b to a, the output current waveform is changed from $3'$ to $2'$. It is obvious that the non-linearity of the magnetization curve leads to a substantial harmonic distortion.

When the operating points are retained in the linear region of the $\boldsymbol{B}-\boldsymbol{H}$ "cluster", the output current waveform can be expected to maintain sinusoidal in a wide control region [6], as shown in Fig. 2.

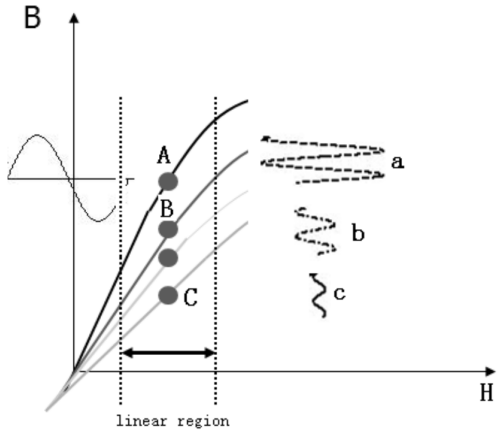

Fig. 2. Operating points in linear region results in sinusoidal waveform

When the DC bias current is changing, the magnetization curve should be decided in the cluster of $\boldsymbol{B}-\boldsymbol{H}$ plane, which maintains in the linear area, so the changing accurately reactance of the reactor depends on the selection of the $\boldsymbol{B}-\boldsymbol{H}$ curve other than the core operating points [6]. In the end, the corresponding permeability of the core is decided.

The key element is a cylinder iron core which is wound by strips of grain oriented silicon steel and two kinds of windings are arranged orthogonally around the cylinder core. The inside winding is the bias coil connected to DC supply, the outside winding is the AC main coil connected to AC supply. The structural scheme is shown in Fig. 3.

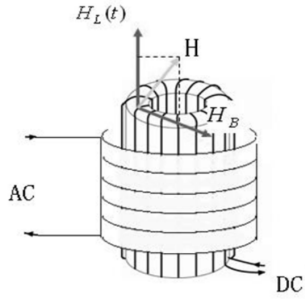

Fig. 3. Structure of the orthogonal core

Based on the above structure of the orthogonal core, AC main winding yields an AC flux in direction of the axis of the cylinder iron core when AC current is applied. The DC control winding is wound through the hollow cylinder and yields a DC flux along the azimuthal direction when DC current plus on. Subsequently, the AC flux and the DC flux are orthogonal in the cylinder core and a semi-rotating magnetic flux is formed. Fig. 4 shows a circumferential flux produced by DC current and axial flux generated by AC current.

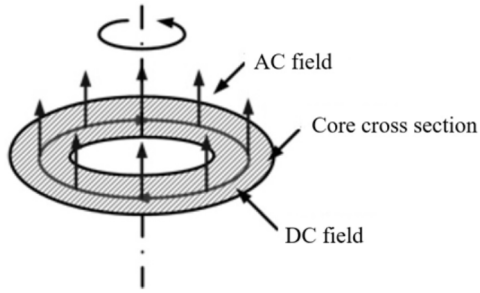

Fig. 4. Fluxes in the orthogonal core

The three-phase controllable reactor consists of two types of elements: up and down yokes which are wounded by strips of grain oriented silicon steel and some control discs which are stocked as three-phase limbs (the number depends on the designed capacity). These control discs are wound also by silicon steel in the way of involute as shown in Fig. 5, which are the key elements for the three-phase reactor, playing the main role to determine the orthogonal flux and making the reactor controllable.

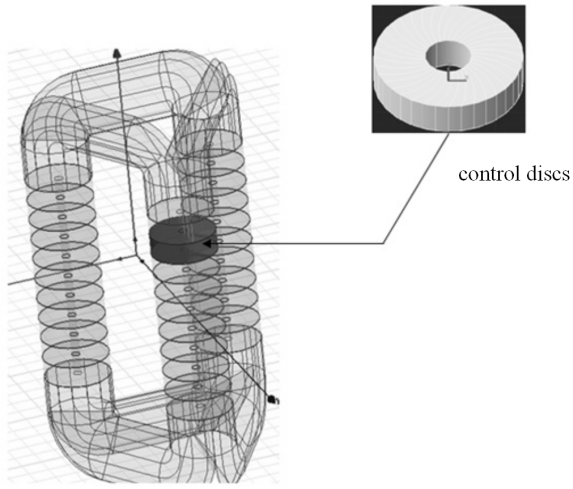

Fig. 5. Structure of three-phase controllable reactor

Each phase limb is the main core of the reactor as well as the return path of other

two phases' flux. For each phase core, AC current yields an AC flux in direction of the axis of the limb. In the meantime, DC current yields a DC flux along the annular direction. Subsequently, the AC flux and the DC flux are orthogonal in the control disc, and a semi-rotating magnetic flux is formed.

3. Result analysis and discussion

Generally, magnetic parameters of grain-oriented silicon steel is presented by magnetic permeability matrix without diagonal items of μ_{xx} and μ_{yy} [7]. However, when the grain-oriented core is subject to orthogonal field, the tensor permeability should be considered instead of above mentioned matrix. In the case a semi-rotating field is formed and the magnetic characteristics are different from that parallel field conditions, the following equation is used to describe the relationship between $\boldsymbol{B}$ and $\boldsymbol{H}$

$$\begin{pmatrix} B_{\mathrm{x}} \\ B_{\mathrm{y}} \end{pmatrix} = \begin{bmatrix} \mu_{xx} & \mu_{xy} \\ \mu_{yx} & \mu_{yy} \end{bmatrix} \begin{pmatrix} H_x \\ H_y \end{pmatrix}. \tag{1}$$

When the inclination between $\boldsymbol{H}$ and grain-oriented steel is different, the ratio of components of flux density B_x/B_y is different, and the permeability tensor is the function of the ratio [8]. The permeability matrix must include inclination items. These added items can be measured with two-dimensional excitation, the magnetic permeability is related to the inclination angle. As shown in Fig. 6.

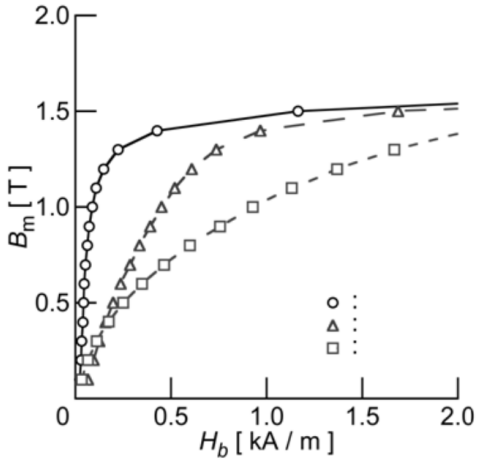

Fig. 6. Permeability relative with inclination angle

Furthermore, the tensor permeability is expressed as following:

$$\begin{pmatrix} \mu_{xx} \\ \mu_{xy} \\ \mu_{yx} \\ \mu_{yy} \end{pmatrix} = \begin{pmatrix} k_{11} & k_{12} & k_{13} & k_{14} \\ k_{21} & k_{22} & k_{23} & k_{24} \\ k_{31} & k_{32} & k_{33} & k_{34} \\ k_{41} & k_{42} & k_{43} & k_{44} \end{pmatrix} \begin{pmatrix} 1 \\ H_x^2 \\ H_x H_y \\ H_y^2 \end{pmatrix}, \tag{2}$$

where k_{ij} is the element of the coefficient matrix [9].

Let us setting AC exciting while $I_{\mathrm{D}} = 0$, AC current creates magnetic field H_1 which establishes a magnetic field density B_1'. The $B - H$ loop depends on the magnetization characteristics of the magnetic material. If H_1 is constant with I_{D} producing H_{D}, the composed field intensity becomes $\boldsymbol{H} = H_{\mathrm{a}}\boldsymbol{e}_x + H_{\mathrm{D}}\boldsymbol{e}_y$ where $\boldsymbol{e}_x$ and $\boldsymbol{e}_y$ are, respectively, the unit vectors in the H_{a} and H_{D} directions. The composed magnetic flux density $\boldsymbol{B}$ is along with the direction of $\boldsymbol{H}$, and its value can be calculated from the $B - H$ curve.

The composed field $\boldsymbol{B}$ can be divided into orthogonal components, as shown in Fig. 7. It is obvious to see $B_1 < B_1'$. Hence, the bias H_{D} is caused the variation of B_1' to B_1 [10].

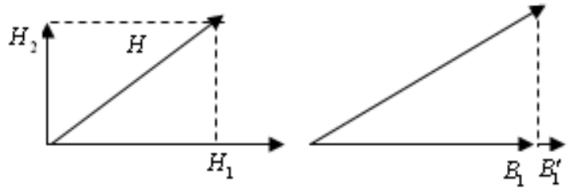

Fig. 7. DC bias field causes $\boldsymbol{B}$ varying

It is clear that the two windings (AC winding and DC winding) are coupled through the tensor of permeability [11]. The DC current changes the $B - H$ curve in the plane into a new one and the magnetic behavior of the core depends on the new characteristics.

Considering the coupling among magnetic moments in the grain-oriented material, the energy E of the magnetic moment in an excitation field with the presence of an orthogonal bias field can be expressed as [12]

$$E = -\mu_0 \left(H_{\parallel} + H_{\perp} + \alpha M \right) , \tag{3}$$

where M is the magnetization, which is determined from both fields (AC flux and DC fluxes), and α is the magnetization coefficient. The resultant direction is not along the direction of the vector sum of the two $\boldsymbol{H}$ fields.

The DC bias field generally reduces the magnetization in the AC flux direction. It is similar to an additional anisotropy along the orthogonal direction [13], and makes a perturbation of the original hysteresis along the excitation field.

When DC bias field is created, an additional anisotropy energy and elastic energy can be effectively calculated and included into the generalized anhysteretic function described previously [5]. The energy E of domains can be described as

$$E = -\mu_0 m(H_{\parallel} + H_{\perp} + \alpha M) + \widetilde{E}_{\mathrm{aniso}} + \widetilde{E}_{\sigma} , \tag{4}$$

where $\widetilde{E}_{\mathrm{aniso}}$ is the anisotropy energy and $\widetilde{E}_{\sigma}$ is the elastic energy.

From minimum energy theory, the magnetic material will get elastic distortion when the magnetization changes, so modeling of domain rotating can be established to analyze the system energy changing. All this phenomena are connected with

magneto mechanical field, which can be described as

$$E_{\text{total}} = E_H + \widetilde{E}_{\text{aniso}} + \widetilde{E_\sigma}\,, \tag{5}$$

where

$$\widetilde{E}_{\text{aniso}} = E_0 + K_1(\cos^2\theta_1\cos^2\theta_2 + \cos^2\theta_2\cos^2\theta_3 + \cos^2\theta_3\cos^2\theta_1)\,, \tag{6}$$

$$E_H = -\mu_0 M_{\text{s}} H(\cos\theta_1\cos\phi_1 + \cos\theta_2\cos\phi_2 + \cos\theta_3\cos\phi_3)\,, \tag{7}$$

$$\begin{aligned}\widetilde{E}_\sigma = {} & -\frac{3}{2}\lambda_{100}\sigma(\cos^2\theta_1\cos^2\beta_1 + \cos^2\theta_2\cos^2\beta_2 + \cos^2\theta_3\cos^2\beta_3) - \\ & - \lambda_{111}\sigma(\cos\theta_1\cos\theta_2\cos\beta_1\cos\beta_2 + \cos\theta_2\cos\theta_3\cos\beta_2\cos\beta_3 + \\ & + \cos\theta_3\cos\theta_1\cos\beta_3\cos\beta_1)\end{aligned} \tag{8}$$

and

$$\overline{\mu_{ij}} = \frac{1}{8\pi^2}\int_0^\pi\int_0^{2\pi}\int_0^{2\pi}\mu_{ij}(\theta,\varphi,\psi)\sin\theta\,\mathrm{d}\psi\,\mathrm{d}\varphi\,\mathrm{d}\theta\,. \tag{9}$$

Here, E_H is the exciting field energy, θ_1, ϕ_1, β_1 are the angles between M, H, effective strain force and grain axial direction, respectively.

The magnetization equation now can be applied to calculate the above problem. After incorporation of the anisotropic and anhysteretic magnetization $\mathrm{M}_{\text{aniso}}$, the magnetization curves can be calculated as the following functions:

$$\frac{\mathrm{d}M}{\mathrm{d}H} = (1-c)\frac{M_{\text{an}} - M_{\text{irr}}}{k\delta - \alpha(M_{\text{an}} - M_{\text{irr}})} + c\frac{\mathrm{d}M_{\text{an}}}{\mathrm{d}H}$$

$$B_z = \frac{\mu_0 M_{\text{sat}} H_z}{\sqrt{(H_z)^2 + (H_\varphi)^2}} + \mu_0 H_z\,. \tag{10}$$

The relationship between M and H is given by "shearing" $M - H$ curves under different DC current biases through computer simulation.

Once the magnetization is obtained, the effective core permeability μ_{eff} may be found. Subsequently, the core inductance L can be obtained from the following approximate expression:

$$L \approx \frac{\mu_{\text{eff}} N_{\text{a}}^2 \pi(D^2 - d^2)}{4l}\,, \tag{11}$$

where N_{a} are the turns of the main coil, l is the core length, D and d are the out diameter and the inner diameter of the cylinder iron core, respectively.

A prototype of the proposed three-phase controllable reactor is fabricated, as shown in Fig. 8.

The overall size of the reactor is $600 \times 450 \times 500\,\text{mm}$. The reactor body includes up yoke, down yoke and center limbs between the yokes. Each limb consists of 5

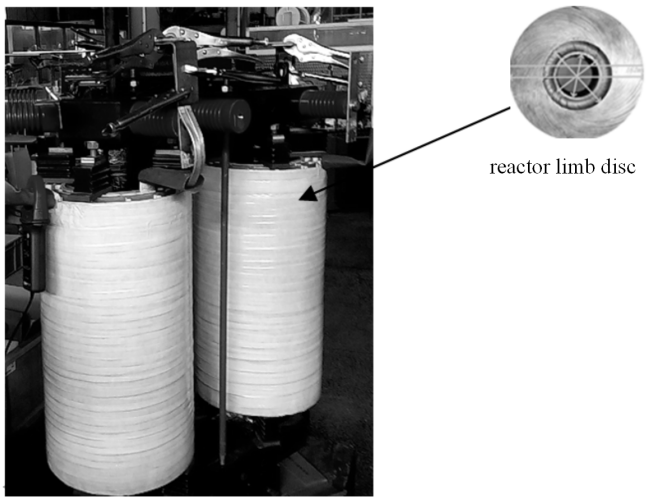

Fig. 8. Three-phase controllable reactor

control discs with outer diameter 160 mm and inner diameter 50 mm. The limb cylinder is with the parameters: $l = 250$ mm, $N_{\mathrm{a}} = 250$ mm and $N_{\mathrm{d}} = 100$ mm.

The prototype was investigated experimentally. The DC bias currents are adjusted to generate 0, 100, 200, 400 A/m orthogonal bias fields, separately. The effective inductance values of the prototype are shown in Fig. 9. It is obvious that the change of DC bias indeed leads to a change of the inductance value.

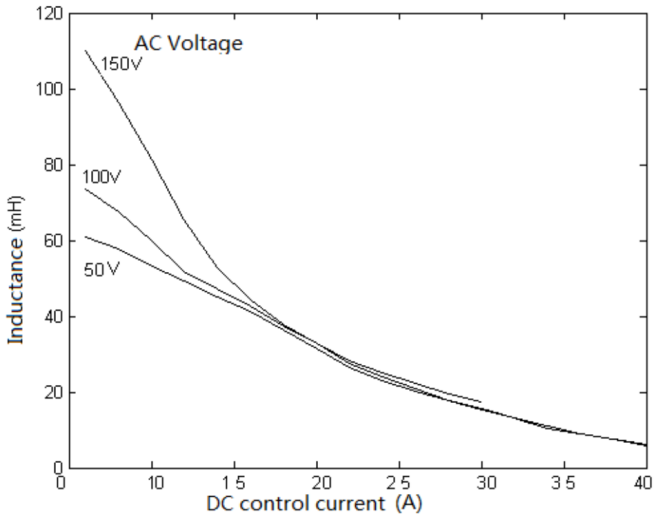

Fig. 9. Control characteristic of the reactor

In order to investigate the relationship between the orthogonal bias current and

the harmonic content, a further experiment was performed. When maintaining the main AC voltage 70 V and varying the orthogonal DC bias current from 0 A to 10 A, the work currents corresponding to different DC bias are gained. The corresponding harmonic analysis shows that with the increasing of the orthogonal bias current, the harmonic contents of the main current are relatively stable. This can be explained very well by the analysis above. The result indicates that variation of the orthogonal bias field does not only change the inductance, but may also lead to a good linearity of the inductance. It is a direction to develop a high quality controllable reactor [14].

4. Conclusion

Based on the quadrature magnetization, the three-phase controllable reactor can adjust the three-phase inductance under the influence of the DC bias current. The advantages of the new controllable reactor include:

1) Realization of the electrical insulation between AC voltage and DC control circuit to ensure the safety of the reactor, when using EVH or interference.

2) Three phase inductance can be adjusted at the same time, which secures balance of interests of the power grid and three-phase load change;

3) Low harmonics can adjust the three-phase inductance, and the current drives the corresponding iron core bias, which is much lower than the saturation point of the magnetic group". The advantage of low harmonic content is the reaction of high quality.

4) The magnetization mechanism can be described as changing the anisotropic magnetic field from the bias magnetic field, thereby providing additional energy for the anisotropy of the nucleus, thereby changing the effective permeability.

5) The new three-phase controllable reactor can be used for filtering or reactive power compensation.

References

[1] S. Sadtler, B. Laube, A. Lasub, A. Nicke, H. Betz, G. Schmalzing: *A basic cluster determines topology of the cytoplasmic M3-M4 loop of the glycine receptor alpha1 subunit.* Journal of Biological Chemistry *278* (2003), No. 19, 16782–16790.

[2] S. F. Shen, Y. J. Tang, L. Ren, Z. H. Wang: *Electromagnetic calculation of a 35 kV/3.5 MVA single-phase HTS controllable reactor with field–circuit coupled-FEM.* IEEE Transactions on Applied Superconductivity *26* (2016), No. 7, Article Sequence Number 5603305.

[3] G. Sutter, L. Faure, A. Molinari, N. Ranc, V. Pina: *An experimental technique for the measurement of temperature fields for the orthogonal cutting in high speed machining.* International Journal of Machine Tools and Manufacture *43* (2003), No. 7, 671–678.

[4] X. Chen, B. Chen, C. Tian, J. Yuan, Y. Liu: *Modeling and harmonic optimization of a two-stage saturable magnetically controlled reactor for an arc suppression coil.* IEEE Transactions on Industrial Electronics *59* (2012), No. 7, 2824–2831.

[5] Y. Wang, S. Zhang, G. Chen: *A novel continuously adjustable magnetic-valve controllable reactor and its modeling.* IEEE International Power Electronics and Motion

Control Conference,2–5 June 2012, Harbin, China, IEEE Conference Publications *1* (2012), 77–80.

[6] J. F. Hoburg, J. R. Melcher: *Internal electrohydrodynamic instability and mixing of fluids with orthogonal field and conductivity gradients.* Journal of Fluid Mechanics *73* (1976), No. 2, 333–351.

[7] Q. Yu, X. Wang, Y. Cheng: *Electromagnetic modeling and analysis of can effect of a canned induction electrical machine.* IEEE Transactions on Energy Conversion *31* (2016), No. 4, 1471–1478.

[8] M. S. Misrikhanov, A. O. Mirzzabdullaev: *Analysis of the reasons for accidents and of protective measures against induced voltage on aerial electrical transmission lines.* Power Technology and Engineering *43* (2009), No. 1, 54–59.

[9] R. P. Verma, W. Z. Fam: *Theory and performance of parametric transformers.* IEEE Transactions on Power Apparatus and Systems *PAS-91* (1972), No. 6, 2494–2504.

[10] J. H. Citriniti, W. K. George: *Reconstruction of global velocity field on the axisymmetric mixing layer utilizing proper orthogonal decomposition.* Journal of Fluid Mechanics *418*, (2000), 137–166.

[11] T. Xu, J. T. Goldbach, T. P. Russell: *Sequential, orthogonal fields: A path to long-range, 3-D order in block copolymer thin films.* Macromolecules *36* (2003), No. 19, 7296–7300.

[12] C. Dinc, I. Lazoglu, A. Serpenguzel: *Analysis of thermal fields in orthogonal machining with infrared imaging.* Journal of Materials Processing Technology *198* (2008), Nos. 1–3, 147–154.

[13] T. Sondergaard, P. F. J. Lermusiaux: *Data assimilation with gaussian mixture models using the dynamically orthogonal field equations. Part II: Applications.* American Meteorological Society, Monthly Weather Review *141*, (2013), No. 6, 1761–1785.

[14] Z. H. Wang, Y. J. Tang, L. Ren, S. Yan, Z. G. Yang, Y. Xu, C. Zhang: *Development of a new type of HTS controllable reactor with orthogonally configured core.* IEEE Transactions on Applied Superconductivity *27* (2017), No. 4, Article Sequence Number 5000205.

Received September 19, 2017

Acta Technica 62 No. 2B/2017, 513–522

Application analysis of Diffusion magnetic resonance imaging in the diagnosis of prostate cancer

Hao Lei[1,2], Gao Yuehua[1,2,3]

Abstract. The surrounding environment of human survival was polluted and damaged to a great extent, and the living habits and eating habits were changing, which caused a rise in the incidence of serious diseases. Cancer was one of the major diseases. The diagnosis of cancer was of great importance. This study was mainly focused on the new technique of magnetic resonance diffusion imaging in the diagnosis of prostate cancer. The theories were summarized and perfected, and were applied to the actual case study, which can provide theoretical basis and scientific support for the application and popularization of cancer diagnosis technology.

Key words. Magnetic resonance imaging, diffusion imaging, prostate, diagnostic techniques.

1. Introduction

With the development of the times, people's living standard has been improved and all kinds of new technologies were emerging. The emergence of new technology brought more convenience to people, but also brought a lot of trouble. The destruction of the environment was a threat to human health because of the pollution of the environment. Among them, cancer has begun to have an increasing trend year by year in today's era [1]. For example, the leakage of nuclear material caused skin cancer and other cancers. The combustion of various fuels created a greenhouse effect, which caused the atmosphere to become empty, thereby increasing the amount of ultraviolet radiation, which led to an increase in the incidence of skin cancer. In recent years, the pollution caused by industrial pollution haze around caused lung cancer and other cancers has been an outbreak of the trend. Cancer was known as a malignant tumor, including more than 100 types of cancer. The tumor cells in the body were activated under the influence of some external factors, thus forming the rapidly growing tumor cells. There was a great difference between tumor cells

[1]College of Electronic Information Engineering, Hebei University, 071002, China
[2]Key Laboratory of Digital Medical Engineering of Hebei Province, Baoding, 071002, China
[2]Corresponding author

and other cells, and it was a kind of apoptosis gene [2]. Because of the rapid growth rate and the lack of apoptosis, tumor cells can cause damage to the surrounding tissues and organs. With the increase of tumor cells, they caused the related tissue and cell swelling, resulting in tissue and organ stress. Malignant tumor cells will be separated from the original tissue into the body environment, and they spread from the original tissue to other tissues or organs in the internal environment through the tissue fluid circulation, which caused the whole body damage, and even cause human death [3].

This study focused on prostate cancer as the main research object. Prostate cancer was one of the most common malignant tumors in male patients. According to statistics, prostate cancer was after lung cancer in all the incidence of cancer [4]. There were many factors that led to prostate cancer, which were affected by many factors, such as the body's own heredity and so on. With the improvement of people's living standard in recent years, more and more people eat more pickled foods, and because of the bad habit of smoking in men's living habits, the incidence of prostate cancer has been rising in recent years. Because of the continuous improvement of medical technology, people's medical detection technology has been used in the monitoring of tumor. Therefore, the current data showed that the incidence of prostate cancer in men was increasing with the development of the age [5]. The increasing incidence of prostate cancer has begun to attract the attention of many scholars. A number of disease detection techniques and theories have been used to detect prostate cancer. Moreover, there was a lot of theoretical analysis on the mechanism of related diseases. Through the analysis of the relevant data, we can determine the pathogenesis and the related gene expression level. On the basis of a large amount of data, the pathogenesis can be analyzed to determine and activated genes in cancer cells, which provided a theoretical basis for the treatment of prostate cancer, and provided scientific support for the supplement and improvement of the theory. This study was mainly to study the diagnostic methods of prostate cancer, and many methods are used in the diagnosis of prostate cancer. The method of magnetic resonance diffusion imaging was selected and the related theory and application were analyzed in this paper so as to provide theoretical basis for the improvement of the theory, and to provide theoretical support for the application and analysis of other prostate cancer diagnosis methods.

2. State of the art

2.1. Research status of prostate cancer at home and abroad

Prostate cancer was one of the most common malignant tumors in men, and it showed a rising trend with age. The overall incidence of prostate cancer increased year by year due to changes in people's eating habits and living habits in recent years [6]. There were a lot of studies on the research of prostate cancer, and the research mainly focuses on the data analysis of the incidence of cancer, the pathogenesis of prostate cancer and the detection of related control genes. Based on the pathogenesis of the relevant treatment methods, and with the improvement of human health, the

detection of prostate cancer technology has begun to be used. This study was based on the previous scholars for the relevant theoretical research and summary. Prostate cancer showed a growing trend with age. With the increase of the pathogenesis of prostate cancer in recent years, the early diagnosis of prostate cancer has been greatly developed, and the incidence of prostate cancer was increasing year by year in recent years. However, due to the application of the new technology, the recovery rate of prostate cancer after surgery has also been a certain upward trend, especially in the era of emerging disease diagnosis technology. The recovery rate of patients with prostate cancer was increasing for the effective diagnosis and prevention of prostate cancer.

2.2. Research status of prostate cancer diagnosis technology at home and abroad

At present, the clinical diagnosis of prostate cancer mainly included the extraction of the serum of the examiner and the corresponding prostate cancer specific antigen. The results could be used to determine whether the examiner had prostate cancer. The rectal cavity of the examiner was examined by ultrasonography, and the patient's condition was determined by the results of the examination. The possibility of prostate cancer was analyzed based on the results of microscopic examination in some hospitals. The following will summarize several common methods:

(1) Some specific antigens which were used in the diagnosis of prostate cancer were commonly used in the early diagnosis of prostate cancer. This specific antigen was a glycoprotein that was synthesized from prostate gland cells. The secretion of some lesions in the prostate gland will continue to rise because of prostate cancer. However, due to the low expression level of tumor cells and the degree of specificity was relatively low, only the antigen with high specificity can be identified and combined with it so as to enhance the possibility of fusion between antigen and antibody. In view of these characteristics, the advantage of specific antigen recognition ability can be played to identify the relevant regional lesions of secretion, which can make the fusion and lesions secretions better, and the fluorescence quantitative analysis was performed by fusion results. The final outcome of the quantitative analysis of fluorescence was used to determine whether prostate cancer had occurred. This method can effectively reduce the subjective factors in the diagnosis process, and the objective result analysis can make the diagnosis result more credible and convincing [7].

(2) The method of rectal cavity examination mainly determined the physiological and biochemical indexes of the chamber. The physiological and biochemical components in the tissue fluid were classified and the content was determined through the extraction of some internal environment tissue fluid, and some of the physiological and biochemical indexes related to prostate cancer were compared with the normal concentration. Through the comparison of the results, the relevant mathematical model was used for a comprehensive analysis [8]. According to the results of the final data analysis, the incidence of prostate cancer and the health of the body were evaluated so as to achieve the purpose of diagnosis of prostate cancer. This method had a more objective credibility. However, when the physiological and biochemical

indexes were measured, it may have a certain degree of impact on the final results due to the influence of physiological and biochemical parameters on the extraction and determination of the relevant steps, which may lead to bias in the results of the analysis.

(3) Rectal examination. The doctors examined the rectum by means of a microscope and conducted prediction and diagnosis of prostate cancer incidence by number and size of lesions. This method was easy to operate. Although the disease can be predicted and diagnosed according to the related lesions, the diagnosis of prostate cancer was influenced by the subjective consciousness of the doctors by using this method, which may have some influence on the diagnosis results.

(4) Application of other technologies. Now, with the development of medical technology, more and more new technologies have begun to be applied in the diagnosis of prostate cancer. A combination of imaging theory and prostate cancer diagnosis techniques has led to the widespread use of imaging diagnostic techniques (Fig. 1). Imaging technology was based on the principle that it can be quickly formed according to the density and the formation of the tissue, which played an important role in the diagnosis of prostate cancer and other diseases [9]. Compared with the CT technology, the imaging results are more authentic and reliable, which can be used in the diagnosis of prostate cancer.

Fig. 1. Magnetic resonance diffusion imaging in the diagnosis of diseases

3. Methodology

3.1. Magnetic resonance diffusion imaging technology concept and application status analysis

Magnetic resonance imaging technique can be used to scan the related lesions, and the image data was generated by the chemical fluorescence signal during the scanning process. We can measure the size of the tumor by affecting the data, and we can also study and analyze the different stages of the lesions through the data of the image data so as to determine the development process of the lesions, and ultimately determined the location of the lesions. It can be seen that the research and application of magnetic resonance technology was of epoch-making significance in the diagnosis of prostate cancer. However, the study of prostate cancer in China started late and it cannot form a more systematic research system. Therefore, the diagnosis technology of prostate cancer was still in the basic research stage. For the application of magnetic resonance diffusion imaging in the diagnosis of prostate cancer, we had a relatively low awareness of prostate cancer because of the late prostate cancer. When prostate cancer was detected, the patient has entered the advanced stage of cancer, which delayed the best treatment period and indirectly affected the level of treatment of patients so that cannot be better for the patient's recovery and rehabilitation [10]. In order to solve these problems, this paper made a further summary and analysis of the concept of magnetic resonance diffusion imaging, and clearly related to the theory and operation process so as to lay a foundation for the implementation of relevant theory and application in the diagnosis of prostate cancer in China disease areas, which also provided technical support for combination with other diagnostic methods.

3.2. The research process of this study

This experiment was mainly based on the analysis of some relevant information and summary. Information needed to query included not only the domestic and foreign research related to the diagnosis of prostate cancer in technology to query Chinese HowNet system database, and included the relevant aspects of the data. In addition to the data query of the relevant theory, this study also selected the data of the medical records of a hospital to carry on the statistics and analysis of prostate cancer related data. The statistical indicators included the relevant methods used in the early diagnosis of prostate cancer and the related physiological and biochemical indexes and the evaluation criteria [11]. In addition to the data collection and statistics, the article also interviewed some well-known doctors and experts and scholars in order to document their experience with many years and knowledge of the technical aspects of the diagnosis and treatment of prostate cancer. Based on this, some suggestions were put forward to supplement the deficiencies of the above theory so as to better realize the integrity and credibility of the theory and data [12]. The collection process of hospital related cases was as follows:

(1) Collection of clinical data information. This study was conducted to analyze the data of patients with prostate cancer who were admitted to the hospital from

2015 to 2016. Through the inquiry and statistics of all the cases, the examiner's almanac was removed in all of the patients with prostate cancer who were admitted to the hospital and the choice of the examiner was checked, and the statistical analysis of the number of cases and the proportion of the various inspection methods were conducted.

(2) Physical fitness standards for the subjects. Based on the statistical results of the above data, the reasons for the selection of the diagnostic methods were analyzed. On the basis of voluntary examination, a group of people with no heart disease and normal liver and kidney function were selected as the subjects of this study. There were no other diagnostic methods for the diagnosis of the disease, and there was no fracture in the near future (the fixation of the fracture will produce some deviation to the scanning result).

(3) Scanning and analysis of magnetic resonance diffusion imaging. The subjects should be informed of the emptying of the body in advance, and there was no food intake in the application of magnetic resonance diffusion imaging (MRI). Participants needed to keep on lying state table scan in the trial process. Relieve respiratory rhythm can reduce the tension caused by the experimental process. The experimenter should be informed in time to stop the experiment to ensure the safety of the subjects in case of any discomfort and condition. We used a dual gradient whole-body MRI system in this experiment. The operating parameters of the instrument were shown in Table 1.

Table 1. Display of operation parameters of whole body magnetic resonance imaging instrument

Scanning parameters	TR (ms)	TE (ms)	View (FOV cm)	Encouraging times (NEX)	Matrix	Thick layer (mm)	Zeng interval
Numerical value	5250	71–83	28	2.0	128×128	3.5	0.5

Prostate cancer inspection process is shown in Fig. 2.

3.3. Data processing

All the data obtained were conducted statistical processing and the software used included Excel 2007 and SPSS 22. Excel 2007 was mainly used for data statistics and simple data analysis, and SPSS 22 software was used to analyze and deal with the correlation and significance of all the data.

4. Result analysis and discussion

4.1. The concept of magnetic resonance diffusion imaging and its application

People's eating habits and unhealthy living habits caused that the incidence of some diseases of human being was increasing year by year in the current era [13].

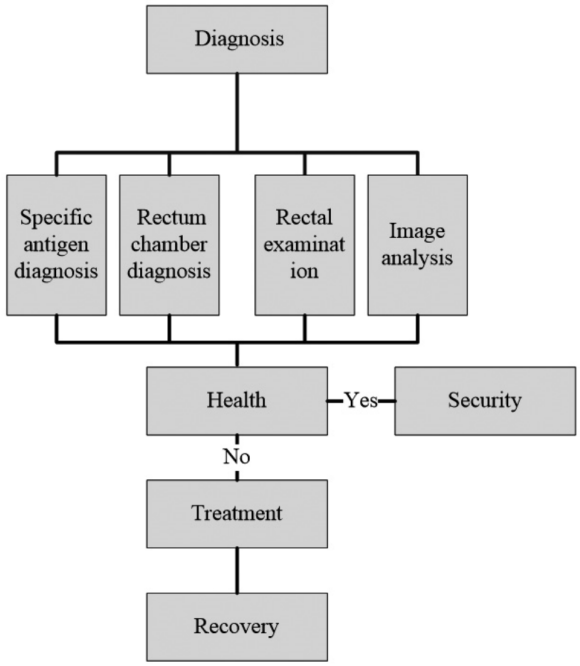

Fig. 2. Summary of prostate cancer diagnosis and treatment process

Human life production caused serious pollution of the living environment, and their genetic causes made that cancer has become a threat to human health and was the main form of disease. And there were experts counted that lung cancer was the first cancer incidence in the outbreak of cancer. Prostate cancer was the most common form of cancer that has the highest incidence except lung cancer for men. Because of some of the characteristics of cancer cells, the treatment of cancer has not been able to prevent the spread of cancer cells from cancer so that the treatment of cancer has shown poor results. The disease still needed to be taken from its source for cancer, and the diagnosis of cancer also played an important role in the treatment of cancer. The disease can be found earlier through the diagnosis and the earlier findings for the treatment of late cancer was also better [14]. The diagnosis of cancer has remained on the basis of technology for a long time. However, it has been proved by practice that the basic diagnostic techniques had some disadvantages, so the reliability of diagnosis results was not high. This study was focused on the diagnosis and application of diffusion tensor imaging (DWI) in the diagnosis of prostate cancer. Diffusion magnetic resonance imaging (MRI) was mainly used to scan the blood flow of the lesion tissue through the relevant data query and statistics, and its velocity and other changes were analyzed to generate a kind of image data finally. We can diagnose the presence of prostate cancer by analyzing the image data. The method had the advantages of high sensitivity, and overcame the problems of the traditional influence of imaging detection technology such as the signal intensity was too strong or too weak. At the same time, the advantages of non-invasive and non-

ionizing radiation accelerated the application and popularization of this technique in diagnosis [15].

4.2. Application of magnetic resonance diffusion imaging in the diagnosis of prostate cancer

62 patients with prostate cancer were examined by magnetic resonance diffusion imaging. It can be seen that a total of 35 patients with prostate cancer were found and a total of 27 cases with hyperplasia. The results checked are shown in Table 2.

Table 2. Analysis of magnetic resonance diffusion imaging

	Incidence of disease	Number of cases	Place of occurrence	Number of cases
Magnetic resonance diffusion imaging	Prostatic cancer, Benign prostatic hyperplasia, Incidence of disease prostatic cancer	35	Peripheral zone	19
			Central gland	12
			Peripheral and central gland involvement	4
			Extracapsular spread	5
			Distant metastasis	2
	Benign prostatic hyperplasia	27		27
	Total	62		62

4.3. Analysis of ADC and MRS values in prostate cancer

In order to better determine the incidence and the incidence of prostate cancer in all subjects, the present study was performed to investigate the actual situation of the lesion. The ADC value and MRS value of the lesions were analyzed by magnetic resonance diffusion imaging software. SPSS 22 was used to analyze all the data. The results of data analysis were shown in Table 3 and Table 4. The results showed that there was a significant difference between the ADC value and MRS value in the cancer and non-cancerous regions ($P<0.001$), which passed to test and the t values were higher. Thus the results were of great reliability. Therefore, magnetic resonance diffusion imaging can be applied to the diagnosis of prostate cancer, and its application had a greater degree of credibility.

Table 3. ADC value of cancer and non-cancer

Partition	Number of cases	Average value	T value	P value
Cancer area	35	0.47±0.17	15.833	0.000
Non-cancerous area	27	1.09±0.25	-	-

Table 4. MRS value of cancer and non-cancer

Partition	Number of cases	Average value	T value	P value
Cancer area	35	1.64±0.63	11.826	0.000
Non-cancerous area	27	0.61±0.28	-	-

5. Conclusion

With the continuous improvement of the production and living standards, the surrounding environment of human being has been affected to a great extent. And because of the impact of different physical fitness, unhealthy habits and eating habits even caused a number of disease incidence increased. Taking the prostate cancer as a research object, the concept and definition of magnetic resonance diffusion imaging diagnostic techniques were summarized in this study and a clear theory of MR diffusion imaging was established finally. And the study made this technique used in the application of prostate cancer diagnosed, which provided a theoretical basis and scientific support for the popularization and application of new technology in the diagnosis of prostate cancer, and laid a theoretical foundation for the introduction of new diagnostic techniques in other cancers.

References

[1] S. D. Forman, J. D. Cohen, M. Fitzgerald, W. F. Eddy, M. A. Mintun, D. C. Noll: *Improved assessment of significant activation in Functional Magnetic Resonance Imaging (FMRI): Use of a cluster-size threshold.* Magnetic Resonance in Medicine *33* (1995), No. TOC5, 636–647.

[2] M. A. Al-Ghazo, I. F. Ghalayini, I. I. Matalka: *Ultrasound-guided transrectal extended prostate biopsy: A prospective study.* Asian Journal Androl *7* (2005), No. 2, 165–169.

[3] N. Morakkabati-Spitz, P. J. Bastian, J. Gieseke, F. Träber, C. K. Kuhl, N. P. Wattjes, S. C. Müller, H. H. Schild: *MR imaging of the prostate at 3.0T with external phased array coil - preliminary results.* European Journal of Medical Research *13* (2008), No. 6, 287–291.

[4] K. J. Macura: *Multiparametric magnetic resonance imaging of the prostate: Current status in prostate cancer detection, localization, and staging.* Seminars in Roentgenology *43* (2008), No. 4, 303–311.

[5] Y. J. Choi, J. K. Kim, N. Kim, K. W. Kim, E. K. Choi, K. S. Cho: *Functional MR imaging of prostate cancer.* Radiographics *27* (2007), No. 1, 63–75.

[6] D. M. Cornfeld, J. C. Weinreb: *MR imaging of the prostate: 1.5T versus 3T.* Magnetic Resonance Imaging Clinics of North America *15* (2007), No. 3, 433–448.

[7] J. K. Kim, S. S. Hong, Y. J. Choi, S. H. Park, H. Ahn, C. S. Kim, K. S. Cho: *Wash-in rate on the basis of dynamic contrast-enhanced MRI: usefulness for prostate cancer detection and localization.* Journal of Magnetic Resonance Imaging *22* (2005), No. 5, 639–646.

[8] G. M. Villeirs, W. Oosterlinck, E. Vanherreweghe, G. O. de Meerleer: *A qualitative approach to combined magnetic resonance imaging and spectroscopy in the diagnosis of prostate cancer.* European Journal of Radiology *73* (2010), No. 2, 352–356.

[9] K. Kitajima, Y. Kaji, Y. Fukabori, K. Yoshida, N. Suganuma, K. Sugimura: *Prostate cancer detection with 3T MRI: Comparison of diffusion-weighted imaging and*

dynamic contrast-enhanced MRI in combination with T2-weighted imaging. Journal of Magnetic Resonance Imaging *31* (2010), No. 3, 625–631.

[10] M. A. Haider, T. H. van der Kwast, J. Tanguay, A. J. Evans, A. T. Hashmi, G. Lockwood, J. Trachtenberg: *Combined T2-weighted and diffusion-weighted MRI for localization of prostate cancer.* American Journal of Roentgenology *189*, (2007), No. 2, 323–328.

[11] M. D. Fox, M. E. Raichle: *Spontaneous fluctuations in brain activity observed with functional magnetic resonance imaging.* Nature Reviews Neuroscience *8* (2007), No. 9, 700–711.

[12] P. Kozlowski, S. D. Chang, R. Meng, B. Mädler, R. Bell, E. C. Jones, S. L. Goldenberg: *Combined prostate diffusion tensor imaging and dynamic contrast enhanced MRI at 3T–quantitative correlation with biopsy.* Journal of Magnetic Resonance Imaging *28* (2010), No. 5, 621–628.

[13] S. M. Noworolski, D. B. Vigneron, A. P. Chen, J. Kurhanewicz: *Dynamic contrast-enhanced MRI and MR diffusion imaging to distinguish between glandular and stromal prostatic tissues.* Journal of Magnetic Resonance Imaging *26*, (2008), No. 8, 1071–1080.

[14] S. A. Reinsberg, G. S. Payne, S. F. Riches, S. Ashley, J. M. Brewster, V. A. Morgan, N. M. de Souza: *Combined use of diffusion-weighted MRI and 1H MR spectroscopy to increase accuracy in prostate cancer detection.* American Journal of Roentgenology *188* (2007), No. 1, 91–98.

[15] J. Kurhanewicz, M. G. Swanson, S. J. Nelson, D. B. Vigneron: *Combined magnetic resonance imaging and spectroscopic imaging approach to molecular imaging of prostate cancer.* Journal of Magnetic Resonance Imaging *16* (2002), No. 4, 451–463.

Received September 19, 2017

Acta Technica *62* No. 2B/2017, 523–532

Motion rehabilitation detection system based on artificial fish swarm intelligent algorithm

Ma Chao[1], Zhang Henan[1], Wu Dongmin[2]

Abstract. The motion rehabilitation system based on artificial fish swarm intelligence algorithm has a positive impact on the recovery of motor function in patients with disabilities. In order to better apply this detection system to the clinical treatment of disabled patients in our country, in this paper, the motion rehabilitation detection system based on artificial fish swarm intelligent algorithm was constructed. Then, the running performance was tested. It is found that the vortex signal frequency obtained by the system is 118.60 Hz, which can effectively collect the weak signals of the sensor, and the control ability of the limbs is improved after the disabled patients use the system. Therefore, the motion rehabilitation detection system is beneficial to the recovery of motor function in patients with disabilities. The purpose of this study is to provide a theoretical basis for the improvement of motion rehabilitation detection system.

Key words. Artificial fish swarm intelligent algorithm, motion rehabilitation, detection system.

1. Introduction

Since the beginning of the new century, medical care has become one of the most important issues affecting social development in the current situation. Diseases such as bone diseases and brain tissue injuries are the main diseases that affect the normal life of the people because of their high incidence and disability in the population. With the rapid development of the society, the improvement of medical level has provided some positive effects on the diagnosis and treatment of some diseases, and has reduced the mortality of patients effectively. However, due to a variety of complications and sequelae, many patients have disabling symptoms in different degree, thus weakening the ability of the self-help movement, and directly or indirectly affecting the normal life and work of patients. The rehabilitation of the damaged nervous system is one of the key links in the later diagnosis and treatment

[1]The National Police University for Criminal justice, Baoding, Hebei, China, 071000
[2]Baoding Vocational and Technical College, Baoding, Hebei, China, 071000

of the disabled. The development of rehabilitation medicine has prompted some techniques for rehabilitation training to be developed and gradually applied to the recovery of neurological deficits in patients with disabilities. However, there are still some problems in the movement rehabilitation training, such as the movement of the therapist and the inaccuracy of the exercise, so that the rehabilitation testing system needs further improvement and development. In view of this situation, the motion rehabilitation detection system based on artificial fish swarm intelligent algorithm was studied in this paper, so as to provide theoretical basis and support for the improvement of motion rehabilitation training mode and theory in China.

2. State of the art

In the process of rapid development of the times, the medical level of the world has also been greatly improved. Although studies have suggested that improvements in medical standards provide technical support for the reduction in mortality from diseases, many patients still suffer from some damage to the nervous system, which weakens their motor function, and then affects their psychological and life [1]. In the 80 s of last century, researchers put forward that the motion rehabilitation testing can be applied in the diagnosis and treatment of some diseases, and can be further developed into an auxiliary means of clinical medical treatment [2]. In 1991, the Massachusetts Institute of Technology designed and developed the world's first rehabilitation equipment for human upper limb rehabilitation exercises, which can collect information about the movements of the upper limbs of the patient and provide visual feedback for the therapist [3]. With the continuous development of science and technology, motion rehabilitation testing system with better algorithms and more sensors has been constantly researched and developed, thus promoting the rehabilitation of patients and increasing the effectiveness of rehabilitation training [4]. However, with the development of motion rehabilitation testing system, many researchers gradually realized that the detection of the weak feedback signals from sensors can have a positive impact on the improvement of the motion rehabilitation system. Under this demand, due to the strong adaptability, artificial fish swarm intelligent algorithm is gradually combined with the traditional motion rehabilitation system, and has achieved great development [5].

3. Methodology

3.1. Motion rehabilitation detection system

Under the development of our national economy, unhealthy lifestyles affect people's normal production and life directly or indirectly, thus causing damage to the nerve center of the body movement and causing frequent diseases [6]. Although the medical level of our country has improved in the development of the times, and the cure rate of the national disease has also improved, the related diseases and complications may cause the rise of our national physical disability rate [7]. China's motion

rehabilitation field has made great progress and development. However, compared with the developed countries in the west, China's relative theories and techniques are still relatively backward, and most of the studies are only in the initial stage, and thus are in lack of mature practical application of theory and products. Nowadays, many colleges and universities in China have developed a multifunctional rehabilitation system for motion rehabilitation to interact with a variety of secondary modes. These related systems can detect the state of the user in real time, and improve the structure of the system, so that it can be more effective in practical clinical applications. In addition, it provides some technical support for some patients to recover their normal body through the auxiliary training of motion rehabilitation system in a more efficient manner (Fig. 1).

Fig. 1. Clinical application of motion rehabilitation test system

3.2. Artificial fish swarm intelligent algorithm

The motion rehabilitation testing system has been developed greatly, and has provided a clinical auxiliary role for the recovery of motor function in the disabled population. However, in the process of studying the related system, the collection of the weak signals of the system sensors and the understanding of the causes of the system have become the most important parts in the motion rehabilitation testing system [8]. In the course of mechanical operation, the stochastic resonance among the links may cause noise pollution to the weak signals of sensors [9]. Therefore, in practical applications, only by further improving the relevant algorithm of the system operation can the resonance problem among the mechanical links be effectively controlled, so as to provide scientific support for the accurate operation of the whole motion rehabilitation system. Therefore, in this demand, a large number of algorithm models have been studied and applied to the rehabilitation of clinical patients in our country. As a new and scientific intelligent algorithm theory (Fig. , 2), artificial fish swarm algorithm provides some ideas and methods for solving the

problem of resonance in mechanical operation [10]. In this study, by reading relevant literature, the related theories of artificial fish swarm intelligent algorithm were summarized. The algorithm, derived from the observations of Li Xiaolei and others on the foraging behavior, clustering and pursuit of fish stocks, is the type of algorithm that can obtain the best purpose according to the related behavior. Compared with the traditional genetic algorithm, the artificial fish swarm intelligent algorithm can more easily and quickly optimize the local extremum [11]. Since the artificial fish swarm intelligent algorithm can select the best factor from various factors, its optimization function is usually expressed as follows: the x and y in the function represent the main influencing factors of the project respectively. And its specific algorithm steps are detailed as follows:

(1) The establishment of related parameters of fish stocks includes the scale of fish, the number of iterations, the range of perception, the maximum moving distance of fish stocks and the crowding degree of fish stocks.

(2) In the set of parameters, a certain number of fish are selected randomly and defined as the initial fish group of the algorithm.

(3) The concentration of food consumed by fish stocks is used as the objective function of fish swarm algorithm, and the optimal value is calculated and defined as the announcement value.

(4) The best behavior strategy is select by calculating the rear end collision and swarm behavior of fish stocks. The optimal behavior strategy is defined as the movement strategy of fish, and the foraging behavior of fish is defined as the default behavior. And according to these parameters, the optimal target parameters of each fish are calculated and compared with the announcement value:

$$Maxf(x,y) = \sin\sqrt{(x-10)^2+(y-10)^2}/\sqrt{(\overline{x}-10)^2+(\overline{y}-10)^2}\,. \tag{1}$$

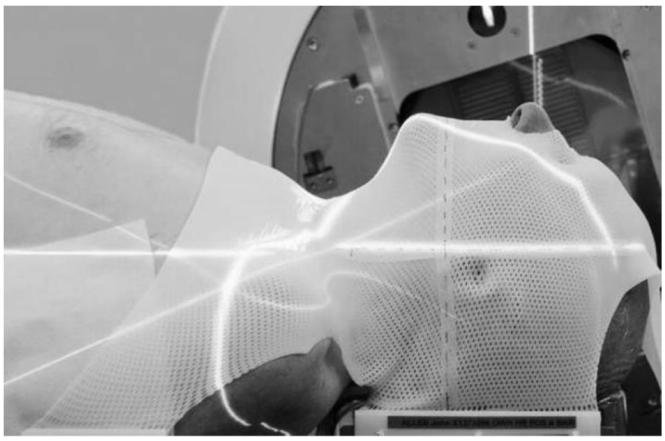

Fig. 2. Application of artificial fish swarm intelligent algorithm in motion rehabilitation detection system

3.3. Development of motion rehabilitation detection system based on artificial fish swarm intelligent algorithm

On the basis of fully understanding the related theories, the motion rehabilitation detection system based on artificial fish swarm intelligent algorithm was developed and constructed. In the process of building the system, the visual programming tool of Lab VIEW was introduced, and the design of the rehabilitation system was carried out, the operation mode of which was mainly accomplished by the mixed programming methods of Lab VIEW and MATLAB. Then, artificial fish swarm intelligent algorithm was embedded into the system, and then a motion rehabilitation detection system suitable for this study was built, providing the research foundation for the subsequent rehabilitation training. Therefore, on the basis of understanding the relevant theories, first of all, the motion rehabilitation testing system involved in this study was constructed. Then, artificial fish swarm intelligent algorithm was introduced into the system, thus providing theoretical support for the rational rehabilitation scheme of the later treatment [12]. Then, in the design of the motion rehabilitation system, the mixed programming mode of Lab, VIEW and MATLAB was mainly used. Only by combining the two programming methods can the optimization process of artificial fish swarm intelligent algorithm mentioned in this study be more efficient [13]. Thus, the whole movement rehabilitation system can be in a relatively stable running state, so as to further promote the whole system to intelligently detect the weak signals emitted by the sensors, and provide certain technical support for the accurate collection of the patient's rehabilitation data [14]. Part of the program diagram of the motion rehabilitation system based on artificial fish swarm intelligent algorithm developed in this research is shown in Fig. 3. The performance parameters of the whole motion rehabilitation system are shown in Table 1. Then, the performance of the system was evaluated and analyzed.

Table 1. Summary of the performance parameters of the motion rehabilitation test system designed in this paper

Parameter name	Function	Numerical value
Working space	Translation	Φ160×110 mm
	Rotate	240×140×180 deg
	Grab	25 mm
Freedom	Translation	3
	Rotate	3
	Grab	1
Power	Sustaining power	12.0 N
	Grasping force	±8.0 N
Resolving power	Linear displacement	<0.01 mm
	Angle	0.09 deg
	Grab	0.006 mm
Interface	Standard	USB2.0
	Refresh frequency	Up to 8 kHz

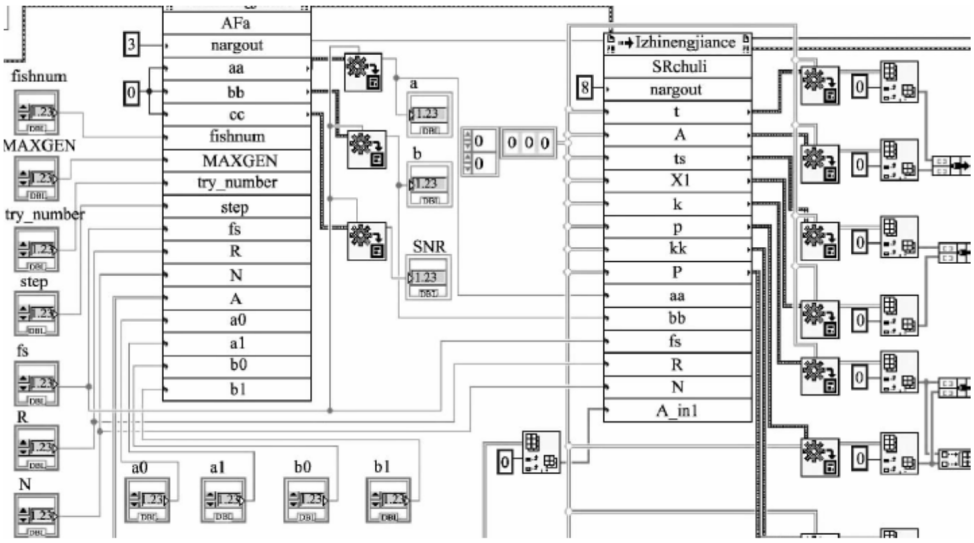

Fig. 3. Part of the program diagram of the motion rehabilitation system based on artificial fish swarm intelligent algorithm

4. Result analysis and discussion

4.1. The test of motion rehabilitation detection system based on artificial fish swarm intelligent algorithm

The motion rehabilitation system based on artificial fish swarm intelligent algorithm is mainly divided into two parts: the test of the system itself and the test of its application effect. All aspects of testing indicators and procedures are described below:

(1) Test of vortex signal Vortex signal is mainly used in the measurement of system running flow. In traditional algorithms, vortex signals in the process of running a motion rehabilitation system may be disturbed due to the irrationality of some links. And the result of the test is low, and even unable to obtain the relevant data, so that the system's detection results can't be timely fed back to the user, thus affecting the normal use of motion rehabilitation detection system [15]. In this study, the related parameters of artificial fish swarm intelligent algorithm were set up, the collection of vortex signals was analyzed, and then the feasibility of this algorithm in rehabilitation system is confirmed.

(2) Application test of motion rehabilitation test system The performance of the motion rehabilitation system based on the artificial fish swarm intelligent algorithm is not only reflected in the operation of the system itself, and it is also necessary to evaluate the effect of motion rehabilitation objectively, and evaluate the effectiveness of the algorithm from the practical point of view. In this study, two patients with upper limb hemiplegia were taken as an example, and relevant data of catching movements at different stages was collected after applying the motion rehabilitation

detection system based on artificial fish swarm intelligent algorithm. And then, the kinematics indexes such as the upper limb rate and the whole motion smoothness were evaluated. Thus, the application effect of the detection system was illustrated. The formulas for calculating the speed and the smoothness of the whole motion are as follows:

$$v = \frac{S}{t}\,, \tag{2}$$

where v represents the rate at which upper limbs move, S represents the trajectory displacement of motion and t stands for the exercise time. Further

$$NJS = \sqrt{\frac{1}{2}\int \left(\left(\frac{\mathrm{d}^3x}{\mathrm{d}t^3}\right)^2 + \left(\frac{\mathrm{d}^3y}{\mathrm{d}t^3}\right)^2 + \left(\frac{\mathrm{d}^3z}{\mathrm{d}t^3}\right)^2\right)\mathrm{d}t\left(\frac{t^3}{S^2}\right)}\,, \tag{3}$$

where NJS represents the overall smoothness of the limbs, x, y, z represent the coordinates of the limb movements obtained by the sensors, S represents the trajectory displacement of motion and t stands for the exercise time.

4.2. Detection results of vortex signals in motion rehabilitation system based on artificial fish swarm intelligent algorithm

On the basis of the design of the system, it is necessary to evaluate and analyze the performance of the system further, so as to determine the feasibility and accuracy of the system. As one of the important parameters in the operation of the whole system, traffic flow effectively reflects the data information collected by the sensors in the whole system and the efficiency of the transmission. And the vortex flowmeter provides technical support for accurate flow measurement. Therefore, in order to better determine the performance of the motion rehabilitation detection system based on artificial fish swarm intelligent algorithm designed in this paper, the vortex signal collected by vortex flow meter is detected during the operation of the system. The parameters of the designed rehabilitation system are as follows: the number of system runs is 100 times, the system detection displacement is 0.1, the system perception of distance Visual is 2.5, and the number of system iterations is 50 times. Then, the system runs, and the vortex signal frequency is 118.60 Hz, which proves that the artificial fish swarm algorithm can effectively achieve the collection of weak signals.

4.3. Test results of motion rehabilitation system based on artificial fish swarm intelligent algorithm

The ultimate goal of the motion rehabilitation detection system of artificial fish swarm intelligent algorithm is to apply it to the actual rehabilitation of patients. Therefore, two disabled patients were included in the study, the catching movements of patients before and after applying the motion rehabilitation detection system were mainly used as evaluation actions, and the moving speed and the smoothness of the

whole movement were tested. The rate of movement of the patient before and after applying the rehabilitation system is shown in Fig. 4. The results show that the motion rehabilitation system based on artificial fish swarm intelligent algorithm has certain influence on patient movement rate. After using the system, the rate of catching movement of the two patients tended to be relatively stable, indicating that the patient's ability to control the body was stronger after the use of the motion rehabilitation test system.

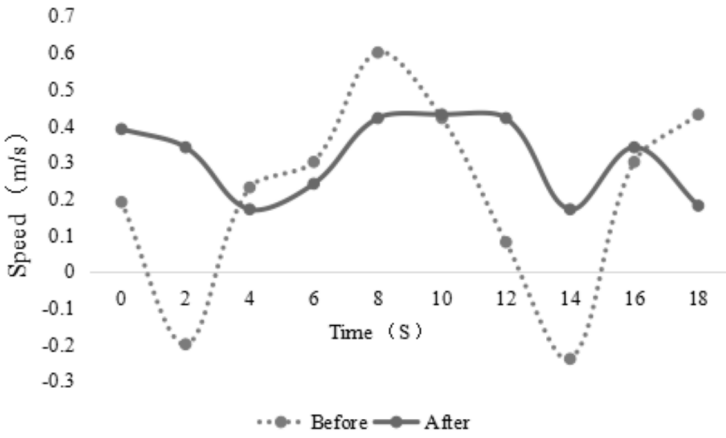

Fig. 4. Changes of catching movement before and after training

Furthermore, the number of catch, the quality and time of the grasping object after the rehabilitation treatment were examined, and the formula (2) was used to calculate the smoothness of the patient's movement. The relevant data is shown in Table 2. The results show that with the increase of training time, the catching movement of patients is increasing, and the weight of what the limbs can take is also increasing. Furthermore, the scores of limb movement smoothness are also increased, which shows that the system has a very important positive effect on limb rehabilitation in patients with disabilities, and has practical value.

Table 2. Analysis of the experimental results before and after applying the motion rehabilitation detection system based on artificial fish swarm intelligent algorithm

Catch quantity				Pinch power		
Time	The sixth day	The thirteenth day	The nineteenth days	Time	The twenty-fourth day	The thirty-first day
Catch number	2	5	8	Object weight	0.15 kg	0.45 kg
NJS (points)	13	22	37	NJS (points)	39	53
Brunnstrom	I	I	II	Brunnstrom	II	III

5. Conclusion

With the development of the times, more diseases have further affected people's normal life and production. However, with the improvement of the medical level, although the cure rate of disease has increased, complications after disease treatment may cause people physical disability, and directly or indirectly affect the development of the whole society. As a supplementary means of limb rehabilitation, the rehabilitation test system has a positive effect on the recovery of the motor function of the disabled patients. Artificial fish swarm intelligent algorithm, as a perfect algorithm of motion rehabilitation system, can select the best parameters from the system and provide some data support for the patient's rehabilitation training. In this study, based on the understanding of the relevant theories, the motion rehabilitation detection system based on artificial fish swarm intelligent algorithm was constructed, and the operation performance and the effect of the patients were analyzed. The results show that the system has a positive effect on the rehabilitation of disabled patients. However, due to the limitations of the theoretical level, there are still some shortcomings in the study, but the study can still provide a reference for follow-up research.

References

[1] V. Malmo, B. M. Nes, B. H. Amundsen, A. E. Tjonna, A. Stoylen, O. Rossvoll, U. Wisloff, J. P. Loennechen: *Aerobic interval training reduces the burden of atrial fibrillation in the short term: randomized trial.* Circulation *133* (2016), No. 5, 466–473.

[2] S. S. Risom, A. D. Zwisler, T. B. Rasmussen, K. L. Sibilitz, T. L. S. Madsen, J. H. Svendsen : *Cardiac rehabilitation versus usual care for patients treated with catheter ablation for atrial fibrillation: Results of the randomized CopenHeartRFA trial.* American Heart Journal *181* (2016), 120–129.

[3] M. Zeren, R. Demir, Z. Yigit, H. N. Gurses: *Effects of inspiratory muscle training on pulmonary function, respiratory muscle strength and functional capacity in patients with atrial fibrillation: A randomized controlled trial.* Clinical Rehabilitation *30* (2016), No. 12, 1165–1174.

[4] I. Frederix, D. Hansen, K. Coninx, P. Vandervoort, D. Vandijck, N. Hens, E. van Craenenbroeck, N. van Driessche, P. Dendale: *Effect of comprehen-*

sive cardiac telerehabilitation on one-year cardiovascular rehospitalization rate, medical costs and quality of life: A cost-effectiveness analysis. European Journal of Preventive Cardiology *23* (2016), No. 7, 674–682.

[5] J. Y. Kim, S. J. Lee, J. H. Kim, C. M. Choi, S. R. Yoon, K. I. Jung: *Effects of atrial fibrillation on the outcome of the rehabilitation in patients with cerebral infarction.* Annals of Rehabilitation Medicine *38* (2014), No. 6, 766–774.

[6] S. K. Berg, P. U. PedersenU, A. D. Zwisler, P. Winkel, C. Gluud, B. D. Pedersen, J. H. Svendsen: *Comprehensive cardiac rehabilitation improves outcome for patients with implantable cardioverter defibrillator. Findings from the COPE-ICD randomised clinical trial.* European Journal of Cardiovascular Nursing *14* (2015), No. 1, 34–44.

[7] W. Shen, X. Guo, C. Wu, D. Wu: *Forecasting stock indices using radial basis function neural networks optimized by artificial fish swarm algorithm.* Knowledge-Based Systems *24* (2011), No. 3, 378–385.

[8] N. B. Giacomantonio, S. S. Bredin, H. J. Foulds, D. E. Warburton: *A systematic review of the health benefits of exercise rehabilitation in persons living with atrial fibrillation.* Canadian Journal of Cardiology *29* (2013), No. 4, 483–491.

[9] G. Guyatt, A. D. Oxman, S. Sultan, J. Brozek, P. Glasziou, P. Alonso-Coello, D. Atkins, R. Kunz, V. Montori, R. Jaeschke, D. Rind, P. Dahm, E. A. Akl, J. Meerpohl, G. Vist, E. Berliner, S. Norris, Y. Falck-Ytter, H. J. Schünemann: *GRADE guidelines: 11. Making an overall rating of confidence in effect estimates for a single outcome and for all outcomes.* Journal of Clinical Epidemiology *66* (2013), No. 2, 151–157.

[10] G. H. Guyatt, A. D. Oxman, N. Santesso, M. HelfandM, G. Vist, R. Kunz, J. Brozek, S. Norris, J. Meerpohl, B. Djulbegovic, P. Alonso-Coello, P. N. Post, J. W. Busse, P. Glasziou, R. Christensen, H. J. Schünemann: *GRADE guidelines: 12. Preparing summary of findings tables-binary outcomes.* Journal of Clinical Epidemiology *66*, (2013), No. 2, 158–172.

[11] G. H. Guyatt, K. Thorlund, A. D. Oxman, S. D. Walter, D. Patrick, T. A. Furukawa, B. C. Johnston, P. Karanicolas, E. A. Akl, G. Vist, R. Kunz, J. Brozek, L. L. Kupper, S. L. Martin, J. J. Meerpohl, P. Alonso-Coello, R. Christensen, H. J. Schunemann: *GRADE guidelines: 13. Preparing summary of findings tables and evidence profiles-continuous outcomes.* Journal of Clinical Epidemiology *66* (2013), No. 2, 173–183.

[12] R. A. Mustafa, N. Santesso, J. Brozek, E. A. Akl, S. D. Walter, G. Norman, M. Kulasegaram, R. Christensen, G. H. Guyatt, Y. Falck-Ytter, S. Chang, M. H. Murad, G. E. Vist, T. Lasserson, G. Gartlehner, V. Shukla, X. Sun, C. Whittington, P. N. Post, E. Lang, K. Thaler, I. Kunnamo, H. Alenius, J. J. Meerpohl, A. C. Alba, I. F. Nevis, S. Gentles, M. C. Ethier, A. Carrasco-Labra, R. Khatib, G. Nesrallah, J. Kroft, A. Selk, R. Brignardello-Petersen, H. J. Schünemann: *The GRADE approach is reproducible in assessing the quality of evidence of quantitative evidence syntheses.* Journal of Clinical Epidemiology *66* (2013), No. 7, 736–742.

[13] T. N. Nguyen, S. N. Hilmer, R. G. Cumming: *Review of epidemiology and management of atrial fibrillation in developing countries.* International Journal of Cardiology *167* (2013), No. 6, 2412–2420.

[14] J. L. Reed, A. E. Mark, R. D. Reid, A. L. Pipe: *The effects of chronic exercise training in individuals with permanent atrial fibrillation: A systematic review.* Canadian Journal of Cardiology *29*, (2013), No. 12, 1721–1728.

[15] J. M. L. Hendriks, H. M. J. Vrijhoef, H. J. G. M. Crijns, H. P. B. L. Rocca: *The effect of a nurse-led integrated chronic care approach on quality of life in patients with atrial fibrillation.* Europace *16* (2014), No. 4, 491–499.

Received September 19, 2017

Acta Technica *62* No. 2B/2017, 533–540

Service optimization model of mechanical manufacturing under cloud manufacturing mode

Yeyingzi Guo[1]

Abstract. The service optimization model of mechanical manufacturing under the cloud manufacturing model has played an important role in the development of manufacturing industry. In order to perfect the related technologies and theories in the manufacturing industry of our country, the related theories of cloud manufacturing model and machining were summarized in this paper. Furthermore, a customer demand and manufacturing company were taken as the cases. And based on the mathematical model of multi-granularity manufacturing service optimization, the operation efficiency of different modes was contrasted and analyzed. The results show that the service optimization model of machining manufacturing in the cloud manufacturing model has certain practical significance for the development of manufacturing companies. The purpose of the study is to provide theoretical research for follow-up studies.

Key words. Cloud manufacturing model, machining manufacturing, service optimization model.

1. Introduction

With the development of the times, "peace and development" has gradually become the theme of the development of the world. All the industries in the world have been greatly developed and improved, which has brought a very important driving role and practical significance for the promotion of the comprehensive strength of each country. In the new era of development needs, science and technology have gradually become an important productive force in the rapid development of the times, and various new technologies have been constantly researched and produced, thus providing important impetus for the development and prosperity of some industries and fields, and bringing positive effects on the revival of some countries and peoples. In the process of rapid development of the times, the important influence brought by the progress of science and technology has provided more opportunities and challenges for the development of various industries and fields.

[1] Jiangsu Vocational College of Agriculture and Forestry, Jurong, Jiangsu, China, 212400

2. State of the art

As an important industry in the development of the times, the mechanical manufacturing industry can provide certain parts and components for the development of related industries, so as to be one of the basic industries of the world economic development [1]. With the development of various industries in the world, the machinery manufacturing industry is becoming more and more important. However, in the traditional mechanical manufacturing industry, because more procedures are carried out by manpower, there are some shortcomings such as low productivity, so that the further improvement of the world economic level has been negatively affected to some extent [2]. Nowadays, many scholars have put forward new technologies and theories and applied them to the development of actual manufacturing industry. As a new technology, computer technology has a positive impact on the development of the world manufacturing industry [3]. Many researchers have believed that because computer aided technology can collect relevant data information, machinery manufacturing industry based on computer aided technology can connect the enterprise with the advanced world level, and then recognize the shortcomings, improve the efficiency of enterprise development, and thus enhance the overall level of enterprise [4]. Many researchers have believed that today's computer technology is also affected by the increasing amount of data [5].

3. Methodology

With the development of the times, China's various industries have achieved greater progress and promotion, which has positively affected the comprehensive level of our country, and has further enhanced the international status of our country [6]. Under the influence of the rapid development of the world economic level, the development of China's various industries has also been affected. Manufacturing enterprises, as one of the important pillar industries in the rapid development of China's current economic level, has provides some basic support for the development of other related industries in China [7]. However, in the traditional machinery manufacturing industry in our country, the manufacture of related mechanical parts is done more manually, which may result in poor accuracy of components due to some subjective factors, thereby affecting the further development of other related industries. In addition, manual work may be affected by physical strength, and the work efficiency may be low in the whole work process, thus to produce a negative impact on the continuous development of the industry, and further affect the comprehensive level of China's machinery manufacturing industry. Statistics show that, in the larger machinery manufacturing industry in China, more is the introduction of other developed countries or industries due to defects in some manufacturing processes, which directly or indirectly improves the production cost of our country, and has a negative impact on the development of other industries [8]. Therefore, many scholars in China have put forward more perfect theory and technology of machine building industry, and have gradually introduced these technologies into the actual mechanical manufacturing process, thus making the level of China's technology in-

dustry greatly improved. Now, the machinery manufacturing industry in China is moving towards a more vigorous development direction, and its important influence is also gradually increased. Through the statistics of the output value of the machine processing industry in China from 2008 to 2016, with the continuous development of its industry, the output value of China's machinery manufacturing industry has shown an increasing trend year by year [9]. This has provided a certain degree of scientific and technological support for further development of other industries, and has provided a very important driving force for the overall development of China's economic industry.

In order to better determine the advantages and development of the machining industry in the cloud manufacturing mode, through the combination of theory and practice, the follow-up related research was carried out. And the research methods are as follows:

1. On the basis of a clear understanding of the relevant theories, the relevant tasks in the mechanical manufacturing services were further optimized. And the optimization model of process level and component level manufacturing service in the process of mechanical manufacturing service was constructed.

2. Then, the mathematical model of multi-granularity manufacturing service optimization was constructed, and the related characteristics of the constructed mathematical model were analyzed (Cheng et al. 2014) [12]. Thus, the relevant index values of each influence factor were determined. The relevant mathematical models used in the study are as follows:

$$f(t) = f(t_{\mathrm{t}}) + f(t_{\mathrm{s}})\,, \tag{1}$$

$$f(t_{\mathrm{s}}) = \sum_{i=1}^{m}\sum_{j=1}^{n_i} x_{ij}t(ij)\,, \tag{2}$$

$$f(t_{\mathrm{t}}) = \alpha\sum_{j=1}^{n_1} x_{1j}t(0j) + \sum_{i=1}^{m-1}\sum_{j=1}^{n_i}\sum_{k=1}^{n_{i+1}} x_{ij_{(i+1)k}}t(ij,(i+1)k) + \beta_{mj}t(mj)\,. \tag{3}$$

Here, $f(t_{\mathrm{t}})$ and $f(t_{\mathrm{s}})$ represent the running time of the whole machine manufacturing operation process and the processing time of each process for the related products. The formula (2) represents the total time cost of the whole machining process for the manufacture of the product, and the formula (3) represents the final time cost of the whole mechanical manufacturing process, which consists of three different operating processes: $\alpha\sum_{j=1}^{n_1} x_{1j}t(0j)$ represents the total process time required by a customer to book a mechanical product to the manufacturing process, $\sum i = 1^{m-1}\sum_{j=1}^{n_i}\sum_{k=1}^{n_{i+1}} x_{ij_{(i+1)k}}t(ij,(i+1)k)$ represents the running time between processes in different mechanical products, and $\beta_{mj}t(mj)$ represents the total time spent from the processing of the product to the end of the customer's premises.

3. Finally, a mechanical manufacturing enterprise in our country was taken as an example. And the operation cost, operation efficiency and operation income of the enterprise before and after the application of the service optimization model of mechanical manufacturing under cloud manufacturing mode were compared and analyzed. Thus, the advantages of this technology for the production of machinery manufacturing industry in China were determined, and the technical support for the improvement of other technologies and theories was also provided.

4. Result analysis and discussion

Under the trend and background of the times, the promotion of the comprehensive strength of various industries has become one of the important criteria for the national economic strength and comprehensive level. After China's reform and opening up, more innovative technologies and theories have been introduced, so that the comprehensive strength of China's various industries has been developed to a certain extent. In this context, the machinery manufacturing industry has gradually become an important pillar industry of China's economic development. With the continuous improvement of the industrial model, a variety of new technologies are gradually integrated with the industry, making the overall level of the industry further developed. Cloud manufacturing technology is a new technology which obtains relevant results through the cloud computing of basic data in the background of the rapid development of information technology. In the development of this technology, there are many advantages and characteristics of service oriented and converged with network technology. The main architecture includes physical resource layer, basic information resource layer, central service, application layer and other main structures (Fig. 1). In actual use, in the operation process of the platform technology, the industry related manufacturing information resources are input to the platform center, and then the manufacturing service is formed. After entering the relevant platform, the customer can understand and analyze the status of the enterprise's production, so as to determine some of the services they want to obtain and release the requirements. Then, enterprises and customers form relevant contracts and carry out related work. In this technique, cloud computing is used to run traditional operating processes, so that the operation efficiency of the whole operation process is improved, the resource sharing is further increased, the time cost is reduced, and the overall production efficiency of the enterprise is higher, and the overall economic strength of the enterprise is improved.

On the basis of a clear understanding of the relevant theories, in this paper, a service model framework for machining manufacturing in the cloud manufacturing model was proposed. It consists of three levels: task release level, service level and final decision interface layer, in which, the framework of service hierarchy. The process is mainly in the related platform of manufacturer's related product production information input value. Then, the system sets the platform's daily maximum access and access time parameters. When the customers meet these two requirements, they can browse the relevant information and release their own demand. Thus, the

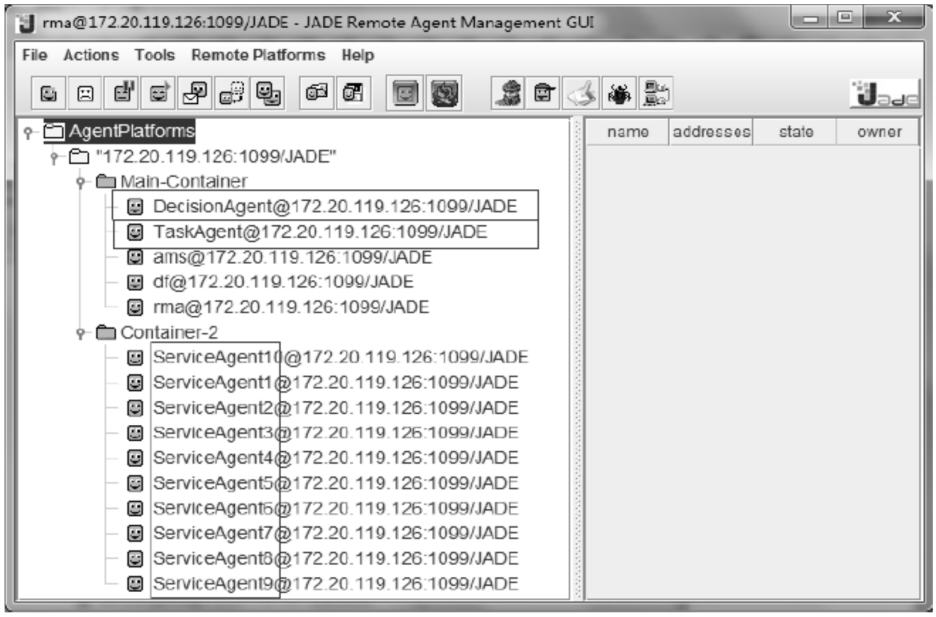

Fig. 1. Development of cloud manufacturing model

connection between the customer and the producer and the sharing of relevant information resources are realized, thereby reducing the cost increase caused by the restriction of time and space in the traditional communication process.

Then, taking the mechanical manufacturing industry in a city as an example, the application of cloud manufacturing technology in the process of mechanical manufacturing was analyzed. First of all, it was assumed that a customer needed to order a batch of outer products in a stepped bearing. The information about all the product processing is shown in Table 1. The two kinds of information was input to the mechanical processing of the above construction manufacturing service system, so that customers were able to query the relevant information to obtain relevant information about the machinery manufacturing enterprises.

Based on the input of relevant information, the model of multi-granularity manufacturing service optimization was applied to evaluate the service model of mechanical manufacturing and the efficiency of the acquisition of related tasks for different manufacturing companies. And the whole process of mechanical product transportation were contrasted and analyzed. Its results are listed in Table 2. The results show that compared with the traditional mechanical manufacturing and operation mode, the production efficiency and operation efficiency of each company in the cloud manufacturing mode are increased to some extent, and the operation cost is reduced. Therefore, from an example point of view, compared with the traditional machining manufacturing services, the service optimization model of mechanical manufacturing in the cloud manufacturing model can produce relatively high operational efficiency. Through the comparison of the three companies, it can be found that, compared with other companies, there is higher production efficiency in Com.2, which can

better meet the actual needs of customers.

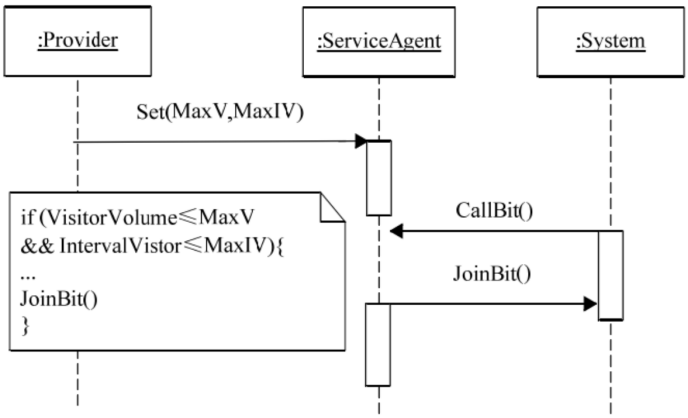

Fig. 2. Sequence diagram of service behavior in mechanical manufacturing

Table 1. Task information for manufacturing products outside the circle

Demand side name (customer)	User1
Address	U.1
Machining process	The car outside the circle and chamfer
Type	Lathe
Material	Steel
Main feature	The outer circle
Diameter (mm)	500
Length (mm)	700
Accuracy class	9
Indicates roughness (Ra)	2.5
Part weight (g)	20
Total ceiling (yuan)	1000
Quantity (unit)	20
Start time	2016-09-04
Harvest time	2017-09-11

Table 1. Task information for manufacturing products outside the circle

Model	Company	$f(t_t)$	$f(t_s)$	Total operating cost (yuan)	Operation efficiency
A service optimization model for mechanical manufacturing in cloud manufacturing	Com.1	4	12	1327	0.67
	Com.2	2	11	1149	0.71
	Com.3	3	13	1424	0.59
Traditional mechanical manufacturing service model	Com.1	5	17	1539	0.44
	Com.2	4	15	1227	0.52
	Com.3	4	18	1644	0.38

5. Conclusion

With the development of the times, manufacturing industry has gradually become one of the most important economic pillar industries in the world. And the development of computer technology has further promoted the comprehensive strength of manufacturing industry. As a new theory in the manufacturing industry, the development of the cloud manufacturing model has a positive impact on the operation efficiency of the whole machinery manufacturing industry. In order to perfect and analyze the technology and theory, in this paper, the relevant data was read and summarized, and the relevant theory was confirmed and clarified. On this basis, the relevant model formulas used for the study were constructed. Then, a customer demand and different mechanical manufacturing companies were taken as examples, and customer requirements and related information about company production and logistics were systematically input. Then, based on the mathematical model of multi-granularity manufacturing service optimization, the operation efficiency of different models and different companies were compared and analyzed. The results show that the service optimization model of mechanical manufacturing under cloud manufacturing model has a positive effect on the development of related industries. Because the cognition of the relevant theories is not perfect enough, there are still some shortcomings in the study, but it can provide reference for the study of related major.

References

[1] X. Xu: *From cloud computing to cloud manufacturing.* Robotics and Computer-Integrated Manufacturing *28* (2012), No. 1, 75–86.

[2] X. V. Wang, X. W. Xu: *An interoperable solution for cloud manufacturing.* Robotics and Computer-Integrated Manufacturing *29* (2013), No. 4, 232–247.

[3] D. Wu, M. J. Greer, D. W. Rosen: *Cloud manufacturing: Strategic vision and state-of-the-art.* Journal of Manufacturing Systems *32* (2013), No. 4, 564–579.

[4] D. Wu, J. Lane Thames, D. W. Rosen, D. Schaefer: *Enhancing the product real-*

ization process with cloud-based design and manufacturing systems. Journal of Computing and Information Science in Engineering *13* (2008), No. 4, paper 041004.

[5] X. Yang, G. Shi, Z. Zhang: *Collaboration of large equipment complete service under cloud manufacturing mode.* International Journal of Production Research *52* (2014), No. 2, 326–336.

[6] Y. Laili, F. Tao, L. Zhang, L. Ren: *The optimal allocation model of computing resources in cloud manufacturing system.* IEEE International Conference on Natural Computation, 26–28 July 2011, Shanghai, China, IEEE Conference Publications *4* (2011), 2322–2326, International Journal of Advanced Manufacturing Technology *63* (2011), Nos. 5–8, 2322–2326.

[7] B. M. Li, S. Q. Xie, Z. Q. Sang: *Step-based data sharing and exchange in one-of-a-kind product collaborative design for cloud manufacturing.* Advances in Mechanical Engineering (2015), Article ID No. 135291, 1–16.

[8] L. Mertz: *New world of 3-D printing offers "completely new ways of thinking": Q&A with author, engineer, and 3-D printing expert Hod Lipson.* IEEE Pulse *4* (2013), No. 6, 12–14.

[9] Y. Laili, F. Tao, L. Zhang, B. R. Sarker: *A study of optimal allocation of computing resources in cloud manufacturing systems.* International Journal of Advanced Manufacturing Technology *63* (2012), Nos. 5–8, 671–690.

[10] B. Huang, C. Li, C. Yin: *Cloud manufacturing service platform for small- and medium-sized enterprises.* International Journal of Advanced Manufacturing Technology *65*, (2013), Nos. 9–12, 1261–1272.

Received September 19, 2017

Acta Technica *62* No. 2B/2017, 541–552

Application of hybrid compression and converging technology in wireless sensor network routing protocol in China[1]

Yang Chen[2]

Abstract. In order to give full play to the advantages of wireless sensor and make use of the restriction of it, it is very important to study and design the proper routing protocol and data fusion. In this paper, the basic structure, characteristics and classification of wireless sensor networks were discussed systematically, and several typical routing protocols were introduced and compared. Based on the analysis of existing network layer routing protocols and key technologies, the network layer routing protocols and their key technologies in wireless sensor networks were studied. Finally, the conclusions that the data compression rate is basically a fixed value, and the influence of the depth of the ternary tree is very small, which can greatly increase the scalability of the network were drawn.

Key words. Wireless sensor networks, hybrid routing model, data fusion.

1. Introduction

In the past ten years, the rapid development of network information technology has made the connection between people in every corner of the world more and more close, and people can talk and communicate conveniently anytime and anywhere. Because of the passive nature of things, the communication between people and things will not be very smooth. Therefore, in order to make the physical world useful to us, other tools and techniques must be used to explore everything in the world, such as various sensors. Based on the development of communication technology, sensing technology and micro electromechanical systems, sensors are so small that they can be encapsulated into a millimeter scale chip, with low cost, but high

[1]The study was supported by the Key natural science research project supported by Anhui province (KJ2016A303) Research on data fusion technology of wireless sensor network for privacy protection; Quality engineering project supported by Anhui province (2016sjjd041) Anhui Xinhua University & Hefei City Cloud Data Center Co., Ltd, practice education base.

[2]College of Information Engineering, Anhui Xinhua University, Hefei, Anhui, China, 230088

robustness and more powerful functions. The "intelligence" of sensors can help people complete the collection, arrangement and communication of data, thus greatly expanding the application field of sensors. Wireless sensor networks will fundamentally change the interaction between human and the natural world, and make the virtual network world and the physical world and the various fields communicate with people. People can get rich and reliable information from the physical world by means of tools, and realize the desire of "ubiquitous computing". It is no exaggeration to say that the widespread application of wireless sensor networks is the trend of the development of science and technology, which will always lead to changes in the wireless sensor and related research fields to the human world.

2. State of the art

Wireless sensor networks are at the forefront of new technologies, and there are still a lot of hot issues to be discussed, such as data fusion. In recent years, a large number of routing protocols have been developed in the process of data collection, most of which can support data fusion functions, so as to reduce energy consumption and communication costs [1]. In the process of building a cluster, considering the influence of the residual energy and the distance from the sink node to the routing protocol design, a routing protocol supporting data fusion was designed. The node structure was upgraded to heterogeneous, and the establishment of cluster and data transmission path under heterogeneous condition were analyzed [2]. Considering the coverage of nodes, the most comprehensive information was transmitted with the least nodes. Linear regression model was used to fuse data and reduce data transmission. At present, most data fusion research focuses on the shortest path tree junction, but the focus of different application scenarios is certainly different. Much of the work of data fusion is focused on intra-data fusion in wireless sensor networks [3]. For fusion queries, a certain amount of computation within the network is acceptable. The sensor sensing data is processed into individual parts and then constantly updated during the delivery to the sink node or base station. Each sensor node only delivers one or relay a small amount of data to other nodes, thus forming an energy efficient method [4]. Current data fusion protocols are mainly divided into three categories: cluster based data fusion, tree based data fusion, and multipath based data fusion [5].

2.1. Methodology

A large number of wireless sensor nodes are deployed in a certain range of monitoring target areas, and a network is generated among nodes through self-organizing and adaptive methods, and the structure of the wireless sensor network is shown in Fig. 1.

The whole network is usually composed of sensor nodes, sink nodes sink, Internet and satellite console in the monitoring area. The working principle is as follows: a large number of sensor nodes are randomly distributed within a certain range of target regions, and the data parameters in the region are collected according to

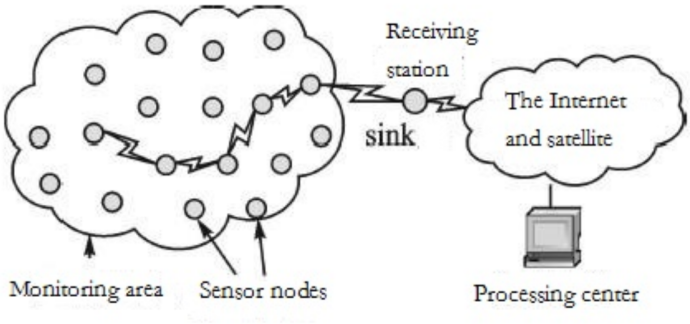

Fig. 1. Structure of wireless sensor network

specific requirements. And a single hop or multi-hop communication mode is used to send the collected data to the sink node. Then, after the connection with the console and the satellite, the user can find data at the end of the console or send instructions to each node in the network [6].

In general, sensor nodes can be considered as a micro embedded system powered by batteries, and the storage capacity and communication processing capability are weak, which limits the direct communication between the sensor nodes and the sink node. From the point of view of network function, in addition to local data acquisition and fusion, sensor nodes also relay and forward data from other nodes, which acts as double roles of terminals and repeaters [7]. The sink node can be a powerful node with enough energy support and more memory and processing capabilities, and can also be used as a gateway device to connect the wireless sensor network and realize the conversion between the two protocol stacks.

Wireless sensor network protocol stack provides the necessary software support for communication between sensor nodes. According to the identification of the majority of scholars, wireless sensor network protocol stack is divided into five layers, namely application layer, transport layer, network layer, data link layer and physical layer. And there are three supporting parts, energy management platform, mobile management platform and task management platform stack [8].

Data fusion technology includes the collection, transmission, synthesis, filtering, correlation and synthesis of useful information given by various information sources, so as to assist people in the determination, planning, detection, verification and diagnosis of situation environment [9]. Sensor data fusion technology needs to get the internal relations and rules of various information, and combine with the spatio-temporal correlation of sensor nodes, thus to eliminate redundant and erroneous information, retain the key and correct information components, and ultimately simplify and optimize the information. A single sensor may only obtain partial information segments of the environment or the object under test, while the multi-sensor information can reflect the characteristics of the environment perfectly and accurately after fusion. Data fusion technology plays an irreplaceable role in the research of intelligent information processing technology [10].

According to the level classification, data fusion can be divided into pixel level fusion, feature layer fusion and decision level fusion. Pixel level fusion is the fusion directly on the original data layer, which is synthesized and analyzed before the raw data of various sensors are preprocessed, belonging to a low level of convergence. Feature layer fusion extracts features from the original data of the sensor, and analyzes and processes the features comprehensively, belonging to the intermediate levels of convergence [11]. For each sensor, the decision level fusion firstly completes the basic processing locally such as preprocessing, feature extraction, recognition or decision, and establishes the preliminary conclusion, and then makes decision fusion by association processing, and finally obtains the joint inference result, which belongs to high-level fusion.

When the deployment density of nodes is large, the sensor sensed data will be redundant, that is, multiple neighboring sensor nodes will acquire the same information. In order to save the energy of sensor nodes, it is necessary to remove the redundant information and reduce data transmission [12]. In a network with thousands of sensor nodes, the energy consumed to deliver a message is far greater than the energy consumed by the computation, and data fusion can remove the redundant information very well, which makes the transfer of information small.

Space means that different kinds of data come from different places and spaces, while time means that the database can adapt to changes in the objective environment over time. If the nodes in a wireless sensor network are similar in the near or continuous time period, then the sensed data or attribute values are similar or have a regular change. Even if there are still a few nodes that fail to be sensed at a certain point in time, a set of data can also be obtained by using the similarity of data to have very little error or a slight change to real data. Then, these nodes have time correlation [13]. In a wireless sensor network, because of the random deployment of nodes, especially in some remote locations, the use of aircraft to broadcast nodes will result in high density of some nodes. At the same time, the data sensed by some geographically similar nodes have a high degree of similarity. And then the data induced by these nodes have spatial correlation.

In order to store and find the convenience, the tree structure is used to store and transmit data, and a complete trinomial tree can be constructed. A child node transmits only a set of coefficients to its parent node, which is used for data fusion and data query, greatly reducing energy consumption and effectively prolonging the life cycle.

In a network where a large number of sensors are deployed, the minimum spanning tree is used to solve the problem of how the sensor nodes pass to the base station via the optimal path. Greedy algorithm is a commonly used algorithm. But the greedy algorithm is a local optimal algorithm, which just makes what seems the best choice at the moment, and if it is not considered from the overall optimum, it is only a locally optimal solution in some sense [14]. In this paper, a complete trinomial tree is constructed for propagating data. The role of each node of a fully ternary tree is the cluster head of a hierarchical network that performs only the functions of receiving data, transmitting data, and merging data. And the structure of the CTETREG data fusion tree is shown in Fig. 2.

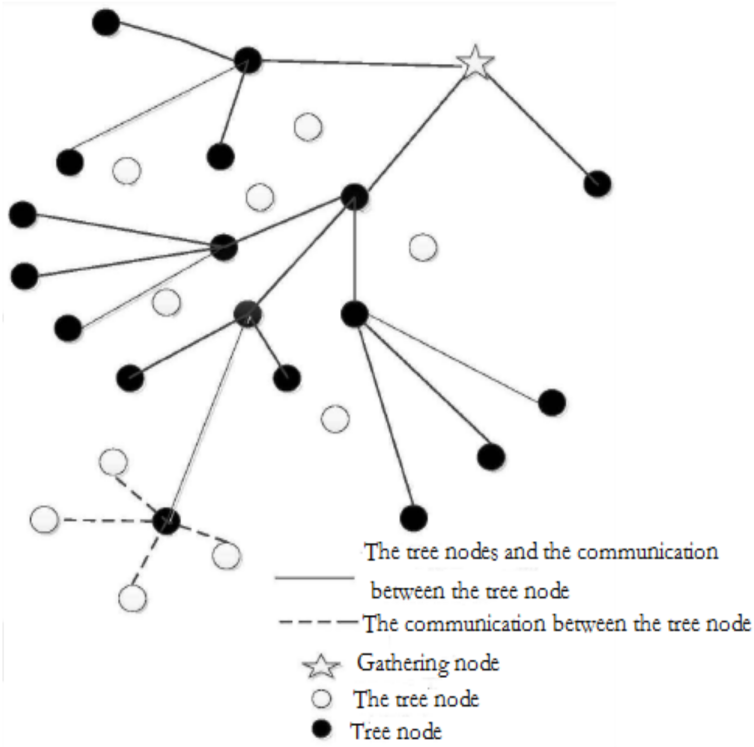

Fig. 2. The structure of the CTETREG data fusion tree

For the choice of roots, in order to facilitate the coordinate representation, the wireless sensor network area is set to a square area, and the length is L. If the length of each subregion is L_{s}, then, the whole network can be divided into L/L_{s} subregions. The roots of adjacent areas must be as close as possible to meet the needs of querying multiple regions while minimizing the propagation path. So, the root of each query subtree is best deployed in the corner of the square sub region. For odd sub regions, the root is selected in the upper right corner of the subregion, while the even region is selected in the upper left corner, so that the roots of the neighboring four sub regions are clustered together [15].

When the roots of each tree are determined, tree analysis and selection are necessary. Using the topological structure of the complete trinomial tree, each parent node has a 3 child node, which ensures the full coverage of the tree and the accuracy of the data processing. The entire sensor network area is S, and the total number of nodes deployed is N, and then the node density N/S is ρ, each subregion is S_s, and the average number N_{s} of nodes in a subregion is ρS_{s}.

In a full trinomial tree, the total number of nodes is N_{at} as shown in equation (1):

$$N_{\mathrm{at}} = \frac{3^{p+1} - 1}{2}. \tag{1}$$

Here, p is the depth of the tree of the complete trigeminal tree.
Tree depth can be obtained by type 1, as shown in type 2:

$$p = \log_3 \left(\frac{2N}{n_s + 1} \right) - 1 \,. \tag{2}$$

Here, n_s is the number of non-tree nodes corresponding to a tree node.
Using formula (2), the following formulae (3) and (4) are obtained:

$$N = n_s N_{at} + N_{at} \,, \tag{3}$$

$$N_{at} = \frac{N}{n_s + 1} \,. \tag{4}$$

In this paper, it is assumed that there are $N = 3000$ nodes in sensor networks, area$S = 800 \times 800$ is a square area, and the subregion is $S_s = 400 \times 400$. The average number of nodes in each subregion is

$$N_s = \rho S_s = \frac{N}{S} S_s = \frac{3000}{800 \times 800} \times 400 \times 400 = 750 \,.$$

The depth of the tree is $p = 3$, and the number of tree nodes in each subregion is

$$T_c = N_{at} = \frac{3^{p+1} - 1}{2} = 40 \,.$$

Further, $n_s = 15$, and, therefore, the number of nodes in the subregion is

$$n_s t + t = 15 \times 40 + 40 = 640 < 750 \,.$$

From the above calculation, it can be seen that the maximum tree depth $p = 3$ is appropriate.

In a wireless sensor network, a large number of distributed nodes are constantly sensing the data of the surrounding environment and transmitting it to other nodes. If the environment changes suddenly or the sensor node receives interference, an abnormal signal value is generated. In order to keep the accuracy of the data, it is necessary to identify abnormal data in time and analyze them or discard them directly. which was very important in some application fields. For example, in forest fire monitoring, a large number of sensor nodes are deployed, and each sensor node will continue to transmit information to the base station in an active or passive manner. In general, the temperature of sensor induction is within a fixed range. Once a fire occurs, the sensor sends out an abnormal data value that touches the warning signal, which requires timely identification to control the spread of the fire. But sometimes because of human factors, for example, when outdoor enthusiasts cook in the forest, just the furnace is located near a sensor, the abnormal data value will also be generated. If the node is restored to normal in a short time, and the value of the neighboring sensor is normal, it can be done without any processing.

There are three performance indexes of CTETREG data fusion tree, percentage error, compression ratio and fusion data output size.

Percentage error is the representation of the error between the induced data and the real data in the form of a percentage.

The compression ratio is the ratio between the number of output data of the neutron nodes in the query tree and the total data received by the other query tree nodes and the non-query tree nodes, which is the ratio between output and input. The greater the compression ratio, the smaller the ratio of the reduction will be, and the more redundancy of the data will be. And the smaller the compression ratio, the less redundancy of the data will be. Generally, the smaller the compression ratio, the better the effect can be. However, considering the completeness and accuracy of data, the compression ratio is not as small as possible.

For the fusion data output size, it is expected that when the tree depth is different and the node density is changed, the output of the data is a fixed value, which is beneficial for network expansion and energy savings.

3. Result analysis and discussion

Based on the conclusions obtained by the simulation platform MATLAB, the advantages of the method were compared. The specific simulation reference data is shown in Table 1.

Table 1. Simulation parameters

Notation	Value	Unit
Z	800×800	m^2
R	40	m
S	3000	
ρ	0.0047	
Z_s	400×400	m^2
p^n	0.33	
p	3	
n_s	15	

The simulation results are shown in Fig. 3. Symbol Z is measured by the width of the node coverage in the monitoring area, and R is measured in terms of the accuracy of the area being covered. Node Z_s is randomly distributed in the 400 m×400 m squared plane region.

As shown in the figure, when the tree depth was 1, there were only 4 nodes in each subregion for processing the whole sub region parameter value. In the distribution of dense nodes, the received data was limited, and sometimes the real data value can't be accurately reflected, so that the percentage error was 120 %. When the tree depth was 2, the node of the tree reached 13. Compared with the 4 nodes, the number of nodes involved in the data fusion increased, and the accuracy of the data fusion

value was improved. However, the simulation can also see up to 65 %, but when the tree depth was 3, the fusion effect was greatly improved, and the percentage error rate was only about 5 %. All of the above results were better than two fork tree, even if the two fork tree was deep; its percentage error rate was 5 %.

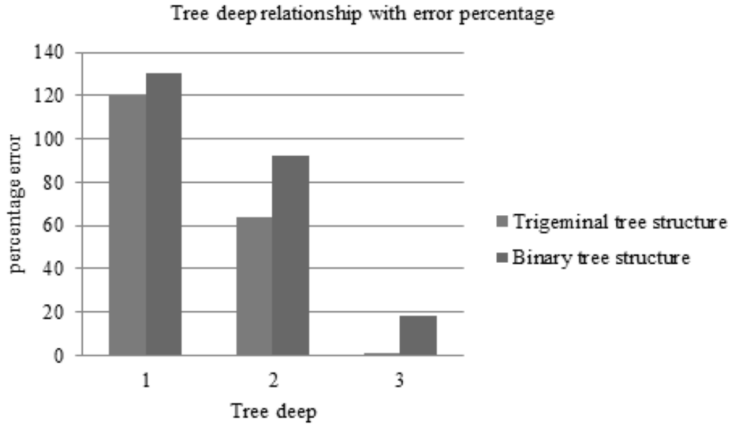

Fig. 3. Comparison of the error percentage and tree depth of the complete two fork tree and the complete trinomial tree

Figure 4 shows the comparison of the compression ratio and tree depth of the full two-fork tree and the complete trinomial tree.

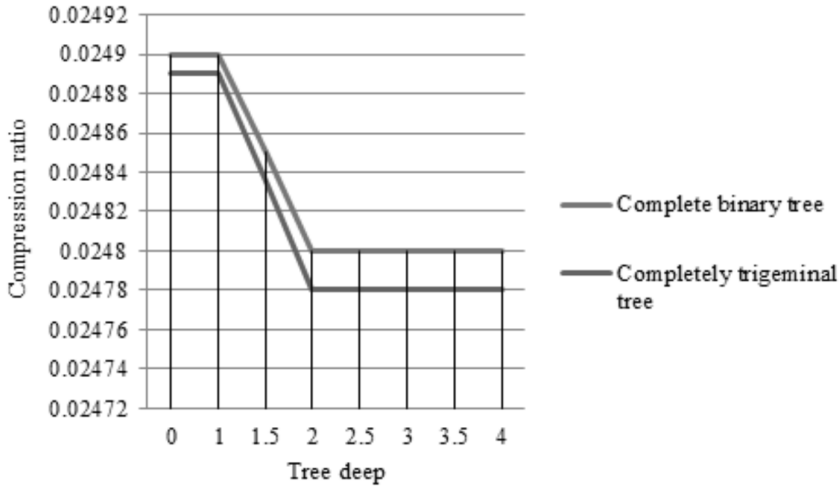

Fig. 4. Comparison of the compression ratio and tree depth of the full two-fork tree and the complete trinomial tree

A low compression ratio can reduce data redundancy, reduce broadband duty cycle and save transmission energy. As can be seen from the simulation Fig. 2, the

compression ratio of a fully two fork tree was between 0.0248 and 0.0249, while the compression ratio of the complete trinomial tree was almost 0.02478 to 0.02489. The full trinomial tree node was more than the full two fork tree, and the data was much more. The base of the denominator was large, but the compression ratio was smaller. Therefore, the amount of data transmission was less, but the difference between the two was not large, thus having little impact on the accuracy of the data. From the change of the compression ratio, it can be seen that the range of change was very small, basically a constant, which was beneficial to the expansion of wireless sensor network.

From the simulation Fig. 5, it can be seen that the output size of the data fusion was $(S_x + S_y + S_c)$ bit value based on the regression approximation of the trinomial tree model. When a node was passed to another node and base station, the final output data value was a constant, which also confirmed that the data values included the coefficients and coordinate ranges obtained from data fusion. In theory, the coefficient is a fixed number, and the coordinate range is a value, and the length of the data added by it is considered to be a constant value. From the simulation results, it also can be seen that the output of the data was independent of the number of nodes and the tree depth, which greatly increased the scalability of the network, and facilitated the application of this method in a wider range.

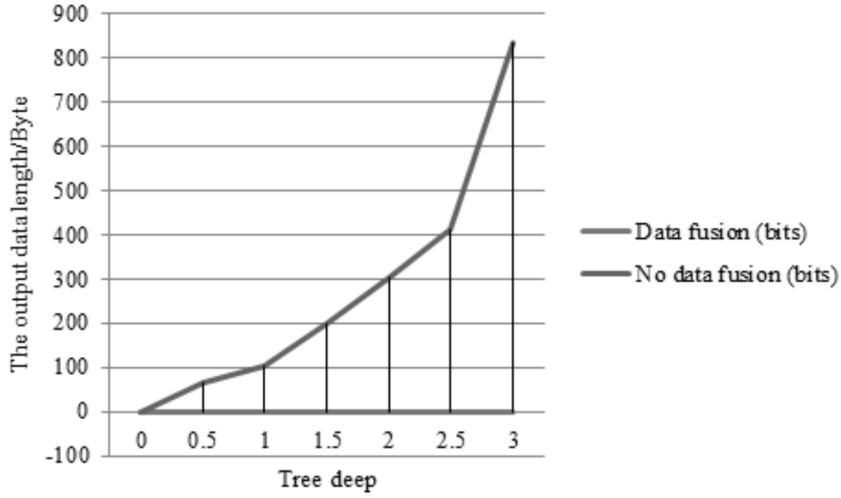

Fig. 5. The effect of a full Trident tree with and without data fusion

4. Conclusion

In order to solve the limitations of wireless sensor and make full use of its advantages, in this paper, on the basis of studying the systematicness of routing protocols, the application scope of the protocol was extended and simulated, and the energy saving and security of data fusion in data transmission were studied. Some con-

clusions were drawn as follows: a regression analysis data fusion algorithm based on full trinomial tree structure was proposed to reduce the data transfer and the energy consumption. Moreover, the data packets transmitted by each tree node were always of the same size, and even if the number of nodes and the tree depth increased, the size of packet transmission would not be affected, so that there was a good scalability in the network. In addition, every parent node of a full trinomial tree had more child nodes than that of a full two fork tree. In the same case, the complete trinomial tree required less tree depth, which makes its performance better than that of the fully two fork tree. Simulation results show that, compared with the algorithm of fully two tree structure, the data fusion method based on the complete trinomial tree structure can greatly prolong the network life cycle. Of course, there are some problems that deserve further study, such as how to apply fuzzy control and intelligent control to data fusion.

References

[1] C. Karlof, D. Wagner: *Secure routing in wireless sensor networks: Attacks and countermeasures.* IEEE International Workshop on Sensor Network Protocols and Applications, 11–11 May 2003, Anchorage, AK, USA, IEEE Conference Publications (2003), 113–117.

[2] C. Sha, R. C. Wang, H. P. Huang, L. J. Sun: *Energy efficient clustering algorithm for data aggregation in wireless sensor networks.* Journal of China Universities of Posts and Telecommunications *17* (2010), Suppl. No. 2, 104–109, 122.

[3] D. Kumar, T. C. Aseri, R. B. Patel: *EEHC: Energy efficient heterogeneous clustered scheme for wireless sensor networks.* Computer Communications *32* (2009), No. 4, 662–667.

[4] H. F. Chen, H. Mineno, T. Mizuno: *Adaptive data aggregation scheme in clustered wireless sensor networks.* Computer Communications *31* (2008), No. 15, 3579–3585.

[5] M. Mostafizur, R. Mozumdar, G. F. Nan: *An efficient data aggregation algorithm for cluster-based sensor network.* Journal of Networks *4* (2009), No. 7, 598–606.

[6] W. M. Lee, V. M. S. Wong: *E-Span and LPT for data aggregation in wireless sensor networks.* Computer Communications *29* (2006), Nos. 13–14, 2506–2520.

[7] W. H. LiaoH, Y. C. Kao, C. M. Fan: *Data aggregation in wireless sensor networks using ant colony algorithm.* Journal of Network and Computer Applications *31* (2008), No. 4, 387–401.

[8] Y. Y. Mao, F. R. Kschischang, B. Li, S. Pasupathy: *A factor graph approach to link loss monitoring in wireless sensor network.* IEEE Journal on Selected Areas in Communications *23* (2005), No. 4, 820–829.

[9] Y. Yu, R. Govindan, D. Estrin: *Geographical and Energy Aware Routing: A recursive data dissemination protocol for wireless sensor networks.* Marine Pollution Bulletin *20* (2011), No. 1, paper 48.

[10] J. Kulik, W. Heinzelman, H. Balakrishnan: *Negotiation-based protocols for disseminating information in Wireless Sensor Networks.* Wireless Networks *8*, (2002), Nos. 2–3, 169–185.

[11] G. Anastasi, M. Conti, M. Di Francesco, A. Passarella: *Energy conservation in wireless sensor networks: A survey.* Ad Hoc Networks *7* (2009), No. 3, 537–568.

[12] B. H. Liu, W. C. Ke, C. H. Tsai, M. J. Tsai: *Constructing a message-pruning tree with minimum cost for tracking moving objects in Wireless Sensor Networks is NP-complete and an enhanced data aggregation structure.* IEEE Transactions on Computers *57* (2008), No. 6, 849–863.

[13] J. Lian, K. Naik, G. Agnew: *Data capacity improvement of wireless sensor networks using Non-uniform sensor distribution* . International Journal of Distributed Sensor Networks *2*, (2006), No. 2, 121–145.

[14] V. Rajendran, K. Obraczka, J. J. Garcia-Luna-Aceves: *Energy-efficient collision-free medium access control for wireless sensor networks.* Journal Wireless Networks *12* (2006), No. 1, 63–78.

[15] B. Khaleghi, A. Khamis, F. O. Karray, S. N. Razavi: *Multisensor data fusion: A review of the state-of-the-art.* Information Fusion *14* (2013), No. 1, 28–44.

Received September 19, 2017

Acta Technica *62* No. 2B/2017, 551–560

Analysis of the key technologies of practical application based on embedded reconfigurable computing system

Jingshu Cao[1,2], Wenxin Li[1]

Abstract. With the continuous development of science and technology, reconfigurable computing has become one of the current research hotspots as a new computing model. However, with the increasing complexity of the embedded reconfigurable computing system, it is increasingly necessary to design from the system level to improve the design effect. Therefore, the practical application technology of the reconfigurable computing system has become a very important research topic. In this paper, the development of the subject was understood, the relevant theory of the subject was analyzed, the key technology was researched and analyzed, the example experiment was carried out, and the results were compared and analyzed, which proves the feasibility and effectiveness of the study, and is of great significance to the development of key technologies.

Key words. Reconfigurable computing, system level design, operating system.

1. Introduction

Traditional computing systems usually use two different methods to implement the algorithm. Firstly, the use of special integrated circuits, this method has a very high execution speed and accuracy of the operation. Once designed, its function cannot be changed. In order to implement different algorithms, it is necessary to redesign the circuit, the development cycle and the cost is high, and only the mass production can show its superiority. Secondly, the use of general-purpose microprocessors, the flexibility of the method is high, and once the requirements change, the function of the system can be changed by software instruction, but the serial execution of the instruction and the bottleneck of memory access bandwidth make the

[1]Lanzhou Institute of Physics, GanSu, LanZhou, 730000, China
[2]Corresponding author

performance of general-purpose microprocessors often difficult to meet the actual requirements. A single processor-based software implementation does not provide good support for complex algorithms with potential parallelism [1]. Semiconductor industry has been in accordance with the generalization and specialization of the alternating development, once every twenty years. The first common and dedicated loop is characterized by pure hardware design, that is, through the hard wired way to achieve the algorithm. The second loop is characterized by sequential programming of software, that is, through the order to achieve the algorithm. The third cycle is characterized by structural programming, that is, through the reconfigurable logic device to implement the algorithm [2]. As a new way to calculate, reconfigurable computing is in line with the development trend of semiconductor technology. It combines the advantages of generalization and specialization, uses the FPGA to reconfigure the logic unit functions and interconnection characteristics, which is a form based on the application requirements of the dynamic configuration of the circuit and has the high performance of hardware implementation and software implementation flexibility [3]. Reconfigurable systems based on reconfigurable computing techniques can be simply defined as computing systems that contain at least one reconfigurable hardware module. The function of the hardware module can be modified by the end user. The modification process is realized mainly by refactoring or partially reconstructing the programmable logic device in the system. The reconfigurable system can combine the advantages of software implementation and hardware implementation with only a small amount of hardware resources. Its appearance makes the boundaries of hardware and software in the traditional sense become blurred, the hardware system to be software [4]. Reconfigurable systems have been presented with powerful computational performance and data processing capabilities in a number of data-intensive applications, particularly in the presence of large parallelism and waterborne applications within the algorithm. One of the most representatives is the Splash 2 developed by the US Supercomputer Research Center in 1992 [5].

2. State of the art

2.1. Reconfigurable computing overview

Estrin of the University of California, USA, first proposed a reconfigurable concept and developed a prototype system. The system consists of non-flexible but programmable processors and flexible digital logic components reconstructed by program control. Although the abstraction level of the system software and hardware is not high, it can be programmed and reconstructed [6]. As the implementation of the technology is not yet perfect, the system developed by Estrin is only a rough approximation of the design concept, but it is the core of the reconfigurable computing system.

In 1986, Xilinx companies developed the world's first FPGA chip, and obtained a very good application effect in practice. To the early nineties of last century, there has been some FPGA-oriented development for a certain type of application computing equipment. The common practice is to combine one or more FPGAs,

CPUs, and memories together. As part of the coprocessor accelerator program that can be executed in parallel (typically the loop body), the FPGA is managed by the refactoring [7]. The computing device of this structure was known as a reconfigurable computer. This way of working is also called refactoring.

From a different research point of view, the understanding of reconfigurable computing is not the same. We see it as a class of computer organizational structure, and has the following characteristics which are different from other organizational structure, that is, the chip customization capabilities after manufacture (different from the ASIC), can achieve the mapping of the algorithm to the computing engine to a large extent (different from the general microprocessor) [8].

Reconfigurable computing is a numerical model of the spatiotemporal domain which uses FPGA as the technical basis, changes the function of the logical unit in FPGA and the interconnection mode of the connection according to the programming information in the reconfigurable device configuration file, thus changing the function of the computing system. It can use custom reconfigurable devices to customize the computing components while designing the implementation, and can reuse the computational resources to achieve a number of different computational tasks [9]. Reconfigurable computing makes up for the performance gap between microprocessor implementation and ASIC implementation, the calculation speed is comparable to that of ASIC at the same time, which has the flexibility similar to the microprocessor, and provides a flexible and effective computing solution for a wide range of applications.

2.2. Research at home and abroad

As the reconfigurable system has broad application prospects and potential market value, programmable device manufacturers Xilinx and Altera are represented. Industry has carried out in-depth research on reconfigurable devices since the mid-1990s. The goal is to improve the device reconstruction speed, there have been some partially reconfigurable devices, as well as reconfigurable devices using compressed configuration files [10]. In addition, field-specific reconfigurable chips have also been successful, such as reconfigurable multiprocessor systems developed by IMEC and Freescale semiconductors, reconfigurable communication chip series which are capable of handling 50 channels at a chip rate of CDMA 2000 developed by Chameleon Systems, and the dynamic reconfigurable processor "DAPDNA-2" developed by Japan IPFlex for image processing and so on.

At the same time, the academic research on reconfigurable system has made great progress, and many new architectures, algorithms and tools have emerged. According to the degree of coupling, the reconfigurable computing platform is divided into system-level loose coupling system, chip-level loose coupling system and on-chip tight coupling system. In order to improve the speed of reconstruction, the researchers put forward a number of strategies and methods, some of which have been implemented in commercial products, such as partial reconfiguration. In addition, scholars have proposed to use multi-context and configuration data Cache to reduce the configuration time [11]. In terms of compilation tools, the Single-Assignment C

project already has the ability to compile some C fragments into assembly language and map it to a reconfigurable system.

With the progress of the level of programmable devices and integrated circuits, reconfigurable computing has been widely used in many areas from embedded systems to high performance computing, including digital image processing, network security, bioinformatics and supercomputing, However, for the further application of reconfigurable computing, there are still many key problems that need to be solved and improved. In the aspect of system design support, with the increasing complexity of embedded reconfigurable computing system design, it is necessary to design from the system level at the same time. In the aspect of running environment support, because the traditional operating system can't adapt to the new reconfigurable system application requirements, it is one of the most important problems to be solved that how to manage the reconfigurable computing resources through the operating system, how to shield the details of the implementation, and how to provide the hardware and software unified programming model to the application developers [12].

In the domestic, Zhejiang University, China University of Science and Technology, Xi'an University of Electronic Science and Technology, National University of Defense Technology and the Chinese Academy of Sciences Institute of Computing and other research institutes have carried out fruitful research on the related problems in reconfigurable operating system. Our labs use the improved unified multitasking model to design the SHUM-UCOS operating system for reconfigurable computing, which has been able to support the dynamic creation of hardware tasks and provide a variety of topology and communication support.

3. Methodology

3.1. Reconfigurable device foundation

FPGA is the most commonly used reconfigurable device. The most widely used is based on SRAM technology. It uses the configuration SRAM to store configuration information for logical and routing resources, and the configuration information is written to the internal configuration SRAM of the FPGA to change the logic functions and interconnections between the logical units [13]. As shown in Fig. 1, Q is determined by the circuit design or hardware description language, and the corresponding configuration is controlled by programming "read" or "write".

The island structure is an early programmable device structure, and it is also a commonly used device model for academic discussion. The island structure consists of a logical cell array, routing resources, and input and output pins. Fine-grained logical units are small lookup tables (LUTs).

Existing reconfigurable devices mainly support the following reconfiguration models:

Single context model: In this model, each rewrite of configuration information must override the entire configuration memory.

Multi-context model: The main idea of this model is to prepare a plurality of

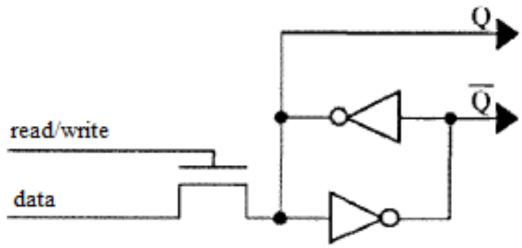

Fig. 1. SRAM-based FPGA programming principles

configuration files for the logical array of devices and store them in different addresses.

Dynamic partial reconstruction model: In this model, only some of the resources on the reconfigurable device can be reconfigured selectively without affecting the other resources on the device [14].

3.2. Dynamic reconfigurable system architecture

In this paper, the dynamic reconfigurable system based on bus connection is studied. The system is mainly composed of CPU, reconfigurable device, system memory, configuration controller and communication controller, as shown in Fig. 2.

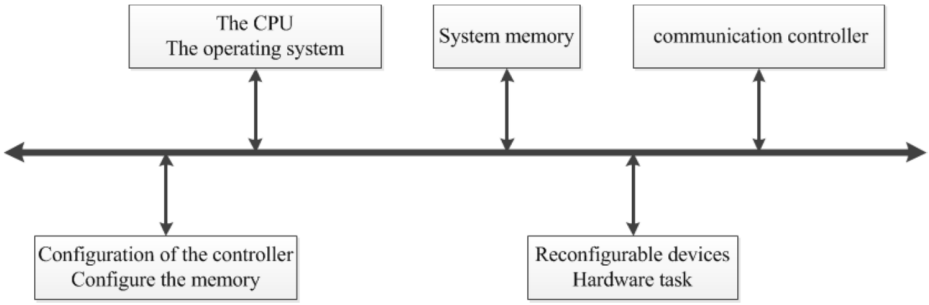

Fig. 2. Dynamic reconfigurable system based on bus connection

In Fig. 2, the operating system runs on CPU, which is responsible for managing the entire reconfigurable computing system and handling software tasks. As an additional computing unit other than the CPU, the reconfigurable device contains a number of CPUs for performing coarse-grained computationally intensive tasks. The communication controller is responsible for handling the underlying communication details and provides support for inter-task communication. The system has a dynamic partial refactoring capability that can be reconstructed on a reconfigurable device to load new hardware tasks without affecting the other running parts. Refactoring refers to the process in which the configuration controller reprograms the RPU in units of frames according to the corresponding hardware task configuration information in the configuration memory.

3.3. Experimental platform and operating environment

The experimental platform consists of XC2VP30 FPGAs and related peripherals that support DPR. The PPC 405 hardcore CPU and reconfigurable computing resources are included in the FPGA, both sharing the OPB bus, CPU clock frequency and bus frequency are 100 MHz [15]. According to the Xilinx EAPR reconfigurable system design flow, the platform is designed to be divided into AES encryption/decryption PRM and the basic design except PRM. They are located in FPGA dynamic PRR and static area. Due to the limited resources within the FPGA, the experimental platform contains only one PRR, the PRR and the static region are communicated via the bus macro, and the routing results are shown in Fig. 3.

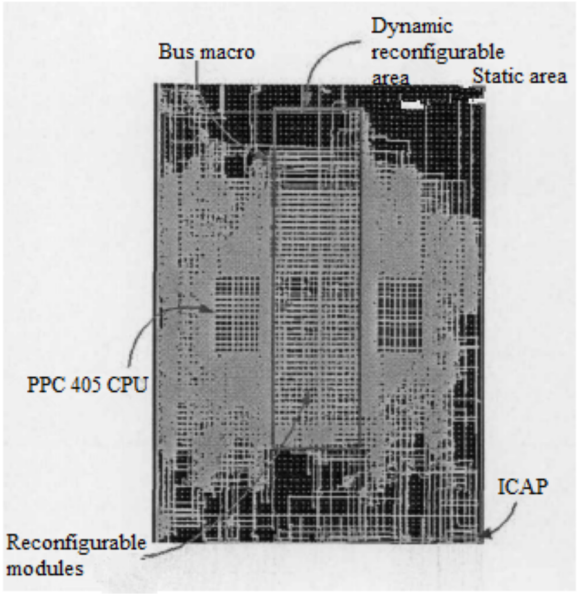

Fig. 3. XC2VP30 FPGA wiring diagram

The extended Xilkernel 3.0 operating system kernel is loaded on the above experimental platform, in addition to support priority preemptive scheduling, dynamic/static buffer allocation and semaphore synchronization, the kernel also added PRR resource management and hardware task management module. In the process of extending the thread concept from the software, the computing resource management is extended from CPU to PRR. As Xilkernel itself supports Pthread multi-threaded programming model, on this basis, it is further extended to support the creation of hardware threads, control and data transmission, to provide designers with dynamic reconfigurable hardware and software unified multi-threaded programming model SHUMDR.

Taking the AES application driven by data flow as an example, it is assumed that the data source to be processed is stored in Compact Flash in binary file format.

The application is divided into multiple threads for processing. Among them, the data producer software thread acquires the data block to be processed, the data encryption hardware thread, the thread of the data decryption hardware sharing the PRR resources, and the data block is processed. Data consumer software thread will handle the results of the data block output, through the serial port on the host. The process first allocates two shared data buffers, and then creates three threads. Among them, when hardware encryption thread was created, the dynamic binding of the pile thread, the thread between the pile thread and the producer software thread, the consumer software thread can achieve an orderly access to the shared buffer through two semaphores to complete the communication between software and hardware. According to SHUMDR, when the system is running, the operating system can dynamically reconstruct the PRR according to the resource usage and hardware task description. Once the hardware encryption thread is exited, the PRR resource is released and the data decryption thread can be created to decrypt the data. The data decryption process is similar to the data encryption process.

4. Result analysis and discussion

4.1. Hardware thread resource usage

In the previous experimental platform, the hardware thread is the hardware logic module which is run on the PRR through the HTI package, and is communicated with the CPU through the OPB bus, and is accepted by the operating system. The results are shown in Table 1.

Table 1. Usage of HTI resources

	HTI resource usage	Number of XC2VP30 FPGA resources	HTI resource occupancy
Slice	433	13696	3.20 %
FF	773	27382	2.80 %
LUT	574	27392	2.10 %
BRAM	2	136	1.40 %

As shown in the table above, the number of Slice used is only 3.2 % of the review.

4.2. Hardware thread creation

Table 2 shows the time required to create encryption and decryption hardware thread. The average creation time of the software thread set by the default attribute is 19 μs; and the hardware thread creation time includes task configuration time, task management time, and stub thread creation time.

As can be seen from Table 2, if the hardware task configuration hits, there is no need to reconfigure, the hardware thread creation time only includes task man-

agement time as well as the thread creation time for 50 µs. If the hardware task configuration is invalid, task reconfiguration is needed. In order to reduce the creation time of the hardware task configuration failure, SHUMDR uses CBB in the system memory to improve the data transmission rate. With AES encryption hardware thread, for example, task configuration time reduced from 821.9 ms to 32.29 ms. As can be seen from Table 2, the use of CBB significantly shortens the hardware thread creation time.

Table 2. Hardware thread creation time

	AAES encrypts hardware threads (bit stream file size: 307525Bytes)		AES decrypts the hardware thread (bit stream file size: 293821Bytes)	
	Use CBB	Not used CBB	Use CBB	Not used CBB
Task configuration time	32.29	821.90	31.48	776.63
Task management time+ Pile thread creation time	005	0.05	0.05	0.05
Create time for hardware task configuration failure	32.34	821.95	31.53	776.68
Create time for hardware task configuration hit	0.05		0.05	

4.3. Communication and synchronization between threads

Table 3 describes that when data cache (D-Cache) is turned on, shared buffer size is 2 K, 4 K, 8 KByte, CPU direct data I / O read and write mode is used to extend the communication time between threads corresponding to the communication API. Among them, the extended communication API combined with different shared buffer allocation, which is corresponding to different data transmission delay.

As can be seen from Table 3, compared with the way that CPU is directly responsible for data transmission, SHUMDR uses the DMA in the communication controller, which effectively improves the communication efficiency between threads. Among them, the dynamically allocated buffer is located in the D-Cache buffer memory area, while the static allocated buffer is located in the non-buffer address area. Compared with the static buffer allocation method, because of the need to maintain the consistency of Cache data, the communication time of dynamic buffer allocation is relatively long, which is characterized by better communication flexibility and programming transparency.

Table 2. Hardware thread creation time

Shared buffer size (bytes)	Communication time from software thread to hardware thread			
	Dynamic buffer allocation		Static buffer allocation	Direct I/O read and write
	D-Cache update	Data transmission	Data transmission	Data transmission
2 K	85.64	18.46	24.52	184.29
4 K	167.56	33.50	43.12	369.21
8 K	331.41	63.45	81.22	739.02
Shared buffer size (bytes)	Communication time from software thread to hardware thread			
	Dynamic buffer allocation		Static buffer allocation	Direct I/O read and write
	D-Cache void	Data transmission	Data transmission	Data transmission
2 K	83.47	18.46	24.52	184.29
4 K	165.59	33.50	43.12	369.21
8 K	329.10	63.45	81.22	739.02

5. Conclusion

As a new computing model, reconfigurable computing has high performance and flexibility, which is one of the hot research areas of the current architecture. It can configure the realization of the circuit according to the application requirements and can be used in the field of embedded system design. In this paper, through the analysis and research of the previous technology, the key technologies of practical application were deeply studied, the experimental platform was built, and the case analysis was carried out.

In this paper, a model-driven design method for reconfigurable embedded systems was proposed to design and implement a dynamic reconfigurable operating system prototype guided by a unified multitasking model, which provides designers with a unified multi-threaded programming model of hardware and software combined with the programming model. Performance of load applications was analyzed and predicted. From the different semantics and implementation of hardware and software tasks, an operating system framework based on unified multitasking model was designed.

In this paper, the key issues in system-level design and operational environment support were discussed, some progress was achieved, but there are still many areas to be improved. For example, in the prototype of reconfigurable operating system, the communication between hardware tasks still needs to be realized by the task of the pile, and the communication efficiency between hardware tasks has not been fully exploited. It is necessary to further improve the existing hardware task interface and

the inter task communication mechanism, so as to reduce the communication and synchronization overhead between the hardware tasks, to improve the performance of the operating system.

References

[1] K. Compton, S. Hauck: *Reconfigurable computing: A survey of systems and software.* ACM Computing Surveys *34* (2002), No. 2, 171–210.

[2] K. Bondalapati, V. K. Prasanna: *Reconfigurable computing systems.* Proceedings of the IEEE *90* (2002), No. 7, 1201–1217.

[3] G. Estrin: *Reconfigurable computer origins: The UCLA fixed-plus-variable (F+V) structure computer.* IEEE Annals of the History of Computing *24* (2002), No. 4, 3–9.

[4] W. A. Najjar, W. Bohm, B. A. Draper, J. Hammes, R. Rinker, J. R. Beveridge, M. Chawathe, C. Ross: *High-level language abstraction for reconfigurable computing.* Computer *36* (2003), No. 8, 63–69.

[5] D. Andrews, D. Niehaus, R. Jidin, M. Finley, W. Peck, M. Frisbie, J. Ortiz. E. Komp, P. Ashenden: *Programming models for hybrid FPGA-cpu computational components: A missing link.* IEEE Micro *24* (2004), No. 4, 42–53.

[6] M. Vuletic, L. Pozzi, P. Ienne: *Seamless hardware-software integration in reconfigurable computing systems.* IEEE Design & Test of Computers *22* (2005) No. 2, 102–113.

[7] J. M. P. Cardoso, P. C. Diniz, M. Weinhardt: *Compiling for reconfigurable computing: A survey.* Journal ACM Computing Surveys (CSUR) *42* (2010), No. 4, Article No. 13.

[8] T. El-Ghazawi, E. El-Araby, M. Huang, K. Gaj, V. Kindratenko, D. Buell: *The promise of high-performance reconfigurable computing.* Computer *41* (2008), No. 2, 69–76.

[9] M. B. Taylor, J. Kim, J. Miller, D. Wentzlaff, F. Ghodrat, B. Greenwald, H. Hoffman, P. Johnson, J. W. Lee, W. Lee, A. Ma, A. Saraf, S. Seneski, N. Shnidman, V. Strumpen, M. Frank, S. Amarasinghe, A. Agarwal: *The Raw microprocessor: A computational fabric for software circuits and general-purpose programs.* IEEE Micro *22* (2002), No. 2, 25–35.

[10] C. A. Moritz, Y. Donald, A. Agarwal: *Simple fit: A framework for analyzing design trade-offs in Raw architectures.* IEEE Transactions on Parallel and Distributed Systems *12*, (2001), No. 7, 730–742.

[11] S. C. Goldstein, H. Schmit, M. Budiu, S. Cadambi, M. Moe, R. R. Taylor: *PipeRench: A reconfigurable architecture and compiler.* Computer *33* (2000), No. 4, 70–77.

[12] T. J. Callahan, J. R. Hauser, J. Wawrzynek: *The garp architecture and C compiler.* Computer *33* (2000), No. 4, 62–69.

[13] E. Fuller, M. Caffrey, A. Salazar, C. Carmichael, J. Fabula: *Radiation testing update, SEU mitigation, and availability analysis of the virtex FPGA for space reconfigurable computing.* Third Military and Aerospace Programmable Logic Devices International Conference (MAPLD'2000), 26–28 Sept., Maryland, USA, 2000.

[14] M. Sanchez-Elez, H. Du, N. Tabrizi, Y. Long, N. Bagherzadeh, M. Fernandez: *Algorithm optimizations and mapping scheme for interactive ray tracing on a reconfigurable architecture.* Computers & Graphics *27* (2003), No. 5, 701–713.

[15] N. Gude, T. Koponen, J. Pettit, B. Pfaff, M. Casado, N. McKeown, S. Shenker: *NOX: Towards an operating system for networks.* ACM SIGCOMM Computer Communication Review *38* (2008), No. 3, 105–110.

Received September 12, 2017

Acta Technica *62* No. 2B/2017, 563–572

The large data particle clustering algorithm based on minimum variance response[1]

Zeng Jun[2]

Abstract. Large data clustering has good application value in the field of pattern recognition and fault diagnosis. A large data clustering algorithm based on minimum variance response is proposed. Firstly, the standard particle swarm algorithm is analyzed, the principle of minimum variance response and large data clustering is studied. Using the method of particle swarm optimization to reconstruct and extract the feature vector of large data information flow. Two approaches are proposed based on the limitation conditions of the minimum variance distortionless response beamforming [1]. The first one translates the uncertainty Constraints into the uncertainty for the whole extended steering vector. The second one uses the structure information of signal. Simulation results show that the algorithm can effectively improve the accuracy of data classification, reduce the error rate and improve the performance of data mining and feature extraction.

Key words. Large data clustering, particle swarm, minimum variance distortionless, response, beamforming.

1. Introduction

With the development of information computing science, the research of biology is applied in computational science, which realizes the design of intelligent bionic optimization algorithm and improves the processing and analysis ability of large data. The intelligent bionic algorithm mainly includes ant colony algorithm, Particle swarm optimization and quantum swarm optimization. Through the biomimetic principle of this kind of biological group or particle, the mathematical model of man and nature is simulated to realize the design of group intelligent optimization algorithm. The group intelligent optimization algorithm has better performance in

[1]This work was supported by the Project of Education Commission in Chongqing: Research on parallel mining of large data based on Hadoop architecture, KJ15012021 and "Chunhui" project of Ministry of education: Preliminary application of big data on intelligent agriculture platform of Internet of things, S2016038.

[2]College of Computer Engineering of Yangtze Normal University, Chongqing, China, 408100

artificial intelligence design, data clustering analysis and computer control [2].Large data clustering has a good application value in the fields of pattern recognition and fault diagnosis. In this paper, we introduce particle swarm optimization algorithm to improve the data clustering algorithm, and propose a large data particle clustering algorithm based on minimum variance response. Particle Swarm Optimization (PSO) is a population-based adaptive stochastic optimization algorithm, which is derived from Kennedy and Eberbar's research on foraging behavior of bird population. Now particle swarm optimization (PSO) is widely used in pattern recognition, data mining and intelligent control. In this paper, the standard particle swarm algorithm is analyzed, and the principle of large data clustering is studied by particle swarm optimization algorithm. Particle swarm space recombination method is used to reconstruct and extract the feature vector of large data flow, and optimize clustering is realized. Finally, performance tests were carried out by simulation experiments, showing better data clustering performance.

2. Standard particle swarm optimization and data clustering

2.1. Standard particle swarm optimization

Particle swarm optimization (PSO) is based on the simulation of biological activities, and a new intelligent optimization algorithm is constructed by simulating the ability of the group to cooperate with each other. But the particle swarm algorithm itself comes from the phenomenon of biological groups, the theoretical basis is not complete. And because of its stochastic approximation optimization algorithm, it is mainly applied to continuous region, so the algorithm has the disadvantages of premature convergence and difficulty in applying discrete problem. Therefore, it is very important to study the theoretical analysis, algorithm improvement and discretization of particle swarm optimization [3].

The standard particle swarm algorithm and the discrete binary particle swarm algorithm are analyzed and improved. We obtain the following results: (1) Particle swarm algorithm is a heuristic stochastic optimization algorithm, each particle chase its own optimal particle and global optimal location search, and chase with random factors. Particle swarm algorithm in this random search process, the particles eventually converge to the group optimal particles. In this paper, it is theoretically proved that the trajectories of the particles converge to the optimal particle position of the population under the condition of increasing the randomness and the optimization of the particle optimal point. According to the theoretical results of the analysis, the principle of algorithm weight selection is further explained.

(2) Since the particle trajectory finally converges to the population optimal particle, this paper defines the concept of similarity between particles, and designs the concept of calculating the diversity of the population particles. By calculating the average similarity of the population particles and the optimal particles of the population, and measure the diversity of particle groups. Based on the population clustering degree and its similarity with the optimal particle size, each particle is randomly generated [4]. Thus, an improved algorithm for the standard algorithm is

constructed to improve the global search ability of the algorithm, to avoid premature convergence, and to improve the standard performance of the algorithm.

(3) The weight of the standard algorithm is the parameter of the global search and local search ability of the equilibrium algorithm, and its value affects the performance of the algorithm.The weights of the standard algorithm are linearly decreasing from the early to the later, but the weight of each particle is the same. In this paper, according to the similarity between particles and the optimal particles of the population, different weights are given to different particles, so that the weight of each particle is different, and it changes with the iteration of the algorithm. This constructs a particle swarm algorithm with dynamic change of weight.

(4) The theoretical analysis of the algorithm constructs a mathematical model, and the mathematical model clearly reflects the mathematical meaning of the algorithm itself from a mathematical point of view [5].By using this mathematical model instead of the updating formula of the original algorithm speed and position, a new evolutionary algorithm is obtained, and the selection of new evolutionary algorithm parameters is analyzed. The new algorithm can directly reflect the mathematical thinking of the algorithm. The simulation results show that the new algorithm is not worse than the standard algorithm.

2.2. The basic flow of particle swarm optimization

The basic particle swarm algorithm is as follows:

Step 1: Initialization: The position and velocity of the particles are randomly generated in the dimension space of the problem space.

Step 2: Evaluation of particles: For each particle, evaluate the applicable value for the dimension optimization function.

Step 3: Update the best: 1) Compare the particle value and its individual optimal value p_{best}, if better than p_{best}, its p_{best} position is set to the current particle position. 2) Compare the value of the particle to the population's optimal value g_{best}. If the current value is better than g_{best}, set the g_{best} position to the current particle position.

Step 4: Update the particles: change the speed and position of the particle.

Step 5: Stop condition: the loop returns to Step 2 until the termination condition is met, usually satisfying the applicable value and the maximum iteration algebra.

Corresponding to the above algorithm flow, the basic framework of particle swarm algorithm is shown in Fig. 1.

2.3. Clustering algorithm overview

Traditional clustering algorithms such as hierarchical, average-linkage clustering algorithm, segmented K-Means clustering algorithm, neural network-based pre-SOM clustering algorithm and density-based DBSSAN algorithm, etc. They have been proven effective in many applications, but they also have some problems: scholars have not yet proved that they can produce the global optimal cluster, and these clustering algorithms can not be efficient and accurate processing of high-dimensional

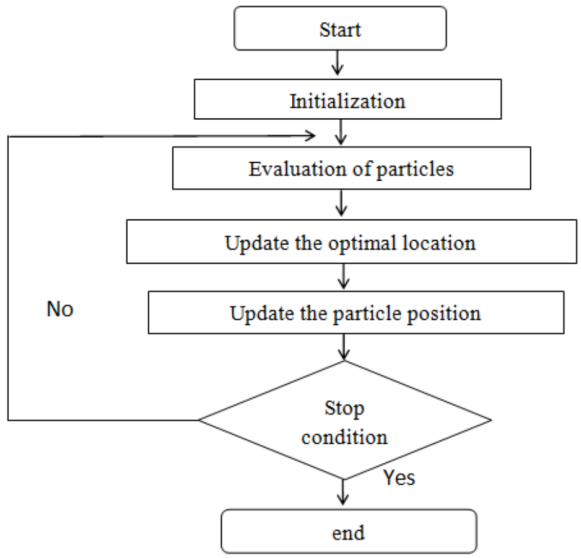

Fig. 1. The basic framework of particle swarm optimization

large number of data clustering. So we propose a large data clustering algorithm based on the nature and characteristics of the minimum spanning tree MST in graph theory. The algorithm tries to simplify the clustering problem into the edge of the MST. It is also the edge of the maximum weight of the MDT. The MST is divided into several sub-trees [6]. Each sub-tree is an optimal cluster. The process does not need to consider the size of the data and the distribution of the data shape, not only solve the above problems, but also efficient and accurate processing of large quantities of data. The algorithm can find abnormal points, and can be used in combination with other clustering algorithms, which has some expansibility.

Based on the theory of graph theory, the data set is preprocessed by quantifying the interrelatedness of each data object point. The data clustering analysis based on the network is based on the large data of Kth high dimension. Constructing adjacency: W data points are vertices, and the adjacency matrix between the data is the weight of the edge, and a full graph is constructed: and then the MST of the whole graph is generated. According to the actual problem and the distribution state of the data, A sub-tree is the sub-tree of the smallest spanning tree, and a sub-tree is an optimal clustering of the data set.

An adjacency matrix is a data matrix that uses a two-dimensional data set to represent the relationship between data points. If graph G is the weighted network graph, we can define it as:

$$A_{ij} = \begin{cases} w_{ij} & \text{if } (v_i, v_j) \text{ or } < v_i, v_j > \in E(G), \\ 0 & \text{if } (v_i, v_j) \text{ or } < v_i, v_j > \notin E(G). \end{cases} \tag{1}$$

Here, w_{ij} represents the weight of the edge, and Figs. 2 and 3 show the process of generating the adjacency matrix from the graph

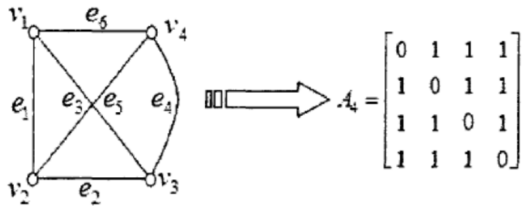

Fig. 2. The original distribution of large data

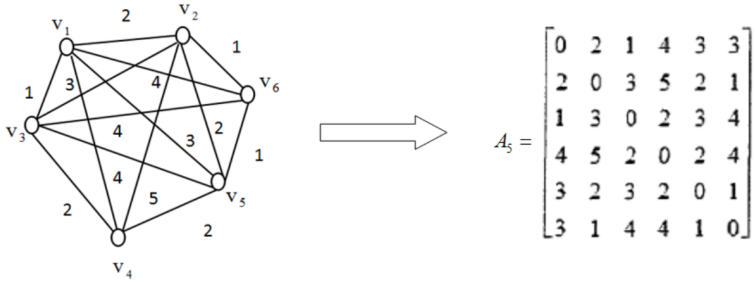

Fig. 3. Generate adjacency matrix by empowering the whole graph

From this we can see that the adjacency matrix of the network graph is a symmetric matrix, and the elements of the ith row in the matrix are the distances w_{ij} between the vertex V_i and the vertex V_j in the weighted graph.

In this paper, we obtain the adjacency matrix between the data object points, so we get the full graph represented by the adjacency matrix, and let the weight of the data object point. The algorithm of the minimum tree gets the MST of the full graph, and then divides the edge of the smallest tree. And then in accordance with the size of the MST edge of the division of the smallest tree edge, get a number of the smallest tree subtree. Each subtree is an optimal Cluster.

The clustering algorithm is an unsupervised machine learning method, which is a method of dividing data between the degrees of data objects. It can classify data with high similarity or high relevance as a cluster, but the algorithm's own subjectivity is very strong; the algorithm uses different, the starting point assumes that the difference in the number of clusters specified or pre-defined will make the results different.

2.4. Realization of large data optimization clustering

The method of particle swarm optimization is used to reconstruct and extract the feature vector of large data flow. The optimization of the algorithm is described as follows: The hybrid algorithm based on particle swarm optimization is a pair of chromosomal data with three segments. In the process of calculating the use of each

region of the data parallel operation to improve efficiency [7], as a basis for large data clustering to get clustering center vector distance:

$$(d_{ik})^2 = ||x_k - V_i||^2 . \tag{2}$$

The particle swarm optimization is performed to obtain the particle recombination state:

$$\sum_{i=1}^{c} \mu_{ik} = 1, \ k = 1, 2, ..., n . \tag{3}$$

Set the population size M, the total number of iterations of the algorithm T, the current number of iterations T_N, and obtain the phase shift velocity $V_i = (v_{i1}, v_{i2}, ..., v_{iD})^{\mathrm{T}}$ and position $x_i = (x_{i1}, x_{i2}, ..., x_{iD})^{\mathrm{T}}$ of the zero point trajectory of the multi-beam particles. Based on the constraint condition, the maximum value of the clustering objective function is obtained by using the particle swarm depth zero point trajectory optimization theorem [8]

$$\mu_{ik} = \frac{1}{\sum_{j=1}^{c} \left(\frac{d_{ik}}{jk} \right)^{\frac{2}{m-1}}} , \tag{4}$$

$$V_i = \frac{\sum_{k=1}^{m} (\mu_{ik})^m x_k}{\sum_{k=1}^{n} (\mu_{ik})^m} . \tag{5}$$

The disturbance variables loaded into the population of individuals are

$$x_{n,G} = x_{n,G} + \Delta x_i . \tag{6}$$

For each particle, a random number between [0, 1] will be generated. If $r \leq m$, and the subscript is the $i \neq g_{\mathrm{best}}$, the large data stream is reconstructed and extracted according to the information of each particle in the population P_i and P_g, we obtain the characteristic space of the multi-beam particle group depth zero locus:

$$x_i = (x_{i1}, x_{i2}, ..., x_{iD})^{\mathrm{T}} . \tag{7}$$

The multi-beam particles are added into the population to produce the recombination Schwefel 1.2 function z of the particle swarm space, which is the C×D dimension. Through the above processing, the particle swarm optimization data clustering algorithm is improved [9].

3. Simulation experiment and result analysis

In order to test the performance of this algorithm in the realization of large data clustering, we conducted a simulation experiment, the experimental use of personal PC as a hardware environment, PC operating system: Windows 7, the processor Intel (R) Core (TM) 2 Duo CPU frequency 2.93 GHz. The number of particles is $N_{\mathrm{s}} =$ 200, 500, 700, and 1000. The sampling interval is 1024 dB, the interference signal

to noise ratio is -3 dB, the other parameters are $n = 30$ K, $m = \{20,\ 50,$ and 100, the data is sampled at a sampling time of 20 s, Each component of the cluster population is between (0, 1) [10]. According to the simulation environment and parameter design, the large data clustering simulation is carried out. First, the distribution of the large data samples is given as shown in Fig.4.

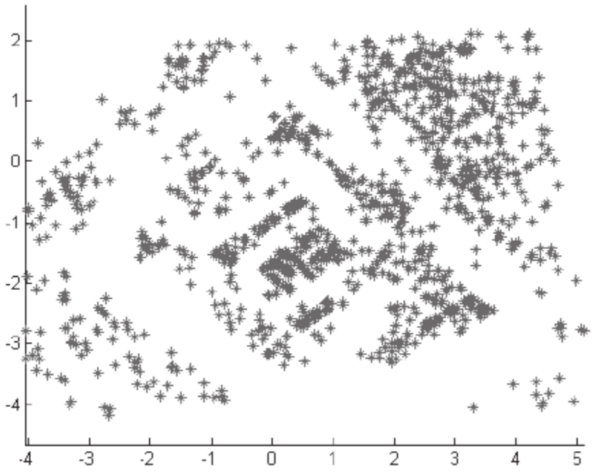

Fig. 4. The original distribution of large data

With the above data as test samples, large data feature extraction and classification processing, improve the data fusion and mining capabilities, we get clustering results shown in Fig. 5, we can see from the figure, this algorithm can effectively achieve large data clustering. The accuracy of clustering is 99.39 %, the precision is higher, the error rate is 12 % lower than that of the traditional method, and the application value is better.

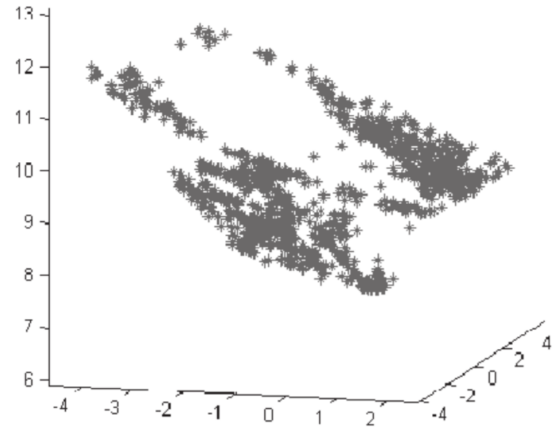

Fig. 5. The original distribution of large data

Simulation experiments are carried out to simulate the algorithm in this paper. Based on the minimum variance response, the large data particle clustering algorithm has obvious advantages both in the accuracy of the result, the complexity of the calculation or the efficiency of the calculation. This algorithm has the advantages of dealing with high - dimensional large - scale data, and it is an accurate, efficient and fast clustering algorithm, which can solve the shortcomings of traditional clustering algorithm. And in today's large data for the mainstream of the era of the algorithm has a very good practicality, can quickly and efficiently solve the problem.

4. Conclusion

This paper expounds the importance of data mining under the era of large data, and points out that the main content of this paper is based on the analysis of large data particle clustering based on minimum variance response. As an important means of data mining, clustering analysis is a kind of important data mining method, which divides the similarity data objects into the same data class cluster through certain criterion. Each subset in the sample cluster has some similar Attributes. However, the traditional clustering algorithm presents the shortcomings of low clustering efficiency, low precision and long calculation time when faced with high-dimensional large data set. Based on the nature of the minimum variance response, this paper proposes a clustering analysis of large data by using particle swarm optimization method. The adjacency matrix between each data object is constructed by correlation analysis. Through simulation experiment using the clustering method, we compare the algorithm with the traditional clustering algorithm: the large data particle clustering algorithm based on the minimum variance response, regardless of the accuracy of the result, the complexity of the calculation or the efficiency of the calculation. The algorithm has the advantages of dealing with high-dimensional large-scale data.

References

[1] I. S. Dhillon, D. S. Modha: *Concept decompositions for large sparse text data using clustering.* Machine Learning *42* (2001), Nos. 1–2, 143–175.

[2] H. Takizawa, H. Kobayashi: *Hierarchical parallel processing of large scale data clustering on a PC cluster with GPU co-processing.* Journal of Supercomputing *36* (2006), No. 3, 219–234.

[3] R. J. Hathaway, J. C. Bezdek: *Extending fuzzy and probabilistic clustering to very large data sets.* Computational Statistics & Data Analysis *51* (2006), No. 1, 215–234.

[4] S. Asharaf, M. N. Murty: *An adaptive rough fuzzy single pass algorithm for clustering large data sets.* Pattern Recognition *36* (2003), No. 12, 3015–3018.

[5] J. Cervantes, X. Li, W. Yu, K. Li: *Support vector machine classification for large data sets via minimum enclosing ball clustering.* Neurocomputing *71* (2008), Nos. 4–6, 611–619.

[6] R. Mendes, J. Kennedy, J. Neves: *The fully informed particle swarm: Simpler, maybe better.* Journal IEEE Transactions on Evolutionary Computation *8* (2004), No. 3, 204–210.

[7] Y. del Valle, G. K. Venayagamoorthy, S. Mohagheghi, J. C. Hernandez, R. G. Harley: *Particle swarm optimization: Basic concepts, variants and applications in power systems.* IEEE Transactions on Evolutionary Computation *12* (2008), No. 2, 171–195.

[8] I. C. Trelea: *The particle swarm optimization algorithm: Convergence analysis and parameter selection.* Information Processing Letters *85* (2003), No. 6, 317–325.

[9] C. A. C. Coello, G. T. Pulido, M. S. Lechuga: *Handling multiple objectives with particle swarm optimization.* IEEE Transactions on Evolutionary Computation *8* (2004), No. 3, 256–279.

[10] M. Wolfel, J. McDonough: *Minimum variance distortionless response spectral estimation.* IEEE Signal Processing Magazine *22*, (2005), No. 5, 117–126.

Received September 12, 2017

Acta Technica *62* No. 2B/2017, 573–584

The application of reactive power compensation technology in electrical automation engineering

LiMin Xu[1]

Abstract. In recent years, with the rapid development of China's social economy and the continuous improvement of science and technology, the power industry has begun to develop in the direction of electrical automation. And the reactive power compensation is of great significance for China's electrical automation. In this paper, based on the application of reactive power compensation technology in electrical automation, firstly, the key technology of reactive power compensation was introduced. Secondly, the way for realizing the application of reactive power compensation technology was discussed. Finally, the application measure of reactive power compensation technology in electrical automation was put forward, so as to provide some reference for the reactive power compensation technology in electrical automation.

Key words. Electrical automation, reactive power compensation technology, application.

1. Introduction

Reactive power compensation technology is developed recently in China, according to adjust the electronic power supply system, the maximum power grid power is achieved, and its utilization is improved. In this process, the power supply transformer and transmission line consumption is minimized, so as to improve the power efficiency in the whole electric automation, and continually improve the power supply environment [1]. With the continuous improvement of the level of electrical automation, the non-linear and unstable changes in electrical equipment increase the reactive power of the transmission line to a certain extent. While in electrical automation, the rational use of reactive power compensation technology cannot effectively improve the energy efficiency of electrical equipment, while the reactive efficiency in the automation process can be reduced, at the same time, to a certain extent, the stability and reliability of the electrical equipment operation can be improved [2]. From the current actual situation to see, China's power operation

[1]School of Electrical and Electronic Engineering, North China Electric Power University, Beijing, 102206, China; e-mail: plxwy@163.com

mode is divided into three kinds: low-voltage network, medium-voltage network and high-voltage network. In these three power operation modes, the medium-voltage network is relatively stable, and compared to high-voltage network, the low-voltage network unstable. And then, how to ensure the stability of low-voltage network and high-voltage network becomes an important issue that is urgent to be solved in the power industry [3]. Through the use of reactive power compensation technology, the stability of low-voltage network and high-voltage network has been significantly improved. Reactive power compensation technology can effectively reduce the loss of network operation and improve the utilization rate of power resources, thus increasing the capacity of power supply equipment, and effectively controlling the voltage of distribution system and power supply system in electrical automation [4]. Then, the application of reactive power compensation technology in the process of electrical automation can better maintain the stability of the power grid, thereby reducing the damage of the break current to the internal components caused in the electrical automation process, which has a good improvement role [5].

2. State of the art

2.1. The development situation and realization way of reactive power compensation technology in electrical automation

In essence, the reactive power compensation technology is mainly used to improve the high power factor of electrical automation, according to the fundamental way by combining with the current filtering technology, to achieve the purpose of harmonic compensation, and reducing the negative sequence. From the development of reactive power compensation technology at this stage, China has made considerable achievements in the research work of this technology [6]. In recent years, according to apply the reactive power compensation technology to the problem of harmonic control, to a large extent, a role in improving the power factor is played, so that the ultimate purpose of filtering or counteracting the harmonics in electrical automation is achieved.

Under the normal circumstances, in the electrical automation, the application of the effective way of reactive power compensation technology can be divided into the following several. Firstly, the simple filter design, which can be achieved by installing a fixed capacitor and reactor, but before designing this filter, the actual power should be considered, so as to ensure that the reactive power compensation technology can improve the power factor and reduce the negative sequence. Secondly, the design of vacuum circuit breaker, which has the characteristics of small investment and easy operation, however, due to at the time of closing, the vacuum circuit breaker will bring high-voltage withstand pressure for the capacitor, resulting in that dynamic compensation effect is affected. Thirdly, the hybrid voltage regulator, that is, the device consists of the fixed filters, capacitors and reactors, etc.; in general, it is to use the bus bar voltage of the regulated step-down transformer to adjust the filter or reactor voltage, so as to achieve the purpose of reactive power change. In addition,

theoretically speaking, through the thermistor on-off regulation, tap-changer no-load regulation, the electrical life will not be limited [7].

2.2. The problems of reactive power compensation technology in electrical automation

Line wear problem. Because of the restriction of the development of China's actual uncompensated compensation technology, in a large number of use processes, the current in China's electrical automation circuit is transferred in a variety of high-voltage transformer, then, through the transmission line, the current is conveyed to middle and low voltage substation with the indirect help of external machines and lines, so it is conveyed to the electricity enterprises or units that have different demands step by step [8].

Effect of harmonic content on the capacitor, in the operation of electrical automation, the capacitor in the reactive power compensation technology has a certain degree of anti-harmonic ability, and if the harmonic content in the circuit exceeds the national standard, then, the capacitor life will suffer certain impact, and it will be greatly shortened, or even appears in serious problems, resulting in that the capacitor cannot work, and the overall operation of the system is affected, which brings running errors and troubles for the whole system.

Reactive power compensation capacity configuration is unreasonable. The application of reactive power compensation technology in the field of electrical automation in China is still in a primary stage, for the reactive power compensation technology, in all relevant operations, such as the configuration coordination, it is inevitably that there will be loopholes, which causes that in the process of electric automatic operation, the power factor is too low at high load, or the phenomenon of compensation will often occur when the load is low, and this seriously affects the quality of electrical automation application [9].

2.3. Significance for applying the reactive power compensation technology in the development of electrical automation

At the same time of the rapid development of China's economy, the scientific and technological fields have also secured big development, especially the development in the field of electrical automation. Whether it is in the substation or the high-speed rail traction system, the degree of application of the electrical automation is very high. However, there is a more serious problem in the application of electrical automation technology, that is, the load problem of conventional single-phase electric traction, the variation of the load is very complex, which results in the unnecessary power increase, and then, it will affect the utilization rate of electrical automation system, which is not conducive to improving the overall efficiency. For the application of reactive power compensation technology in electrical automation, its advantages can be divided into the following points: Firstly is to provide stable support for the electrical automation system, this can not only stabilize the entire system's voltage, but also greatly improve the entire power grid quality and safety,

at the same time, the regulator can also be configured properly, so as to improve the transmission capacity of the whole system. Secondly, the partial electrical appliances will produce overheating, and the main cause of the problem is due to the existence of high harmonics, then, the use of reactive power compensation technology can avoid that better [10]. The working principle is to set the static reactive power compensator in the electrical automation system, thereby improving the voltage load in the power grid, and avoiding the phenomenon of overheating temperature, so as to protect the capacitor. Thirdly, if we meet the case of three-phase load imbalance, the reactive power compensation technology can be used, and this can balance the power. Besides, the rational application of reactive power compensation technology in electrical automation technology can effectively improve the stability and anti-interference of the electrical system.

3. Methodology

3.1. The principle of reactive power compensation

Reactive power compensation, which is referred to as reactive power compensation, it plays a role of improving the power factor of the power grid in the power supply system, reducing the power supply transformer and transmission line loss, improving the power efficiency and the power supply environment. Therefore, in the power supply system, reactive power compensation device is in an indispensable and very important position. The reasonable choice of the compensation device can minimize the loss of the power grid and improve its quality [11]. On the contrary, if the choice or use is improper, it may cause the increase of the power supply system, voltage fluctuations, harmonics and many other factors.

Power output power includes two parts: Firstly is the active power: direct consumption of electricity, the electrical energy is transformed into mechanical energy, heat, chemical energy or sound energy, according to use these work, this part of the power is known as active power; secondly is the reactive power: electricity consumption, this is only to change the electrical energy into another form of energy, which is the essential condition for the electric device to be able to work, furthermore, this energy can conduct the periodic transformation with the electric energy in the power grid, which is called as reactive power (such as the occupied electric energy for the electromagnetic components to establish the magnetic field, the occupied electric energy for the capacitor to establish the electric field) [12].

3.2. The significance of reactive power compensation

Compensating the reactive power can increase the proportionality constant of active power in the power grid.

Reducing the design capacity of power supply equipment, reducing the investment, for example, when the power factor $\cos\varphi = 0.8$ increases to $\cos\varphi = 0.95$, the capacitor that takes 1 kvar can save equipment capacity 0.52 kW; conversely, for the original equipment, increasing 0.52 kW is equivalent to increase the power

supply equipment capacity. Therefore, the new construction and alteration of the engineering should take full account of reactive power compensation, so that the design capacity can be reduced, thereby reducing investment.

Reducing the line loss, the formula for calculating the change of power factor is shown in Fig. 1.

$$\Delta P\ (\%) = 1 - \frac{\cos\theta}{\cos\varphi} \times 100\,\%\,. \tag{1}$$

It can be derived from (1), that $cos\varphi$ is the power factor after the compensation, $cos\theta$ is the power factor before the compensation, then: $cos\varphi > cos\theta$, Therefore, after increasing the power factor, the line loss rate is reduced, besides, reducing the design capacity and the investment, increasing the transmission ratio of active power in the power grid, and reducing the line loss directly determine and affect the economic benefits of power supply enterprises [13].

3.3. Function of reactive power compensation technology in electrical automation

The continuous advancement of electromechanical integration and the application of electrical automation have greatly accelerated the development speed of power system. The reactive power compensation technology system of electrical automation is shown in Fig. 1, and its function is shown in Table 1.

Table 1. Function of the reactive power compensation technology of the electrical automation

1	When the three-phase load appears in the unbalanced conditions, the reactive power compensation technology can balance the three-phase apparent power, which plays an important role in improving the overall performance and anti-interference of power system.
2	Because the power network composed of a large number of power transmission lines can be divided into three modes: high, medium and low. In most cases, the flow voltage of the high-voltage network and low-voltage network is very unstable, and then, the use of reactive power compensation technology can improve the stability and reliability of the electrical automation system, so that the power system can greatly improve the transmission quality in more secure conditions. Moreover, in actual use, the corresponding regulator can be equipped with, and then, according to cooperate with the reactive power compensation technology, the overall performance of the system operation is improved, and the system's anti-interference is enhanced.
3	Application of reactive power compensation technology in electrical automation can improve the power factor of the power grid and its load, and reduce the capacity of each part of the electrical equipment as much as possible, thus saving the operating costs and energy consumption.
4	In addition, the reactive power compensation technology can also configure the corresponding static vary compensator for the system, on the one hand, it can regulate the voltage of the power grid in the operation of electric automation; on the other hand, it can also provide safety guarantee for the cable and capacitor in the operation of electrical automation, so as to prevent the local heating failure caused by the high-frequency harmonics.

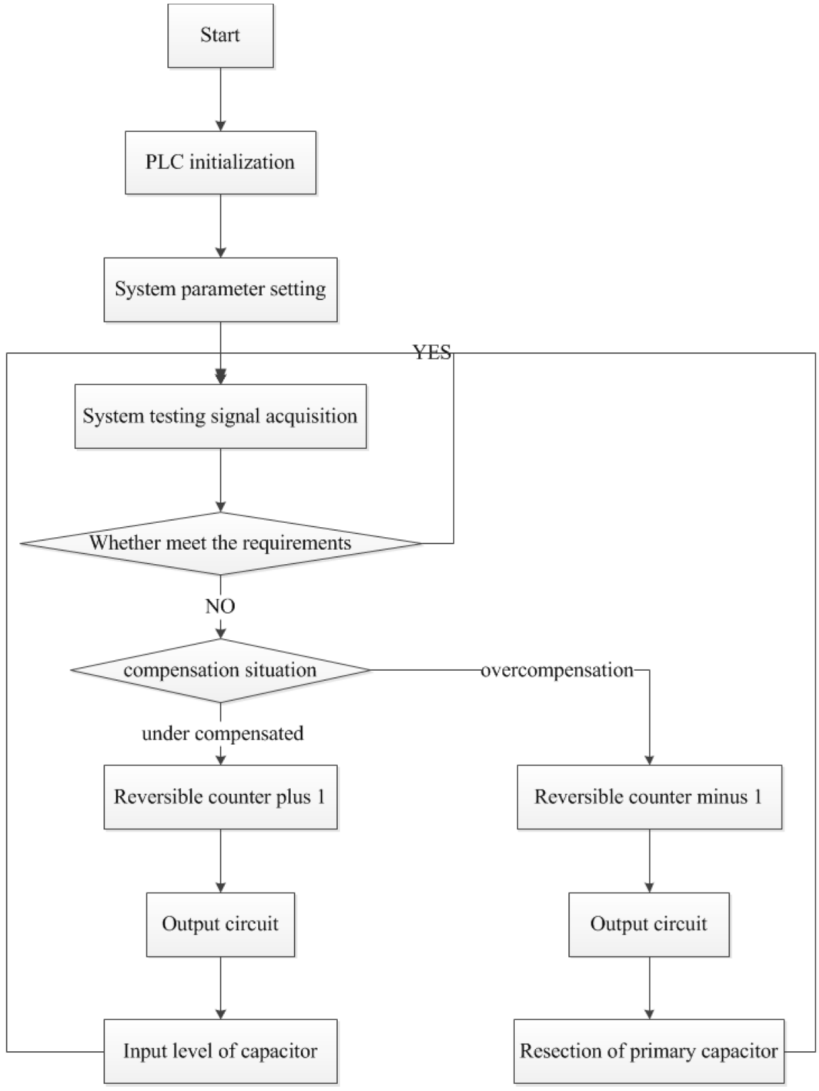

Fig. 1. Reactive power compensation system of the electrical automation

3.4. The key technology of reactive power compensation

Power factor was introduced as follows in this paper. The so-called power factor mainly refers to the proportion of the active power supplied by the apparent power of the transformer and the line in the power network. In the operation of power network, the power factor should be increased as much as possible. Because the bigger the power, the better it is. If the power factor is large, most of the active power can be supplied by the apparent power of the power equipment. Therefore, the transmission of reactive power and the loss of active power are reduced [14].

The power factor of the power supply equipment can be improved and the quality of the voltage can be guaranteed by improving the power factor of the users within a reasonable range. In this case, when Q is 0, the power factor is 1. Therefore, in order to reduce the reactive power consumption of power equipment, it is necessary to improve the power factor.

The method of compensating reactive power of shunt capacitor is as follows. The adjustment of reactive compensation voltage: the removal and input of shunt compensation capacitor will have certain influence on the voltage change of transformer load side. Therefore, the quality of the voltage can be improved by the removal and input of the capacitor. Firstly, the capacitor input is adjusted to the load side voltage of the transformer, which is shown in formula (2). The adjustment of the voltage measured by the transformer when the capacitor is cut out is shown in formula (3).

$$U_{\mathrm{H}} = \sqrt{\sum_{n=2}^{\infty} U_n^2}, \quad I_{\mathrm{H}} = \sqrt{\sum_{n=1}^{\infty} I_n^2}\,, \tag{2}$$

$$U_{\mathrm{h}} = \sqrt{\sum_{k=1}^{25} X_k I_k}\,. \tag{3}$$

Here, U_{h} is harmonic voltage limit, X_k is the impedance of the kth harmonic, ${}_I k$ is the current of the kth harmonic.

3.5. Design method of reactive power compensation technology in electrical automation

Table 2 summarizes the design method of reactive power compensation technology in electrical automation.

3.6. Solving measures of the reactive power compensation technology in the application of electrical automation

Strengthening the management of the user side, according to strengthen the energy saving and management of the user side, the users can be fully aware of the importance of reactive power compensation technology in electrical automation, and then set up a consciousness of correctly treating the relationship between reactive power compensation technology and power loss, so that to a large extent, the loss of electrical energy in transmission lines can be reduced from the internal part.

Determining the actual capacity of substation reactive power compensation, in determining the actual capacity size of the substation reactive power compensation, people should be fully aware of the actual situation in different regions, and besides, there are differences in the regulation of substation [15]. On this basis, the reactive power compensation technology is used to conduct the reactive power compensation for the low load, transformer of the transformer substation. And the latest technology, equipment and technology, the reasonable compensation capacity of power industry are used. In addition, it is necessary to strengthen the skill training of staff,

and try to reduce and prevent the occurrence of reactive power back phenomenon.

Table 2. Design method of reactive power compensation technology in electrical automation

Method	Concrete content
The method of combining the thyristor adjustment reactor phase with the stable filtering equipment	Through the method of combining the thyristor adjustment reactor phase with the stable filtering equipment, the inductive current of the inflow loop can be influenced at the time of adjusting the saturation degree of saturation reactor, so as to enable the extra capacitive power in the parallel filter to achieve a balance. At the same time, because the filter can be put into irregularly, to a certain extent, the use of thyristors is reduced, and the processing speed of the system is greatly guaranteed, but the drawback will be generated by filtering.
Method of combining with a stable filter, the capacitor adjustment pressure and capacitor	Before using this method, it is necessary to adjust the bus voltage of the two sides of the transformer low voltage, so as to connect the filter on the low-voltage bus or the voltage on reactor, and achieve the purpose of changing reactive power. However, in terms of the present situation, the technical level for achieving the combination of stable filter, capacitor adjustment pressure and capacitor is not mature and perfect enough.
Method of combining with the stable filtering harmonic device and controllable saturation reactor	Series reactors and anti-parallel thyristors can play a role of balancing and paralleling the compensating current of the additional capacitive reactive power of filter, so as to meet the requirements of the power factors. Relatively speaking, this technology has several advantages: high investment time, easy to operate, fast adjustment speed, and does not produce resonance and other advantages, while because this technology has higher technical requirements, the risk is higher, the cost is relatively expensive and other factors, resulting in that this technology cannot be well applied.

Effectively compensating the low-voltage side of the distribution network capacitor group, in this regard, it is necessary to pay attention to the reduction of the power and electric power caused by the transformer and line passing through the reactive current transmission, while for the common transformer unit that its load is relatively large, it is necessary to consider whether setting the capacitor bank at the side of low-voltage distribution network, and then to implement the effective compensation.

4. Result analysis and discussion

4.1. Cyclic switching test of simplified structure of reactive power compensation system

Intelligent low-voltage reactive power compensation system simplified architecture consists of two intelligent compensation capacitor integrated modules, and the two integrated modules are equipped with two three-phase capacitors that the capacity is 5 kVAr. After power-on, firstly is to set the ID number of the capacitor

and the corresponding capacity; then, it is to set one of them as the main controller mode, and the other is the non-controller mode. The experimental results of connecting the reactive power compensation system into the power grid are shown in Table 3.

Table 3. Experimental results of simplified structure of reactive power compensation system

	Three-phase voltage U (V)	Current value I (A)	Apparent power S (KVA)	Reactive power Q (kVAr)	Power factor $\cos\varphi$
Before compensation	211	106	22	15.3	0.73
After compensation	217	78	16.8	5.4	0.95

It can be found that, firstly, the thyristor conduction, that is corresponding to the first capacitor, the capacitor is put into the grid, indicating to compensate 5 kVAr of amount of reactive power; and after a period of time, the thyristor conduction, that is corresponding to the second capacitor, the capacitor is put into the grid, then, there is no capacitor to be put into. After the three-phase motor's operation is stopped, the first capacitor is first removed, then, followed by the second capacitor, indicating that the desired effect of the recirculation is achieved.

4.2. Optimized switching test for standard architecture of reactive power compensation system

Intelligent low-voltage reactive power compensation system standard architecture consists of a reactive power compensation controller and two intelligent compensation capacitor integrated modules, and among them, the capacity of one integrated module is 5 kVAr three-phase capacitor and 10 kVAr three-phase capacitor; then, another integrated module has 20 kVAr three-phase capacitor and 40 kVAr three-phase capacitor. According to connecting this set of reactive power compensation system to the power grid, the experimental results after operation are shown in Table 4.

Table 4. Experimental results of the standard architecture of reactive power compensation system

	Three-phase voltage U (V)	Current value I (A)	Apparent power S (KVA)	Reactive power Q (kVAr)	Power factor $\cos\varphi$
Before compensation	211	106	22	15.3	0.73
After compensation	218	82	17.6	4.9	0.96

Through the experiment, it can be found that after the compensation capacitor of the reactive power compensation system, the power factor of the power grid is

compensated from the original 0.73 to 0.96, and the voltage value is increased from 211 V to 218 V. After the capacitor is put into the power grid, the reactive power value is reduced a lot, and the quality of the power grid is highly improved.

5. Conclusion

In electrical automation, the use of reactive power compensation technology not only enhanced the coordination and integrity of the entire system, but also played a key role in improving its stability, at the same time, it also provided the conditions for the use and utilization of the resources and energy of the whole system more effectively, which played an important role in ensuring that the equipment could be safely used in the electrical automation system. Then, according to discuss the development status, ways of realization, design method of reactive power compensation technology in the electrical automation, as well as the problems in the application process, a reasonable and effective way to solve these problems was found, so that the efficiency of electronic automation was further improved, and the loss of power energy during transmission was reduced. Moreover, in order to further promote the reform and development of electrical automation industry, it is necessary to strengthen relevant technical personnel's research and development efforts, and strengthen the improvement of technology and equipment, then solve the problems existing in the application of reactive power compensation technology in electrical automation.

References

[1] J. Sauer, B. S. Wiese, B. Rüttinger: *Ecological performance of electrical consumer products: The influence of automation and information-based measures.* Applied Ergonomics *35* (2004), No. 1, 37–47.

[2] W. Yue, G. Tao, S. Wang, B. Tian: *2-D numerical simulation of digital rock experiments with lattice gas automation for electrical properties of reservoir formation.* Geophysical Journal International *183* (2010), No. 3, 1316–1323.

[3] S. Musa: *Perceptions of automation industries towards the automation curriculum of the electrical equipment and installation technology course at Malaysia France Institute.* Textbook, Universiti Teknologi Malaysia (2000).

[4] Y. Koseki, H. Maruhashi, H. Miyadera: *Fundamental study of LCA method for electrical appliances and office automation equipment.* Chemical Engineering and Materials Research Information Center *24* (1998), No. 6, 934–939.

[5] L. A. Moran, J. W. Dixon, R. R. Wallace: *A three-phase active power filter operating with fixed switching frequency for reactive power and current harmonic compensation.* IEEE Transactions on Industrial Electronics *42* (1995), No. 4, 402–408.

[6] A. Luo, Z. Shuai, W. Zhu, Z. J. Shen: *Combined system for harmonic suppression and reactive power compensation.* IEEE Transactions on Industrial Electronics *56* (2009), No. 2, 418–428.

[7] Z. Shu, S. Xie, Q. Li: *Single-phase back-to-back converter for active power balancing, reactive power compensation, and harmonic filtering in traction power system.* IEEE Transactions on Power Electronics *26* (2011), No. 2, 334–343.

[8] S. Bolognani, S. Zampieri: *A distributed control strategy for reactive power com-*

pensation in smart microgrid. IEEE Transactions on Automatic Control *58* (2013), No. 11, 2818–2833.

[9] M. Singh, V. Khadkikar, A. Chandra: *Grid synchronisation with harmonics and reactive power compensation capability of a permanent magnet synchronous generator-based variable speed wind energy conversion system.* IET Power Electronics *4* (2011), No. 1, 122–130.

[10] D. Das: *Reactive power compensation for radial distribution networks using genetic algorithm.* International Journal of Electrical Power & Energy Systems *24*, (2002), No. 7, 573–581.

[11] C. S. Lam, W. H. Choi, M. C. Wong, Y. G. Han: *Adaptive DC-link voltage-controlled hybrid active power filters for reactive power compensation.* IEEE Transactions on Power Electronics *27* (2012), No. 4, 1758–1772.

[12] G. E. Valderrama, P. Mattavelli, A. M. Stankovic: *Reactive power and imbalance compensation using STATCOM with dissipativity-based control.* IEEE Transactions on Control Systems Technology *9* (2001), No. 5, 718–727.

[13] F. Li, J. D. Pilgrim, C. Dabeedin, A. Chebbo, R. K. Aggarwal: *Genetic algorithms for optimal reactive power compensation on the national grid system.* IEEE Transactions on Power Systems *20* (2005), No. 1, 493–500.

[14] R. Majumder: *Reactive power compensation in single-phase operation of microgrid.* IEEE Transactions on Industrial Electronics *60* (2013), No. 4, 1403–1416.

[15] M. Prodanovic, K. de Brabandere, J. van den Keybus, T. Green, J. Driesen: *Harmonic and reactive power compensation as ancillary services in inverter-based distributed generation.* IET Generation, Transmission & Distribution *1* (2007), No. 3, 432–438.

Received September 12, 2017

Acta Technica *62* No. 2B/2017, 585–596

Environmental forecast of the solar greenhouse based on the weighted Markov chain[1]

Dongsheng Zhou[2,3,5], Yikui Bai[3,5,6], Rongfei Zhao[3,5], Yingchun Jiang[4,5]

Abstract. The prediction of Greenhouse environment is greatly important for solar greenhouse modeling. Solar irradiation, humidity and soil temperature are the main influence factors of the temperature in the greenhouse. The paper builds the weighted Markov chain model, it uses sequential cluster to realize the state classification of sample output, it calculates the coefficients and weights of each order autocorrelation, in order to simulate and predict the parameters in the short term, which include the average solar irradiation, the average humidity and soil temperature, and then it predicts the average temperature of the greenhouse. Simulation results show that environmental forecast interval is reasonable; the short term prediction modeling is accurate. It provides a theoretical basis for the greenhouse temperature prediction, which has important guiding significance in the light of the analysis of uncertainty parameter in greenhouse. It is easy to bring about, it is less time to calculate, and provides a broader prospects

Key words. Solar greenhouse, simulation, sequential cluster, the weighted Markov chain, environment prediction.

1. Introduction

Chinese solar greenhouse is the main production style of vegetables and fruits in the north of China in the winter. Solar irradiation is the main source of energy, and it

[1]This work was supported by NSFC (51508345), modern agricultural industry technology system special Funds (CARS-25-C-01), Chinese postdoctoral science foundation project(2014M561250), and general project of Education department of Liaoning province (LSNYB201618).

[2]College of Information and Electrical Engineering, Shenyang Agricultural University, Shenyang 110866, China

[3]College of Water Conservancy, Shenyang Agricultural University, Shenyang 110866, China

[4]College of Engineering, Shenyang Agricultural University, Shenyang 110866, China

[5]Engineering & Technology Research Center of Protected Agricultural Environment and Equipment of Liaoning Province, Shenyang 110866, China

[6]Corresponding author

is affected by the season and weather; humidity reduces with temperature rises, and humidity rises with temperature reduces; soil temperature rises or reduces with the temperature of greenhouse [1, 2]. So mastering the relation of temperature and the three influence factors is of great significance for the production of the greenhouse.

Research of environment of greenhouse focuses on the irradiation, temperature and humidity. Light model is established to calculate the direct solar radiation and scattered radiation [3, 4], time series method [5], nerve network [6], constrained predictive control model and self-adapting mechanism model to forecast the temperature of the solar greenhouse [7, 8]. The paper puts forward improving extreme learning machine algorithm [9], grey prediction model to forecast the temperature and humidity [10]. Daily change and math-expression method is used to analyze the temperature variation [11]. Markov chain is used to simulate and predict the PV output and wind speed in recent years, and got the better effects [12–15].

2. Materials and methods

2.1. Data analysis

The experimental greenhouse is located in the Shenyang Agricultural University scientific research base (123.4 °E, 41.8 °N). The greenhouse toward for 5 ° south by west, the length is 60 m, the span is 10 m, the angle of south roof is 30.5 °, the height of roof is 5 m, the height of back wall is 3.2 m, the wall is multilayer that is combined bricks and benzene board, the film is PE. The structure of greenhouse is main structural style in the Liaoning China.

The samples were selected from December 1st, 2015 to January 19th, 2016, a total of 50 days of data. The experiment measured the data of solar irradiation that entered greenhouse, inner temperature of greenhouse, inner soil temperature, inner humidity and outer temperature through using the wireless meteorological station made by ADCON, spectral range of pyranometer is between 400 nm and 1100 nm, operating temperature is between –30 ° and 70 °C, sensitivity is between 60 V $W^{-1}m^{-1}$ and 100 V W^{-1} m^{-1}, max irradiation is 2000 W m^{-2}, accuracy of temperature sensor is $< \pm 0.2$ °C, measure range is between –40 °C and 60 °C. The equipment records data every 15 minutes. We selected the data from 9:00 to 15:00 and calculated the total solar irradiation, average humidity, average inner temperature and average outer temperature.

The environmental data samples in solar greenhouse are shown in Figure 1. The distribution curve shows random distribution characteristics, and there is distinct boundaries interval range. Therefore, Markov chain short-term prediction is suitable for matching the characteristics of temperature interval distribution. In the actual engineering design, the temperature specific values in solar greenhouse are undetermined, but their state boundaries can be predicted to achieve by Markov chain. So the feasible range is provided for engineering design by means of Markov chain prediction.

Inner temperature of greenhouse is a main indicator that measures greenhouse. Solar irradiation, outer temperature and soil temperature are major impact factors.

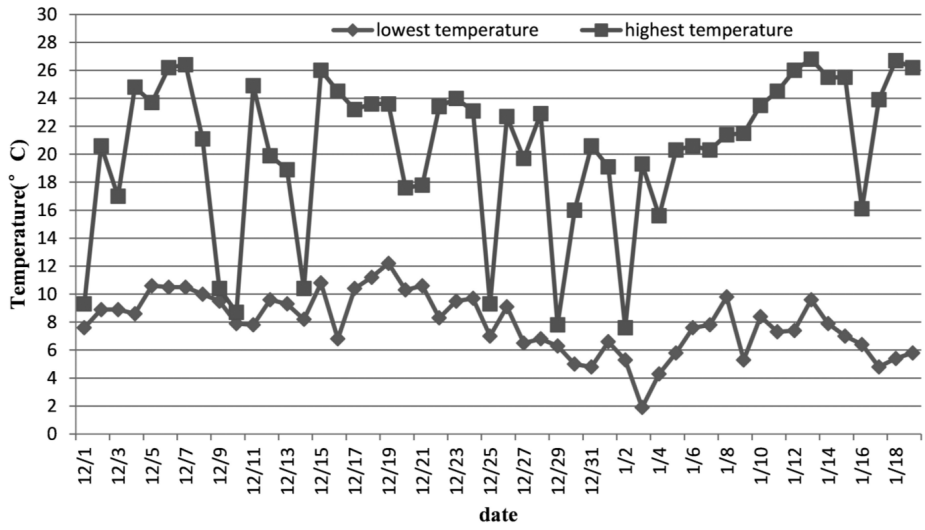

Fig. 1. Temperature range of data samples

The linear relationship analysis is based on SPSS 20.0 and significance level is less than or equal to 0.05. The analysis result is shown in Table 1.

Table 1. The linear relationship analysis of impact factors and inner temperature

Impact factor	Association	Sig.	R^2
Solar irradiation	0.711	0.000	0.769
Soil temperature	–0.790	0.000	
Humidity	0.789	0.000	

Analyzed from Table 1, the three impact factors and inner temperature exhibit a linear relationship. Multivariate regression linear equation is $y = 0.907 + 0.10x_1 - 0.65x_2 + 1.111x_3$.

For next processing, Consider the method presented by Fisher in 1958. It is used to deal with sequential data. The steps of classification are as follows: Ordinal sample is X, $b\,(n,k)$ represents the kth classifications of n samples. Symbol G represents one of the classifications and contains parameters $\{X_{(i),}X_{(i+1),}\ldots\ldots,X_{(j),}\}\,(j>i)$. The average vector

$$\bar{X}_G = \frac{1}{j-i+1}\sum_{t=i}^{j} X_{(t)}\,.$$

Let $D\,(i,j)$ represents diameter of the classification,

$$D(i,j) = \sum_{t=i}^{j}\left(X_{(t)} - \bar{X}_G\right)'\left(X_{(t)} - \bar{X}_G\right)\,.$$

If $m = 1$, then $D(\mathrm{i}, j) = \sum_{t=i}^{j} \left| X_{(t)} - \bar{X}_G \right|$, $\bar{X}_G$ representing the median of data. Define the error function L

$$L[b(n,k)] = \sum_{i=1}^{k} D(i_t, i_{t+1} - 1) \ . \tag{1}$$

If $L[b(\mathrm{n}, \mathrm{k})]$ is smaller, the sum of deviations is also smaller. The classification is then more reasonable. Then, based on the equation (1), we achieve the optimal segmentation through the iterative method.

Obtain the optimal solution. First, find j_k as the point of division, make the result of (1) the smallest possible, and obtain G_k. Now, based on the above method, obtain all classifications G_1, G_2, G_3, ..., G_k. This can be written as

$$p(n,k) = \{G_1, G_2, \ldots, G_{1k}\} \ . \tag{2}$$

2.2. Weighted Markov chain

Markov Chain is a random process that meets two hypothesizes as follows:

1. Probability distribution of system state at the $T + 1$th moment relates with Tth moment, and has nothing to do with phenomena before Tth moment.

2. State transition from Tth to $T + 1$th moment has nothing to do with the Tth moment. A Markov Model is represented by triple $E = (S, P, Q$, where S represents the state space, P represents the state transition probability and Q represents the initial probability density.

The weighted Markov Chain is an improved Markov chain. It can be used to describe a lot of dynamic in economic, weather forecast, etc. It can predict the current state based on the number of past states, then predict and analyze through weight on the basis of the relationship of the current state and the past states, achieve the aim of prediction adequately and reasonably. The method is suitable for prediction in short term.

3. Case study and discussion

The experimental greenhouse lies in the science and research base of Shenyang Agricultural University. Select 50 sets of data of total irradiation, average humidity and average soil temperature. Adopt the Weighted Markov Chain to predict total irradiation, average humidity and average soil temperature. Based on the three indicators, analyze the range of inner temperature of greenhouse. Explain the process based on the irradiation. The steps are as follows:

Step (1). Classify the data in accordance with the Sequential Clustering Method, generate the classification standard. In the example, the data is classified five classes, which includes total irradiation, average humidity and average soil temperature. The standard is shown in Table 2.

Table 2. Classification standard of data

State	Total irradiation	Average humidity	Average soil temperature
1	$<1000\,\mathrm{W/m^2}$	>85	$<12.5\,^\circ\mathrm{C}$
2	$1000\sim3000\,\mathrm{W/m^2}$	$75\sim85$	$12.5\sim14\,^\circ\mathrm{C}$
3	$3000\sim4500\,\mathrm{W/m^2}$	$65\sim75$	$14\sim15\,^\circ\mathrm{C}$
4	$4500\sim5900\,\mathrm{W/m^2}$	$58\sim65$	$15\sim17\,^\circ\mathrm{C}$
5	$>5900\,\mathrm{W/m^2}$	<58	$>17\,^\circ\mathrm{C}$

Step (2). Transform the irradiation value into the corresponding state, which is shown in Fig. 2.

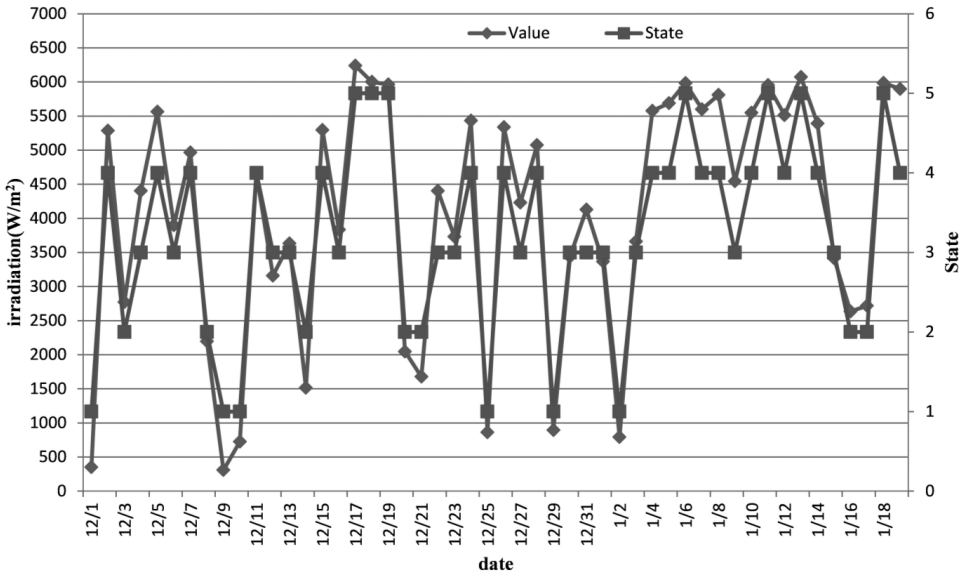

Fig. 2. Irradiation and state classification

Step (3). Calculate autocorrelation coefficient of every order $r_k,\ k \in E$.

$$r_k = \frac{\sum_{l=1}^{n-k} (x_l - \overline{x})\,(x_{l+k} - \overline{x})}{\sum_{l=1}^{n} (x_l - \overline{x})^2}\,. \tag{3}$$

In the equation, r_k represents autocorrelation coefficient of the kth order, x_l represents irradiation of the lth moment, and $\bar{x}$ represents average irradiation. The autocorrelation coefficient is shown in Table 3.

Table 3. Autocorrelation coefficient of orders from 1 to 8

	1	2	3	4	5	6	7	8
r_k	0.9542	-1.3977	-1.3171	-2.9484	1.3758	0.9132	1.2616	0.9707
z_k	0.0857	0.1255	0.1182	0.2647	0.1235	0.0820	0.1133	0.0871

Step (4). Normalize the autocorrelation coefficient.

$$w_k = \frac{|r_k|}{\sum_{k=1}^{m} |r_k|} \,. \tag{4}$$

Here, w_k represents the weight of the kth order, m represents the max order. The weights are also shown in Table 3.

Step (5). Calculate respectively eight-order transfer matrices, the matrices representing the probability rules of state transitions.

$$P^{(1)} = \begin{bmatrix} 1/6 & 0 & 1/3 & 1/2 & 0 \\ 1/7 & 2/7 & 2/7 & 1/7 & 1/7 \\ 1/14 & 1/7 & 2/7 & 3/7 & 1/14 \\ 2/15 & 2/15 & 2/5 & 2/15 & 1/5 \\ 0 & 1/7 & 0 & 4/7 & 2/7 \end{bmatrix},$$

$$P^{(2)} = \begin{bmatrix} 0 & 1/6 & 1/2 & 1/3 & 0 \\ 1/7 & 0 & 3/7 & 2/7 & 1/7 \\ 3/14 & 3/14 & 3/14 & 3/14 & 1/7 \\ 1/15 & 1/15 & 4/15 & 7/15 & 2/15 \\ 0 & 1/3 & 1/6 & 1/6 & 1/3 \end{bmatrix},$$

$$P^{(3)} = \begin{bmatrix} 0 & 0 & 2/3 & 1/3 & 0 \\ 0 & 0 & 1/3 & 1/2 & 1/6 \\ 3/14 & 0 & 3/14 & 5/14 & 3/14 \\ 2/15 & 1/5 & 1/5 & 4/15 & 1/5 \\ 0 & 1/2 & 1/3 & 1/6 & 0 \end{bmatrix},$$

$$P^{(4)} = \begin{bmatrix} 1/3 & 1/6 & 1/6 & 1/6 & 1/6 \\ 1/5 & 0 & 1/5 & 2/5 & 1/5 \\ 1/14 & 1/7 & 2/7 & 5/14 & 1/7 \\ 1/15 & 1/15 & 4/15 & 2/5 & 1/5 \\ 0 & 1/3 & 1/2 & 1/6 & 0 \end{bmatrix},$$

$$P^{(5)} = \begin{bmatrix} 0 & 1/6 & 1/2 & 1/3 & 0 \\ 1/5 & 1/5 & 1/5 & 1/5 & 1/5 \\ 1/13 & 1/13 & 2/13 & 6/13 & 3/13 \\ 1/5 & 2/15 & 1/3 & 4/15 & 1/15 \\ 0 & 1/6 & 1/3 & 1/6 & 1/3 \end{bmatrix},$$

$$P^{(6)} = \begin{bmatrix} 0 & 0 & 1/3 & 2/3 & 0 \\ 1/5 & 2/5 & 1/5 & 1/5 & 0 \\ 3/13 & 0 & 4/13 & 3/13 & 3/13 \\ 0 & 3/14 & 2/7 & 3/14 & 2/7 \\ 1/6 & 1/6 & 1/6 & 1/2 & 0 \end{bmatrix},$$

$$P^{(7)} = \begin{bmatrix} 0 & 1/6 & 1/2 & 1/6 & 1/6 \\ 1/5 & 1/5 & 1/5 & 2/5 & 0 \\ 1/13 & 2/13 & 4/13 & 4/13 & 2/13 \\ 1/7 & 1/7 & 2/7 & 2/7 & 1/7 \\ 1/5 & 0 & 0 & 2/5 & 2/5 \end{bmatrix},$$

$$P^{(8)} = \begin{bmatrix} 1/3 & 0 & 0 & 1/6 & 1/2 \\ 1/5 & 0 & 2/5 & 2/5 & 0 \\ 0 & 4/13 & 4/13 & 4/13 & 1/13 \\ 1/13 & 1/13 & 5/13 & 3/13 & 3/13 \\ 1/5 & 0 & 1/5 & 3/5 & 0 \end{bmatrix},$$

Step (6) Calculate the state probability of the moment. $P_i^{(k)}$, $i \in E$, $k = 1, 2, \ldots, m$ Predict the irradiation state on the January 20. The results are shown in Table 4.

Table 4. Prediction table of total irradiation on January 20

Initial day	State	Hysteresis time (day)	Weight	State					Probability resource
				1	2	3	4	5	
Jan.19	4	1	0.0856645	2/15	2/15	2/5	2/15	1/5	$P^{(1)}$
Jan.18	5	2	0.1254783	0	1/3	1/6	1/6	1/3	$P^{(2)}$
Jan.17	2	3	0.1182479	0	0	1/3	1/2	1/6	$P^{(3)}$
Jan.16	2	4	0.2647003	1/5	0	1/5	2/5	1/5	$P^{(4)}$
Jan.15	3	5	0.1235196	1/13	1/13	2/13	6/13	3/13	$P^{(5)}$
Jan.14	4	6	0.0819807	0	3/14	2/7	3/14	2/7	$P^{(6)}$
Jan.13	5	7	0.1132639	1/5	0	0	2/5	2/5	$P^{(7)}$
Jan.12	4	8	0.0871448	1/13	1/13	5/13	3/13	3/13	$P^{(8)}$
P_i (the sum of weights)				0.103	0.087	0.224	0.337	0.249	

Step (7). The weighted sum of every same state prediction probability is taken as the prediction probability of the state

$$P_i = \sum_{k=1}^{m} w_k P_i^k, \ i \in E, \tag{5}$$

where $\max\{P_i,\ i \in E\}$ is the prediction probability. In Table 5, the state of total irradiation on the Jan. 20 is 4, the result agrees with the actual value. And so on, we predict the state for the next 5 day; the results are also shown in the Table 5.

The same method is used for calculation of prediction of humidity and soil temperature. The results are shown in Table 6 and Table 7, respectively.

Table 5. The results simulation and prediction of total irradiation

Date	State					Prediction state	Actual state	Actual value
	1	2	3	4	5			
Jan. 20	0.1032	0.0870	0.2235	0.3373	0.2490	4	4	5767.4
Jan. 21	0.1500	0.1198	0.2598	0.3238	0.1466	4	4	5680.0
Jan. 22	0.0921	0.2133	0.3332	0.2417	0.1198	3	3	4424.4
Jan. 23	0.0922	0.1639	0.2690	0.3165	0.1583	4	4	5803.4
Jan. 24	0.1502	0.1324	0.2677	0.3298	0.1199	4	4	5066.9

Table 6. The results simulation and prediction of humidity

Date	State					Prediction state	Actual state	Actual value
	1	2	3	4	5			
Jan. 20	0.4948	0.1450	0.2042	0.0854	0.0706	1	1	39.320
Jan. 21	0.5123	0.1360	0.2270	0.0749	0.0500	1	1	41.540
Jan. 22	0.5003	0.1576	0.2368	0.0517	0.0536	1	1	45.716
Jan. 23	0.4406	0.1725	0.2745	0.0581	0.0542	1	1	39.204
Jan. 24	0.4633	0.1535	0.2974	0.0497	0.0361	1	1	43.808

Table 7. The results simulation and prediction of soil temperature

Date	State					Prediction state	Actual state	Actual value
	1	2	3	4	5			
Jan. 20	0.2321	0.1363	0.1482	0.3286	0.1548	4	4	16.412
Jan. 21	0.3115	0.1432	0.0590	0.1474	0.3389	5	5	17.596
Jan. 22	0.1384	0.1309	0.1637	0.0743	0.4928	5	5	17.221
Jan. 23	0.1344	0.1282	0.1975	0.0337	0.5062	5	5	17.412
Jan. 24	0.1017	0.2254	0.1801	0.1930	0.2998	5	5	17.152

In the practical production, the temperature of inner greenhouse is major consideration. When the temperature is over 20 °C, the environment is suitable of the growth of vegetable, so the indicator that the temperature is over 20 °C is a very important parameter. Through predicting inner irradiation, humidity and soil temperature, we can establish a relationship of the three and temperature of inner greenhouse. The results are shown in Table 8.

Table 8. The relationship of temperature and the three (irradiation, humidity and soil temperature)

Parameter	Value	The count of temperatures >20 °C	Value	Temperature > 20 °C
Irradiation	$> 4400\,\mathrm{W/m^2}$	> 13	$< 2000\,\mathrm{W/m^2}$	0
Humidity	< 60	> 18	> 80	0
Soil temperature	$> 15.5\,^\circ\mathrm{C}$	> 12	$< 13.5\,^\circ\mathrm{C}$	0

From the above table, we can observe that the prediction state is matched with actual state. This indicates that the method is effective, and we can use the method to predict the environmental parameters of greenhouse.

Predicting the main impact factors of the inner environment of solar greenhouse with Weighted Markov Chain, which has been built, presents the predictive state of irradiation, humidity and soil temperature in the solar greenhouse, and shows the actual state and actual values.

In summary, the above data show that the effect of simulation and prediction of impact factors is satisfactory, the prediction agrees well with the actual situation, and the model is successful. Table 8 shows that irradiation, humidity and soil temperature are the important impact factors. When irradiation value is over $4400\,\mathrm{W/m^2}$, the count of the inner temperature over 20 °C is over 13, when irradiation value is under $2000\,\mathrm{W/m^2}$, the count is 0. When humidity value is under 60, the count of inner temperature over 20 °C is over 18 when the value is over 80, the count is 0. When soil temperature is over 15.5 °C, the count is over 12, when the value is under 13.5 °C, the count is 0. So we can predict whether the weather is suitable for the growth of plants in the short term, and provide the basis for the environment control.

4. Conclusion

In the study, the Weighted Markov Chain method was adopted to predict the major environment impact factors in the solar greenhouse. The results show that predictive accuracy of the model is high, and predictive states are according with the actual states. The predictive results are objective and reasonable, and the impact factors have a strong nonlinear relationship. Therefore, the model can be applied to forecast the indicators (including irradiation, humidity and soil temperature).

Adopted Sequential Clustering Method to classify the data, make the data groups more reasonable. With the help of MATLAB, it is easy to classify the data.

Weighted Markov Chain method is adopted to forecast the inner environment of solar greenhouse and which will be targeted to improve the management level in the solar greenhouse. It can also provide a realistic approach to environment control in the greenhouse.

References

[1] G. Tong, D. M. Christopher, T. Li, T. Wang: *Passive solar energy utilization: A review of cross-section building parameter selection for Chinese solar greenhouses.* Renewable and Sustainable Energy Reviews *26* (2013), 540–548.

[2] o. Ozgener, A. Hepbasli: *Experimental performance analysis of a solar assisted ground-source heat pump greenhouse heating system.* Energy and Buildings *37* (2005), 101–110.

[3] Y. Han, X. Xue, X. Luo, L. Guo, T. Li: *Establishment of estimation model of solar radiation within solar greenhouse.* Transactions of the Chinese Society of Agricultural Engineering *30* (2014), No. 10, 174–181.

[4] C. W. Ma, S. M. Zhao, J. Y. Cheng, N. Wang, Y. C. Jiang, S. Y. Wang, B. M. Li: *On establishing light environment model in Chinese solar greenhouse.* Journal of Shenyang Agricultural University *44* (2013), No. 5, 513–517.

[5] Z. Y. Zuo, H. P. Mao, X. D. Zhang, J. Hu, L. Han, J. Ni: *Forecast Model of Greenhouse Temperature Based on Time Series Method.* Transactions of the Chinese Society for Agricultural Machinery *41* (2010), No. 11, 173–177,182.

[6] G. A. Meehl, W. M. Washington, T. M. Wigley, J. M. Arblaster, A. Dai: *Solar and greenhouse gas forcing and climate response in the 20th century.* Journal of Climate *16* (2003) 426–444.

[7] W. Zhou, X. C. Wang: *Constrained predictive control model for greenhouse temperature.* Xinjiang Agricultural Sciences *51* (2014), No. 6, 1015–1021.

[8] P. Taalas, J. Kaurola, A. Kylling, D. Shindell, R. Sausen, M. Dameris, V. Grewe, J. Herman, J. Damski, B. Steil: *The impact of greenhouse gases and halogenated species on future solar UV radiation doses.* Geophysical Research Letters *27* (2000), No. 8, 1127–1130.

[9] P. S. Magnusson, M. Christensson, J. Eskilson, D. Forsgren, G. Hallberg, J. Hogberg, L. Larsson, A. Moested, B. Werner: *Simics: A full system simulation platform.* Computer *35* (2002), No. 2, 50–58.

[10] R. G. Sargent: *Verification and validation of simulation models.* Winter Simulation Conference, 4–7 December 2005, Orlando, FL (2005), European Journal of Operational Research *66*, (2013), No. 2, 250–258.

[11] F. Xu, C. Ma: *Daily change and math-expression method of outside temperature in winter for greenhouse environmental analysis.* Transactions of the Chinese Society of Agricultural Engineering *29* (2013), No. 12, 203–209.

[12] A. J. Hamilton, G. Hepworth: *Accounting for cluster sampling in constructing enumerative sequential sampling plans.* Journal of Economic Entomology *97* (2004), No. 3, 1132–1136.

[13] P. Jiang, Y. Huo, L. Zhang, J. Luo, H. Li: *A wind speed time series model based on advanced first-order Markov chain approach.* Automation of Electric Power Systems *38* (2014), No. 19, 22–27.

[14] Y. Li, L. He, J. Niu: *Forecasting power generation of grid-connected solar PV system based on Markov chain.* Acta Energiae Solaris Sinica *35* (2014), No. 4, 611–616.

[15] X. Yang, H. Liu, B. Zhang, Y. Xiao: *Similar day selection based on combined weight and photovoltaic power output forecasting.* Electric Power Automation Equipment *34* (2014), No. 9, 118–122.

Received September 12, 2017

Acta Technica *62* No. 2B/2017, 597–606

Anti-collision algorithm and security authentication mechanism of radio frequency identification system[1]

Jinyan Liu[2], Quanyuan Feng[2]

Abstract. Radio frequency identification (RFID) is a non-contact automatic identification communication technology. Based on the requirement analysis of anti-collision algorithm and security authentication function of radio frequency identification system in this paper, the improved binary search anti-collision algorithm and the RFID security authentication protocol based on Hash function and state locking were proposed respectively, so as to ensure the promotion of the efficiency and security of radio frequency identification system. The results show that the improved binary search anti-collision algorithm has a shorter data transmission length, and is more efficient for large-scale object label recognition, and the RFID security authentication protocol based on Hash function and state locking can avoid illegal attack and complete tag authentication effectively through Hash function, symmetric encryption, ID updating and K value.

Key words. Anti-collision algorithm, RFID, binary search, hash function.

1. Introduction

With the innovation of information technology, it is possible to establish communications between object information through information sensing devices, identification systems and the Internet, so as to realize the automatic and intelligent system of information system in the development of modern industry [1]. Radio frequency identification (RFID) system, as an important component of the perception layer in the architecture of Internet of things, is the key module to support the Internet of things. RFID technology allows contactless and unique identifying objects, and the Internet of things transfers this information from the sense layer to the application layer through the network layer, so that the interconnected neural net of things is formed.

[1]This work is supported by the National Natural Science Foundation of China under Grant 61531016.

[2]School of Information Science and Technology, Southwest Jiaotong University, Chengdu, Sichuan, China, 610031

Compared with other identification technologies, RFID technology can adapt to long distances, and it can make a batch and other advantages, so it has been widely concerned and applied to the logistics, access control and other industries [2]. Although the RFID technology in the world has been widely studied and applied, there are still some problems such as high costs of electronic tags, overlapping aliasing of multiple labels and information security, which restricts the popularization and promotion of RFID technology. Based on this, the research on anti-collision algorithm and security mechanism of RFID technology was launched in this paper, so as to improve the operation efficiency of RFID system and guarantee the security of data and channel.

2. State of the art

In RFID system, information collision refers to the superposition of multiple tag information when multiple tags are identified at the same time, thus, it is difficult for readers to recognize the tag information, which seriously reduces the operation efficiency of RFID system [3]. The anti-collision algorithm based on RFID system is built on the principle of time division multiplexing (TDMA), and scholars have also done a lot of researches on anti-collision algorithms of RFID system, but in the past research on anti-collision algorithm, it will still face such problems. On the one hand, some anti-collision algorithms have too long recognition times and high requirements on the moving speed of tags, so the efficiency is too low; on the other hand, if it simply increases the recognition efficiency by increasing the amount of control in a timely manner, it will result in a substantial increase in operating costs [4]. Therefore, it is an urgent problem for RFID system to improve the operation efficiency without increasing the system cost.

The security authentication mechanism of RFID system is concerned with many aspects, such as system security protection and privacy protection. Only by ensuring the data security of RFID system, can the effective application of Internet of things be realized [5]. In order to prevent the illegal attack on RFID system and the leakage of information of individuals, goods and enterprises, it is necessary to realize the encryption of information and the security authentication of users through security protocol. There are more mature security protocols, such as DES and AES, but what cannot be ignored is that these security protocols can guarantee the operation safety of system to a certain extent, and there is also an increase in costs resulting from the increased logical processing units. At the same time, limited to the calculation and storage capabilities of the tag, it is difficult for the existing security protocols to be popularized in applications of the RFID system. Therefore, lightweight security protocol is also the focus of RFID system research.

2.1. Methodology

2.2. An improved binary search anti-collision algorithm

In this paper, through the study of the current status of RFID system operations and the application of the survey results, it is found that the binary search algorithm has high recognition rate for electronic tags, which is more suitable for large-scale identification of objects. Therefore, in this paper, a binary search anti-collision algorithm was used as the object of study, and on this basis, the improved binary search anti-collision algorithm was analyzed and studied.

The binary search algorithm requires Manchester encoding (Manchester) to provide accurate bit locations for multiple electronic tags to enter the identification area, so that the tag search can then be carried out according to the corresponding rules [6]. The encoding setting map is listed in Table 1.

Table 1. Electronic tag encoding settings

Tag number	Coding (8-bit)
Label 1	01010101
Label 2	01010111
Label 3	01110101
Label 4	01100110
Label 5	01010100

In this study, the sleep counting method was adopted; then, the search time of the reader was then shortened by identifying an electronic tag state. The anti-collision command in this algorithm is divided into request command Request (x, m), activation command Active, removing command Unselect and Read-Data and so on [7]. The function of the request command is to detect the difference between the high value of the tag conflict and the binary value of the 1 bit. If the value is consistent, it will be answered and returned, otherwise, the label is converted to sleep, and the corresponding sleep level is 1 or 1.; the activation command is used to reduce the sleep label, and make it become the standby state by reducing the 1 sleep level of the sleeping tag; the removing command is to change the selected label into "silent", without responding to the commands issued by the reader [8]. In this study, the tag code was set as 8 and the number was 5, as shown in Fig. 1.

When the tag enters the identification area, a request command is issued to all tags in the area. The diagram is shown in Fig. 1, and the process is as follows:

The first request command: for the label entering the reading area, the system sends the Request (NULL, 8) command to it, and then the UID data obtained is 01XX01XX. The maximum collision bit index is 5, which is used as the parameter setting for the second request command, and at the second time, it executes the Request (0, 5) command.

The second request command: after the execution of the first command, the standby fifth-bit response labels are numbered Label, 1, Label 2, and Label 5. The UID data obtained at this time is 010101XX, and the maximum collision bit index

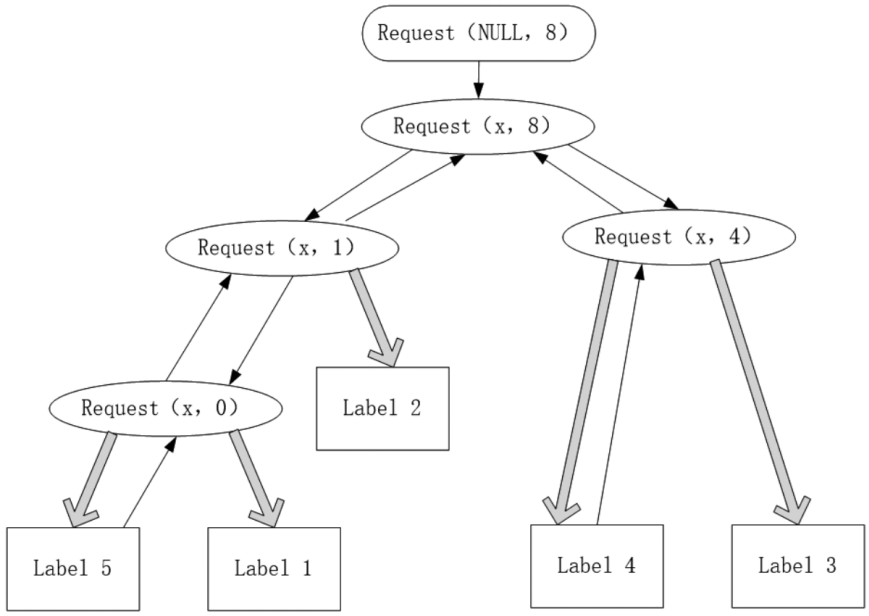

Fig. 1. Collision algorithm identification schemes

is 1, so the Request (0, 1) command is required for the third time. In addition, the command sets label 3 and label 4 to be in a sleeping state (the fifth is 1), and the label 1, label 2, and label 5 still keep a standby state.

The third request command: at this point, label 1 and label 5 which are on a standby state will respond to the Request (0, 1) command issued by the reader, and the maximum collision bit index is 0, and the fourth request command can be executed. The command parameter is Request (0, 0). In addition, the value of the sleep level of label 2 is 1, and label 3 and label 4 are added to 1.

The fourth request command: the execution process has no collision and can be accurately identified, and it will execute other commands in turn, and it will also execute the living command Unselect at the end of the execution and place it in "silent". When a tag is correctly identified, the system sends the activation command Active to all tags, and the dormant degree of corresponding labels has been reduced by 1, and the rebound strategy has been taken. Unlike the beginning, the first parameter is 1.

The fifth request command: the system sends a request command to each tag, and at this time the parameter is set as Request (1, 0), which means that the label whose zeroth digit value is 1 should make a response. Comparing the coding of the five tags, it is found that each of them does not produce collisions, so that the tags can be correctly identified and other operations can be performed sequentially.

The sixth request command: the command parameter is Request (1, 1), and Label 2 responds to the reader and can be correctly identified.

The seventh request command: the command that the system sends to the tag is

Request (1, 5), and when both Label 3 and Label 4 make a response (both of which are standby labels with the fifth digit value of 1), and the maximum collision bit index is 4, which is the parameter of the next request command.

The eighth request command: according to the above operation, the operation result shows that the request command is Request (0, 4), and Label 4 makes a response (the encoding is a standby label with the fourth digit value of 0), and the collision does not happen.

As shown in Fig. 1, the binary tree structure has 4 sub-nodes behind the root node of the tree structure to ensure the accurate identification of each tag. It is characterized by bidirectional search between root nodes and sub nodes, and it reduces the number of searches that are required for multiple tag identification in the anti-collision algorithm design [13]. In the process of the identification of the 5 tags set by the experiment, it can be found that the number of searches is 9, and $S(5) = 2(5\text{-}1) + 1 = 9$. Thus, the binary search anti-collision algorithm requires the number of searches that are required to identify the n tags should be $S(n) = 2(n-1)+1 = 2n-1$.

As shown in Table 2, it is the improved binary search anti-collision algorithm and the binary search algorithm [14]. Compared with the dynamic binary search algorithm, it has a shorter data transmission length and greatly improves the recognition efficiency of the anti-collision algorithm [15]. With the increase of the number of identification tags, the efficiency advantage of this algorithm is more obvious.

Table 2. The sum of the length of the transmitted binary data

Algorithm	The total length of the transmitted binary data
The binary search algorithm	$L_1 = \frac{m(m+1)}{2} N$
The dynamic binary search algorithm	$L_2 = \frac{m(m+1)}{2} \frac{N+1}{2}$
The improved binary search algorithm	$L_3 = (2m-1) \times \log_2^N + 1$

2.3. Research of RFID security authentication protocol based on Hash function and state locking

Radio frequency identification (RFID) needs to add secure and lightweight security protocols to ensure the security and efficiency of the identification system [9]. According to the characteristics of Hash function in RFID security authentication, in this paper it was combined with the state locking module organically. The authentication system is characterized by mutual authentication between the reader and the tag [10]. The legitimacy of the tag is validated by the backend database [11]. In the process of authentication, new ID and key values are constantly formed, which can prevent illegal attacks and avoid information leakages and system paralysis [12].

The schematic diagram of the authentication protocol is shown in Figure 2, and the authentication procedure is as follows:

1. It generates random number r and then passes it to the data to form cipher text and request authentication through the encryption algorithm.

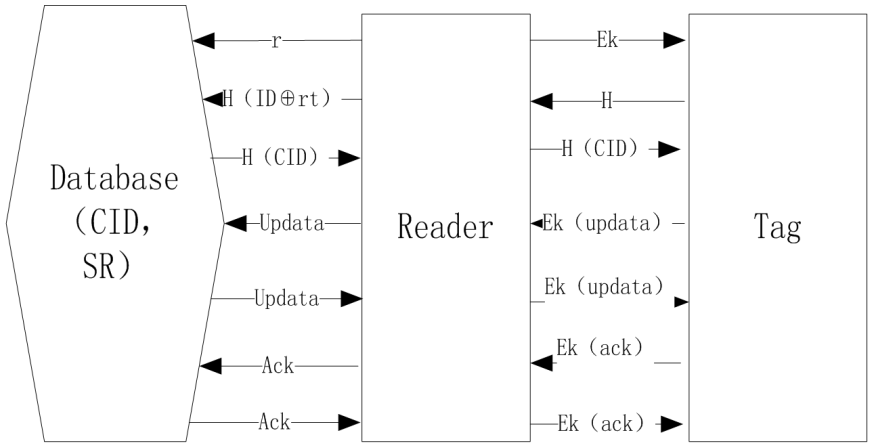

Fig. 2. The schematic diagram of authentication protocol based on Hash function and state locking

2. Database accepts the r value, and then the tag extracts Query and the r value is transmitted to the reader by encryption.

3. H (ID source RT) value is sent to the back-end database.

4. It is necessary to query the CID field, so as to judge whether the numerical values of H (ID source RT) and H (CID source RR) are unanimous.

5. H (CID) is forwarded to the tag to determine whether the H (CID) and the H (ID) values are consistent, or it will pass the authentication, otherwise, the authentication fails.

6. The update data is extracted, and passed to the database.

7. The CID value is updated.

8. The key of the reader is updated.

9. The label ID and key are updated.

10. The ack value is extracted and passed to the database. After setting the SR value to 00, the ack value is passed to the reader.

11. When the tag extracts the ack message, the ST is set to 00.

The meanings of particular symbols in agreement are listed in Table 3.

3. Result analysis and discussion

3.1. Algorithm simulation analysis

The binary search algorithm and the improved binary search anti-collision algorithm were simulated by using MATLAB software. In the simulation experiment, the tag length is 16 bits, as shown in Fig. 3, left part. When the number of processing tags is 10, the binary search algorithm searches 80 times, while the improved binary search anti-collision algorithm searches only 19 times, and search times are reduced by 76 % after improvement; when the number of processing tags is 80, the

binary search algorithm searches 159 times, while the improved binary search anti-collision algorithm searches only 726 times, and search times are reduced by 76 % after improvement. Therefore, the improved binary search anti-collision algorithm can effectively reduce the number of searches with equal number of tags, and improve the operational efficiency. At the same time, as the number of tags increases, the number of search decreases, and it has more advantages in improving the efficiency of large-scale tagging.

Table 3. The meaning table of symbol in the agreement

Sequence number	Symbol	Meaning
1	K	shared key
2	ID	Tag identification number
3	ST	Label state
4	rt	Tag stored in the random number
5	r	Reader stored in the random number
6	CID	Backend database to store the current tag identification number
7	SR	State of the reader
8	PID	Backend database to store the last tag identification number
9	Rr	Random Numbers are stored in the database background
10	Random ()	Random function
11	E()	Symmetric encryption algorithm
12	D()	Nverse execution of symmetric encryption algorithm
13	H()	Hash function
14	Updata	Both sides agreed updates
15	Ack	Both sides agreed confirmation
16	II	Join operation
17	$\oplus$	Exclusive or operation

In Fig. 3, right part, the binary search algorithms and the improved binary search anti-collision algorithms are used for tag identification, and sums of the length of the binary data positively rise with the increase of the number of tags. But from the slope of the two curves, the improved binary search anti-collision algorithm can obviously reduce the total length of binary data transmission. When the number of processing tags is 80, the binary search algorithm has a total binary data length of 14328, while the improved binary search anti-collision algorithm searches only 854 times, and the total length of the improved binary transmission data is reduced by

94 %, which greatly improves the recognition efficiency of the anti-collision algorithm.

The improved algorithm can effectively reduce the number of searches and the total length of binary data transmissions, thus greatly improving the channel saving. In recent years, with the development of computer and Internet, the logistics industry and the new business model have been developing rapidly, which makes it difficult for people to identify, collect and record the information of goods, and it is hard to satisfy the pursuit on efficiency in the information age, moreover, manual labor can also greatly waste labors and cause unavoidable operational errors. The improved binary search anti-collision algorithm can better reflect the advantages of the algorithm when dealing with a large number of larger labels, which can effectively improve the processing efficiency of RFID system and solve the interference problem of simultaneous responses of multiple tags in the operation of RFID system, thus avoiding manual operations in the identification process to the greatest extent.

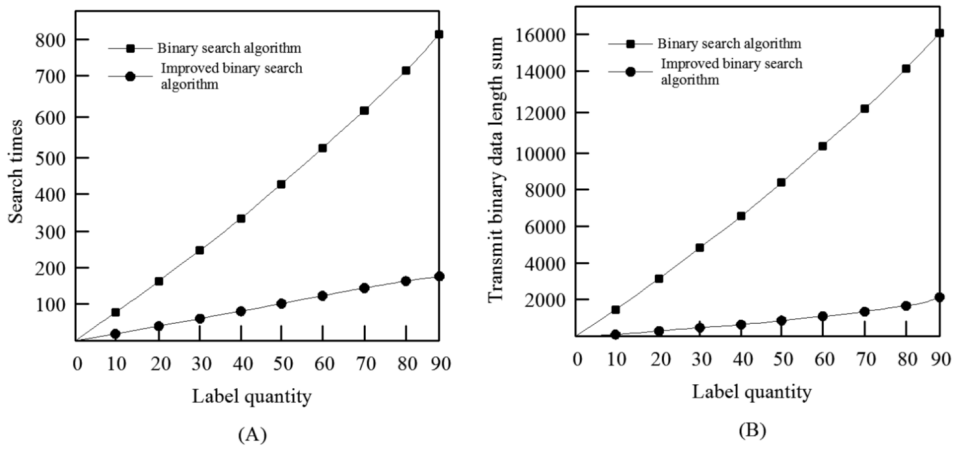

Fig. 3. Number of searches (left) and the total length (right) of transmission data

3.2. Security analysis of the security authentication protocol

In the previous analysis of the security authentication process (Fig. 2), the authentication protocol has high data confidentiality, tag anonymity, forward security and mutual authentication. Among them, the data confidentiality is manifested in the identification process of the tag system, and the data involved is encrypted by the encryption algorithm or Hash function, which ensures the confidentiality of the information passed by the tag and reader [16]. The anonymity of the tag means that the information received by the reader is changing constantly and randomly, which also means that the intercepted label information is erratic for the attacker; the function of the forward security is to update the ID and K values of the tag synchronously, so that even if the attacker has obtained the ID and K values of the current tag, it is also difficult to reverse the tag information before it is launched; the mutual authentication shows that readers and labels need to complete mutual

information comparisons in this secure authentication protocol, so as to realize the mutual authentication and complete the information reading.

In addition, this security authentication protocol also has the following two advantages: on the one hand, the timely updating of ID and K values of the tag ensures that it is difficult for the attacker to retrieve the ID value of the tag again when the reader has finished identifying the tag, that is, the reader will not be re-authenticated; on the other hand, the protocol can lock each step of the system, and the operation of the state is unique. Even if the attacker steals all the information, it is difficult to find the status of the reader's identification on the tag, and the attacker's illegal instructions will not be responded. RFID security authentication protocol based on Hash function and state lock integrates many modules, such as information encryption, status lock and background database, which ensures that every program in the system is locked into a specific state in the process of security authentication. While realizing the mutual authentication between the reader and the tag, the information security risk of the RFID authentication system is effectively avoided by updating the label ID and K value.

4. Conclusion

The optimization of anti-collision algorithm and the construction of security authentication mechanism are two important aspects in the research of radio frequency identification technology. In the research of the improved binary search anti-collision algorithm, it is found that the improved binary algorithm has shorter data transmission length compared with the binary search algorithm and the dynamic binary search algorithm, which greatly enhances the recognition efficiency of the anti-collision algorithm, and with the increase of the number of identification tags, the efficiency advantage of this algorithm is more obvious. At the same time, the research of RFID security authentication protocol based on Hash function and state locking can effectively protect the information security of each process of RFID system in the process of label authentication, and through the application of background database, the updating of label ID and K value and the locking of label status, data confidentiality, label anonymity, forward security and mutual authentication are realized at the same time, which effectively reduces the risk of information security caused by illegal attacks. But limited to the research time and effort, the binary search algorithm in anti-collision algorithm and the RFID security authentication protocol based on Hash function and state locking were discussed and simulated in this paper, and the application research of RFID system was not done. There may be a short board in the design and connection of other components of the RFID system, which will affect the practical performance of the algorithm, and further researches are needed.

References

[1] X. Liu, B. Xiao, K. Li, J. Wu, A. X. Liu, H. Qi, X. Xie: *RFID estimation with blocker tags.* IEEE/ACM Transactions on Networking *25* (2017), No. 1, 224–237.

[2] Y. H. Chen, S. J. Horng, R. S. Run, J. L. Lai, R. J. Chen, W. C. Chen, Y. Pan, T. Takao: *A novel anti-collision algorithm in RFID systems for identifying passive tags.* IEEE Transactions on Industrial Informatics *6* (2010), No. 1, 105–121.

[3] J. Zhao, N. Li, D. A. Li, R. Bai, B. Zhu, X. Liu: *Collision alignment: An RFID anti-collision algorithm assisted by orthogonal signal detection and analogy principle.* Telecommunication Systems *66* (2017), No. 1, 131–144.

[4] J. Su, X. Zhao, D. Hong, Z. Luo, H. Chen: *Q-value fine-grained adjustment based RFID anti-collision algorithm.* IEICE Transactions on Communications *E99.B* (2016), No. 7, 1593–1598.

[5] K. C. Shin, S. B. Park, G. S. Jo: *Enhanced TDMA based anti-collision algorithm with a dynamic frame size adjustment strategy for mobile RFID readers.* Sensors (Basel) *9* (2009), No. 2, 845–858.

[6] H. P. Zhang, J. J. Li, Z. L. Chen, B. Wang: *A rapid anti-collision method for RFID tag identification.* Applied Mechanics and Materials *738–739* (2015) 1123–1128.

[7] X. Tan, H. Wang, L. Fu, J. Wang, H. Min, D. W. Engls: *Collision detection and signal recovery for UHF RFID systems.* IEEE Transactions on Automation Science and Engineering *PP* (2016), No. 99, 1–12.

[8] D. J. Deng, H. W. Tsao: *Optimal dynamic framed slotted ALOHA based anti-collision algorithm for RFID systems.* Wireless Personal Communications *59* (2011), No. 1, 109–122.

[9] X. Q. Yan, Y. Liu, B. Li, X. M. Liu: *A memoryless binary query tree based successive scheme for passive RFID tag collision resolution.* Information Fusion *22* (2015), 26–38.

[10] H. Safa, W. El-Hajj, C. Meguerditchian: *A distributed multi-channel reader anti-collision algorithm for RFID environments.* Computer Communications *64*, (2015), 44–56.

[11] C. T. Nguyen, A. T. H. Bui, V. D. Nguyen, A. T. Pham: *Modified tree-based identification protocols for solving hidden-tag problem in RFID systems over fading channels.* IET Communications *11* (2017), No. 7, 1132–1142.

[12] S. L. Garfinkel, A. Juels, R. Pappu: *RFID privacy: An overview of problems and proposed solutions.* IEEE Security & Privacy *3* (2005), No. 3, 34–43.

[13] X. Liu, X. Xie, K. Li, B. Xiao, J. Wu, H. Qi, D. Lu: *Fast tracking the population of key tags in large-scale anonymous RFID systems.* IEEE/ACM Transactions on Networking *25* (2017), No. 1, 278–291.

[14] C. Wang, Z. Shi, F. Wu: *An improved particle swarm optimization-based feed-forward neural network combined with RFID sensors to indoor localization.* Information *8* (2017), No. 1, paper 9.

[15] F. Zhu, B. Xiao, J. Liu, L. J. Chen: *Efficient physical-layer unknown tag identification in large-scale RFID systems.* IEEE Transactions on Communications *65* (2017), No. 1, 283–295.

[16] Z. Zhou, L. Shangguan, X. Zheng, L. Yang, Y. Liu: *Design and Implementation of an RFID-based customer shopping behavior mining system.* IEEE/ACM Transactions on Networking *25* (2017), No. 4, 2405–2418.

Received September 12, 2017

Acta Technica *62* No. 2B/2017, 607–618

Optimization study of hybrid virtual network mapping algorithm (VNE) based on cost optimization and energy efficiency optimization theory

Yanli Wang[1]

Abstract. The virtual network mapping algorithm can effectively change the phenomenon that the energy consumption of network technology is large in our country. In order to optimize the virtual network mapping algorithm better, based on the related literature summary, theories of virtual network mapping algorithm were clarified and model of virtual network mapping algorithm proposed was constructed in this study. By using the related optimization model, the running cost and the rate of network request acceptance of virtual network mapping model were calculated. The results show that the virtual mapping algorithm can reduce the running cost and increase the acceptance rate compared with the traditional mapping algorithm. The purpose of this research is to provide a reference for the optimization of related algorithms.

Key words. Cost optimization, energy efficiency optimization, mixed virtual network mapping algorithm.

1. Introduction

With the development of the times, various new science and technologies in modern time appear constantly and have been improved greatly. As a new technology which is developing more rapidly, information technology has a strong resource sharing. And the combination of this technology and other industries is strong, so it has been widely used in other industry development. As the advantages of this technology continue to increase, a variety of more systematic and scientific theoretical studies have been initiated, which has further promotes the further improvement and development of information technology. However, the rapid development of information technology has brought great convenience to people's production and life. At the same time, some uncoordinated problems have been further exposed, such as energy consumption. How to reduce the energy consumption of information technology

[1]Engineering Technology College, Xi'an Fanyi University, Xi'an, Shaanxi, China, 710105

through more perfect new technology has become an important problem to be solved urgently in the development of science and technology in the times. Based on the related theories of cost optimization and energy efficiency optimization, the hybrid virtual network mapping algorithm (VNE) of information technology was optimized in this study. A kind of new information technology with lower energy consumption was determined, which provided certain theoretical support and reference for the follow-up research.

2. State of the art

The development of information technology has brought the extremely important influence and the positive promotion function for the progress of other industries in the present era. As an important science and technology in the development of the times, information technology is often used to fulfill the user's needs by running some applications on the server. Although this technology has brought great convenience to people's production and life, the traditional network information technology has greatly consumed some network resources and energy [1]. Statistics show that the most technologically advanced supplier of information technology in the world today is the Akamai Company in the United States. The vigorous development and advancement of the information technology of the company has caused great consumption for the use of electricity cost in the current era. As a big country in the economic and scientific and technological power in the current era, the rapid development of mobile internet companies has further caused the extensive use of related resources in China [2]. Therefore, the energy consumption of information technology has become one of the most important subjects in the development of information technology. Some researchers have pointed out that network virtualization should be the main direction of network development in the future development of network information technology. The technology should be based on the shared network platform and make use of a variety of different virtual resources so as to improve the operation efficiency of network system, and further reduce the physical resources borne by the amount of resources in order to achieve the purpose of energy conservation [3]. There are many techniques that have already been put into use. As a novel theory, the hybrid virtual network mapping algorithm has a very important positive impact on the energy saving in the development of the whole information technology [4]. Many researchers have begun to pay attention to it and constantly improve the relevant theories, which provide technical support for the development of information technology [5].

2.1. Methodology

With China's entry into the new century, China's various technologies have been greatly improved and developed, and people's living standards have also been improved greatly. Now, many new techniques have begun to gradually enter the people's field of vision, and have brought great convenience to the production and life of the people [6]. With the development of mobile internet technology, more and more

new businesses are emerging. This better meets the actual needs of some industries or individuals in our country to a certain extent (Fig. 1).

Fig. 1. Rapid development of network technology

However, with the rapid development and application of network information technology in our country, some drawbacks have begun to emerge. The whole network technology is beginning to show a rigid phenomenon. According to statistics, data traffic used by China's network users reached 20523 PB due to certain network activities in 2015. And most of the data traffic is mainly used for network video viewing [7]. Network users in our country usually look at the rate of VOD on some network video. Based on the rate of request, the video you might want to watch is determined. Then through the use of the client, the publication of network video online shop is connected so as to obtain relevant video resources. However, in this process, some servers may have a higher hot spot of video resources, which may lead to a larger load on the server terminal because of excessive user access. This can directly lead to low efficiency of resource delivery and limit the scalability of traffic (Fig. 2). Especially in the application of network technology of traditional TCP/IP architecture, the perfection of its structure is relatively poor. A large number of accessing customers may make the network technology system unable to load larger amounts of data. This situation makes the operation of the network system a certain resistance. A large number of energy materials are consumed, which makes the traditional network technology system facing more severe use challenges [8]. In addition to the expansion of network traffic caused by the excessive amount of user access mentioned in the above articles, another issue that needs further attention is the scalability of the routing problem. In the development of traditional network information technology, IP addresses can be used to mark the location and identity of network nodes. Therefore, when the location of some physical devices changes, it may affect the communication process of the entire network. This limits the freedom of certain network physical devices to a certain extent. It has a negative impact on the expansion of routing, and indirectly affects the efficiency of the use of the network, resulting in waste of resources [9].

In view of the above problems, many researchers in our country put forward the application of network virtual technology in the development of actual network

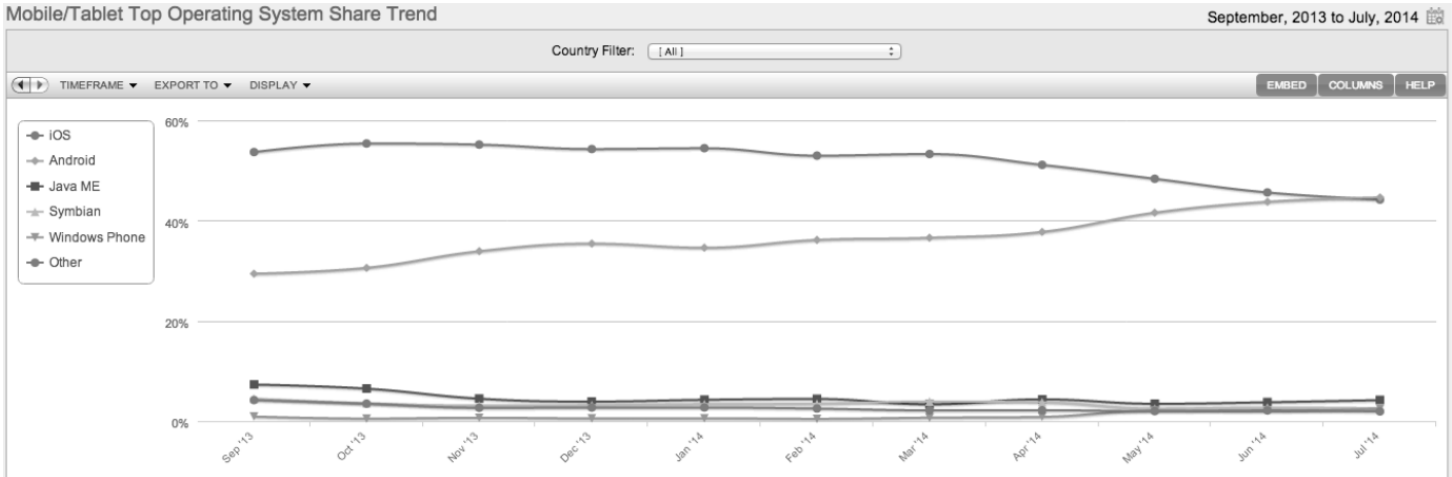

MONTH	IOS	ANDROID	JAVA ME	SYMBIAN	WINDOWS PHONE	OTHER
September, 2013	53.68%	29.42%	7.31%	4.48%	0.92%	4.20%
October, 2013	55.39%	30.58%	6.47%	3.58%	0.50%	3.48%
November, 2013	55.17%	33.89%	4.49%	3.12%	0.67%	2.66%
December, 2013	54.27%	35.41%	3.90%	3.18%	0.55%	2.70%
January, 2014	54.46%	34.60%	4.26%	3.41%	0.56%	2.72%
February, 2014	52.96%	36.14%	4.44%	3.50%	0.45%	2.51%
March, 2014	53.29%	36.58%	3.36%	3.92%	0.69%	2.17%
April, 2014	51.11%	37.75%	4.36%	3.77%	0.83%	2.18%
May, 2014	48.34%	41.58%	3.46%	2.52%	2.10%	2.00%
June, 2014	45.61%	43.75%	3.77%	2.73%	1.99%	2.15%
July, 2014	44.19%	44.62%	4.19%	2.57%	2.49%	1.94%

Fig. 2. Data flow related data logging

technology. And through the further improvement of the technology, higher resource saving rate and data transmission efficiency are obtained [10]. Nowadays, the research of this kind of technology in our country is mainly in the realization of the technology and all aspects of its mapping. However, because our research on this technology is still in the initial stage, the related theories and techniques are not mature enough, so the generalization is still poor. In this context, it is necessary to put forward and improve the relevant technical algorithms so as to achieve further optimization of the whole technical performance [11]. On the basis of consideration of the operation cost and energy consumption of the technology, it also needs to discuss its application reliability and science in the course of the study, so as to form a more perfect new network technology and provide some technical support for the development of other industries. This study will discuss and analyze the related aspects of hybrid virtual network mapping algorithm (VNE) based on two aspects of cost optimization and energy efficiency optimization. Moreover, on the basis of optimizing the original algorithm, better technical algorithm is determined, so as to provide a certain reference for the later research. The related research methods are as follows:

(1) First of all, through the reading of relevant information, the relevant main theoretical basis for the study was identified and clarified. On the basis of a clear understanding of the relevant theoretical foundations, the related application technologies of the traditional virtual network mapping model were analyzed, and then the relevant research ideas of node segmentation in this study were obtained.

(2) On the basis of understanding the relevant theories, in order to better guarantee the design of the associated virtual network mapping algorithm model has lower operating costs, a more optimized mathematical model formula was introduced in the construction of the related network mapping algorithm model. Index value experiment was carried out to obtain data through related mapping algorithm. Then, the performance of the model was compared and analyzed with the traditional network mapping algorithm. The mathematical model of correlation optimization used in this study is as follows:

Objective function:

$$\min \sum_{(u,v)\in E} \sum_{i=1}^{k} c_i(u,v) f_i(u,v)\,. \tag{1}$$

Here, E represents all links and u and v represent different nodes respectively. Function $f_i(u,v)$ represents the traffic data that flows through the associated nodes and $c_i(u,v)$ represents the cost of the unit flow through different nodes.

Capacity restriction formula:

$$\sum_{i=1}^{k} f_i(u,v) \le b(u,v)\ \forall (u,v) \in E\,. \tag{2}$$

Here, $b(u,v)$ represents the maximum flow capacity that a link can afford.

Range restriction formula:

$$f_i(u,v) \geq 0,\ 1 \leq i \leq k\ \forall (u,v) \in E\,. \tag{3}$$

The formula is a non-negative restriction on the traffic capacity carried by a link.

(3) The designed network virtual technology was optimized by using the relevant optimization mathematical model, so as to construct a virtual network mapping algorithm with lower cost and better energy efficiency. Moreover, the energy saving strategy in this algorithm was discussed in depth, and the main modes of energy saving were analyzed. Then, the performance of the adaptive algorithm was calculated and compared by the experimental method of the actual case.

3. Result analysis and discussion

Development of times makes the network information technology gradually become one of the important science and technology in the development of the times. However, due to the influence of network structure, traditional network information technology may cause the limitation of energy consumption when facing large traffic load. And the mapping algorithm of network virtual network is proposed, which provides some positive effects on the solution of this limitation. Nowadays, all countries in the world have begun to search for a more efficient and efficient network virtual network mapping algorithm, so as to solve the main problems faced by traditional network technology [12]. The virtual network mapping model refers to the sharing of the same network physical resources between different virtual networks. The virtual network is mainly replaced by a number of different virtual nodes. Then, the virtual link is used to connect all the virtual nodes with the network physical resources, so as to realize the related data transmission path and share the data resources. The proposed network mapping model can better meet the actual needs of people and reduce the use of related energy consumption due to the shared processing of a variety of architectures [13].

Relevant information was read and summarized in this study firstly. Based on the understanding of the underlying network graph of traditional network technology and the relevant theories, the segmentation of virtual network technology was introduced. Thus, the model of network virtual technology was created, as shown in Fig. 3 [14]. Among them, the letters in the model represented different element nodes, and the dotted line represented the element link between the different element nodes.

On the premise of segmenting the link mapping path of the related model, the study generalized the parameters of the whole model and applied it to later model optimization. The list of related parameters is shown in Table 1.

Table 1. List of related model parameters for this design

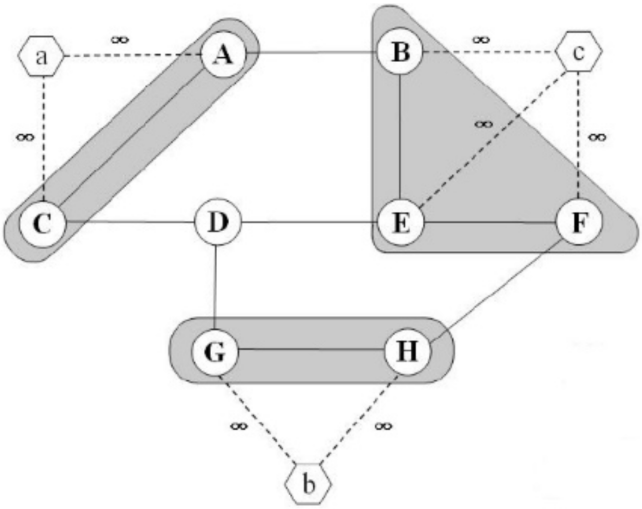

Fig. 3. Network virtual technology model constructed by this research

Parameter name	Parameter nominal
$R_E(u,v)$	The residual bandwidth capacity of the underlying link u,v
$R_N(n^{\mathrm{s}})$	The residual CPU capacity of the underlying node N^{S}
$b\left(e_i^v\right)$	Article i bandwidth requirements for virtual link e_i^v
$c\left(n^{\mathrm{v}}\right)$	The residual CPU capacity of the underlying noden^{v}
$c_0\left(n^{\mathrm{v}}\right)$	CPU capacity requirements for traffic independent parts of virtual node n^{v}
$B\left(n^{\mathrm{v}}\right)$	The maximum amount of traffic that virtual node n^{v} needs to handle

On the basis of understanding the related parameters of the virtual network technology model that has been constructed, the performance of the mapping algorithm of the virtual network mapping algorithm and the traditional network technology was compared and analyzed through the relevant experimental data in this study. In order to speed up the optimization speed of the related algorithms, the method of direct solution of the above mathematical formula model was studied so that it was possible to study the efficiency of the data in this study. Since the actual network cannot be studied, this study is mainly to simulate the whole experiment through some virtual networks. Firstly, the bandwidth distribution of 10 randomly acquired virtual network link requests was studied. The bandwidth requirement is shown in Table 2. Through the analysis of the optimization of all bandwidth values, this study considers that when the bandwidth value is set to 0.5, the interval of the bandwidth distribution is even.

Table 2. Bandwidth requirements for virtual links in this study

Load	Evenly distributed intervals of bandwidth
0.1	[2, 3]
0.2	[4, 6]
0.3	[6, 9]
0.4	[8, 12]
0.5	[10, 15]
0.6	[12, 18]
0.7	[14, 21]
0.8	[16, 24]
0.9	[18, 27]
1.0	[20, 30]

In order to simplify the relative process of experiment, the values of all virtual nodes were set to 0.1 in this study. Then, the cost weights values of the virtual network mapping algorithm were set differently. When carrying out different mapping cost weighting values, the conclusion of average mapping cost of the virtual network mapping algorithm and the traditional network mapping algorithm was carried out by using the above mathematical model. The results are shown in Table 3. The results show that the running cost of the mapping algorithm is related to the cost weight and the setting of bandwidth. With the increase of bandwidth settings, the running cost of the network virtual mapping algorithm (VNE) and the traditional mapping algorithm show an increasing trend. The two mapping algorithms have positive correlation with the mapping weight value (β). With the increase of mapping weight (β), it shows a gradually increasing trend. Therefore, when optimizing different mapping algorithms, it is necessary to consider the optimization of the bandwidth and the setting of the mapping weight value as much as possible. The research further compares the operation cost of the network virtual mapping algorithm and the traditional mapping algorithm. The results show that the operating cost of the network virtual mapping algorithm is lower than that of the traditional network technology regardless of the setting of any weight value. However, the savings rate of different weight values is also different. When the weight value is relatively small, the cost savings of the network mapping algorithm compared to the traditional mapping algorithm are significantly lower than the cost savings when the weight value is set larger. This is probably because when the mapping weight value of the node is set to smaller value, the segmentation mapping has less impact on the total cost. Thus, the total operating cost can be reduced as much as possible so that the final rate of saving is relatively large [15].

Table 3. Comparison of the cost of the network virtual mapping algorithm and the traditional mapping algorithm when different mapping weights are used

	$\beta = 0.2$			$\beta = 1$			$\beta = 5$		
Load	VNE	tradition	Cost saving rate	VNE	tradition	Cost saving rate	VNE	tradition	Cost saving rate
0.1	19.0	25.3	24.9 %	30.6	36.2	15.5 %	88.6	90.9	2.5 %
0.2	43.1	57.2	24.7 %	67.3	80.1	16.0 %	188.4	194.3	3.0 %
0.3	72.2	93.3	22.6 %	107.3	126.8	15.4 %	281.4	291.7	3.5 %
0.4	113.5	141.9	20.0 %	159.4	185.4	14.0 %	388.1	403.2	3.7 %
0.5	154.3	185.7	16.9 %	214.2	242.7	11.7 %	513.6	528.3	2.8 %
0.6	179.4	203.8	12.0 %	252.3	272.4	7.4 %	586.4	608.8	3.7 %
0.7	200.8	233.7	14.1 %	281.6	310.8	9.4 %	670.2	696.6	3.8 %
0.8	235.6	250.0	5.8 %	327.8	354.9	7.6 %	786.2	806.9	2.6 %
0.9	251.5	276.3	9.0 %	356.8	380.0	6.1 %	827.9	860.3	3.8 %
1.0	277.3	312.9	11.4 %	393.4	421.9	6.8 %	910.1	967.0	5.0 %

Finally, the acceptance rate of network requests under different mapping algorithms was calculated. The results are shown in Fig. 4. The results show that the network virtual mapping algorithm (VNE) has higher acceptance rate for the virtual network request than the traditional mapping algorithm when the bandwidth load is large. This may be because it saves more running costs and thus accommodates a larger amount of data request commands.

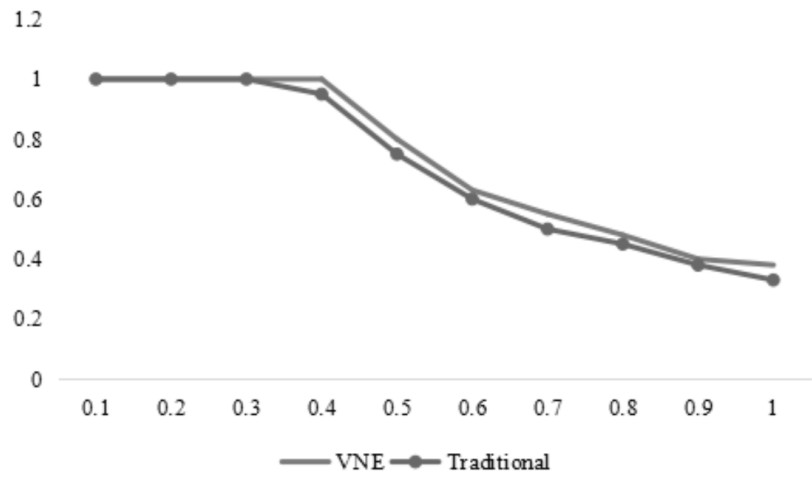

Fig. 4. Average acceptance ratio of network virtual mapping algorithm (VNE) and traditional mapping algorithm for virtual network requests

4. Conclusion

With the development of the times, network information technology has been improved greatly, while the technology has brought great convenience to people's production and life, some incompatible factors have begun to appear. In the traditional network technology, the expansion of flow is weak, and the demand for energy consumption is increasing due to the limitation of the operation structure. As an important direction of the development of network information technology, the network virtual mapping algorithm can improve the operation efficiency of network technology and reduce the related cost effectively. In order to better optimize the design of network virtual mapping algorithm in our country, the related theories were analyzed, and a simple virtual mapping algorithm model was designed in this study. Then, the mapping cost and acceptance rate were calculated by the relevant optimization model. The results show that the mapping algorithm has relatively low mapping cost, and the acceptance rate of virtual requests is high, and then it can be applied to the subsequent improvement of related technologies. However, this research is more simulation virtual process and lacked practical application, which may cause the result to have certain limitation and insufficiency. However, this study can still provide some reference and scientific support for the improvement of related technologies and theories in China.

References

[1] J. F. Boreto: *Optimal mapping of virtual networks with hidden hops.* Telecommunication Systems *51* (2012), No. 4, 273–282.

[2] N. M. M. K. Chowdhury, M. R. Rahman, R. Boutaba: *Virtual network embedding with coordinated node and link mapping.* IEEE INFOCOM, 29–25 April 2009, Rio de Janeiro, Brazil, IEEE Conference Publications (2009), 783–791.

[3] A. P. BianzinoP, C. Chaudet, D. Rossi, J. L. Rougier: *A survey of green networking research.* IEEE Communications Surveys & Tutorials *14* (2010), No. 1, 3–20.

[4] J. F. Botero, X. Hesselbach, M. Duelli, D. Schlosser, A. Fischer, H. de Meern: *Energy efficient virtual network embedding.* IEEE Communications Letters *16* (2012), No. 5, 756–759.

[5] N. M. M. K. Chowdhury, R. Boutaba: *A survey of network virtualization.* Computer Networks *54* (2010), No. 5, 862–876.

[6] J. B. Park, K. S. Lee, J. R. Shin, K. Y. Lee: *A particle swarm optimization for economic dispatch with nonsmooth cost functions.* IEEE Transactions on Power Systems *20* (2005) No. 1, 34–42.

[7] J. S. Kong, D. M. Frangopol: *Life-cycle reliability-based maintenance cost optimization of deteriorating structures with emphasis on bridges.* Journal of Structural Engineering *129* (2003), No. 6, 818–828.

[8] P. Kelle, A. Akbulut: *The role of ERP tools in supply chain information sharing, cooperation, and cost optimization.* International Journal of Production Economics *93–94* (2005), 41–52.

[9] K. C. Sarma, H. Adeli: *Life-cycle cost optimization of steel structures.* International Journal for Numerical Methods in Engineering *55* (2002), No. 12, 1451–1462.

[10] M. Yu, Y. Yi, J. Rexford, M. Chiang: *Rethinking virtual network embedding: substrate support for path splitting and migration.* Newsletter ACM SIGCOMM Computer Communication Review *38*, (2008), No. 2, 17–29.

[11] C. Isheden, Z. Chong, E. Jorswieck, G. Fettweis: *Framework for link-level energy efficiency optimization with informed transmitter*. IEEE Transactions on Wireless Communications *11* (2013), No. 8, 2946–2957.

[12] D. W. K. Ng, E. S. Lo, R. Schober: *Wireless information and power transfer: Energy efficiency optimization in OFDMA systems*. IEEE Transactions on Wireless Communications *12* (2013), No. 12, 6352–6370.

[13] C. Diakaki, E. Grigoroudis, D. Kolokotsa: *Towards a multi-objective optimization approach for improving energy efficiency in buildings*. Energy and Buildings *40* (2008), No. 9, 1747–1754.

[14] S. Zhang, X. Xia: *Modeling and energy efficiency optimization of belt conveyors*. Applied Energy *88* (2011), No. 9, 3061–3071.

[15] A. Zappone, P. Cao, E. A. Jorswieck: *Energy efficiency optimization in relay-assisted MIMO systems with perfect and statistical CSI*. IEEE Transactions on Signal Processing *62* (2014), No. 2, 443–457.

Received September 12, 2017

Acta Technica *62* No. 2B/2017, 619–630

Application of the steel structure model based on modular coordination in optimization design of residential system in China[1]

Zhang Jinge[2]

Abstract. In order to promote the development of housing industry from extensive to intensive, and to realize the formation and perfection of industrialized construction system, in this paper, the current situation of serious lack of application research of modular design in residential building of steel structure in our country was put forward. On the basis of explaining the characteristics of steel structure residence, the design process, design method and selection of basic modulus were expounded. Then the modular location of steel structure residence was carried out, the positioning method was based on the installation way of the enclosure system, and the coordination of the outer protection system and the main structure was taken as the principle. The final research results show that the steel structure house can minimize the number of non-standard components and the number of installation nodes, and can increase the level of industrialization construction.

Key words. Modular coordination, steel structure residential building, systematic design.

1. Introduction

With the high PM2.5 and the intensification of Urban Haze, the quality of the living environment and the sustainable development of society have become the focus of attention. The real estate industry has begun to explore new patterns of development. It is a consensus that the building should be covered with a "green coat". Building a green and low carbon city has become the main theme of the times, and creating a scientific and healthy housing has also become a new trend in the development of the real estate industry. In the 12th Five-Year "planning" development goals, it is easy to see that energy-saving and green buildings have become

[1]This work was supported by the Research on Protection of Traditional Rural Culture and Development of Beautiful Countryside. Research on Nanyang "Painter Village" Intangible Culture's Protection and Countryside Development (2017-ZZJH-384, Education Department of Henan).

[2]School of Arts and Design, Nanyang Normal University, Nanyang, Henan, China, 473061

the development trend of China's residential industry. Therefore, in recent years, the relevant departments of the state have issued a series of guidance documents and norms on steel structure residential buildings to promote the development of China's steel residential buildings. The level of industrial production is the key to comprehensive evaluation of steel structure residential buildings, this is because industrialisation housing is standardized based on modularization. Industrialisation is constructed through standardization, and industrialization is strengthened through industrialisation. Standardization is the basis of industrial production. Modular design and standardization are the primary tasks of the establishment of steel structure housing system and its industrialization.

2. State of the art

The practice of steel structure housing system began in 1980s. For example, the Exhibition Hotel, built in 1987, adopted a steel structure system, with seven main buildings, surrounded by 3 layers of conjoined houses. And the steel used in the building mainly came from Canada, welding of square steel column and H type steel beam [1]. In November 1994, China completely built the first steel structure house entirely by itself in Beicai, Shanghai, which was the test type steel structure residential system of 8 layers. At present, the domestic steel structure system is mostly used in high-rise residential buildings, and with the continuous development of technology, the practice of steel residential structure is increasing year by year. Residential buildings with steel structure residence system have the advantages of flexible layout, green energy saving, good seismic performance and short construction period [2]. However, at present, the construction period of most of the steel residential buildings is no less than that of other residential buildings. This is mainly because that in the component of enclosure structure, the industrialized production of industrial products and the assembly characteristics of the construction site has not been realized. The selection of materials for the component of enclosure structure is limited, the rate of finished components is low, and the connection structure is imperfect [3]. Through the engineering practice, the experience of the scheme design, structure, equipment and technology of the steel structure house has been effectively accumulated, summarized as three points: the advantages of the steel structure are exploited, and the structure selection is more freedom. Different from the previous residential limitations of the "small bay layout", many cases adopt the "layout of large spaces". In order to realize the standardization of building components, the design of residence plane and space form is simple and regular, and the architectural details are less changed. In the course of the design of steel structure residence design, although there is a standardized design of structural parts, there is no systematic design method, and only the traditional design methods are used to consider the standardization of building structures and components [4].

3. Methodology

Building modulus is a unified value-added unit, which is used to harmonize building scales, so as to achieve large-scale production of industrialization, and to make the construction parts and components of different materials, different forms and different manufacturing methods with certain versatility and interchangeability [5]. Building modulus is also the basis for scale coordination of architectural design, building construction, building materials and products, building equipment, building components and other departments, the purpose of which is to make the fittings fit together and be interchangeable.

Modulus coordination is a standard scale system for the design, manufacture and installation of buildings and their components, formerly called modular systems. The purpose of building a modular coordination system for buildings is to realize the industrialization of building products and building components by means of standardization [6]. Requirements for modular coordination of buildings: the modulus series is used to adjust the dimensional relationship between the assembled monolithic building and the components (parts), and to optimize the dimensions and types of the building parts (parts); when the components (parts) are assembled, the sizes and positions of the parts (parts) can be clearly defined, so that the design, manufacture and installation can be easily matched with each other, so as to meet the requirements of the integrity, efficiency and economy of the assembly type architectural design.

The modular mesh is a modular space grid composed of three orthogonal coordinates with modulus dimensions, and the projection on the horizontal and vertical surfaces is called the modular mesh. The unit scale of a grid is a fundamental modulus or an enlarged modulus. Different amplification modulus can be used in three directions or the same direction of the grid [7].

The locating axis is the basis of the position of the component in the 3D mesh space. In the grid, each component is positioned in three directions by means of the boundary locating plane and the alignment line (or alignment line). The boundary location refers to that the boundary of the number of fingerprints is located in the component of the grid line, while the middle (or alignment line) refers to that the number of grid positioning line is located in the center line of the component (or partial center line) [8].

Construction Standardization refers to the establishment and implementation of relevant standards, specifications, rules and other procedures in construction [9]. The purpose of building standardization is to make rational use of raw materials, promote the versatility and interchangeability of structural parts, realize the industrialization of construction, and achieve the best economic results. Modularization is a form of standardization, for general purpose.

The steel structure residential system refers to the residential construction system whose main load-bearing component is steel, and the enclosure and partition members are new lightweight wall materials. The structural system of steel structure residence is the structural type composed of each load-bearing component with steel structural component as the main part [10]. The frame system is mainly com-

posed of beams and columns. The steel frame is generally made of concrete-filled steel tubular columns, and H steel is often used as steel frame columns. The high frequency dry type thin-wall steel beam, narrow flange shaped steel or other swing connecting I-beam are used as steel frame beam, and each type steel member has its own product series. The types of common dteels and their properties are listed in Table 1.

Table 1. Types of common steel and their sectional dimensions (in mm)

Type of steel	Section H steel (beam) (A×B)	Light channel steel (H×A×C)	Square steel tube (A×B)	Round steel tube (external diameter)
Common size	100–600×50–200	60–250×30–75×10–25	50–175×50–175	21.7–1219.2

The system has small dead weight, long vibration cycle and good seismic resistance, but its lateral displacement stiffness is small. Under the action of wind load and earthquake, the lateral displacement and the total lateral displacement cannot meet the requirements, and a variety of lateral resistance system must be set up. The lateral force resisting system is composed of connection support, shear wall and core tube of each frame [11]. Therefore, the structural system of steel residential structure is divided into the following, as shown in Table 2.

Table 2. Classification of steel structure residential structure system

Structural system name	Brief introduction
Pure steel frame system	Along the longitudinal and transverse sides of the house, the frame is used as the main component for weighing and resisting the side force
Steel frame (Center/ eccentric) support structure system	On the basis of the frame system of the building, a certain number of vertical supports are arranged in the longitudinal and transverse directions of the building
Steel frame shear wall structure system	In the frame structure, a certain shear wall is arranged, and the frame is combined with the shear wall
Steel frame core tube structure	A rigid or hinged steel frame is formed of a reinforced concrete core tube and an outer ring
Staggered truss steel structure system	It consists of columns, plane trusses and floor panels; the plane is rectangular or rectangular

The structural system, performance characteristics and the number of floors used in various steel residential structures are shown in Table 3. In the residential design, the selection of the steel structure residential system should follow the principles of safety, convenience and economy, and combine with the specific requirements of the function, modulus and maintenance of the house. At the same time, the use function of the house should be satisfied, so as to save investment.

Table 3. Comparison of structural performance of multi-story residential buildings

Resi-dential layers				Structural system name	Lateral resistance	Amount of steel used	Industrialized factory make-up	Structure construction difficulty and speed	Advantage	Disadvantages
Below 6				Steel frame	Bad	High	All frame system	Simple and fast	Simple structure rapid construction	Construction of sectional dimensions, uneconomical
	6–12			Bar truss	Very good	Low	Steel structure part	Relatively simple and fast	Good lateral resistance and large depth of bay	The truss has an influence on the graphic design of residential buildings
				Steel frame-bracing	Good	Preety low	All frame system	Relatively simple and relatively fast	Good lateral resistance and simple structure	The support has an influence on the opening of doors and windows and the adjustment of partition walls
		12–40		Steel frame-shear wall	Good	Low	Steel structure part	Relatively simple and relatively fast	Good lateral resistance and relatively simple structure	The shear wall has an influence on the opening of doors and windows and the adjustment of partition walls
			More than 40	Steel frame-core tube	Very good	Low	Steel structure part	Complex and slow	Good lateral resistance and good flexibility of the outer frame	Wet operation of some concrete

Through Table 3, it can be found that the structural system affects the graphic design of residential buildings. In order to avoid exposing the frame structure in the plane space, the wall and the beam column structure should be arranged on

the same line as much as possible. The steel frame column that is often used in residential system is about 6–7.5 m, and the construction area occupied by a single structural component should not be too large. As a whole, the cross section of the pure steel frame member is larger, which affects the plane space size. The frame in staggered frame will affect the plane arrangement. And the supporting elements in the steel frame bracing system can affect the layout of the facade doors and windows. In addition, in the frame shear wall, shear wall position will affect the position and arrangement of the partition door. The arrangement of the bracing system of the frame core tube is flexible and free from structural constraints, but there will be some wet work on site, the construction is more complex, and construction speed is slow. Therefore, in the design of steel residential structure, the structural system should be chosen according to the specific conditions.

Traditional residential design is the design process from a small proportion of macro architectural layout to a large proportion of technical details. However, the systematic design should coordinate the construction, the structure, the equipment, the construction and the production of the factory, and the goal is to produce a unique design process of the building system [12]. The design process is applicable to a large class of buildings. Before the specific architectural design, according to the characteristics of the building itself, technical issues should be given priority and systematized, so as to apply to the architectural series design in the system. As opposed to the traditional design process, the design process is called "reverse design process", and the design flow chart of the system house is shown in Fig. 1.

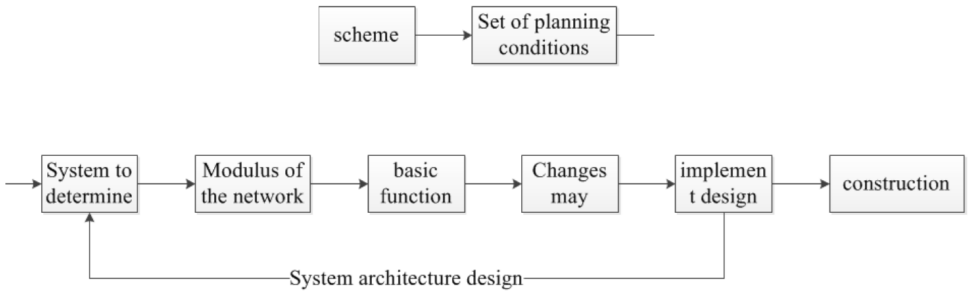

Fig. 1. Design flow chart of system house

Industrialized residential buildings are required to move from the site to the factory and from the extensive to the fine. Industrialized housing is a residential product with a manufacturing mode. Therefore, industrial residential design should combine the benefits of large-scale production and the market demand of small-scale production. Modularization is one of the techniques to fuse these two patterns. The highly standardized parts are simple in shape, and the standard function modules are rapidly configured by combining with the modular technology, so that a series of new products can be quickly obtained to meet the market demand, shorten the product life cycle, and accelerate the development process of the product. In other words, the internal diversity of performance is reduced, and the external diversity of production patterns is expanded [13]. Similarly, architectural modulus coordination can unify and simplify the specifications of building components, thus to make the

structure simpler, the construction more convenient, and to meet the diverse needs of building users. At the same time, the facade of the steel structure house needs the aesthetic effect of continuous rhythm and so on.

The modular mesh method is a design method based on geometry. A space grid is arranged in a size line, and the mesh gap is called modulus, and the design is carried out on the mesh. When the middle gap of the grid system is larger, the component specification is less, and the flexibility of the assembly is smaller. The smaller the middle gap of the grid system is, the more the component specifications are, and the stronger the flexibility of the combination is [14]. 100 mm is widely used as the fundamental modulus M in the world, and the division modulus and amplification modulus are developed on the basis of the fundamental modulus. The main application areas of modular modulus are: structural joints, product specifications, building materials, building cracks, and tolerances of building products. Enlarged modulus is mainly used for building branch spacing, span and height dimensions, and the range of its sequence directly affects the degree of simplification of the control dimension. Different types of building use different expansion modulus, and at present our country has stipulated different amplitude. The modular grid method is one of the most basic systematic design methods, because modulus is the basic unit of measurement for systematic architecture. The specifications, sizes (except thickness or sectional dimension) of the main components of the system shall be as much as possible to meet the design modulus or enlarged modulus. Moreover, the structural members of the modular grid can give full play to the structural properties of a balanced extension of a steel structure plane. The module network can be divided into building modulus network and structure modulus network. The building modular network is mainly used for the arrangement of function space and space combination, which can mark the net outline of the space, reflect the thickness of the wall, and facilitate the arrangement of the equipment and the design of the decoration. The structural modulus network is the basis of the structural component combination, which can indicate the axis of the column and the wall, so that the selection of the structural parameters and the rationality of the structural arrangement should be taken into account. The main parameters of the structure are the formulation of the production program and the modular setting of the housing factory. And the rationality of structural arrangement refers to the size and layout of the component, which is the basis of architectural design [15]. The grid of the main structure is different from that of the building space, but they should be consistent with each other. For example, when the space division function and the structure bearing function are the same, the building modulus network and the structural modulus network can replace each other. When the two are inconsistent, two different modular network systems are needed.

4. Result analysis and discussion

In the process of investigation, the plane of some steel structures in our country is drawn up. It can be found that the central location method is adopted in the residential part of steel structure in our country at present, and the basic moduli

are mostly 3M and 6M. An arrangement of modulus networks for a modular steel house is shown in Figs. 2–5.

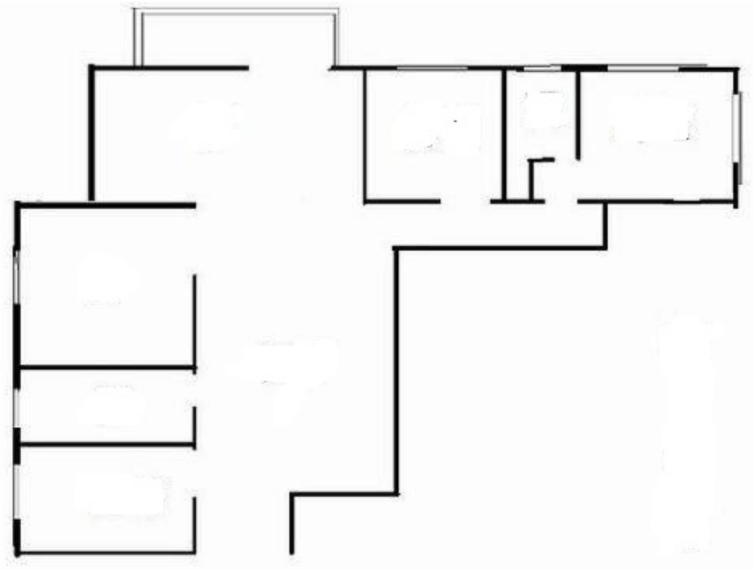

Fig. 2. Building 3 (apartment type), Jin Chen apartment, Beijing

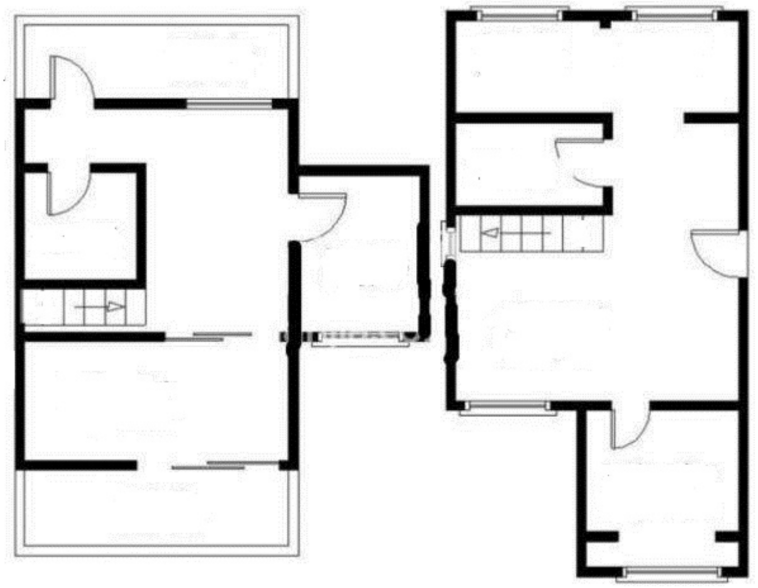

Fig. 3. Yizhuang youth apartment (drive)

Through Figs. 2–3, it can be found that in the current steel residential building, corridor style and unit type are designed by case 6M basic module, especially in the

unit type. In the investigation, there is no application of 6M basic design modulus in point house. Therefore, an existing case is selected to locate and transform it and the plan before and after the transformation is shown in Figs. 4–5.

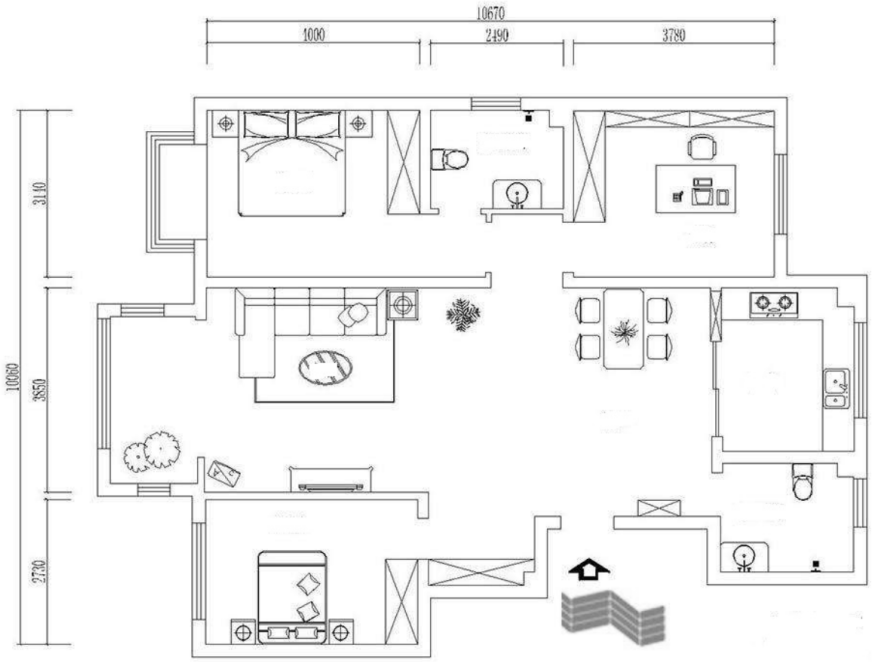

Fig. 4. The standard house of No. 1 building of Laiwu Iron and steel garden

Through the comparison of Figs. 4–5, it can be found that the function space of the plane changes little after using the basic design modulus of 6M, and can still meet the application requirements. Therefore, the design of 6M can also be used in our country's steel house.

There are different positioning methods in horizontal direction of steel structure residence. In order to ensure the interchangeability of parts and positions, and meet the requirements of functions, in actual project design, different positioning methods or hybrid positioning methods can be adopted to achieve economic and effective results. In view of the embedded exterior retaining component and the plug-in type outer enclosure component, the modulus coordination can be carried out by means of the net distance modulus method, or the positioning mode of combining the center line of structural column beam with modulus mesh. For the specific situation, the vertical direction can be coordinated by means of the linear high speed module or the high layer modulus.

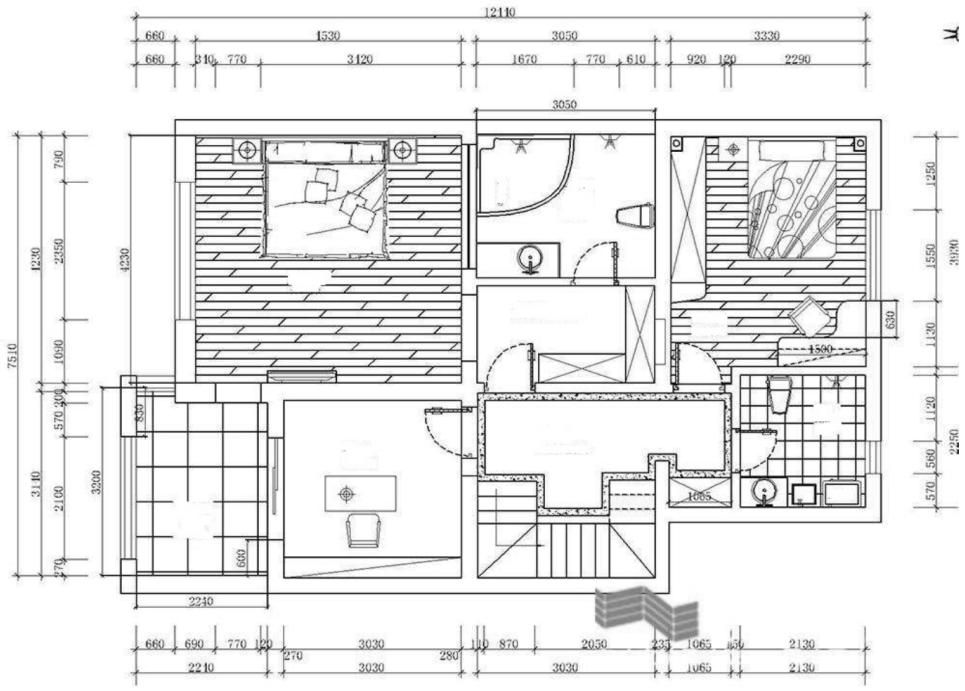

Fig. 5. Location of flat 6M of No. 19 Building of Sakura garden in Laiwu Iron

5. Conclusion

In order to study the application of the steel structure model based on modulus coordination in the optimization design of housing system in our country, in this paper, the system design was mainly analyzed, and the development process, system structure, design process and design method were studied. And system design method was the core of this paper. Through the previous research, the system design method was summed up. Through the research, some conclusions were drawn as follows: there are two main methods for the design of steel structure residence in our country: the modular grid method and the basic combination method. The modular grid method is the most basic system design method, whose purpose is to reduce the use of nonstandard components. There are two main parts of the research: the determination of basic modulus and location method. Moreover, there are three kinds of modulus positioning methods: central line positioning method, interface positioning method and fixed distance method. Central location method is a single structural system positioning method, and the interface location method and the fixed distance localization method are all aimed at the envelope system positioning method. The basic combination method is another method of system design, which is mainly used to solve the contradiction between standardized design and diversified requirements. Thus, in the future research, scholars can study how

to design the basic unit modules according to the modulus of the basic combination design.

References

[1] Q. L. Zhang, G. W. Feng, Y. Q. Zhang, B. X. Zhu: *Syntheses, structures, and luminescence properties of anion-controlled heterometal modular coordination polymers based on a metalloligand*. RSC Advances *4* (2014), No. 22, 11384–11392.

[2] E. Hofman, H. Voordijk, J. Halman: *Matching supply networks to a modular product architecture in the house-building industry*. Building Research & Information *37* (2009), No. 1, 31–42.

[3] L. March: *Rudolph M. Schindler: Space reference frame, modular coordination and the "Row"*. Nexus Network Journal *5* (2003), No. 2, 51–64.

[4] C. de Marchis, M. Schmid, D. Bibbo, I. Bernabucci, S. Conforto: *Inter-individual variability of forces and modular muscle coordination in cycling: A study on untrained subjects*. Human Movement Science *32* (2013), No. 6, 1480–1494.

[5] M. H. Filby, J. W. Steed: *A modular approach to organic, coordination complex and polymer based podand hosts for anions*. Coordination Chemistry Reviews *250* (2006), Nos. 23–24, 3200–3218.

[6] P. D. Jovančić, D. Ignjatović, M. Tanasijević, T. Maneski: *Load-bearing steel structure diagnostics on bucket wheel excavator, for the purpose of failure prevention*. Engineering Failure Analysis *18* (2011), No. 4, 1203–1211.

[7] M. K. Kuzman, J. Hrovatin, P. Grošelj: *Comparison of various types of residential building structures*. Građevinar *63* (2011), No. 9, 869–874.

[8] F. Fu, J. Sun, C. Pasquire: *Carbon emission assessment for steel structure based on lean construction process*. Journal of Intelligent & Robotic Systems *79* (2015), Nos. 3–4, 401–416.

[9] M. K. Kuzman, P. Grošelj: *Wood as a construction material: Comparison of different construction types for residential building using the analytic hierarchy process*. Wood Research *57* (2012), No. 4, 591–600.

[10] H. Takabatake, T. Nonaka: *Numerical study of Ashiyahama residential building damage in the Kobe Earthquake*. Earthquake Engineering & Structural Dynamics *30* (2001), No. TOC 6, 879–897.

[11] Y. Li, Z. Shen, X. Yao, R. Ma: *Experimental investigation and design method research on low-rise cold-formed thin-walled steel framing buildings*. Journal of Structural Engineering *139* (2013), No. 5, 818–836.

[12] D. Y. Seo, C. Koo, T. Hong: *A Lagrangian finite element model for estimating the heating and cooling demand of a residential building with a different envelope design*. Applied Energy *142* (2015), 66–79.

[13] J. Li, T. P. White, L. O'Faolain, A. Gomez-Iglesias, T. F. Krauss: *Systematic design of flat band slow light in photonic crystal waveguides*. Optics Express *16* (2008), No. 9, 6227–6232.

[14] A. I. Papadopoulos, M. Stijepovic, P. Linke: *On the systematic design and selection of optimal working fluids for Organic Rankine Cycles*. Applied Thermal Engineeringh *30* (2010), Nos. 6–7, 760–769.

[15] J. S. Jensen, O. Sigmund: *Systematic design of photonic crystal structures using topology optimization: Low-loss waveguide bends*. Applied Physics Letters *84* (2004), No. 12, 2022–2024.

Received September 12, 2017

Acta Technica *62* No. 2B/2017, 631–642

Application of building integrated photovoltaic (BIPV) system in green building[1]

Jiawei Cai[2], Zhenfei Zhang[2]

Abstract. Solar energy is an important direction of the development and application of modern clean energy, and great achievements have been made in the development of photovoltaic technology in China. However, in the specific practical applications, the photovoltaic technology and green building have not been unified to form a comprehensive function of the integrated building. In order to study the building integrated photovoltaic (BIPV) in the green building, the energy consumption and solar radiation heat gain of solar panels installed in a green building in China were simulated and analyzed by using Energy Plus software and the CTF method. Through the analysis, it can be found that solar panels can effectively reduce the cooling energy consumption of the air-conditioning system in summer, and it has no significant effect on the solar radiation in winter.

Key words. Photovoltaic, air conditioning energy consumption, energy saving, BIPV.

1. Introduction

With the development of modern economy, the use of natural resources and the destruction of ecology are becoming more and more serious, which is not conducive to the long-term, sustainable and healthy development of human society [1]. In addition, with the further increase of energy demand in recent years, the energy problem has become an urgent problem that human society needs to solve [2]. People are trying to find new energy sources to solve the energy crisis now facing, such as water, nuclear power, solar energy and so on. Among them, the utilization of solar energy is one of the effective ways to solve the human energy crisis [3]. Solar energy is clean, pollution-free, inexhaustible, and very applicable. From the beginning of 1990s, people put forward the building integrated photovoltaic (hereinafter referred

[1]This work was supported by the Henan Province Key Science and Technology Research Projects (Field of Social Development), Research and Demonstration of the Technology Integration of Renewable Energy & Green Buildings' Combination Based on the Concept of Industry 4.0.

[2]Nanyang Institute of Technology, Nanyang, Henan, China, 473000

to as BIPV). The building and the components of solar photovoltaic power generation were combined and used efficiently, which could effectively use solar energy that was absorbed by the building's outer surface and improve the indoor thermal environment with many advantages [4]. At present, the combination of green building and green photovoltaic energy saving technology has become a major trend in the development of modern architecture [5]. Although our country has carried on certain research in this aspect, it is still relatively few in the actual application. Therefore, it is necessary to make further application research and apply it to the design and implementation of our architecture, which has a far-reaching and important impact on China's long-term sustainable and healthy development.

2. State of the art

In recent years, many developed countries have put solar power in the primary position of sustainable renewable energy utilization. Since 1970s, China has increased the investment in resources and the formulation of policies in this aspect, thus promoting the utilization and development of solar energy [6]. As of 2008, Spain's new installed capacity of photovoltaic power generation exceeded 2500 MW, and Germany's new PV installed capacity in 2010 was more than 4.8 GW [7]. Since 2010, China has entered the rapid development of photovoltaic power generation. Now it has the world's largest photovoltaic industry, becoming the world's largest photovoltaic component production and export country [8]. For buildings, a variety of ways can be used to carry out the sun shading, including the building of mutual sun shading, outdoor shading, indoor shading and green shading. The combination of photovoltaic power generation and green building can simultaneously play its role of sun shading and effectively reduce indoor energy consumption. One of the typical forms of photovoltaic integrated building is photovoltaic shading system. In summer to ensure lighting is reasonable, it can be as much as possible to reduce solar radiation and the energy consumption of air conditioning. In addition, it can obtain more solar radiation heat and reduce the energy consumption of heating in winter [9]. Therefore, in building design, it is necessary to consider the performance optimization problem of the whole year, and combine the self-generating function to make it possible to achieve the optimal annual power generation situation [10].

3. Methodology

3.1. Simulation analysis of building energy consumption

With EnergyPlus software, the simulation analysis of energy consumption based on building integrated photovoltaic is carried out. The software is used because of its integration method of load/device/system simulation. In the process of use, the user can select the time step, and each module simulation is synchronized. In addition, the time step results are feedback to each other, which is more accurate than the traditional sequential simulation method [11]. The comparative analysis of integrated

synchronous and sequential analog load/device/system simulation methods is shown in Fig. 1. The building system simulation includes heat and mass balance simulation, equipment simulation, air conditioning system simulation and so on. Data transfer and overall control of each part are simulated based on analog manager [12].

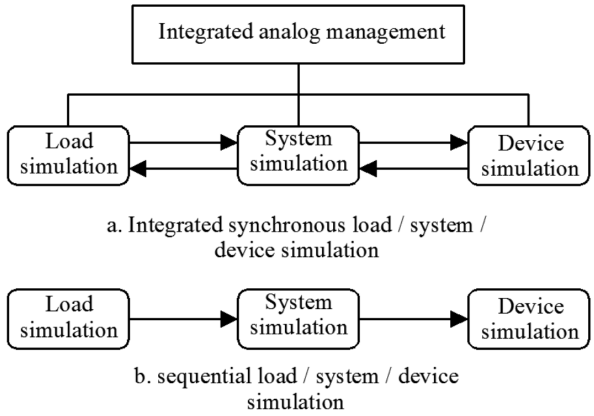

Fig. 1. Comparison of integrated, synchronous, and sequential load/system/device simulations

When using EnergyPlus software, the CTF method is used to simulate the transient heat transfer of the roof, floor, wall and so on, in which the essence is the response coefficient method [13]. The method is based on the interior surface temperature of the enclosure structure, and the results of calculation are more accurate. It is assumed that the long wave radiation heat exchange rate of the surface is q''_{lwx}, the heat flux of the wall is q''_{ki}, the convection heat exchange rate of regional air is q''_{conv}, the absorption of solar radiation through the injected region is q''_{sol}, long wave radiation heat flow from the interior surface receiving net shortwave and equipment in the area are q''_{sw} and q''_{lws}, respectively. The heat transfer process of the inner and outer surfaces of the enclosure is shown in Fig. 2. Thus, the internal surface heat balance equation can be obtained in the form

$$q''_{\mathrm{lwx}} + q''_{\mathrm{sw}} + q''_{\mathrm{lws}} + q''_{\mathrm{ki}} + q''_{\mathrm{sol}} + q''_{\mathrm{conv}} = 0\,. \tag{1}$$

Heat flow is assumed to be q''_{ko} based on heat conduction into the wall. The convective exchange volume between the outer surface and the air is q''_{conv}. The net heat exchange volume of the outer surface and the long wave radiation of air and environment are q''_{lwr}. The radiant heat flux of the outside surface absorption, direct scattering and scattering is $q''_{\alpha\mathrm{sol}}$. Now, the heat balance equation of the exterior surface of the enclosure structure can be obtained im the form

$$q''_{\alpha\mathrm{sol}} + q''_{\mathrm{lwr}} + q''_{\mathrm{conv}} - q''_{\mathrm{ko}} = 0\,. \tag{2}$$

The starting point of the energy simulation process is load simulation, which provides the required parameters for the simulation of the air conditioning system.

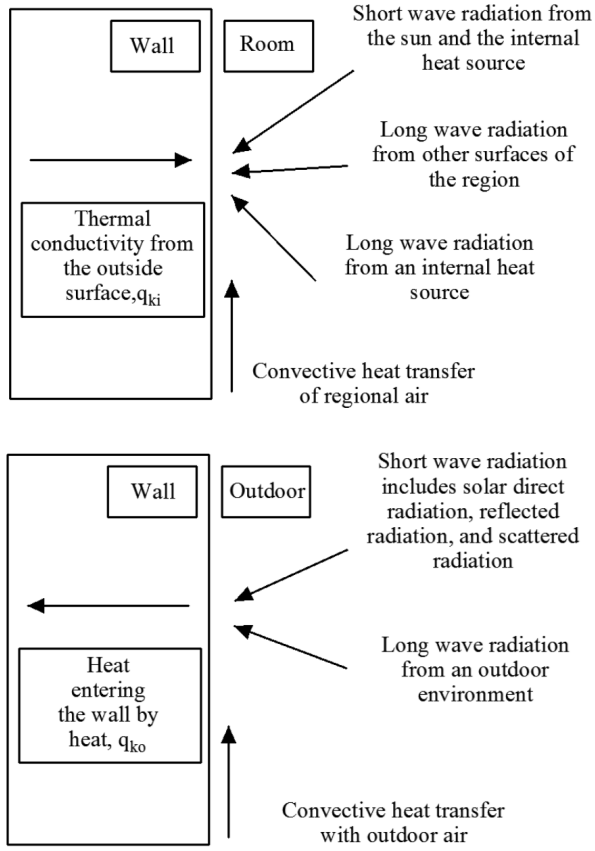

Fig. 2. Sketch of heat transfer of inner and outer surface of enclosure

The key to simulate the load by heat balance method is to calculate the regional air heat balance equation [14]. It is assumed that the heating capacity of the air conditioning system is $\dot{Q}_{\mathrm{s}}$, the outdoor air temperature is T_{∞}, the mass flow rate between the simulated area and ambient air is $\dot{m}_{\mathrm{st}}$, the air temperature of simulated solution area and adjacent area is $T_{\mathrm{z}i}$, the air mixing mass in the region and adjacent area is $\dot{m}_i$, the regional surface temperature is $T_{\mathrm{s}i}$, the surface area of the solution area is A_i, the convective heat transfer coefficient of the zone surface is h_i, the number of heat sources, surfaces and adjacent areas in the solution area is N_{sl}, N_{s} and N_{z}, respectively, the convection heat transfer of the internal heat source in the solution is $\dot{Q}_i$, the area temperature is T_{z}, the area air specific heat is C_{p} and the

regional heat capacity is C_{z}. Thus, we can obtain the thermal balance as follows:

$$C_{\mathrm{z}}\frac{\mathrm{d}T_{\mathrm{z}}}{\mathrm{d}t} = \sum_{i=1}^{N_{\mathrm{sl}}}\dot{Q}_i + \sum_{i=1}^{N_{\mathrm{s}}} h_i A_i \left(T_{\mathrm{s}i} - T_{\mathrm{z}}\right) +$$

$$+ \sum_{i=1}^{N_{\mathrm{z}}}\dot{m}_i C_{\mathrm{p}}\left(T_{\mathrm{z}i} - T_{\mathrm{z}}\right) + \dot{m}_{\mathrm{st}} C_{\mathrm{p}}\left(T_{\infty} - T_{\mathrm{z}}\right) + Q_{\mathrm{s}}\,. \tag{3}$$

If the heat capacity of the regional air is not considered, and the air heat storage in the solution area is 0, the output quantity of the steady air conditioning system can be obtained:

$$-\dot{Q}_{\mathrm{s}} = \sum_{i=1}^{N_{\mathrm{sl}}}\dot{Q}_i + \sum_{i=1}^{N_{\mathrm{s}}} h_i A_i \left(T_{\mathrm{si}} - T_{\mathrm{z}}\right) + \sum_{i=1}^{N_{\mathrm{z}}}\dot{m}_i C_{\mathrm{p}}\left(T_{\mathrm{z}i} - T_{\mathrm{z}}\right) + \dot{m}_{\mathrm{st}} C_{\mathrm{p}}\left(T_{\infty} - T_{\mathrm{z}}\right)\,. \tag{4}$$

The cold and heat load in the simulated area is eliminated by the hot and cold air supplied by the air conditioning system. The energy output from the air conditioning system can be calculated by using the air supply rate and the air supply temperature difference [15]. The air supply rate and the air supply temperature of the air-conditioning system are $\dot{m}_{\mathrm{s}}$ and T_{s}, respectively. In this way we obtain

$$\dot{Q}_{\mathrm{s}} = \dot{m}_{\mathrm{s}} C_{\mathrm{p}}\left(T_{\mathrm{s}} - T_{\mathrm{z}}\right)\,. \tag{5}$$

After completing the calculation of the dynamic heat balance of each time step, the software will issue instructions to the system simulation manager to update the indoor environment and the air conditioning system simulation. The system is simulated by EnergyPlus software with modular method. The air conditioning system type and configuration are made into modules, including the direct evaporative system, ground source heat pump, cooling system, and VAV system. Among them, the cold and heat source equipment is simulated by curve fitting method.

3.2. Construction of calculation model of building energy consumption

In this paper, an office building in a southern city of our country is used as a model of calculation. The floor plan of the standard layer is shown in Fig. 3. The building is facing the south with a total of 8 stories and the height of 3.5 m. The length and width are 60 m and 20 m respectively, and the total construction area is 9600 m^2. The height of windowsill and window height are 0.8 m and 1.8 m, respectively, and the ratio of window to wall is 50 %. The building is equipped with photovoltaic sun shading board with the size of 0.8 m×1.2 m×1.6 m, installed in the East, South and West of the office building in three directions. The length of each row of photovoltaic shading panels is outer wall length.

In the simulation of building energy consumption, it is assumed that there are no other objects around the building for shelter, and the artificial parameters of the

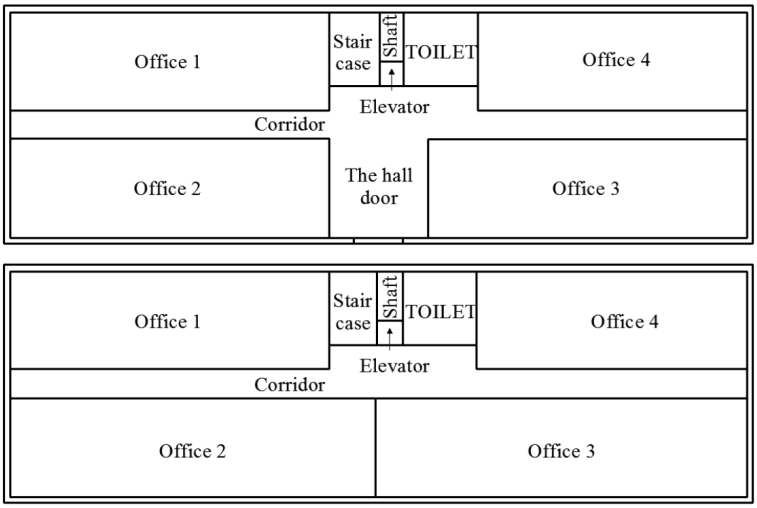

Fig. 3. Layout of building plan

building envelope will not change as the temperature changes. The main thermal parameters are shown in Table 1.

Table 1. Thermal parameters of enclosure structure of building model

Name of enclosure structure	Total heat transfer coefficient W/ (m^2 K)	Concrete construction situation
Interior wall	0.671	Plaster plaster layer + aerated concrete brick + plaster plaster layer
Exterior wall	0.453	Tile and cement mortar + polystyrene board + aerated concrete brick + plaster plaster layer
Roof	0.362	Asphalt and glass fiber cotton + polystyrene board + reinforced concrete pouring + plastering layer
Outside the window	2.716	Glass + hollow sandwich + glass aluminum alloy window frame
Floor	0.630	Plastering layer + reinforced concrete + floor tile

The air conditioning system for an office building is a full air system. In the summer, the chiller uses a chiller and a gas-fired boiler for heating in winter. Among them, the heating efficiency of the gas filter used in the winter heating is 0.9. In the building, corridors and staircases are non-air conditioning area, air-conditioning system operating period is determined to refrigeration 134 days with the heating period of 101 days. The temperature in summer and the amount of radiation in the simulated area are large, and the temperature in winter is low and the radiation

quantity fluctuates greatly. Using local weather data as a specific meteorological data, the hourly solar radiation intensity of the whole year is obtained, as shown in Fig. 4.

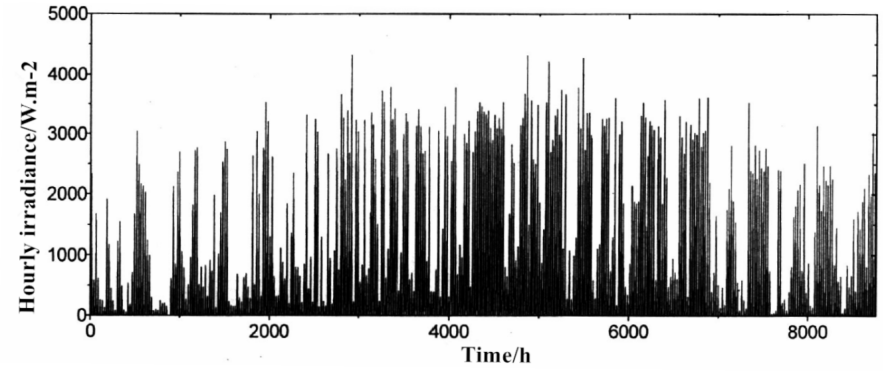

Fig. 4. Hourly solar radiation intensity in simulated region

The computation time step of energy consumption simulation is chosen as 05 h. When the absolute load error or the absolute temperature error of the room is lower than 0.04 W or 0.4 °C, the calculation convergence is considered. In summer, the energy consumption of the air conditioning system in the office is mainly the power consumption of pumps, fans and water-cooled units. In winter, the heating energy consumption of the air conditioning system in the office building is mainly composed of fans, pumps and boilers, and natural gas consumption. As the main energy consumption before and after are different, mainly for electricity and natural gas energy, the two in the taste also has a big difference. Therefore, in order to facilitate the simulation analysis and comparison, the equivalent electrical method is used to calculate the energy of other different types of power. Where the gas is converted into electricity, the coefficient is calculated as 65.9 %. The final simulation calculates that the energy consumption of the reference cooling and heating of the office building is 442.6 MWh and 214.2 MWh, respectively, in the absence of photovoltaic systems. The total energy consumption of air conditioning reached 656.8 MWh, and then the annual energy consumption of air conditioning in unit area was 68.4 MWh/m^2.

4. Result analysis and discussion

By simulating the different angles and widths, the refrigeration and heating energy consumption of the office buildings and the total energy consumption of the air conditioning system are simulated and analyzed. Preliminary analysis shows that the energy consumption of the refrigeration decreases with the increase of the width of the photovoltaic plate, and it decreases with the decrease of the inclination angle. No matter what the width of the photovoltaic panel is, when the dip angle is 60 °, the energy consumption reaches the minimum. With the increase of photovoltaic panels, the energy consumption of air conditioning system is gradually reduced. No

matter what the width of the photovoltaic panel is, the energy consumption is the minimum when the inclination angle is 60 °. Thus, whether it is cooling in summer or heating in winter, the installation angle of solar photovoltaic panels is determined at 60 degrees, and the minimum energy consumption of the air-conditioning system can always be obtained.

Compared with the benchmark building, for different forms of photovoltaic panels installed on green buildings, the total energy saving Q and the energy saving q per unit area of the air-conditioning system are shown in Figs. 5 and 6, respectively. As can be seen from the diagrams, as the width of the photovoltaic plate decreases, q increases gradually, but Q decreases. However, for Q and q, they both can achieve maximum energy consumption at the angle of about 60 °, which is determined by the geographical location of the simulated area. Therefore, when it is installed, we can perform the design with reference to this parameter.

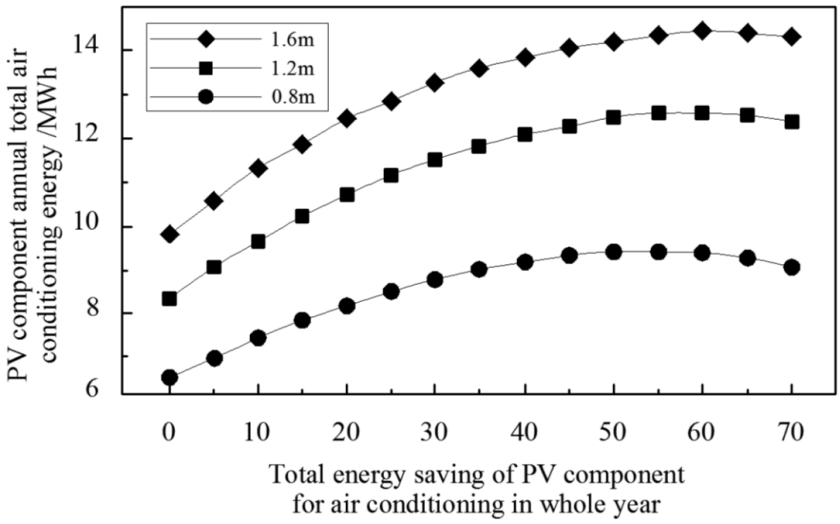

Fig. 5. Solar energy photovoltaic component, annual air conditioning, total energy saving

The effect of photovoltaic sunshade to the building outside the window of the solar heat gain is further studied. Photovoltaic panels can effectively block sunlight from passing through window glass into the room, thus avoiding excessive radiant heat caused by sunlight. Especially in summer, indoor solar heating can be avoided by photovoltaic panels, which can reduce indoor cooling load and reduce energy consumption of air-conditioning system. However, in the winter, too much will cause too small indoor solar heat gain and increase the indoor heating load. In this case, during the choice of photovoltaic panels, we need a compromise consideration. In this paper, the typical summer meteorological days in the simulated area are analyzed. The specific parameters are as follows: solar radiation is direct radiation; the average temperature is 32 °; the maximum temperature is 37.3 °, and the lowest

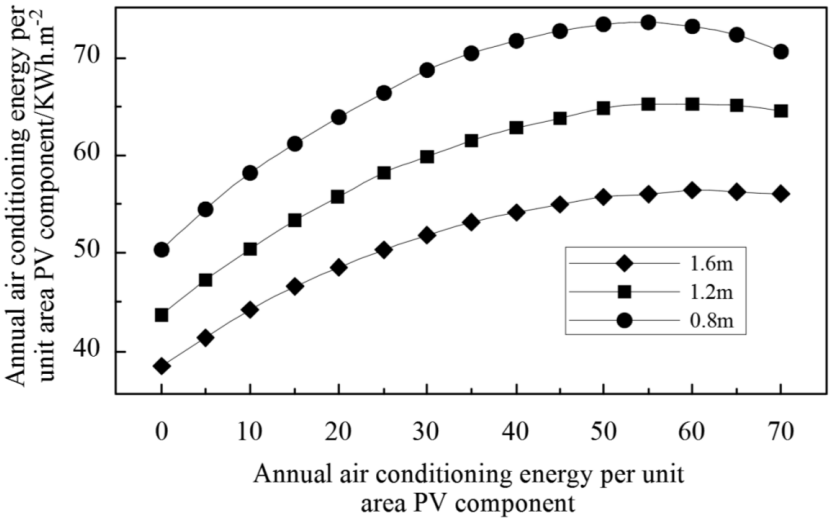

Fig. 6. Annual air conditioning energy per unit area solar photovoltaic component

temperature is 26.7 °. The reduction rate of building solar photovoltaic installation visor case and corresponding heat are respectively compared. The results of the simulation analysis are shown in Fig. 7.

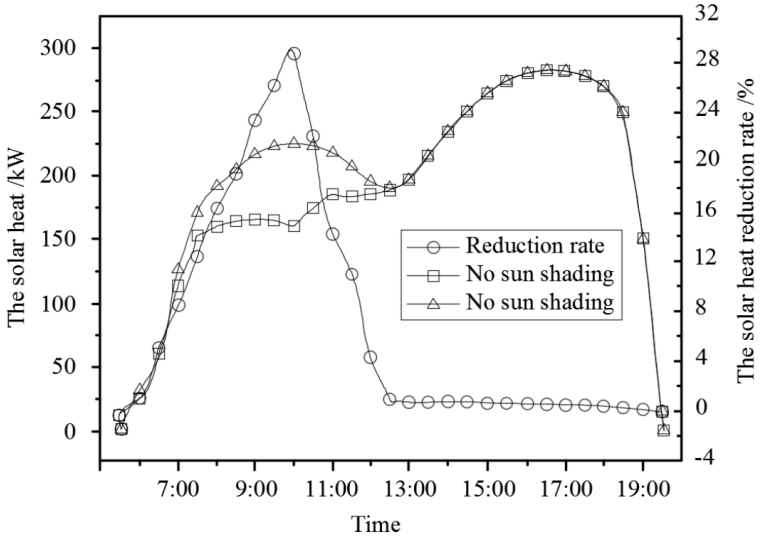

Fig. 7. The influence of the building photovoltaic sunshade window solar heat gain

It can be seen from the figures that without the installation of photovoltaic sun visor, the solar heat of the outside window has two peaks at 10:00 a.m. and 16:30, and the middle period is relatively low stage. It is because that the big sun

elevation angle at noon forms a small plane angle between the building facade, and the direct radiation intensity outside the window on the reflection to the building is very small. In the morning and afternoon, the sun high angle is small, and the plane angle between the sun and the building facade is big with too large solar heat. The comparison of two peaks in the morning and afternoon shows that the afternoon heat insulation peak is higher than that of the solar heat morning peak because of greater sun radiation intensity in the afternoon.

From the reduction rate, the heat reduction rate during 7:00 a.m.–11:30 a.m. is around 12 %. At the time of 12:00, the solar thermal reduction rate is reduced to 0. This is because the sun has the smallest azimuth and the height angle at noon. In addition, the plane angle between sun and the building facade is large, which leads to large direct solar radiation intensity. But from the different installation orientations, the effect of installing photovoltaic panels on the east side is the best, far better than the south. Similarly, the effect of the installation of winter photovoltaic shading panels on buildings can also be obtained. Around the noon, there is little difference between the amount of heat and the rate of decrease in the days of winter, but the reduction rate is slightly higher point at noon. From the time all day long, the solar thermal reduction rate maintains at around 4 %. This is because the solar radiation in winter mainly presents scattered radiation, and there is very little direct radiation. Although the sun visor can play a very good shielding effect on the solar radiation, the effect of scatter radiation is not obvious. In conclusion, solar photovoltaic panels can effectively block solar radiation in summer and reduce indoor refrigeration energy consumption. In winter, solar photovoltaic panels have small effect on diffuse solar radiation and little influence on the indoor energy consumption.

5. Conclusion

In this paper, EnergyPlus software was used to simulate and analyze the energy consumption of the building integrated photovoltaic, so as to effectively carry out the data transmission and overall control simulation analysis of the building envelope and indoor. On this basis, an office building in a southern city of our country was chosen as a calculation model, and photovoltaic shading panels were installed in the east, south and west of the office building in three directions. Combined with the local weather data simulation results, it can be seen that no matter what width of photovoltaic shading board is adopted, the minimum energy consumption of air conditioning system can be obtained when the inclination angle is 60 °. However, the change of its width has different effects on the total energy saving of the air conditioning system and the energy per unit area, so that the width parameter should be considered in the design. Further analysis shows that in the summer time, photovoltaic solar panels can effectively prevent direct sunlight into the room, thereby effectively reducing the cooling energy consumption. In winter, the photovoltaic solar panels have little influence on the solar radiation, so the indoor heating energy consumption does not increase. On the whole, solar panels can effectively reduce the energy consumption of air-conditioning systems, and contribute to energy saving design. However, this study does not carry out in-depth study of the impact of

photovoltaic power on the overall energy consumption, which is also a major part of the impact.

References

[1] F. Cucchiella, I. D'Adamo, S. C. L. Koh: *Environmental and economic analysis of building integrated photovoltaic systems in Italian regions.* Journal of Cleaner Production *98* (2015), 241–252.

[2] S. Sharma, A. Tahir, K. S. Reddy, K. Tapas, K. Mallick: *Performance enhancement of a building-integrated concentrating photovoltaic system using phase change material.* Solar Energy Materials and Solar Cells *149* (2016), 29–39.

[3] A. K. Shukla, K. Sudhakar, P. Baredar: *Simulation and performance analysis of 110 kWp grid-connected photovoltaic system for residential building in India: A comparative analysis of various PV technology.* Energy Reports *2* (2016), 82–88.

[4] A. M. Pal, S. Das, N. B. Raju: *Designing of a standalone photovoltaic system for a residential building in Gurgaon, India.* Sustainable Energy *3* (2015), No. 1, 14–24.

[5] T. Yang, A. K. Athienitis: *Experimental investigation of a two-inlet air-based building integrated photovoltaic/thermal (BIPV/T) system.* Applied Energy *159* (2015), 70–79.

[6] G. N. Tiwari, H. Saini, A. Tiwari, A. Deo, N. Gupta, P. S. Saini: *Periodic theory of building integrated photovoltaic thermal (BIPVT) system.* Solar Energy *125* (2016), 373–380.

[7] H. Baig, N. Sellami, T. K. Mallick: *Performance modeling and testing of a building integrated concentrating photovoltaic (BICPV) system.* Solar Energy Materials and Solar Cells *134* (2015), 29–44.

[8] M. S. Buker, B. Mempouo, S. B. Riffat: *Experimental investigation of a building integrated photovoltaic/thermal roof collector combined with a liquid desiccant enhanced indirect evaporative cooling system.* Energy Conversion and Management *101* (2015), 239–254.

[9] H. S. Park, C. Koo, T. Hong, J. Oh, K. Jeong: *A finite element model for estimating the techno-economic performance of the building-integrated photovoltaic blind.* Applied Energy *179* (2016), 211–227.

[10] M. Tripathy, P. K. Sadhu, S. K. Panda: *A critical review on building integrated photovoltaic products and their applications.* Renewable and Sustainable Energy Reviews *61* (2016), 451–465.

[11] Y. Zhang, C. Q. He, B. J. Tang, Y. M. Wei: *China's energy consumption in the building sector: A life cycle approach.* Energy and Buildings *94* (2015), 240–251.

[12] M. Aksoezen, M. Daniel, U. Hassler, N. Kohler: *Building age as an indicator for energy consumption.* Energy and Buildings *87* (2015), 74–86.

[13] R. Galvin: *How many interviews are enough? Do qualitative interviews in building energy consumption research produce reliable knowledge?.* Journal of Building Engineering *19* (2015), 2–12.

[14] M. S. Gul, S. Patidar: *Understanding the energy consumption and occupancy of a multi-purpose academic building.* Energy and Buildings *87* (2015), 155–165.

[15] J. A. Fonseca, A. Schlueter: *Integrated model for characterization of spatiotemporal building energy consumption patterns in neighborhoods and city districts.* Applied Energy *142* (2015), 247–265.

Received September 12, 2017

Acta Technica *62* No. 2B/2017, 641–650

Designing a quality gain-loss function for smaller-the-better characteristic under not neglecting the linear term loss[1]

Bo Wang[2], Tianyu Fan[2], Jing Tian[2], Xiangtian Nie[2 3]

Abstract. Because the smaller-the-better quality characteristic cannot achieve zero in practice, it is unreasonable to express the quality gain-loss function only by the compensation and the loss of quadratic term, and it is unreasonable to directly delete the loss of the linear term, therefore a new quality gain-loss function for smaller-the-better characteristic is designed. When the linear term loss is not ignored and the compensation amount is kept constant, the expression form of the smaller-the-better gain-loss function is studied, the determination method for the loss coefficient of the linear term and quadratic term in quadratic quality gain-loss function is researched, and the linear term and the quadratic term loss in quadratic gain-loss function are compared and analyzed.

Key words. The smaller-the-better characteristic, gain-loss function, loss coefficient, compensation amount.

1. Introduction

Ever since the quality loss function was proposed by Taguchi, many scholars have done a lot of research about product quality loss model. Aimed at the limitations of the quality loss function, the inverted-normal distribution functions were used to solve an unbounded quality loss function [1]. For the weight-loss problem of asymmetry, an asymmetric quality loss function model was proposed using the theory of

[1]The authors are grateful to the support of National Natural Science Foundation of China (No. 51709116), the Key Scientific Research Projects of Henan Province Universities and Colleges (No. 17B570003) and Foundation for Dr in North China University of Water Resources and Electric Power (No. 10030). Special thanks for the reviewers and their constructive comments and suggestions in improving the quality of this manuscript.

[2]College of Water Conservancy, North China University of Water Resources and Electric Power, Zhengzhou, Henan, 450011, China

[3]Corresponding author

piecewise functions to extend the quality loss function, and established the quality loss function model [2–5]. Fuzzy logic was used to present the concept of fuzzy quality loss, and the fuzzy quality loss function model was established [6]. While most studies have focused on single characteristics of the quality loss function, a multiple quality characteristics model of total mass loss and the method of tolerance design were presented [7]. The method of scaling and multivariate Taylor series expansion of the function to propose a more general form of multiple-parameter quality loss model was applied [8, 9]. Because the smaller-the-better quality characteristic cannot achieve zero in practice, a quadratic quality loss function for the smaller-the-better characteristic under not neglecting the linear term loss was proposed [10]. Because the quality loss function could not describe the quality compensation effect in production practice, due to its giving the constant term in the Taylor series expansion a physical meaning—the quality of compensation—the concept of quality gain-loss function was proposed and the quality gain-loss model of transmitting and a method of tolerance optimization for quality characteristics were studied[11], [12].

In the literature of studying on quality gain-loss function, the quality loss was almost represented only by a quadratic term, it not only neglects the linear terms but also the higher-order terms. It is possible to express the quality gain-loss function only with a quadratic term for target characteristic, but this is inappropriate for the smaller-the-better characteristic. For the quality characteristic target value can be realized and the minimum can be reached. When the compensation amount is kept constant, the quality gain-loss function for the smaller-the-better characteristic is the Taylor expansion of the quality characteristic value at zero quality characteristic point. According to the core idea of the quality gain-loss function, the quality loss is 0 when the quality characteristic value reaches zero quality characteristic point, and the first derivative is 0 for the quality loss value reaching the minimum as the quality characteristic value goes to zero quality characteristic point. Although the quality characteristics value does not necessarily reach zero quality characteristic point, the quality characteristic value is relatively small and the higher-order terms above the second order are relatively small, so the higher order terms can be omitted. Thus, there is only a constant term and a quadratic term in the Taylor expansion, i.e., the quality gain-loss function is represented only by the constant term and the quadratic term.

The smaller the smaller-the-better quality characteristic, the better, but the product quality characteristic value is always finite in practice, neither the zero quality characteristic point nor the minimum can be reached. Therefore, the first derivative of Taylor expansion is not equal to 0. It is unreasonable to directly delete the linear term loss of the quality gain-loss function. In this paper, the quality gain-loss function is appropriately expressed in the quadratic term under not neglecting the linear term loss function and keeping the compensation amount constant, and the determination method for the loss coefficient of the linear term and the quadratic term in quadratic quality gain-loss function is proposed simultaneously.

2. The quality gain-loss function for the smaller-the-better characteristic

Assume that the quality characteristic value of a product is y and the quality gain-loss function corresponding to quality characteristic value y is $G(y)$. The smaller-the-better characteristic quality gain-loss function comes from the Taylor expansion of $G(y)$ at point $y = 0$ [1]

$$G(y) = G(0) + \frac{G'(0)}{1!}y + \frac{G''(0)}{2!}y^2 + o(y^2)\,. \tag{1}$$

Assuming that the quality compensation is constant, for the smaller-the-better quality characteristics, the quality gain-loss reaches the minimum when the quality characteristic value reaches zero. In other word, $G(0) = \sigma$, $\sigma \in R$. Because the quality gain-loss reaches the minimum at 0, $G'(0) = 0$. Omitting the higher-order terms above the second order, we obtain

$$G(y) = G(0) + k\,y^2\,. \tag{2}$$

The smaller the smaller-the-better characteristic, the better, but the smaller-the-better quality characteristic value cannot really reach zero and the maximum point (zero point) cannot be reached in practice. Therefore we cannot directly let $G'(0) = 0$ in (1), as $G(\infty) \neq 0$. In other words, the loss of the linear term is not negligible. Since the loss of the linear term is not ignored directly, the quality gain-loss function should be expressed in quadratic form.

In the model of the quadratic quality gain-loss function, an intersection exists between the linear term function curve and the quadratic term function curve, so that the amount of the linear term loss and quadratic term loss can change with the changes of the quality characteristic value. Then, make the linear term quality loss function $G_1(y) = k_1/y$ and the quadratic term quality loss $G_2(y) = k_2/y$. The relationship between the linear and quadratic term quality loss functions for the smaller-the-better characteristic is shown in Fig. 1.

It can be seen in Fig. 1 that when $y < y_0$, the loss of the linear term is higher than that of quadratic term; when $y > y_0$, the loss of the linear term is less than that of quadratic term. And when $y = y_0$, the loss of the linear term is equal to that of the quadratic term. From Fig. 1 we can see that only when $y < y_0$ reaches a certain value and the loss of the linear term is far less than that of the quadratic term loss, the loss of the linear term can be ignored.

3. The design of quadratic form quality gain-loss function for the smaller-the-better characteristic

In the Taylor expansion of the quality gain-loss function, although the linear term quality loss cannot be ignored directly, for the smaller-the-better quality characteristic the quality characteristic value is small and the higher-order terms above the second order are very small, so the higher-order terms can be omitted. Because

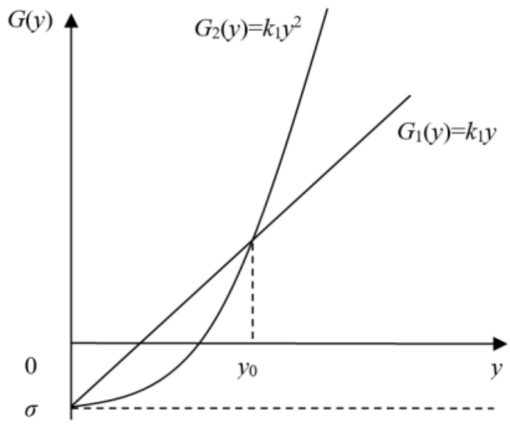

Fig. 1. The relationship between the linear and quadratic term quality loss functions for the smaller-the-better characteristic

the quality compensation quantity is constant, the quality gain-loss function for the smaller-the-better characteristic is:

$$G(y) = \sigma + k_1\, y + k_2\, y^2\,. \tag{3}$$

When the compensation quantity is assumed to be constant in the theory of quality gain-loss function, the greater the deviation of the quality characteristic value from the target value, the greater the quality gain-loss, so $k_1 \geq 0$, $k_2 > 0$ and $\sigma \in R$. The product is defective when the quality characteristic value exceeds the specification limit (tolerance Δ). In this case, the required cost of reworking or repairing the product is A. The product losses are now determined by the function when the quality characteristic value exceeds the functional limit (i.e., the deviation is greater than Δ_0); in this case the quality gain-losses caused by the product being scrapped is A_0. Therefore, by formula (3) we get

$$A = \sigma + k_1\, \Delta + k_2\, \Delta^2$$

and

$$A_0 = \sigma + k_1\, \Delta_0 + k_2\, \Delta_0^2\,. \tag{4}$$

From (4) we have

$$k_1 = \frac{(A-\sigma)\Delta_0^2 - (A_0-\sigma)\Delta^2}{\Delta\Delta_0(\Delta_0-\Delta)}$$

and

$$k_2 = \frac{(A_0-\sigma)\Delta - (A-\sigma)\Delta_0}{\Delta\Delta_0(\Delta_0-\Delta)}\,. \tag{5}$$

Putting both equations (5) into (3), we obtain the quality gain-loss function in

the form

$$G(y) = \sigma + \frac{(A-\sigma)\Delta_0^2 - (A_0-\sigma)\Delta^2}{\Delta\Delta_0(\Delta_0-\Delta)}y + \frac{(A_0-\sigma)\Delta - (A-\sigma)\Delta_0}{\Delta\Delta_0(\Delta_0-\Delta)}y^2\,. \tag{6}$$

To analyze the effect of the quality gain-loss function for the smaller-the-better characteristic, the quadratic form quality gain-loss function for the smaller-the-better characteristic can be divided into linear term loss, quadratic term loss, and constant term compensation as

$$G_1(y) = \frac{(A-\sigma)\Delta_0^2 - (A_0-\sigma)\Delta^2}{\Delta\Delta_0(\Delta_0-\Delta)}y\,, \tag{7}$$

$$G_2(y) = \frac{(A_0-\sigma)\Delta - (A-\sigma)\Delta_0}{\Delta\Delta_0(\Delta_0-\Delta)}y^2\,, \tag{8}$$

$$G_3(y) = \sigma\,. \tag{9}$$

The ratio of the linear and the quadratic term equals π, so that

$$\pi = \frac{G_1(y)}{G_2(y)} = \frac{(A-\sigma)\Delta_0^2 - (A_0-\sigma)\Delta^2}{(A_0-\sigma)\Delta - (A-\sigma)\Delta_0}\,\frac{1}{y} =$$

$$= \frac{\left(\frac{\Delta_0}{\Delta}\right)^2 - \left(\frac{A_0-\sigma}{A-\sigma}\right)^2}{\frac{A_0-\sigma}{A-\sigma} - \frac{\Delta_0}{\Delta}}\,\frac{\Delta}{y}\,. \tag{10}$$

According to the value of π in equation (10), the following cases were discussed:

When $\pi = 1$, $G_1(y) = G_2(y)$. Let $y = y_0$ be the point of intersection of the linear and quadratic functions in Fig. 1, that is

$$y_0 = \frac{\left(\frac{\Delta_0}{\Delta}\right)^2 - \left(\frac{A_0-\sigma}{A-\sigma}\right)^2}{\frac{A_0-\sigma}{A-\sigma} - \frac{\Delta_0}{\Delta}}\,\Delta\,.$$

.

At this point, whether the loss of the linear term relative to the quadratic term is negligible, depends on the value of y_0. For the smaller-the-better quality characteristic, if y_0 is very small, that is $1/y_0 \to \infty$, then the linear term loss is smaller than that of the quadratic term, and the linear term loss is negligible. Otherwise, it is not negligible.

When

$$\frac{A_0-\sigma}{A-\sigma} \to \left(\frac{\Delta}{\Delta_0}\right)^2\,,$$

then $\pi \to 0$, so that the linear term loss is negligible compared with the quadratic term loss, and the intersection of the linear term function curve and the quadratic

function curve goes to zero $y_0 \to 0$.

When

$$\frac{A_0 - \sigma}{A - \sigma} \to \frac{\Delta}{\Delta_0}$$

and $\pi \to \infty$, then y_0 is high and the linear term loss is greater than the quadratic term loss. Then, the intersection of the linear term function and quadratic term function y_0 is very high, which is the most common situation in practice. Although the consumers expect the smaller-the-better quality characteristic value, and the smaller the better, the actual value of the characteristic is not small, and the linear term loss cannot be neglected at this time. The linear term can be ignored, as shown in Fig. 2, and the linear term cannot be ignored, as shown in Fig. 3.

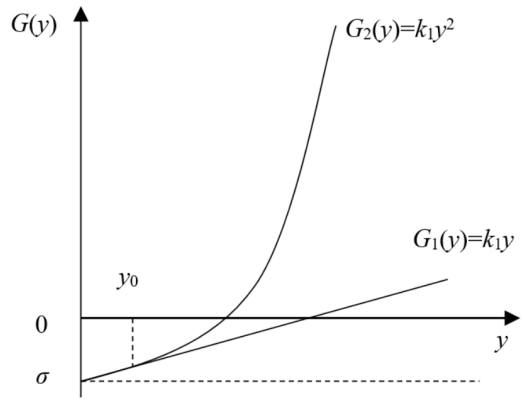

Fig. 2. The linear term can be ignored

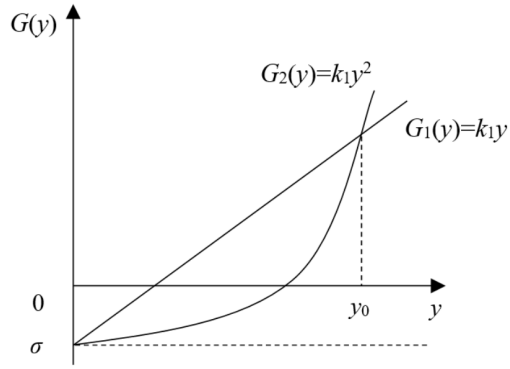

Fig. 3. The linear term cannot be ignored

When

$$\frac{\Delta}{\Delta_0} < \frac{A_0 - \sigma}{A - \sigma} < \left(\frac{\Delta}{\Delta_0}\right)^2,$$

then the ratio $G_1(y)/G_2(y)$ can determine whether the linear term can be neglected. Substitute $\bar{y}$ for y in (10), so that the equation now reads

$$\frac{G_1(y)}{G_2(y)} = \frac{\left(\frac{\Delta_0}{\Delta}\right)^2 - \left(\frac{A_0-\sigma}{A-\sigma}\right)^2}{\frac{A_0-\sigma}{A-\sigma} - \frac{\Delta_0}{\Delta}} \frac{\Delta}{\bar{y}} = \pi\,. \tag{11}$$

For the smaller-the-better quality characteristic, remove the human factors, which means $\bar{y} < \Delta$ under normal circumstances. When the actual value of π is very small, generally because the linear term loss is much less than the quadratic term loss, then the linear term loss can be neglected. Otherwise, it cannot be neglected. In the actual application process, a specific criterion can also be determined: the linear term loss can be neglected if it is less than 10 % of the quadratic term loss

$$\frac{A-\sigma}{A_0-\sigma} = \left(\frac{\Delta}{\Delta_0}\right)^2 .$$

Since $k_1 \geq 0$ and $k_2 > 0$ in the equation (3), then

$$(A-\sigma)\Delta^2 - (A_0-\sigma)\,\Delta_0^2 \geq 0\,,$$

and

$$(A_0-\sigma)\Delta_0 - (A-\sigma)\,\Delta > 0\,.$$

Hence

$$\frac{A_0-\sigma}{A-\sigma} \leq \left(\frac{\Delta}{\Delta_0}\right)^2 \text{ and } \frac{\Delta}{\Delta_0} < \frac{A_0-\sigma}{A-\sigma}\,.$$

In the actual application process, if the parameter is reasonable, then

$$\frac{A_0-\sigma}{A-\sigma} > \left(\frac{\Delta}{\Delta_0}\right)^2$$

or

$$\frac{\Delta}{\Delta_0} \geq \frac{A_0-\sigma}{A-\sigma}$$

cannot occur.

When $k_1 \geq 0$ in equation (3), it may happen that $k_1 = 0$. In such a case

$$\frac{A-\sigma}{A_0-\sigma} = \left(\frac{\Delta}{\Delta_0}\right)^2$$

. Now, the quality gain-loss function for the smaller-the-better characteristic is

$$G(y) = \sigma + k\,y^2 \tag{12}$$

In the classic quality gain-loss function where the compensation is constant, as shown in equation (12), the tolerance of quality characteristic can be determined by

the functional limit, and the quality gain-loss caused by discarded product is

$$\Delta = \sqrt{\frac{A-\sigma}{A_0-\sigma}}\,\Delta_0\,. \tag{13}$$

4. The analysis of practical problems

To show that a quality gain-loss function for the smaller-the-better characteristic under not neglecting the linear term loss and keeping the compensation amount constant is superior to the quadratic term quality gain-loss function, it is good to analyze a concrete case.

A dam concrete construction project mainly includes concrete production, concrete transportation, concrete pouring and concrete maintenance. Among them, the key quality indicators of concrete production have the outlet temperature of the concrete mixture (unit: days), it is the smaller-the-better characteristic. Assume that the design target value of the concrete mixture outlet temperature is 7 °C, and when deviation from the design target temperature value $y \geq 2$°C, the product is not qualified. That is, the design target temperature value tolerance $\Delta = 2$°C and the loss caused by it is 75 yuan/m^3. When the deviation from the design target temperature value $y \geq 5$°C, the products lose their function. That is, the functional limit of deviation from the design target temperature value $\Delta = 5$°C, and the loss caused by it is 200 yuan/m^3. Assume that the quality compensation of the next process for this process or the compensation produced by parallel processes through mutual cooperation $\sigma = -10$ yuan/m^3. To evaluate the quality of concrete production, 10 concrete mixture samples were randomly selected during a particular period to obtain the deviation from the design target temperature in the quadratic term gain-loss function and the function under not neglecting the linear term gain-loss.

4.1. Evaluation using the quadratic term gain-loss function

When $\Delta = 2$°C, $A = 75$ yuan/m^3, $\sigma = -10$ yuan/m^3, the quadratic term gain-loss function is

$$G(y) = -10 + 21.5y^2\,. \tag{14}$$

The number of the sample is used in equation (14), and then the average of it is determined to obtain the average of quality gain-loss: $G_{\mathrm{a}} = 11.9$ yuan/m^3.

4.2. Evaluation using the function under not neglecting the linear term gain-loss

When $\Delta = 2$°C, $A = 75$ yuan/m^3, $\Delta_0 = 5d$, $A_0 = 200$ yuan/m^3, $\sigma = -10$ yuan/m^3, the function under not neglecting the linear term gain-loss is

$$G(y) = -10 + 37.5y + 2.5y^2\,. \tag{15}$$

The number of the sample is used in equation (15), then its average is deter-

mined to obtain the average of quality gain-loss: $G_{\mathrm{b}} = 25.6\,\mathrm{yuan/m^3}$, the average linear term loss, $L_1 = 33\,\mathrm{yuan/m^3}$, and the average of quadratic term loss $L_2 = 2.6\,\mathrm{yuan/m^3}$.

When the quality compensation is constant, the quality gain-loss vale when maintaining the linear term is 13.7 yuan $/\mathrm{m}^3$ more than the value of the quadratic term quality gain-loss function, because the quadratic term quality gain-loss function neglects the linear term loss. Judged on the amount of the linear term loss and the quadratic term loss of the average quality gain-loss function equation under not neglecting the linear term loss for the smaller-the-better characteristic, the quadratic term loss is less than the linear term loss, so the linear term loss cannot be neglected. Of course, when not neglecting the linear term loss, the loss coefficient equation of the linear term and the quadratic term has changed, so the corresponding quadratic term loss is not equal to the quality gain-loss expressed only by the quadratic loss function.

5. Conclusion

When the quality gain-loss function is represented only by the compensation function and the quadratic term, it is not only neglects the linear term in the Taylor expansion but also the higher-order terms above the second order. However, it is not appropriate for the smaller-the-better characteristic to function like this. The quality gain-loss function for the smaller-the-better characteristic is studied from theoretical and practical perspectives in this paper, and the form of quadratic quality gain-loss function for the smaller-the-better characteristics under not neglecting the linear term loss and keeping the compensation amount constant and the corresponding loss coefficient equation of the linear term and quadratic term were put forward, and the amount of the linear term loss and the quadratic term loss for the smaller-the-better characteristics are compared. This study shows that the original quadratic term quality gain-loss function is a special case considering the linear term quality gain-loss function.

References

[1] F. A. Spring: *The reflected normal loss function.* The Canadian Journal of Statistics *21* (1993), No. TOC 3, 321–330.

[2] F. A. Spring, A. S. Yeung: *General class of loss functions with industrial applications.* Journal of Quality Technology *30* (1998), No. 2, 152–162.

[3] C. C. Wu, G. R. Tang: *Tolerance design for products with asymmetric quality losses.* International Journal of Production Research *36* (1998), No. 9, 2529–2541.

[4] Y. M. Zhao, D. S. Liu, J. Zhang, Q. Liu: *Quality loss cost model and its application to products with multi-quality characteristics.* Journal of Central South University (Science and Technology) *43* (2012), No. 5, 1753–1763.

[5] C. Balamurugan, A. Saravanan, P. D. Babu, S. Jagan, S. R. Narasimman: *Concurrent optimal allocation of geometric and process tolerances based on the present worth of quality loss using evolutionary optimization techniques.* Research in Engineering Design *28* (2017), No. 2, 185–202.

[6] Y. L. Cao, J. X. Yang, Z. T. Wu, L. Q. Wu: *Robust tolerance design based on fuzzy quality loss.* Journal of Zhejiang University (Engineering Science) *38* (2004), No. 1, 1–4.

[7] C. L. Lee, G. R. Tang: *Tolerance design for products with correlated characteristics.* Mechanism and Machine Theory *35* (2000), No. 12, 1675–1687.

[8] M. F. Huang, Y. R. Zhong, Z. G. Xu: *Concurrent process tolerance design based on minimum product manufacturing cost and quality loss.* International Journal of Advanced Manufacturing Technology *25* (2005), Nos. 7–8, 714–722.

[9] S. B. Amara, J. Dhahri, N. B. Fredj: *Process true capability evaluation with the consideration of measurement system variability and expected quality loss.* Quality and Reliability Engineering International *33* (2017), No. 5, 937–944.

[10] Y. Y. Zhang, M. S. Song, Z. J. Han, X. L. Chen: *Design of quality loss function under the smaller the better characteristic without neglecting the linear term.* Industrial Engineering Journal *14* (2011), No. 6, 81–84.

[11] B. Wang, Z. Y. Li, Y. Y. Gao, H. Vaso: *Critical quality source diagnosis for dam concrete construction based on quality gain-loss function.* Journal of Engineering Science and Technology Review *7* (2014), No. 2, 145–151.

[12] B. Wang, H. G. Zhou, Z. Y. Li, X. T. Nie: *Tolerance optimization for quality characteristics of the dam concrete construction based on quality gain-loss function.* Journal Mathematics in Practice and Theory *46* (2016), No. 23, 90–99.

Received September 12, 2017

Acta Technica *62* No. 2B/2017, 653–662

Analysis of ink-jet printing and seal timing experiment by confocal Raman spectroscopy

Feng Chao[1], Luo Dongdong[2,4], Xie Peng[3]

Abstract. Confocal Raman spectroscopic technique has very important influence for the verification and identification of ink-jet writing and seal timing. In order to better discuss this technology, the related theories of this technology were first summarized in this paper. Scanning curves of Raman linewidth of different timing seals were compared. The results show that the Rapp spectral curve prints linewidth and timing have some relevance. Through questionnaires, the judicial personnel's approval degree of this technique can be further determined. The purpose of this study is to provide theoretical basis and technical support for follow-up research.

Key words. Confocal microscopy, Raman spectroscopy determination, ink-jet printing, seal timing.

1. Introduction

With the development of the times, the current social economy has made great progress and promotion. In this trend, each industry has gained more opportunities for development, which makes the development of the industry more comprehensive and scientific. However, with the rapid economic development of various industries, many uncoordinated phenomena have been further exposed. In the process of social development in the current era, some phenomena such as economic crimes and civil disputes appear. In the development of various industries, because some economic criminals alter the contract and some relevant notes, it is difficult to identify the whole late related materials, which causes certain restrictions for the late development of enterprises. Especially in some cases of economic crime, the validity and reliability of the investigation are reduced to a certain extent due to the alteration of

[1]Key Laboratory of Evidence-Identifying in Universities of Shandong (Shandong University of Political Science and Law), Jinan, 250014, Shandong, China
[2]Anhui Public Security College, Hefei, 230000, Anhui, China
[3]Criminal Investigation Police University of China, Shenyang, 110854, Liaoning, China
[4]Corresponding author; e-mail: Fengcha100@qq.com

these important materials and evidence. In addition, it has an impact on the overall fairness of justice, which makes the detection of judicial cases disturbed. Therefore, only a more accurate examination of the handwriting in relevant documents can effectively provide a more positive impact on the relevant case cracking, and become a key factor in cracking the case justice. Many scholars have begun to pay attention to the methods of identifying handwriting. However, the traditional handwriting identification may cause damage to the relevant testing documents, which makes the integrity of the physical evidence damaged. In this paper, the analysis and discussion of the more advanced confocal spectroscopic techniques are conducted to determine the more mature techniques and means for related handwriting identification.

2. State of the art

In the process of the development of the times, many enterprises and industries have been given some opportunities for development. However, with the rapid development of the industry, some cases of economic crimes or some civil disputes have made the evidence of certain document nature become the key to the detection [1]. In the evidence, because it can make some key handwriting fraud, it affects the detection credibility of the case. Therefore, many scholars begin to gradually use some related techniques to identify handwriting, which brings certain advantages and positive effects for the detection of the case [2]. Some scholars have used chromatography to identify some important documents. Although they have been some credible results, this method directly or indirectly causes a certain degree of damage to the documentary evidence, which makes the integrity and credibility of the relevant evidence subject to some doubt [3]. In this context, many scholars begin to put forward and further apply new detection technologies in the handwriting detection, such as confocal microscope Rapp spectroscopy. While carrying on the effective verification to the related handwriting, it also has promoted the reasonable explanation and the solution of industry economy crime, and provided certain technical support for the further development of the industries [4].

The relevant experimental design in this study is as follows:

(1) In the study, the laser scanning of the confocal Raman spectrometer was carried out for different ink jet printing fields at first. The related Raman spectra of the text in different fields were made, and the results were shown in Fig. 1. Wherein, the two rows of curves were the writing of the first section of ink jet printing field; the relatively flat four lines in the middle were the writing of the second section of ink jet printing field; the last two lines were the writing of the third section of the ink jet field.

(2) On the basis for accurate scanning fields in all of the paragraphs, the relevant documents were handled through the use of print and stamp different order. Processing methods mainly include two kinds of printing methods: the first print then stamp and the first stamp then print.

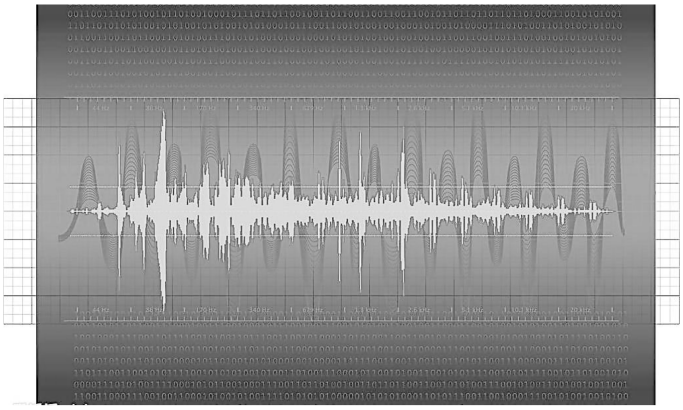

Fig. 1. Scanning confocal microscopy curves for different sections of inkjet printing fields

(3) All documents and materials were scanned by micro confocal Raman laser with different energy to determine the relatively stable laser energy, in order to prepare follow-up related experiments. Then, the SRS channel theory and the time series model in the confocal Raman spectroscopy were used to compare the laser scanning energies of different materials [7]. Through the calculation of the spectral curve, the accuracy and reliability of the confocal microscopy Raman spectroscopy and laser scanning technology in the identification of the relevant documents were further determined. Finally, through the introduction of actual cases, the actual analysis of related technologies was conducted to determine the related advantages and performance of this technology, and to provide some advantages for the promotion of technology. The related SRS signal channel theory and timing theory computational models were shown in formula (1) and (2). First, the digestibility of the relevant curves obtained by all scans was computed [8]. The correlation model is shown below:

$$x^{(3)}(\omega_{\mathrm{p}}) = x^{(3)}_{\mathrm{NR}} + \frac{x^{(3)}_{\mathrm{R}}}{\Delta - iT}\,, \tag{1}$$

where, $x^{(3)}(\omega_{\mathrm{p}})$ is the polarizability obtained by scanning the related document data, $x^{(3)}_{\mathrm{NR}}$ is the standard curve obtained after the determination of the multiple standard document value, $x^{(3)}_{\mathrm{R}}$ represents the signal intensity measured values obtained after scanning the file, Δ represents the numerical value of the representative system and iT is the linewidth of the correlation curves obtained after scanning confocal Raman microscopy.

The scanning correlation coefficients of all curves were calculated by formula (2), and the formula is as follows:

$$I_{\mathrm{CARS}} = \left\{ \left| x^{(3)}_{\mathrm{R}}(\Delta) \right|^2 + \left| x^{(3)}_{\mathrm{NR}} \right|^2 + 2x^{(3)}_{\mathrm{R}} \mathrm{Re}\left[x^{(3)}_{\mathrm{R}}(\Delta) \right] \right\} I^2_{\mathrm{P}} I_{\mathrm{S}} Z^2\,, \tag{2}$$

where I_{CARS} are the calculated indexes values for all relevant parameter and $x^{(3)}_R(\Delta)$

mainly represents different signal intensities, including three main parts: resonant part, non-resonant part and the cross section. Symbols I_{P}^2, I_{S} and Z^2 represent the probability coefficients, the speed coefficients and the curve deviation coefficients of the scanning transmission of the measured files, respectively.

Finally, through the investigation and analysis of some judicial investigation departments, the advantages of micro confocal Raman spectrometry in practical judicial investigation were further confirmed. The information related to the questionnaire was set out in Table 1.

Table 1. Main questionnaire setting information used in this study

No.	Related questions setting	Excellent	Good	Poor
1	Completeness of evidence obtained at the end of the scan	10	5	3
2	Reliability and accuracy of scanning after scanning relevant document data	10	5	3
3	The scanning method is easy to operate and related program and hardware operation performance	10	5	3
4	The credibility of the final result	10	5	3
5	The final resolution of the handwriting obtained in scanning the relevant document data	10	5	3
6	The ultimate effectiveness of judicial decisions	10	5	3

3. Result analysis and discussion

Since entering the era of reform and opening up, the country's economic level has been greatly improved. The status of the state in the international community has increased gradually. In this trend, China's social industry has been a common development and promotion. Under the background of the rapid development of economic strength and comprehensive level, China's overall economic level has been improved greatly. However, many discordant phenomena are further exposed in this context [9]. China's economic crimes and civil disputes are gradually increasing with the promotion and progress of the economic level, which has made all sectors of China's common sustainable development restricted and hindered. In the relevant criminal activities, certain evidence documents cannot provide better evidence for the subsequent judicial review process after the writing has been altered [10]. Under this trend, many judicial departments begin to gradually introduce some novel handwriting data identification and scanning tools, and these tools are gradually applied to the actual document scanning, and certain results are achieved. However, with the development of criminals' false handwriting techniques in some materials, it has caused some difficulties for the identification of relevant documents. Thus, the fairness justice have been restricted to a certain extent, and the whole social environment and the steady development of economy have also been restricted [11].

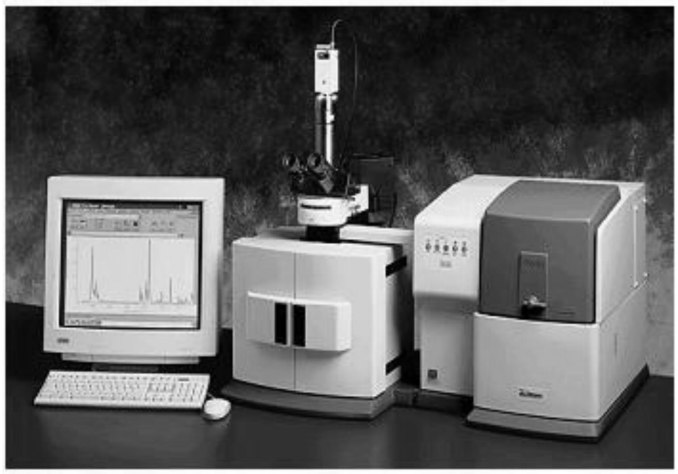

Fig. 2. Development of confocal Raman spectroscopy

Under the demand of the times, more new handwriting identification techniques are beginning to emerge. Especially, with the rapid development of computer technology, this new technology brings more important impetus and positive influence for the development of the handwriting identification technology of relevant documents. The technique of confocal Raman spectroscopy is higher than other handwriting identification techniques because of its high sensitivity to related handwriting identification and the reliability of relevant handwriting identification results in the development of today's times. Therefore, this technique has been gradually applied to the actual judicial identification, and it also ensures the integrity of the relevant evidence in the process of effective identification of relevant handwriting. Moreover, it provides some positive influence and impetus for the judicial justice to be more fair and complete, and gradually becomes the key handwriting identification technology in the current era [12]. The application of confocal Raman spectroscopy in handwriting identification is mainly based on the SRS effect theory. The main principles of the use of the theory are that when scanning certain handwriting by using confocal Raman spectroscopy, the scanning light produced by the relevant equipment or instrument touches some of the substances in the handwriting and scatters [13]. And most of the light does not change the elastic scattering due to the scattering wavelength associated with the writing medium. There is also a portion of the light that will be inelastic with the relevant documentation of the document's medium. When the light scattering does not have to dry, there will be micro confocal scattering. The main scattering process is shown in Fig. 3.

In addition, there are many research find that different frequencies of light with blue and red shift occurs between the light and the writing medium Rapp in the process of Raman scattering by collisions of light with matter. And the whole scattering process shows the relative and weak process of light. Therefore, the frequency of this scattering phenomenon is also relatively low. In the light of Rapp enhancement-processing, the re-emergence of new superimposed light and scattering

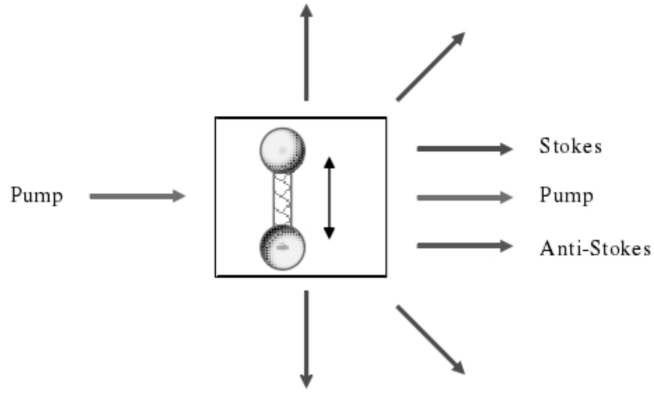

Fig. 3. Rapp light scattering process map

processes increases the ultimate efficiency of scattering, which is shown in Fig. 4 [14]. Therefore, this process is applied to the process of handwriting identification gradually. The light scattering efficiency of this increased the light scattering process may be about 105 times the average scattering efficiency of the process, and even shows a scattering of higher efficiency, which makes the final determination results have higher credibility, and provides a positive impact and impetus for the latter part of the handwriting verification [15]. It needs to be explained that the use this kind of technology considers energy of Rapp light, and analyze and discuss the final frequency on the scattering. Therefore, the accuracy of this technique is higher.

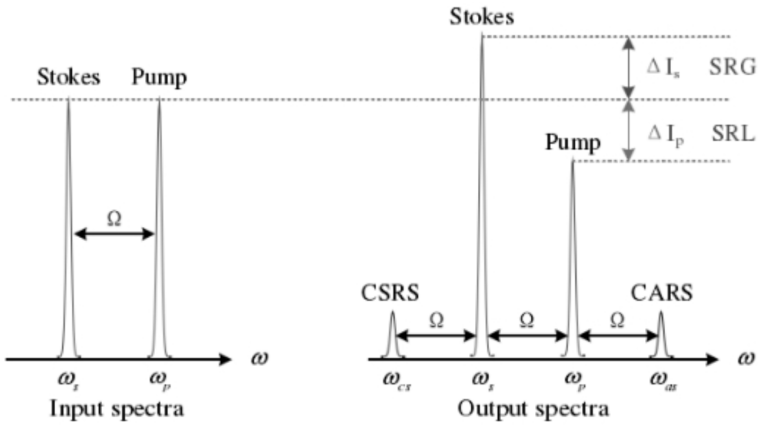

Fig. 4. Input and output spectrum of coherent light scattering process

On the basis of a clearer understanding of the relevant theories, a document was taken as an example for analysis in this paper. The micro confocal spectroscopy technique was used for Rapp jet to the file. All the fields and paragraph seals were scanned accurately. Then file data was processed through the experiment of different timing (first printed stamp and first cover printing printing). Finally,

measuring instrument spectral results by the confocal microscope Rapp spectra were analyzed. Relevant mathematical models were utilized to perform data calculations. The experimental results of two different timing were studied, such as the original spectral line scan results. The contrast results were shown in Table 2. The results showed that the line width of the scanning line of the original paragraph of different passages was analyzed with the results of the spectral line-width of two different time series after the input of the relevant parameters. The line width of the scan lines of all the segments was related to the processing time of the files. It could be seen through the results that line width of a segment scan line of the processing order of seal materials after the first print file was close to the width of the original file material. The first stamp printing order showed great difference relative to the original scanning line width. Research showed that this kind of technology could be used for timing analysis of ink-jet printing and print handwriting, and the result had certain reliability and accuracy.

Table 2. Linewidth analysis of scanning lines of different segments with confocal microscope spectroscopy

Paragraph	Parameter input			Spectral line width result output		
	Peak center	Width	Area under the peak	Original	First print then stamp	First stamp then print
1	2850.46 (3.44)	28.41	24.45	9.34	8.24	5.33
2	2869.59 (10.39)	33.97	26.94	15.62	14.55	10.49
3	2887.48 (13.41)	33.30	23.15	16.93	16.47	14.50
4	2907.08 (16.46)	40.61	28.31	18.95	17.98	13.22
5	2931.74 (10.59)	53.24	72.94	18.86	18.01	15.14
6	2958.01 (11.00)	39.04	18.92	13.93	13.37	11.27
7	2989.90 (14.94)	40.61	8.77	5.87	5.22	4.95

Finally, through the questionnaire of a judicial unit staff survey, the main characteristics of confocal micro Raman spectroscopy and traditional scanning technology were compared, and the results in Table 3 and Fig. 5. The results showed that the confocal Raman spectroscopy technique had higher score than the traditional scanning technique, and it also indirectly indicated that the technique was more suitable for the scanning of document handwriting in modern times.

4. Conclusion

With the development of the times, today's various industries have been greatly improved. In the process of rapid development of various industries and enterprises, some uncoordinated phenomena such as economic crimes or civil disputes are gradu-

ally exposed. And the related text material is the more important link in the related judicial activity. However, with the progress of science and technology, a lot of criminals have the ability to fake relevant handwriting that has a certain confusion and negative influence on the judicial expertise. With this phenomenon, many handwriting identification techniques have been applied and some achievements have been achieved. Confocal micro Raman spectroscopy is used for the analysis and identification of ink-jet printing and the print timing, which is a kind of scientific technology. In this study, the main concepts of this technology were analyzed and different word processing methods were introduced as examples. Through the use of relevant models for settlement, the results were finally compared through the questionnaire method. The results show that this technique is of great importance to the identification of handwriting. However, due to the simple analysis of one technology, the study has a poor contrast and some defects. But it can provide a theoretical basis for further studies.

Table 3. Questionnaire results

No.	Related questions setting	Raman spectra	Traditional techniques
1	Completeness of evidence obtained at the end of the scan	8	4
2	Reliability and accuracy of scanning after scanning relevant document data	7	7
3	Scanning method, operation simplicity and related program and hardware operation performance	7	5
4	The credibility of the final result	9	4
5	The final resolution of the handwriting obtained in scanning the relevant document data	10	4
6	The ultimate effectiveness of judicial decisions	10	6
7	Total	51	30

References

[1] Z. Movasaghi, S. Rehman, I. U. Rehman: *Raman spectroscopy of biological tissues.* Applied Spectroscopy Reviews *42* (2007), No. 5, 493–541.

[2] B. G. Saar, C. W. Freudiger, J. Reichman, M. Stanley, G. R. Holtom, X. S. Xie: *Video-rate molecular imaging in vivo with stimulated Raman scattering.* Science *330* (2010), No. 6009, 1368–1370.

[3] C. L. Evans, X. S. Xie: *Coherent anti-stokes Raman scattering microscopy: Chemical imaging for biology and medicine.* Annual Review of Analytical Chemistry (Palo Alto Calif) (2008), No. 1, 883–909.

[4] W. Min, C. W. Freudiger, S. Lu, X. S. Xie: *Coherent nonlinear optical imaging:*

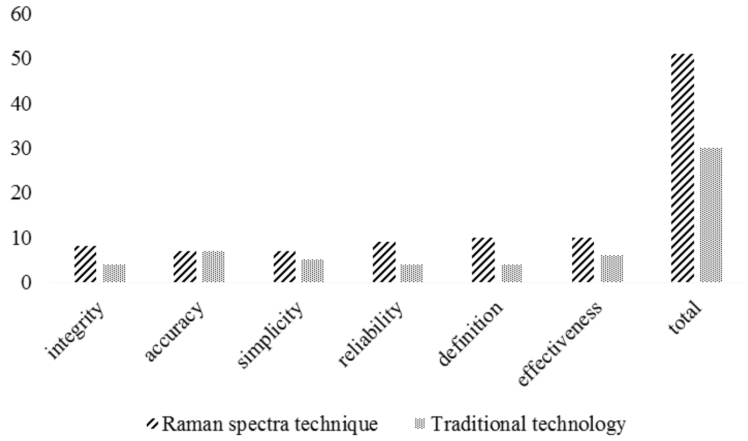

Fig. 5. Questionnaire results

Beyond fluorescence microscopy. Annual Review of Physical Chemistry *62* (2011), 507–530.

[5] D. Zhang, P. Wang, M. N. Slipchenko, J. X. Cheng: *Fast vibrational imaging of single cells and tissues by stimulated Raman scattering microscopy.* Accounts of chemical research *47* (2014), No. 8, 2282–2290.

[6] C. Krafft, I. W. Schie, T. Meyer, M. Schmitt, J. Popp: *Developments in spontaneous and coherent Raman scattering microscopic imaging for biomedical applications.* Chemical Society Reviews *45* (2016), No. 7, 1819–1849.

[7] M. Winterhalder, A. Zumbusch: *Beyond the borders–biomedical applications of non-linear Raman microscopy.* Advanced Drug Delivery Reviews *89* (2015), 135–144.

[8] I. W. Schie, C. Krafft, J. Popp: *Applications of coherent Raman scattering microscopies to clinical and biological studies.* Journal Analyst–Royal Society of Chemistry *140* (2015), No. 12, 3897–3909.

[9] H. Tu, S. A. Boppart: *Coherent anti-stokes Raman scattering microscopy: Overcoming technical barriers for clinical translation.* Journal Biophotonics *7* (2014), Nos. 1–2, 9–22.

[10] A. Zumbusch, W. Langbein, P. Borri: *Nonlinear vibrational microscopy applied to lipid biology.* Progress in Lipid Research *52* (2013), No. 4, 615–632.

[11] C. Y. Chung, E. O. Potma: *Biomolecular imaging with coherent nonlinear vibrational microscopy.* Annual Review of Physical Chemistry *64* (2013), 77–99.

[12] C. Zhang, D. Zhang, J. X. Cheng: *Coherent Raman scattering microscopy in biology and medicine.* Annual Review of Biomedical Engineering *17* (2015), 415–445.

[13] J. X. Cheng, X. S. Xie: *Vibrational spectroscopic imaging of living systems: An emerging platform for biology and medicine.* Science *350* (2015), No. 6264, Aaa8870–Aaa8870.

[14] V. V. Yakovlev, G. I. Petrov, H. F. Zhang, G. D. Noojin, M. L. Denton, R. J. Thomas, M. O. Scully: *Stimulated Raman scattering: Old physics, new applications.* Journal of Modern Optics *56* (2009), Nos. 18–19, 1970–1973.

[15] Y. Ozeki, F. Dake, S. Kajiyama, K. Fukui, K. Itoh: *Analysis and experimental assessment of the sensitivity of stimulated Raman scattering microscopy.* Optics Express *17* (2009), No. 5, 3651–3658.

Received September 12, 2017

Acta Technica *62* No. 2B/2017, 663–672

Characteristic model based on structural noise of heavy duty vehicle engines

Jiao Hongtao[1]

Abstract. With the improvement of people's living standard, people's requirements for living environment are getting higher and higher, and their attention to noise pollution is also getting higher and higher. In order to establish the characteristic model for structural modeling of heavy duty vehicle engines, and obtain the noise reduction method, in this paper, according to take four-stroke six-cylinder diesel engine as an example, the modern design theory and method were used to conduct a comprehensive analysis to the mechanism of diesel engine noise, main radiation noise sources and so on; then, the internal combustion engine noise source identification method that was suitable for engineering practice was proposed, the surface vibration velocity level of internal combustion engine was obtained by the improved surface vibration velocity method, the contribution of radiated noise, sound power level and radiated noise of each component was predicted successfully. The final experimental results show that the proposed method which is in good agreement with the measured results can be used to predict the sound power of the engine and identify the main radiated noise source of the engine, which is very practical for the low noise design and prediction of the engine.

Key words. Heavy vehicle engine, noise, noise control.

1. Introduction

Noise can cause people's mental instability, emotional instability, resulting in headache, dizziness, insomnia and other illnesses, in serious period, it can damage people's hearing organs, resulting in noise deafness; besides, it also has a negative impact to the nervous system, the cardiovascular system, and the gastrointestinal system, etc.; noise will reduce the work efficiency; high-frequency noise causes the structural sound fatigue, so that buildings and equipment are damaged [1]. The vehicle noise is one of the main sources of ambient noise. According to the statistics, the average of heavy-duty vehicles is 100 dB (A), the public transport is 90 dB (A), and the maximum noise that a person can bear in the car compartment is 70 dB

[1]Zhengzhou Railway Vocational & Technical College, Henan, Zhengzhou, 450052, China

(A). If the noise generated by the vehicle reaches a certain intensity, it will cause that the driver's auditory sense suffers long-term stimulation, this will not only significantly reduce the auditory organ sensitivity, but also produce uncomfortable feeling and impatience, tension and other negative emotions, thus affecting traffic safety, resulting in the hidden dangers of life and property of the people [2]. In addition, the noise can also make people's vision change abnormally, in the role of 90 dB (A) noise, the sensitivity of human eyes to distinguish the brightness will be reduced, and the reflect time to identify low light will be lengthened; then, 85-110 dB (A) noise can magnify people's pupil; 112–120 dB (A) of the stable noise can also reduce the stability of vision clarity. Noise affects the normal feeling of the visual system through the human auditory system, which will undoubtedly bring great risks to traffic safety [3]. The engine noise source is analyzed and researched by using the analytic hierarchy process (AHP) and the cluster analysis method. According to combine with the experiment, the contribution of engine's noise in the center frequency of the 1/3 octave frequency within the working speed range is analyzed, and the contribution of each component to important frequency segments is also analyzed, moreover, the weight index value is given, which provides specific quantitative indicators for the future of low-noise engine design [4]. In the test case, the noise sources that their noise contribution to the machine is located in the top three are oil pan, air inlet and intake pipe. Especially in the idling conditions, the radiation noise of the oil pan occupies part of the total noise, which should be an important part of engine noise reduction, thereby improving the whole machine noise. On the basis of surface vibration test and sound intensity test method, the contribution of sound power contribution is analyzed. The results of this study can show the contribution of component radiated noise to the noise power of the whole machine, which provides quantitative guidance for the improvement design of the low noise in diesel engine engineering [5].

2. State of the art

Whether there's good vibration, noise, running smoothness is one of the key factors to determine the excellent performance of internal combustion engine. Since 1950s, the vibration and noise problems of the internal combustion engine have begun to be studied deeply abroad. According to start from the vibration and noise sources of an internal combustion engine, the mechanism of their generation, transmission and radiation is analyzed, and the classification analysis on the noise of internal combustion engine is also carried out [6–7]. From the end of 1960s to the end of 1970s, with the introduction of noise standards in various countries, the research focused on the study of combustion noise, the distribution of surface noise radiation in an internal combustion engine, the noise reduction effect of various special materials, and the improvements in the traditional structure of an internal combustion engine, etc. From the 1980s onwards, with the development of computer science and mechanics, modern analysis and calculation methods and test methods have been widely cited in the vibration and noise analysis of internal combustion engine, and then, there has been a phenomenon of using finite elements, boundary

element technology to calculate and analyze the internal combustion engine vibration and noise problems, besides, the sound intensity method has also been used to measure near-field noise, etc., and a lot of results have been made at the aspects of the vibration and noise prediction [8]. Since the 1990s, the research of vibration and noise of internal combustion engine has entered a new stage. And the concept of new concept design and the technical direction of subjective evaluation of vehicle sounds are put forward. Then, the combination of virtual prototyping design and test technology is carried out to control the structural vibration and noise [9]. With the continuous development of related technologies and the constant improvement of requirements of people on the internal combustion engine vibration and noise, the future car noise target is to reach 71 dB (A).

3. Methodology

3.1. Study on the relationship between surface vibration and radiated noise of diesel engine

1/3 octave band analysis is well fit for noise analysis of rotating machinery, because it does not involve the directional effect of noise. If a large rigid piston (that is, the piston vibrates at the same phase) vibrating on an infinite baffle is considered, and the size of the piston is very large, in this case, the direction of the radial sound of a vibrating piston is perpendicular to its surface, the acoustic power that the piston radiating enters into the surrounding medium is expressed as the force multiplied by the speed, and then multiplied by the area, as shown in the formula

$$W_{\text{rad}} = \pi a^2 p_{\text{rms}} u_{\text{rms}} \,. \tag{1}$$

Here, p_{rms} is the root mean square radiation pressure of a point in space, u_{rms} is the corresponding root mean square velocity at the same point and a is the radius of the piston.

From the acoustic pressure equation it can be obtained, $p = u\rho_0 c$, thus, the calculation formula can be obtained in the form

$$W = \rho_0 c S \left\langle \bar{u}^2 \right\rangle \,. \tag{2}$$

Here, $S = \pi a^2$, $< >$ represents the time average and "" represents the space average.

The above derivation is based on the ideal state, and an arbitrary structure of the acoustic radiation takes this as a comparison. Thus, the radiation ratio σ of any structure is defined as the acoustic power of a structure radiating into half space (i.e., the side of the structure) that is it divided by the sound power radiated by a large piston with the same surface area and the same root mean square velocity as the structure. Thus, the radiation ratio can be used to describe the efficiency of acoustic radiation. When compared with the same area of the piston, the structure radiates the sound by this efficiency, that is, the piston has a radiation ratio that

it's 1. So for any structure, a formula for calculating acoustic power of structural radiation is shown in the relation

$$W_{\mathrm{rad}}(f) = \rho_0 c S_{\mathrm{rad}} \sigma_{\mathrm{rad}}(f) < U_0^2(f) > \ . \tag{3}$$

The mean square velocity by area average is actually the mean square value of the normal vibration velocity of the vibration surface. The radiation ratio provides a strong relationship between the structural vibration and the associated radiated sound power. Then, the mean square value of the normal vibrational velocity of the sound radiation surface of vibrating object can be obtained by experiment or theoretical calculation. If the value or relationship of the radiation ratios of different types of structural units can be established, the noise radiation can be estimated to establish the relationship between structural vibration and radiated noise. The radiation ratio $\sigma_{rad}(f)$ value in the formula is in the range between 1–2.

$$W_{\mathrm{rad}}(f) = \frac{p^2(f)}{\rho_0 c} S_{\mathrm{trav}} \, . \tag{4}$$

In the above formula, S_{trav} is the surface area of a spherical surface of the acoustic sensor, then, the measured pressure level from the sound source r can be expressed in formula

$$p^2(f) = (\rho_0 c)^2 \left(\frac{S_{\mathrm{rad}}}{S_{\mathrm{trav}}} \right) \sigma_{\mathrm{rad}}(f) < U_0^2(f) > \ . \tag{5}$$

Formula (5) is represented in logarithmic form, as shown in the equation

$$\mathrm{SPL}(f) = L_{\mathrm{v}}(f) - 101 \log_{10} \left(\frac{S_{\mathrm{rad}}}{S_{\mathrm{trav}}} \right) + 101 \log_{10} \sigma_{\mathrm{rad}}(f) + K. \tag{6}$$

For each 1/3 octave band, the sound pressure level is calculated as shown in the following formula

$$\mathrm{SPL}(f) = L_{\mathrm{V}}(f) - 101 \log_{10} \left[\pi \left(\sqrt{\frac{S_{\mathrm{rad}}}{2}} + 2 \right)^2 \right] + 101 \ \log_{10} \sigma_{\mathrm{rad}}(f) + 138 \tag{7}$$

and is given in dB.

The total sound pressure level is obtained by adding the sound pressure levels of each of the 1/3 octave bands. The main noise frequency of the diesel engine falls between 500–3000 Hz, so that the total noise level can be properly represented by the A-weighted sound level. For this reason and the size of the engine, the noise radiation ratio can be regarded as 1 unit, that is, $101 \log_{10} \sigma_{\mathrm{rad}}(f) = 0$, in this case, the radiated noise generated by the engine surface is determined using by one of the formula

$$\mathrm{SPL}(f) = L_{\mathrm{V}}(f) - 10 \log_{10} \left(\frac{S_{\mathrm{trav}}}{S_{\mathrm{rad}}} \right) + 138 \, \mathrm{dB}, \ [L_{\mathrm{V}}(f)_{\mathrm{ref}\, 0.39 \, \mathrm{m/s}}] \tag{8}$$

or formula

$$\mathrm{SPL} = L_{\mathrm{V}}(f) - 10\log_{10}\left(\frac{S_{\mathrm{trav}}}{S_{\mathrm{rad}}}\right) - 33.7\,\mathrm{dB},\ \left[L_{\mathrm{V}}(f)_{\mathrm{ref\ ln\,m/s}}\right]. \tag{9}$$

Here,

$$S_{\mathrm{trav}} = \pi\left[\left(\frac{S_{\mathrm{rad}}}{\pi}\right)^{\frac{1}{2}} + 2\right]^2,\ L_{\mathrm{V}}(f)_{\mathrm{ref\ ln\,m/s}} = L_{\mathrm{V}}(f)_{\mathrm{ref}\,0.39\,\mathrm{m/s}} + 172\,\mathrm{dB},.$$

Therefore, as long as the average vibration speed level based on the area average $L_{\mathrm{V}}(f)$ is calculated accurately, the sound power of the components and the whole machine radiation noise can be calculated, so that the contribution of components to the whole machine noise power can be derived.

3.2. Identification of main radiated noise sources of diesel engine by surface vibration velocity method

The identification research of the main radiated noise source of diesel engine is carried out by using the surface vibration velocity method. Then, the test uses the surface vibration test and analysis system, as shown in Fig. 1, which mainly includes piezoelectric crystal accelerometer, LMS SCADA3 acoustic vibration test and analysis system and the corresponding analysis software. Based on the vibration characteristics of the diesel engine, the analysis frequency is set as 4 kHz.

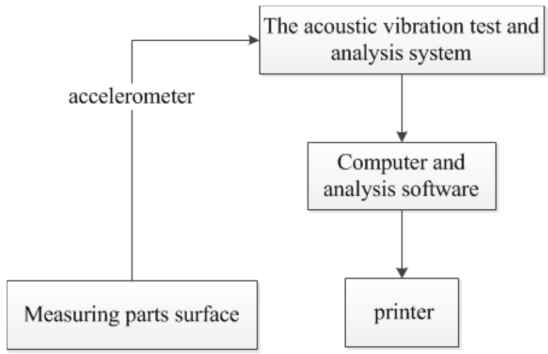

Fig. 1. Test system diagram

Surface vibration measurement uses a piezoelectric crystal accelerometer, which mainly takes into account that the accelerometer can highlight the high-frequency vibration signal, and furthermore, the actual use situation also proves the reliable performance of the accelerometer. The acceleration signal is collected and stored by the acoustic analyzer, after the compute using the software, the analysis and processing are carried out, then, the surface vibration velocity signals can be obtained after the obtained surface vibration acceleration signals are integrated in frequency domain, so that the acoustic power of each component is obtained. In the test, in

order to measure the average area of the vibration acceleration, each component measures the vibration acceleration at many different locations as much as possible, and then, according to average these accelerations, the acceleration of the entire component is obtained. In order to eliminate the influence of the accelerometer weight on component vibration, a smaller weight accelerometer should be used as much as possible.

4. Result analysis and discussion

4.1. 1/3 octave spectrum of each noise radiation part of the diesel engine under four working conditions

For the 1/3 octave band, the value of 20 log 10 $(f/4)$ is shown in Table 1.

Table 1. 1/3 octave band of 20 log 10 $(f/4)$ value

1/3 octave band center frequency (Hz)	500	800	1000	1600	2000	2500	4000	5000
20 log 10 $(f/4)$ (dB)	42	46	48	52	54	56	60	62

According to the structural characteristics and surface vibration characteristics of the diesel engine prototype, the measured engine was divided into the following main noise radiating parts: air inlet (cast aluminum square pipe), intake pipe (round thin wall metal pipe), oil pan, timing gear chamber cover, exhaust pipe, body, crankcase, fuel pump and flywheel shell and other 12 parts, then the surface vibration measurement on the above parts was carried out respectively. A total of four operating conditions (idle, 1500 rpm, 1850 rpm, 2200 rpm) were tested, which were the rated speeds. Through the processing of the surface vibration data of the measuring part, the octave frequency spectrum of the noise radiating parts of the diesel engine under four working conditions was calculated. The noise radiation spectrum diagrams that take the intake pipe as an example are shown in Fig. 2–Fig. 4.

It could be seen from the spectrum that in a wide frequency range, the intake pipe had a larger radiation noise, and there was a higher value in 500–3500 Hz, which was consistent with the noise radiation frequency range of the diesel engine.

4.2. Contribution of radiation noise of components to the sound power of the whole machine

As the noise was actually a form of energy, each band of sound power could be superimposed according to the noise synthesis method, and the sound power level of components was secured, then, the components' sound power was integrated to gain the machine sound power. According to calculate the proportion of radiant noise energy of the main components in the total noise energy of the engine, the contribution of the main components to the total noise was obtained, that was, the

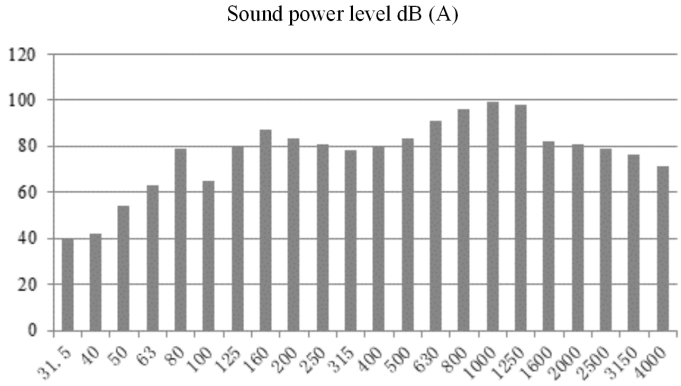

Fig. 2. 1/3 octave center frequency of intake pipe under 1500 rpm condition

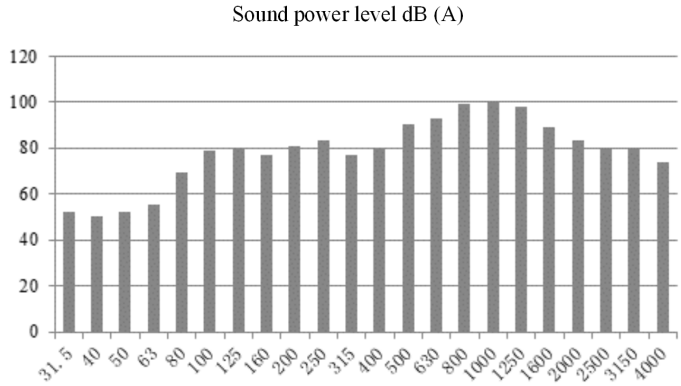

Fig. 3. 1/3 octave center frequency of intake pipe under 1850 rpm condition

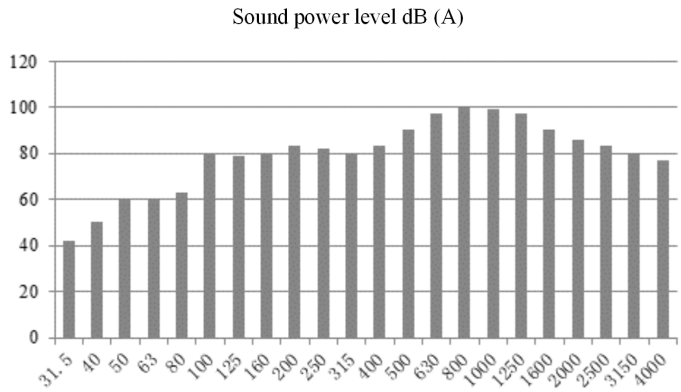

Fig. 4. 1/3 octave center frequency of intake pipe under 2200 rpm condition

order of the main noise sources of the engine. The contribution of the components of the diesel engine to the overall noise is shown in Table 2. And then, the sound power levels of the main parts in different working conditions are shown in Table 3.

Table 2. Contribution of parts of the airframe to noise radiation of the whole machine

%	Idle speed	1500 rpm	1859 rpm	2200 rpm
Oil pan	67	25	20	20
Water jacket side cover	5	7	6	4
Exhaust pipe	1	6	7	6
Valve compartment cover	3	4	6	6
Fuel pump	2	5	7	6
Air inlet	7	22	19	26
Intake pipe	10	17	20	15
The upper part of the body	2	4	4	4
Body skirt	0	0	1	1
Lower crankcase side wall	1	5	4	6
Flywheel shell	1	3	4	4
Timing gear cover	1	2	2	2

The relationship between surface vibration velocity and radiated noise was systematically analyzed. Then, the surface vibration velocity method was used to test the surface vibration of engine under four working conditions: idle speed, maximum torque point, 1850 rpm and rated speed. Among them, the calculated value of the sound power level of the whole unit integrated by the diesel engine under the rated speed condition was basically the same as that of the actual measured engine sound power level. The calculated result was 0.6–1 dB (A) lower than the actual measured result of the sound power. Analyzing the main reason: the measuring part did not completely include all the accessories of the engine, such as: air pump, pulley and generator, etc. Because the pulley was a high-speed moving part, and it is difficult to arrange the sensor on the surface. Besides, as the sensor had a certain quality, which would have a certain impact for measuring the vibration characteristics of parts, especially for some thin-walled stamping parts, however, the impact on the casting was very small.

Table 3. The power level dB (a) of the main components under different working conditions

	Idle speed	1500 rpm	1859 rpm	2200 rpm
Body	83.7	94.9	97.3	98.9
Crankcase	78.9	94.4	96.3	99.2
Air inlet	88.1	101.3	102.7	105.9
Intake pipe	90.5	100.2	102.9	103.5
Valve compartment cover	84.4	94.3	97.6	99.3
Oil pan	98.6	101.8	103.1	105
Water cover side cover	87	96.3	97.7	97.6
Flywheel shell	81.3	92.7	96.3	97.2
Gear chamber cover	79.7	89.8	92.4	94.5
Fuel pump	83.8	94.8	98.2	99.2
Exhaust pipe	81.5	95.8	98.2	99.3
Calculate the total sound power	100.4	107.8	110	112
Measure the total sound power	101	108.4	110.8	113

5. Conclusion

The internal combustion engine noise source identification method that it was suitable for engineering practice was proposed. And then, the surface vibration velocity of the internal combustion engine was obtained by using the improved surface vibration velocity method, and the sound power level of the engine radiated noise and the contribution of the radiation noise of each component were successfully predicted. Then, the method was used to predict and identify the acoustic power levels and the main radiated noise sources of the studied diesel engines, and the predictions were especially consistent with the actually measured results. In addition, the method could also be used to predict the sound power of the engine, identify the main source of radiation noise of the engine, which had a strong practicality for the low noise design and prediction of the engine. And next, the contribution of combustion noise and mechanical noise to the sound power of the whole machine under different diesel engine operating conditions was studied, meanwhile, the contribution of combustion noise and mechanical noise to the engine noise under different engine speed and load was also researched, which laid a good foundation for the adopting different noise control methods to control the sound power of the radiation noise of the whole machine.

References

[1] X. Zhang, C. Li, C. Huang: *Analysis on the role of transport equipment standardization in the development of multimodal transport.* International Symposium for Intelligent Transportation and Smart City (ITASC), Springer Nature, Book Series (SIST) *62* (2017), 139–148.

[2] C. Lim: *Railway technology of South Manchuria railway and workers in China.* The Development of Railway Technology in East Asia in Comparative Perspective, Springer Nature, Book Series (SEH) (2017), 67–103.

[3] Ö. Can, E. Öztürk, H. S. Yücesu: *Combustion and exhaust emissions of canola biodiesel blends in a single cylinder DI diesel engine.* Renewable Energy *109* (2017), 73–82.

[4] R. Powell, J. Wu, S. Gangel, C. Shue: *Total noise solution for a directional drill.* ATZ Off-Highway Worldwide *10* (2071), No. 1, 38–43.

[5] L. D. Simio, M. Gambino, S. Iannaccone: *Experimental and numerical study of hydrogen addition in a natural gas heavy duty engine for a bus vehicle.* International Journal of Hydrogen Energy *38* (2013), No. 16, 6865–6873.

[6] T. Tousignant, K. Govindswamy, G. Eisele, C. Steffens, D. Tomazic: *Optimization of electric vehicle exterior noise for pedestrian safety and sound quality.* SAE International, Technical Paper 2017-01-1889 (2017).

[7] B. Jang, J. H. Kim, S. M. Yang: *Application of rack type motor driven power steering control system for heavy vehicles.* International Journal of Automotive Technology *17* (2016), No. 3, 409–414.

[8] X. Zhao, Y. Cheng, L. Wang, S. Ji: *Real time identification of the internal combustion engine combustion parameters based on the vibration velocity signal.* Journal of Sound and Vibration *390* (2017), 205–217.

[9] S. K. Singh, S. Jain, T. Ahuja, Y. Sharma, N. Pathak: *Performance evaluation of biosignal ring for reduction of pollution level in diesel and petrol engines.* International Journal of Innovative Research in Science, Engineering and Technology *6* (2017), 13814–13824.

Received October 10, 2017

Acta Technica *62* No. 2B/2017, 673–682

Construction of model for performance comparison between SNA and TCP/IP in computer network communication

Hengjie Zhang[1]

Abstract. TCP/IP is known as a communication protocol. SNA is the exclusive network framework developed by IBM. The industry's analysis of TCP/IP and SNA is almost saturated, but there are no corresponding laboratory data to compare the performance of the two in multiple scenarios. In this paper, the transmission protocols of TCP/IP and SNA were studied. IBM was used to achieve the SNA network construction process, as well as a simple end-to-end network and multi-client network were designed. On this basis, a multi-client network context was proposed and used to test two parties, and simple end-to-end network and multi-client network were implemented. On the basis of this, the test comparison in different conversation situations was carried out. Practice has proved that TCP/IP has better transmission efficiency, and SNA can guarantee fairness better.

Key words. TCP/IP, SNA, performance comparison.

1. Introduction

Computer network communication combines computer technology with communication technology and designs data communication mode according to requirements [1]. Computer network communications can connect hosts, terminals and other network devices located in different regions. Combined with the application software corresponding to the host, a complete communication system is formed. The resource sharing in the system is realized through this communication system [2]. TCP/IP is known as a communications protocol that replaced the old network control protocol in 1983 and becomes the cornerstone of the Internet in twenty-first Century [3]. In the middle of the 90s of the last century, TCP/IP began to flourish. Today, TCP/IP has become the mainstream of computer network communication, and has a decisive position [4]. TCP/IP is a layered communication protocol, which consists of four layers and they are application layer, transport layer, network layer and network interface layer [5].

[1]Shijiazhuang University of Applied Technology, Shijiazhuang, Hebei, China, 050081

SNA is the proprietary network framework of IBM, and is widely used in IBM host environment [6]. SNA is the major networking protocol of IBM's large and medium-sized machines, and is a large group of network protocol and standard, which contains configuration in IBM mainframe network environment and managing system resource services [7]. The reason why SNA is concerned is that SNA appears earlier than OSI. As early as the 70s of last century, the proprietary network architecture has been widely used [8]. Initially, a single host is designed to connect to the terminal. As technology matures, multi host communications are allowed until SNA joins and supports LAN and any topology [9]. The SNA network includes both the physical part and software part. The physical part consists of a processor, a communication controller and a terminal controller. The software part includes access mode, application subsystem, user application program and network control program [10].

2. State of the art

The development route of TCP/IP has a great relationship with the development track of internet. Since 1960, American Gordon research network began to sprout, which was the rudiment of international network. The advanced research planning network begins with experimental packet switching system linking computers and slowly transitions to the host to host network control protocol by using master-slave architecture. As early as the beginning of the Internet development, the demand for network interconnection based on different protocols has been paid attention, and the development of network connection technology is on the rise. Network connection technology has been developing very rapidly in the past few decades, which makes it easy and fast for users to access resources and information. But at the same time, there is a difficult problem. Problems can arise when integrating different types of networks. Therefore, people need to solve them through open protocols and public applications. Subsequently, the TCP protocol is invented. Until the late 70s of the last century, TCP development was basically completed.

SNA was created in the 70s of last century and was widely used in IBM host environment. In order to provide inter procedural communication, IBM introduces APPCAPPC which is a high-level program for program communication. In order to combat the threat of TCP/IP, IBM then introduces an advanced peer-to-peer network. This peer to peer network is regarded as the second generation SNA network, which is named APPN. The presence of APPN ensures the diversity of host systems. At the same time, APPN can provide enterprises with a non-centralized network computing [14]. Peer-to-peer operations of large and small systems can be completed on the APPN network and IBM' strategies are embodied clearly in the networking program. That is to say, the inclusive industry standard protocols such as TCP/IP continue to support APPN, but SNA is still at a disadvantage in the competition between SNA and TCP/IP.

3. Methodology

3.1. TCP/IP network building

In order to compare the overall performance of the SNA and the TCP/IP in the practical application, a series of different end-to-end network scenario tests were designed in this paper and they were discussed from multiple perspectives, so as to choose the protocol with better performance to use. The hierarchical communication protocol for TCP/IP is shown in Table 1. In the TCP/IP hierarchical model, the lower layer is the upper layer structure service, and it can provide additional function for the upper layer structure. But each layer is usually communication with the peer layers in the remote computer. For example, the network layer is responsible for forwarding data to the computer in the best way and providing services to the transport layer. The TCP transport layer communicates with the TCP peer layer of the remote computing when processing congestion control and stream control. By collaboration, the two TCP transport layers provide service for the application layer.

Table 1. Layered list of TCP/IP

Application layer	FTP, Telnet, DNS, SMTP, HTTP, ...
Transport layer	TCP, UDP
Network layer	IP, ICMP, IGMP, ARP, ...
Network interface layer	LAN, X25, SNA, ATM

The TCP/IP transport layer protocol serves each task and another process communication. The port number is 16 bits. The host to host protocol is used to identify the protocol, and the incoming message must be forwarded to high-level protocol or application program. However, these high-level application programs such as Telnet and FTP are protocols in the TCP/IP tables. So it is needed to use the same port in your implementation. The port with number 23 is used for Telnet and port with number 20 is used for FTP. Ports that have been assigned port numbers are called well-known ports. In order to avoid two different applications by using the same port number of a host, when applications are written, they can get a usable port by sending a request to the TCP/IP. However, the port assigned is dynamic, so the port numbers that are called each time are not the same. Ports used by UDP and TCP are interlinked. A socket is a special type of file handle that is requested by a process from the operating system. In other words, sockets are used for naming and addressing in the network, and are used in communication terminal nodes. UDP is the application interface to IP, which is shown in Fig. 1. UDP does not provide additional possibilities, flow control, and congestion control. It can only send or receive IP data as a multiplexed signal multiplexer, and use the port to forward datagrams.

TCP cannot recognize data patterns in any application. It can only write data to a byte stream of the TCP window cache as the sending application program.

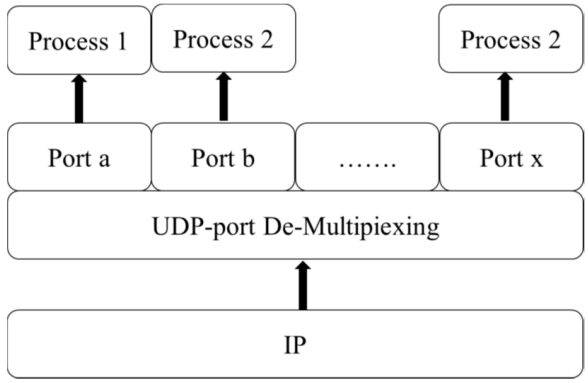

Fig. 1. UDP-based multi-channel signal resolution

TCP uses the three-grip technique to establish the connection, and the TCP data sequences sent are shown in Fig. 2. The network node A initiates the TCP link and executes the CONNECT primitive. The specified parameters are as follows: destination IP address and port, MSS received and other TCP optional parameters. These parameters are waiting for reply. When the network node B receives the SUN, it replies SYN and ACK. The TCP option corresponds only to the TCP optional parameter sent by the node A. After the network node A receives the SYN and ACK, it replies the ACK segment to the network node B and confirms it at the network node B. The TCP connection is completed.

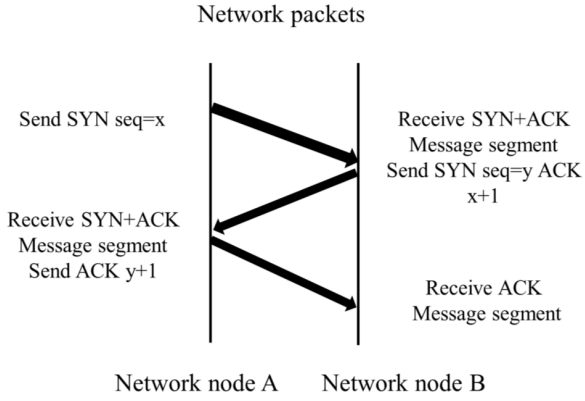

Fig. 2. Simple connection process of TCP

3.2. SNA network construction

SNA is a network architecture developed by IBM, including a large set of network standards and protocols. SNA defines a centralized architecture of mainframe and control terminals that is applied to the IBM host environment. SNA has received

extensive attention because SNA appears very early. It not only defines the logical structure of the data communication network, and describes network configuration to control the network cyber source, information transmission and other operation orders. The SNA network includes the physical part and software part. The purpose of designing SNA is end-to-end communication, which allows users to pass the complex data communication system through the application so that users can feel the head shape of the communication system. SNA has 7 protocol layers, including transaction service layer, indicates service layer, data flow control layer, transmission control layer, path control layer and data link control layer as well as physical layer, which is shown in Fig. 3.

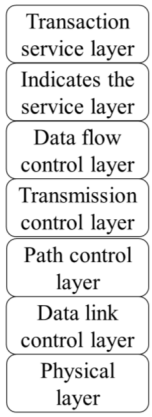

Fig. 3. Seven-tier structure of SNA

The APPN architecture has a number of features. Among them, three important basic characteristics form the basic functions of APPN. These three basic characteristics are the transport group, the network addressable unit and the address and session identifier. An array is a link between APPN nodes, and the underlying APPN schema can only support single link arrays. A network addressing unit is any part that can establish sessions with corresponding components in APPN environment, such as control nodes and logical units. Addressing and session identifiers play a very important role in session management and routing. In traditional SNA subarear, each resource is assigned a unique network element. In the APPN environment, routing information is session oriented. The address selected by the APPN transmission head is one to one. The address used by the HPR/IP transport header contains not only the HPR session identifier, but also the IP address involved in the terminal node.

Enterprise extender is based on the implementation of SNA over ATM. Among them, the UDP port identifies the destination of the datagram. IP implements the routing function as a UDP host. The mapping to the UDP port number is the SNA transport priority. Because many IP routers can be configured to the data flow of Venus line according to the port number, the five UDP ports have been registered for EE use, which is also called the enterprise expander use. Table 2

shows the correspondence among the APPN priority, the IP preamble and the UDP port number.

Table 2. APPN priority, IP precedence and UDP port number

APPN priority, IP precedence and UDP port number		
N/A	B'llO'	12000
Network	B'llO'	12001
High	B'lOO'	12002
Medium	B'OlO'	12003
Low	B'OOl'	12004

4. Result analysis and discussion

4.1. Simple end-to-end network testing

Sensitivities of applications program to operating systems and host performance are considered. This creates errors and affects data results. Therefore, several hosts with the same configuration and installed Windows 2003 server operating system at the same time are selected as the test system in this paper. The windows platform integrates the TCP/IP protocol. The SNA network still relies on the IBM communications server for windows installation to achieve communications server for windows fully supporting APPN, HPR and DLUR functions, and provides a full set of enterprise network solutions. Users can achieve a variety of ways to connect through the system. Because Windows NT has only one TCP/IP protocol, and only one EE port can be defined. Therefore, defining the EE process is relatively simple in the CS for OS/390 process. First of all, SNA node Configuration is initiated to create a new configuration file and then create nodes. Nodes are virtually invisible in the APPN network environment, which is similar to the hosts in the TCP/IP network.

The fully qualified control node name consists of two parts. One part is the NETID of the SNA network and the other is the server. The control node name in the SNA network is unique. The name of the control node in the same NETID network can't be repeated. Moreover, the control node is unique in the APPN network. This uniqueness is similar to the host naming of the TCP/IP network. Another point to note is that CP alias, which is the alias of the control node. Typically, the terminal nodes participating in the SNA network are IBM communication server for windows. But sometimes it can be set as terminal node. For example, when there is no need to route SNA sessions in actual applications, nodes should be set to terminal nodes.

Cstest is defined as server and scwin35 is defined as client. The following tests are designed in this paper. File FTP transfer test is carried out between server and client nodes and connections are established. When the server sends data to the client, the connection is closed after the end of the transmission. Measuring time is the total time to establish connection and disconnect and file transfer time. In addition, socket buffers received and sent by FTP are the SNA MODE setting of

2048 bytes. The result is shown in Fig. 4.

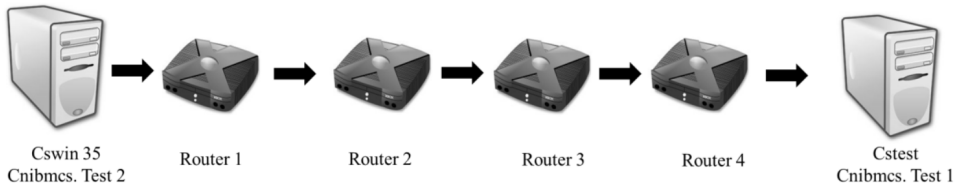

Fig. 4. Simple end-to-end network

The test uses 500MB's large file for transmission, which is designed to avoid interference from broadcast traffic in the network and to facilitate the distinction between results. It is found that large file transfer has higher transmission rate in TCP/IP protocol in single process. Moreover, the average transmission rate is nearly 50 % higher than the RTP transmission rate. Therefore, the gap between the two is very obvious. In addition, the TCP/IP protocol can be transmitted quickly at the beginning of the link. It can also be maintained at a higher transmission rate during transmission, so flow control of TCP based on sliding window can be implemented. At the same time, data can be sent at any point. TCP/IP peer to peer window design is to provide traffic control for the receiver. The window is designed to receive the data range of the byte stream allowed by the other party, but it can only send bytes in the byte stream within the window.

In order to indicate the size of the receiving port, the TCP/IP Baotou contains window fields 16 bits. When the receiver receives the data, sending the ACK indicates that the receiver has successfully received the byte. When the maximum receive window is filled, the sending end must stop sending data.

4.2. Multi-client network analysis

In a multi-session file transfer scenario, the TCP/IP protocol connection can transmit data at a higher rate. As a result, the TCP/IP protocol can still hold the edge in multi session file transmission. However, the network stability will decrease with the increase of session, which will lead to a decrease in the quality of the service. In the RTP connection, the speed drops as each session transfers speed begins. However, the relative balance is maintained, so the network stability is very good and will not be affected by the increase in the number of sessions. The session in the TCP/IP protocol corresponds to a TCP connection, and a number of TCP connections are established from the same end to the end path, which can not only improve the utilization of broadband networks, but also increase the speed of network transmission. At the same time, the number of TCP connections can be optimized so that the network can reach the highest transmission speed. GridFTP-APT algorithm explains the relationship between broadband and connection numbers and buffers, as well as link bottleneck bandwidth and round trip time. This relationship can be

expressed by the following formula

$$G = \min\left(\frac{NW}{R}, \frac{N(1-p*)}{2R}\left(-3+\frac{\sqrt{6+21p*}}{\sqrt{p*}}\right)\right), \tag{1}$$

where

$$p* = \left(-2+\frac{2BR}{N}+\frac{2}{3}\left(\frac{BR}{N}\right)^2\right)^{-1}. \tag{2}$$

Here, N represents the number of TCP connections and W represents the size of the TCP connection socket buffer. Symbol B represents link bottleneck bandwidth and R represents the round-trip time of the TCP link. As the number of TCP connections increases, the system bandwidth increases. When the connection is too large, the system bandwidth drops.

After each server of the client node establish a link, the server starts sending data to the client. When the transfer is finished, the connection is closed. Test time is the sum of the time to establish connection and disconnection, and the time of file transfers. The transmission file size is 500 MB. The socket buffer received and sent of FTP is 2048 bytes, which corresponds to the SNA MODE design.

Table 3. The results of two client transfers

TCP	timel (s)	speed l (Kbytes/s)	time2 (s)	speed 2 (Kbytes/s)
1	23.15	21294. 95	23.25	21686. 63
2	22.79	21747.08	22.50	22222. 89
3	23. 25	21702.35	23. 29	21686. 63
4	22.39	22350.47	22. 49	22222.59
5	22.57	21872. 7	22.39	21030. 44
rtp	timel (s)	speed l (Kbytes/s)	time2 (s)	speed 2 (Kbytes/s)
1	52.53	9142. 88	53.39	9156. 89
2	53. 49	9119.97	53. 79	9165. 10
3	52. 79	9112.80	54.15	9164. 29
4	53.17	9150. 57	53.29	9183. 32
5	54. 13	9167. 86	54. 28	9103. 44

When the TCP/IP protocol is used in multi-client transmission, there is no obvious change in the transmission time. The SNA protocol shortens the data transmission time, so that the transmission efficiency has been greatly improved. And in the multi-client scenario, the total bandwidth of the TCP does not change, and server throughput is unchanged. Therefore, the performance changes are not obvious. However, the RTP process has changed. Unlike multiple sessions reusing the same RTP connection from single end to end networks, the RTP sets up separate RTP connections for each client's FTP session.

In summary, TCP maintains high transmission efficiency in the multi-client scenario. However, with the increase of data transmission, the TCP protocol cannot solve the problem of link fairness. The existence of this problem will lead to a

sudden instability in the network, and higher bandwidth will increase the burden on the network. Practical tests show that servers in TCP/IP networks consume more resources and affect the overall network speed. In the multi-client scene, the transmission rate of the SNA protocol is slow, but it takes into account the fairness. Therefore, the stability of the transmission data stream can still be maintained.

5. Conclusion

Computer network communication is a new communication type. It combines computer technology with communication technology to meet the needs of data communication. In this paper, the development status of SNA and TCP/IP were introduced, and the transport layer of TCP/IP protocol and the network structure of SNA were expounded. The theoretical comparison between the two protocols was made and tests under different session scenarios were carried out. According to the performance of the two networks, the performance of the main transport protocols in TCP/IP and SNA networks was compared. It is found through the test that with the complexity of the application scene and the influences from external factors, network instability and other factors, the number of TCP connections increases and is at a very fast rate, which leads to worse network performance and worse serious deterioration. The ARB flow control and session connected by RTP can independently adjust and execute commands independently. They do not affect each other. As a result, SNA networks can remain stable, so TCP/IP has better transmission efficiency and SNA could better guarantee fairness. However, affected by objective factors such as experimental conditions, complex topologies are not designed in this paper. In simple networks, routing performance is not adequately represented. Therefore, further research on network routing performance can be carried out.

References

[1] J. Bian, X. Zhou: *Hidden Markov models in bioinformatics: SNV inference from next generation sequence.* Methods in Molecular Biology - Journals - NCBI, *1552* (2017), 123–133.

[2] J. Grobelny, R. Michalski: *Applying hidden Markov models to visual activity analysis for simple digital control panel operations.* Proc. International Conference on Information Systems Architecture and Technology (ISAT), 19–20 September 2016, Karpacz, Poland, Springer Nature, Book Series (AISC) *523* (2016), Part III, 3–14.

[3] R. Mattila, C. R. Rojas, V. Krishnamurthy, B. Wahlberg: *Asymptotically efficient identification of known-sensor hidden Markov Models.* IEEE Signal Processing Letters *24* (2017), No. 12, 1813–1817.

[4] J. Li, W. Pedrycz, I. Jamal: *Multivariate time series anomaly detection: A framework of Hidden Markov Models.* Applied Soft Computing *60* (2017), 229–240.

[5] J. Alerini, M. Cottrell, M. Olteanu: *Hidden-Markov Models for time series of continuous proportions with excess zeros.* Proc. International Work-Conference on Artificial Neural Networks, 14–16 June 2017, Cadiz, Spain, Advances in Computational Intelligence, Book Series(LNCS) *10306* (2017), 198–209.

[6] L. Yang, A. Maezawa, J. B. L. Smith, E. Chew: *Probabilistic transcription of sung melody using a pitch dynamic model*. IEEE International Conference on Acoustics, Speech and Signal Processing (ICASSP), 5–9 March 2017, New Orleans, LA, USA, IEEE Conference Publications (2017), 301–305.

[7] M. Karg, D. Kulić: *Modeling movement primitives with hidden markov models for robotic and biomedical applications*. Methods in Molecular Biology - Journals - NCBI *1552* (2017), 199–213.

[8] C. Sharp, J. Bray, N. G. Housden: *Diversity and distribution of nuclease bacteriocins in bacterial genomes revealed using Hidden Markov Models*. PLoS Computational Biology *13* (2017), No. 7, paper e1005652.

[9] M. Sesia, C. Sabatti, E. J. Candès: *Gene hunting with knockoffs for hidden Markov Models*. Statistics > Methodology (2017), arXiv:1706.04677.

[10] M. Li, B. M. Bolker: *Incorporating periodic variability in hidden Markov models for animal movement*. Movement Ecology *5* (2017), No. 1, paper 1.

Received October 10, 2017

Acta Technica *62* No. 2B/2017, 683–692

Design and implementation of new glass CNC sand blasting engraving machine and information system[1]

Wenli Yang[2], Yuchun Zhu[2], Xianghui Lu[2]

Abstract. With the gradual improvement of people's living standards, the demand for stone handicrafts tends to rise. Glass, stone and other carved handicrafts have formed an important industry. At present, the degree of engraving automation in our country is generally low, and the traditional engraving processing technology has the problems of high energy consumption and high labor intensity. Therefore, the demand for new glass CNC sand blasting engraving machine is more and more intense. Drawing on the advanced processing ideas and methods at home and abroad, a new type of glass CNC sand blasting and engraving machine with higher intelligence was designed in this paper. Combined with the idea of CAD intelligent processing, the 3D model of glass and stone was constructed, and finally the process of robot machining integration was realized.

Key words. CNC engraving machine, information system, stone carving.

1. Introduction

Carving process is to remove and correct the surface of the carved material, and to make it a handicraft with a sense of space and three-dimensional beauty. This craft requires a natural or mission image that can be touched and perceived [1]. According to the morphological classification, sculpture can be divided into emboss, model sculpture and image sculpture. The living standard of people is undergoing great changes. People's pursuit of cultural life is not just a simple entertainment, but a deeper appreciation of art [2]. According to the basic requirements of artistic features and ornamental features, the sculpture industry, such as glass and stone, is rising quietly in recent years. The homogeneity of traditional sculpture craft in our country is higher, and the possibility of higher value added is not very high. Therefore, the

[1]In this paper, high technology to transform Hebei province 2017 key research projects and promote the traditional industry "special glass Intelligent NC spraying carving technology research and application": 17211810D.

[2]Hebei Construction Material Vocational and Technical College, Qinhuangdao, Hebei, China, 066000

development of new products is slow [3]. The quality of traditional engraving is entirely dependent on the experience and craftsmanship of the master. If the number of craftsmen who train the craftsman spirit is constantly decreasing, the carving process will be confronted with the shortage of technicians [4]. Glass, stone and other arts and crafts urgently need a higher degree of automation equipment to solve the problem of engraving technology and technical personnel shortage. Therefore, the significance of this study lies in this.

2. State of the art

Glass and stone have many steps during the engraving process. Even for the companies that carry out the process are very mature, they rely heavily on manual work to do the necessary work processes. In particular, the basic carving of the crafts with complex shape is completed by hand [5]. Although the processing equipment of complex structures made in China has been applied in many fields, there is no CNC machining which can realize intelligent processing [6]. The main research results are also concentrated in the design phase of small CNC engraving machines. In foreign countries, the research on the engraving equipment for stone, glass and other crafts has entered a relatively mature stage. Industrial CCNC machine tools have been able to realize automatic integration of robots and machines [7]. The latest research results show that foreign CNC engraving machine has been able to automatically change tools, and automatically form cutting path. But the disadvantage is that equipment is expensive and manufacturing technology is basically blocked [8].

Industrial robots are widely used in industrial automation production process. They include advanced manufacturing technologies such as machinery, electronics, computers and artificial intelligence [9]. Since the design and manufacture of the first industrial robot, the robot has been bursting with great potential. Since 1970s, industrial robot technology has been developed rapidly. Many countries began to pay attention to the future development of industrial robots, and constantly put in a lot of manpower and material resources [10]. At present, CNC machine and industrial robots have been widely used in the field of automobile manufacturing and aerospace, and later developed into food processing, timber and furniture industries. The adoption of CCNC machine technology and intelligent robot manufacturing ideas into glass, stone and other crafts sculpture manufacturing will give full play to the multi axis flexibility of CNC machines and industrial robots to meet the processing requirements for the maximum space range and the special structure.

2.1. Methodology

Based on computer aided technology, a whole set of new glass numerical control sand blasting engraving machine system is designed. The system makes rough machining and finishing of glass, stone and other materials. Fig.1 shows the scheme design of engraving system. The whole CNC engraving system is divided into the mechanical structure part, the electrical control part, the modulation part, the displacement machine design, and the processing tool movement track. Besides the

design of robot body, the design and application of displacement machine is also an important structure of engraving machine system. The positioner is the special robot auxiliary equipment. It is more suitable for the rotary machining of materials with complicated structure, which can obtain ideal engraving and machining positions. The positioner, the operating machine and the electric welding machine are fully matched and used. They are connected with the welding machine system to realize the linkage operation. The positioner is applied to CNC engraving system, which can realize multi-directional machining and effectively handle machining dead angle. The use of positioner is mainly supported by the manufacturers of robots for sale, and the core manufacturing technology is also the manufacturer's business secrets. In this study, the application principle of positioner has broken through the manufacturing technology of CNC engraving machine.

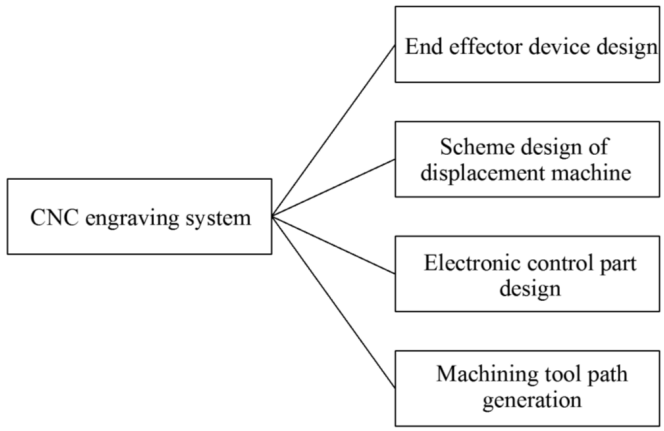

Fig. 1. Scheme design of engraving system

Fig. 2 shows the machining process of CNC engraving machine. The whole CNC engraving process is as follows. 3D modeling software UG and Solidworks are used for three-dimensional modeling design of the sculpture image. Then, the modeling image is imported into the CAM computer aided program to generate the reasonable running track of the CNC machining tool. The CNC machine tool is used to track the tool path according to the machining trajectory. Before optimizing the tool path, it is necessary to predict the possible machining problems in the process of machining and eliminate the interference that may exist in the process of tool movement. After obtaining the processing program of CNC engraving machine, it is embedded in the controller to do engraving. According to the reports, the correlation between cutting speed and cutting stress in stone and glass processing is relatively high. The feed speed and the change of cutting depth have a great influence on the cutting stress. Overall, however, the cutting depth has the greatest impact on the cutting force of the tool path.

The reason is that after increasing the feed rate, the arc area of cutting has no change in length direction, but only increases the maximum cutting thickness and normal contact stress. Therefore, in the phase of the efficiency of utilization

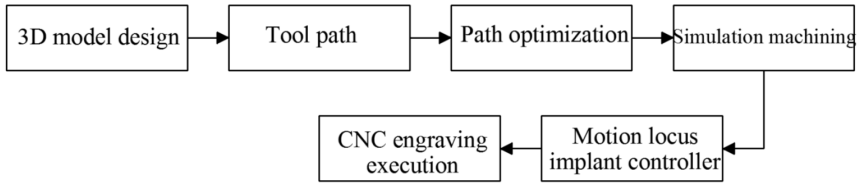

Fig. 2. Machining process of CNC engraving machine

involves cutting tools, it is better to increase the cutting speed and minimize the cutting depth in the allowable range of CNC machine tools, so as to minimize the material damage caused by cutting stress. The speed of cutting is closely related to the surface quality of the stone. Therefore, the high-speed motor is selected in this paper, which can improve the cutting rate of the tool better, and then improve the quality of the surface material of the stone [11].

Power driven cutting tools can process materials. The power unit is an important part of the structure. Therefore, when it comes to this part of the component, the appropriate engraving machine power device should be chosen. The end effector should have the basic functions of driving tools, and choose different cutters according to different machining conditions. Because of the material difference of cutting, the speed of engraving tool is different, and the maximum speed can reach 10000 rpm /min. During the general carbide processing, cutting process requires a fast tool's rotate speed. The main driving force is the speed control function of the power unit, which meets the requirements of machining performance. The two stages of finishing and roughing require different tool properties. The machine tools with higher degree of automation can replace the manual suspension of tool change. It is considered that the replacement of cutting tools is not only inefficient, but also has great security risks [12].

Motor spindle is a new technology for CNC machine, and the main purpose is to effectively combine the spindle and motor. The motor spindle is widely used. The motor spindle with high rotating speed can replace the traditional gear box. During the operation, the vibration is small, the noise is relatively low, and the response rate is relatively fast [13]. Considering the drive requirements of the motor spindle, the main spindle of the motor should be lightweight and the speed change function should be fine. It can satisfy the function of the automatic replacement tool. Therefore, it is believed that the power unit of CNC sand blasting engraving machine is the main shaft of the motor. The selection of motor spindle combines the main process and parameters of cutting to calculate the cutting stress and the steering torque. The type of motor spindle is selected by power and tool interface parameters. In this paper, 120TD18Z5.5A motor spindle is selected by calculation. The maximum rotating speed of the shaft is 1820 rpm, and the rated power during operation is about 5.6 kW. Loose and tightened sensors are installed to meet the requirements of material engraving of different structures. The $U - f$ curve of the motor spindle is shown in Fig. 3.

The electronic control system needs to satisfy the communication, emergency

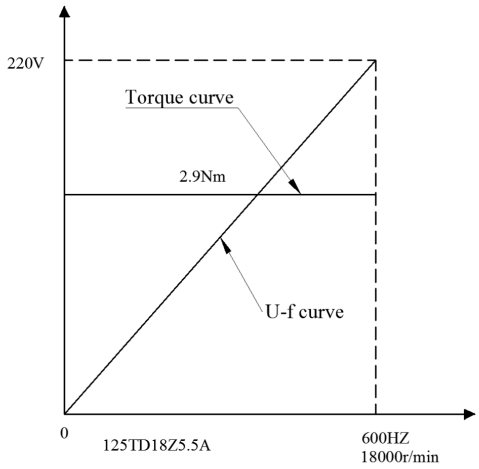

Fig. 3. $U - f$ curve of main shaft of CNC engraving machine

stop or open, I/O port allocation and other control functions, in which the I/O port allocation is affected by the control of the displacement machine. The controller of engraving machine can be selected as the central controller component of different material carving system, and the technical actions in the process are completed by the intelligent controller. The intelligent controller passes the machine information through the I/O and the outside. With the addition of the port of the SDI input signal of the link and the SDO output port, the feedback of signal reception and release is completed through the input and output ports. The output signal wiring diagram is depicted in Fig. 4.

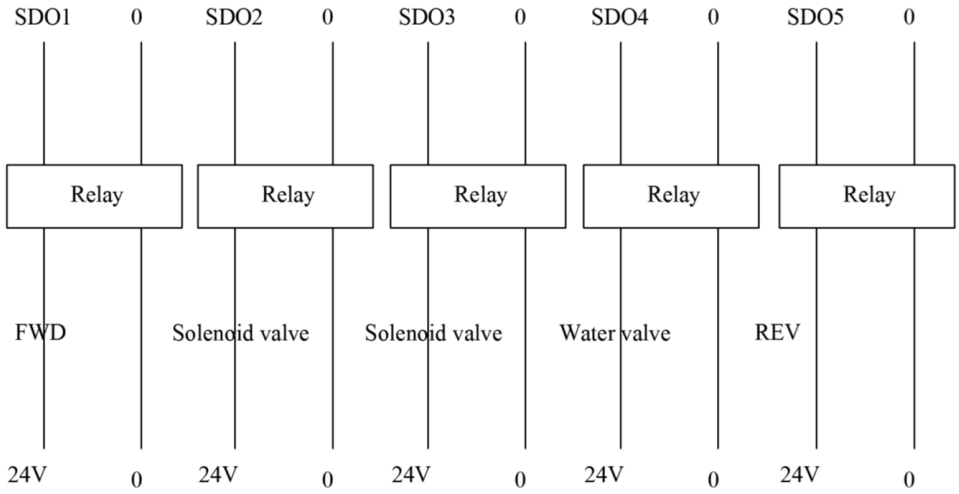

Fig. 4. Output signal wiring diagram

The design of control cabinet for CNC sand blasting and engraving system needs

to be analyzed and designed according to the function of system components. The inverter in the control cabinet has heat to emit at work. The components need to reserve a certain gap around. The heat dissipation part needs to be designed larger, so as to reserve the basic space for heat dissipation. The frequency conversion design is shown in Fig. 5. At the same time, the cooling part of the control cabinet needs to be designed with a cooling fan with higher power. A fan hole is designed and installed nearby the fan, which is equipped with warning, lifting and so on.

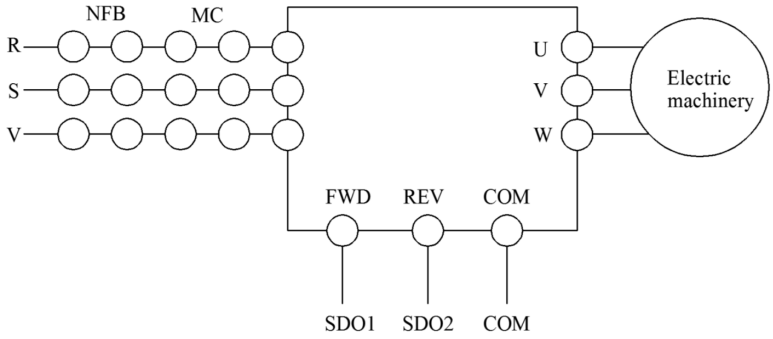

Fig. 5. Frequency converter wiring diagram

The design of mechanical structure mainly includes the grip design of motor spindle, the design and manufacture of the fixed platform, the choice of the tool and so on. The main shaft of the motor is connected with the machine control device by means of a grip. If the cutting speed is too high, the vibration will lead to the reduction of cutting accuracy. Choosing the right material and grip can reduce the weight and minimize the weight load of the CNC machine. Processing materials are generally heavy in weight. Therefore, in order to ensure the accuracy of cutting, it is necessary to use a relatively stable processing platform as a guarantee, and design reasonable processing fixed platform through a certain calculation. The tool has a great impact on the effect of CNC bed's processing and quality. Engraving machine cannot be separated from the use of tools. Because the cutting material is different, the engraving machine tool should also be installed with the corresponding tool. The engraving process is divided into two parts: roughing and finishing. Roughing is the removal of wool to obtain approximate outline features, usually with relatively large amount of cutting. The finishing stage is the process of engraving process in order to obtain the theoretical requirements of the surface. The final form and structure of the product is actually determined by the finishing stage.

When machining large size sculptures and craft products, proper displacement machines are needed to coordinate CNC machine for omnidirectional, multi angle continuous machining. In this paper, I/O conversion information is realized according to the coordinated motion principle of the positioner and the CNC machine, and the coordinate movement of the machine is controlled by the coordinate machine. The intelligent controller is the main core control element of the positioner, which coordinates the operation efficiency of the overall positioner. The intelligent controller keeps the same initial speed as the positioner, so that the intelligent controller

keeps the same running state as the positioner. The time point of the received port signal is the point at which the first instruction point begins. In particular cases, lag angles may be generated, and the angle and time can be used to determine how much the positioner is growing.

Through the preliminary design of the three-dimensional model of the new glass CNC sand blasting machine, the method of generating tool path is set up, and the theoretical research and simulation before and after the cutting process are made. The structure of CNC engraving machine and the design method of information system have been formed. It is necessary to test the CNC engraving machine to establish the consistency between the data in the simulated environment and the actual data. According to the problems of different material processing, information feedback is carried out, and a large amount of data is analyzed and summarized. After the actual stone processing in the processing system, it can verify the system's scientific validity of the new glass CNC sand blasting engraving machine designed in this paper. The basic design problems are found in the experiment, so that the optimization of the stone and glass engraving experiments will be improved in the future research work.

3. Result analysis and discussion

The structure design of the new glass CNC sand blasting engraving machine and the design scheme of the system are given in the paper. In order to verify the operation of the hardware, the test experiment of the positioner is given. The way to build the experiment is to connect the worm to the motor. The worm connects the turbine and drives the turntable. The transmission ratio of worm and turbine selected in this paper is about 50:1. The circuit is connected before the experiment, and the positioner is adjusted according to the results of the running parameters of the computer. When the performance of the worm drive reaches a stable state, the turntable is driven to rotate. After turning, the CNC machine sends out signals through I/O. The turntable motion depends on the transmission of the motor. The actual relative displacement of the robot depends on the motor encoder to feed back to the CNC machine, or after the relative error is calculated, the actual relative displacement at the next stage is calculated according to the error. The motion speed of the next stage is calculated according to the displacement, and each pulse signal can be adjusted by different stages of the relative error. The control point of the robot's tail clamp of CNC machine needs to keep consistent with the movement curve track of the machine turntable. The effect of the study is the coordinated tracking of the two.

In the experiment of the positioner, the software needs to accumulate the error of moving track continuously. The output errors of each stage are recorded through the Notepad output platform. The concept described by VR is the operation speed of CNC machine. Nrepresents the relative cycle of motion. STEP describes the amount of movement per relative cycle. The movement speed of the displacement machine is V. The average machining cycle of CNC machine is about 20000-pulse, and other operating parameters are unchanged. If the moving speed of the glass CNC sand

blasting machine changes, the speeds are defined as 10 mm/s and 20 mm/s. The speed of the engraving machine is controlled and the relative error of motion in each cycle is obtained, as shown in Fig. 6.

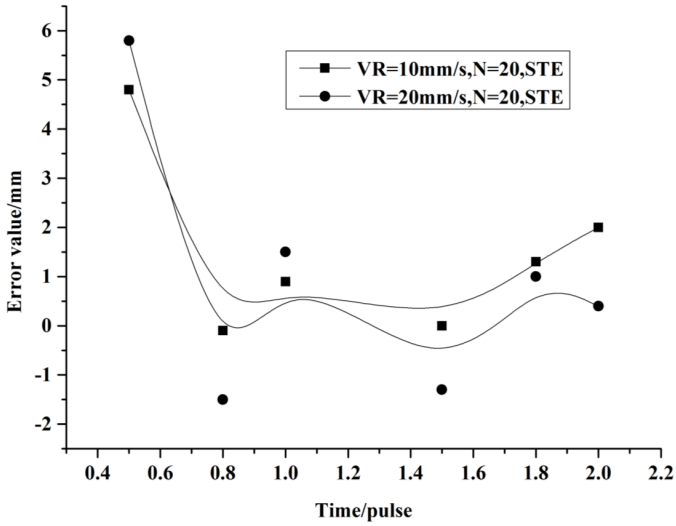

Fig. 6. The error value varies with the movement time

Through the above experimental data, it can be seen a relatively close trend of movement. In the process of starting the positioner, the error of engraving machine is relatively large. After continuous tracking adjustment, the error is gradually reduced, and finally tends to a range of changes. In the process of movement, the operation speed of CNC engraving machine needs constant adjustment, and the error value fluctuates as well. If the machine is stalled at one stage and the speed is accumulated, the next stage will run too fast and a certain rate of conflict will occur. Controller's changes will reduce the speed of operation and affect the speed of the next stage. Delays also cause errors to fluctuate within a certain range. As shown in Fig. 7, the calculated unit data show that the variance data for the first three sets are 1.26, 2.58, and 2.70, respectively, and the variance of the latter three sets is 0.22, 0.36, and 0.62, respectively. The results show that after the movement speed of CNC engraving machine is increased, the variation of the error is increased. When the exercise cycle is reduced, the trend becomes more gradual. When the movement speed of CNC engraving machine is reduced, the movement accuracy of the control position machine can be controlled by adjusting the cycle time.

4. Conclusion

According to the design and application defects of domestic stone and glass engraving equipment, a more advanced design method of new glass CNC sand blasting engraving machine was put forward in this paper. Through the CAD/CAM com-

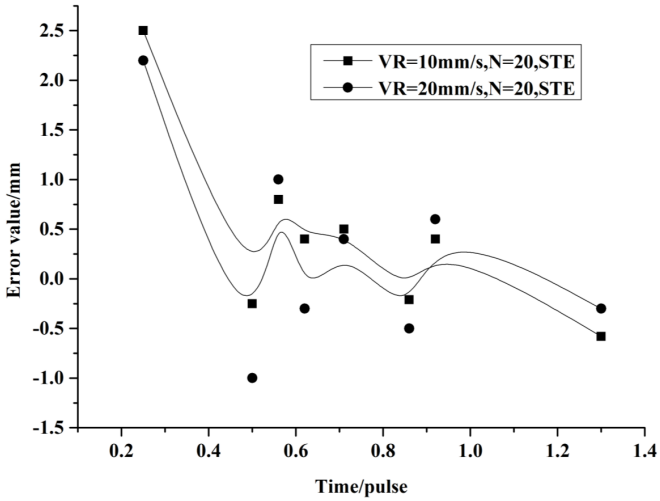

Fig. 7. The error value varies with the movement time

puter application assistance technology, the integration processing process from the three-dimensional model to the different materials was completed. The problems of small processing range and low machining accuracy of the domestic numerical control engraving machine were overcome. Referring to the basic characteristics of glass, stone and other processing processes, the overall design of the process was first designed. The design of the mechanical structure, selection, and installation process were mainly completed. In order to extend the space axis of CNC engraving machine, the hardware of the experiment was matched and the software was coordinated. The software program was programmed by C++ development platform to realize the synchronous and coordinated movement of the shifting machine and CNC engraving machine. The experimental results of the displacement machine experiment obtained in this paper can be used for the design of the large positioner with more complex structure. Combined with certain control method, the CNC sand blasting engraving machine can be designed and manufactured independently.

References

[1] A. C. Lee, M. T. Lin, Y. R. Pan, W. Y. Lin: *The feedrate scheduling of NURBS interpolator for CNC machine tools.* Computer-Aided Design *43* (2011), No. 6, 612–628.

[2] S. Weyer, M. Schmitt, M. Ohmer, D. Gorecky: *Towards Industry 4.0 - Standardization as the crucial challenge for highly modular, multi-vendor production systems.* IFAC-PapersOnLine *48* (2015), No. 3, 579–584.

[3] Z. Jia, Y. Chen, W. Liu, K. Zhao, L. Wang, X. Tu: *The control system for precise five-axis laser/micro-milling machine tool.* International Journal of Industrial and Systems Engineering *22* (2016), No. 2, paper 073960.

[4] H. Yang, J. Yan: *DXF file identification with C# for CNC engraving machine system.* Intelligent Control and Automation *6* (2015), No. 1, 20–28.

[5] Y. X. Chen: *Design and development of economic type mechanical engraving machine.* Applied Mechanics and Materials *644–650* (2014), 813–816.

[6] Z. Pandilov, N. Veselinkovski: *Improvements and benefits of upgrading CNC Maschine for engraving and cleaning metal parts.* Acta Technica Corvininesis - Bulletin of Engineering *9* (2016), No. 2, 111–114.

[7] G. M. Martinov, A. I. Obuhov, L. I. Martinova, A. s. Grigoriev: *An approach to building a specialized CNC system for laser engraving machining.* Procedia CIRP *41* (2016), 998–1003.

[8] H. L. Wu, Z. Q. Zeng, Y. Y. Zhang: *Experiment design for crafts design and fabrication based on CNC engraving technology.* Research & Exploration in Laboratory *33* (2014), No. 12, 229–232.

[9] X. Chen, J. Shen: *Numerical and experimental investigation on splitting-and-recombination micromixer with E-shape mixing units.* Microsystem Technologies *23* (2017), No. 10, 4671–4677.

[10] Q. M. Liang, H. J. Yin: *Modeling and simulation of the feed drive system for a type of CNC engraving and milling machine.* Mechanical Research & Application (2013), No. 2.

[11] X. Zhang, Y. Liu, B. Gou, L. Han: *Design and rigidity analysis of key components in five-axis wood engraving machine.* Machine Tool & Hydraulics (2014), No. 1.

[12] Y. Liu, C. Ai, Y. Yang: *Development of motion control module for flame cutting machine CNC system.* Machine Tool & Hydraulics (2015), No. 10, paper 051.

[13] T. A. Dow, J. Nowak, J. R. Kessing: *Design of elliptically-vibrating ultrasonic actuator for nanocoining.* Precision Engineering *45* (2016), 301–310.

Received October 10, 2017

Acta Technica *62* No. 2B/2017, 693–702

Determination of the content of hypericin in Huanghua Ningshen granules based on HPLC[1]

Jiang Xiaomei[2,3], Jin Yongxin[2,3,4], Liao Qun[2,3], Hua Daping[2,3], Shang Keyi[2,3], Huang Yubo[2,3], Xiang Rong[2,3]

Abstract. In this study, the HPLC method was used to determine the content of hypericin in huanghua ningshen granules. The Fortisil-C18 chromatographic column (4.6 mm×250 mm, 5 μm) was used with mobile phase of dipotassium hydrogen phosphate solution: acetonitrile (88:12), 1 mL/min^{-1} flow rate, detection wavelength of 360 nm. The results showed that the content of hypericin was linear in the range of 6.6–67.0 μg mL^{-1} (r = 0.9991). The average recovery was 99.43 %, and RSD was 0.94 %. This method can be used to determine the content of hypericin in Huanghua Ningshen granules.

Key words. Huanghua Ningshen granule, hypericin, HPLC method.

1. Introduction

In today's society, more and more people suffer from varying degrees of depression [1]. This may be due to faster and faster pace of life, more and more intense social competition, and work and life and other aspects of the pressure is also increasing. Depression is the neuropsychiatric disorder caused by a variety of factors and with depression as the main symptoms. Depression is a disease with high incidence, high disability rate and high recurrence rate [2]. The main manifestations of depression include slow thinking, difficulty falling asleep, serious self-mutilation, suicide and other acts. WHO statistics show that depression ranked in the top fourth in the

[1]The work presented in this paper is supported by the Special fund for basic research of Central University of Northwest University For Nationalities (Item number 31920150093).

[2]The Second Clinical Medical College, Northwest University For Nationalities, Lanzhou 730030, Gansu, China

[3]Gansu Second People's Hospital, Lanzhou 730030, Gansu, China

[4]Corresponding author

ten major diseases. By 2020, it may become the second largest disease after cardiovascular and cerebrovascular diseases, becoming the highest burden of disease in developed countries [3]. Prevention and treatment of depression has attracted the medical profession and the community's attention [4].

Depression is not caused by a single cause, and the causes are very complex. The influence of various factors, such as genetic factors, biochemistry, immunity, psychology, health, society and environment, may lead to different degrees of depression. It is a complex disease caused by multiple etiologies [5]. At present, its pathogenesis is not clear, which is still in the stage of hypothesis. It is thought that the occurrence of depression is closely related to the abnormal metabolism of biogenic amines [6]. There are many hypotheses about its pathogenesis. At present, there are 5 kinds of hypotheses which are recognized by the medical profession, that is, the 5- (5-HT) hypothesis, the norepinephrine hypothesis, the dopamine hypothesis, the amino acid neurotransmitter system hypothesis and the acetylcholine hypothesis [7].

At present, the main treatment of depression is drug therapy with Western medicine, SSRI classic antidepressants as the main medicine. However, the drug cost is high, the effect is slow, and there are some side effects. There are 70 % patients with residual effect, and the effect is not ideal [8]. Therefore, the key is to reduce the side effects of drugs and shorten the onset time of drugs. Therefore, a large number of studies began to focus on natural medicines, including traditional Chinese medicine. Chinese medicine has great potential in the treatment of depression, and it also shows a very bright future. Traditional Chinese medicine multi-target, comprehensive treatment has low adverse reaction, which is the absolute superiority superior to Western medicine. Especially for patients with longer course of disease, its curative effect is better than Western medicine [9].

Huanghua Ningshen granule is compound preparation by 12 kinds of herbs including yellow, rehmannia, Acacia flowers, vinegar Cyperus, turmeric, licorice, floating wheat, wheat, tuckahoe, lily, calamus, and jujube according to a certain proportion. Its main function is the curative effect of restoring consciousness and inducing liver and relieving depression, which has better clinical effect on treating depression. Based on the reports on the determination of the content of hypericin in the Huang Ning ning granules, in this paper, HPLC method was used to determine the content, which provided a new basis for quality analysis, evaluation and control.

2. State of the art

2.1. Clinical study of Chinese medicine in the treatment of depression

Traditional Chinese medicine (TCM) is an important part of Chinese traditional culture. Traditional Chinese medicine a very influential and valuable subject at home and abroad and it has been extensively studied [10]. Chinese medicine is a kind of medicine which is produced under the guidance of the basic theory of traditional medicine with a wide application, and it has played an important role to cure various diseases and human health in the whole world, and it has made

outstanding contributions [11]. Because of its unique curative effect, mechanism of action and therapeutic effect, more and more attention has been paid to the study of medicine at home and abroad.

At present, the main treatment of depression is drug therapy with Western medicine, SSRI classic antidepressants as the main medicine. However, the drug cost is high, the effect is slow, and there are some side effects. Some people are not suitable for the treatment of Western medicine. In this case, traditional Chinese medicine or acupuncture can be used to treat the disease and to reverse the development of the disease.

For patients with self-mutilation or even suicidal tendencies with major depression, taking a slower onset of Western medicine can increase the risk and it may delay the treatment of the last period. High medical expenses also let many patients give up treatment. Therefore, the key to the development of new drugs is the ability to solve the problem of timeliness and rapid onset.

In clinical application, it is found that the yellow flower has sedative and hypnotic effect, so it has a series of clinical research. The results show that the yellow flower has a better effect of sleep calming, and it may improve the quality of sleep. And there are no greater adverse reactions with fewer side effects, which have a good guiding role in clinical medication. The flower of silk tree albizzia belongs to the leguminous plant, and the taste is good. It can be found that the flower can play a role in relieving depression. Flowers can be used for the treatment of depression, insomnia and other symptoms. The extract of the flower of silk tree albizzia was found to have the function of resisting depression and hypnosis. Glycyrrhizin has obvious antidepressant effect, and its mechanism is to reduce the probability of BV2 cell death induced by glutamate injury. In the study on the pharmaceutical composition of liquiritia glycyrrhiza, it is found that most of the antidepressant drugs in Glycyrrhiza are flavonoids. Therefore, the antidepressant effect of flavonoids is one of the important references for current drug screening. In the clinical treatment, the patient has a certain improvement in the short term after taking Acorus calamus. With continuous administration of the drug, the patient's mental state will be significantly improved as well as better quality of sleep. Rhizoma cyperi belongs to Cyperus sedges, and it has a bitter taste. It has the effect of soothing the liver and relieving depression. In the analysis of TCM syndrome of depression, liver qi stagnation is an important cause of depression. Therefore, Rhizoma cyperi can treat on liver qi stagnation in clinical. After the drug composition analysis of Rhizoma Cyperi, it is found that the main component is the same kind of brass. In addition, it has includes the carrier of saponins. This not only can play a neuroprotective role in anti-oxidation, but also has important pharmacological effects of anti-allergy and reducing blood sugar, with mechanism of increasing the content of DA and Cyperus 5-HT. Shengdi belongs to Scrophulariaceae Rehmannia injection, and its water extract has a protective effect on organisms. Its function is to protect the brain tissue of rats, and can promote the repair of nerve function. Turmeric belongs to Zingiberaceae plants, and it can improve the sport level of depressive rats effectively, including vertical movement and horizontal movement level, and reduce consumption of sugar, which has verified the antidepressant effects of turmeric.

2.2. Study on Chinese medicine preparation

Chinese medicine has made good progress in the treatment of depression, and it also has played a positive role in guiding clinical medication. After a number of repeated rigorous clinical studies, it has confirmed the support of compound drugs in the treatment of depression has a better clinical effect: multiple targets, rapid onset, less side effects, especially in the regulation of neural plasticity and inflammation. Therefore, it is of great significance to explore the active ingredients of traditional Chinese medicine and the prescription of Chinese herbal medicines in the comprehensive understanding of the role of Chinese medicine in the treatment of depression.

Most of the traditional Chinese medicine is based on decoction. The decoction is in accordance with a certain proportion of all kinds of water and medicine in the prescription were mixed, and then after a certain time of boiling. It is not easy to carry, not easy to store, less suitable for the crowd, which limits the widespread use of Chinese herbal medicine decoction.

Huanghua Ningshen granule is a kind of dry extract granule of Chinese traditional medicine extract, which is developed by extraction, concentration, drying and so on. Compared with the decoction, the preparation process is simple, easy to carry and store, providing convenience for most patients. This solves a series of problems caused by the limitation of the conditions, which is more applicable to the crowd and greatly promotes the popularization.

3. Methodology

3.1. Instrument

The main experimental instruments used in this study are as follows: Ultimate 3000 high performance liquid chromatography system, purchased from the United States Diane; Electronic balance, bought from METTLER & TOLEDO instruments Shanghai Co.; The constant temperature water bath box and chromatography analysis platform of Tianjin Test Instruments Company; Ultrasonic cleaning machine of Kunshan, Shanghai.

3.2. Selection of extraction methods

In this study, three methods of extracting hypericin were selected, and the extraction efficiency was compared in the same time. Hot ethanol reflux extraction: To accurately weigh the amount of the Huanghua Ningshen granules. After crushing and screening, 1g was added to the flask of 50 ml. 25 ml of 70 % ethanol was refluxed for 1 h and the loss of 70 % ethanol was made up for fully shaking. After filtration, the former 2 ml filtrate was discarded. Then following 2 ml filtrate was added to the 10 ml flask. Finally, 70 % ethanol was added to the scale and shade well to complete the extraction process.

Ultrasonic concussion: To accurately weigh the amount of the Huanghua Ning-

shen particles. After crushing and screening, 1 g was added to the flask of 50 ml. 25 ml of 70 % ethanol was weighed for 20 min of ultrasonic treatment. After the completion of the ultrasound, it was put with natural cooling to room temperature. Then the loss of 70 % ethanol was made up for fully shaking. After filtration, the former 2 ml filtrate was discarded. Then following 2 ml filtrate was added to the 10 ml flask. Finally, 70 % ethanol was added to the scale and shade well to complete the extraction process.

Soxhlet extraction method: To accurately weigh the amount of the Huanghua Ningshen particles. After crushing and screening, 1 g was added to a Soxhlet extractor. 25 ml of 70 % ethanol was refluxed for 1 h and the loss of 70 % ethanol was made up for fully shaking. After filtration, the former 2 ml filtrate was discarded. Then following 2 ml filtrate was added to the 10 ml flask. Finally, 70 % ethanol was added to the scale and shade well to complete the extraction process.

3.3. Chromatographic condition

Fortisil-C18 chromatographic column (4.6 mm×250 mm, 5 μm), 40 °C as the column temperature, flow rate of 1 ml/min, the sample volume of 10 μL. The mobile phase of acetonitrile (A) - 0.2 % phosphoric acid (B) was used for gradient elution. The detection wavelength was 360 nm.

The hypericin comparative sample in Huanghua Ningshen granules was accurately weighed. The sample obtained was dissolved by methanol, and the solution of 0.5 mg/ml was obtained. The 1 g sample powder was precisely weighed and added to the flask with 25 ml of 70 % ethanol solution after No. 3 sieve filtration. Then the total weight was recorded. It was carried out with water bath heating reflux for 45 min, and put at the room temperature for 1 h. Weigh again, and use 70 % ethanol to make up for the loss of weight. After fully mixed and filtration by 0.45 μm membrane, the filtrate was the prepared sample solution. The reference solutions respectively 0.1, 0.2, 0.5, 1, 2, 4, 8 ml was put into 7 flasks of 10 ml. They were diluted with 70 % ethanol to the scale, shade well, and added to high performance liquid chromatography to determine its peak area. The peak area of the sample was the ordinate, the sample volume was the abscissa, and the linear regression was used to obtain the linear concentration range and correlation coefficient r.

3.4. Precision test and stability test

With precision weigh of Huanghua Ningshen God granules for crushing and screening, the same sample was tested for 6 times under the same chromatographic conditions. According to the measured peak area of hypericin, we could determine whether it met the requirements. Similarly, with the same sample, different time points were measured. This study selected 0, 2, 4, 8, 16 h for test, according to the measured peak area of hypericin to determine whether to meet the requirements.

Take about 0.5 g granules with the known concentration, taking 6 pieces. The sample solution was prepared by adding the reference solution of 0.4 ml, and added to the liquid chromatograph. The peak area was determined, and the recovery rate

was calculated according to the established conditions. The results showed that the average recovery rate was 99.43 % and RSD was about 0.94 %, which was in line with the requirements. In this paper, the sample solution using 0.2 g granules was prepared according to the method described in this paper. 20 µl was added to the liquid chromatography column, and the content of hypericin was determined according to the optimized chromatographic conditions.

4. Result analysis and discussion

4.1. The established of the HPLC method to analyze the results

The results showed that the extraction efficiency of hot ethanol reflux had the highest in the same extraction time. In this paper, the hot ethanol reflux and the HPLC method was used for the determination of the content of hypericin in the granules, and the main instrument was Ultimate 3000 high performance liquid chromatography (Fig. 1). The chromatographic conditions could be used to measure the separation of the peaks of the hypericin and other components in the granules (Fig. 2), which showed a good linear relationship in the range of 2.5–50.0 µg ml^{-1} (Table 1). The recovery was 99.43 % and for RSD see (Table 2). Therefore, the method established in this paper could be used to determine the content of hypericin.

Fig. 1. Diane ultimate high performance liquid chromatography system

Table 1. The linear analysis of the hypericin content in the granules

Component	Regression equation	Correlation coefficient	Linear range (mg/ml)
Hypericin	$y = 0.5134x - 0.4612$	0.9991	0.66–67.00

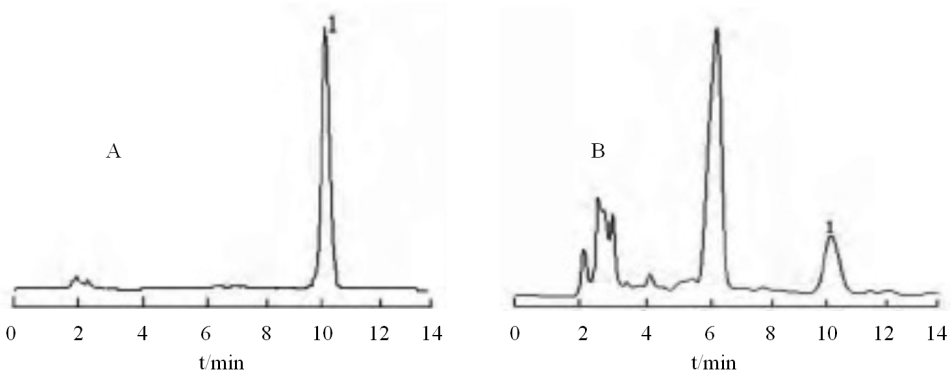

Fig. 2. HPLC chromatogram (A: hypericin reference product; B: sample; 1: hypericin)

Table 2. The results of the recovery of Hypericum in the granules

Component	Sample weight (mg)	Sample content (mg)	Addition amount (mg)	Measured quantity (mg)	Rate of recovery (%)	Average recovery (%)	RSD (%)
Hypericin	0.5021	0.3364	0.3350	0.6681	99.58	9.43	0.94
	0.5053	0.3367	0.3350	0.6781	99.49		
	0.5019	0.3379	0.3350	0.6693	99.14		
	0.5037	0.3372	0.3350	0.6721	99.34		
	0.5042	0.3352	0.3350	0.6737	99.94		
	0.5007	0.3382	0.3350	0.6601	99.05		

4.2. Determination of the content of Hypericum in Huanghua Ningshen granules

According to the established chromatographic conditions, the solution of the sample was analyzed, and the content of hypericin was determined.

Table 3. Results of the determination of the content of hypericin

No.	Content of hypericin (%)	Average concent	RSD (%)
1	0.35	0.35	0.97
2	0.33		
3	0.35		
4	0.36		
5	0.35		

5. Conclusion

At present, the treatment of depression is mainly based on drug treatment of Western medicine with SSRI classic antidepressant drugs. But the drug is expensive, slow onset and there are large side effects. Chinese medicine has made good progress in the treatment of depression, and has played a positive role in guiding clinical medication. Repeated rigorous clinical studies have confirmed the good clinical effect of compound medicine to support in anti-depression, multi targets, fast acting, less side effects, especially played an important role in the process of clinical neural plasticity and neural regulation of inflammation (Chaki 2003) [15]. Therefore, closely combining the basic theoretical knowledge of Chinese medicine, rich clinical experience, advanced technology and the latest application of neural science and biology to carry out the systematic research to multiple templates between multiple disciplines will promote the whole society can more in-depth understand the clinical value and scientific connotation of traditional Chinese medicine compound preparation in the treatment of depression.

In this study, the sample was extracted with 70 % ethanol and then determined by Ultimate high performance liquid chromatography (HPLC) system. The operation was very simple and reliable with short operation time. With acetonitrile (A) - 0.2 % phosphoric acid (B) as mobile phase for gradient elution, the peak separation effect was good, and the hypericin could be separated from other miscellaneous peaks obviously. In the process of detection wavelength, the maximum absorption peak could be detected by the 360 nm wavelength, and the lowest degree of interference of the magazine could be guaranteed. There was a good linear relationship in the range of 2.5–50.0 $\mu g\,ml^{-1}$. The recovery was 99.43 %, and RSD was 0.94 %. After repeated experiments, it was found that the method used in this study was accurate and reliable, which could provide a new basis for quality analysis, evaluation and control.

References

[1] V. L. Feigin, G. A. Roth, M. Naghavi, P. Parmar, R. Krishnamurthi, S. Chugh, G. A. Mensah, B. Norrving, I. Shiue, M. Ng, K. Estep, K. Cercy, C. J. L. Murray, M. H. Forouzanfar *Global burden of stroke and risk factors in 188 countries, during 1990–2013: A systematic analysis for the Global Burden of Disease Study 2013.* The Lancet Neurology *52* (2016), No. 9, 913–924.

[2] S. Z. Langer: *α_2-Adrenoceptors in the treatment of major neuropsychiatric disorders.* Trends in pharmacological sciences *36* (2015), No. 4, 196–202.

[3] S. Bhavsar, A. Sarkar, R. Ram, P. Pithadia, J. P. Mehta, D. Parmar: *Lifestyle practices related to health promotion among adult males in urban areas of Jamnagar city, Gujarat.* Journal of Research in Medical and Dental Science *1* (2013), No. 2, 36–39.

[4] H. I. Kuo, W. Paulus, G. Batsikadze, A. Jamil, M. F. Kuo, M. A. Nitsche: *Acute and chronic effects of noradrenergic enhancement on transcranial direct current stimulation-induced neuroplasticity in humans.* The Journal of physiology *595* (2017), No. 4, 1305–1314.

[5] T. Guo, Y. T. Xiang, L. Xiao, C. Q. Hu, H. F. Chiu, G. S. Ungvari,

C. U. Correll, K. Y. Lai, L. Feng, Y. Geng, Y. Feng, G. Wang: *Measurement-based care versus standard care for major depression: a randomized controlled trial with blind raters.* American Journal of Psychiatry *172* (2015), No. 10, 1004–1013.

[6] T. H. Chao, P. K. Fu, C. H. Chang, S. N. Chang, F. C. Mao, C. H. Lin: *Prescription patterns of Chinese herbal products for post-surgery colon cancer patients in Taiwan.* Journal of Ethnopharmacology *155* (2014), No. 1, 702–708.

[7] Y. Guo, J. Zhu, X. Su, J. Yang, Y. Li, Q. Wang, W. Wei: *Efficacy of Chinese herbal medicine in functional dyspepsia: A meta-analysis of randomized, double-blind, placebo-controlled trials.* Journal of Traditional Chinese Medical Sciences *3* (2016), No. 3, 147–156.

[8] S. S. Qu, Y. Huang, Z. J. Zhang, J. Q. Chen, R. Y. Lin, C. Q. Wang, G. L. Li, H. K. Wong, C. H. Zhao, J. Y. Pan, S. C. Guo, Y. C. Zhang: *A 6-week randomized controlled trial with 4-week follow-up of acupuncture combined with paroxetine in patients with major depressive disorder.* Journal of Psychiatric Research *47* (2013), No. 6, 726–732.

[9] S. C. Man, B. H. Huang, R. M. Ng, X. C. Yu, H. Cheung, M. P. M. Fung, L. S. W. Li, Kei P. Leung, Kwok P. Leung, K. W. Y. Tsang, E. Ziea, V. T. Wong, Z. J. Zhang: *A pilot controlled trial of a combination of dense cranial electroacupuncture stimulation and body acupuncture for post-stroke depression.* BMC Complementary and Alternative Medicine *19* (2014), No. 14, paper 255.

[10] R. Y. Wu, D. D. Zhu, Y. C. Xia, H. S. Wang, W. W. Tao, W. D. Xue, B. M. Xia, L. Ren, X. Zhou, G. C. Li, G. Chen: *A role of Yueju in fast-onset antidepressant action on major depressive disorder and serum BDNF expression: a randomly double-blind, fluoxetine-adjunct, placebo-controlled, pilot clinical study.* Neuropsychiatric Disease and Treatment *11* (2015), 2013–2021.

[11] M. J. Ramaker, S. C. Dulawa: *Identifying fast-onset antidepressants using rodent models.* Molecular Psychiatry *22* (2017), No. 5, 656–665.

Received October 10, 2017

Acta Technica *62* No. 2B/2017, 703–712

Dielectric properties of single layer pyrrole coated fabric based on polypyrrole absorbing mechanism

Liu Xiaolan[1], Duan Zhonghang[1], Lu Guizhen[2]

Abstract. Single layer pyrrole coated fabrics based on the absorbing mechanism of polypyrrole play an active role in the absorption of electromagnetic radiation of electronic products. In this study, the doping ratio model of dopant that has great influence on the dielectric properties of polypyrrole absorbing materials was studied. The morphology and dielectric properties of microwave absorbing materials with different mixing modes were compared. The results show that when the ratio of dopant/monomer is 0.1, the absorbing efficiency is the best, and the suitable dopant in the absorbing material is CBDS. The purpose of this study is to provide theoretical basis and technical support for further research.

Key words. Polypyrrole, absorbing wave, single layer pyrrole coated fabric, dielectric properties.

1. Introduction

With the development of the times, the current world has begun to enter the "electronic products" era. The development of computers, mobile phones and other household appliances has brought great fun and convenience to people's life, and has gradually brought positive impetus to the development of the world. The development of the electronic equipment has gradually become an important trend in the development of the times. However, some discordant phenomena are further revealed. With the increasing number of electronic equipment, the electromagnetic radiation caused by electronic products is gradually becoming more and more serious. Many studies suggest that some electronic radiation generated by electronic products not only brings certain restriction and negative influence to the operation and progress of other subsidiary electronic equipment, but also does harm to people's health. In this study, we mainly study the dielectric properties of single layer pyrrole coated fabric based on the mechanism of polypyrrole absorbing wave, ana-

[1]Information Engineering School, Communication University of China, Beijing, 100024, China

lyze and discuss the advantages of the whole electronic industry and industry. The purpose of the research is to provide a theoretical basis and scientific support for the development of new type of absorbing materials.

2. State of the art

Under the theme of new era development, electronic information technology has gradually become an important innovation technology in the new era. The development of these technologies has brought a lot of modern electronic equipment for many enterprises and industries, and it has also provided a positive impetus for the development of related industries [1]. However, the rapid development of the electronic equipment has also brought a series of problems such as electromagnetic pollution. Many researchers in different fields have studied the electromagnetic radiation and pollution. They think that if people are in the environment of electromagnetic radiation for a long time, they may have a series of diseases and variations such as tumor. Moreover, the development of some advanced electromagnetic weapons also poses certain threats to the security and environment, ecology and ecological balance in some areas [2]. Therefore, how to better solve this series of electromagnetic pollution problems has gradually become an important research topic of all countries in the world. In order to better to solve these problems, many researchers begin looking for related materials with a better absorbing performance, and analyze related properties of these materials, so as to obtain the relevant materials that can deal with electromagnetic pollution. Single layer pyrrole coated fabrics based on polypyrrole wave absorption mechanism have better dielectric properties [3]. Therefore, the study of this material has gradually become the main subject of study. The main effect of this kind of wave absorbing material is that it has certain electromagnetic absorption and treatment efficiency. It has gradually be applied in medical, military and other related industries, which has brought a positive and effective role in promoting the development of these industries. At the same time, absorbing materials with stronger wave absorbing efficiency and cost performance have also been gradually developed and applied to the actual production and life [4].

2.1. Methodology

The study on the current single pyrrole coated fabrics based on the mechanism of polypyrrole absorption was analyzed. Different morphologies of wave absorbing agents were prepared by using different preparation methods. Polypyrrole was prepared by using different materials in the study. The effect of these factors on the wave absorbing efficiency of the absorbing materials was determined by different proportioning methods and different production schemes [5]. The optimization of the related manufacturing process is to provide a theoretical basis and scientific support for the further study of related materials, and to provide a certain guarantee for the ecological balance and people's health in China. The main materials and methods of this study are as follows:

The experimental reagents used in this study were mainly used for the preparation

of wave absorbing agents doped with polypyrrole. The main reagents are shown in Table 1.

Table 1. Main reagents used in this experiment

Reagent name	Purity	Production company
Pyrrole (Py)	CP	Sinopharm Chemical Reagent Co., Ltd.
Ferric chloride chloride ($FeCl_36H_2O$)	AP	Wuhan Huashun Biotechnology Co., Ltd.
Twelve sodium alkylbenzene sulfonate (SDBS)	AP	Beijing Aoboxing Biotechnology Co., Ltd.
Two (2-hexyl) sodium sulfosuccinate (AOT-Na)	AP	Tianjin Kermel Chemical Reagent Co., Ltd.
Sodium p-toluene sulfonate (pTSNa)	AP	Sinopharm Chemical Reagent Co., Ltd.
Camphor sulfonic acid (CSA)	AP	Sinopharm Chemical Reagent Co., Ltd.
Absolute ethanol (C_3H_3OH)	AP	Dongli Tianjin Tyrande Chemical Reagent Factory

First of all, a certain volume of deionized water was prepared before the preparation of polypyrrole absorbing material. The amount of 0.01 mol substance was doped into the sterilized deionized water of 100 ml, and a magnetic stirrer was used to mix the solution until a relatively stable milky liquid was formed. A pyrrole drug with the amount of 0.05 mol was added to a relatively stable emulsion. It was mixed using magnetic mixer, added into the three-flask, and placed at 0 °C to control the temperature of the solution. After the preparation of the mixed solution was complete, the deionized water solution mixed with ferric chloride was slowly dripped into the prepared mixed liquid with a gel dropper, and placed in a quiet state for about 6 hours. When the reaction state was stable, a certain amount of acetone was added to react. The final state was washed by deionized water until all the reaction systems exhibited a colorless and transparent state. The final reaction system was placed in a vacuum drying chamber of 60 °C for drying treatment. The dried product was grinded until it reached the powder state, so as to obtain the final polypyrrole (Cho, et al. 2014) [6]. In this study, polypyrrole without addition of any dopant was used as a control group. Samples of polypyrrole with different modes and ratios were obtained by adding different dopants. The related samples are shown in Table 2.

In this study, the infrared spectra of the samples related to polypyrrole based on different dopants were firstly determined by infrared spectrophotometer. In the determination of samples, the sample preparation was mainly dependent on the tabletting method. The wavelength range of the infrared spectrophotometer used can reach about 4000–400 cm^{-1}, so that it has a more reliable measurement accuracy [7].

Table 2. Labeling of polypyrrole samples doped with different dopants

Sample number	PPy-1	PPy-2	PPy-3	PPy-4	PPy-5	PPy-6	PPy-7	PPy-8
Dopant	$FeCl_3$	AOT-Na	SDBS	CSA	pTSNa	SDBS	SDBS	SDBS
Dopant/ monomer	0.1	0.1	0.1	0.1	0.1	0.2	0.4	1.0

The product of certain weight polypyrrole products was measured by elemental analyzer and X-ray technique, so as to ensure that there was no experimental deviation in the obtained polypyrrole product due to nonstandard experimental operation. In addition, it can provide certain protection and support for the accuracy improvement of follow-up related characteristics (Andrade, et al. 2014) [8].

On the basis of analyzing the external characteristics of polypyrrole products by using related software, the absorbing property of the polypyrrole was calculated and analyzed (Luo et al. 2013) [9]. In this study, the reflection coefficients of the wave absorbing agents at different ratios and times were calculated. The formula is

$$\Gamma = \frac{Z - Z_0}{Z + Z_0},\ Z = \sqrt{\frac{\mu_r}{\varepsilon_r}},\ Z_0 = \sqrt{\frac{\mu_0}{\varepsilon_0}}\,, \tag{1}$$

where, Z_0 stands for the characteristic impedance properties of different absorbing materials in relatively free space, Z represents the normalized value of characteristic impedance properties of some absorbing materials. The dielectric constant and permeability of the wave absorbing materials with different mixing ratio and different configuration time were calculated [10]. The main formulas are

$$\varepsilon_r = \varepsilon_r' - \mathrm{j}\varepsilon_r''\,, \tag{2}$$

$$\mu_r = \mu_r' - \mathrm{j}\mu_r''\,, \tag{3}$$

where, ε_r and μ_r represent the dielectric constant and magnetic permeability of various absorbing materials, respectively, ε_r' and $varepsilon_r''$ represent the variable values and loss measurements of some absorbing materials, respectively, μ_r' and μ_r'' represent the magnetization variables and loss measurements of some absorbing materials, respectively. On the basis of the calculation of the correlation characteristics, the tangent of the dielectric loss angle δ of various absorbing materials with different mixing ratio and different configuration time was calculated.

The relevant formulas are as follows:

$$\tan\delta = \tan\delta_\varepsilon + \tan\delta_\mu = \varepsilon''/\varepsilon' + \mu''/\mu'\,, \tag{4}$$

where, δ_ε and δ_μ show hysteresis in each absorbing material compared with the applied electric field and magnetic field. Therefore, only when the tan value shows a relatively large value can the further confirmation of this kind of absorbing mate-

rial be made. Compared with other absorbing materials, it has stronger absorbing properties [11].

Finally, the absorption properties of different dopants and different modes were compared and analyzed by means of the acquisition and calculation of related parameters, so as to provide theoretical basis and technical support for the study of absorbing materials with relatively high wave absorbing efficiency.

3. Result analysis and discussion

With China's reform and opening up, China's various industries and fields have made great progress and development. Electronic equipment industry, as one of the most important technologies in the development of the times, is very important to the development of our country's industry. With the increasing proportion of China's investment in this field and industry, China's electronic equipment industry has already been developed in the world. However, the development of electronic equipment has posed a certain threat to the environment, ecological balance and health of our country. At present, China has gradually become aware of the risk of electronic radiation caused by electronic equipment, and the main way to solve this threat is to use some wave absorbing materials. Today, China has achieved some achievements in the study of related absorbing materials, and has made great progress in the use of related materials in various industries. The research and development of microwave absorbing materials and the gradual increase of frequency make our country begin to increase the development of related technologies (Fig. 1). In the absorbing materials, the main factor affecting the wave absorbing strength of materials is the selection of wave absorbing agents. How to better improve the performance of the absorbing material not only studies the selection of wave absorbing agents, but also needs to study and design all aspects of the overall properties and state of the related absorbers in the entire material. Therefore, the research and future trends of absorbing properties of materials in our country are mainly aimed at the following aspects:

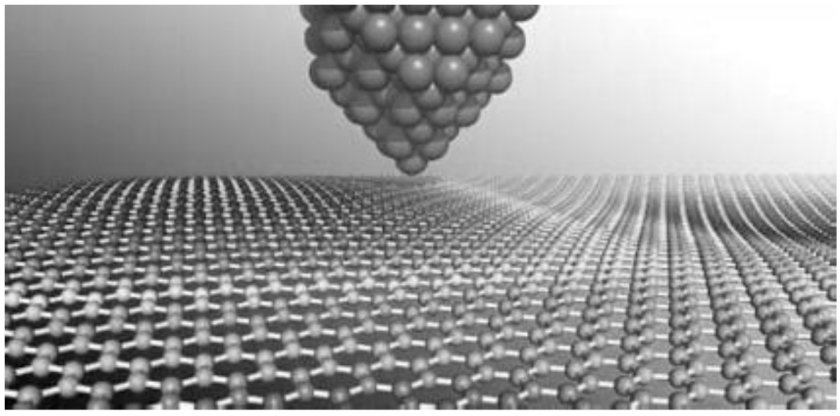

Fig. 1. Development of polypyrrole absorbing materials

For the main absorbers for absorbing materials already used in our country, we should further optimize the main characteristics of the relevant material and improve the related properties of the whole wave absorbing material through the relevant treatment methods to improve the absorbing material for absorbing electromagnetic radiation based on the analysis and comparison of its performance.

The characteristics of all used wave absorbers are analyzed. The microwave absorbing agents with strong wave absorbing property can be synthesized and used to make them perform their unique properties and advantages, and then form a new wave absorbing composite. The use of related materials is not only a single use of a material, but more complex forms of "1+1>2".

We should continue to develop some new wave absorbing materials and wave absorbers with stronger wave absorbing efficiency. Nano wave absorbing materials, which have been gradually developed and used in the current era, can be used as follow-up research contents. Many industries in our country have begun to introduce new ideas and apply them to the real estate industry. These new wave absorbing materials can obviously reduce the overall conductivity of the whole wave absorbing material, and further optimize the overall wave absorption structure, so as to better absorb the electromagnetic radiation. As a result, emerging materials, if used properly, may have stronger wave absorbing effectiveness.

On the basis of a thorough understanding of the development trend of polypyrrole absorbing materials, it is believed that the absorbing properties of materials and the morphology and size of absorbing material is related more closely by reading the relevant literature (Fig. 2). With the gradual development of processing technology, now in the design of related wave absorbing materials, usually the shape and size are specifically designed. The usual methods of manufacture include hard template method and soft template method. In the fabrication of the template method, it is usually classified according to the position of the absorber of polypyrrole. Some polypyrrole materials may grow on the inner side of the template. In this case, the method is often referred to as the inner template. Some may grow on the outer side of the entire template space, which is called the outer side. Two different template methods have their respective advantages and disadvantages. Therefore, after considering the size of the absorbing materials and their design materials and the future scope of the application, the two template methods are chosen to improve the microwave absorbing properties of the whole wave absorbing material. Because the hard template method has relatively tedious steps in the removal process of the template, it makes the whole production process of absorbing materials limited, which may affect the subsequent material absorbing efficiency. Under this trend, the soft template method has been gradually researched and produced. This method not only takes advantage of the hard template method, but also avoids the process of template removal, which makes the production process of the related wave absorbing materials show a more efficient trend. In this study, the polypyrrole absorbing material is designed by the soft template method.

On the basis of understanding and understanding of the related theories, this study designed and fabricated the absorbing products and materials of polypyrrole by different ratio methods. The main external morphologies and related character-

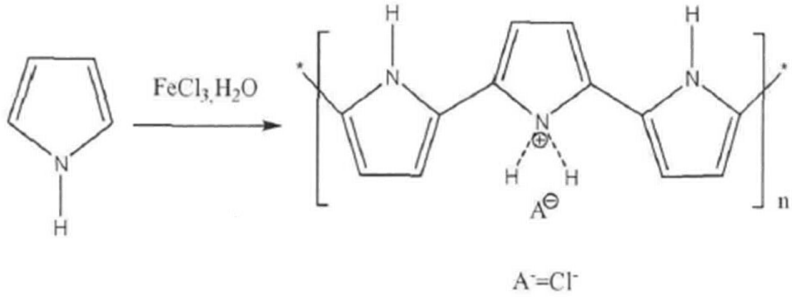

Fig. 2. Schematic diagram of the preparation of polypyrrole (soft template method, taking $FeCl_3$ as an example)

istics were analyzed by various techniques. The results are as follows.

Firstly, the ratio of dopant and monomer was studied. In this study, the wavelength of polypyrrole absorbing material under different ratios was analyzed by using infrared spectrophotometer and X-ray technique. The results are shown in Fig.3. Among them, a, b, c, d and e represented the ratio of the dopant and monomer for 0, 0.1, 0.2, 0.3 and 0.4, respectively. The results showed that when the ratio was 0.1, which was b spectrum, the spectrum peak value was higher compared to other energy state, which could be considered as the best ratio. This was also similar to the ratio scheme used in this study. The result of infrared spectrum analysis also showed that it was difficult to observe the vibration peak when the doping degree was relatively high. Therefore, the preparation of polypyrrole absorbing material was difficult to choose with relatively high doping degree.

The elemental composition of the polypyrrole absorbing materials with different doping levels was analyzed by elemental analyzer. The results are shown in Table 3. The results showed that the conductivity of the absorbing material was relatively high when the dopant ratio was low because a lower proportion of dopants had a positive effect on the flow of electrons. When the dopant ratio was high, it might hinder the electron flow and further reduce its absorbing capacity.

Table 3. Elemental analysis of polypyrrole with different doping levels

No.	SDBS/Py	Component				S/N	Conductivity (S/m)
		C	H	O	N		
PPy-3	0.1	57.86	5.37	13.09	2.76	0.21	9.07
PPy-6	0.2	60.09	5.99	11.36	3.49	0.31	4.98
PPy-7	0.4	61.07	5.34	10.54	4.49	0.43	3.91
PPy-8	1.0	66.49	7.11	9.19	5.64	0.61	0.93

The conductivity of polypyrrole absorbing materials with different dopant modes was calculated. The results are shown in Table 4. The results showed that the conductivity decreased and the wave absorbing efficiency decreased with the increase

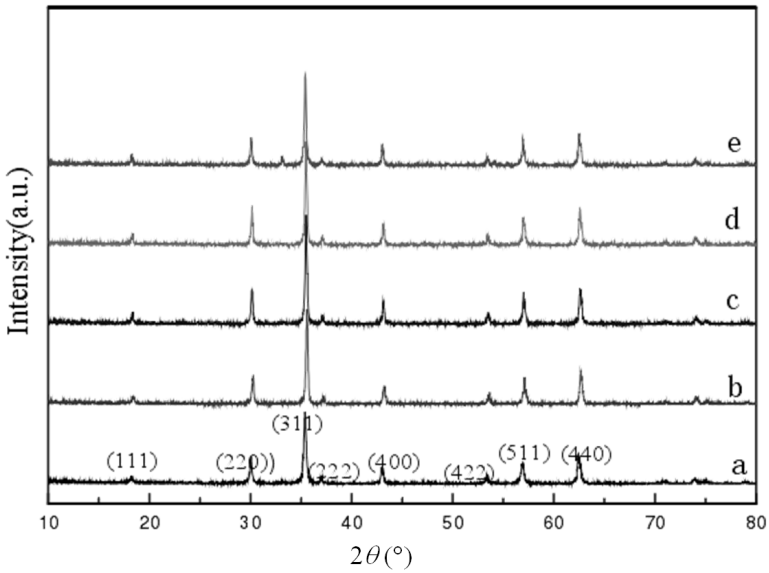

Fig. 3. X-ray diffraction patterns of polypyrrole absorbing materials with different doping ratios

of dopant ratio. However, the conductivity of the polypyrrole absorbing materials made by different dopants was also different. When SDBS was used as dopant, the conductivity of the absorbing material was the highest and the wave absorbing efficiency was the strongest.

Table 4. Conductivity of polypyrrole samples doped with different dopants

No.	PPy-1	PPy-2	PPy-3	PPy-4	PPy-5	PPy-6	PPy-7	PPy-8
Conductivity	2.70	9.44	9.07	3.21	4.98	4.98	3.91	0.93

4. Conclusion

With the development of the times, now the emergence of computers and other electronic products have brought great convenience for people's production and life, which has played a certain driving significance for people's industry and economic development. However, in the trend of the rapid development of electronic products, some uncoordinated phenomena are further exposed. For example, when working or using electronic products, they may cause a series of hazards such as electromagnetic radiation, which have a negative impact on human health and ecological balance. For this problem, a better solution is to do the preparation of some absorbing materials. The absorbing materials based on the principle of polypyrrole absorbing wave have begun to attract more and more attention, and have achieved a certain degree of

progress and development. Under this trend, our country has begun to increase the study of wave absorbing materials. In this study, the mixing modes of dopant factors which have the greatest influence on dielectric properties of absorbing materials were compared and analyzed. The morphology and dielectric properties of microwave absorbing materials with different mixing modes were compared. The appropriate ratio and dopant were determined. The purpose of the study is to provide theoretical basis and technical support for follow-up studies. In this study, only the important factors have been analyzed, and there are some defects. However, it can provide technical support for the development of subsequent absorbing materials.

References

[1] E. Koposova, X. Liu, A. Kisner, Y. Ermolenko, G. Shumilova, A. Offenhäusser, Y. Mourzina: *Bioelectrochemical systems with oleylamine-stabilized gold nanostructures and horseradish peroxidase for hydrogen peroxide sensor*. Biosensors and bioelectronics *57* (2014), 54–58.

[2] Z. Mosleh, P. Kameli, A. Poorbaferani, M. Ranjbar, H. Salamati: *Structural, magnetic and microwave absorption properties of Ce-doped barium hexaferrite*. Journal of Magnetism and Magnetic Materials *397* (2016), 101–107.

[3] M. Tahara, M. Okubo: *Detection of free radicals produced by a pulsed electrohydraulic discharge using electron spin resonance*. Journal of Electrostatics *72* (2014), 222–227.

[4] A. V. Ivanshin, O. T. Litvinova, A. A. Sukhanov, N. A. Ivanshin, S. Jia, S. L. Bud'ko, P. C. Canfield: *Dual nature of electron spin resonance in $YbCo_2Zn_{20}$ intermetallic compound*. JETP Letters *99* (2014), No. 3, 153–157.

[5] K. Ishii, S. Terauchi, R. Murakami, J. V. Swain, R. Mutoh, H. Mino, K. Maki, T. Arata, M. Ishiura: *Site-directed spin labeling-electron spin resonance mapping of the residues of cyanobacterial clock protein KaiA that are affected by KaiA–KaiC interaction*. Genes to Cells *19* (2014), No. TOC4, 297–324.

[6] C. Cho, D. Y. Lee, J. S. Bae, S. Park: *Crossover of uniaxial magnetic anisotropy direction mediated by interfacial strain of $CoFe_2O_4$ films*. Journal of Magnetism and Magnetic Materials *368* (2014), No. 24, 149–154.

[7] S. Pourbafarani: *The effect of alkali concentration on the structural and magnetic properties of Mn-Ferrite nanoparticles prepared via the coprecipitation method*.Metallurgical and Materials Transactions A *45* (2014), No. 10, 4535–4537.

[8] J. M. Marín, Y. A. Rojas, G. A. P. Alcázar, B. Cruz, M. H. M. Barreto: *Effect of sintering conditions on the magnetic and structural properties of $Fe_{0.6}Mn_{0.1}Al_{0.3}$ synthesized by mechanical alloying*. Hyperfine Interactions *224* (2014), Nos. 1–3, 35–42.

[9] Z. Luo, H. Jiang, J. Jiang, W. Rhodes: *Synthesis of cerium-doped Gd3(Al,Ga)5O12 powder for ceramic scintillators with ultrasonic-assisted chemical coprecipitation method*. Journal of the American Ceramic Society *96* (2013), No. 10, 3038–3041.

[10] X. Yang, Q. Jin, Z. Chen, Q. L. Li, B. Liu: *Fabrication and microwave absorbent properties of Cobate zinc substituted W-type $BaCoZnFe_{16}O_{27}$*. Journal of Magnetism and Magnetic Materials *367* (2014), No. 46, 64–68.

[11] M. Khairy: *Polyaniline-Zn 0.2Mn 0.8Fe_2O_4 ferrite core-shell composite: Preparation, characterization and properties*. Journal of Alloys and Compounds *608* (2014), No. 12, 283–291.

Received October 10, 2017

Acta Technica *62* No. 2B/2017, 713–722

Dynamic analysis method of voltage stability in power system based on power flow betweenness[1]

Li Ting[1]

Abstract. With the rapid development of power system technology, power system represented by large power grid, large generator unit, long distance and high voltage has become the direction of the future development of power system. Under this background, a method for dynamic analysis of power system voltage stability based on power flow betweenness was proposed in this paper. The common fault analysis methods of power system were expounded in detail; then, the power flow system was simulated by the method of power flow betweenness; finally, the IEEE39 node system was used to validate the method. The results show that the power flow betweenness of the key nodes in the power system can reflect the possible problems in the power system under the influence of voltage and other factors.

Key words. Power system, voltage, power flow betweenness, fault simulation.

1. Introduction

The operation of modern society cannot be separated from the support of energy. Natural gas, oil and electricity are among the most common sources of energy in the society [1]. With the emergence of environmental protection problems, the use of natural resources, such as oil and natural gas, has gradually been limited. Electric energy has been widely used in social production and life. In particular, water, wind, solar, geothermal and other power generation methods are not only environmentally friendly, but also provide a continuous supply of energy for the normal functioning of human society [2]. As a result, electric energy is used more and more widely in current social production and life [3].

At present, large power grid, large unit, long distance and high voltage are the main directions of the development of power technology [4]. These technologies are of great importance to the current energy demand and ecological environment protection, but they bring great problems as well as positive tendency [5]. These

[1]Department of Electrical Engineering, Guang Xi Technological College of Machinery and Electricity, Guangxi, Nanning, 530007, China

new technologies pose a major challenge to the safety of power grid systems. For example, the increase of power supply and the limit of power grid have also begun to disturb the power system. Therefore, how to maintain the safe operation of power grid system has become the main research direction in the field of power [6]. In this context, a method for dynamic analysis of power system voltage stability based on power flow betweenness is proposed, which provides a reference for power system operation.

2. State of the art

In power systems, faults are often caused by voltage problems. When the power system fails, it will affect a considerable range of production and life. Therefore, how to judge the fault of power system has become the main problem of power system [7]. In the past, the power system fault diagnosis includes two kinds of computation models: unauthorized topology and weighted topology. The calculation method is similar to the betweenness calculation of communication network in information technology. However, it is built on the shortest route propagation of power flow, which is a fatal flaw. Therefore, the application of the two models has great limitations [8]. Therefore, according to the characteristics of power flow propagation in power grid based on Kirchhoff's law, an electrical betweenness model is designed. The model is more close to the actual situation of power flow propagation [9].

In the electrical betweenness model, the premise of the betweenness is that the power grid is undirected weighted network [10]. Although the electrical betweenness model is more close to the physical characteristics of the power grid than the two models of unauthorized topology and weighted topology, there are some defects in the model [11]. In the model of electrical betweenness, many problems such as the mode of operation of power system, the direction of power flow, the reactive power of grid and the voltage of power grid are not in the model of electrical betweenness. Therefore, there are many problems and defects in the calculation process. The stability research of power system has been continuously improved by many experts and scholars.

3. Methodology

3.1. Calculation of power flow betweenness in power system nodes

In the research of power system stability, from the earliest unauthorized topology and weighted topological model to the electrical betweenness model, the related technology and theory have been constantly changing and improving. However, there are still some defects and problems in these methods. For example, the electrical betweenness model that is closest to the physical characteristics of the power system has considered problems, such as voltage problems in power systems. Therefore, in the study with the method of dynamic analysis of power system voltage stability

based on power flow betweenness, the calculation of AC model is added to the calculation of the electrical betweenness model. In other words, when calculating the betweenness of power system, the method of power flow calculation is adopted. The problem of stability of each node in power system is measured by power flow vectors, so as to judge the possible problems and the faults in power system. Nodes in power systems can be divided into three types of power generation, load and connection according to their nature. Supposing that the power flow betweenness of a node n is $B_f(n)$, the following formula can be used to express it:

$$B_f(n) = \sum_{i \in G. j \in L} \sqrt{W_i W_j} P_{ij}(n) . \tag{1}$$

Here, G and L in the above formula represent the set of two nodes of the generator and the load, respectively, and (i, j) represents all the "power-load" pairs in the power system. Index i represents the generator node, and index j represents the load node. Symbols W_i and W_j, respectively, represent the weight of the two nodes of power generation and load, and the weight represents the importance of the two nodes of power generation and load in the power system. Finally, $P_{ij}(n)$ represents the active power on the node n in the power system. The power flow betweenness of the power system is basically the same as that of the other betweenness indexes. That is to say, it can reflect the situation of power flow occupancy nodes in the whole power system by quantizing. But the power flow betweenness has more advantages in reflecting the voltage, power flow direction and operation mode of power system.

Before calculating the power flow betweenness of the whole power system, it is necessary to determine the active power flow between the power generation and load, and the power flow path between the two. This process can be achieved by tracing the flow. Fig. 1 shows the flow calculation process.

The whole calculation process is divided into six steps. The power flow needs to be calculated according to the basic parameters of the power system. Therefore, before the power flow calculation, the basic parameters of the whole power system should be determined. The first step of the power flow calculation is to calculate the AC flow in the power system by using the Newton-Raphson method. According to the calculation results, the power loss and the charging power of the whole power system are judged, and the magnitude and direction of the power flow in all the lines of the power system are determined.

In the second step, the power flow direction of the power system is judged according to the first step, and the power loss in each loop of the power system is incorporated into the power flow terminal node by the equivalent load. The charging power in the grid is incorporated into the nodes at both ends of the line in the same way.

The third step is to determine the shunt ratio of each node in the power system. Supposing that the injection power is for node i in the whole power system, the calculation method of the shunt ratio $K_{j,i}$ at the node J is as follows.

$$K_{j,i} = \frac{S_{O,j}}{\sum_{j=1}^{N} S_{O,j}} . \tag{2}$$

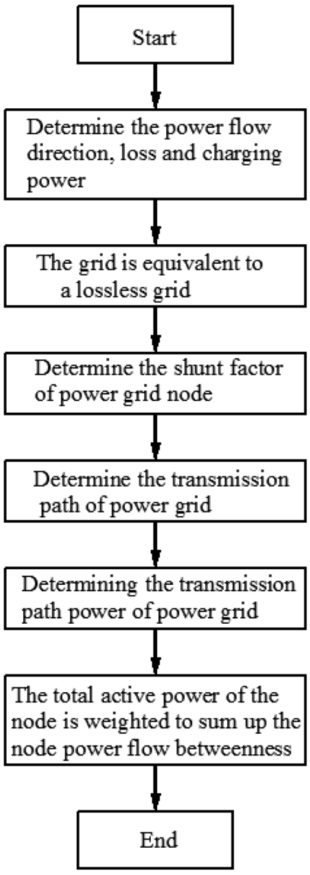

Fig. 1. Calculation procedure of power flow betweenness

In the above formula, $S_{O,j}$ represents the active power flowing out of the circuit system node J, M represents the number of injected power branches associated with the node, and N represents the number of branches that flow out at the node position.

The fourth step is to search the whole load node of the whole power grid from the starting point of the power system, which is the generator node, along the direction of the power flow, and to determine the transmission path between the two.

The fifth step starts from the initial node, calculates the load allocation of all generators in the power grid according to the results obtained in the third step, and then determines the power in each transmission path of the grid. Assuming that the transmission branch is i, the formula for the allocation $S_{j,i}$ of the injected power at the Jth branch is

$$S_{j,i} = K_{j,i} S_{I,i} \,. \tag{3}$$

Here, $K_{j,i}$ in the above formula is the allocation factor of third steps, and $S_{I,i}$ represents the active power injected on the ith branch.

The sixth step is to sum up all the active power of the nodes, and finally get all the power flow betweenness of the node. Through the power flow betweenness of the node, the fault of the node can be determined.

3.2. Power grid simulation based on power flow betweenness

After defining the calculation method and procedure of power flow betweenness, power system based on power flow betweenness is simulated in this paper. The simulation also considers the voltage of the grid in the power system as a whole. The possible problems in the whole power system are judged by simulation. In the process of power flow simulation based on power flow betweenness, the optimal load shedding model is adopted in this paper. The model can be expressed in the formulas.

$$\min C_{\mathrm{p}} = \sum_{i \in N} C_{\mathrm{p}i}\,, \tag{4}$$

$$\begin{cases} P_{\mathrm{g}i} - P_{\mathrm{d}i} - U_i \sum U_j \left(G_{ij}\cos\theta_{ij} + B_{ij}\sin\theta_{ij}\right) = 0, \\ Q_{\mathrm{g}i} - Q_{\mathrm{d}i} - U_i \sum U_j \left(G_{ij}\sin\theta_{ij} - B_{ij}\sin\theta_{ij}\right) = 0, \\ \left(P_{\mathrm{d}i} - C_{\mathrm{p}i}\right) / \left(Q_{\mathrm{d}i} - C_{\mathrm{q}i}\right) = P_{\mathrm{d}i}/Q_{\mathrm{d}i}, \\ P_{\mathrm{g}i}\min \le P_{\mathrm{g}i} \le P_{\mathrm{g}i,\max}, Q_{\mathrm{g}i,\min} \le Q_{\mathrm{g}i} \le Q_{\mathrm{g}i,\max}, \\ U_{i,\min} \le U_i \le U_{i,\max} \\ 0 \le C_{\mathrm{p}i} \le P_{\mathrm{d}i}, 0 \le C_{\mathrm{q}i} \le Q_{\mathrm{d}i}, \\ P_{ij}^2 + Q_{ij}^2 \le T_{ij,\max}^2. \end{cases} \tag{5}$$

In formula (4), $_{\mathrm{p}i}$ represents the total load shedding for each load node in the grid and $_{\mathrm{p}i}$ represents the reduction of the active load at the node i. In formula (5), $P_{\mathrm{g}i}$ and $P_{\mathrm{d}i}$ represent the active power and active load at the node, $Q_{\mathrm{g}i}$ and B_{ij} represent the reactive power generation and reactive power load, $C_{\mathrm{q}i}$ represents the reactive load curtailment of the node i, G_{ij} and B_{ij} represent the real and imaginary parts of the element at the row i and column j of the admittance matrix, P_{ij} and Q_{ij} represent the active power and reactive power on the power network branch$i-j$, $P_{\mathrm{g}i,\max}$ and $Q_{\mathrm{g}i,\max}$ indicate the active power upper limit of the starting node (generator) i and the upper limit of reactive power output, $P_{\mathrm{g}i,\min}$ and $Q_{\mathrm{g}i,\min}$ represent the active power lower limit of the starting node (generator) i and the lower limit of reactive power output, $\theta_{ij} = \theta_i - \theta_j$ represents the difference of the phase angle at the two ends of the branch $i-j$, and $T_{ij,\max}$ represents the rated capacity of the branch $i-j$. The constraints in the formula are the constraints of node active power, reactive power, and the constant power factor before and after the load shedding, the output range of the generator set, the upper and lower limits of the node voltage, the node clipping load and the power flow of the grid lines.

4. Result analysis and discussion

In order to verify the applicability of power flow simulation method based on power flow betweenness, IEEE39 node system is used in this paper to verify. The degree of node in power system has a great influence on the fault of power system. If the degree of the node is relatively high, the number of transmission paths through the node will be relatively more, and the power flow betweenness will be relatively large. Fig. 2 shows the statistics of the cumulative distribution of the power flow betweenness in the IEEE39 node system. As can be seen from the diagram, the power flow betweenness is relatively high among several critical nodes in the IEEE39 node system. According to the statistical results, the nodes with more than 50 of the power flow account for only 6.79 % of the IEEE39 node system. The results show that the power flow node can reflect the importance of nodes in the power system. The voltage of these parts should be paid more attention to, and then the possible faults in the power system are warned in advance. In addition to these small number of key nodes, nearly 80 % of the node's power flow betweenness is between 0–30, which shows that the voltage concerns of these nodes can be lower than those of the critical nodes.

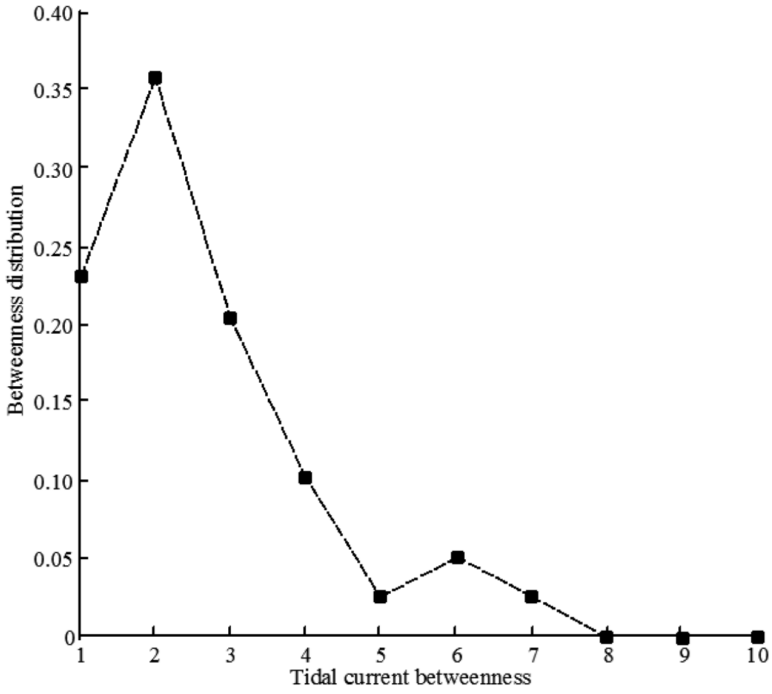

Fig. 2. Statistical analysis of power flow betweenness of power grid node

Table 1 shows the statistical results of the influence of the removal of nodes with different power flow betweenness on cascading failures. From the statistics in the table, it can be seen that in the simulation of power system faults based on power

flow betweenness, the overall load shedding after power system failures is small. This kind of results can reflect the actual situation of power system more than the simple electric betweenness. The main reason for the results is that the power flow direction and the voltage of the power system are taken into account in the calculation of the flow betweenness. In other words, the power flow betweenness combines the actual conditions of the voltage of the power system, which can reflect the possible problems of power system more practically. The results also show that the voltage is larger when the flow is larger, and the contact node has a greater impact on the power system.

Table 1. Influence of different betweenness on power system faults

Node number	Betweenness sorting	Tidal current betweenness	Percentage of minimum load loss	node number	Betweenness sorting	Tidal current betweenness	Percentage of minimum load loss
1	30	10.17	1.66	21	19	16.70	11.01
2	17	19.85	0.21	22	9	29.36	13.22
3	28	12.00	5.15	23	15	20.69	11.54
4	8	32.15	8.00	24	24	14.32	13.34
5	4	46.02	10.36	25	20	16.60	6.82
6	1	66.60	26.64	26	31	8.94	5.01
7	16	20.53	3.74	27	34	7.60	10.99
8	6	34.51	8.35	28	36	6.40	3.29
9	39	2.85	0.10	29	25	12.77	8.42
10	2	50.57	7.19	30	32	8.04	5.80
11	11	28.30	10.02	31	5	38.43	5.97
12	37	5.33	0.14	32	3	50.57	3.59
13	14	22.26	8.82	33	13	26.74	10.47
14	22	16.10	9.29	34	38	5.08	7.49
15	18	18.63	18.99	35	10	29.36	9.02
16	7	32.96	14.09	36	33	8.03	9.11
17	27	12.15	12.52	37	212	16.60	2.75
18	29	10.80	6.65	38	26	12.77	32.60
19	12	26.74	17.90	39	35	7.47	17.65

Figure 3 shows the influence of margin coefficients on power system failures. When the power system fails due to voltage or other reasons, the effect on other nodes in the power system is mainly determined by the betweenness threshold of the nodes.

As can be seen from Fig.3, with the increase of the margin coefficient of different tidal currents, the percentage of minimum load loss in power system shows a downward trend. Moreover, for different fault nodes, when the margin factor is greater than 1.7, the minimum percentage of loss between the three essentially assumes a linear state, i.e., the percentage of minimum load loss is no longer changing. The results show that the power system is sensitive to single node faults when the margin coefficient is lower due to voltage and other reasons. With the increase of the margin coefficient, the resistance of the power system to the fault is improved to a certain extent.

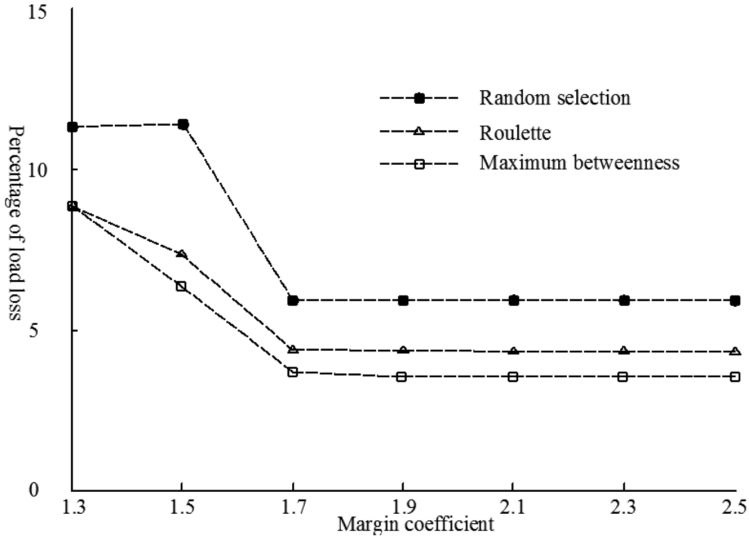

Fig. 3. Influence of margin coefficient on power system failure

5. Conclusion

With the increasing awareness of environmental protection, the application of fossil fuels represented by oil and natural gas in the production and life of human society has been more and more limited. Clean energy, such as power energy, has gradually been favored by all countries, and has been vigorously developed. However, electric power has many defects and problems while satisfying the requirements of human society for environmental protection. Therefore, in this context, the dynamic analysis method of voltage stability in power system was proposed in this paper. Various nodes in the power system were calculated by the power flow betweenness and the actual voltage in the power system. The influence of voltage and other factors on the fault of power system was analyzed by calculating the results. The method was validated by IEEE39 node system. The verification results show that the key nodes in the power system have the greatest impact on the power system, such as voltage and other factors. Therefore, the voltage of these nodes should be paid more attention to ensure the normal operation of the power system.

References

[1] A. Morandi: *State of the art of superconducting fault current limiters and their application to the electric power system.* Physica C: Superconductivity *484* (2013), 242–247.

[2] M. Q. Suo, Y. P. Li, G. H. Huang, D. L. Deng, Y. F. Li: *Electric power system planning under uncertainty using inexact inventory nonlinear programming method.* Journal of Environmental Informatics *22* (2013), No. 1, 49–67.

[3] R. A. Bakkiyaraj, N. Kumarappan: *Optimal reliability planning for a composite electric power system based on Monte Carlo simulation using particle swarm optimization.* International Journal of Electrical Power & Energy Systems *47* (2013), 109–116.

[4] R. M. M. Pereira, C. M. M. Ferreira, F. P. M. Barbosa: *Comparative study of STATCOM and SVC performance on dynamic voltage collapse of an electric power system with wind generation.* IEEE Latin America Transactions *12* (2014), No. 2, 138–145.

[5] D. Malagueta, A. Szklo, R. Soria, R. Dutra, R. Schaeffer, B. S. M. C. Borba: *Potential and impacts of Concentrated Solar Power (CSP) integration in the Brazilian electric power system.* Renewable Energy *68* (2014), 223–235.

[6] H. C. Jo, S. K. Joo, K. Lee: *Optimal Placement of Superconducting Fault Current Limiters (SFCLs) for protection of an electric power system with Distributed Generations (DGs).* IEEE Transactions on Applied Superconductivity *23* (2013), No. 3, paper 5600304.

[7] D. Malagueta, A. Szklo, B. S. M. C. Borba, R. Soria, R. Aragão, R. Dutra, R. Schaeffer: *Assessing incentive policies for integrating centralized solar power generation in the Brazilian electric power system.* Energy Policy *59* (2013), 198–212.

[8] M. Ghasemi, S. Ghavidel, M. M. Ghanbarian: *Multi-objective optimal electric power planning in the power system using Gaussian bare-bones imperialist competitive algorithm.* Information Sciences *294* (2015), 286–304.

[9] E. Kötter, L. Schneider, F. Sehnke: *The future electric power system: Impact of Power-to-Gas by interacting with other renewable energy components.* Journal of Energy Storage *5* (2016), 113–119.

[10] M. Stua: *Evidence of the clean development mechanism impact on the Chinese electric power system's low-carbon transition.* Energy Policy *62* (2013), 1309–1319.

[11] Y. Huang, Z. H. Yu, C. Xie, X. Zhou: *Study on the application of electric power big data technology in power system simulation.* Proceedings of the CSEE *35* (2015), No. 1, 13–22.

Received October 10, 2017

Acta Technica *62* No. 2B/2017, 723–732

Feature extraction of pulse wave signal[1]

Xu Yan[2,4], Chang Rui[2], Yue Zhanwei[3], Lv Lingling[2], Xu Xiaokun[2]

Abstract. Nowadays cardiovascular disease has become "the number one killer" of human life and health. Most of the clinical diagnosis is invasive means, in which the patients have pain without real-time monitoring. Aiming at the problems of pulse wave in the diagnosis of cardiovascular diseases, the method of pulse wave time domain and frequency domain analysis was used in this paper. The parameters related to coronary heart disease were found out from the characteristic parameters by the feature recognition technology, which were used to establish the identification model. And the simple parameter report was associated with the disease diagnosis. For the first time, the complex parameter–wavelet entropy analysis method was introduced into the field of pulse wave feature detection.

Key words. Pulse wave, wavelet transform, fuzzy recognition.

1. Introduction

The vascular system of the human body is a whole body composed of heart, blood vessels and blood. Under the condition of mutual coordination and restriction and the control of the central nervous system, the whole process of blood circulation is completed. The pulse signal is generated by the heart beat to push blood along the blood vessels. Therefore, according to the modern scientific viewpoint, the pulse signal can be regarded as the output and mapping of the internal motion of the heart in the human body (Wang et al. 2002) [1]. The pulse wave is mainly formed by the contraction and relaxation of the heart and the interaction of various resistances along the blood vessels. So when the pulse wave spreads from the heart to the arterial system, it is not only affected by the heart itself, but also affected by various physiological factors, such as vascular resistance and blood vessel wall

[1]The work presented in this paper is supported by natural science foundation of China (No. U1604148).

[2]School of Electric Power, North China University of Water Resources and Electric Power, Zhengzhou 450045, Henan, China

[3]Operation Company, Zhengzhou Metro, Zhengzhou 450000, Henan,China

[4]Corresponding author; e-mail: 605973249@qq.com

elasticity. Therefore, the pulse wave signal contains a great deal of physiological and pathological information of cardiovascular system. The waveform characteristics and harmonic information of pulse wave are closely related to the change of characteristic parameters in the cardiovascular system (Qiao et al. 2000) [2]. There is a close relationship between traditional Chinese medicine pulse and Waveform shape of pulse wave. Over the years, researchers have made great achievements in the non-invasive diagnosis of cardiovascular diseases by exploiting the relationship between physiological parameters such as pulse wave parameters and pathology, and summarized a large number of parameters related to cardiovascular disease in time domain and frequency domain. However, there are a large number of parameters, and an effective evaluation criteria is needed for which parameters are more relevant to cardiovascular pathology (Mollet et al. 2005) [3]. It is difficult to understand the relation between the single parameter and the physiological information with poor systematicness, which can only provide single index evaluation and no disease diagnosis. All these problems make the application of research results in hospital clinic and patients' daily health care subject to a certain degree of limitation (Yang et al. 2002) [4]. In addition, the research on the characteristic parameters of pulse wave in time and frequency domain is very large, so it is necessary to develop new research ideas (Wang et al. 2001) [5].

2. State of the art

In 1775, the famous Swiss mathematician Euler studied quantitatively the law of pulse wave propagation in human body for the first time. Since then, it has been one of the most important problems in the field of biomechanics and biomedicine to detect the information of human pulse system and establish the dynamic model of human cardiovascular system [6–8]. For the first time, Erasistratos found that the pulse was a kind of wave propagation. However, because of the lack of the concept of blood circulation, it was also very superficial understanding of the pulse. He believed that the blood from the heart contracts pushed forward the blood column in the blood vessel, which was the periodic expansion of the blood vessels and the "driving" theory. Until the beginning of seventeenth century, British physician Harvey first discovered and recognized the phenomenon of blood circulation. In 1775, Leonard Eular first gave the governing equations describing the flow of incompressible ideal fluid in an elastic tube. Since then, people had been really starting to develop a correct description of the pulse system. Thomas Young, Ernst Heinrich Weber, Korteweg, Lamb, Witzig and others had improved and obtained different pulse wave velocity formula in different cases. In 1898, Otto Frank proposed a quantitative model of the artery as an elastic cavity. The elastic cavity model gave a better approximation of the pressure and flow waves in the large arteries. The modern analysis of pulse wave propagation began in 1950s. During 1950s to 1970s, the most representative researchers included Womersley, Mc Donald, Bergel, Fung and Gang Xiaotian. They established a linearized model of the pulse wave in the arterial segment, developed the Windkessel model and discussed he law of pulsatile flow on the basis of this. Cox et al. extended the thin wall model used by Womersley to the

case of finite thickness wall, which made the results more likely to correspond to the actual arterial wall [9–11].

3. Methodology

3.1. The relationship between pulse wave and cardiovascular disease

The resistance to cardiac ejection is composed of two parts: non pulsatile components and pulsatile components. The former is peripheral resistance, while the latter is produced by the effects of arterial compliance and reflected waves. When arterial stiffness increases, due to speed up and reflection points of pulse wave velocity to near the heart, reflected wave appeared earlier in the systolic pressure curve, which increased systolic blood pressure and pulse pressure, reduced diastolic pressure, resulting in increased left ventricular afterload and easily leading to left ventricular hypertrophy. Because the coronary blood supply mainly depends on the diastolic pressure and the length of diastole, diastolic blood pressure lowering can lead to coronary hypoperfusion. Increased left ventricular afterload causes an increase in left ventricular oxygen demand, and perfusion of the left ventricle is decreased due to coronary insufficiency. Both of the two can aggravate myocardial ischemia and hypoxia, resulting in ischemic heart disease. In fact, it has been shown that the increase of aortic stiffness, reflex wave and pulse pressure in patients with essential hypertension is closely related to left ventricular hypertrophy in patients. Atherosclerosis can change the pulse wave transmission and reflection, causing systolic hypertension. Therefore, it can be inferred that the abnormal reflex wave caused by arterial dysfunction is an important risk factor for cardiovascular disease.

3.2. Selection of characteristic points of pulse wave signal

Human pulse wave is generally considered to have 6 characteristic points, as shown in Fig. .1. Point b1 is the opening point of aortic valve, point c1 is the highest systolic pressure point, point d is the aortic dilation pressure point, point e is the starting point of left ventricular diastolic, point f is the starting point of anti-tidal wave, and point g is the highest pressure point of the anti-tidal wave. They reflect different states of the cardiovascular system.

In the analysis of the experimental results, through the analysis of the relationship between the characteristics of the points, the difference between patients and normal people is compared. Based on the recognition of pulse feature point, we define the index as shown in Fig. 2. The left one is the measurement of the amplitude and time interval of the pulse, and the right is the measurement for the parameters of the pulse area.

Each index is as follows: h_1 is primary wave amplitude (mm), h_2 is the amplitude of the pre-pulse wave (mm), h_3 is the lower middle lobe amplitude (mm), h_4 is pulse wave amplitude (mm), t_1 is the time from the beginning of the main wave to the peak of the main wave (ms), t_2 is the time from the beginning of the main wave to

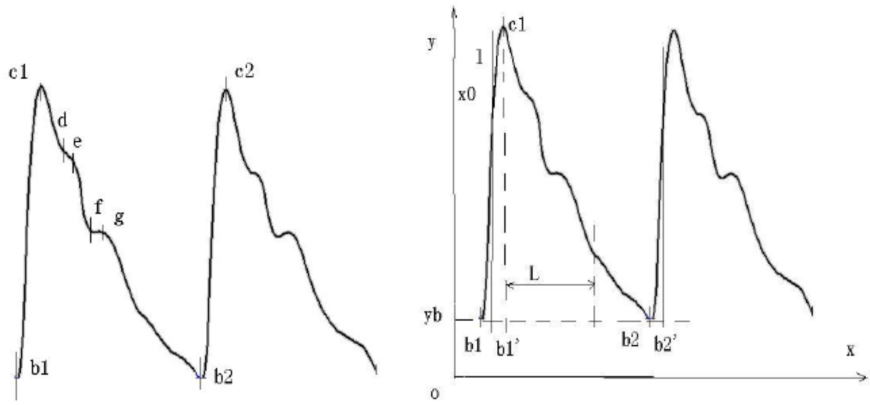

Fig. 1. The six characteristic points of pulse wave and the reference map

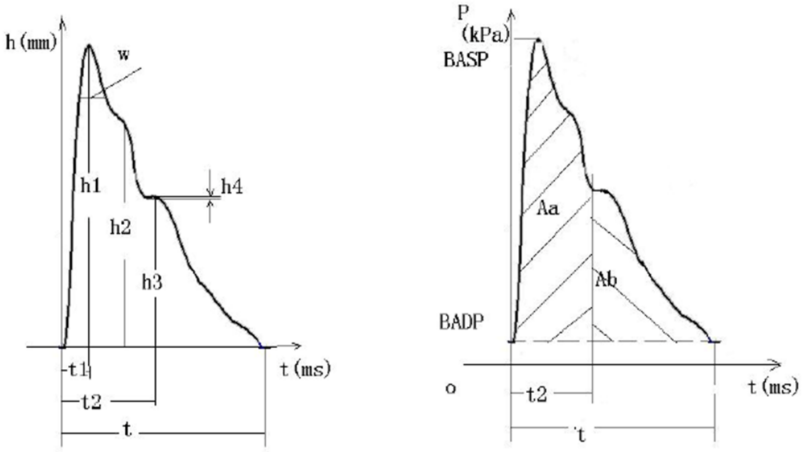

Fig. 2. Side view of pulse wave index

the bottom of the Canyon (ms), t is pulse cycle time (ms), A_a denotes the systolic area of pulse graph, and A_b denotes the diastolic area of pulse graph.

The vertical distance from the highest point to the baseline is set to h_1, and the feature normalization highly correlated with the time domain waveform of the pulse wave is h_2/h_1, h_3/h_1, and h_4/h_1, respectively. Similarly, a pulsation cycle time t is set to 1, and the time related parameters are normalized to t_2/t and t_1/t. The total area $A_\mathrm{a} + A_\mathrm{b}$ of the pulse wave time domain waveform is set to 1, so the area related parameters can be normalized to area $A_\mathrm{a}/(A_\mathrm{a} + A_\mathrm{b})$.

3.3. Study on fuzzy pattern recognition using genetic algorithm

From any initial population of genetic algorithm, populations evolve from generation to generation for better areas until the optimal solution with the genetic operations of selection, crossover and mutation. Because of its inherent parallelism and not easy to fall into local optimum, it is very suitable for large scale space search optimization. The first step: input control parameters: population size P, crossover probability C, and mutation probability M.

The second step: the initial population G is generated randomly, and the fitness of each individual in the population and the total fitness of the population are calculated.

The third step: genetic operators (that is, selection, crossover, mutation) are used to produce a new generation G of groups, and calculate individual fitness, in order to evaluate the individual.

The fourth step: convergence condition judgment. If the average fitness difference of adjacent generations is less than a threshold ε or the specified evolution algebra is completed, the search is terminated. According to the fitness, the results are sorted by the individual, and the highest fitness value is selected as the optimal solution. Otherwise, turn to the third step.

4. Result analysis and discussion

4.1. Experimental method

From April 2007 to June 2007, form patients in the Second Department of Cardiology, the Second Affiliated Hospital of Tianjin University of Traditional Chinese Medicine, and sixty eligible patients were selected and included in this study. There were 30 cases in the control group and the others in the control group. The test instrument was calibrated before the measurement. The subjects' name, sex, height, weight and other basic parameters were input into the computer. The subjects sat for 15 minutes before the test. The instrument was used to record the pulse wave of the left wrist of the tested person and save into the computer. Patients for echocardiographic measurements should be given a brief rest before the examination to avoid tension and activity affecting blood flow velocity. Echocardiography included two-dimensional, M type and Doppler echocardiography, with probe frequency of 2.5 MHz.

4.2. Verification of time domain feature recognition model of pulse wave

In this paper, the fitness function of genetic algorithm optimization was Fisher criterion function. According to the definition of Fisher criterion function, the feature selection program of the Matlab genetic algorithm was compiled, and the Fisher criterion function was returned. The criterion was that if the value of Fisher crite-

rion function was more than 0.5, it was considered as feature selection; otherwise, it would be removed out. As shown in Table 1, the Fisher criterion function values returned by each parameter for parameters feature selection of the pulse wave time domain were listed.

Table 1. Fisher criterion function of time domain parameter

h_2/h_1	h_3/h_1	h_4/h_1	t_1/t	t_2/t	$A_a/(A_a + A_b)$
0.9355	0.7942	0.9669	0.602	0.4733	0.6595

According to the results of the above table, we could see that, in addition to t_2/t, other parameters were up to the selection criteria, which could be used as the selected parameters of the next model training. The model test results are shown in Fig. 3.

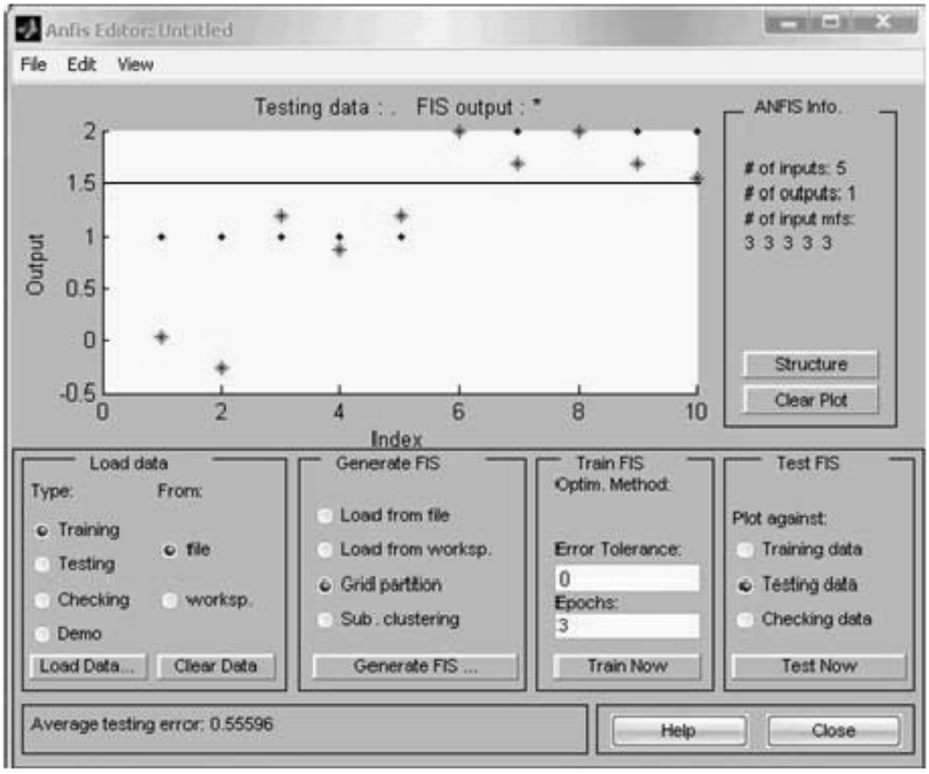

Fig. 3. Test results of fuzzy recognition model

Set the results of the classification threshold: the patient classification code was set to 1, and the normal classification code was set to 2. In the results of the model training, if the test sample classification code identification was less than 1.5, the sample was more close to category 1; if more than 1.5, the sample was more close

to category 2.

5. Verification of frequency domain feature recognition model of pulse wave

In this paper, the fitness function of genetic algorithm optimization was Fisher criterion function. According to the definition of Fisher criterion function, the feature selection program of the Matlab genetic algorithm was compiled, and the Fisher criterion function was returned. The criterion was that if the value of Fisher criterion function was more than 0.5, it was considered as feature selection; otherwise, it would be removed out. As shown in Table 2, the Fisher criterion function values returned by each parameter for parameters feature selection of the pulse wave frequency domain were listed.

Table 2. Fisher criterion function of frequency domain parameter

Pera6	Pera5	Pera4	Pera3	Pera2	Pera1	we
0.4057	0.5678	0.6458	0.9159	0.9862	0.6049	0.9781

According to the results of Table 2, we could see that all parameters except the pulse wave frequency domain Pera6 achieved the optimization criteria, which could be used as the parameters of the next model training. The Fisher criterion function value of Perd3, Perd2 and we was the largest, which indicated that the spectral energy of the pulse wave signal in the interval of the pulse wave frequency range of 5–20Hz was smaller than that of the pulse wave signal, known as wavelet entropy. The pathological features of the patients with obvious coronary heart disease and normal subjects were included.

Table 3 showed the coordinates of the center of gravity of each category in space. After the calculation of the specific coordinates of each observation and their distance from the center of gravity, we could determine their classification.

Table 3. Barycentric coordinates of each category (1 for patients with coronary heart disease, and 2 for normal persons)

Group	Function
1.00	–1.084
2.00	1.084

It could be seen from Table 3 that the correct rate of the recognition of coronal heart disease patients and normal persons was 83.3 % and 90 %, respectively. The results of cross validation showed that the pulse wave characteristic parameters could be used to distinguish between patients with coronary heart disease and normal subjects.

6. Verification of hybrid feature recognition model

The parameters of pulse wave frequency domain and time domain of 30 patients with coronary heart disease and 30 normal subjects were selected as the training samples. The marker variable group was used to divide them into two groups, namely, the coronal heart disease patients and the normal subjects. Table 4 shows the coordinates of the center of gravity of each class in space. As long as we could calculate the coordinates of each observation in the front and the distance from the center of gravity, we could know their classification.

Table 4. Barycentric coordinates of each category (1 for coronary heart disease, and 2 for normal persons)

Group	Function
1.00	–1.298
2.00	1.298

The results of the evaluation of the model performance by interactive verification were shown in Table 5.

Table 5. Correct classification of interactive verification)

Classification	Patients with coronary heart disease	Normal persons
Patients with coronary heart disease	80.0 %	20.0 %
Normal persons	16.7 %	83.3 %

It could be seen from Table 6 that the correct rate of the recognition of coronal heart disease patients and normal persons was 80 % and 83.3 %, respectively. The results of cross validation showed that the pulse wave characteristic parameters could be used to distinguish between patients with coronary heart disease and normal subjects.

6.1. Conclusion

In this paper, the method of pulse wave signal in time domain and frequency domain parameters identification of cardiovascular disease patients and normal persons was studied, which were mainly focused on the definition and selection of parameters of pulse wave in time domain and frequency domain, parameter optimization and the establishment of identification model. The clinical trial data as the basis of this research, the echocardiographic results of echocardiography and ECG results measured by multi lead ECG as the basis for clinical diagnosis of patients with coronary heart disease, the criteria for screening patients with coronary heart disease were as criteria for screening cases. Under the premise of this standard, the original pulse wave shape data of patients with coronary heart disease and normal people were collected, and the parameters of time and frequency domain were calculated.

The method of feature selection based on genetic algorithm was used to optimize the parameters of pulse wave. By setting the value of Fisher criterion function, the characteristic parameters of the return criterion function value less than 0.5 were removed. To some extent, the composition of the pulse wave characteristic parameters was optimized, which laid a good foundation for the establishment of the model. This method was suitable for feature selection with a large number of feature parameters. In this paper, genetic algorithm was introduced to optimize the parameters of human pulse wave information, which laid a foundation for future research work.

A preliminary study on the diagnosis of coronary heart disease by using the parameters of time and frequency of pulse wave and the establishment of the model of feature recognition was made in this paper. The results of this study achieved the primary objective of the theory. However, due to the problem of small sample size, the correction of the model and the improvement of the recognition accuracy needed to be further implemented. For the first time, the complexity parameter was introduced into the field of pulse wave analysis. However, there are many more analytical methods can be applied to the analysis of pulse wave signal, and further research is needed in the future research.

References

[1] J. M. Jornet, I. F. Akyildiz: *Femtosecond-long pulse-based modulation for terahertz band communication in nanonetworks.* IEEE Transactions on Communications *62* (2014), No. 5, 1742–1754.

[2] A. S. Liberson, J. S. Lillie, W. S. Day, D. A. Borkholder: *A physics based approach to the pulse wave velocity prediction in compliant arterial segments.* Journal of Biomechanics *49* (2016), No. 14, 3460–3466.

[3] X. Chen, J. Li, Z. Zhang, Y. Wang, Z. Jia, K. Pu, D. Yu: *A new algorithm for calculating optimal viewing angles in coronary angiography based on 4-D cardiac computed tomography.* Journal of X-ray science and technology *22* (2014), No. 2, 137–145.

[4] R. Singh, A. Khare: *Fusion of multimodal medical images using Daubechies complex wavelet transform–A multiresolution approach.* Information Fusion *19* (2014), 49–60.

[5] C. W. Chang, S. H. Wang, M. Y. Jan, W. K. Wang: *Effect of black tea consumption on radial blood pulse spectrum and cognitive health.* Complementary Therapies in Medicine *31* (2017), 1–7.

[6] U. R. Acharya, H. Fujita, V. K. Sudarshan, S. Bhat, J. E. W. Koh: *Application of entropies for automated diagnosis of epilepsy using EEG signals: A review.* Knowledge-Based Systems *88* (2015), 85–96.

[7] H. Xiao, I. Tan, M. Butlin, D. Li, A. P. Avolio: *Arterial viscoelasticity: Role in the dependency of pulse wave velocity on heart rate in conduit arteries.* American Journal of Physiology-Heart and Circulatory Physiology *312* (2017), No. 6, H1185–H1194.

[8] M. U. Qureshi, VG. D. A. Vaughan, C. Sainsbury: *Numerical simulation of blood flow and pressure drop in the pulmonary arterial and venous circulation.* Biomechanics and modeling in mechanobiology *13* (2014), No. 5, 1137–1154.

[9] X. Lu, G. V. Naidis, M. Laroussi, K. Ostrikov: *Guided ionization waves: Theory and experiments.* Physics Reports *540* (2014), No. 3, 123–166.

[10] D. Wang, D. Zhang, G. Lu: *A novel multichannel wrist pulse system with different sensor arrays.* IEEE Transactions on Instrumentation and Measurement *64* (2015), No. 7, 2020–2034.

[11] S. Y. Shin, E. B. Fauman, A. K. Petersen, J. Krumsiek, R. Santos, J. Huang, M. Arnold, I. Erte, V. Forgetta, T. P. Yang, K. Walter, C. Menni, L. Chen, L. Vasquez, A. M. Valdes, C. L. Hyde, V. Wang, D. Ziemek, P. Roberts, L. Xi, E. Grundberg, (MuTHER) Consortium, M. Waldenberger, J. B. Richards, R. P. Mohney, M. V. Milburn, S. l. John, J. Trimmer, F. J. Theis, J. P. Overington, K. Suhre, M. J. Brosnan, C. Gieger, G. Kastenmüller, T. D. Spector, N. Soranzo: *An atlas of genetic influences on human blood metabolites.* Nature genetics *46* (2014), 543–550.

Received October 10, 2017

Acta Technica *62* No. 2B/2017, 733–742

Mapping data acquisition and processing of hybrid small unmanned aerial vehicle (UAVs)

Chen Chen[1]

Abstract. Unmanned aerial vehicle (UAV) is becoming more and more popular and recognized, and it can be used in many situations, such as search, rescue, surveillance and mobile sensor networks. In this paper, the automatic analysis of moving objects was introduced to generate real-time road points for the design and implementation of the four-rotating machines that the continuous reconnaissance was interested in. The system was equipped with an autopilot that controlled flight and on-board image processors. The processor analyzed the image to create a real-time estimate of the target's direction and speed. An algorithm for creating flight plans from captured imaging data was described. In addition, an algorithm for generating optimal trajectories through position and yaw angle sequences was developed.

Key words. Hybrid power, small unmanned aerial vehicle (UAV), mapping, data acquisition, processing methods.

1. Introduction

UAV is becoming more and more popular and recognized, and it can be applied to many occasions, such as search, rescue, surveillance and mobile sensor networks [1]. UAVs currently used for military surveillance applications include MQ-9, Reaper, RQ-7, Shadow, and RQ-11 Raven [2]. These systems include aircraft with sensor packages and data links for transmitting sensor data to related ground stations. The aim is to provide combat personnel with almost real-time situational awareness of battlefield [3]. As of 2010, the United States Army has been more than 4000 unmanned aircraft systems, and more programs for developing military drones.

Current UAV system technology has been able to autonomously operate, including automatic takeoff and landing, or following flight plans. The ground control station (GCS) is used to receive data collected from the system and control the UAS [4]. The project aims to increase autonomy in the control of UAV Systems and reduce the workload of combat personnel [5]. The ability to automatically process

[1]Hebei University of Water Resources and Electric Engineering, Cangzhou, Hebei, China, 061001

UAS sensor data is a key function in urban environments or indoor operations. With the development of embedded system technology, sensor data can be processed on chip to determine the required motion for UAS [6]. This increases the degree of autonomy that the system can operate and allows the user to receive data without the need to control the UAS.

2. State of the art

Recently, with the advent of modern microcontrollers and advances in sensor technology, an upsurge in the design of four rotors has been brought about. Today, there are more and more suppliers and platforms in the machine market. The use and application of these platforms are being studied and extended [7]. Multi-users usually provide high flexibility at the expense of search scope. Multiple helicopters must have the lift generated by propellers, and they are dominated by the wings (such as fixed wing aircraft) [8]. A company in San Francisco aims to transport food through the use of multiple devices. These innovative platforms are also frequently used in some unexpected places [9].

Obtaining flight performance and aerodynamic data for small UAVs is a complex task because of UAV size constraints, weight constraints, and power limitations [10]. The integration of sensors and flight controllers is another issue. Most commercial drones have their own data acquisition systems. These systems usually include the inertial measurement unit (IMU) with six or ten degrees of freedom, GPS modules with dedicated uplink and downlink, pilot probe or ground control station (GCS) [11]. Small UAVs for research purposes are expensive, which is a complex task. There are many devices on the international market to monitor the flight performance of non-commercial UAVs. Low-cost flight data monitoring system has great research significance because most of the equipment is expensive.

2.1. Methodology

2.2. System architecture for UAVs

The first is the weight based airframe design that uses MathCAD to optimize the target weight of the four rotators. Manufacturers estimate that each engine produces about 1000 g of thrust combined with 8×4.3 propellers. Four motors provide a total of 4000 g of thrust to lift the fuselage. The manufacturer cannot obtain the torque curve, so four rotators are selected at a 45 % duty ratio. Autodesk Inventor is used to estimate the total weight of the components, calculate 1800 grams of thrust and give about 4 pounds of target weigh.

The picture of the investigated microdrone is in Fig. 1

The system contains an Arduino compatible GPS/GPRS/GSM module that is used to locate the drone's GPS capabilities. The compact IMU sensor SEN-00126 with ten degrees of freedom (10-DOF) is selected. The sensor is a combination of MPU9255 sensors and BMP180 sensors. The MPU9255 sensor can measure 9 inertial parameters: 3 axial angular accelerations, 3 axial gyroscopic motions (scroll,

Fig. 1. Microdrone md4-200 with a Ricoh GR3 compact camera

pitch and yaw), and 3 axial magnetic/Compass headings. The BMP180 is an atmospheric pressure sensor that measures airspeed in terms of pressure. Using IMU sensors instead of accelerometers alone, gyroscopes, magnetometers, and barometers can reduce circuit complexity, and consume less space and cost effectiveness. The Arduino SD card module is used as a data logger for transmitting data from various sensors and stored in SD cards. One of the most important goals of this research is to reduce costs rather than using expensive commercial data acquisition devices. Therefore, locally available and cost effective hardware is selected. Obtaining flight performance and aerodynamic data for small UAVs is a complex task because of UAV size constraints, weight constraints, and power limitations. The integration of sensors and flight controllers is another issue. Most commercial drones have their own data acquisition systems. These systems usually include the inertial measurement unit (IMU) with six or ten degrees of freedom, the GPS module with dedicated uplink and downlink, pilot probe or ground control station (GCS).

The drive uses the ArduCopter suite. The software set used by the autopilot is an open source project called ArduCopter (ArduCopter 2012). ArduCopter aims to create an easy to install and fly platform for multi-rotor UAVs. The project provides software for controlling helicopters in flight. The interface of RC receiver allows manual control and coverage. For debugging purposes, the Bluetooth link is used as a wireless serial data link to the ground station. ArduCopter is a popular project that receives regular updates from its developers. The version 2.0.48 is the latest version of APM. As of May 2012, the 2.5.5 version was widely used.

The open source projects are used for project design, and it provides a GUI interface to configure APM, monitor flight status, enter waypoints, analyze log files and change flight patterns. The software is used for functional testing APM, and loading firmware changes, which usually runs on the Windows desktop. Although Mono is running on other operating systems (Ardupilot itself uses program mono 2011 on the Ubuntu Linux), the scheduler cannot run on the development board under Linux.

The power distribution system must provide sufficient current for all critical flight components, so as to achieve a successful flight. The main power comes from two

12 V lithium polymer batteries. The capacity of each battery is 5000mAh, and the rated power is 200 A for continuous discharge. The main load on the system is four motors. The maximum current consumption of each motor is 28 A when it is stopped. The load generated by the four motors is 112 A, which can be easily handled by a single battery. The power from the battery is fed to the four electronic speed controllers (ESC) via the power switch. Each ESC can continuously supply up to 30 A of an electric motor with a voltage of 12 V. Each ESC also offers 2 A in 5 V, which powers the autopilot and image processor. The four ESCs together create a 5 V track capable of 8 A. The autopilot and image processor are small loads that consume 3 % of the total power. The autopilot receives the 5 V power from the ESC. The image processor is connected to the 5 V rail on the autopilot. Although the ESCs filter most of the high frequency noise of the motor, it adds extra protection to the image processor. The LC filter between the autopilot and the image processor filters out any additional noise and stabilize the current. The overall power distribution block diagram is shown in Fig. 2.

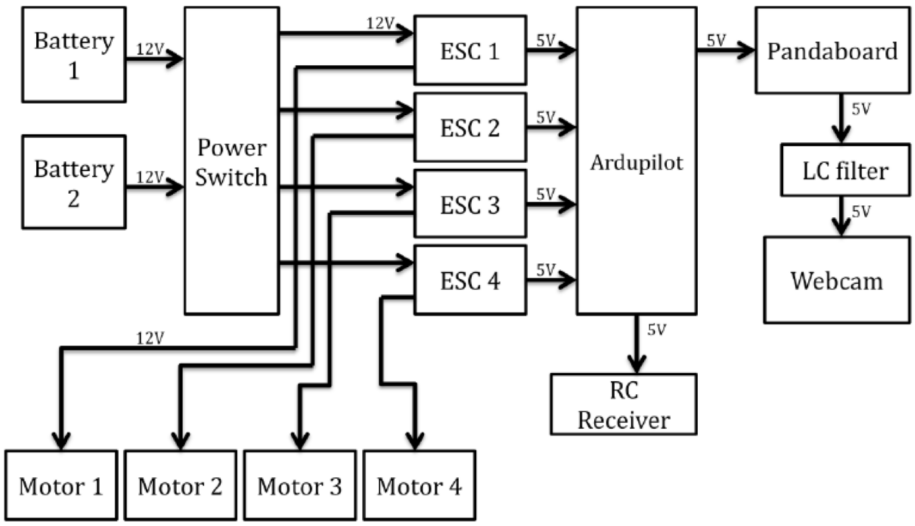

Fig. 2. Power distribution block diagram

2.3. Data acquisition system

In today's software projects, code modularity and reusability are always the most important. Because of the rapid development of hardware, evaluating a piece of code is not just about running speed, but modularity, reusability, and scalability. In order to meet these requirements, there are many options available in the data acquisition system. In this case, the actual observer is the specific sensor that is connected to the device. All sensors, regardless of their function, must implement an abstract interface that has the function of configuring and controlling sensors. The coordinators store the list of registered observers (devices). When it wants to

control them, it will walk through the list and call one of the generic functions. The task of the coordinator is not to understand every particular detail of each additional device, but to implement and use well-defined interfaces that are used and known by the coordinator.

Imaging sensor is an important component of the system that provides imaging feedback to the image processor. After considering various imaging sensors, only video sensors are purchased due to cost. Cameras provide high quality video. However, due to 167 grams of high weight and unable to convert the output video stream to the Linux operating system in real time, the camera is replaced. Logitech C310 network camera is selected because it is low in weight and compatible with Linux (C310 technical specification 2012).

Next is the design of the UAV message marshalling library. The library is used to provide a two-way interface between the image processor and the autopilot. The protocol has the characteristics of high transmission speed and good security performance, so it is usually used in ground control station (GCS) to MAV architecture. Python scripts are used to implement protocols, and the language used is 8 bytes with a maximum payload of 255 bytes. The USB serial interface provides 115200 BPS of bandwidth per second, or about 56 MAVLink packets. In this application, the development board can send MAVLink messages to the APM of the four - way transponder. With the functions of the cover RC channel, more independent procedures are developed, and "arms" and "removal" functions are written. Various functions along with takeoff to a certain height are landed to achieve autonomy. Although a framework has been set up, further development is needed to create a fully autonomous product. The image processing software uses the supplied MAVLink code for processing and output.

Processing data captured from a camera to detect the target and its attributes. The image analysis identifies the position of the target relative to the four rotators and determines the set point required for the PID motion controller. OpenCV is a real-time computer vision library (OpenCV 2012). It contains an optimization algorithm for general image processing. All of the codes are written by C++ with OpenCV 2.3 version.

The camera is attached to the moving object for detecting and analyzing the operation of the object software under the Linux operating system, and the multiple iterations of the image detection software set are carried out. After the video stream is turned on, the image is resized to 320 pixels×240 pixels. Images are shielded by upper and lower bounds to isolate objects. The objects are successfully isolated in the image. The object is placed 5 meters away from the camera. The first method of motion analysis is by sensing the circular contour and recording the position in the loop buffer. The buffer is then used to calculate the movement of the target, and a block diagram of the data output is given below.

3. Result of analysis and discussion

The primary purpose of the first field test is to view and measure the range of the radio module. The test settings are made up of two design versions of PCB. One uses

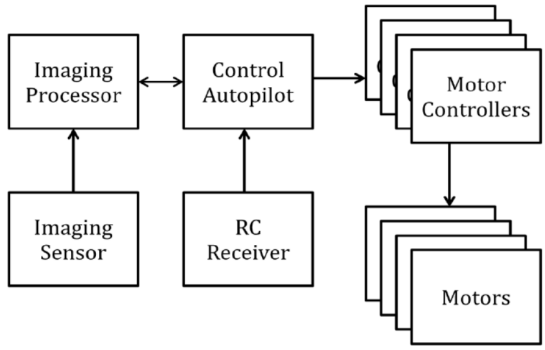

Fig. 3. Data flow diagram

the linear converter as the power source, and the other uses a buck converter. Test scenario: a node of communication is placed in the fix, and the predefined location is not move throughout the experiment. It is programmed to send data packets over a radio interface (Radiocrafts, RC-1280). The second sensor node has been installed with the GPS module. It is programmed to receive any incoming data from the wireless module and write the received data along with the timestamp and the GPS coordinates on the SD card. Basically, this test checks the functions of the SD card, the radio module, the GPS module, the voltage regulator, and several GPIO pins used to control certain states of the LED. The model after the overall installation is shown in Fig. 4.

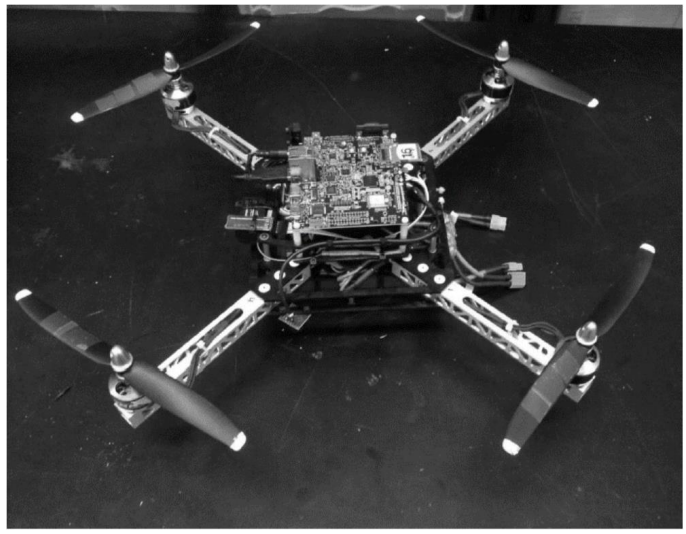

Fig. 4. Quadrotor airframe and electronics

After the sensor nodes are incorporated into the transmitted data, the second mobile sensor has moved from a distance of about 1 km from the fixed sensor. The test result is ideal: the maximum distance between the two modules is 660 m, which

corresponds to the potential area of a circle with a diameter of 1.3 km. Although the test conditions are not ideal, the result makes it possible to successfully implement the effective communication between the UAV and the sensor nodes at that distance.

The next test is to check the feasibility of the entire communication process. The main difference from previous tests is that a test module is added to these tests. The UAV used is the X8 flying wing, and its active components include a development board and several mechanical/electrical modules. The program and setup use the DUNE software framework introduced in the previous chapter. The development board can run under the Linux system. And a DUNE task has been written to read the incoming data from the serial port and package it into the IMC message. Thereafter, the received message is transmitted to the DUNE via the 5 GHz link.

The sensor nodes are set up on the ground in advance, and each parameter is adjusted. The UAV is controlled to fly over it to collect its data and forward data to the base station. The next image shows a snapshot of the test process. In this test, the sensor nodes have been programmed to sample data. The collected data is sent to UAV as a sample and recorded on the SD card, and no sleep mode is adopted. The data sent by the sensor node is composed of temperature readings and their GPS coordinates. The UAV's development board starts running the DUNE task, reads data from the sensor nodes and records it. Some data is sent back to the sensor node. The received sensor data is forwarded to the base station by forwarding 5 Hz through the UDP connection. The base station is a computer that runs the DUNE software, and the comparison of the captured images is shown in Fig. 5.

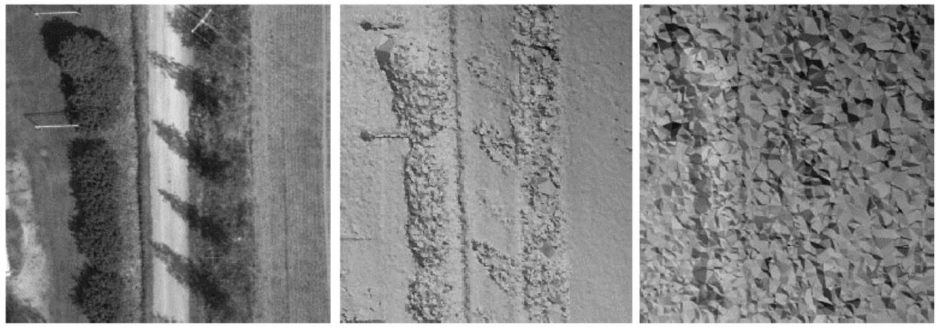

Fig. 5. Image acquisition contrast

The test takes 14 minutes of flight time. During the whole process, sensor nodes, UAVs and base stations have valid data links. Sensor nodes have been previously placed on the map representing the center of the red circle. The maximum distance between the UAV and the sensor node is 100 m on the horizontal axis, and the height is 100 m. The number of messages sent from the sensor node to the UAV (GPS position and temperature) is about 438. All of these messages are accompanied by check and field, and they are checked only once throughout the flight. It means that the packet lost from the sensor node to the UAV is the smallest. There are different cases in which messages are sent back from the UAV to the sensor nodes. Packets sent from UAV to sensor nodes should be commands and configuration files. In this

test scenario, the received data (command) is not explained explicitly and is directly logged on the SD card. The results are also good. In Table 1, the received data is edited and compared to the actual data. Because the CRC field is not added to these packets, the damaged field is recorded. In the range of 3 m×3 m, the relative density of the acquired images is evaluated, and the results are as follows. It can be seen that the collection situation is different in different areas, and the relative density of different objects is different. From the results of the table, it can be seen that the collected density is relatively large, which can reach 0.87–0.90.

Table 1. Points per square meter and relative point densities evaluated in different objects in 3 m×3 m areas

	Points per square meter				Relative point density			
	Field	Grass	Forest	Asphalt	Field	Grass	Forest	Asphalt
UC NGATE	82.1	86.9	47.6	89.6	0.82	0.87	0.48	0.90
GF NGATE	278.2	361.8	136.0	233.0	0.70	0.90	0.34	0.58
Photosynth	2.9	2.4	2.1	2.4	-	-	-	-

4. Conclusion

So far, autonomic search and tracking models have been successfully simulated. In this paper, the automatic analysis of moving objects was introduced to generate real-time road points for the design and implementation of the four-rotating machines that the continuous reconnaissance is interested in. The system is equipped with an autopilot that controls flight in flight and on-board image processors. Simulations can reach maturity that accurately reflects the intent of the action language model. Both models and simulations provide a powerful basis for allowing the development of autonomous agents for a variety of applications. The current prototype is able to stabilize flight and provide sufficient battery life and agility for further development. The components of the problem are usually motors and propellers. Platforms do not have built-in redundancy, and problems that occur can lead to catastrophic failures. Motor faults are traced to connectors that fail at high vibration, thus resulting in intermittent signal integrity problems. These connector failures cause a sharp drop in the motor RPM and crash, and the basic design is carried out from the APM and development boards. Although some achievements are made in image processing software and data acquisition system, it needs further improvement, such as object recognition and so on.

References

[1] D. H. Ho, P. B. Sujit, T. A. Johansen, J. B. Sousa: *Optimization of wireless sensor network and UAV data acquisition.* Journal of Intelligent & Robotic Systems *78* (2015), No. 1, 159–179.

[2] S. Say, H. Inata, J. Liu, S. Shimamoto: *Priority-based data gathering framework*

in UAV-assisted wireless sensor networks. IEEE Sensors Journal *16* (2016), No. 14, 5785–5794.

[3] A. Mazayev, N. Correia, G. Schütz: *Data gathering in wireless sensor networks using unmanned aerial vehicles*. International Journal of Wireless Information Networks *23* (2016), No. 4, 297–309.

[4] I. Jawhar, N. Mohamed, J. Al-Jaroodi, S. Zhang: *A framework for using unmanned aerial vehicles for data collection in linear wireless sensor networks*. Journal of Intelligent & Robotic Systems *74* (2014), Nos. 1–2, 437–453.

[5] L. A. Villas, D. L. Guidoni, G. Maia, R. W. Pazzi, J. Ueyama, A. A. F. Loureiro: *An energy efficient joint localization and synchronization solution for wireless sensor networks using unmanned aerial vehicle*. Wireless Networks *21* (2015), No. 2, 485–498.

[6] C. Keleshis, S. Ioanno, M. Vrekoussis, Z. Levin, M. A. Lange: *Data Acquisition (DAQ) system dedicated for remote sensing applications on Unmanned Aerial Vehicles (UAV)*. International Conference on Remote Sensing and Geoinformation of the Environment, 12 August 2014, Paphos, Cyprus, Proceedings of SPIE *9229* (2014).

[7] G. Bareth, A. Bolten, M. L. Gnyp, S. Reusch, J. Jasper: *Comparison of uncalibrated RGBVI with spectrometer-based NDVI derived from UAV sensing systems on field scale*. ISPRS - International Archives of the Photogrammetry, Remote Sensing and Spatial Information Sciences *XLI-B8* (2016), 837–843.

[8] S. Say, M. E. Ernawan, S. Shimamoto,: *Cooperative path selection framework for effective data gathering in UAV-aided wireless sensor networkss*. IEICE Transactions on Communications *E99.B* (2016), No. 10, 2156–2167.

[9] F. Chiabrando, A. Spanò, G. Sammartano, L. T. Losè: *UAV oblique photogrammetry and lidar data acquisition for 3D documentation of the Hercules Fountain*. Virtual Archaeology Review *8* (2017), No. 16, 83–96.

[10] M. Smigaj, R. Gaulton, S. L. Barr, J. C. Suárez: *UAV-borne thermal imaging for forest health monitoring: Detection of disease-induced canopy temperature increase*. ISPRS - International Archives of the Photogrammetry, Remote Sensing and Spatial Information Sciences *XL-3/W3* (2015), 349–354.

[11] E. Honkavaara, H. Saari, J. Kaivosoja, I. Pölönen, T. Hakala, P. Litkey, L. Pesonen: *Processing and assessment of spectrometric, stereoscopic imagery collected using a lightweight UAV spectral camera for precision agriculture*. Remote Sensing *5* (2013), No. 10, 5006–5039.

Received October 10, 2017

Acta Technica *62* No. 2B/2017, 743–752

Settlement calculation method of rivet pile composite foundation under embankment load[1]

Mingquan Liu[2,3], Chunyuan Liu[2], Xiaozhi Li[2,4]

Abstract. The settlement calculation method of rivet pile composite foundation under embankment load is a basic problem often encountered by engineering. Generally, the composite elastic modulus method is used to calculate the settlement of the rivet pile. But in this process, there is still a "mass" role between the rivet piles, and the calculated value is quite different from the actual situation. In this paper, the interaction effect of rivet pile was discussed based on the basic data of existing research and practical measurement. A method of calculating composite foundation with two layers settlement was put forward for a composite foundation of rivet pile. The actual effect of the algorithm was verified by a practical engineering example.

Key words. Embankment load, composite foundation, rivet pile, settlement calculation.

1. Introduction

In recent years, China's highway infrastructure construction and development has entered a stage of rapid development, especially in the eastern coastal areas with better economic development. The ground base of coastal cities is weak because the area affects the structure of soft soil in this area. But during the construction of expressway, the soil layer structure of soft layer is the inevitable basic problem in engineering construction [1]. During the practice of soft layer treatment, many basic problems of soft soil are found, such as surcharge preloading and reinforcement. Although these design methods have their own advantages, many construction defects are inevitable [2]. The method of preloading can really deal with the insufficient depth of soft soil layer, and the cost of using pure rigid piles is high. This provides

[1]Project is supported by both the National Natural Science Foundation of China (51378331) and Department of Housing & Urban-Rural Development Hebei (2014-289).

[2]School of Civil and Communication Engineering, Hebei University of Technology, Tianjin, 300401, China

[3]School of Civil Engineering, Tangshan University, Tangshan, Hebei, 063000, China

[4]Corresponding author

opportunities for the development of soft soil treatment methods for rivet piles, while the two-way "rivet pile" application is put forward in such a context [3]. For the application of concentrated load rivet pile, there are still few researches on quantitative calculation of consolidation and deformation. Generally, the engineering design of the foundation uses the settlement as the standard foundation. In addition to the necessary bearing capacity of the project, it is necessary to calculate the coincidence between the calculated results of settlement and the actual conditions. This requires the calculation accuracy of the rivet pile composite foundation, so the optimization of the calculation method is imperative [4].

2. State of the art

The two-way foundation characteristics of the rivet pile composite foundation under the embankment load determine the cause and effect of settlement calculation, and also limit the coordination relationship between rivet pile and soil [5]. It is necessary to consider the sharing of the rivet pile and the land load under the action of the external load and the carrying capacity of the land. In addition, the problem of larger end of rivet pile needs to be analyzed, which makes the calculation method of composite foundation settlement of rivet pile become complicated. Rivet pile is a new type of composite foundation combined pile. It has high application value in construction of composite foundation. However, the research literature about it is very rare [6]. Some scholars have simulated and analyzed the larger end design capacity of rivet pile. On the basis of the same geological or soil foundation, the ultimate load carrying capacity of rivet pile is larger than that of ordinary pile. Therefore, it is necessary to put forward the calculation of the bearing capacity of rivet pile [7].

For the same soil foundation construction, through the comparison of the load test of rivet pile and conventional pile, it can be seen that the deformation data of composite foundation have big experimental data difference [8]. On the whole, it can be found that the foundation depth of the rivet pile is uniform, and the depth of the conventional pile is inversely proportional to the strong support of the pile. For some application parameters of rivet pile, the conclusion is less, but it is necessary to analyze and discuss some construction parameters [9]. The calculation of bearing capacity of composite foundation with rivet piles needs to be studied deeply. The settlement calculation of composite foundation of rivet pile is not perfect, and the role between rivet piles is not clear [10]. The surface of the soil layer in the eastern coast is hard, and the middle layer is a soft soil layer. It makes it possible to analyze the bearing capacity and settlement characteristics of the lower layer of the hard layer foundation when using rivets to reinforce the composite foundation.

2.1. Methodology

There is a certain pile group effect in the rivet pile under the embankment load. It is found in the literature that there is a mass effect in the enlarged part of the composite foundation settlement of the rivet pile under the embankment load. Some

scholars have designed the method to transfer the load of an independent rivet pile, and calculated the value of the settlement of the foundation. However, the results obtained are not consistent with the actual measured values, which seriously ignore the interaction mechanism between rivet piles. Based on the applicability of the basic research and practical construction, the soft soil structure of the coastal cities in the eastern part of the country needs to be dealt with. The settlement is mostly the composite settlement of pile groups. Therefore, the group effect of rivet pile must be considered in the design of settlement calculation method of composite foundation [11]. In order to study and discuss the regional settlement effect of composite pile foundation with rivet piles, the basic model of composite foundation is set up. The larger end of the element body is enlarged, and the depth of the rivet pile at the lower part is divided into three bearing layers for calculation. The reinforcement layer is solved by compound modulus calculation method. Enlarging the composite modulus of rivet head needs to consider the mass effect of rivet pile, and the lower part of pile cannot be considered. By applying the method of gradual stress diffusion, the applied stress of the underlying lower layer is calculated in advance. The settlement value of composite foundation is calculated by the method of layer synthesis calculation.

In the course of soil bearing capacity of soft soil layer with hard layer, with the increase of load, the internal stress of hard layer is composed of two stages: elastic layer and ultimate elastic layer. It is assumed that the embankment is less than a certain height, and the composite base is in an elastic deformation stage. The hard layer will bear most of the load and transfer the load to the outside of the embankment. In this way, the stress transmitted to the soft soil layer is greatly weakened. In such a state, the compression settlement of the soft soil layer will be relatively small. Although the stress of the hard layer of the soil is relatively large, the rigidity of the hard layer is relatively large. The hard layer capture is compressed too much without exceeding the limit compression capability. Therefore, the overall settlement of the foundation is small and it will soon be restored.

It is assumed that the original elastic working state is broken by the height of the embankment, and the thickness of the plastic change layer increases gradually. Then the rigidity of the hard layer will be weakened, the stress of the soft soil layer will be increased, and the distance of settlement will gradually increase. This is referred to in the literature that when the embankment exceeds a certain height, the settlement value of the hard layer foundation will change qualitatively. In the process of increasing load, the ultimate state of composite foundation will be bigger and bigger. The deformation of the foundation may be very large. The hard and soft layers have been adjusted to the limit, but the hard layer still maintains relatively high shear strength. The strength difference between the hard and soft layers is stress distribution and foundation ratio, and the trend will tend to the upper part of the foundation. The hard layer and the upper soft soil bear the greater load on the composite foundation. The stress of the lower soft soil is small, and the compression of the composite foundation is relatively small. The compressibility of the upper soil determines that the total settlement is less than the foundation without the hard layer structure.

The double deck structure of composite foundation means that in the foundation

construction process, the reinforcing layer and the soft soil layer form the condition of upper firm and lower soft, so as to improve the deformation characteristics of the bearing capacity change. In the treatment of soft soil foundation of expressway, the rivet pile is embedded in soft soil layer, which is a typical strengthening structure. The surface of reinforcing area is hard layer, and the lower layer is soft soil layer structure. The bearing stratum is the soil layer between the two forces. In different soil layer structures, distinct strength and stiffness differences are formed. The strength and stiffness difference of the bearing capacity of the composite foundation is similar to the bearing capacity of some kind of slab. Different laminates form different compression deposition effects. The plate body is more obvious for the diffusion stress of the embankment load, which can effectively weaken the additional embankment stress in the soft soil layer, so that the bearing capacity and settlement characteristics of the composite foundation can be effectively improved.

Through a large number of field tests, it is believed that the deformation of the rivet pile is different from that of the rivet pile under the action of the external load of the rivet pile, and the key problem is the deformation coordination between the rivet piles. Compared with reinforced concrete, the stress and compressive modulus of rivet pile are relatively small. Therefore, after the static loading test, the curve is generally smooth curve. There is no obvious inflection point, and the force is closer to the soil structure, rather than rivet pile. At present, the larger end of the rivet pile is slightly higher than the height of the hard soil layer. The area of the enlarged head is larger than the straight section of the lower part. The composite growth value of the enlarged head is larger than that in the lower part. Under the action of embankment load, the group effect of rivet pile composite foundation is more obvious.

It is assumed that the composite foundation of rivet pile is a composite foundation with double deck. The thickness of the first layer composite foundation is the middle extended depth range. The thickness of the second layer composite foundation is the depth area of the lower pile in the strengthening area, as shown in Fig. 1. The depth change of composite foundation in the first layer is S_1, and it is S_2 for the second layer and S_3 for the third layer. The total settlement of the composite foundation of the last rivet pile is

$$S = S_1 + S_2 + S_3 \,. \tag{1}$$

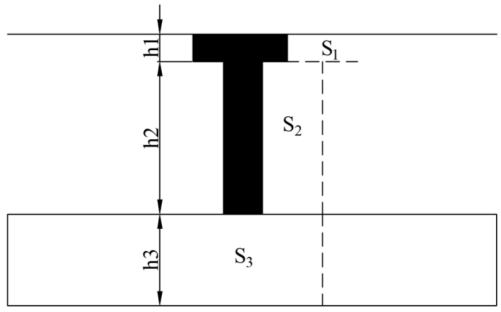

Fig. 1. Calculation model of settlement of rivet pile

The empirical values show that the relationship between 85 % of the actual strength of the rivet piles and the soil properties and soil age parameters is as follows:

$$q_{\mathrm{M}} = \mathrm{e}^{-1.28}(\omega/\omega_{\mathrm{L}})^{-0.819}(C/\omega)^{0.972}t^{0.156}\,. \tag{2}$$

In the above formula , ω represents the soil water content probability, ω_{L} represents the liquid limit ratio of the soil body, C represents the amount of cement used, and t represents the time limit for the use of the cement in the soil. If the number of rivet piles is relatively large, the group effect of rivet pile should be considered. Finally, the group effect of rivet pile is established with the calculation formula

$$E_{\mathrm{SP}} = [\beta_1, \beta_2][E_{\mathrm{p}}, E_{\mathrm{s}}]\,. \tag{3}$$

In formula (3), β_1 and β_2 respectively represent the proportion coefficient of rivet pile composite modulus, including the basic factors of influence. Symbols E_{p} and E_{s} represent the deformation modulus before and after the deformation of the pile.

Taking the 6 rivet piles as an example, the interaction between adjacent rivet piles takes into account only the relation between the 1# rivet pile and the 2#–5# rivet pile. The distance between the piles outside the rivet pile is so far away that such a long distance can be neglected. For the cube rivet pile, each pile outside has its influence on pile rivet. For a plum shaped rivet pile, there are 6 rivet piles outside each rivet pile, as shown in Fig. 2. Assuming that the influence of the modulus of elasticity between the square rivet piles can be calculated, the calculation method and formula for the rivet pile with plum blossom shape and even more shapes can be deduced.

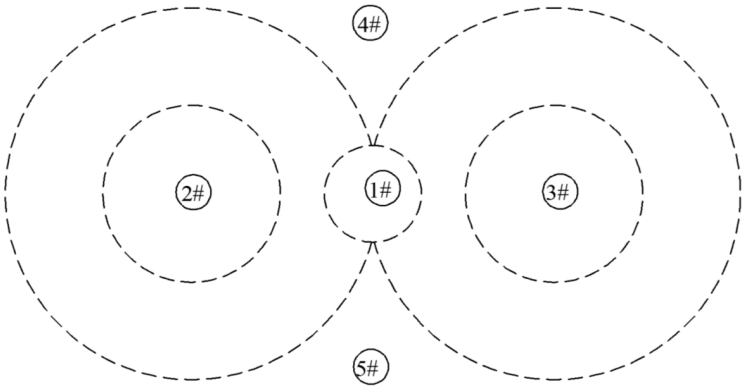

Fig. 2. Influence of pile forming process on soil composite modulus

The expression for the influence between the rivet piles is:

$$E_{\mathrm{sp}} = \beta_1 E_{\mathrm{p}} + \beta_2 E_{\mathrm{s}}\,. \tag{4}$$

Based on the theory of elastic deformation, the composite modulus is solved to calculate the settlement of the reinforcement region.

The depth range of the enlarged part is calculated as

$$s_1 = \frac{(p + p_1)H}{2E_{sp1}} \tag{5}$$

The depth range of the lower part is calculated as:

$$s_2 = \frac{(p_1 + p_2)L}{2E_{\mathrm{sp2}}}\,. \tag{6}$$

In the formula, p represents the load on the surface of the rivet pile composite foundation (kPa), p_1 represents the equivalent applied stress on the top of the enlarged part of the rivet pile (kPa), p_2 represents the equivalent additional stress under the rivet pile composite foundation (kPa), H represents the height of the enlarged head of the rivet pile (m), L represents the height of the pile at the lower part of the rivet pile (m), E_{sp1} represents the composite modulus at the upper depth of the composite foundation of the rivet pile (MPa), and E_{sp2} represents the composite modulus at the lower depth of the composite foundation of the rivet pile (MPa).

According to the design codes' requirements of building foundation, the depth deformation degree of building foundation is calculated as

$$\Delta s'_n \leq 0.025 \sum_{i=1}^{n} \Delta s'_i\,, \tag{7}$$

where, $\Delta s'_i$ represents the calculated soil depth of the ith layer within the calculated depth range, $\Delta s'_n$ represents the calculated soil depth for the thickness Δz within the calculated depth range.

Assuming that the adjacent load of the rivet pile is affected, and the design range of the foundation is from 1 m to 30 m, the calculation formula of the foundation deformation depth is:

$$Z_n = b(2.5 - 0.4 \ln b)\,. \tag{8}$$

The concept of "b" described in formula (8) is the base width, and the unit is m. The depth of settlement of composite foundation is calculated according to the above formula. When there is a soft soil layer, it should continue to be calculated downward until the experimental results in the soft soil meet the required position.

3. Result analysis and discussion

The highway test area of a high speed section is used as the object of study. The experimentation area is located in soft soil areas, and the surface width of the embankment is about 34 m. The height of embankment after filling is about 5.8 m, and the ratio of slope to angle is about 1:1.4. The width of the embankment surface is about 52 m, and the lower water level is flush with the surface of the ground, as shown in Fig. 3.

In the structure of soil layer, the main physical and mechanical indexes are shown

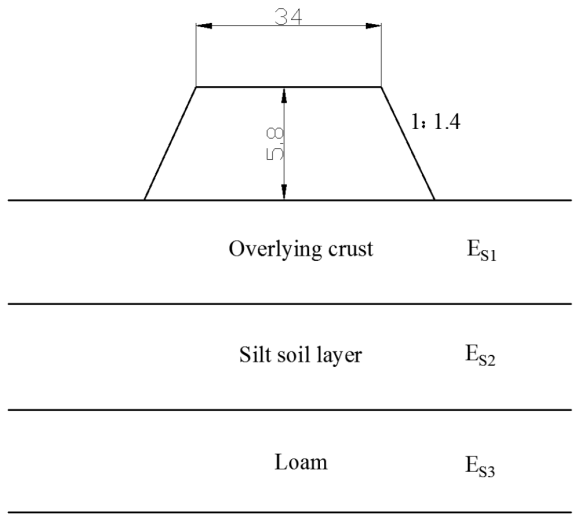

Fig. 3. Embankment profile

in Table 1.

Table 1. The main physical and mechanical indexes of soil layer structure

i	0	1	2	3	4
Layer	Embankment fill	Hard layer	Silt layer	Loam	Bearing stratum
Height m)	6	2	13	2	48.5
r (kN/m^3)	20	19.3	17.5	19.5	20
E_{si} (MPa)	20.4	11.7	2.8	13.2	20.4

The area in which the experimental area is located is the plain area of a lake. The surface is medium compressed soft plastic sub clay with the thickness of 4 m and the settlement is the silty clay with the thickness of 14 m. The water content of the soil layer is about 50 %. The natural average land porosity ratio in the lake is about 1.42, and the bearing layer is sub clay. The project is located in a high speed section of Jiangsu and Zhejiang, and the rivet pile used is "K30+140". In the experimental stage, composite foundation of rivet pile is used to soften foundation. The length of the designed rivet pile is about 16 m, and the diameter of the rivet pile is about 500 mm. The upper height is about 4 m, and the lower height is about 12 m. The spacing of rivet piles is 2 m, and the distribution rule is plum blossom shape. The severe value of rivet pile is 21 kN/m^3. In this experiment, the change of the modulus of rivet pile with the soil layer is only considered, so the compression modulus is 83.3 MPa.

In order to verify the practicability of the settlement calculation of composite foundation in this paper, the author considers that the method of simulation and composite modulus can be adopted. The design concept of double layer composite

foundation is put forward. The research object of this paper is the standardized calculation of composite foundation settlement. Various calculations are shown in Table 2. The calculation method and measured results of the calculation examples are given in Table 2. Through the comparative analysis, the calculation method of composite modulus ignores the group effect of the hard soil layer, and the interchange function of the rivet pile is relatively exaggerated, so that the settlement value of the calculated reinforcement area is too small. The simulation results are close to the actual measured values. However, for the general engineering and technical personnel, it is difficult to master this method in a short period of time. The settlement calculation method of double layered composite foundation is easy to understand and feasible in practice. The design parameters of the rivet pile are considered at the same time. The settlement value is too large, but it is also within the design error range.

Table 1. The results of various methods of calculation

Number	1	2	3	4
Computing method	Complex modulus method	Research methods in this paper	FLAC3D	Measured settlement value
Calculation result (mm)	264.4	318.3	285	281

4. Conclusion

In practical engineering practice, the settlement calculation of rivet pile composite foundation is widely used. Based on the existing research results and measured data, the group effect of rivet pile composite foundation was analyzed in this paper. A double-layer composite foundation method was put forward for settlement calculation of double-layer structure of rivet pile composite foundation reinforcement. The results were verified by a practical case analysis and satisfactory results were obtained. Based on the study of the settlement calculation method of composite foundation with rivets, the group effects of the hard layer and soft soil foundation were taken into account. A model of double-layer composite foundation strengthened with rivet pile composite foundation was put forward, and the settlement value of composite foundation was calculated. Calculation method of ground settlement was induced by double-layer composite foundation model. The experimental results show that the double layered composite foundation can be combined with the method of rivet pile reinforcement to calculate the ground drop value. The double-layer composite foundation settlement calculation model was used to determine the calculation parameters of the settlement of pile composite foundation such as deformation modulus of rivet pile, the pile body range of upper and lower enlarged part, thickness and calculated depth of the deformation layer. The calculation methods of settlement of composite foundation with various rivet piles were analyzed. By comparing the results of the double-layer riveted pile composite foundation proposed in

this paper, it is proved that the group effect of rivet pile is scientific and effective.

References

[1] W. Liu, S. Qu, H. Zhang, Z. Nie: *An integrated method for analyzing load transfer in geosynthetic-reinforced and pile-supported embankment.* KSCE Journal of Civil Engineering *21* (2017), No. 3, 687–702.

[2] J. Zhang, X. Cui, D. Huang, Q. Jin: *Numerical simulation of consolidation settlement of pervious concrete pile composite foundation under road embankment.* International Journal of Geomechanics *16* (2016), No. 1, B4015006.

[3] M. J. Zhang, Q. Luo, X. Q. Zhan, L. Zhang: *Research on settlement calculation empirical coefficient of end-bearing CFG pile composite foundation.* Rock and Soil Mechanics (*34* 2008), No. 2, 519–525, 545 (in Chinese).

[4] M. H. Zhao, M. Liu, R. Zhang, J. Long: *Calculation of load sharing ratio and settlement of bidirectional reinforced composite foundation under embankment loads.* Chinese Journal of Geotechnical Engineering *36* (2011), No. 12, 2161–2169.

[5] C. Wang, B. Wang, P. Guo, S. Zhou: *Experimental analysis on settlement controlling of geogrid-reinforced pile-raft-supported embankments in high-speed railway.* Acta Geotechnica *10* (2015), No. 2, 231–242.

[6] W. M. L. Lü: *Calculation method of pile-soil stress ratio of rigid pile composite foundation.* Journal of Southeast University(Natural Science Edition) *43* (2013), No. 3, 624–628.

[7] W. Z. Liu, J. H. Zhang, H. Zhang: *Analysis on pile-soil stress ratio of composite foundation with sparse capped-piles under lime-soil embankment load.* Applied Mechanics and Materials *501–504* (2014), 124–131.

[8] Y. U. Hui, X. M. Ding, Y. R. Lv: *Analysis on calculation method for widen expressway settlement with x-section cast-in-place concrete pile composite foundation.* Journal of Disaster Prevention and Mitigation Engineering *33* (2013), No. 1, 84–90.

[9] X. Cui, N. Zhang, S. Li, J. Zhang, L. Wang: *Effects of embankment height and vehicle loads on traffic-load-induced cumulative settlement of soft clay subsoil.* Arabian Journal of Geosciences *8* (2015), No. 5, 2487–2496.

[10] C. Wang, S. Zhou, B. Wang, H. Su: *Differential settlements in foundations under embankment load: Theoretical model and experimental verification.* Geomechanics and Engineering *8* (2015), No. 2, 283–303.

[11] N. Ravichandran, V. Mahmoudabadi, S. Shrestha: *Analysis of the bearing capacity of shallow foundation in unsaturated soil using Monte Carlo simulation.* International Journal of Geosciences *8* (2017), No. 10, 1231–1250.

Received October 10, 2017

Acta Technica *62* No. 2B/2017, 753–760

STATCOM current detection method and control technology based on instantaneous reactive power theory[1]

Xuehai Pan[2]

Abstract. With the widespread application of impulsive loads and nonlinear loads in the power grid, reactive power and harmonic pollution of the power grid are also rising, which have a certain impact on people's lives. STATCOM can effectively suppress harmonics and reactive power, and has become the main mode of power quality control. STATCOM system model was set up in this paper. On the basis, two control techniques, hysteresis control and triangle wave control, were designed and simulated. The results show that the two techniques can track the instruction currents fast and accurately, and realize effective harmonic suppression and reactive power compensation. In practical application, the appropriate hysteresis width and triangle wave frequency should be chosen to achieve the optimal tracking compensation performance of STATCOM.

Key words. STATCOM, reactive power compensation, control technology.

1. Introduction

In recent years, with the extensive application of electronic power technology, people's living standards have been greatly improved. While enjoying the convenience of scientific and technological progress, its negative effects are gradually emerging [1]. On the one hand, many applications of electric equipment, such as electric arc furnace, electric locomotive, and frequency converter, bring more new challenges to power grid, such as voltage fluctuation, harmonic, over-voltage and under voltage. On the other hand, with the wide application of the Internet era of computer and electronic technology, some precision instruments and equipment for power quality is more and more sensitive, such as voltage sag and swell, flicker and other power quality problems, which may cause serious loss of sensitive load [2]. According to the statistics conducted by experts in American Academy of Electric Power, the United States loses hundreds of billions of dollars per year due to power quality

[1]This work is for fund projects: Shandong province science and technology development project (No. 2011GGA03156).

[2]Zibo Vocational Institute, Zibo, Shandong, 255314, China

problems. Disputes arising from the quality of power supply are also numerous, and its losses are incalculable [3]. Therefore, in order to realize the efficient, green and stable operation of power system, some necessary measures should be taken to control the power grid and reduce pollution. At present, the most widely used static synchronous compensator (STATCOM) not only can solve the power quality problems comprehensively, but also has the advantages of dynamic, adjustable, fast and so on [4]. Therefore, it has gradually become the development direction of reactive power compensation device in modern power system, and has extremely important engineering application value and very broad market potential.

2. State of the art

The basic principle of STATCOM is that by adjusting the amplitude and phase of the AC output voltage of the circuit, it absorbs from the grid or sends reactive current to the grid to compensate for the constant voltage of the access point, so as to realize reactive power current compensation of power grid [5]. The emergence of new electronic power devices has greatly promoted the development of STATCOM. STATCOM's early switching devices are mainly high voltage and high power gate turn off thyristors (GTO). With the progress of electronic power technology, insulated gate transistor (IGBT) and integrated gate commutated thyristor (IGCT) become the main force, which can compensate reactive power more quickly and more accurately. Compared with the traditional static var compensator (SVC), STATCOM has the characteristics of small size, high accuracy, high speed, and wide range [6]. Currently, STATCOM presents two major research trends. The scope of research is more and more widespread, not only in the high-voltage transmission system, but also in the user side. Two is the continuous use of new power electronic device system performance [7]. In the study of STATCOM dynamic control model, the control strategy and control design are also very important research points [8–10]. The controller of STATCOM consists of two parts: inner loop controller and outer loop controller [11]. The inner loop controller mainly generates a synchronous driving signal, and establishes dominant relation between the output current and the reactive command. The main task of the outer loop controller is to assist the inner loop controller and provide the reactive power reference value for the inner loop controller.

2.1. Methodology

The basic principle of hysteresis width selection in the control system is that the actual value i_{st} of the compensation current is compared to the reference value i_{ref} of the compensation current, and the current tracking difference Δi is obtained. When Δi is greater than the maximum value of the hysteresis width, $T1$ is energized, $T2$ is switched off, and the actual current is increased. When Δi is less than the maximum value of the hysteresis width, $T1$ is switched off, $T2$ is energized, and the actual current is reduced. In hysteresis control, the hysteresis width of hysteresis comparator has a great influence on the following performance of the compensation

current. The equivalent structure of the hysteresis control circuit of the single-phase voltage source inverter is shown in Fig. 1.

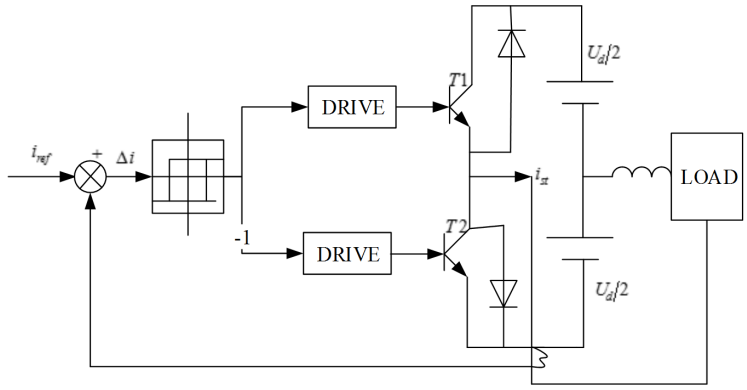

Fig. 1. Single phase hysteresis control structure diagram

Parameter design of PI regulator in control system is one of the most important parts of the system. In this paper, hysteresis control and triangle wave are used to control the two control modes. The control is divided into inner loop control and outer loop control. The current inner loop control system mainly consists of four parts: PI regulator, time delay, voltage inverter and current filter feedback. The reactive current channel control system diagram is shown in Fig. 2.

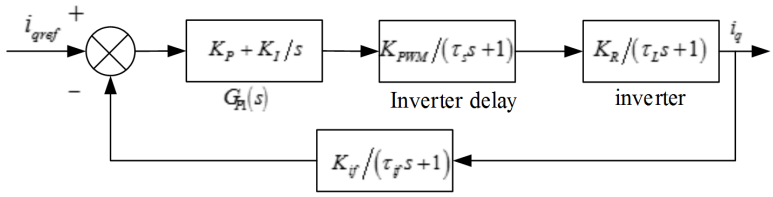

Fig. 2. Internal loop current control system diagram

Here, $G_{\mathrm{P1}}(s)$ represents the PI regulator, $K_{\mathrm{P}} + K_{\mathrm{I}}/s$ refers to the delay link, $K_{\mathrm{R}}/(\tau_L s + 1)$ represents a voltage inverter; $K_{\mathrm{if}}/(\tau_{\mathrm{if}} s + 1)$ represents current filtering feedback, K_{P} stands for the proportion of the PI regulators; K_{I} represents the integral coefficient of the PI regulator, K_{PWM} represents the magnification of the rectifier, τ_{s} indicates that the delay of the converter, which is equal to half the switching period, τ_{L} represents the inductance time constant, $\tau_{\mathrm{L}} = L/R$, $K_{\mathrm{R}} = 1/R$; K_{if} represents the amplification factor of the feedback channel, and τ_{if} represents the time constant of the feedback channel.

Therefore, the transfer function of the current controller is represented as:

$$H(s) = \frac{K_{\mathrm{I}} K_{\mathrm{PWM}} K_{\mathrm{R}} K_{\mathrm{if}} (\tau_{\mathrm{x}} s + 1)}{s(\tau_{\mathrm{L}} s + 1)(\tau_{\mathrm{s}} s + 1)(\tau_{\mathrm{if}} s + 1)} \tag{1}$$

where $\tau_{\mathrm{x}} = K_{\mathrm{P}}/K_{\mathrm{I}}$. In formula (1), it is assumed that $\tau_{\mathrm{x}} = \tau_{\mathrm{L}} = L/R$. The time constant of the feedback channel τ_{if} and the time delay of τ_{s} converter are very small. The first order system is replaced by a secondary order system, and the closed loop function is represented as

$$H_1(s) = \frac{\varphi_{\mathrm{n}}^2}{s^2 + 2\theta\varphi_{\mathrm{n}} + \varphi_{\mathrm{n}}^2}. \tag{2}$$

where θ represents the load damping ratio of the two order system, $\theta = \sqrt{1/K\tau_{\mathrm{sf}}}\Big/2$, $\varphi_{\mathrm{n}} = \sqrt{K/\tau_{\mathrm{sf}}}$, $\tau_{\mathrm{sf}} = \tau_{\mathrm{s}} + \tau_{\mathrm{if}}$, $K = K_{\mathrm{I}}K_{\mathrm{PWM}}K_{\mathrm{R}}K_{\mathrm{if}}$.

When the load damping ratio of the secondary order system is $\theta = 0.707$, the overshoot and the tuning time of the system are optimal, and K can be calculated. Therefore, the values of parameters K_{P} and K_{I} can be obtained.

The voltage outer loop control system mainly consists of three parts: PI regulator, time delay and voltage inverter. The capacitor voltage control diagram is shown in Fig. 3.

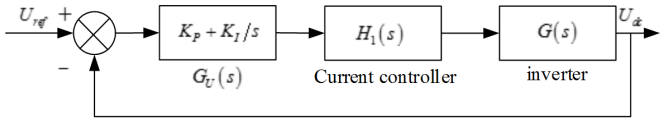

Fig. 3. External loop voltage control system diagram

The transfer function between the input current and the output current and voltage is:

$$G(s) = K_0\frac{1 - s\tau_{\mathrm{z}}}{1 + s\tau_{\mathrm{p}}} \tag{3}$$

Where, there is $K_0 = 3R_{\mathrm{L}}U_{\mathrm{m}}/(4U_{\mathrm{dc}})$,$\tau_{\mathrm{p}} = 0.5R_{\mathrm{L}}C$, $\tau_{\mathrm{z}} = L/R_{\mathrm{i}}$. R_{i} represents the input impedance of the inverter, $R_{\mathrm{i}} = U_{\mathrm{m}}/I_{\mathrm{m}}$.

$$G_{\mathrm{U}}(s) = K_{\mathrm{up}} + K_{\mathrm{ul}}/s = K_{\mathrm{ul}}(\tau_{\mathrm{u}}s + 1)/s. \tag{4}$$

where $G_{\mathrm{U}}(s)$ stands for the PI regulator, $\tau_{\mathrm{u}} = K_{\mathrm{up}}/K_{\mathrm{ul}}$, K_{up} and K_{ul} are the ratios of PI regulator and integral coefficient, respectively.

The same as the regulation process of current inner loop control, the first order inertial system is used instead of the secondary order system, which is represented by $H_1(s)$.

$$H_1(s) = 1/(2\tau_{\mathrm{sf}}s + 1). \tag{5}$$

Therefore, the transfer function of the voltage controller is represented as:

$$W(s) = \frac{K_{\mathrm{ui}}K_0(\tau_{\mathrm{u}}s + 1)(1 - \tau_{\mathrm{z}}s)}{s(\tau_{\mathrm{p}}s + 1)(2\tau_{\mathrm{sf}}s + 1)}. \tag{6}$$

It is assumed that $\tau_{\mathrm{u}} = \tau_{\mathrm{p}}$, and $K_{\mathrm{I}} = K_{\mathrm{ui}}K_0$. Quantity τ_{z} has little influence on

the peak response time and the rising time of the system, which can be neglected. Then the closed loop transfer function is:

$$W_1(s) = \frac{\varphi_{\mathrm{n}}^2}{s^2 + 2\theta\varphi_{\mathrm{n}} + \varphi_{\mathrm{n}}^2}. \tag{7}$$

where, $\theta = \frac{1}{2}\sqrt{1/2K\tau_{\mathrm{sf}}}\,(1 - \tau_{\mathrm{z}}K_l)$ and $\varphi_{\mathrm{n}} = \sqrt{K/2\tau_{\mathrm{sf}}}$. Similarly, the values of $\theta = 0.707$, parameters K_{uP} and K_{uI} can also be calculated.

3. Result analysis and discussion

Through the above analysis, Matlab is used for modeling and simulation, and the triangle wave control and hysteresis control are simulated in two ways. The waveforms of the current under two control modes are obtained.

Hysteresis control simulation analysis: two hysteresis widths 6 % and 3 % are selected. The waveforms obtained by simulation are shown in Fig. 4 and Fig. 5.

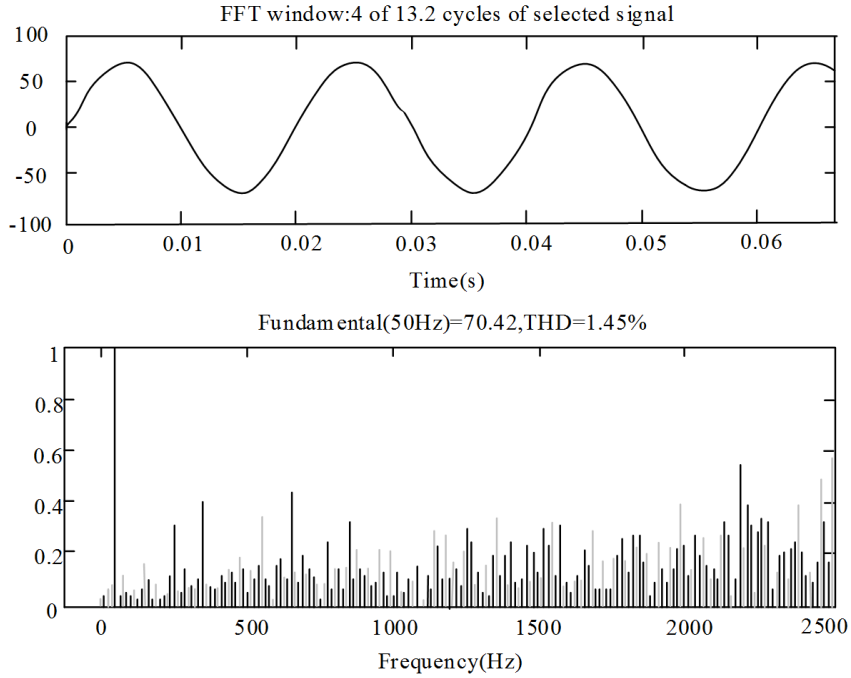

Fig. 4. A phase compensation current i_{st} and spectrum generated by STATCOM at 6 % of the hysteresis width

Two conclusions can be drawn from Fig. 4 and Fig. 5. One is the hysteresis control, which can track the reference wave rapidly and accurately under two conditions with the hysteresis width of 6 % and 3 %. The other is that the hysteresis width is

bigger, the tracking reference current error is bigger, and the compensation current harmonic is also bigger.

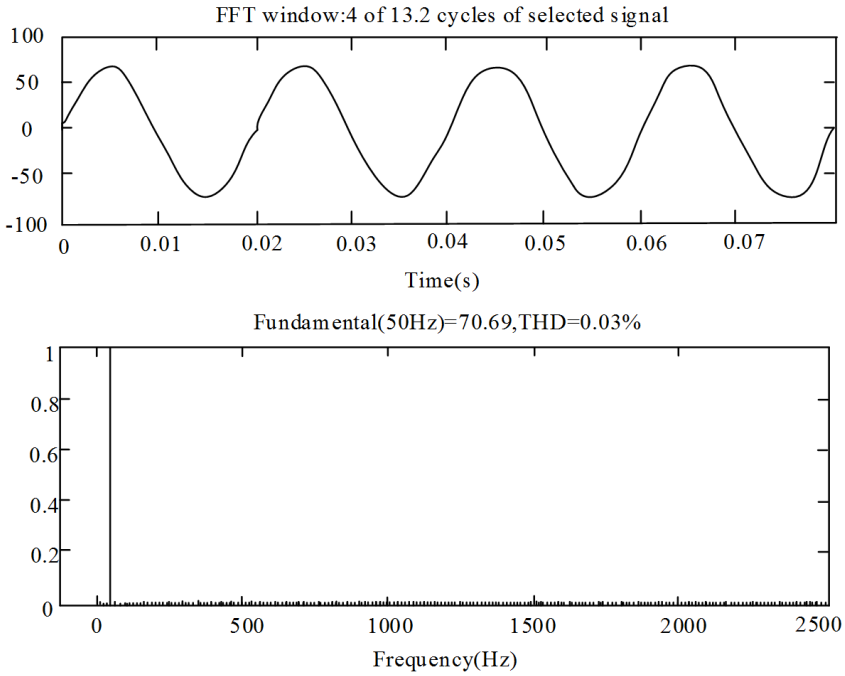

Fig. 5. A phase compensation current i_{st} and spectrum generated by STATCOM at 3 % of the hysteresis width

Simulation and analysis of triangle wave control: parameter setting in triangle wave control mode: frequency is set to 2 kHz; parameter of current controller $K_P = 8$, $K_I = 140$; parameter of voltage controller $K_{uP} = 0.5$, $K_{uI} = 1.5$. By simulation, the compensation current and its spectrum analysis results of phase A are shown in Fig. 6.

It can be seen from the Fig. 6 that the triangle wave control mode can track the reference wave quickly and accurately, but the distortion component of the compensation current is the same as that of the triangle wave.

Comparing the two control methods, the two control methods have their respective advantages and disadvantages. Therefore, according to the actual requirements of the STATCOM compensation effect and the switching frequency limits of the electronic power devices, STATCOM can have the best tracking compensation performance by choosing proper hysteresis width, triangle wave frequency and various parameters.

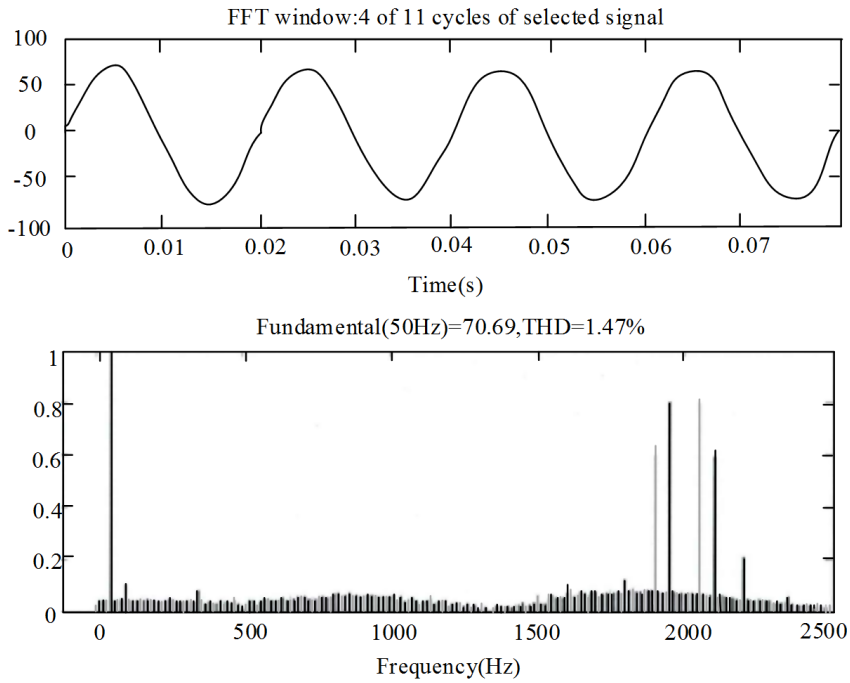

Fig. 6. The phase A compensation current i_{st} and spectrum generated by STATCOM of Triangular wave control

4. Conclusion

In this paper, the research of device pole control in STATCOM control technology was mainly studied. Device level control was mainly divided into PWM tracking technology control and square wave tracking technology according to the driving pulse. PWM tracking control waves were generated by space vector PWM or SPWM sinusoidal modulation. The hysteresis loop control method and the triangle wave control method in PWM tracking technique were simulated. The simulation results show that the switching frequency of the hysteresis control mode is not fixed. The smaller the hysteresis width, the higher the switching frequency, and the greater the switching loss will be. At the same time, the error of the compensating current tracking reference current is smaller, and the harmonic content in the compensation current is low. The switching frequency of the triangle wave control mode is fixed. This control method can track the reference wave rapidly and accurately. However, the high-frequency distortion component of the same frequency as the triangle wave will be introduced into the compensating current. According to the simulation results, in the actual STATCOM control system, the appropriate hysteresis width, triangle wave frequency and various parameters of the PI regulator should be selected according to the actual demand of the compensation effect and the switching frequency limit of the electronic power device. The research on the

control technology of STATCOM is limited to the device level control level. Three kinds of integrated control technology, including system level control, device level control and device level control, should be further studied to improve STATCOM control technology.

References

[1] O. Hasnaoui, M. Allagui: *Dynamic performance improvement of wind farms equipped with three SCIG generators using STATCOM.* Journal of Energy in Southern Africa *25* (2014), No. 4, 128–135.

[2] J. I. Y. Ota, Y. Shibano, H. Akagi: *A phase-shifted PWM D-STATCOM using a modular multilevel cascade converter (SSBC)—Part II: Zero-voltage-ride-through capability.* IEEE Transactions on Industry Applications *51* (2015), No. 1, 289–296.

[3] R. Xu, Y. Yu, R. Yang, G. Wang, D. Xu, B. Li, S. Sui: *A novel control method for transformerless H-bridge cascaded STATCOM with star configuration.* IEEE Transactions on Power Electronics *30* (2015), No. 3, 1189–1202.

[4] X. Zhao, L. Shi, L. Chen, Z. Xia, A. R. Bendre: *Modeling and current control strategy for a medium-voltage cascaded multilevel STATCOM with LCL filter.* Journal of Power Technologies *95* (2015), No. 1, 1–13.

[5] R. Xu, Y. Yu, R. Yang, D. Xu: *Strategy based on passivity theory for nonlinear control of STATCOM with cascaded H-bridges.* Electric Power Automation Equipment *35* (2015), No. 1, 50–57.

[6] L. Prakash, A. M. Sundaram, K. Durairaj: *Digital implementation of a constant frequency hysteresis controller for dual mode operation of an inverter acting as a PV-grid interface and STATCOM.* Turkish Journal of Electrical Engineering and Computer Sciences *24* (2016), No. 5, 4406–4428.

[7] W. Hua, J. Qi, M. Jia: *An inductance Fourier decomposition-based current-hysteresis control strategy for switched reluctance motors.* AIP Advances *7* (2017), No. 5, paper 543.

[8] X. Zhao, L. Shi, L. Chen: *A new current control strategy of cascaded STATCOM with composite control.* Power System Protection and Control *43* (2015), No. 17, 98–106.

[9] S. Guo, P. Sun, S. Jing, Z. Wang: *Research on modeling and simulation of power control method for STATCOM based on predictive model.* Power System Protection and Control *43* (2015), No. 1, 88–92.

[10] S. Wu, Y. Kobori, N. Tsukiji, H. Kobayashi: *Transient response improvement of DC-DC buck converter by a slope adjustable triangular wave generator.* IEICE Transactions on Communications *E98.B* (2015), No. 2, 288–295.

Received October 10, 2017

Acta Technica *62* No. 2B/2017, 761–768

Application of chemical bio-sensor based on nano-conductive rubber in sports rehabilitation

Qiang Li[1]

Abstract. With the development of robot technology, it is more and more important for the research of flexible multi-dimensional tactile chemical sensors for intelligent robots, especially bionic robots and service robots. Because flexible multidimensional tactile chemical sensor has the function of measuring the pressure distribution of any material and free surface, it has wide application prospect in many fields such as sports training, rehabilitation medicine, sports biomechanics and so on. In this paper, the new liquid-formable pressure-sensitive conductive rubber material was studied, which not only has good mechanical and electrical properties, but also the production cost is low and the preparation process is simple and easy. Flexible multidimensional array tactile chemical sensor not only has the flexibility of human skin, but also has the function of obtaining 3D direction force information. The research work and achievements of this thesis have laid a good foundation for further research on the application of robot sensitive skin and flexible tactile chemical sensor.

Key words. Missing.

1. Introduction

Based on high molecular material silicone rubber, conductive rubber is added with various conductive fillers to form a composite system with conductive function [1]. It not only has a conductive function, but also has many excellent properties of polymer materials [2]. Depending on the requirements, we can adjust the electrical and mechanical properties of the material. Conductive rubber is a good function of anti-static products and anti-electromagnetic shielding device composite materials [3]. Therefore, it is widely used. In addition, people use the conductive rubber force sensitive or temperature-sensitive effect developed a variety of electronic key materials, touch components, temperature sensitivity and force sensitive chemical sensor materials, which makes the application of conductive rubber continues to expand. The current multi-dimensional array of tactile chemical sensors cannot

[1]Northwest University of Politics and Law, 710063, Shaanxi, China

have both flexibility and measurement of multi-dimensional force characteristics of information. We propose a new flexible multidimensional array tactile chemical sensor based on pressure sensitive conductive rubber. The research work and the results can provide a new idea for the interdisciplinary research of materials science, instrument science, chemical sensor technology and artificial intelligence, so as to lay a good foundation for the further study of the application of robot sensitive skin and flexible tactile chemical sensor. It is expected to promote the development of bionic robots and service robots. In many fields, such as sports training, rehabilitation medicine, human body modeling and simulation, sports biomechanics, it has wide application prospect.

2. Materials and experiments

2.1. Matrix material

The flexible pressure sensitive conductive rubber matrix belongs to the polymer material. The mechanical properties of flexible pressure sensitive conductive rubber are largely dependent on the properties of the matrix material, since the matrix material has a significant effect on the properties of the composites after the addition of the conductive filler [4]. For example, adding a large number of conductive filler in the rigid matrix, although the conductivity is good, it will make the composite material brittle. However, for the flexible tactile chemical sensor used in the field of robotics, we need to choose the material with smaller and more flexible molecular force. As a continuous phase and composite of composite materials, the polymer matrix plays two roles, one is the matrix material, and the other is the fixed packing [5, 6]. The choice of polymer matrix material has a great influence on the comprehensive performance of conductive composites [7]. In general, the greater the crystallinity of the polymer, the higher the conductivity. It is generally believed that the conductive particles are distributed in the amorphous phase of the crystalline polymer matrix, and the increase of the crystallinity of the matrix is helpful to improve the concentration of the conducting particles in the amorphous phase, which is favorable for the formation of conductive path and the resistivity of the material [8].

2.2. Conductive material

Conductive filler is an important part of pressure sensitive conductive rubber. For a polymer material having an insulating property, a conductive polymer composite material can be usually made by adding conductive particles. Depending on the nature of the conductive filler itself and its content in the rubber matrix material, it determines the conductive properties and pressure sensitive properties of the pressure sensitive conductive rubber [9]. Therefore, according to actual needs, we choose the appropriate type, shape and dosage of conductive material. Commonly used conductive fillers include metal-based fillers, carbon-based fillers, metal oxide-based fillers, and composite fillers.

Conductive carbon black is a kind of carbon material with special microstructure, particle morphology and surface properties. Its main ingredient is carbon, containing a small amount of hydrogen, oxygen and sulfur and other elements, which determines the chemical properties of carbon black. Compared with other conductive particles such as metal, carbon black particles are the largest amount of conductive filler. A conductive polymer with carbon black as filler, its conductivity depends on the structure, particle size, specific area and porosity of carbon black to a large extent. The results show that the smaller the particle size of carbon black, the more complex the structure. The carbon black properties have a significant effect on the conductivity of the composites. Thus, the conductivity of the carbon black filled polymer composite depends on the type and amount of carbon black.

2.3. Nano - modified materials

Nanomaterial and nanotechnology will be the core material and core technology in new material and new technology. In the fields of microelectronics, metallurgy, chemical industry, electronics, national defense, nuclear technology, aerospace, medical and biological engineering, nano-materials research has been widely used. At the same time, it will also improve people's living environment and protect people's health. Nanomaterials generally refer to particles in a particle size. It is neither a typical microscopic system nor a typical macro system, but a typical mediated system. As the particle size into the nano-scale, the structure compared with conventional materials have undergone great changes. It has many unique physical and chemical properties in catalysis, photoelectricity, magnetism, heat, mechanics and so on. In recent years, nanomaterials have been used in polymers to improve the performance of polymer materials, and have achieved considerable results.

As shown in Table 1, we conducted experiments on the conductivity, material softness and piezoresistive properties of the samples. Among them, the proportion of nano-modified materials and silicone rubber is the percentage of mass. The piezoresistive characteristics of the samples of different nano-modified materials are shown in Fig. 1. On the basis of ensuring the softness of pressure sensitive rubber, nano-silica and aluminum oxide material can be better modified pressure-sensitive conductive rubber mechanical properties, piezoresistive properties, conductivity and other comprehensive performance.

Table 1. Comparison of different nano-modified materials

Sample	T1	T2	T3	T4
nanomaterials	zinc oxide ZnO	calcium carbonate CaCO	silica SiO_2	aluminum oxide Al_2O_3
carbon black CB3100/silicone rubber	8 %			
nano - materials/silicone rubber	3 %			

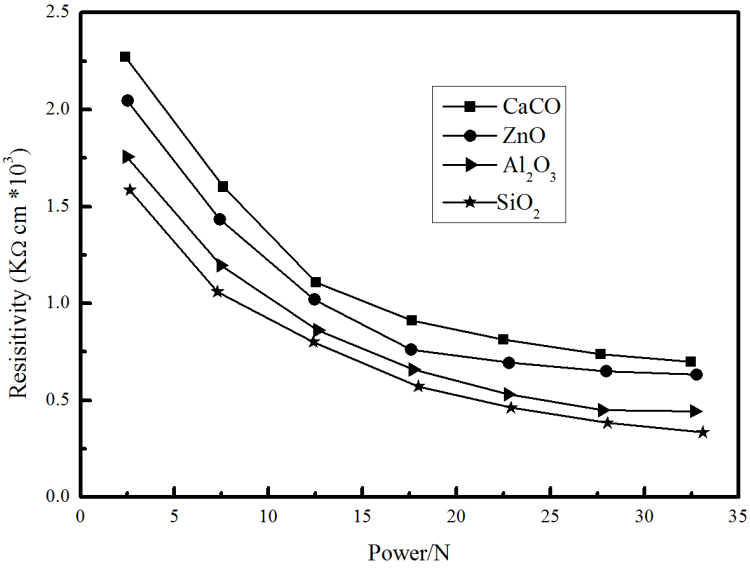

Fig. 1. Piezoresistive properties of different nano-modification materials

3. Research results and discussion

3.1. Experimental phenomena and results of dispersion treatment

Under normal circumstances, nano-conductive filler and nano-modified materials have a high surface energy, so it is very easy to reunite.In order to make the prepared conductive composite material has good uniformity and good conductivity, nano-conductive filler and nano-modified materials need to be dispersed. For nano-conductive filler, if the dispersion is not good, conductivity is not good. In the polymer matrix, the nanoparticles can be orderly distributed or disordered. In general, the aggregation of nanoparticles is aggregated particles, and the size of aggregates is always greater than the primary particle size of nanoparticles. Even if the coupling agent has been added to the silicone rubber to make the particles dispersed evenly, and the compatibility of the particles with the matrix is improved, it is difficult to disperse the particles to the primary particles. As the nano-modified materials have more surface-active light base and a large surface energy, thus limiting the nano-modified materials to enhance the effect.

The dispersion of nanoparticles refers to the process of uniform distribution in the liquid phase of the powder particles. It usually consists of three phases: liquid wetting the solid particles; through the external force to make the larger aggregates dispersed into smaller particles; to ensure that the powder particles in the liquid medium long-term uniform dispersion, and to prevent the scattered particles to re-aggregation. According to the different methods of dispersion, it can be divided into

physical and chemical treatment methods.

From the above experiments, we can see that nano-carbon black in the form of aggregation dispersed in the rubber matrix. At the same time, the results also explain the importance of the dispersion of nanoparticles on the structure and properties of the material forming. With the combination of mechanical agitation and ultrasonic agitation, we can make nanoparticles better dispersed in the polymer. Through the combination of mechanical stirring and ultrasonic dispersion method, the conductivity and stability of the material can get a relatively good effect. Therefore, combined with the effect of various factors, the first step is to use the mechanical stirring method to obtain the small aggregates from micron to hundreds of nanometers. Then, through the ultrasonic dispersion method, we get hundreds of nanometers to tens of nanometers nanometer particles. In the decentralized treatment, through the experiment, we can be preferred for nano-conductive filler and nano-modified materials with better dispersion effect of the dispersant and dosage.

3.2. The effect of the loading of conductive particles

The content of the conductive filler filled with pressure sensitive conductive rubber plays a key role in the electrical properties, mechanical properties and softness of the prepared sample. After the material is molded, it not only has a certain flexibility, but also has a suitable conductivity and pressure sensitive characteristics. Table 2 is the use of different proportions of conductive filler samples of each sample mass percentage. Figure 2 is the hardness of the sample at different addition ratios. Figure 3 shows the conductivity of the sample at different fill ratios.

Table 2. Experimental samples of conductive fillers at different addition ratios*

Samples		S1	S2	S3	S4	S5	S6	S7	S8
Component proportion	CB3100/RTV	4 %	6 %	7 %	8 %	9 %	10 %	12 %	15 %
	naphtha/RTV	50 %		60 %		70 %		80 %	100 %
	SiO_2/RTV	2 %							
	Si-69/RTV	3 %							

*CB3100 is carbon black, RTV is silicone rubber, and Si-69 is a silane coupling agent.

As can be seen from these two figures, under the premise of ensuring the flexibility of the composite material after molding, the filling ratio of the conductive filler is more suitable for the content of the pressure-sensitive conductive rubber. In this proportion, we can adjust the different conductivity requirements and pressure sensitive range.

3.3. Experiment and discussion

The mass ratio of conductive rubber should be within the percolation zone, so we test the temperature of the diafiltration sample. The temperature range of the experiment is 30 °C–90 °C. The temperature of the sample is recorded at a tempera-

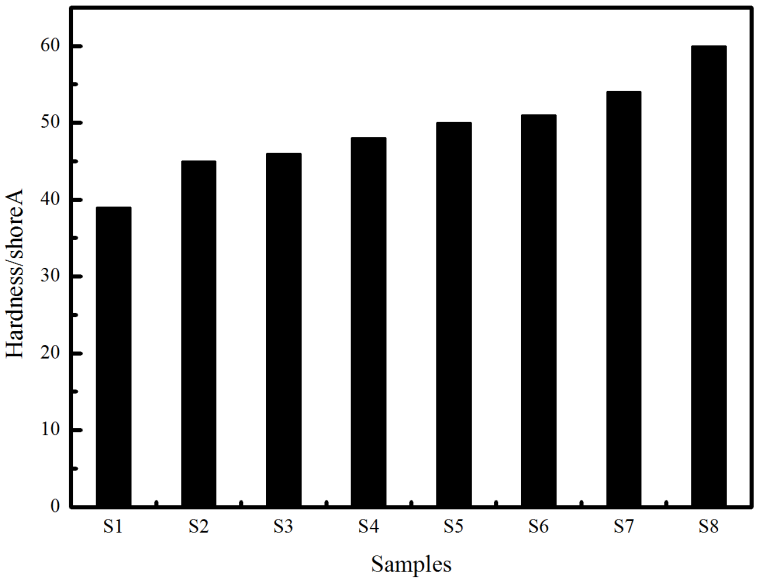

Fig. 2. The hardness values for different addition ratios

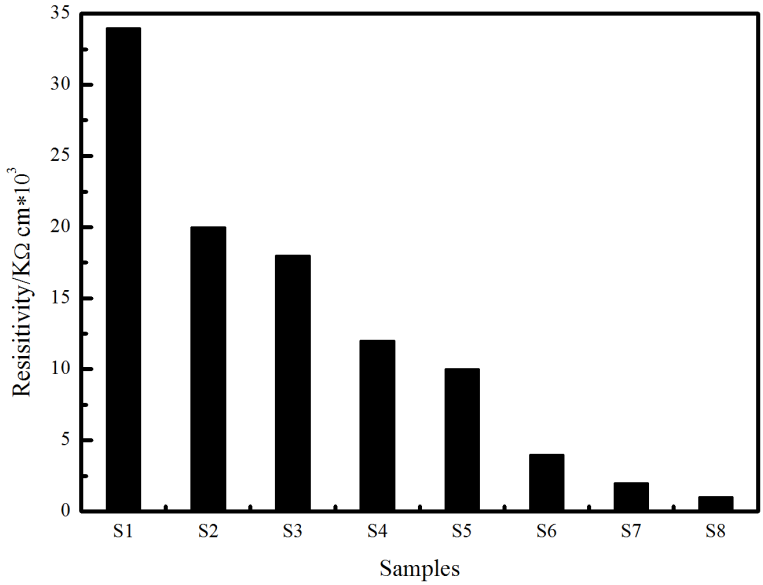

Fig. 3. Different proportionality of the conductive properties

ture of 10 °C for 20 minutes. The resistance temperature characteristics of pressure sensitive conductive rubber samples are shown in Figure 4. From the figure, we can see that the resistivity of samples N3, N4, N5 with the temperature rise are fluctu-

ated, especially the low filling of the sample is more significant. This shows that the effect of temperature on the tunnel effect is more obvious, that is, the thermal disturbance plays a leading role. As a result, the resistivity of the sample is decreasing, and it exhibits a negative temperature coefficient characteristic.

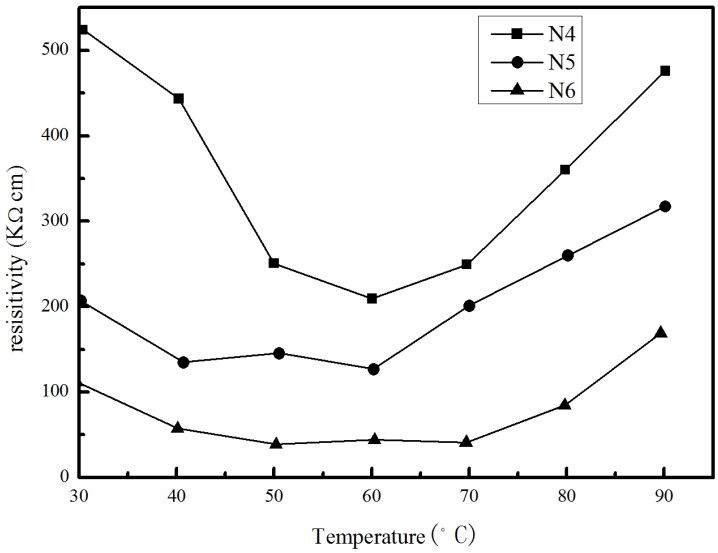

Fig. 4. Resistance temperature characteristics of pressure sensitive conductive rubber

After the temperature reaches a certain value, due to the different thermal expansion rate of the conductive carbon black particles and silicone rubber, resulting in a larger gap between the carbon black particles and the destruction of some conductive networks. As a result, the resistivity of the sample increases, and the thermal expansion at this time plays a dominant role, which exhibits positive temperature coefficient characteristics. In addition, it can be seen from Figure 5, with the increase in the content of carbon black, pressure-sensitive conductive rubber resistivity gradually reduced, and the temperature stability is getting better and better. This reduces the effect of thermal disturbances and also counteracts the thermal expansion of colloids. Therefore, under the high filling ratio, the interaction of thermal and thermal expansion can improve the resistance temperature characteristics of the sample. At the same time, by the temperature effect experiment, it further validates the effect of the conductive mechanism of the tunneling effect under the low packing concentration in the percolation zone.

4. Conclusion

In this paper, we studied the pressure-sensitive conductive rubber materials, the performance of each component and preparation technology. Firstly, analyzing the

mechanical properties of the base material of flexible pressure sensitive conductive rubber and the conductivity, surface structure, physical and chemical properties of various conductive fillers, we obtained pressure sensitive conductive rubber matrix material and conductive filler with good mechanical and electrical properties. Then, we studied the properties and composition of various nano-modified materials suitable for improving the performance of pressure-sensitive conductive rubber. Finally, we studied the effects of material dispersion treatment, material forming process and various auxiliary materials, which provided economically feasible material formulation and process for the preparation of pressure sensitive conductive rubber. However, the current study is just preliminary. The design of the structure, the calculation model, and the self-characteristics of the pressure-sensitive conductive rubber material need to be improved and perfected. With further model correction, we can improve the detection accuracy of flexible multidimensional array tactile chemical sensors. The research results can not only meet the urgent needs of the robot field, but also can be used in sports training, rehabilitation medicine, sports biomechanics and many other areas.

References

[1] T. N. Tallman, J. A. Hernandez: *The effect of error and regularization norms on strain and damage identification via electrical impedance tomography in piezoresistive nanocomposites*. NDT & E International *91* (2017), 156–163.

[2] X. Guo, Y. Huang, X. Cai, C. Liu, P. Liu: *Capacitive wearable tactile sensor based on smart textile substrate with carbon black/silicone rubber composite dielectric*. Measurement Science and Technology *28* (2017), No. 4, paper 045105.

[3] H. Ying, M. Wei, L. Li, W. Cai, Q. Yang, Y. Ge: *Research and experiment of electrodes for 3D force flexible tactile sensor*. Journal of Electronic Measurement and Instrument *27* (2013), No. 1, 57–63.

[4] M. Ha, S. Lim, J. Park, D. S. Um, Y. Lee, H. Ko: *Bioinspired interlocked and hierarchical design of ZnO nanowire arrays for static and dynamic pressure-sensitive electronic skins*. Advanced Functional Materials *25* (2015), No. TOC19, 2841–2849.

[5] S. H. Li, Y. J. Ge, Y. Huang, Y. B. Wang, H. B. Cao, J. X. Ding: *Application of conductive rubber filled by carbon black for 3-D force measurement*. Applied Mechanics and Materials *300–301* (2013), 547–550.

[6] M. Ohmukai, Y. Kami, K. Ashida: *Conducting rubber force sensor: Transient characteristics and radiation heating effec*. Journal of Sensor Technology *3* (2013) No. 3, 36–41.

[7] M. H. M. Som, K. Nagamune, S. Kawaguchi: *Performance comparison of conductive rubber-based sensor array calibration using cubic spline and back propagation neural network*. International Journal on Information *18* (2015), No. 2, 673–688.

[8] S. G. Woo, I. H. Lee, K. C. Lee: *Hybrid fabrication process of additive manufacturing and direct writing for a 4*4 mm matrix flexible tactile sensor*. Journal of Mechanical Science and Technology *29* (2015), No. 9, 3905–3909.

[9] S. Jung, J. H. Kim, J. Kim, S. Choi, J. Lee, I. Park, T. Hyeon, D. H. Kim: *Reverse-micelle-induced porous pressure-sensitive rubber for wearable human-machine interfaces*. Advanced Materials *26* (2014), No. TOC28, 4825–4830.

Received October 12, 2017

Acta Technica *62* No. 2B/2017, 769–778

Design and research of test platform for grounding device technology based on DSP builder

Qingqing Zeng[1], Junxia Lang[2]

Abstract. The grounding device is always an important problem to be solved in power network, which is directly related to the safety of people and equipment. However, the measurement of traditional grounding devices has the characteristics of instability and low reliability. Therefore, the design and research of the test platform for grounding devices based on DSP Builder was proposed in this paper. The working mechanism of grounding device was described, and the test platform of grounding device based on DSP Builder was constructed. Finally, through the test of the performance of the platform, it was concluded that the design of the platform for the grounding device based on DSP Builder is reasonable. In addition, the measured data has small difference from the actual values with good accuracy and stability.

Key words. DSP Builder, grounding device, technical test, platform design.

1. Introduction

With the continuous development of economy and science and technology, people's demand and demand for power systems are also increasing. The larger the scale of the grid, the greater the current required for ground short circuit, and the higher the grounding requirements. At the same time, the grounding is also closely related to the whole power system and the safety of people and equipment [1]. In the past power system, the power equipment was damaged because of the defects of the grounding device, which made the power plant shutdown or even serious accidents. As the complexity of the power system increasing, in order to avoid more unnecessary people and equipment property losses caused by serious accidents, the study of grounding device and grounding device testing has become the focus of research in recent years, which is of great significance.

[1]Department of Energy Engineering, Chongqing Energy College, 400041 Chongqing, China
[2]Department of Architectural design & Engineering Management, Chongqing Energy College, 400041, Chongqing, China

2. State of the art

At the beginning of people's understanding of the power grid, the measurement of the characteristic parameters of the grounding device was mainly to measure the ground resistance, and the experiment was carried out in the traditional way. An electrode was installed at a relatively far distance from the grid, and the result was the ground resistance by comparing the measurement of the auxiliary electrode resistance, the current and voltage at the two ends of the grid [2]. This traditional method was not only complicated, but also needed a lot of work. At the same time, the influence of the auxiliary electrode on the potential distribution was not considered in the process of measurement. Moreover, the auxiliary electrode was easily disturbed in the strong magnetic field and could not be effectively measured. With the development of technology, it was found that the measurement method of grounding device had many errors, and the reliability was low. Therefore, after 1960, people gradually accepted the principle of potential drop measurement. Up to now, the potential drop method can still be used in the ANSI/IEEE standard [3]. The method of potential drop measurement is the installation method of the auxiliary electrode, that is, the grounding body and the voltage potential drop curve are measured by changing the position of the constant voltage pole, and then the grounding resistance is obtained by analyzing the curve. In the same way, a lot of work is needed, and complex things such as potential drop curves are also needed. It is not easy to perform relevant operations at the scene [4]. Therefore, in the following research, some experts have proposed a relatively simple theory, in which the three-pole potential compensation method is one of the most widely used methods.

In order to reduce the interference of grounding resistance measurement, the related researchers have improved on the basis of the three-pole compensation method, and obtained a lot of advanced measurement methods, such as inverting method [5]. However, due to technical and environmental limitations, the final measurement results of these methods are inaccurate. Because the interference signal is uncertain in actual situations, the measured values are different. Therefore, in order to better remove the interference in the signal, it is necessary to ensure that the ground resistance has a more accurate measurement value [6]. Later, some scholars put forward the grounding resistance measurement method based on white noise, the phase compensation method, variable frequency and small current method.

3. Methodology

3.1. Grounding device technology and its basic principles

The grounding of the power system is to make the metal objects on the ground or some nodes in the circuit connect reliably through the wires and the earth, so that the potential of the metal objects or the nodes is consistent with the earth. In essence, in the case of normal, accident and lightning strikes, the power system can use the earth as a component of a ground current loop to hold the ground to the ground potential [7]. Therefore, the main function of grounding is to prevent

damage to devices and lines in the power system when struck by lightning, and prevent electrostatic damage and personal electric shock, so as to ensure the normal operation of the power system and the personal safety [8]. According to the different purposes of electrical equipment, the grounding is divided into three kinds. The first is the protective grounding, which is mainly to protect the personal safety, avoid the damage of the insulation materials in the equipment and the risk of electric shock. The second is the working grounding, which is mainly to ensure the normal operation of the power system. The third is grounding for lightening, which is to drain the lightning into the earth to get rid of the dangerous voltage [9].

A hemispherical ground body and its potential distribution in a homogeneous soil are shown in Fig. 1. The resistance of the current to the earth after passing through the grounding body is the dispersion resistance. The contact resistance between ground and soil is much smaller than the dispersion resistance, so the grounding resistance is practically equal to the dispersion resistance [10].

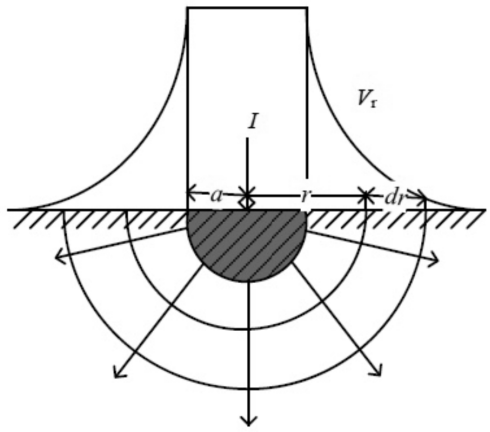

Fig. 1. Hemispherical ground body and its potential distribution in homogeneous soil

Let I be the current that from the earth electrode flows into the earth, and a is the radius of the grounding electrode. The earth is assumed to be homogeneous, and its resistivity is ρ. The current density in the soil with the center distance of r is J and the electric field corresponding to this is shown in the formula

$$E = J\rho = \frac{I\rho}{2\pi r^2} \tag{1}$$

As shown in formula (2), the resistance of hemispherical ground electrode from radius a to radius r is

$$R' = \frac{V_{ar}}{I} = \frac{\int_a^r E\,\mathrm{d}r}{I} = \int_a^r \frac{\rho\,\mathrm{d}r}{2\pi r^2} = \frac{\rho}{2\pi}\left(\frac{1}{a} - \frac{1}{r}\right) = \frac{\rho}{2\pi a}\left(1 - \frac{a}{r}\right). \tag{2}$$

When $r \to \infty$, there will be

$$R = R'_{\infty} = \frac{\rho}{2\pi a}\,.$$

3.2. Design and construction of technical test platform for grounding device based on DSP builder

In this article, the test platform for grounding device technology is designed and constructed mainly through the DSP Builder technology. Therefore, the test system for grounding device technology can achieve accurate measurement and tracking of the impact grounding resistance. In actual situation, better voltage and current signal acquisition requires the test system has a fast response speed and reliable stability. The hardware diagram of the test platform is shown in Fig. 2. As can be seen there , DSP is mainly the core of the system's control processing, including voltage divider, impact current generator, data acquisition, data preprocessing part, LCD display, keyboard and other peripheral circuits. The following describes the principle of grounding device test platform based on DSP Builder. First, after the measurement command is received by DSP, a trigger pulse is generated to control the impulse current generator, and an incident current injection grounding device is generated. The voltage divider and diverter will sample the response voltage signals and the current signals according to a certain proportion, and then send them to the AD converter after the signal conditioning to carry out the data acquisition of the two channels' signals. After the DSP's corresponding data processing and calculation, finally the operation results are displayed by the LCD.

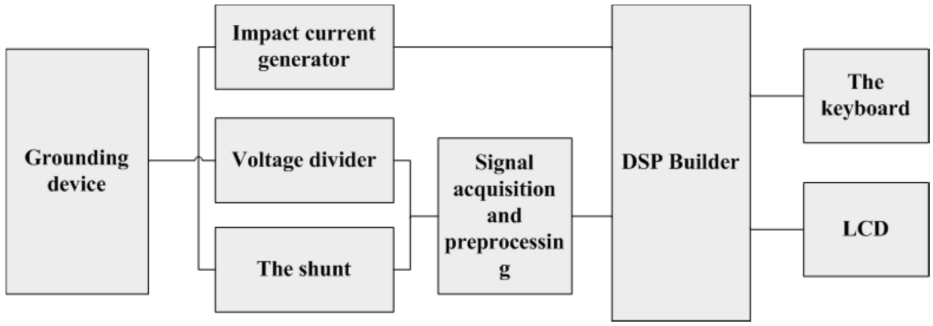

Fig. 2. Schematic diagram of test platform hardware

This paper is based on DSP Builder technology to carry out the design of testing platform for grounding device technology. The design based on DSP Builder is a fully up and down design process. Both the description of the platform system and the implementation of hardware can be completed in a complete design environment. The following is the design steps for DSP Builder. First of all, the design of the platform is mainly modeled by Simulink module and DSP Builder module. The main modeling environment is MATLAB/Simulink, and the corresponding parameters of each module are set. At the same time, through the Simulink platform, the system functions of the DSP system and the corresponding modules are simulated and

verified.

Secondly, Signal Compiler module in DSP Builder toolbox is used to compile the model which has already been built in the platform. At the same time, the Simulink file is transformed into VHDL description code, and the TCL script is used for synthesis, emulation, and compiling. After we get the VHDL file, the system will provide two options, the automated process or the manual process. An automated process is a process that can almost ignore hardware. Quartus and other EDA software can be automatically called to complete adaptation such as synthesis and netlist generation, until the FPGA configuration is downloaded from MATLAB. The manual process is basically the same as the design process of EDA standards based on the VHDL, except for design input and behavior level simulation validation.

Finally, the hardware is simulated for the VHDL generated by the previous step, and the function simulation is done by automatically generating the TCL script and the simulation of the simulation incentive file. Download the configuration files generated by the Quartus II to the target device and form the required hardware system. In the experiment of test platform for grounding device technology based on DSP Builder, it is necessary to test and calculate the grounding resistance. The formula (3) shows the mathematical expression of the impulse current signal with double exponential wave in theory.

$$i\left(t\right) = I_{\mathrm{m}}\left(\mathrm{e}^{-\frac{t}{T_2}} - \mathrm{e}^{-\frac{t}{T_1}}\,,\right) \tag{3}$$

where I_{m} represents the peak of the impact current, T_1 represents the time at which the theoretical wave head appears and T_2 represents the time at which the theoretical coda appears. From equation (3) we can see that the amplitude and steepness of impulse current waveform formed by different parameter values are different. The amplitude of standard lightning impulse current waveform adopted by this algorithm is 5000 A, and the time of wave head and wave tail is $2.6/50$ μs.

According to formula (2), the maximum values of the corresponding impulse voltage $u_2'(n)$ and standard lightning current waveform sequence $i_2(n)$ that be found by the software. The theoretical impulse grounding resistance R_{ch}' is calculated as shown in equation

$$R_{\mathrm{ch}}' = \frac{u_{2m}'(n)}{i_{2m}(n)} \tag{4}$$

where, $u_{2\mathrm{m}}'(n)$ and $i_{2\mathrm{m}}(n)$ are the maximum values of $u_2'(n)$ and $i_2(n)$, respectively.

In addition to hardware design, the grounding technology test platform based on DSP Builder still needs to design the software. The management of system measurement and control, data collection and analysis are realized by corresponding software. According to the actual demands, TMS320F2812 DSP is adopted as the core of the measurement system. According to the characteristics of TMS320F2812 DSP and the existing problems, the high-level language C is used to do the corresponding software design, so as to improve the readability and portability of the program and reduce the difficulty of software programming. As a platform software program code to edit and debug software, Code Composer Studio 2.21 (CCS) provides program code editing tools, which has painting capabilities and real-time debugging capabil-

ities. The following is the basic idea of the master program of the platform system, that is, after the initialization of the DSP system, all commands, states, and related storage units are restored to their initial state. Upon entering the test process, the DSP system issues a capacitor charging command that causes the pulse to trigger the thyristor of the current generator. In this way, the impulse current is simulated in the grounding device. Meanwhile, the AD switch is started to collect the voltage and current signals. After the AD conversion technology, the current and voltage data will be analyzed and judged. Then the corresponding calculation of voltage and current data is carried out by measuring and calculating program. Finally, the grounding resistance value is displayed on the display. This cycle goes into the next measurement calculation process of grounding resistance.

4. Result analysis and discussion

According to the above mentioned, the construction of the grounding device technology test platform based on DSP Builder has been carried out. In order to better test the performance of the platform, the measurement platform of grounding device based on DSP Builder is simulated. The generation of impulse current and the adjustment signal and the measurement and calculation of impulse grounding resistance are tested. Fig.3 shows the analog impulse current and voltage waveform. As can be seen from the diagram, the corresponding impulse voltage waveform is collected at channel 1, and the impulse current waveform is acquired by channel 2. As can be seen from the waveform diagram, the response of the voltage signal to the wave head and wave tail is about $8/59\,\mu s$, and the current signal's wave head and wave tail is about $12/59\,\mu s$. It shows that the simulated impulse current waveform in the platform is similar to that of the previous standard lightning impulse waveform. That is to say, the design of the test platform is in line with the requirements. Based on the comparison of the data and waveform, it can be seen that the time of the wave head of the voltage waveform is faster than that of the wave head in the current waveform, and the response voltage waveform is less smooth as that of the current. This is mainly due to the fact that the load ground model contains inductance components so that the current signal lags behind the voltage signal. At the same time, inductance exists in the load ground model, which has great influence on the current waveform. The larger the inductance is, the greater the influence of the current waveform is, and the longer the wave head time lags.

Table 1 shows the resistance values measured under different model parameter conditions. From the data in the table can be seen, the measured values of the resistance of test platform for grounding device technology based on the DSP Builder are relatively stable. Moreover, there is little error between the actual measured values and the theoretical values. This shows that the calculation and measurement algorithm based on the DSP Builder grounding device technology's test platform is correct, and the principles of the clipping algorithm are feasible to measure the impulse grounding resistance.

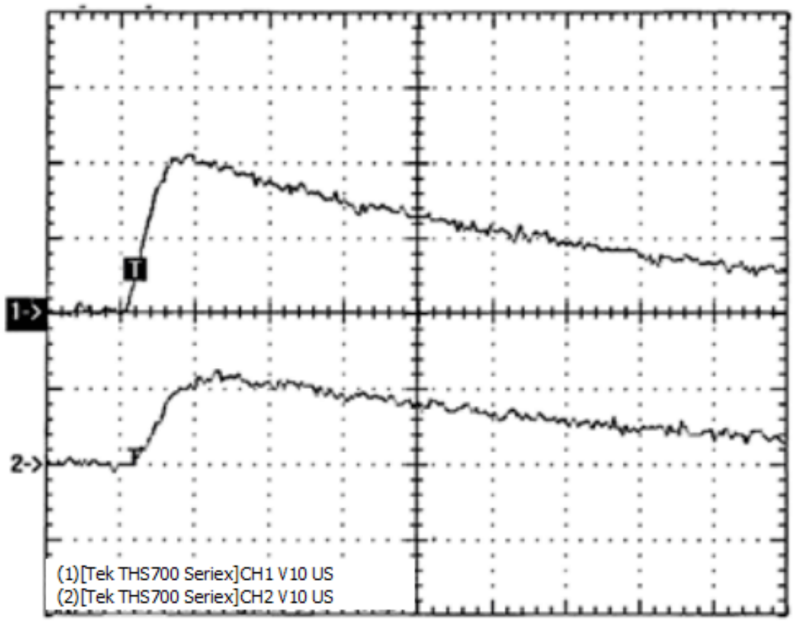

Fig. 3. Analog impulse current and voltage waveform

Table 1. Resistance values measured under different model parameters

R (Ω)	L (μH)	Measured impulse grounding resistance (Ω)			Calculated value (Ω)
49	125	18.08	18.21	17.95	16.25
25	125	14.2l	13.88	14.35	13.02
15	125	10.12	10.50	10.67	9.52
10	125	7.77	7.94	7.88	7.14
49	220	26.56	26.16	26.79	24.21
25	220	17.55	17.40	17.07	16.15
15	220	11.90	11.78	12.13	11.13
10	220	8.64	8.85	8.95	8.03
49	350	32.03	31.77	32.26	28.88
25	350	19.82	20.09	19.68	18.11
15	350	13.21 1	13.05	13.28	12.04
10	350	9.27	9.38	9.16	8.45

In summary, the experimental process of simulating shock current generation, conditioning signals, and calculating impulse grounding resistance shows that the design of test platform for grounding device technology based on DSP Builder is reasonable and feasible. It can capture the impact current and resistance signal and present the corresponding waveform more accurately. Compared with the previous testing technology, it has better stability and accuracy, and has higher practical

value. However, there are some deficiencies in the test platform for grounding technology based on DSP Builder. For example, the hardware and software design of the platform's system needs to be further optimized, and more testing environments need to be considered. All of these need further research and improvement.

5. Conclusion

With the expansion of power grid scale, the requirement of docking device technology is increasing day by day. In order to better protect the safety of people and equipment, and avoid unnecessary accidents and property losses, the measurement of grounding device technology has become the focus of research in recent years. In this paper, the problems existing in the traditional grounding device and the mechanism of the grounding device were expounded. On the basis of grounding device mechanism and DSP Builder, the design and construction of the test platform for the grounding device technology were carried out. Finally, for the test platform for the grounding device technology based on DSP Builder, the simulated generation of impact current, conditioning signals as well as measurement and calculation of impulse ground resistance were tested. The results analysis shows that the simulated impulse current waveform in the platform is consistent with the previous standard lightning impulse waveform, that is, the design of the platform is reasonable. At the same time, the measured values of the resistance measurement based on DSP Builder grounding device test platform are relatively stable, and the errors between the actual measured values and the theoretical calculated values are not large. Therefore, the test platform measurement of grounding device technology based on DSP Builder is accurate and stable. However, there are still some problems in the design of the test platform for the grounding technology based on DSP Builder, which need further research and improvement.

References

[1] B. D. Rodrigues, S. Visacro: *Portable grounding impedance meter based on DSP.* IEEE Transactions on Instrumentation and Measurement *63* (2014), No. 8, 1916–1925.

[2] P. Beckett, R. Heiko: *Run–time control of subthreshold current using double–gate device technology.* IEEE International Symposium on Electronic Design, Test & Applications, 13–15 Januar 2010, Ho Chi Minh City, Vietnam, IEEE Conference Publications (2010), 245–249.

[3] J. Stephen: *Ion implantation in semiconductor device technology.* Radio and Electronic Engineer *42* (1972), No. 6, 265–283.

[4] M. Masahara, Y. Liu, K. Endo, T. Matsukawa, E. Suzuki: *Vertical double-gate MOSFET device technology.* Electronics & Communications in Japan *91* (2008), No. TOC1, 46–51.

[5] T. Netzel, H. Hein, Y. Hein: *APAP device technology and correlation with patient compliance.* Somnologie - Schlafforschung und Schlafmedizin *18* (2014), No. 2, 113–120.

[6] P. Falcaro, R. Ricco, C. M. Doherty, K. Liang, A. J. Hill, M. J. Styles: *MOF positioning technology and device fabrication.* Chemical Society Reviews *43* (2014) No. 16, 5513–5560.

[7] T. Goto, H. Igarashi, Y. Kumagai, K. Keisuke, S. Atsushi: *New method about measurement of ground resistance for where surfaced with asphalt.* J-Global, Papers of Technical Meeting on Transportation and Electric Railway, IEE Japan *TER13* (2013), Nos. 16–32, 23–28.

[8] H. J. Gil, D. W. Kim, G. S. Kil: *A study on the improvement of electrode installation for measurement of ground resistance through investigation on the spot in buildings.* Journal of Korean Institute of Illuminating and Electrical Installation Engineers (KIIEE) *25* (2011), No. 5, 92–97.

[9] D. W. Kim, H. J. Gil, D. O. Kim, K. Y. lee, H. W. Moon, H. K. Kim: *Measurement error analysis of ground resistance using the fall-of-potential method according to the locations of auxiliary probes.* Transactions of the Korean Institute of electrical engineers *59* (2010), No. 2, 222–231.

[10] M. A. Salam: *Grounding resistance measurement by grid electrode in Brunei Darussalam.* International Journal of Energy Technology and Policy *8*, (2012), No. 2, 196 to 208.

[11] L. E. Ring: *RDHWT/MARIAH II Systems integration studies review.* IAerodynamic Measurement Technology and Ground Testing Conference (AIAA), 28 June–1 July 2004, Portland, Oregon, AIAA Meeting Papers 2004–2486.

Received October 12, 2017

Acta Technica *62* No. 2B/2017, 779–788

Construction of prison wireless management system based on active RFID wireless sensor

Hongyan Sun[1]

Abstract. With the increasing population base and crime ways, the population of prison inmates increased a lot, which raised higher requirements on prison management. Based on this, wireless management system is proposed to enhance the intelligent management of prison. This paper conducted a research on the construction of prison wireless management system based on active RFID wireless sensor. First, the paper analyzed RFID technology, discussed the application advantage of active RFID sensor in prison wireless management system, and then analyzed the demands of designing wireless management system, including the access control management subsystem, regional management system, prison factory personnel positioning subsystem and auxiliary systems, etc. On this basis, the research combined software systems to construct the management system and improve the functionality and reliability of the prison management system.

Key words. Active RFID, prison, wireless management.

1. Introduction

With the continuous development of computer technology and communication technology, traditional prison system can no longer satisfy the actual demands. Prison information management is an inevitable trend for the development of modern prison management. The innovative combination of all the prison systems can improve the management mechanism, organizational structure and personnel quality of the prison, promote a scientific, fair, safe and effective development of prison management based on the principles of optimization, improvement and recombination, and better perform the nature intelligence of the prison. The prison wireless management system based on active RFID wireless sensor is an effective prison management system which plays an important role in the prison management system and can satisfy various demands.

RFID (radio frequency identification) technology is originally used to improve the performance of radar recognition on target planes in World War II [1]. But

[1]Henan Judicial Police Vocational College, 450046, Henan, China

limited to the high cost, RFID technology is not widely applied. Since the 21st century, RFID technology started to enter people's daily life. With the development of integrated circuit and network communication technology, RFID technology, featuring an accurate and rapid recognition on moving objects, entered the commercial industry as a recognition technology with its own characteristics of multi-target and non-contact recognitions, and can be used for various kinds of recognition and monitoring systems [2]. At present, RFID presented enormous development space and prospects, which is considered as one of the most potential technologies in the 21st century. Especially in the IT industry, RFID is widely concerned and is regarded as the next "gold mine" for the IT industry. Nowadays, all the software factories showed great interests in RFID and have conducted a large amount of investments on this aspect.

In recent years, with the soaring population base, current prison armed forces and traditional defense methods can no longer satisfy the actual demands, and it becomes imperative to promote the prison wireless management system. The automatic information recognition and acquisition that RFID possessed matches well with the prison detection system. Especially on monitoring moving objects, RFID has an incomparable advantage against other monitoring technologies [3]. This paper will conduct a research on the construction of prison wireless management system based on active RFID wireless sensor.

2. RFID system

2.1. Composition of RFID system

As a non-contact automatic recognition technology, RFID technology obtains the target information mainly by launching radio frequency signals. This technology is applicable for various environments without requiring human intervention. Different from traditional recognition technologies which are limited by single recognition, RFID can recognize multiple labels with certain operation convenience. RFID system mainly consists of label, reader and antenna [4].

The label mainly includes label antenna, modem, clock, storage and code generator. The label is featured with uniqueness. Each label represents one piece of information which is similar to the barcode in traditional recognition technologies. The labels in the recognizable region of RFID can be effectively recognized and the recognition process is mainly accomplished by reading and writing information through the storage. Some active electronic labels are integrated with extension units such as MEMS sensor.

The reader is a device for label reading and writing. There are mainly two types of readers: handheld reader and stationary reader. Currently, the microprocessors of many readers continued the embedded system, which has the functions of signal state control and error correction. The reader mainly consists of radio frequency module and reader module [5].

RFID antenna is designed for the spatial transmission of radio frequency signals for the label and the reader. RFID antenna is usually installed on the reader or

connects the reader through cables. In practical use, the main factors that influence the recognition distance of RFID antenna include the system power and the structure of the antenna [6].

2.2. Working principle of RFID system

The working principle sketch of RFID is shown as Fig. 1.

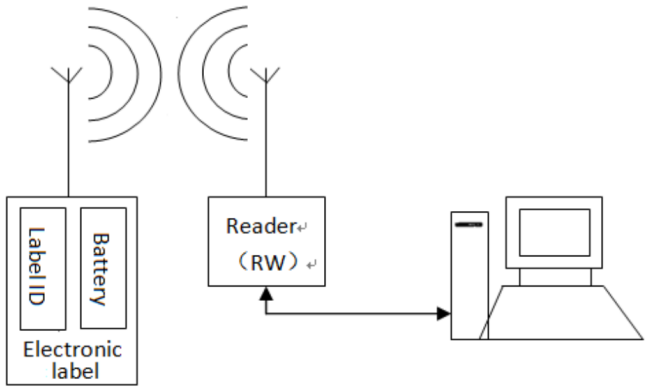

Fig. 1. RFID working principle sketch

According to Fig. 1, the RFID system working principle is shown as below: First, set the data and radio carrier signal mode through the reader as "send out by antenna". At this time, the monitoring is started in a certain area. When a RFID label enters the area, it will be detected and transmitted to the system through the antenna after checking the information code in the reader. When receiving the carrier signals of the RFID label, the system will transmit the signals to the reader and decode the signals through the modem and then deliver to the backend computer controller. After that, the computer controller will judge the validity of the RFID label by logic operation, make corresponding control treatment on different settings, and send commands to control the actions of the actuator. Upon receiving the signals, the actuator will execute the corresponding commands. Through the computer communication network, all the monitoring points can be effectively connected to compose a general information control platform and realize the expected functions by designing different software for different projects [7].

2.3. Active RFID system

According to different working initiatives, RFID technologies can be divided into active RFID and passive RFID [8]. In real applications, active RFID and passive RFID can be combined to accomplish specific projects. However, in the future development, active RFID technology will certainly become an important development direction. Passive RFID technology is only applicable for simple and short-distance recognition, which cannot be used for positioning and multi-target and wide-range

management. Essentially, the performance of active RFID is much better than passive RFID. Active RFID technology possesses the sensing ability between label and reader, interaction ability between label and reader, anti-collision ability, ability of avoiding the influences from human body, metal and fluid, ability of loading sensing technology and data security, etc. In addition, active RFID technology can be used to search specific persons or objects, with externally embedded sensor or LED lights available. The positioning computation of active RFID technology is conducted by maximum likelihood method, as shown in Fig. 2 [9].

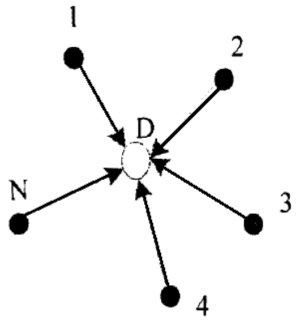

Fig. 2. Maximum likelihood method

Assume the coordinates of $1-N$ points in Fig. 2 are (x_1, y_1), (x_2, y_2),...(x_n, y_n), respectively, then the distances between these points to the nodes are $d_1, d_2, ...d_n$, respectively, and the coordinate of point D is (x, y). Then:

$$\begin{cases} (x_1 - x)^2 + (y_1 - y)^2 = d_1^2, \\ \quad\quad ... \\ (x_n - x)^2 + (y_n - y)^2 = d_n^2. \end{cases} \tag{1}$$

That is

$$\begin{array}{c} x_1^2 - x_n^2 - 2(x_1 - x_n)x + y_1^2 - y_n^2 - 2(y_1 - y_n) = d_1^2 - d_n^2, \\ x_{n-1}^2 - x_n^2 - 2(x_{n-1} - x_n)x + y_{n-1}^2 - y_n^2 - 2(y_{n-1} - y_n) = d_{n-1}^2 - d_n^2. \end{array} \tag{2}$$

The linear equation $AX = b$:

$$A = \begin{bmatrix} 2(x_1 - x_n) & 2(y_1 - y_n) \\ ... & ... \\ 2(x_{n-1} - x_n) & 2(y_{n-1} - y_n) \end{bmatrix},$$

$$b = \begin{bmatrix} x_1^2 - x_n^2 + y_1^2 - y_n^2 - d_1^2 + d_n^2 \\ ... \\ x_{n-1}^2 - x_n^2 + y_{n-1}^2 - y_n^2 + d_n^2 - d_{n-2}^2 \end{bmatrix}. \tag{3}$$

So the coordinates of point D will be

$$\hat{X} = \left(A^{\mathrm{T}}A\right)^{-1} A^{\mathrm{T}}B\,. \tag{4}$$

3. General design of prison wireless management system based on active RFID sensor

3.1. Demand analysis of the system design

As an integrated comprehensive system, prison management system mainly contains computer control, automatic control, sensor and communication network technology, including RFID personnel management system, positioning and digital video monitoring system [10–12], Active detection system. Considering the technical integrity and functional complexity, the designing of the management system shall stick to the principles of standardization, security and reliability, advancement, openness and extensibility, easy in implementation, and maintainability.

Prison management system is an application system integrated with hardware and software, which is specially designed for prison monitoring. In its real application, the system can recognize the personnel type safely and reliably, employ an intelligent one-to-one management between prisoners and system recorded personnel, and realize a true automatic information management. The system can manage the population and personal information of the inmates in each control area of the prison, prevent them escaping from the prison, and effectively reduce the probabilities of criminals making trouble in the prison. In addition, the system can adopt private monitoring for high-level criminals, keep a close eye on the prison to avoid violent incidents, and assure the stable operation of the prison as well as the safety of the inmates to the maximum. Meanwhile, the system can monitor the population of specific areas, detect the outbound personnel dynamically, and reduce the workloads of the prison personnel. When an emergency occurs, the system can position all the police officers rapidly.

Access control: The system will conduct real-time monitoring at each entrance, take real-time videos of all the personnel entering and exiting the prison, automatically record the time and the information of the personnel, and report an alarm when abnormal situation is detected; Real-time monitoring: a real-time monitoring will cover all the workplaces, important monitoring areas, prison hospital, washrooms and recreation yards, etc. The system will set an information feedback interval cycle, and submit a personnel monitoring report to the center at each cycle. When the monitoring personnel is out of the designated area, an alarm will be triggered, and the real-time information of the violator will be reported the management personnel; Police sentry positioning: the system will position the personnel on duty to assure they act in a certain area. As soon as they are away from the sentry unexpectedly, the system will send a warning, and restrict the personnel at the non-duty area. In case any non-duty personnel enters the duty area, the system will deliver a warning automatically; Prison factory management: during the prison period, labor inmates shall not leave their workplaces. They are under a whole process of monitoring. For inmates who leave their workplaces unexpectedly, the system will send a warning, report the information to the management personnel, and record the position of the inmate (s) in real time; for inmates working at farms or mines, handheld devices can be used to conduct real-time monitoring on certain personnel in the area. Once

escape occurs, the device will report an alarm and inform all the police officers to take arrestment; video monitoring and control: a remote real-time monitoring is conducted at the connection between the prison and the outside world. In addition, the system will control the monitoring devices, environment light and sound equipment respectively according to different priority levels so that to accurately monitor the places with frequent situations.

3.2. Construction of prison wireless management system based on active RFID wireless sensor

The prison wireless management system based on active RFID wireless sensor mainly consists of access control management subsystem, regional management subsystem, prison factory personnel positioning subsystem and auxiliary system.

Software design. Software design mainly includes personnel management and data base. VB 6.0 is used to develop personnel management part, and SQL Server is used to design the data part. The designing rule of the personnel management part is similar to the above, including access control management subsystem, regional management subsystem and prison factory personnel positioning subsystem. An effective control on the personnel can be realized by establishing related data sheet and inputting them in the system. For example, an access record table as shown in Table 1 can be established.

Table 1. Access record table

Field name	Content	Type	Length	Remarks
ID	Card no.	Text	5	NOT NULL
DoorID	Gate no.	Text	4	NOT NULL
InDate	Entry date	Date	8	NULL
InTime	Entry time	Time	6	NULL
OutDate	Exit date	Date	8	NULL
OutTime	Exit time	Time	6	NULL
State	Access control state	Yes/No	2	NULL
Alart	Alarm	Yes/No	2	NULL

Access control management subsystem. As a modern security management system, access control management subsystem plays an important role in working environment security and personnel attendance, which is an effective measure taken by prisons to conduct security guard management. The working principle is to make various magnetic cards according to different activity areas of the personnel, set the activity area in the magnetic cards, establish access controls at important places as the entrances, elevators, equipment control center and warehouse of the main management areas inside the prison building, assure the security of all the areas through real-time monitoring, and realize the real-time monitoring and control of all the regions only by the control center. When entering related area, the entrant should use a magnetic card with related permission to release the access control. The system would also perform a real-time monitoring through the active RFID sensors installed

at each access control, and lock the facial information of the personnel. As soon as the violator enters unauthorized area, the system will effect an alarm, lock the real-time position of the violator, inform the police officers of other areas to head for the site to take actions. In actual designing, separated structured active RFID sensors are used to conduct access control management on related personnel. As the access control recognition device, the active RFID sensors are installed at key positions of the monitoring areas respectively, which are connected to the control center through Ethernet network to assure the flexibility, communication and real-time monitoring and control of the system.

Regional management subsystem. This part mainly includes roll call of the personal in the region, sentry inspection of the on-duty police officer, and work of laborers. The prisoners need to be gathered in a certain area when proceeding roll calls, recreation, dining or working. At this time, the prison guard should know the number of the inmates in the area, and notice when there is any absence or departure. Except for the management on the inmates, the on-duty prison guard should be also managed to enhance a full play of their monitoring and management functions. At this time, active RFID sensors can be used for the real-time management on the inmates and the prison guard. The actual design of regional management subsystem continued the way of access control management subsystem. The hardware mainly consists of active RFID sensor and label. In a certain gathering area, the inmates and prison guard are under a real-time monitoring, and their real-time information will be transmitted to the control center every 10 seconds. Based on the standard data entered in the data base, if any abnormal situation occurs, a notice and warning will be delivered. The regional management function sketch is shown as Fig. 3.

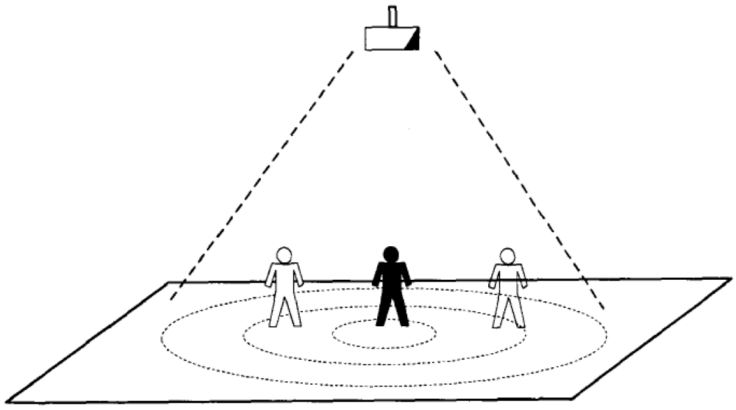

Fig. 3. Regional management function sketch

Prison factory personnel positioning subsystem. Due to the particularity of the factors (environment and personnel, etc.) in the prison factory, it should be assured that the inmates shall not escape the required area during the prison time, and the required area should be under real-time management. The analysis is conducted by taking the factory internal management during the labor reforming process as the

example. In real management, based on the positioning performance of active RFID, the control range of RFID sensor is set as 80 meters. The number of installations is calculated according to the range of each workshop, which can satisfy the real-time monitoring demands of all the workshop ranges. Then, the working positions of the personnel are decided through the positioning algorithm, and the RFID label is positioned to realize the label roll call and warning functions.

Auxiliary system. Except for the above system and related software systems, auxiliary systems are also required to satisfy the management demand of the prison. Generally speaking, the management with active RFID wireless sensor can satisfy the normal management demand of prison. However, the inmates may tend to resist the management of the prison. Hence, during the management process, some inmates may destroy the active RFID wireless sensor intentionally or discard the label maliciously. Hence, auxiliary management systems are also required on the basis of wireless management system. The auxiliary management system mainly includes video monitoring system, infrared boundary system and boundary escaping prevention system. With these systems as the backup for RFID wireless management system, even malicious prison break occurs, the auxiliary management system will detect the situation and inform the management personnel to take arrestment.

4. Conclusion

As a non-contact automatic recognition technology, RFID technology mainly obtains and recognizes the target information by sending radio frequency signals. This technology is applicable for various environments without requiring human intervention. Different from traditional recognition technologies which are limited by single recognition, RFID can recognize multiple labels simultaneously with certain operation convenience. RFID system mainly consists of label, reader and antenna. Active RFID technology possesses the sensing ability between label and reader, interaction ability between label and reader, anti-collision ability, ability of avoiding the influences from human body, metal and fluid, ability of loading sensing technology and data security, etc. As an integrated comprehensive system, prison management system based on active RFID sensor mainly contains computer control, automatic control, sensor and communication network technology, including RFID personnel management system, positioning and digital video monitoring system, active detection system. This management system can realize the functions of access control management, real-time monitoring, police sentry positioning, prison factory management, video monitoring and control, etc. The prison wireless management system based on active RFID wireless sensor mainly includes access control management system, regional management subsystem, prison factory personnel positioning subsystem and auxiliary systems, etc. Combined with hardware and software designing, the management system functionality can be improved gradually to assure the effective running of prison.

References

[1] Y. Zhao, N. Patwari, P. Agrawal, M. Rabbat: *Directed by directionality: Benefiting from the gain pattern of active RFID badges.* IEEE Transactions on Mobile Computing *11* (2012), No. 5, 865–877.

[2] G. Strazdins, A. Elsts, K. Nesenbergs, L. Selavo: *Wireless sensor network operating system design rules based on real-world deployment survey.* Journal of Sensor and Actuator Networks *2* (2013), No. 3, 509–556.

[3] W. Boonsong, W. Ismail: *Wireless monitoring of household electrical power meter using embedded RFID with wireless sensor network platform.* International Journal of Distributed Sensor Networks *10* (2014), No. 6, Article ID 876914.

[4] D. Djenouri, E. Karbab, S. Boulkaboul, A. Bagula: *Car park management with networked wireless sensors and active RFID.* IEEE International Conference on Electro/Information Technology (EIT), 21–23 May 2015, Dekalb, IL, USA, IEEE Conference Publications (2015), 373–378.

[5] M. Daito, N. Tanida: *Agent-based simulation approach for disaster rescue using active RFID.* Review of Socionetwork Strategies *1* (2008), No. 2, 23–39.

[6] D. Djenouri, E. Karbab, S. Boulkaboul, A. Bagula: *Networked wireless sensors, active RFID, and handheld devices for modern car park management: WSN, RFID, and Mob Devs for car park management.* International Journal of Handheld Computing Research *6* (2015) No. 3, 33–45.

[7] J. S. Yuan, J. Zhang: *Development of wireless sensor network based on ZigBee and RFID technology.* Applied Mechanics and Materials *341–342* (2013), 1175–1180.

[8] N. Wang, P. Guan, H. Du, Y. Zhao: *Implementation of asset management system based on wireless sensor technology.* Sensors & Transducers Journal *164* (2014), No. 2, 136–144.

[9] H. Jia: *Mobile HCI optimization based on RFID and wireless sensor networks.* Sensors & Transducers Journal *167* (2014), No. 3, 161–169.

[10] C. Z. Zulkifli, H. N. Hassan, W. Ismail, S. N. Semunab: *Embedded RFID and wireless mesh sensor network materializing automated production line monitoring.* Acta Physica Polonica A *128*, (2015), No. 2-B, 86–89.

[11] S. P. Tseng, K. Y. Hwa, I. Chang, W. Li: *An automatic RFID and wireless sensing system on a GHS-based hazardous chemicals management platform.* IEEE International Conference on Embedded and Multimedia Computing, 10–12 December 2009, Jeju, Korea (South), IEEE Conference Publications (2009), 1–6.

[12] R. Goncalves, S. Rima, R. Magueta, P. Pinho, A. Collado, A. Georgiadis, J. Hester, N. B. Carvalho, M. M. Tentzeris: *RFID-based wireless passive sensors utilizing cork materials.* IEEE Sensors Journal *15* (2015), No. 12, 7242–7251.

Received October 12, 2017

Acta Technica *62* No. 2B/2017, 789–798

Simulation analysis of energy storage and power system of rooftop solar system[1]

Peng Wang[2]

Abstract. The research on the utilization of solar energy resources was of great significance. The problems of energy storage and power system simulation of rooftop solar energy system were analyzed in this paper. The main contents of digital simulation technology and solar energy storage technology were introduced. At the same time, the main contents and research methods of the solar system as well as the power system model were described. Finally, the research results were analyzed and discussed. The results showed that the parallel computation of power system with serial computation had a good effect, which provided a favorable research direction for the improvement of energy efficiency in the future.

Key words. Solar energy system, power system, energy storage, simulation analysis.

1. Introduction

Tsiganis [1] argued energy storage technology played an important role in improving the stability and power quality of solar energy system. The energy storage device not only can absorb and release a certain power, but also can reduce the network loss of the solar system effectively. At the same time, the energy storage device can also play the most important role in the power system. Vidal [2] considered that energy storage technology included energy storage technology, compressed air energy storage technology, battery energy storage technology and pumped storage technology. Generally speaking, power storage technology had higher power and response speed. Solar energy had low density and poor stability. The energy storage technology can adjust the system load and production cost effectively and improved the utilization efficiency of solar energy to a certain extent in the process of the roof solar energy system. Bhattarai [3] considered that the simulation technology of power system had high accuracy, rapidity and flexibility. Gene rally speaking, the

[1]The author acknowledge the Science & Technology Innovation Teams in the Universities of Henan Province (Grant No. 14IRTSTHN022).

[2]School of Electrical Engineering, Xuchang University, 461000, Xuchang, China

digital simulation technology of power system can realize the simulation calculation of power network and adjusted the simulation data reasonably. At the same time, the numerical simulation technology of power system can be combined with other fields such as environment and economy. Nema [4] considered that the simulation experiment of power system can be carried out through several remote experimental equipment, and the main way of simulation calculation was cloud computing and collaborative computing. The application of data fusion technology can integrate the large amount of data in the simulation experiment of power system effectively. In general, the data of simulation experiments were mainly based on linear and nonlinear equations, characteristic equations and nonlinear programming equations to solve and calculate.

In summary, as people paid more and more attention to the use of solar energy, it was very important to study the energy storage and power system simulation of rooftop solar energy system. The energy storage and power system simulation of rooftop solar energy system were analyzed and studied based on the relevant theories at home and abroad in this paper. The connotation of digital simulation technology and solar energy storage technology was expounded in the second section. The main content of the power system and simulation model in the third quarter of rooftop solar energy storage system were introduced, and the research methods of rooftop solar energy storage system analysis and Simulation of power system was discussed in this paper. The simulation data were listed and analyzed in the fourth section. Finally, the conclusions were drawn in the fifth section.

2. State of the art

2.1. Digital simulation technology

Morbidelli [5] thought that the digital simulation of power system is the process of constructing the mathematical model of the power system running by computer and solving the problem by mathematical simulation. There was little difference between the simulation efficiency of the power system and the dynamic efficiency of the actual system. Different simulation requirements needed to build different mathematical models. Figure 1 shows the effectiveness of the power system simulation. Uzunoglu [6] considered that these models included linear or nonlinear, continuous or discrete, lumped or distributed parameters, deterministic or stochastic. However, some of the secondary factors were often ignored in the construction of mathematical models and such models belonged to the simplified model. Different power system simulation software will use different simulation methods based on the different operating conditions of the system. The simulation methods of power system mainly included three kinds of electromagnetic transient process simulation, electromechanical transient process simulation and medium and long term dynamic process simulation. The digital simulation of electromagnetic transient process simulated the real power system by the method of data operation. It was necessary to fully consider the characteristics of the power line parameters and the transient process of the generator and the various characteristics of the lightning arrester in the process of electromag-

netic transient simulation. Therefore, the mathematical model of electromagnetic transient simulation must establish the algebraic or differential and partial differential equations of these components and systems. The numerical integration method used in this paper was implicit integration method. Mateus [7] believed that it also involved the transient process of the network and used differential equations to describe so that the simulation of electromagnetic transient simulation program was limited because the electromagnetic transient simulation required not the detailed nonlinear model of the power system dynamic components. In general, the power system was simplified when the electromagnetic transient simulation was carried out.

Fig. 1. Simulation results

Raymond [8] believed that real-time simulation of power system can be divided into digital simulation, physical simulation and digital analog hybrid simulation. The simulation speed was exactly the same as that of the actual system. The real time simulation of power system was realized by the simulation system of the moving film. The hardware of the power system dynamic simulation laboratory were usually composed of a number of scaled down motors, a certain number of line models, power supply, load, switch model and corresponding monitoring and control system. Argiriou [9] believed that these devices had high intuitive and rich physical meaning. The price of these devices was high and the area was too large. In addition, the limitations, scalability and compatibility of these devices were poor. The equipment and hardware of power system dynamic simulation laboratory had important function. Most of the components of the digital analog hybrid real-time simulation system were basically the same as those of the power system dynamic simulation system. These components had high flexibility and wide application range. Digital analog hybrid real-time simulation system can simulate the whole process of power system in real time. Digital analog hybrid real-time simulation system had high stability and large simulation scale. Analog and digital hybrid analog circuits, transformers and other components were analog components. The whole simulation system will not produce numerical oscillation when these analog elements and the generator and other digital components were decoupled completely.

2.2. Solar energy storage technology

The integration of solar energy, energy storage and electric vehicles was the trend of new energy development. Solar energy and energy storage technologies had their own advantages. Figure 2 shows the actual scene of solar photovoltaic applications. Gommed [10] believed that solar power can achieve zero carbon emissions without additional costs. Energy storage technology can provide backup power, frequency modulation and other grid services, and the combination of the two can get further advantages. In particular, it can achieve continuous power supply at night, increased the available power generation time and improved the flexibility of the grid. Some authors believe that the combination of solar energy and energy storage technologies in distributed communities and rooftop systems can also reduce the pressure on the distribution network, delayed or reduced infrastructure investment. At the macro level, energy storage and solar power can increase the popularity of solar facilities without major changes, thereby reducing carbon emissions. Energy storage technology combined with solar power can be used as a fast channel for emerging markets electrification. In mature markets, the main drivers for the integration of distributed solar energy and energy storage technologies were cost savings and reduced dependence on the grid. From the cost point of view, the main driving force for consumers or communities to invest in this technology was to reduce electricity bills. Photovoltaic power generation was a leading technology, and can increase the utilization of solar power according to energy storage, thereby increasing economic benefits. The combination of these two technologies was the main driving force to solve the problem of power grid instability in emerging markets. Consumers can enjoy uninterrupted power after buying energy storage system. Solar power can support the energy storage system to extend the power supply time, and further improved the value of the energy storage system. The imbalance of the development of these two technologies has been very obvious. Some parts of Germany, Japan and the United States had economic considerations, and they have adopted rooftop photovoltaic systems quickly, but were not equipped with energy storage systems in most cases. India has established a mature lead-acid battery supply chain to help end users solve the problem of power supply instability in the absence of solar power facilities.

At present, energy storage technology played an important role in the development and utilization of electric energy and new energy. The application of energy storage technology such as pumped storage was large, but the application of other energy storage technologies was limited by economic factors. Energy storage technology can be divided into three categories: physical energy storage, chemical energy storage and electromagnetic energy storage. Different energy storage technologies had different characteristics. Flywheel energy storage, superconducting electromagnetic energy storage and super capacitor energy storage technology can be applied in the case of instantaneous voltage drop and high pulse power. At the same time, these technologies can improve the power quality and power system stability effectively. The application of pumped storage, compressed air energy storage and electrochemical battery storage were suitable for large system peaking and emergency power

Fig. 2. Practical application of solar energy storage

supply, renewable energy into large scale and large capacity etc. Electromagnetic energy storage includes superconducting energy storage, capacitance energy storage and super capacitor energy storage. Superconducting magnetic energy storage system had some advantages in energy storage and transmission power. At the same time, the system also has a higher corresponding speed and conversion efficiency. Superconducting energy storage system can also achieve large number of effective energy conversion. Superconducting energy storage system can meet the requirements of the power grid, such as voltage support, power compensation, frequency adjustment and the ability to lift the system, etc. Super-capacitors were developed according to the theory of electrochemical double layer, which provided powerful pulse power. When the electrode was in an ideal state of polarization, the charge will attract the opposite ions in the electrolyte solution, which was attached to the surface of the electrode to form a double charge layer. Superconducting energy storage system had a wide range of applications. This system can realize the optimization of power quality and power in a short time.

3. Methodology

3.1. Roof solar system simulation mathematical model

The application of photovoltaic technology in solar energy system has led to the development of rooftop photovoltaic devices. At present, China's national science and Technology Commission has begun to develop and optimize the roof solar system into the overall plan of national science and technology gradually. More and more attention has been paid to the effective combination and application of roof solar energy system and building. This is mainly because the system has many obvious advantages. First, the roof solar system covered a small area. Secondly, the system can achieve in situ use and power generation, and reduced the power transmission loss and roof temperature rise to a certain extent. Finally, the system can enhance the beauty of the building to a certain extent and meet the requirements of safe use

of electricity.

$$f(u) = I_0 \left\{ \exp\left[\frac{qu}{AKT}\right] - 1 \right\} . \tag{1}$$

Here, u is the voltage, I_0 is the output current, A denotes the diode characteristic fitting coefficient, K is the Boltzmann constant and T is the temperature.

When the light intensity was constant, the photocurrent did not change with the working state of the photovoltaic cell. Therefore, a constant current source can be used to simulate the power system module library and there was no direct current source module. The function of the voltage detection module was shown in formula (1), and the expression of the output value was the formula (2). The simulation experiment was carried out mainly through the MATLAB software for data experiments in this paper. MATLAB application software had great advantages in data calculation and graphic display. In general, it was more convenient to use MATLAB software for data operation and simulation analysis. At the same time, it also had high programming efficiency.

$$u = V + IR_{\mathrm{S}} , \tag{2}$$

where V is the voltage of the PV battery, I is the input current of the diode and R_{S} is the serial resistance.

3.2. Mathematical model of power system simulation

The construction of mathematical model mainly referred to the process of applying mathematics to the physical system. The mathematical model of the system contains diesel engine torque balance model, governor model, synchronous generator model, phase compound excitation device of voltage adjusting model, induction motor load model, static load model, the reactive power compensation device model, emergency alarm system model, power model and so on. In practical power system, the impedance, voltage and current which are connected with the unit property were called the known values. And the rest of the other properties without the unit value were called the value. The reference value was the relative value of the index. The flux linkage equation represented by the scalar value, which was shown in equation (3).

$$\begin{bmatrix} \psi_{\mathrm{dq0}} \\ \\ \psi_{\mathrm{fDQ}} \end{bmatrix} = \begin{bmatrix} X_{\mathrm{SS}} & X_{\mathrm{SR}} \\ \\ X_{\mathrm{RS}} & X_{\mathrm{RR}} \end{bmatrix} \begin{bmatrix} -i_{\mathrm{dq0}} \\ \\ i_{\mathrm{fDQ}} \end{bmatrix} . \tag{3}$$

Here, f denotes field winding, d, q, D and Q represent the rotor and armature axes, φ with appropriate indexes denote the magnetic fluxes and X stand for self and mutual inductances of the rotor and stator.

The electromagnetic torque equation was equivalent to the resistance and inductance of the winding of synchronous motor. At the same time, this equation was based on the assumption of ideal motor to convert the motor into a multi-winding linear electromagnetic system. Among them, the well-known equation for the electromagnetic torque is shown in formula (4). The rotor motion equation was

a mathematical explanation of the dynamic process of the rotor system by Newton's law of motion. The equation of motion was one of the basic equations of synchronous generators. The electromagnetic time constant of synchronous generator set was much lower than that of electromechanical time constant. Generally speaking, it was assumed that the unit speed was constant in the calculation of the stator voltage equation in the process of studying the change of the excitation. Under the condition that the rotor speed change was small, the error of the system operation was small. The mathematical model of synchronous generator should be simplified and simulated. The seven order model had a great advantage in describing the dynamic change of the system. These dynamic changes included the transient process of the rotor, the process of the rotor damping winding, the transient process of the excitation winding, the transient process of the shaft winding and the dynamic process of the rotor.

$$T_{\mathrm{e}} = p_{\mathrm{p}} \frac{3}{2} \left(\psi_{\mathrm{d}} i_{\mathrm{q}} - \psi_{\mathrm{q}} i_{\mathrm{d}} \right) . \tag{4}$$

Here, p_{p} expresses the number of pole-pairs, T_{e} denotes the electromagnetic torque, $i_{\mathrm{d}}, i_{\mathrm{q}}$ and ψ_{d}, ψ_{q} are currents and magnetic fluxes in axes d and q, respectively.

The mathematical model was built to ensure the correctness and accuracy of the results. At the same time, the test process of mathematical model was also very important. MATLAB was a kind of application software with high efficiency and high visualization. This software had a strong ability of numerical calculation and graphic display. First of all, we needed to design and test all kinds of graphics control. Then, the simulation system control layout was carried out according to the actual needs. Finally, its characteristics were added and set according to the function of the control in the process of power system simulation system interface design.

4. Result analysis and discussion

The results obtained by the method described above were shown in the following tables:

Table 1. Comparison results of 10 simulation tasks

Serial number threshold calculation task	computing time	Speedup ratio	Parallel efficiency
5	30.403	1.36	0.68
3	35.237	1.17	0.59
2	43.520	0.95	0.48
1	49.516	0.84	0.42

It can be seen from Table 1 that the calculation time, speedup ratio and parallel efficiency of the simulation experiments of the power system when the 10 simulation tasks were parallel. The total computation time of the 10 simulation tasks was 41.381 s, and the optimal time of parallel computation is 30.403 s. The speedup was 1.36, and the parallel efficiency was about 0.68. It can be seen from Table 2 that the computational time, speedup and parallel efficiency of the simulation results of the 50 simulation tasks were parallel. The parallel serial time of the 50 simulation tasks was 211.31 s, and the speedup was 1.65, and the parallel efficiency was up to 0.83. In contrast, the results of the 50 simulation tasks were better than the experimental ones. This was mainly because of the increase of the task to make the simulation process more time-consuming. When the serial threshold was 2 and 1, the efficiency was lower than the serial. It can be seen that serial threshold setting had a direct impact on the parallel efficiency and computing time. A reasonable set of serial threshold can make the simulation tasks be divided equally and achieved the best effect of parallel computing.

Table 2. Comparison results of 50 simulation tasks

Serial number threshold calculation task	computing time	Speedup ratio	Parallel efficiency
25	127.824	1.65	0.83
13	132.036	1.60	0.80
7	142.115	1.49	0.74
4	161.884	1.31	0.65
1	211.862	1.00	0.50

It can be seen from Fig. 3 that the results of the simulation of the rooftop solar system. The data showed that the current, light intensity and temperature were basically the same. The maximum value of the current is 225, which was approximately the same as that of the solar system. We can see from Fig. 4 that the results of the simulation of the power current of rooftop solar system.

The results showed that the trend of power, light intensity and temperature are basically the same. The power between half past eight and half past five PM was more than 6.7 kW, which can meet the requirements of rated power. At the same time, the simulation results showed that the maximum current was not the same as that of the solar system. It can be seen that the variation trend of the current, light intensity and temperature of the solar system were basically the same. At the same time, the trend of power, light intensity and temperature of the roof solar system were basically the same. The power of each period of the simulation experiment can meet the requirement of the rated power.

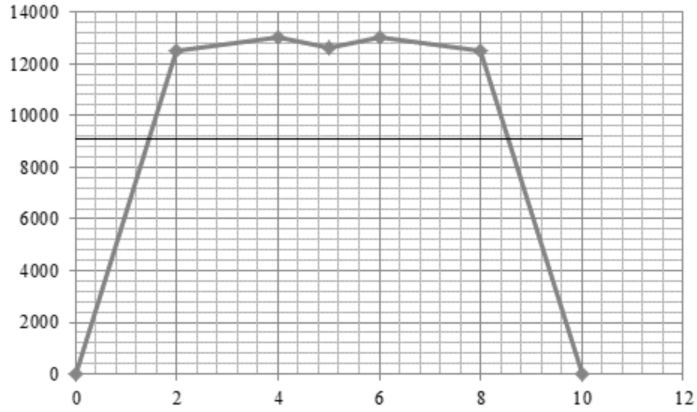

Fig. 3. Current trend

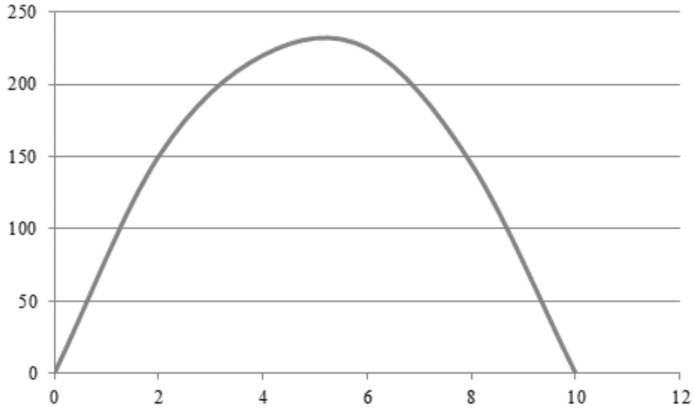

Fig. 4. Trend of power change

5. Conclusion

With the increasing attention to the use of energy, solar energy storage has become a hot research topic in recent years. Therefore, it was very important to study the energy storage and power system simulation. The results of the 50 simulation experiments showed that the results were satisfactory and the parallel effect was better in the research process of solar energy storage and power system simulation experiment. This was mainly because of the increase of the task to make the simulation process more time-consuming. When the serial threshold was 2 and 1, the efficiency was lower than the serial. At the same time, the simulation results showed that the current, light intensity and temperature of the solar system were basically the same. At the same time, the trend of power, light intensity and temperature of the roof solar system were basically the same. The power of each period of the simulation experiment can meet the requirement of the rated power. In summary, the parallel effect of serial computing power system was better. Therefore, designers

can optimize the energy efficiency of rooftop solar system and power system from the point of view of simulation operation and system power in the process of the solar system and power system improvement in the future.

References

[1] K. Tsiganis, R. Gomes, A. Morbidelli, H. F. Levison: *Origin of the orbital architecture of the giant planets of the solar system.* Nature, International Journal of Science*435* (2005), No. 7041, 459–461.

[2] H. Vidal, S. Colle, G. dos Santos Pereira: *Modelling and hourly simulation of a solar ejector cooling system.* Applied Thermal Engineering *26* (2006), No. 7, 663–672.

[3] S. Bhattarai, J. H. Oh, S. H. Euh, G. K. Kafle, D. H. Kim: *Simulation and model validation of sheet and tube type photovoltaic thermal solar system and conventional solar collecting system in transient states.* Solar Energy Materials and Solar Cells *103* (2012), 183–193.

[4] P. Nema, R. K. Nema, S. Rangnekar: *A current and future state of art development of hybrid energy system using wind and PV-solar: A review.* Renewable and Sustainable Energy Reviews *13* (2009), No. 8, 2096–2103.

[5] A. Morbidelli, K. Tsiganis, A. Crida, H. F. Levison, R. Gomes: *Dynamics of the giant planets of the Solar System in the gaseous protoplanetary disk and their relationship to the current orbital architecture.* Astronomical Journal *143* (2007), No. 5, 1790–1798.

[6] M. Uzunoglu, O. C. Onar, M. S. Alam: *Modeling, control and simulation of a PV/FC/UC based hybrid power generation system for stand-alone applications.* Renewable Energy *34* (2009), No. 3, 509–520.

[7] T. Mateus, A. C. Oliveira: *Energy and economic analysis of an integrated solar absorption cooling and heating system in different building types and climates.* Applied Energy *86* (2009), No. 6, 949–957.

[8] S. N. Raymond, D. P. O'Brien, A. Morbidelli, N. A. Kaib: *Building the terrestrial planets: Constrained accretion in the inner solar system.* Icarus *203* (2009), 644–662.

[9] A. A. Argiriou, C. A. Balaras, S. Kontoyiannidis, E. Michel: *Numerical simulation and performance assessment of a low capacity solar assisted absorption heat pump coupled with a sub-floor system.* Solar Energy *79* (2005), No. 3, 290–301.

[10] K. Gommed, G. Grossman: *Experimental investigation of a liquid desiccant system for solar cooling and dehumidification.* Solar Energy *81* (2007), No. 1, 131–138.

Received October 12, 2017

Acta Technica *62* No. 2B/2017, 799–808

Intelligent analysis method of automatic welding quality based on X-ray imaging[1]

Yan Hou[1]

Abstract. In the oil engineering construction and operation maintenance project, welding and nondestructive testing are the key construction processes. The timeliness and accuracy of welding quality analysis are important guarantees for the quality of petroleum engineering construction. Most of the petroleum engineering work environment is very complex. The welding quality of conventional detection technology has been unable to meet the demand, therefore, the automatic welding quality analysis based on X-ray imaging has become the main research technique at home and abroad. Under this background, in this paper, the welding quality analysis technology and the research status of X-ray image acquisition technology in China and abroad were analyzed; the principles of X-ray welding and the key technologies of visual inspection were analyzed; evaluation index was proposed for X ray imaging based on the welding quality; wireless transmission network based on regression model of welding was used, quality evaluation was optimized; through simulation experiment, its accuracy and feasibility were analyzed. This research has made certain contributions to the intelligent analysis method of automatic welding quality based on X-ray imaging.

Key words. Petroleum engineering, X-ray imaging, automatic welding, quality analysis.

1. Introduction

The total amount of petroleum resources in our country is insufficient, and the time and space distribution is uneven, besides, the oil field resource combination is not coordinated. With the development of oil field infrastructure and the increasing scale of oil and gas transportation system, long distance oil pipeline in China occupies an increasingly large proportion of oil and gas transportation. This has played an important role in China's national economic development and national strategic security reserves. The method of weld quality analysis based on X-ray imaging is of great value to the construction of petroleum engineering, especially for the welding quality inspection of long-distance oil pipeline. This is the most widely used method

[1]College of Electrical Engineering, Henan University of Technology, 450001, Zhengzhou, China

in the present stage of the weld quality inspection [1]. The intelligent analysis of weld quality based on X ray imaging is of great significance to ensure the quality of welded components.

A method for automatic detection of weld defects using defect tracking technique is proposed by Shao. This method uses the improved Hof transform to avoid the false defects caused by more noises, so as to ensure the accuracy of the welding defect detection. Vilar proposed a method to classify the defects of X-ray image automatically. This method can reduce the noise and enhance contrast to deal with the image of welding defects. Using the threshold selection, label technique and feature extraction method, it splits the welding defects [2]. After getting all the characteristic parameters, input it to the artificial neural network for processing (Artificial Neural Networks, ANNs), so as to realize the identification of defects. In order to get the best performance of the artificial neural network, the proposed method has been improved by using a variety of different methods to improve the neural network. In the input layer, the principal component analysis technique is used to reduce the number of feature variables. When dealing with the image of welding defects, Wang uses the three steps of image preprocessing, feature extraction and welding defects classification [3]. In the defect segmentation of image preprocessing, the two methods are proposed, which are background elimination method and histogram thresholding method. In the feature extraction step, a series of information parameters are extracted to describe the shape of welding defects. And in the third step, detect the defects of the welding classification. This step uses the fuzzy k- nearest neighbor algorithm and MLP neural network to send these two kinds of technology. Experiments show that, for the welding defects classification, the treatment effect of these two kinds of technology is excellent, reaching more than 90 % of the correct rate of judgment [4]. Du used the mean filter to do noise reduction processing for X-ray weld seam image, and achieved good results. Guo Dong analyzed the factors that affect the image quality of the weld, and put forward the application of computer aided image processing technology in the detection of weld radiographic. On this basis, the automatic recognition system of the weld negative image defect is developed. Based on the GB3323-87 standard, the system can assess the detected defects [5]. Zhang Quan proposed a digital image processing method based on the TV camera, and developed a corresponding image processing system and processing methods [6]. By using the method of gray level analysis, Wang Gang has carried out a series of noise reduction processing to the image, and proposed an S-T nonlinear gray image transformation method which can significantly improve the image sharpness and contrast. On this basis, the gray gradient method is used to extract the weld defects. This method can effectively enhance the effect of defects in the weld, but the contrast is not high, and the defect information will be lost [7]. X-ray digital imaging detection can be understood as direct digital imaging. In this method, the intensity of the radiographic image is converted to the visible light image in real time, and the test results are evaluated. For the inspection and evaluation of the weld quality of long distance oil pipeline with strong specificity and application limitation, the applicability of the present research is insufficient, so it is difficult to achieve the weld of pipeline inspection of complex geological environment

under the cross region remote. At the same time, it also lacks the evaluation method and system which is suitable for the objective condition.

2. State of the art

2.1. Status of X-ray image acquisition research

At present, the X-ray detectors used in the electronic industry are basically foreign products. Among them, the most typical representative is the flat panel detector P3H271 which appeared in the end of 1990s. The flat plate type X-ray imaging detector uses two methods to convert X-ray photon conversion: direct and indirect methods. The structure of these two ways is different. The direct way uses a photoelectric conductor to convert the X-ray into electric charge. In the indirect mode, the photoelectric diode is used to convert the visible light photons into electric charge [8]. Compared with the direct method, the indirect method has more than one layer of the scintillation to convert the incident X-ray photons into visible light. In the detection of electronic industry, the commonly used methods of X-ray imaging data acquisition are mainly divided into film imaging and non-film imaging. Film imaging has the longest history, but its biggest disadvantage is that it cannot be detected and evaluated in real time, and the result is not suitable for long-term preservation. Non film imaging replaces film imaging with X-ray sensitive devices, which can be simulated images or digital images. This imaging technology can be real-time detection and evaluation. With the development of image processing technology, the technology has been widely used [9]. In 1950s, researches on X-ray image intensifier gained rapid development. The basic principle of the X-ray imaging device is electronic vacuum tube approach. Although it has the advantages of low price, fast imaging, its disadvantages are also obvious. For example, it can withstand a small range of X-ray energy, as well as a small area of visible light image and so on. In order to better collect data, in the end of 1990s, the X-ray digital radiography detection technology based on flat panel detector appeared, and began to be applied in the field of industrial radiographic testing. In order to improve the higher spatial resolution, the linear array detector appeared. This is a digital imaging device. A new type of X-ray detecting unit is arranged in an array, and the array is directly connected with the large scale integrated circuit to complete the whole process of ray receiving, photoelectric conversion, and digitalization. This direct conversion method reduces the distance of signal transmission, and reduces the noise generated during the transformation process. Using the corresponding filter circuit, we can obtain the image of low noise and high sensitivity. In wireless sensor networks, one of the major research challenges is to save severely limited energy resources and effectively extend the life cycle of the network [10]. The energy consumption of a sensor node can be divided into three parts: sensing loss, data processing loss, and transmission consumption. According to the survey of N. Kimura and S. Latifi, each sensor node has about 80 % of the energy loss for data transmission. Therefore, reducing the size of the data will reduce the transmission consumption. In order to realize the communication connection fault tolerance, the sensor node uses the

redundant deployment way. Wireless sensor networks naturally show the high redundancy of temporal spatial sampling. Sampling redundant attributes can reduce the data flow in the network, which can reduce the energy consumption. The following picture is the scene of oil engineering.

Fig. 1. Oil engineering site

3. Methodology

The process of automatic welding quality analysis for X-ray imaging is shown Fig. 2

3.1. Multivariate linear regression models

Based on the simple linear regression model, we need to further explore the more complex multivariate situation. In wireless sensor networks, sensor nodes can monitor multiple variables. In addition, multivariate correlations are usually strong. Correlation is the data collected from one or more attributes of each sensor node at a given time. This is the nature of the observed physical phenomena. Simple linear regression models are able to study correlations, but it cannot study the multivari-

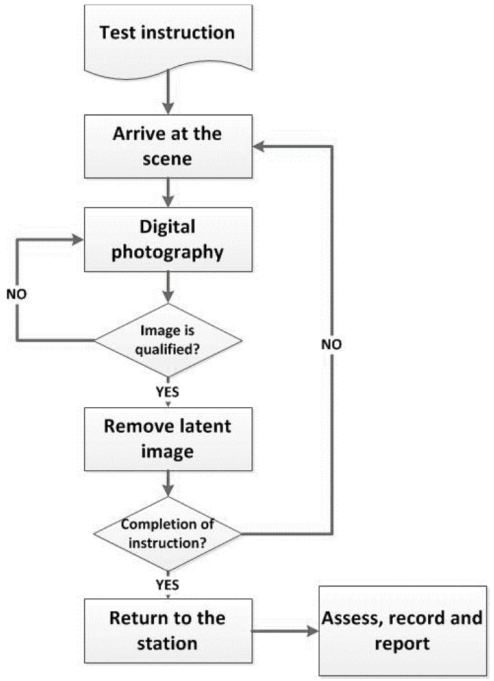

Fig. 2. Automatic welding process of X-ray image

ate correlations (more than one variable). In our solution, we use multiple linear regression models to study multivariate correlation. In wireless sensor networks, multi-variable correlation method is used to reduce the data transmission and the prediction accuracy of the proposed method.

Suppose a sensor node has p sensing units, and the collected properties are $x_j,\ j = 1, 2 \ldots, p$. The overall independent variable compression scheme is operated as follows:

$$y_i = 1 + \beta_1 x_{i,1} + \beta_2 x_{i,2} + \cdots + \beta_p x_{i,p-1}\,. \tag{1}$$

Here, y_i represents the response value attribute, while the $x_{i,1}, x_{i,2}, \ldots, x_{i,p-1}$ are the remaining $p-1$ properties at a given time i. We can express all the actual measured values as an m-dimension vector

$$Y = \begin{pmatrix} y_1 \\ y_2 \\ \vdots \\ y_m \end{pmatrix}. \tag{2}$$

We can express all the predictive factors in the form matrix $m \times (p-1)+1$

$$X = \begin{pmatrix} 1 & x_{11} & x_{12} & \cdots & x_{1(1-p)} \\ 1 & x_{21} & x_{22} & \cdots & x_{2(1-p)} \\ \vdots & \vdots & \vdots & \vdots & \vdots \\ 1 & x_{m1} & x_{m2} & \cdots & x_{m(1-p)} \end{pmatrix}. \tag{3}$$

Now the regression coefficient may be written as a p-dimensional vector:

$$\beta = \begin{pmatrix} 1 \\ \beta_1 \\ \vdots \\ \beta_{p-1}. \end{pmatrix} \tag{4}$$

Using a linear algebra symbol (1) may be represented as $Y = X\beta$. In order to estimate β, we can use the least square method:

$$\sum_{i=1}^{m} [y_i - (1 + \beta_1 x_{i,1} + \beta_2 x_{i,2} + \cdots + \beta_p x_{i,p-1})]^2 = \min, \tag{5}$$

so that

$$\beta = \left(X^{\mathrm{T}} X\right)^{-1} XY. \tag{6}$$

3.2. Parameter setting of distributed regression algorithm

In wireless sensor networks, the substitution method of transmitting all measured values is to establish a regression model of the network data and only transfer the model coefficients. This processing method can reduce the transmission of packets and reduce the redundancy, which helps to extend the network life cycle. For example, replace the original measured value that extracted from the node every 10 seconds. Suppose that we have ten original readings for each attribute in the sampling time, as shown in the following Table 1.

4. Result analysis and discussion

In order to analyze the validity of the regression method and verify the correctness of the proposed model and algorithm, we design the experiment in this section to verify the performance of the proposed method. In a small wireless sensor network, implement regression strategy. In the experiment, the initial energy of each node is only 0.5 J and the 200 byte control packet at the beginning. Cluster head node at the beginning of each round is determined to continue for more than and 20 seconds. When the sensor is transmitting or receiving the data in the network, or performing the regression operation, the node will produce the energy consumption. The following Fig. 3 shows that in the protocol and LEACH protocol, how the total

amount of energy consumption per round of network changes with the time of the simulation.

Table 1. Ten raw data for the properties

frequency	wind power	flow	voltage	instrument temperature	pipe temperature	sink temperature	sink level	time
50.00	6.29	11.32	378.00	11.16	21.20	28.91	1.21	1
50.00	6.29	11.40	377.00	11.18	21.22	28.92	1.21	2
49.78	5.98	11.05	377.00	11.18	21.21	28.91	1.21	3
49.15	5.79	10.88	378.00	11.18	21.22	28.91	1.21	4
50.00	6.14	11.10	379.00	11.18	21.22	28.91	1.21	5
49.52	5.95	11.02	381.00	11.21	21.21	28.91	1.21	6
49.71	6.11	11.29	383.00	11.22	21.20	28.92	1.21	7
50.00	6.09	11.20	378.00	11.23	21.23	28.92	1.21	8
50.00	6.07	11.05	372.00	11.22	21.22	28.90	1.21	9
49.04	5.60	10.55	365.00	11.22	21.21	28.91	1.21	10

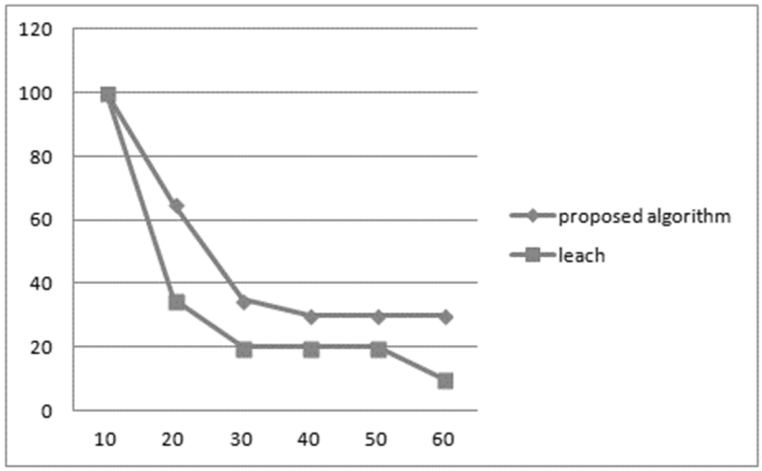

Fig. 3. Total energy consumption per round

From the analysis of the experimental results, we can see that, for each attribute, the absolute value of the error is very small. For power sampling, sampling time error at the end of the absolute value is the maximum and is as high as 9.5 %, which is lower than some preset error thresholds.

5. Conclusion

In the process of the construction of oil engineering, especially of the long oil pipeline, welding and nondestructive testing of pipeline and pipeline are the keys of the construction process. The quality of welding is an important guarantee for the construction quality of the project. X-ray detection is an important means to detect the quality of welding. For along, the welding spot detection mainly uses the X-ray film photography method, but the film photographic method has the problems of high cost, long cycle, low efficiency, serious pollution and so on. X-ray imaging provides a good technical support for solving this problem. In non-destructive testing of long oil pipeline, the method of weld quality inspection and analysis based on X-ray imaging technology can enhance the core technology competitiveness, improve the efficiency of welding seam detection, and reduce the production cost. This provides strong technical support for the construction of oil field infrastructure and the construction of large scale oil and gas transmission pipeline network. With the analysis of the weld quality detection characteristics of long distance oil pipeline and the comparison of several common methods of X-ray image, this paper solved the problem of weld quality evaluation. Based on the comprehensive application of X-ray weld quality detection and analysis technology, this paper presents an intelligent evaluation method of weld quality based on X-ray digital imaging. The hybrid intelligent mechanism is applied to the identification and evaluation of the weld quality, which realizes the intelligent method for the identification and evaluation of the quality of the weld seam. In this paper, we put forward the evaluation index of welding quality based on X-ray image, and use the wireless transmission network based on the multi-variable linear regression model to optimize the welding quality evaluation. Through simulation experiments, the accuracy and feasibility of this method are determined, which provides a theoretical support for the intelligent analysis method of automatic welding quality based on X-ray imaging.

References

[1] D. Mery, I. Lillo, H. Loebel, V. Riffo, A. Soto, A. Cipriano, J. M. Aguilera: *Automated fish bone detection using X-ray imaging.* Journal of Food Engineering *105* (2011), No. 3, 485–492.

[2] X. Li, S. K. Tso, X. P. Guan, Q. Huang: *Improving automatic detection of defects in castings by applying wavelet technique.* IEEE Transactions on Industrial Electronics *53* (2006), No. 6, 1927–1934.

[3] Z. Wang: *An imaging and measurement system for robust reconstruction of weld pool during arc welding.* IEEE Transactions on industrial electronics *62* (2015), No. 8, 5109–5118.

[4] Y. Wang, Y. Sun, P. Lv, H. Wang: *Detection of line weld defects based on multiple thresholds and support vector machine.* NDT & E International *41* (2008), No. 7, 517 to 524.

[5] Y. Li, Y. F. Li, Q. L. Wang, D. Xu, M. Tan: *Measurement and defect detection of the weld bead based on online vision inspection.* IEEE Transactions on Instrumentation and Measurement *59* (2010), No. 7, 1841–1849.

[6] C. B. Singh, R. Choudhary, D. S. Jayas, J. Paliwal: *Wavelet analysis of signals*

in agriculture and food quality inspection. Food and Bioprocess Technology *3* (2010) No. 1, 2–12.

[7] M. Menaka, M. Vasudevan, V. Balasubramaniam, B. Raj: *Estimating bead width and depth of penetration during welding by infrared thermal imaging.* Insight-Non-Destructive Testing and Condition Monitoring *47* (2005), No. 9, 564–568.

[8] S. Shirmohammadi, A. Ferrero: *Camera as the instrument: the rising trend of vision based measurement.* IEEE Instrumentation & Measurement Magazine *17* (2014), No. 3, 41–47.

[9] B. Pan, K. Qian, H. Xie, A. Asundi: *Two-dimensional digital image correlation for in-plane displacement and strain measurement: A review.* Measurement Science and Technology *20* (2009), No. 6, paper 062001.

[10] Y. Wang, D. L. Gao, M. F. Liao: *Application status and development Of nondestructive testing in welding.* Nondestructive Testing (2003), No. 3, paper 008.

Received October 12, 2017

Acta Technica *62* No. 2B/2017, 809–818

Research progress of optimized operation technology of natural gas pipelines

Dong Ye[1]

Abstract. In recent years, the large application of natural gas has led to a severe shortage of the operation efficiency of its pipelines, which has been unable to meet the rapid growth demand. Therefore, the study of natural gas pipeline transportation optimization plays a very important role in maintaining the steady economic development of our country. In this paper, through the empirical analysis, the natural gas pipeline optimization operation technology was studied, the existing problems of natural gas pipeline transportation were analyzed first, and the scheme and countermeasure of natural gas pipeline operation optimization design were obtained; then through the experimental analysis, the optimization design scheme of natural gas pipeline was verified. It can be concluded that the scheme can effectively improve the optimal operation level of natural gas pipeline.

Key words. Natural gas pipeline, optimal operation, technical research.

1. Introduction

After the reform and opening up, China's economic development speed is obvious to all, so the rapidly rising energy consumption of the industries is particularly prominent [1]. In China's energy consumption structure, Oil consumption accounts for a large proportion, the proportion of natural gas consumption is also great, which has reached more than 30 % [2]. Therefore, natural gas has become an important part of China's energy consumption [3]. Not only that, in recent years, the use of natural gas in China has been increasing, which has increased the burden of natural gas pipeline and put forward higher demands on the operation efficiency of natural gas pipeline [4]. Therefore, how to improve the efficiency of natural gas transportation pipeline operation and maintain the construction and optimization of natural gas pipeline has become one of the more difficult problems in the chemical industry [5].

[1]Inner Mongolia Technical College of Mechanics and Electrics, 010070, Hohhot, Inner Mongolia, China

At present, more and more researchers have been involved in the study of the optimization design of natural gas pipelines, and have had some research experience on the current situation and existing problems of natural gas pipeline operation [6]. The state has invested a lot of money and resources to develop a number of natural gas delivery projects to meet the growing demand for natural gas use [7]. However, for the optimal design of natural gas pipeline operation, our research is still in a relatively weak stage, so for the researchers concerned, this is a major problem that needs to be overcome [8].

2. State of the art

Because of the lack of experience in the design of natural gas pipelines in China, the current design is still based on the mathematical approach that has been consistently used in the past, which relies on the construction of a mathematical model to design natural gas pipelines [9].

Since the 1970s, the development of natural gas pipeline projects has become an important part of economic construction in the world [10]. And because of the uneven distribution of natural gas resources between countries, a large amount of natural gas trade has been needed between countries, which has greatly increased the distance and demand of natural gas transportation As a result, many countries have had the need to build long-distance, large-diameter natural gas pipelines Before the 90 s of last century, the Soviet Union had already owned a 2698-kilometer natural gas pipeline. By the time of the 1990s, large diameter natural gas pipelines built by Russia have exceeded 60 % of the total natural gas pipeline Compared with the 1219 mm diameter of Western European countries, Russia's 1420 mm pipeline caliber has a great advantage.

In the past more than 20 years, on the basis of absorbing the advanced experience of foreign natural gas transportation technology, China's natural gas transportation technology has also developed rapidly. In order to realize the rapid development of China's western region economy, the "West-East Gas Pipeline Project" in China has promoted the improvement of the technical level of natural gas pipeline and provided technical guarantee for the rapid economic development.

2.1. Methodology

2.2. Problems in operation of natural gas long-distance pipeline

In terms of technology, natural gas pipelines are generally laid along the road. Therefore, when they passes through some larger buildings and bridges and other ground environment, it is necessary to use some methods to solve, which puts forward high requirements for the construction technology. In the process of building natural gas pipelines, some people who steal natural gas tend to appear due to economic interests. These personnel will drill some of the pipes and then use some means to steal natural gas for sale, which makes the natural gas transmission process

suffer greater losses, and is also likely to cause major safety incidents, such as leaking pipelines. In addition to man-made destruction, natural gas pipelines are also vulnerable to natural disasters. Natural gas pipelines are often conduits with very long distances, so they passes through a lot of areas, and the natural environment is also complex, which usually has a lot of natural factors that cannot be controlled. As a result, natural gas pipelines often encounter a variety of ground subsidence, debris flow, earthquakes and other harsh natural environment, which threatens natural gas pipelines. The following figure shows the actual operation and transmission of natural gas pipeline, which is the actual laying of natural gas pipeline.

Fig. 1. The actual laying of natural gas transmission pipelines

In the whole natural gas pipeline project development process, the construction of oil and gas pipeline is a very important part, which will greatly affect the stability and reliability of natural gas transportation. So this step is a very important step. In the case of oil and gas pipelines, it is necessary to understand the natural and weather conditions of the installation area before the installation, and to make full technical preparations, so as to strictly control the entire construction process in the construction process and perform a test of performance after completion. Once there is a problem in any of these links, it will affect the operation efficiency and operation safety of the whole natural gas transmission pipeline. When welding the pipe, it is necessary to check the safety and integrity of the device material, and to make a timely remedy for the damaged pipe, so as to avoid mistakes from construction personnel at any time and prevent the emergence of various construction defects and other issues, thus ensuring the efficient and safe operation of natural gas pipeline.

Today, natural gas has entered the people's lives, and has become an indispensable part of people's lives, so the use of the natural gas is gradually increased. However, although the number of people who use natural gas is very large, there is no effective protection measure, the people are less aware of the precautions and knowledge in the use of natural gas, but also lack security awareness. Therefore, in the process of using, people's safety cannot be fully guaranteed.

2.3. Measures for optimizing design of natural gas pipeline operation

Based on the analysis of the problems that are easy to occur in the construction of the above natural gas pipeline, the corresponding effective measures for the optimization of the operation of the long-distance natural gas pipeline can be explored. Figure 2 below shows the design of the natural gas transmission pipeline, in which the specific values and the standard of the pipeline have been designed and marked in detail, so as to ensure that the natural gas transmission pipeline can guarantee a more precise size when building.

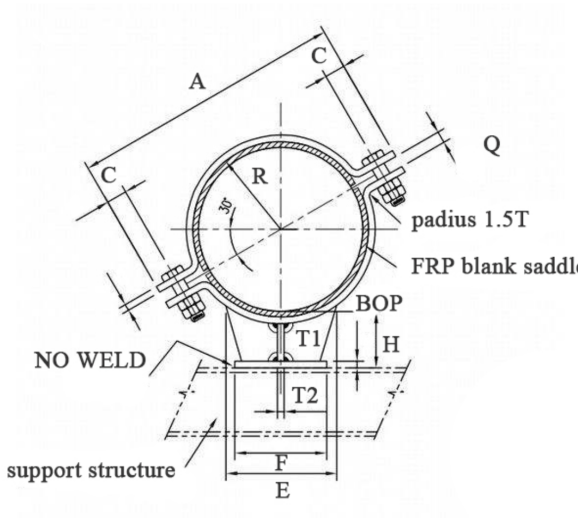

Fig. 2. Design diagram of a natural gas transmission pipeline

In the optimization of the design of flat lots of pipelines, it is necessary to take full account of various special circumstances encountered when laying the natural gas pipelines, different pipe elevation determines the safety of different pipe, which puts forward higher requirements for the design of natural gas pipeline. Therefore, the design must take full account of the natural environment of the natural gas pipeline during the laying, and allow the natural gas pipelines to be fully safe at the time of operation and have effective measures to minimize losses after its emergence of a security incident. For the environment and conditions, it is necessary to take into account the various important large buildings that pass through the pipeline and to understand the special natural environment of the area. In the optimization of the construction of natural gas pipeline in the river crossing phase, it is necessary to take full account the situation when the pipe passes through the river. Because natural gas pipelines are vulnerable to water erosion, it is necessary to avoid these problems as much as possible during design. In order to avoid all kinds of damage to the natural gas pipeline, casing and other methods can be used to protect the safety of the pipeline. In order to prevent the occurrence of rotations in the pipeline, the outside of the natural gas pipeline can be coated with a cathodic protection sub-

stance. In the optimization of mountain and other stages of the natural gas pipeline, it is necessary to fully take into account all sorts of circumstances that appear when suffering landscape scour. Because the laying distance of natural gas pipelines is very long, pipelines often go through many countries and regions. Therefore, it is necessary to fully understand the standards and specifications of the natural gas industry in these countries and regions, so as to strictly implement these standards and specifications at the time of design. The laying of natural gas pipeline will be carried out along the ridge, because the amount of water collected in the ridge area is relatively small, which will not cause extensive erosion of the pipeline, and can greatly improve the safety of the pipeline.

2.4. Empirical analysis of optimized design of natural gas pipeline operation

Firstly, the emptying time and volume of gas in the pipeline are calculated by reasoning, and the formula is derived. Combined with the company's current diameter specifications and pressure condition, the formula is applied, and the evacuation of the chamber between two valves is calculated separately. Through the formula analysis, some conclusions can be drawn, so as to provide the scientific basis for our production scheduling decision, the dispatching of the gas volume and the reasonable organization of the accident repair, which has the practical guiding significance to ensure the stable supply of the pipeline. The figure below shows the pipeline pressure setting in the natural gas pipeline design. The air pressure setting of the natural gas pipeline can adequately ensure the safety of the pipeline and can determine the speed and efficiency of the natural gas in the transmission process. Therefore, the pressure control of the pipeline is a very important part.

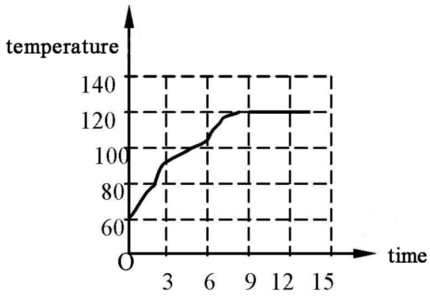

Fig. 3. Gas pressure setting of natural gas transportation pipeline

Assume that the length of a pipeline is L, the pipe diameter is 9Dx, and the average line pressure is P_1 (absolute pressure). The pipeline is emptied by the air release valve, and P_2 is the venting time and volume required when the pressure drops. Assuming that the pipeline temperature T remains the same the process is described by equations listed according to the conservation of mass:

$$V\,\mathrm{d}p = G\,\mathrm{d}t\,, \tag{1}$$

where G is the mass flow and V is the volume of the empty tube, p is the valve opening (abscissa) and t is the venting time. Because

$$p = \frac{PM}{RT}\,, \tag{2}$$

where M represents the relative molecular mass of the vent gas, T is the pipe temperature, P is the absolute pressure before and after venting and $R = 848\,\mathrm{kg}$, we can write

$$V\,\mathrm{d}\left(\frac{PM}{RT}\right) = G\,\mathrm{d}t\,. \tag{3}$$

As the mass flow rate G of the gas in the critical state is

$$G = FP\sqrt{\frac{KMg}{ZRT}\left(\frac{2}{K+1}\right)^{\frac{K+1}{K-1}}}\,, \tag{4}$$

where F represents the cross-sectional area when the vent valve is fully open, K represents the adiabatic index, $g = 9.81$ and Z represents the natural gas compression factor.

Then

$$V\mathrm{d}\left(\frac{PM}{RT}\right) = \left(FP\sqrt{\frac{KMg}{ZRT}\left(\frac{2}{K+1}\right)^{\frac{K+1}{K-1}}}\right)\,\mathrm{d}t\,, \tag{5}$$

and, hence

$$t = \frac{V}{F}\sqrt{\frac{\frac{M}{ZRT}}{Kg\left(\frac{2}{K+1}\right)^{\frac{K+1}{K-1}}}\ln\frac{P_1}{P_2}}\,. \tag{6}$$

It is necessary to conduct a certain instance of the calculation, and the gas between the two valves is vented, pipeline specifications is $426\times7\,\mathrm{mm}$, the length is $30\,\mathrm{km}$, and tube pressure is $3.5\,\mathrm{MPa}$ (gauge pressure), the temperature is $17\,^{\circ}\mathrm{C}$, vent tube specifications is $9108\times6\,\mathrm{mm}$, and the valve opening height and diameter ratio is: $h/d = 1.0$. It is now calculated that, firstly, the emptying time and volume required when the natural gas in the pipeline is vented is equal to the atmospheric pressure; secondly, the emptying time and volume required when the natural gas in the pipeline is vented until the pipe pressure is $1.5\,\mathrm{MPa}$

By using the formula above, the calculation can be obtained:

When the natural gas in the pipe is completely emptied to the atmospheric pressure, the venting time is 128 minutes, and the discharge volume is $140724.5\,\mathrm{m}^3$.

The emptying time is 50 minutes when the pressure is $1.5\,\mathrm{MPa}$, and the vent volume is $80446\,\mathrm{m}^3$.

3. Result analysis and discussion

After analyzing the optimization design of the natural gas pipeline, the author also made an empirical analysis of the pipeline to construct the overall structure of the natural gas pipeline design. Before the construction and operation of the above design plan, the integrity and safety of its natural gas pipeline design must be tested to ensure the safety and efficiency of the gas pipeline when it is running. The figure below shows the overall structure of the natural gas pipeline design. Through the interconnection between the various hardware facilities, the basic system of the operation and management of the natural gas pipeline can be established, which can manage the operation of the whole natural gas pipeline in an orderly way and ensure the efficiency of its natural gas transmission.

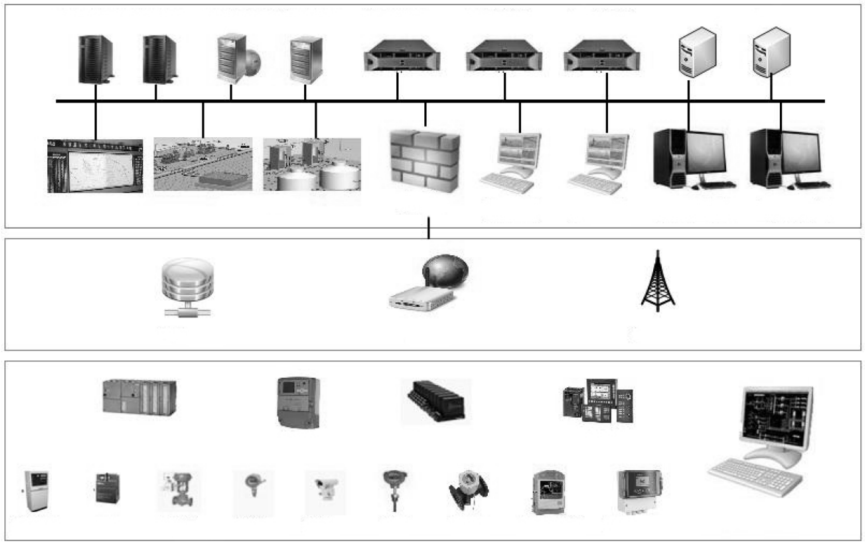

Fig. 4. The overall structure of the natural gas pipeline design

The integrity and safety of gas pipeline design must be analyzed on the basis of a large amount of experimental data collected. Therefore, at the time of this test, the author collected some of the actual operation data, and collated and analyzed the data, and obtained a certain analysis results from the data analysis. Table 1 shows the experimental data for the operation of natural gas pipelines, including pipeline integrity data, safety data, barometric data, operational efficiency data, and operating speed data.

Evaluation of pipeline integrity: pipeline integrity management refers to that risk and integrity evaluation is carried out through the collection and classification and analysis of potential risk factors for pipeline, and the evaluation results are processed to ensure the integrity and safety of pipeline operations, which mainly adopts GIS and database, risk assessment, risk detection, applicability evaluation, pipeline geological hazard assessment, pipeline maintenance decision and emergency

response and other key technologies. The corresponding safety risk control measures are developed and the identified adverse factors are continuously improved, so that the safety risk level of the pipeline operation is controlled within a reasonable and acceptable range, so as to reduce the occurrence of pipeline accidents and ensure the safe operation of the pipeline.

Table 1. Natural gas pipeline operation experimental data

	Integrity	safety	Air pressure	Operating efficiency	Running speed
P1	0.56	1.11	0.97	0.24	1.45
P2	0.83	1.13	0.06	0.45	1.22
P3	0.59	1.15	0.04	0.77	1.13
P4	0.76	1.43	0.34	0.46	1.13
P5	0.88	1.26	0.13	0.33	1.14
P6	0.90	1.21	0.46	0.57	1.46
P7	0.34	1.14	0.31	0.24	1.25
P8	0.34	1.45	0.62	0.34	1.09
P9	0.56	1.62	0.72	0.32	1.05
P10	0.28	1.09	0.53	0.14	1.04

Optimized detection technology: in order to ensure the safety of gas pipelines, domestic and foreign advanced technology can be actively absorbed and introduced to ensure the safe operation of the pipeline, the safety supervision and prevention of gas pipelines in the area where natural conditions are harsh and social environment is complex can be strengthened. Through field investigation, safety management can be carried out. At the same time, corrosion tests of pipeline and production base equipment can be continuously strengthened to improve safety management levels.

4. Conclusion

Because research experience of natural gas pipeline design technology of our country is less, and the research starts late, so it is still in a relatively primary stage, technical level is not high. The design of natural gas pipelines can affect the safety and efficiency of pipeline operation. Therefore, the optimization of pipeline design technology is very necessary. In this paper, through the analysis of the problems in the operation of long-distance natural gas pipeline, measures of natural gas pipeline operation optimization design were designed; then from the three perspectives of optimizing the flat pipelines, optimizing river pipelines, and optimizing mountainous pipelines, the description was carried out; finally, through the empirical analysis, the natural gas pipeline optimization scheme was designed, and the experimental data of the safety and operation efficiency of the gas pipeline were collected and the experimental results were analyzed, so as to show the effectiveness of the natural gas pipeline optimization design in this paper and promote the development of China's natural gas pipeline optimization design technology.

References

[1] R. Z. Ríos-Mercado, C. Borraz-Sánchez: *Optimization problems in natural gas transportation systems: A state-of-the-art review.* Applied Energy *147* (2015), 536 to 555.

[2] J. GaoJ, F. You: *Shale gas supply chain design and operations toward better economic and life cycle environmental performance: MINLP model and global optimization algorithm.* ACS Sustainable Chemistry & Engineering *3* (2015), No. 7, 1282–1291.

[3] M. Ma, H. Zhao, X. Su, K. Li: *The current development status and prospect of oil and gas pipeline plugging and emergency repair technology.* China Petroleum Machinery *42* (2014), No. 6, 109–112,118.

[4] Z. Dai, R. D. Noble, D. L. Gin, X. Zhang, L. Deng: *Combination of Ionic liquids with membrane technology: A new approach for CO_2 separation.* Journal of Membrane Science *497* (2016), 1–20.

[5] A. Zlotnik, L. Roald, S. Backhaus, M. Chertkov, G. Andersson: *Coordinated scheduling for interdependent electric power and natural gas infrastructures.* IEEE Transactions on Power Systems *32* (2017), No. 1, 600–610.

[6] C. G. Xu, X. S. Li: *Research progress of hydrate-based CO_2 separation and capture from gas mixtures.* RSC Advances *4* (2014) No. 35, 18301–18316.

[7] Z. Huang, Z. Chen, Q. Li, R. Zhu, S. Jing, Y. Zhou, Y. Ma, N. Wang, W. Chang: *Experimental research on the drag reduction mechanism of natural gas drag reduction agent and its industrial field test.* Industrial & Engineering Chemistry Research *53* (2014), No. 31, 12494–12501.

[8] S. Kumar, J. H. Cho, I. Moon: *Ionic liquid-amine blends and CO_2 BOLs: Prospective solvents for natural gas sweetening and CO_2 capture technology–a review.* International Journal of Greenhouse Gas Control *20* (2014), 87–116.

[9] G. Pi, X. Dong, C. Dong, Z. Ma: *The status, obstacles and policy recommendations of shale gas development in China.* Sustainability *7* (2015), No. 3, 2353–2372.

[10] L. Yang, X. Ge, C. Wan, F. Yu, Y. Li: *Progress and perspectives in converting biogas to transportation fuels.* Renewable and Sustainable Energy Reviews *40*, (2014), 1133–1152.

Received October 12, 2017

Acta Technica *62* No. 2B/2017, 819–828

Simulation study of automotive electronics mechanical braking system based on self-tuning fuzzy PID control

Junyan Xu[1], Jianrong Bu[1]

Abstract. On the basis of the analysis of vehicle longitudinal dynamic control system, the control problem of longitudinal automatic tracking based on two vehicles is discussed. The second order model of two-car following motion is established and the logic switching rule of acceleration/braking is designed. The three parameters of PID are adjusted by parameter self-tuning fuzzy PID control to control the variation range of the error between the vertical relative distance and vertical relative velocity of the controlled vehicle and the navigating vehicle to achieve the purpose of longitudinal control of the vehicle. The sufficient conditions for the stability of fuzzy PID control system are obtained by using the small gain theorem. The simulation results show that this method can reduce the overshoot of the system compared with the general fuzzy control, and enhance the dynamic anti-jamming ability. It has certain robustness and can solve the contradiction between the fastness and small overshoot.

Key words. Vehicle, kinetic control, longitudinal control, parameter self-tuning, fuzzy PID.

1. Introduction

The vehicle anti-lock braking control system (for short ABS) is a kind of active safety device, which can automatically adjust the wheel braking torque in an electronic control way according to the motion state of the vehicle in the braking process so as to achieve the purpose of preventing wheel locking. Nowadays, active safety of vehicle has become a hot research focus in the automotive field. As an active safety part of vehicle, the vehicle longitudinal dynamic control system consists of upper control system and lower control system [1–3]. The lower control system of vehicle longitudinal dynamics transfers the output of the upper control system to the controlled vehicle system to achieve the desired acceleration / deceleration. Its control model includes the braking system model, the engine model, the drive system model and the vehicle movement model four parts [4].

[1]Zhejiang Industry Polytechnic College, 312000, Shaoxing, China

The lower control system combined with the upper control system of the vehicle longitudinal dynamics to constitute the vehicle longitudinal dynamics control system. It is a complex nonlinear system, its actual characteristics is difficult to accurately describe with the linear model [5]. The parameter self-tuning fuzzy PID control method is used to control the longitudinal dynamic system of the vehicle. The real-time and effectiveness of the control system are studied in order to realize and improve the control performance of the vehicle longitudinal dynamic system.

2. Literature review

From the initial development point of view, the first application of the electronic mechanical braking is on the aircraft, and then slowly transforms into the vehicle. It is still in the applied research and improvement stage of the automotive field. Applied research in the car was first proposed by the Bosch Company in the 20th century 90 years. Bosch introduced a research project of "Brake 2000". The goal of the project is to study a braking system with faster response and significant braking effect. The electronic sensor braking system is the world's first set of fully-controlled braking system in the birth of this request. The system was first loaded in the high-end Mercedes-Benz SL500. At present, Bosch, Siemens and other companies have made some research results, but only in the experimental stage, and there is no mass production. In 2004, Australia's PBR International Limited announced that developed the first wired vehicle. Haldex Company in Sweden vigorously promoted the wire-controlled braking technology, but also launched its own electronic mechanical braking system. The significant results of the research and application of the fuzzy theory are focus on the United States, Japan and Europe and other countries and regions [6]. On the basis of the fuzzy ABS controller, Georg E. Mauer et al. introduced a slip rate predictor, which can be used to infer the discreet value of the slip rate due to the system lagging based on the measured current slip rate and braking torque. And the corresponding control rules are selected to identify the current pavement behavior by real-time judgment of the relationship between the slip rate and the braking torque. The simulation results on the single-wheel model show good control effect and can adapt to different changes of road surface, and it is not sensitive to external disturbance, and improves the robustness [5–7]. C. Jun combines various model-based control methods such as PID controller, sliding-mode controller and fuzzy controller, and it proves that the combination of controllers and improves the adaptability of different pavement by comparing with PID controller, and achieved better control effect. Mark Akey designed the ABS fuzzy controller, which uses three fuzzy control sets and seven logic variables. Its working principle is that the first two control sets are based on the measured wheel acceleration, the extremum of the angular acceleration, the vehicle speed, the status value of the solenoid valve and the current value to determine the current anti-lock phase and solenoid valve state. The third control set is based on this, and then according to the cycle and the brake pressure to determine the amount of regulation of the final pressure. The simulation results achieve the desired purpose, but the controlled quantity to be measured is too much control, the control is complex and the cost is much.

The research on the application of fuzzy theory in our country is relatively late, but it develops rapidly. In recent years, many domestic universities and automotive research institutions have done a lot of theoretical and experimental research in the fuzzy control technology, and laid a foundation for the development of fuzzy control [7]. On the basis of the simplified automobile model, Guokonghui, a famous scholar, designed ABS fuzzy controller and adaptive fuzzy controller to make the vehicle achieve better control under the variable operating conditions, and overcome the shortcomings of control singleness. Li Jun, Yu Fan, Zhang Jian-wu, et al. Put forward the control strategy of road surface recognition during vehicle steering braking. This method can calculate the optimal target slip rate in real-time according to the road surface attachment condition and vehicle motion state, and the vehicle's braking and lateral stability has been greatly improved by adopting the corresponding control strategy. Chen Jiong, Wang Hui-yi, Song Jian designed a fuzzy controller based on slip rate and deceleration, and simulated on a degree of freedom vehicle model, which proved that the controller was more adaptive than the logic threshold method.

From the research status quo at home and abroad, although the fuzzy control exhibits a great development, there are still some shortcomings of fuzzy control, and the establishment and analysis of fuzzy control system is still in the initial stage, the stability theory is not mature. Secondly, the modeling of fuzzy systems, the establishment of fuzzy rules, and the fuzzy reasoning methods have not been well resolved. Therefore, it needs further study and discussion in theory or in the application [8].

3. Research contents and methods

3.1. The longitudinal relative distance model of vehicles

The control quality of longitudinal relative distance between vehicles is an important index to evaluate the active safety of the vehicle. The control parameter is the longitudinal relative distance between vehicles [9]. Considering the dynamic response characteristics of the control system, in order to improve the precision of the model, the change rate of the longitudinal relative distance between vehicles is taken as the other parameter of the control system, and the second order model of two-car following motion is established. The role of the switch logic control system of engine throttle/brake master cylinder is to determine the switch of the engine throttle / brake master cylinder, and transfer the desired acceleration/subtraction value to the lower control system of the vehicle longitudinal dynamics. The one-dimensional model of relative longitudinal error of vehicles is

$$\delta'_{\mathrm{d}} = (x_{\mathrm{h}} - x) - L - H\,, \tag{1}$$

where H is the desired value of the longitudinal relative distance between vehicles. Symbol L denotes the length of the vehicle, x_{h} and x, respectively represents the vertical coordinate of the tail bumper of the navigation vehicle and controlled

vehicle, and δ'_d is the longitudinal relative distance error between vehicles. The one-dimensional control model is simple in structure and easy to control, but under the actual longitudinal driving conditions, the longitudinal relative distance error between vehicles is related to the longitudinal displacement rate of the controlled vehicle. Considering the influence of the controlled vehicle speed on the accuracy of the model, Swaroop et al. proposed a two-dimensional model of the relative distance between vehicles

$$\delta_{\mathrm{d}} = (x_{\mathrm{h}} - x) - L - H - \lambda v\,, \tag{2}$$

where δ_{d} is the relative longitudinal distance error between vehicles, λ is the compensation time of the controlled vehicle converging to δ'_{d}. and v is the speed of controlled vehicle.

3.2. Relative longitudinal velocity model between vehicles

The relative error of longitudinal relative velocity between vehicles is

$$\delta_v = v_{\mathrm{h}} - v\,, \tag{3}$$

where δ_v is the relative longitudinal velocity error between vehicles and v_{h} is the speed of the navigation vehicle.

3.3. Second order model of two-car following motion

The longitudinal relative distance two-dimension control and the relative velocity control model are adopted to establish the second order longitudinal relative distance control model between vehicles.

$$\delta_{\mathrm{d}} = (x_{\mathrm{h}} - x) - L - H - \lambda v\,,$$

$$\delta_v = v_{\mathrm{h}} - v \tag{4}$$

and the state space equation of the model is given as:

$$X = AX + Bu + \Gamma w = \begin{bmatrix} 0 & 1 \\ 0 & 0 \end{bmatrix} X + \begin{bmatrix} -\lambda \\ -1 \end{bmatrix} u + \begin{bmatrix} 0 \\ 1 \end{bmatrix} w\,, \tag{5}$$

where X is the state vector of the control system, $X^{\mathrm{T}} = [x_1, x_2] = \delta d, \delta v$, u is the control variable of control system (controlled vehicle acceleration/deceleration a), w is the disturbance variable of the control system (navigation vehicle acceleration/deceleration ah). The second-order model contains the longitudinal displacement, velocity and acceleration/deceleration information of the navigation vehicle and the controlled vehicle, which can reflect the real-time and dynamic characteristics of the longitudinal automatic tracking control system of the vehicle team [10]. The control system is a two-input single-output control system, the input variable is the longitudinal relative distance error between vehicles and the relative speed error,

and the output variable is the expected controlled vehicle acceleration/deceleration.

4. Results and simulated analysis

4.1. Parameter self-tuning fuzzy PID controller

Parameter self-tuning fuzzy PID control is a kind of fuzzy compound control. In order to meet the requirement of the self-tuning of PID parameters at different error e and error change rate ec, PID parameters are modified online by using fuzzy control rules. The basic idea of parameter self-tuning fuzzy PID control is that the fuzzy relationship between three PID parameters and error e and error change rate ec is found out firstly, the e and ec are tested constantly in the running, and then three parameters are modified online based on fuzzy control theory to meet the different requirements of different e and ec on the control parameters, and to achieve the purposes of desired control.

The self-tuning requirements for the parameters K_{P}, K_{I} and K_{D} at different e and ec can be summarized as the following rules:

1) When $|e|$ is large, larger K_{P} and smaller K_{D} should be taken (to make the system response faster) and $K_{\mathrm{I}} = 0$ (the integral effect is removed to avoid a large overshoot).

2) When $|e|$ is medium, a smaller K_{P} (to make the system response has a smaller overshoot), appropriate K_{P} and K_{D} (especially the value of K_{D} has a greater impact on the response of the system) should be taken. When $|e|$ is small, larger K_{P} and K_{I} should be taken (to make the system have better steady-state performance) and K_{D} should be appropriate to avoid oscillation near the equilibrium point. The absolute values of error $|e|$ fuzzy and the error rate of change $|e|$ fuzzy are taken as the input language variables. For fuzzy input quantities, the combination of $|e|$ and $|ec|$ states can be set based on the design of the above rules, and the corresponding memberships can be calculated.

4.2. Selection and simulation of controller parameters

The fuzzification quantization factor of the input variables e and ec and the defuzzification scale factor of the output variables P, I and D (denoted by R) are selected: $Ke = 7.2$, $Kec = 8$,$RP = 0.6$, $RI = 1.3$, $RD = 1.0$. In different states, the setting value is obtained by the conventional PID parameter tuning method

$$K'_{\mathrm{P1}} = 1,\ K'_{\mathrm{I1}} = 0,\ K'_{\mathrm{D1}} = 0.00\,,$$

$$K'_{\mathrm{P2}} = 2,\ K'_{\mathrm{I2}} = 0,\ K'_{\mathrm{D2}} = 1.25\,,$$

$$K'_{\mathrm{P3}} = 3,\ K'_{\mathrm{I3}} = 0,\ K'_{\mathrm{D3}} = 2.50\,,$$

$$K'_{\mathrm{P4}} = 4,\ K'_{\mathrm{I4}} = 0,\ K'_{\mathrm{D4}} = 3.75\,,$$

$$K'_{\mathrm{P5}} = 5,\ K'_{\mathrm{I5}} = 2,\ K'_{\mathrm{D4}} = 5.00\,,$$

The MATLAB/Simulink platform is used for simulation control research, and the control block diagram is shown in Fig. 1 .

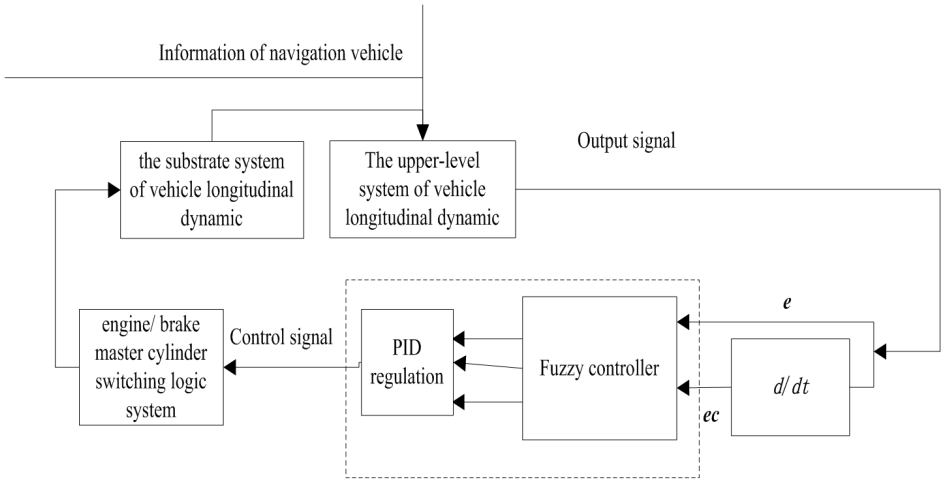

Fig. 1. The longitudinal dynamic fuzzy PID control system of automobile

Figures 2–5 are the simulation results of parameters self-tuning fuzzy PID control system of vehicle longitudinal dynamic.

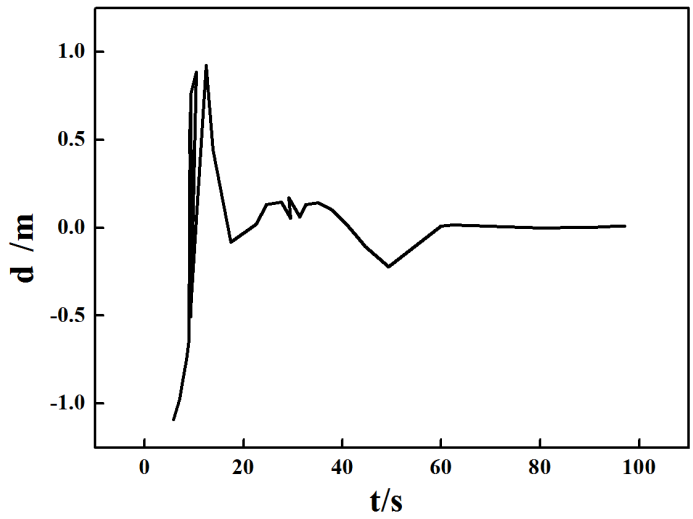

Fig. 2. Longitudinal relative distance errors of vehicles

Figures 2 and 3 show that when the navigation vehicle is in the variable acceleration/deceleration mode, the controlled vehicle is controlled by the parameters of self-tuning fuzzy PID, the change range of the longitudinal relative distance error between the navigation vehicle and the controlled vehicle is –1–1 m, which is

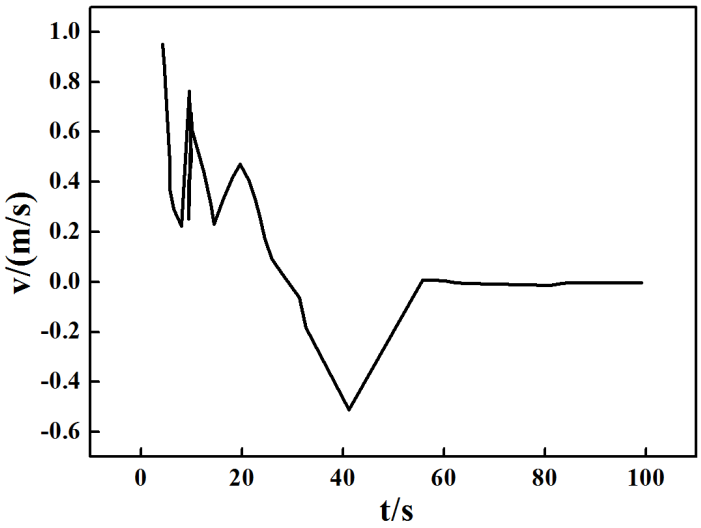

Fig. 3. Longitudinal relative velocity errors of vehicles

smaller than the distance error 1.4 m achieved by using single fuzzy control. While the change range of the longitudinal relative velocity error is only –0.6–1 m/s, which is smaller than velocity error 1 m/s achieved by using single fuzzy control, and the change is gentle and finally converges to zero, thus realizing that the controlled vehicle can automatically track the navigation vehicle, and the robustness is better than that using the fuzzy control.

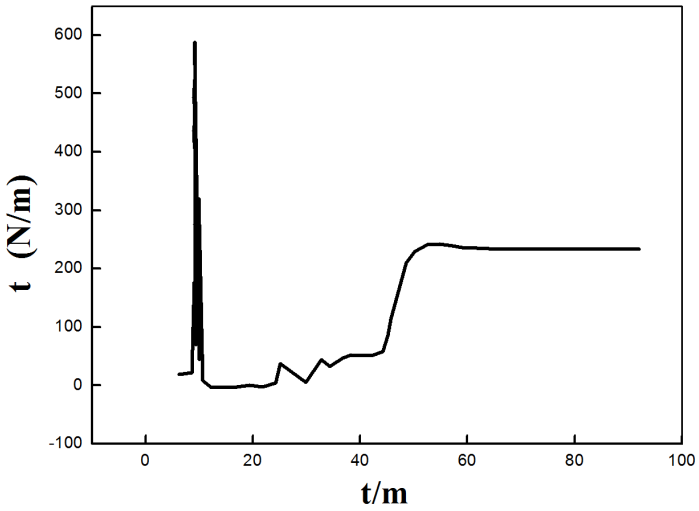

Fig. 4. Retarding torque

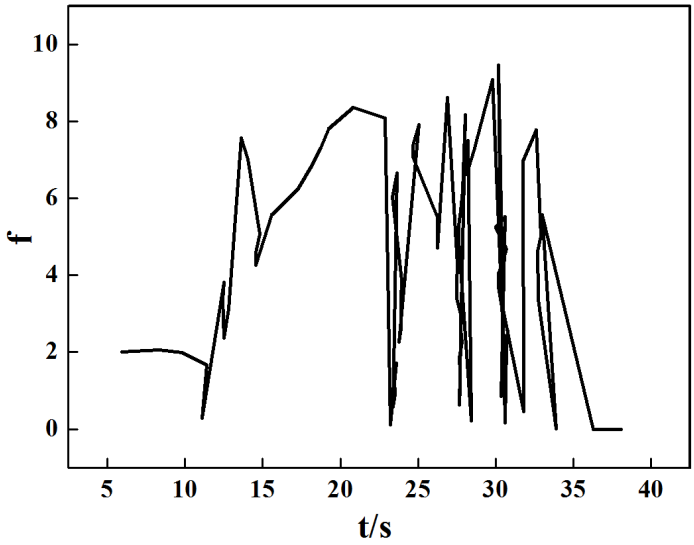

Fig. 5. Throttle percentage angle

Figures 4 and 5 are the braking torque t of the controlled vehicle and the throttle percentage angle f response. When the angle of the controlled vehicle throttle percentage is greater than zero, the car accelerates, and the brake torque associated with the brake is zero. Otherwise, when the angle of throttle percentage is less than zero, the car decelerates, and the brake torque is greater than zero. It can be seen that the simulation curve with parameter self-tuning fuzzy PID control accord with this logic, and it can transit smoothly during most of the time, but at the same time, the frequent switching of the dynamic torque and throttle percentage angle happen because of the frequent alternation between accelerator acceleration and brake deceleration between 20 s and 35 s.

5. Conclusion

Through the above analysis, we can see that the longitudinal dynamic system of the automobile and the parameter self-tuning fuzzy PID control can achieve the automatic control of the safe distance of the two vehicles. Because it uses the fuzzy control to express the advantages of irregular events and learns the tuning function of PID control, so compared with the single fuzzy control, it can reduce the overshoot volume, and also enhance the dynamic anti-jamming ability and improve the robustness, which solves the contradiction between the fastness and the small overshoot. However, this method has a problem that the switching of the braking torque and the throttle percentage angle is frequent due to the frequent alternation of the acceleration of the accelerator and the deceleration of the brake, which needs further improvement.

References

[1] J. Xu, J. Bu: *Simulation study of automotive electronics mechanical braking system based on self-tuning fuzzy PID control.* Journal of Residuals Science & Technology *13* (2016), No. 5.

[2] I. Souza-De-Assis, R. Oliveira, M. A. C. Fernandes: *Speed fuzzy control applied to autonomous electric vehicles.* WSEAS Transactions on Systems and Control *9* (2014), No. 67, 640–651.

[3] D. D. Mu, G. F. Wang, Z. S. Fan: *Design of adaptive neural tracking controller for pod propulsion unmanned vessel subject to unknown dynamics.* Journal of Electrical Engineering & Technology *12* (2017), No. 6, 2365–2377.

[4] G. A. Elnashar: *Dynamics modelling, performance evaluation and stability analysis of an autonomous underwater vehicle.* International Journal of Modelling, Identification and Control *21* (2014), No. 3, 306–320.

[5] Y. Lu, D. Yan, D. Levy: *Parameter estimation of vertical takeoff and landing aircrafts by using a PID controlling particle swarm optimization algorithm.* Applied Intelligence *44* (2016), No. 4, 793–815.

[6] M. H. Khooban: *Design an intelligent proportional-derivative PD feedback linearization control for nonholonomic-wheeled mobile robot.* Journal of Intelligent & Fuzzy Systems: Applications in Engineering and Technology *26* (2014) No. 4, 1833–1843.

[7] M. Cipek, D. Pavković, J. Petrić: *A control-oriented simulation model of a power-split hybrid electric vehicle.* Applied Energy *101* (2013), 121–133.

[8] A. Shokuhfar, B. Arab: *The effect of cross linking density on the mechanical properties and structure of the epoxy polymers: Molecular dynamics simulation.* Journal of Molecular Modeling *19* (2013), No. 9, 3719–3731.

[9] G. Ren, G. Ma, N. Cong: *Review of electrical energy storage system for vehicular applications.* Renewable and Sustainable Energy Reviews *41* (2015), 225–236.

[10] O. Laldin, M. Moshirvaziri, O. Trescases: *Predictive algorithm for optimizing power flow in hybrid ultracapacitor/battery storage systems for light electric vehicles.* IEEE Transactions on Power Electronics *28*, (2013), No. 8, 3882–3895.

Received October 12, 2017

Acta Technica *62* No. 2B/2017, 829–838

Wearable computer device design for environmental perception system

Xin Xu[1]

Abstract. With the growing popularity of smart devices, wearable computer devices are being more and more attention. The environment perception system of the wearable computer equipment design and research of this subject was analyzed in this paper, the connotation of environment perception technology and its effect were mainly introduced, at the same time, the wearable computer equipment content and research methods of the paper were explained, finally the research results were discussed and analyzed. The results show that the wearable computer equipment can better realize the function of human computer interaction with the support of environmental sensing technology, which provides a favorable research direction for the design of wearable computer equipment.

Key words. Environmental perception, wearable computer, equipment design, application research.

1. Introduction

Stana believes that the development of wearable computers dates from the mid-1950s. The first wearable computer is limited by the hardware and software, therefore, the first wearable computer in all aspects is at a low level [1]. The wearable computer has only a few simple buttons, the size of which is similar to that of a cigarette case. At the same time, the first wearable computer can only control their own data acquisition device to get the speed of the disc and the results of the data of feedback and transmission. Therefore, the first wearable computer is relatively low, but this does not have a negative impact on the continuous development of wearable computers. By the end of 60s, the wearable computer has the function which can read lips and eyes that is worn on the human body function. At the same time, some researchers use a filter to achieve the display of the function of pronunciation. Wearable computers in this period are still in the primary stage of a single function does not have the ability to program. Mann believes that the continuous development of the integrated circuit manufacturing industry in 80s provides a good basis

[1]Chongqing College of Electronic Engineering, 401331, Chongqing, China

for the continuous improvement of wearable computers. At the same time, a lot of researchers and institutions also pay more and more attention to the research of wearable computing. According to the needs of different industries, they have made a lot of research on the functional applications of wearable computers [2].

International Conference on wearable computer in 1997 by MIT and Carnegie Mellon jointly organized by many universities in the United States, and the U.S. Department of defense research institutions and Boeing also give support to wearable computer conference. Lin believes that wearable computer has become a very important academic research object; its potential value is also in many different industries gradually demonstrated. European research institutions in many developed countries have carried out a lot of researches of wearable computer technology and have formed a relatively stable industrial chain [3]. Our country's wearable computer research is from the beginning of 90s. In the early stage of our country, the related research is realized through the interaction between the host computer and the peripheral devices and sensors. Chongqing University in 2000 withdraws the wearable computer prototype. Leder believes that the centralized structure needs to be equipped with a large number of sensors and human-computer interaction devices. Although this structure can collect data, it has a certain degree of negative impact on human comfort [4]. Therefore, wearable computer is currently the most widely used in embedded watches and hat and other control chip. So far, the most popular product of wearable computer is the Google Corporation Glass Project. This product has completed its research and begins to sale. But the high price of this product has not been popular with the public. The purchase of this product is more scientific research staff. In recent years, our country for wearable computer research has just started, the research institutions most are the professional institutions. In summary, with the development of the globalization of the computer network and the intelligent equipment, it is very important to design and research the wearable computer equipment for the environmental sensing system. Based on the relevant theories at home and abroad, this paper analyzes and studies the design and research of wearable computer equipment in the system of the environmental perception system through the method of system experiment and model construction. In the second section, the connotation of environmental awareness technology and its role in the design of wearable computer devices are described. In the third section, the main content of wearable computer equipment design is introduced, and the research method of the design of wearable computer device which is opposite to the environment perception system is described. In the fourth section, it lists the specific data and the analysis and discussion of the system experiment and model construction. At the end of the fifth section, the results of this research are discussed.

2. State of the art

2.1. Environmental sensing technology

Parson believes that the continuous application of environmental sensing technology in life has brought more and more benefits to the production and life, thus

promoting the continuous research of environmental awareness technology. With the development of science and technology and the tendency of intelligence, there are more and more researches on the technology of environmental perception [5]. Figure 1 is the study and discussion of the environmental perception system of the academic activities of the scene.

Fig. 1. Environmental awareness technology conference

Bogner thinks environment perception is an important technology of pervasive computing, which involves the main content of this technique of environment information of modeling, information acquisition, processing and other aspects of rule reasoning excuse the main content of this technique. The difference between the actual environment and the purpose of the application is different, so that people form a different definition of the environment [6]. Most of the researchers understand the environment around the application environment and the actual situation, also includes the application execution environment overall, the main computing environment, physical environment and user. Generally speaking, the environment refers to the user's location, the surrounding people and other objects and their changes. Lien thinks from the point of view of the system function, the environment perception system, the user's location, and people around the user and resources have a certain understanding. Environment is constantly changing [7]. Pellerin thinks the main contents of green space environment that sent including computing environment, user environment and the physical environment in three aspects. Table 1 is the detailed content of the environment space. Environmental perception calculation can be made through the perception of environmental information and its response to the examination and interpretation [8]. Environment perception calculation is based on the user and the system's environment information to carry on the dynamic change and adaptation. For environmental perception system, the ability to perceive the environment in the character and material information and the characters of the interactive command figure is the basis, and then make the reasoning on

this basis judge and adapt the service strategy. Therefore, environmental awareness technology can help users reduce the unnecessary burden on the interactive process and develop the level of the characters in a certain extent. The development of environmental sensing technology has made its application scope more and more extensive. Figure 2 shows the research of the present robot that has been applied to the environmental sensing technology.

Table 1. The content of the environment space

Category	Content
Computing environment	Processor input, Device, Computing costs
User environment	Position, Crowd around, Social status
Physical environment	Temperature, Humidity, Illumination

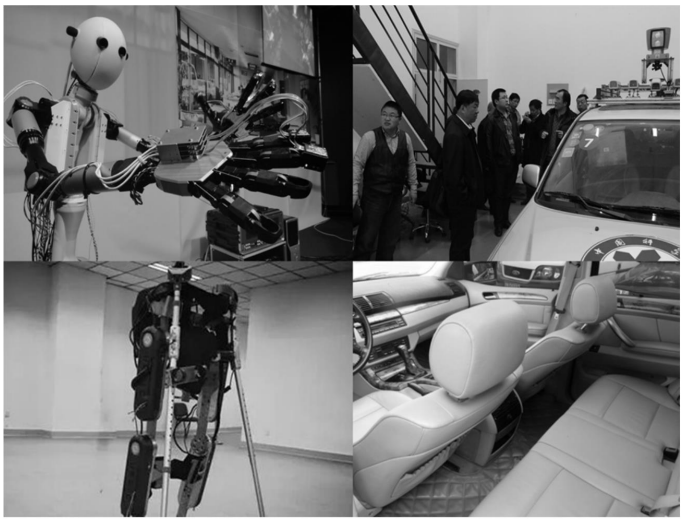

Fig. 2. Application of environmental awareness technology

Hassan believes that the perception of the environment structure is equivalent to a lot of different types of heterogeneous devices, such as sensors, mobile terminals and other software and hardware collection. The service provided by the system is completed by different devices [9]. This is mainly because the amount of information that the independent equipment cannot meet the requirements of the system and the user, with a certain degree of dispersion. Information of different equipment is different in form and way of acquisition, which is usually presented in an abstract way. At present, there are different levels of differences in the data structure of the modeling of the environmental sensing system, and the ways and methods of modeling are different. Sang believes that in the traditional environment, the access to information is generally achieved by direct access to the way the sensor device. This leads to the limitation of hardware binding in the development process [10]. The way of obtaining this information is not flexible enough, but it is most convenient

in operation. Based on the hardware sensor abstraction and processing by middleware, shielding upper application direct the operation of the underlying hardware can be abstracted hardware package and bind with the application layer, in a certain extent, which greatly improves the flexibility and expansion performance, which greatly reduces the limitations of hardware binding. Oliver thinks that the difference of the interface of the environment perception system is decided by the different users. The common interface of the environment perception system mainly includes three kinds of traditional API interface, database interface and event callback. The traditional API interface is usually the application program interface. The system provides access to the upper level application directly to the processing procedure interface, which is similar to the dynamic link library, and provides the interface style. At present, many network operators for their products with a suitable application interface to meet the needs of different developers. This kind of application program interface has the function of sharing, in a certain degree; it provides the convenience for the programmer. The interaction between the perceptual system and the database is inevitable. Database interface is essential between the two. The database interface is also designed for the data operation of the environment perception system. Callback method is a method of automatic operation after the end of the operation. Event and callback have a certain similarity in the mechanism. But, relatively speaking, the event is much easier to use than the callback. Environment perception system has its own rules. When the environment happen some changes, the system should take the environmental information and the environmental rules as the basis to carry on the adaptive change. Environmental rules mainly refer to the rational reasoning of environmental information behavior, which is based on the reasoning and conflict detection of middleware. Environmental reasoning is based on the environmental information database, which is built according to the environment model, and the reasoning mechanism of each environment model is different. Modeling the environment perception system mainly marked configuration model, value model, graph model and object-oriented models. The tag configuration model is a model that uses a markup language with a hierarchical structure to represent the environmental information. The main carrier of this model is the transmission of Internet information. The accuracy and convenience of this model are very high, but the relationship between the environmental information is difficult to distinguish. The graph model is more common, and its content is rich, and the model also has the characteristics of visual expression. But the graphics model needs to be abstract and has the computer language conversion processing.

3. Methodology

3.1. An overview of wearable computer device design

Ross believes wearable computer can be classified into the user's personal space; the user can operate and control the computer. Wearable computer has certain stability in the operation and interaction. Wearable computer has a certain continuity of the open state, at the same time, wearable computer access has its characteristics

at any time But Bulling believes wearable device mainly refers to the clothing and accessories and equipment, these devices can be provided for people to wear, one for wearable devices play the role of the carrier. Wearable device is a kind of portable equipment, which is based on the human capacity and equipment function, to a certain extent, to achieve the concept of human products. Thus, the concept of wearable devices is people-oriented, human and machine integration. At the same time, the realization of wearable device function is closely related to computer equipment and technology. The continuous progress of science and technology makes people tend to understand the understanding of wearable devices. In fact, the wearable device is not just simple smart equipment, in addition to its wearable function; it can also provide more specific services for people. In the globalization of the Internet today, wearable devices have been equipped with a variety of electronic hardware and the application software is provided for user. Wearable devices and most of the traditional electronic equipment, there is a big difference. Wearable devices have a lot of different ways of wearing, at the same time; these devices can also be worn at different locations in the human body. With the continuous development of wearable device design technology, the interaction between people and the machine will produce a variety of different ways. On the whole, different wearable devices have their own different characteristics.

Wearable computer equipment and the definition of a wide variety of devices, the standard measure of wearable devices also have a lot of different types and Haas Moto believes that the classification of wearable devices also have a lot of standards. From the perspective of the shape, wearable devices can be divided into glasses, watches, helmets and accessories, etc. A glass type wearable device is the main representative of wearable devices, Google glasses is a typical wearable device glasses. Some enterprises in our country also produce and sell similar products. However, this product is not yet more practical and in line with the user's products, most of the glasses wearable devices are still in the initial stage of the enterprise. The glasses type wearable device in general is mainly composed by battery energy, interactive systems and data processing core components. The main function of this kind of product is to realize the function of the intelligent mobile phone through the glasses. Smart glasses are prominent features of their interaction system. This system can help the smart glasses through speech and eye movement to achieve human-computer interaction throughout the process, in a certain extent; it is liberation of the people's hands. In addition, the smart glasses achieve a realistic and virtual space conversion to make human-computer interaction more humane. Wearable devices are generally semi covered or full coverage of the product. Starr leaf believes that helmet wearable devices and glasses wearable devices in the shape of little difference. However, there is a big difference between the technology and the smart glasses in the technology application. At present, the helmet wearable device is mainly applied to the VR virtual reality technology. Virtual reality helmet will provide a virtual three-dimensional space, when the user to wear a helmet after exposure to this virtual environment, the user generated an immersive feeling. Virtual reality is a completely virtual environment, this technology is characterized by its application to a lot of specific environment of the training and game scenes. There-

fore, many companies believe that the virtual reality helmet has a great space and value in the future development. Watch type wearable devices in the form and the traditional sense of the watch is similar. Wearable devices, however, it has a built-in computer smart chip and operating system. At present, the wearable watch is no longer a simple timing tool, but also has the function of smart phones. Wearable devices and wearable devices have the same structure. The user can operate and control the watch by touch and voice. Many companies have studied and released an equipment of wearable watches. Apple Corp's Watch Apple is a typical representative. In fact, the wearable device is a watch type of smart phones. From the point of view of market sales, its popularity is quite general. Users do not like the smart watch is mainly due to the neglect of the smart watch style wearable devices lack of its own characteristics. In addition, the performance of this type of wearable devices is generally wearable devices. But the role of Apple smart watches in the health and medical field is still worth the affirmative.

3.2. Research method of wearable computer device design for environmental sensing system

This paper mainly uses the method of system experiment and model construction to study and analyze the research and analysis of the design and research of wearable computer equipment for the environment perception system. The specific method of the system experiment is to verify the rationality and practicability of the wearable device design by testing the response of the environmental sensing system. In the process of building the main application formula (1) and the formula (2) reduce the degree of freedom of the algorithm, while the formula (3) and the formula (4) are for vector iteration. After the model is constructed, the process of the whole system experiment is finished by the test method of the system's requirement and the result output.

$$\{x_n\} = -\left[K_{nn}\right]^{-1}\left[K_{nm}\right]\{x_m\}\ , \tag{1}$$

$$[U] = -\left[K_{nn}\right]^{-1}\left[K_{nm}\right]\ , \tag{2}$$

$$[\phi] = [K]^{-1}[M]\,[\varphi]_{\text{old}}\ , \tag{3}$$

$$[\varphi]_{\text{new}} = [\phi]\,[Q]\ . \tag{4}$$

3.2.1. Result analysis and discussion The results obtained by the method of system test and model construction are shown below.

Figure 3 shows the change of the feedback information of the wearable device to obtain the feedback information of the environment, and also can see the dynamic change of the wearable device in the process of human-computer interaction. The coefficient of the model of the wearable device is low, and the linear correlation between the click time and the difficulty coefficient of the corresponding model can be reflected to a certain extent. From the results of the system test, the wearable

device is difficult to control. This is mainly by the operating mode of the device is more single, more with the thumb alone operation. Compared with other wearable devices, this problem should pay more attention in the design process of wearable devices.

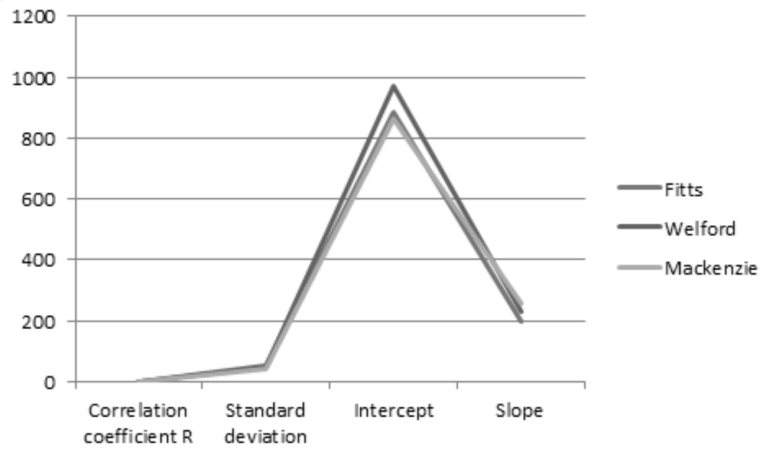

Fig. 3. Experimental results of Twiddler

Figure 4 depicts other wearable devices to a certain extent than wearable devices such as wearable devices and other visual perception wearable device model coefficient is higher. At the same time, the dynamic changes of the situation are also more stable. This is mainly because the other wearable devices operating mode is more convenient. Compared with the single mode of operation, the operation mode of the device is improved greatly, and the user experience is improved. This has a very important positive impact on the application of wearable devices. In addition, from the point of view of the feedback information, the performance indicators of these wearable devices are also higher than the first wearable device.

Figure 5 depicts through different test environments and different models of the construction and test of the results of the comparison of the various coefficients. Both of these two regression models reflect the length of the reaction time and the difficulty of operation to a certain extent. Under different test conditions, the operation difficulty of the wearable device is not changed, and the performance index of other wearable devices is relatively stable under different conditions. Thus it can be seen that the operation of the device is difficult to wear and the user experience is closely related to the user experience. At the same time, it can be seen that the application environment of wearable device has low impact on its use effect and its own performance. Therefore, in the actual design process, the staff can be from the perspective of environmental awareness technology to improve the simplicity of the operation of the product to carry on the reasonable design of wearable devices.

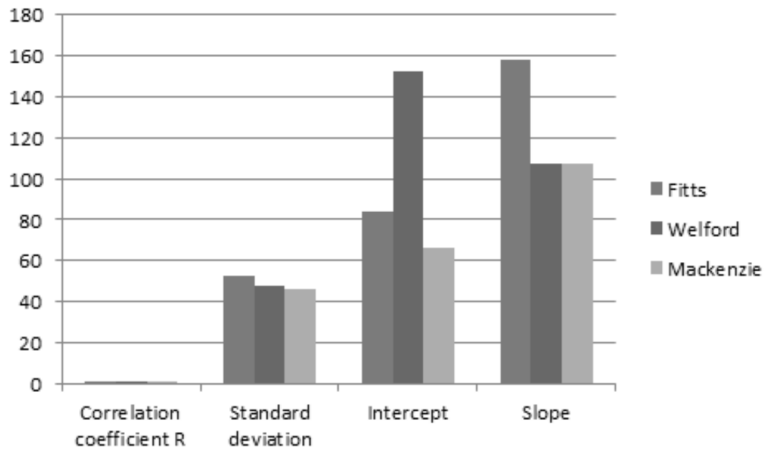

Fig. 4. Experimental results of Mouse

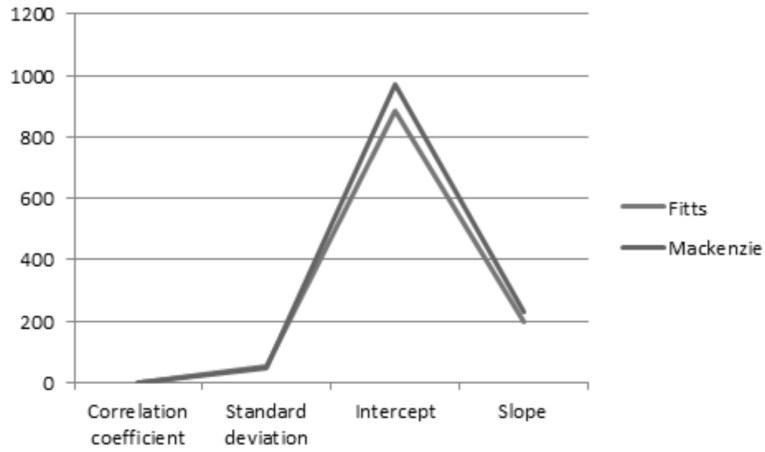

Fig. 5. Results of model data comparison

4. Conclusion

With the popularity of smart phones and applications, the wearable devices which can be used got more and more people's attention and welcome. Therefore, it is very important to design and research the wearable computer equipment for the environmental sensing system. Environmental sensing technology to a certain extent, it has promoted the development of wearable computer equipment. In the process of design and research of wearable computer equipment for environmental sensing system, wearable computer equipment is more widely used. Compared with other wearable computer equipment, the performance coefficient of the head mounted computer equipment is slightly lower than that of other wearable computer equipment. In the operation mode, the head mounted computer equipment has some disadvantages,

and the single operation mode has a certain degree of negative impact on the user experience. And other wearable devices in different test conditions, the performance index of the level is relatively stable.

In summary, the wearable computer equipment for environmental perception system still exist some problems. In the actual design process, the staff should improve the degree of attention of the user experience; from the perspective of equipment operating mode effectively improve the equipment, so as to promote the development of wearable devices.

References

[1] V. G. Motti, K. Caine: *Human factors considerations in the design of wearable devices.* Human Factors and Ergonomics Society Annual Meeting, Santa Monica, CA, SAGE Publications *58* (2014), No. 1, 1820–1824.

[2] I. Schnell, O. Potchter, Y. Epstein, Y. Yaakov, H. Hermesh, S. Brenner, E. Tirosh: *The effects of exposure to environmental factors on heart rate variability: An ecological perspective.* Environmental Pollution (2013), No. 183, 7–13.

[3] S. F. Foley, D. Gronenborn, M. o. Andreae, J. W. Kadereit, J. Esper, D. Scholz, U. Pöschl, D. E. Jacob, B. R. Schöne, R. Schreg, A. Vött, Da. Jordan, J. Lelieveld, C. G. Weller, K. W. Alt, S. Gaudzinski-Windheuser, K. C. Bruhn, H. Tost, P. J. Crutzen: *The Palaeoanthropocene – The beginnings of anthropogenic environmental change.* Anthropocene *3* (2013), 83–88.

[4] X. Liu, D. Liu, Y. Zhang, Q. Wang, S. Zhang, H. Wang: *Optimal support vector regression algorithms for multifunctional sensor signal reconstruction.* TELKOMNIKA Indonesian Journal of Electrical Engineering *12* (2014), No. 4, 2762–2768.

[5] A. Ogawa, E. Macaluso: *Audio–visual interactions for motion perception in depth modulate activity in visual area V3A.* Neuroimage (2013), No. 71, 158–167.

[6] P. Majaranta, A. Bulling: *Eye tracking and eye-based human–computer interaction.* Advances in physiological computing, Springer Nature, Book Series (HCIS) (2014) 39–65.

[7] N. K. F. Tsang, L. Y. S. Lee, C. K. L. Liu: *Understanding the shopping motivation of mainland Chinese tourists in Hong Kong.* Journal of China Tourism Research *10* (2014), No. 3, 323–346.

[8] H. T. Dinh, C. Lee, D. Niyato, P. Wang: *A survey of mobile cloud computing: architecture, applications, and approaches.* Wireless Communications and Mobile Computing *13* (2013), No. 18, 1587–1611.

[9] S. Yi, C. Li, Q. Li: *A survey of fog computing: Concepts, applications and issues.* Workshop on Mobile Big Data, 21 June 2015, Hangzhou, China, ACM Procedings Mobidata'15 (2015), 37–42.

Received October 12, 2017

Acta Technica 62 No. 2B/2017, 839–848

Analysis of the protective effect of POLYSWITCH on resistor based on the construction of mathematical model[1]

Huandong Wang[1], Yingxin Wang[2], Qiang Shao[1]

Abstract. The resistance value changes as the temperature increases. However, when it is beyond a certain range, the enthalpy of the resistor will continue to rise and damage may occur. In view of this, in this paper, the protective effect of POLYSWITCH on resistor was analyzed based on the mathematical model. First of all, the current status of application and research of resistor and integrated circuit in China were introduced; then, the protective effect of POLYSWITCH on resistor was analyzed based on the ANSYS mathematical model; finally, the protective effect of common thermal resistor and POLYSWITCH resistor under the ANSYS mathematical model were tested by different current values. Studies show that POLYSWITCH can make resistors more resistant to current shock and voltage resistance, thus ensuring the durability of resistors for long term use.

Key words. Construction of mathematical model, POLYSWITCH, protective function of resistor.

1. Introduction

Resistors, as a kind of important and versatile electronic components, have more than 100 years of history. The latest developments in the scale and quality of electronic resistors have reached a new level. The reliable resistors with a precision of up to 0.001 can be produced technically with a very small size, which can be adapted to the resistor network that is required for the integrated circuit. In electronic equipment, the resistance component accounts for most of the total number of electronic components [1]. Therefore, all countries attach great importance to the development of RC devices. Improving the performance is the goal of resistance devices manufacturers all over the world. They constantly study and use new materials, fundamentally improve the performance of RC components and expand their

[1]Hebei University of Water Resources and Electric Engineering, Cangzhou, Hebei, China, 061001
[2]Chengde Petroleum College, Chengde, Hebei, China, 067000

applications. In recent years, the components made in China are stable, and the output of the products continues to rise, moving forward at a pace of doubling in three years [2].

Metal film resistors, manufactured in 1950s, are a variety of high stability, high quality resistors. The development of integrated circuit in 1960s has made the miniaturization of electronic components in a new era. The development of large-scale and VLSI circuits in the 1980s has made profound changes in the structure of the electronics industry [3]. The advantages of integrated circuits are obvious, but the integrated circuit cannot completely replace the discrete components. There are still many components that are not integrated, and discrete components are needed to make up for them. It will take a long time for so many varieties of resistors to continue to develop, including resistor networks, potentiometers, and a variety of sensitive resistors [4].

2. State of the art

The use of POLYSWITCH thermistors for overcurrent protection is becoming increasingly widespread. In recent years, with the rapid development of science and technology and electronic communications, online distribution of the main distribution frame has reached hundreds of millions. Especially in the relatively complex environment of the rural areas, because of lightning, electromagnetic interference and power line collision, a short circuit can cause damage to the circuit board of the distribution module or switchboard, and can cause serious flame combustion [5]. All of these have caused great potential danger to communication security, so the protection of communication equipment is an important issue for the communication industry. Previously, this protection was done using a hot coil or protective circuit. Because the quality is not uniform, the protection effect is not obvious. Now using excellent UI function of POLYSWITCH components, the POLYSWITCH thermistor is designed for the over-current protection on program-controlled switches and wiring boards. The problem has been solved and the number has risen sharply [6]. At present, there are a lot of integrated circuits and modules in communication equipment. The problems, such as low working voltage, strong current and low overcurrent, exist. Relatively high lightning protection and high voltage resistance of communication lines is required [7]. The maximum rated voltage of the POLYSWITCH thermistor is between 30 V and 265 V, and the communication equipment (line) has over-current protective effect. The maximum rated voltage used by the POLYSWITCH component is between 250 V and 650 V. Therefore, the over-current protection type POLYSWITCH thermistors exhibit high temperature cycle requirements [8].

3. Methodology

3.1. ANSYS mathematical model analysis method

The most critical task of the simulation method is to construct an objective mathematical model and match the exact underlying database. Its advantage is that it provides great convenience for the future grounding resistance, structure optimization, performance simulation and so on. However, building models and basic databases takes a lot of time and cost, and the deviations between the mathematical model and the basic parameters directly affects the accuracy of the results. The ANSYS software was created and developed by Dr. John Swanson, a professor at the University of Pittsburgh in 1970. It can analyze the physical fields such as structures, heat, electromagnetic fields, fluids, acoustic fields and coupled fields. In addition, it can be used in many fields, such as mechanical, aircraft design, energy, traffic, water conservancy, architectural design, circuit simulation, medical teaching, and so on. ANSYS software provides CATIA, UG, PRO/E and other mainstream CAD software data interface. The finite element model is established to load, solve and examine the results [9].

In this study, the main steps of finite element analysis are to build finite element models, load and solve, and post process results and examine the effects. According to the analysis described in the POLYSWITCH (polymer composite thermistor), the material properties include conductivity, material density, specific heat of the material, resistivity of the material, and temperature coefficient of resistance. Applied loads include convection loads and initial temperatures [10].

The thermal field analysis of polymers is mainly determined by the physical field of polymer composites, and the thermal complex of all polymers can be analyzed by two general analytical methods: ordered polymer thermal composites and direct polymer thermal composites. The sequential polymer thermal compounding refers to that two or more physical fields are analyzed in a certain order, and then the results of the previous analysis are applied as a load to the polymer thermal fit for the next analysis. The direct polymer thermosensitive composite consists of only one analysis, and the units used contain two or more field degrees of freedom.

ANSYS software is attached with a variety of thermistor coupling units. Through the simulation experiments, it is found that solid 69 thermistor coupling unit is the most appropriate. The use of such units can be directly coupled to the current field directly on the model temperature field and operation, which greatly reduces the workload. SOLID 69 is a three-dimensional eight-node hexahedral element which consists of two degrees of freedom: voltage and temperature. It can achieve the Joule heat generated by the current, transient and steady state analyses. Common thermistors are shown in Fig. 1.

3.2. POLYSWITCH resistor protection analysis process under ANSYS mathematical model

Every ANSYS analysis must include material properties. For example, at least the relative permeability of the material is input during electromagnetic field analy-

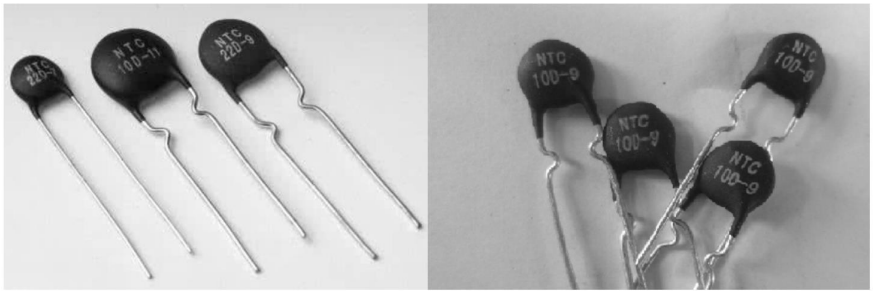

Fig. 1. Common thermistors

sis; and the modulus of the material is used as an input to structural analysis. The main components of the resistor include lead, protective layer, metal cap, melt and ceramic substrate. The main material of lead is copper, and the surface is coated with tin thin layer, the main purpose of which is to weld better. Because the tin layer is very thin, the fused wire has little influence on the fusing performance of the resistor. Therefore, the simulation results only require the material properties of copper wire, which will not affect the results of simulation.

POLYSWITCH resistance is characterized by the aspects as follows: hardness is Rockwell hardness, namely HRA80-90, which is second only after diamond and far exceeds the wear resistance of wear-resistant steel and stainless steel; abrasive resistance is excellent, the abrasive resistance of manganese steel and high chromium cast iron is very good, but the abrasive resistance of alumina ceramics is 266 times and 171.5 times than the two, and it can extend at least ten times the equipment life or more under the same operating conditions; the weight is light, and the density is half of the steel, thereby reducing the load on the equipment. The specific physical parameters of the components of the POLYSWITCH resistor are shown in Table 1.

Table 1. Specific physical parameters of the components of the POLYSWITCH resistor

Material	Density (kg/m^3)	Thermal conductivity (W/m K)	Specific heat capacity (J/kg)	Resistivity (Ωm)	Resistance temperature coefficient (TRC)
Copper	8920	400	390	1.75×10^{-8}	-
Protective layer	2650	1.3	795	-	-
Iron	7900	80	448	1.0×10^{-7}	-
Alumina ceramic	3600	25	-	-	-
Nickel chromium wire	8300	16.75	460	1.08×10^{-6}	-

Because the temperature range of the POLYSWITCH resistor melt is large, the variation of resistivity with temperature cannot be neglected. By using the following formula, the resistivity at different temperatures can be calculated.

$$\rho = \rho_0(1 + \alpha t)\,, \tag{1}$$

where ρ_0 is the resistivity of the melt at room temperature, and α is the resistance temperature coefficient.

The first is the formula method, which is used to define the relationship between parameters and temperature changes. In each step of the ANSYS iterative operation, the temperature values of each node are first read, and then the corresponding parameter values are calculated by a formula for continuous operation. If the phase transition occurs at a certain temperature, the simulation results obtained by the formula will be incorrect, because the change trend of the parameters before and after the phase transition temperature is different. Another method is the look-up table method. The physical parameter values and temperature values corresponding to the table are obtained by a test or other method in a certain temperature range, i.e., each temperature parameter corresponds to the parameter value. In calculations, the ANSYS automatically reads the temperature corresponding to the calculated parameter in the form. Melting involves phase transition. Phase change analysis must take into account the potential heat of the material, i.e., enthalpy. In ANSYS, the enthalpy of input is used as the material parameter to calculate the enthalpy of the material. Since the enthalpy is a temperature change, the enthalpy is nonlinear.

When the object is solid, the temperature is T_{S}, and the heat capacity is C_{S}. When the object is liquid, the temperature is T_τ, and the heat capacity is C_τ. The two temperatures are defined and the latent heat is obtained in the finite element analysis. The enthalpy calculation method at different temperatures is as follows:

Below the solid temperature

$$H = pC(T - T_\tau)\,. \tag{2}$$

When the object is in liquid state

$$H = H_{\mathrm{s}} + pC(T - T_\tau)\,, \tag{3}$$

The enthalpy of the body can be obtained from the above formula. The values at particular temperatures are given in Table 2.

Table 2. Values of heat enthalpy of an object at various temperatures

Temperature (K)	Enthalpy (J)
0	0
1399	5.34E9
1401	1.12E10
2000	1.42E10

In addition, meshing is a very important step in the ANSYS simulation process,

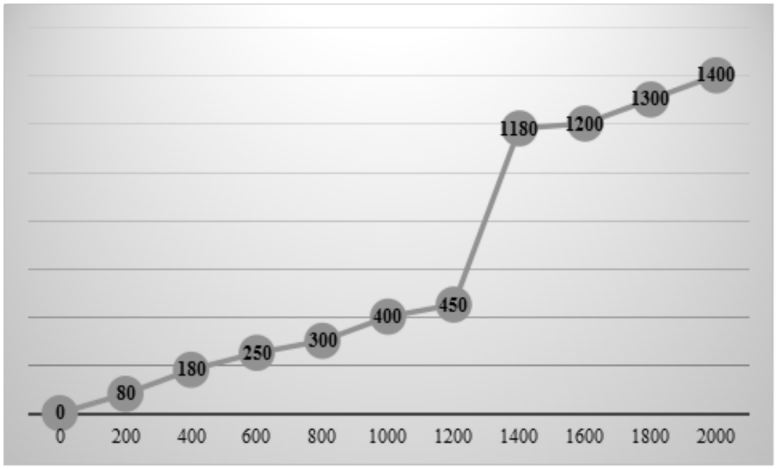

Fig. 2. Change curve of enthalpy value of resistor with temperature

because the correctness of ANSYS finite element calculation is mainly determined by the quality of the mesh. For free mesh, unit shape has no special requirement. The shape regular or irregular model can be divided into surface automatic generation triangle or quadrilateral mesh, and the body automatically generates tetrahedral mesh. The scanning mesh is mainly used in 3D model, which is to scan the whole cell from the source grid element.

For POLYSWITCH resistor, the load is first set as the initial condition. In general, the initial temperature of the model node is 20 °C. Secondly, the boundary conditions should be set up: thermal analysis conditions. Both ends of the load resistance force convection are assumed so that the temperature at both ends stays at 50 °C.

4. Result analysis and discussion

According to the project target, and combined with the current test hardware and software conditions, the project was selected through simulation test method. Through the test data, the actual heating parameters of POLYSWITCH resistance were obtained, and protection suggestions were put forward according to these parameters. According to the actual situation of the southern power grid, this study used typical structure, the hangers ZDZ66-10-10 POLYSWITCH resistors with the largest number to carry out the simulation test. The test was divided into two parts: single chip resistance heating test of common thermistor and POLYSWITCH resistance heating test.

The test was to apply frequency current on a common thermistor single resistor, so that the temperature rise of the time curve and the final heat balance temperature or blowing temperature were measured under different currents. The DZ alloy resistor which was reliably welded and secured to a special bracket was powered by

a 8000 kVA test transformer and regulated with a 500 kVA regulator. The test current was monitored by the 1000/5 current transformer and the T24 ammeter. The impedance parameters of the line and equipment were obtained by several small current tests before and after the test. Then, the enthalpy and voltage of each test current were calculated. Three current values of 200 A, 300 A, and 400 A were tested each time. The results are as listed in Table 3

Table 3. Results of temperature rise test of monolithic thermistor

Current (A)	Time (s)	Hot spot temperature rise (K)	Enthalpy (J)
200 A	50	192	57
	100	307	84
	150	390	136
	200	436	172
	300	471	274
300 A	50	280	63
	100	435	89
	150	495	144
	200	530	179
	300	629	279
400 A	50	460	105
	100	660	132
	150	742	183
	200	814	229
	300	885	323

According to the results of above test several test current, it can be seen that under the action of 200 A and 300 A frequency power, the heating temperature of the hot spot is relatively mild, and the enthalpy of the two current is about 5 thresholds. The ordinary thermistor can reach the thermal equilibrium state at 373 K under 200 A power frequency. There is no abnormal heating process, and the appearance of the resistor has no obvious change after cooling. The common thermistor can achieve the thermal balance under the 300 A power frequency and the 612 K temperature. The heating time is 300 s, without abnormal heating process. After the cooling, the appearance resistance chip has slight change in color. But under the 400 A power frequency and current, the hot spot reaches 885 °C in 300 seconds, without any abnormal heating process. After cooling, the appearance color of the resistance film has changed significantly.

A frequency current was applied to the POLYSWITCH resistance to measure the temperature rise at different currents and possible thermal equilibrium temperatures. The products A, ZDZ66-10-10 type POLYSWITCH resistor was tested, which was powered by the 8000 kVA test transformer. The test voltage was adjusted by 500 kVA regulator and monitored by 1000 V current transformer and T24 ammeter. The current was tested (current was less than 100 A clamp current meter, and the test ensured measurement accuracy), and the infrared imaging equipment, automatic temperature and full video were used. Before the formal test, the impedance

parameters of the line and the equipment were obtained by small current test. By calculating the test current, the voltage was applied to the required voltage. Each test was carried out in accordance with three current values of 200 A, 300 A, and 400 A. The resistor grid was only allowed to be opened in a short period of temperature measurement. The resistor gate was kept as close as possible during the rest of the time, so that the analog resistor was in the best test state. The test results are listed in Table 4.

Table 4. Test results of temperature rise of POLYSWITCH resistor

Current (A)	Time (s)	Hottest point temperature rise (K)	Enthalpy (J)	Hot spot
200 A	10	23.1	15.6	Central region
	20	48.7	25.9	Upper central region
	50	182	36.7	Upper area
	80	299	52.4	Upper area
	100	361	71.5	Uppermost central region
300 A	10	37	17.3	Central region
	20	76	29	Upper central region
	50	270	41	Upper area
	80	353	55.4	Upper area
	100	405	75.9	Uppermost central region
400 A	10	43	26.8	Central region
	20	115	43.7	Upper central region
	50	387	54	Upper area
	80	436	63.2	Upper area
	100	523	88	Uppermost central region

From the data above, it can be found that the POLYSWITCH resistor cannot achieve thermal balance in the range of 385 K under the action of 200 A frequency current. After experiencing the heating time of 95 s, the hottest point temperature rise of the resistor reaches 405 K, and the hot spot is located in the uppermost middle region. There is no abnormality during the test, and the appearance of the resistor after cooling has no obvious change. When the POLYSWITCH resistor is under the action of 250 A frequency current, the thermal balance state cannot be reached in the range of 385 K. After the heating time of 75 s, the hottest point temperature rise of the resistor reaches 405 K, and the hot spot is located in the uppermost middle region. There is no abnormality during the test, and the appearance of the resistor after cooling has no obvious change. When the POLYSWITCH resistor is under the action of 400 A frequency current, the thermal balance state cannot be reached in the range of 385 K. After the heating time of 100 s, the hottest point temperature rise

of the resistor reaches 523 K, and the hot spot is located in the uppermost middle region. There is no abnormality during the test, and the appearance of the resistor after cooling has no obvious change. In summary, compared with the ordinary thermistor under the same current test condition, the POLYSWITCH resistor has lower enthalpy value, relatively stable temperature and better protective effect of the electric appliance. In addition, it has more stable physical properties and improves durability.

5. Conclusion

With the introduction of all kinds of electrical equipment, the electrical equipment commonly used in thermistors has been used for the first time to protect them. Application areas continue to expand in communications equipment. Small power input saturation and battery charger products have been applied. The fuse tube equipment can be replaced by thermistors to play over voltage protection, and over-current protection. In this paper, the protective effect of POLYSWITCH on resistor based on mathematical model was studied. Firstly, the research and application of resistors at home and abroad were introduced; then, the main steps of constructing the mathematical model were analyzed; with this model, the protection of POLYSWITCH resistor was discussed; finally, the mathematical model was used to compare the protective effects of common thermistors and POLYSWITCH resistors. Research shows that based on the role of POLYSWITCH, the associated resistors can save electricity costs and achieve a safe and efficient power plan. Therefore, the choice of POLYSWITCH resistor is the inevitable trend of the development of high-end electronic products. In addition, POLYSWITCH heating resistors need to be evenly distributed through various methods, so as to improve the reaction time and improve the working efficiency of the appliance.

References

[1] J. R. Shih, J. H. Lee, H. L. Hwang, B. K. Liew, S. Y. Chiang: *Analytical model of human body model electrostatic discharge current distribution and novel electrostatic discharge protection structure.* Japanese Journal of Applied Physics: Part 1 *38* Part 1 (2014), No. 8, 4632–4641.

[2] X. Y. Wang, H. Zhang, X. P. Ma, Q. Cheng, C. G. Li, M. X. Li, T. N. Chen, P. Zhang, J. Q. Shao: *Degradation behavior and mechanism of polymer films for high-ohmic resistor protection in a heat and humid environment.* Microelectronics Reliability *57* (2016), 79–85.

[3] S. Roy, D. Kanabar, C. Dodiya, S. Pradhan: *Development of a prototype hybrid DC circuit breaker for superconducting magnets quench protection.* IEEE Transactions on Applied Superconductivity *24* (2014), No. 6, Article Seq. No. 4702006.

[4] A. Sahebi, H. Samet, T. Ghanbari: *Method to secure the performance of the differential protection in presence of fault current limiter applied into the neutral line.* IET Science, Measurement & Technology *10* (2016), No. 8, 880–888.

[5] J. Mondal, A. Marques, L. Aarik, J. Kozlova, A. Simões, V. Sammelselg: *Development of a thin ceramic-graphene nanolaminate coating for corrosion protection of stainless steel.* Corrosion Science *105* (2016), 161–169.

[6] D. Xu, Y. Wang, Z. Y. Li, H. Gao, Z. Hong, Z. Jin: *Coupled analysis and protection of the HTS DC magnet for DC induction heater in dynamic disturbance.* IEEE Transactions on Applied Superconductivity *25* (2015) No. 3, Article Seq. No. 4602605.

[7] M. F. B. Abdullah, Z. Baharudin, N. H. B. Hamid: *The third harmonic model for salient pole synchronous generator under balanced load.* IEEE Transactions on Energy Conversion *29* (2014), No. 2, 519–526.

[8] J. Asaadi, J. M. Conrad, S. Gollapinni, B. J. P. Jones, H. Jostlein, J. M. S. John, T. Strauss, S. Wolbers, J. Zennamo: *Testing of high voltage surge protection devices for use in liquid argon TPC detectors.* Journal of Instrumentation *9* (2014), No. 9, P09002.

[9] C. Y. Lin, M. D. Ker, Y. W. Hsiao: *Design of differential low-noise amplifier with cross-coupled-SCR ESD protection scheme.* Microelectronics Reliability *50* (2010), No. 6, 831–838.

Received October 12, 2017

Acta Technica *62* No. 2B/2017, 849–858

Application and design of mobile intelligent terminal security protection system based on android platform

Zhang Qi[1], Wang Haoxin[2], Hu Jing[3]

Abstract. With the rapid development of mobile Internet information technology, a large number of mobile systems are surging up just like the waves, and people's daily life is also increasingly inseparable from these mobile systems. However, at the same time of that the mobile system brings convenience to people, it can't be ignored that it may reveal people's personal privacy information and even endanger people's lives and property. Therefore, how to improve the security of the mobile phone system has become an urgent need to solve the problem. In this paper, the application of the mobile intelligent terminal security protection system based on Android platform was devised, and then, a system with perfect function, good interface and excellent performance was formed by constantly updating the system version and repairing some loopholes and defects of the system.

Key words. Mobile intelligent terminal, security protection, system application.

1. Introduction

As we all know, with the development and popularization of smart phones, the mobile phone security management functions are becoming more and more important. Based on the actual needs, this paper designs and implements an application of mobile intelligent terminal security protection system based on Android platform. Android is a system platform and operating system based on the Linux kernel [1]. As an open source operating system, Android's technical architecture is easy to master, and furthermore, it is easy to implement the system solutions. At the same time, Android platform open source promotes that the application system based on the Android platform in the smart phone market is increasing [2]. Therefore, there are various problems that need to be solved in security and experience, for example:

[1]Computer Center of Experiment, Chengde Medical College, Chengde, Hebei, China, 67000
[2]Educational Administration Office, Hebei Normal University for Nationalities, Chengde, Hebei, China, 067000
[3]College of Business, Hebei Normal University for Nationalities, Chengde, Hebei, China, 067000

some illegal systems may threaten the performance and security of mobile phones, and ultimately cause time and economic losses to the mobile phone users whose guard consciousness is weak [3]. Based on the above reasons, it is imperative to design an application of the mobile intelligent terminal security protection system based on application with better performance.

2. State of the art

At present, the domestic Android phone security protection system is 360 security protection system, the proportion of users is far ahead, which ranks first in the industry, and furthermore, it continues to lead the mobile security market [4]. 360 security protection system's main features include: mobile phone antivirus, mobile phone physical examination, mobile phone acceleration, harassing SMS / phone interception, personal privacy protection, call attribution display and query, mobile phone physical examination, commonly used number inquiries. In the statistics of Ai media, Tencent mobile housekeeper has the second largest number of users. Tencent QQ mobile phone management is a mobile phone security protection system launched by Tencent for users [5]. At first, the purpose of designing Tencent mobile phone housekeeper is to protect the user's QQ account Internet security. Then, this system is widely praised by people because of its superior performance, and it gradually develops into a versatile antivirus system. At the same time, from the user's point of view, some small functions that are close to the actual needs of users are developed, which are fit for the pursuit of the fashion of users. Tencent mobile phone housekeeper is not only a security expert, and moreover, it is also the user's intimate butler.

In contrast, foreign applications do better in users' privacy. However, it is inevitable that many malicious systems run secretly in the background, steal the traffic and information. Therefore, foreign countries also attach great importance to mobile phone security, which release a variety of security applications [6]. AVG is currently an anti-virus system widely used on the Android platform, it has a powerful virus scanning capabilities, provides personalized security information services, at the same time, it also has GPS function, which can carry out the reverse tracking to the mobile phones lost, and then protect users' mobile phone security from all aspects. Kaspersky Anti-Virus System is the leader in foreign security systems. At present, it has been extended to the mobile field [7]. Whether it is in the antivirus or privacy protection, the system shows a very good advantage, which is a very professional antivirus system.

3. Methodology

3.1. System architecture design

MVC is a system design pattern. MVC is divided into three levels, and the three letters of MVC are the abbreviation of three words, which are respectively the Model

layer, View layer, Control layer. The first is the Model layer, which is primarily the core functionality of the packaging system. The second is the View layer, which is mainly responsible for the human-computer interactive part, processing the user's request and displaying the processing results [8]. And then, the main business logic processing is encapsulated in the Controller layer, the users' related requests are implemented in this layer. The design idea advocates to respectively realizing the system interface, data processing, business logic processing, etc., so as to achieve that the system will not cause the tedious change works and make mistakes because of the complexity of the system code association when it needs to modify or extend the relevant functions in the development or even the latter part of the maintenance process [9]. In addition, the business logic functions and the program interfaces are separated, which can also allow developers to focus more on achieving the customization of system function business, rather than rigidly adhering to the redundant and complex configuration of the framework. The system logical architecture diagram is shown in Fig. 1 below.

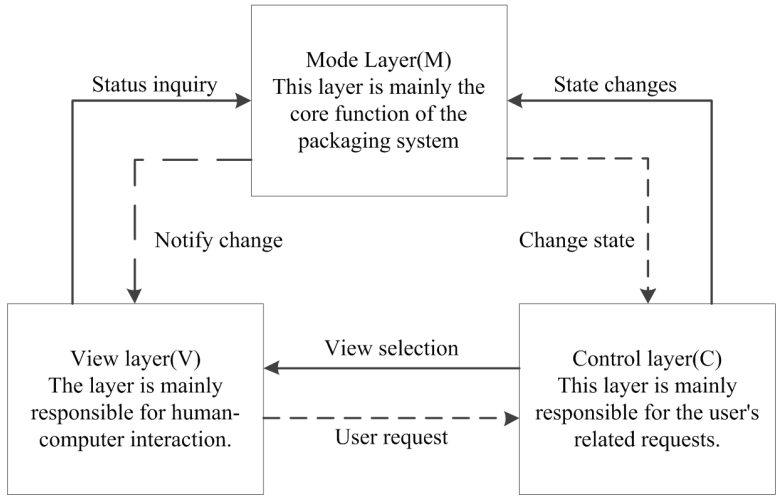

Fig. 1. System logic architecture diagram

The system client of the system adopts the Android program written by Java language, while the server uses the ThinkPHP framework to conduct design. Then, Nginx + Apache architecture builds a distributed cluster server by coordinating with keepalived [10]. This distributed master-slave server architecture can transfer the failure point to the backup server, so that the corresponding system functions can be directly transferred to the backup server when the system function failure appears, thus ensuring that the system can run properly. Moreover, in order to improve the overall data privacy security of the system and the reliability of the system data transmission, for some critical data of the system, the RSS encryption algorithm is used to carry out the encrypted transmission. In addition, in the design process of the system, it is necessary to strictly follow the RBAC access authority design principles, strictly control the system access operation authority among different roles, so as to

ensure that the user permissions between different user roles in the system operation process are not the same, thereby achieving the fundamental purpose of protecting the system data information security. The physical architecture diagram of the system is shown in Fig. 2 below.

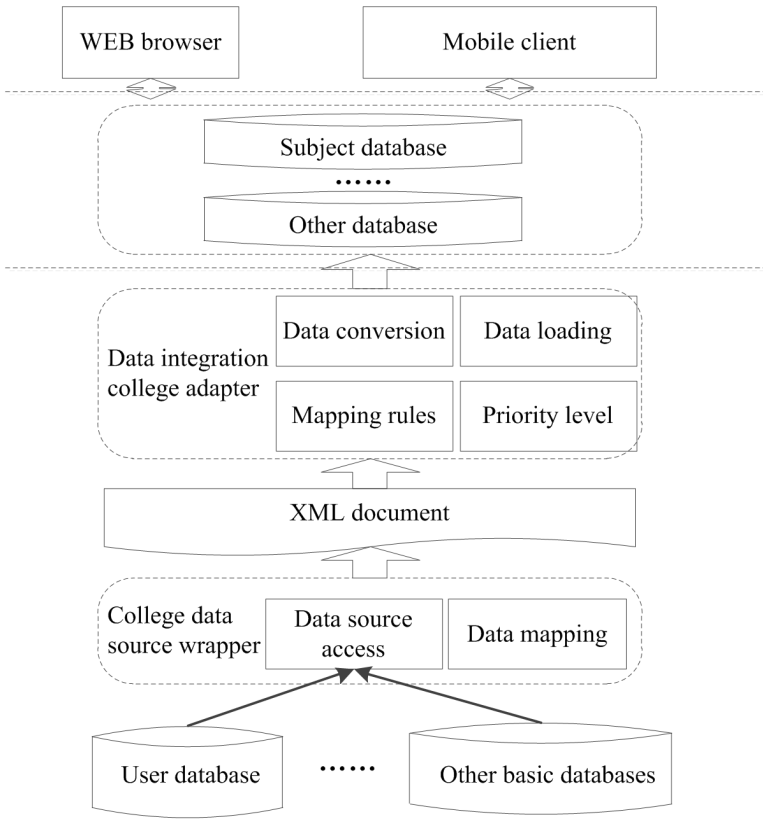

Fig. 2. System physical architecture diagrams

3.2. System database design

The database is used to store data and provide support for the business functions of the system. Therefore, in the final analysis, the database design is to achieve two goals: the first is to meet the requirements of system transaction processing, that is, to meet the function that the system needs to achieve. However, it is still not enough to be satisfied with the functions that the system needs to meet, because the business system needs to achieve a certain processing efficiency. If the access to the database makes that the system performance is greatly reduced, it can only indicate that the design of the database is unreasonable; the second is to store the data. Business systems will produce a lot of data every day, these data do not have a big effect currently, but a lot of regular data are hided there, which can be found

by a large number of data. Therefore, the E-R modeling method needs to be used to build the basic model architecture of the database. The mobile intelligent terminal security protection system based on the Android platform includes five major functional modules: mobile phone anti-theft function, remote command control function, mobile phone antivirus function, process management functions, system upgrades. At present, the mobile phone anti-theft function is the core function of the security system, and the main purpose for designing this function is to protect that the user's personal information will not be leaked because the cell phone was stolen. When the mobile phone is lost, the user can directly send the appropriate operation instructions to destroy the remaining data information in the phone through this function.

When a user discovers that his cell phone is stolen or lost, he can directly send the appropriate command to the lost phone to remotely control the phone to destroy personal information through the remote command function. Mobile antivirus function is mainly to use Pack Manager to compile all of the program packages in the system. According to compare the package name digital signature of different procedures with the virus digital signature in database, when the match is successful, the program can be identified as a virus program, and then it is unloaded from the mobile phone system. System upgrade function is mainly to conduct the phased upgrade for the anti-virus database information in the system, so as to ensure that the system's virus killing ability can maintain long-term effective. The system interface implementation diagram is shown in Fig. 3.

Fig. 3. System interface implementation diagram (Chinese version)

4. Result analysis and discussion

4.1. Test overview

Software testing is one of the important aspects of project construction, which is a comprehensive and complete detection to the code developed before. According to test the system that has been developed, the existing problems or hidden problems of the code can be found. And then, after timely repairing the problems found, the regression testing is carried out, so as to make the code keep constantly robust and stable in the test again and again.

The system of the software developed is tested through the corresponding test method. During the testing process, some errors are obtained and the bugs are fixed, so as to ensure that the system can maintain long-time stable operation. At the same time, people also hope to be able to find some subtle loopholes that are not found or even not noticed in the software development process at the time of testing, and then rapidly repair them. The software test needs to first simulate a set of data, the data should cover all possible situations as much as possible, and then enter them into the system. If the desired output can be obtained, it indicates that the software system is correct; if the desired output can't be obtained, it indicates that the software system is wrong and the software needs to be modified. After the modification is complete, the data needs to be tested again, thereby ensuring that the final software system is correct.

4.2. Test content

At present, the software testing process has several common test methods. The first is white box and black box test method: white box test refers to the tester is very clear about the internal structure of the software, the white box testing is generally carried out through the exhaustive path. Black box testing is also known as functional testing, while its meaning is the opposite of the white box test, the tester is not clear about the internal structure of the software, which tests the software functions completely in accordance with the requirements specification and detailed design specifications. Gray box testing is based on the white box testing and the black box testing, which not only pays attention to the internal structure of the program, but also concerns about the specific function of the software. The second is static test method: static method checks the source code syntax, structure, process, interface, so as to identify the software defects. While the dynamic test method does not care about the source program itself, which only concerns about the difference between the operation results and the expected results of the program. The third is unit test method: this method is also known as the module test. The integrated test is also known as assembly test or joint test, it is the test after assembling all software modules into a system. Before the final deployment of the software, the acceptance test is conducted. The acceptance test is the last test link after completing the unit test, the integration test and the validation test. After the acceptance test is completed, the product can be released and used. The task of the acceptance test is

to ensure that the software has entered the ready state, and then to verify whether the functionality of the software is consistent with the user's requirements. The regression test is to carry out the second after modifying the error of the software test. Alpha testing and beta testing are software testing during the commissioning.

The security protection system of the mobile intelligent terminal based on Android platform designed in this paper mainly used the black box to carry out test. According to use Load Runner software, a whole test was conducted to the performance of the system. Different levels of user access simulation for the system were mainly carried out, and then, the overall response time of the system was tested, so as to determine whether the system met the actual requirements of the actual bearing. According to carry out the systematic testing and other operations to the main functions of the program, the 10 minutes of testing was carried out in accordance with the 50, 100 and 200 concurrent number, the average user pass time and the pass time of 90 % users were recorded at each time. And the performance test situation of the partial operation obtained is shown in Table 1.

Table 1. A test table that is concurrent with some users of the system

Function	Test the user login process				
Purpose	Verify the concurrency of the system when the performance is reached 200 times				
Methods	Virtual maximum maximum limit of 250 concurrent, minimum 50 concurrent test scripts				
Concurrency	Average response time (seconds)	Transaction maximum response time (seconds)	Average transactions per second	Transaction success rate	Clicks per second
50	0.6	1.4	102.154	100%	50.00
100	0.9	1.6	117.941	100%	125.941
150	1.8	3.2	231.667	100%	154.742
200	2.8	4.7	292.173	100%	245.851
250	10.5	22.4	180.411	100%	271.212
Number of concurrent users	CPU utilization	Utilization rate of MEM	Disk I/O situation	DB parameter (M)	The other parameters not listed in the table
50	3 %	4.53	451.319	3500/400	3 %
100	21 %	8.16	579.951	3500/400	21 %
150	26 %	12.32	671.532	3500/400	26 %
200	35 %	19.21	785.435	3500/400	35 %
250	47 %	31.13	800.233	3500/400	47 %

According to the result display of the above test, the following conclusions are obtained: in the case of that the concurrent data was equal, the registration submission processing capacity was better than the login module home page display. And then, in the case of that the number of concurrent was 100, the system could support the normal use for about 150.000 online active users within 8 hours. After testing, all kinds of operations met the user response time requirements, which were mainly that at the time of browsing the tutorial course list, the loading speed did not affect the sense of experience for users to use this function.

4.3. Test result

Program function test cases covered multiple levels of functional testing. The most prominent was the function of security and protection system of mobile intelligent terminal based on Android platform. The functional test results are shown in Table 2.

Table 2. Functional test results table

Function module	The total number of cases	The total number of defect	Resolved	Unsolved
Mobile phone anti-theft function	134	25	18	0
Cell phone anti-virus function	156	27	19	0
Process management function	100	16	14	0
Remote command control	213	28	29	0

According to conduct the tracking debugging and regression testing to the design defects existing in the main function of the program, 45 numbers of Bug were solved ultimately. Therefore, the program function test was feasible. The test method used by the software program should be applied to the program management according to the standard, and the program development requirements should be pointed out according to the different test results. Then, the management level should be described in accordance with the general requirements, so that the function of the entire program can be achieved, and the normal operation of the program can be promoted stably and safely.

5. Conclusion

As we all know, with the development and popularization of smart phones, mobile phone security management functions become more and more important. This article is to develop a convenient, practical mobile phone security system based on the Android system to manage the mobile phone security, and then protect people's privacy to a certain extent, so that users can safely use the phone. The system

mainly includes several core functions: mobile phone anti-theft function, remote command control function, mobile phone antivirus function, process management function, system upgrade. These functions are designed primarily for the actual needs of the user's mobile phone, and the purpose is to protect the user's personal privacy information. At the same time, the system also has a function that is similar to system performance optimization, which is mainly to manage the system background process, and optimize the system cache file and background process, so as to make the system have certain safety protection function, as well as certain practicability. The function of the system is to choose the most valuable application function, so that users can quickly start using in the process, rather than too many functions of most anti-virus systems in the market, thus resulting in dazzling. In addition, the system also implements the open source free principle, which does not embed the advertising information forcibly, and this allows users to avoid the advertising troubles in the use process. At this stage, such an anti-virus system has a certain market prospect.

References

[1] L. C. Huang, H. C. Chang, C. C. Chen, C. C. Kuo: *A ZigBee-based monitoring and protection system for building electrical safety.* Energy and Buildings *43* (2011), No. 6, 1418–1426.

[2] G. Q. Huang, K. L. Mak: *Issues in the development and implementation of web applications for product design and manufacture.* International Journal of Computer Integrated Manufacturing *14* (2001), No. 1, 125–135.

[3] S. J. Mao, Q. X. Liu, M. Li: *Design and development of safety production management information system based on a digital coalmine.* Procedia Earth and Planetary Science *1* (2009), No. 1, 1121–1127.

[4] B. Jin, X. Liu, Q. Bai, D. Wang, Y. Wang: *Design and implementation of an intrinsically safe liquid-level sensor using coaxial cable.* Sensors *15* (2015), No. 6, 12613–12634.

[5] Y. Wu, X. Shui, Y. Cai, J. Zhou, Z. Wu,J. Zheng: *Development, verification and validation of an FPGA-based core heat removal protection system for a PWR.* Nuclear Engineering and Design *301* (2016), 311–319.

[6] D. E. Knoop, A. T. Tershak, M. Thieneman: *An adaptive demand defrost and two-zone control and monitor system for refrigeration products.* IEEE Transactions on Industry Applications *24* (1988) No. 2, 337–342.

[7] J. Jeon, J. Lee, D. Shin, H. Park: *Development of dam safety management system.* Advances in Engineering Software *40* (2009), No. 8, 554–563.

[8] P. Zito, A. Lampasi, O. Baulaigue, S. Gharafi, L. Novello, M. Matsukawa, K. Shimada, F. Fasce, M. Portesine, A. Dorronsoro, D. Vian, K. Celaya, B. Eikelboom: *Design and testing of crowbar protection system for the JT-60SA superconducting magnet power supplies.* Fusion Engineering and Design *124* (2017), 131–136.

[9] C. Zhang, J. M. Kovacs: *The application of small unmanned aerial systems for precision agriculture: A review.* Precision Agriculture *13* (2012), No. 6, 693–712.

[10] A. R. Miller, K. S. Hess, D. L. Barnes, T. L. Erickson: *System design of a large fuel cell hybrid locomotive.* Journal of Power Sources *173*, (2007), No. 2, 935–942.

Received October 12, 2017